SEISMIC HAZARD ANALYSIS

FOR ROCKY FLATS PLANT

Final Report

Prepared for
EG&G Rocky Flats, Inc.
Golden, Colorado

JAN 1995
RECEIVED
Environmental
Library

by

Risk Engineering, Inc.
Boulder, Colorado

September 29, 1994

Prepared By: Robin K. McGuire — Date 9-27-94

QA Review: Thomas P. Stone — Date 9-27-94

Risk Engineering, Inc.: Robin K. McGuire — Date 9-27-94

REVIEWED FOR CLASSIFICATION/UCN
By J. N. CONYERS
Date 9/27/94

352/352

Future Resources Associates, Inc.

2039 Shattuck Avenue Suite 402 Berkeley, CA 94704 510-644-2700

23 September 1994

Mr. Faris M. Badwan
Systematic Evaluation Program Manager
EG&G-Rocky Flats, Inc.
Golden, Colorado 80402

SUBJECT: Final Report of the Peer Review Panel for the "Seismic Hazard Study, Rocky Flats Plant"

Dear Mr. Badwan:

This is the second and final report of the Peer Review Panel that has been assembled by EG&G Rocky Flats, Inc. to review report of the "Seismic Hazard Study, Rocky Flats Plant, Jefferson County, Colorado" that has been produced by Risk Engineering, Inc. study team under contract to EG&G.

The Peer Review Panel's activities began with a review of the July 27 version of the REI draft report, followed by an initial review meeting on August 11-12. The result of that meeting was our initial report dated September 9 (Attachment A), containing technical comments on 18 issues. The REI study team responded with a memorandum dated September 21 (Attachment B), which described how they proposed to deal with each of our 18 issues, as well as an updated version of the project report, incorporating their proposed changes The memorandum and the updated REI report were the focus of discussion at our second review meeting on September 22.

Based on commitments made by the study team at the close of our meeting on September 22 to make a few changes to the report, the Peer Review Panel is fully satisfied with the final report, and recommends that the sponsor, EG&G Rocky Flats, should accept the report and should publish it in the public domain as soon as feasible.

For the Panel:

Robert J. Budnitz
Chairman

Panel: Bruce A. Bolt
Vicki Cowart
John Lysmer
Michael W. West

TABLE OF CONTENTS

Page

Executive Summary ES-1

Section 1. INTRODUCTION 1

Section 2. SEISMIC HAZARD CALCULATIONS 4

2.1 INTRODUCTION 4
2.2 BASIC SEISMIC HAZARD MODEL 4
2.3 TREATMENT OF UNCERTAINTY 8
2.4 SUMMARY 10

Section 3. SEISMIC HAZARD RESULTS 11

3.1 PROBABILISTIC RESULTS 11
3.2 DETERMINISTIC RESULTS 15
3.3 SEISMIC HAZARD ISSUES 16

Section 4. CONCLUSIONS 24

Section 5. REFERENCES 26

APPENDIX A. DETAILED SEISMIC SOURCE CHARACTERIZATION A-1

INTRODUCTION A-1
SEISMIC SOURCE CHARACTERISTICS A-1
FAULT SOURCE CHARACTERISTICS A-7
AREAL SOURCE ZONE CHARACTERISTICS A-23
REFERENCES A-30

APPENDIX B. GEOMORPHIC ANALYSIS B-1

INTRODUCTION B-1
GEOMORPHIC STUDIES OF THE WALNUT CREEK FAULT B-2
REGIONAL TECTONIC GEOMORPHIC STUDIES
OF THE RANGE FRONT B-9
SUMMARY OF THE GEOMORPHIC ANALYSES B-12
REFERENCES B-13

APPENDIX C. REEVALUATION OF THE EPICENTER AND MAGNITUDE FOR THE 1882 COLORADO EARTHQUAKE C-1

OBJECTIVE C-1
BACKGROUND C-1
EPICENTER ESTIMATION C-2
INTENSITY MAP FOR THE 1882 COLORADO EARTHQUAKE C-3
ANALYSIS C-4
MAGNITUDE ESTIMATION C-6
INTENSITY DATA BASE AND INTERPRETATION C-7
ANALYSIS C-7
SUMMARY C-8
REFERENCES C-10

APPENDIX D. HISTORICAL SEISMICITY STUDIES D-1

INTRODUCTION D-1
HISTORICAL SEISMICITY D-1
EARTHQUAKE CATALOG INCOMPLETENESS D-8
HISTORICAL EARTHQUAKE HAZARD D-11
ACTIVITY RATES AND *b*-VALUES D-13
CONCLUSIONS D-18
REFERENCES D-19

APPENDIX E. ATTENUATION RELATIONSHIPS E-1

INTRODUCTION E-1
EMPIRICAL ESTIMATES OF GROUND MOTION E-2
ANALYTICAL ESTIMATES OF GROUND MOTION E-10
ESTIMATES OF SPECTRA E-19
VERTICAL GROUND MOTIONS E-20
CONCLUSIONS E-20
REFERENCES E-22

APPENDIX F. SOIL AMPLIFICATION STUDIES F-1

INTRODUCTION F-1
EMPIRICAL ESTIMATES OF SOIL AMPLIFICATION F-2
ANALYTICAL ESTIMATES OF SOIL AMPLIFICATION F-5
EFFECTS OF FRONT RANGE BEDROCK GEOLOGY F-9
OBSERVATIONS OF EARTHQUAKE INTENSITY F-12
CONCLUSIONS F-13
REFERENCES F-16

APPENDIX G. SOIL LIQUEFACTION POTENTIAL G-1

INTRODUCTION G-1
SUMMARY OF SITE GEOLOGY G-1
METHODOLOGY AND SCOPE OF GEOTECHNICAL DATA REVIEW G-2
SUBSURFACE SITE CONDITIONS G-3
ASSESSMENT OF POTENTIAL FOR LIQUEFACTION G-5
SUMMARY AND CONCLUSIONS G-9
REFERENCES G-11

APPENDIX H. STABILITY OF GEOTECHNICAL STRUCTURES H-1

INTRODUCTION H-1
SUMMARY OF SITE GEOLOGY H-1
METHODOLOGY AND SCOPE OF GEOTECHNICAL DATA REVIEW H-3
SUBSURFACE SITE CONDITIONS H-3
SHEAR STRENGTH PROPERTIES H-4
EVALUATION OF SEISMIC STABILITY H-5
SUMMARY AND CONCLUSIONS H-8
REFERENCES H-9
ADDENDUM H-1: SOIL PROFILES SELECTED FOR EVALUATION OF SEISMIC STABILITY H-20
ADDENDUM H-2: COMPUTER PRINTOUTS OF SLOPE STABILITY ANALYSES H-31

APPENDIX I. DEVELOPMENT OF ARTIFICIAL EARTHQUAKE GROUND MOTIONS I-1

INTRODUCTION I-1
GROUND MOTION CHARACTERISTICS I-1
METHODOLOGY I-2
SELECTION OF REAL RECORDS I-2
NRC REQUIREMENTS I-2
RESULTS I-3
REFERENCES I-4

APPENDIX J. DETERMINISTIC GROUND MOTION J-1

INTRODUCTION J-1
DEAGGREGATION OF PSHA RESULTS J-2
USE OF CAPABLE FAULTS AND AREA SOURCES J-5
SUMMARY J-7
REFERENCES J-9

LIST OF TABLES

TABLE 2-1 SUMMARY OF SEISMICITY PARAMETERS 29

TABLE 3-1 MEAN CALCULATED HAZARD FOR ROCK (FOR 5% DAMPED SPECTRA) 30

TABLE 3-2 MEAN UNIFORM HAZARD SPECTRA FOR ROCK 31

TABLE 3-3 MEAN CALCULATED HAZARD FOR SOIL 32

TABLE 3-4 MEAN UNIFORM HAZARD SPECTRA FOR SOIL 33

TABLE 3-5 VALUES OF AND FOR PSV(10 Hz) AND PSV(1 Hz) 34

LIST OF FIGURES

Figure 2-1. Seismic hazard computational model (modified from McGuire and Arabasz, 1990). 35
Figure 2-2. Historical seismicity and area sources used to represent seismicity in Colorado. 36
Figure 2-3. Potential active faults in the vicinity of Rocky Flats included in the project. . . 37
Figure 2-4. Comparison of PGA estimates on rock vs distance for **M** = 6.5, using the seven attenuation equations derived in this project. 38
Figure 2-5. Comparison of PSV(1 Hz) estimates on rock vs distance for **M** = 6.5, using the seven attenuation equations derived in this project. 39
Figure 2-6. Soil amplification factors vs frequency from empirical and analytical methods. 40
Figure 2-7. Logic tree representation of uncertain parameters for seismic hazard analysis. . 41
Figure 3-1. Total hazard curves, PGA on rock. 42
Figure 3-2. Total hazard curves, PSV(25 Hz) on rock. 43
Figure 3-3. Total hazard curves, PSV(10 Hz) on rock. 44
Figure 3-4. Total hazard curves, PSV(5 Hz) on rock. 45
Figure 3-5. Total hazard curves, PSV(2.5 Hz) on rock. 46
Figure 3-6. Total hazard curves, PSV(1 Hz) on rock. 47
Figure 3-7. Contribution to rock PGA hazard by seismic source. 48
Figure 3-8. Contribution to rock PSV(1 Hz) hazard by 49
Figure 3-9. Sensitivity to 1882 earthquake, PGA on rock. 50
Figure 3-10. Sensitivity to 1882 earthquake, PSV(1 Hz) on rock. 51
Figure 3-11. Sensitivity to M_L conversion, PGA on rock. 52
Figure 3-12. Sensitivity to M_L conversion, PSV(1 Hz) on rock. 53
Figure 3-13. Sensitivity to seismicity rate, PGA on rock. 54
Figure 3-14. Sensitivity to seismicity rate, PSV(1 Hz) on rock. 55
Figure 3-15. Sensitivity to RMA/Derby source slip rate, PGA on rock. (The weight of each hypothesis is indicated in the legend.) 56
Figure 3-16. Sensitivity to RMA/Derby source slip rate, PSV (1 Hz) on rock. 57
Figure 3-17. Sensitivity to Golden-Boulder slip rate, PGA on rock. 58
Figure 3-18. Sensitivity to Golden-Boulder slip rate, PSV(1 Hz) on rock. 59
Figure 3-19. Sensitivity to *b*-value, PGA on rock. 60
Figure 3-20. Sensitivity to *b*-value, PSV(1 Hz) on rock 61
Figure 3-21. Sensitivity to M_{max}, RMA/Derby source, PGA on rock. 62
Figure 3-22. Sensitivity to M_{max}, RMA/Derby source, PSV(1 Hz) on rock. (The weight of each hypothesis is indicated in the legend.) 63
Figure 3-23. Sensitivity to M_{max}, Golden-Boulder fault, PGA on rock. 64
Figure 3-24. Sensitivity to M_{max}, Golden-Boulder fault, PSV(1 Hz) on rock 65
Figure 3-25. Sensitivity to RMA/Derby source representation, PGA on rock. 66
Figure 3-26. Sensitivity to RMA/Derby source representation, PSV (1 Hz) on rock. 67
Figure 3-27. Sensitivity to RMA/Derby source seismicity region, PGA on rock. 68
Figure 3-28. Sensitivity to RMA/Derby source seismicity region, PSV(1 Hz) on rock. 69
Figure 3-29. Sensitivity to RMA/Derby source geometry, PGA on rock. 70
Figure 3-30. Sensitivity to RMA/Derby source geometry, PSV(1 Hz) on rock. 71
Figure 3-31. Sensitivity to attenuation, PGA on rock. 72

Figure 3-32. Sensitivity to attenuation, PSV(1 Hz) on rock. 73
Figure 3-33. Comparison of historical vs. seismic hazard results for PGA on rock. 74
Figure 3-34. Comparison of historical vs. seismic hazard results for PSV(10 Hz) on rock. . . 75
Figure 3-35. Comparison of historical and seismic hazard results for PSV(1 Hz) on rock. . . 76
Figure 3-36. Uniform hazard spectra for $2x10^{-3}$ annual probability on rock. 77
Figure 3-37. PSA vs period for $2x10^{-3}$ annual probability on rock. 78
Figure 3-38. Uniform hazard spectra for 10^{-3} annual probability on rock. 79
Figure 3-39. PSA vs period for 10^{-3} annual probability on rock. 80
Figure 3-40. Uniform hazard spectra for $4x10^{-4}$ annual probability on rock. 81
Figure 3-41. PSA vs period for $4x10^{-4}$ annual probability on rock. 82
Figure 3-42. Uniform hazard spectra for $2x10^{-4}$ annual probability on rock. 83
Figure 3-43. PSA vs period for $2x10^{-4}$ annual probability on rock. 84
Figure 3-44. Uniform hazard spectra for 10^{-4} annual probability on rock. 85
Figure 3-45. PSA vs period for 10^{-4} annual probability on rock. 86
Figure 3-46. Mean uniform hazard spectra on rock 87
Figure 3-47. Mean spectra on rock plotted as PSA vs period. 88
Figure 3-48. Total hazard curves, PGA on soil. 89
Figure 3-49. Total hazard curves, PSV(25 Hz) on soil. 90
Figure 3-50. Total hazard curves, PSV(10 Hz) on soil. 91
Figure 3-51. Total hazard curves, PSV(5 Hz) on soil. 92
Figure 3-52. Total hazard curves, PSV(2.5 Hz) on soil. 93
Figure 3-53. Total hazard curves, PSV(1 Hz) on soil. 94
Figure 3-54. Uniform hazard spectra for $2x10^{-3}$ annual probability on soil. 95
Figure 3-55. PSA vs period for $2x10^{-3}$ annual probability on soil. 96
Figure 3-56. Uniform hazard spectra for 10^{-3} annual probability on soil. 97
Figure 3-57. PSA vs period for 10^{-3} annual probability on soil. 98
Figure 3-58. Uniform hazard spectra for $4x10^{-4}$ annual probability on soil. 99
Figure 3-59. PSA vs period for $4x10^{-4}$ annual probability on soil. 100
Figure 3-60. Uniform hazard spectra for $2x10^{-4}$ annual probability on soil. 101
Figure 3-61. PSA vs period for $2x10^{-4}$ annual probability on soil. 102
Figure 3-62. Uniform hazard spectra for 10^{-4} annual probability on soil. 103
Figure 3-63. PSA vs period for 10^{-4} annual probability on soil. 104
Figure 3-64. Mean uniform hazard spectra on soil. 105
Figure 3-65. Mean spectra on soil plotted as PSA vs period. 106
Figure 3-66. Contribution to hazard by magnitude and distance for PGA = 0.08g, all sources. 107
Figure 3-67. Contribution to hazard by magnitude and distance for PGA = 0.25g, all sources. 108
Figure 3-68. 5% damped spectra for M = 5.9, R = 27 km on rock. 109

Consultants Letters 110

EXECUTIVE SUMMARY

OVERVIEW

This study of the seismic hazard at the Rocky Flats Plant (RFP), Jefferson County, Colorado, has both probabilistic and deterministic aspects and conclusions. On the probabilistic side, a state-of-the-art probabilistic seismic hazard analysis (PSHA) has been conducted to evaluate the probabilities of exceedence of various levels of seismic shaking. Uncertainties in states of knowledge and understanding of earthquake sources, characteristics, and ground motions are represented explicitly and are translated into uncertainties in the probabilistic hazard results. This leads to conclusions on the major contributors to current uncertainties in the seismic hazard at the RFP. On the deterministic side, studies are conducted of the soil liquefaction potential, and of the stability of slopes at the site (subject to seismic shaking). Combining these studies with results from the PSHA allow conclusions regarding the hazard of liquefaction and slope deformation. Also, deterministic ground motion spectra are calculated for the magnitude and distance that dominate the seismic hazard at annual probabilities in the range of interest (10^{-3} to 10^{-4}) for seismic re-evaluation of critical facilities. Throughout this study the emphasis is on ground shaking as represented by peak ground acceleration and by response spectral amplitude in the frequency range 25 Hz to 1 Hz.

This is the most comprehensive seismic hazard study conducted to date for the RFP in that it considers multiple alternative hypotheses on earthquake sources, magnitude distributions, ground motion attenuation equations, and soil amplification factors. The results are robust with respect to changes in assumptions about earthquake distribution parameters and ground motions. Large changes in the PSHA results would occur only if new, active faults were identified in the immediate vicinity of the RFP or if currently-identified faults thought to be active were proven to be inactive.

SEISMIC SOURCES

A comprehensive evaluation of earthquake sources in the vicinity of the RFP was conducted to identify faults or areal sources that might affect seismic hazard at the site. This included the review of previous studies of potentially active faults in Colorado and on-site leveling studies and drainage basin topographic surveys to identify possible differential vertical displacements in bedrock that might be caused by faulting. Also, areal sources were derived based on crustal geology to account for earthquakes not attributable to identified faults.

Fault sources that were identified were the Golden-Boulder segment of the Front Range fault system (herein called the "Golden-Boulder fault"), the Valmont fault, the Walnut Creek fault, and the Rock Creek fault. All of these structures lie within 25 km of the RFP and contribute to seismic hazard at the site. The probability of activity, P_a, of these faults was assessed by an explicit, structured analysis that included possible association with historical seismicity, evidence of late Quaternary slip, structural association with another seismogenic fault, crustal dimensions, and orientation. The following P_a values were assessed for these faults: Golden-Boulder, 0.4; Valmont, 0.4; Walnut Creek, 0.3; and Rock Creek, 0.3. The maximum magnitude of each fault was assessed using relations based on fault length, width, and slip. The results were represented by a discrete probability distribution because there is considerable uncertainty in this parameter. Maximum

magnitudes for these faults were assessed to be in the following ranges: Golden-Boulder, 7 to 7 1/2; Valmont, 5 3/4 to 6 3/4; Walnut Creek, 5 3/4 to 6 3/4; and Rock Creek, 5 3/4 to 6 3/4. Slip rates also were assessed based on offsets of identified geologic units, and again a discrete probability distribution was used to quantify uncertainty in slip rate. These slip rates were used to assess the seismicity rate on the above faults.

The RMA/Derby source lies approximately 15 to 25 km east of Rocky Flats. This source lies close to the Rocky Mountain Arsenal, where considerable earthquake activity was induced by deep-well injection of liquid waste in the 1960s. The locations of these earthquakes led to identification of the RMA/Derby source as a potentially active source by the Colorado Geological Survey. Seismicity rates for the RMA/Derby source were based on hypothesized slip rates and on historical seismicity data; for the latter analysis only earthquakes that were thought to be naturally-occurring (not induced) were included. P_a was assessed to be 0.5 for the RMA/Derby source and its maximum magnitude was determined to be in the range of 5 1/2 to 7.

Five area sources were identified in Colorado to represent the occurrence of earthquakes that cannot be associated with known faults. These area sources, with $P_a = 1$, have seismic activity estimated from the historical record. Maximum magnitudes were assessed based on historical activity and analogies with other regions, and ranged from 5.5 to 7.0 for the host source representing the Denver Basin, to 6.5 to 7.5 for the source representing western Colorado.

STUDIES OF HISTORICAL SEISMICITY

The historical record of earthquakes in Colorado was analyzed in detail to provide a solid data base for statistical evaluations. Conversion of Modified Mercalli Intensity (MMI) to magnitude was examined using recent earthquake data in the region, and uncertainty in this conversion was represented with two relationships for estimation of magnitudes for pre-instrumental shocks in Colorado. Studies of the historical rates of activity allowed evaluation of the periods over which reporting was estimated to have been complete for various magnitude levels, and these interpretations were used to calculate rates of activity in area sources and for the RMA/Derby source. The generally low number of earthquakes in Colorado meant that there is some uncertainty in rates of activity and in the *b*-value of the exponential distribution used to represent earthquake magnitudes, and these uncertainties were represented explicitly.

A specific study was conducted of the 1882 Colorado earthquake, the largest seismic shock in Colorado history. Available studies were reviewed and MMI maps independently redrawn to evaluate whether new inferences could be obtained from original MMI data. This study concluded that there is still considerable uncertainty on the location of the 1882 earthquake; it may have occurred anywhere in northcentral or northwestern Colorado, southern Wyoming, or eastern Utah. Its moment magnitude was assessed with a discrete probability distribution to be between 5.0 ± 0.4 and 6.9 ± 0.2, with the most likely value 6.4 ± 0.3, based on estimates developed from the earthquake's maximum epicentral intensity, the total felt area, and the areas enclosed by the MMI V and VI contours. No additional sources of historical data are evident that would resolve current uncertainties.

GROUND MOTION ATTENUATION EQUATIONS

There are no strong motion records of earthquakes in Colorado, so earthquake ground motions on rock must be estimated by other than strictly empirical procedures. For this study two methods were adopted from California experience, one based on modifying empirical equations derived in California to represent Colorado conditions, and the other based on using an analytical procedure that has achieved wide success in California and in the eastern U.S. The empirical equations are based on an analysis that modified formulas published respectively by Joyner and Boore, Sadigh and Campbell (which are based on California ground motion records) to account for the difference in crustal attenuation between California and Colorado. This led to three predictive equations for the ground motion parameters of interest. The analytical method consisted of using Random Vibration Techniques to model strong ground motion with band-limited white noise, taking explicit account of characteristics of the earthquake source spectrum, attenuation in the crust and attenuation in the near-surface rock. Uncertainties in all of these characteristics were modeled explicitly so that four attenuation equations could be derived to represent the range of predictions of ground motion based on the analytical technique. The two methods give consistent estimates of the amplitudes of ground shaking and provide a range that represents current uncertainty; the empirically-based method and the analytically-based method were weighted 0.5 each to allow a quantitative assessment of ground motion uncertainty.

SOIL AMPLIFICATION

Soils at the RFP consist of Rocky Flats alluvium (a mixture of sand, clay, gravel and boulders) which is about 20 feet thick and which overlies weathered sedimentary units. At a depth of about 100 feet, sedimentary units are competent and have a shear wave velocity of about 2000 ft/s. These soil conditions have the potential to amplify incoming ground motions, so a study of possible amplification was undertaken. Again, both empirical and analytical techniques were used. For the analytical method, a technique is used that is equivalent to the program SHAKE in that it is based on the vertical propagation of shear waves through horizontally-layered soils and is an equivalent-linear method. This technique used Random Vibration Theory to obtain a solution in the frequency domain and hence does not require a time history as input. The shear-wave velocities measured at the RFP in 1993 and 1994 are used as input, along with strain-dependent soil modulus and damping curves. This results in soil amplification factors that are both frequency- and amplitude-dependent. For the empirical method, a technique based on observations in California was modified to account for the average shear-wave velocity for shallow soil layers measured during down-hole testing at the RFP in 1993 and 1994. This method is linear (so the results apply to all amplitudes of ground motion) and is frequency-dependent. The two methods give consistent results, with the empirical amplification factors equivalent to those calculated from the analytical method for about 0.3g peak acceleration of the input motion. The largest amplification occurs around 1 to 3 Hz, and less amplification (and for some amplitudes in the analytical procedure, deamplification) occurs at higher frequencies. The final recommended soil amplification factors are based on the analytical procedure, because it accounts for the amplitude-dependence of soil response. These factors may be used for general evaluation purposes, but specific building analysis or design should incorporate site-specific analyses of soil amplification.

PROBABILISTIC RESULTS

All of the above results are combined into a PSHA to evaluate the annual probabilities with which various amplitudes of ground motion will be exceeded at the RFP for both rock and soil conditions. Explicit account is taken of uncertainties in inputs, and these result in uncertainties in seismic hazard curves and in uniform hazard spectra (the response spectra corresponding to the selected annual probabilities of $2x10^{-3}$, 10^{-3}, $4x10^{-4}$, $2x10^{-4}$, and 10^{-4}). The major source contributing to the hazard at high frequencies is the RMA/Derby source (from 10^{-3} to $2x10^{-5}$ annual probability). The RMA/Derby fault dominates because of its proximity to the RFP, because its maximum magnitudes are in the range 5 1/2 to 7, and because it has an inferred moderate level of activity, based on small naturally-occurring earthquakes in its vicinity. At low frequencies, area Source III dominates the hazard within the $2x10^{-3}$ to 10^{-4} annual probability range. Source III dominates the lower frequencies because it has relatively high rates of activity and has maximum magnitudes in the range 6 1/2 to 7 1/2. Current uncertainties in hazard are typical for a site in a region with few earthquakes and no strong-motion records, and there are no obvious studies that would reduce current uncertainties substantially.

Seismic hazard curves and uniform hazard spectra are illustrated in Figures ES-1 and ES-2, respectively, for rock conditions. The first figure shows seismic hazard for peak ground acceleration; the second figure shows mean 5% damped spectra for the annual probabilities indicated above. Figure ES-3 shows the contribution by magnitude and distance to the hazard of exceeding a peak ground acceleration of 0.25g, which corresponds to a total annual probability of 10^{-4}. Most of the contribution comes from a distance of 27 km, which corresponds to the RMA/Derby source. Other contributions to hazard come from shorter distances because of the area sources in the vicinity.

DETERMINISTIC RESULTS

Deterministic response spectra are presented in this study for the mean magnitude and distance that dominate seismic hazard in the annual probability range of 10^{-3} to 10^{-4}. These spectra show the sensitivity to the ground motion attenuation equations and are also presented for the mean spectrum over all ground motion equations.

Deterministic studies were also conducted of the potential for soil liquefaction and slope instability. Because of the nature of alluvium at the site, where sand layers are generally intermixed with clay and silt, and where most fill and alluvium is cohesive, it is concluded that the potential for soil liquefaction is negligible. With respect to slope stability, under high ground motions (exceeding 0.4g), some slopes of cohesionless alluvium 30 feet in height, with a high water table, may experience permanent deformations up to 30 cm. For slopes that are lower in height, or that consist of cohesive soils or fills, or where the water table is deeper, permanent deformations are estimated to range from 15 cm to negligible.

SUMMARY

This project has conducted a state-of-the-art seismic hazard study that incorporates all relevant hypotheses on earthquake occurrences, characteristics, and ground motions, to estimate seismic hazard at the RFP. Potentially active faults identified by the Colorado Geological Survey have been included as well as area sources used to represent seismicity that occurs away from known faults. The results are presented here for a range of annual probability of exceedence levels and can be used for seismic safety evaluation of plant structures and equipment.

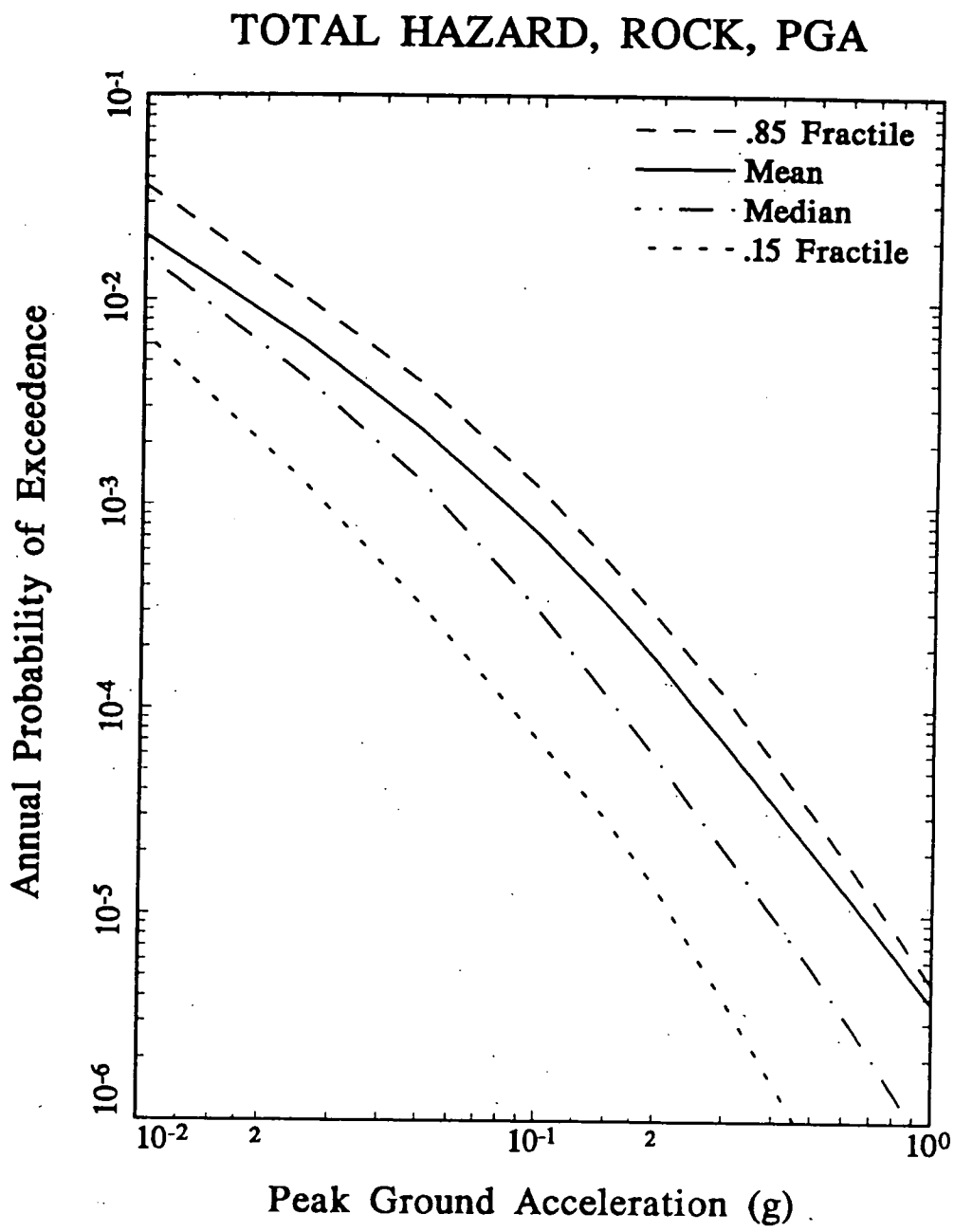

Figure ES-1. Total hazard curves, PGA on rock.

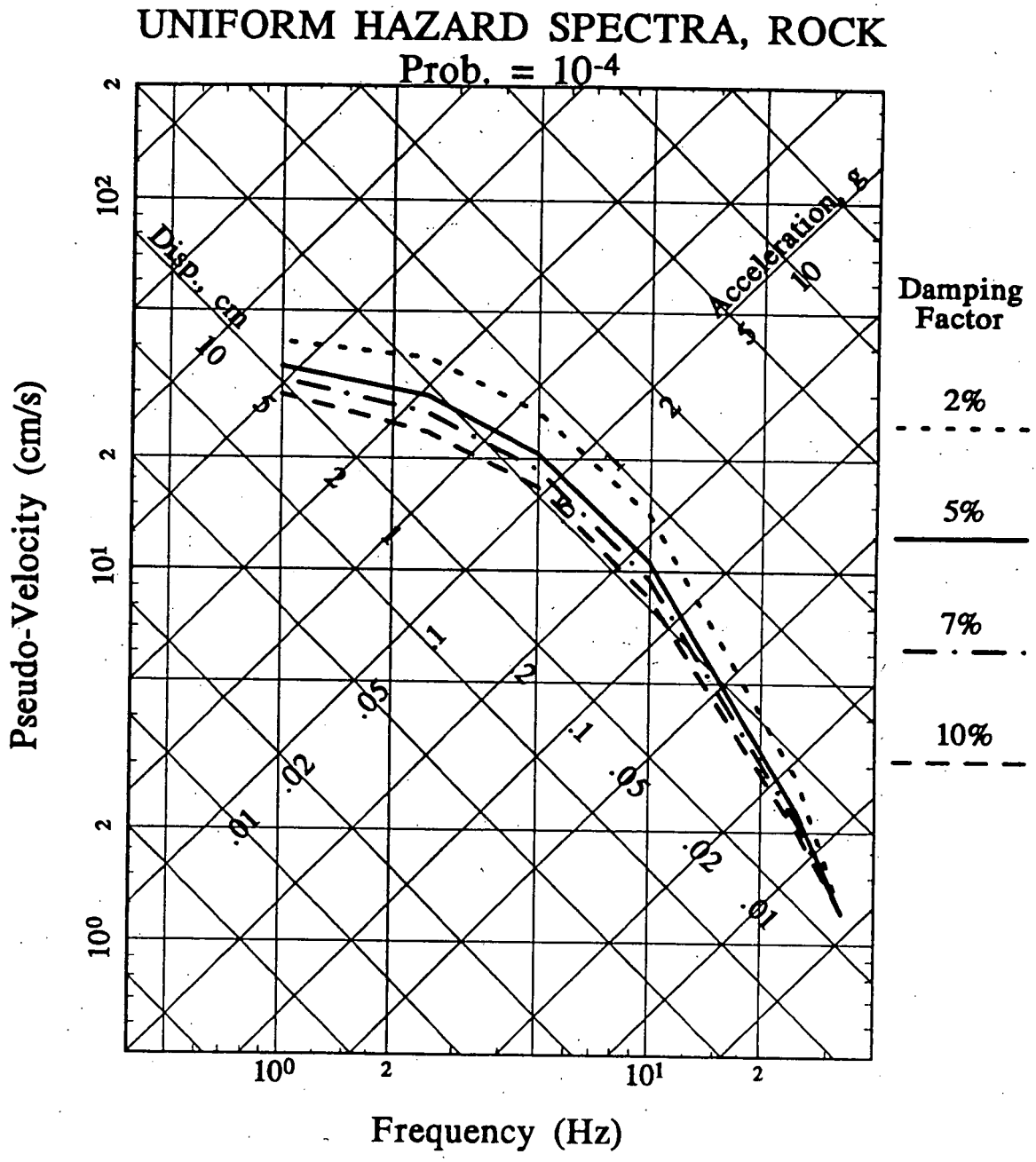

Figure ES-2. Mean uniform hazard spectra on rock.

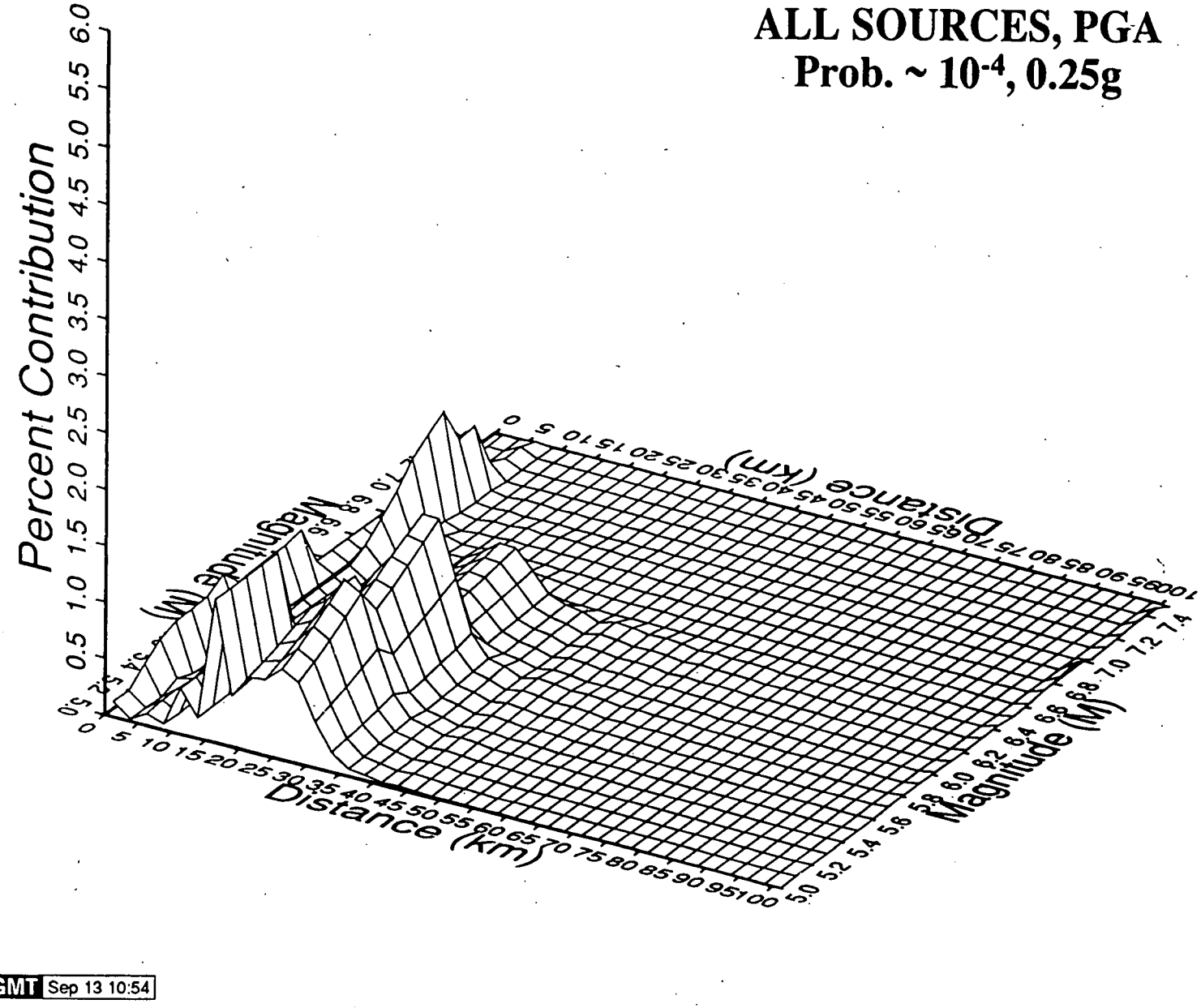

Figure ES-3. Contribution to hazard by magnitude and distance for PGA = 0.25 g, all sources.

Section 1

INTRODUCTION

1. INTRODUCTION

This evaluation of seismic hazard at the Rocky Flats Plant (RFP), Jefferson County, Colorado, has two purposes. The first is to perform a probabilistic seismic hazard analysis at the site to evaluate the probability of exceedence of various levels of ground shaking. The second purpose is to examine several deterministic issues to evaluate whether any has an important impact on the level of seismic hazard at the RFP. This report describes the studies carried out and the conclusions reached for both of these purposes.

The RFP is located at longitude 105.203° west and latitude 39.892° north. Site conditions consist of several tens of feet of alluvium, underlain by weathered claystone to a depth of approximately 100 ft, which in turn is underlain by 13,000 ft or more of sedimentary units. Crystalline bedrock underlays all of these units. The site is located approximately 5 km east of the Front Range of the Rocky Mountains.

There are several products of the study. From the probabilistic analysis, seismic hazard curves have been computed, along with uniform hazard spectra for several return periods. Artificial time histories of earthquake ground motion have been derived corresponding to uniform hazard spectra with specific return periods. From the deterministic analysis, specific spectra have been computed for the mean magnitude and distance that dominate the hazard at the RFP. Also, conclusions have been drawn for each of ten specific seismic hazard issues identified at the start of the project as important to the evaluation of seismic safety at the RFP.

All of these products are described in this report, along with a description of the methodologies used to obtain them. An important aspect of modern seismic hazard studies is the incorporation and quantification of uncertainties in inputs, and the representation of the effects of these in terms of uncertainties in results. Uncertainties are represented explicitly in this study, both for deterministic spectra (showing the result of uncertainty in attenuation equations) and for seismic hazard results (showing the effects of uncertainties in tectonic, seismicity, and ground motion interpretations). This attention to explicit uncertainty representation allows the results to be understood in terms of the precision of available data and models used as input.

Appendices A through I provide details on the inputs used for the studies and on the detailed models and methods used to draw conclusions. Several organizations contributed to this report and to the creation of the Appendices, as follows:

Risk Engineering, Inc. (R.K. McGuire, T.P. Stone, and G.R. Toro) conducted the probabilistic and deterministic seismic hazard evaluations, coordinated the study, compiled the report, wrote the main body of the report, and wrote parts or all of Appendices D, E, F, I, and J.

Geomatrix Consultants, Inc. (K.J. Coppersmith, F. Makdisi, R. Perman, and M. Angell) derived seismic sources in Colorado for input to the seismic hazard analysis and performed the soil

liquefaction and geotechnical stability analyses. This group also wrote Appendices A, B, G, and H of the project report.

EQE International, Inc. (K.W. Campbell) and Pacific Engineering and Analysis (W.J. Silva) conducted ground motion attenuation and soil amplification studies, and wrote parts of Appendices E and F.

Dr. G.A. Bollinger, consultant, conducted the evaluation of the 1882 Colorado earthquake and wrote Appendix C.

Drs. W.J. Arabasz (University of Utah) and C.A. Cornell (Stanford University) provided input and interpretation for the analysis of historical seismicity and conducted reviews of the historical seismicity analysis (Appendix D) and the main report.

Multiple reviews of this work have been conducted by personnel at EG&G Rocky Flats, Inc., and by an external review panel consisting of R. Budnitz (consultant and chair), B. Bolt (University of California, Berkeley), V. Cowart (Colorado Geological Survey), J. Lysmer (University of California, Berekeley) and M. West (consultant).

The report is organized as follows. Section 2 describes the methodology used for probabilistic seismic hazard calculations, and summarizes the inputs to the calculations. Details on the inputs are contained in the Appendices. Section 3 presents recommendations based on the probabilistic results and on deterministic considerations, in several subsections. Subsection 3.1 describes the probabilistic seismic hazard results in terms of seismic hazard curves, uniform hazard spectra, and artificial ground motions derived to match specific uniform hazard spectra. Subsection 3.2 describes deterministic results, which are the calculated spectra for worst-case earthquakes in each seismic source (source area or fault), that being the maximum magnitude event located at the closest distance. This subsection also reviews the results from the soil liquefaction and geotechnical stability studies that were conducted. Subsection 3.3 presents ten seismic issues that were identified at the beginning of the project and summarizes the conclusions reached on each. These issues are as follows:

Issue No. 1: Size, location, and seismotectonic significance of the November 7, 1882 earthquake (Colorado)

Issue No.. 2: Implications of the October 18, 1984 Laramie Mountains (Wyoming) earthquake to seismotectonics of the Colorado Front Range

Issue No.. 3: Amplification of ground motions associated with surficial/bedrock geology of the Colorado Front Range

Issue No. 4: Continuing seismicity in the Rocky Mountain Arsenal area

Issue No. 5: "Potentially active faults" as defined by the Colorado Geological Survey (1981)

Issue No. 6: Implications of seismotectonic studies conducted for Two Forks Dam (Denver Water Department)

Issue No. 7: Structure of the Front Range in the vicinity of Rocky Flats based on oil/gas drilling and geophysical data

Issue No. 8: Origin of the Quaternary graben near Golden and its structural/tectonic relation to the Golden fault

Issue No. 9: DOE interim position on seismic evaluations

Issue No. 10: Ground motion attenuation in the Front Range region

Each of these issues has been addressed based on the studies conducted as part of this project, and the relevance of these issues to seismic hazard at the RFP is discussed. Finally, Section 4 draws overall conclusions from the project, and Section 5 contains references used in the main body of the report.

Appendices follow the main body of the report, as follows:

Appendix A: Detailed Seismic Source Characterization

Appendix B: Detailed Geomorphic Analysis

Appendix C: 1882 Colorado Earthquake

Appendix D: Historical Seismicity Studies

Appendix E: Vibratory Ground Motion

Appendix F: Soil Amplification Studies

Appendix G: Soil Liquefaction Potential

Appendix H: Stability of Geotechnical Structures

Appendix I: Artificial Ground Motions

Appendix J: Deterministic Ground Motions

Each of these Appendices gives details of the specific studies undertaken to provide the input to probabilistic and deterministic analyses described in Sections 2 and 3 of this report. Sections 2 and 3 summarize these studies, but the Appendices should be referenced for details.

Section 2

SEISMIC HAZARD CALCULATIONS

2.1 INTRODUCTION

This Section describes the methodology used to calculate seismic hazard for this project. Specific inputs to the methodology are summarized here and are described in detail in the relevant Appendices.

State-of-the-art seismic hazard studies calculate ground-motion exceedence probabilities using earth-science hypotheses about the causes and characteristics of earthquakes in the region being studied. Scientific uncertainty about the causes of earthquakes and about the physical characteristics of potentially active tectonic features and regions lead to uncertainties in the inputs to the seismic hazard calculations. These uncertainties are quantified using the tectonic interpretations developed by earth scientists familiar with the region. These analysts evaluate the likelihood associated with alternative tectonic features and regions and with alternative characteristics of these potential sources. Similarly, geophysicists and earthquake engineers develop equations estimating strong ground shaking in the region, expressing uncertainties in scientific understanding with alternative hypotheses on magnitude and distance scaling.

These uncertainties are carried through the entire analysis. The result of the analysis is a suite of hazard curves and their associated weights. These curves quantify the seismic hazard at the site and its uncertainty, and can be used to make decisions regarding seismic safety and possible retrofit.

2.2 BASIC SEISMIC HAZARD MODEL

2.2.1 Overview

The methodology to calculate seismic hazard at a site is well established in the literature (Cornell, 1968, 1971; Der Kiureghian and Ang, 1975; McGuire, 1976, 1978) Calculation of the hazard requires specification of three inputs:

1. Source geometry: the geographic description of the seismic source. A seismic source is a portion of the earth's crust associated with a fault, with a concentration of historic seismicity, or with a general region of the earth's crust with similar geologic characteristics, that may be capable of producing earthquakes. Source geometry determines the probability distribution of distance r from the earthquake to the site: $f_R(r)$.

2. Seismicity: the rate of occurrence ν_i, b-value, and magnitude distribution $f_{M(i)}(m)$ of earthquakes occurring in each source i. Magnitude is usually characterized by the moment magnitude scale **M** in California and the Rocky Mountain region, and by the body-wave magnitude m_b in the central and eastern U.S.

3. Attenuation functions: a relationship that allows the estimation of ground motion at the site as a function of earthquake magnitude and distance. Additional factors quantifying the amplification/deamplification of surficial soils are used to include the effects on those soils on ground motions.

These inputs are illustrated in Figure 2-1, parts a through c. Figure 2-1a shows the geometry of a seismic source. From the source's geometry, $f_{R(i)}(r)$, can be derived. The density function on magnitude $f_{M(i)}(m)$ is often specified as the doubly truncated exponential distribution for area sources and the characteristic magnitude distribution (Schwartz and Coppersmith, 1984) for faults, as illustrated in Figure 2-1b. Seismicity for a source with the exponential magnitude distribution is completely specified by the minimum magnitude m_o and parameters a and b. Parameter a is a measure of seismic activity, b is a measure of relative frequency of large versus small events, and $\log[\, v_i\, f_{M(i)}(m)]$ is proportional to $a + b\, m$ for $m_o < m \leq m_{max}$. For the characteristic magnitude distribution, it is necessary in addition to specify the "characteristic" part of the distribution, i.e. the magnitude range of earthquakes that act in a characteristic way, and the annual rate of occurrence of magnitudes in that range.

The ground motion is modeled by an attenuation function, as illustrated in Figure 2-1c. Attenuation functions are usually of the form $\ln[A] = f(M,R) + \epsilon$, where A is ground-motion amplitude, M is magnitude, R is distance, and ϵ is a random variable that represents scatter. The attenuation function is used to calculate $G_{A|m,r}(a^*) = P[A > a^*|m,r]$: the probability that the ground-motion amplitude is larger than a^*, for a given M and R. The seismic hazard over all sources is calculated as a summation:

$$\frac{P[A > a_* \text{ in time } t]}{t} = \sum_i v_i \int\int G_{A|m,r}(a_*)\, f_{M(i)}(m)\, f_{R(i)}(r)\, dm\, dr \qquad (2\text{-}1)$$

in which the summation is performed over all seismic sources i and in which the probability is calculated per unit time.

2.2.2 Tectonic and Seismicity Interpretations

The specification of potential sources of future earthquakes is the first step in the evaluation of earthquake hazards. Seismic sources indicate <u>where</u> earthquakes may occur; analysis of historical seismicity within those defined sources indicates the probabilities of occurrence and characteristics of future earthquakes (i.e., a magnitude distribution is fit to historical data within the source, once the source is defined).

A seismic source is taken by definition to be a fault or area with a single probability of being active, a single magnitude distribution, and a single distribution for maximum magnitude. Within a seismic source the seismicity is usually taken to be spatially homogenous, i.e., earthquakes are assumed to be equally likely to occur at any location within the source. Some studies (e.g. the EPRI/SOG study) use spatially-varying seismicity, but this generalization is not adopted here.

In general, seismic sources are defined based on faults, tectonic features, or other evidence (including, in some cases, merely a spatial cluster of historical seismicity). Because of this derivation there is, conceptually, some <u>causal</u> association of earthquakes within a source: they are

releasing crustal stresses of the same orientation and amplitude, and/or they are caused by slip on faults with the same general depth, orientation, and sense of slip. Because of these similarities the delineation is consistent with the seismic source definition with regard to maximum magnitude and probability of activity.

Figure 2-2 illustrates the area sources derived for this study, and Figure 2-3 illustrates the faults in the region of the RFP that are considered potentially active with a non-zero probability. The faults were determined using available studies on potentially active faults in Colorado, and the area sources were drawn using available knowledge of crustal geology and stress characteristics in the Colorado region.

The tectonic and seismic source interpretations were made by a team from Geomatrix Consultants, Inc. Details on the methods used to derive these area sources and faults are described in Appendix A.

2.2.3 Seismicity Parameters

Seismicity parameters for earthquake sources are estimated using the rate of tectonic slip for active faults, and using historical seismicity for area sources. The rate of slip on faults is important because multiple methods of estimation can be applied, including measured offsets of datable horizons, crustal strain measurements or inferences, mechanistic tectonic block models of crustal plates, and paleoseismicity studies. For area sources, earthquake catalogs are analyzed to collect all seismic events that have occurred within each source. For each magnitude level, periods of completeness are picked and the rate of occurrence for that magnitude level is calculated as the number of events divided by the time of complete observation. These data are then fit using the maximum-likelihood procedure (Weichert, 1980) to obtain estimates of a and b.

When the characteristic magnitude distribution is used, the rate of occurrence of events with the characteristic size must generally be estimated using data other than historical seismicity. This is the case because there are few places in the U.S. where a sufficient number of cycles of seismicity have been observed historically to calculate a rate of characteristic events from observations. For some faults (e.g. the San Andreas), paleoseismic evidence gives some indication of the rate of occurrence of the characteristic earthquakes.

Maximum magnitude distributions are estimated using a combination of techniques (e.g., Coppersmith et al., 1986; Bollinger et al., 1992). Among these are fault length-magnitude relations, comparison with other regions of similar characteristics, consideration of geophysical characteristics that relate to M_{max}, and consideration of the amount of information known about the region under consideration. Ultimately the specification of the M_{max} distribution must be made by analysts familiar with the region. It is important to note that M_{max} values assigned to the fault sources in Appendix A correspond to the middle of the characteristic magnitude interval, whereas the main report adds 0.25 to these magnitudes to represent the upper end of the characteristic magnitude interval.

The choice of minimum magnitude m_o is based on the characteristics of small earthquakes (i.e., on how damaging are the ground motions associated with these earthquakes), analysis of structural response for the facilities being studied, and field observations of structural performance during low-

intensity ground motions. Convention in current studies is to use a moment magnitude of 5.0 for m_o, which is supported by studies of the damageability of ground motions from small magnitude earthquakes (McCann and Reed, 1988a, 1988b).

Table 2-1 summarizes the magnitude distributions and the range of seismicity parameters determined for the faults and area sources of Figures 2-2 and 2-3. For the Golden-Boulder, Walnut Creek, Rock Creek, and Valmont faults, a characteristic magnitude distribution was used, and the seismicity rate was estimated from slip rate. For the RMA/Derby source both a characteristic and an exponential magnitude distribution (fault and area representation) were used and the seismicity rate was estimated from the slip rate and the surrounding historical seismicity that is not associated with the deep-well injection activities at the Rocky Mountain Arsenal in the 1960s. Appendix A describes this source characterization in more detail. The uncertainty in *b*-value for the RMA/Derby source covers the possibility that a characteristic magnitude process might be at work, and expresses a realistic distribution on seismicity rate given the small earthquakes that have occurred historically. The derivation of slip rates, *b*-values, and M_{max} values for faults is documented in Appendix A. The historical seismic activity rates and *b*-values for area sources (and for the RMA/Derby source) are documented in Appendix D, and M_{max} values for these area sources are described in Appendix A. A range of interpretations is shown for each parameter, because the available data on fault slip rate and on historical seismicity in Colorado are not sufficient to estimate seismicity parameters with high precision. The uncertainty in parameters indicated by the ranges in Table 2-1 is treated using the methods described below in Section 2.3.

Seismicity parameters were estimated from historical seismicity by a team from Risk Engineering, Inc. Details of the methods and results are given in Appendix D.

2.2.4 Ground Motion Attenuation Equations

Equations estimating seismic ground motion are required for both seismic hazard calculations and for deterministic spectra calculated for each fault and area source. Because there are no strong motion records available from Colorado earthquakes, ground motion attenuation equations must be modified from other regions to be consistent with known crustal properties in Colorado. In general, two major methods are available to estimate attenuation equations for seismic hazard studies: empirical and analytical. Both methods are used here, by modifying empirical and analytical techniques developed elsewhere for Colorado crustal characteristics. Equations are derived for all measures of interest for the study, which are peak ground acceleration (PGA) and pseudo-velocity (PSV) for frequencies in the range of 25 Hz to 1 Hz. (Results are also presented in terms of pseudo-acceleration, PSA.) Ground motion estimates exhibit randomness, and the standard assumption in seismic hazard analyses is to characterize the randomness using a lognormal distribution with a specified standard deviation of ln[ground motion]. Typically the value of $\sigma_{\ln[\text{ground motion}]}$ varies as a function of structural frequency, and it may also vary with magnitude of the earthquake.

The attenuation equations derived for this study for rock site conditions are compared on Figures 2-4 and 2-5 for M = 6.5. Three of the equations (labelled "Campbell," "Sadigh," and "Joyner and Boore") were derived by modifying available empirical equations from California. Four of the equations (labelled "Analy. no. 1" through "Analy. no. 4") were developed from analytical techniques used in California and eastern North America and adapted here to Colorado conditions.

Ground motions were derived by a team from EQE International, Inc., Pacific Engineering and Analysis, and Risk Engineering, Inc. Appendix E describes in detail these attenuation equations and their derivations.

2.2.5 Site Effects

The alluvial and soft bedrock conditions at the RFP modify any rock motion that occurs at the base of the soil column. To estimate this effect, both empirical and analytical techniques again were used, as no site-specific measurements of soil motion are available at the RFP. Both of these methods used shear-wave velocity measurements made at the RFP in 1993 and 1994 at depths down to 500 feet. The analytical estimates were based on an equivalent linear, vertically propagating shear wave model that is equivalent to the program SHAKE except that it used random vibration methods in place of time domain integration. The resulting soil amplification factors are amplitude-dependent. The empirical estimates of soil amplification modified California results using the average measured shear-wave velocity in the upper layers at the RFP, to obtain an empirically-based estimate of soil amplification at the RFP that was used for all amplitudes. Figure 2-6 compares the amplification factors for the two methods, as a function of frequency. The analytical results show a predominant amplification at 1 to 4 Hz, with lesser amplification at 10 Hz. At frequencies above 10 Hz the PGA controls the response amplitudes, so the ratio increases. The amplitude-dependent site factors were used for the calculations, and the empirical site factors were used to check for reasonableness. Appendix F gives details of the procedures used to derive both the empirically-based and analytically-based soil amplification factors.

2.2.6 Calculations

Equation 2-1 is formulated using the assumption that earthquakes (most particularly, successive earthquakes) are independent in size and location. In all seismic hazard applications, primary interest is focused on computing probabilities for high (rare) ground motions. As a result, the probability of two exceedences in time t is negligible. The same argument holds when considering hazard at a site from multiple sources. Thus, the summation on the right side of Equation 2-1 -- which is the *rate* of earthquakes with $A > a^*$ -- is a good approximation to the *probability* of exceeding amplitude a^* in time t. This is why Equation 2-1 is an approximation (but an accurate one), not a strict equality.

The calculation of hazard from all sources is performed for multiple values of a^* in order to generate the hazard curve, which gives the annual probability of exceedence as a function of a^*. This calculation is performed in the current study for six measures of ground motion: PGA and PSV at five frequencies (25, 10, 5, 2.5, and 1 Hz, all at 5% damping).

2.3 TREATMENT OF UNCERTAINTY

State-of-the-art seismic hazard studies distinguish between two types of variability: randomness and uncertainty. "Randomness" is probabilistic variability that results from natural physical processes. The size, location and time of the next earthquake on a fault and the details of the ground motion are examples of random events. In concept, these elements cannot be predicted even with collection of additional data, so the randomness component of variability is irreducible. The second category

of variability is "uncertainty," which is parametric or modeling variability that results from lack of knowledge about the true state of nature. In principle this variability can be reduced with the collection of additional data.

These two types of variability are treated differently in advanced seismic hazard studies, as follows. Integration is carried out over probabilistic variabilities to get a single hazard curve (as indicated by Equation 2-1). Modeling uncertainties are expressed by multiple assumptions, hypotheses, or parameter values.

There are uncertainties associated with each of the three inputs to the seismic-hazard evaluation, as follows:

- Uncertainty about seismic sources and faults (i.e. about which tectonic features in a region are actually earthquake sources) arises because of lack of knowledge about which, if any, faults created in a previous tectonic environment have been reactivated in the current tectonic environment. P_a, the probability that a source is tectonically active, is assessed using explicit criteria based on earth science information. Uncertainty may also arise about the geometry of a seismic source.

- Uncertainty in seismicity is generally divided into uncertainty in maximum magnitude and uncertainty in seismicity parameters v and b. Uncertainty about M_{max}, the maximum magnitude that a given source can generate, arises from incomplete knowledge about how a fault, perhaps created in a different tectonic stress regime, might release crustal stress in the current regime. Estimates of M_{max} are obtained from physical characteristics of the source and from historical seismicity. Uncertainty in seismicity parameters v and b arises from statistical uncertainty caused by few observations, from lack of knowledge about how completely earthquakes have been reported, and from uncertainty about the accuracy of various catalogs of historical seismicity available with which to estimate parameters. For the characteristic magnitude distribution, additional uncertainties are the magnitude range of the characteristic event and its annual rate of occurrence.

- Uncertainty in the attenuation functions arises from alternative hypotheses about the ground motion characteristics associated with earthquakes. This uncertainty often is large, particularly in areas where few direct recordings of strong motion are available.

These multiple interpretations are used to calculate alternative seismic hazard values according to Equation 2-1, resulting in a suite of hazard curves. The probability for each seismic hazard curve is calculated from the probabilities given to each of the uncertain inputs used to calculate it; the final probability is calculated as the product of the probabilities of the input variables. From the suite of hazard curves, each with an associated probability, fractile curves or a mean seismic hazard curve are derived.

In order to organize and display the multiple hypotheses, assumptions, parameter values and their possible combinations, a logic tree approach is used in this study. Logic trees are a convenient means to express alternative interpretations and their probabilities. Each node of the logic tree represents an input assumption, model, or parameter that is uncertain. The branches emanating from that node represent possible alternative choices of the assumption, model or parameter. The

probability assigned to each branch represents the assessed likelihood that the choice represented by that branch is "correct," given our current knowledge, and these choices (and probabilities) may depend on values of the preceding parameters.

The logic tree in Figure 2-7 illustrates the treatment of parameter uncertainty. There is one hazard curve associated with each terminal node; this hazard curve corresponds to certain sources being active, each active source having a certain M_{max} and certain seismicity parameters, and a certain attenuation function being the "correct" attenuation model. The probability associated with that end branch is the product of the probabilities of all branches traversed to reach that end branch.

Logic trees are a convenient way of organizing the uncertainties incorporated into a seismic hazard analysis, and of documenting them as well. Examples are contained in Appendix A on seismic source characterization.

2.4 SUMMARY

Probabilistic seismic hazard analysis requires as input a delineation of seismic sources, a specification of seismicity characteristics for those sources consisting of magnitude distributions and associated parameters, and a selection of ground motion attenuation equations for the region of interest. In concept all possible earthquakes in the region are modeled, as are the associated ground motions. Uncertainties in active faulting, areal sources, characteristics of seismicity, and ground motion are incorporated explicitly as multiple alternative hypotheses. The effects of these uncertainties are represented as uncertainty in the hazard curves, and sensitivity studies show the influence of each input uncertainty on the resulting calculated hazards. Thus the hazard analysis is an overall methodology that can represent both randomness and uncertainty in earthquake occurrences, characteristics, and ground motions, for the purpose of decision-making regarding seismic risk mitigation.

Section 3

SEISMIC HAZARD RESULTS

3.1 PROBABILISTIC RESULTS

Probabilistic results are presented in this Section in the form of total seismic hazard curves, sensitivities of seismic hazard to uncertainties in input assumptions, and uniform hazard spectra. These results have been calculated using the methodology and inputs described in Section 2. Sensitivity results are presented for both PGA (as a high-frequency representation of the ground motion) and PSV(1 Hz). These results are shown for rock conditions, because the rock hazard curves do not introduce the complicating factor of soils response and may be used as input to a soil-structure interaction model, for example. The sensitivities for hazard at the soil surface are similar.

The total hazard curves with uncertainties are illustrated in Figures 3-1 through 3-6 for PGA and for PSV at 25 Hz, 10 Hz, 5 Hz, 2.5 Hz, and 1 Hz. The mean, median, 15% and 85% fractile curves are shown for contributions from all fault and area sources. As an example of the range in hazard, at $2x10^{-4}$ annual probability the difference in PGA between the 85% and 15% fractile is about a factor of 4. For PSV in the frequency range 25 Hz to 1 Hz the uncertainty in ground motion is about the same as for PGA. The mean hazards are documented numerically in Table 3-1. The slopes of these total hazard curves are about -2 (on log-log scale), and the ratio of mean/median probability is about a factor of 2 to 5 across the frequency range studied.

Figures 3-7 and 3-8 show the mean hazard by fault and area source for PGA and PSV(1 Hz), respectively. These are mean hazard curves in the sense that the mean hazard is computed over all uncertainties in fault geometry, seismicity parameters, and attenuation equation. The P_a is incorporated into the calculation of these curves, as it is in the total hazard curves. From these two plots it is clear that the RMA/Derby source dominates the hazard for annual probabilities between 10^{-3} and $2x10^{-5}$ (for PGA) and between 10^{-4} and 10^{-5} (for 1 Hz PSV). At low ground motion levels (e.g. PGA ~ 0.02g) Source III contributes most because of its high rate of activity. Note that the RMA/Derby source is modeled mathematically as an area source and a fault source because of uncertainty in its location, geometry, and seismicity rate (this source has been inferred on the basis of seismicity patterns--see Appendix A).

The small contributions of sources I through V to the total seismic hazard (except for some contribution at low frequencies and low amplitudes by source III) means that the exact delineation of these sources is not critical. Most interpretations of seismic sources show a separate source in the western part of the state, where historical seismicity is higher (see Figure D-23), and the normalized seismic activity rates in sources I and II are similar (meaning that the boundary between the two is not critical to hazard estimates). All of this means that detailed modeling of uncertainty in the source boundaries would have little effect on the seismic hazard at the RFP.

Results showing the sensitivity of hazard to the input assumptions are presented next. These plots show the mean hazard conditional on fixing several of the input assumptions to specific values, so that the variation in hazard can be examined and judged as to its contribution to the total uncertainty. Approximate numerical sensitivities are also reported as the approximate percentage by which the

ground motion amplitude varies at the $2x10^{-4}$ annual probability level (which is in the range of annual probability levels consistent with typical seismic design levels for critical facilities), as a function of changing each input assumption.

Sensitivity to whether the 1882 earthquake occurred inside or outside of Source I is illustrated in Figures 3-9 and 3-10 for PGA and PSV(1 Hz), respectively. Inclusion of this earthquake increases the ground motion by a factor of about 2 to 2.4 (depending on natural frequency) at the $2x10^{-4}$ annual probability level, over the calculation without the 1882 earthquake. The primary effect of including the 1882 earthquake is to lower the *b*-value estimated from the historical record and to raise the estimated M_{max} values.

The conversion of MM intensity to magnitude is an uncertainty that received substantial effort in the analysis of the historical earthquake catalog. Figures 3-11 and 3-12 indicate the sensitivity to the alternative conversions for Source I. Using the M_{L1} magnitudes results in ground motions that are a factor of 1.5 higher than for the M_{L2} conversion, at $2x10^{-4}$ annual probability.

The rate of occurrence of earthquakes on the RMA/Derby source has an important influence on the hazard, and this is demonstrated in Figures 3-13 and 3-14. Here the sensitivity to seismicity rate is shown for three values that derive from the uncertainty in rate of occurrence (see Appendix D). The rates based on slip rate are not included in these figures but are depicted in Figures 3-15 and 3-16. Uncertainty in seismicity rate resulting from application of the two methods is large. This results in a large uncertainty in hazard (Figures 3-13 through 3-16).

Changes in rate of earthquake occurrence on the Golden-Boulder fault (as well as others) are controlled by changes in the estimated slip rate. Sensitivity to this parameter is illustrated in Figures 3-17 and 3-18. There is a one-to-one relationship between hazard and estimated slip rate, so the range of a factor of 30 in slip rates leads to a factor of 30 range in hazard. The ground motion at $2x10^{-4}$ changes greatly, because the lowest slip rate results in fewer than $2x\ 10^{-4}$ earthquakes per year.

The *b*-values used for the exponential magnitude distribution have an important influence on hazard, and this is illustrated for the RMA/Derby source on Figures 3-19 and 3-20. The total range in ground motion is a factor of 4 to 10 at $2x10^{-4}$ annual probability, from the highest to the lowest *b*-value. Note that, in comparing these two figures to Figures 3-3 and 3-4, incorporation of this large range in *b*-values leads to a much smaller increase in mean ground motion (a factor of 1.2 to 1.4) over the central *b*-value estimates. Stated another way, if one starts with the hazard result from the central *b*-value only, and adds uncertainty in *b*-value estimates (as shown in Figures 3-17 and 3-18), the mean ground motion increases by a factor of 1.2 to 1.4, depending on natural frequency.

The sensitivity to maximum magnitude M_{max} is illustrated for the RMA/Derby source in Figures 3-21 and 3-22 for the area representation of this source. There is no sensitivity at low levels of ground motion, but the importance of M_{max} increases at higher amplitudes to a factor of 1.3 to 1.7 at $2x10^{-4}$ annual probability. For this source, in which seismicity was estimated from historical events, increasing M_{max} increases the hazard.

The opposite effect takes place for the Golden-Boulder fault, where seismicity rates are estimated from fault slip rates. This is shown in Figures 3-23 and 3-24, where separate curves are shown for

the two seismogenic depths specified for this fault. In this case, for a given slip rate, a lower value of M_{max} means that more earthquakes must occur to explain that slip rate, and this higher rate of events causes higher hazard. (The lower value of M_{max} is more than compensated for by the higher rate of activity.) Conversely, a higher value of M_{max} means fewer earthquakes will explain the given slip rate, and the hazard is lower.

The seismicity of the RMA/Derby source is obtained using both an exponential magnitude distribution applied to the historical activity rate (area source) and a characteristic magnitude distribution applied to the seismicity rate (fault source) based on slip rate. Comparison is made on these two representations in Figures 3-25 and 3-26. The two equally-weighted representations show a large difference in hazard at all ground motion levels, primarily as a result of the differences in estimated seismicity rates.

Two representations of uncertainty were made in modeling the RMA/Derby source as an area source, and it is useful to look at their importance. First, two regions were used to collect seismicity for the historical analysis: Region A and Region B (see Appendix D for a definition of these). Region A is larger, it includes more historical events, and leads to slightly higher hazard, as illustrated in Figures 3-27 and 3-28. Second, two geometries were used to characterize the spatial extent of the source, Geometry 1 and Geometry 2 (see Appendix D for a definition of these). Geometry 1 extends closer to the RFP and leads to slightly higher hazard, as illustrated in Figures 3-29 and 3-30. Neither of these uncertainty models has a large influence on the hazard, as illustrated by Figures 3-27 through 3-30.

The effect of attenuation uncertainty is illustrated on Figures 3-31 and 3-32, which shows the mean hazard curves for each of the seven attenuation equations for PGA and PSV(1 Hz), respectively. Ignoring the two extreme analytical equations (nos. 1 and 4, which have very low weight), the range of ground motion at 2×10^{-4} annual probability is about 2.2 for PGA and 2.9 for PSV(1 Hz), which implies an important contribution to uncertainty in hazard.

To summarize the sensitivities, major contributions to uncertainty in hazard come from attenuation equation uncertainty, M_{max} uncertainty, seismicity rate (including source representation) and *b*-value uncertainty on the RMA/Derby source. The location uncertainty on the 1882 earthquake, and M_L-MMI conversion uncertainty, are important for Source I. Of the above sources of uncertainty, the attenuation equations are most important, as they affect all sources simultaneously.

We can gain some insight into the accuracy of the hazard results by comparing calculated seismic hazard with the historical analysis presented in Appendix D. Figures 3-33 through 3-35 show the medians, upper and lower fractiles from the two sets of analyses (the seismic hazard results are presented for the 15% and 85% fractiles, the historical results are presented in Appendix D for the 10% and 90% fractiles). The three figures show results for PGA, PSV(10 Hz), and PSV(1 Hz), respectively. The uncertainty bands generally overlap, with the analytical results showing more uncertainty than the historical results. There is a good reason for this. The seismic hazard results include, and for PGA in the annual probability range 10^{-2} to 10^{-3} are dominated by, earthquakes on the RMA/Derby source. This feature has not had a historical earthquake greater than M = 4 (except for events caused by the Rocky Mountain Arsenal disposal well), so no contribution to the historical hazard comes from the RMA/Derby source. (Recall that the lower-bound magnitude for both analyses was M = 5). The RMA/Derby source contributes to the seismic hazard for the range 10^{-3}

to 10^{-4}, as is clear from Figures 3-3 and 3-4, and uncertainties in parameters for this source are large, so the analytical hazard results have larger uncertainties than the historical results.

The rock hazard curves are presented in the form of uniform hazard spectra as both tripartite plots and acceleration vs. period plots in Figures 3-36 through 3-45 for mean spectra corresponding to damping values of 2%, 5%, 7%, and 10%. These are shown for the following annual probabilities and return periods:

Annual Probability	Return Period
$2x10^{-3}$	500 yrs
$1x10^{-3}$	1,000 yrs
$4x10^{-4}$	2,500 yrs
$2x10^{-4}$	5,000 yrs
$1x10^{-4}$	10,000 yrs

The mean rock spectra are presented together for the five return periods in Figures 3-46 and 3-47 for 5% damping, and Table 3-2 documents these mean spectra in terms of the ground motion values associated with the above return periods. Note that the values are the PGA values plotted at the high-frequency (short period) end of the spectra at 33 Hz on these plots.

Artificial ground motions have been derived whose response spectra match those calculated for each annual probability (return period) given in the above table. These artificial motions can be used as input to soil-structure interaction analysis for specific structures at the RFP. Details of these ground motions are documented in Appendix I.

Hazard results for soil were computed from the rock hazard calculations by using the computed soil amplification factors to determine seismic hazard at the free-field soil surface. The uncertainty in soil hazard curves was considered to be the same as the uncertainty in rock hazard curves, i.e. no additional uncertainty in the soil amplification was taken into account, following the recommendation of EPRI (1993; p. 9-55). The soil hazard curves are illustrated on Figures 3-48 through 3-53 for PGA and PSV at 25, 10, 5, 2.5, and 1 Hz, respectively. These are similar to the rock hazard curves but they take into account the calculated soil amplification/deamplification. The mean seismic hazards for soil conditions are documented in Table 3-3. The soil results are not recommended for analysis or design of specific buildings.

Figures 3-54 through 3-63 illustrate the uniform hazard spectra for soil, for the same return periods documented above for rock, and Figures 3-64 and 3-65 plots together the mean uniform hazard spectra for soil, for the five return periods. Table 3-4 documents the numerical values for the mean uniform hazard spectra.

In addition to the direct hazard results, the hazard has been deaggregated to show the contribution by magnitude and distance. Appendix J gives the details of this deaggregation, and Figures 3-66 and 3-67 illustrate the magnitude-distance contribution for PGA = 0.08g and 0.25g, respectively.

These PGA levels correspond to 10^{-3} and 10^{-4} annual probabilities of exceedence. The figures indicate that the RMA/Derby source at 27 km dominates the hazard for PGA from 0.08g to 0.25g. Similar results are presented in Appendix J for 1 Hz frequency.

3.2 DETERMINISTIC RESULTS

This section presents deterministic results in the form of spectra computed for a representative magnitude and distance important to hazard at the RFP, and in terms of conclusions from the soil liquefaction and geotechnical stability parts of the project.

Deterministic Spectra

A set of spectra are plotted on Figure 3-68 for = 5.9 and R = 27 km. These values are the modal (most likely) magnitude M and distance R for events causing exceedences in the 10^{-3} and 10^{-4} annual probability range, where the RMA/Derby source dominates the hazard. Table 3-5 illustrates values of M and R for several amplitudes and natural frequencies for the RMA/Derby source. Figure 3-66 illustrates the sensitivity of the median spectral shape to attenuation equation, and also shows the average of the median spectra.

Additional examples of deterministic spectra are presented in Appendix J.

Soil Liquefaction and Geotechnical Stability

Appendices G and H present an analysis of "Soil Liquefaction Potential" and "Stability of Geotechnical Structures," respectively. These studies were conducted as part of the current project.

Appendix G on soil liquefaction finds that soil conditions at the RFP consist of stiff clays, medium dense to very dense sands, medium dense to very dense gravels, and stiff cohesive fill. Where sand occurs, it is generally clayey or gravelly. The conclusion is that under any ground motions envisioned for the RFP, there is very little likelihood of liquefaction due to the nature of the Rocky Flats alluvium.

With respect to the stability of slope surfaces, the analysis conducted and reported in Appendix H indicates that some slopes may undergo some amount of permanent displacement under extreme loadings and conditions. If ground motions at the 10^{-4} annual probability level are considered for seismic evaluations, the corresponding ground motions are 0.25g to 0.35g at the mean level (see Figure 3-1). If soils comprising slopes at the RFP are cohesionless, if they are about 30 ft in height, and if the water table is within 10 ft of the crest of the slope, these slopes can be expected to have permanent displacements that might approach 30 cm. For slopes comprised of cohesive soil or fill, the permanent displacements would be less than this, perhaps as much as 15 cm. A lower water table or a slope that is less than 30 ft could be expected to undergo less displacement. Note that these conclusions were reached using conservative assumptions on shear strength parameters, as detailed site parameters were not available for this study.

3.3 SEISMIC HAZARD ISSUES

Ten seismic hazard issues have been addressed by this project, in addition to the calculation of seismic hazard. These issues are stated in this Section, along with their degree of resolution and potential impact on seismic hazard given current knowledge.

Issue No. 1: Size, location, and seismotectonic significance of the November 7, 1882 earthquake (Colorado).

The location, size, and association of this earthquake with a particular tectonic structure or province has been the focus of significant study (e.g. Hadsell, 1968; Coffman and Von Hake, 1973; Dames and Moore, 1981, McGuire et al., 1982; Oaks et al., 1985; Kirkham and Rogers, 1986, 1988). The most recent studies estimate its size at about magnitude 6 to 6 1/2 and place its epicenter in north-central Colorado. Despite its obvious importance as the largest historical earthquake in the state, the significance of the 1882 event to seismic hazard, given our present knowledge of the event, is limited, as we proceed to explain.

Under this project, Dr. G.A. Bollinger has reviewed available data and interpretations of the 1882 earthquake and has quantified his uncertainties on the epicentral location and magnitude of the event (see Appendix C). Given currently-available data, the epicenter may have been anywhere in north-central or northwestern Colorado, southern Wyoming, or northeastern Utah, and the moment magnitude is estimated to have been in the range 5.0 ± 0.4 to 6.9 ± 0.2, with a best estimate of 6.4 ± 0.3.

Evidence has not been found that will allow association of the 1882 earthquake with a particular fault. As a result, the event must be treated for hazard analysis using an areal source and cannot be tied to any particular position other than within the source zone boundaries. Sensitivity studies indicate a moderate sensitivity of the seismic hazard to whether the 1882 earthquake is in source area I (the host source), but this source does not contribute significantly to seismic hazard at Rocky Flats. The primary effects of including this earthquake in the historical seismicity analysis for a source are that estimates of the *b*-value based on historical seismicity are reduced, and maximum magnitudes are increased. Both effects increase the frequency of events with $M > 6$.

The seismotectonic significance of this earthquake is that it shows that magnitude 6 to 6 1/2 earthquakes are possible in the area. This is not surprising, given the level of earthquake activity in the area and the topographic relief associated with the Rocky Mountains. Earthquakes of this size are taken into account both by the source areas derived for this study and by the faults delineated as earthquake sources. Thus while the size and location of this earthquake cannot be resolved, the effect of uncertainties in these parameters are taken into account in the current hazard study.

Issue No. 2: Implications of the October 18, 1984 Laramie Mountains (Wyoming) earthquake to seismotectonics of the Colorado Front Range.

This earthquake had a magnitude (M_L) of 5.5 and was located over 300 km from the Rocky Flats Plant. This means that the causative fault will have little effect on strong ground motions at the site. The broader question of how this earthquake affects seismotectonic interpretations within Colorado revolves around what has been learned about the characteristics of the event.

Efforts to find the causative fault for the earthquake have not been successful (Langer and Snyder, 1988; Langer et al., 1991). Studies of the intensity distribution (Stover, 1985) and focal mechanisms (Langer et al., 1991) provide information on the source parameters for the event and its aftershocks.

The dominant style of faulting during the mainshock and aftershocks was strike-slip and normal, suggesting a predominately extensional stress regime with T-axis in the northeastern quadrant (Langer et al., 1991). This is common for the Rocky Mountain province and does not indicate an unusual style of faulting or type of earthquake that requires special modeling in a hazard analysis. Focal depths for the earthquakes and its aftershocks of about 20 to 25 km (Langer et al., 1991) are unusual for earthquakes in the region and should not be considered typical in the sense that future earthquakes should be modeled with these depths.

The confirmation of extensional stresses in the area is useful in helping to delineate the location and nature of the boundary between the compressional stress regime of the mid-continent and the extensional stresses of the Rio Grande rift and Colorado Plateau. The specific importance of these assessments to seismic hazard at the site is relatively small.

Issue No. 3: Amplification of ground motions associated with surficial/bedrock geology of the Colorado Front Range.

Amplification of ground motions at Rocky Flats might come from two causes. First, the Rocky Flats alluvium overlying claystone may amplify vertically-propagating wave amplitudes in the frequency range of engineering interest. Second, the sedimentary units underlying Rocky Flats become more shallow to the west, and ultimately the sedimentary/crystalline interface comes to the surface at the Front Range of the Rocky Mountains. This geometry might generate surface waves and trapped body waves, increasing low frequency ground motions over those that would occur for horizontally-layered units. Both potential phenomena are explored in this study.

To examine the effects of alluvial layers on ground motion amplitudes, we have used two methods. Both methods rely on the downhole shear wave velocities measured in 1993 and 1994 in boreholes at Rocky Flats. The first uses an analytical method employing vertically-propagating shear waves to estimate soil response. The method uses a random vibration theory equivalent linear approach, which is equivalent to the program SHAKE except that time histories are not required. The second method uses empirically-based predictions of soil response in California, and modifies those predictions using the Rocky Flats shear wave velocities. Both methods indicate that the predominant amplification occurs at low frequencies (below 5 Hz). The analytical method results in amplitude-dependent amplification factors, and these factors are used to generate spectra for the soil surface.

The effects of this soil amplification is relevant to the seismic hazard at Rocky Flats, and the soil amplification factors are used in this project to calculate hazard at the soil surface. The techniques used here are state-of-the-practice in that similar techniques are used in like projects for similar facilities. The only better way to obtain soil amplification factors for Rocky Flats would be to deploy several downhole arrays of strong motion seismographs and wait to record multiple strong earthquakes, which is not practical. Thus the soil amplification caused by overlying Rocky Flats

alluvium has been resolved to the extent possible, and is incorporated into the hazard estimates for the soil surface.

For site-specific analyses that employ soil structure interaction (SSI) investigations or detailed building-specific soil columns, it is recommended that the rock outcrop motions be used as control motions. The control point should be taken at a depth of about 100 feet with a bedrock velocity of 2000 ft/sec (610 m/sec) and the base case profile used (Figure F-4). If a local building-specific profile is used, it should extend to a depth where the material has a velocity of about 2000 ft/sec (610 m/sec). For profiles which do not extend to a sufficient depth, they may be merged to the base case profile. The rock motions (both horizontal and vertical) should be propagated to the surface using an appropriate computational scheme that can accommodate both horizontal and vertical motions. This approach reflects state-of-practice site-specific analyses and is the only approach available.

For a generic analysis of structures at the soil surface, the soil motions (both horizontal and vertical) presented in this report should be used. These represent the effects of soil for the base case profile (Figure F-4) and represent an average conversion of horizontal to vertical motions. Therefore, these motions are appropriate for a generic analysis.

With regard to the amplification caused by geometric effects of sedimentary bedrock juxtaposed against older igneous and metamorphic units, a 2-dimensional, time-domain, explicit finite-difference model was used to determine the extent to which ground motions (including surface waves) might be amplified at Rocky Flats. Properties of the sedimentary and crystalline units were estimated from available sonic logs and reflection lines. The analysis indicated no significant amplification at frequencies of 1 Hz and higher.

An additional, empirical analysis was conducted of intensity observations from the 1984 Laramie Mountains (Wyoming) earthquake. This analysis examined whether intensities in the Front Range area were systematically higher than in other locations for this well-observed earthquake. There was no statistically-significant effect of location near the Front Range that indicated higher-than-average intensities for this earthquake.

Our conclusion with respect to this geometric amplification is that the location of the RFP close to the Front Range, where sedimentary units are juxtaposed against crystalline bedrock, does not amplify ground motions at frequencies of 1 Hz and higher. Therefore amplifications of this type should not be incorporated into a seismic hazard analysis.

Issue No. 4: Continuing seismicity in the Rocky Mountain Arsenal area.

The Rocky Mountain Arsenal, located about 30 km east of the RFP, operated a deep fluid injection well between November 1961 and February 1966. A temporal and spatial association of earthquakes with the volume of injected fluid was noted by Evans (1966) and Healy et al. (1966, 1968), among others. Three earthquakes with reported magnitudes in the lower 5 range, which were the largest shocks of the sequence, occurred in 1967 after injection had stopped. These three largest shocks had seismic moments that imply moment magnitudes of 4.5 to 4.8 (Herrmann et al., 1981). Seismicity in the vicinity of the injection well subsequently decreased after the late 1960s. Convincing arguments have been made that the local earthquakes in the vicinity of the Rocky

Mountain Arsenal were caused by tectonic stresses whose release was triggered by the fluid injection (e.g., Hsieh and Bredehoeft, 1981; Nicholson and Wesson, 1990; Davis and Frohlich, 1993). It is likely that similar tectonic stresses exist elsewhere in Denver and Front Range areas.

The seismicity record of the Rocky Mountain Arsenal area includes eleven earthquakes that either precede or cannot convincingly be associated with the deep-well injection of the 1960s. Four of these earthquakes occurred between 1902 and 1924 and included two shocks of MMI IV; the other two were recorded as "felt." The remaining seven earthquakes occurred subsequent to 1972 when the effects of injection are estimated to have dissipated (Hsieh and Bredehoeft, 1981). The fluid-injection-related earthquakes did not behave like an aftershock sequence in time, so a rate-decay model such as typically used in estimating the change from aftershocks to normal background activity could not be applied successfully. The process of pore pressure build-up and diffusion does not change crustal stresses, either in space or time, the same way a main shock does.

The RMA/Derby source, with which one can arguably make a spatial association with the Rocky Mountain Arsenal seismicity, has been identified by the Colorado Geological Survey (Kirkham and Rogers, 1981) as "potentially active." Therefore, we include the RMA/Derby source in our analysis, using historical earthquakes in its vicinity not associated with the deep-well injection activities to estimate historical rates of occurrence. The maximum magnitude on the RMA/Derby source is estimated using the fault length and width.

With these historical observations and identification of the RMA/Derby source as "potentially active," it is important to include this fault in the seismic hazard analysis. This has been done in this study, using a probability of activity of 0.7 (see Appendix A) and using historical seismicity to estimate rates of activity (see Appendix D). The RMA/Derby source is relevant to seismic hazard at Rocky Flats, at least for annual probabilities of about 2×10^{-4} and greater. (At lower annual probabilities, other sources indicate larger contributions to the hazard.) Current uncertainties on the activity of this fault cannot easily be resolved, as there is no surface expression of this feature. Kirkham and Rogers (1981) determined the fault to be potentially active on the basis of earthquake epicenters from seismicity induced at the Rocky Mountain Arsenal. Also, the association of historical (non-induced) events with the fault is uncertain. That uncertainty has been incorporated here explicitly with multiple hypotheses on the events used to estimate the historical rate of activity. Thus current uncertainties are accounted for in the seismic hazard analysis; there is no apparent way in which these current uncertainties could be reduced to better resolve the hazard from the RMA/Derby source.

Issue No. 5: "Potentially active faults" as defined by the Colorado Geological Survey (1981).

The faults identified as "potentially active" in the mapping by Kirkham and Rogers (1981) have potential importance to the seismic hazard assessment in two ways: faults in close proximity to Rocky Flats (50 km or less) could contribute to site ground motions; and faults at some distance lying within tectonically-analogous regions to the site could be diagnostic of the seismic potential of sources closer to the site. The closest mapped "potentially active" fault to the site is the Golden-Boulder section of the Front Range fault system and was the subject of detailed investigation along the main trace previously (Dames and Moore, 1981; Darrow and Krusi, 1981). These studies indicated that the mapped Golden fault is not capable by USNRC criteria (i.e. the most recent displacement occurred prior to 600,000 year-old Verdos-age alluvium). However, deep seismic

reflection profiling along a profile from the Front Range past Rocky Flats indicates some possibility for current activity along the Front Range fault system, in particular on the Golden-Boulder sections of this system. Thus the Golden-Boulder fault has been included in the current seismic hazard study, with a probability of activity of 0.4. Close to the site other relevant earthquake sources are the Valmont fault, RMA/Derby source (discussed in Issue No. 4 above), Walnut Creek fault, and Rock Creek fault. The first two were identified by the Colorado Geological Survey as potentially active, the others were not. All four have been included in the hazard calculations presented here. Other faults at progressively greater distances from the site include the Floyd Hill, Kennedy Gulch and Jarre Creek faults. These faults were the subject of detailed investigations in conjunction with the geologic and seismotectonic investigations by the Denver Water Department (1986). All of these faults are interpreted to not displace deposits at least as old as late Pleistocene in age. Uncertainties exist because the relationship between the faults and Quaternary deposits can only be established intermittently along their traces and because of uncertainties in the age of deposits. However, the conclusion is that these faults are not active in the present tectonic regime.

In sum, the mapped "potentially active" faults identified by the Colorado Geological Survey in the nearby vicinity of the site have all undergone fairly detailed field investigations elsewhere and have been reviewed in detail for this study. They have largely been found to be inactive, with some possibility (probability of 0.4) of the Golden-Boulder fault being active (see Appendix A).

The potential activity of faults in the vicinity of Rocky Flats is critical to the seismic hazard. The calculation of hazard is dominated by hypothesized faults in the area (represented, for example, by the RMA/Derby source and Golden-Boulder fault), and these have been characterized as well as possible given current knowledge and investigations of these faults.

Issue No. 6: Implications of seismotectonic studies conducted for Two Forks Dam (Denver Water Department).

The studies conducted by the Denver Water Department (1986) mark a significant contribution to understanding of the seismotectonic environment of the central Front Range. The area that has significance to the seismic hazard at the Rocky Flats site is the investigation of several "potentially active" faults within 100 km of Rocky Flats. The regional fault studies and Quaternary geologic studies provided local calibration for regional Rocky Mountain chronosequences and demonstrated that local fluvial stratigraphy and soils could be tied to regional glacial episodes for purposes of dating the age of most recent displacement on the faults. The seismic hazard issues associated with the "potentially active" faults investigated by the Denver Water Department are discussed above in Issue No. 5.

An issue that is addressed in the Denver Water Department studies but not resolved is the issue of the state of tectonic stress in the central Front Range. From the standpoint of seismic hazard analysis, stress state is important inasmuch as areal seismic source boundaries are drawn taking into account stress provinces, and because the orientation of stress axes relative to that of particular faults may be an indicator of their potential for activity. Denver Water Department (1986) concludes that microseismic monitoring in the central Front Range indicates strike slip displacements consistent with the Larimide compressional stress regime. They attribute these stresses to "remnant stresses" inherited from earlier tectonism (Warner, 1986). However, other more regional studies have concluded that the central part of Colorado lies within a large region of extension (e.g. Wong, 1986;

Zoback, 1988) marked by a relative uniformity in the orientation of the least principal stress axis lying in the northeast quadrant. The origin of these extensional stresses is uncertain, although Wong (1986) suggests that they may be related to development of the Rio Grande rift and Zoback (1988) suggests that the stress may be related to the same thermal uplift affecting the Basin and Range province. Ultimately, the issue of the implications of stress orientations to the activity of a particular fault is minor. Geologic criteria for activity, such as the age of the most recent displacement, override considerations of the favorability of the orientation of a fault to the tectonic stress regime. Thus issues related to the state of tectonic stress addressed by the Denver Water Department (1986) do not have large implications on the seismic hazard at Rocky Flats.

Issue No. 7: Structure of the Front Range in the vicinity of Rocky Flats based on oil/gas drilling and geophysical data.

Although the structure of the central Front Range is extremely important to an understanding of the geologic history of the region and the potential for hydrocarbons, it is potentially important to the seismic hazard at the site in only a restricted sense. The nearby structure is only important if faults contained therein have the potential for earthquake generation within the present tectonic environment. The Front Range structures developed in a previous tectonic regime, and reactivation in the contemporary tectonic regime is probably occurring only locally. Studies all over the world have shown that the best indicator of the potential for future fault activity is the presence of Quaternary deformation along a fault zone (Allen, 1975). Recent experience with blind seismogenic faults would broaden the definition of "deformation" somewhat to include Quaternary folding above a blind fault (Coppersmith, 1991) as well as brittle surface displacement. Therefore the most appropriate way to address the importance of the complex Front Range structure to seismic hazard is to focus on the issue of whether or not such structures show evidence of Quaternary, particularly late-Quaternary, deformation. If they do, then unraveling the details of their structure is warranted. If not, detailed data gathering and structural analysis is simply not justified from the standpoint of seismic hazard assessment.

Faults that are shown to be associated with Quaternary deformation are characterized in the current study as fault sources for the seismic hazard analysis and, to the extent that downdip geometries are known, this information is incorporated into their characterization. A key uncertainty in assessing the earthquake potential of reactivated faults is the length of the fault that has been reactivated (which is therefore the maximum possible rupture length). Reactivated faults in close proximity to the Rocky Flats site are significant to the site hazard, particularly for very long return period ground motions.

An effective approach that has been used here to evaluate the potential for Quaternary deformation across the entire Front Range-Great Plains boundary is to carry out a tectonic geomorphic analysis across the boundary and to the east past the location of the Rocky Flats Plant. Tectonic geomorphology (Bull, 1984) was evaluated using existing Quaternary maps (e.g. Trimble and Machette, 1979) and digital topographic data available from the USGS. The object of these studies was to use particular geomorphic surfaces of known age as "strain gauges" to assess whether or not they have been deformed. These techniques have been applied in extensional environments (Bull, 1984, 1990), compressional environments (Bullard and Lettis, 1990), and low-strain rate environments of the southeastern U.S. (Hanson and Bullard, 1992). An advantage of these techniques is that they are capable of discerning either brittle surface fault displacement or near-

surface folding related to deep-seated fault slip. Quaternary data were also combined with available interpretations of the deeper structure in the vicinity of the site in a balanced cross section analysis. Quantitative cross section balancing techniques developed in recent years relate secondary fault-related features observed at the surface (e.g. folding, tilting) to the location, shape, and slip of a primary fault at depth. By incorporating the Quaternary geologic data (both Quaternary deposits as well as associated geomorphic surfaces), the balanced sections help identify any evidence for recent deformation. These tectonic geomorphic and cross section techniques have recently been used in a licensing context for a very similar geologic problem of assessing the possibility of reactivation of Tertiary faults and folds in California (Pacific Gas and Electric Co., 1993), and for evaluating the activity of lower Tertiary faults in South Carolina (Hanson and Bullard, 1992).

No evidence of deformation was observed from this analysis, thus providing a stronger basis for concluding that the Front Range structures in the immediate site vicinity are not active or are active only at a very low rate.

Issue No. 8: Origin of the Quaternary graben near Golden and its structural/tectonic relation to the Golden fault.

The Quaternary graben near Golden has been the focus of several studies (e.g. Scott, 1970; Kirkham, 1977; Kirkham and Rogers, 1981; Dames and Moore, 1981, 1983). The feature itself is relatively short and its potential importance lies in its possible association with the Golden fault.

The above studies conclude that the graben is far better expressed geomorphically than the Golden fault and that the graben faults displace strata that contain a 600-700 ka ash deposit (Kirkham and Rogers, 1981). Evaluation of the graben by Dames and Moore (1981) resulted in the conclusion that the feature probably has a limited lateral extent, can be explained by both tectonic and nontectonic mechanisms for its origin, and is likely not tectonically or structurally related to the Golden fault. A non-tectonic mechanism for the observed displacements at the graben has been proposed involving surface subsidence over a burnt coal bed (Dames and Moore, 1981, 1983; U.S. Department of Energy, 1981). These studies would imply that both the Quaternary graben as well as the Golden fault itself are inactive and would not be significant to the site seismic hazard.

The limited lateral extent of the graben (less than few kilometers) would imply a limited earthquake potential (i.e., small source area and small magnitudes) as an individual seismic source. Therefore, the importance of the graben for purposes of this study is the degree to which a structural association with the Golden fault might imply geologically recent deformation on the Golden fault. Since the structural association of the graben with the Front Range fault system cannot be resolved unequivocally, the activity of the Golden-Boulder segment of the Front Range fault system is modeled with a probability of 0.4.

Issue No. 9: DOE interim position on seismic evaluations.

This issue is of high relevance, but is not so much an issue of how to conduct a seismic hazard study as it is how to derive guidelines and recommendations once the hazard results have been computed. The DOE Interim Position on Seismic Evaluations is still in draft form, but sufficient hazard results (over the annual probability range 10^{-2} to 10^{-5}) have been produced to cover any unexpected changes in recommended probability levels. With respect to the seismic hazard study, a state-of-the-art study

has been performed, incorporating all relevant uncertainties and sources of earthquakes. Multiple reviews of the work have been undertaken. Thus the results should be acceptable to DOE as being consistent with the Interim Position.

Issue No. 10: Ground motion attenuation in the Front Range region.

This issue addresses the appropriate ground motion equation to use in the region surrounding the Rocky Flats Plant. Because there are no strong ground motion data available from Colorado, this issue cannot be resolved unequivocally. The uncertainty associated with strong ground motion is common, however, even in the central U.S. where data are not available for magnitudes above 5. Uncertainties are handled by multiple hypotheses in state-of-the-art seismic hazard analyses, and this procedure has been adopted here. Thus non-resolution of an accurate attenuation equation for the Colorado region does not have an adverse effect on the seismic hazard results vis-a-vis those for other regions. Addressing the uncertainty in an explicit, quantitative way with both analytical and empirical methods, as done here, documents current uncertainties and adds credibility to the study. This is the best (and only available) way of handling this uncertainty.

Section 4

CONCLUSIONS

This study has made a seismic evaluation of the hazard of ground shaking at the Rocky Flats Plant (RFP), Jefferson County, Colorado. This has been done both on a probabilistic and deterministic basis, with a range of investigations to look at various sources of hazard and resulting effects on soils at the RFP.

The RMA/Derby source dominates the contribution to seismic hazard. This is not a new source of seismicity in Colorado; it was identified; in 1981 by the Colorado Geological Survey as "potentially active" (Kirkham and Rogers, 1981). The quantitative probability of activity assessed in this study for this source is 0.5.

A probabilistic seismic hazard analysis has been performed under this study to evaluate probabilities with which various amplitudes of ground motion might be exceeded. This is a state-of-the-art study in the sense that multiple hypotheses on earthquake sources, characteristics, and ground motions have been incorporated into the study, so that quantitative statements of the uncertainty in hazard can be made. The sources of that uncertainty can also be traced back to the uncertainties in interpretations, and this has been done to identify the major contributors to uncertainty in hazard.

From the probabilistic hazard results, ground motions for annual probabilities between $2x10^{-5}$ and 10^{-3} and greater are dominated by earthquake occurrences on the RMA/Derby source, which lies at its closest extension about 13 km from the RFP. The RMA/Derby source has a maximum magnitude estimated to be between 5 3/4 and 7, and was identified by the Colorado Geological Survey based on earthquakes that were caused by deep-well injection of liquid waste at the Rocky Mountain Arsenal in the 1960s. The rate of earthquake activity for the RMA/Derby source was estimated in this study from historical seismicity in its vicinity and estimated slip rate. Historical seismicity was evaluated removing all events thought to be associated with the 1960 injection activity and keeping only earthquakes that are thought to be naturally-occurring.

Dominant contributors to uncertainty in seismic hazard are the uncertainty in activity on the RMA/Derby source, the estimates of the rate of seismic activity (whether derived from historical seismicity or slip rate) for this source, the ground motion attenuation equations, and the representation of the RMA/Derby as an area source or fault source. For the attenuation equations, estimates of ground motion were made for Colorado earthquakes using both empirical and analytical techniques, modifying equations developed elsewhere for Colorado conditions. This was necessary because there are no strong-motion records from Colorado earthquakes on which to base a purely empirical procedure.

Soils at the RFP will amplify ground motions predominantly at lower frequencies (below about 5 Hz). This conclusion is reached from both empirically- and analytically-based studies. Shear wave velocity measurements taken at the RFP in 1993 and 1994 were used as input to these studies, so that site-specific data could be incorporated into the soil amplification estimates. The final recommended soil amplification factors are based on an analytical procedure that is amplitude

dependent, and the levels of soil amplification are confirmed by the application of an empirical procedure.

The 1882 Colorado earthquake was investigated by examining available studies on this earthquake, and making quantitative estimates of its magnitude and location uncertainties. This earthquake is modeled with areal sources; its location uncertainty has an important contribution to uncertainty in hazard for those sources (in particular the host source), but those sources do not dominate the hazard at the RFP, as noted above. Therefore uncertainty in the interpretation of the 1882 earthquake has a minor effect on the total hazard evaluated for the RFP.

Deterministic results consist of response spectra calculated for all of the potentially-active area sources in the region (including the RMA/Derby), a study of soil liquefaction potential, and a study of slope stability under seismic loads. For the spectra, which were calculated with the maximum magnitude earthquake at the closest location to the RFP, the RMA/Derby indicates the highest ground motions, due to its large maximum-magnitude earthquake and close distance.

The soil liquefaction study indicates that there is a negligible chance of soil liquefaction at the RFP. This is the case because soils consist of medium-to-very dense gravels, clays, and sands that are clayey or gravelly, which are not likely to liquefy.

The study of slope stability indicates that, under certain conditions, soil slopes may undergo some permanent displacement, up to about 30 cm, during earthquake motions. The conditions estimated to lead to these permanent displacement are a slope of at least 30 ft in height, a high water table (within 10 ft of the crest of the slope), cohesionless soils, and ground motions of 0.4g or greater. For lower slopes, a deeper water table, slopes comprised of cohesive soils or fill, or lower ground motion, less permanent displacement will occur.

Several qualifications to this study are appropriate. As defined in the scope of work, no field investigations of faults was undertaken; we relied on information available in the literature to identify potentially active faults and to make assessments of fault activity, slip rates, and maximum magnitude. Also, no new information was developed on historical seismicity; we relied on available seismicity catalogs, resolving discrepancies where appropriate. No soil borings or tests were conducted for the soil liquefaction or slope stability studies, and estimates of the shear strength of soils was made on a generic basis using the soil classification and available blow count data from soil reports of other contractors to the Rocky Flats facilities. We have no reason to believe that conducting any of the extra field studies or other data collection described above would lead to higher or lower hazard than estimated here, except that site-specific data on soil shear strength would likely indicate higher strength than used here (conservative values were chosen because of the lack of detailed data).

In summary, this study has been a state-of-the-art evaluation of seismic hazard at the RFP, incorporating uncertainties where appropriate and investigating the relationship between inputs to the seismic hazard calculation and results. The results of this study are appropriate for decision-making regarding seismic safety at the RFP.

Section 5

REFERENCES

Allen, C.R. (1975). Geological Criteria for Evaluating Seismicity, *Geological Society of America Bulletin*, v. 86, p. 1041-1057.

Bollinger, G.A., M.S. Sibol and M.C. Chapman (1992). Maximum Magnitude Estimation for an Intraplate Setting--Example: The Giles County, Virginia, Seismic Zone, *Seismological Research Letters*, 63:2, April-June.

Bull, W.B. (1984). Tectonic geomorphology, *Journal of Geological Education*, v. 32, p. 310-324.

Bull, W.B. (1990). Stream-terrace genesis: implications for soil development, *in* P.L.K. Kneupfer and L.D. McFadden, eds., Soils and Landscape Evolution, *Geomorphology*, v. 3, p. 351-367.

Bullard, T.F. and W.R. Lettis (1990). Characterization of Quaternary Surface Deformation in the Vicinity of the 1987 Whittier Narrows Earthquake, Los Angeles Basin, California (abs.), *Geol. Soc. Am. Abs. with Prog.*, v. 22, p. 11.

Coffman, J.L. and C.A. Von Hake (1973). *Earthquake History of the United States*, Pub. 41-4, Rev. Edition (through 1970), N.O.A.A., Washington, D.C., pp. 59-60.

Coppersmith, K.J. (1991). Seismic Source Characterization for Engineering Seismic Hazard Analysis, *Proceedings of the Fourth International Seismic Zonation Conference*, v. 1, p. 1-60.

Coppersmith, K.J., A.C. Johnston, and W.J. Arabasz (1986). Assessment of Maximum Earthquake Magnitudes in the Eastern United States, *Earthquake Notes*, 57-1:1.

Cornell, C.A. (1968). Engineering Seismic Risk Analysis, *Bulletin of the Seismological Society of America*, 58(5):1583-1606, October.

Cornell, C.A. (1971). *Dynamic Waves in Civil Engineering*, Chapter 27: Probabilistic Analysis of Damage to Structures Under Seismic Loads, Wiley Interscience, 1971.

Dames & Moore (1981). Geologic and seismologic investigations for Rocky Flats Plant, Rept. to U.S. Dept. of Energy, July 9, Chapter 8, "1882 Earthquake Investigation."

Dames & Moore (1983). Rubey Clay-Mine Subsidence Hazard Study, Golden, Colorado, Report to Adolph Coors Co., August 30.

Darrow, A.C. and A.P. Krusi (1981). Geologic Investigations of the Seismic Hazards Associated with the Golden Fault, Colorado (abs.), Colorado Tectonics, Seismicity and Earthquake Hazards: Proc. and Field Trip Guide on a Symposium held in Denver, Colorado, June 4-6, p. 32.

Davis, S.D. and C. Frohlich (1993). Did (or will) fluid injection cause earthquakes? Criteria for a rational assessment, *Seism. Res. Letters*, 64, 3-4, 207-224, July-December.

Denver Water Department (1986). Geologic and Seismotectonic Investigations Central Front Range, Colorado, Geotechnical Advisory Committee, Denver Water Department, Denver, Colorado, January.

Der Kiureghian, A. and A.H.S. Ang (1975). *A Line Source Model for Seismic Hazard Risk Analysis*, Technical Report UILU-ENG-75-2023, University of Illinois, October 1975, pp. 134, 6-67, U.S.

Electric Power Research Institute (1993). "Guidelines for determining design basis ground motions," Electric Power Research Institute, Palo Alto, California, Vol. 1, EPRI TR-102293.

Evans, D. (1966). The Derby Earthquakes, *Mountain Geologist*, 3, 1, p. 23.

Hadsell, F.A. (1968). History of earthquake activity in Colorado, *in*, J.C. Hollister and R.J. Weimer (eds.), Geophysical and geological studies of the relationship between the Denver earthquake and the Rocky Mountain Arsenal well, *Colorado School of Mines Quarterly*, 63, pp. 57-72.

Hanson, K.L. and T.F. Bullard (1992). Quaternary and Neotectonics of the Savannah River Site, South Carolina, Savannah River Site Earth Sciences Advisory Committee Meeting, Field Trip Guide, 41 p.

Healy et al. (1966). Microseismicity Studies at the Site of Denver Earthquakes, *in* J.H. Healy and others, Geophysical and Geological Investigations Relating to Earthquakes in the Denver Area, Colorado, U.S. Geological Survey Open-File Report, pt. 5.

Healy, J.H., W.W. Rubey, D.T. Griggs and C.B. Raleigh (1968). The Denver earthquakes, *Science*, 161, 3848, September 27, p. 1301-1310.

Herrmann, R.B., S.K. Park and C.Y. Wang (1981). The Denver earthquakes of 1967-1968, *Bull. Seis. Soc. Am.*, 71, 3, 731-745, June.

Hsieh, P.A. and J.D. Bredehoeft (1981). A reservoir analysis of the Denver earthquakes: a case of induced seismicity, *Jour. Geophys. Res.*, 86, 903-920, February 10.

Kirkham, R.M. (1977). Quaternary movements on the Golden fault, Colorado, *Geology*, v. 5, p. 689-692.

Kirkham, R.M. and W.P. Rogers (1981). Earthquake Potential in Colorado--A Preliminary Evaluation, Colorado Geological Survey, Bulletin 43, 171 p.

Kirkham, R.M. and W.P Rogers (1986). An interpretation of the November 7, 1882 Colorado earthquake, *in* W.P. Rogers and R.K. Kirkham, eds., Contributions to Colorado Seismicity and Tectonics--A 1986 Update, Colorado Geological Survey Special Publication 28, p. 122-144.

Kirkham, R.M. and W.P. Rogers (1988). The November 7, 1882, Colorado earthquake and its significance to seismic hazard estimation, *Geol. Soc. Am. Abstr. with Prog.*, 20, A15p

Langer, C.J. and G.L. Snyder (1988). The Laramie Mountains, Wyoming, Earthquakes of 18 October 1984: Its Aftershocks and a Search for Holocene Surface Displacements (abs.), *Geol. Soc. Am. Abstr. with Prog.*, v. 20, p. A14.

Langer, C.J., R.A. Martin, C.K. Wood, G.L. Snyder and G.A. Bollinger (1991). The Laramie Mountains, Wyoming, earthquake of 18 October 1984, A report on its aftershocks and seismotectonic setting, U.S. Geological Survey Open-File Report 91-258, 41 p.

McCann, M.W. and J.W. Reed (1988a). *Selection of a Lower Bound Magnitude for Seismic Hazard Assessment*, Technical Report, Electric Power Research Institute, Palo Alto, California.

McCann, M.W. and J.W. Reed, editors (1988b). *Engineering Characterization of Small-Magnitude Earthquakes*, Electric Power Research Institute, Palo Alto, California.

McGuire, R.K. (1976). *FORTRAN Computer Program for Seismic Risk Analysis*, Open-File Report 7, Geological Survey, 1976, pp. 1-90.

McGuire, R.K. (1978). *FRISK: Computer Program for Seismic Risk Analysis Using Faults as Earthquake Sources*, U.S. Geological Survey, Open-File Report 78-1007, 70 p., 1978.

McGuire, R.K. and W.J. Arabasz (1990). An Introduction to Probabilistic Seismic Hazard Analysis, *in* S.H. Ward, ed., *Geotechnical and Environmental Geophysics*, Society of Exp. Geophys., Tulsa.

McGuire, R.K., A. Krusi and S.D. Oaks (1982). The Colorado earthquake of November 7, 1882: Size, epicentral location, intensities, and possible causative fault, *The Mountain Geologist*, v. 19, p. 11-23.

Nicholson, C. and R.L. Wesson (1990). *Earthquake Hazard Associated With Deep Well Injection--A Report to the U.S. Environmental Protection Agency*, U.S. Geological Survey Bulletin 1951, Washington, D.C.

Oaks, S.D., M.G. Hopper, L.M. Barnhard and S.T. Algermissen (1985). November 7, 1882, Colorado earthquake reinterpreted in light of the October 18, 1984, Wyoming earthquake, *Earthquake Notes*, 55, 24 p.

Pacific Gas and Electric Co. (1993). Evaluation of fault behavior and earthquake potential in the Sierra foothills of California, Geosciences Department, San Francisco, California.

Schwartz, D. and K.J. Coppersmith (1984). Fault Behavior and Characteristic Earthquakes: Examples from the Wasatch and San Andreas Fault Zones, *Journal of Geophysical Research*, 89:5681-5698, 1984.

Scott, G.R. (1970). Quaternary Faulting and Potential Earthquakes in East-Central Colorado, *in* Geological Survey Research 1970, Chapter C, U.S. Geological Survey Prof. Paper 700-C, p. C11-C18.

Stover, C.W. (1985). Preliminary Isoseismal Map and Intensity Distribution for the Laramie Mountains, Wyoming, Earthquake of October 18, 1984, U.S. Geological Survey Open-File Report 85-137, 9 p.

Trimble, D.E. and M.N. Machette (1979). Geologic map of greater Denver area, Front Range urban corridor, Colorado, Misc. Inv. Series Greater Denver Area, Colorado, Map I-856-H.

U.S. Department of Energy (1981). Geologic and Seismologic Investigation for Rocky Flats Plant, Report submitted July 13.

Warner, L.A. (1986). Strain Rates, Stress Distribution, and Seismic Potential in Central Colorado, *in* Contributions to Colorado Seismicity and Tectonics--A 1986 Update, W.P. Rogers and R.M. Kirkham, eds., Colorado Geological Survey Spec. Pub. 28, p. 28-42.

Weichert, D.H. (1980). Estimation of the Earthquake Recurrence Parameters for Unequal Observations Periods for Different Magnitudes, *Bulletin of the Seismological Society of America*, 70:1337-1346.

Wong, I.G. (1986). Tectonic Stresses in Colorado and Their Implications to Seismicity, *in* Contributions to Colorado Seismicity and Tectonics--A 1986 Update, W.P. Rogers and R.M. Kirkham, eds., Colorado Geological Survey Spec. Pub. 28, p. 17-27.

Zoback, M.L. (1988). State of stress in the Rocky Mountain region (abs.), Geol. Soc. Am. Abs. with Prog., v. 20, p. A12.

TABLE 2-1

SUMMARY OF SEISMICITY PARAMETERS

Fault/Area Source	Prob. of Activity	Mag. Distrib.	Slip rate, mm/yr		v5.0		b-value		Mmax	
			mean	range	mean	range	mean	range	mean	range
RMA/Derby	0.5	Exp. & Char.	.0194	.002-.06	3.20E-3	2E-6 to 4E-2	0.75	0.46-1.04	6.2	5.5-7
Golden-Boulder	0.4	Char.	0.0099	.002-.06	7.01E-5	6E-6 to 1E-3	0.75	---	7.2	7.0-7.6
Rock Creek	0.3	Char.	.0106	.001-.04	6.35E-5	2E-7 to 1E-3	0.75	---	6.2	5.8-6.8
Valmont	0.4	Char.	.0135	.007-.02	8.09E-5	1E-6 to 5E-4	0.75	---	6.2	5.8-6.8
Walnut Creek	0.3	Char.	0.0033	.0005-.01	1.98E-5	8E-8 to 3E-4	0.75	---	6.2	5.8-6.8
I	1	Exp.	---	---	7.51E-3	4E-3 to 2E-2	0.79	0.64-0.85	5.8	5.5-6.5
II	1	Exp.	---	---	8.90E-3	3E-3 to 2E-2	0.78	0.66-0.85	6.2	5.5-7.0
III	1	Exp.	---	---	7.78E-2	5E-2 to 1E-1	0.72	0.67-0.76	7	6.5-7.5
IV	1	Exp.	---	---	1.29E-2	7E-4 to 3E-2	0.93	0.75-1.11	5.8	5.5-6.0
V	1	Exp.	---	---	1.85E-3	---	0.75	0.55-0.95	5.8	5.5-6.0

TABLE 3-1

MEAN CALCULATED HAZARD FOR ROCK (FOR 5% DAMPED SPECTRA)

Amplitude *	Parameter					
	PGA	PSV(25 Hz)	PSV(10 Hz)	PSV(5 Hz)	PSV(2.5 Hz)	PSV(1 Hz)
1	2.08E-2	5.28E-4	5.32E-3	1.46E-2	2.49E-2	2.82E-2
2.5	6.46E-3	8.11E-5	1.47E-3	4.44E-3	8.41E-3	1.09E-2
5	2.36E-3	1.72E-5	4.58E-4	1.58E-3	3.04E-3	4.30E-3
10	7.33E-4	3.41E-6	1.13E-4	4.66E-4	9.29E-4	1.37E-3
15	3.29E-4	1.32E-6	4.50E-5	2.04E-4	4.25E-4	6.32E-4
20	1.76E-4	6.71E-7	2.25E-5	1.08E-4	2.35E-4	3.50E-4
30	6.91E-5	2.49E-7	8.03E-6	4.19E-5	9.66E-5	1.45E-4
50	2.05E-5	6.40E-8	2.11E-6	1.20E-5	3.00E-5	4.54E-5
75	7.71E-6	1.84E-8	7.28E-7	4.25E-6	1.17E-5	1.80E-5
100	3.78E-6	6.66E-9	3.41E-7	1.98E-6	5.91E-6	9.39E-6

* % g for PGA, cm/s for PSV

TABLE 3-2

MEAN UNIFORM HAZARD SPECTRA FOR ROCK

Return Period, yrs	PGA (g)	damping	Amplitude (g) for				
			PSA(25 Hz)	PSA(10 Hz)	PSA(5 Hz)	PSA(2.5 Hz)	PSA(1 Hz)
500	.055	2%	.085	.170	.176	.130	.059
		5%	.072	.129	.137	.102	.051
		7%	.068	.116	.124	.092	.047
		10%	.065	.105	.112	.082	.043
1,000	.083	2%	.130	.268	.267	.195	.088
		5%	.109	.201	.207	.153	.075
		7%	.103	.182	.188	.138	.070
		10%	.099	.163	.170	.122	.064
2,500	.136	2%	.222	.457	.445	.314	.140
		5%	.183	.343	.345	.247	.120
		7%	.173	.308	.312	.223	.111
		10%	.165	.276	.282	.197	.101
5,000	.189	2%	.313	.645	.626	.437	.193
		5%	.257	.483	.484	.345	.166
		7%	.243	.434	.439	.310	.153
		10%	.231	.389	.395	.275	.139
10,000	.256	2%	.445	.905	.856	.600	.264
		5%	.361	.676	.662	.473	.226
		7%	.340	.607	.599	.425	.209
		10%	.321	.543	.539	.377	.190

TABLE 3-3

MEAN CALCULATED HAZARD FOR SOIL

Amplitude *	PGA	PSV(25 Hz)	PSV(10 Hz)	PSV(5 Hz)	PSV(2.5 Hz)	PSV(1 Hz)
1	3.23E-2	9.14E-4	8.67E-3	2.58E-2	3.78E-2	3.03E-2
2.5	1.13E-2	1.11E-4	2.37E-3	8.80E-3	1.48E-2	1.20E-2
5	4.43E-3	1.44E-5	7.05E-4	3.39E-3	6.22E-3	4.97E-3
10	1.49E-3	2.21E-6	1.19E-4	1.07E-3	2.21E-3	1.70E-3
15	7.33E-4	8.52E-7	2.55E-5	4.89E-4	1.13E-3	8.41E-4
20	3.98E-4	4.26E-7	6.47E-6	2.46E-4	6.77E-4	4.93E-4
30	1.51E-4	1.52E-7	2.02E-6	6.96E-5	3.10E-4	2.22E-4
50	3.53E-5	3.61E-8	5.28E-7	7.72E-6	1.01E-4	7.65E-5
75	8.65E-6	9.52E-9	---	1.90E-6	3.42E-5	3.20E-5
100	3.58E-6	---	---	8.38E-7	1.37E-5	1.73E-5

* % g for PGA, cm/s for PSV

TABLE 3-4

MEAN UNIFORM HAZARD SPECTRA FOR SOIL

Return Period, yrs	PGA (g)	damping	Amplitude (g) for				
			PSA(25 Hz)	PSA(10 Hz)	PSA(5 Hz)	PSA(2.5 Hz)	PSA(1 Hz)
500	.085	2%	.121	.236	.291	.216	.067
		5%	.104	.180	.225	.170	.058
		7%	.100	.163	.204	.153	.053
		10%	.097	.148	.183	.136	.049
1,000	.126	2%	.178	.354	.431	.328	.102
		5%	.154	.270	.333	.259	.087
		7%	.148	.245	.301	.233	.081
		10%	.143	.222	.271	.206	.073
2,500	.200	2%	.282	.552	.680	.537	.167
		5%	.244	.421	.526	.423	.143
		7%	.234	.383	.475	.381	.132
		10%	.226	.347	.428	.338	.120
5,000	.270	2%	.367	.709	.901	.755	.237
		5%	.321	.544	.697	.595	.203
		7%	.310	.496	.631	.536	.188
		10%	.300	.451	.568	.475	.171
10,000	.350	2%	.477	.874	1.131	1.019	.332
		5%	.417	.675	.877	.803	.284
		7%	.402	.617	.795	.723	.263
		10%	.390	.564	.717	.641	.239

TABLE 3-5

VALUES OF $\hat{M}$ AND $\hat{R}$ FOR PSV(10 Hz) AND PSV(1 Hz)

Freq.	Amp, cm/s	Approx. RP, yrs	RMA/Derby source	
			$\hat{M}$	$\hat{R}$, km
10 Hz	2.5	1,800	5.5	27
	10	21,000	5.6	27
	20	142,000	5.7	26
1 Hz	10	3,600	5.7	27
	20	11,000	5.8	27
	50	78,000	6.0	27

A. Seismic Source I
(Earthquake locations in space lead to a distribution of epicentral distances $f_R(r|m)$

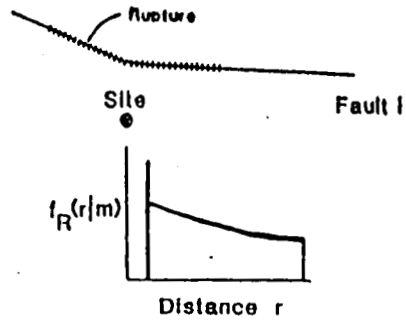

B. Magnitude distribution and rate of occurrence for Source I:

$f_M(m), \nu_I$

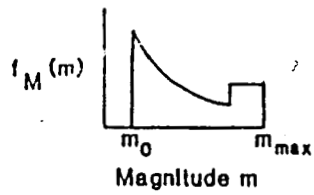

C. Ground motion estimation:

$G_{A|m,r}(a^*)$

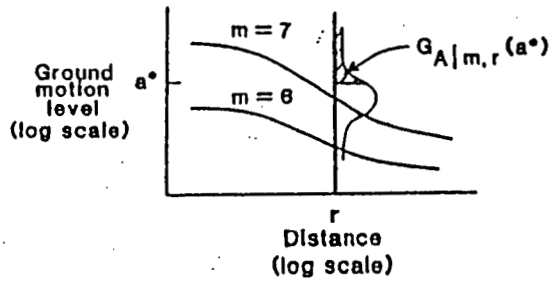

D. Probability analysis:

$$P[A > a^* \text{ in time } t]/t = \sum_I \nu_I \iint G_{A|m,r}(a^*)\, f_M(m)\, f_R(r|m)\, dm\, dr$$

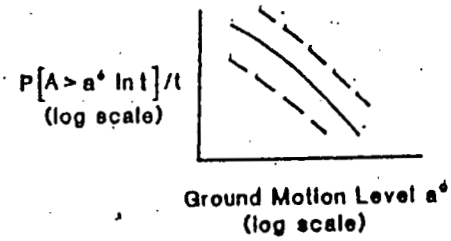

Figure 2-1. Seismic hazard computational model (modified from McGuire and Arabasz, 1990).

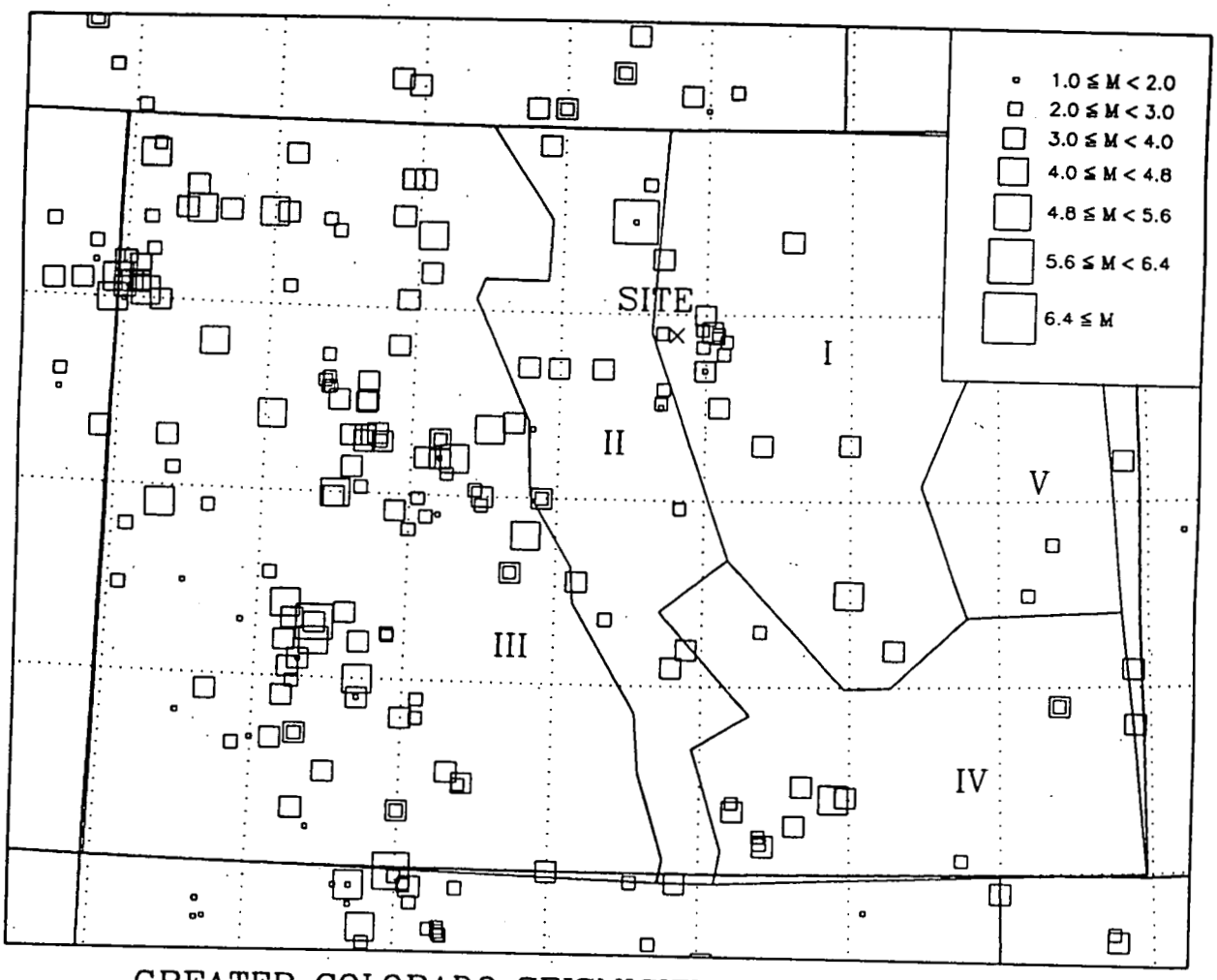

GREATER COLORADO SEISMICITY 1870 – MAY 1993

Figure 2-2. Historical seismicity and area sources used to represent seismicity in Colorado.

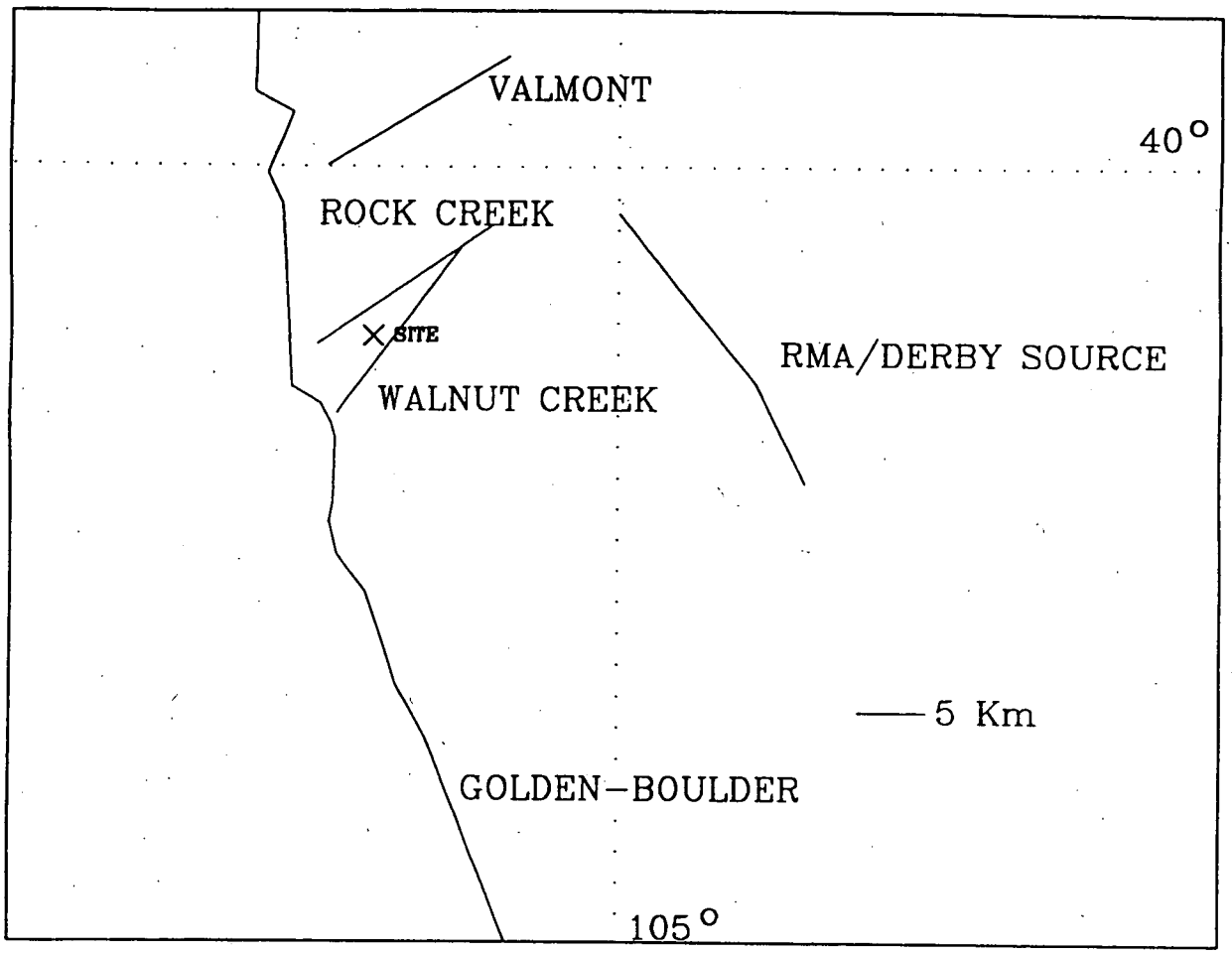

FAULTS NEAR ROCKY FLATS

Figure 2-3. Potential active faults in the vicinity of Rocky Flats included in the project.

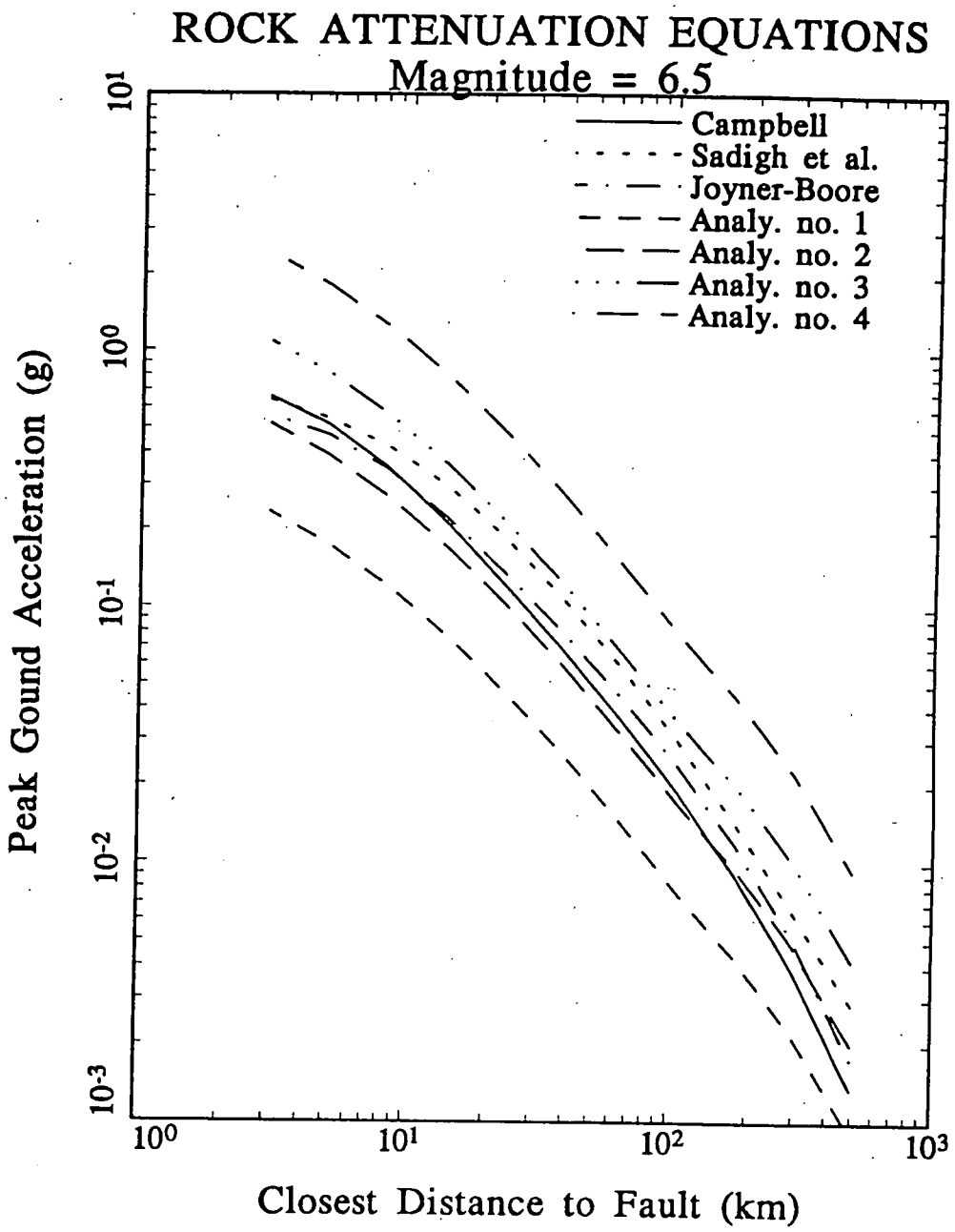

Figure 2-4. Comparison of PGA estimates on rock vs distance for **M** = 6.5, using the seven attenuation equations derived in this project.

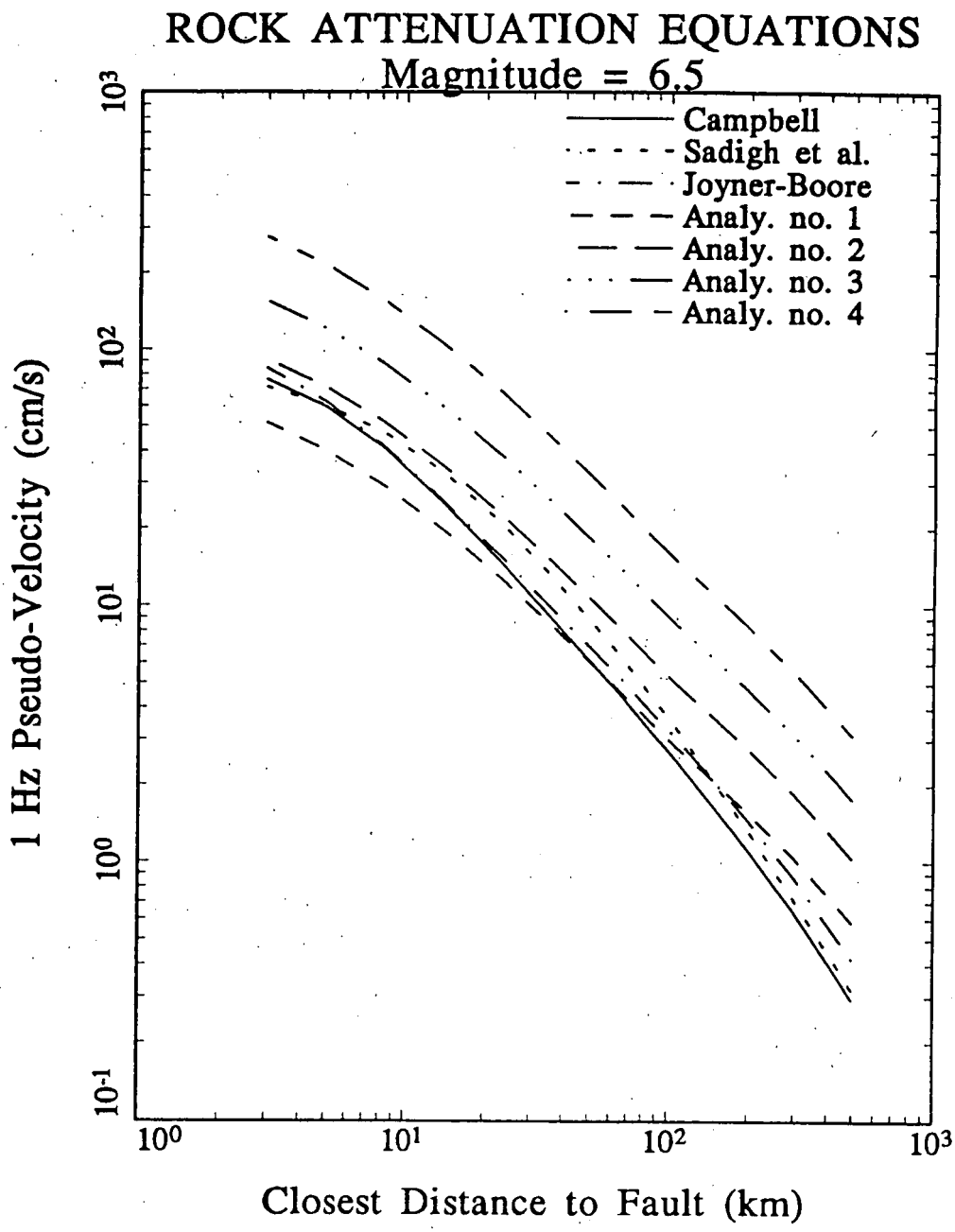

Figure 2-5. Comparison of PSV(1 Hz) estimates on rock vs distance for **M** = 6.5, using the seven attenuation equations derived in this project.

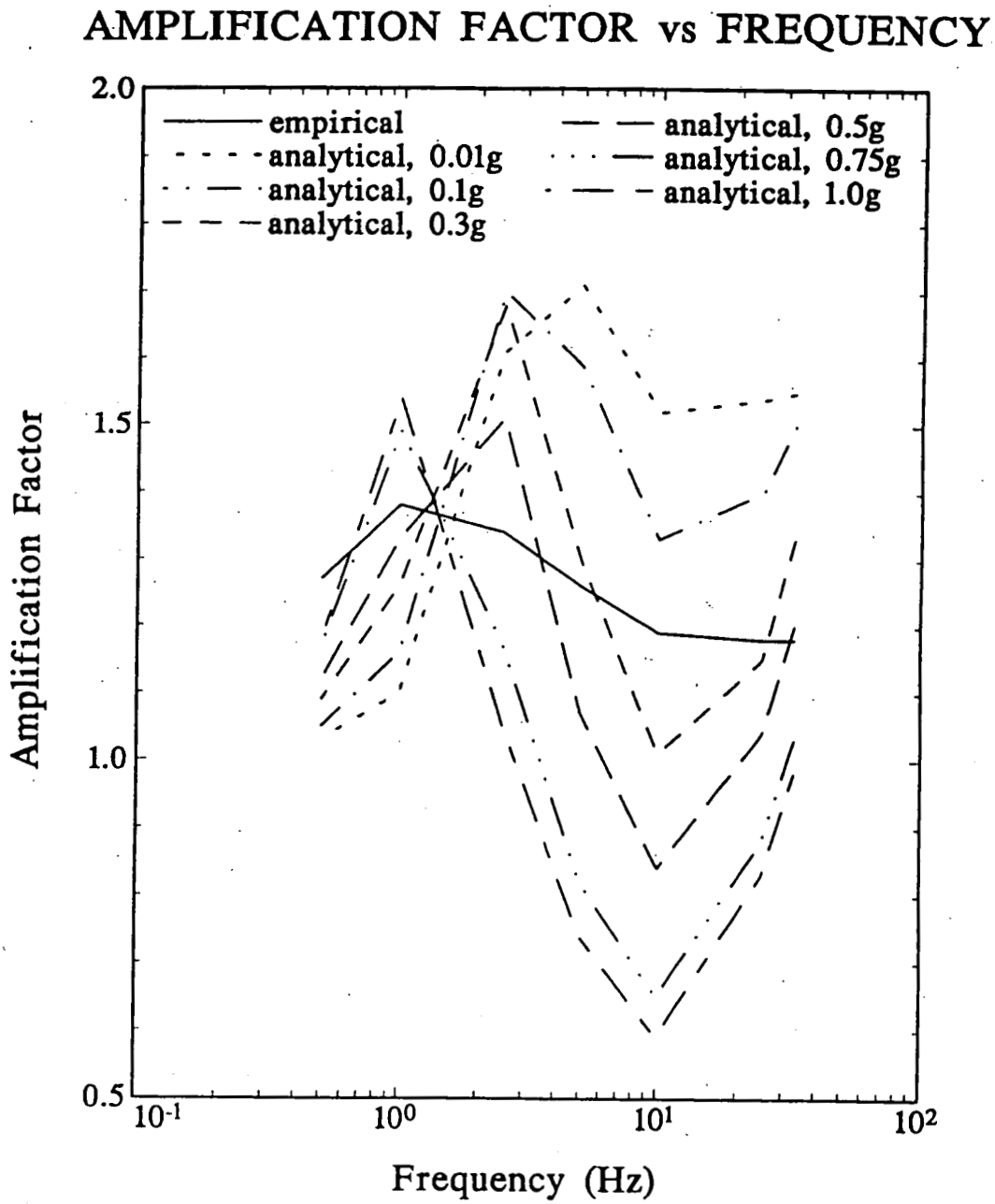

Figure 2-6. Soil amplification factors vs frequency from empirical and analytical methods.

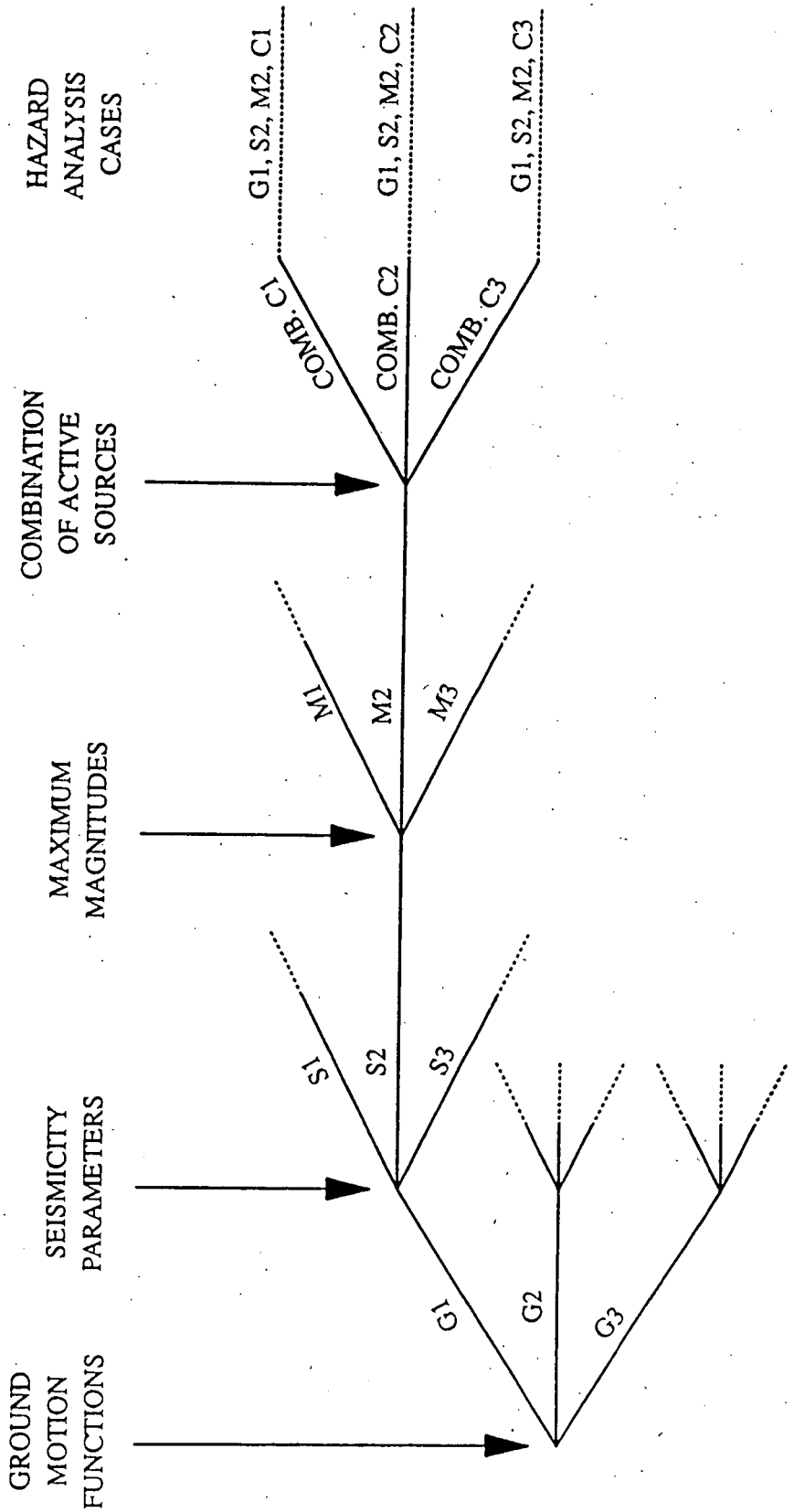

Figure 2-7. Logic tree representation of uncertain parameters for seismic hazard analysis.

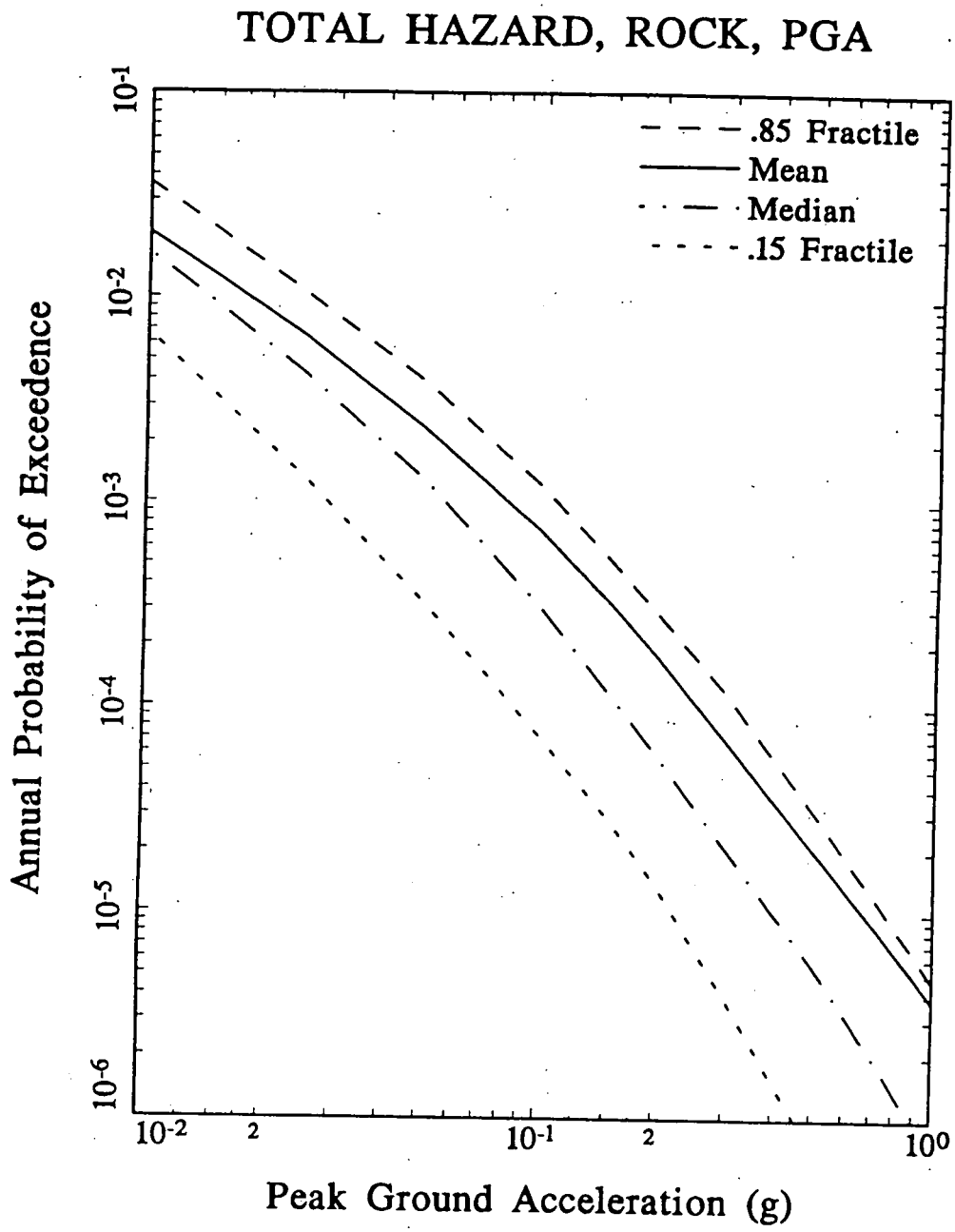

Figure 3-1. Total hazard curves, PGA on rock.

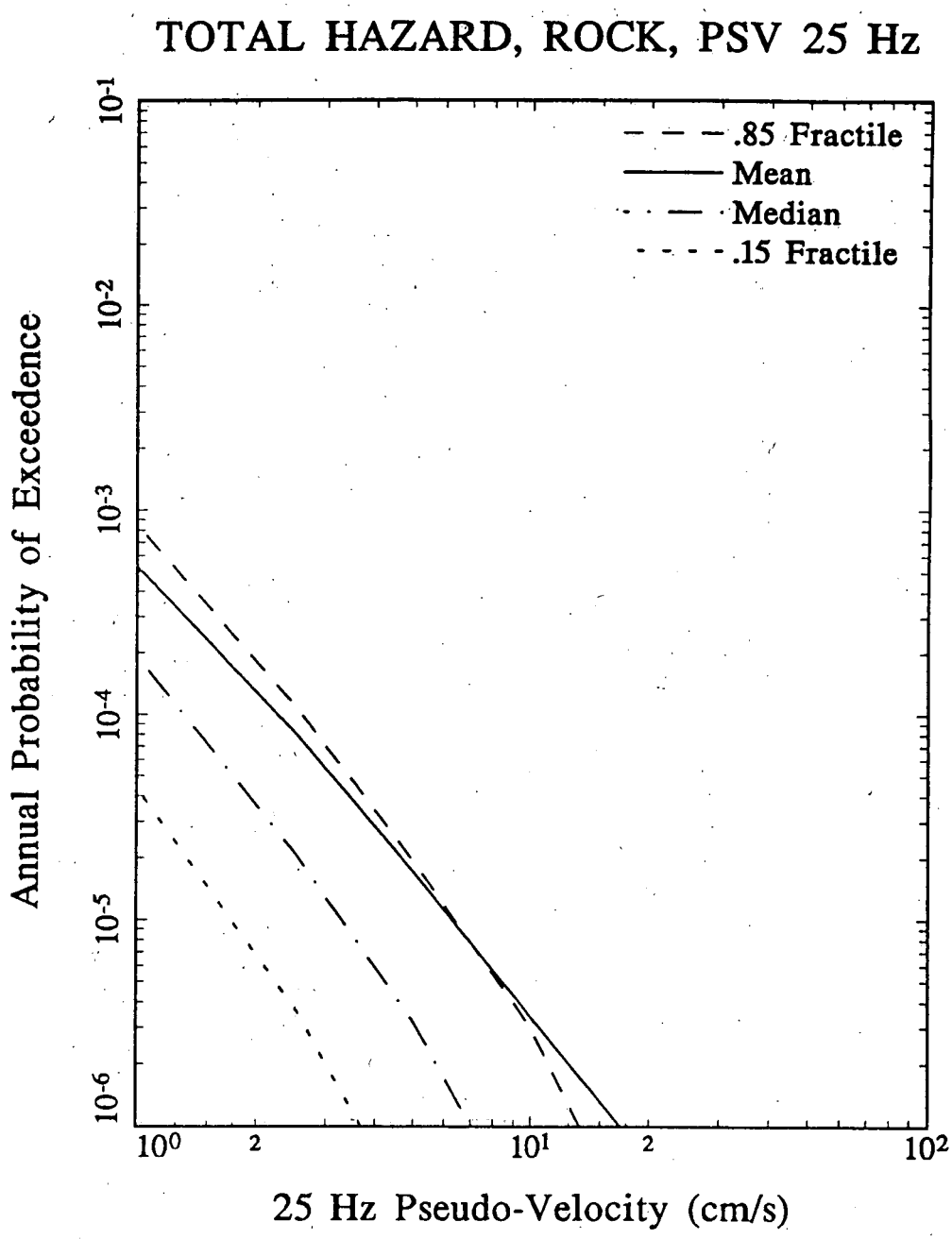

Figure 3-2. Total hazard curves, PSV(25 Hz) on rock.

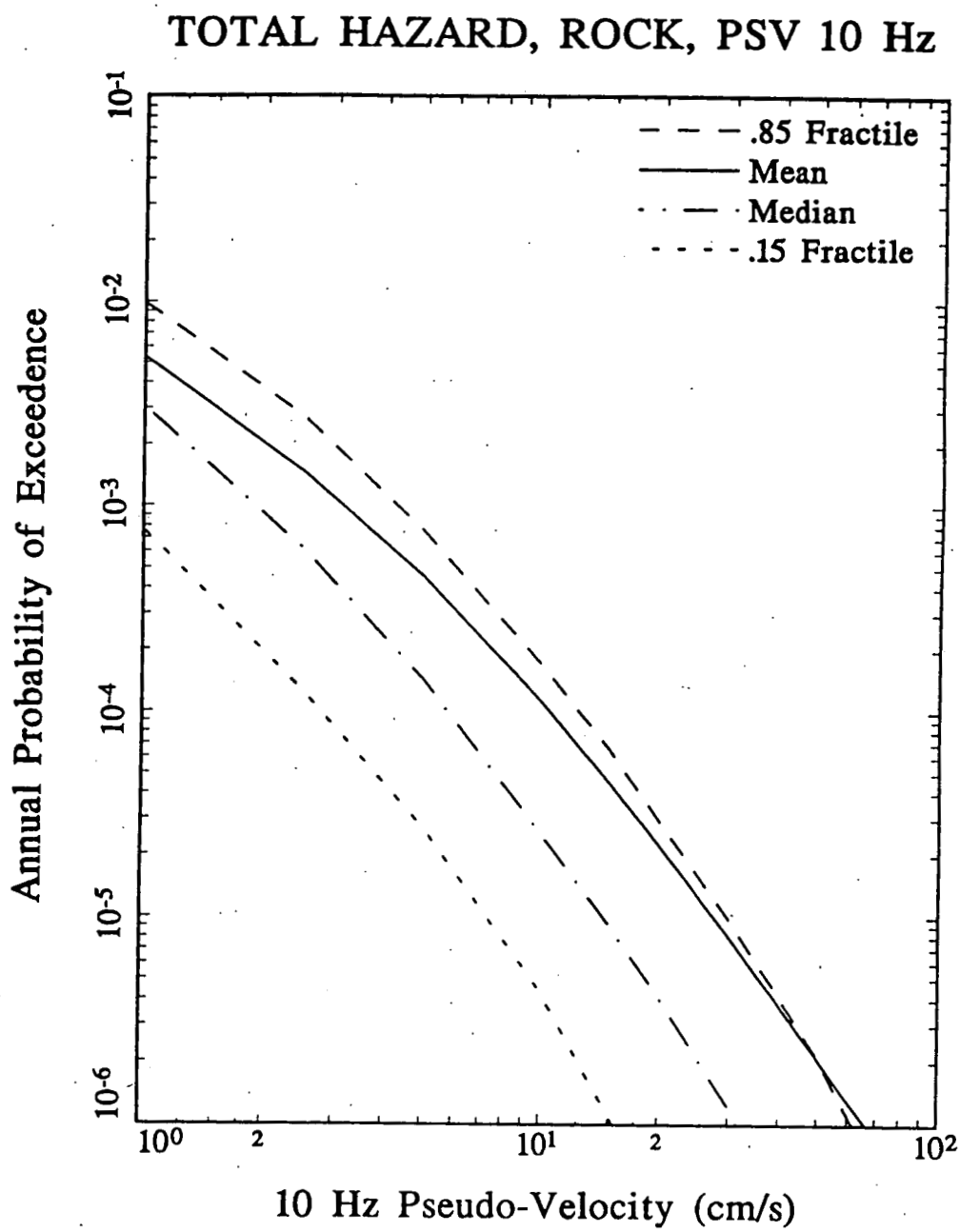

Figure 3-3. Total hazard curves, PSV(10 Hz) on rock.

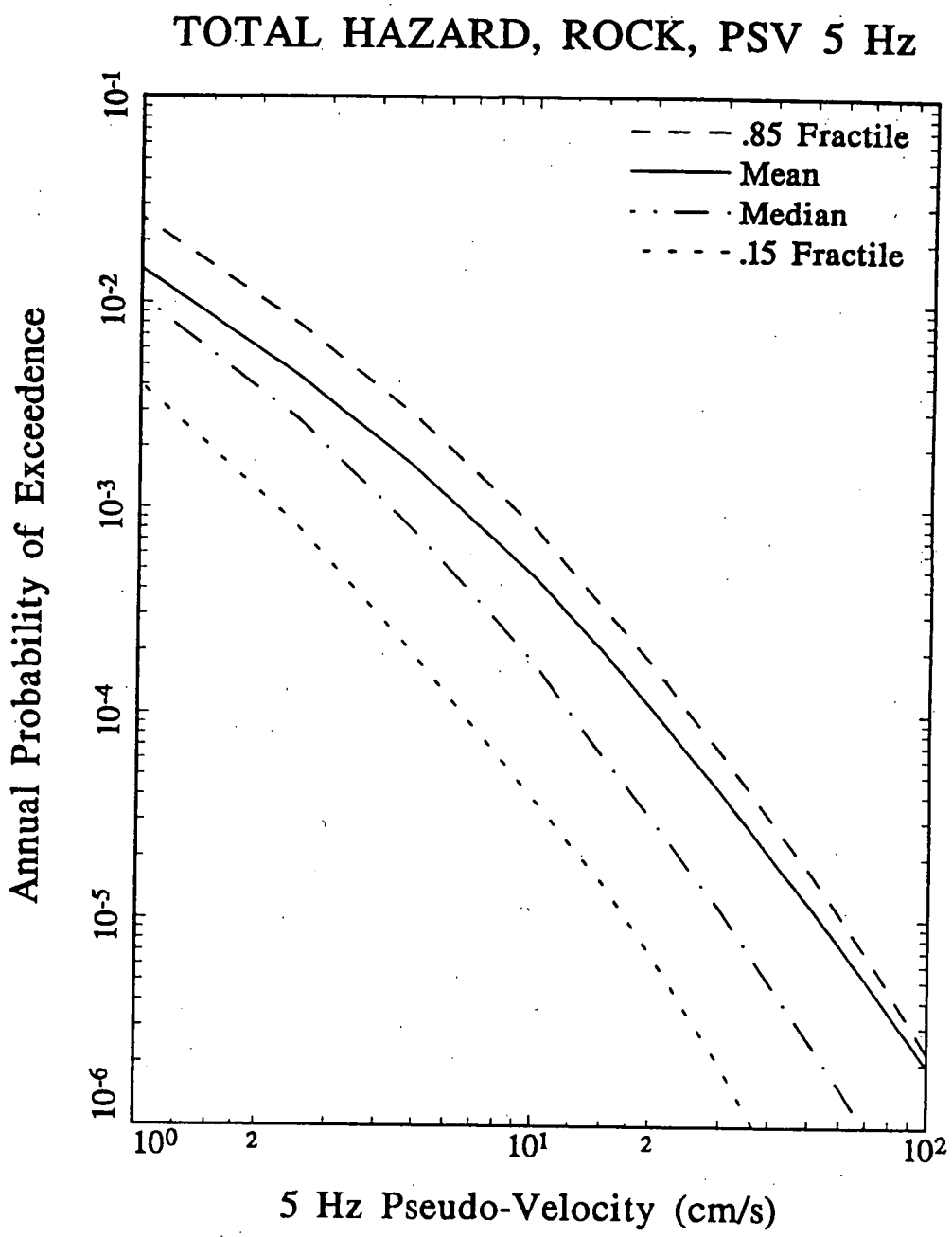

Figure 3-4. Total hazard curves, PSV(5 Hz) on rock.

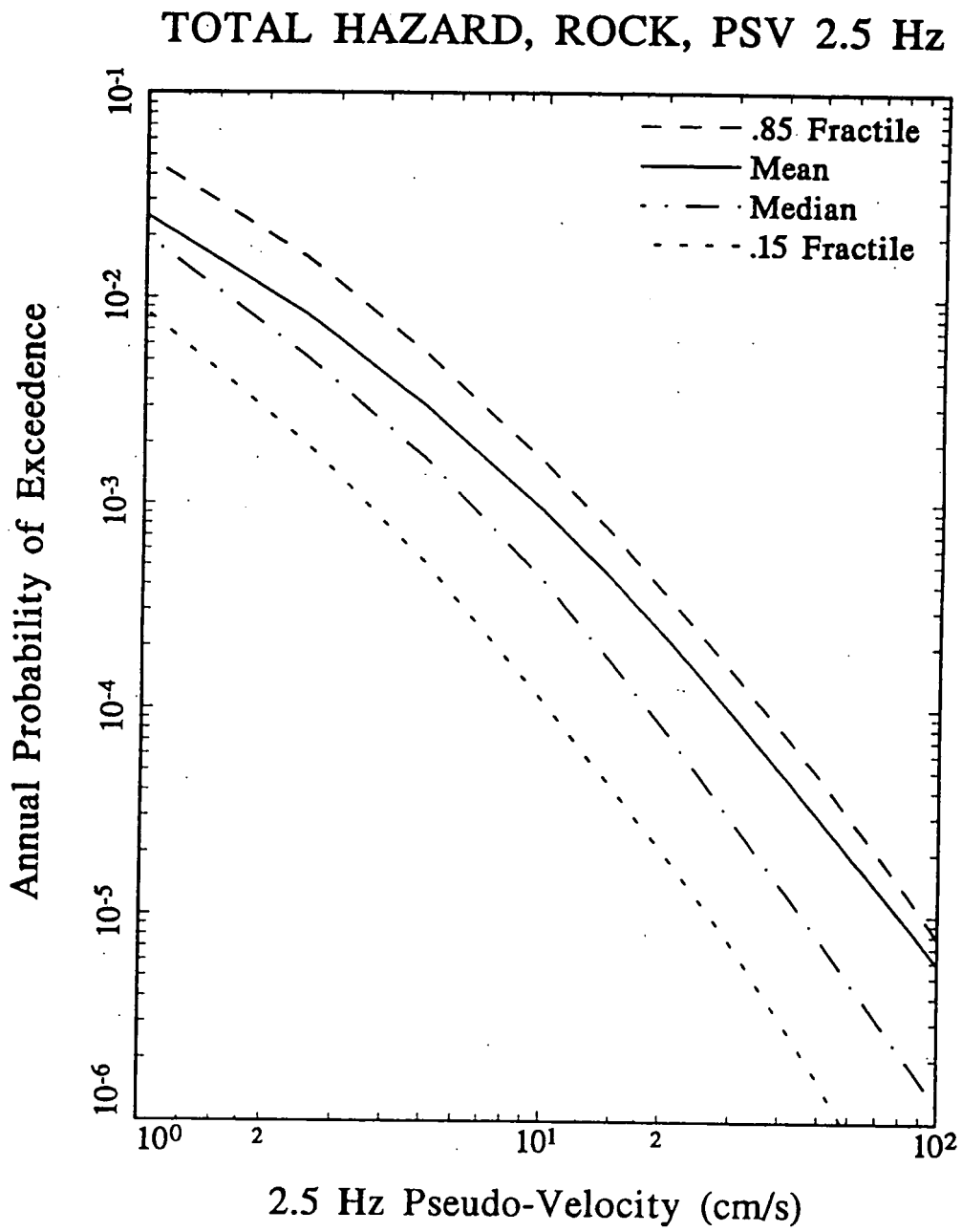

Figure 3-5. Total hazard curves, PSV(2.5 Hz) on rock.

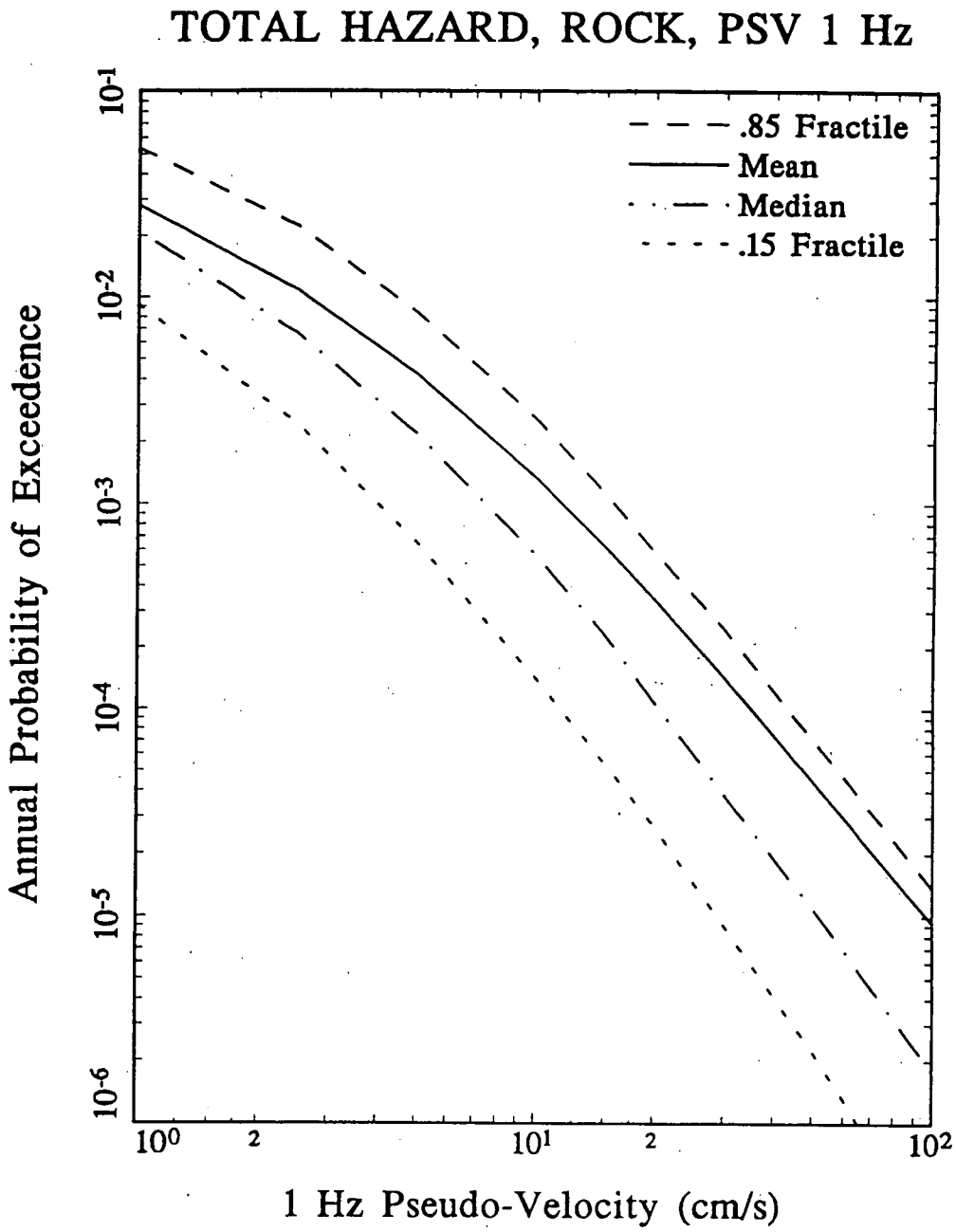

Figure 3-6. Total hazard curves, PSV(1 Hz) on rock.

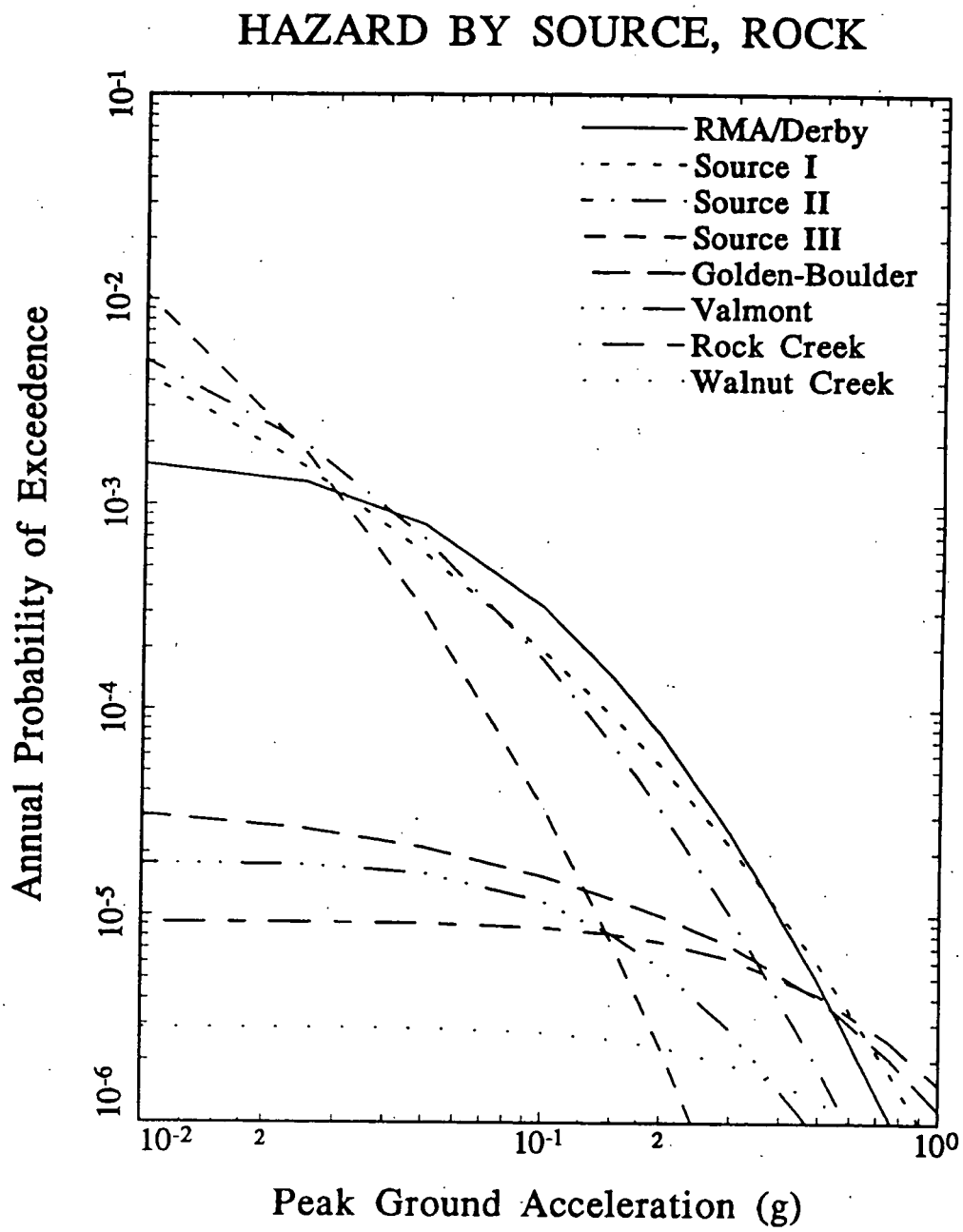

Figure 3-7. Contribution to rock PGA hazard by seismic source.

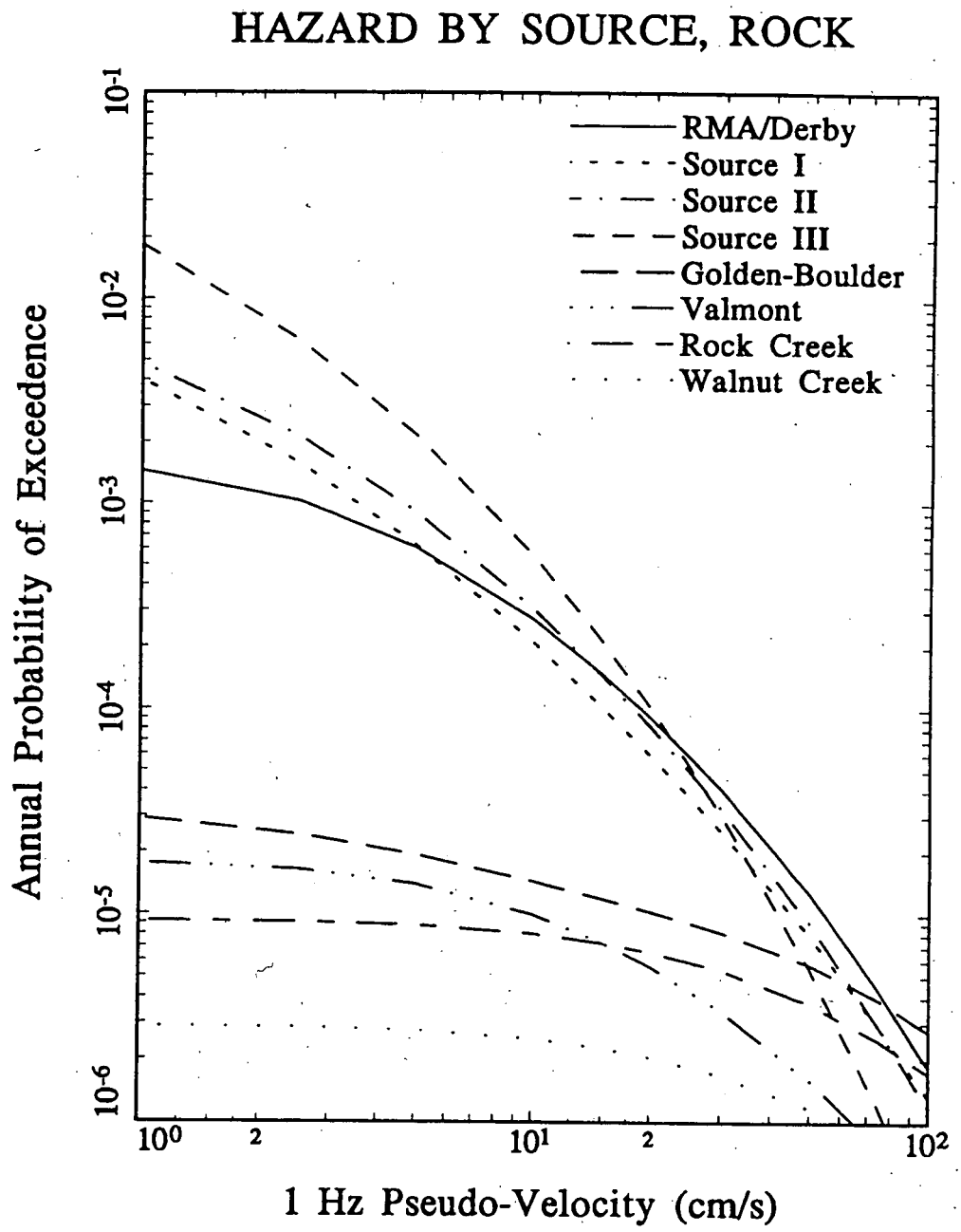

Figure 3-8. Contribution to rock PSV(1 Hz) hazard by seismic source.

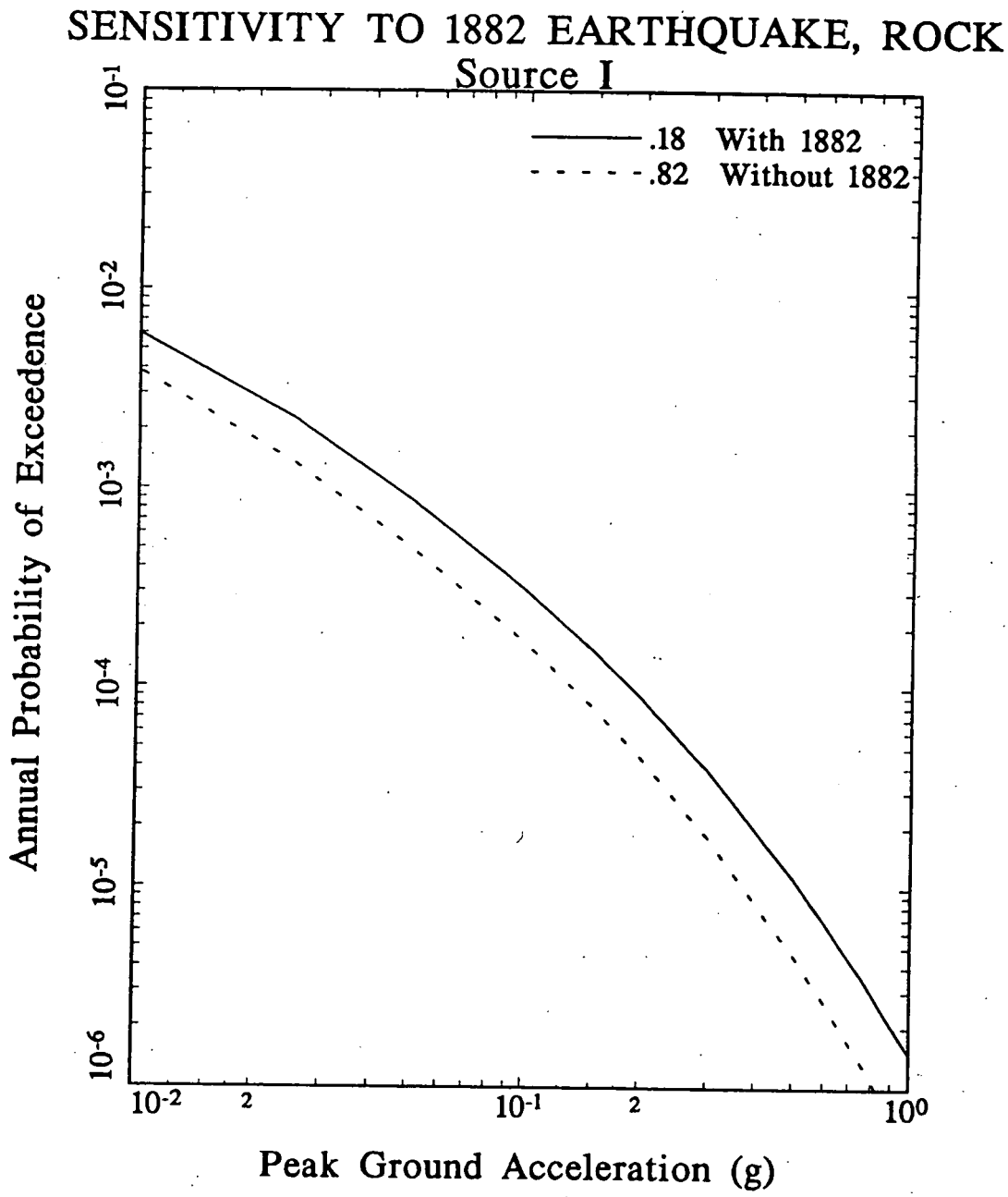

Figure 3-9. Sensitivity to 1882 earthquake, PGA on rock.
(The weight of each hypothesis is indicated in the legend.)

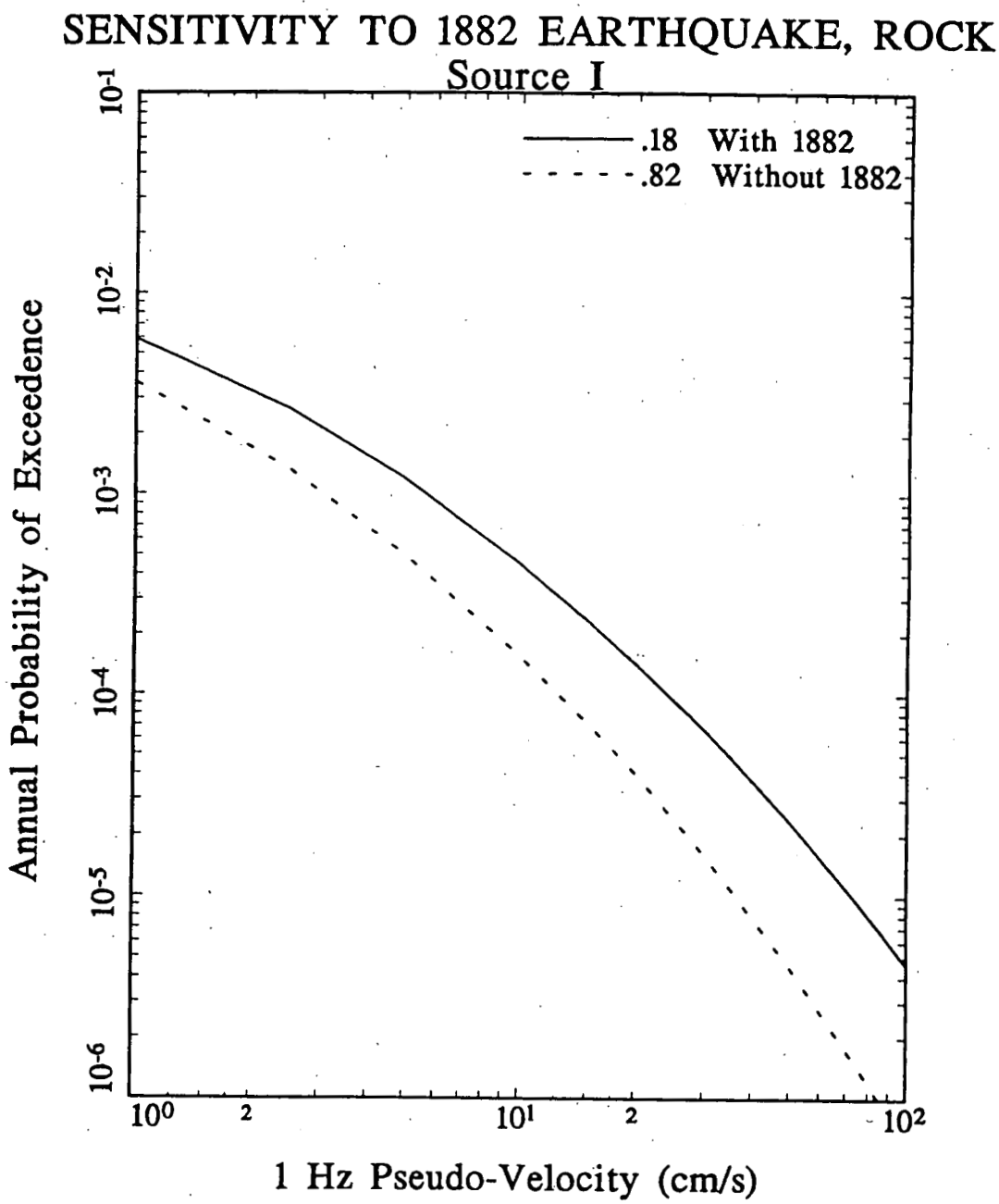

Figure 3-10. Sensitivity to 1882 earthquake, PSV(1 Hz) on rock.
(The weight of each hypothesis is indicated in the legend.)

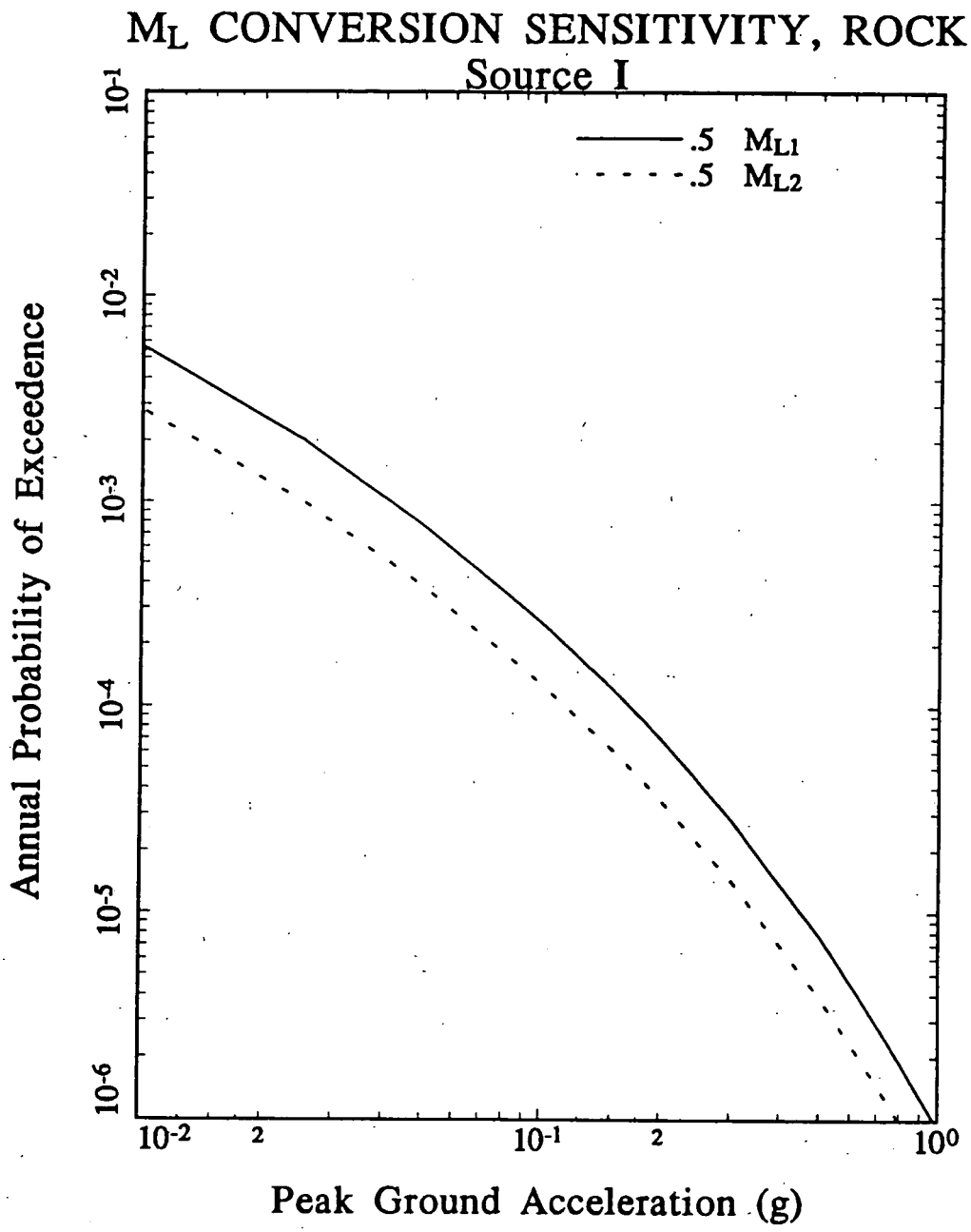

Figure 3-11. Sensitivity to M_L conversion, PGA on rock.
(The weight of each hypothesis is indicated in the legend.)

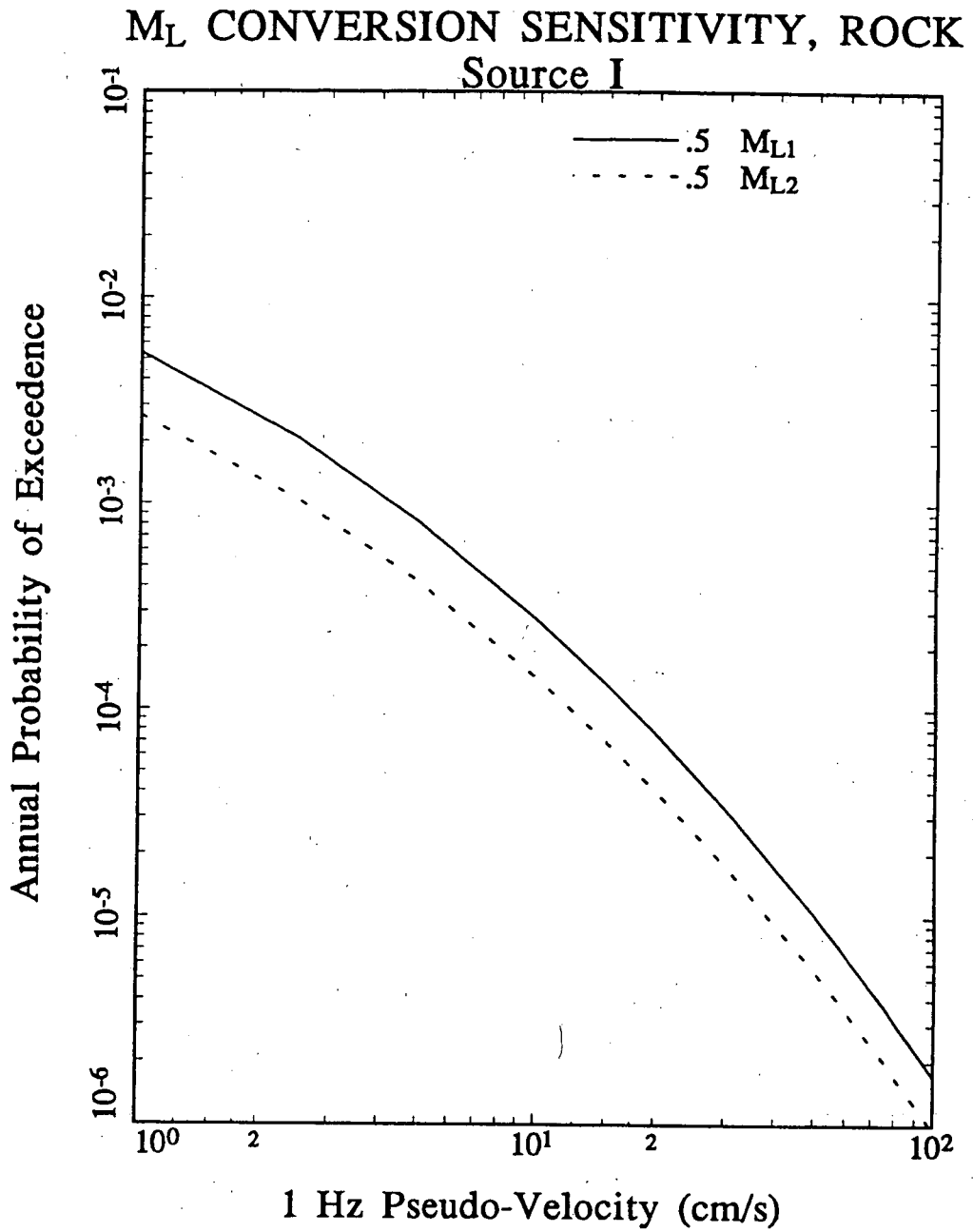

Figure 3-12. Sensitivity to M_L conversion, PSV(1 Hz) on rock.
(The weight of each hypothesis is indicated in the legend.)

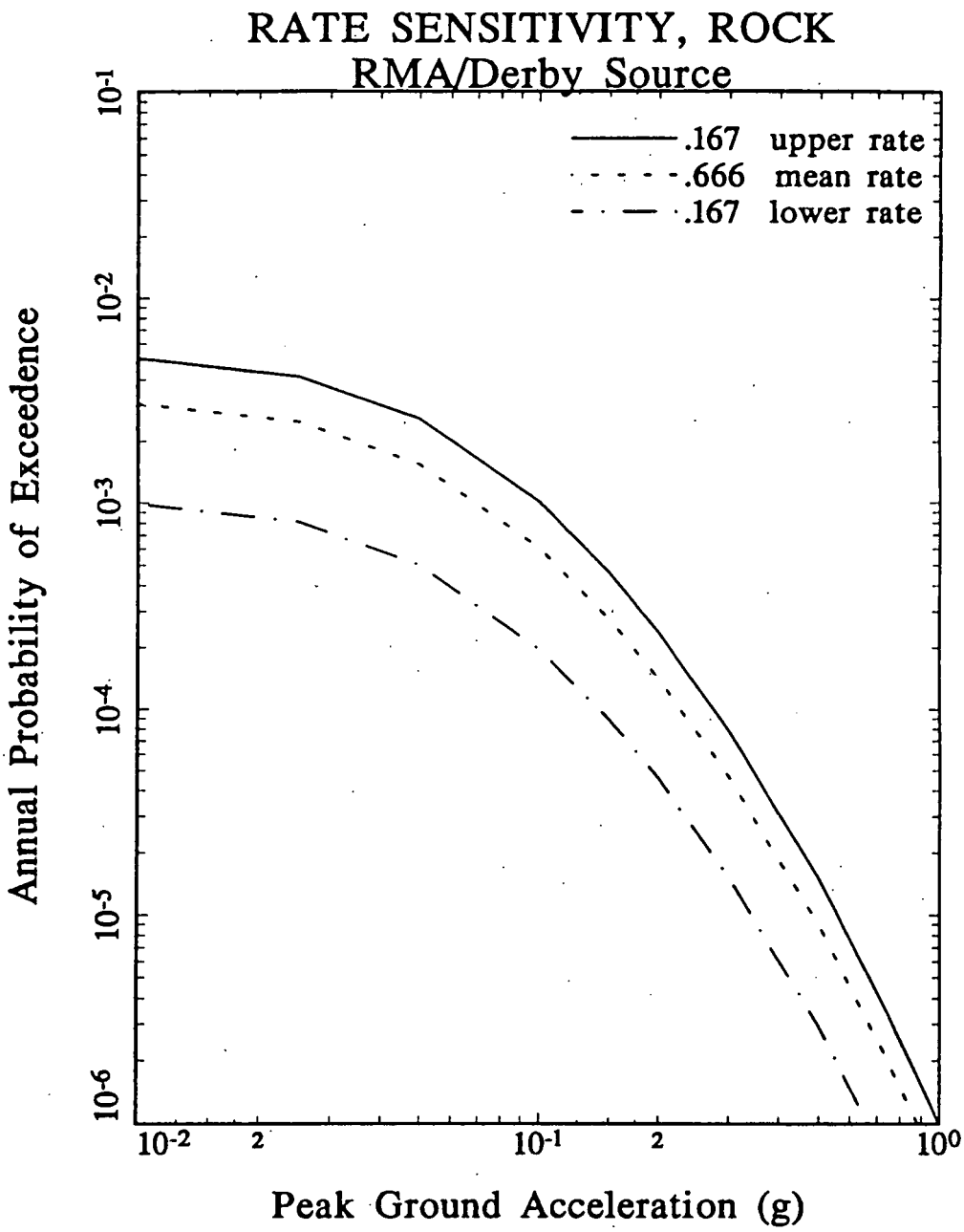

Figure 3-13. Sensitivity to seismicity rate, PGA on rock.
(The weight of each hypothesis is indicated in the legend.)

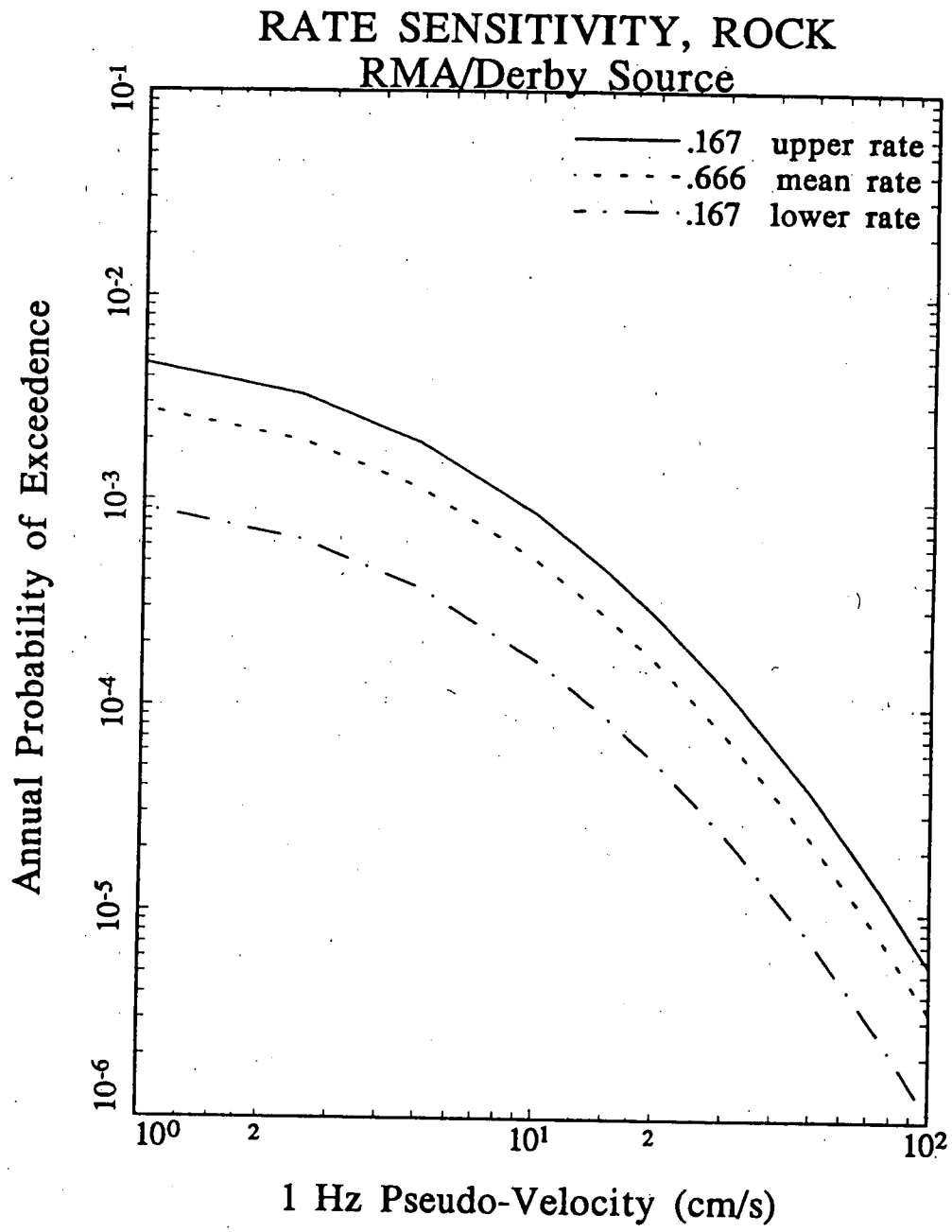

Figure 3-14. Sensitivity to seismicity rate, PSV(1 Hz) on rock.
(The weight of each hypothesis is indicated in the legend.)

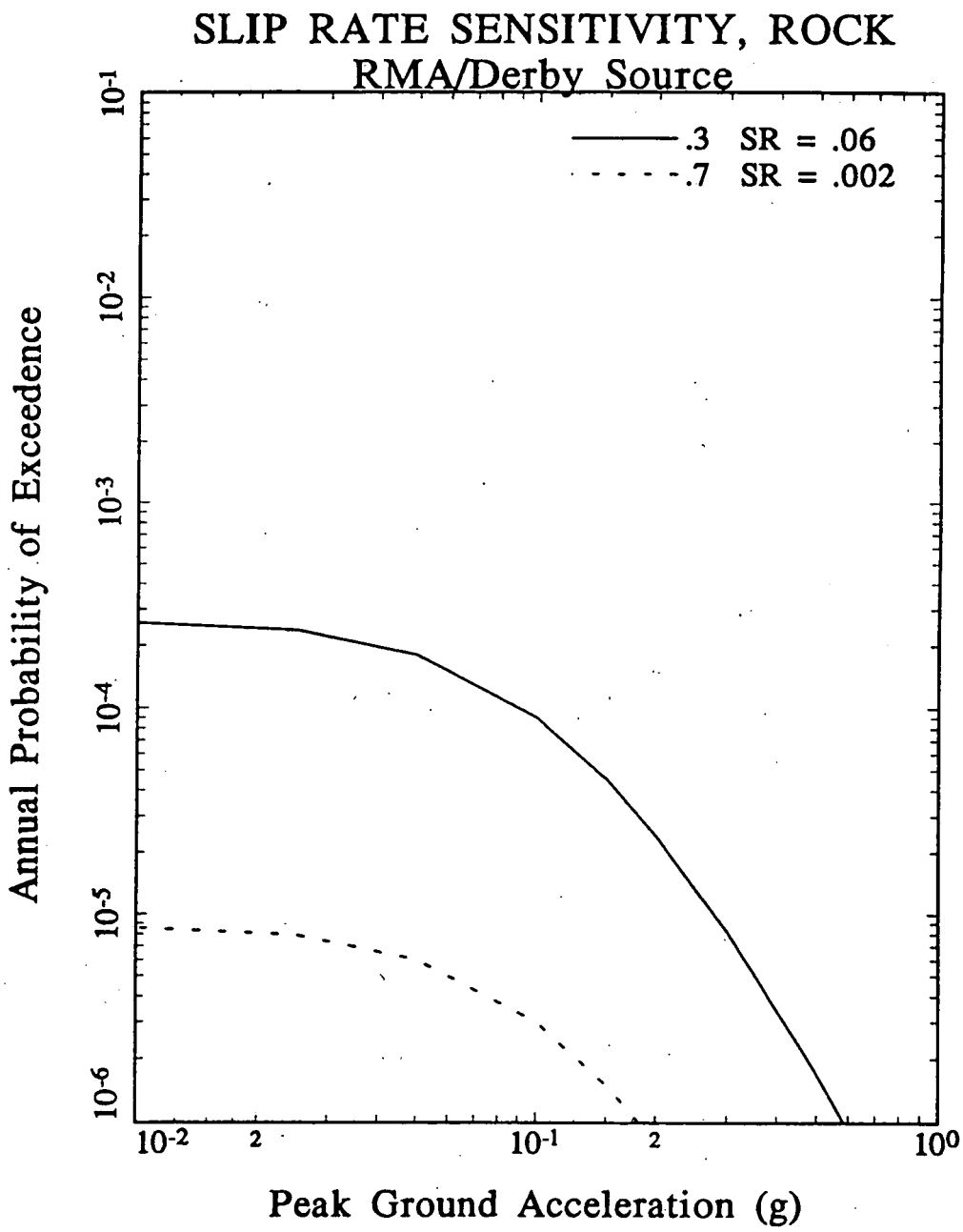

Figure 3-15. Sensitivity to RMA/Derby source slip rate, PGA on rock.
(The weight of each hypothesis is indicated in the legend.)

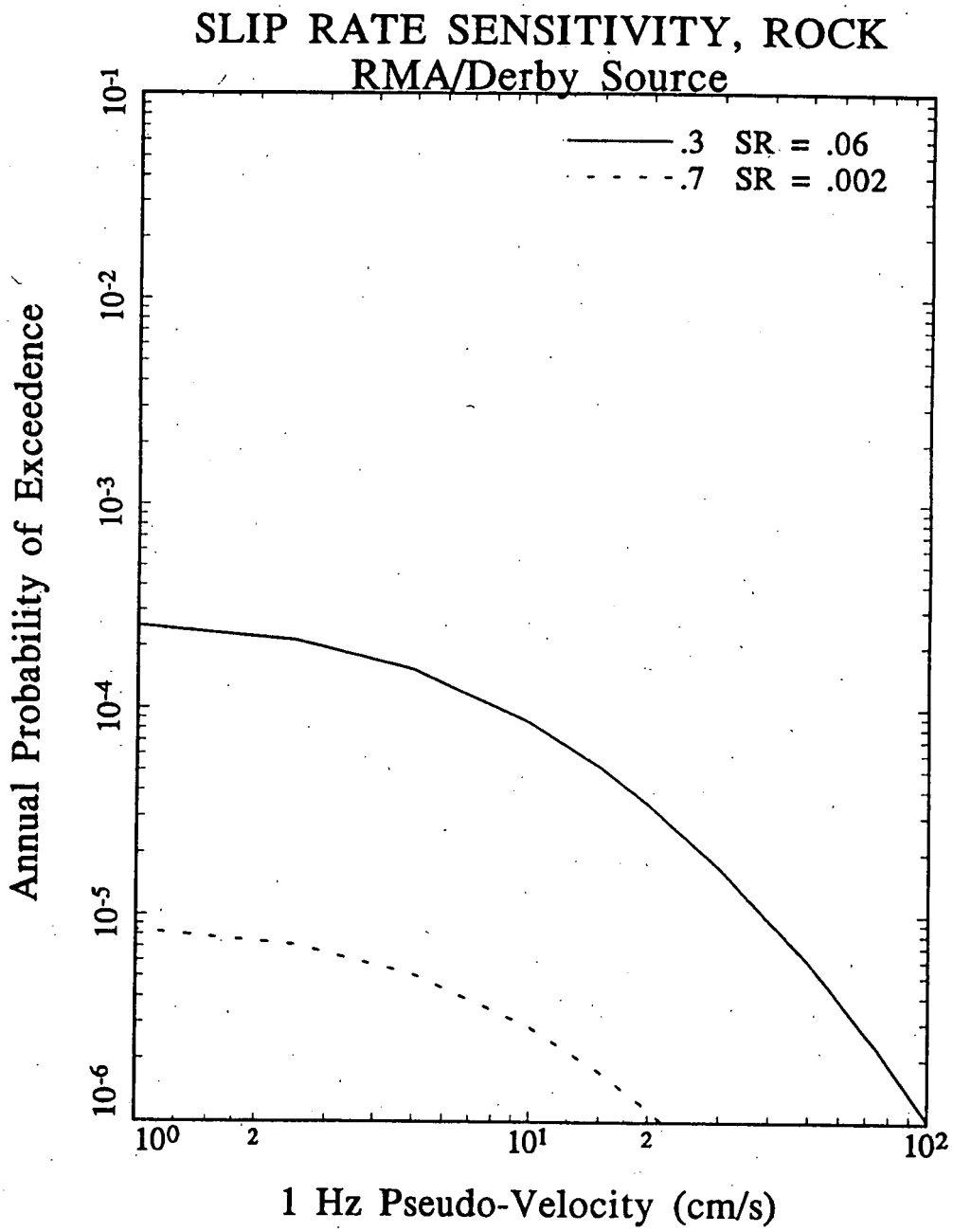

Figure 3-16. Sensitivity to RMA/Derby source slip rate, PSV (1 Hz) on rock. (The weight of each hypothesis is indicated in the legend.)

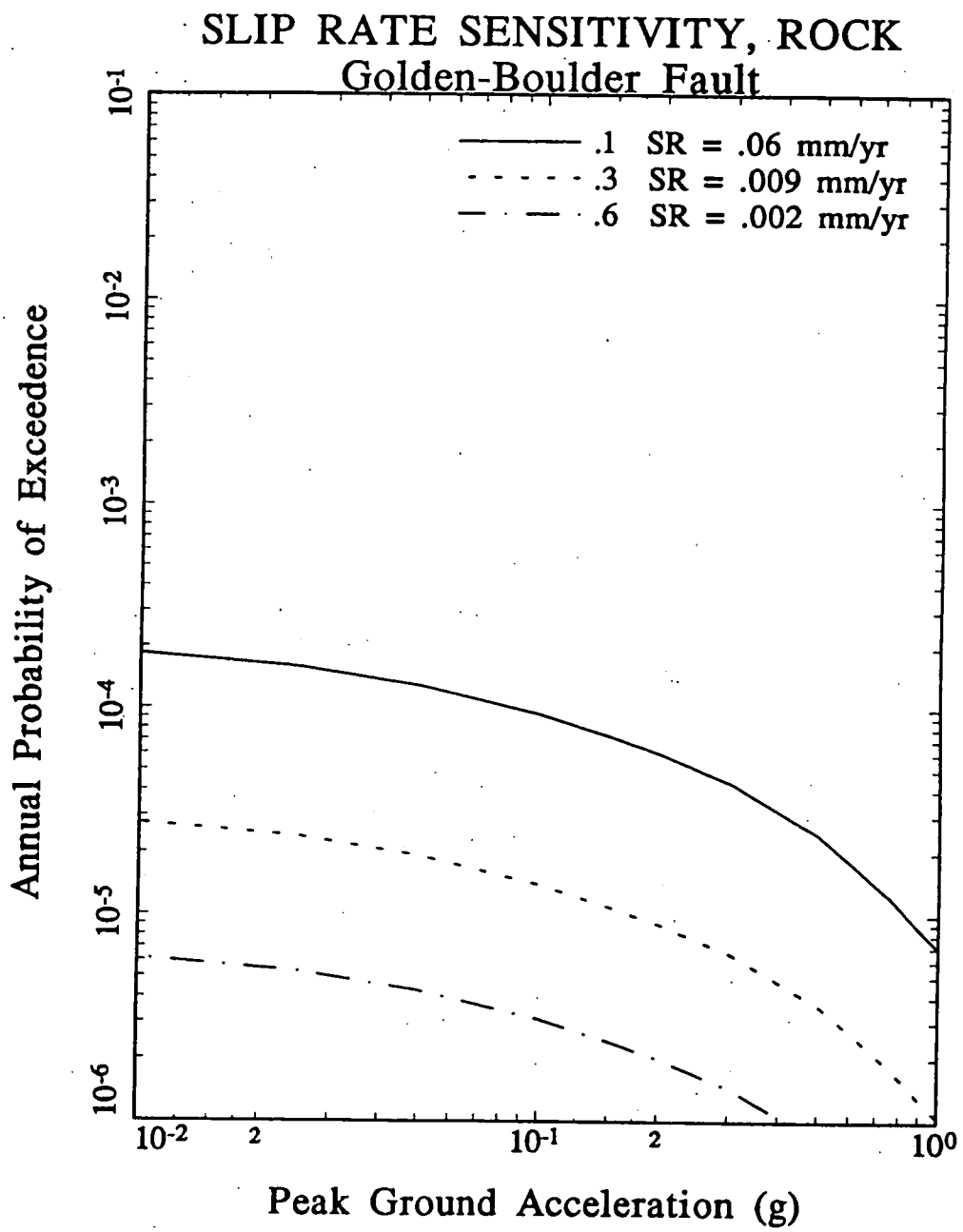

Figure 3-17. Sensitivity to Golden-Boulder slip rate, PGA on rock.
(The weight of each hypothesis is indicated in the legend.)

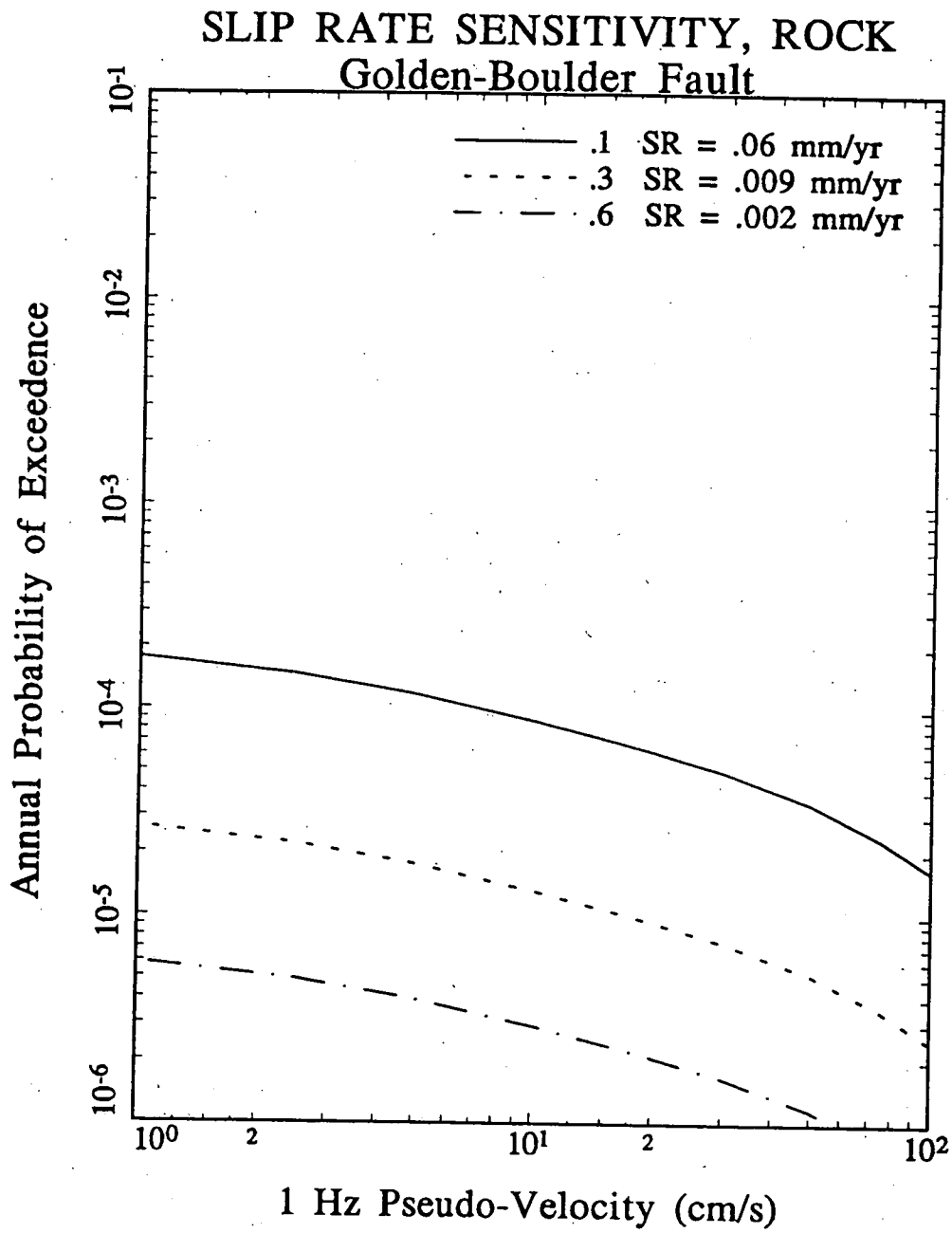

Figure 3-18. Sensitivity to Golden-Boulder slip rate, PSV(1 Hz) on rock. (The weight of each hypothesis is indicated in the legend.)

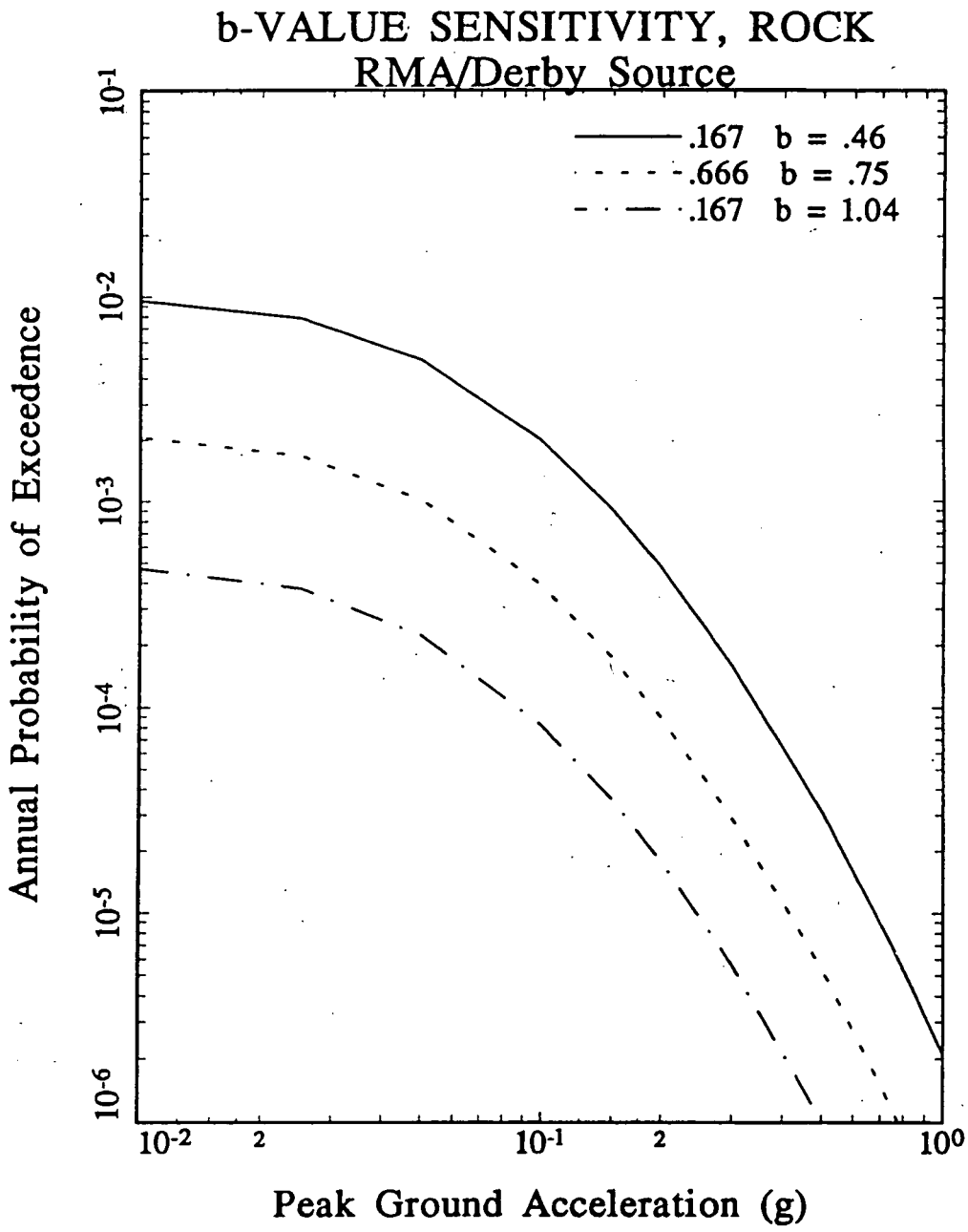

Figure 3-19. Sensitivity to *b*-value, PGA on rock.
(The weight of each hypothesis is indicated in the legend.)

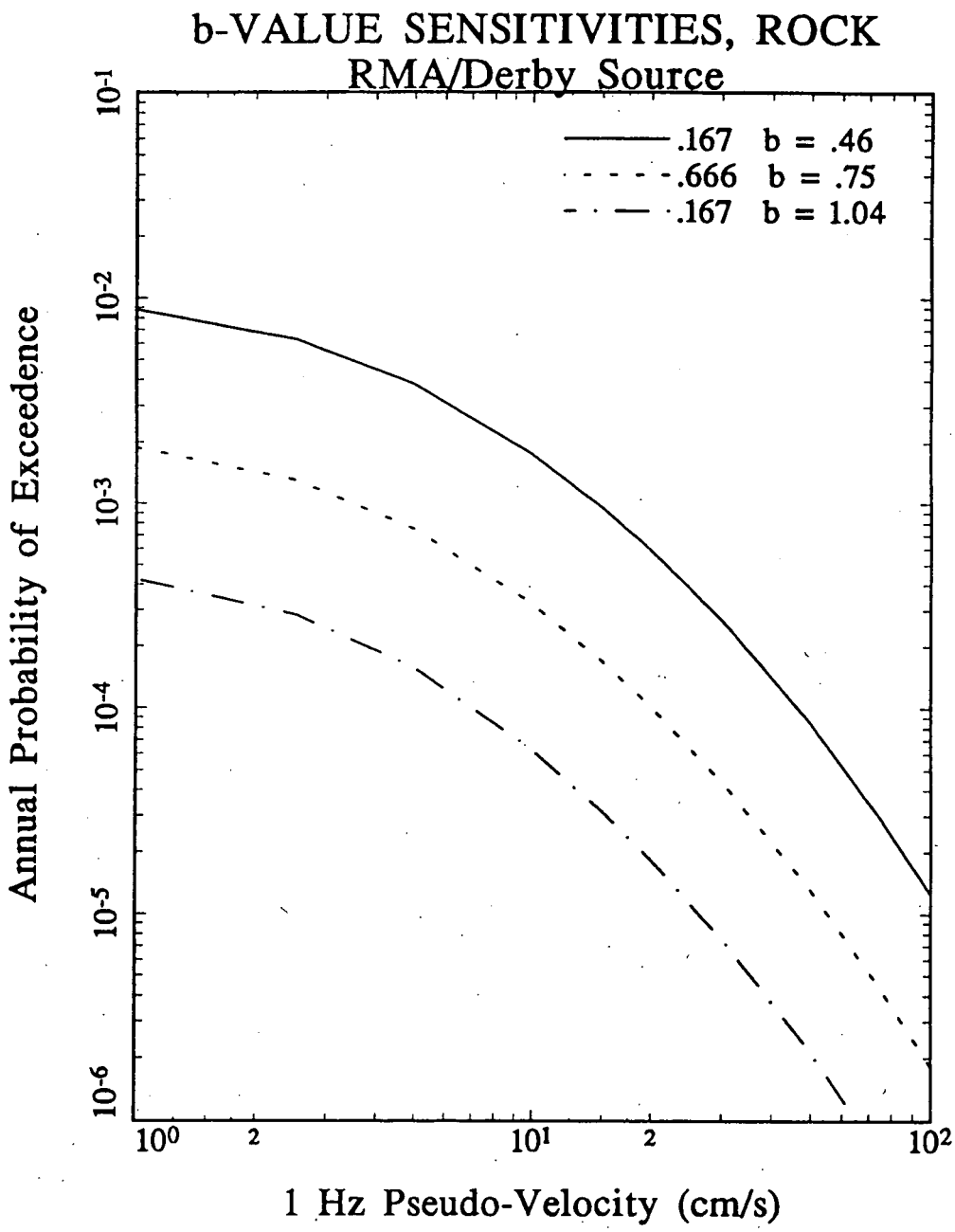

Figure 3-20. Sensitivity to *b*-value, PSV(1 Hz) on rock.
(The weight of each hypothesis is indicated in the legend.)

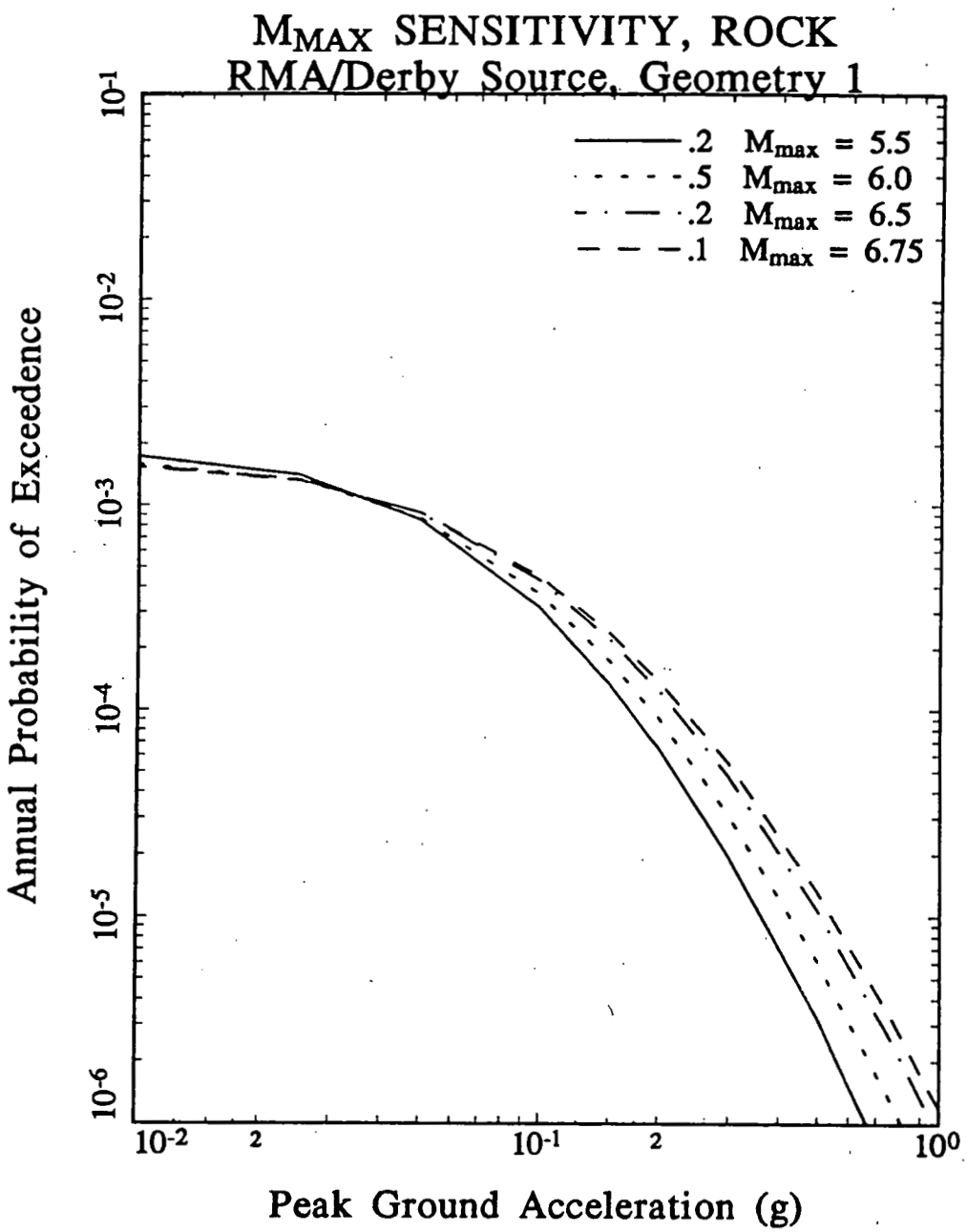

Figure 3-21. Sensitivity to M_{max}, RMA/Derby source, PGA on rock. (The weight of each hypothesis is indicated in the legend.)

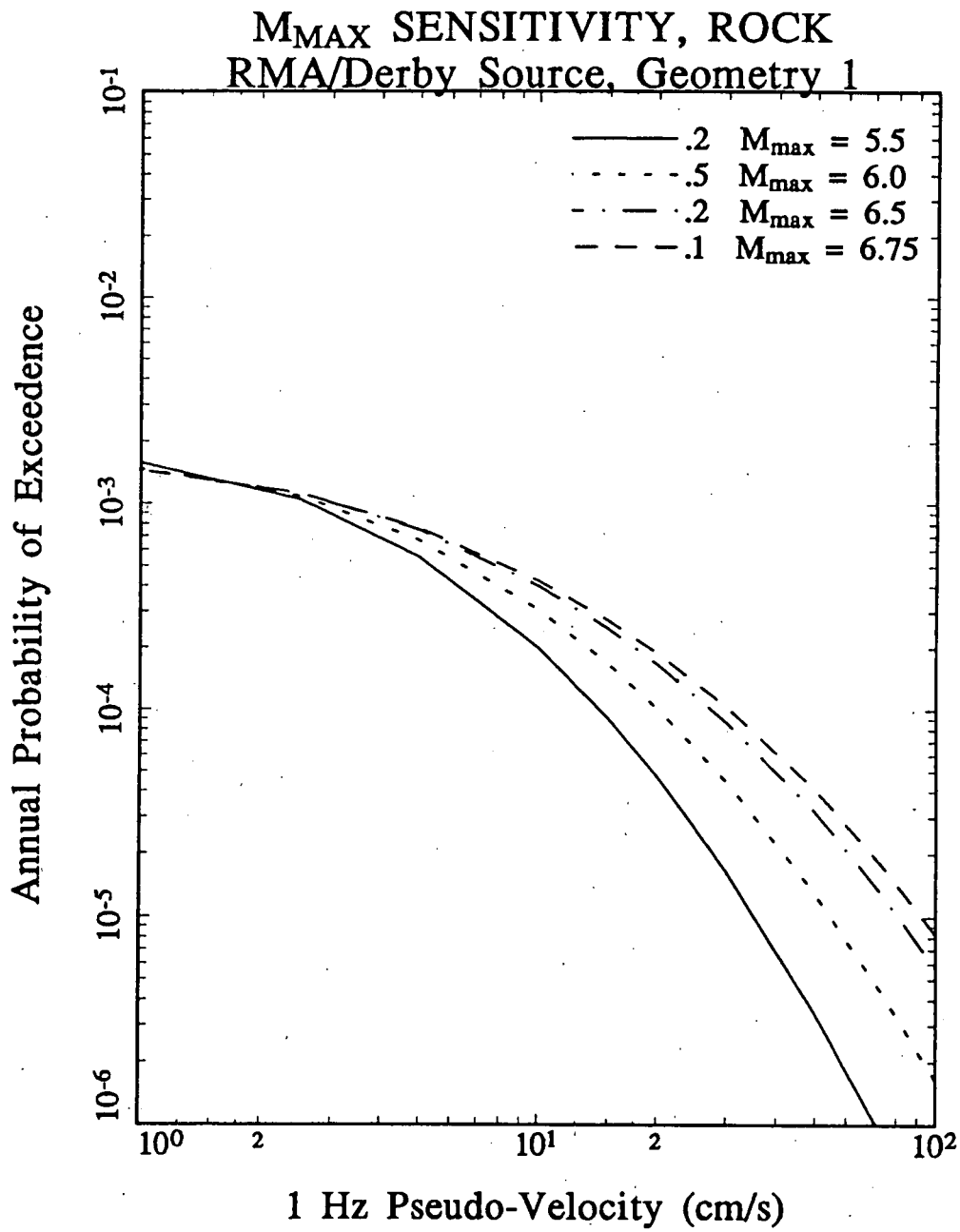

Figure 3-22. Sensitivity to M_{max}, RMA/Derby source, PSV(1 Hz) on rock. (The weight of each hypothesis is indicated in the legend.)

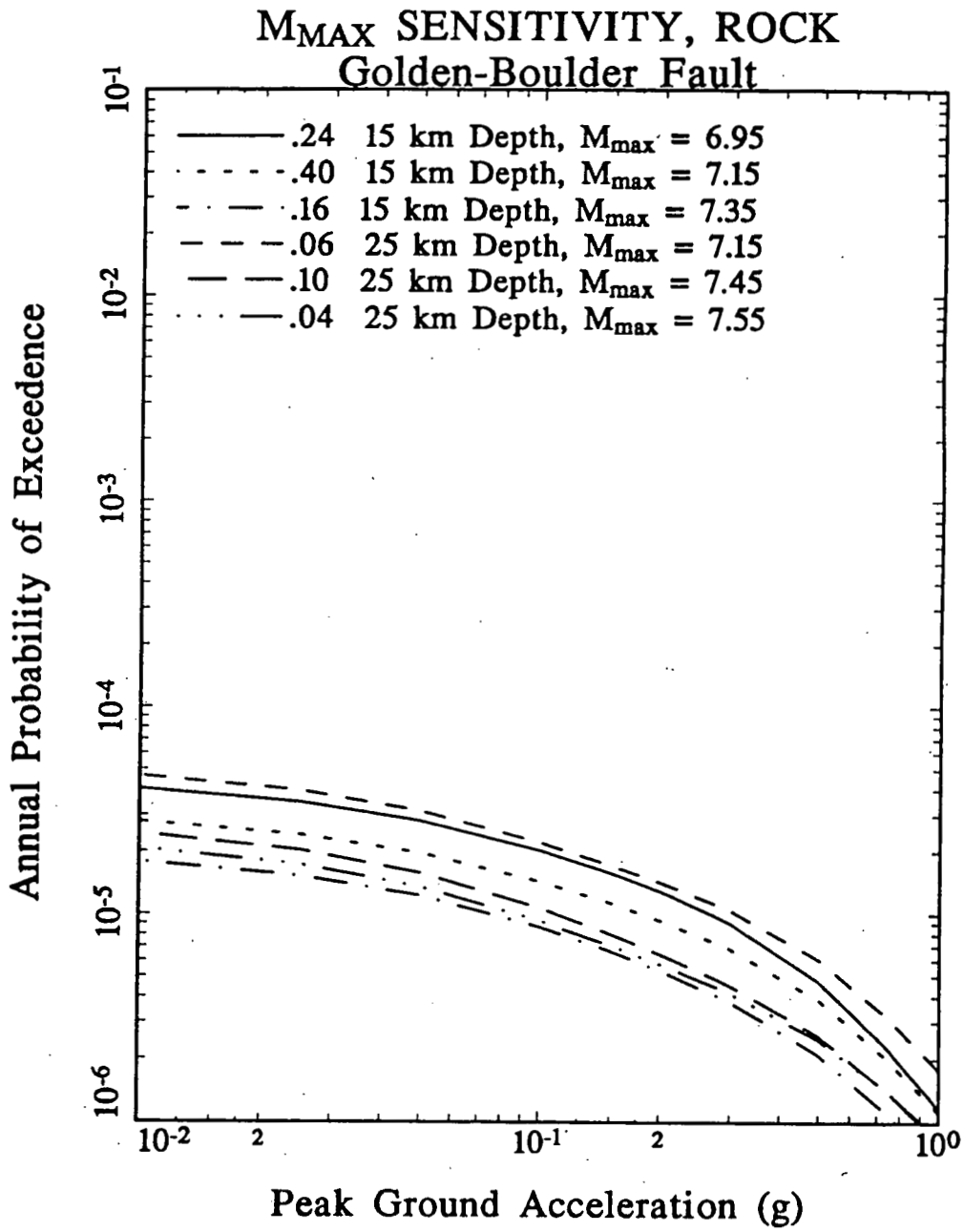

Figure 3-23. Sensitivity to M_{max}, Golden-Boulder fault, PGA on rock. (The weight of each hypothesis is indicated in the legend.)

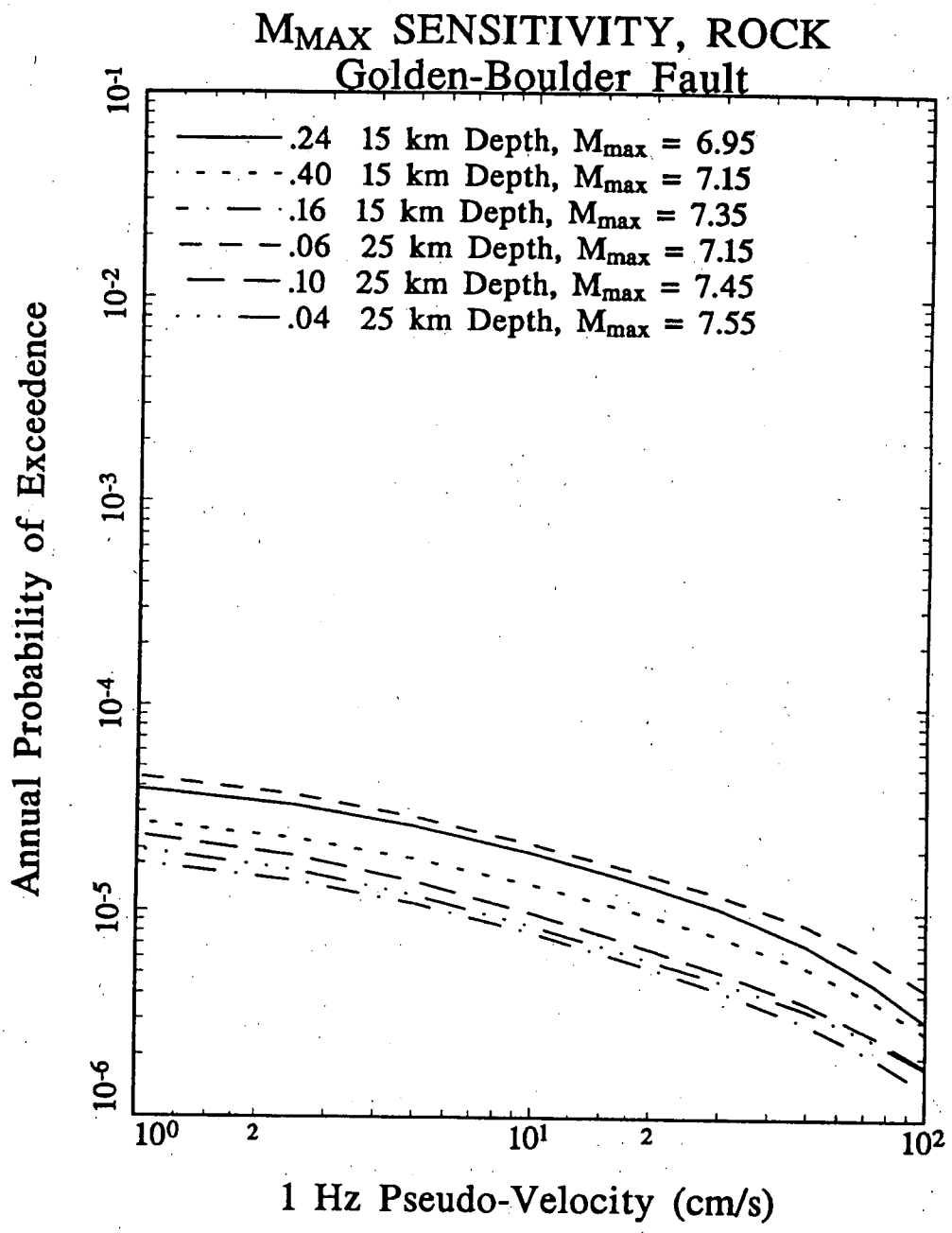

Figure 3-24. Sensitivity to M_{max}, Golden-Boulder fault, PSV(1 Hz) on rock. (The weight of each hypothesis is indicated in the legend.)

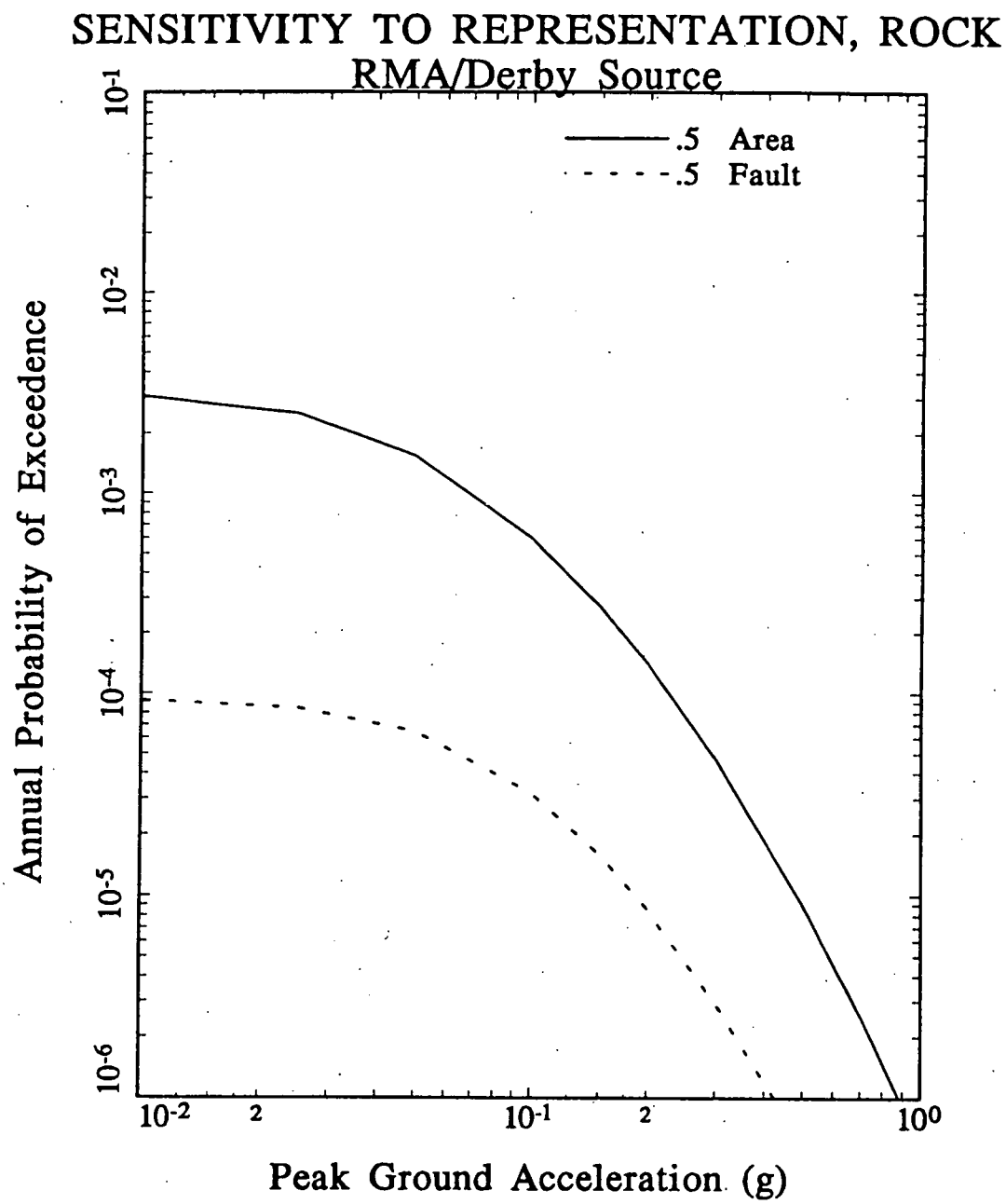

Figure 3-25. Sensitivity to RMA/Derby source representation, PGA on rock. (The weight of each hypothesis is indicated in the legend.)

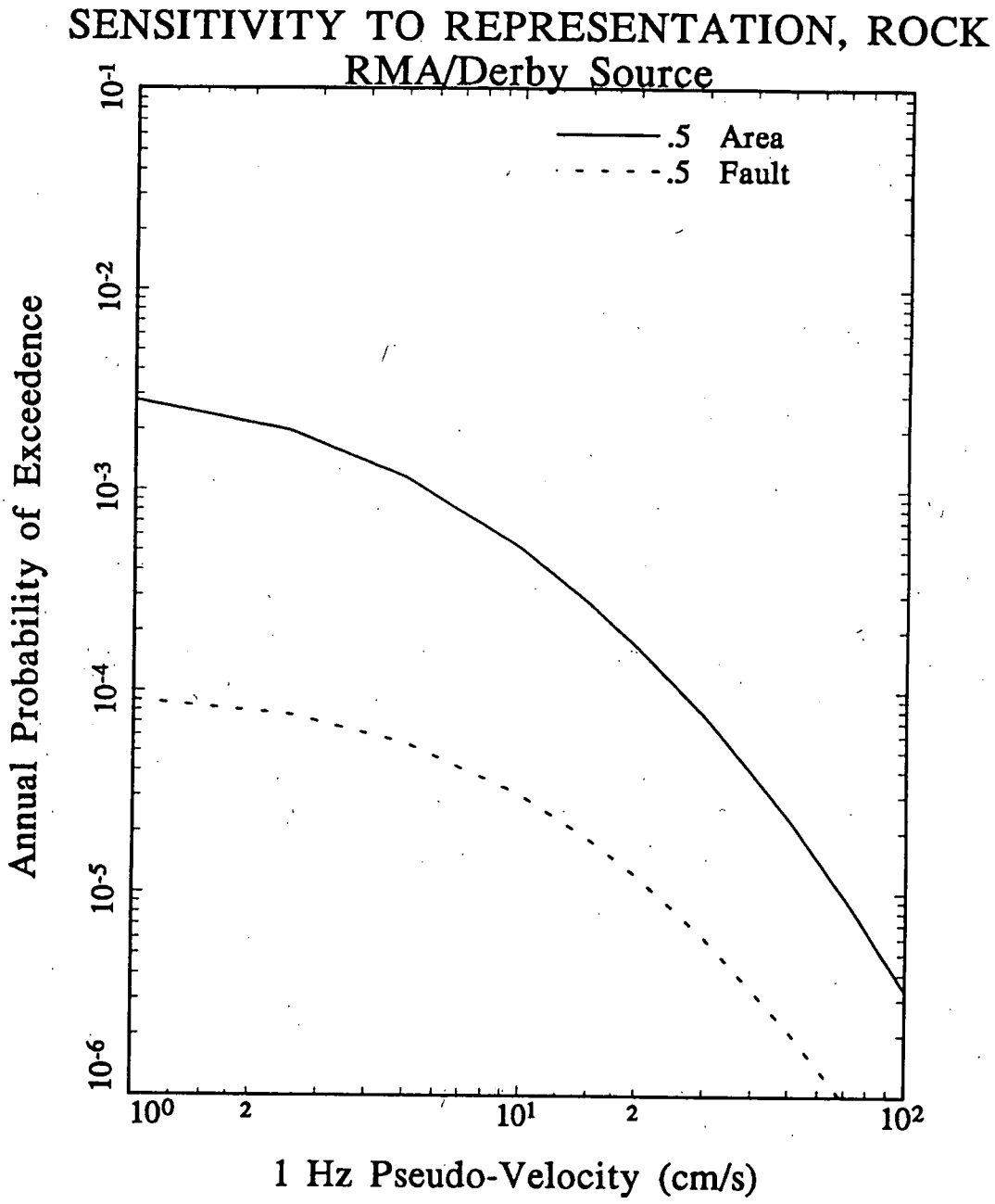

Figure 3-26. Sensitivity to RMA/Derby source representation, PSV (1 Hz) on rock. (The weight of each hypothesis is indicated in the legend.)

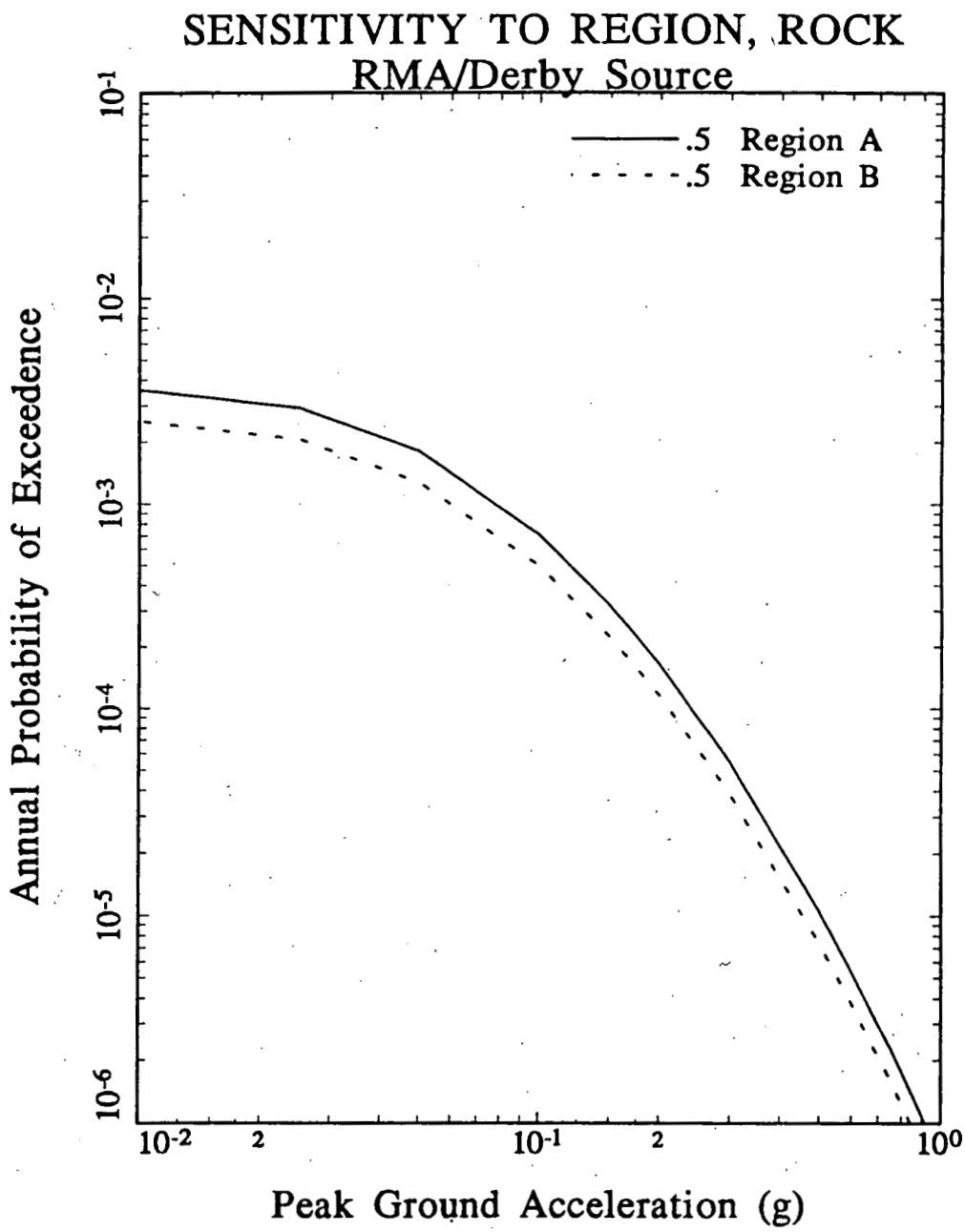

Figure 3-27. Sensitivity to RMA/Derby source seismicity region, PGA on rock. (The weight of each hypothesis is indicated in the legend.)

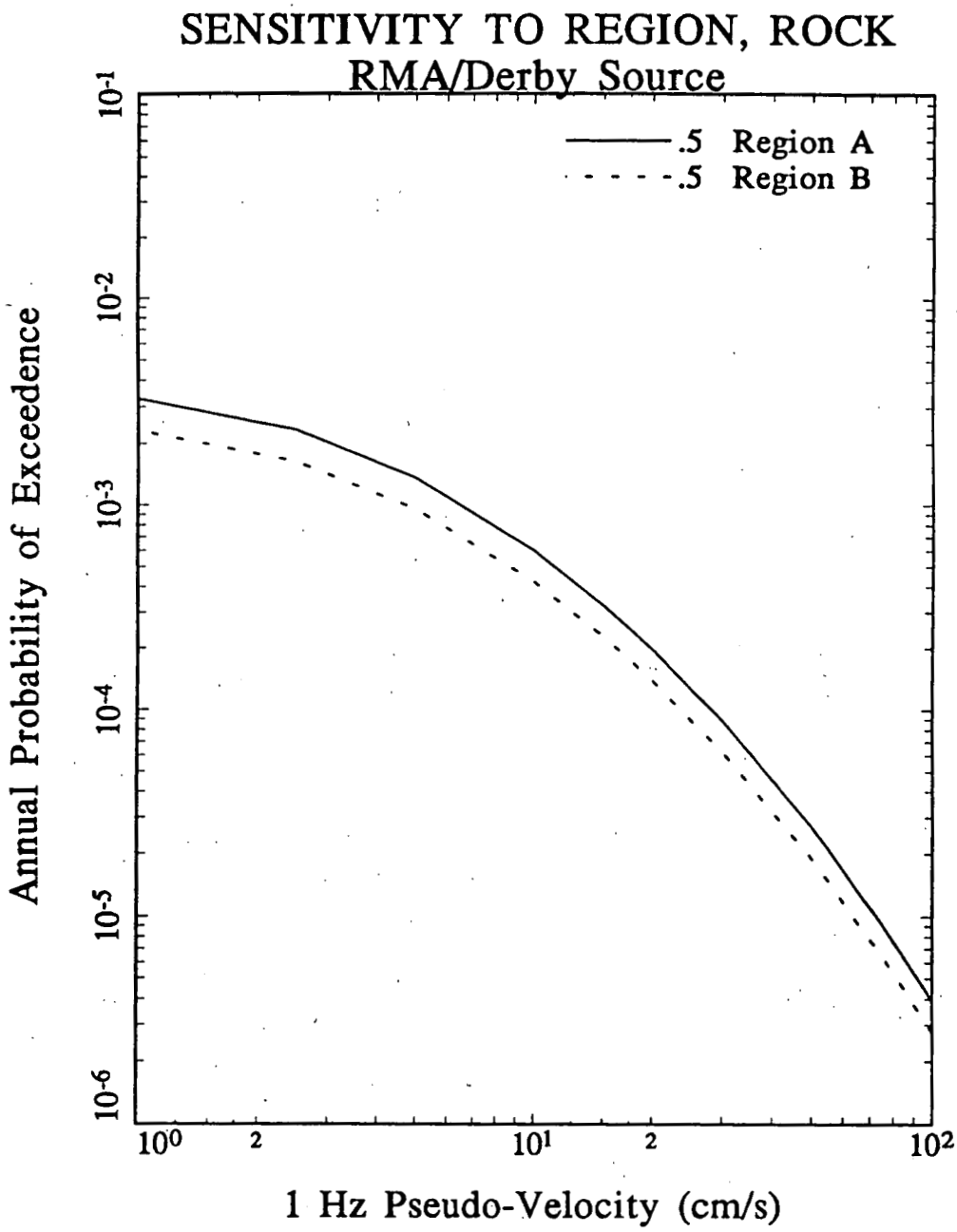

Figure 3-28. Sensitivity to RMA/Derby source seismicity region, PSV(1 Hz) on rock. (The weight of each hypothesis is indicated in the legend.)

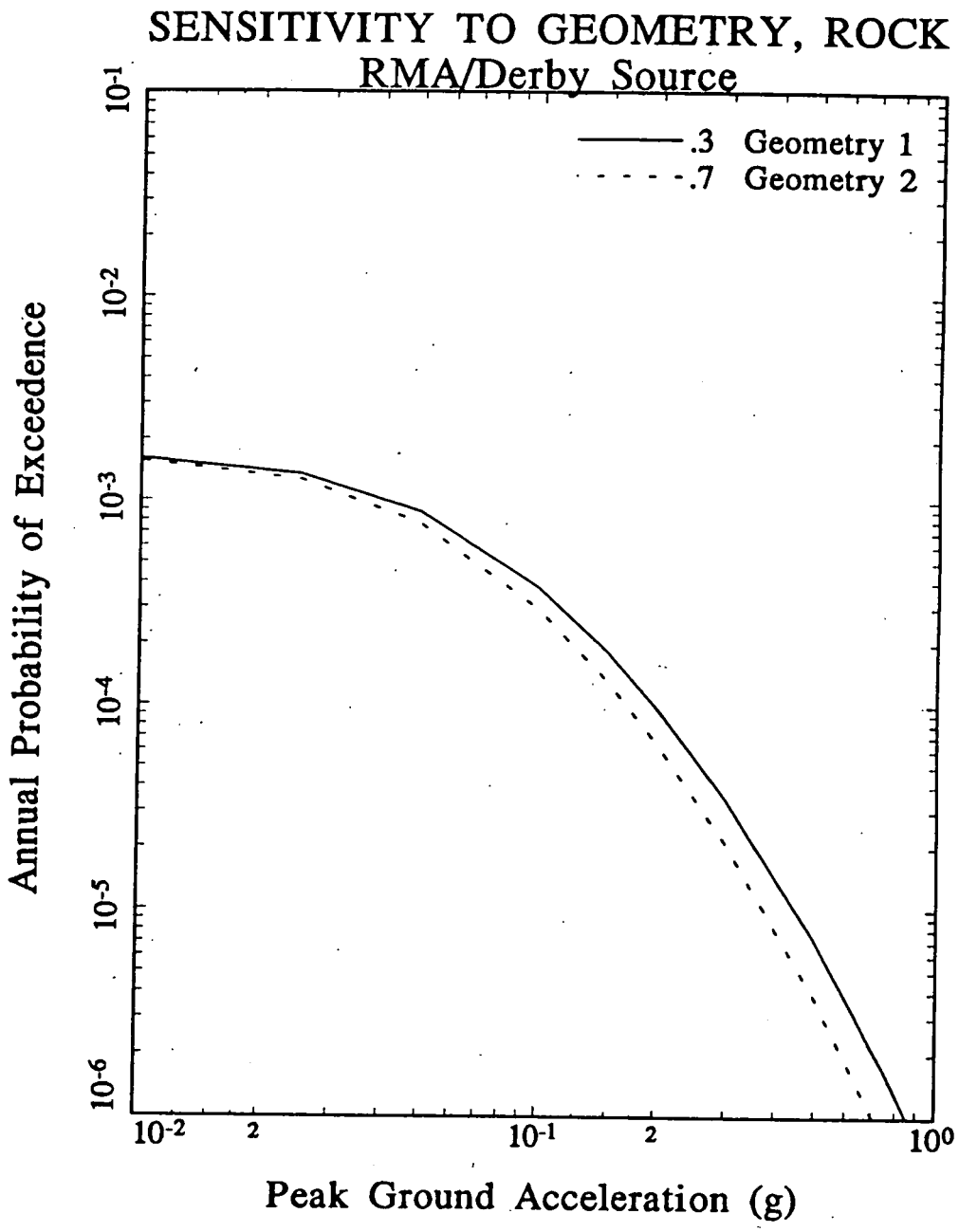

Figure 3-29. Sensitivity to RMA/Derby source geometry, PGA on rock. (The weight of each hypothesis is indicated in the legend.)

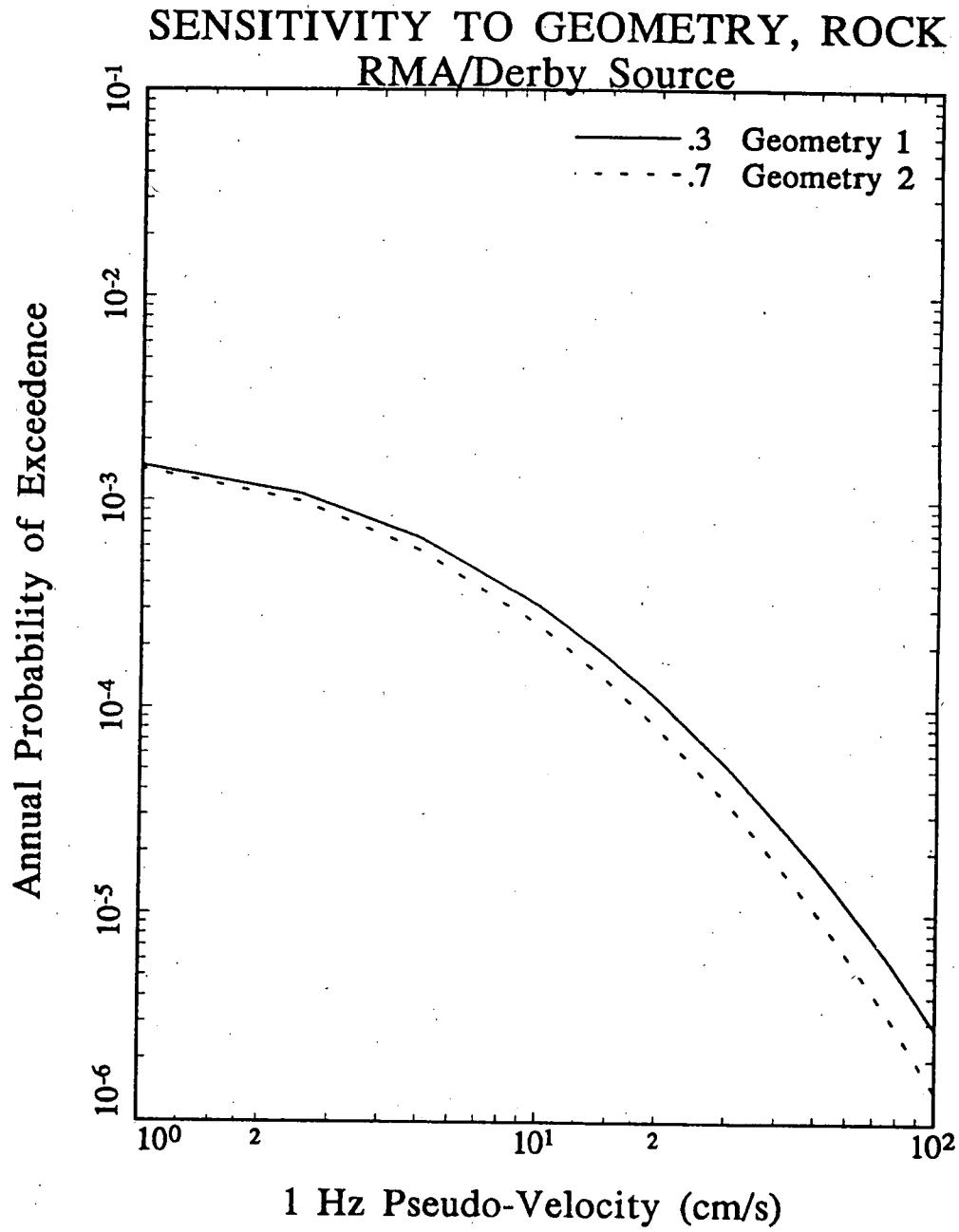

Figure 3-30. Sensitivity to RMA/Derby source geometry, PSV(1 Hz) on rock. (The weight of each hypothesis is indicated in the legend.)

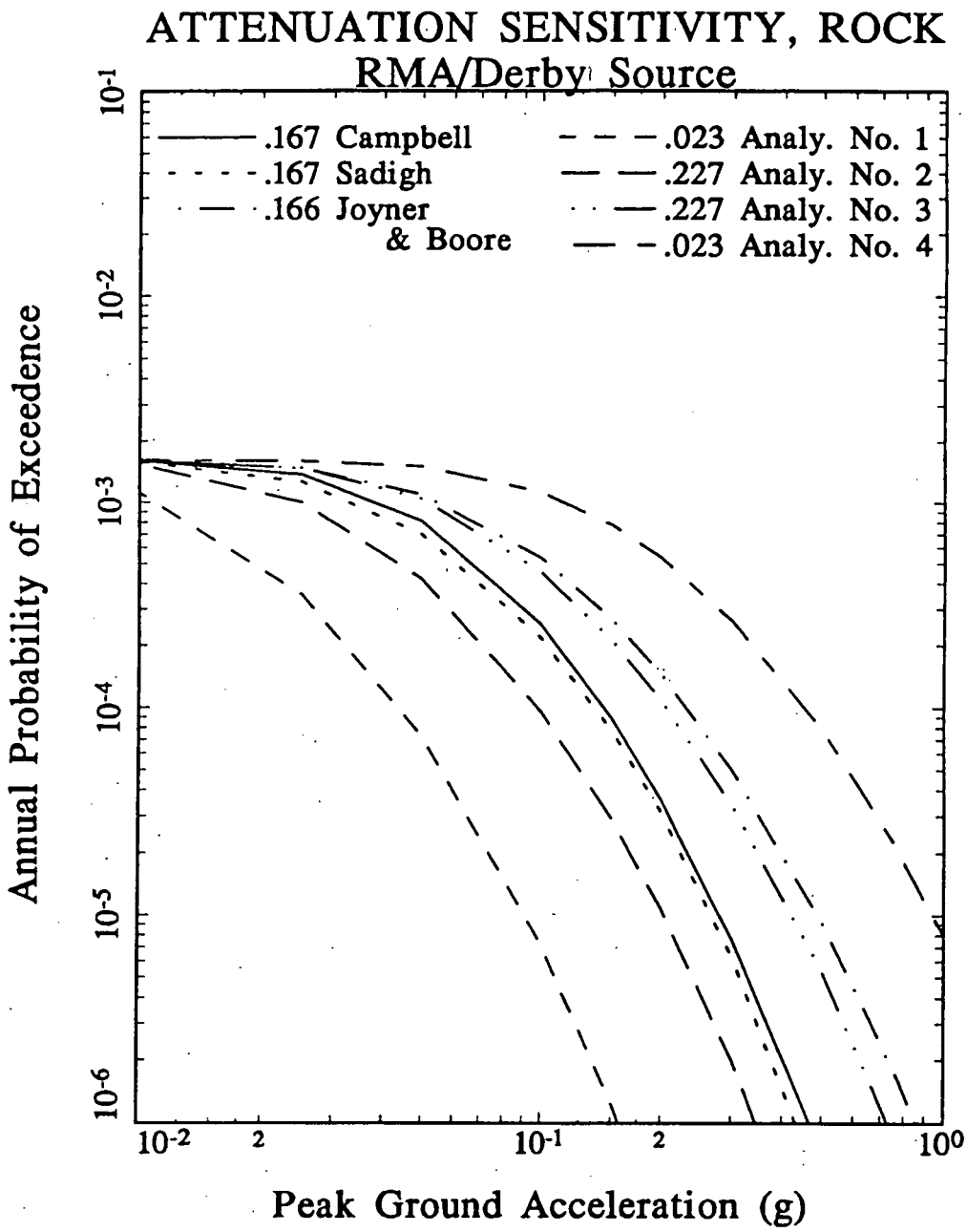

Figure 3-31. Sensitivity to attenuation, PGA on rock.
(The weight of each hypothesis is indicated in the legend.)

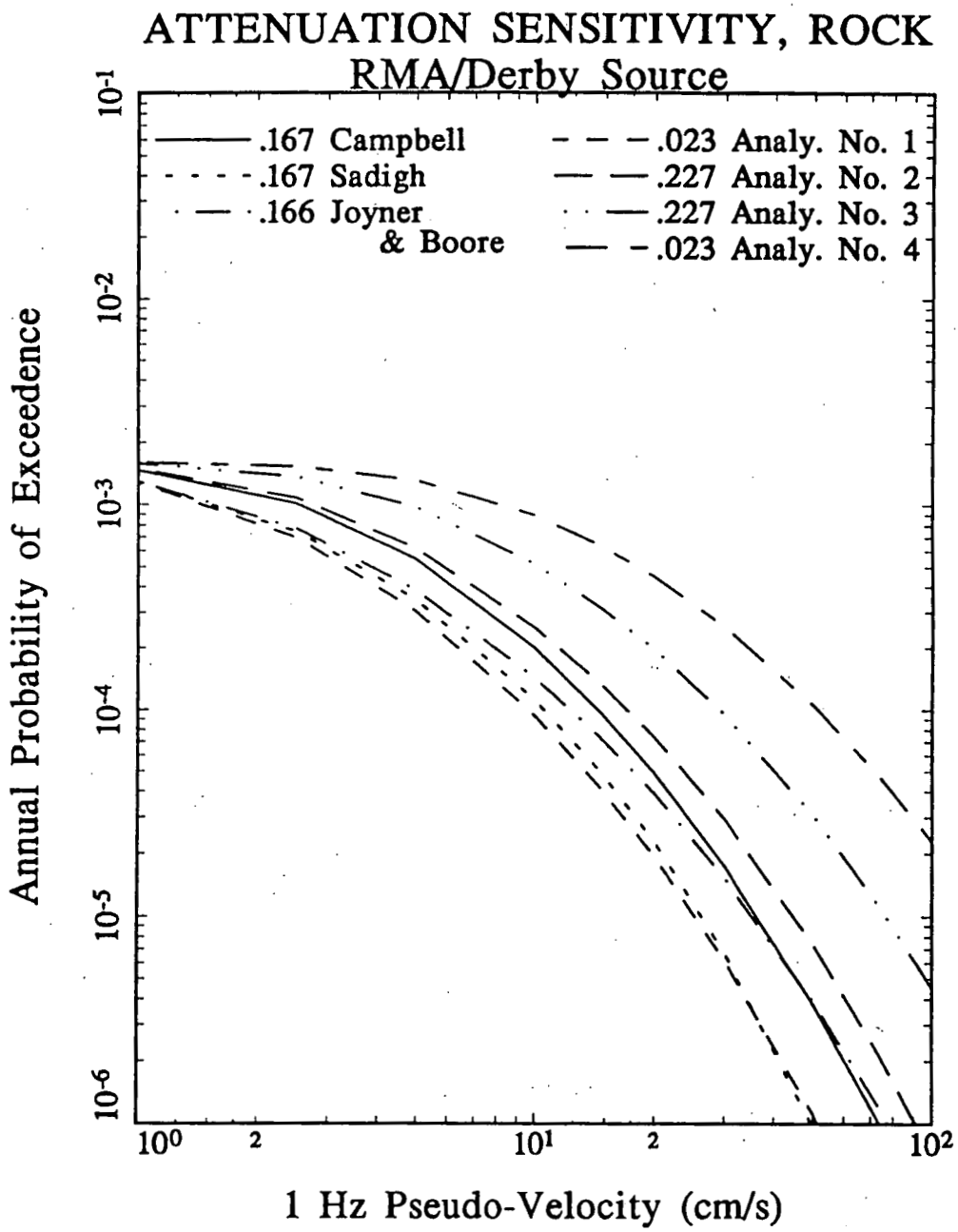

Figure 3-32. Sensitivity to attenuation, PSV(1 Hz) on rock.
(The weight of each hypothesis is indicated in the legend.)

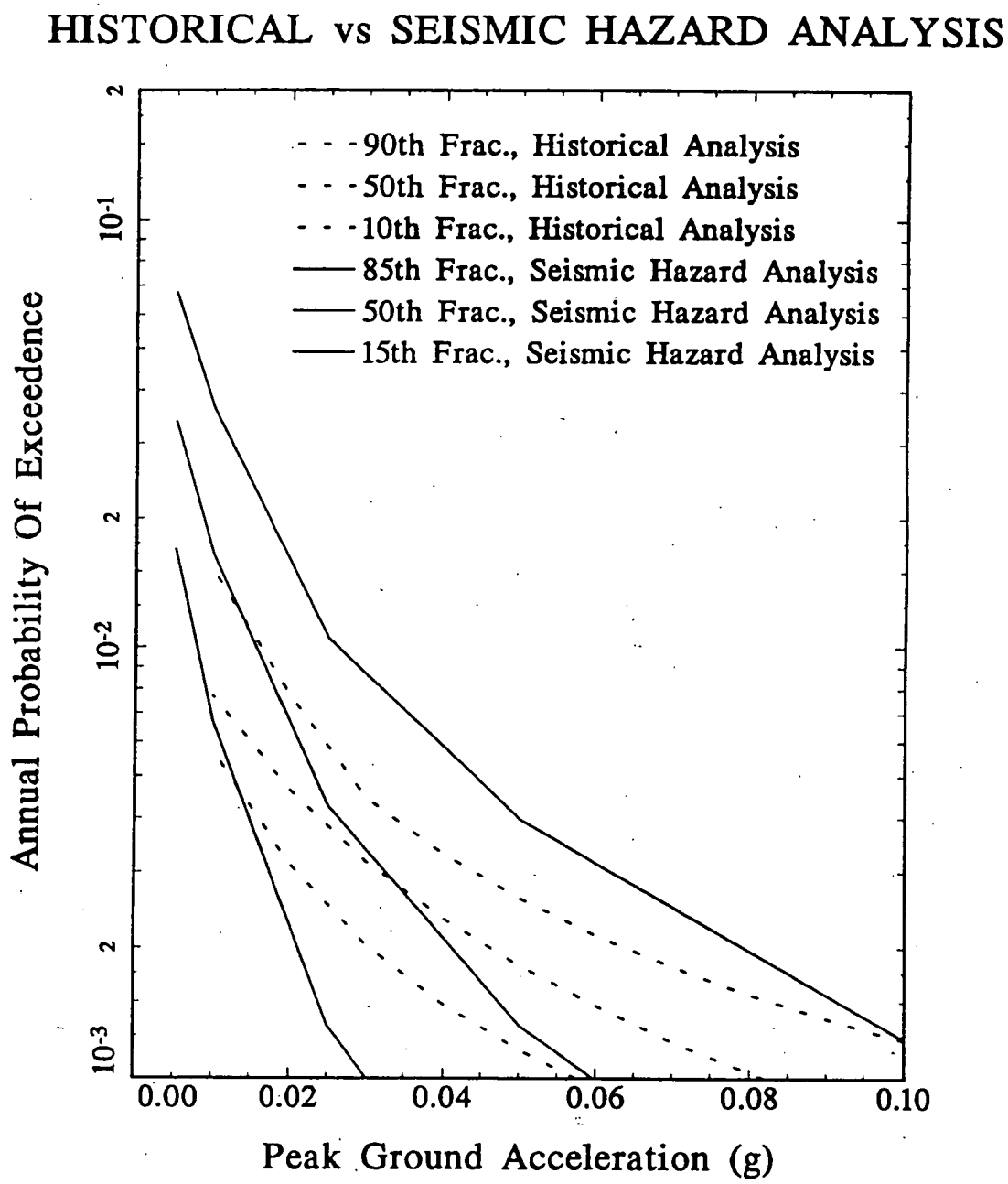

Figure 3-33. Comparison of historical vs. seismic hazard results for PGA on rock.

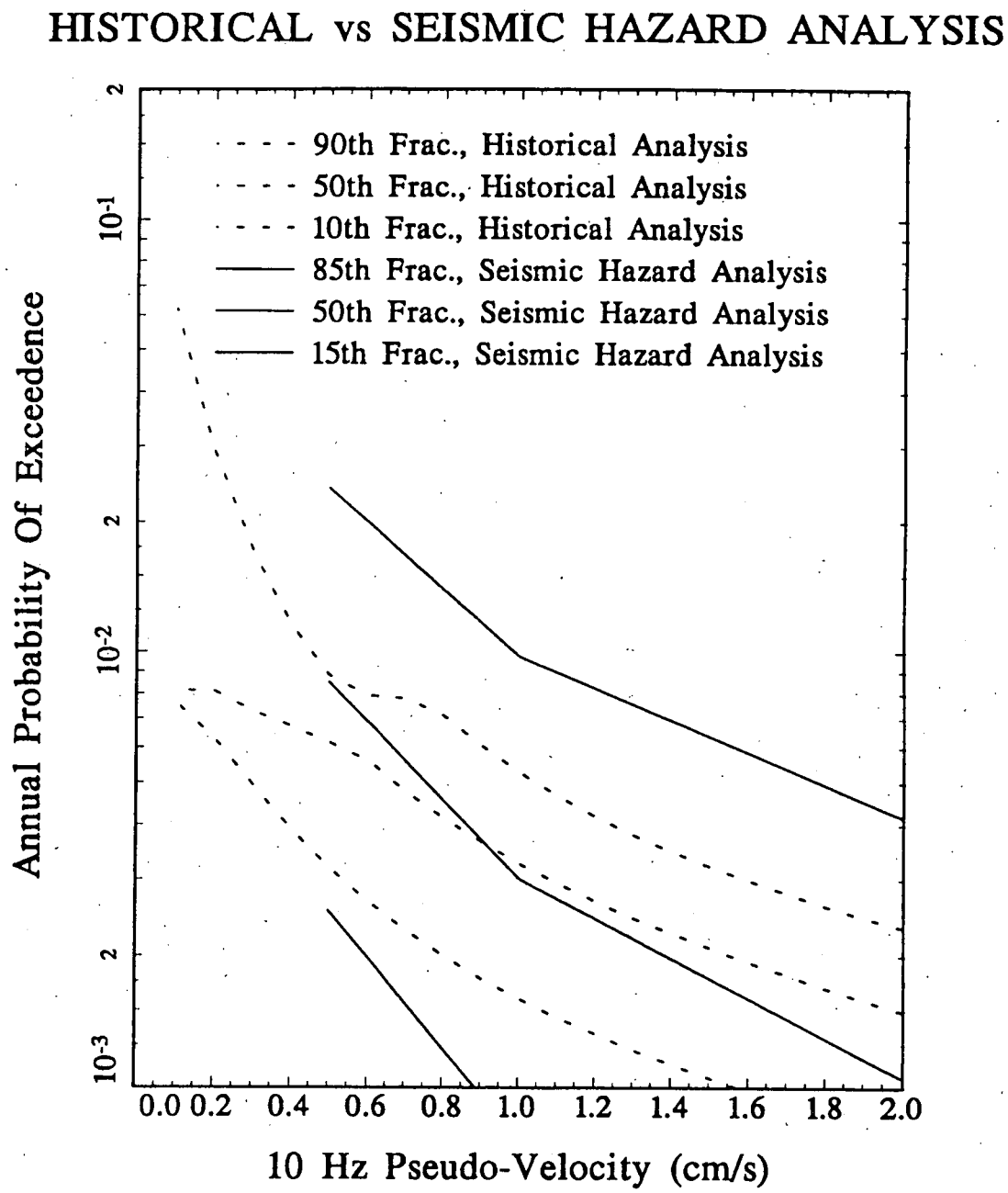

Figure 3-34. Comparison of historical vs. seismic hazard results for PSV(10 Hz) on rock.

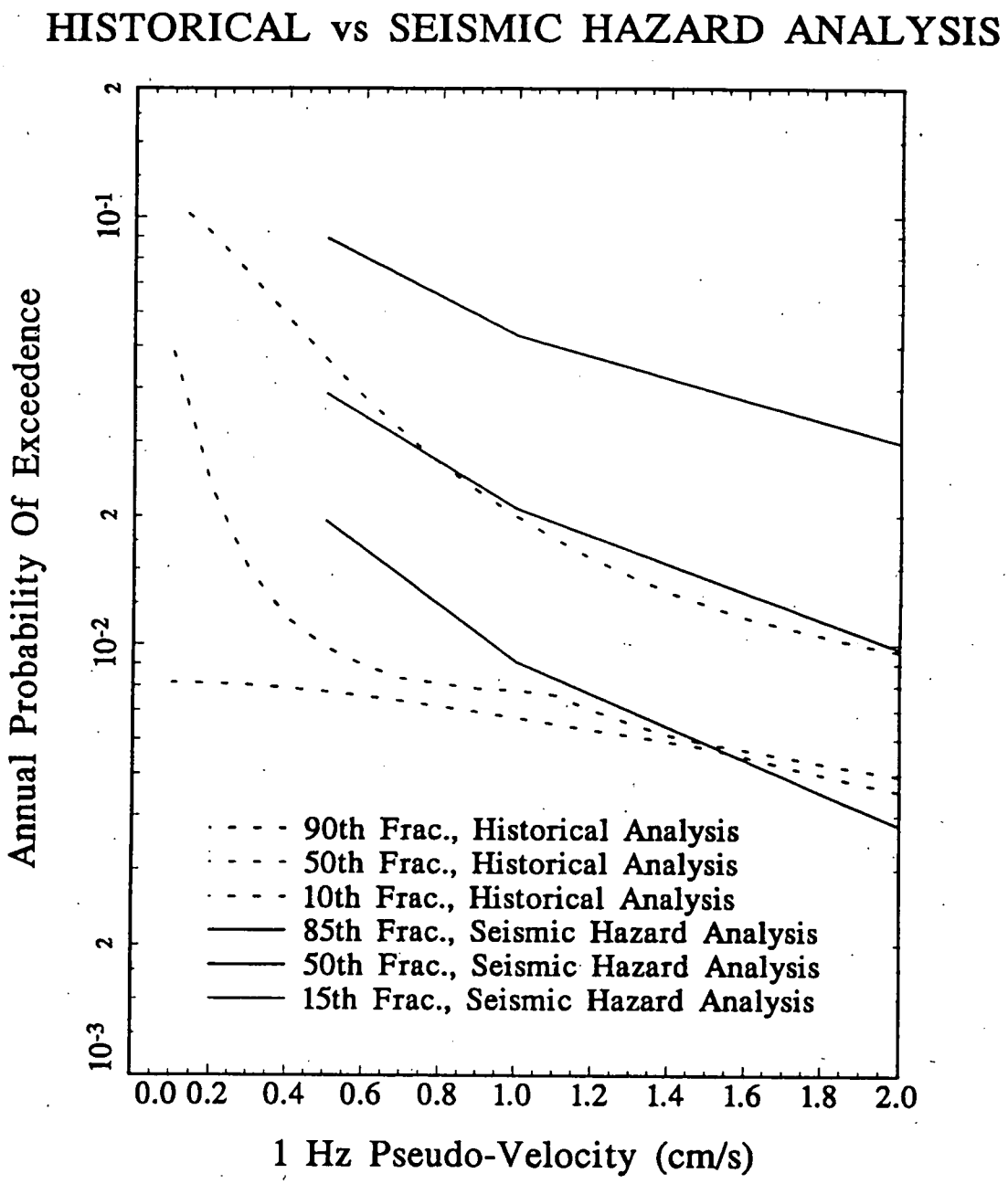

Figure 3-35. Comparison of historical and seismic hazard results for PSV(1 Hz) on rock.

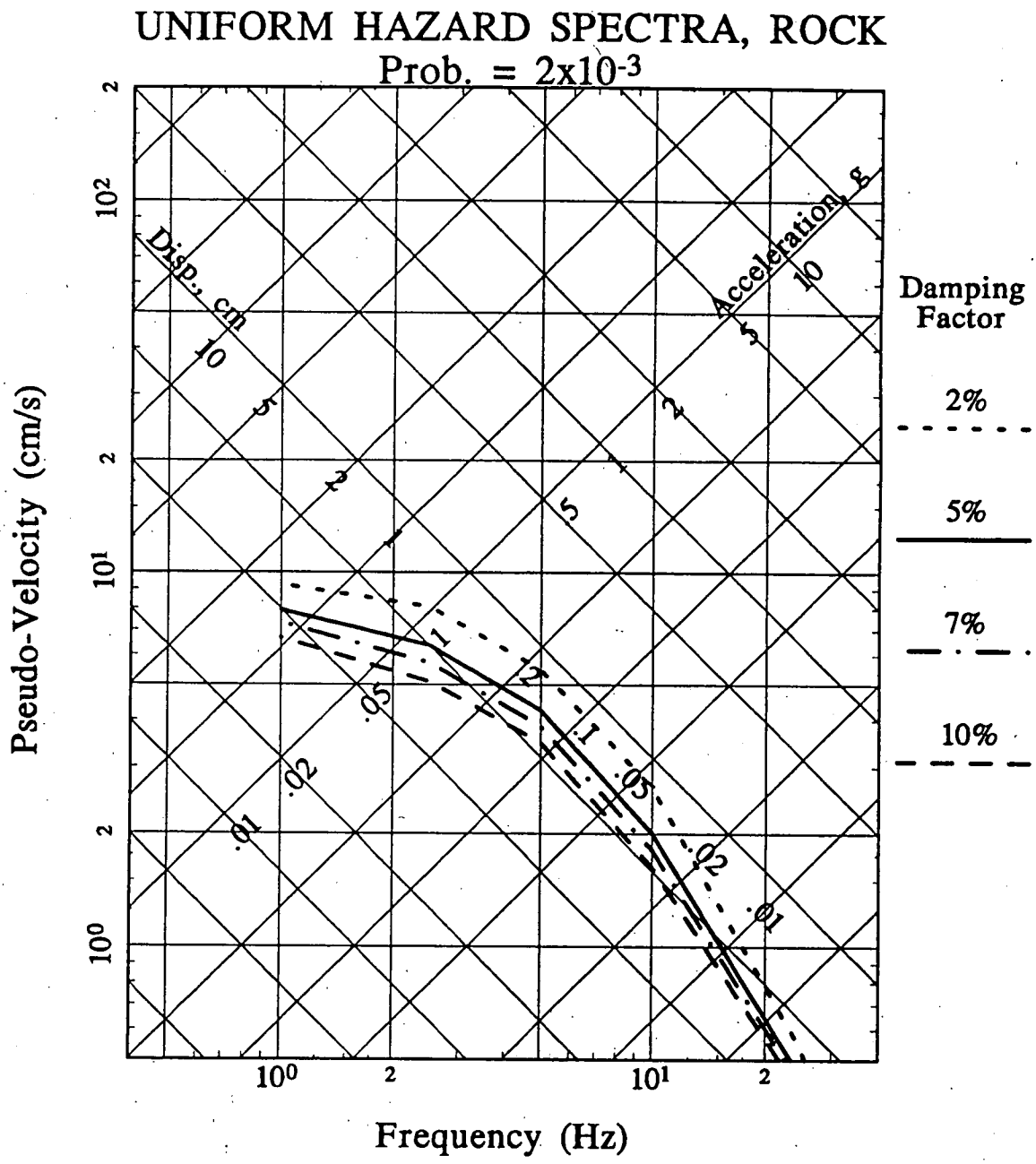

Figure 3-36. Uniform hazard spectra for $2x10^{-3}$ annual probability on rock.

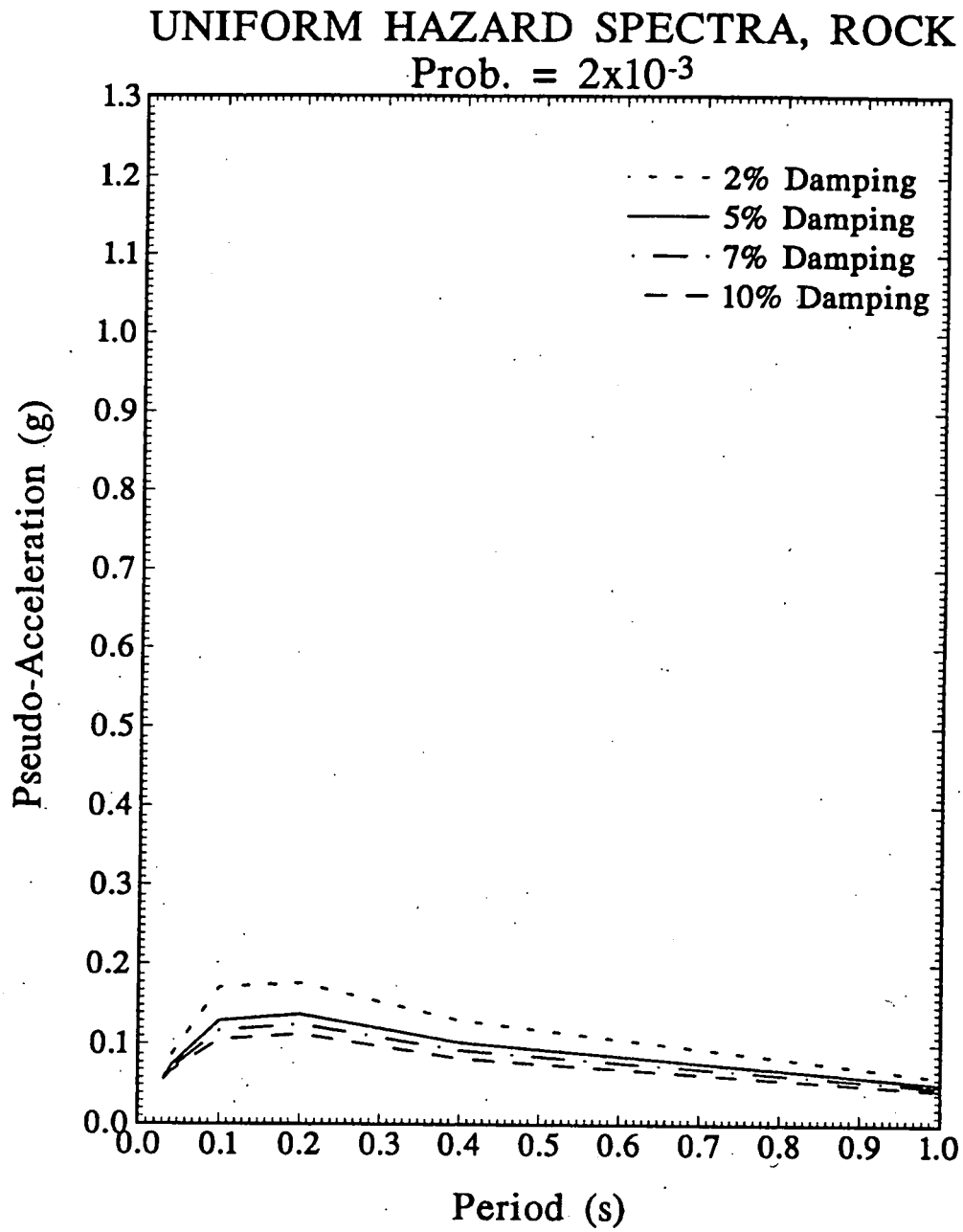

Figure 3-37. PSA vs period for $2x10^{-3}$ annual probability on rock.

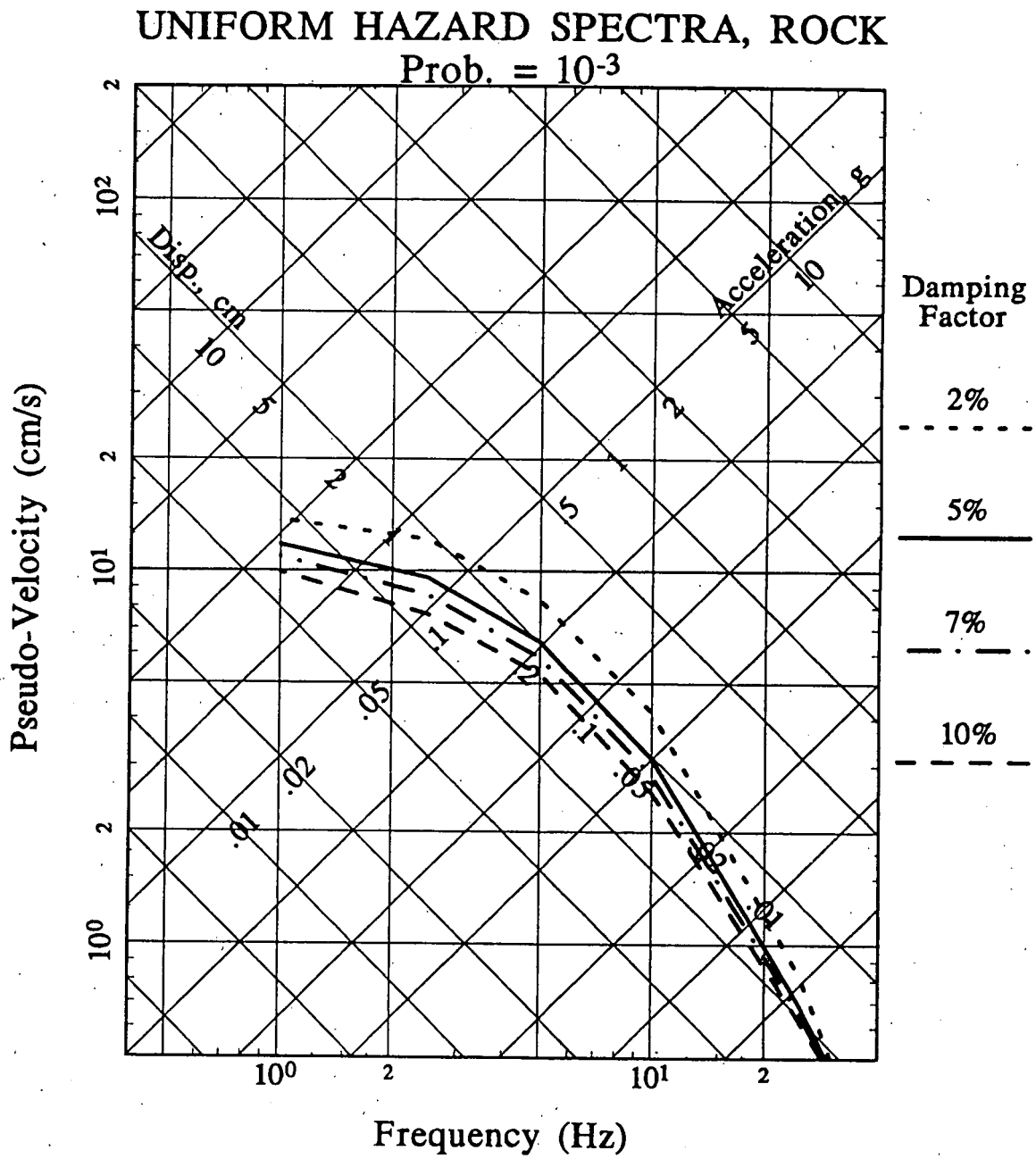

Figure 3-38. Uniform hazard spectra for 10^{-3} annual probability on rock.

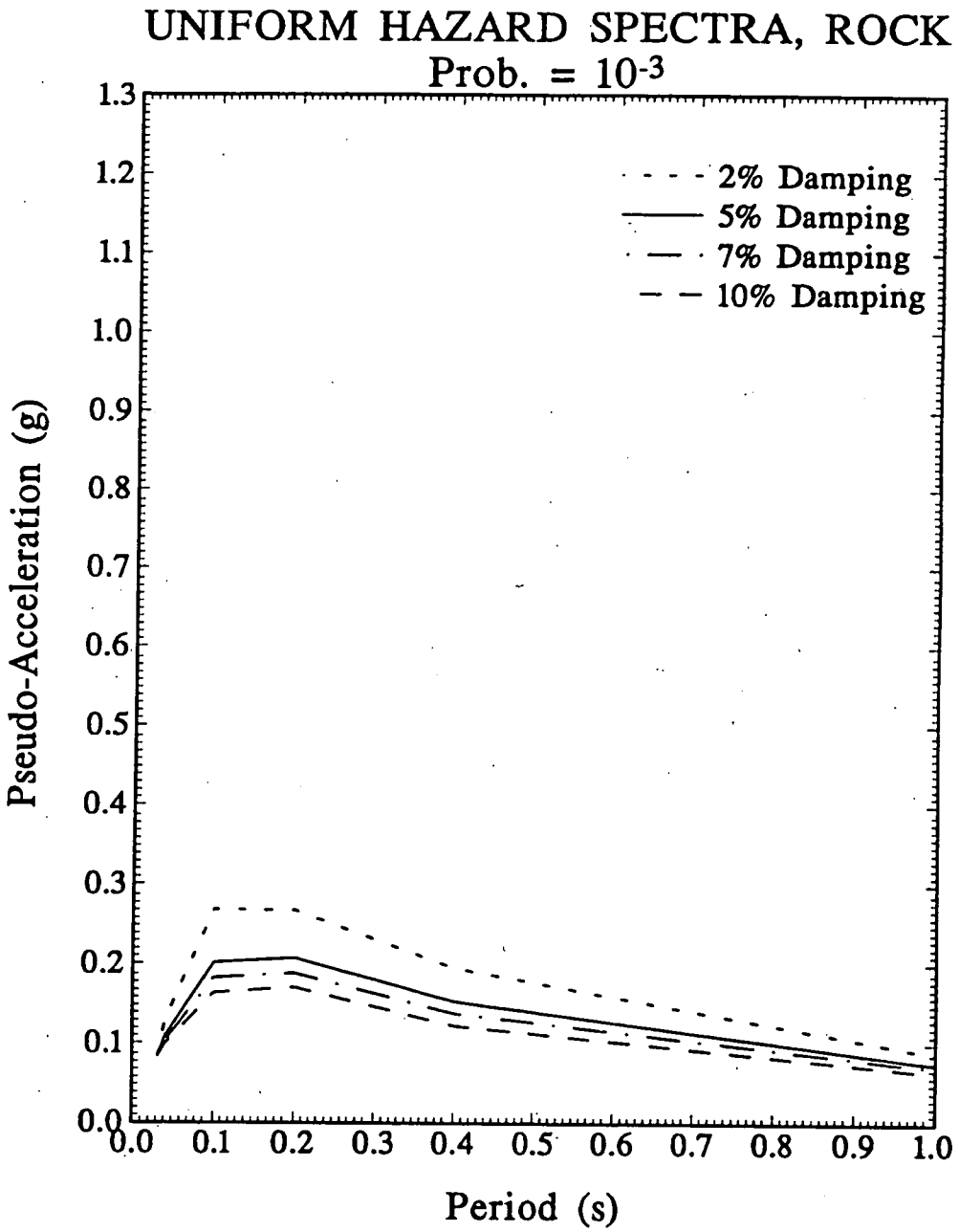

Figure 3-39. PSA vs period for 10^{-3} annual probability on rock.

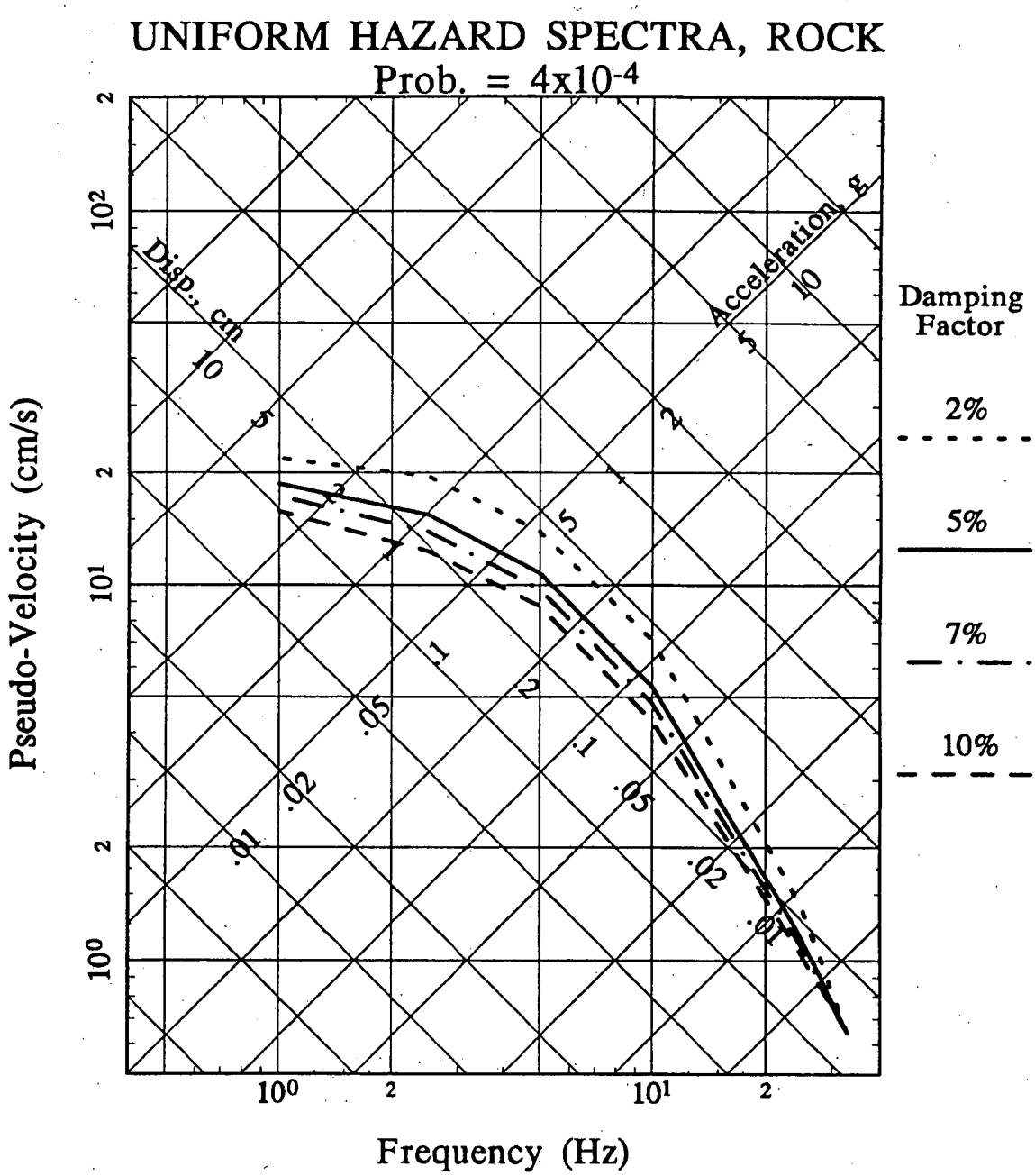

Figure 3-40. Uniform hazard spectra for 4×10^{-4} annual probability on rock.

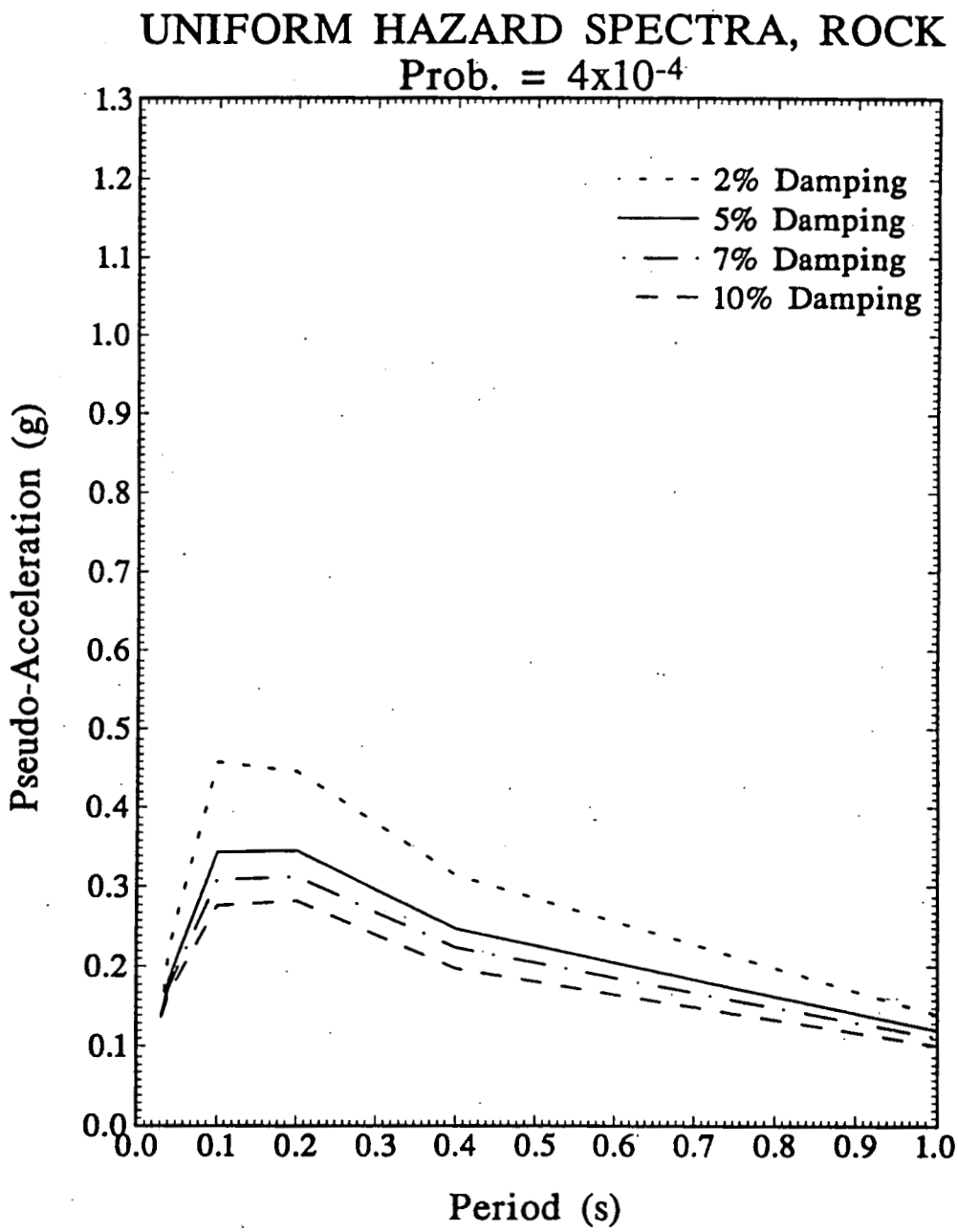

Figure 3-41. PSA vs period for 4×10^{-4} annual probability on rock.

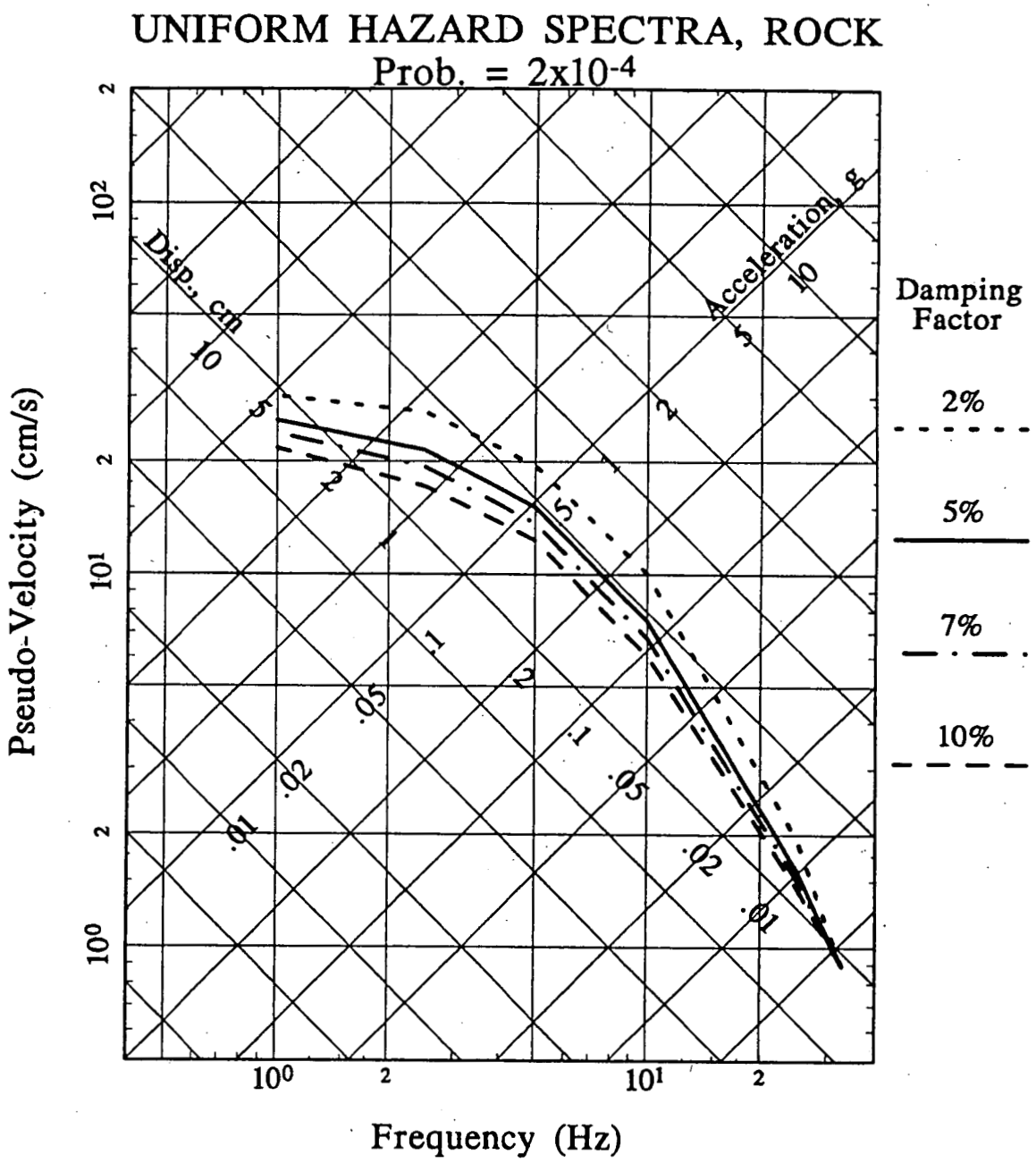

Figure 3-42. Uniform hazard spectra for $2x10^{-4}$ annual probability on rock.

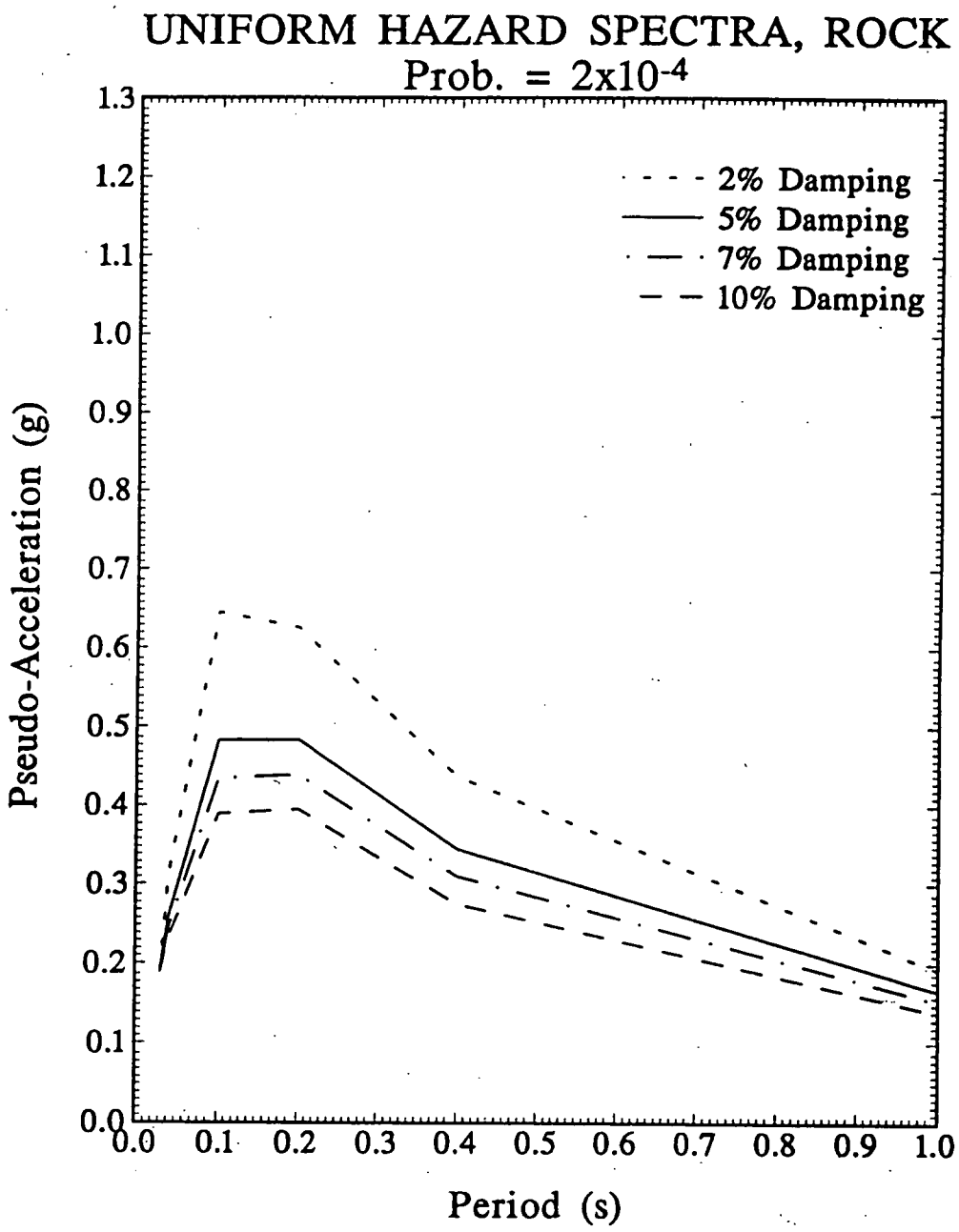

Figure 3-43. PSA vs period for 2×10^{-4} annual probability on rock.

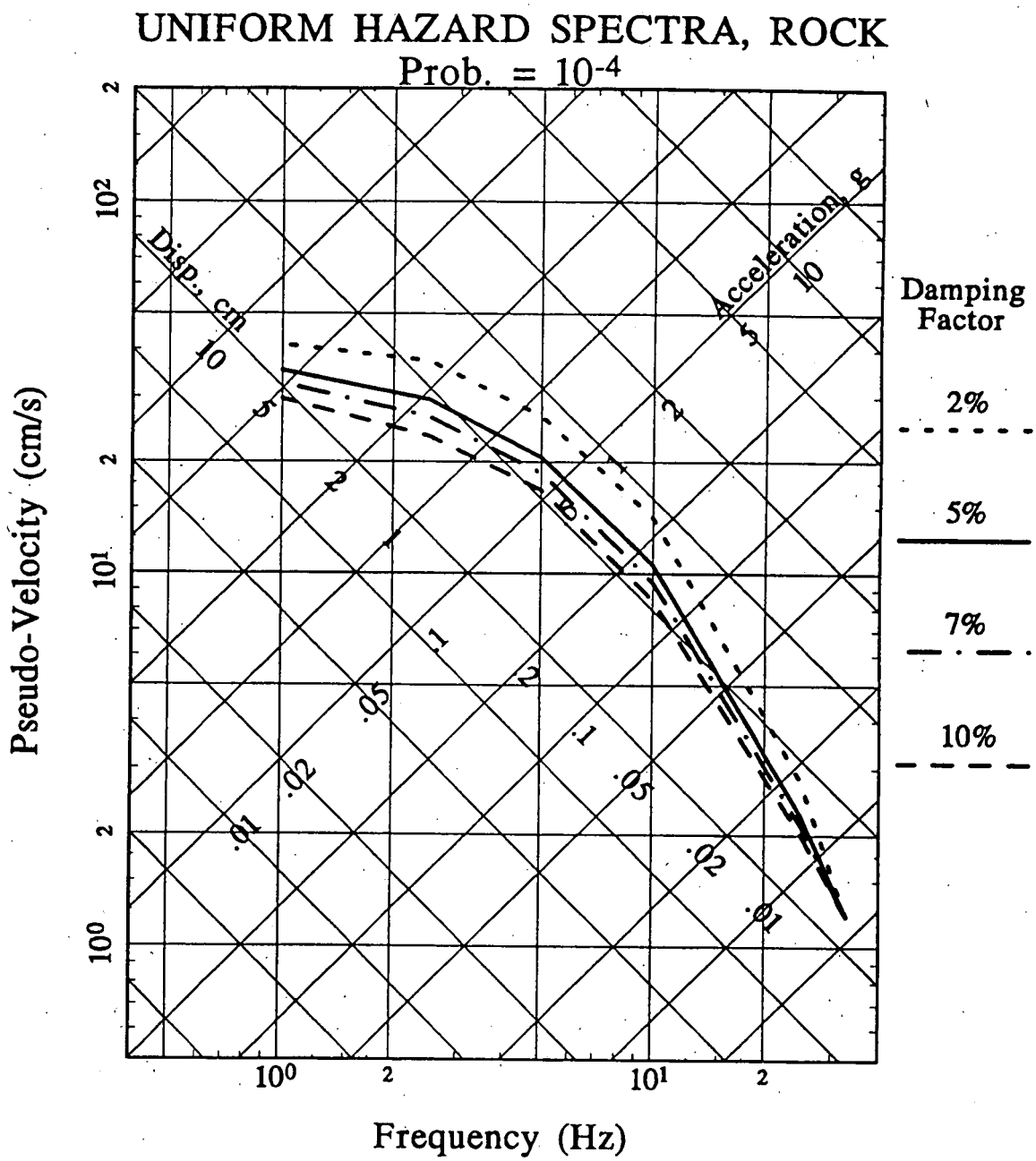

Figure 3-44. Uniform hazard spectra for 10^{-4} annual probability on rock.

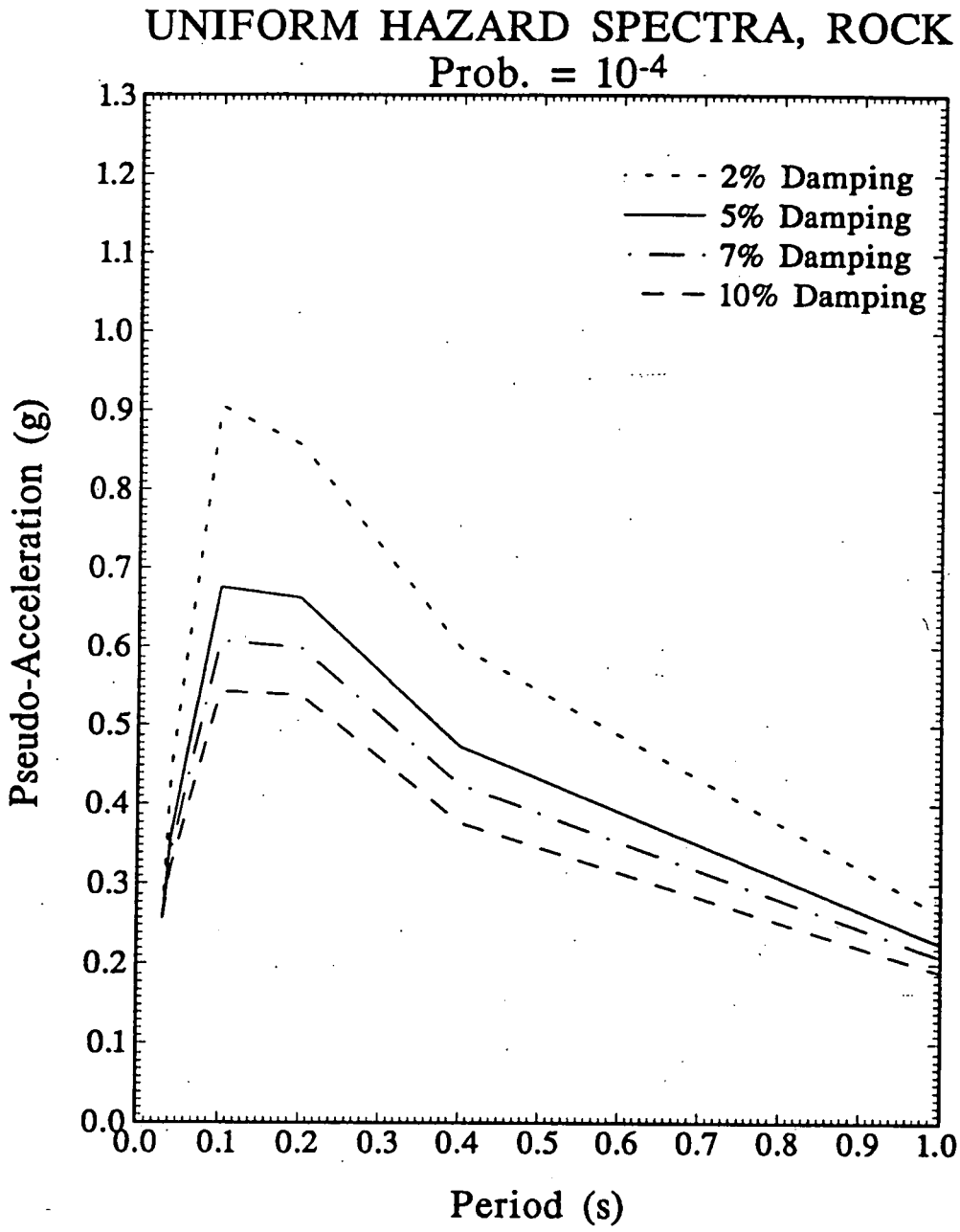

Figure 3-45. PSA vs period for 10^{-4} annual probability on rock.

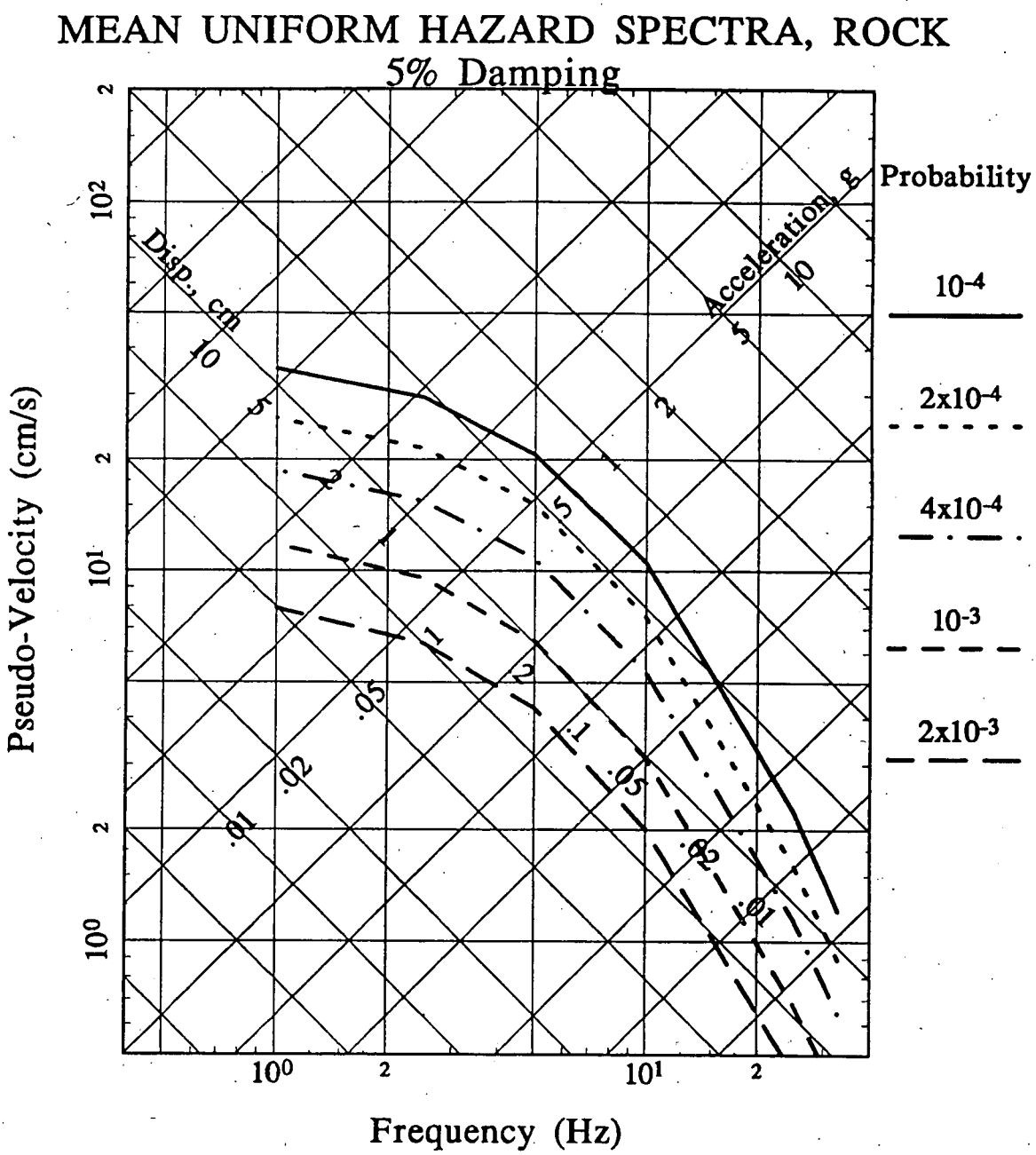

Figure 3-46. Mean uniform hazard spectra on rock.

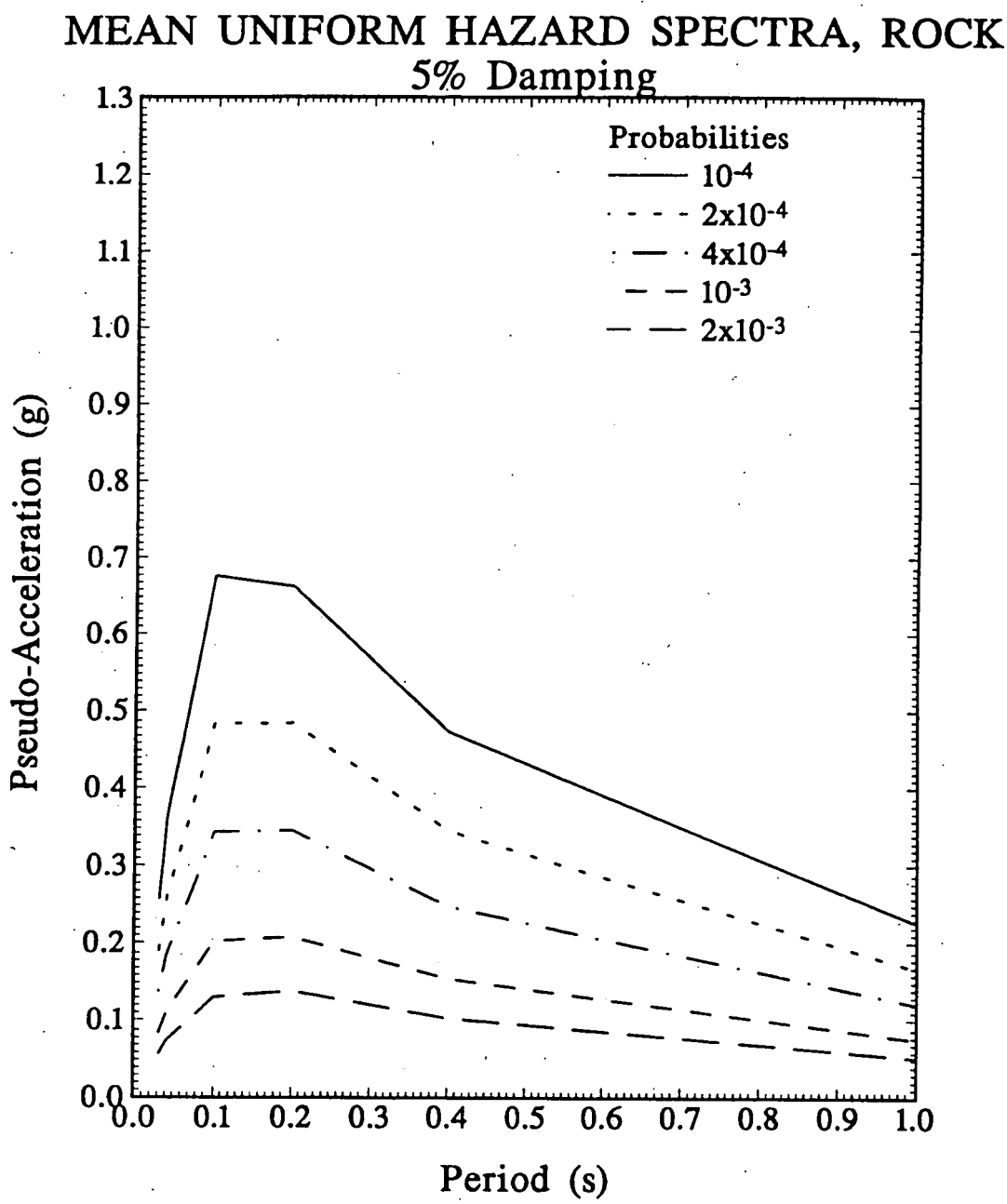

Figure 3-47. Mean spectra on rock plotted as PSA vs period.

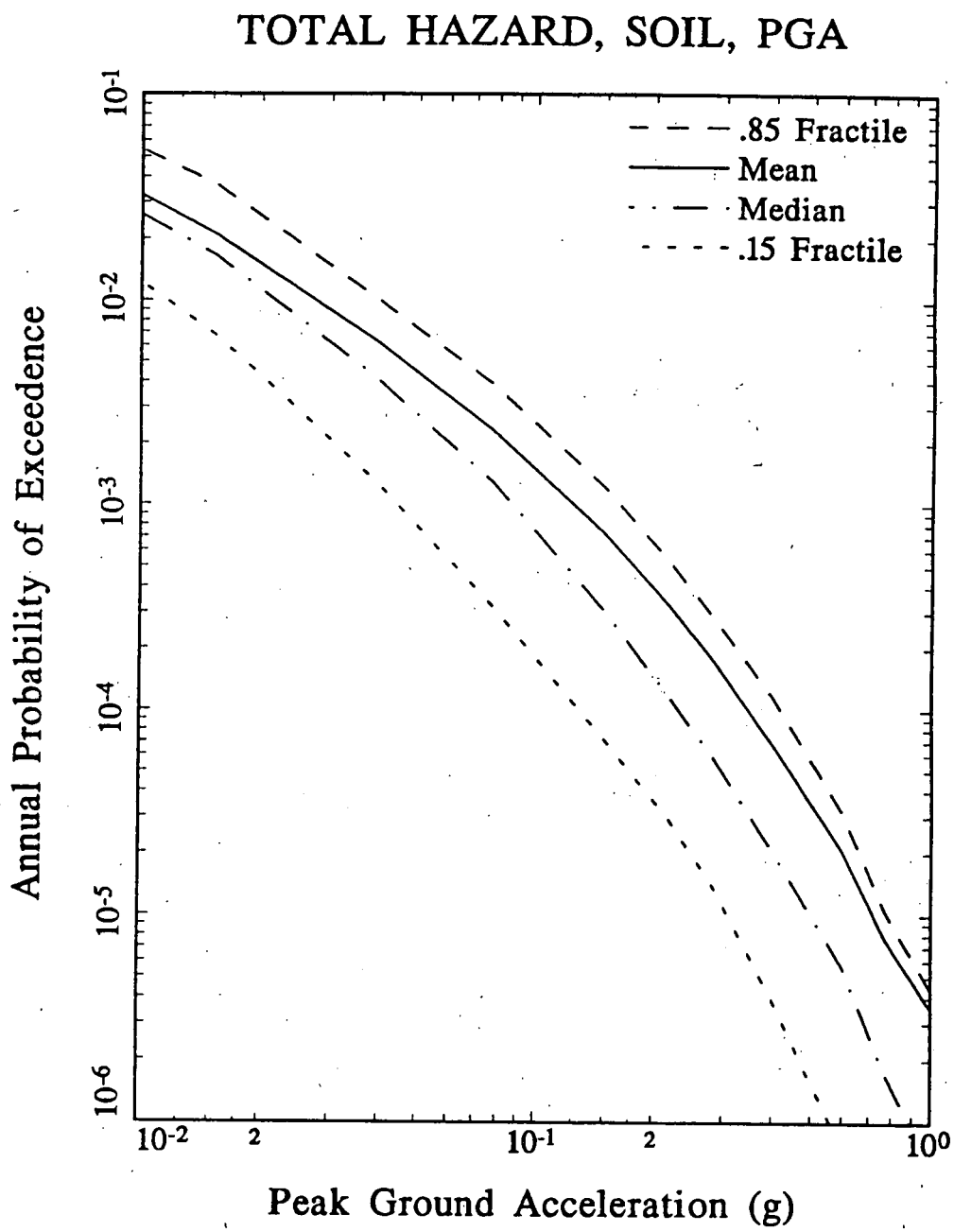

Figure 3-48. Total hazard curves, PGA on soil.

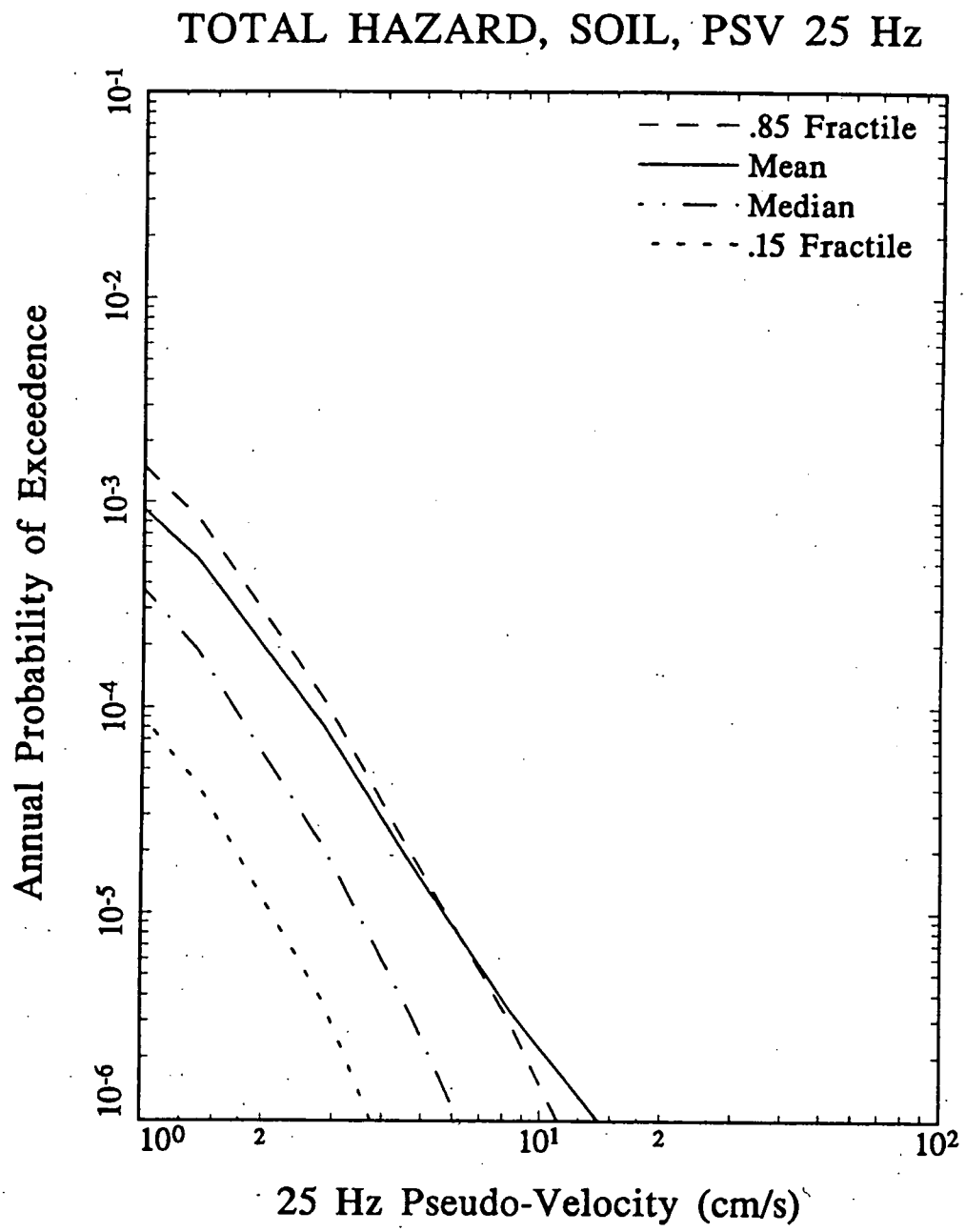

Figure 3-49. Total hazard curves, PSV(25 Hz) on soil.

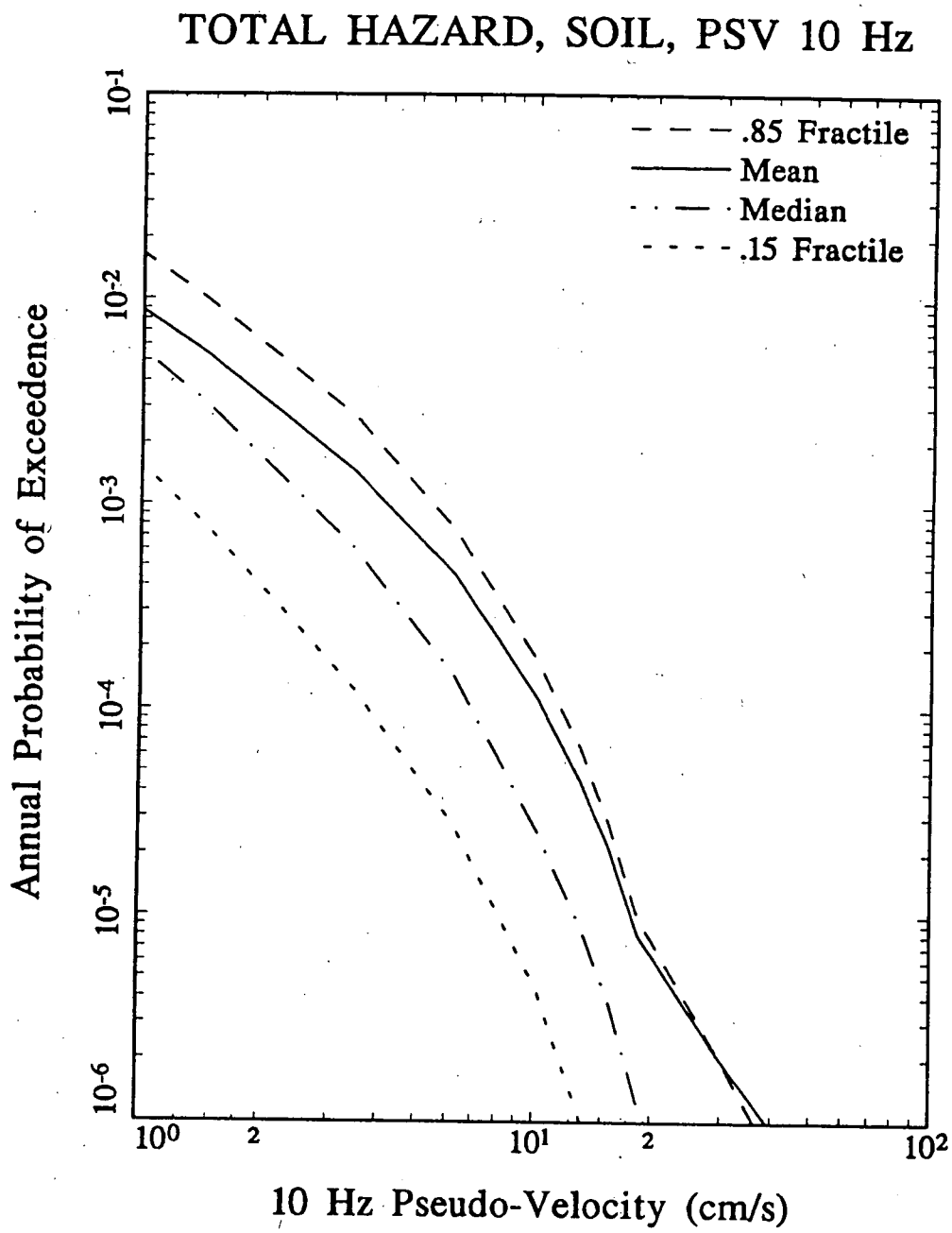

Figure 3-50. Total hazard curves, PSV(10 Hz) on soil.

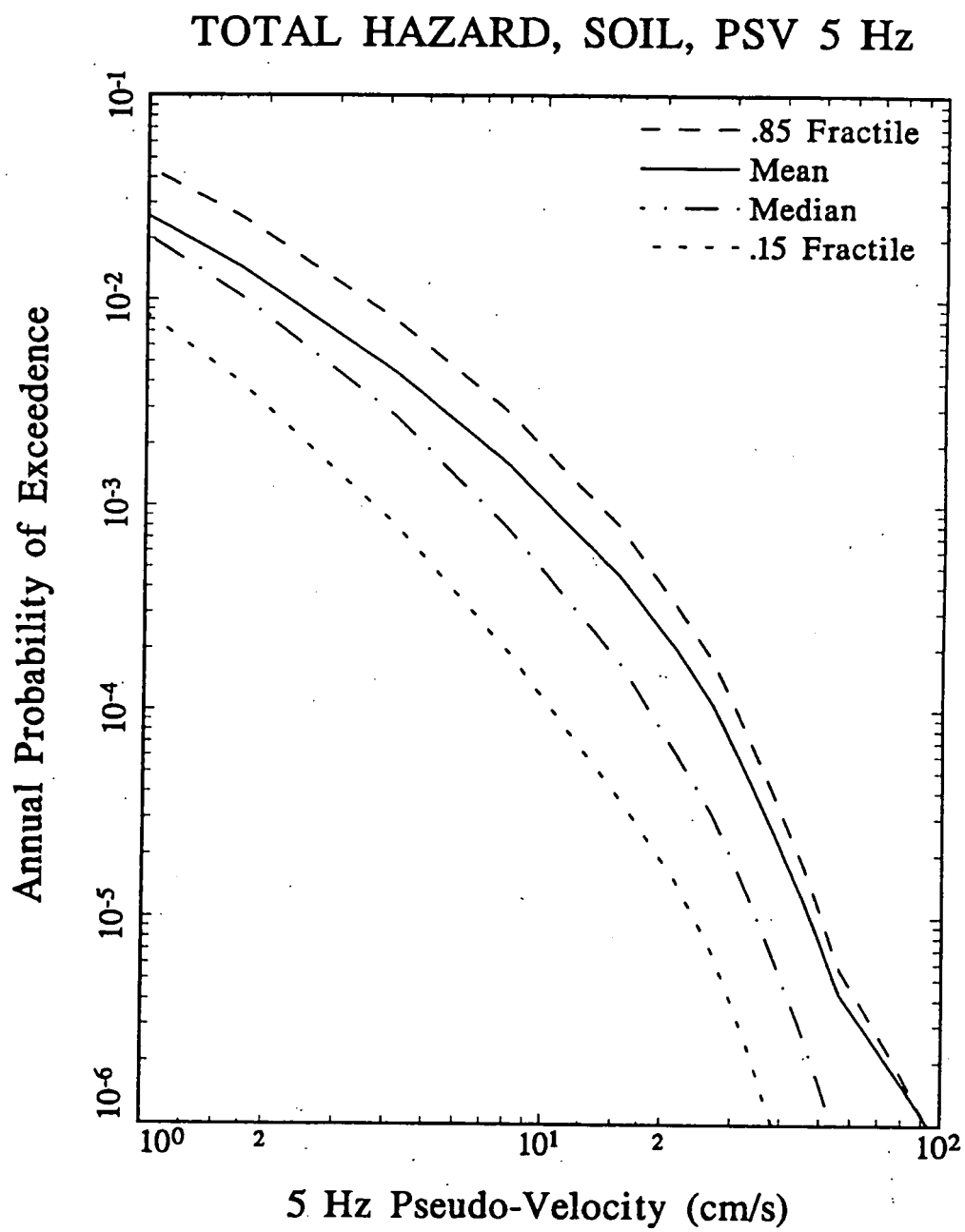

Figure 3-51. Total hazard curves, PSV(5 Hz) on soil.

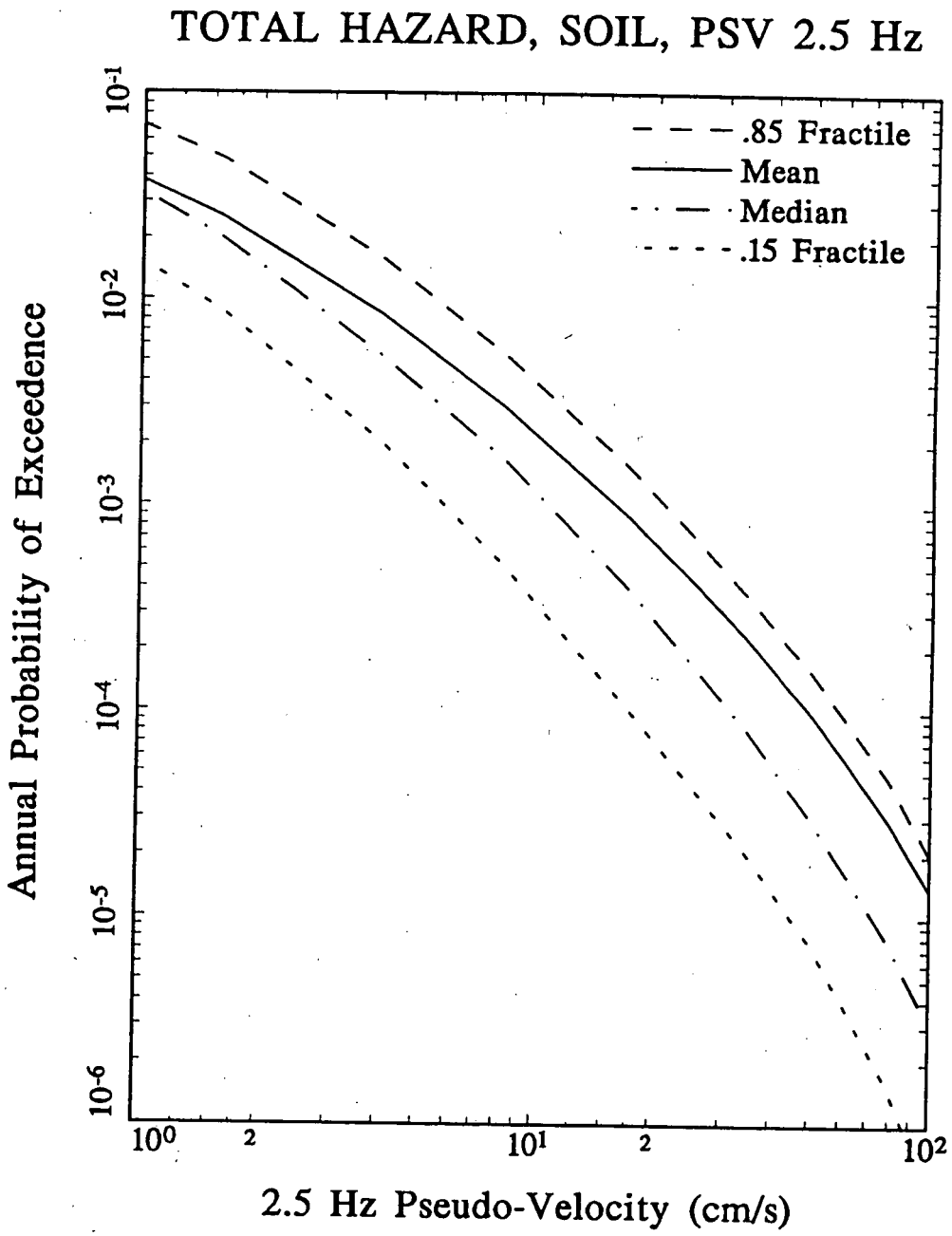

Figure 3-52. Total hazard curves, PSV(2.5 Hz) on soil.

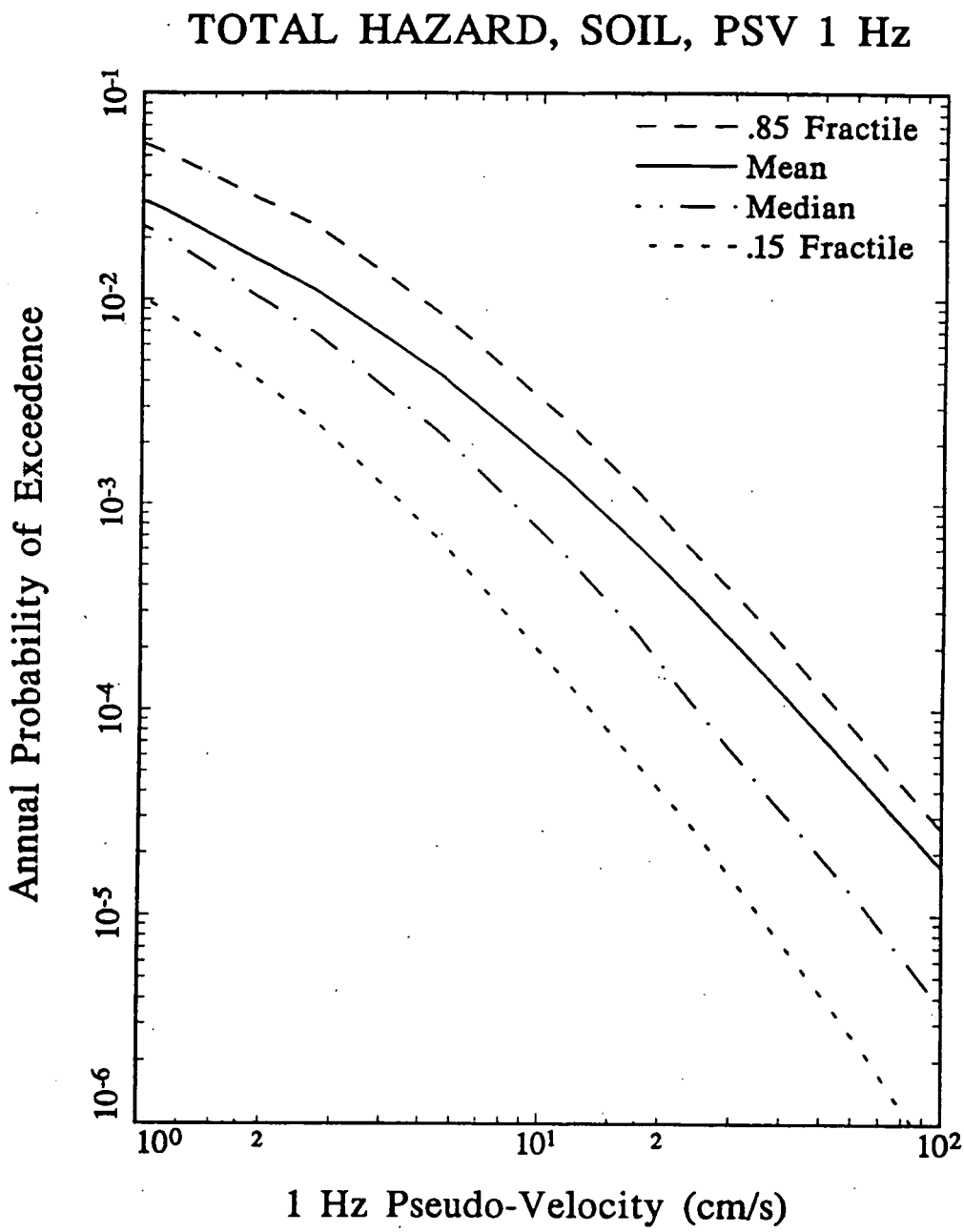

Figure 3-53. Total hazard curves, PSV(1 Hz) on soil.

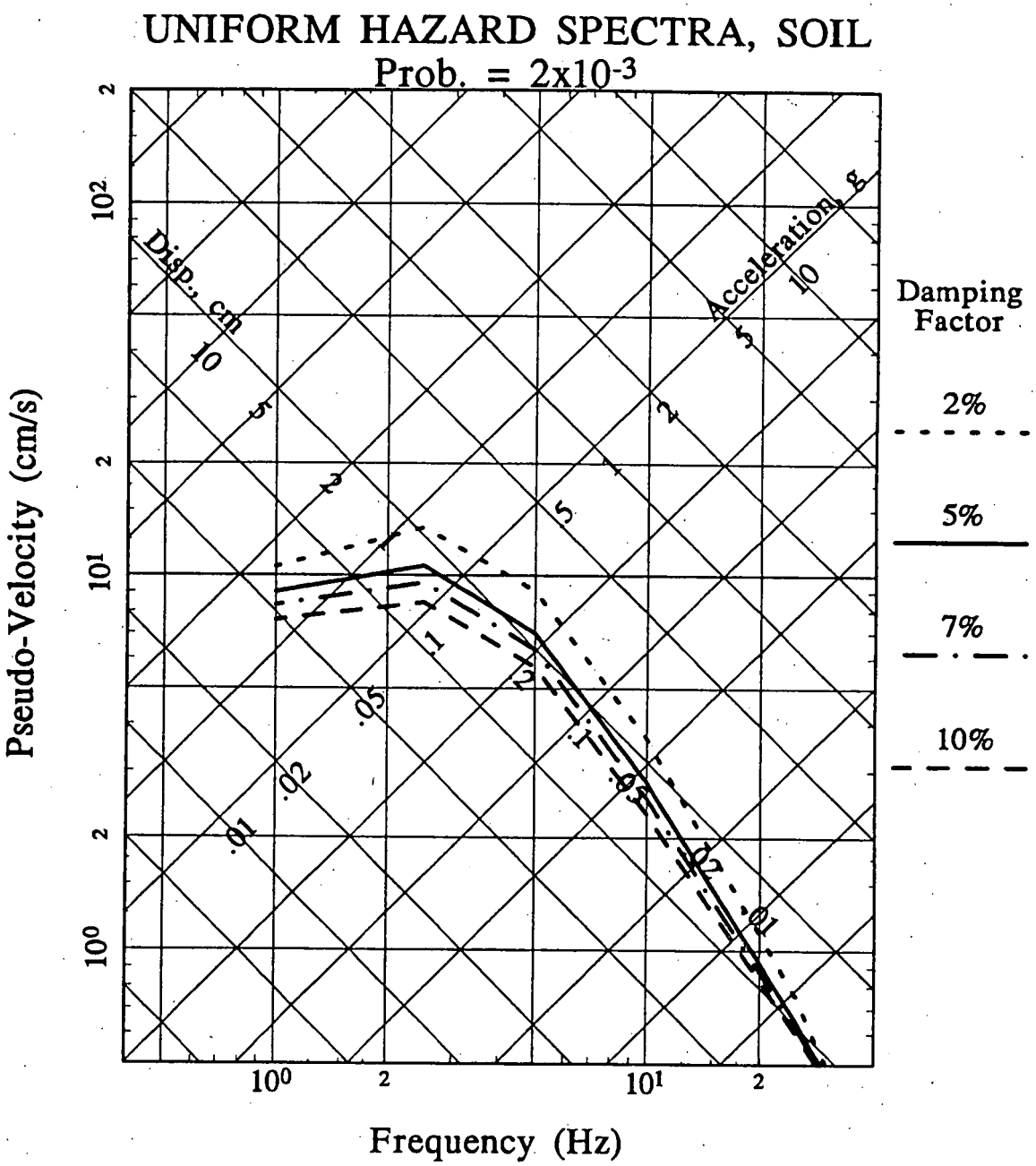

Figure 3-54. Uniform hazard spectra for $2x10^{-3}$ annual probability on soil.

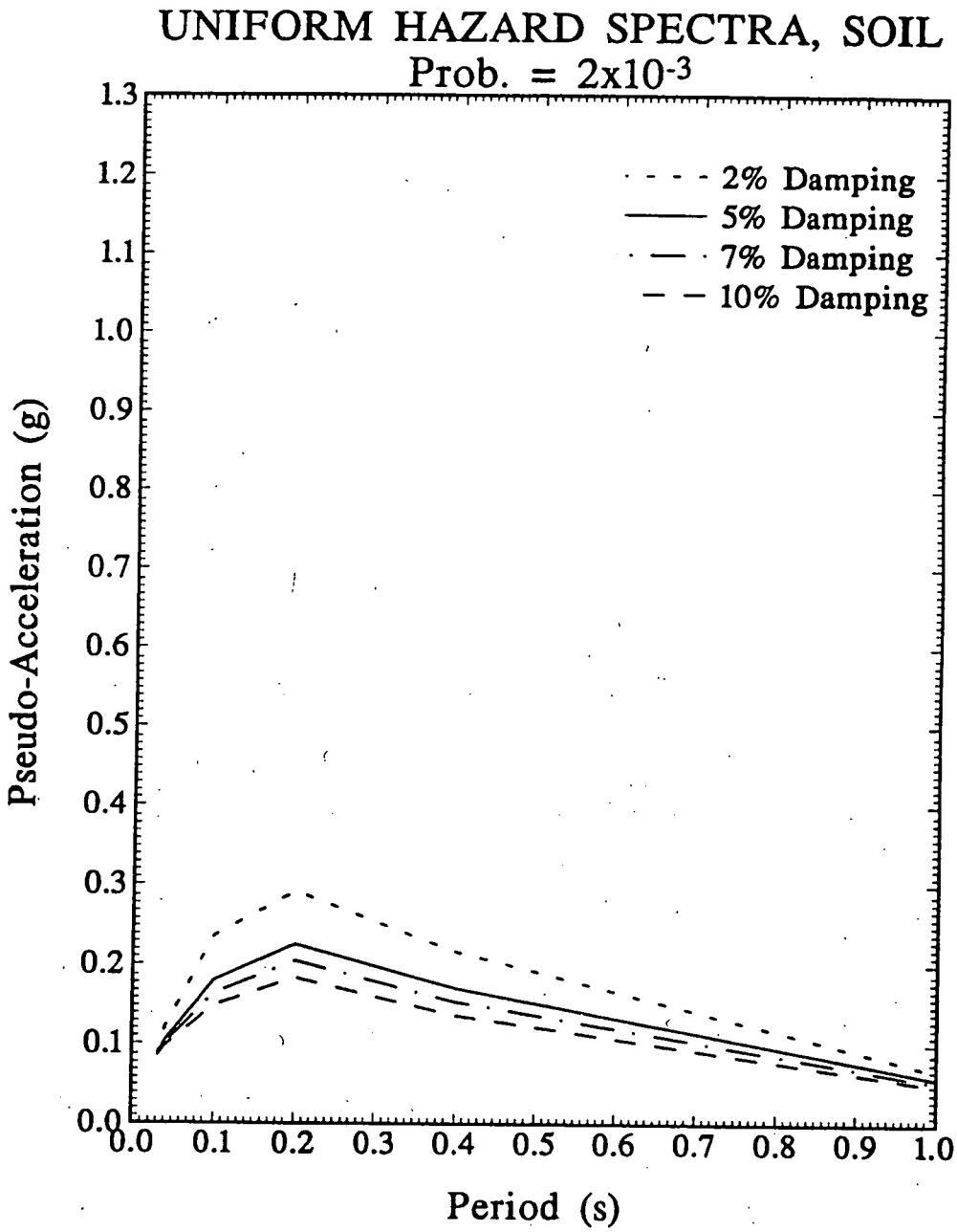

Figure 3-55. PSA vs period for $2x10^{-3}$ annual probability on soil.

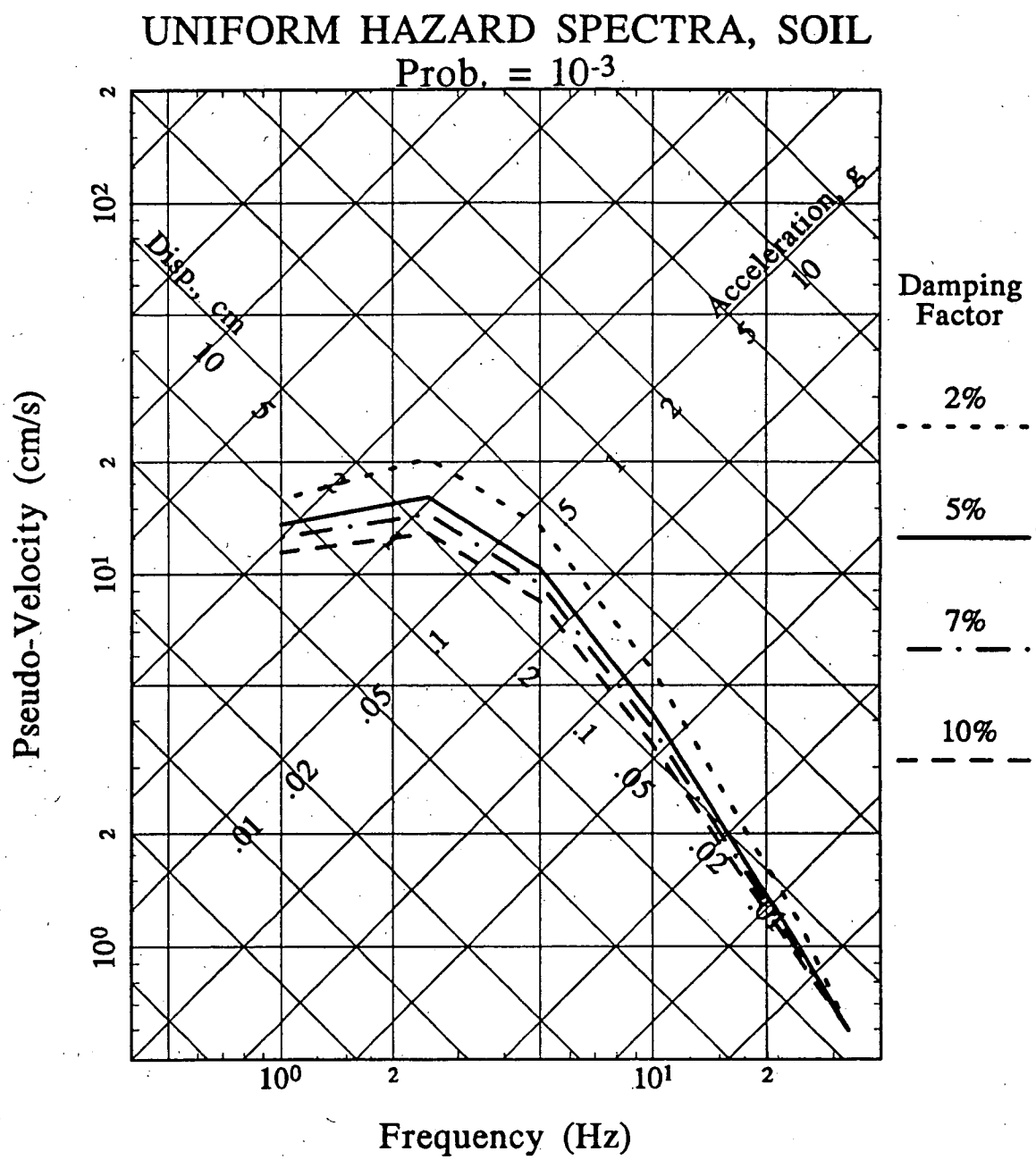

Figure 3-56. Uniform hazard spectra for 10^{-3} annual probability on soil.

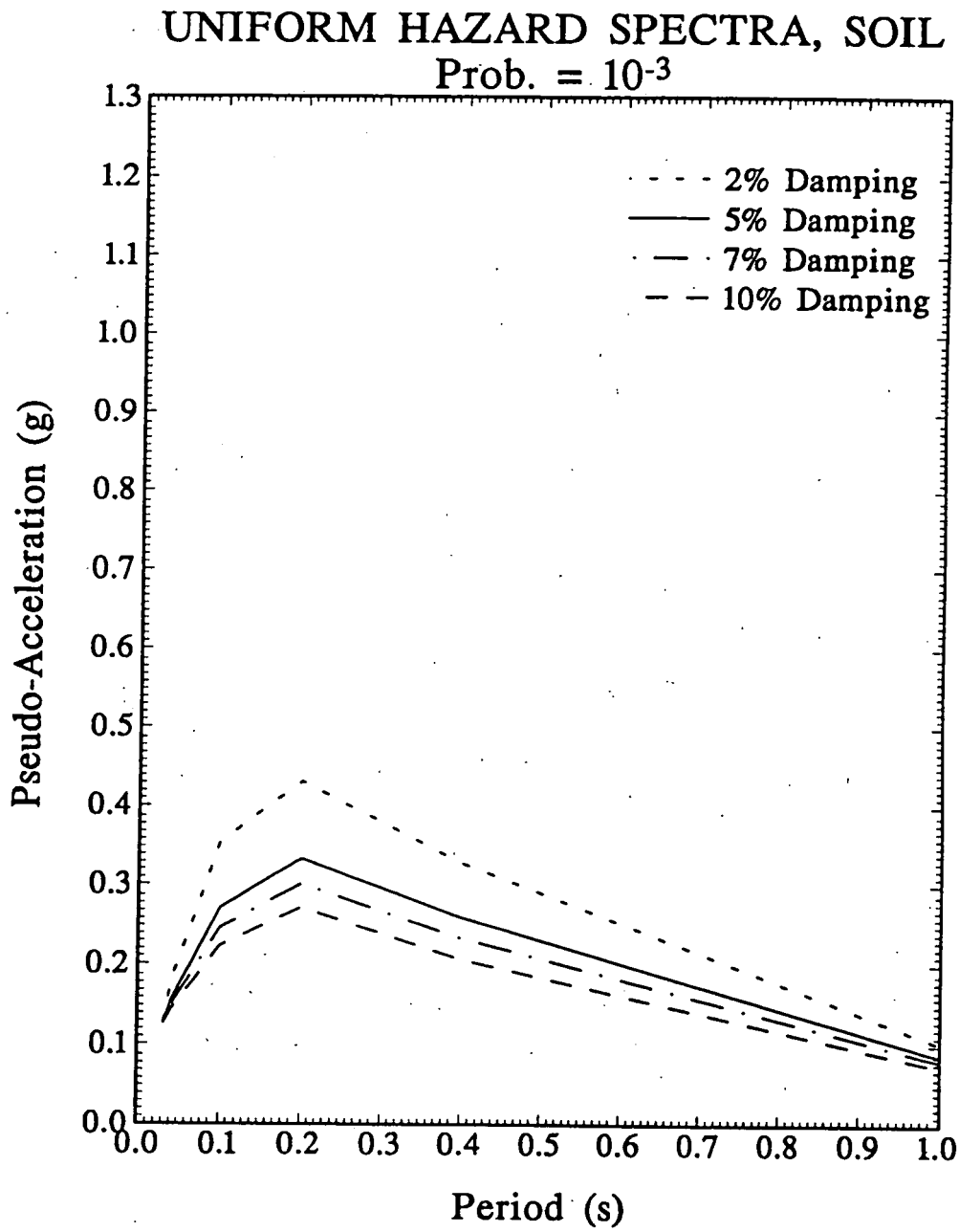

Figure 3-57. PSA vs period for 10^{-3} annual probability on soil.

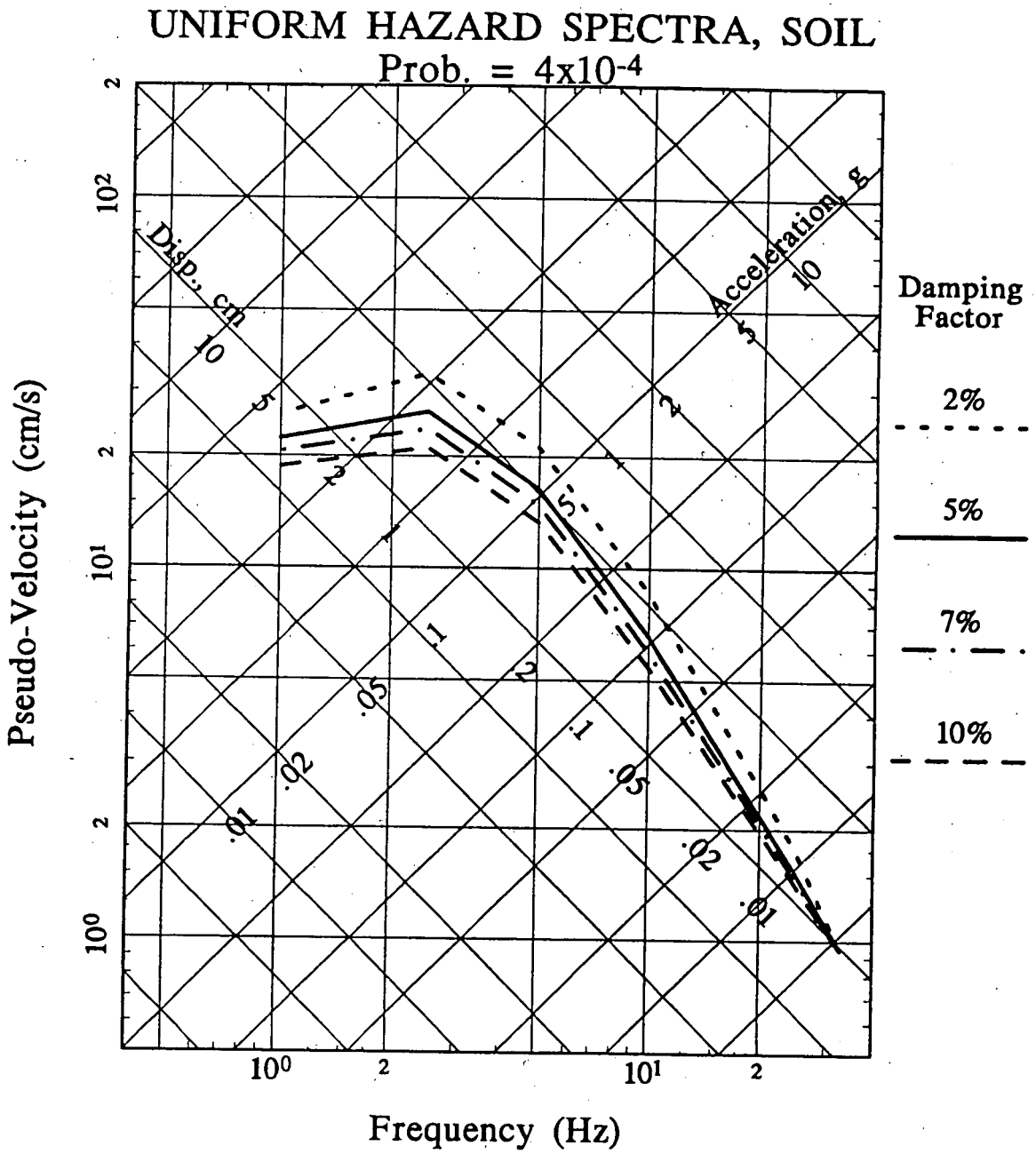

Figure 3-58. Uniform hazard spectra for 4×10^{-4} annual probability on soil.

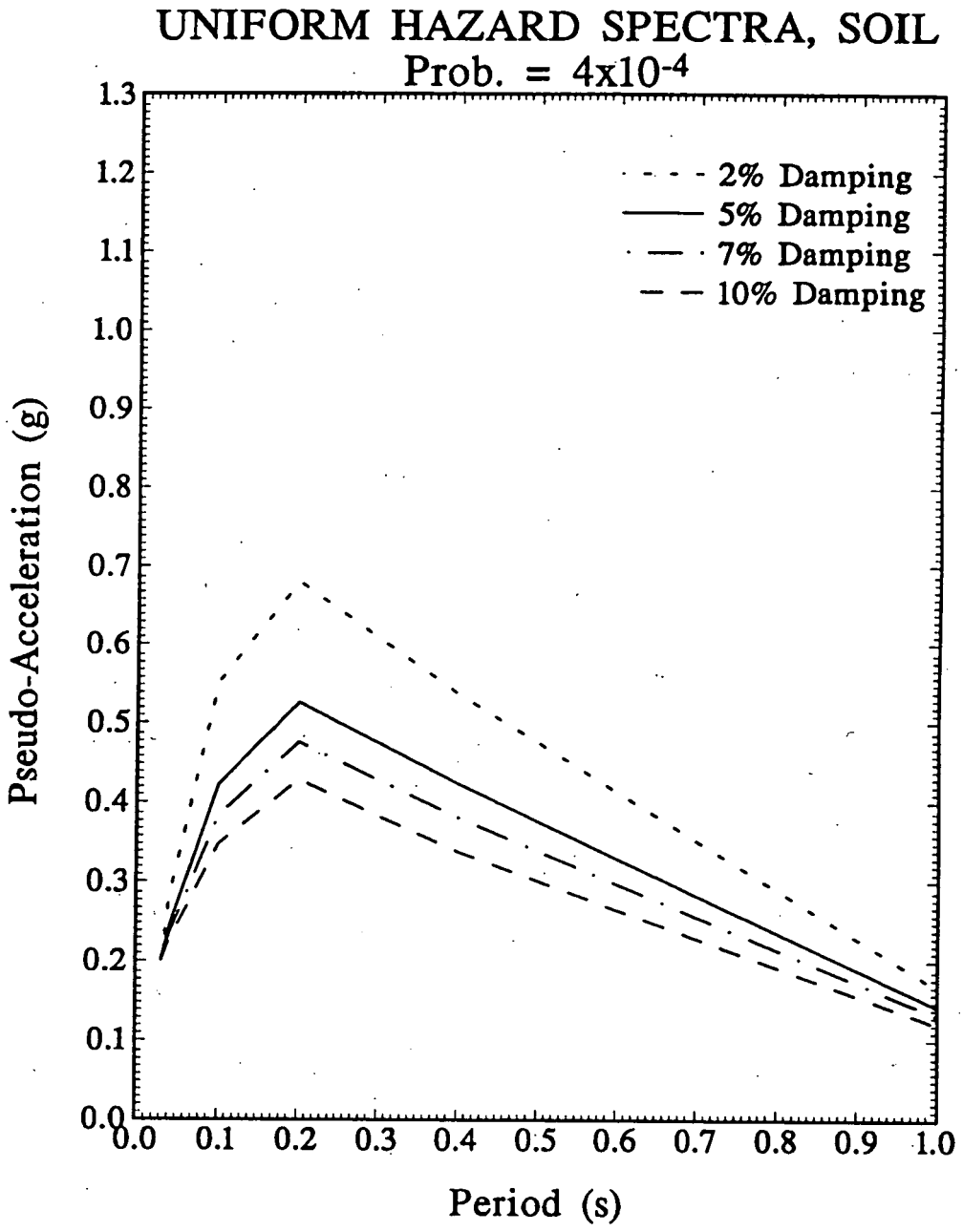

Figure 3-59. PSA vs period for 4×10^{-4} annual probability on soil.

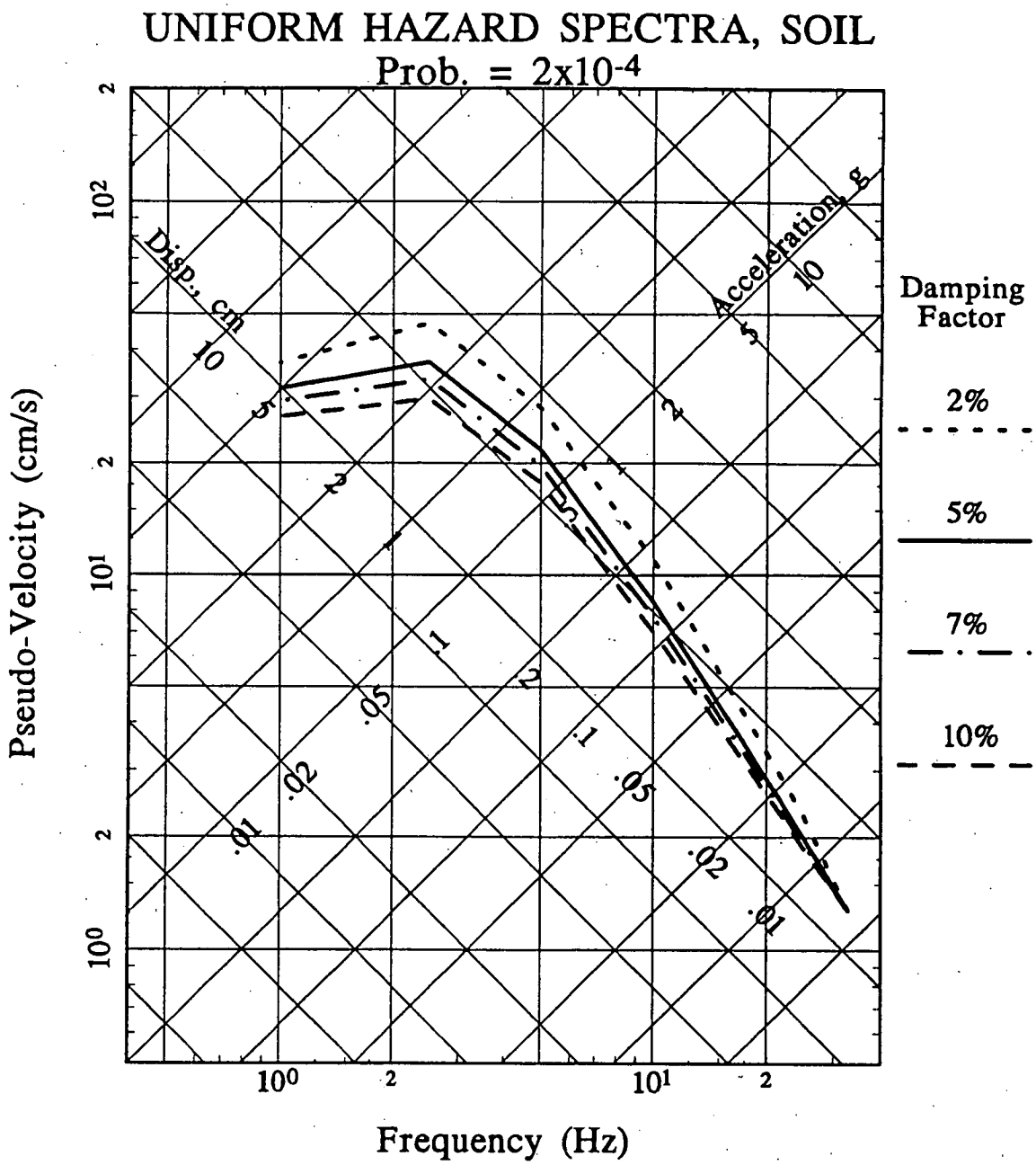

Figure 3-60. Uniform hazard spectra for $2x10^{-4}$ annual probability on soil.

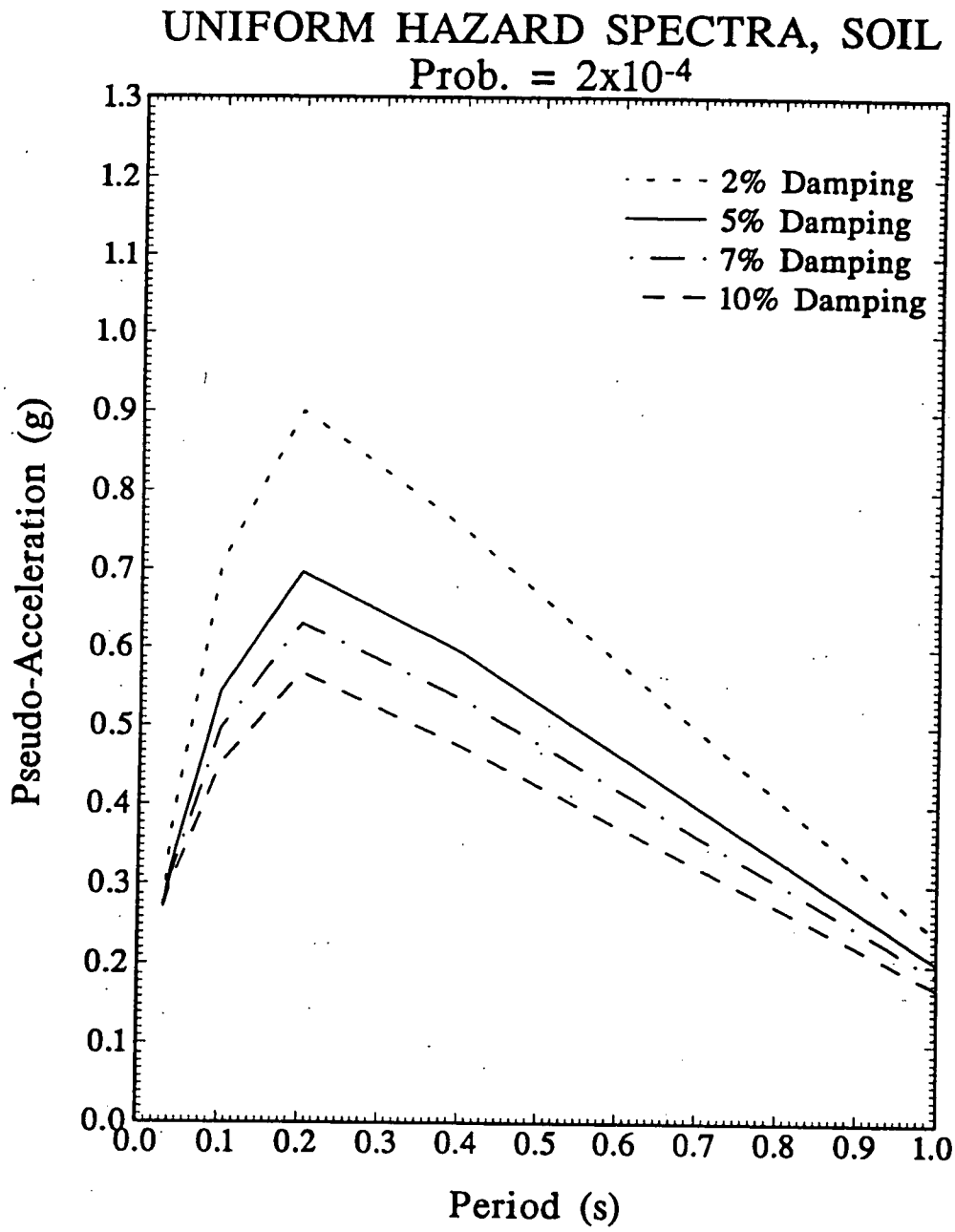

Figure 3-61. PSA vs period for $2x10^{-4}$ annual probability on soil.

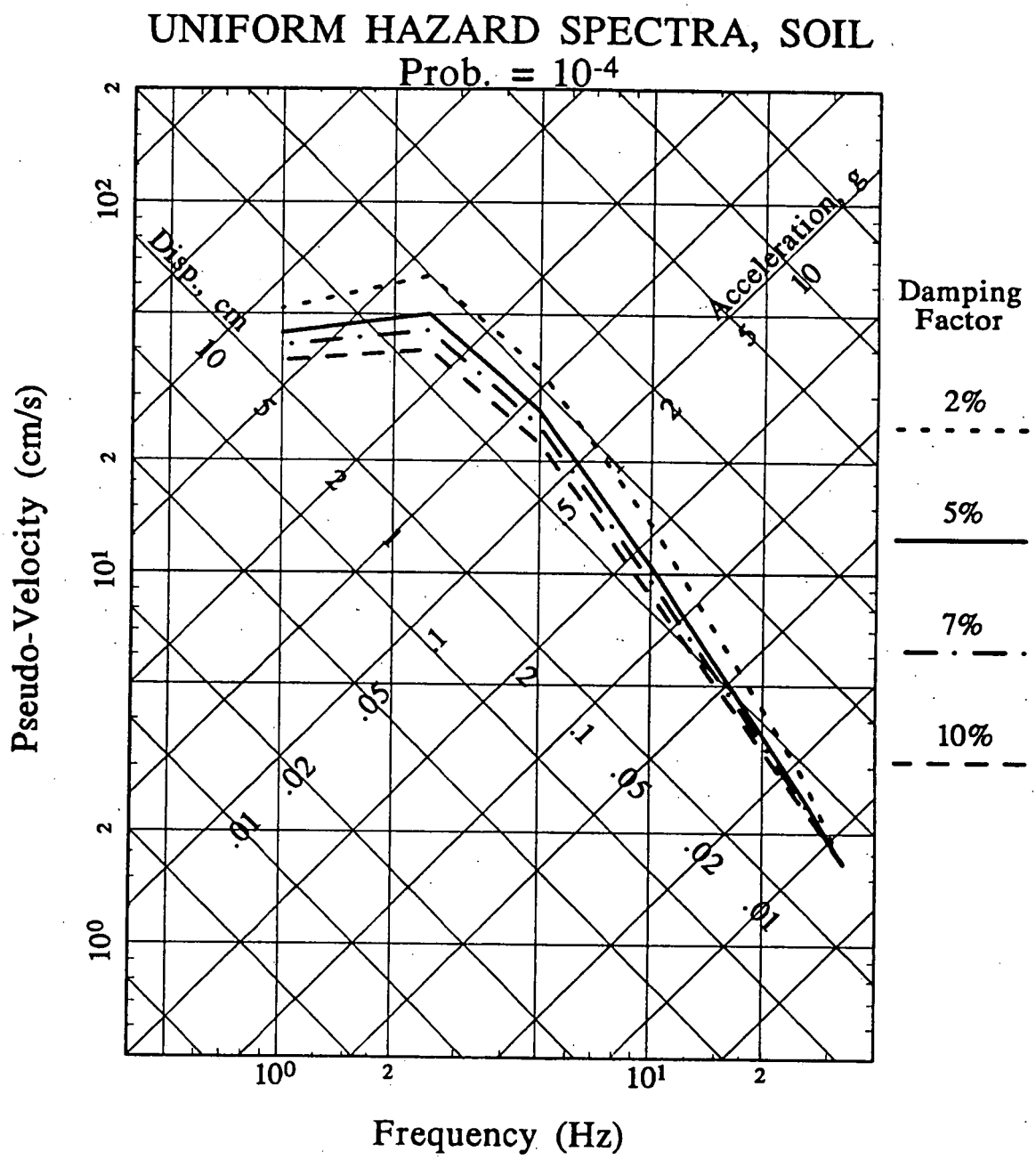

Figure 3-62. Uniform hazard spectra for 10^{-4} annual probability on soil.

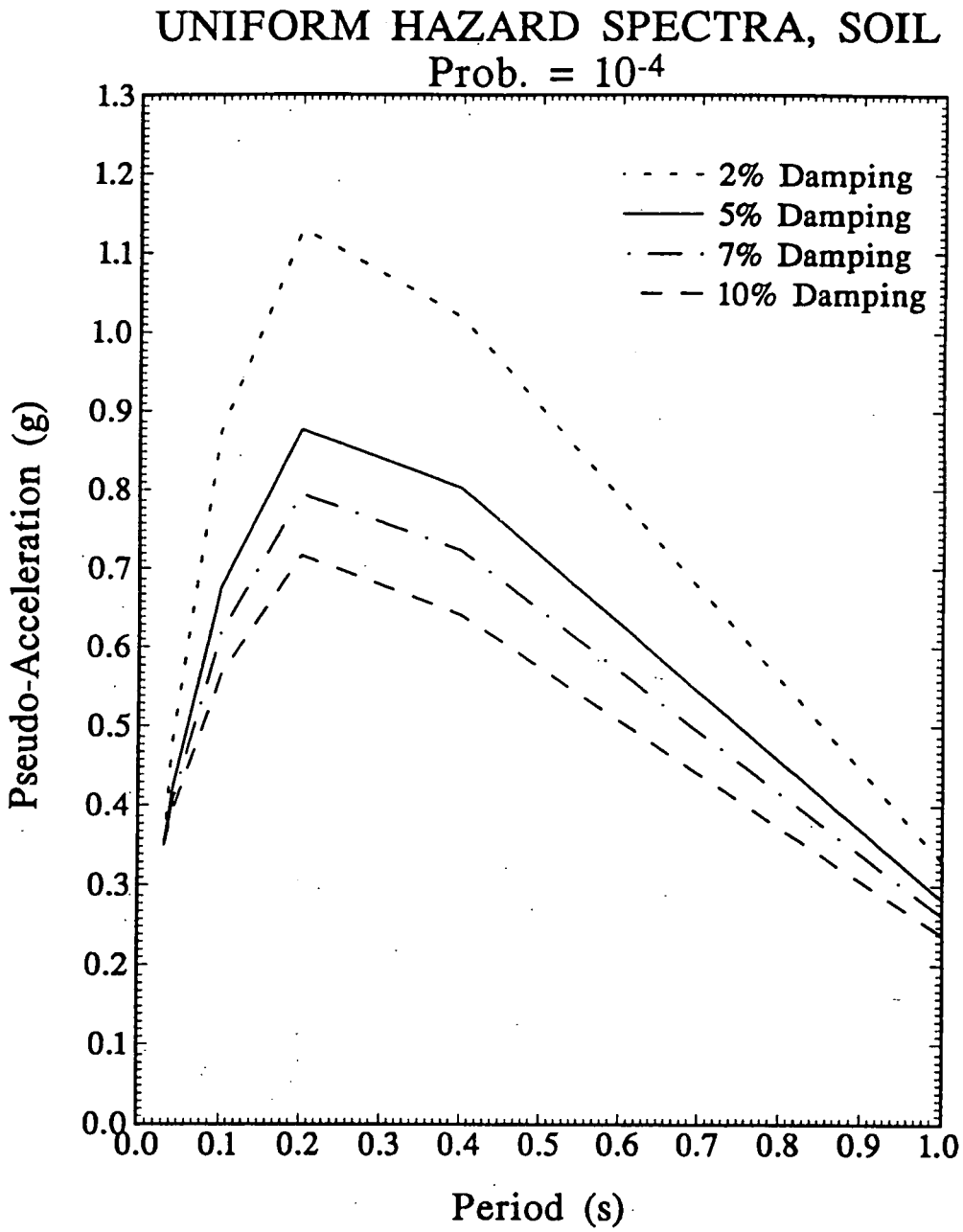

Figure 3-63. PSA vs period for 10^{-4} annual probability on soil.

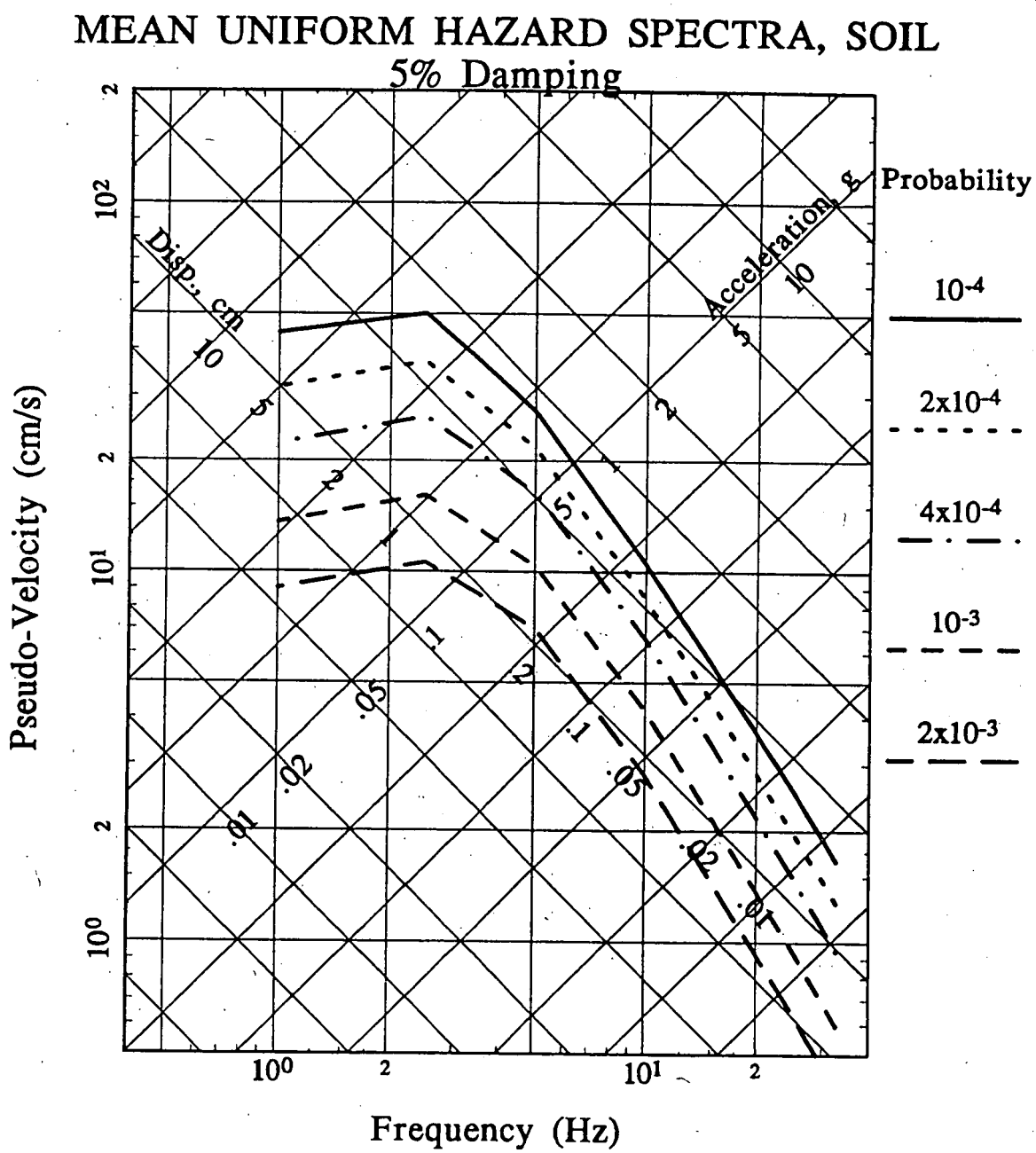

Figure 3-64. Mean uniform hazard spectra on soil.

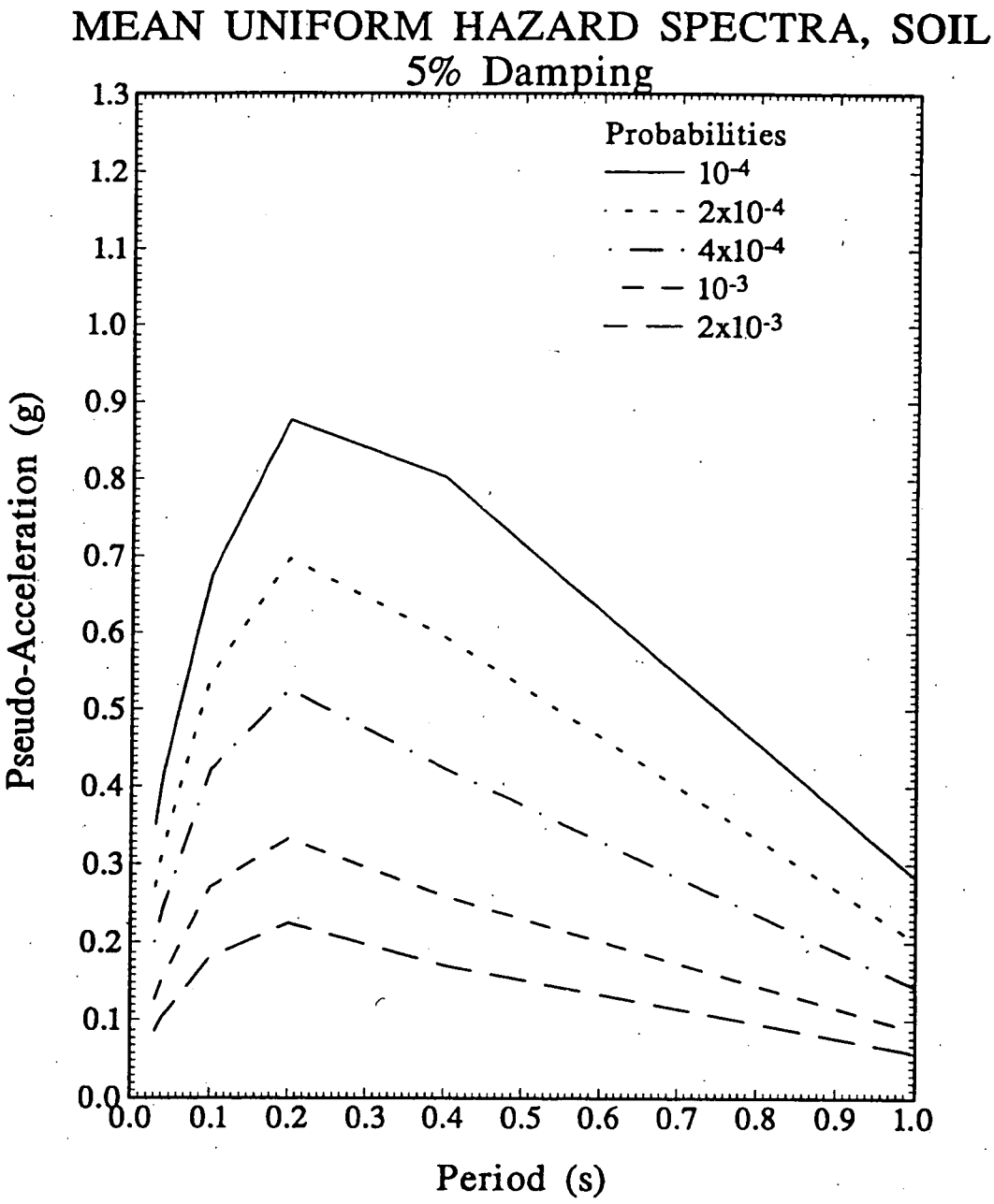

Figure 3-65. Mean spectra on soil plotted as PSA vs period.

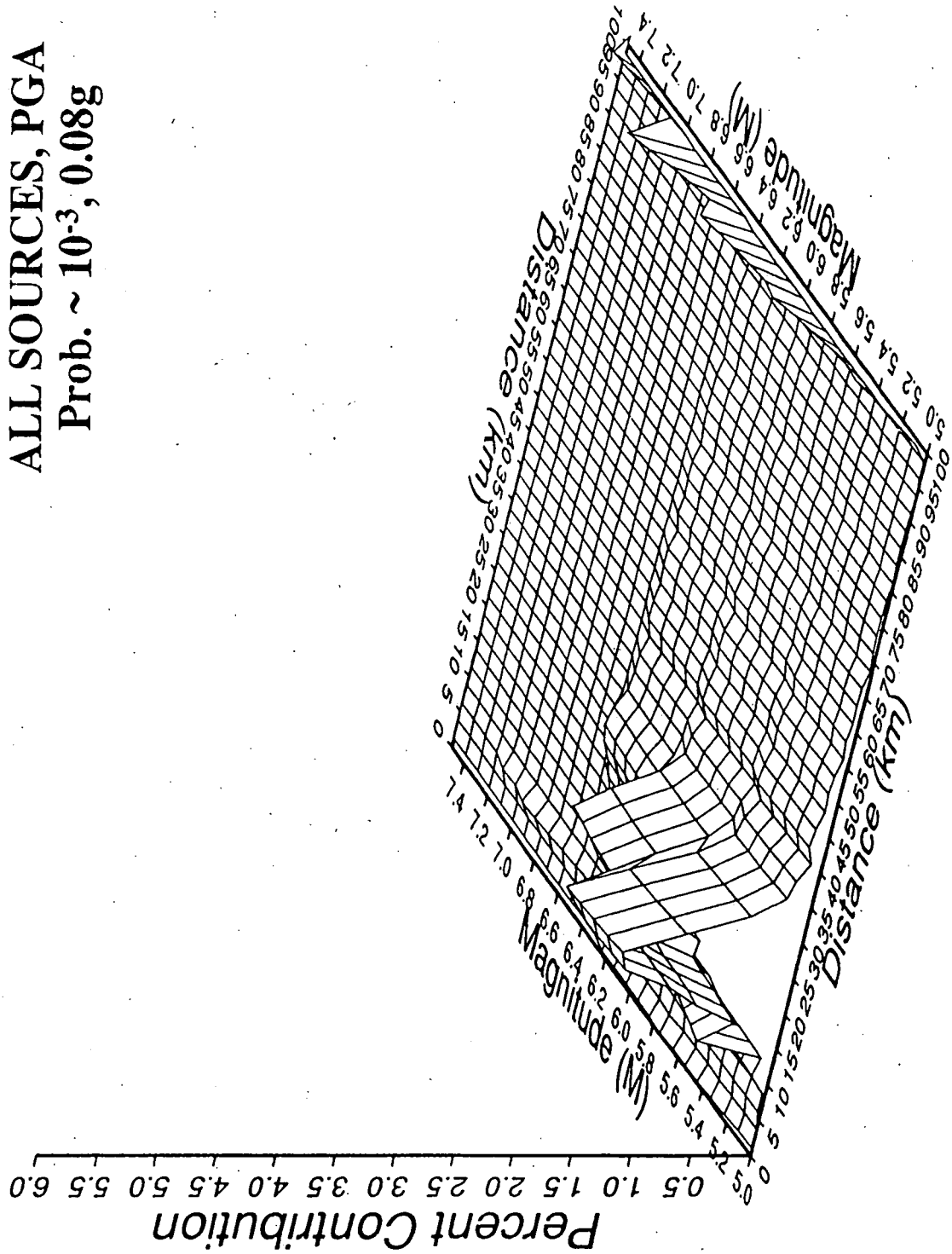

Figure 3-66. Contribution to hazard by magnitude and distance for PGA = 0.08g, all sources.

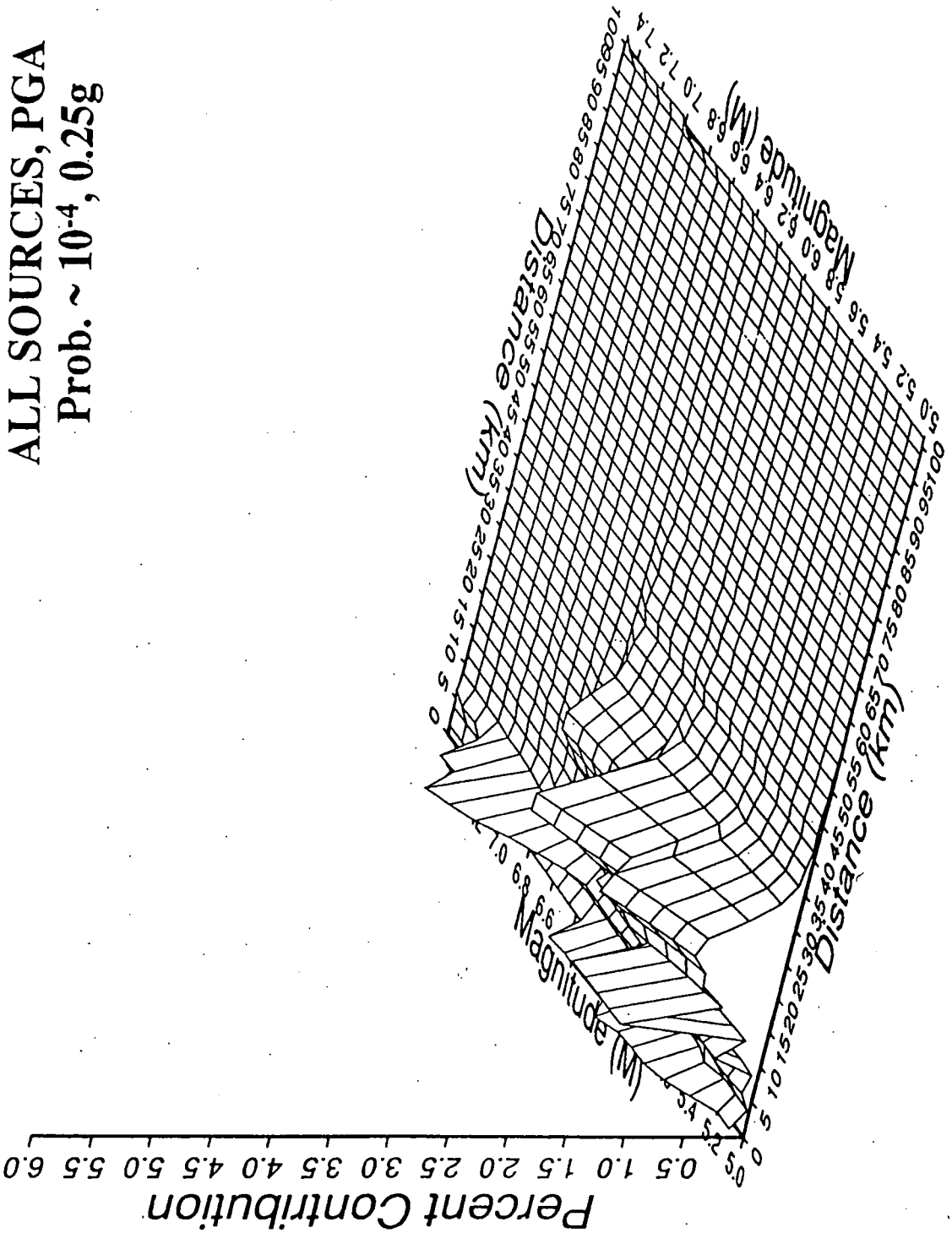

Figure 3-67. Contribution to hazard by magnitude and distance for PGA = 0.25g, all sources.

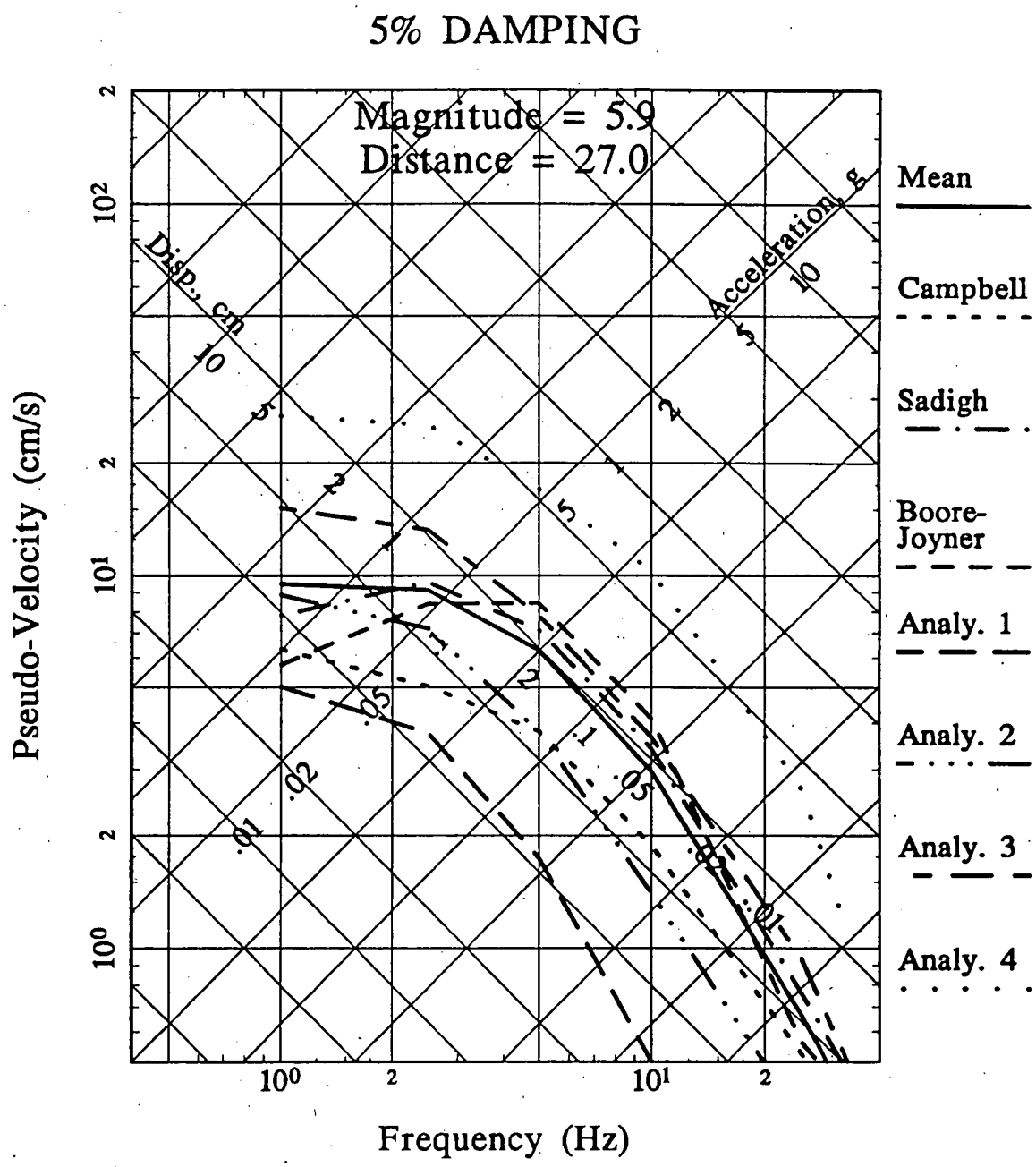

Figure 3-68. 5% damped spectra for M = 5.9, R = 27 km on rock.

705 W.C. Browning Bldg.
University of Utah
Salt Lake City, UT 84112-1183
September 21, 1994

Dr. Robin K. McGuire
Risk Engineering, Inc.
4155 Darley Avenue, Suite A
Boulder, Colorado 80303

Re: Report on *Seismic Hazard Analysis for Rocky Flats Plant*

Dear Robin:

In response to your request, this letter is to confirm in writing that I performed multiple reviews of Appendix D, "Historical Seismicity Studies", of the subject report. I provided you with detailed, written review comments on September 5, 1993, on May 13, 1994, and, most recently, on July 15, 1994—for a late-stage revised version of the draft report given to me to review. The latter review included a review not only of Appendix D but also the whole main body of the report.

Based on a revised version I have in hand of the full report dated July 27, 1994, I can confirm that all of my review comments have been satisfactorily addressed and resolved. I endorse the analyses and conclusions of Appendix D on "Historical Seismicity Studies" without any residual reservations. I also endorse the main body of the report with my resolved comments, insofar as my area of expertise in seismicity and seismotectonics allows meaningful endorsement.

If any further feedback is needed regarding my reviews, please contact or refer any concerned party to me.

Sincerely,

Walter J. Arabasz

Walter J. Arabasz, Ph.D.
tel. (801) 581-6274

DR. C. ALLIN CORNELL

P. O. Box 9260
Stanford, CA 94305

PLEASE REMIT TO:
110 Coquito Way
Portola Valley, CA 94028
Phone/Fax: (415) 854-8053

September 14, 1994

Dr. R. K. McGuire
RISK ENGINEERING INC.
4155 Darley Avenue, Ste. A
Boulder, Colorado 80303

Subject: Rocky Flats
Seismic Hazard Analysis

Dear Dr. McGuire:

This letter will confirm that I have reviewed in detail: (1) the main body of the Rocky Flats Seismic Hazard Analysis report and (2) Appendices D and J, related to statistical analysis of the seismicity data and "deterministic" ground motions. I have been given sufficient time and resources to review them in depth.

I have sent my detailed comments on drafts of these documents to you. We have discussed those comments to clarify them. You have responded by properly and effectively investigating any issues I raised and by incorporating your responses in the final versions. I am fully satisfied that you have responded well to all my substantive comments.

I endorse the final versions of these three documents.

Congratulations, it's a well done job.

Yours very truly,

C. Allin Cornell

CAC:bb

[wplet.60\mcguire.ltr]

APPENDIX A

DETAILED SEISMIC SOURCE CHARACTERIZATION

by

Geomatrix Consultants, Inc.
San Francisco, California

INTRODUCTION

The purpose of the Seismic Source Characterization activities is to characterize the earthquake sources of potential significance to the Rocky Flats Plant (RFP). The products of this effort include maps of seismic sources, maximum earthquake magnitudes, and earthquake recurrence rates for each source. These products are used in the seismic hazard analysis to assess ground motions at the site. This Appendix documents these activities.

The source characterization documented in this Appendix captures a full range of credible parameter values, based on available data and information. Data sources are principally the professional literature, project reports, and interim reports for ongoing RFP projects. Limited new field data gathered as part of this study were also used in making source interpretations. The credibility of alternative models and parameters is evaluated based on their degree of support in the available data. The interpretations of the data and the assessments of the credibility of alternative parameter values were made by the source characterization contractor, Geomatrix Consultants Inc. The technical basis for the parameter values and their relative credibilities are documented in this Appendix.

The ground motions evaluations for RFP will have both deterministic and probabilistic components. From the standpoint of source characterization, the characteristics required for the deterministic assessment (maximum credible earthquakes and closest distance to the site) are a subset of the characteristics required for the probabilistic assessment. Therefore, the following discussion will focus on the elements required for the probabilistic hazard analysis. It should be noted that all references to magnitude in this report shall be "moment magnitude" (Hanks and Kanamori, 1979) unless otherwise specified.

The report begins with a discussion of the elements of seismic source characterization followed by a source-by-source discussion. Appendix B presents tectonic geomorphic analyses conducted to assess activity of potential seismic sources. Appendix C presents a reevaluation of the location and magnitude of the 1882 Colorado earthquake.

SEISMIC SOURCE CHARACTERISTICS

The basic elements of probabilistic seismic hazard analysis are seismic source characterization, ground motion attenuation, and probabilistic hazard calculations (see Reiter, 1991, for discussion). The principal components of seismic source characterization include definition of source locations, maximum earthquake magnitudes, and earthquake recurrence rates (see Coppersmith, 1991, for

discussion of these components and methodologies for their assessment). State-of-the-art seismic hazard analyses include the full range of possible interpretations and parameter values for characterizing sources and explicitly quantify and include uncertainties (e.g., see National Research Council, 1988, for methodologies). Experience with seismic hazard analyses has shown that the seismic sources that lie within about 25 km of the site of interest usually control probabilistic ground motions and, typically, earthquake recurrence rates for these nearby sources are the most significant characteristic to site hazard. As in the case of the RFP, nearby faults are often important contributors to hazard and, because the historical record of observation is usually too short to establish earthquake recurrence rates, geologic data (e.g., slip rates) commonly provide the primary basis for recurrence estimates. Based on these common observations, the RFP seismic hazard study has focused specifically on these technical issues in characterizing seismic sources.

The uncertainty in modeling natural phenomena is incorporated into the hazard analysis through the use of the logic tree methodology. The logic tree formulation for seismic hazard analysis (Kulkarni and others, 1984; Youngs and others, 1985, 1987, 1988; Coppersmith and Youngs, 1986; National Research Council, 1988) involves specifying discrete alternative hypotheses or parameter values, expressed as the branches at each node of the logic tree. The relative likelihood that each discrete alternative is the correct value or state of the input parameter is expressed as a probability ranging from 0 to 1. The probabilities are based typically on professional judgment, but may be specified by an objective statistical analysis if the available data allow such an assessment. The components of the seismic source characterization logic trees are given below.

Figure A-1 displays the general logic tree representing the key components of the seismic source characterization analysis. The logic tree consists of nodes and branches. Each node is a particular component of the analysis; branches are alternative models or parameter values of each component. For example, the maximum magnitude node is associated with alternative magnitude values displayed on the branches. Each branch is assigned a probability or relative weight that expresses the degree of credibility that the value has, given the available data. The sum of the probabilities at each branch is unity. For each seismic source, such trees are developed and the technical basis for both the values on the branches and their probabilities are documented in this report. The general components of the seismic source logic tree shown in Figure A-1 are discussed below.

Uncertainties in Seismic Source Characterization for RFP

The uncertainties associated with characterizing seismic sources for the RFP are comparable to those associated with other site-specific seismic hazard analyses. An explicit goal in this seismic hazard analysis has been to identify and incorporate a full range of interpretations. To do so a variety of methods have been used to identify the diversity of interpretations that exist regarding seismic sources of importance to the site. These methods include: review of published literature; review and compilation of available reports conducted for engineering analysis; review of available data gathered for the RFP; interviews with researchers at federal, state, and academic institutions; reconnaissance review of key field localities cited in available reports; new analyses of intensity data for the 1882 earthquake; and limited gathering of topographic field data. The entire range of interpretations regarding the seismic sources of importance to the site have been included in the analysis and no interpretations have been eliminated. These interpretations are discussed in detail in terms of the elements of source characterization for each seismic source. The advantage of the logic tree approach is that individual hypotheses, models, and parameters are identified explicitly

and the basis for assessments of their relative credibility are given in the text. In conclusion, it is believed that the treatment of uncertainties in the seismic source characterization is an adequate and proper representation of the range and diversity of interpretations regarding earthquake sources of importance to the seismic hazard at RFP.

Seismic Sources

Individual logic trees are developed for each seismic source of potential significance to ground motions at the RFP. Two types of seismic sources are considered: fault sources and areal sources. The methods used in this study to characterize the seismic sources are state-of-the-art and provide for the inclusion of geologic information on fault behavior (e.g., Coppersmith, 1991). The fault sources in the RFP region, with the exception of the RMA/Derby source associated with the Rocky Mountain Arsenal, have not been associated with significant levels of seismicity during the historical and instrumental period. Therefore, much of their characterization relies on geologic and geomorphic data sets. The areal sources are of two types: a local source defining the boundaries of a subsurface fault system, and regional source zones that are "background" zones. Following standard practice, the location of earthquakes within the areal sources is assumed to be randomly distributed.

Seismogenic Potential

A key uncertainty in the RFP region is the assessment of whether or not individual faults are seismogenic. "Seismogenic" in this context is defined as capable of generating moderate-to-large earthquakes (M>5). Uncertainty in this assessment, which is specific to each seismic source, is represented by the relative probabilities on the yes and no branches. In the hazard analysis, the "yes" branch means that the fault will be treated as a source that localizes seismicity; the "no" branch means that the fault will not localize seismicity. In all cases, the large regional sources are assumed to be seismogenic with a probability of 1.0. The probability that any given fault is seismogenic varies as a function of evidence for its activity.

Because of the importance of this component of the analysis to the hazard assessment, it is useful to make explicit the technical criteria that are used to assess whether or not a fault is seismogenic, and to define the relative value that each criterion has in making the evaluation. The criteria and their relative weights (on a scale of 1 to 10) are summarized in the table and discussed below:

SEISMOGENIC CRITERION	RELATIVE WEIGHTS,W (1-10)
Spatially associated with large-magnitude (M>5) earthquakes	7
Spatially associated with small-magnitude (M<5) earthquakes	6
Displays geologic evidence for recent (late-Quaternary) slip	9
Structurally associated with another seismogenic fault	5
Extends downdip through seismogenic crust	2
Favorably oriented relative to stress/ tectonic analogy	1
Sum of weights	$\sum 30$

The criteria above are the types of information that would indicate whether or not a fault is seismogenic (i.e., capable of generating M>5 earthquakes in the future). Note that most of these criteria are those that have been recognized as diagnostic of "activity" or "capability" in various regulations. These criteria are best suited for potential sources with unclear evidence of activity, but should not be used if certain evidence is well-documented. For example, if a fault has been definitely associated with a large-magnitude historical earthquake or shows unequivocal evidence of repeated late-Quaternary displacements then that fault would be considered to be seismogenic with a probability of 1.0. If, however, uncertainties relative to the above criteria exist for a particular fault, then they can be used to evaluate the fault's probability of being seismogenic.

The relative weight assigned to each criterion expresses the degree to which that criterion is diagnostic of a fault being seismogenic. Of course, it is recognized that any given fault will display some or all of these characteristics to varying degrees. The criteria and weights are the professional judgments of the project team and are discussed further below.

The first criterion is the spatial association of a fault with one or more moderate-to-large earthquakes that have occurred historically. Typically, the historical record is short relative to the recurrence intervals of larger earthquakes, such that the occurrence of only a single such event historically is not uncommon. For the same reason, the *absence* of large earthquakes historically is also not uncommon, thus diminishing the value of this criterion. It is often difficult to associate older historical events with particular faults because of uncertainties in epicenter locations, and sometimes even instrumentally-located events are not easily associated with mapped faults. This criterion is given a moderately high value in assessing activity, but is less than geologic criteria on recency of faulting. This is because the geologic record spans a much longer period of time.

The second criterion is the spatial association of a fault with small-magnitude earthquakes only (M<5 earthquakes) in the historical record. It is common for seismogenic faults to be associated with small-magnitude earthquakes, but the association of a fault with such events does not

necessarily indicate that the fault can also generate larger events. For this reason, the criterion is given a moderately high rating but less than geologic or historical evidence for large-magnitude occurrence.

The third criterion is evidence for geologically young displacement (generally late Quaternary). The advantage of the geologic record is that it spans a longer time period than the historical record. Further, because the geologic record captures the larger earthquakes that rupture the surface, they were likely M>6 events (e.g., Wells and Coppersmith, 1994). Uncertainties in using this criterion come from uncertainties in dating the age of slip and recognizing coseismic displacements. The criterion is given a high rating in assessing seismogenic potential.

A fourth criterion is the structural association of a fault with another fault that is known to be seismogenic. Such an association may be by a mechanical linkage, such as a branching or *en echelon* pattern between two fault zone, or direct tectonic linkage, such as faults bounding either side of an actively uplifting crustal block. Application of this criterion can be difficult, however, such as when two faults are not in proximity but part of the same tectonic regime, or when the structural relationships are poorly understood. For this reason, the criterion is given moderate weight.

Because of the rupture dimensions associated with moderate-to-large earthquakes, seismogenic faults extend throughout the seismogenic crust. The fifth criterion expresses the degree to which a knowledge of the downdip crustal extent of a fault provides an indication of whether or not it is seismogenic. The relatively low rating assigned to this criterion reflects the judgment that crustal extent is a necessary but not sufficient condition for assessing seismogenic potential. This conclusion is supported in many geologic environments, such as much of the eastern U.S., where abundant large, crustal faults exist but few are believed to be seismogenic.

The final criterion incorporates two concepts: the favorable orientation of a fault relative to the contemporary tectonic stress regime, and analogy to other tectonic environments. By definition, seismogenic faults are favorably oriented relative to tectonic stresses, because earthquakes are a manifestation of the release of tectonic stresses. But in the absence of other evidence, determination of how "favorably" a fault is oriented involves a good knowledge of the three-dimensional geometry of the fault, orientations of principle stress directions, and rheologic properties (Zoback, 1992). Without this information, it is often possible to identify only grossly unfavorably oriented faults. Again, this criterion appears to be a necessary component, but is not sufficient alone for assessing seismogenic potential. The second part of this criterion allows for drawing analogies between the tectonic environment of the fault in question and other tectonic environments. For example, the seismogenic potential of a fault associated with an intracontinental rift system may be assessed by comparing it to another fault of known seismogenic potential within an analogous rift system. Because of the large uncertainties in drawing such analogies and their implications to earthquake potential, as well as the difficulties in applying the orientation relative to stress method, this criterion is assigned a relatively low weight.

As part of the seismic source characterization for this study, each of the criteria above have been evaluated for each of the potential fault sources. The fault-specific assessment evaluates the degree to which each criterion characterizes that particular fault (e.g., whether or not it has been associated with M>5 earthquakes or shows evidence of geologically-recent slip). These assessments are then

multiplied by the relative weight or value of each criterion, the products then are summed, and divided by the sum of the criterion weights (30) to arrive at a probability that the fault is seismogenic. By disaggregating the assessment this way into its component parts, the technical basis for the assessment is made clear. It should be noted that, although the assessment is made more explicit by dissecting it into its component parts, the assessment of the probability of the fault being seismogenic is still one that includes professional judgment. That judgment is reflected in the relative weights assigned above to each criterion and in the probabilities assigned for each fault source. The technical basis for the assessments is given for each fault in this report. The other elements of the source logic tree are discussed first (Figure A-1).

Sense of Slip

The sense of slip on faults that comprise the fault sources in the seismic hazard analysis for the Rocky Flats Plant are classified into three categories: normal, reverse, and strike slip. The sense of slip is estimated based on one or more of the following data: 1) direct geologic observation of fault surfaces in rock outcrop, 2) indirect observations of stratigraphic relationships, 3) stratigraphic relationships determined from subsurface well data, 4) observations of seismic reflection data, 5) slip directions inferred from focal mechanisms of local earthquakes and, 6) orientation of the structures with respect to the regional stress direction.

The tectonic setting, including stress conditions, are different today than when many of the faults first were formed toward the end of the Laramide orogeny in the late Cretaceous-early Paleocene. Therefore, due to the very large disconformity (approximately 65 million years) between the late Cretaceous bedrock (Fox Hills, Laramie, Arapahoe Fms.) and the overlying late Pliocene-early Pleistocene Rocky Flats alluvium at the plant site, determination of the *recent* sense of slip on faults using geologic observations within bedrock are not as reliable as observations within the Rocky Flats alluvium. Sense of slip determined using criteria that are related to the modern stress field (i.e. stress data, earthquake focal mechanisms) are considered more reliable.

Source Geometry

The source geometry component of the source logic tree (Figure A-1) expresses the three-dimensional configuration of the source. Faults are modeled as planar features described by their mapped location at the surface, dip, total length, and downdip width. Uncertainties in all of these parameters are included in the assessment on a source-by-source basis (for example, see the logic tree for the Walnut Creek fault in Figure A-6). The geometry of areal source zones is given by their mapped boundaries and it is assumed that the spatial distribution of seismicity is uniform within a zone.

Maximum Magnitude

Each seismic source is associated with a maximum magnitude estimate. For the probabilistic assessment, the maximum magnitude assessment will result in a distribution of values that reflects the uncertainties in the data and methods for assessing maximum magnitudes. For the deterministic assessment, a single maximum credible earthquake (MCE) is selected.

Maximum magnitudes are assessed for fault sources based on a consideration of the possible lengths of rupture and associated rupture areas (Coppersmith, 1991). If such data exist, estimates of displacement per event from geologic studies also provide a basis for maximum magnitudes. The empirical relationships between moment magnitude and rupture length, rupture area, and displacement per event given in Wells and Coppersmith (1994) are used for the magnitude estimates.

For areal source zones, the maximum magnitude is estimated based on a consideration of the largest historical earthquake, as well as consideration of the largest earthquakes that can occur within the source without leaving a clear geologic signature (e.g., surface rupture or recognizable Quaternary deformation).

Slip Rate/Recurrence Rate

Activity rates or recurrence rates are defined for each source using either fault slip rate information or observed seismicity data. Recurrence rates for fault sources are assessed based on the slip rate estimated for the fault (see Youngs and Coppersmith, 1985; Coppersmith, 1991, for discussion of approach). A fault's slip rate is assumed to represent the average rate of seismic energy release along the fault and the product of the slip rate, total fault area, and shear modulus defines the seismic moment rate along the fault (e.g., Anderson, 1979). This moment rate is then partitioned into earthquakes of various size according to two magnitude distribution models: the characteristic earthquake model (Youngs and Coppersmith, 1985) and the exponential model (Anderson, 1979). Youngs and Coppersmith (1985) and Youngs and others (1993) have shown that the characteristic earthquake model is more appropriate for fault sources and areal source zones are typically modeled using the exponential recurrence model.

Recurrence rates for regional areal source zones are developed from the historical and instrumental catalog of events falling within the source zone boundaries.

FAULT SOURCE CHARACTERISTICS

In this section of the Appendix the characteristics of the seismic sources are given and the technical basis for them is described. The following discussion focuses on the potential seismic sources that are closest to the RFP. In particular, fault sources include the Walnut Creek, Rock Creek, and Valmont faults, and Golden-Boulder reaches of the Front Range fault system. Because of their proximity to the RFP, the source characterization effort for Task 7 has focused on these potential sources. The documentation below also reflects this prioritization, with more discussion accorded those sources of potentially greatest significance to the site hazard.

Walnut Creek Fault

The Walnut Creek fault (Figure A-2) is a previously unidentified possible Quaternary fault that lies adjacent to the RFP (Figure A-3) and is described in the RFP Site Characterization Report (EG&G, 1992; Figure A-4). The fault was first identified from observations made at surface outcrops and was later confirmed with subsurface data. The fault is marked by an apparent down-on-the east vertical discontinuity or "step" of over 100 feet of a conglomeratic sandstone marker bed at the base

of the Cretaceous Arapahoe Formation, near the Arapahoe-Laramie Formation contact. The borehole data suggest a vertical drop of over 100 feet over a horizontal distance of less than 1000 feet (EG&G, 1992). The boreholes used to identify the 100 foot "step" are shown in Figure A-5. Shallow boreholes and high resolution seismic reflection data have also indicated a vertical step in the contact between the Arapahoe Formation and overlying Quaternary Rocky Flats Alluvium of up to about 30 feet (9 meters) (EG&G, 1991a). Within the resolution of the available data, the step at the base of the Rocky Flats Alluvium appears to coincide with the step at the base of the Arapahoe Formation. The distribution of depths to bedrock from borehole data defines the approximate location of the Walnut Creek fault immediately east of the RFP (Figure A-5).

Three alternative explanations are given in the Site Characterization Report to explain the 100 foot vertical discontinuity at the base of the Arapahoe Formation (EG&G, 1992): folding, a stratigraphic discontinuity (leading to improperly correlating a sandstone marker in the boreholes), and faulting. Resolution of the issue is left open, although problems are discussed with the folding and stratigraphic explanations. Further, it is noted that the 100 foot step appears to coincide with the bedrock-alluvium step, and deep seismic reflection data as well as surface mapping are noted as showing evidence for faulting in the area east of RFP (EG&G, 1992).

Seismogenic Potential. The logic tree for the Walnut Creek fault is given in Figure A-6. The first assessment is whether or not the Walnut Creek fault is seismogenic. To make this assessment, the criteria discussed earlier are considered and are tabulated below.

CRITERION	PROBABILITY, P	P x W
Association with M>5 seismicity	0.01	0.07
Association with M<5 seismicity	0.1	0.6
Geologically recent slip	0.6	5.4
Structural association	0.3	1.5
Crustal extent	0.4	0.8
Favorable to stress/tectonic analogue	0.2	0.2

Given above is the probability that the Walnut Creek fault displays each of the criteria used to define seismogenic potential, with strong evidence resulting in probabilities near 1.0, and weak evidence resulting in probabilities near 0. Each of the assessments is discussed below.

The only historical M>5 earthquake in the region that could have occurred on the Walnut Creek fault is the 1882 Colorado earthquake. Although there is uncertainty in its location (Appendix C), it appears that all interpretations would place it at least 100 km north and west of the Walnut Creek fault. Therefore, a very low probability (0.01) is assigned to this criteria.

Small-magnitude seismicity is sparse east of the range-front at the latitude of the RFP, with the exception of the seismicity associated with the Rocky Mountain Arsenal and scattered seismicity (see Appendix D). We therefore assign a low probability (0.1) to the Walnut Creek fault being associated with small-magnitude seismicity.

The assessment of the recency of slip of the Walnut Creek fault is difficult because much of the inferred trace is covered by undifferentiated late Quaternary-Holocene surficial deposits (Figure A-4). The fault is identified from high resolution seismic reflection data and boreholes to vertically displace the base of the Cretaceous Arapahoe Formation about 100 feet. However, EG&G (1992) suggest that on the basis of available seismic data the Laramie-Fox Hills contact, which is downsection from the Arapahoe-Laramie contact, is not vertically displaced. The resolution of the data supporting this interpretation is not discussed. They conclude that if the Walnut Creek fault exists at the base of the Arapahoe Formation, it must become listric (i.e., decrease in dip with depth) within the Laramie to avoid displacing the Fox Hills contact. Shallow boreholes indicating the depth to the contact between the bedrock and Quaternary Rocky Flats alluvium show a distinct down-on-the-east "step" and strongly suggest that the faulting postdates this unconformable contact (Figure A-5). The age of this contact is uncertain but is probably close to that of the overlying Rocky Flats Alluvium. The age of the Rocky Flats Alluvium and its terrace surface are estimated to be from 900 ka (thousand years) to 1.9 Ma (million years) based on soils development, age constraints on the Verdos alluvium containing the Pearlette Type O ash, identification of the Bishop ash, and alteration of magnetite (Van Horn, 1972; Trimble, 1975; Scott, 1975; Van Horn, 1976; Trimble and Machette, 1979).

One plausible hypothesis that would account for the vertical "step" in the unconformity at the base of the Rocky Flats Alluvium and yet not imply post-unconformity faulting is the following. A fault zone may have been present in Laramie Formation rocks; during erosion of the unconformity the fault zone may have served to localize erosion perhaps along a channel leading to a topographic scarp on the bedrock surface; subsequent deposition of the Rocky Flats Alluvium over this scarp would then have proceeded until the flat alluvial terrace surface was developed. The test for this hypothesis would be to determine whether or not faults within the bedrock actually displace the unconformity and the alluvium above the unconformity.

To further constrain the estimates of recency of slip on the Walnut Creek fault, previous detailed geologic studies searching for evidence of Quaternary deformation were reviewed (i.e., Dames & Moore, 1981). At the time of the Dames & Moore studies, the Walnut Creek fault was not identified. However, as part of their "site vicinity investigations," Dames & Moore evaluated the potential southeastward projection of a fault mapped near Eggleston Reservoir into the area immediately east of RFP. As part of those studies three excavations were made that lie near the mapped position of the Walnut Creek fault (Figure A-7). A bulldozer cut (labeled SWC-1 on Figure A-7) exposed rocks entirely within the Laramie Formation. Faults and deformation were observed that were tentatively interpreted to be due to syndepositional processes. A "slip plane" with a southwesterly trend was identified in SWC-1 that could not be ruled out as being tectonic. Two additional trenches were excavated to the southwest along the trend of the "slip plane" on top of the Rocky Flats alluvial surface, but no evidence for faulting was found in the bedrock and the bedrock-alluvium contact was not found to be faulted. Based on our current knowledge of the likely location of the Walnut Creek fault based on the location of the step in the bedrock-alluvium unconformity, it is likely that the two Dames & Moore trenches did not cross the Walnut Creek fault (Figure A-7).

Because of the importance of determining the seismogenic potential of the Walnut Creek fault due to its proximity to the site, additional geomorphic studies were carried out as part of this project. These studies are described in detail in Appendix B and pertinent conclusions are given here. The geomorphic studies consisted of development of surface profiles and drainage basin analysis. These techniques were used because they are capable of revealing subtle signs of tectonic deformation, both those due to surface faulting and those due to surface folding associated with blind faulting. Longitudinal stream profiles and basin analysis show subtle suggestions of tectonic deformation associated with the Walnut Creek fault (Appendix B).

Review of aerial photographs shows a fairly distinct step in the bedrock-alluvium contact expressed in the topography east of the RFP (Figure A-8). Because of differences in the erodability of the Rocky Flats Alluvium and the Laramie Formation, the contact between the two units is identifiable in the geomorphology, and comparison of the position of the contact to the east and to the west of the point marked "A" in Figure A-7 shows a down-to-the-east step in the bedrock-alluvium contact. The Rocky Flats alluvial surface provides an extremely useful time horizon or "strain gauge" for assessing possible deformation across the Walnut Creek fault because it is sufficiently old to capture even low rates of vertical slip and, where it has not been eroded away or modified by cultural activities, it is remarkably planar. Longitudinal profiles of the surface based on existing topographic maps show no evidence of vertical displacement at the surface projection of the fault, within the resolution of the 20 foot (7 meter) contour interval. Detailed topographic profiles developed for this study using a Wild Total Station surveying instrument show no evidence of vertical displacement, within a resolution of about 1 to 2 meters (e.g., Figures A-9, A-10, and A-11).

The general conclusion from the available data is that the Walnut Creek fault is present within Cretaceous rocks and probably displaces the contact between the Cretaceous Laramie Formation and Quaternary Rocky Flats Alluvium. Whether or not the fault has been active throughout the Quaternary is not clear. As will be discussed later, if the fault is presently active, its slip rate must be extremely low because the total post-Rocky Flats Alluvium vertical strain is constrained to be less than 1 to 2 meters. On the basis of the available data, it is concluded that the probability that the Walnut Creek fault has undergone late Quaternary slip is assessed to be 0.6.

The Walnut Creek fault appears to strike to the northeast based on the distribution of the abrupt change in thickness of the Rocky Flats Alluvium from boreholes (Figure A-5), the strike of faults seen in trench SWC-1 (Dames & Moore, 1981), and the distribution of bedrock deformation features (EG&G, 1992). As such, it may be one of a series of northeast-trending faults (Figure A-12) that have been mapped in the RFP area northward (e.g., Spencer, 1961, 1986; Weimer, 1973; Davis, 1974; Colton, 1978; Kittleson, 1992). As will be discussed later, the Valmont fault, which shows evidence of Quaternary activity, is likely one element of this northeast-trending zone. These faults were originally interpreted as listric normal syndepositional faults within the upper Cretaceous section (Davis, 1974), but recent detailed stratigraphic analysis (Kittleson, 1992) indicates they are reverse faults, consistent with Laramide compression. This zone of faults is treated as a local areal source zone in this study (see below). The structural association of various elements of this zone with each other is not clear. For this assessment, the likelihood of a structural association of the Walnut Creek fault with seismogenic faults that may be included in the northeast-trending zone is assessed to be 0.3. This relatively low weight reflects the uncertainty in a direct mechanical linkage of the Walnut Creek fault with other faults of the zone, and the uncertainty that other faults are themselves seismogenic.

The downdip crustal extent of the Walnut Creek fault is not well-constrained from available data. The absence of associated seismicity precludes the use of hypocenters to assess downdip extent. As noted in EG&G (1992), high resolution seismic reflection lines from Operating Unit 2 (EG&G, 1991a) show apparently undeformed, gently southeast-dipping reflectors in the lower Laramie and Fox Hills sandstones. This may indicate that the Walnut Creek fault becomes listric and is a shallow structure floored within the Laramie Formation (EG&G, 1992). A deep seismic reflection profile through the site (Ebasco, 1991; Figure A-13) shows an undisturbed contact between the Fox Hills and underlying Pierre Formation, within the level of resolution of the data. Further, if the Walnut Creek fault were interpreted to represent an updip extension the faults observed within the Pierre Formation (Figure A-12), these faults do not appear to disrupt the contact with the Lower Cretaceous-Paleozoic section. The caveat in these interpretations from the deep seismic lines is that the level of resolution of these data is insufficient to preclude small amounts of displacement. Assuming reasonable velocities, the resolution of the Fox Hills-Pierre and Pierre-Lower Cretaceous

contact is about 100 meters on the deep seismic reflection profile. Thus, although there is no evidence for displacements downdip along the Walnut Creek fault, the displacements observed from borehole data of the Arapahoe-Laramie contact (about 30 meters) likely would not be observed on the deep seismic data. On the basis of the available data, the likelihood that the Walnut Creek fault extends throughout the seismogenic crust is assessed to be 0.4. This assessment reflects the interpretation that the available data support the interpretation that the fault does not extend below the base of the Pierre Formation, but allow for a downdip extension that, because of a lack of high resolution, would continue to the base of the seismogenic crust.

The state of crustal stress in the RFP region is not well known, due to an absence of seismicity. Current interpretations place the region in the Cordilleran extensional province (e.g., Zoback and Zoback, 1991) and the most local borehole breakout data (Dart, 1985) suggest maximum horizontal extension in the northeast quadrant. Wong (1986) and Zoback and Zoback (1991) note that the juxtaposition of strike slip and normal faulting focal mechanisms in this region suggest that the magnitude of the maximum and intermediate compressive stresses are probably about equal. The maximum compressive stress is likely vertical in the region and the intermediate compressive stress is in the northwest quadrant. This orientation is not particularly favorable for the Walnut Creek fault and the other northeast-trending structures. A possible tectonic analogue to the Walnut Creek fault is the Cheraw fault southeast of Colorado Springs. The Cheraw fault also has a northeast strike, displaces Rocky Flats alluvium up to 12 meters, and appears to show geomorphic evidence for late Quaternary displacement (Scott, 1970; Sharps, 1976; Kirkham and Rogers, 1981). Unfortunately, detailed field studies have not been conducted along the Cheraw fault such that its late Quaternary behavior is not well-understood. Consequently, drawing a tectonic analogy between the Walnut Creek fault and the Cheraw fault is difficult based on available data. On the basis of the available information, the likelihood that the Walnut Creek fault is favorably oriented relative to tectonic stresses or tectonically analogous to another seismogenic fault is assessed to 0.2.

To arrive at the probability that the Walnut Creek fault is seismogenic, the probabilities associated with each criterion, P, are multiplied by the relative weight associated with each criterion, W, in assessing whether or not a fault is seismogenic. The sum of these (P x W) products is 8.57. This sum is divided by the sum of the weights (30) to arrive at a probability of 0.29, rounded off to 0.3, that the Walnut Creek fault is seismogenic. This assessment is included in the logic tree (Figure A-6) and all of the other assessments, discussed below, are conditional on the fault being seismogenic.

Sense of Slip

In considering style of faulting, the Walnut Creek, Rock Creek and Valmont fault sources are treated together as members of the northeast-trending fault system having similar origin and source characteristics. A similar origin and geometry for these sources is supported by recent sub-regional subsurface stratigraphic studies of the Cretaceous bedrock in the Boulder-Weld coal field (Kittleson, 1992) and a regional fault kinematic study in the vicinity of Rocky Flats Plant (Selvig, 1993).

Based on surficial mapping and limited subsurface data, Spencer (1961) interpreted the northeast-trending faults as planar normal and reverse faults bounding a horst and graben bedrock geometry. Subsequent detailed subsurface mapping of portions of the Boulder-Weld coal field by seismic reflection, (Davis, 1974; Davis and Weimer, 1976) interpreted the northeast-trending faults as shallow-rooted syndepositional listric normal growth faults. More recently, Spencer (1986) demonstrated uniform thickness of Cretaceous coal seams across the faults, contradicting a normal growth origin. Based on correlation of well data within the Boulder-Weld coal field, Kittleson (1992) demonstrated widespread repetition of strata across northeast-trending faults indicative of

reverse, not normal, displacements. This analysis also defines a bedding-parallel detachment within the Pierre shale at a depth of about 1000'.

Bedrock exposures of the northeast-trending faults in the area surrounding Marshall, Colorado, southwest of the Boulder-Weld coal field were studied in detail by Selvig (1993). In this study the attitudes of over 200 faults were recorded and the direction of slip determined for approximately half of the exposures. The data reveal a predominance of low-angle reverse faulting with an oblique component, and no normal components of slip. A stress analysis performed on the fault data for the Marshall area faults during the study indicates a sub-horizontal NW-SE orientation for maximum compression. In contrast, stress analysis of the Front Range fault system indicates a SSW-NNE direction of maximum compression during their formation. On the basis of these data and analyses, Selvig (1993) concurs with Kittleson (1992) and favors a gravity-driven model for the formation of the Marshall faults in which the low-angle reverse faults sole into a bedding-parallel detachment within the Pierre shale.

Recent compilations of stress data (e.g., Zoback and Zoback, 1991) suggest that the axis of maximum horizontal stress is likely in the northwest quadrant, which is compatible with reverse faulting on the northeast-trending faults. Although less likely, the regional stress regime may also be compatible with strike slip faulting.

Based on these data, the sense of slip on the Walnut Creek, Rock Creek, and Valmont fault is assessed to be: reverse (0.5), normal (0.2), and strike slip (0.3).

Geometry: Dip, Total Length, and Depth of Faulting. As shown in Figure A-6, the characteristics related to the geometry of the Walnut Creek fault are the dip (as measured from the horizontal), total fault length, and depth of faulting (which, together with the dip, defines the downdip width of the fault). Because the Walnut Creek fault is not clearly exposed at the surface, the dip of the fault must be estimated from indirect evidence. All of the available evidence suggests that the fault is steeply dipping to vertical, with a dip direction to the northwest. Solving a three-point problem using the EG&G (1992) map (Figure A-4) and topography suggests a dip of about 75 degrees. The constraints on the location of the step in the bedrock-alluvium contact (Figure A-5) also strongly suggest that the dip of the fault is steep. Based on these observations, the dip of the Walnut Creek fault is assessed to be 75 to 90 degrees, with probabilities of 0.6 and 0.4, respectively. There is a slight preference for the 75 degree dip because of the geologic evidence for a steep dip.

The total length of the Walnut Creek fault is highly uncertain, due mostly to a lack of detailed surface mapping over the area. The inferred length based on existing mapping is about 3 km (EG&G, 1992). It is also considered possible that the total length is greater, if an analogy is drawn to other northeast-trending faults. If the Walnut Creek is considered to be a member of the northeast-trending faults mapped in the Marshall area (Spencer, 1961) and the Boulder-Fort Collins-Greeley area by Colton (1978) that are interpreted from seismic reflection data by Davis (1974), then the total length of the Walnut Creek fault is assessed from the typical mapped length of faults within this zone. A typical length is about 15 km and this value is included in the logic tree as a possible length of the Walnut Creek fault with a probability of 0.3. The 3 km length is given greater weight (0.7), because the existing geologic mapping in the site vicinity has not identified a fault of longer than 3 km (i.e., such a fault has not been required to explain the mapped geologic relationships).

The next node of the logic tree (Figure A-6) is the depth of faulting, which expresses the vertical extent of the fault within the seismogenic part of the crust. The vertical depth of faulting is combined with the dip of the fault to arrive at the downdip width of the fault within the seismogenic crust. For example, if the depth of faulting is assessed to be 10 km and the dip of the fault is

estimated to be 45 degrees, the downdip width of the fault would be about 14 km. Clearly, for the case where the fault is vertical, the depth of faulting is equivalent to the downdip width.

In the Walnut Creek logic tree, the assessment of the depth of faulting is made conditional on the total length of the fault. Assuming a total length of 3 km, the depth of faulting (and the downdip width for the 90 degree dip case) is assessed to be either 6 km or 15 km. Compilations of length-to-width aspect ratios for historical ruptures (e.g., Purcaru and Berkhemer, 1982) indicate that, for dip-slip faults, minimum ratios are about 1:1. Allowing for an extreme ratio of 1:2, the width would be 6 km for an assumed length of 3 km. The 15 km width is based on the maximum depth of seismicity for M>5 in the central U.S. region (Langer and others, 1991), and would result in a highly unusual aspect ratio of 1:5. The 6 km width is given more weight because it appears to be more physically realistic than the 15 km width, based on our understanding of coseismic ruptures. Given a total length of 15 km, a single downdip width of 15 km is considered, which is the approximate maximum depth of seismicity in the region (Langer and others, 1991). For the case where the Walnut Creek fault is assumed to dip 75 degrees, the downdip widths are calculated from the depths of faulting.

Maximum Earthquake Magnitude. Estimates of maximum magnitude for the Walnut Creek fault are made based on considerations of the dimensions of coseismic rupture areas that might be possible, supported by considerations of the threshold of surface faulting. The maximum magnitude possible on the Walnut Creek fault is a function of the length of ruptures and rupture areas (length times downdip width). Because in all cases the total length estimates for the Walnut Creek fault are short (Figure A-6) relative to most seismogenic faults, it is assumed that the entire length of the fault will rupture in a single event. The total lengths are multiplied by their respective downdip widths to arrive at rupture area estimates. The empirical relationships between rupture area and moment magnitude (Wells and Coppersmith, 1994) are then used to calculate magnitudes for given rupture areas.

To evaluate the magnitude threshold at which surface faulting occurs, Wells and Coppersmith (1994) have compiled data on about 275 crustal earthquakes for which an assessment has been made of whether or not surface faulting occurred and a reliable moment magnitude estimate has been made. Their results indicate that at about magnitude 5 1/2 only about 20% of their earthquakes were associated with surface faulting; at about magnitude 6 1/2 about 80% were associated with surface rupture. At about magnitude 6, about one-half of the earthquakes in the dataset experienced surface rupture and one-half did not. It is concluded that the "threshold" of surface faulting occurs at about moment magnitude 6, plus or minus one-half magnitude unit (Wells and Coppersmith, 1994). The Walnut Creek fault is known to exist in the shallow subsurface (at the bedrock-alluvium contact) and is not well-expressed at the surface geomorphically. This is true despite the fact that surfaces, such as the Rocky Flats alluvial terrace surface, are quite old and should have been subjected to multiple surface-rupturing events. It is therefore concluded that the maximum magnitudes on the Walnut Creek fault should be very near the magnitudes associated with the threshold of surface faulting (in the range of 5 1/2 to 6 1/2).

Based on the above consideration of rupture dimensions, and supported by a consideration of the threshold of surface faulting, the distribution of maximum magnitudes given in the logic tree is: 5 1/2 (0.36), 6 (0.46), 6 1/2 (0.18).

Slip Rate. Because fault slip rate is used in the hazard analysis to constrain the earthquake recurrence rate, the most recent slip rate is to be used. The youngest geologic unit across the Walnut Creek fault is the Rocky Flats Alluvium and its terrace surface, which are dated at between 900 ka and 1.9 Ma. As discussed previously, the maximum vertical displacement of the bedrock-Rocky Flats Alluvium unconformable contact is about 9 m. Detailed topographic profiles were developed

for this study with the specific purpose of searching for evidence of vertical displacement across the Walnut Creek fault (Appendix B). No unequivocal evidence for displacement of the Rocky Flats surface was observed, within the resolution of the data. If a vertical down-on-the-east displacement is "forced" to exist, the maximum displacement would be no more than one to two meters (Figures A-10 and A-11). Using these data constraints and the range of ages for the Rocky Flats alluvium, the following slip rates are calculated: 0.01 mm/yr based on 9 m in 900 ka; 0.002 mm/yr based on 2 m in 1 Ma; and 0.0005 mm/yr based on 1 m in 2 Ma. The high and low values are unlikely interpretations and are both assigned a weight of 0.2; the central value is assigned a weight of 0.6 (Figure A-6).

Rock Creek Fault

The existence of the Rock Creek fault (Figure A-2) is inferred on the basis of an interpreted 400 ft (120 m) down-on-the-east vertical displacement of the basal contact of the Laramie Formation (EG&G, 1992). The surface trace of the fault is mapped coincident with a strong tonal lineament that appears on a regional Landsat infrared image (EG&G, 1992). Along nearly all of its mapped length, the fault does not intersect post-Cretaceous materials (with the exception of recent alluvium) and therefore the assessment of its seismogenic potential is difficult. A small patch of "undifferentiated alluvium" is mapped just north of Rock Creek, which the fault is mapped to cross without any significant displacement at mapping scales of 1:24,000 (EG&G, 1992; Figure 17).

The proximity, similar trend, and probable analogous tectonic role of the Rock Creek and Walnut Creek faults leads to the conclusion that they should be characterized the same for this analysis (i.e., same probability of being seismogenic, geometry, and maximum magnitudes), with one exception. The cumulative slip of the Arapahoe-Laramie contact along the Rock Creek fault appears to be two to four times as great as the cumulative slip across the Walnut Creek fault (EG&G, 1992). The timing of this post-Cretaceous slip is not known, but, if the slip occurred on the faults over the same time period, the Rock Creek fault would have a slip rate that is two to four times that on the Walnut Creek fault. Allowing for this possibility and in lieu of late-Quaternary slip rate information on the Rock Creek fault, it is assumed for this analysis that the slip rate on the Rock Creek fault is also two to four times that on the Walnut Creek fault (Figure A-6). Note that the considerable uncertainties in the slip rates means that there is significant overlap in the range of slip rates assumed for the two faults.

Valmont Fault

The Valmont fault (Figure A-2) was first mapped by Scott and Cobban (1965) and also appears on the Niwot quadrangle geologic map of Trimble (1975). Evidence for Quaternary activity was first described by Scott (1970) as a northeast-trending minor fault juxtaposing Cretaceous Fox Hills Formation against late Quaternary Slocum Alluvium. The trace location shown in Figure A-2 is taken from Scott and Cobban (1965). The logic tree for the Valmont fault is shown in Figure A-14.

Seismogenic Potential. The Valmont fault lies in a tectonically similar position as the Walnut Creek fault: both are northeast-trending, have down-on-the-east displacement, lie within a larger zone of northeast-trending faults observed within the Cretaceous section, and both show evidence of Quaternary faulting. All of the criteria used to assess the seismogenic potential of the Valmont fault are identical to those used for the Walnut Creek fault, with the exception of the geologic evidence for late Quaternary displacement. As part of this study, the exposure photographed by Scott (1970) was examined and a reconnaissance field log was developed (Figures A-15 and A-16). Examination of the exposure confirms the presence of a significant fault zone within Cretaceous Fox Hills siltstone and the juxtaposition of what is apparently Slocum alluvial gravel against Fox Hills and overlying younger colluvium. Detailed field correlations have not been established to confirm

that this is Slocum alluvium or to confirm that the juxtaposition is due to faulting and not some other mechanism (e.g., channel incision). The Slocum gravels are interpreted to be Illinoian (~300 ka) to Sangamon (~120 ka) in age, thus confirming late Quaternary displacement if the juxtaposition is due to faulting.

All of the assessments for the probability of Valmont fault being seismogenic are the same as for the Walnut Creek fault, with one exception. The probability that the Valmont fault is associated with evidence for geologically-recent displacement is assessed to be 0.9. Therefore the sum of the probabilities times the weights of each criterion (P x W) is 11.27, which when divided by the total sum of the weights (30), results in a probability of 0.38. Therefore, the probability that the Valmont fault is seismogenic is assessed to be 0.4.

The sense of slip assessed for the Valmont fault is the same as that assessed for the Walnut Creek and Rock Creek faults: reverse (0.5), normal (0.2), and strike slip (0.3).

Geometry: Dip, Total Length, and Depth of Faulting. The dip on the Valmont fault is estimated based on the roadcut exposure and by analogy to the Walnut Creek fault. The main zone of foliated gouge in the Fox Hills Formation has a dip of about 50 degrees to the north (Figure A-16) and this dip is given the highest weight to define the fault. By analogy to the Walnut Creek fault, which likely lies within the same zone of northeast-trending faults, an alternative dip of 75 degrees is also considered.

The mapped length of the Valmont fault on Scott and Cobban's (1965) map is about 3 km. For the same reasons as described for the Walnut Creek fault, a total length of 15 km is also considered. Similarly, alternative downdip widths are developed for the Valmont fault using the same arguments as for the Walnut Creek fault.

Maximum Earthquake Magnitude. Because the total length scenarios and downdip widths (corrected for dip) are essentially identical to the Walnut Creek fault, the maximum magnitudes assessed for the Valmont fault are also the same. The maximum magnitude distribution is: 5 1/2 (0.36), 6 (0.46), 6 1/2 (0.18).

Golden-Boulder Reaches of the Front Range Fault System

The uplifted Front Range of the Colorado Rocky Mountains is structurally juxtaposed against the relatively undeformed crust of the Great Plains along its eastern range front by a narrow fault system called the Front Range fault system (Figure A-13). The Front Range fault system consists of both emergent faults exposed and mapped at the surface, and blind faults that do not extend to the surface but are expressed indirectly by deformation of the overlying sedimentary cover rocks. The principal elements of the Front Range fault system formed to accommodate uplift of the Front Range during the late Cretaceous-Paleocene Laramide orogency, though some may have re-activated Paleozoic structures formed during uplift of the ancestral Rockies (Tweto, 1975).

Interpretations of the subsurface geometry of the Front Range fault system have evolved from the predominantly high-angle/vertical style of faulting inferred by "thick-skinned" tectonics (e.g., Harms, 1964; Prucha and others, 1965; Stearns, 1971, 1978; and Matthews and Work, 1978) to the more shallow-dipping master faults associated with "thin-skinned" tectonic models (e.g., Brewer and others, 1982; Lowell, 1983; Erslev and others, 1988). Recent general acceptance of the "thin-skinned" model of low-angle compressional faulting involving basement is due largely to evidence from recent subsurface geophysical investigations (e.g., Smithson and others, 1979; Brewer and others, 1982; Bieber, 1983) and successful application of modern structural analysis and modeling techniques (e.g., Erslev, 1986, 1988; Narr and Suppe, 1989, 1990; Schmidt and others, 1993). A

simple blind thrust wedge fault geometry consistent with "thin-skinned" tectonics theory is adopted as the structural framework of the Front Range fault system for this report.

A recent deep seismic reflection profile that extends across the Rocky Flats alluvial fan surface from just inside the range front at Coal Creek canyon, through the Rocky Flats Plant and ending in the vicinity of Indiana Street east of the plant site is shown in Figure A-13. The characterization of the subsurface geometry of seismic sources as faults of the Front Range fault system is derived largely according to the structural relationships depicted in the interpreted seismic section of Figure A-13a. The main structural components of the wedge model are:

- A primary fault (A) dipping moderately to the west that extends upward from mid-crustal depths (based on analogy to similar structures observed on deep seismic profiles of the Rocky Mountain range front to the north) to a ramp-flat transition at a depth of about 3.5 km, near the base of the range front.

- A subhorizontal decollement (B) lying near the base of the flat-lying sedimentary cover rocks east of the ramp/flat transition.

- A east-dipping fault (C) that splays upwards from the decollement along the upturned basement/cover contact (formed as the Laramide roof thrust that defines the top of the wedge).

- A steeply west-dipping "breakthrough" fault (D) splays upwards from fault (A) below the ramp/flat transition to the surface.

- A series of high-angle conjugate reverse faults (E) within the flat-lying sedimentary cover rocks east of the range front.

According to this model, faults A, B, C, and E formed simultaneously, while the "breakthrough" fault (D) formed later, splaying upwards from primary fault (A) below the ramp/flat transition and cutting the Laramide roof thrust (C).

The general similarity in structural style along the range front and the interpretation of major faults from both surface mapping and subsurface studies leads to the conclusion that, for the purposes of seismic source characterization, a fault or fault zone similar to that shown in Figure A-13 should be assumed to exist along the entire range front at least from Boulder to Colorado Springs. The reaches of the Front Range fault system closest to the RFP are the Golden fault as mapped by Van Horn (1972) and Smith (1964) and what is termed for this study as the "Boulder reach" (Figure A-2). For the purpose of this analysis, the Golden fault is equivalent to fault A + D of Figure A-13a, and the Boulder reach is equivalent to fault A of Figure A-13a.

The Golden fault extends from just south of the RFP to near Mount Carbon, a length of about 30 km. The Boulder reach of the Front Range fault system is not coincident with a mapped surface fault, but is inferred to be a blind or buried structure from Coal Creek Canyon 4 km west of the RFP to Rabbit Mountain to the north. The length of the Boulder reach is about 50 km. The Golden fault and Boulder reach are the faults that are the closest elements of the Front Range fault system to the RFP and, for this analysis, they are the faults of the Front Range fault system have the most potential significance to the seismic hazard at the site. As appropriate, information related to other parts of the system are used to assist in characterizing the Golden-Boulder reaches.

The logic tree for the Golden-Boulder reaches is shown in Figure A-18 and is discussed below.

Seismogenic Potential. Using the criteria for seismogenic potential discussed previously, the assessments for the Golden-Boulder reaches of the Front Range fault system are the following:

Criterion	Probability,P	P x W
Association with M>5 seismicity	0.2	1.4
Association with M<5 seismicity	0.2	1.2
Geologically recent slip	0.5	4.5
Structural association	0.7	3.5
Crustal extent	0.9	1.8
Favorable stress/tectonic analogue	0.8	0.8

The only M>5 earthquake that has occurred in the historical record that could have occurred on the Golden-Boulder reaches is the 1882 Colorado earthquake. Original assessments of the location of this earthquake (Hadsell, 1968) placed it near Boulder with a magnitude between 5.0 and 6.7. Subsequent studies (Dames & Moore, 1981; McGuire and others, 1982) placed the epicenter in northwest Colorado with a magnitude of about 6.5, based on a detailed review of original intensity reports. Kirkham and Rogers (1986) reviewed some additional felt reports, re-interpreted many of the original reports of shaking, and made an analogy with the 1984 Laramie Mountains earthquake to conclude that the epicenter was near Estes Park at 40.5°N, 105.5°W, with a magnitude of about 6.2. By analogy to the deep 1984 Laramie Mountains earthquake, Kirkham and Rogers (1986) conclude that it is probable that the 1882 earthquake was also a deep event and that no or only very minor surface faulting may have resulted.

A reassessment of the magnitude and location of the 1882 earthquake was carried out for this study (Appendix C). Shown in Figure C-3 are the possible epicentral areas for the earthquake, as a function of the judged degree of confidence. In all cases only the extreme eastern edge of the possible epicentral areas would allow for the Front Range fault system to have been the causative fault for the earthquake. These findings are consistent with those of previous workers in assessing the preferred location for the event to have been within the Rocky Mountains. It is therefore concluded that there is a low probability (0.2) that the event was associated with the Golden-Boulder reaches of the Front Range fault system.

Compilations of the historical and instrumental seismicity in central Colorado show a few scattered small magnitude earthquakes in the eastern Rocky Mountains-Denver Basin region. A few of these events appear to be spatially associated with the range front, but there are too few events to arrive at a conclusion that the Golden-Boulder reaches, or any other reaches of the Front Range fault system, have a clear association with small-magnitude seismicity. Therefore, it is concluded that there is a low probability (0.2) that the fault zone is associated with M<5 seismicity.

Previous evaluations of evidence for geologically-recent slip have focused on the Golden fault, have attempted to evaluate fault "capability" (using 500 ka criteria of Appendix B to 10 CFR 100), and have concluded that there is no evidence suggesting that the Golden fault is capable. Dames & Moore (1981) investigated the Golden fault using literature search, remote sensing, field mapping, trenching at three sites, and a microearthquake survey. They also conducted field studies of the

"Quaternary graben" near Golden and concluded that there is no evidence to suggest that the graben is tectonically or structurally related to the Golden fault.

Since the time of the Dames & Moore (1981) studies, tectonic geomorphic techniques have been developed that are capable of identifying fairly low rates of activity and surface deformation that may result from buried or blind faulting. As part of the present study, some of these techniques have been applied in a preliminary way along the frontal zone of the Front Range as a means of assessing evidence for post-Cretaceous deformation along the range front boundary. These analyses are presented in Appendix B and are summarized here. The evaluation of Quaternary deformation across this boundary is very difficult because of a general lack of Quaternary geologic units that lie across the boundary. For example, the Rocky Flats Alluvium terrace surface that provides a remarkable time horizon and "strain gauge" for assessing fault displacement east of the front, is virtually absent west of the front. Detailed studies to identify and correlate terrace remnants in stream valleys within the range have not yet been carried out. A second reason that evaluations of possible Quaternary deformation are difficult is the likely low rates of deformation that are occurring. The general absence of geomorphic evidence of young faulting along the range front clearly indicates that the rate of fault slip, if occurring at all, is low.

A third reason for the difficulty in assessing young deformation is the fact that the tectonic mechanisms for such deformation are likely complex. Much of the range front boundary is marked by major blind reverse faults and folds formed during Laramide compression. The present stress regime is likely extensional (see further discussion below) and the manner in which the Laramide structures might be reactivated in this extensional stress regime is not clear. Experience in other tectonic environments that are characterized by low rates of tectonic deformation has shown that reactivation occurs along only a limited number of "favorably oriented" structures. For example, in the western Sierra foothills of eastern California, major Paleozoic and Mesozoic reverse-fault systems, several hundred kilometers long, have been mapped that accommodated subduction-related compression. However, the contemporary stress regime in this area is extensional and late Cenozoic deformation is occurring at very low rates. Detailed studies of late Cenozoic faulting (Schwartz and others, 1978, 1979; Pacific Gas and Electric Co., 1993) show the following: 1) late Cenozoic normal-slip faulting occurred as a result of reactivation of preexisting Mesozoic reverse faults, 2) late Cenozoic fault reactivation occurred only along limited portions of the Mesozoic faults and at extremely low rates, and 3) those portions of fault zones being reactivated show evidence for multiple episodes of fault displacement. Another example of reactivation is the Meers fault in Oklahoma, where the 600-km-long Wichita frontal fault zone has been reactivated locally in the late Quaternary along the 40-km-long Meers fault (e.g., Slemmons, 1991; Swan, in press). The Meers fault also shows evidence for multiple late Quaternary displacements.

Based on these examples, the reactivation of the Front Range fault system in general and the Golden-Boulder reaches in particular may be occurring along limited portions of the zone and, where reactivation has occurred, multiple displacements should be evident. The only documented case of Quaternary deformation along the range front is along the Rampart Range fault near the Air Force Academy (Dickson, 1986) and the "Quaternary graben" near Golden (Kirkham, 1977; Kirkham and Rogers, 1981; Dames & Moore, 1981). The graben near Golden is considered later in this evaluation. The Rampart Range fault is interpreted to show the best geomorphic expression of any Quaternary fault of the Front Range fault system (Kirkham and Rogers, 1981). Geomorphic analyses of range-front sinuosity show that this portion of the range front also suggests younger tectonism (Appendix B and Figure A-20). Profiles of the range crest, piedmont-mountain front junction, Eocene erosional surface, and Rocky Flats terrace remnants suggest that post-Eocence deformation has occurred and can be used to identify discrete range front segments, particularly the segment including the Rampart Range fault (approximately Fountain Creek to the South Platte River on Figure A-19). In the Golden-Boulder portion of the range front, however, the geomorphology

is more difficult to interpret. A short segment west of the RFP appears to show low sinuosity (higher rate of tectonic activity) and the Eocene erosion surface appears to be warped. Terrace remnants of the Rocky Flats alluvium do not appear to show similar warping. It is therefore concluded that geologic evidence for young deformation is present but equivocal, and the Golden-Boulder reaches are assigned a probability of displaying geologically recent slip of 0.5.

In assessing the structural association of the Golden-Boulder reaches with other active faults, we consider two possible associations: with the Rampart Range fault and with the Quaternary graben near Golden. As part of investigations conducted for the Denver Water Department (Denver Water Department, 1986; Dickson, 1986), trenches were excavated across a trace of the Rampart Range fault at the Air Force Academy and showed down-on-the-west displacement of the Douglas Mesa Gravel. Varnes and Scott (1967) correlate the Douglas Mesa Gravel with Verdos Alluvium, which contains a 600 ka ash deposit. The presence of late Quaternary displacement is consistent with the strong geomorphic expression of the Rampart Range fault zone (Kirkham and Rogers, 1981). Because the Rampart Range fault zone is in a similar tectonic position as the Golden-Boulder reaches and likely part of the same fault system, the likelihood that the two zones are structurally associated is judged to be fairly high. The large distance between the Rampart Range fault and the Boulder-Golden reaches, however, leads to some uncertainties in their structural association.

Studies of the Quaternary graben near Golden concluded that the graben is far better expressed geomorphically than the Golden fault and that the graben faults displace strata that contain a 600-700 ka ash deposit (Kirkham and Rogers, 1981). Evaluation of the graben by Dames & Moore (1981) resulted in the conclusion that the feature probably has a limited lateral extent, can be explained by both tectonic and nontectonic mechanisms for its origin, and is likely not tectonically or structurally related to the Golden fault. The limited lateral extent of the graben (less than few kilometers) would imply a limited earthquake potential (i.e., small source area and small magnitudes) as an individual seismic source. Therefore, the importance of the graben for purposes of this study is the degree to which a structural association with the Golden fault might imply geologically recent deformation on the Golden fault.

One model for how the graben might relate to the Golden fault is through an evolutionary model proposed by West (1992) for the development of normal fault systems within preexisting thrust fault terrains. The graben may represent the surface manifestation of a preexisting thrust fault that, during intermediate stages of evolution in West's model, ruptures the surface and tectonically beheads reactivated thrusts toward the leading edge of the thrust system (Fault K in Figure 12 of West, 1992). In this case the range front (Golden fault) would be the primary seismogenic fault and the graben a result of extension in the shallow parts of the crust. The principal argument against this interpretation is that the short lateral extent of the graben suggests that it is not a major preexisting thrust fault.

Based on a consideration discussed above of the possible association of the Golden-Boulder reaches with the Rampart Range fault zone, it is concluded that there is a 0.7 probability that the Golden-Boulder reaches of the Front Range fault system are structurally associated with another seismogenic fault. The relationship with the Quaternary fault near Golden is not resolved, but may also suggest an association with another seismogenic fault.

As defined for this study, the Golden-Boulder reaches of the Front Range fault system are the boundary between the eastern Rocky Mountains and the Great Plains province. This boundary is a fundamental crustal boundary that affects the entire crust. Locally, the deep seismic reflection line across the RFP west into the Front Range clearly shows a major reverse fault zone (Figure A-11). Therefore, on the basis of available data, the probability that the Golden-Boulder reaches extend to significant crustal depths is assessed to be high (0.9).

The strike of the Golden-Boulder reaches is roughly north-south and the contemporary stress field in the region is likely extensional with the maximum axis of horizontal extension in the northeast quadrant (e.g., Dart, 1985; Zoback and Zoback, 1991). The Quaternary geologic evidence at the Air Force Academy trench site on the Rampart Range fault and the graben near Golden both show normal faulting with the down-on-the-west displacement. From the available stress and geologic data the likelihood that the Golden-Boulder fault is favorably oriented relative to contemporary stresses is assessed to be fairly high (0.8).

Based on the probabilities assessed for each criterion and the products of these probabilities and their weights (P x W), the sum of the products is 13.2. Dividing this value by the total sum of the weights (30) results is a probability of 0.44. Therefore the probability that the Golden-Boulder reaches of the Front Range fault system is seismogenic is assessed to be 0.4.

Sense of Slip

Bedrock exposures of the Front Range fault system along the Golden-Boulder reach reveal a complex reverse fault system that contains both primary west-dipping and secondary east-dipping faults (Van Horn, 1957; Spencer, 1961; Van Horn, 1972; Bryant et al., 1981; Selvig, 1993). This is supported by subsurface information from deep wells near the fault zone in the Golden area (Berg, 1962) and from seismic reflection data gathered across the fault zone south of Rocky Flats Plant in the vicinity of Golden (Domoracki, 1986), and west of Rocky Flats Plant in Coal Creek Canyon (Ebasco, 1991). These data are restricted to the bedrock geometry of the fault system and do not resolve offsets within the Quaternary section.

The only direct observation of sense of slip on the Front Range fault system where it affects Quaternary age deposits is in one of the Air Force Academy trenches excavated across the Rampart Range reach of the Front Range fault system (Dickson, 1986). This exposure reveals down-on-the-west normal displacement on west-dipping bedding-parallel faults within Cretaceous bedrock that affect the overlying Douglas Mesa Quaternary gravels. Extensional deformation of Quaternary deposits is observed in the Golden graben near Clear Creek Canyon (Kirkham, 1977; Kirkham and Rogers, 1981), but this exposure can not be unequivocally associated with the Golden fault, nor is there net displacement across the feature.

The level of seismicity in the area surrounding Rocky Flats Plant is very low and therefore few earthquake focal mechanisms are available to assess fault kinematics. The only earthquakes having well constrained locations and focal mechanisms are those associated with the Rocky Mountain Arsenal swarms of 1967-68 and 1981. Focal mechanism solutions for the 1967-68 earthquakes reveal predominately normal displacement along a northwest-striking plane (Herrmann and others, 1981). Focal mechanism solutions for the March-April 1981 sequence a combination of reverse and strike-slip faulting along an approximately WSW-ENE trending plane (Bollinger and others, 1983).

A compilation of stress indicators in the region indicates a N15°W direction for the maximum horizontal stress direction (Dart, 1985; Zoback and others, 1990). These data include wellbore breakouts, downhole hydraulic fracturing experiments, and the Rocky Mountain Arsenal earthquakes. The Front Range faults west of the Rocky Flats Plant strike approximately N20°W. This parallel orientation of the regional maximum horizontal stress direction and the strike of the Front Range faults suggests that they will be activated as extensional faults in the present tectonic regime.

Based on these observations, the following sense of slip on the Golden-Boulder reaches of the Front Range fault system is assessed: normal (0.6), reverse (0.3), and strike slip (0.1).

Geometry: Dip, Total Length, and Depth of Faulting. As shown in the logic tree for the Golden-Boulder reaches (Figure A-18), the dip, total length, and depth of faulting are the elements that define the geometry. Two directions of dip are provided for in the analysis: toward the west and toward the east. A 60° west dip is estimated based on exposures of the Golden fault near Golden, interpretation of borehole data south of Pleasant View (Berg, 1962; Smith, 1964), and the interpretation of deep seismic reflection data near Coal Creek Canyon (Ebasco, 1991). As shown in Figure A-13, the major subsurface faults associated with the Front Range fault system are large west-dipping reverse faults (faults "A" and "D"). The seismic reflection profile in Figure A-13 is a time section rather than a depth section; depth correction indicates that westerly dips of these large reverse faults is about 60° consistent with the limited borehole data (Berg, 1962). The deep seismic reflection data also show an east-dipping fault at the base of the steeply-east dipping late Cretaceous-Paleozoic section (fault "C" in Figure A-13). In the analysis, strong preference (0.8) is given to the hypothesis that the Golden-Boulder reaches of the Front Range fault system have a westerly dip and are coincident with the west-dipping reverse faults seen on the seismic reflection profile. The possibility that the Golden-Boulder reaches have an easterly dip (coincident with the fault "C" in the profile) is also allowed in the analysis. This east-dipping scenario is given less weight (0.2) because there is no evidence for displacement of the flat-lying late Cretaceous-Paleozoic section on the seismic reflection profile, thus suggesting that the east-dipping fault is more likely a back-thrust and not a major seismogenic fault extending through the entire seismogenic crust.

The total length of the Golden-Boulder fault zone is uncertain and two alternative lengths are considered for this analysis. The first length is 75 km, which, after accounting for overlap, is the combined length of the two faults extending from Rabbit Mountain south to near Mount Carbon. A second scenario would extend the southern limit to include the entire range front to about Colorado Springs, a total length of about 165 km. Differences in the surface expression of faulting and structural styles leads to the slight preference of the 75 km length (0.6) over the 165 km alternative (0.4). It should be noted that the total length is used in the hazard analysis to model the location of earthquakes. In this case, the closest distance of the Golden-Boulder reaches to the RFP site is the same for both total length scenarios. Hence, the effect of the choice of total length on the hazard results is expected to be minor.

The downdip width (depth of the seismogenic crust) is estimated for the Golden-Boulder reaches based on earthquake focal depths. The typical maximum focal depths in the region and in the central U.S. in general are about 15 km (Langer and others, 1991) and that value is given greatest weight (0.8). Studies of the 1984 Laramie Mountains earthquake have shown that the focal depths for the main shock and aftershocks occurred at depths of 20 to 25 km (Langer and others, 1991). The Laramie Mountains earthquake occurred well within the Rocky Mountains tectonic province and is highly unusual for focal depths in the region to the east of the Rocky Mountains. It is therefore assessed that these anomalously deep focal depths are probably not representative of the focal depths along the range front. However, a 25 km seismogenic crustal width is allowed for in the analysis, with a low weight (0.2).

Maximum Earthquake Magnitude. To evaluate possible maximum magnitudes on the Golden-Boulder reaches, potential rupture segment lengths are first considered (Figure A-17). Three alternative lengths are considered: 30, 50, and 75 km. 30 km is the approximate length of the Golden fault and 50 km is the approximate length of the Boulder reach (Figure A-2). Although the Golden fault is mapped as a more continuous fault zone and may be a considered a possible rupture segment, the Boulder reach is likely also a relatively continuous fault in the shallow subsurface, and may more likely represent a maximum rupture segment. The range-front profile (Figure A-19; see Appendix B for discussion) indicates the elevation of various datums including the range front, the piedmont-mountain front junction, the Eocene erosional surface, and the Rocky Flats alluvial terrace

surface. The profile strongly suggests that the range front is segmented. The coincident rise and fall of all four surfaces suggests that a fairly clear 75-km-long segment exists between Fountain Creek and the South Platte River and would include the Rampart Range fault zone. North of the South Platte River in the reaches of the Front Range of importance to the RFP, the segmentation is less clear and may consist of shorter segments, such as an approximately 30-km-long segment between Clear Creek and Boulder Creek, or an approximately 50-km-long segment between the South Platte River and Boulder Creek. Based on the lengths of the Golden fault and the Boulder reach, as well as the evidence for segmentation suggested in Figure A-20, rupture lengths of 30 km and 50 km are assessed with probabilities of 0.3 and 0.5, respectively. For purposes of this study, a 75 km rupture segment length is also considered, which would, after accounting for overlap, approximate the combined lengths of the Golden and Boulder fault zones. Because this interpretation is not well-supported by the considerations of segmentation in the Golden-Boulder reaches of the fault system, this alternative is given lower weight (0.2).

After correcting downdip widths for the various fault dips, rupture areas are calculated and moment magnitudes are determined for each rupture area. The resulting distribution of maximum magnitudes is the following: 6 3/4 (0.24), 7 (0.62), and 7 1/4 (0.14).

Slip Rate. There are no direct data on the slip rate on the Golden-Boulder reaches. To make the assessment, slip rates developed from data on the Rampart Range fault and the graben near Golden are used, together with comparisons of the geomorphic expression of these faults with the Golden-Boulder reaches. Faults in the AF-1 trench at the Air Force Academy show down-to-the-west vertical displacement of the Douglas Mesa Gravel deposits (Dickson, 1986). The cumulative displacement for the 25 faults exposed in trench AF-1 totals 29.3 m (Dickson, 1986). Using simple geometric relationships and assuming all displacement occurs on a single fault, the total vertical slip is inferred to be 37.6 m. The Douglas Mesa Gravel has been correlated with the Verdos Alluvium, which contains a 600 ka ash deposit (Varnes and Scott, 1967). Using a range of 29.3 to 37.6 m, vertical slip rates of 0.049 to 0.063 mm/yr are derived. In the exposure of the graben near Golden, a down-to-the-west vertical displacement of 5.5 m is observed in Quaternary strata that contain a 600-700 ka ash deposit. This implies a vertical slip rate of 0.008 to 0.009 mm/yr.

Although the data and interpretations discussed above provide reasonable estimates of slip rate for the faults studied, the rates are most likely higher than the rates appropriate for the Golden-Boulder reaches of the Front Range fault system. This is because the Rampart Range fault and the graben near Golden display the best geomorphic expression of Quaternary faulting along the Front Range boundary. Recall that the Quaternary graben near Golden may not be tectonic and cannot be unequivocally associated with the Golden-Boulder reaches. The Golden-Boulder reaches lack such expression despite the fact that the rock type, climate, and other factors affecting geomorphic expression are equivalent along the boundary. This suggests that the rate along the Golden-Boulder reaches is lower. As an estimate of slip rates that are possible without the presence of geomorphic expression, we use the estimated slip rate for the Walnut Creek fault. Therefore, the three slip rates used and their relative weights are the following: 0.06 mm/yr (0.1), which is the rate of the Rampart Range fault; 0.009 mm/yr (0.3), which is the rate of the graben near Golden; and 0.002 mm/yr (0.6), which is the average estimated rate for the Walnut Creek fault.

Recurrence Relationships for Fault Sources

Based on the slip rate information summarized above and the magnitude-distribution model given by Youngs and Coppersmith (1985), earthquake recurrence relationships are developed for each of the fault sources. The mean recurrence curves for the Walnut Creek, Rock Creek, Valmont, and Golden-Boulder reaches of the Front Range fault system are shown in Figure A-22. The "characteristic earthquake" magnitude-distribution model of Youngs and Coppersmith (1985) is

selected because recent studies (e.g., Youngs and others, 1993) have shown this model to be more appropriate than the exponential model for characterizing the recurrence for individual faults. The *b*-value of the exponential portion of the curves is 0.75 based on the average *b*-values of the regional source zones (see Appendix D). Also shown in Figure A-22 is the recurrence relationship for the RMA/Derby source, which is based on independent instrumental seismicity (devoid of injection-related events) within a 10-km wide corridor. The observed events are assumed to follow an exponential distribution within this fault corridor and the *b*-value for this source is 1.16.

AREAL SOURCE ZONE CHARACTERISTICS

Two types of areal source zones are considered in this analysis: a local source zone (Figure A-2) and regional source zones (Figure A-23). In developing the regional source zones, other hazard studies were reviewed. Generally, our regional sources follow well-known geologic boundaries (e.g., Denver Basin), and are very similar to the zones identified by Kirkham and Rogers (1981). The basis for the zones identified for the USGS national seismic hazard maps is not documented and is not apparent based on geologic or seismicity comparisons. Studies for the "eastern" U.S. (e.g., Bernreuter et al., 1989; EPRI, 1985) focused on the region to the east of 105.00 degrees longitude and, therefore, interpretations for this region are judged to be unreliable for this study.
The basis for the definition of areal source zones is given below.

Local Source

The local source is intended to enclose a group of northeast-trending faults that are known to exist north and east of the RFP and are inferred to exist in the vicinity of the site. A zone of faults lying north of the RFP in the Marshall area are mapped by Spencer (1961) on the basis of structural/stratigraphic relationships in Cretaceous rock outcrops and inferred from local borehole data. These faults are continuous along strike to the northeast with a larger group of faults that appear on the 1:100,000 geologic map of Boulder-Fort Collins-Greeley area by Colton (1978) that are interpreted from seismic reflection data by Davis (1974). These faults occur primarily in Cretaceous strata. Faults in the Boulder-Weld coal field had been interpreted as high-angle normal faults (Spencer, 1986) or growth faults developed during the deltaic deposition of the surficial sedimentary rocks (Davis and Weimer, 1976). However, through detailed subsurface mapping, Kittleson (1992) showed that the coal beds are displaced along reverse faults that splay upwards from an underlying subhorizontal decollement.

The sharp truncation of the mapped faults of this zone (Figure A-12) is a function of the boundary of the edge of Colton's (1978) map and the faults likely are present to the southwest in the RFP vicinity. EG&G (1992, p.133) note that from RFP northward, Rock Creek, Coal Creek, and South Boulder Creek exhibit a northeast-southwest alignment that appears to be controlled by northeast-trending structures. They also note that the Upper Cretaceous stratigraphic section in this area has little coherence, due presumably to faulting. The deep seismic reflection profile through the RFP (Ebasco, 1991; Figure A-13) shows evidence of faults in the Pierre shale beneath the RFP. It is reasonable to infer that these faults are part of the regional northeast-trending fault set. The origin of the northeast-trending zone is not clear. Although the trend is consistent with the trend of some Precambrian basement structures, such as the Idaho Springs-Ralston Shear Zone, in the Front Range (Spencer, 1961), there is no apparent lateral offset of the Dakota Group sedimentary rocks (Kittleson, 1992), suggesting that the Ralston shear zone has not been active in post-Cretaceous time.

The Walnut Creek, Rock Creek, and Valmont faults are likely members of the northeast-trending fault set. They are treated separately and independently as potential seismic sources. However, the

potential activity of these faults (assessed to have probabilities of 0.3, 0.3, and 0.4, respectively) suggests that other faults of the zone may also be potentially seismogenic. Using a probability that is the average of that assessed for the three faults, a probability of 0.3 is assessed that the local areal source zone is seismogenic. Note that in the application of this assessment in the hazard analysis, there is a 0.3 probability that both the local source zone is seismogenic as well as the Denver Basin regional source I (Figure A-1). Conversely, there is a 0.7 probability that the local source is not seismogenic and, in this case, only the Denver Basin regional source I is seismogenic.

The maximum earthquake magnitude for the local source zone is assessed to be the same as that for the Walnut Creek, Rock Creek, and Valmont faults, which may be a typical elements of the fault system: 5 1/2 (0.36), 6 (0.46), 6 1/2 (0.18). The maximum credible earthquake (MCE) for the local source zone is selected to be moment magnitude 6.

Rocky Mountain Arsenal (Derby) Source Zone (RMA/Derby)

The RMA/Derby source zone is the name given to the seismogenic structure inferred as the source for the swarm of earthquake activity within the western Denver Basin triggered by borehole injection of waste fluids at the Rocky Mountain Arsenal (RMA) beginning in March 1962 (Healy and others, 1966). The seismic source is referred to as the Rocky Mountain Arsenal fault in the early literature. More recently, the source was named the "Derby fault" after a lake that lies within Rocky Mountain Arsenal near the fluid injection well. As discussed below, there is no mapped fault coincident with the zone of seismicity there. This report retains the original designation and for purposes of the hazard analysis it is referred to as the Rocky Mountain Arsenal/Derby source zone.

The location of the RMA/Derby source zone and associated source zonation is shown in Figure D-29. The RMA/Derby source zone is defined by epicenters of the 1967-8 and 1981 earthquake swarms. The 1967-8 earthquakes are characterized by normal faulting along a fault plane striking N50W with most of the events occurring at depths of between 3 and 8 km (Herrmann and others, 1981). The composite focal mechanism for the earthquake sequence of March to April 1981 shows a combination of reverse and strike-slip faulting with nodal planes of N58W/60NW and N76W/40SW (Bollinger and others, 1983). The occurrence of the 1981 sequence, well after the end of deep fluid injection, as well as the change in style of faulting between 1967-8 and 1981 is not well understood. The possibility of a complex array of fractures in a source volume has been suggested (Bollinger and others, 1983). The fact that the earthquakes occur adjacent to a change in the ambient stress field from extensional in the west to compressional in the east (Zoback and Zoback, 1991) may also be a factor. The logic tree for the RMA/Derby source zone is shown in Figure A-21 and is discussed below.

Seismogenic Potential. In discussing the "Derby fault," Kirkham and Rogers (1981) stated that they found no geophysical or geological evidence for disruption of late Tertiary strata. According to these authors, possible evidence for Quaternary fault activity prior to the post-injection swarm consists of: unusual geomorphic features in the vicinity of the RMA noted by De Voto (1968); and personal communications with J.L. Hamilton and K.E. Brand, who separately suggested that late Cretaceous and Paleocene rocks may be disrupted by faulting on the northern and southern limits of the mapped fault. Kirkham and Rogers concluded that the existence of the "Derby fault" is uncertain and that "...a great deal remains to be learned about this fault."

Healy and others (1966) conducted detailed geologic, geophysical, and seismologic investigations into the earthquake activity at the RMA, which at that time was only suspected of being associated with borehole injection of waste fluids. Lindvall (Part 1 in Healy and others, 1966), in writing on the geology of the RMA area, noted that there are no known faults that cut either the exposed bedrock surface or overlying surficial deposits in the mapped area. The closest known faults to the

site displace Cretaceous and Paleocene rocks and lie far to the west in the Morrison and Golden quadrangles and in the Louisville quadrangle near Superior about 15 mi northwest of the RMA. Scott (1970) reported a fault with apparent Quaternary displacement west of Superior near Boulder.

De Voto (1968) conducted Quaternary geologic mapping studies in the RMA area and found no apparent evidence for faulting over the past 5 ka and equivocal evidence for Pleistocene fault activity. He noted a pronounced 20-foot step in the Broadway terrace (pre-Wisconsin age) northwest of the RMA disposal well that falls within the elliptical zone of earthquake epicenters defined by Healy and others (1966). This feature also is aligned with a northwest-trending, bedrock paleovalley that he suggested may be the buried trace of a pre-Yarmouth age fault. From this evidence De Voto suggested pre-Wisconsin surface faulting May have occurred, perhaps related to the RMA/Derby source. He also noted that these same features (topographic step in the terrace, bedrock outlier) can be explained by normal geomorphic processes without requiring tectonic faulting.

Therefore, the sole dataset for the existence of the RMA/Derby source zone, and hence for evaluating its seismogenic potential, is observed seismicity. Clearly, the association of the source zone with small-magnitude earthquakes confirms that it is capable of generating M<5 events. On the basis of the dimensions of the zone, its downdip extent, and continuing seismicity well after termination of fluid injection, it is concluded that the ongoing seismicity represents tectonic stress release (Bollinger and others, 1983). Because of the unusual nature of the RMA/Derby source zone relative to the other faults evaluated for this assessment (e.g., there is no known geologic structure coincident with what is called the "RMA fault" or the "Derby fault"), it is difficult to apply the evaluation criteria for faults. Although it is clear that the RMA/Derby source is capable of generating M<5 earthquakes, there is some uncertainty in its ability to generate larger earthquakes. There is no unequivocal evidence for deformation of Quaternary deposits and available geologic and geophysical studies show no clear evidence of faulting. The probability that the Derby fault is seismogenic is therefore assessed to be 0.5.

Sense of Slip

Because the RMA/Derby source zone is not a fault zone, there is no geologic evidence for the sense of slip. Instead, the estimates of the sense of slip come from earthquake focal mechanisms and considerations of the regional stress regime. Focal mechanisms associated with the 1967-68 sequence show primarily normal fault mechanisms along northwest-trending faults (Herrman and others, 1981). Composite focal mechanisms for the 1981 sequence shows a combination of reverse and strike slip mechanisms (Bollinger and others, 1983). Regional considerations of stress (e.g., Zoback and Zoback, 1991) indicate that the axis of maximum extension is in the northeast quadrant, suggesting that normal faulting would be favored along northwest-trending faults, as inferred for the RMA/Derby source zone. Based on these data and interpretations, the sense-of-slip models and their relative weights are the following: normal (0.4), reverse (0.3), and strike slip (0.3). Clearly, there is considerable uncertainty in this assessment. Slightly greater weight is given to the normal faulting model because it is consistent with the regional tectonic stress field.

Geometry. In their discussion of the 1960's RMA earthquakes, Kirkham and Rogers (1981) cite the U.S. Geological Survey study by Healy and others (1966) indicating that 62 earthquakes recorded over a 2-month period in January and February of 1966 occurred in an N60W-trending ellipsoidal zone about 10 km long and 3 km wide. The earthquakes in this zone ranged from 5 to 6 km depth. It was inferred that these earthquakes were defining the active part of a fault or fracture zone, which Kirkham and Rogers (1981) refer to as the Rocky Mountain Arsenal fault. Healy and others (1968) pointed out that two lines of evidence point toward a tectonic origin for the earthquakes in the area: (1) the pre-1967 earthquakes have a frequency-magnitude relationship

similar to that found in tectonically active areas, and (2) the distribution of earthquakes, consistent fault plane solutions, and presence of fracturing in cores from the borehole suggest a zone of vertical fracturing. The fault-plane solutions (Healy and others, 1966, 1968) indicated right-lateral strike-slip movement on a near vertical fault plane.

Other sources of information (Hsieh and Bredehoeft [1981]; Hermann and others [1981], and Bollinger and others [1983]) make little mention the existence of a fault associated with the RMA earthquakes. Hsieh and Bredehoeft (1981) use a map of epicenters to define an elliptical zone about 10 km x 3 km with a trend of about N55W. The location of their source, based on epicenters, is north of the RMA injection well.

Hermann and others (1981) conducted surface wave analysis for earthquake events that occurred in April, August, and November of 1967 and joint hypocentral relocation studies for 289 earthquakes recorded between 1967 and early 1969. The surface wave studies showed T- and P-axis orientations indicative of normal faulting. The joint hypocentral relocation studies did not yield a definite fault plane, but defined a hypocenter pattern trending N50W with most events occurring about 5 km northwest of the injection well and at depths of 3 to 8 km. While the joint hypocenter relocation studies did not clearly define a fault plane, clustering of hypocenters provided weak evidence for a southwest-dipping fault plane above 5 km and a vertical to slightly northeast dipping fault plane below 5 km. A review of microearthquake data and simulation of seismoscope traces performed in this study also support the interpretation of a northwest-trending normal fault.

The available evidence can be used to develop two alternative geometries for the RMA/Derby source zone. The dimensions of the zones are derived from the epicentral location of earthquakes recorded from 1902 through 1989, excluding the seismicity considered to be resultant of high pressure fluid injection. Earthquake events from 1981 through 1984 and most of the 1967 and 1968 events fall within a relatively tight zone that trends to the northwest. This elliptical pattern of earthquake epicenters is given as Geometry 2 in Figure D- 29. This is our preferred zonation and receives a 0.7 weighting for the hazard model. The remainder of events within the zone given as Geometry 1. Because this zone is controlled by some older poorly located earthquakes (e.g., the 1902 earthquake on the north end whose location is indicated to be at the degree). This alternative geometry is given a weight of 0.3.

Maximum Earthquake Magnitude. Maximum earthquake magnitudes are estimated for the RMA/Derby source zone based on considerations of possible rupture areas, defined from the pattern of seismicity, as well as considerations of the absence of surface expression. Two alternative maximum depths are considered: 8 km, which is the approximate maximum depths of well-recorded seismicity; and 15 km, which is the average maximum depth of seismicity in the region. Higher weight is given to the 15 km (0.7) because, if the source is a seismogenic source, it will likely have maximum downdip dimensions that are comparable to those of estimates of the thickness of the seismogenic crust regionally.

A critical observation in the assessment is the absence of geomorphic or geologic evidence for Quaternary faulting. Reconnaissance following the earthquake swarms did not find evidence for surface rupture. Available evidence suggests that the Quaternary alluvial terrace deposits are not disturbed by faulting in the RMA/Derby source zone area, with the possible exception of a 20 foot `step' in the pre-Wisconsin (about 115 ka) Broadway terrace. This `step' is not a scarp (occurs over a horizontal distance of about 2,000 feet) and is present only along a short part of the zone of observed seismicity.

As shown on the logic tree for the RMA/Derby source zone (Figure A-21), the assessment of maximum earthquake magnitude is made conditional on which geometry is assumed. As discussed

previously in the context of the Walnut Creek fault, the absence of surface faulting and surface expression suggests that the maximum magnitude should lie between 5 1/2 and 6 1/2. The maximum length of the zone in Geometry 2 is about 15 km, which is compatible in length with ruptures of about magnitude 6 (see Wells and Coppersmith, 1994). Therefore, assuming Geometry 2, the maximum magnitude distribution for the RMA/Derby source zone is 5 1/2 (0.2), 6 (0.6), 6 1/2 (0.2). Assuming Geometry 1, the maximum dimension of the source zone is about 30 km. Although the observed seismicity does not suggest a continuous fault along this length, a low probability scenario is allowed that would imply the rupture of this entire 30 km length and would result in a magnitude 6 3/4. This scenario is given a low weight of 0.1. The combination of the low weight (0.1) for this magnitude with the low weight assigned to Geometry 1 (0.3) results in a very low weight (0.03) for the 6 3/4 maximum magnitude estimate. The maximum magnitude distribution assuming Geometry 1 is the following: 5 1/2 (0.2), 6 (0.5), 6 1/2 (0.2), 6 3/4 (0.1).

Recurrence Approach

The assessment of earthquake recurrence for the RMA/Derby source zone is uncertain. Two approaches are considered: the use of observed seismicity to constrain recurrence rates, and estimated fault slip rates. These two approaches are given equal weight (0.5). The assessment of the recurrence rate for the RMA/Derby source zone using observed seismicity data is discussed in Appendix D and includes the removal of events that are assessed to be related to injection. To evaluate recurrence using fault slip rate, slip rates for the source were estimated, as described below.

Fault Slip Rate

Because the RMA/Derby source zone is not coincident with a known mapped fault, there are no direct geologic data from which to evaluate the fault slip rate. However, estimates can be made based on observations of the geomorphic expression of the possible causative fault. De Voto (1968) identified a 20 foot (6 meter) `step' in the Broadway terrace that he postulated could be related to faulting. Assuming an approximate age of 115,000 yr for the Broadway terrace, the derived slip rate would be 0.06 mm/yr. An alternative estimate of slip rate is the estimated rate of the Walnut Creek fault, 0.002 mm/yr. This rate is believed to be credible for the RMA/Derby source because it is a rate that appears to be compatible with faulting at a rate low enough to preclude geomorphic expression. Because the evidence for possible deformation of the Broadway terrace is equivocal and is limited to a single location (i.e., no geomorphic evidence for faulting is noted along most of the trend of the RMA/Derby source zone), a lower weight is given to the slip rate based on the 20 foot displacement (0.3) and a higher weight is given to the rate compatible with an absence of surface expression (0.7).

Denver Basin (Regional Source I)

The RFP site lies within the Denver Basin regional source (Figure A-23). The configuration of this areal source is drawn according to the outline of the Denver basin depicted in the Petroleum Information Corp. Oil and Gas map of the United States (1983). The unconformable contact between Pennsylvanian and Ordivician age sediments defines the structural contour of the basin boundary (Anderman and Ackman, 1963). The deepest portion of the basin lies along a synclinal axis directly adjacent and parallel to the range front of the Rocky Mountains. Late Cretaceous subsidence of the basin accompanied uplift of the Colorado Front Range and therefore the basin likely represents a foreland basin to the Laramide contractional orogen.

The level of seismicity with the Denver Basin source has been low during the historical and instrumental period. The majority of seismic activity within the Denver Basin Source occurs in the Denver area and scattered along the eastern range front of the Front Range. Most of the earthquake activity in the Denver area is related to induced seismicity associated with waste disposal by well

injection at the Rocky Mountain Arsenal (discussed previously as the RMA/Derby source in this analysis). Several historical events located by intensity data occur at the southern end of the source. It is interesting to note that these events are located in the vicinity of two potentially Quaternary active faults, the Fowler and Cheraw faults (Kirkham and Rogers, 1981) that are nearly coincident with the southern basin boundary.

Assessments of the location of the 1882 Colorado earthquake (Appendix C) conclude that it is unlikely that the earthquake occurred within the Denver Basin source. However, if the earthquake did occur in the source, it would be important to estimates of the maximum magnitude. The magnitude of the 1882 earthquake is defined by the following:

5.0 0.3 weight = 10%
6.4 0.3 weight = 80%
6.9 0.2 weight = 10%

The assessment of maximum magnitude for the Denver Basin source is made as a function of whether or not the 1882 earthquake is assumed to have occurred within the Denver Basin source. If the 1882 earthquake is assumed to have occurred within the source, the maximum magnitude for regional Source I is assessed to be: 5 1/2 (0.3), 6 1/2 (0.6), and 7 (0.1). This maximum magnitude distribution takes into account the uncertainties in the size of the 1882 event, as well as the apparent absence of significant Quaternary faults within the source (see discussion of the threshold of surface faulting in the Walnut Creek maximum magnitude description). If the 1882 earthquake is assumed to <u>not</u> have occurred within regional source I, the maximum magnitude is assessed to be the following: 5 1/2 (0.5), 6 (0.5). This maximum magnitude distribution is based on a consideration of the historical seismicity and the absence of significant Quaternary geologic structures. The largest historical earthquake within this source is magnitude 4.3 to 5.0. The Denver Basin source specifically excludes the fault sources in the site vicinity, the RMA/Derby source, the local areal source, as well as the Golden-Boulder fault.

Eastern Rocky Mountains (Regional Source II)

The boundaries of the Eastern Rocky Mountains Source (Figure A-23) are drawn on the basis of both topographic and tectonic characteristics and generally conform to the Eastern Mountain Province of Kirkham and Rogers (1981). The western boundary is drawn along, but does not include, structures associated with the Rio Grande rift. To the north, where the rift is not present or is insufficiently defined, the boundary is drawn along the range front of the Medicine Bow Mountains and includes the Middle and South Parks. The eastern boundary is shared with the Denver basin and continues south along the eastern range front of the Rocky Mountains. The southeastern margin is drawn along the eastern boundary to the Rio Grande rift in the Sangre De Cristo Range and includes the Wet Mountains.

Seismic activity in this source is very low and earthquake epicenters do not appear to be associated spatially with mapped faults within the range. As discussed in Appendix C, there is some likelihood that the 1882 Colorado earthquake occurred within this source. Therefore, the assessment of the maximum magnitude for regional Source II is made conditional on whether or not the 1882 earthquake occurred within it. If the event is assumed to have occurred within the source, the maximum magnitude distribution is assessed to be the following: 5 1/2 (0.1), 6 1/2 (0.8), 7 (0.1). This distribution approximates the uncertainties associated with the magnitude of the 1882 earthquake. If the 1882 earthquake is assumed to <u>not</u> have occurred within the source, the maximum magnitude distribution is: 5 1/2 (0.2), 6 (0.6), 6 1/2 (0.2). The largest historical earthquake (excluding the 1882 event) is 3.6 to 4.3. The maximum magnitude distribution reflects the low magnitudes of historical earthquakes as well as the apparent absence of significant Quaternary faults,

such that earthquakes likely occur at or below the threshold of surface rupture (see Walnut Creek maximum magnitude discussion of the threshold of surface rupture).

The Western Colorado/Rio Grande Rift Source (Regional Source III)

The Western Colorado Source contains the Rio Grande Rift, the western Rocky Mountains and the Colorado Plateau. The eastern boundary (Figure A-23) is shared with the Eastern Rocky Mountains Source and the western, northern and southern boundaries are defined by the border of the state of Colorado.

The majority of seismic activity in the state of Colorado is located within this source. Much of the seismicity is associated with the Rio Grande rift system in southern and south-central Colorado. There is a diffuse pattern of seismic activity in the Colorado Plateau with no apparent regional causative structure. The largest historical earthquake within this source is the 1882 Colorado earthquake or, if the 1882 event is not assumed to have occurred within the source, 4.3 to 5.0.

The Rio Grande Rift system contains abundant late Quaternary normal faults and it is possible that the extensional stresses that characterize this source could lead to reactivation of preexisting faults within other parts of the source. Because of the presence of major Quaternary faults and the likelihood that the 1882 earthquake occurred within this source, the maximum magnitude distribution assessed is assessed to be: 6 1/2 (0.2), 7 (0.6), 7 1/2 (0.2).

The Great Plains Sources (Regional Sources IV & V)

The Great Plains physiographic province lies east of the Rocky Mountains range front in the south and east of the Denver Basin in the north (Figure A-23). The province is divided into a northern and southern source in the state of Colorado at approximately 38°30" N latitude. The boundary between the northern and southern Great Plains sources is somewhat arbitrary; however the southern source represents an area of higher relief and exposure of bedrock at the surface. Only diffuse and minor earthquake activity is present in the southern source and is entirely absent in the northern source zone. The largest historical earthquake within this source is magnitude 4.6.

Given the small historical earthquakes and the lack of mapped Quaternary faults, the maximum magnitudes for the Great Plains sources is 5 1/2 (0.5), 6 (0.5).

REFERENCES

Anderman, G.G. and E.J. Ackman (1963). Structure of the Denver-Julesburg Basin and Surrounding Areas, *in* Guidebook to the Geology of the Northern Denver Basin and Adjacent Uplifts - Rocky Mountain Association of Geologists, 14th Field Conference, 1963 - Rocky Mountain Association of Geologists, Denver, Colorado, p. 170-173.

Anderson, J.G. (1979). Estimating the seismicity from geological structure for seismic risk studies, *Bulletin of the Seismological Society of America*, v. 69, p. 135-158.

Berg, R.R. (1962). Subsurface interpretation of the Golden fault at Soda Lakes, Jefferson County, Colorado, *American Association of Petroleum Geologists Bulletin*, v. 46, no. 11, p. 704-707.

Bernreuter, D.L., J.B. Savy, R.W. Mensing and J.C. Chen (1989). Seismic hazard characterization of 69 nuclear plant sites east of the Rocky Mountains, U.S. Nuclear Regulatory Commission NUREG/CR-5250, UCID-21517, 8 volumes.

Bieber, D.W. (1983). Gravimetric evidence for thrusting and hydrocarbon potential of the eastern flank of the Front Range, *in* J.D. Lowell, ed., Rocky Mountain foreland basins and uplifts, Rocky Mountain Association of Geologists, Denver, Colorado, p. 245-256.

Bollinger, G.A., M.J. Adams, R.F. Henrisey and C.J. Langer (1983). The Denver Earthquake Sequence of March-April 1981, *Earthquake Notes*, Vol. 54, No. 2, p. 3-12.

Brewer, J.A., R.W. Allmendinger, L.D. Brown, J.E. Oliver and S. Kaufman (1982). COCORP profiling in southern Wyoming, Part 1: Laramide structure, *Geological Society of America Bulletin*, v. 93, p. 1242-1252.

Bryant, B., L.W. McGrew and R.A. Wobus (1981). Geologic map of the Denver 1° x 2° quadrangle, north-central Colorado: U.S. Geological Survey Miscellaneous Investigations Series Map I-1163.

Colton, R.B. (1978). Geologic Map of the Boulder-Fort Collins-Greeley Area, Colorado, U.S. Geological Survey Misc. Geol. Inv. Map I-855-G, Scale 1:100,000.

Coppersmith, K.J. (1991). Seismic source characterization for engineering seismic hazard analysis, *Proceedings of the Fourth International Seismic Zonation Conference*, v.1, p. 1-60.

Coppersmith, K.J. and R.R. Youngs (1986). Capturing uncertainty in probabilistic seismic hazard assessments within intraplate environments, *Proceedings of the Third National Conference on Earthquake Engineering*, v. 1, p. 301-312.

Dames & Moore (1981). Geological and seismological investigations for Rocky Flats Plant, Final Rep., July 9, 1981, Contract No. DI-AC04-80AL10890, U.S. Dept. of Energy.

Dart, R. (1985). Horizontal-stress directions in the Denver and Illinois basins from the orientations of borehole breakouts, U.S. Geological Survey Open-File Report 85-733.

Davis, T.L. (1974). Seismic Investigation of Late Cretaceous Faulting Along the East Flank of the Front Range, Colorado School of Mines Ph.D. Thesis 1681, 65 p.

Davis, L.T. and R.J. Weimer (1976). Late Cretaceous growth faulting, Denver Basin, Colorado, Professional Contributions of the Colorado School of Mines, No. 8, p. 280-300.

Dart, R. (1985). Horizontal Stress Directions in the Denver and Illinois Basins from the Orientations of Borehole Breakouts, U.S. Geological Survey Open-File Report 85-733, 41 p.

Denver Water Department (1986). Geologic and seismotectonic investigations central Front Range, Colorado, Geotechnical Advisory Committee, Denver Water Department, Denver, CO, January.

De Voto, R. (1968). Quaternary history of the Rocky Mountain Arsenal and environs, Adams County, Colorado, *in*, J. Hollister and R. Weimer, eds., Geophysical and geological studies of the relationships between the Denver earthquakes and the Rocky Mountain Arsenal well, Part A, *Colorado School of Mines Quarterly*, v. 63, p. 113-127.

Dickson, P.A. (1986). Investigation of the Rampart Range Fault at the Air Force Academy Trench Site, Colorado Springs, Colorado, *in* W.P. Rogers and R.M. Kirkham, eds., Contributions to Colorado Seismicity and Tectonics - A 1986 Update - Colorado Geological Survey Special Publication 28, p. 211 - 227.

Domoracki, W.J. (1986). Integrated geophysical survey of the Golden thrust north of Golden, Colorado: Masters thesis, Colorado School of Mines.

Ebasco (1991). EG&G Rocky Flats line RFD-1, (unpublished seismic reflection profile, processed by Vector Seismic Data Processing Inc.)

Ebasco (1991). Task 3, Shallow, high-resolution seismic reflection profiling inoperable unit 2 (903 pad, east trenches, and mound) at the Rocky Flats Plant, final report, prepared for EG&G Rocky Flats and U.S. DOE.

EG&G (1990). Draft Geologic Characterization Report: Prepared for the U.S. Department of Energy, Rocky Flats Plant.

EG&G (1991a). Task 3, Shallow, High Resolution Seismic Reflection Profiling in Operable Unit 2 (903 Pad, Mound, and East Trenches) at the Rocky Flats Plant, Final Report, Prepared for the U.S. Department of Energy, Rocky Flats Plant, Submitted by EBASCO, March.

EG&G (1991b). Geologic Characterization Report, Prepared for the U.S. Department of Energy, Rocky Flats Plant, July.

EG&G (1992). Phase II Geologic Characterization - Data Acquisition, Final Report, Prepared for the U.S. Department of Energy, Rocky Flats Plant, Submitted by EBASCO, March.

Electric Power Research Institute (EPRI) (1985). Seismic hazard methodology for the Central and Eastern United States, EPRI NP-4726.

Erslev, E.A. (1986). Basement balancing of Rocky Mountain foreland uplifts, *Geology*, v. 14, p. 259-262.

Erslev, E.A., J. Rogers and M. Harvey (1988). The northeastern Front Range revisited: Compression and crustal wedging in a classic locality for vertical tectonics, *in* G.S. Holden, ed., Geological Society of American faitle trip guidebook 1988: Colorado School of Mines Professional Contribution 12, p. 122-133.

Hadsell, F.A. (1968). History of earthquake activity in Colorado, *in*, J. Hollister and R. Weimer, eds., Geophysical and geological studies of the relationships between the Denver earthquakes and the Rocky Mountain Arsenal Well, *Colorado School of Mines Quarterly*, v. 63, no. 1, p. 57-72.

Hanks, T.C. and H. Kanamori (1979). A moment-magnitude scale, *Journ. Geophy. Res.*, v. 84, no. B5, p. 2348-2350.

Harms, J.C. (1964). Structural history of the Southern Front Range, *The Mountain Geologist*, Vol. 1, No. 3, p. 93-101.

Healy, J.H. and others (1966). Geophysical and geological investigations relating to earthquakes in the Denver area, Colorado, U.S. Geological Survey Open-File Report, Parts 1-5, 90 p.

Healy, J.H., W.W. Rubey, D.T. Griggs and C.B. Raleigh (1968). The Denver earthquakes, *Science*, v. 161, no. 3848, p. 1301-1310.

Herrmann, R.B., S.Y. Park and C.-Y.Wang (1981). The Denver Earthquakes of 1967-1968, *Bulletin of the Seismological Society of America*, Vol. 71, No. 3, p. 731-745.

Hsieh, P.A. and J.D. Bredehoeft (1981). A reservoir analysis of the Denver earthquakes, a case of induced seismicity, *Journ. Geophy. Res.*, v. 86, no. B2, p. 903-920.

Kirkham, R.M. (1977). Quaternary movements on the Golden fault, Colorado, *Geology*, v. 5, p. 689-692.

Kirkham, R.M. and W.P Rogers (1981). Earthquake Potential in Colorado - A Preliminary Evaluation, Colorado Geological Survey, Bulletin 43, 171 p.

Kirkham, R.M. and W.P. Rogers (1986). An interpretation of the November 7, 1882 Colorado earthquake: *in* W.P. Rogers and R.M. Kirkham, eds., Contributions to Colorado Seismicity and Tectonics-A 1986 Update, Colorado Geological Survey Special Publication 28, p. 122-144.

Kittleson, K. (1992). Decollement faulting in the northwest portion of the Denver Basin, *The Mountain Geologist*, v. 29, p. 65-70.

Kulkarni, R.B., R.R. Youngs and K.J. Coppersmith (1984). Assessment of confidence intervals for results of seismic exposure analysis, *Proceedings of the Eighth World Conference on Earthquake Engineering*, v. 1, p. 263-270.

Langer, C.J., R.A. Martin, C.K. Wood, G.L. Snyder and G.A. Bollinger (1991). The Laramie Mountains, Wyoming, earthquake of 18 October 1984, A report on its aftershocks and seismotectonic setting, U.S. Geol. Survey Open-File Report 91-258, 41 p.

Lowell, J.D., ed. (1983). Rocky Mountain foreland basins and uplifts, Rocky Mountain Association of Geologists, Denver, Colorado, 392 p.

Matthews, V., III. and D.F. Work (1978). Laramide folding associated with basement block faulting along the northeastern flank of the Front Range, Colorado, *in* V. Matthews, III, ed.., Laramide folding associated with basement block faulting, Geological Society of America Memoir 151, p. 101-124.

McGuire, R.K., A. Krusi and S.D. Oaks (1982). The Colorado earthquake of November 7, 1882: Size, epicentral location, intensities, and possible causative fault, *The Mountain Geologist*, v. 19, p. 11-23.

Narr, W. (1990). Deformational behavior and kinematics of basement-involved structures and joint spacing in sedimentary rocks, Ph.D. thesis, Princeton, New Jersey, Princeton University, 243 p.

Narr, W. and J. Suppe (1989). Kinematics of low-temperature, basement-involved compressive structures, Geological Society of America Abstracts with Programs, v. 21, no. 6, p. A137.

National Research Council (1988). Probabilistic Seismic Hazard Analysis, National Academy Press.

Pacific Gas and Electric Company (1993). Evaluation of fault behavior and earthquake potential in the Sierra foothills of California, Geosciences Department, San Francisco, California.

Petroleum Information Corp. (1983). Oil and Gas Map of the United States Including Basins, Uplifts and Basement Rocks, Petroleum Information Corporation.

Prucha, J.J., J.A. Graham and R.P. Nickelson (1965). Basement-controlled deformation in Wyoming Province of Rocky Mountain foreland, *American Association of Petroleum Geologist Bulletin*, v. 49, p. 966-992.

Purcaru, G. and H. Berkhemer (1982). Quantitative relations of seismic source parameters and a classification of earthquakes, *Tectonophysics*, v. 84, p. 57-128.

Reiter, L. (1991). *Earthquake Hazard Analysis, Issues and Rights*, Columbia University Press, New York, 254 p.

Schmidt, C.J., R.B. Chase and E.A. Erslev, eds. (1993). Laramide Basement Deformation in the Rocky Mountain Foreland of the Western United States, Boulder, Colorado, Geological Society of America Special Paper 280, 365 p.

Schwartz, D.P., D.M. Hitchcock and M.E. Perkins (1978). Basement control of late Cenozoic extensional faulting in the Sierra foothills, California (abs.), *Earthquake Notes*, v. 49, p. 89.

Schwartz, D.P., L.S. Cluff and K.J. Coppersmith (1979). Fault reactivation: an example from the western Sierra foothills, CA (abs.), *EOS Trans. American Geophysical Union*, v. 60, p. 320.

Scott, G.R. (1970). Quaternary Faulting and Potential Earthquakes in East-Central Colorado, in Geological Survey Research 1970, Chapter C, U.S. Geological Survey Prof. Paper 700-C, p. C11-C18.

Scott, G.R. (1975). Laramide (Late Cretaceous-early Tertiary) orogeny in the southern Rocky Mountains, *in* B.F. Curtis, Cenozoic history of the southern Rocky Mountains, Geological Society of America Memoir 144, p. 1-44.

Scott, G.R. and W.A. Cobban (1965). Geologic and biostratigraphic map of the Pierre Shale between Jarre Creek and Loveland, Colorado, U.S. Geological Survey Miscellaneous Geologic Investigations Map I-439.

Selvig, B.J. (1994). Kinematics and structural models of faulting adjacent to the Rocky Flats Plant, Central Colorado: Masters thesis, Colorado State University, Fort Collins, Colorado, 132 p.

Sharps, J.A. (1976). Geologic map of the Lamar quadrangle, Colorado and Kansas, U.S. Geol. Survey Misc. Geol. Inv. Map I-944.

Slemmons, D.B. (1991). Introduction, *in* D.B. Slemmons, E.R. Engdahl, M.D. Zoback and D.D. Blackwell, eds., Neotectonics of North America, Boulder, Colorado, Geological Society of America Decade Map Volume 1.

Smith, J.H. (1964). Geology of the Sedimentary Rocks of the Morrison Quadrangle, Colorado, U.S. Geological Survey Misc. Geol. Inv. Map I-428, Scale 1:24,000.

Smithson, S.B., J. Brewer, S. Kaufman and J. Oliver (1979). Structure of the Laramide Wind River uplift, Wyoming, from COCORP deep reflection data and from gravity data, *Journal of Geophysical Research*, v. 84, p. 5955-5972.

Spencer, F.D. (1961). Bedrock Geology of the Louisville Quadrangle, Colorado, U.S. Geological Survey Quad. Map GQ-151, Scale 1:24,000.

Spencer, F.D. (1986). Coal geology, and coal, oil and gas resources of the Erie and Fredrick Quadrangles, Boulder and Weld counties, Colorado, U. S. Geological Bulletin 1619, 50 p.

Stearns, D.W. (1971). Mechanisms of drape folding in the Wyoming province, Wyoming Geological Association, 23rd Annual Field Conference, Wyoming Tectonics Symposium, Guidebook, p. 82-106.

Stearns, D.W. (1978). Faulting and forced folding in the Rocky Mountain foreland, *in* V. Matthews, III., ed., Laramide folding associated with basement block faulting in the western United States, Geological Society of America Memoir 151, p. 1-37.

Swan, F.H. "Paleoseismic studies of the Meers fault, Oklahoma," U.S. Nuclear Regulatory Commission Contract No. NRC-04-077 to Geomatrix Consultants, San Francisco, California (in preparation).

Trimble, D.E. (1975). Geologic Map of the Niwot Quadrangle, Boulder County, Colorado, U.S. Geological Survey Quad. Map GQ-1229, Scale 1:24,000.

Trimble, D.E. and M.N. Machette (1979). Geologic map of the greater Denver area, Front Range urban corridor, Colorado, Misc. Inv. Series Greater Denver Area, CO, Map I-856-H.

Van Horn, R. (1957). Geologic quadrangle maps of the United States, bedrock geology of the Golden quadrangle, Colorado: U.S. Geological Survey Map GQ-103, scale 1:24,000.

Van Horn, R. (1972). Surficial and Bedrock Geologic Map of the Golden Quadrangle, Jefferson County, Colorado, U.S. Geological Survey Misc. Geol. Inv. Map I-761-A, Scale 1:24,000.

Van Horn, R. (1976). Geology of the Golden quadrangle, Colorado, U.S. Geological Survey Professional Paper 872, 116 p.

Varnes, D.J. and G.R. Scott (1967). General and Engineering Geology of the United States Air Force Academy Site, Colorado, U. S. Geological Survey Prof. Paper 551, 93 p.

Weimer, R.J. (1973). A guide to uppermost Cretaceous stratigraphy, central Front Range, Colorado: Deltaic sedimentation, growth faulting, and early Laramide crustal movement, *The Mountain Geologist*, v. 10, p. 53-97.

Weimer, R.J. (1972). Deltaic sedimentation and growth faulting, Upper Cretaceous, Colorado, AAPG Bulletin, v. 56, p. 661.

Wells, D.L. and K.J. Coppersmith (1994). Empirical relationships among magnitude, rupture length, rupture area, and surface displacement, *Bulletin of the Seismological Society of America*, in press.

West, M.W. (1992). An integrated model for seismogenisis in the intermountain seismic belt, *Bulletin of the Seismological Society of America*, v. 82, p. 1350-1372.

Wong, I.G. (1986). Tectonic stresses in Colorado and their implications to seismicity, *in* Contributions to Colorado Seismicity and Tectonics-A 1986 Update, W.P. Rogers and R.M. Kirham, eds., Colorado Geological Survey Spec. Pub. 28, p. 17-27.

Youngs, R.R. and K.J. Coppersmith (1985). Implications of fault slip rates and earthquake recurrence models to probabilistic seismic hazard estimates, *Bulletin of the Seismological Society of America*, v. 75, p. 939-964.

Youngs, R.R., K.J. Coppersmith, C.L. Taylor, M.S. Power, L.A. DiSilvestro, M.L. Angell, N.T. Hall, J.R. Wesling and L. Mualchin (1993). A comprehensive seismic hazard model for the San Francisco Bay region, *Proceedings of the Conference on Seismic Hazards in the Eastern San Francisco Bay Region.*

Youngs, R.R., F.H. Swan, M.S. Power, D.P. Schwartz and R.K. Green (1987). Probabilistic analysis of earthquake ground shaking hazard along the Wasatch Front, Utah: Assessment of Regional Earthquake Hazards and Risk Along the Wasatch Front, Utah, U.S. Geological Survey Open File Report 87-585, v. II, p. M-1-110.

Youngs, R.R., F.H. Swan and M.S. Power (1988). Use of detailed geologic data in regional probabilistic seismic hazard analysis - an example from the Wasatch Front, Utah, *in* Earthquake Engineering and Soil Dynamica Ii - Recent Advances in Ground Motion Evaluation, ASCE Geotechnical Special Publication 20, p. 156-172.

Zoback, M.L. (1988). State of stress in the Rocky Mountain region (abs.), Geol. Soc. Am. Abs. with Prog., v. 20, p. A12.

Zoback, M.D. and M.L. Zoback (1991). Tectonic Stress Field of North America and Relative Plate Motions, *in* D.B. Slemmons, E.R. Engdahl, M.D. Zoback and D.D. Blackwell, eds., Neotectonics of North America, Geological Society of America, Decade Map Volume 1, Boulder, Colorado, p. 339-366.

Zoback, M.L., M.D. Zoback, J. Adams, S. Bell, M. Suter, G. Suarez, K. Jacob, C. Estabrook and M. Magee (1990). Stress map of North America: The Decade of North American Geology, scale 1:5,000,000.

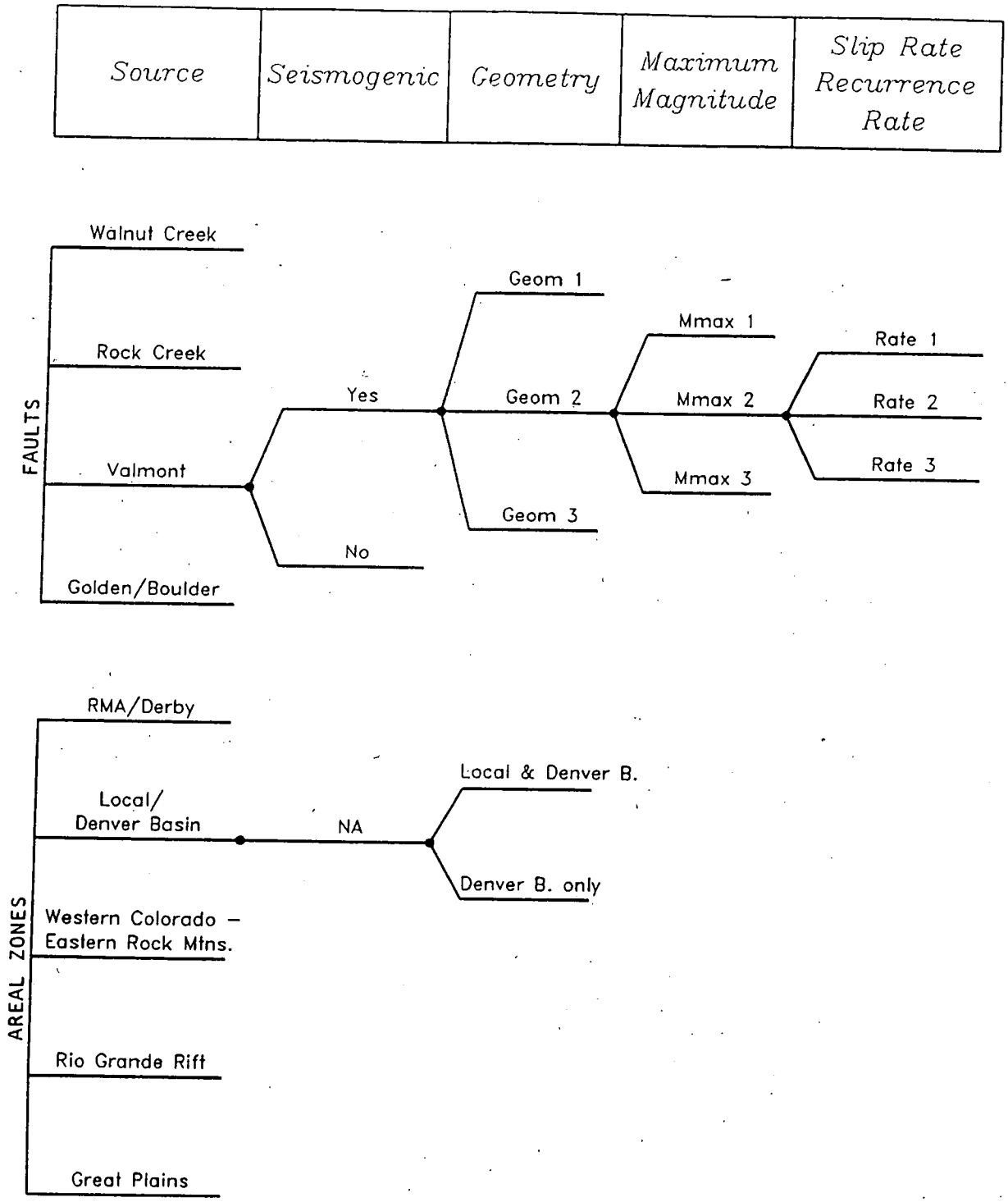

Figure A-1. General seismic source characterization logic tree.

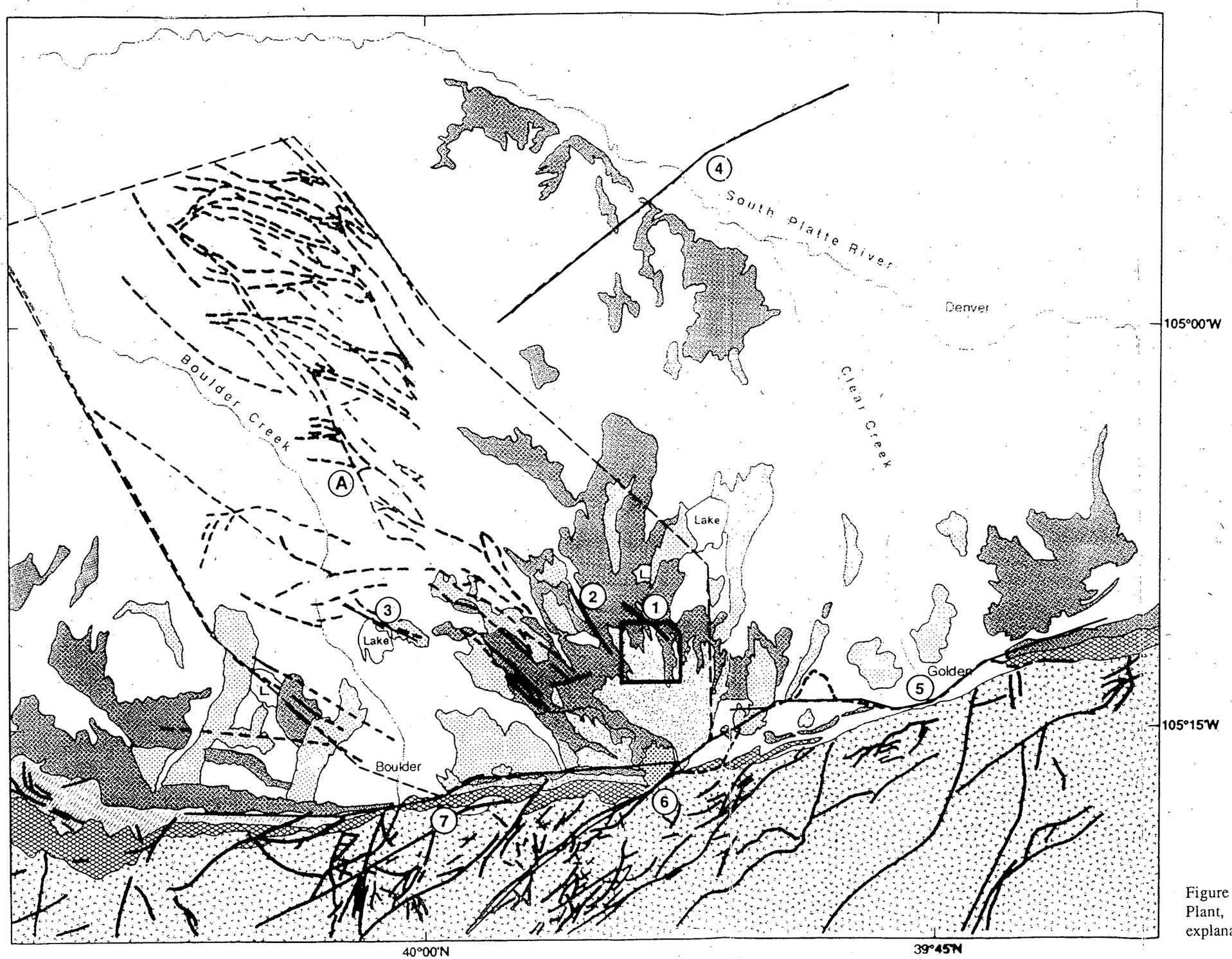

EXPLANATION

- (A) Local source zone containing northeast-trending faults
- (1) Walnut Creek fault
- (2) Rock Creek fault
- (3) Valmont fault
- (4) Derby fault of Kirkham and Rogers (1981)

Rocky Mountain Front Range Fault System

- (5) Golden fault
- (6) Livingston fault
- (7) Boulder fault

Fault source

Source zone boundary

0 3 Miles

0 5 Kilometers

Figure A-2. Local seismic sources, Rocky Flats Plant, Colorado (refer to Figure A-12 for explanation of geology).

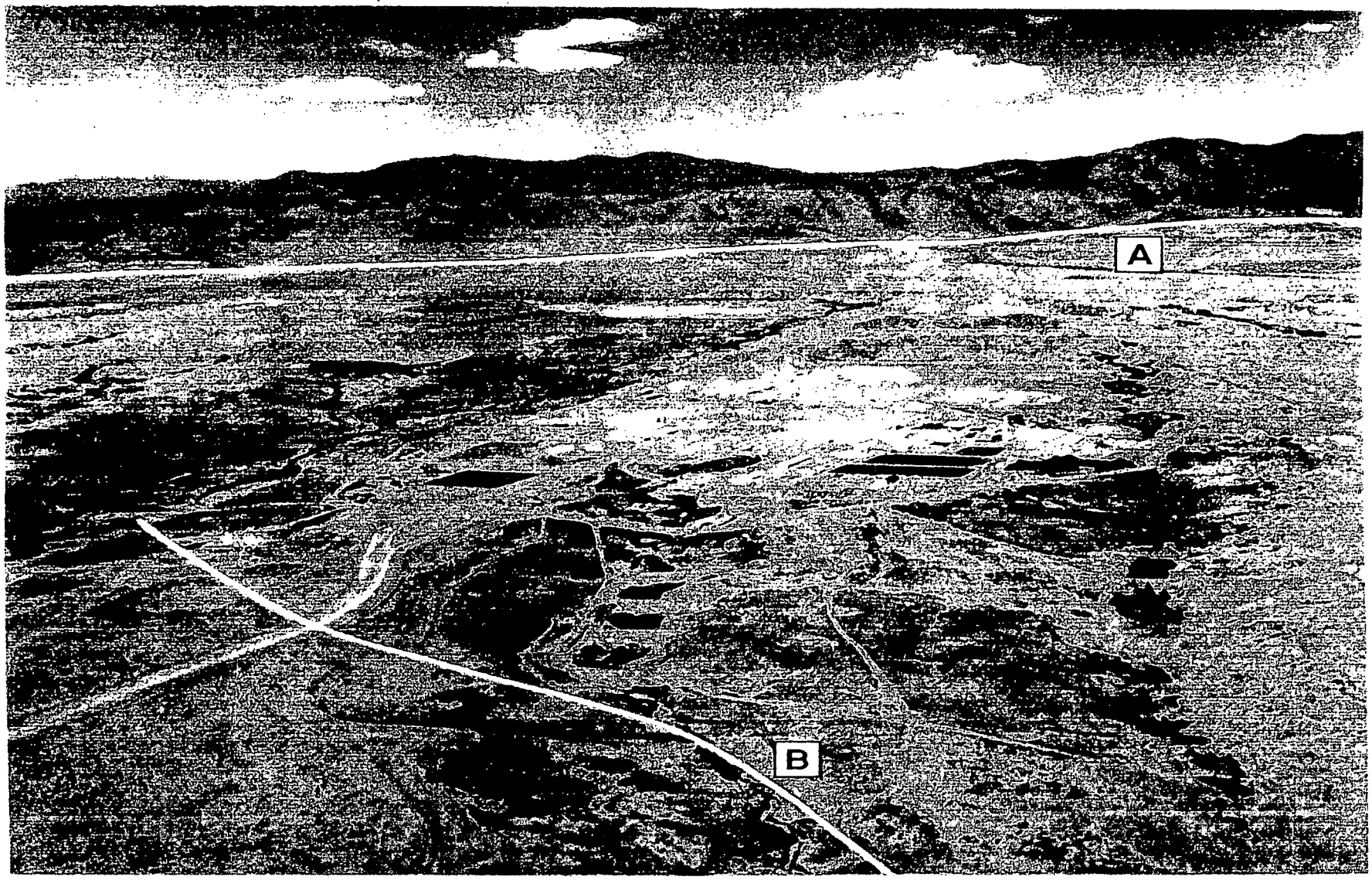

Figure A-3. Oblique aerial photograph of Rocky Flats Plant showing the approximate location of the Rocky Mountain Range Front fault system (**A**) and the Walnut Creek fault (**B**). View is to the southwest.

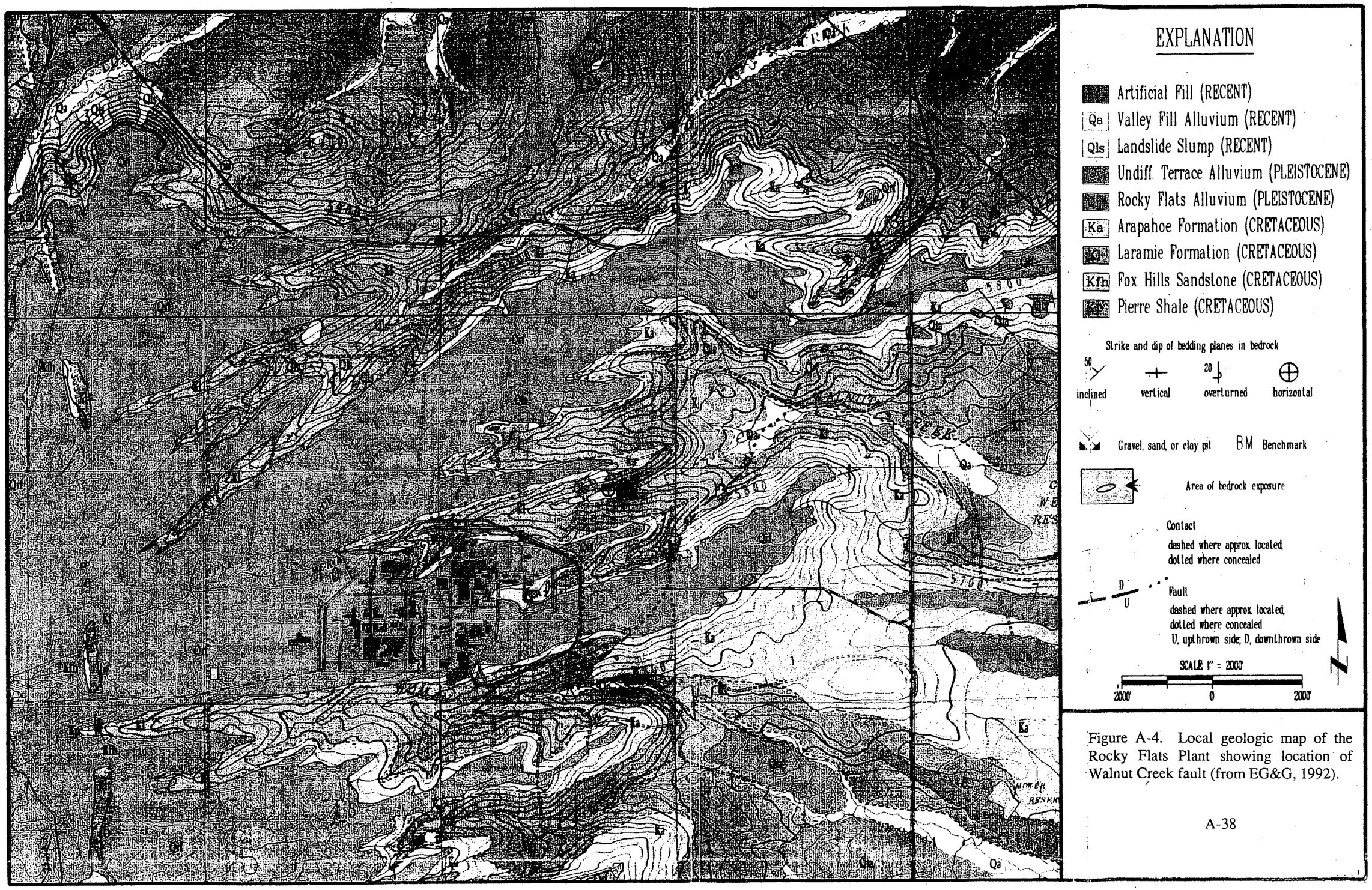

Figure A-4. Local geologic map of the Rocky Flats Plant showing location of Walnut Creek fault (from EG&G, 1992).

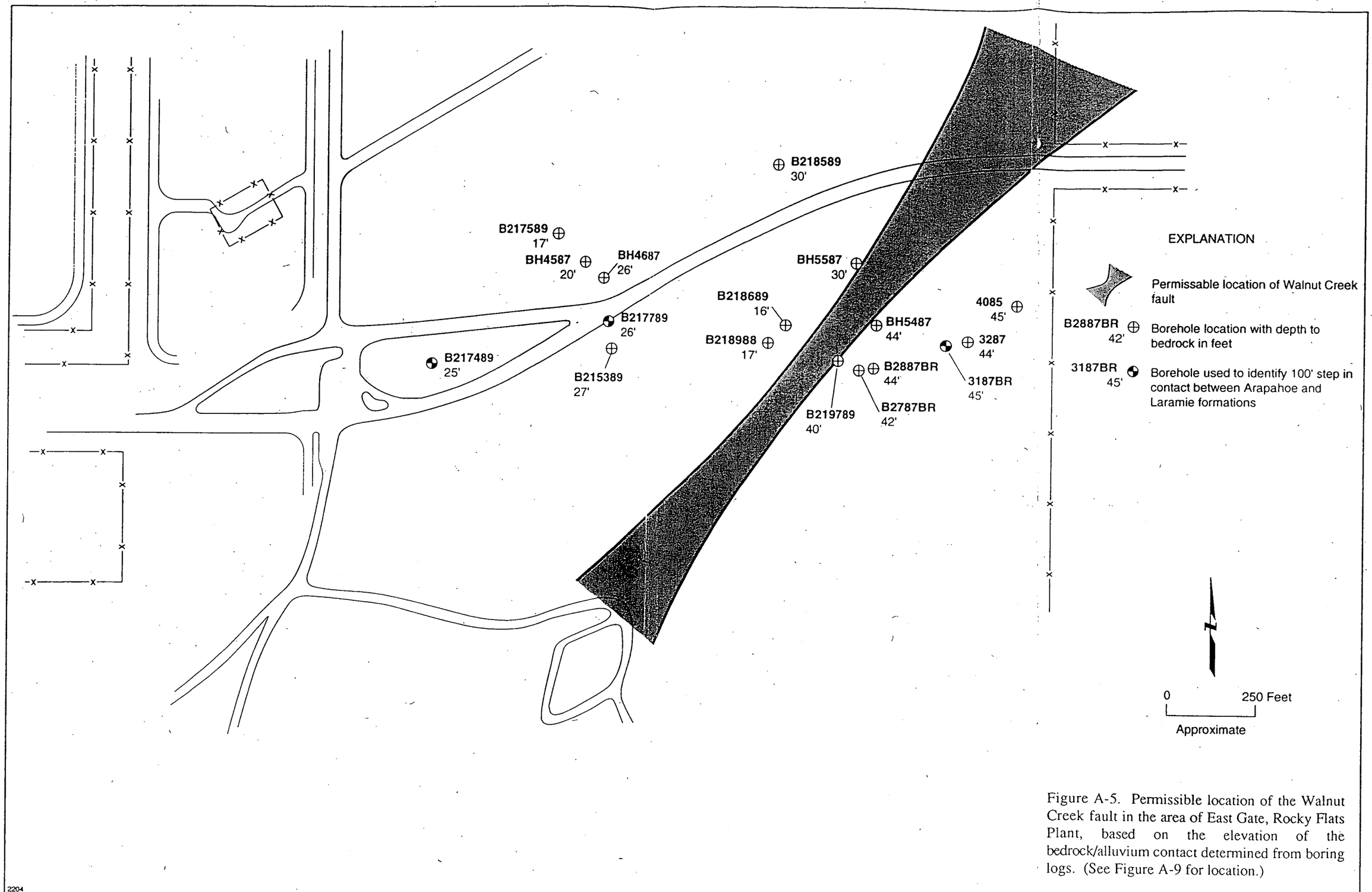

Figure A-5. Permissible location of the Walnut Creek fault in the area of East Gate, Rocky Flats Plant, based on the elevation of the bedrock/alluvium contact determined from boring logs. (See Figure A-9 for location.)

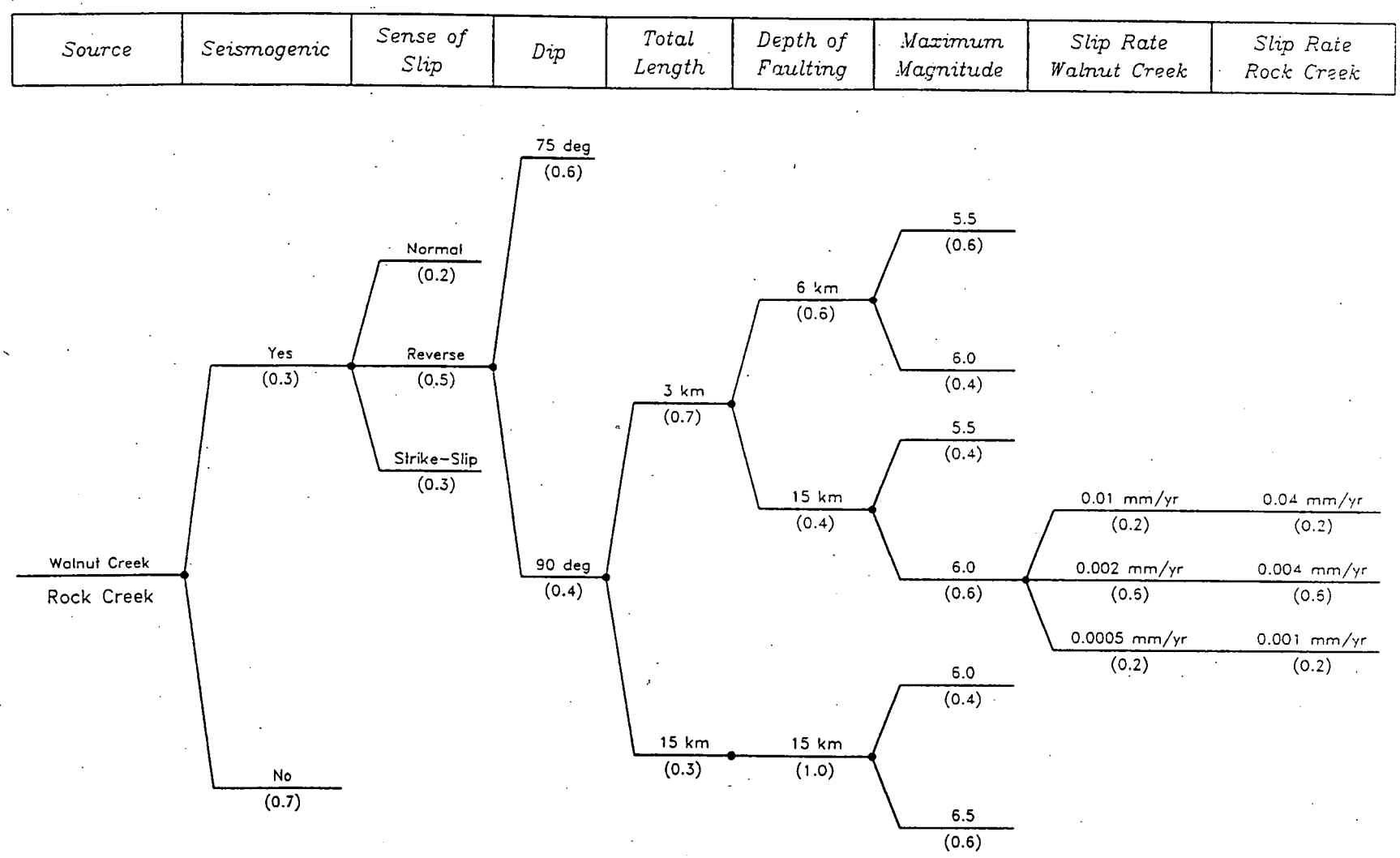

Figure A-6. Logic tree for the Walnut Creek and Rock Creek faults.

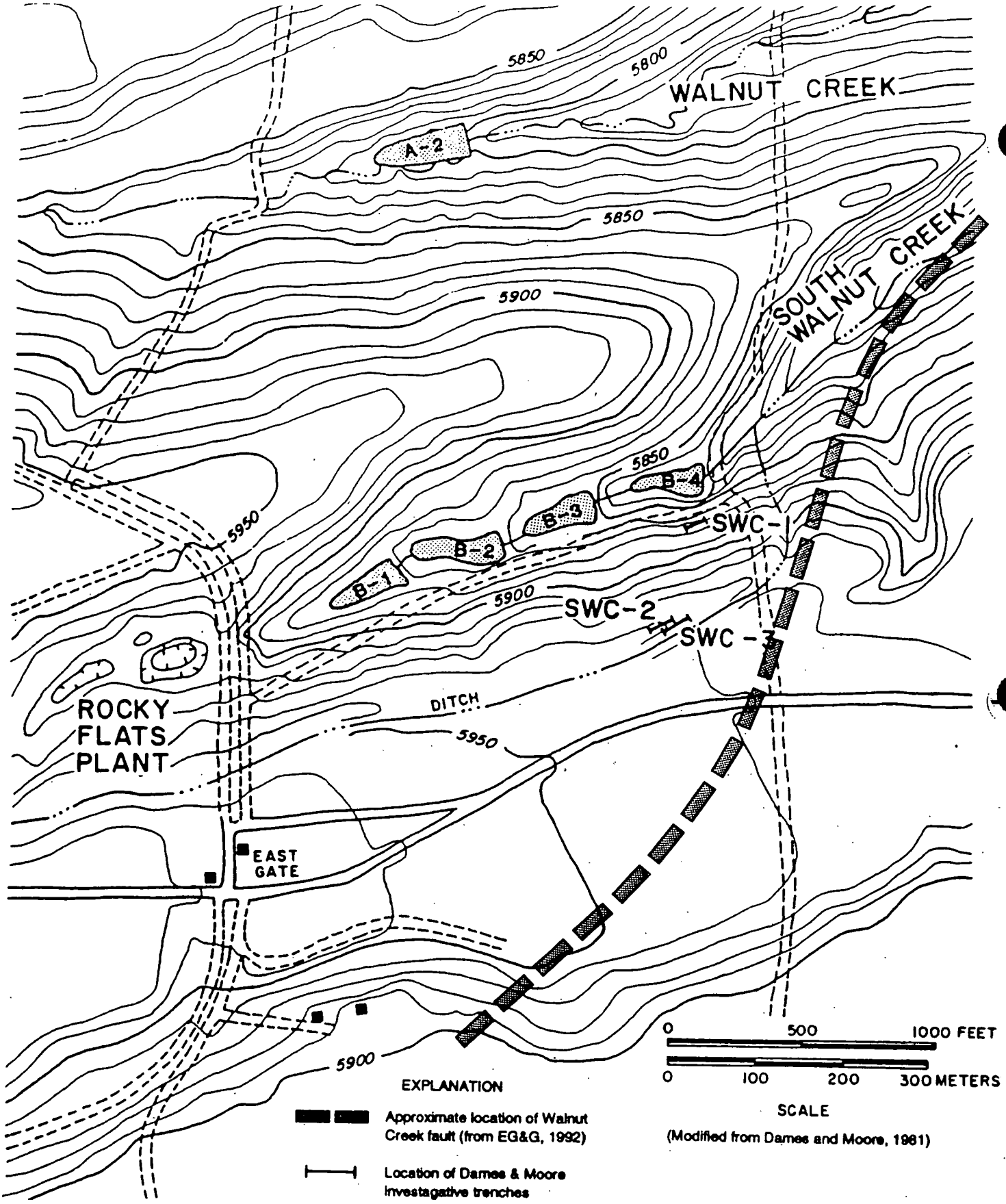

Figure A-7. Location of Dames & Moore's investigative trenches SWC-1, SWC-2, and SWC-3, and location of the Walnut Creek fault according to EG&G (1992). (Modified from Dames & Moore, 1981.)

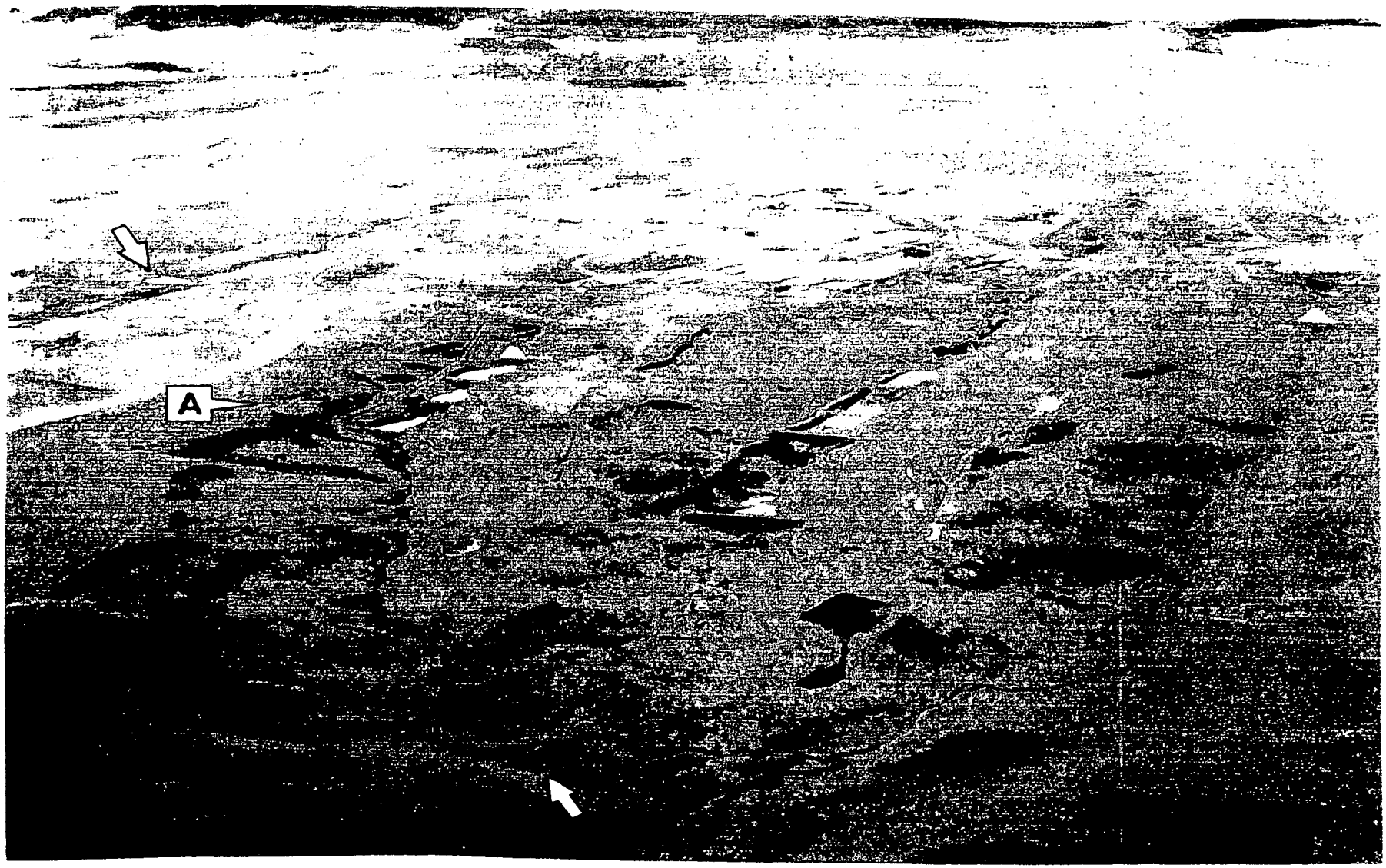

Figure A-8. Oblique aerial photograph of the East Gate area of Rocky Flats Plant. The Walnut Creek fault lies between the arrows. Note the down-on-the-east step in the bedrock/alluvium contact at **A**. View is to the southwest.

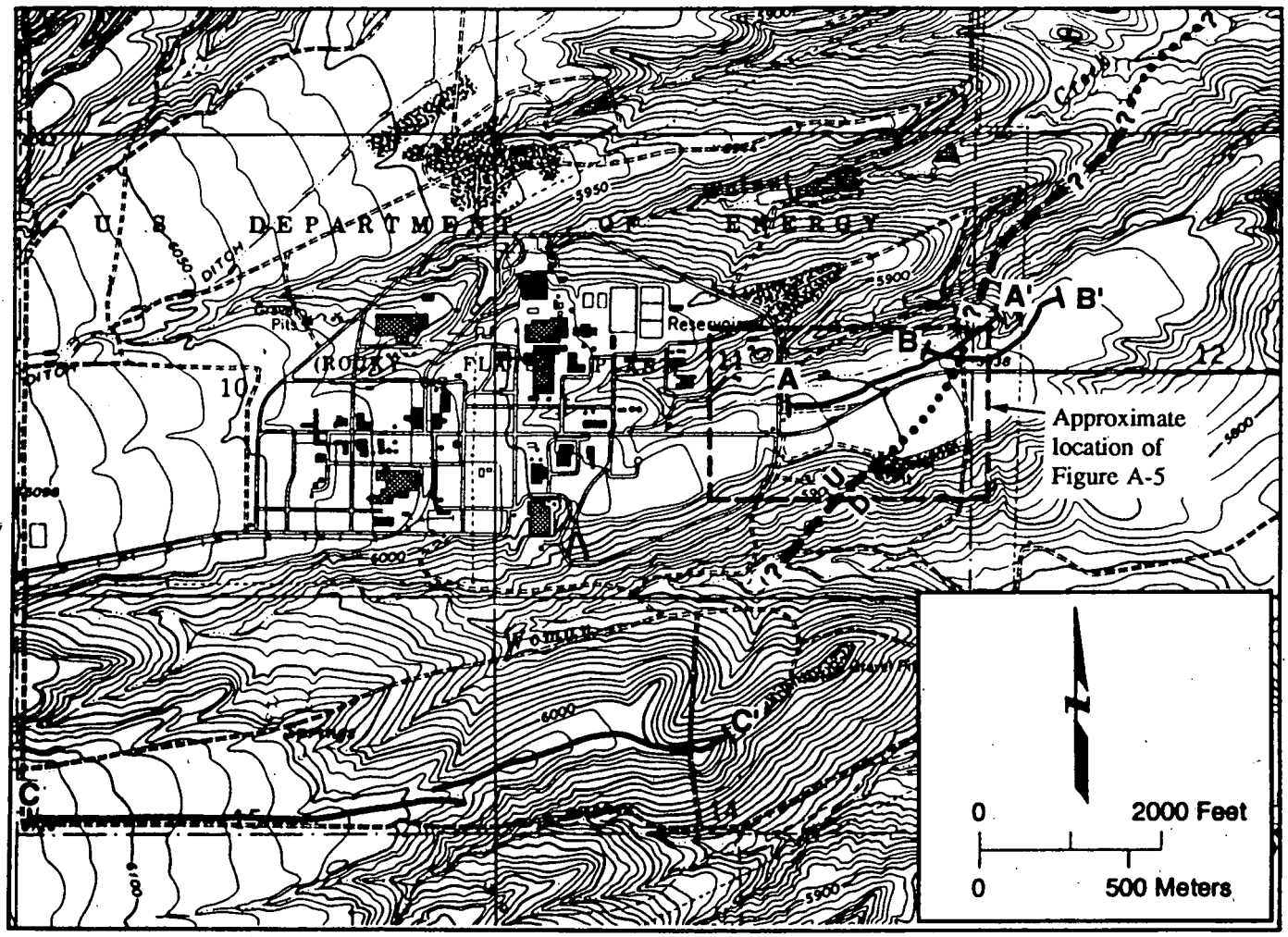

Base map: U.S. Geological Survey, Louisville, Colorado 7.5-minute quadrangle (1957), 1:24,000 scale, contour interval 10 feet.

Figure A-9. Location of topographic profiles A-A', B-B', and C-C' across the Rocky Flats alluvial fan surface, and location of the Walnut Creek fault.

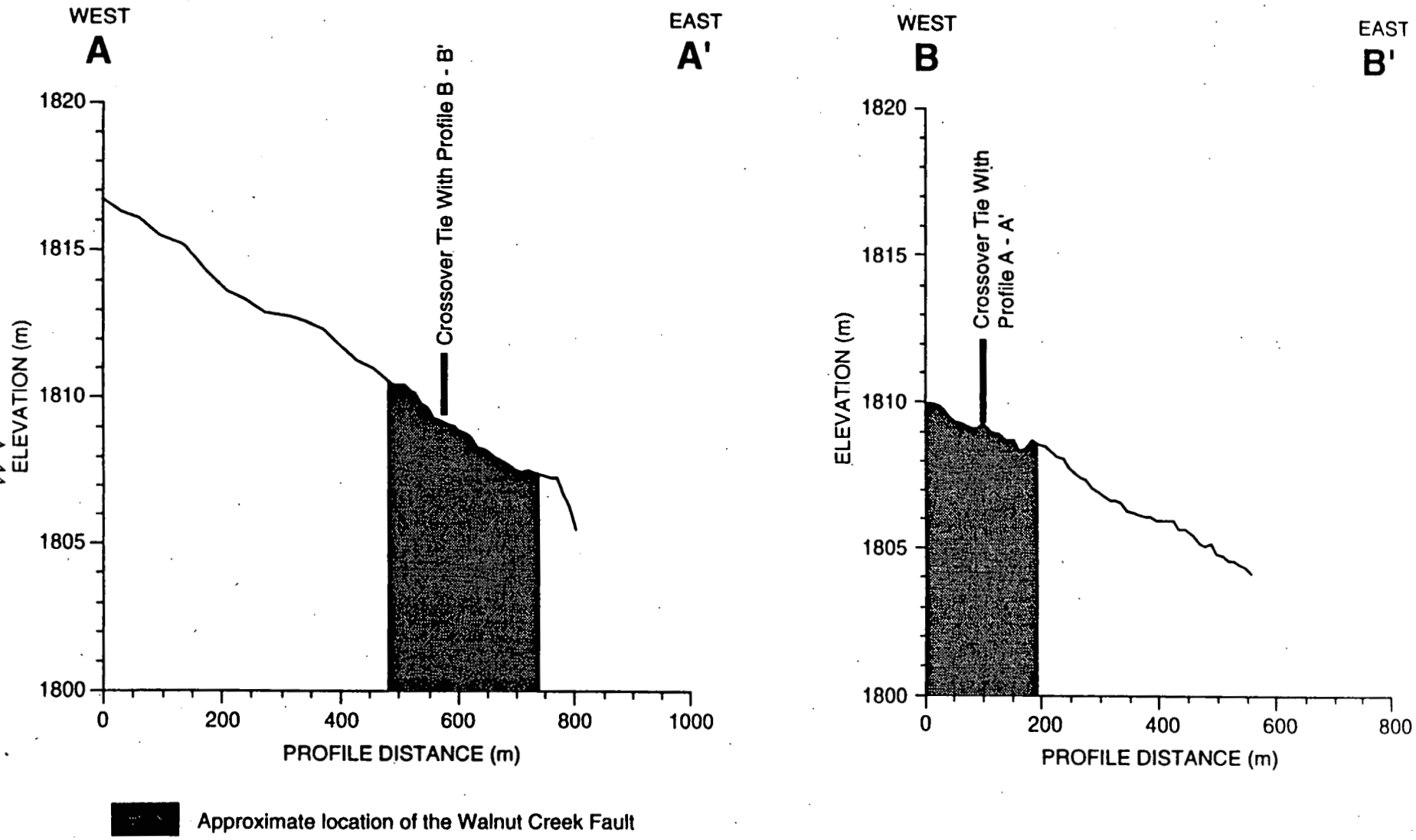

Figure A-10. Profiles A-A and B-B of the Rocky Flats alluvial fan surface in the area of East Gate, Rocky Flats Plant. Profile locations are shown on Figure A-9. Vertical scale is approximately 50 times the horizontal scale.

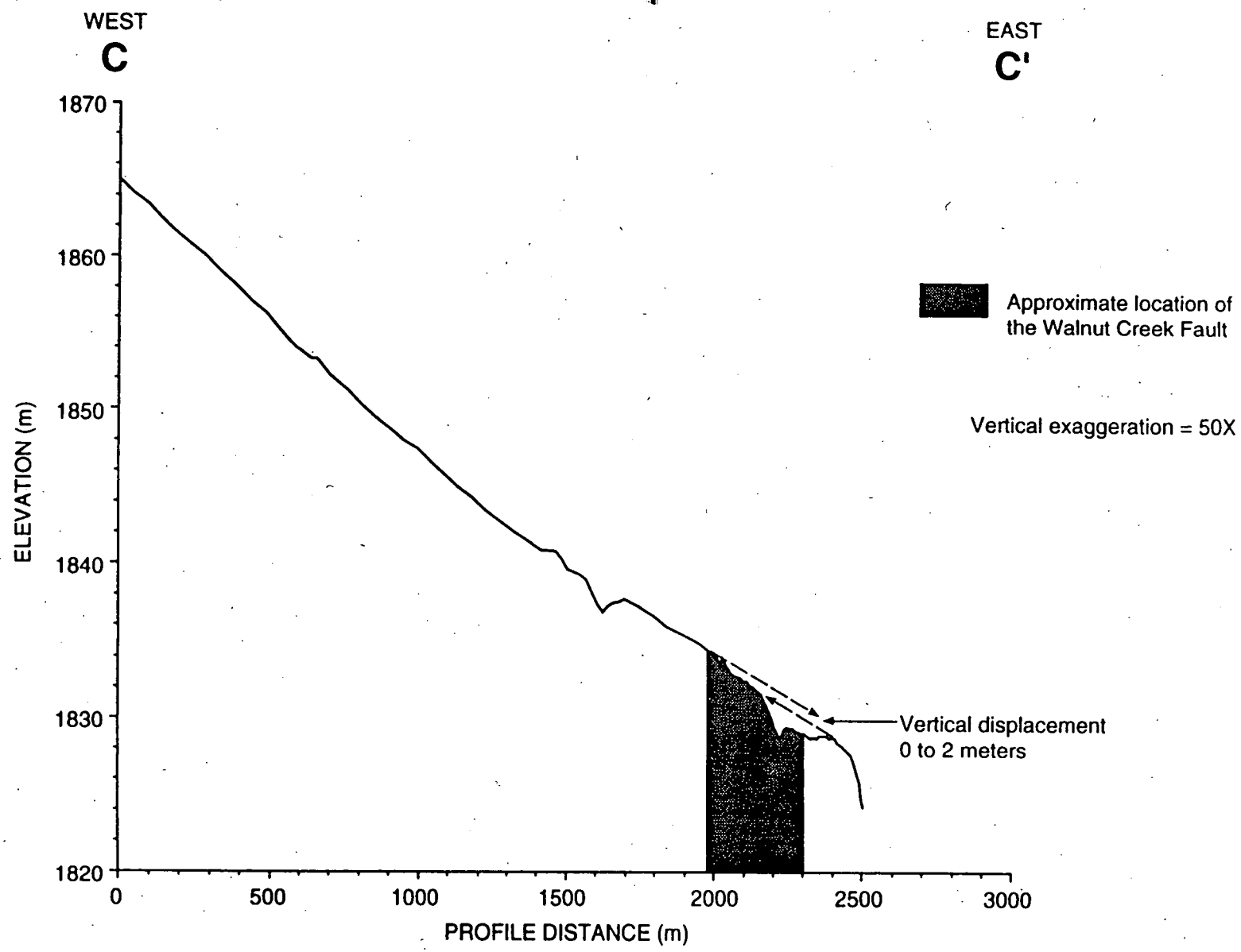

Figure A-11. Profile C-C of the Rocky Flats alluvial fan surface south of the Rocky Flats Plant. Profile locations are shown on Figure A-9. Vertical scale is approximately 50 times the horizontal scale.

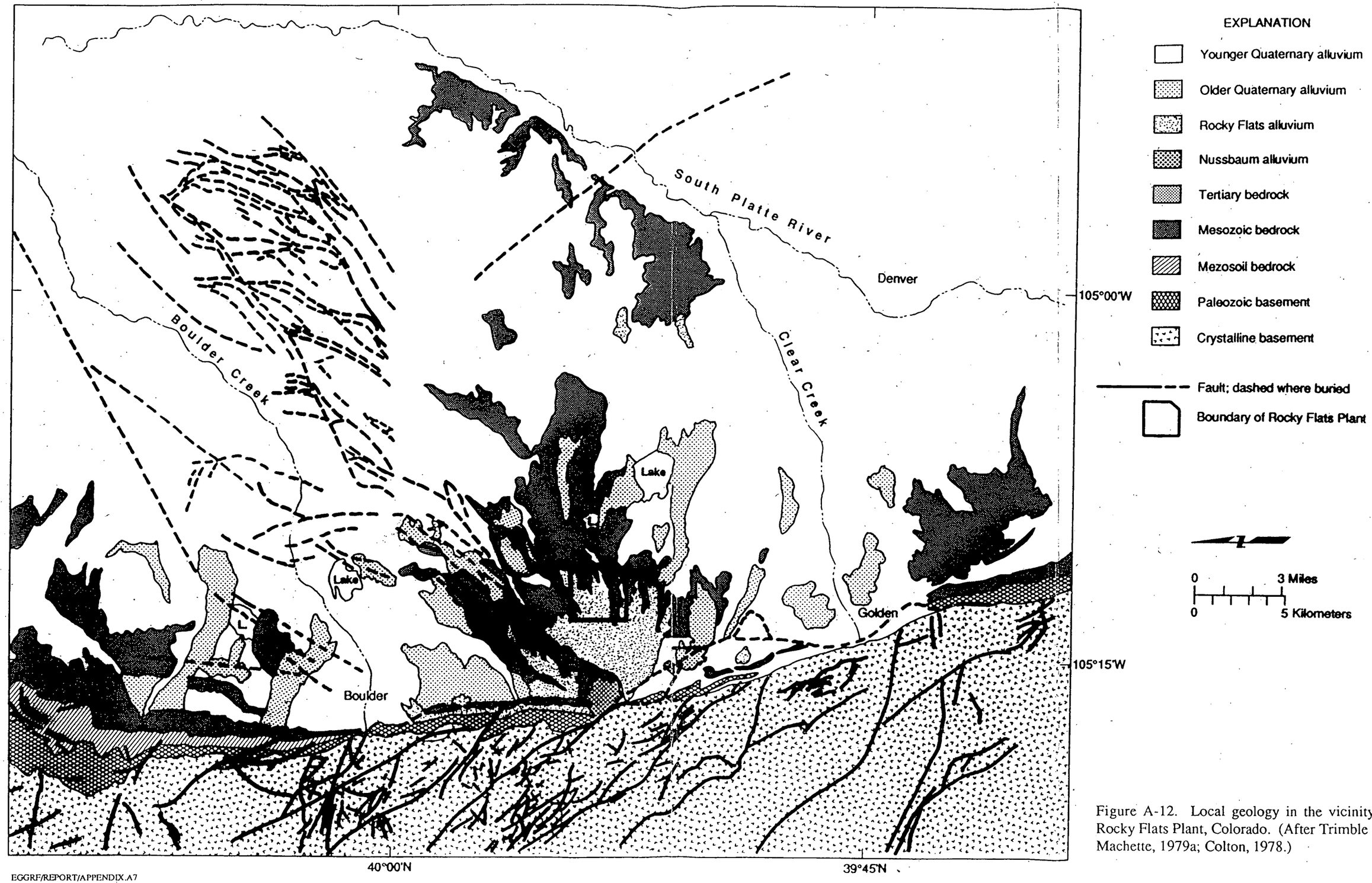

Figure A-12. Local geology in the vicinity of Rocky Flats Plant, Colorado. (After Trimble and Machette, 1979a; Colton, 1978.)

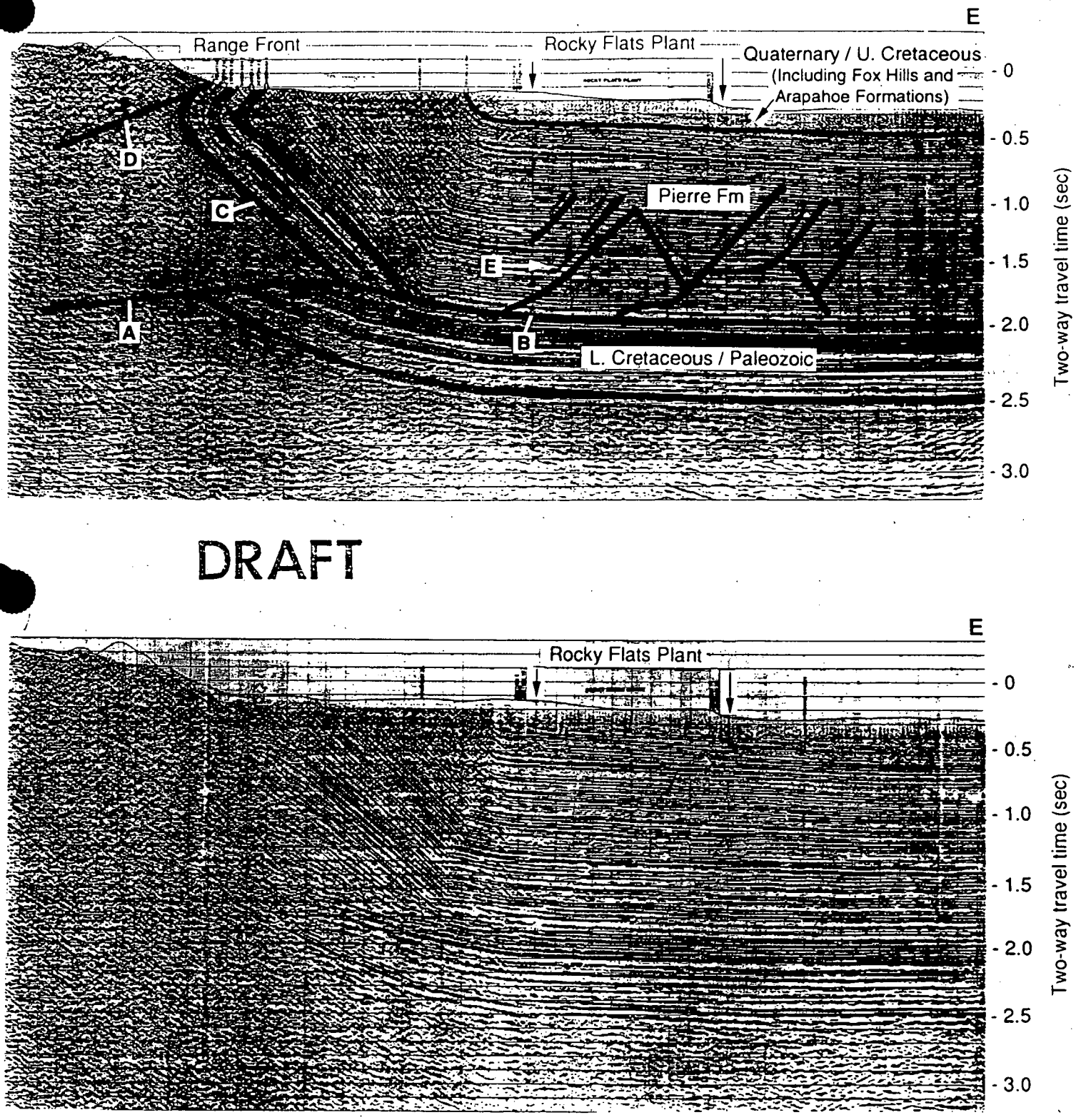

Figure A-13. Interpreted (top) and uninterpreted (bottom) deep seismic reflection profile from Coal Creek Canyon at the range front through Rocky Flats Plant east to Indiana Street. (Modified from Ebasco, 1991.) (See text for discussion.)

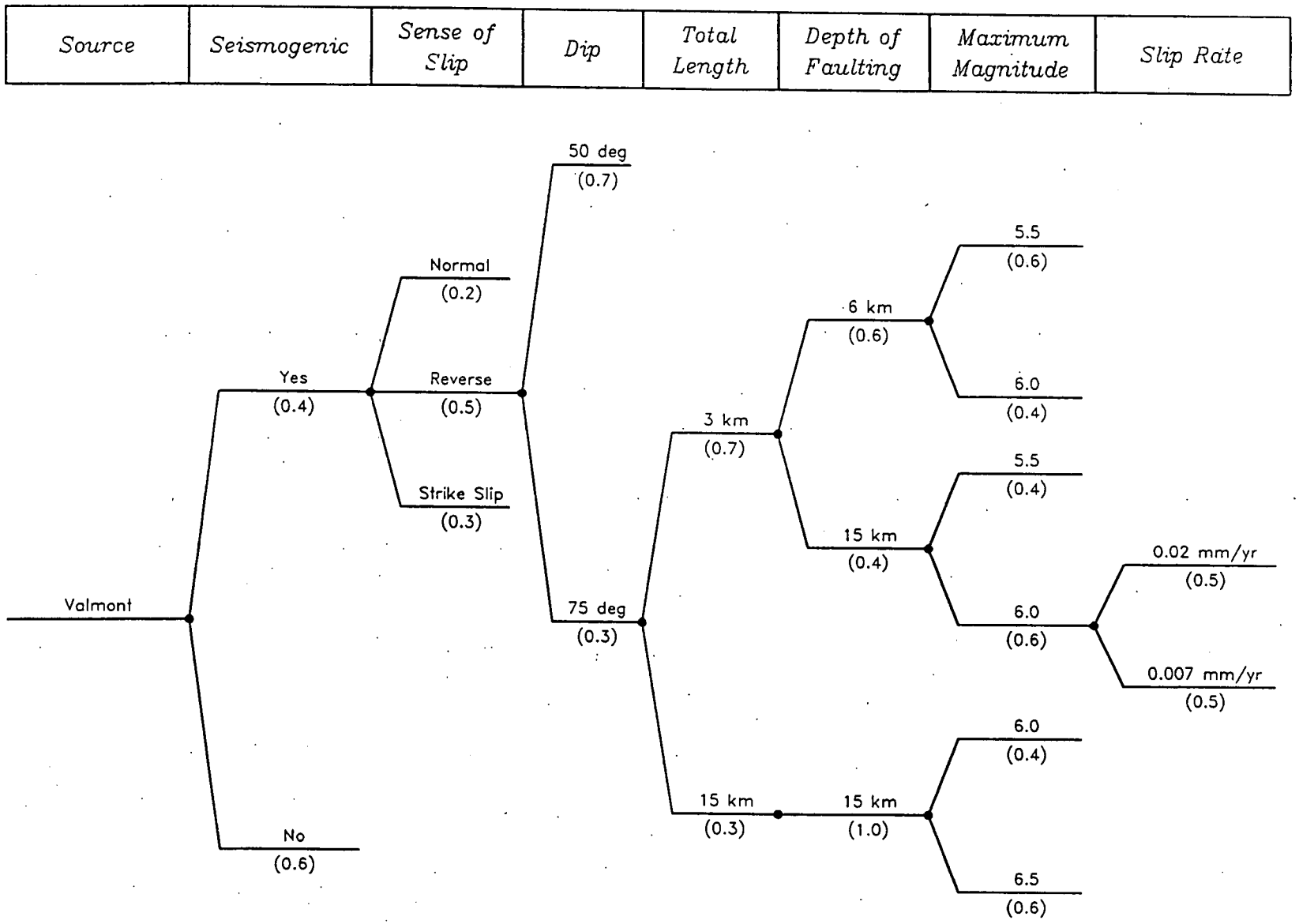

Figure A-14. Logic tree for the Valmont fault.

Figure A-15. Photograph of the Valmont fault exposed in the N. 75th Street roadcut, Valmont, Colorado. Fault trends diagonally across the photograph from upper right to lower left and places Slocum-age alluvial gravel against Cretaceous Fox Hills Formation siltstone and overlying younger colluvium. View is to the northeast.

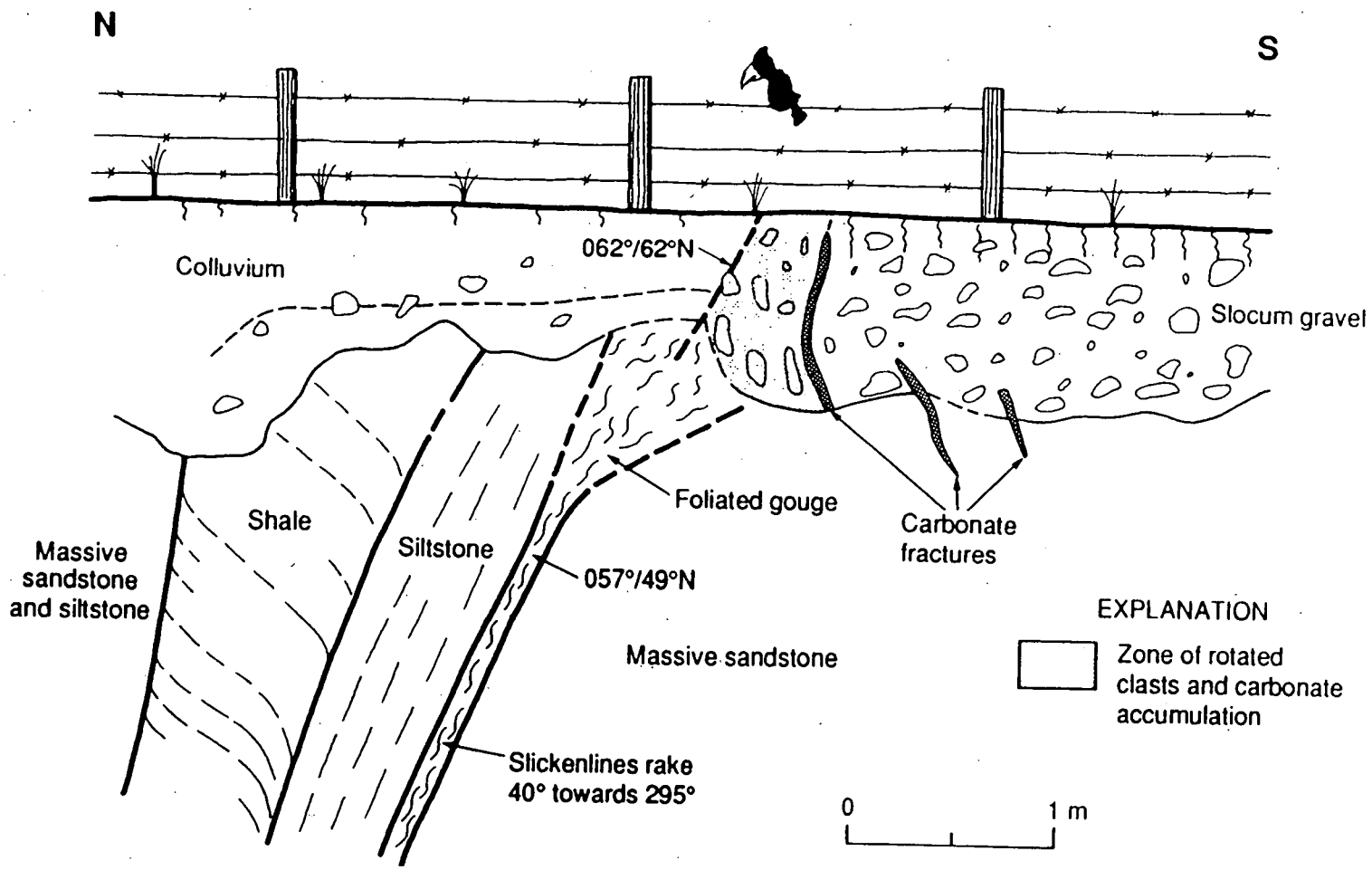

Figure A-16. Sketch log of the Valmont fault exposed in the roadcut on the southeast corner of Valmont Road and N. 75th Street, Valmont, Colorado.

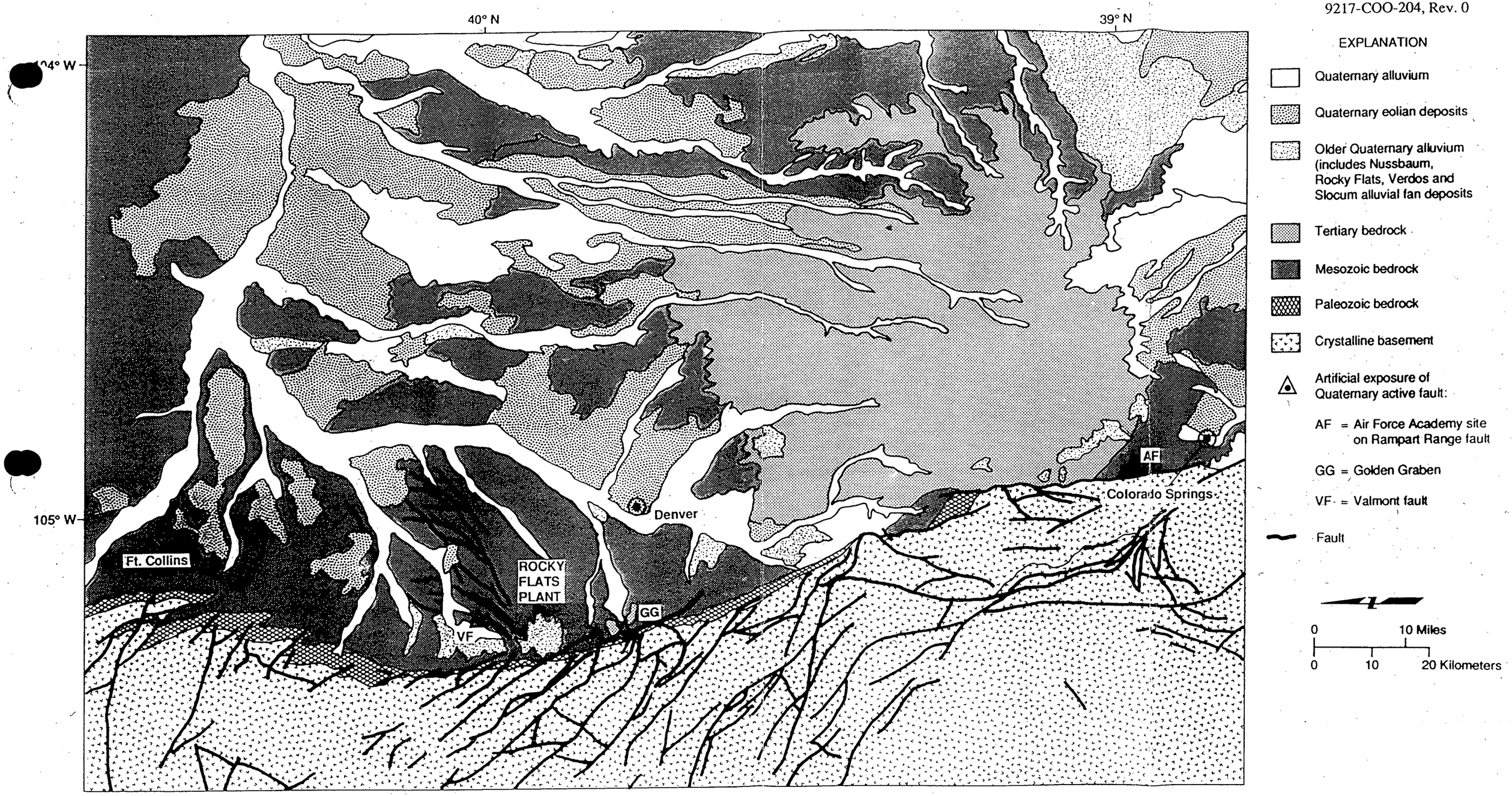

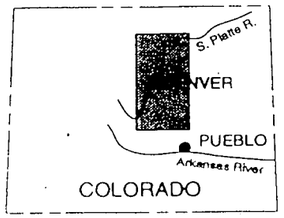

Figure A-17. Geology of the Front Range Urban Corridor, Fort Collins to Colorado Springs, Colorado. (Modified from Tweto, 1975.)

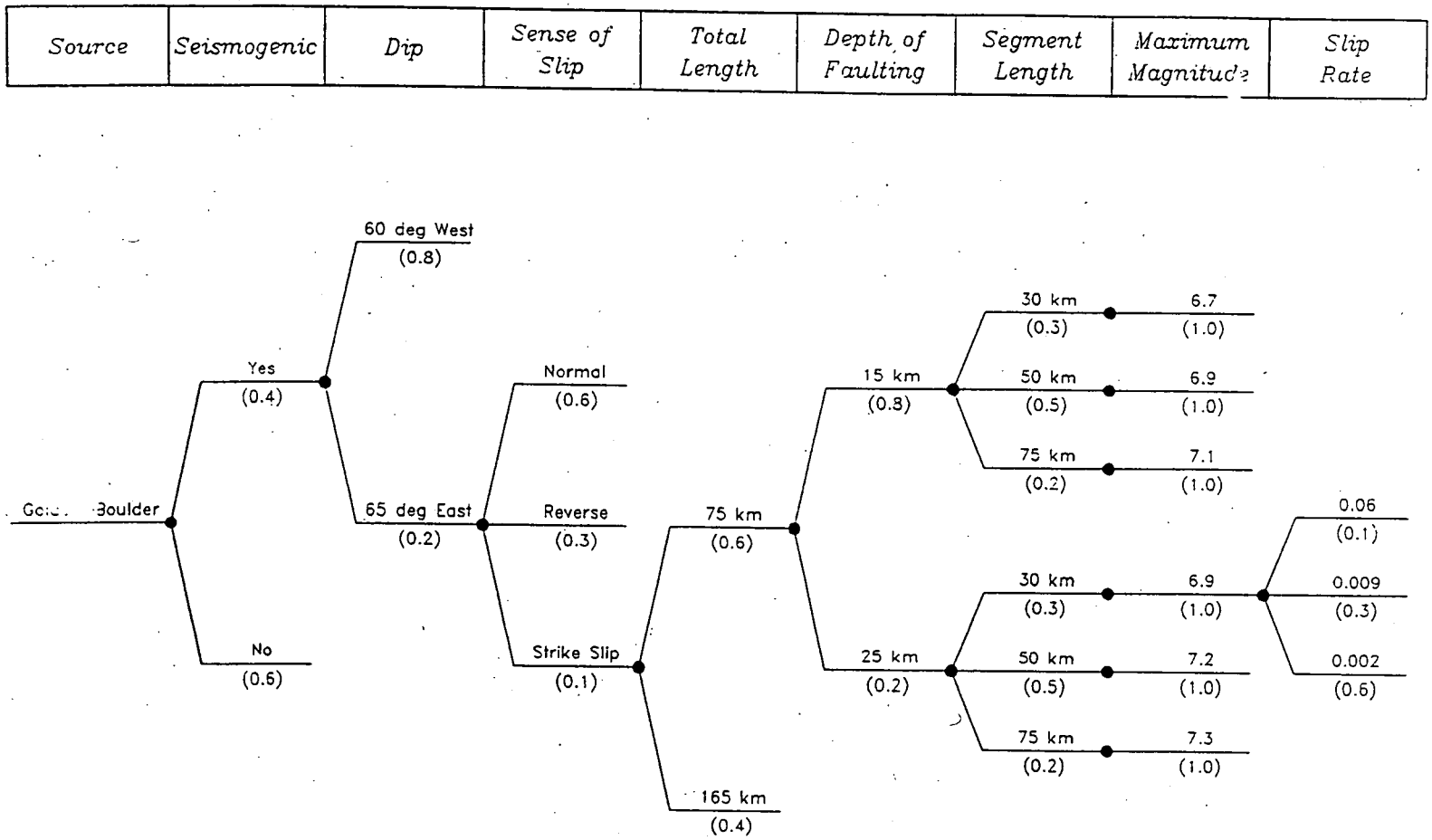

Figure A-18. Logic tree for the Boulder and Golden reaches of the Rocky Mountain Front Range fault system.

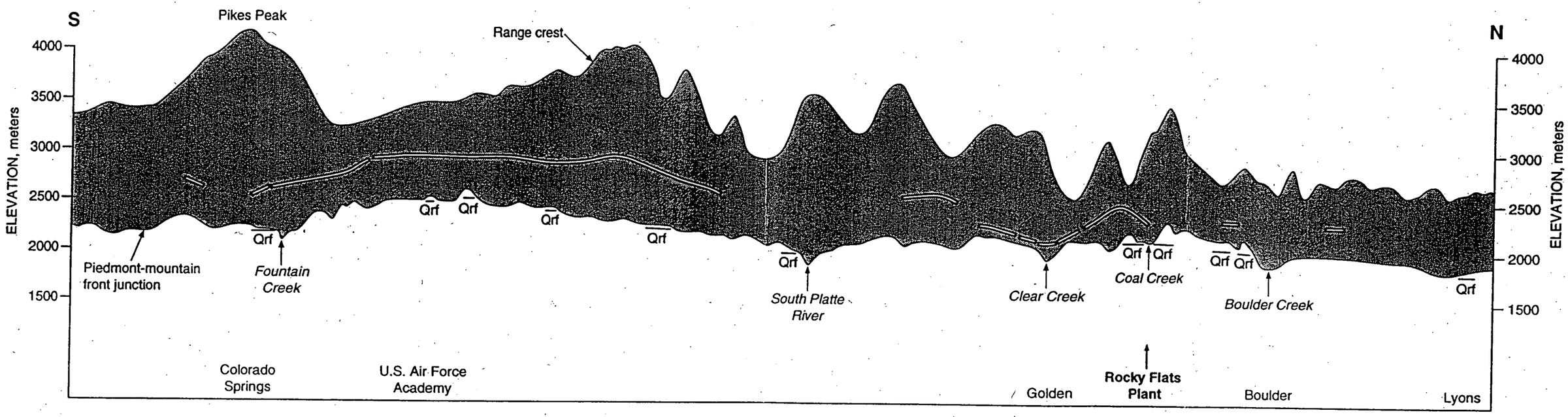

Figure A-19. Profiles of the piedmont-mountain front junction and the Eocene erosional surface projected onto the skyline profile of the Front Range, from Lyons to Colorado Springs, Colorado.

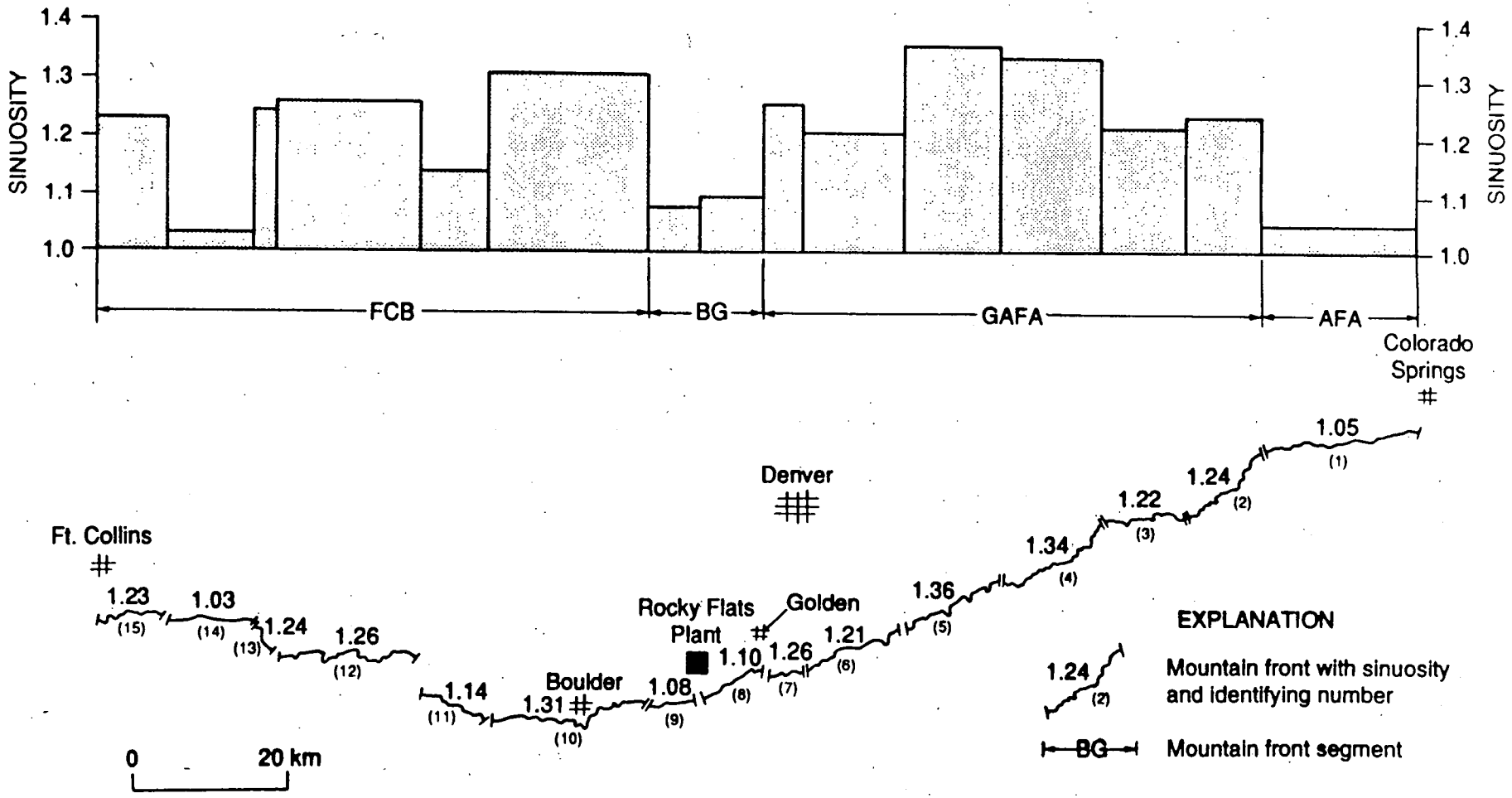

Figure A-20. Graphic (top) and map (bottom) representation of mountain front sinuosity of the eastern range front along the Front Range urban corridor, Fort Collins to Colorado Springs, Colorado. FCB = Fort Collins-Boulder segment; BG = Boulder-Golden segment; GAFA = Golden-Air Force Academy segment; AFA = Air Force Academy segment.

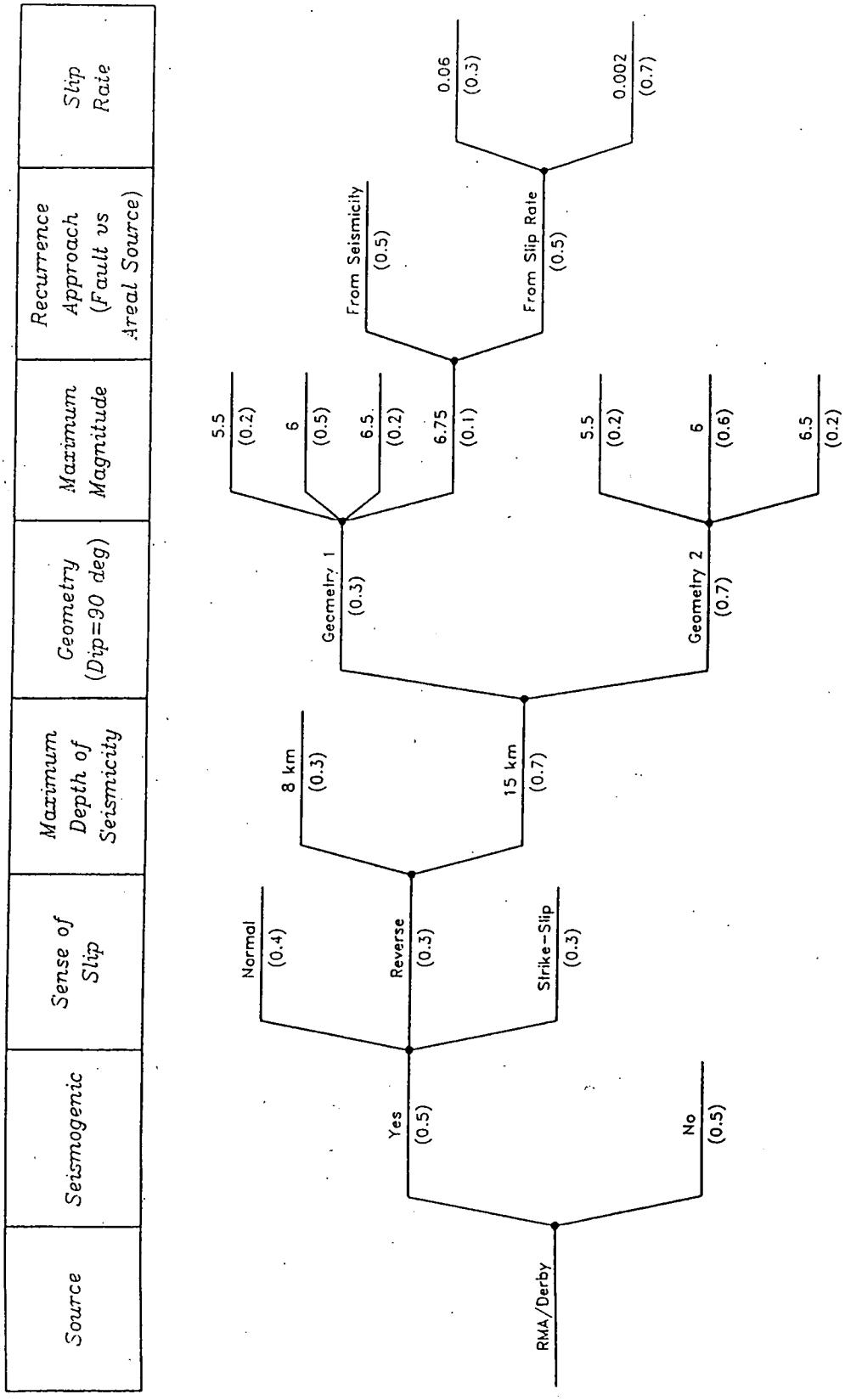

Figure A-21. Logic tree for the RMA/Derby source.

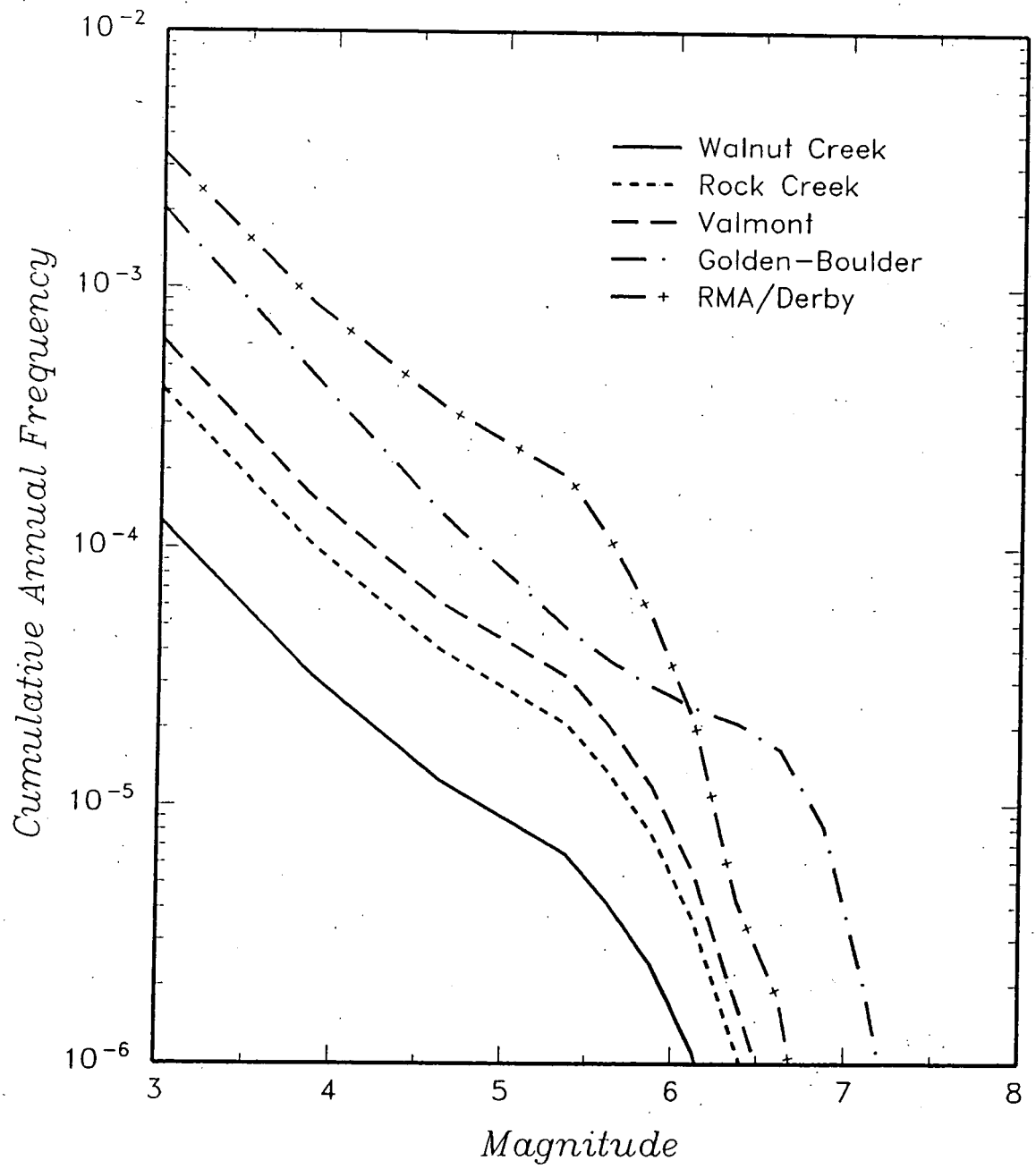

Figure A-22. Mean recurrence curves for fault sources in the vicinity of Rocky Flats Plant, Colorado.

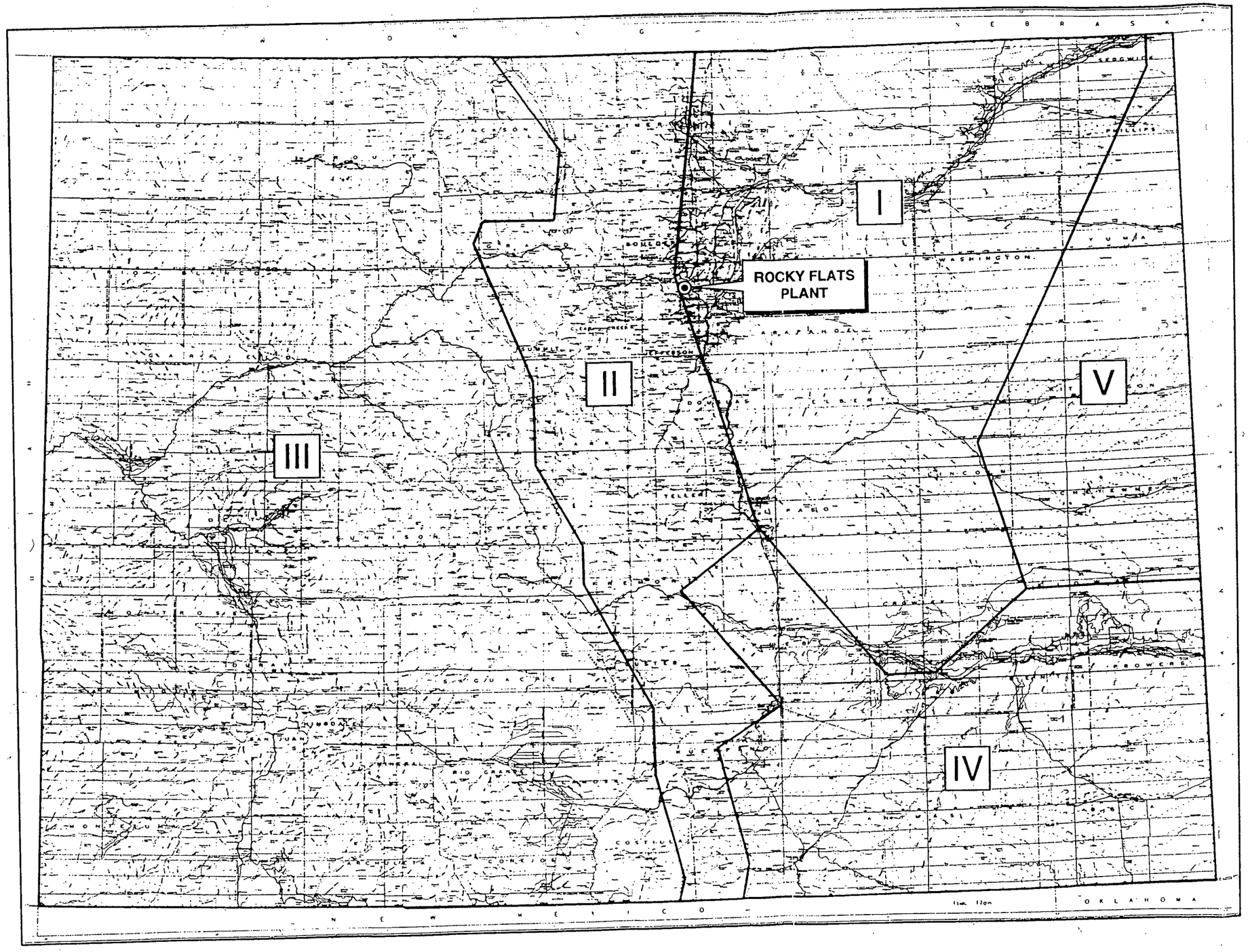

REGIONAL SOURCE ZONES

I Denver Basin

II Rio Grande Rift, and Eastern Rocky Mountain Province

III (Colorado Plateau) and Western Rocky Mountain Province

IV Southern Great Plains

V Northern Great Plains

0 30 Miles
0 50 Kilometers

Figure A-23. Regional seismic source zones, Rocky Flats Plant, Colorado.

APPENDIX B

GEOMORPHIC ANALYSIS

by

Geomatrix Consultants, Inc.
San Francisco, California

INTRODUCTION

Studies concerned with seismic hazard typically rely on techniques and data bases that provide direct evidence of the recency, frequency, and magnitude of earthquake activity. These types of studies focus on geologic (geologic mapping, trenching of active faults, and dating of displaced strata), geophysical (seismic reflection and refraction, gravity, magnetics), geodetic, and seismologic data.

Geomorphic analyses of landscape components (e.g. hillslopes, mountain fronts, drainage basins and stream networks) are employed to evaluate the relative tectonic activity of a region and in some cases, where direct evidence for earthquake activity (e.g. surface rupture of historical seismicity) appears to be lacking, can provide independent evidence that can be used to assess tectonic style and activity. The underlying assumptions for these analyses are as follows: geomorphic processes (e.g. fluvial incision, development of fluvial terraces, processes of landscape degradation and hillslope modification) are sensitive to changes in physical parameters such as slope, relief, and climate; tectonic activity (e.g. faulting, folding, and uplift) can influence those processes; changes in the geomorphic processes are preserved and reflected in the character of the landscape over differing periods. For example, the sudden surface rupture associated with large magnitude earthquakes produces a scarp that has measurable relief and slope. Through time the scarp degrades in an orderly fashion so that careful measurements of scarp height and scarp slope can be used to estimate the age, frequency, and magnitude of faulting (Nash, 1980, 1986; Hanks et al., 1984; Hanks and Wallace, 1985; Menges, 1988; Hanks and Andrews, 1989). Other surface characteristics are affected by faulting such as deformation of the landsurface by folding or tilting.

Earthquakes with very long recurrence may have little associated evidence of surface rupture and earthquakes that are associated with blind thrust faults have no evidence of surface rupture. However, these types of faults may be associated with surface deformation that occurs in response to repeated, long-term deformation and fold growth or deformation of geologic strata at depth. The types of surface deformation above these types of faults include tilted and warped fluvial terraces, regions of pronounced topographic relief, altered drainages including abandoned streams, drainage reversals, changes in slope and sinuosity, and folded geomorphic surfaces (e.g. King and Stein, 1984; Lin and Stein, 1989; Bullard and Lettis, 1989, 1993). Tectonic mountain fronts also exhibit physical characteristics indicating changes in the relative degree of tectonic activity along strike of range bounding faults. The morphology of mountain fronts, such as the sinuosity of the map view trace of the mountain front and deformation of known marker horizons along the mountain front, are useful tools for evaluating segmentation and the relative activity of fault segments.

Methods Applied in This Study

Quaternary morphometric analysis of various landscape components were employed in this study to provide an independent check on assessments of Quaternary tectonic activity in the vicinity of the Rocky Flats Plant (RFP) that are based on a review of previously mapped faults in the region and literature discussing the active structures along the Colorado Front Range.

Several types of analyses were applied, particularly in the vicinity of RFP to assess the recency of tectonic activity of the Walnut Creek fault (WCF) and the range front fault of the Front Range. Analyses included are the following: construction of regional slope maps to assess tilting or warping of the early Pleistocene Rocky Flats alluvial surface; construction of longitudinal and transverse profiles of the Rocky Flats alluvial surface to assess the character of the landsurface slope across mapped faults (constructed from topographic maps with a contour interval of 5 ft); analysis of drainage basin development across the fault; and detailed topographic profiling across the WCF using sophisticated surveying equipment.

At the regional scale, two analyses were performed on the Front Range for purposes of assessing the relative tectonic activity along the Front Range fault system. Mountain front sinuosity was determined for the section from Colorado Springs to Fort Collins, Colorado to help in identifying mountain front segments and assessing relative tectonic activity. A second analysis combined the profiles of the skyline of the Front Range (highest elevations in the front range east of the Continental Divide), the piedmont mountain-front junction profile (the intersection between the range front and the piedmont), remnants of an Eocene-age erosional surface preserved in the Front Range (e.g., Scott and Taylor, 1986), and remnants of the Rocky Flats alluvial surface at the mountain front. The second analysis can be used in conjunction with the mountain front sinuosity to help identify mountain front segments and measure the relative amounts of long term uplift along the length of the mountain front.

GEOMORPHIC STUDIES OF THE WALNUT CREEK FAULT

Geomorphic studies were focused along the Walnut Creek fault (WCF) for several reasons:

- proximity of the fault to RFP
- documented offset of the Pliocene Arapahoe Formation and possible displacement of the Quaternary Rocky Flats alluvium (EG&G, 1992)
- the Rocky Flats alluvium and associated surface is a useful datum that crosses the WCF. The age of the Rocky Flats alluvial surface is estimated to be 900 ka to 1.9 Ma based on soils development, age constraints on the Verdos alluvium containing the Pearlette O ash, identification of the Bishop ash, and alteration of magnetite (Machette, 1975; Scott, 1975; Machette and others, 1976; Van Horn, 1976; Mabee, 1978; Patterson, 1984; Miller, 1988). The duration of time represented by this surface is sufficient to capture potential movement on the WCF and estimate long-term slip rates.

Types of Geomorphic Studies Applied to the Walnut Creek Fault

The types of geomorphic studies applied to the WCF are considered to be the most promising for obtaining information that could aid in the characterization of the WCF as a seismic source. The decision to use certain geomorphic techniques was based on experience with geomorphic analyses in a variety of tectonic environments. Because of the apparent low rates of tectonic activity, techniques that are best suited to the Rocky Flats area are similar to those used in areas of blind thrust fault activity (e.g. Bullard and Lettis, 1993) and the southeastern United States (Geomatrix, 1993; Hanson et al., 1993).

Geomorphic techniques used to assess the tectonic activity of the WCF included slope maps, profiles of the landsurface and streams, and drainage analysis. Slope maps and profiles of the landsurface and streams can provide indirect evidence for tectonic deformation. Analysis of drainage basins also provides indirect, spatial evidence for potential tectonic activity through the measurement of stream morphology (e.g. stream slope and sinuosity). It is assumed that stream morphology is sensitive to changes in relief that force changes in stream slope, sediment/water discharge relationships, and stream sinuosity. Drainage basin characteristics such as overall slope, relief, and derivative products (e.g. relief ratio and hypsometric integral) can reveal potential tectonic influences on drainage basin development such as basin oversteepening caused by tilting or uplift, or spatial differences in erosional development because of faulting or differential uplift.

Slope maps and profiles of the Rocky Flats alluvial surface near RFP. The Rocky Flats alluvial surface and the unconformity between the Rocky Flats alluvium and the underlying Arapahoe Formation comprise near-uniform, east sloping surfaces from the west of RFP to east of RFP and, therefore, serve as unique, time horizons. A contour map of this unconformity (Figure B-1, top) was constructed because it was thought that if there were a strong tectonic signal associated with the WCF, it might manifest itself as an abrupt change in slope of the contact or as a discernible topographic anomaly. The subenvelope map (Figure B-2) is a topographic map of a hypothetical surface eroded to the level of second- or third-order and higher stream segments. Subenvelope maps are useful for identifying areas that may be affected by fault activity (Bullard and Lettis, 1993; Golts and Rosenthal, 1993).

The slope map of the base of the Rocky Flats alluvium (Figure B-1, top) was constructed by determining the elevation of the geologic contact from the existing 1:24,000-scale geologic map of the RFP area (EG&G, 1992) and constructing a topographic map of the elevations. For the slope map of the alluvial surface (Figure B-1, bottom), points of equal surface elevation were determined, plotted in map view, and contoured. The subenvelope map shown in Figure B-2 is constructed using the elevations of the second- and third-order of the stream segments.

The map of the unconformity between the Arapahoe Formation and the overlying Quaternary units (Figure B-1, top) shows an abrupt change in orientation of contour lines along the trace of the WCF; the apparent step down across the fault continues southwest of the mapped trace of the fault. The slope of the Rocky Flats alluvial surface, however, does not show any obvious evidence of tectonic deformation. The subenvelope map (Figure B-2) shows an apparent alignment of topography along the trend of the WCF suggesting that the presence of the fault is recorded in the long-term history of the drainage development.

Longitudinal and transverse profiles of the Rocky Flats alluvial surface. Transverse profiles and longitudinal profiles of the Rocky Flats surface were constructed from 1:24,000 scale topographic maps available for the site area. The transverse profiles cross mapped faults (Spencer, 1961; Trimble and Machette, 1979) in the Marshall Lake area and the longitudinal profiles crossed the Rock Creek fault and the WCF.

The transverse profiles do not show unambiguous evidence for displacement of the Rocky Flats alluvial surface across the faults (Figure B-3). Topographic variation across some faults is opposite the relative sense of fault movement as mapped. For example, the apparent displacement across the North Gorham fault (Figure B-3a) probably reflects differential erosion of the Laramie Formation and the Fox Hills Sandstone.

The longitudinal profiles of the Rocky Flats alluvial surface do not show obvious displacement across the Walnut Creek or Rock Creek structures (Figure B-4), in contrast to the results of the subenvelope map analysis that suggest the surface could be deformed. Because the contour interval of the topographic maps (5 ft) is likely insufficient to adequately assess the location and amount of deformation given the apparent low rate of activity, more detailed field profiles were measured using laser theodolite total station surveys.

Detailed longitudinal profiles of the Rocky Flats alluvial surface. Data for the longitudinal profiles were collected by Geomatrix on October 14 and 15, 1992, using a coaxial Wild T1600 Total Station surveying system. Distance and elevation measurements were taken at approximately 50-meter intervals at distances greater than 50 m from the WCF and every 5 to 10 meters in the immediate vicinity (less than 50 m) of the fault trace (projected to the surface from bedrock). The survey lines were tied into local elevation control bench marks. The location of the detailed field surveys is shown on Figure B-5 and the profiles are shown on Figures B-6 and B-7.

Two profiles were measured across the projected trace of the WCF east of the plant site (Figure B-6). The west end of profile A-A′ shows some topographic irregularities, but these are a result of mechanical disturbance of the ground surface rather than tectonic deformation. Because of surface modification and natural erosional degradation of the surface in the area where the fault is projected to cross the surface, the ability to discern clear evidence of tectonic displacement is limited. The east end of the profile (B-B′) crosses perpendicular to the projection of the trace and shows a slight deflection in the surface (Figure B-6). The amount of possible vertical separation of the Rocky Flats alluvial surface across the fault is less than 2 m suggesting a maximum long-term rate of displacement of 0.001 to 0.002 m/ka.

A third profile was measured across the WCF south of the RFP along the south divide of Woman Creek (Figure B-7, C-C′). The shape of this profile diverges from a smooth, sloping, planar surface. The surface has a concave up profile shape indicative of erosional modification. Localized irregularities in the profile topography are associated with headward extension of drainages into the Rocky Flats alluvial surface. In the area near the projection of the WCF, there is a step in the profile of the Rocky Flats alluvial surface of about 2 m that also suggests a long-term vertical slip rate of 0.001 to 0.002 m/ka. Alternatively, it is possible to make a reasonable pick of the surface that allows for no deflection of the surface.

In summary, detailed longitudinal profiles of the Rocky Flats alluvial surface in the vicinity of RFP show little or no evidence of vertical displacement. Surface modification resulting from human activity and erosional processes has impacted the quality of the profile that can be obtained from detailed measurements of the topography of the surface. Despite the surface modification that has occurred, it is thought that the surface should be capable of preserving measurable evidence of surface deformation. The best resolution of tectonic deformation across the WCF that can be obtained, given estimates for the age of the Rocky Flats alluvium and maximum amount of apparent displacement of the Rocky Flats surface, is < 0.002 m/ka.

Longitudinal profiles of Walnut Creek and Woman Creek. Longitudinal profiles of Walnut Creek and Woman Creek (Figure B-8) have distinctly different forms, but the form of both profiles shows change in the vicinity of the WCF.

The Walnut Creek profile (Figure B-8, top) is convex up in the upper part of the profile suggesting a depositional sediment wedge in the upper stream system. In the vicinity of the projection of the WCF to the surface, the profile form is convex-up and the downstream portion of the profile has a less steep gradient. Both observations are consistent with a tectonic influence having the same relative sense of displacement (i.e., west-side up) as the mapped fault. An increase in relief west of the fault due to either surface rupture or fold deformation related to an active blind fault, most would likely result in local increases in surface slope and stream incision accompanied by a local increase in the stream gradient. As the stream adjusts to the increase in stream slope a sequence of fluvial responses occurs involving incision, transport of sediment through the oversteepened reach, and deposition in the downstream direction (e.g., Schumm, 1977; Ouchi, 1985; Burnett and Schumm, 1983). Unfortunately, there has been abundant surface disturbance and modification of the Walnut Creek valley and this casts doubt on the significance of the deflection in the longitudinal profile.

The longitudinal stream profile of Woman Creek (Figure B-8, bottom) on the other hand has a smooth, concave up shape consistent with a stream that is in a condition of dynamic equilibrium (e.g., Mackin, 1948; Hack, 1960, 1976; Schumm, 1973, 1976; Bull, 1991) with the exception of a short, convex-up section of the profile located in the vicinity of the projected trace of the WCF. The presence of the convexity may be explained by one or more of several possibilities such as changes in bedrock, man-induced disturbance of the valley floor (e.g., construction of dams and ponds), sediment transport processes operating throughout the drainage basin (can be affected by climate change or changing patterns of landuse), or tectonic influence. Bedrock is considered to be uniform in this area and is not thought to influence the shape of the profile. Human disturbance of the valley floor of Woman Creek is much less than in Walnut Creek, especially in the reach where the most pronounced convexity occurs. The presence of a depositional lobe of sediment forming a convexity in the profile cannot be ruled out, although the location and size of the convexity is in marked contrast to the convexity seen in the Walnut Creek longitudinal profile. Both drainage systems have similar shapes, basin sizes, and relief, and should be expected to have similar types of fluvial responses to changes in climate or sediment discharge unless one basin is characterized by a special condition that results in the production and delivery of excessive quantities of sediment, relative to stream discharge, to the trunk stream.

The slopes of stream segments were determined across the WCF to assess the possibility of tectonic influence. The slopes of all tributary stream segments of Walnut Creek (average slope of all segments = 0.1744 m/m) are, in general lower than the stream segment slopes of Woman Creek (average slope of all segments = 0.2493 m/m). There is no apparent difference in stream slopes for north-flowing or south-flowing segments for either Walnut Creek or Woman Creek. The average slope of Walnut Creek is 0.0277 m/m upstream of the trace of the WCF and 0.0164 m/m downstream from the fault (Figure B-8, top). The average slope of Woman Creek ranges from 0.0306 m/m in the headwater reaches, to 0.0250 m/m just upstream of the WCF, to 0.0224 m/m just downstream of the fault, to 0.0206 m/m in the downstream reaches (Figure B-8, bottom). In general, the slope of Woman Creek is more variable than the slope of Walnut Creek.

The average slope of all stream segments for Walnut Creek subbasin 1 and subbasin 2 (Figure B-9) is 0.0397 m/m and 0.0460 m/m, respectively. The average slope of the main stream of subbasin 2 (0.0586 m/m) is steeper than the average slope of the subbasin 1 mainstream (0.0247 m/m). This difference in stream slope for these two small basins located on opposite sides of the WCF probably reflects their location in the landscape and difference in basin size.

Summary of Slope Analysis, Topographic and Longitudinal Profiles

In summary, the slope map analysis, topographic profiles of the Rocky Flats alluvial surface, and longitudinal stream profiles provide inconclusive, and somewhat ambiguous results with regard to tectonic activity. However, the data do confirm that any tectonic displacement that might be present must be occurring at extremely low slip rates--of the order of 10^{-3} mm/yr. The most compelling evidence for recent tectonic activity is the deflection of contours of the subenvelope map, deflection of the Rocky Flats alluvial surface across the WCF, changes in stream slope across the WCF, and a correspondence of stream profile anomalies in the same general area of the WCF. Interpretations of the data tend to give somewhat inconsistent results. For example, if the WCF is active, the Rocky Flats alluvial surface should preserve evidence of the most recent activity, better than the stream channel because of the less erosive force of the unconfined sheet flow across the landsurface than in the stream channels. The slope of the stream, hence channel profile, should adjust to minor tectonic disturbances that cause imbalances in the relationships of stream slope and stream discharge and quickly return to a graded condition. It is possible that rapid natural regrading of the Rocky Flats surface occurs because of the general noncohesiveness of the Rocky Flats alluvium, and a well developed soil which could promote overland flow capable of erosion and transport of surficial material.

The detailed study of stream slope, which is probably the most sensitive indicator of active tectonic deformation, provides ambiguous results. The fact that the stream profiles are not in a graded condition suggests that there has been an external influence (e.g., climate change) on the fluvial system that has forced changes in the internal system (e.g., drainage basin parameters) such that the stream is not in an equilibrium state with respect to sediment and water discharge. The larger stream systems that cross the WCF probably have sufficient stream power to erase the tectonic signal along the WCF. Walnut Creek is the same size as Woman Creek, but the basin is crossed by the fault near the basin outlet. The smaller drainages are much better suited to preserving a tectonic signal; unfortunately, none of the small tributaries in the RFP area actually cross the WCF.

Drainage Basin Analysis Near the Rocky Flats Plant

The assessment of drainage basin development in seismic hazard studies is a relatively new technique (e.g. Bullard and Lettis, 1989, 1993; Geomatrix, 1993; Hanson et al., 1993). The erosional development of a drainage basin is related to available relief in a region and subtle, yet detectable differences in development can provide powerful indirect evidence for tectonic activity. For example, once the basic physical parameters of drainage basins are determined, such as length (L), area (A), perimeter length (P), relief (H_b), stream orders (M), numbers of stream segments (N), and total length of stream channels (C_t), derivative products can be calculated and compared among basins. Basin elongation (S_e) and basin shape (S_b) are both derived from basin area and basin length and provide an indication of the structural control on basin development. The relative perimeter crenulation (S_c) provides a relative measure of the degree of development and amount of drainage divide dissection. Relief ratio (Rr) is derived from total basin relief and basin length and gives an indication of overall basin slope; for two basins of similar size, relief, underlying bedrock, and climatic influences, a large difference in relief ratio can be an indication of tectonic uplift or tilting. The hypsometric integral (HI) is a measure of the distribution of relief and volume in a drainage basin and represents the erosional development of the drainage basin; large values of HI represent youthful drainage basins with high relief (perhaps as a result of tectonic uplift and rejuvenation), whereas lower values are indicative of low relief and large volumes of material removed from the basin (indicating long-term tectonic stability). Stream frequency (F) and drainage density (Dd) are measures of the drainage network development and can be used to identify spatial variation in tectonic deformation of the landsurface.

As a test of the potential usefulness of drainage basin analysis in the RFP area, two drainages were selected for study of their basin characteristics: Walnut Creek and Woman Creek (Figures B-9 and B-10). Two smaller tributaries of Walnut Creek (subbasin 1 and subbasin 2; Figure B-10) that are located on opposite sides of the trace of the WCF also were analyzed (Figure B-9).

The premise for the study is that long-term tectonic activity on the WCF should be manifested in the development of drainages as streams adjust to tectonic deformation of the landscape. Because of the presumed small amount of Quaternary tectonic activity on the WCF, based on about 10 m of displacement of the Pliocene-Quaternary contact, it was hypothesized that the larger drainage basins would have sufficient, available stream power (e.g. Bull, 1979, 1990, 1991) to counteract the low rate of tectonic deformation and, therefore, would not exhibit distinct drainage basin characteristics; whereas, smaller drainages on either side of the WCF would exhibit characteristics indicative of tectonic influence. In particular, the drainages developed on the upthrown block of the fault should have increased relief and exhibit signs of erosional youth in comparison to the drainages on the passive, downthrown fault block.

Drainage basins were selected from the 1:24,000-scale topographic maps for study. Digital elevation data was analyzed using Digital Elevation Models (DEM) to delineate drainage basins (e.g. Mark, 1983; Marks et al., 1984; O'Callaghan and Mark, 1984; Franklin, 1987; Conners et al., 1989; Gardner et al., 1990; and Sasowsky and Gardner, 1991). Software programs designed to automatically extract drainage basin parameters were applied to the DEM basins and derivative morphometric properties were obtained. Table B-1 summarizes the results of the drainage basin geomorphometrics.

For Walnut Creek and Woman Creek (Table B-1), similar values exist for nearly all parameters and derivative products. Without additional drainage basin data from numerous other basins, it is impossible to determine if the differences in drainage basin parameters between the two basins are significant. On inspection of the data, it appears that there is little to no discernible difference in the drainage basin development of Walnut and Woman creeks.

For the smaller subbasins, there are some differences in drainage parameters, but these are probably associated with differences in basin size. Differences in basin elongation and basin shape, relief ratio (indication of steepness), and hypsometric integral are apparent; however, none of the differences appears to be significant enough to warrant inferences about tectonic influence on drainage development.

Drainage basin asymmetry is a relatively quick method of evaluating the impact of tectonic tilting on the position of streams within a drainage basin. Drainage networks typically develop symmetric, leaf-shape patterns. Measurements of the drainage basin area to the left and right of the trunk stream are similar for a symmetric basin. Drainage basins that develop in regions of active tectonics often will have trunk streams that are displaced to one side of the basin if tilting is predominant. These types of basins have unequal areal measurements to the left and right of the trunk stream and are termed asymmetric. Basin asymmetry can also be produced in areas of pronounced structural (bedrock folds or faults) or lithologic influence and where fluvial conditions of tributaries cause the trunk stream to be displaced toward one side of the drainage basin. In the RFP area, bedrock conditions and structural control are considered to have little to no impact on the basin asymmetry.

The results of basin asymmetry analysis in the RFP area are indicated on Figure B-10a and b. The overall asymmetry of the Walnut Creek basin, which is expressed by the leftmost arrow shown on Figure B-10a, is very slight to the northwest (~5% from symmetric). The adjacent tributary basins show asymmetry in opposing directions suggesting that conditions other than tectonic probably influence drainage development. For example, drainages may have developed on a paleodrainage of an ancient surface. A third tributary shows no asymmetry (straight line, most northern and closest to the WCF).

The overall asymmetry of the Woman Creek basin is expressed by the middle north-pointing arrow of Figure B-10b. The arrow in the headwater region of Woman Creek basin indicates that this portion of the trunk stream (treated as a subbasin) actually is asymmetric to the south. Similarly, the arrow in the lower reaches also indicates asymmetry to the south, suggestive of south-directed tilting. In light of the location of the WCF, the change in the direction of asymmetry across the fault may be suggestive of differential tectonic tilting of the basin across the fault.

The hypsometric curves (Figure B-11) for Walnut Creek and Woman Creek show differing shapes suggesting differences in the erosional development in the basins despite having similar values for their basin attributes. The curve for Walnut Creek shows a concave upward curve characteristic of a drainage basin in a mature stage of development; nearly as much material has been removed from the basin as remains. The curve for Woman Creek, on the other hand, has a convex upward shape indicative of more material remaining in the basin than has been removed through erosion. The reason for this discrepancy in hypsometry for these two basin is unknown. Postulated causes for the differences are: the Woman Creek drainage basin is younger than the Walnut Creek drainage

basin; the Walnut Creek drainage basin developed more rapidly than the Woman Creek basin; Woman Creek basin is being rejuvenated by active tectonics and is not able to erode as fast as uplift is occurring. The first possibility is judged not likely based on field observation of landscape elements (e.g., terraces, stable slopes) that indicate that the two basins are of similar age. The second, that Walnut Creek erodes more rapidly is difficult to evaluate, but based on geologic maps and field observations, there appear to be few differences in external conditions. The third hypothesis, that tectonic activity is responsible is possible since Woman Creek is bisected by WCF, whereas the fault passes very close to the outlet of Walnut Creek. The Woman Creek basin could be experiencing tectonic uplift or warping across the central basin axis that could result in erosion just upstream of the fault and deposition just downstream with little or no net basin degradation. Walnut Creek basin is contained entirely in the hanging wall block of WCF and could respond by continual downcutting and erosion in response to uplift.

In summary, the drainage basin development studies were not conducted over a sufficiently large area to provide a range in coverage to determine if there is statistically significant spatial variation in drainage basin parameters that would indicate tectonic influence on drainage evolution. Drainage basin hypsometry reveals some interesting differences in the Walnut Creek and Woman Creek drainages, but these differences are difficult to interpret. Regardless of the origin of the driving forces, if they are tectonic, they have a very low signal to noise ratio and the signals that may be tectonic in origin are not considered to be characteristic of highly active tectonic features.

REGIONAL TECTONIC GEOMORPHIC STUDIES OF THE RANGE FRONT

The Colorado Front Range is well-suited for studies of the tectonic geomorphology of the range front for several reasons. The range front is the demarcation between two major structural and physiographic domains and lithologic characteristics along the range front are readily discerned and can be factored into interpretations of results. In addition, studies of the Rampart Range fault (Dames & Moore, 1984) and the Golden fault (Kirkham, 1977; Kirkham and Rogers, 1981) suggest that the Front Range fault system is probably the most important tectonic feature in this region. The map view expression of the range front indicates a good potential for using mountain front sinuosity as an indicator of relative tectonic activity along the range front. Existing maps of the geology of the Front Range urban corridor from Colorado Springs to Fort Collins (Colton, 1978; Trimble and Machette, 1979a, b) and the late Eocene erosional surface along the Front Range (Scott and Taylor, 1986) provide additional information from which to evaluate relative tectonic activity along the mountain front.

Mountain Front Sinuosity

The map view expression of mountain fronts provides information that can be used to quickly assess the general structural framework (i.e. segmentation) and spatial variation in the relative tectonic activity of mountain fronts. The linearity, or sinuosity, of mountain fronts has been shown to be directly related to tectonic activity along range bounding faults (Bull and McFadden, 1977; Bull, 1984; Menges, 1988; Menges et al., 1987). The sinuosity of mountain fronts is considered to represent the relative magnitude and rate of tectonic activity on range front faults: the most tectonically active faults have rates of uplift that exceed the rate of erosional modification and

therefore preserve linear mountain fronts as an erosional expression of the causative structure; the least tectonically active mountain fronts have uplift rates that are less than the rates of erosional modification such that the mountain front is actively eroded and a sinuous, map-view pattern develops.

The sinuosity of mountain fronts (*Smf*) can be measured quickly. The intersection of the mountain front with the piedmont is delineated on topographic maps. The definition of the piedmont mountain-front junction is dependent on the map scale and contour interval. The intersection is taken as the major topographic change in slope between the piedmont and the mountain front. Typically, a few topographic profiles are constructed to observe the piedmont mountain-front junction between the map and the profile. Then the intersection is visually located and traced on the topographic map. The map view length of this line of intersection is measured with a digitizer and this length is divided by the chord length of the mountain front outboard of the range bounding fault. Mountain front segments are defined on the basis of gross morphological characteristics such as continuity, consistency in trend, and general linearity. Smaller, individual mountain fronts are then delineated to further characterize the larger segment. Relative tectonic activity classes can be assigned for the groupings of *Smf* (e.g., Bull and McFadden, 1977; Menges and others, 1987; Wells and others, 1988).

The analysis was performed at a reconnaissance-scale level to determine the potential for further investigation. The piedmont mountain-front junction was determined from 1:100,000 scale topographic maps. Because of the scale dependence of the analysis, and the use of small-scale maps, classes of relative tectonic activity were not assigned.

Figure B-12 and Table B-2 present the results of the *Smf* study. Figure B-12 shows that the mountain front can be divided into four primary segments: the Fort Collins-Boulder (FCB) segment, the Boulder-Golden (BG) segment, the Golden-Air Force Academy (GAFA) segment and the Air Force Academy (AFA) segment. The histogram above the map view shows the spatial distribution of *Smf* values along the range front; the width of each block represents discrete mountain fronts. The FCB and GAFA segments are characterized by *Smf* values > 1.2 with the exception of mountain fronts 11 and 14 in the FCB segment. These two mountain fronts have *Smf* values of 1.14 and 1.03, respectively; they are considered artificially low values because of inherent problems in identification of the mountain front where the Mesozoic and Paleozoic rock section outcrops prominently along the mountain front. The low *Smf* of the AFA segment (1.05) is thought to reflect the higher degree of relative tectonic activity along the Rampart Range fault. The BG segment has a comparably low *Smf* (1.08) and is statistically distinct from the adjacent FCB and GAFA segments (Table B-3). Since the AFA segment consists of a single mountain front, it is not possible to make a statistical comparison with the other segments. The low *Smf* of the AFA segment is suggestive of relatively high tectonic activity. The implications are that the BG segment and AFA segment are the most tectonically active segments of the Front Range.

Range Crest/Piedmont Mountain-Front Junction Profiles

Profiles of the range crest (*RC*) of the Front Range and the piedmont mountain-front junction (*PMFJ*) provide graphic representations of the spatial variation in topography along the range. In a tectonic environment characterized by uniform uplift rates, the range crest and the topographic

expression of the intersection of the piedmont and the mountain front should be parallel and near-horizontal lines. If there is spatial variation in rates of tectonic activity, the *RC* and *PMFJ* should vary from horizontal lines, but should maintain a certain degree of parallelism unless significant active tectonic elements are present between the range front and the range crest (i.e. interior mountain fronts).

Profiles of the *RC* and *PMFJ* were constructed from 1:100,000 scale topographic maps from Colorado Springs to Lyons. The procedure for defining and delineating the PMFJ is the same as described for mountain front sinuosity. Elevations of the *RC* and *PMFJ* were projected onto a common plane for preparation of Figure B-13. The elevations of remnants of the late Eocene erosional surface at the eastern margin of the Front Range, determined from Scott and Taylor (1986) and remnants of the Quaternary Rocky Flats alluvium determined from the geologic maps of the Front Range Urban Corridor (Colton, 1978; Trimble and Machette, 1979a, b) were also projected onto the same plane in order to assess if known time horizons have been affected by tectonic deformation.

Figure B-13 shows that the *RC* and *PMFJ*, for the most part, rise and fall in parallel. The highest part of the range crest and piedmont occur in similar places which correspond to the segment of the mountain front with the lowest sinuosity (highest relative tectonic activity). Sharp breaks in the *RC* and *PMFJ* topography roughly correspond with defined subsegments of the mountain front (Figure B-12, Table B-2). The *RC* and *PMFJ* elevations decline near the South Platte River and continue to decline until reaching the BG mountain front segment. At the BG segment, the *RC* and *PMFJ* increase in elevation to the north and then decline again north of Boulder. The projections of the Eocene erosional remnants and the Rocky Flats alluvium also mimic the *RC* and *PMFJ* topography indicating that the *RC* and *PMFJ* are deforming together. The elevation of the Eocene erosional surface along the east margin of the Front Range is highest between the southern segment south of the South Platte River and the segment between Boulder and Golden. These topographic relationships substantiate the findings of the *Smf* studies that indicate the BG segment and the segment south of South Platte segments as the most tectonically active.

Summary of Regional Studies

In summary, the regional tectonic geomorphology studies of *Smf* and *RC-PMFJ* profiles help identify mountain front segments and show a distinct spatial variation in the relative tectonic activity along the Front Range from Colorado Springs to Fort Collins. *Smf* studies show that the mountain front is segmented into four major segments. The segment in the vicinity of the Rocky Flats Plant (BG) is statistically distinct from the adjacent segments and has characteristics similar to the Air Force Academy (AFA) segment just north of Colorado Springs. The *RC-PMFJ* profiles with projections of the late Eocene erosional surface and the Quaternary age Rocky Flats alluvium onto the *RC-PMFJ* profiles show similar apparent segmentation of the mountain front and the greatest topographic expression of the *RC*, *PMFJ*, the late Eocene erosional surface, and the Rocky Flats alluvium occurs along the same segments identified in the *Smf* study. It appears that there has been spatial variation in the relative tectonic activity of the Front Range since late Eocene time and through the early Quaternary such that the 0.9 to 1.8 Ma Rocky Flats alluvium has been deformed.

SUMMARY OF THE GEOMORPHIC ANALYSES

All four of the geomorphic analyses utilized, map analysis, field profiling, morphometrics of drainage basins, and tectonic geomorphology of mountain fronts, provide information that can be used to infer tectonic activity. At the local level in the vicinity of the Walnut Creek Fault (WCF), the results of the analyses are equivocal. The subenvelope map and map of the unconformity of the Rocky Flats alluvium and the Arapahoe Formation display anomalies along the WCF that suggest Quaternary fault activity. Map profiles of the Rocky Flats alluvial surface, a reasonably well-constrained early Quaternary datum, showed no clear evidence for tectonic displacement across the WCF. Detailed profiles of the Rocky Flats alluvial surface using sophisticated surveying equipment showed no evidence of vertical displacement across the WCF, within a resolution of about 1-2 meters (due to landscape modification by human activity as well as natural erosion). Using these constraints on maximum surface displacement and the estimated age of the Rocky Flats alluvium (0.9 to 1.9 Ma) yields a long-term maximum slip rate of 0.001 to 0.002 M/ka. Longitudinal profiles of streams that cross the WCF show anomalous shapes in their profile and also are associated with changes in stream gradient across the fault. The anomalous shapes can be explained by tectonic activity, geomorphic responses to tectonic activity, or geomorphic responses to external influences other than tectonic activity. Drainage basin analysis show predictable results of very low resolution of differences in drainage development for basins on either side of the fault. Some results, such as basin hypsometry, show differences that can be explained by tectonic activity. Taken with the results of the longitudinal profiles of streams and surfaces, the hypsometry provides additional evidence to indicate that there are distinct differences between Woman Creek and Walnut Creek drainages that may be related to tectonic activity along the Walnut Creek fault. If the WCF is active, the rate of activity is very low, and possibly below the threshold of detection using geomorphic criteria for recognizing surface deformation associated with tectonic activity.

The regional geomorphic analyses of the range front of the Colorado Front Range provide independent, supportive evidence for tectonic segmentation of the mountain front. A coarse- filter analysis of mountain front sinuosity showed that there are statistically significant differences in the mountain front sinuosity for the segment west of the RFP and the segment along the Rampart Range fault. These results indicate only relative degree of tectonic activity; they cannot be used to estimate rates of activity without further detailed analysis and field checking of factors that can influence the outcome of the sinuosity measurements (e.g. bedrock and structural conditions). The profiles of the piedmont mountain-front junction, range crest, remnants of the Eocene erosional surface, and remnants of the Rocky Flats alluvial surface provide supportive evidence for the notion of tectonic segmentation of the mountain front. For this study, attempts to determine deformation rates based on the elevations of known strain gauges (Rocky Flats alluvium, Eocene erosion surface) are unwise. But in a general sense, the profiles show a distinct spatial variation in apparent tectonic activity along the mountain front. The most active segment is in the region of the Rampart Range Fault. In the vicinity of RFP, the tectonic activity appears to be greater, and perhaps more complex, than adjacent areas.

REFERENCES

Bull, W.B. (1979). Threshold of critical power in streams, *Geological Society of America Bulletin,* v. 90, p. 453-464.

Bull, W.B. (1984). Tectonic geomorphology, *Journal of Geological Education,* v. 32, p. 310-324.

Bull, W.B. (1990). Stream-terrace genesis: implications for soil development, *in* P.L.K. Kneupfer and L.D. McFadden, eds., Soils and Landscape Evolution: Geomorphology, v. 3, p. 351-367.

Bull, W.B. (1991). Geomorphic responses to climatic change, Oxford University Press, New York, 326 p.

Bull, W.B. and L.D. McFadden (1977). Tectonic geomorphology north and south of the Garlock Fault, California, *in* D.O. Doehring, ed., Geomorphology of arid regions: Proceedings, 8th Binghamton Geomorphology Symposium, Allen & Unwin, Boston, p. 115-138.

Bullard, T.F. and W.R. Lettis (1989). Characterization of Quaternary deformation associated with concealed thrust faulting, *in* M. Jacobsen, compiler, National Earthquake Hazards Reduction Program Summaries of Technical Reports, Volume XXIX: U.S. Geological Survey Open File-Report 90-54, p. 112-118.

Bullard, T.F. and W.R. Lettis (1993). Quaternary fold deformation associated with blind thrust faulting, Los Angeles Basin, California, *Journal of Geophysical Research,* v. 98, no. B5, p. 8349-8369.

Burnett, A.W. and S.A. Schumm (1983). Alluvial-river response to neotectonic deformation in Louisiana and Mississippi, *Science*, v. 22, p. 49-50.

Colton, R.B. (1978). Geologic map of the Boulder-Fort Collins-Greeley area, Colorado, U.S. Geological Survey, Miscellaneous Investigations Series Map I-855-G.

Connors, K.F., T.W. Gardner and R.L. Day (1989). Deriving stream parameters for hydrologic modeling from digital elevation data, *in* M.L. Kavvas, ed., New Directions for Surface Water Modeling, Proceedings of the 3rd Scientific Assembly of the International Association of Hydrological Sciences, IAHS Publications No. 181, p. 937-406.

Dames and Moore (1981). Geologic and seismologic investigations for Rocky Flats Plant, Final Report, U.S. Department of Energy Contract Number DE-AC04-80AL 10890.

Davis, J.C. (1986). *Statistics and data analysis in geology*, New York, John Wiley & Sons, 646 p.

EG&G (1992). Phase II Geologic Characterization - Data Acquisition, Final Report, Prepared for the U.S. Department of Energy, Rocky Flats Plant, Submitted by EBASCO, March.

Franklin, S.E. (1987). Geomorphometric processing of digital elevation models, *Computers & Geosciences,* v. 13, p. 603-609.

Gardner, T.W., K.C. Sasowsky and R.L. Day (1990). Automated extraction of geomorphometric properties from digital elevation data, Zeitschrift für Gewomorphologie, Supp. Band 80, p. 57-68.

Geomatrix Consultants, Inc. (1993). Preliminary Quaternary and neotectonic studies, Savannah River Site, South Carolina, Final Report, Lawrence Livermore National Laboratories and Westinghouse Savannah River Company, 59 p.

Golts, S., and E. Rosenthal (1993). A morphotectonic map of northern Arava in Israel, derived from isobase lines, *Geomorphology*, v. 7, p. 305-315.

Hack, J.T. (1960). Interpretation of erosional topography in humid temperate regions, *American Journal of Science* (Bradley Volume), 258-A, pp. 80-97.

Hack, J.T. (1976). Dynamic equilibrium and landscape evolution, *in* W.N. Melhorn and R.C. Flemal, eds., Theories of landform development, 6th Binghamton Geomorphology Symposium, Allen & Unwin, Boston, p. 87-102.

Hanks, T.C., R.C. Bucknam, K.R. Lajoie and R.E. Wallace (1984). Modification of wave-cut and faulting-controlled landforms, *Journal of Geophysical Research,* v. 89, p. 5771-5790.

Hanks, T.C. and R.E. Wallace (1985). Morphological analysis of the Lake Lahontan and Beachfront fault scarps, Pershing County, Nevada, *Bulletin of the Seismological Society of America,* v. 75, p. 835-846.

Hanks, T.C. and D.J. Andrews (1989). Effect of far-field slope on morphologic dating of scarplike landforms, *Journal of Geophysical Research,* v. 94, no. B1, p. 565-573.

Hanson, K.L., T.F. Bullard, M. de Wit and A.L. Stieve (1993). Applications of Quaternary stratigraphic, soil-geomorphic, and quantitative geomorphic analyses to the evaluation of tectonic activity and landscape evolution in the Upper Coastal Plain, South Carolina, 4th Department of Energy Natural Phenomena Hazards Mitigation Conference, in review.

Hines, W.W. and D.C. Montgomery (1980). *Probability and statistics in engineering and management science,* New York, John Wiley & Sons, 634 p.

King, G.C.P. and R.S. Stein (1984). Seismic potential revealed by surface folding: 1983 Coalinga, California Earthquake, *Science*, v. 224, no. 4651, p. 869-872.

Kirkham, R.M. (1977). Quaternary movements on the Golden fault, Colorado, *Geology*, v. 5, p. 689-692.

Kirkham, R.M. and W.P. Rogers (1981). Earthquake potential in Colorado -- A preliminary evaluation, Colorado Geological Survey Bulletin 43, 171 p.

Lin, J. and R.S. Stein (1989). Coseismic folding, earthquake recurrence, and the 1987 source mechanism at Whittier Narrows, Los Angeles Basin, California, *Journal of Geophysical Research,* v. 94, no. B7, p. 9614-9632.

Mabee, S.B. (1978). The use of magnetite alteration as a relative age dating technique: preliminary results, M.S. thesis, University of Colorado, Boulder, 185 p.

Machette, M.N. (1975). The Quaternary geology of the Lafayette quadrangle, Colorado, M.S. thesis, University of Colorado, Boulder, 105 p.

Machette, M.H., P.W. Birkeland, R.M. Burke, M.J. Guccione, R. Hihl and G. Markos (1976). Soil development in Quaternary deposits in the Golden-Boulder portion of the Colorado piedmont, *in* R.C. Epis and E.J. Weimer, eds, Studies in Colorado field geology: Colorado School of Mines, Professional Contributions, no. 8, p. 339-357.

Macklin, J.H. (1948). Concept of the graded river, *Geological Society of America Bulletin*, v. 59, p. 463-512.

Mark, D.M. (1983). Automated detection of drainage networks from digital elevation models, *in* B.S. Wellar, ed., Automated cartography: international perspectives on achievements and challenges, volume II, Auto-Carto Six, 6th International Symposium on Automated Cartography, 288-298.

Marks, D., J. Dozier and J. Frew (1984). Automated basin delineation from digital elevation data, *Geo-Processing*, v. 2, p. 299-311.

Menges, C.M. (1988). The tectonic geomorphology of mountain front landforms in the northern Rio Grande Rift near Taos, New Mexico, Ph.D. dissertation, University of New Mexico, Albuquerque, 339 p.

Menges, C.M., S.G. Wells and T.F. Bullard (1987). Morphometry of tectonic landscapes along a convergent plate boundary, Pacific coast of Costa Rica, *in* W.L. Graf, ed., Geomorphic Systems of North America, Centennial Special Volume 2, Geological Society of America, p. 373-385.

Miller, D. (1988). Correlation and age of Quaternary alluvial sequence using pedogenic clay and carbonate accumulation near Bear, Colorado, Unpublished manuscript, Department of Geological Sciences, University of Colorado, Boulder, 29 p.

Morris, D.G. and R.G. Heerdegen (1988). Automatically derived catchment boundaries and channel networks and their hydrological applications, *Geomorphology*, v. 1, p. 131-141.

Nash, D.B. (1980). Morphologic dating of degraded normal fault scarps, *Journal of Geology*, v. 88, p. 353-360.

Nash, D.B. (1986). Morphologic dating and modeling degradation of fault scarps, *in* Geophysical Research Forum Geophysics Study Committee, Active Tectonics, National Academy Press, p. 181-194.

O'Callaghan, J.F. and D.M. Mark (1984). The extraction of drainage networks from digital elevation data, *Computer Vision, Graphics, and Image Processing*, v. 28, p. 323-344.

Ouchi, S.J. (1985). Response of alluvial rivers to slow active tectonic movement, *Geological Society of America Bulletin*, v. 96, p. 504-515

Patterson, P.E. (1984). A paleomagnetic study of a succession of paleosoils, Unpublished manuscript, Department of Geological Sciences, University of Colorado, Boulder, 35 p.

Sasowsky, K.C. and T.W. Gardner (1991). Watershed configuration and geographic information system parameterization for SPUR model hydrologic simulations, *Water Resources Bulletin*, v. 27, no. 1, p. 7-18.

Schumm, S.A. (1977). *The fluvial system*, John Wiley & Sons, New York, 338 p.

Schumm, S.A. (1976). Episodic erosion, a modification of the Davis cycle, *in* W.N. Melhorn and R.C. Flemal, eds., Theories of landform development, Proceedings of the 6th Annual Binghamton Geomorphology Symposium, Boston, George Allen & Unwin, p. 69-85.

Schumm, S.A. (1973). Geomorphic thresholds and complex response of drainage systems, *in* M. Morisawa, ed., Fluvial and Geomorphology, Proceedings of the 4th Annual Binghamton Geomorphology Symposium, Boston, George Allen & Unwin, p. 299-310.

Scott, G.R. (1975). Cenozoic surfaces and deposits in the southern Rocky Mountains, Geological Society of America, Memoir 144, p. 227-248.

Scott, G.R. and R.B. Taylor (1986). Map showing Late Eocene erosion surface, Oligocene-Miocene paleovalleys, and Tertiary deposits in the Pueblo, Denver, and Greeley 1° x 2° quadrangles, Colorado, U.S. Geological Survey, Miscellaneous Investigation Series Map I-1626.

Siegel, A. (1956). *Nonparametric statistics*, New York, McGraw-Hill, 213 p.

Spencer, F.D. (1961). Bedrock geology of the Louisville quadrangle, Colorado, U.S. Geological Survey, Map GQ-151.

Trimble, D.E. and M.N. Machette (1979a). Geologic map of the Colorado Springs-Castle Rock area, Front Range Urban Corridor, Colorado, U.S. Geological Survey, Miscellaneous Investigation Series Map I-857-F.

Trimble, D.E. and M.N. Machette (1979b). Geologic map of the greater Denver area, Front Range Urban Corridor, Colorado, U.S. Geological Survey. Miscellaneous Investigations Series Map I-856-H.

Van Horn, R. (1976). Surficial ad bedrock geologic map of the Golden quadrangle, Jefferson County, Colorado, U.S. Geologic Survey, Miscellaneous Investigation Series Map I-761-A.

Wells, S.G., T.F. Bullard, C.M. Menges, P.G. Drake, P.A. Karas, K.I. Kelson, J.B. Ritter and J.R. Wesling (1988). Regional variations in tectonic geomorphology along a segmented convergent plate boundary, Pacific coast, Costa Rica, *Geomorphology,* v. 1, p. 239-265.

TABLE B-1
SUMMARY OF DRAINAGE BASIN GEOMORPHOMETRICS IN THE ROCKY FLATS PLANT AREA

Basin	Aspect (%)	L (km)	A (km^2)	P (km)	S_c	S_e	S_b	H_b (m)	Rr	HI	M	N	C_t (km)	F	Dd
Walnut Creek	ENE (64)	6.6	8.3	16.3	32.0	0.438	0.192	178	0.027	0.487	71	141	36.8	16.9	4.4
Woman Creek	ENE (50)	6.7	7.0	16.7	40.2	0.391	0.153	198	0.029	0.568	78	155	33.8	22.2	4.8
Walnut Creek Sub 1 (west of fault)	ESE (110)	2.5	1.34	6.1	28.1	0.472	0.223	86	0.035	0.597	10	19	6.1	14.1	4.5
Walnut Creek Sub 2 (east of fault)	ESE (110)	1.2	0.69	3.5	17.4	0.674	0.454	83	0.067	0.488	6	11	2.7	15.8	3.9

Average Slope for all Stream Segments

Walnut Creek 0.1744 m/m
Woman Creek 0.2493 m/m
Walnut Creek Sub 1 0.0397 m/m
Walnut Creek Sub 2 0.0460 m/m

EXPLANATION

Aspect: Measurement of the dominant slope exposure direction
L: Basin length, measured in straight line from farthest point in basin to the basin outlet
A: Basin area
P: Basin perimeter length measured along the drainage divide
S_c: Relative crenulation of basin perimeter: P^2/A
S_e: Basin elongation: $A^{0.5}/L$; allows assessment of lithologic or tectonic influence on drainage development
S_b: Basin shape: A/L^2; allows assessment of lithologic or tectonic influence on drainage basin development
H_b: Basin relief: greatest elevation within the basin minus the elevation at the basin outlet
Rr: Relief ratio: L/H_b; provides a measure of overall steepness of the basin
HI: Hypsometric integral: measure of the erosional development of a drainage basin
M: Shreve magnitude: method of ordering stream networks; provides the number of tributary branches upstream from any point in basin
N: Total number of stream segments in the basin
C_t: Total length of stream channels in the drainage basin
F: Drainage frequency: the number of stream channels per unit area; $F = (2M-1)/A$
D_d: Drainage density: the length of stream channel per unit area of drainage basin; $D_d = C_t/A$; provides a measure of stream network development in a drainage basin

TABLE B-2
SUMMARY OF MOUNTAIN FRONT SINUOSITY OF THE COLORADO FRONT RANGE FROM COLORADO SPRINGS TO FORT COLLINS

Mountain Front Number	Segment		Lmf	Ls	Smf
1	Air Force Academy (AFA)		21.929	20.817	1.053
	Golden-Air Force Academy (GAFA)	[mean Smf = 1.273]			
2			16.364	13.164	1.243
3			13.170	10.784	1.221
4			20.085	15.013	1.338
5			19.523	14.333	1.362
6			16.491	13.580	1.214
7			5.325	4.231	1.258
	Boulder-Golden (BG)	[mean Smf = 1.087]			
8			9.542	8.690	1.098
9			6.384	5.934	1.076
	Fort Collins-Boulder (FCB)	[mean Smf = 1.199]			
10			26.903	20.611	1.305
11			10.866	9.555	1.137
12			23.365	18.598	1.256
13			4.623	3.739	1.236
14			11.520	11.221	1.030
15			8.479	8.432	1.228

EXPLANATION

Lmf Length of the mountain front measured from 1:100,000 topographic maps
Ls Chord length of the mountain front measured outside of the range block
Smf Mountain front sinuosity: Lmf/Ls

See Figure B-12 for locations of mountain front segments and subsegments.

TABLE B-3
SUMMARY OF WILCOXON TWO-SAMPLE TEST FOR INDEPENDENCE OF SAMPLE MEANS FOR MOUNTAIN FRONT SINUOSITY

H_0: $\bullet_1 = \bullet_2$ the mean sinuosity of the mountain front segments are the same

H_1: $\bullet_1 \neq \bullet_2$ the mean sinuosity of the mountain front segments are not the same

Segment	GAFA	BG	FCB
GAFA	---		
BG	Reject H_o	---	
FCB	Accept H_o	Reject H_o	---

Note:

The Wilcoxon two-sample test for determining independence of sample means is a nonparametric statistical test that is commonly applied to hypotheses concerning geologic data (Davis, 1986). The test is a powerful alternative to parametric statistical tests when sample sizes are small or there are no required distributional assumptions about the underlying population (Siegel, 1956; Hines and Montgomery, 1980). For many situations, the two populations being studied do not even approach a normal distribution, so the parametric t-test is not valid. But if the two populations are normal, the Wilcoxon two-sample test is almost as efficient as the t-test.

For this particular application, the test is used to substantiate the observation that morphological differences are apparent in the mountain front from Colorado Springs to Fort Collins. The null hypothesis (H_0) states that the mean sinuosity of mountain front segments are the same. If the criteria for rejection of the null hypothesis are met, then the alternative hypothesis (H_1), which states that the mean sinuosity of mountain front segments are not the same, must be accepted. The test is simple yet powerful and lends support to arguments concerning the *relative* tectonic activity of the mountain front as expressed by its morphology.

The procedure is as follows (from Hines and Montgomery, 1980): Two samples, n_1 and n_2 are taken and the $n_1 + n_2$ observations are arranged in ascending order and ranked. If two or more observations are tied, use the mean of the ranks that would have been assigned if the observations differed. Let R_1 be the sum of the ranks in the smaller sample, and define

$$R_2 = n_1(n_1 + n_2 + 1) - R_1$$

If the sample means do not differ, then the sum of the ranks should be about equal. If the sum of the sample means greatly differ, it could be concluded that the means are not equal. Statistical tables provide the critical value (R^*_α). The null hypothesis is rejected is either R_1 or R_2 is less than or equal to the critical value. When the samples sizes n_1 and n_2 are large, the sampling distribution of R_1 approaches a normal distribution. For this study, the sample sizes were small and the procedure shown above was used.

The above table gives the results of the testing between mountain front segments. The Air Force Academy segment (segment AFA of Figure B-12) could not be tested because the segment is comprised of one mountain front, which is an insufficient sample size for the statistical test.

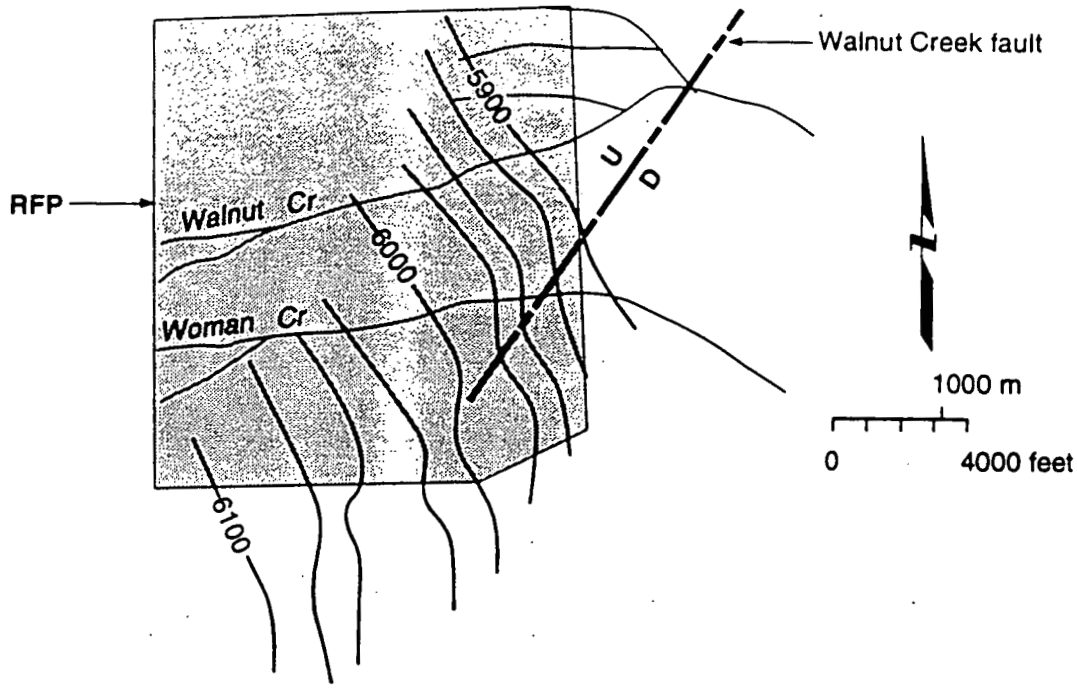

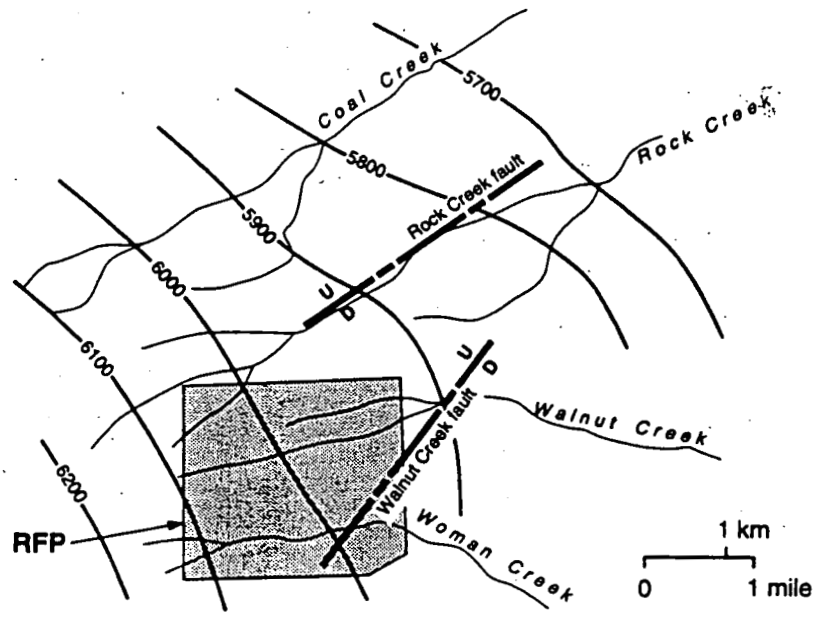

EXPLANATION

6000 —— Contour line, elevation in feet

Figure B-1. Contour map of the unconformity between the Rocky Flats alluvium and Arapahoe Formation (top) and contour map of the Rocky Flats alluvial surface (bottom). Both maps based on 1:24,000 scale geologic map (EG&G, 1992) of the Rocky Flats Plant and vicinity.

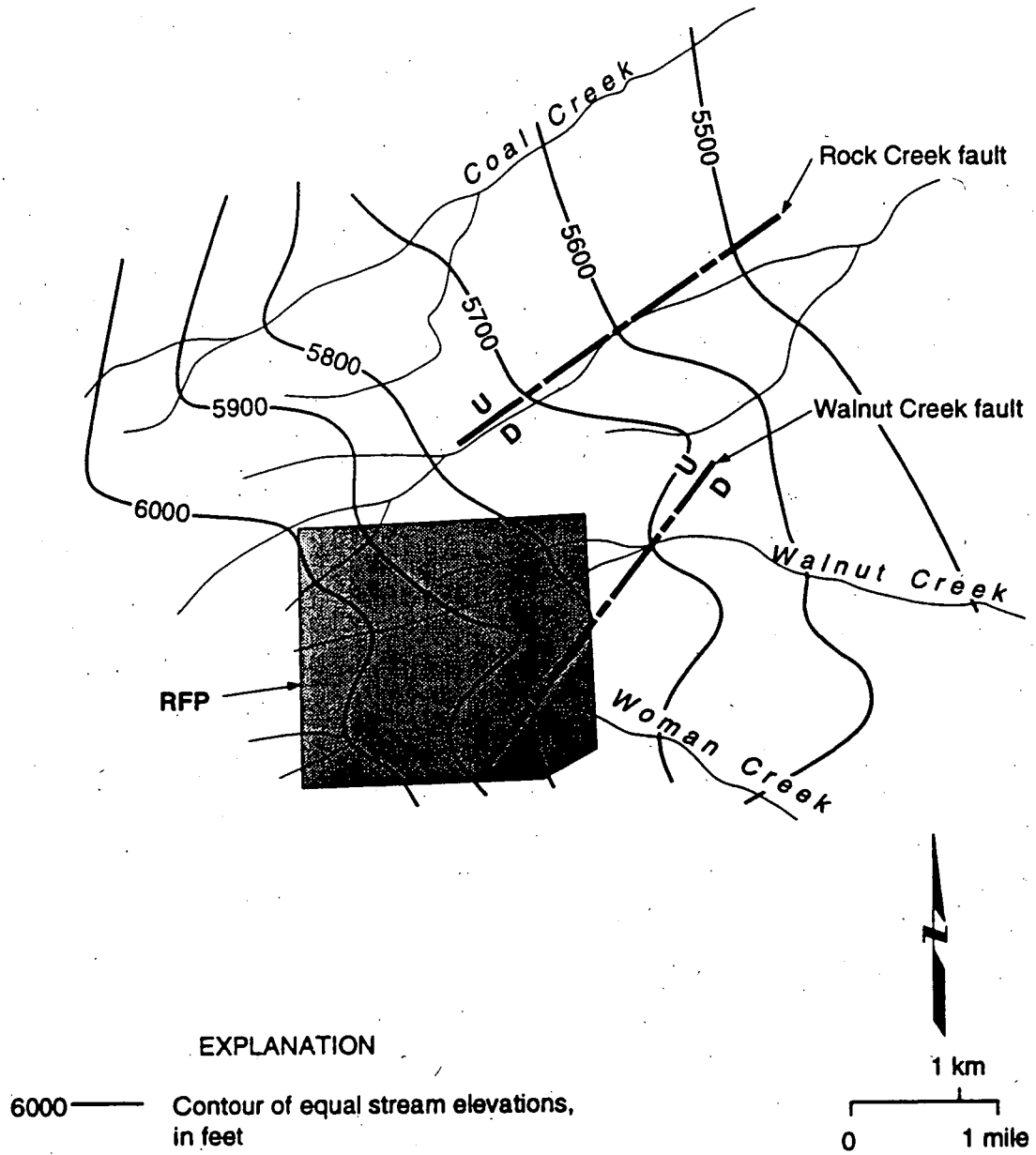

Figure B-2. Subenvelope map of the Rocky Flats Plant area.

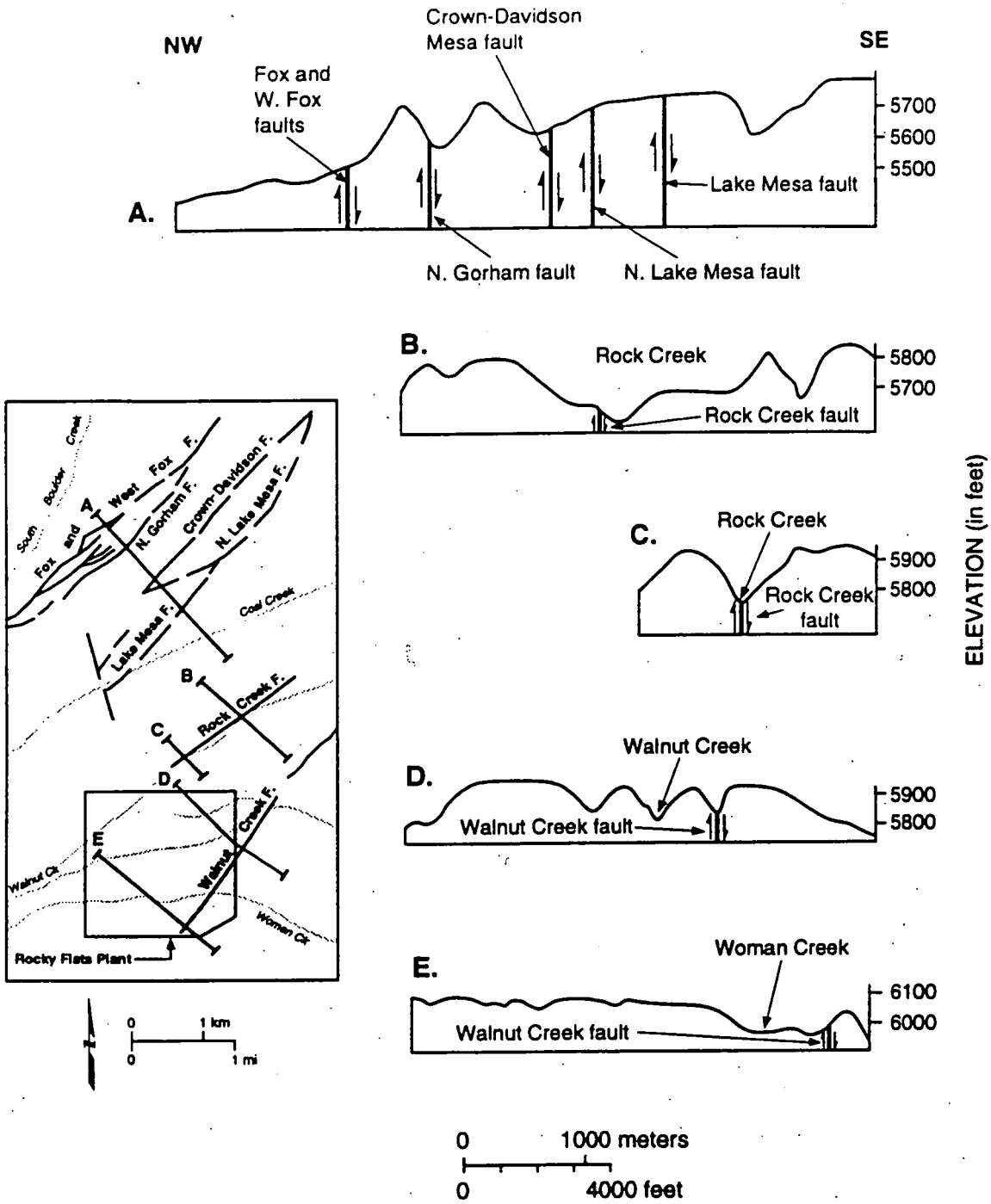

Figure B-3. Topographic profiles across (transverse) the dissected Rocky Flats alluvial surface across the Marshall fault zone (top), the Rock Creek fault (middle two profiles), and the Walnut Creek fault (lower two profiles). Inset map shows location of profiles. Vertical scale is exaggerated about 8 times the horizontal scale.

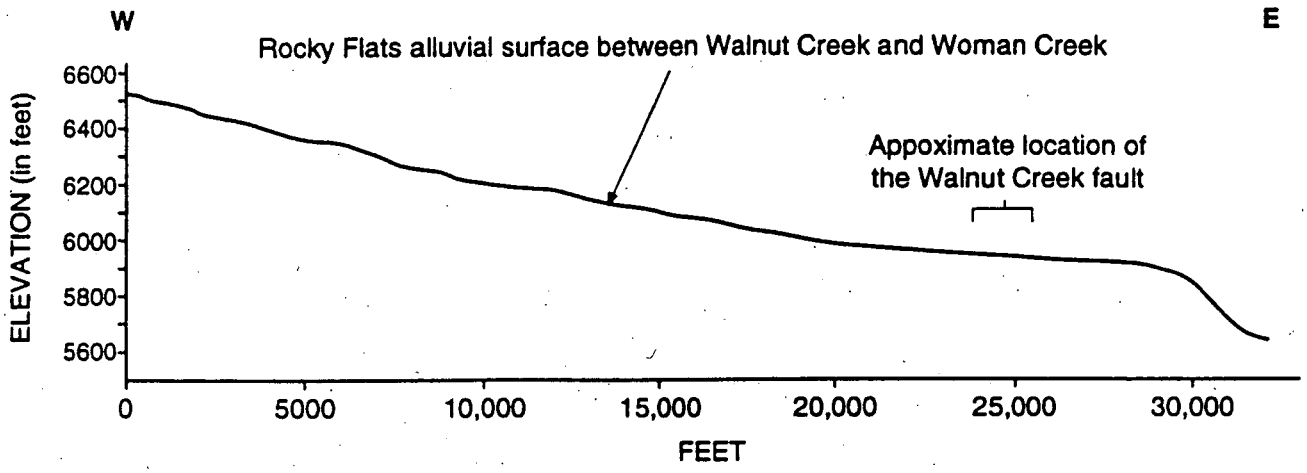

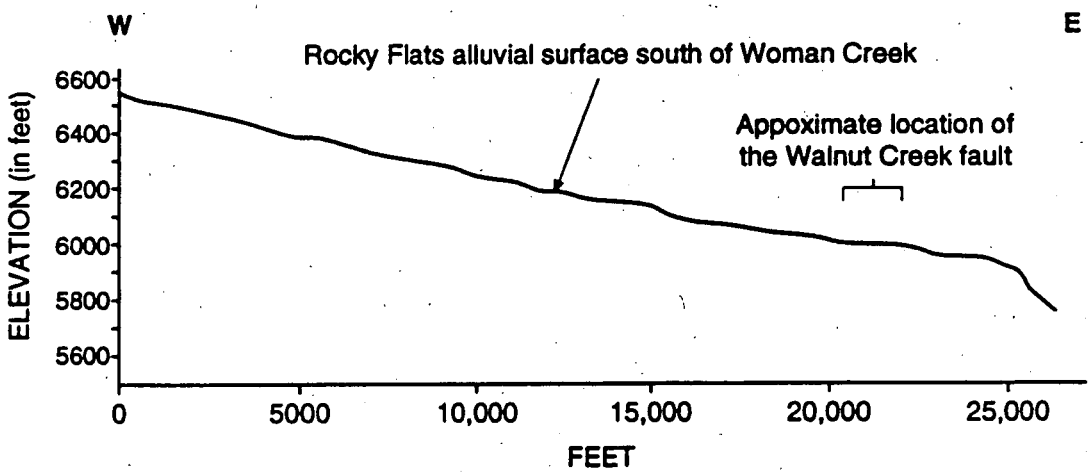

Figure B-4. Longitudinal profiles of the Rocky Flats alluvial surface from USGS. 1:24,000 scale topographic maps (Louisville, 1957; Eldorado Springs, 1965), 10- and 40-ft contour intervals. Vertical scale is exaggerated approximately 8 times the horizontal scale.

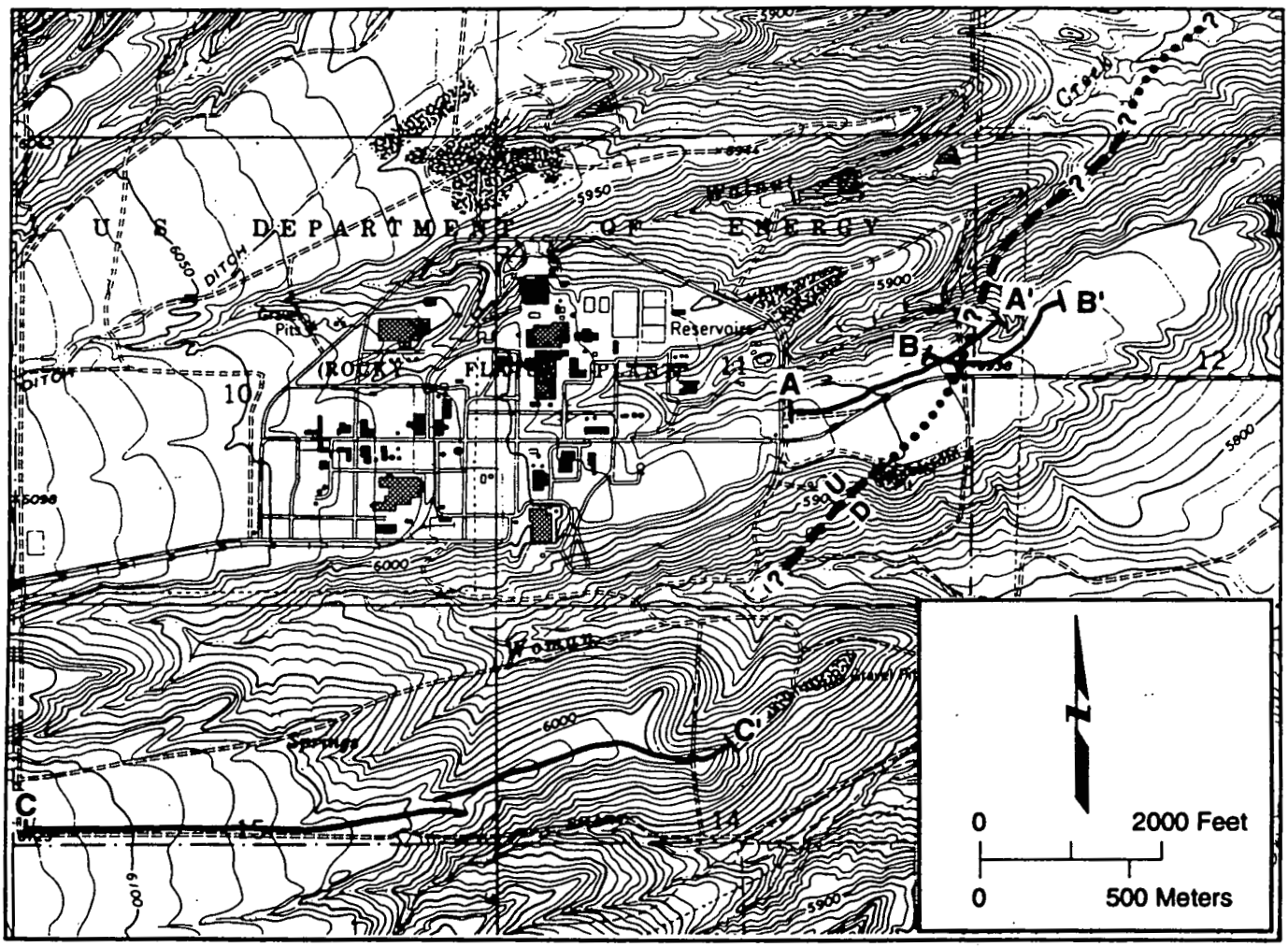

Base map: U.S. Geological Survey, Louisville, Colorado 7.5-minute quadrangle (1957), 1:24,000 scale, contour interval 10 feet.

Figure B-5. Location of Walnut Creek fault and topographic profiles A-A', B-B', and C-C' across Rocky Flats alluvial fan surface. Profiles shown on Figures B-6 and B-7.

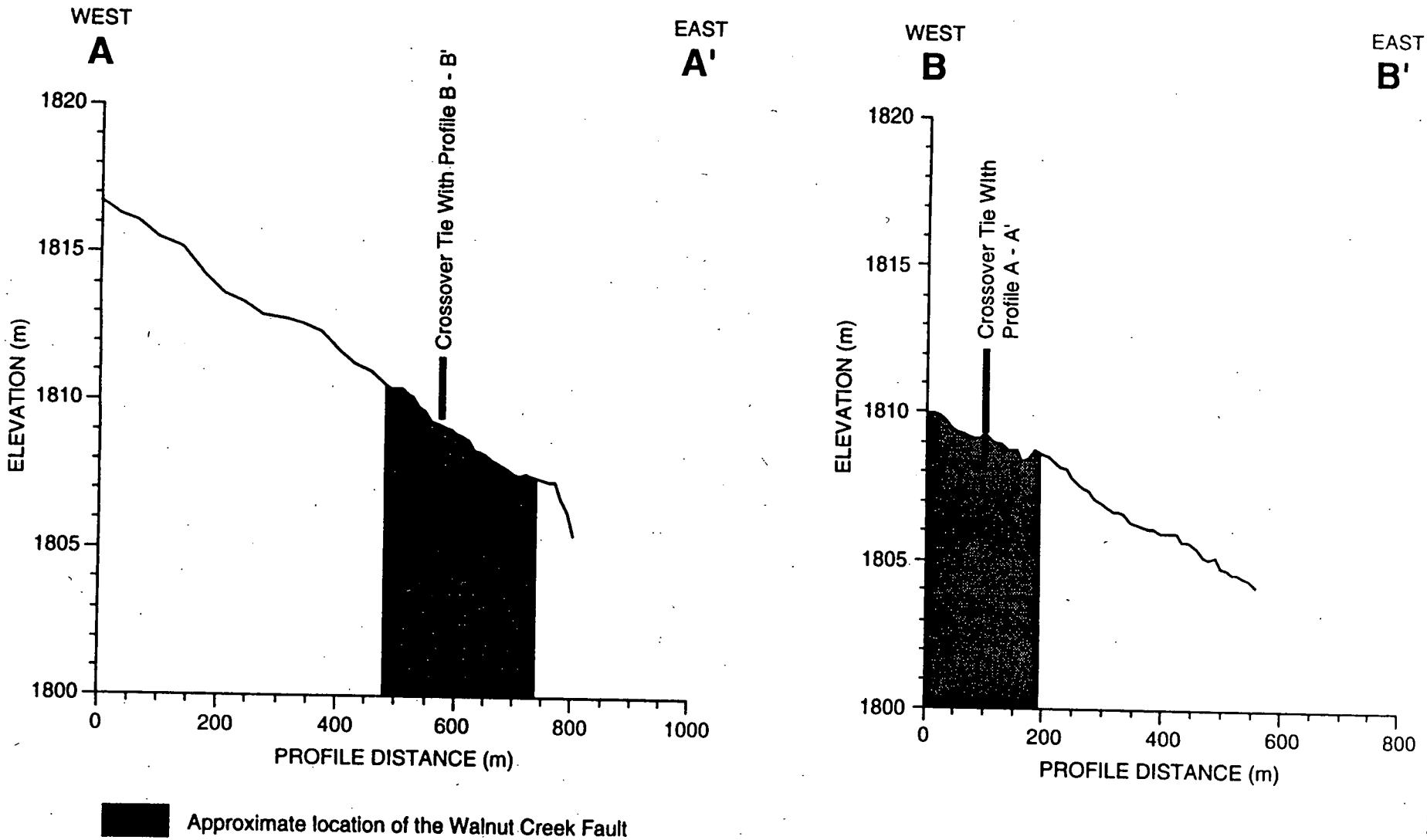

Figure B-6. Profiles A-A and B-B of the Rocky Flats alluvial fan surface to the east of the Rocky Flats Plant facilities. Profile locations shown on Figure B-5. Vertical scale is exaggerated approximately 50 times the horizontal scale.

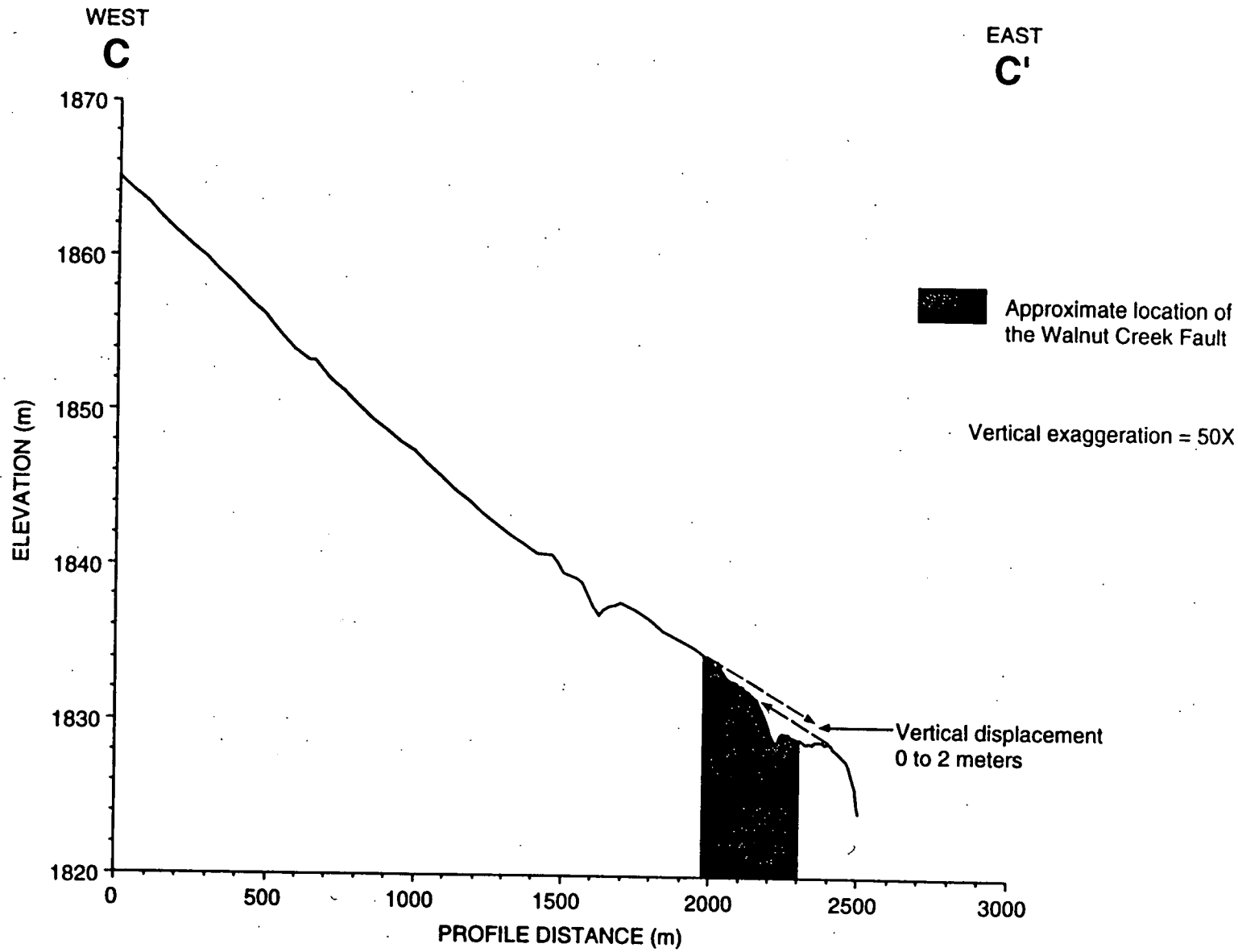

Figure B-7. Profile C-C of the Rocky Flats alluvial fan surface south of Woman Creek. Location of profile is shown on Figure B-5. Vertical scale is exaggerated approximately 50 times the horizontal scale.

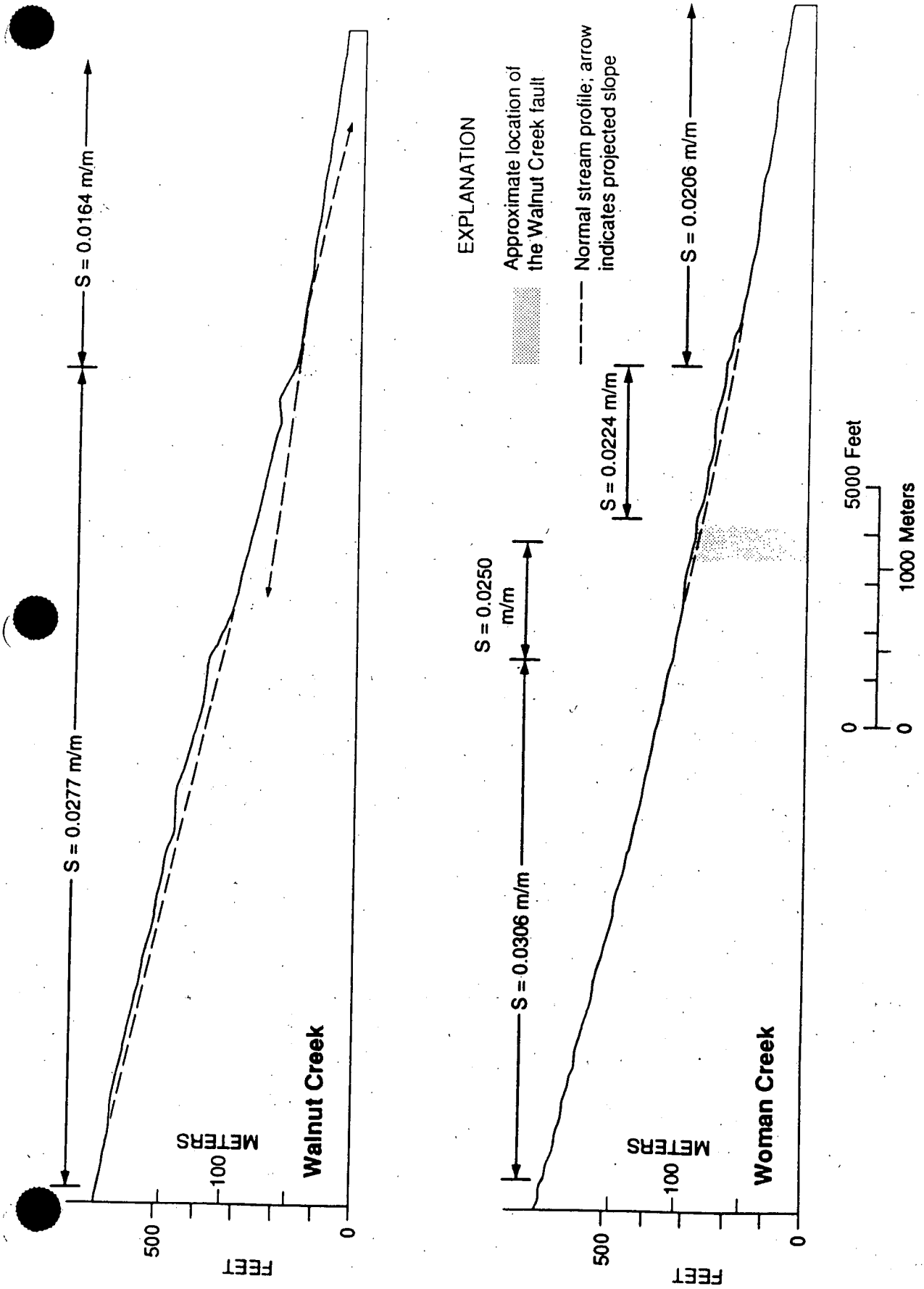

Figure B-8. Longitudinal profiles for Walnut Creek and Woman Creek in the vicinity of Rocky Flats Plant, Colorado. Vertical scale is exaggerated approximately 8 times the horizontal scale.

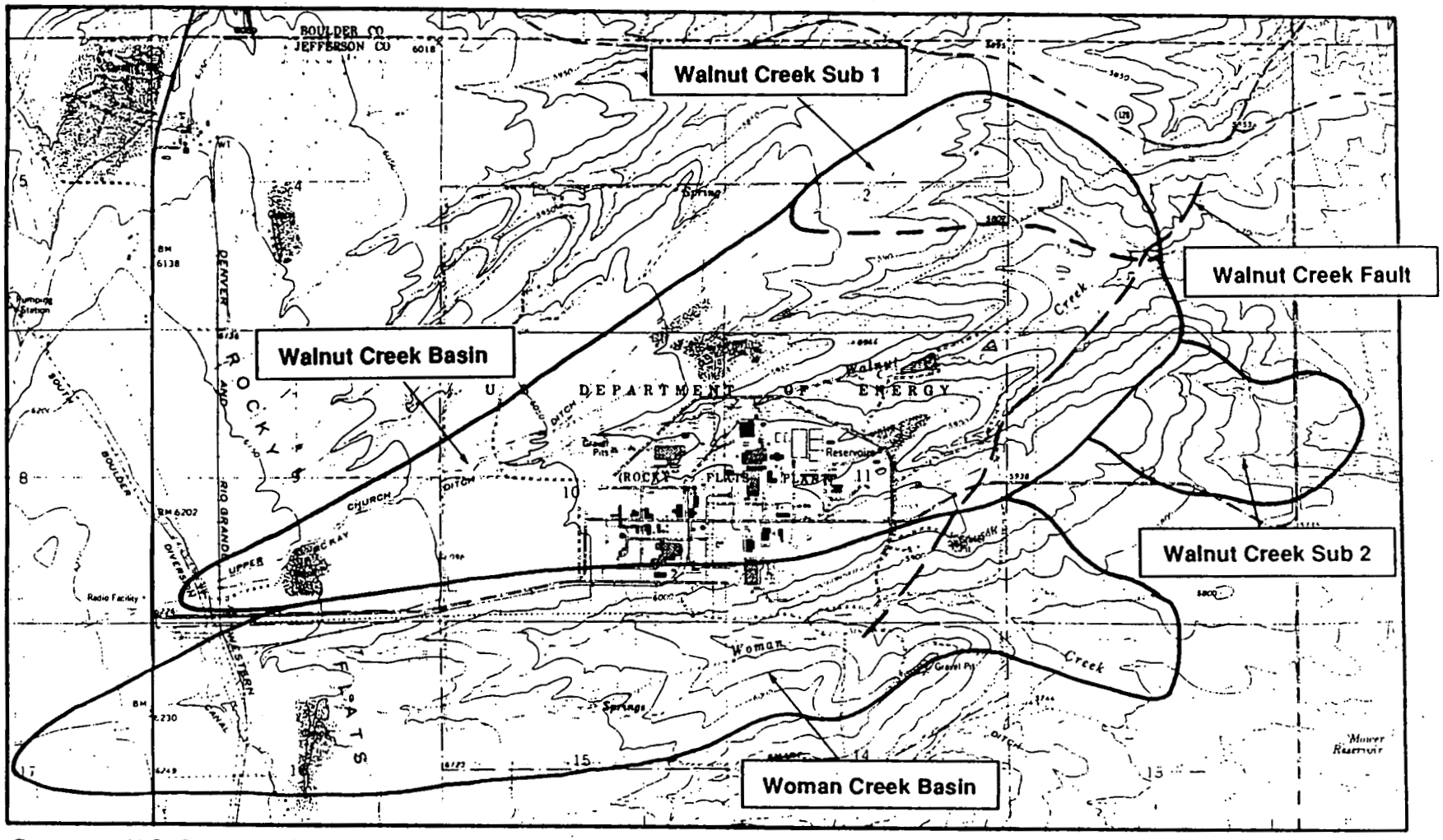

Base map: U.S. Geological Survey, Louisville, Colorado 7.5-minute quadrangle (1957), 1:24,000 scale, contour interval 10 feet.

1 km
0 1 mile

Figure B-9. Map showing the location of the drainage basins selected for study.

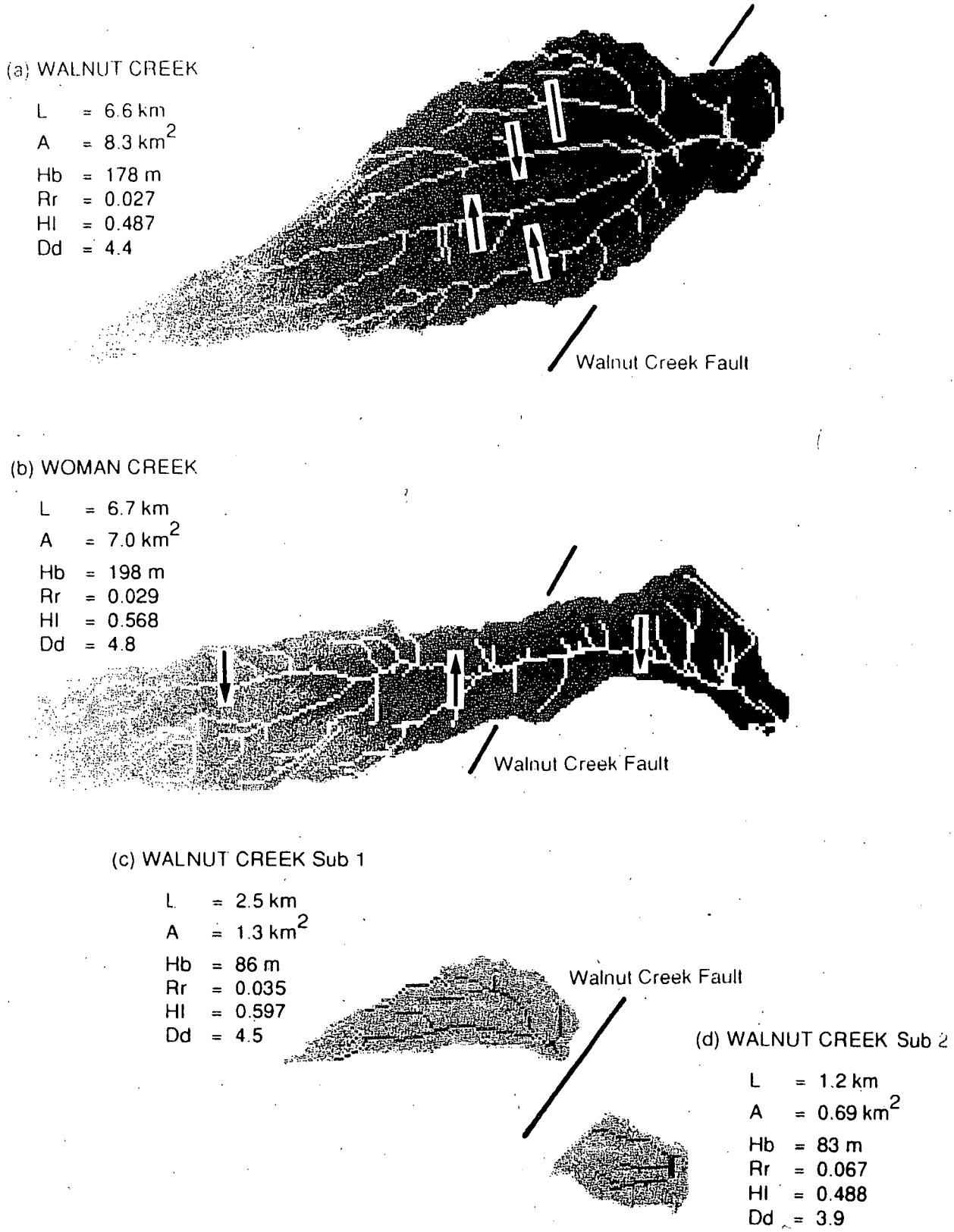

Figure B-10. Drainage basins and stream networks generated from Digital Elevation Models. Stream net for Walnut and Woman creeks shown in white; stream nets for subbasins shown in blue. White arrows show direction of basin asymmetry; line without arrow head indicates a symmetric subbasin. Drainage basin parameters are defined in the text.

APPENDIX C

REEVALUATION OF THE EPICENTER AND MAGNITUDE FOR THE 1882 COLORADO EARTHQUAKE

by

G.A. Bollinger
Buffalo, Wyoming

OBJECTIVE

The objective of this study is to estimate the size and epicentral location of the 1882 Colorado earthquake and to make quantitative assessments of the confidence associated with these estimates. Multiple estimates are to be made as required, along with a quantitative assessment of the credibility of each interpretation unless the properties are found to be well-defined. These estimates are needed (a) to make estimates of maximum possible earthquake size in seismic sources where the 1882 earthquake may have occurred, and (b) to assign a magnitude for historical seismicity analyses in order to determine activity rates and *b*-values.

BACKGROUND

The November 7, 1882, earthquake, apparently centered in Colorado, is the largest shock known to have occurred in that state. The U.S. Geological Survey (Stover and Coffman, 1993) lists its epicentral coordinates as 40.5°N and 105.5°W and its magnitude (based on felt area and equivalent to m_b) as 6.2. Those coordinates place the epicenter approximately 90 km north-northwest of the city of Denver. The earthquake caused minor damage in Denver (MMI VII) and along the Front Range and southern Wyoming (MMI VI). It was felt into Utah and Kansas. An aftershock occurred on November 8 that was reported to be almost as strong as the mainshock according to reports from Denver and Laramie.

At issue here is a critical assessment of the size and location of this earthquake. The pre-instrumental occurrence time dictates that epicentral and size estimates be based on intensity observations. Intensity data are intrinsically qualitative, but the existence of numerous studies on this type of information has proven to be utilitarian in cases such as this one. To accomplish the above-stated objectives, extensive use is made of the results from these studies that have defined intensity characteristics. In particular, a recent study of the size of earthquake damage areas across the United States, just completed by myself and colleagues at Virginia Tech (Bollinger et al., 1993), is useful for the assessments at hand.

EPICENTER ESTIMATION

Earthquake intensity is a number denoting the severity of an earthquake at a particular location, in terms of the effects of the earthquake ground motions on humans, on construction (works of man) and on the natural surface features of the earth. The intensity observed depends on multiple factors, including:

Seismic Factors

Magnitude
Focal depth
Focal mechanism
Distance from source
Path effects (inhomogeneities)

Geologic Factors

Type and thickness of soil and regolith
Character of bedrock geology
Groundwater level
Slope and configuration of the ground surface

Engineering Factors

Type and quality of construction
Natural period of the structure
Interaction between nearby structures

Human Factors

Sensitivity of observer (previous exposure, physical location)
Location of observer (outdoors, indoors, type and floor of building)
Time of day (observer sleeping or awake, active or quiet)
Weather (storms, wind, etc. can mask earthquake effects)
Sounds (can intensify fright)

In the United States, the Modified Mercalli Intensity (MMI) scale is used to categorize earthquake effects into a numerical scheme.

While there can be significant variations, isoseismal contours often have a roughly elliptical to circular shape, sometimes with lobate extensions in one or more directions. In surveys where there is a high density of reliable observations, intensity values can be observed to exhibit rapid spatial variations. For this reason, Richter (1958) recommends that the mode of the intensity data (the value that appears the most often) be contoured rather than trying to honor the individual intensity values vigorously. Indeed, for especially important intensity studies, two maps are sometimes prepared from the same data. One map tends to honor the individual intensity values somewhat closely and this produces a contour map of considerable complexity. This type of map has the

advantage of depicting those areas subject to higher than normal shaking--often such areas are underlain by soft surficial soils as in river valleys. A second map can be prepared that is a highly generalized version with smooth contour geometry. This type of map obscures the more localized variations, and emphasizes the overall radiation pattern of seismic waves from the subject earthquake. Usually, however, only one intensity map is prepared, and, in the literature, examples of both of the above approaches to intensity contouring are found on a given single isoseismal map as well as variations of two basic techniques.

INTENSITY MAP FOR THE 1882 COLORADO EARTHQUAKE

Even after multiple episodes of archival searching, the amount of intensity data available for the 1882 Colorado earthquake is skimpy. Additionally, because of the types of sources available at that time, there is a wide variation in the reliability of the individual observations. This makes the assignment of intensity values and their contouring a difficult task that is subject to considerable uncertainty.

Kirkham and Rogers (1986) have produced the latest intensity map for the 1882 shock (see Figure C-1). They have the benefit of the most recent and complete intensity data set. Their contouring is well done, and the isoseismals are correctly shown as dashed lines. This is effective communication of the lack of an adequate amount and quality of data to accurately define the isoseismal contours. I have reviewed their intensity assignments and their contouring of that data and have no substantive disagreements. I will use their map for this study. That map has a number of interesting features including:

1. A very rapid decrease of intensity toward the east coupled with an apparent elongation of intensity to the west,

2. A roughly triangular shape to the MMI VI and lower contours,

3. Rapid spatial variation of the highest intensity levels (V, VI and VII) along the Front Range urban corridor, and

4. A separate felt area for an aftershock that occurred the day after the mainshock.

Each of these features is discussed briefly in the following paragraphs:

Rapid Decrease of Intensity to the East, Elongation to the West, and a Triangular Shape for the Isoseismals

This type of isoseismal pattern is unusual but not rare. An excellent example from the eastern United States is for the 1973 Knoxville, Tennessee, earthquake (see Figure C-1). There, the epicenter (MMI VI) was displaced toward the rapid decrease (northern) side of the MMI V isoseismal. The same epicenter/isoseismal asymmetry is proposed for the 1882 shock by Kirkham and Rogers (1986). As shown in Figure C-1, when the intensity map for the 1973 earthquake is reoriented so that north on the figure is to the right, there is a marked similarity with the 1882 intensity map.

Rapid Spatial Variation of the Highest Intensity Levels (V, VI and VII) Along the Front Range Urban Corridor

This type of variation is seen often on intensity maps and is usually attributed to population density variations and/or marked changes in character of the ground, e.g. between rock sites and alluvium or soft sediment locations.

Test of the Stability of the Preceding Three Isoseismal Patterns

The intensity data base of Kirkham and Rogers (1986) has been recontoured by myself and three other experienced seismologists (see page C-23 and the isoseismal maps presented in Figures C-2b through C-2e). The preceding three isoseismal patterns (nos. 1 through 3 listed above) were exhibited in all four maps. This affirms the Kirkham and Rogers (1986) map as a valid interpretation of the available data.

A Separate Felt Area for an Aftershock

Kirkham and Rogers (1986) were impressed enough with the aftershock reports along the Front Range that they located the epicenter near the center of its elliptical felt area. They noted that Meeker, Colorado, on the western slope, also reported feeling the same aftershock but gave that report much less weight.

ANALYSIS

Expectably, in the majority of cases where both detailed intensity data and instrumental epicenter locations are available, the epicenter is near the highest intensity or inside of the highest MM level isoseismal. The epicenter is usually not at the exact center of that isoseismal but is often displaced to one side or the other. Conventional practice of specifying epicentral coordinates from intensity maps is intrinsically qualitative and consists of using the centroid of the highest contour, because there is generally no way to know in advance how far or in which direction the actual epicenter might be displaced from that central point.

Epicentral estimation from intensity data for catalog purposes requires that a specific point be defined, usually with an attendant error estimate. Kirkham and Rogers (1986) gave 40.5°N and 105.5°W as their best epicentral location, with a possible error of one-half degree or more for the 1882 shock. For purposes of probabilistic seismic hazard assessment, it is, however, more appropriate to estimate the area within which the epicenter is expected to be and then to assign a confidence associated with that estimate.

I agree with Kirkham and Rogers (1986) that the felt area of the aftershock is a most important indicator of the epicentral locale. This is because aftershocks are generally smaller than the mainshock and thereby have a smaller felt area. Also, they tend to occur near the mainshock epicenter. Different from Kirkham and Rogers (1986), however, I would tend to give the Meeker aftershock somewhat more weight than they did. The Front Range reports do indicate a higher level of shaking, and both Kirkham and Rogers (1986) as well as Stover and Coffman (1993) base their

epicenter assignment on them. I agree with the general interpretation of that locale being the most likely epicentral area.

The area enclosed by the MMI VI is especially large (85,000 km^2). The occurrence of VI level effects in western Colorado as well as southeastern and southwestern Wyoming places those areas at shaking levels comparable to the more populous Front Range corridor. The MMI VI and VII effects south of Colorado Springs appear to me to be an outlier effect and not directly relevant to epicentral location. Also, the intensity assignments there may be a bit high.

Another possible indicator for the location of the 1882 epicenter is the seismicity pattern for the state. That is, where have most of the historical and recent earthquakes occurred? It is more likely that the 1882 shock would occur in that area rather than in some historically aseismic portion of the state. Except for the recent seismic activity associated with the Rocky Mountain Arsenal well, the Decade of North American Geology (DNAG) Project's Seismicity Map of North America by Engdahl and Rinehart (1988) and the Colorado seismicity maps by Kirkham and Rogers (1985) and by Stove and Coffman (1993), all depict most of the historical seismicity in the western part of Colorado, approximately between west longitude 106° and 108°. Thus, a West Slope rather than a Front Range location for the epicenter would be suggested by the historical activity in the state.

In summary, because of:

1. Large areal and east-west extent of MMI VI effects,

2. Aftershocks felt reports from the Front Range corridor and from the West Slope (Meeker), and

3. Historical seismicity mostly in the West Slope area,

three potential epicentral host areas should be considered. These areas are defined as rectangular approximations to the MMI VI contour and to the full and partial aftershock felt area contours (solid and dashed/questioned contours of Kirkham and Rogers [1986]). Figure C-3 shows these areas which have the following latitude-longitude coordinates in degrees:

Area (A + B + C)	(41.7, 110.0), (41.7, 104.8), (39.5, 104.8), (39.5, 108.4), (40.0, 108.4), (40.0, 110.0), (41.7, 110.0)
Area (B + C)	(41.7, 108.4), (41.7, 104.8), (39.5, 104.8), (39.5, 108.4), (41.7, 108.4)
Area (C)	(41.7, 106.0), (41.7, 104.8), (39.5, 104.8), (39.4, 106.0), (41.7, 106.0)

Area (A + B + C), which is essentially the MMI VI contour area, covers some 100,000 km^2 and is assigned a confidence of 95%. Area (B + C), the full aftershock felt area, extends for about 75,000 km^2 and is assigned a confidence of 85%. Area (C), the 25,000 km^2 higher intensity area for the aftershock is given a confidence of 40%.

120

MAGNITUDE ESTIMATION

In 1882 there were no seismographs in operation in the United States. Thus the quantitative measure of earthquake size (magnitude) must be estimated from the level and distribution of its effects as characterized by the qualitative MMI. This procedure consists of employing the several empirical relationships between magnitude and various MMI measures that have been developed from modern earthquake occurrences where both types of measurement are available. Several considerations are relevant here, including the following:

Was the 1882 shock an "eastern" or "western" earthquake?

Because of the marked differences in the anelastic attenuation of seismic waves between the western and eastern parts of the country, magnitude-MMI studies are usually divided into those for earthquakes east of the Rocky Mountains and those for earthquakes west of the Rocky Mountains. For example, the specific quality factor (Q) has values of 200-300 in coastal California and 800-1000 in the central and eastern United States. In some cases, an approximate latitude for the Rocky Mountain boundary, often 105° West longitude, is used to separate the different attenuation regions. The 1882 earthquake was at or near this boundary. The boundary itself, in turn, is uncertain due to the lack of detailed attenuation measurements necessary to specify it more precisely. Accordingly, for this study, both "eastern" and "western" magnitude-MMI relationships will be employed even though I would favor the western equations as the most applicable, given that most of the MMI reports for the 1882 shock occur west of the Front Range's eastern boundary.

The Bollinger et al. (1993) study indicates that MMI VI and VII levels in the East are some five times larger than those in the western United States for the same magnitude earthquake (see Figure C-4). This, in turn, implies that for a given size MMI VI or VII area, the eastern U.S. earthquake will have a magnitude that is, on the average, some 0.8 units smaller than would be the case for a western U.S. shock (see Figure C-5). Clearly, this aspect has very important implications for the task at hand.

Was the focus of the 1882 Colorado earthquake of "normal" depth or was it much shallower or deeper than normal?

Most U.S. earthquakes occur at depths of 5 to 15 km. Those shocks that occur at lesser or greater depths can have MMI distributions that are significantly different. The very shallow earthquakes tend to have an especially high epicentral intensity coupled with an anomalously rapid fall-off of MMI with epicentral distance. The deeper events tend to have lower than normal epicentral intensity levels and usually also exhibit lower than normal attenuation with distance. Thus, shallow earthquakes have very spatially limited MMI distributions while the converse is true for the deeper earthquakes.

The "shallower than normal" MMI characteristics are not observed for the 1882 earthquake. However, by analogy with the October 18, 1984, Laramie Mountains, Wyoming, earthquake which was deeper than normal at 22 km and had a relatively large felt area while the instrumentally determined epicentral locale did not exhibit high intensity levels (only MMI VI), the 1882 shock may indeed have been "deep" (Kirkham and Rogers, 1986). If it was, then somewhat larger than

usual MMI areas, at all intensity levels with respect to the maximum observed intensity (I_o) would result. These differences in intensity area versus focal depth unfortunately have not been quantified due to the small sample of intensity data for deep earthquakes that is available. The "usual" being referred to here is the aforementioned empirical MMI-magnitude relationships derived from the available data base of primarily "normal" focal depth earthquakes.

INTENSITY DATA BASE AND INTERPRETATION

The several episodes of data gathering and the evolving interpretations for this important earthquake have been chronicled by Kirkham and Rogers (1986) and Oaks and Kirkham (1986). As previously mentioned, Stover and Coffman (1993) have critically reviewed all of the available data and results in their preparation of a revision of the U.S. Geological Survey publication, *The Earthquake History of the United States*. Also as previously noted, I have reviewed the assignment of MM values to the individual intensity reports as well as the contouring of those values. I have no substantive disagreement with the Kirkham and Rogers (1986) and Stover and Coffman (1993) results and will use their basic parameters:

MMI_o = VII,
and Felt Area = 485,000 km^2.

My estimates for the area enclosed by the MMI V isoseismal (A_V) and by the MMI VI isoseismal (A_{VI}) are:

A_{VI} = 85,000 km^2,
and A_V = 230,000 km^2.

ANALYSIS

The basic analysis scheme involves the use of published relationships between magnitude and the following intensity parameters:

Maximum Epicentral Intensity	I_o
Total Felt Area	A_f
Area Enclosed by VI Isoseismal	A_{VI}
Area Enclosed by V Isoseismal	A_V

Other relationships, e.g., magnitude versus A_{IV} or A_{VII} are also available in the literature, but they are not applicable to this case. For uniformity, all magnitudes will be converted to moment magnitude (M) according to Bollinger et al. (1993).

A total of 30 separate magnitude estimates were obtained, and Tables C-1 through C-4 present detailed listings of those results. In summary, average values are:

MMI Parameter	Western United States (WUS)	Eastern United States (EUS)
I_o	5.3	4.7
A_V	6.7	6.1
A_{VI}	7.0	6.5
A_f	6.5	4.9

These values vary over two full magnitude units without any obvious outliers. The EUS magnitudes are some 0.6 magnitude units or more smaller than those for the WUS, but this is expectable as previously discussed. Also, the range of WUS magnitude estimates is 1.7 (5.3 to 7.0) is similar to that for the EUS, 1.7 (4.7 to 6.4).

To characterize these apparently non-definitive results, we note that the individual magnitude estimates (Tables C-1 to C-4) can be grouped to give three average estimates of:

M = 5.0, **M** = 6.4, and **M** = 6.9

<u>**M** = 4.99 s.d. = •0.36 n = 19</u>

Derived from three sources: **M** vs I_o (EUS and WUS) and **M** vs A_f for EUS. This is a primarily EUS based result, and the WUS **M** vs I_o is not well constrained (Toppozada, 1975). Also, the 1984 Laramie Mountains, Wyoming earthquake, a deeper, magnitude 5-5.5 shock, had a felt area some 200,000 km^2 smaller than the 1882 shock. Accordingly, I assign a confidence of 10% to its being the correct value.

<u>**M** = 6.44 s.d. = •0.30 n = 7</u>

Also derived from three, primarily EUS, sources: **M** vs A_{VI} (EUS), **M** vs A_V (EUS) and **M** vs A_f (WUS). The agreement of the EUS MMI V and VI areas with the WUS total felt area could be due to a greater-than-normal focal depth as suggested by Kirkham and Rogers (1986). I believe that this magnitude level gives the best balance with the MMI_o of VII and the reported MMI spatial distributions and assign a confidence of 80%.

<u>**M** = 6.90 s.d. = •0.16 n = 4</u>

Derived from two sources: **M** vs A_V and A_{VI} (WUS). While this value is allowed by the WUS empirical relationships, it is not, in my judgment, compatible with the MMI_o of VII level, even for a deeper shock. Also, an earthquake near magnitude 7, would be expected to produce more damage and other surficial effects and have a much stronger aftershock sequence than was reported for 1882 shock. I assign a 10% confidence to the validity of this estimate.

SUMMARY

The preceding discussions and interpretations provide the basis for my interpretation of the 1882 Colorado earthquake's epicentral location and magnitude.

The quantity and quality of the intensity data available for the earthquakes are not adequate to allow a definitive assessment of the location of the epicenter. Rather, three areas are defined as probable host areas. The first area encompasses the highest intensity level reports for the aftershock reported to have followed the day after the mainshock. That area is about 25,000 km^2 and is assigned a 40% confidence. A second area approximates the entire felt area of the aftershock. That area is some 75,000 km^2 and extends from the Front Range westward to Meeker in the western part of the state. A confidence of 85% is assigned to that area. The third area (which includes the other areas) outlines the MMI VI isoseismal contour and is about 100,000 km^2. A confidence of 95% is assigned to this larger area. Specific latitude-longitude coordinates for these three areas are given in the report.

To estimate the size of the 1882 earthquake, 30 moment magnitude estimates are developed from the maximum epicentral intensity, the total felt area and the areas enclosed by the MMI V and VI contours. These values are used to derive the following three moment magnitudes and their associated confidences: 5.0 ± 0.3 (10%), 6.4 ± 0.3 (80%) and 6.9 ± 0.2 (10%).

This analysis takes into account the most recent work of the Colorado Geological Survey on the 1882 earthquake (Kirkham and Rogers, 1986). The current analysis is more comprehensive because it uses analogies with isoseismal patterns of other earthquakes, includes four independently-drawn isoseismal maps of the intensity data, and uses areas of individual isoseismals to estimate magnitude, not simply the felt area. Therefore the current analysis is used to quantify the size and location uncertainty of this earthquake for the seismic hazard analysis.

REFERENCES

Algermissen, S.T. (1981). Letter to R.E. Mast on the subject: Review of "Preliminary Draft Geologic and Seismologic Investigations for Rocky Flats Plant" by Dames and Moore, 7 p.

Bollinger, G.A., C.J. Langer and S.T. Harding (1976). The eastern Tennessee earthquake sequence of October through December, 1973, *Bull. Seism. Soc. Am.*, 66, pp. 525-547.

Bollinger, G.A., M.C. Chapman and M.S. Sibol (1993). A comparison of earthquake damage areas as a function of magnitude across the United States, *Bull. Seism. Soc. Am.*, 83, 4, 1064-1080.

Coffman, J.L. and C.A. von Hake (1973). *Earthquake History of the United States*, Pub. 41-4, Rev. Edition (through 1970), N.O.A.A., Washington, DC, pp. 59-60.

Engdahl, E.R. and W.A. Rinehart (1988). Seismicity Map of North America, Decade North America Geol. Project, Geol. Soc. Am., Boulder, CO (2 sheets).

Gutenberg, B. and C.F. Richter (1942). Earthquake magnitude, intensity, energy and acceleration, *Bull. Seism. Soc. Am.*, 32, pp. 162-191.

Hadsell, F.A. (1968). History of earthquake activity in Colorado, *in*, J.C. Hollister and R.J. Weimer (eds.), Geophysical and geological studies of the relationship between the Denver earthquake and the Rocky Mountain Arsenal well, *Colorado School of Mines Quarterly*, 63, pp. 57-72.

Hanks, T.C. and A.C. Johnson (1992). Common features of the excitation and propagation of strong ground motion for North American earthquakes, *Bull. Seism. Soc. Am.*, 82, pp. 1-23.

Johnston, A.C. (1993). The stable-continent-region earthquake data base, *in*, K.J. Coppersmith and others (eds.), Methods for assessing maximum earthquakes in the central and eastern United States, *Electric Power Res. Inst., Project RP-2556-12*, Palo Alto, CA, in press.

Kirkham, R.M. and W.P. Rogers (1981). *Earthquake Potential in Colorado - A Preliminary Evaluation*, Colorado Geol. Survey, Denver, CO, pp. 94-95.

Kirkham, R.M. and W.P. Rogers (1985). Colorado earthquake data and interpretations - 1867 to 1985, *Colorado Geol. Survey Bulletin 46*, Denver, CO, 106 p.

Kirkham, R.M. and W.P. Rogers (1986). An interpretation of the November 7, 1882, Colorado earthquake *in* W.P. Rogers and R.M. Kirkham (eds.), *Contributions to Colorado Seismicity and Tectonics - A 1986 Update*, Colorado Geol. Survey, Denver, CO, pp. 122-144.

Kirkham, R.M. and W.P. Rogers (1988). The November 7, 1882, Colorado earthquake and its significance to seismic hazard estimation, *Geol. Soc. Am. Abstr. with Prog.*, 20, A15 p.

McGuire, R.K. (1981). *Report on November 7, 1882, Earthquake*, Dames and Moore, Golden, CO, 192 p.

McGuire, R.K., A. Krusi and S.D. Oaks (1982). The Colorado earthquake of November 7, 1882: Size, epicentral location, intensities and possible causative fault, *The Mountain Geologist*, 19, pp. 11-23.

Nuttli, O.W. and J.E. Zollweg (1974). The relation between felt area and magnitude for the central United States, *Bull. Seism. Soc. Am.*, 64, pp. 73-85.

Oaks, S.D. (1981). Appendix H, Historical research data for the November 7, 1882, earthquake in the Rocky Mountain region, *in*, Dames & Moore, *Geologic and Seismological Investigations for Rocky Flats Plant*, 2, unpub. report prepared for U.S. Dept. of Energy, 207 p.

Oaks, S.D., M.G. Hopper, L.M. Barnhard and S.T. Algermissen (1985). November 7, 1882, Colorado earthquake reinterpreted in light of the October 18, 1984, Wyoming earthquake, *Earthquake Notes*, 55, 24 p.

Oaks, S.D. and R.M. Kirkham (1986). Results of a search for felt reports for selected Colorado earthquakes, *Colorado Geol. Survey Info. Series 23*, Denver, CO, 89 p.

Richter, C.F. (1958). *Elementary Seismology*, Freeman and Co., San Francisco, CA, 768 p.

Sibol, M.S., G.A. Bollinger and J.B. Birch (1987). Estimation of magnitudes in central and eastern North America using intensity and felt areas, *Bull. Seism. Soc. Am.*, 77, pp. 1635-1654.

Stover, C.W. and J.L. Coffman (1993). Seismicity of the United States, 1568-1989 (revised), *U.S. Geological Survey Prof. Paper 1527,* 418 p.

Street, R. and A. Lacroix (1979). An empirical study of New England seismicity: 1727-1977, *Bull. Seism. Soc. Am.*, 69, pp. 159-175.

Toppozada, T.R. (1975). Earthquake magnitude as a function of intensity data in California and Nevada, *Bull. Seism. Soc. Am.*, 65, pp. 1223-1238.

TABLE C-1

MAGNITUDE ESTIMATES FOR THE 1882 COLORADO EARTHQUAKE DERIVED FROM TOTAL FELT AREA (A_f) OF 485,000 KM^2

SOURCE	MODEL	MOMENT MAGNITUDE (M)* WESTERN U.S. (REGION)**	EASTERN U.S. (REGION)
Kirkham and Rogers (1985)	M_L vs A_f	6.4 ± 0.3	--
Hadsell (1968) (A_f = 1,200,000 km^2)	--	6.57 ± 0.6	--
McGuire et al. (1982) (A_f = 500,000 km^2)	M_L or M_S vs A_f	6.5	--
Sibol et al. (1987)	m_b vs A_f	--	4.79
Sibol et al. (1987)	m_b vs A_f and I_o	--	4.97
Nuttli and Zollweg (1974)	m_b vs A_f	--	4.77
Toppozada (1975)	M_L vs A_f	6.89	--
Street and Lacroix (1979)	$m_b(L_g)$ vs A_f	--	5.00
Johnston (1993)	M_D vs A_f	--	5.10
	Average	6.52	4.93

* Magnitude conversion scheme:

$$m_b \approx m_b(L_g) \approx M_L;\ \log M_o = 17.8 + 0.654\ M_L + 0.0887\ M_L^2;\ M = \frac{2}{3}\log M_o - 10.7$$

** WNA = western North America; WUS = western United States; CNA = central North America; ENA = eastern North America; EUS = eastern United States

CALCULATIONS FOR TABLE C-1

Sibol et al. (1987)

$$m_b = 2.48 + 0.0769 \log^2 (FA)$$

$$FA = \text{felt area in sq km} = 485{,}000 \text{ km}^2$$

$$m_b = 2.48 + 0.0769 (32.328) = 4.97$$

$$\log M_o = 17.8 + 0.654\, m_b + 0.0887\, m_b^2 = 17.8 + 3.250 + 2.191 = 23.24$$

$$M = \frac{2}{3}(23.24) - 10.7 = 4.79$$

$$m_b = 2.16 + 0.0219\, I_o^2 + 0.0596 \log^2 (FA) = 2.16 + 1.0731 + 1.907 + 5.14$$

$$\log M_o = 17.8 + 0.654\, m_b + 0.0887\, m_b^2 = 17.8 + 3.3616 + 2.3434 = 23.505$$

$$M = \frac{2}{3}(23.505) - 10.7 = 4.97$$

Nuttli and Zollweg (1974)

$$m_b = 2.65 + 0.098 \log (FA) + 0.054 \log^2 (FA) = 2.65 + 0.557 + 1.746 = 4.95$$

$$\log M_o = 17.8 + 0.654\, m_b + 0.0887\, m_b^2 = 17.8 + 3.237 + 2.173 = 23.21$$

$$M = \frac{2}{3}(23.21) - 10.7 = 4.77$$

Street and Lacroix (1979)

$$m_b (L_g) = 2.77 - 0.147 \log (FA) + 0.100 \log^2 (FA) = 2.77 - 0.836 + 3.233 = 5.17$$

$$\log M_o = 17.8 + 0.654\, m_b (L_g) + 0.0887\, m_b^2 (L_g) = 17.8 + 3.381 + 2.371 = 23.55$$

$$M = \frac{2}{3}(23.55) - 10.7 = 5.00$$

Johnston (1993)

$$\log M_o = 47.34 - 10.81 \log (FA) + 1.17 \log^2 (FA) = 47.34 - 61.463 + 37.823 = 23.70$$

$$M = \frac{2}{3}(23.70) - 10.7 = 5.10$$

Toppozada (1975)

$$M_L = -1.88 + 1.53 \log (FA) = -1.88 + 8.700$$

$$M_L = 6.82$$

$$\log M_o = 17.8 + 0.654\, M_L + 0.0887\, M_L^2 = 17.8 + 4.460 + 4.126 = 26.38$$

$$M = \frac{2}{3}(26.38) - 10.7 = 6.89$$

Kirkham and Rogers (1985)

$$M_L = 6.2 \pm 0.3$$

$$\log M_o = 17.8 + 0.654\, M_L + 0.0887\, M_L^2 = 17.8 + 4.055 + 3.410 = 25.265$$

$$M = \frac{2}{3}(25.265) - 10.7 = 6.14$$

Hadsell (1968)

$$M\,(?) = 6.74 \pm 0.6$$

$$\log M_o = 17.8 + 0.654\, M_L + 0.0887\, M_L^2 = 17.8 + 4.080 + 4.029 = 25.91$$

$$M = \frac{2}{3}(25.91) - 10.7 = 6.57$$

McGuire et al. (1982)

$$M_L \text{ or } M_S = 6.5$$

$$\log M_o = 17.8 + 0.654\, M_L + 0.0887\, M_L^2 = 17.8 + 4.251 + 3.748 = 25.80$$

$$M = \frac{2}{3}(25.80) - 10.7 = 6.50$$

TABLE C-2

MAGNITUDE ESTIMATES FOR THE 1882 COLORADO EARTHQUAKE DERIVED FROM THE MM INTENSITY VI AREA (A_{VI}) OF 85,000 KM^2

SOURCE	MODEL	MOMENT MAGNITUDE (M)* WESTERN U.S. (REGION)**	EASTERN U.S. (REGION)
Toppozada (1975)	M_L vs A_{VI}	6.81 (CA&W. NV)	--
Bollinger	M vs A_{VI}	6.96	6.20 (WUS)
Hanks and Johnston (1992)	M vs A_{VI}	7.11	6.70 (SCR)
Bollinger et al. (1993)	M vs A_{VI}	6.96 (WUS)	6.20 (ENA)
	Average	**6.96**	**6.45*** **

* Magnitude conversion scheme:

$$m_b \approx m_b(L_g) \approx M_L;\ \log M_o = 17.8 + 0.654\ M_L + 0.0887\ M_L^2;\ M = \frac{2}{3} \log M_o - 10.7$$

** WNA = western North America; WUS = western United States; CNA = central North America; ENA = eastern North America; EUS = eastern United States; SCR = stable continental regions ("intraplate")

*** The two Bollinger references were treated as one estimate for this average.

CALCULATIONS FOR TABLE C-2

Toppozada (1975)

$M_L = 2.56 + 0.85 \log A_{VI}$

$M_L = 6.75$

$\log M_o = 26.26$

$\mathbf{M} = 6.81$

Bollinger (1993)

ENA: $\mathbf{M} = 1.07 + 1.04 \log A_{VI}$

$\mathbf{M} = 6.20$

WUS: $\mathbf{M} = 1.93 + 1.02 \log A_{VI}$

$\mathbf{M} = 6.69$

Hanks and Johnston (1992)

$\mathbf{M} = 3.26 + 0.24 \log A_{VI} + 0.093 \log^2 A_{VI}$ SCR

$\mathbf{M} = 3.26 + 1.183 + 2.260 = 6.70$

$\mathbf{M} = 2.38 + 0.96 \log A_{VI}$ California

$\mathbf{M} = 7.11$

Bollinger et al. (1993)

$\mathbf{M} = 1.93 + 1.02 \log A$ WUS

$\mathbf{M} = 6.96$

$\mathbf{M} = 1.07 + 1.04 \log A$ ENA

$\mathbf{M} = 6.20$

TABLE C-3

MAGNITUDE ESTIMATES FOR THE 1882 COLORADO EARTHQUAKE DERIVED FROM THE MM INTENSITY V AREA (A_V) OF 230,000 KM^2

		MOMENT MAGNITUDE (M)*	
SOURCE	MODEL	WESTERN U.S. (REGION)**	EASTERN U.S. (REGION)
Toppozada (1975)	M_L vs A_V	6.74 (CA&W. NV)	--
Johnston (1993)	M vs A_V		6.10 (SCR)

* Magnitude conversion scheme:

$$m_b \approx m_b(L_g) \approx M_L;\ \log M_o = 17.8 + 0.654\ M_L + 0.0887\ M_L^2;\ M = \frac{2}{3}\log M_o - 10.7$$

** WNA = western North America; WUS = western United States; CNA = central North America; ENA = eastern North America; EUS = eastern United States; SCR = stable continental regions ('intraplate")

CALCULATIONS FOR TABLE C-2

Toppozada (1975)

$M_L = 2.56 + 0.85 \log A_{VI}$

$M_L = 6.75$

$\log M_o = 26.26$

$\mathbf{M} = 6.81$

Bollinger (1993)

ENA: $\mathbf{M} = 1.07 + 1.04 \log A_{VI}$

$\mathbf{M} = 6.20$

WUS: $\mathbf{M} = 1.93 + 1.02 \log A_{VI}$

$\mathbf{M} = 6.69$

Hanks and Johnston (1992)

$\mathbf{M} = 3.26 + 0.24 \log A_{VI} + 0.093 \log^2 A_{VI}$ SCR

$\mathbf{M} = 3.26 + 1.183 + 2.260 = 6.70$

$\mathbf{M} = 2.38 + 0.96 \log A_{VI}$ California

$\mathbf{M} = 7.11$

Bollinger et al. (1993)

$\mathbf{M} = 1.93 + 1.02 \log A$ WUS

$\mathbf{M} = 6.96$

$\mathbf{M} = 1.07 + 1.04 \log A$ ENA

$\mathbf{M} = 6.20$

TABLE C-3

MAGNITUDE ESTIMATES FOR THE 1882 COLORADO EARTHQUAKE DERIVED FROM THE MM INTENSITY V AREA (A_V) OF 230,000 KM^2

SOURCE	MODEL	MOMENT MAGNITUDE (M)* WESTERN U.S. (REGION)**	EASTERN U.S. (REGION)
Toppozada (1975)	M_L vs A_V	6.74 (CA&W. NV)	--
Johnston (1993)	M vs A_V		6.10 (SCR)

* Magnitude conversion scheme:

$$m_b \approx m_b(L_g) \approx M_L;\ \log M_o = 17.8 + 0.654\ M_L + 0.0887\ M_L^2;\ M = \frac{2}{3}\log M_o - 10.7$$

** WNA = western North America; WUS = western United States; CNA = central North America; ENA = eastern North America; EUS = eastern United States; SCR = stable continental regions ('intraplate")

CALCULATIONS FOR TABLE C-3

Toppozada (1975)

$$M_L = 0.86 + 1.09 \log A_V \ (km^2)$$

$$= 0.86 + 1.09\ (5.3617) = 6.70$$

$$\log M_o = 17.8 + 0.654\ (M_L) + 0.0887\ M_L^2 = 26.16$$

$$\mathbf{M} = \frac{2}{3} \log M_o - 10.7 = 6.74$$

Johnston (1993)

$$\log M_o = 26.90 - 3.10 \underbrace{\log A_V}_{5.3617} + 0.52 \underbrace{(\log A_V)^2}_{28.7481}$$

$$\log M_o = 2.52$$

$$\mathbf{M} = \frac{2}{3} \log M_o - 10.7 = 6.10$$

TABLE C-4

MAGNITUDE ESTIMATES FOR THE 1882 COLORADO EARTHQUAKE DERIVED FROM THE MAXIMUM EPICENTRAL INTENSITY (I_O)

SOURCE	MODEL	MOMENT MAGNITUDE (M)* WESTERN U.S. (REGION)**	EASTERN U.S. (REGION)
Gutenberg and Richter (1942)	M_L vs I_o	5.35 (CA)	--
Toppozada (1975)	M_L vs I_o	5.12 (CA&W. NV)	--
Sibol et al. (1987)	m_b vs I_o	5.09 (WNA)	4.12 (CNA)
Sibol et al. (1987)	m_b vs I_o	5.26 (WNA)	4.41 (CNA)
Sibol et al. (1987)	m_b vs I_o	5.26 (WNA)	4.41 (CNA)
Sibol et al. (1987)	m_b vs I_o discrete distribution-mean	5.39±0.28 (WNA)	5.07±0.46 (ENA)
Sibol et al. (1987)	m_b vs I_o discrete distribution-median	5.23±0.22 (WNA)	5.35±0.30 (ENA)
Stover and Coffman (1993)	average M_L or m_b vs I_o	5.35 (WUS)	4.83 (EUS)
	Average	**5.26**	**4.70**

* magnitude conversion scheme:

$$m_b \approx m_b(L_g) \approx M_L;\ \log M_o = 17.8 + 0.654\ M_L + 0.0087\ M_L^2;\ M = \frac{2}{3}\log M_o - 10.7$$

** WNA = western North America; WUS = western United States; CNA = central North America; ENA = eastern North America; EUS = eastern United States

CALCULATIONS FOR TABLE C-4

Sibol et al. (1987)

Linear Regression Models - WNA

$m_b = 2.03 + 0.461\ I_o$; I_o = VII

$m_b = 2.03 + 3.227 = 5.26$

$\log M_o = 23.69$

M = 5.09

Linear Regression Models - CNA

$m_b = 1.71 + 0.368\ I_o$; I_o = VII

$m_b = 1.71 + 2.576 = 4.29$

$\log M_o = 22.24$

M = 4.12(5)

Sibol et al. (1987)

Linear Regression Models - WNA

$m_b = 3.13 + 0.467\ I_o^2$; I_o = VII

$m_b = 5.418$

$\log M_o = 23.947$

M = 5.265

Linear Regression Models - CNA

$m_b = 2.41 + 0.0444\ I_o^2$; I_o = VII

$m_b = 4.586$

$\log M_o = 22.665$

M = 4.410

Sibol et al. (1987)

Discrete Distribution (Mean) - WNA

$m_b = 5.53 \pm 0.28$

$\log M_o = 17.8 + 3.617 + 2.712 = 24.13$

M = 5.39

Discrete Distribution (Mean) - ENA

$m_b = 5.23 \pm 0.46$

$\log M_o = 17.8 + 3.420 + 2.423 = 23.65$

M = 5.07

Discrete Distribution (Median) - WNA

$m_b = 5.55$

$\log M_o = 17.8 + 3.630 + 2.732 = 23.89$

M = 5.23

Discrete Distribution (Median) - ENA

$m_b = 5.50$

$\log M_o = 17.8 + 3.600 + 2.68 = 24.08$

M = 5.35

Gutenberg and Richter (1942) for California

$$M = 1.3 + 0.6\, I_o = M_L$$

$$I_o = VII$$

$$M_L = 5.50$$

$$\log M_o = 24.08$$

$$\mathbf{M} = 5.354$$

Toppozada (1975) for California and Western Nevada

$$M_L = 1.85 + 0.49\, I_o \qquad I_o = VII$$

$$M_L = 5.280$$

$$\log M_o = 23.73$$

$$\mathbf{M} = 5.12$$

Stover and Coffman (1993)

$M - I_o$ (WUS) = 5.5	$\log M_o = 24.08$	$\mathbf{M} = 5.35$
$M - I_o$ (EUS) = 5.0	$\log M_o = 23.29$	$\mathbf{M} = 4.83$

Notes for Figure C-2

Figures C-2b through C-2e are four independent contourings of the Kirkham and Rogers (1986) intensity data for the 1882 Colorado earthquake. To facilitate comparison, the Kirkham and Rogers (1986) intensity map at the same scale as the recontoured maps, is also shown as Figure C-2a. Note that the three major characteristics of their map:

1. Rapid decrease of intensity eastward and an apparent elongation westward,

2. A roughly triangular shape to the MMI VI and lower contours, and

3. Rapid spatial variation of the highest intensity levels (V, VI, VII) along the Front Range corridor,

are also present to a large degree on the recontoured maps.

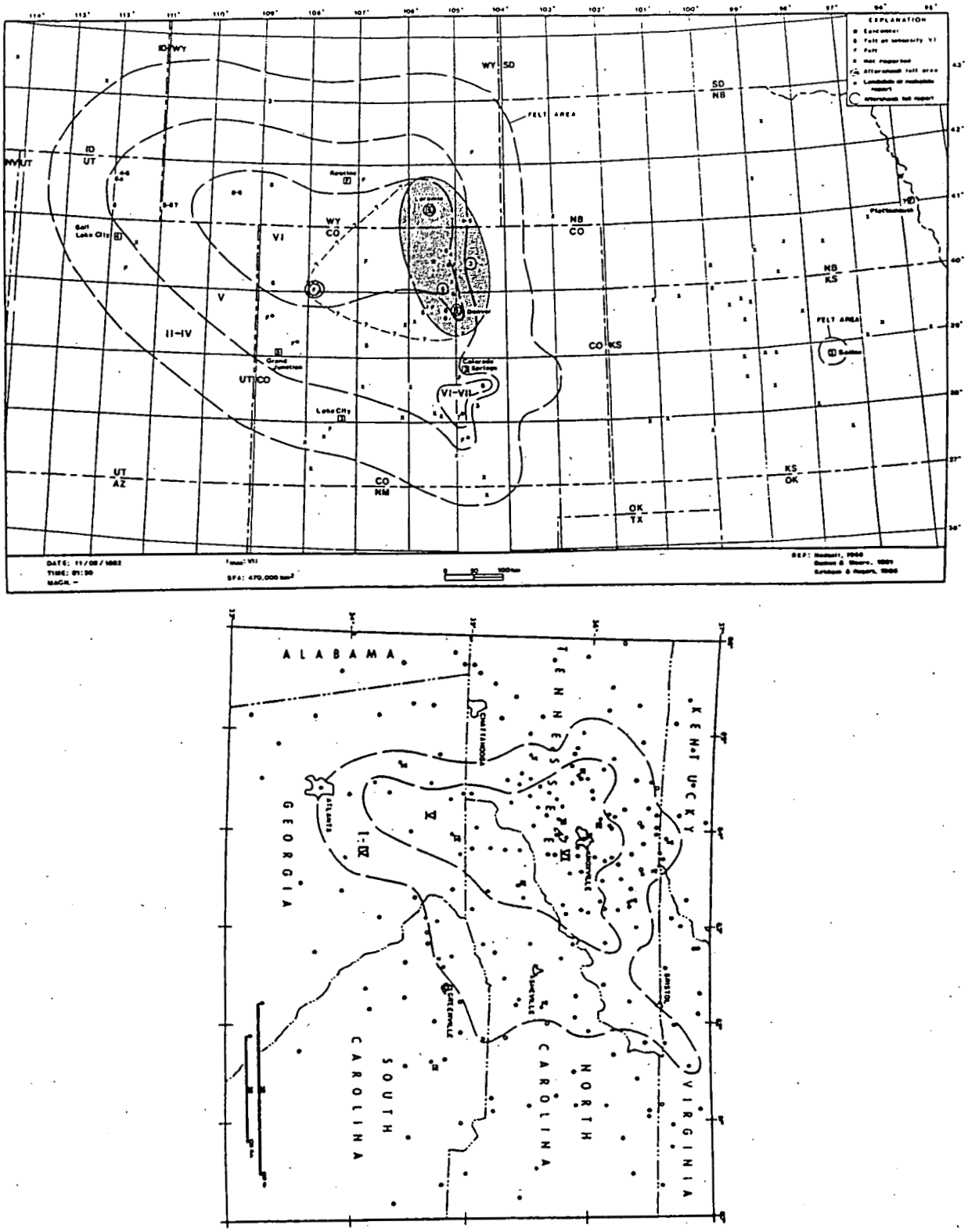

Figure C-1. Isoseismal Maps for the 1882 Colorado earthquake (upper; Kirkham and Rogers, 1986) and the 1973 Knoxville, Tennessee, earthquake (lower; Bollinger and others, 1976, reoriented so that north is to the right). Note the similarities in isoseismal pattern: Rapid decrease in one direction with an elongation in the opposite direction and roughly triangular shape.

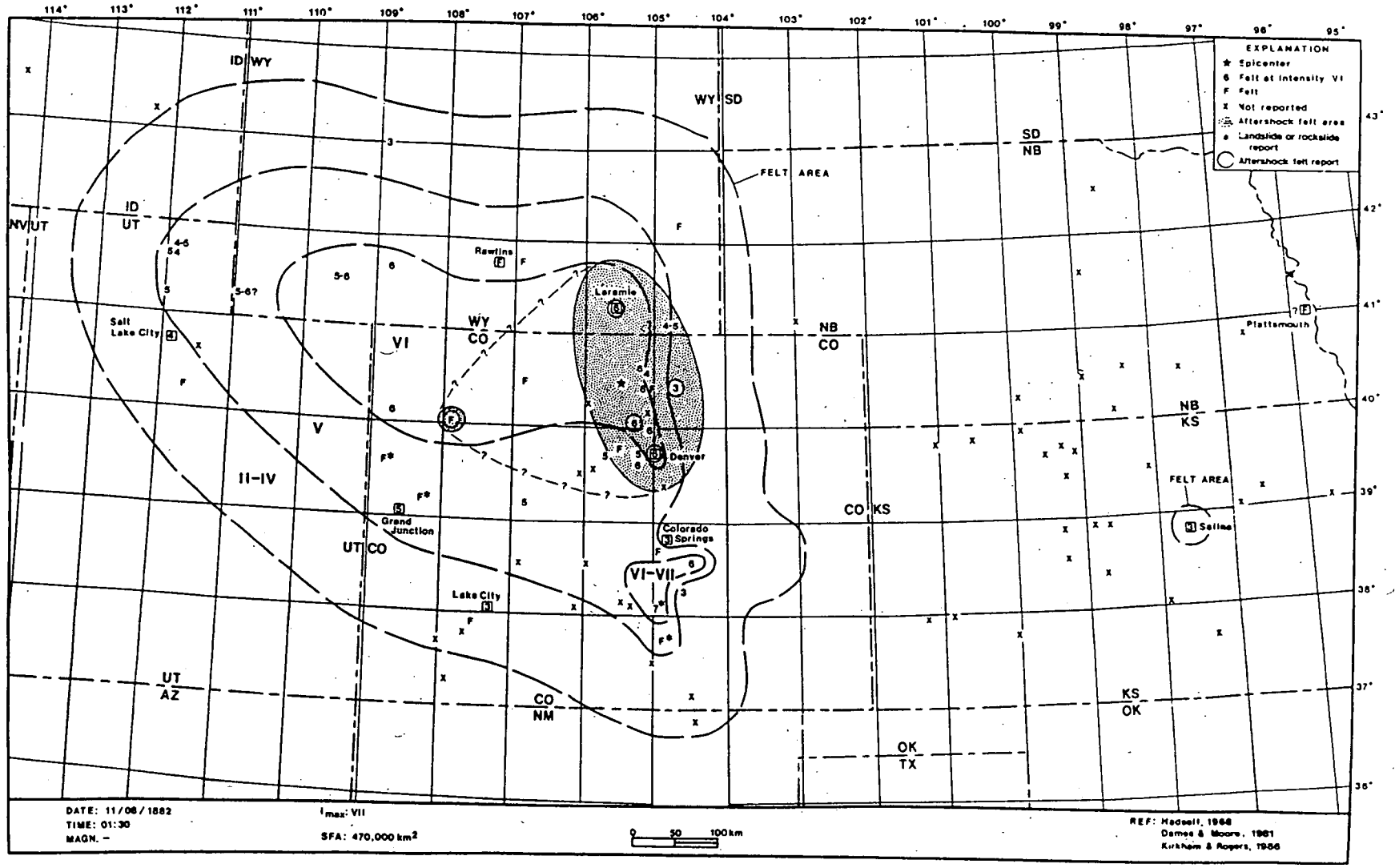

Figure C-2a. Isoseismal map for the 1882 Colorado earthquake. Stippled pattern is felt area of aftershock the next day. Date and time shown is in Coordinated Universal Time.

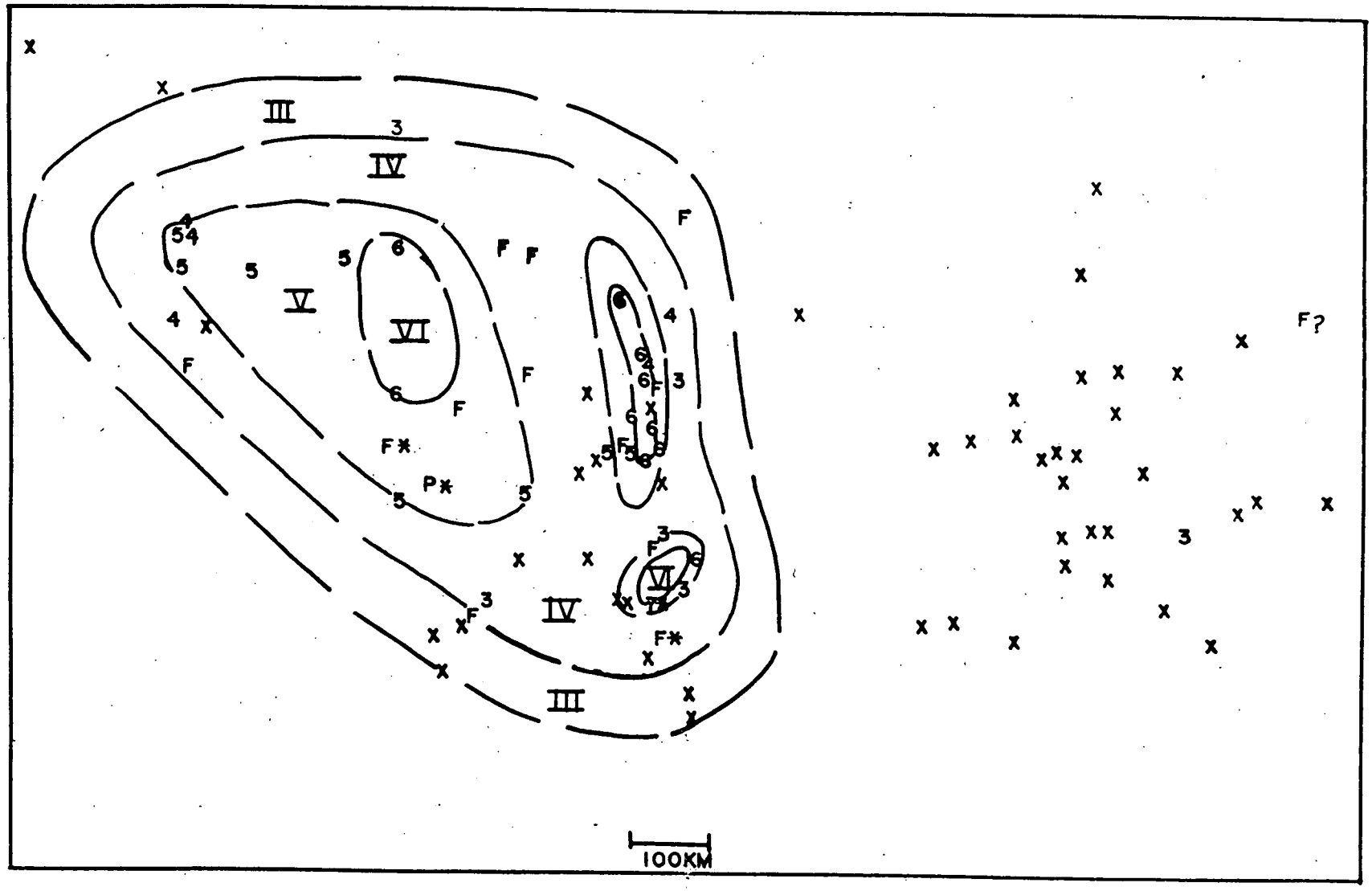

Figure C-2b. First independent contouring of Kirkham and Rogers (1986) intensity data.

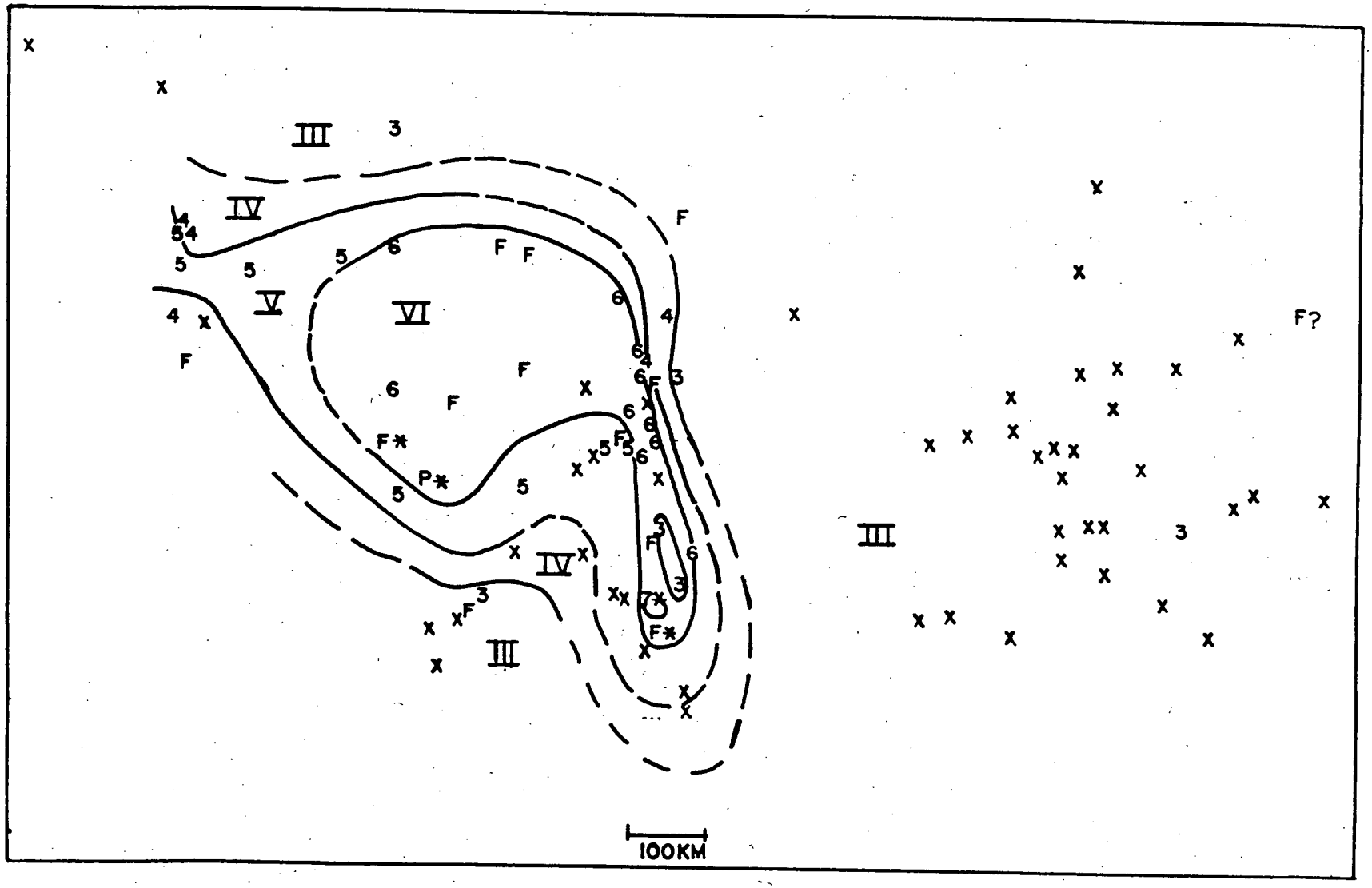

Figure C-2c. Second independent contouring of Kirkham and Rogers (1986) intensity data.

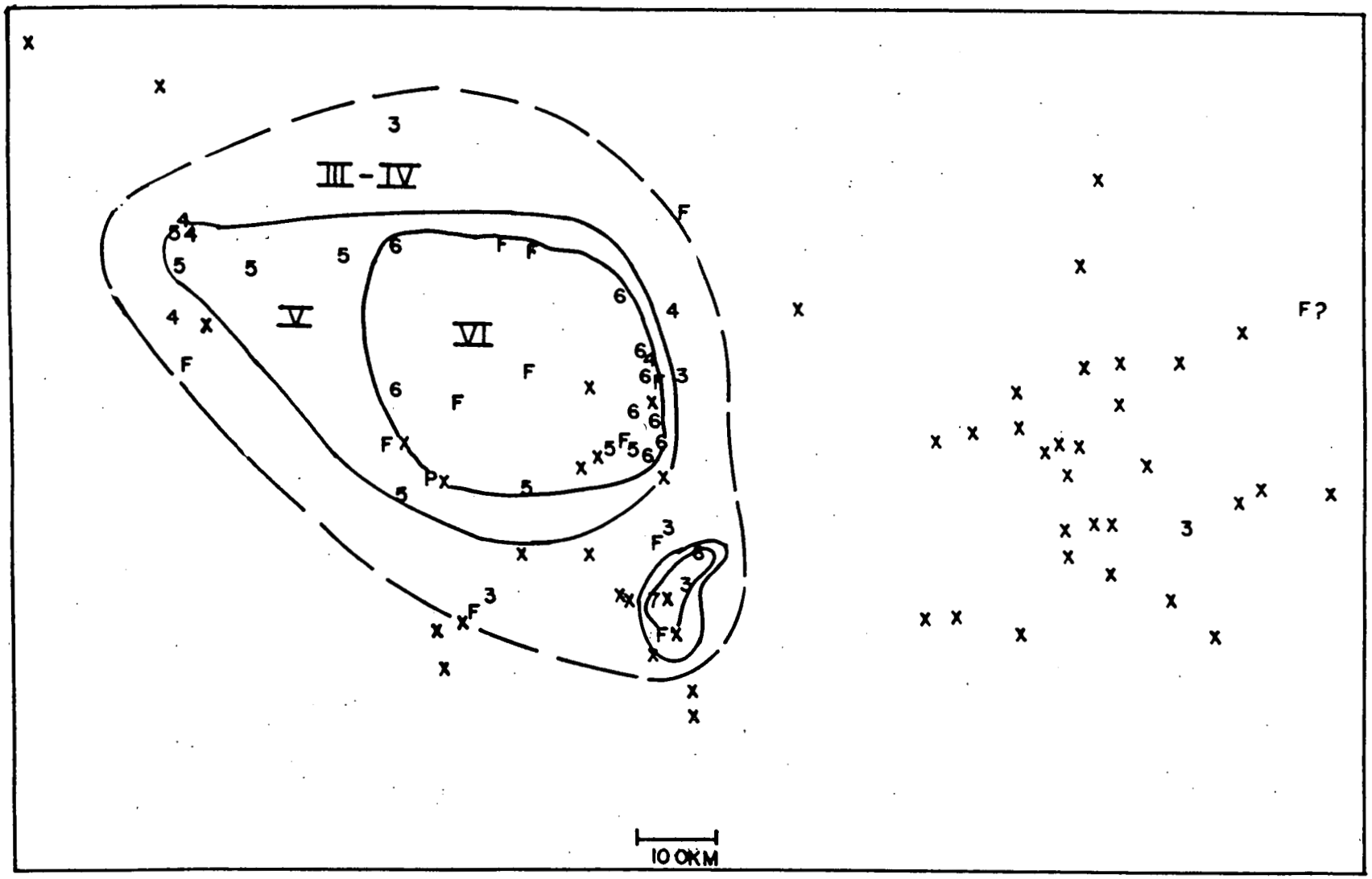

Figure C-2d. Third independent contouring of Kirkham and Rogers (1986) intensity data.

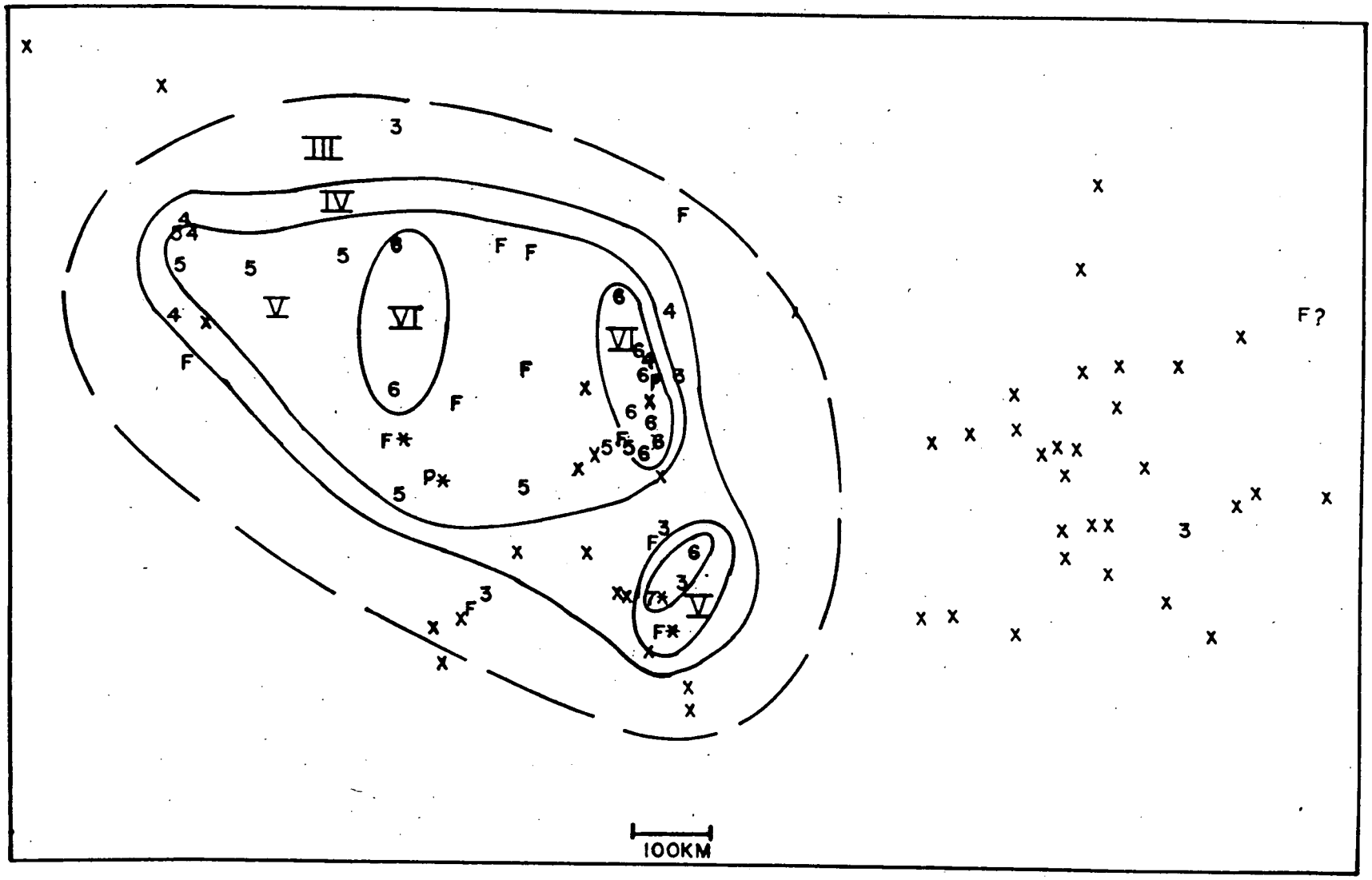

Figure C-2e. Fourth independent contouring of Kirkham and Rogers (1986) intensity data.

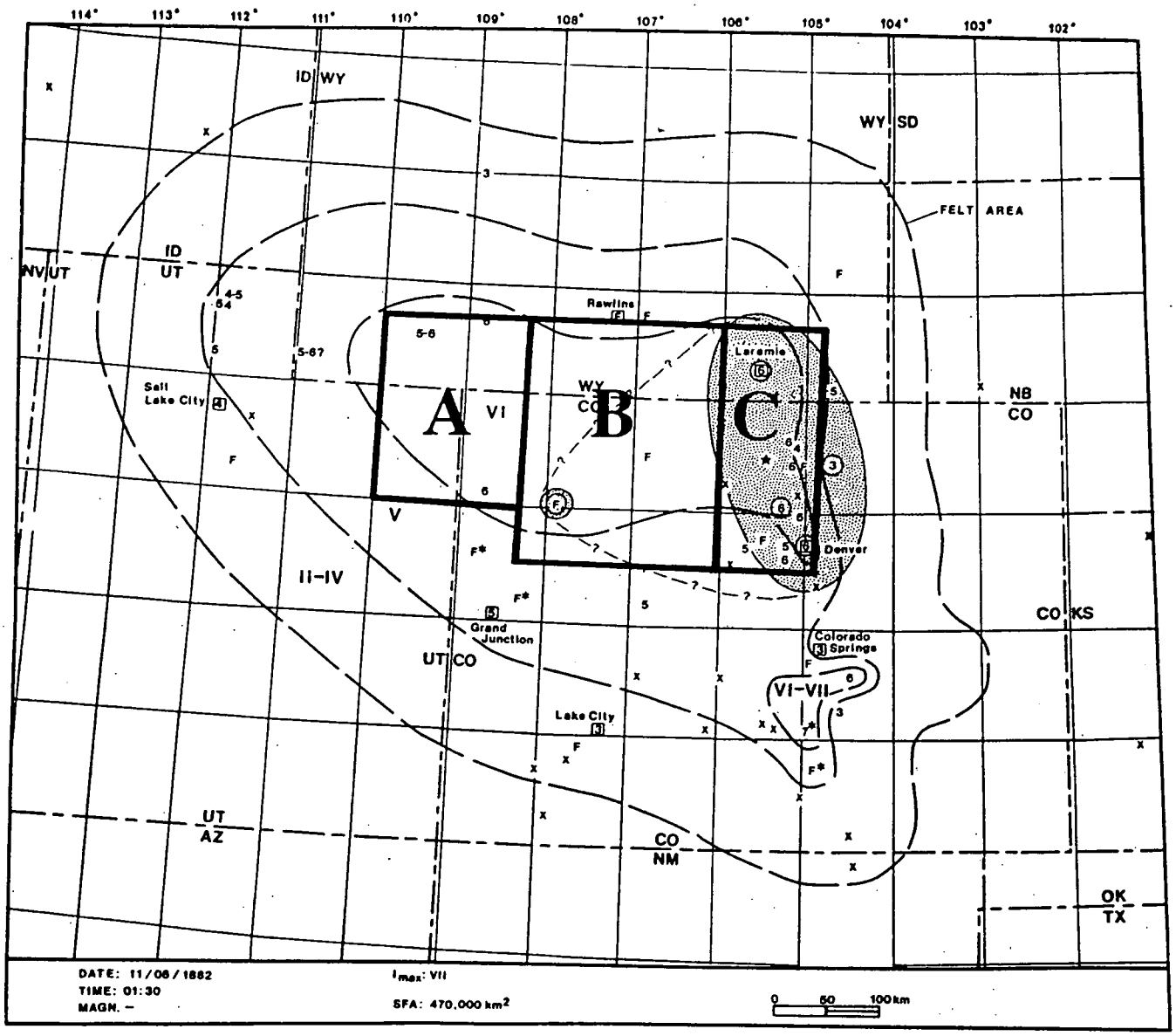

Figure C-3. Definition of epicentral areas (A, B and C) for the 1882 Colorado earthquake. Intensity map from Kirkham and Rogers (1986).

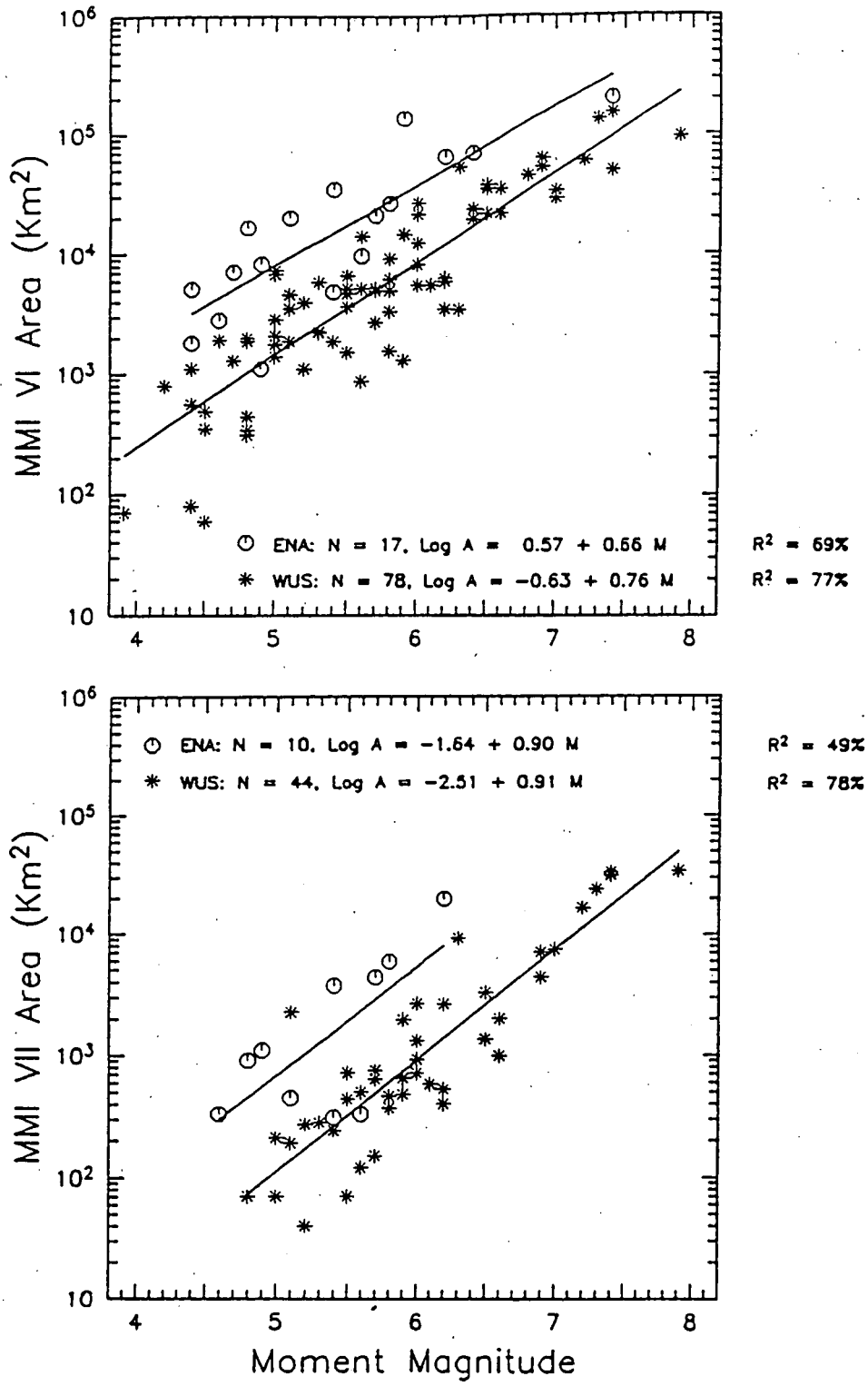

Figure C-4. Isoseismal areas, at the MMI = VI and VII levels, versus moment magnitude for eastern North American earthquakes (ENA) and western U.S. earthquakes (WUS). The straight-line fits indicate the eastern North American damage areas are some five times greater than those resulting from western U.S. earthquakes (Bollinger et al., 1993).

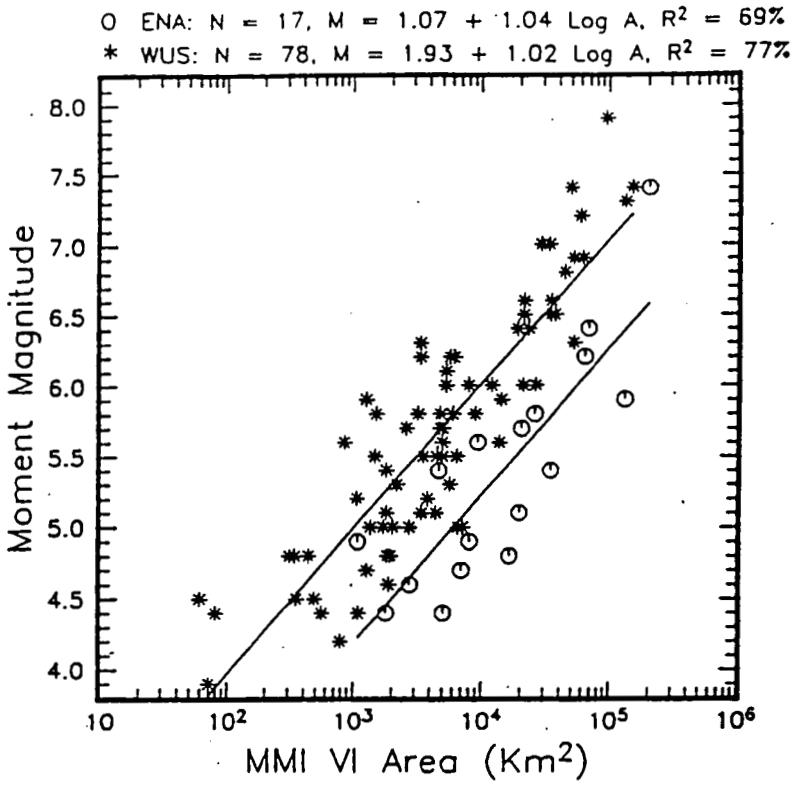

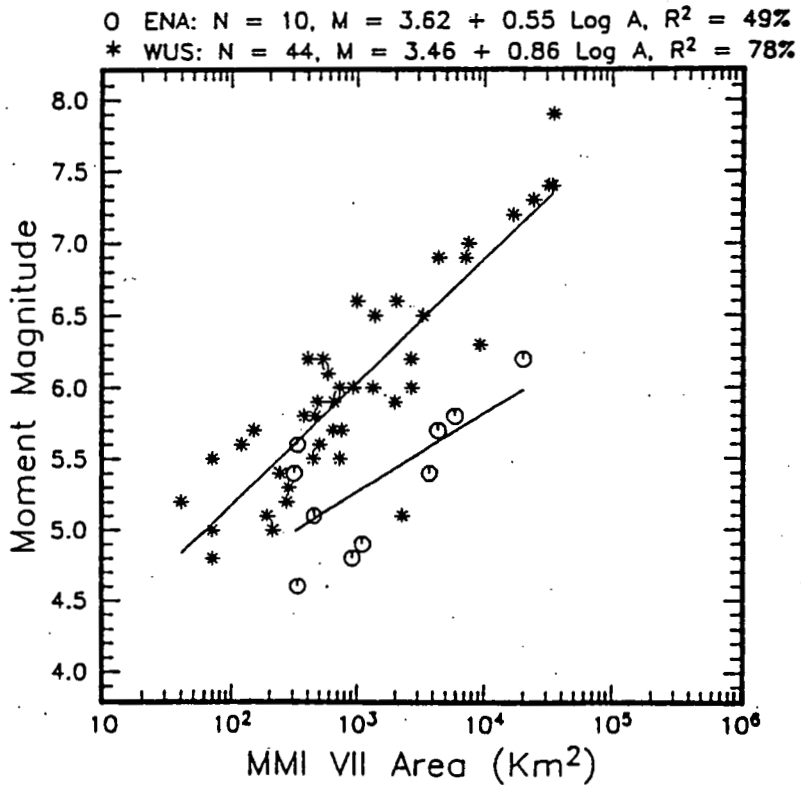

Figure C-5. Moment magnitudes versus MMI VI and VII isoseismal areas for eastern North American earthquakes (ENA; circle symbols) and western U.S. earthquakes (WUS; star symbols). The separation of the straight-line fits is about 0.8 magnitude unit at the MMI VI level. This is the same **M** - MMI area data shown in Figure C-4.

APPENDIX D

HISTORICAL SEISMICITY STUDIES

by

Risk Engineering, Inc.
Boulder, Colorado

INTRODUCTION

This Appendix summarizes the analysis of historical seismicity in Colorado (herein used to imply "the Colorado region" when parts of adjacent states are included) for the seismic hazard study of the Rocky Flats Plant. The purposes of this analysis are (1) to provide a uniform earthquake catalog of mainshocks (independent earthquakes) for Colorado, (2) to estimate how complete the catalog is at different times, (3) to estimate rates of seismic activity and *b*-values for seismic sources, and (4) to estimate the historical seismic hazard (i.e., the ground shaking hazard calculated retrospectively from historical earthquakes) based on the derived catalog and estimates of completeness. The steps used to achieve these purposes are described in the following sections.

State-of-the-art methods are used in this analysis. This means, for example, that the uncertainty in intensity-to-magnitude conversion is treated explicitly with multiple equations, and is carried through the analysis of activity rates and *b*-values. This treatment of uncertainty provides a solid basis with which to calculate seismic hazard for the Rocky Flats Plant.

HISTORICAL SEISMICITY

The analysis of historical seismicity begins by assembling a catalog of historical earthquakes. A catalog referred to herein as "the Colorado catalog" was specially compiled for this project for the region encompassing Colorado and adjacent areas within one-half degree longitude or latitude. Earthquakes are included from 1870 through May, 1993. The catalog involved the concatenation of earthquakes from two prior catalogs. The earthquake list for Colorado and adjacent states was obtained from the U.S. Geological Survey (USGS), which maintains a catalog of earthquakes worldwide. This list for Colorado is itself a compilation of earthquakes from several sources: the USGS (through historical studies such as Stover et al., 1984, and through the PDE [Preliminary Determination of Epicenter] lists), the DNAG catalog (Decade of North American Geology: Engdahl and Rinehart, 1991), and reports from many local networks. Thus the USGS list is the most comprehensive catalog with which to begin a compilation.

The Colorado catalog obtained from the USGS was checked by comparison with the list of earthquakes published by the Colorado Geological Survey (Kirkham and Rogers, 1985). Where discrepancies in the reported magnitudes occurred, the Kirkham and Rogers values were used, as this study is more specific to Colorado than the USGS compilation. Also, any events reported by

Kirkham and Rogers (1985) that were not included in the USGS catalog, were added. Thus the Colorado catalog compiled for this project is a concatenation of events from the two sources. In addition, the study of felt reports conducted by Oaks and Kirkham (1986) was checked to see if any additional changes to event locations or size estimates were warranted. It was concluded that these felt reports did not indicate that any changes to the catalog were appropriate.

A map showing the epicenters of 172 independent mainshocks with either Modified Mercalli intensity ≥ II or magnitude ≥ 1.0 in the Colorado catalog is shown in Figure D-1. The magnitudes for the pre-instrumental earthquakes were estimated using the methods described below. Note that only one location is shown for the 1882 earthquake; the treatment of uncertainty in magnitude and location for this earthquake is described below in the sections entitled "Historical Earthquake Hazard" and "Activity Rates and *b*-Values."

In addition to the Colorado catalog, a larger compilation of events was assembled to provide data for magnitude correlation. This catalog, herein called the Rocky Mountain-Great Plains (RMGP) catalog, is illustrated in Figure D-2.

The magnitude measure of interest to seismic hazard calculations is the moment magnitude **M**, which is used in the attenuation equations (see Appendix E). For values less than 6.5 (which are all earthquakes in the catalog except the 1882 shock, which is evaluated separately), **M** is virtually identical to local magnitude M_L, which is available for many of the earthquakes in the catalog. For other earthquakes that did not have M_L values, data were compiled from the RMGP catalog to provide empirical correlations between M_L and other size measures available. The two most useful measures were maximum reported Modified Mercalli (MM) intensity I_o and body-wave magnitude m_b.

Of the 172 earthquakes in the Colorado catalog, 82 had estimates of M_L provided by original sources. The remaining 90 events had other size measures available in the following numbers:

Size Measure	Number
MM intensity I_o	74
body-wave magnitude m_b	17
duration magnitude	2
Nuttli magnitude	4
magnitude based on felt area	1
Total:	98

The total in the above list is greater than the 90 earthquakes with no direct M_L estimate because some earthquakes had multiple alternative measures listed.

Events with duration magnitudes came from local networks recording small earthquakes. In those cases we contacted the operators of the networks and obtained information on the best method for converting duration magnitude to M_L. The four events with a Nuttli magnitude were considered equivalent to m_b (this was the original intent of Nuttli's magnitude scale), and the magnitude based on felt area was assumed to be M_L.

For events with I_o or m_b reported, we developed empirical conversions based on earthquakes in the RMGP catalog for which both measures were reported. Figure D-3 shows the correlation of M_L with I_o. For this correlation, events with $I_o < 3.0$ were not used because these lower intensities appeared to have a bias in reporting (for $I_o = 2$, the only events in the data base are those for which an instrumental magnitude estimate was available, which restricts them to $M_L > 2$ or so). Figure D-3 shows four equations plotted with the data:

$$M_L = 1.32 + .41\ I_o \tag{D-1}$$

$$M_L = 0.26 + 2/3\ I_o \tag{D-2}$$

$$M_L = 1.3 + 0.6\ I_o \tag{D-3}$$

$$M_L = 1 + 2/3\ I_o \tag{D-4}$$

Equations (D-3) and (D-4) were proposed by Gutenberg and Richter (1942 and 1956, respectively), based on California data. They are similar, and both tend to over-predict the magnitude value for a given I_o. Equation (D-1) is a least-squares fit to the data; it is judged to have too small a slope, particularly for the larger I_o values. (Removing the $I_o = 7$ point on Figure D-3 does not significantly change the fitted slope, within two significant figures.)

As an alternative to the Gutenberg and Richter (1956) relationship, with a slope of 2/3, we developed Equation (D-2). It is the least-squares fit through the data constraining the slope to have a value of 2/3. There are various reasons why, in the Rocky Mountains and Great Plains, earthquakes might tend to have lower values of M_L for a given I_o (or, observationally, higher reported values of I_o for a given M_L) than in California. The low level of seismicity means that more people will be awakened or frightened at a low level of shaking than in California, where such shaking is more common. Also, old, poorly constructed buildings in the Rocky Mountains might be damaged by the infrequent earthquake (indicating I_o = VI), but in our judgment such buildings would have been replaced long ago in California (because of more frequent earthquake occurrences and perhaps previous damage), so only I_o = V would be reported for the same level of shaking in California. Finally, expansion and development in California has replaced many older, vulnerable structures, more so than in the Rocky Mountain region, so less damage would be expected in California for the same levels of shaking.

To give additional guidance on whether Equations (D-2) and (D-4) are reasonable relationships to use, Figure D-4 shows the two relations superimposed on M_L vs I_o data published by Kirkham and Rogers (1985, p. 98) for the Rocky Mountain region. While this is not an independent comparison (many of the same earthquakes are in both data sets), it shows that the two equations provide reasonable estimates of M_L given I_o for the Kirkham and Rogers data set, particularly for $I_o \leq$ VI which comprises all of the data in Colorado for which this correlation is needed.

The data in Figures D-3 and D-4 do not indicate a definitive relationship between I_o and M_L. Therefore we express the uncertainty in M_L value given I_o by using two relationships, Equations (D-2) and (D-4), and weighting these equally. Separate analyses will be conducted of historical seismicity, activity rates, and *b*-values using estimates from the two relationships.

For conversion of m_b to M_L, there is also some uncertainty. Figure D-5 shows the data from the RMGP catalog, and the equation:

$$M_L = m_b - 0.5 \qquad \text{(D-5)}$$

Equation (D-5) is derived from the observation that M_L is directly proportioned to m_b (Herrmann and Nuttli, 1982) but that m_b usually exceeds M_L. Chulick and Herrmann (1986) suggest a constant of -0.3 to -0.4, but we find that a constant of -0.5 fits the data as well as any other, given the scatter in Figure D-5.

These procedures give estimates of M_L for all events in the catalog. We use Equations (D-2) and (D-5) in one analysis, which we designate the M_{L1} magnitudes in the catalog:

$$\left.\begin{aligned} M_{L1} &= 1 + 2/3\ I_o \text{ if } I_o \text{ available} \\ M_{L1} &= m_b - 0.5 \text{ if } m_b \text{ available} \end{aligned}\right\} \qquad \text{(D-6)}$$

and we use Equations (D-4) and (D-5) in a second analysis, which we designate the M_{L2} magnitudes in the catalog:

$$\left.\begin{aligned} M_{L2} &= 0.26 + 2/3\ I_o \text{ if } I_o \text{ available} \\ M_{L2} &= m_b - 0.5 \text{ if } m_b \text{ available} \end{aligned}\right\} \qquad \text{(D-7)}$$

Uncertainties in individual M_L estimates for each earthquake were determined taking into consideration similar work in the eastern U.S. (EPRI, 1986, p. 4-6). This consideration is appropriate because the predictive Equations (D-6 and D-7) were not developed from a pure empirical fit to the data (the empirical standard deviations are reported below, for completeness). Also, empirical data were not available for some of the estimation methods (e.g., duration magnitude and felt area). Standard deviations of estimates of M_L were assigned as follows:

estimator	σ_{ML}	σ_{mb} from EPRI (1986)	empirical σ_{ML}
none; M_L reported in catalog	0.3	0.3 for instrumental	N.A.
I_o	0.6	0.55 for $I_o < 8$	0.635
		0.45 for $I_o > 8$	N.A.
m_b or Nuttli magnitude	0.6	N.A.	0.637
M_L reported based on felt area	0.5	0.35	N.A.
duration magnitude converted to M_L	0.6	N.A.	N.A.

A standard deviation of 0.3 is typical for instrumental magnitude assessments. The values of σ_{ML} for conversions are somewhat higher than used in EPRI (1986, p. 4-6), which we feel is appropriate because the predictive equations have not been derived empirically. The value of 0.6 for conversion of m_b to M_L was selected because the scatter in observed data (Figure D-5) is about the same as for conversion of I_o to M_L (Figure D-3). The value of 0.5 for felt area (the one event in the catalog for which M_L had been reported based on felt area) was chosen to recognize that this method uses more observations and is slightly less uncertain than using I_o alone.

When an M_L value was reported in the catalog, that value alone was used for subsequent analyses (both for the M_{L1} and M_{L2} catalogs). If conversions were required, Equation (D-6) was used for the M_{L1} catalog and Equation (D-7) for the M_{L2} catalog. When multiple predictors were available, estimates of M_{L1} or M_{L2} were made separately using all predictors, and a weighted average was created using:

$$M_{Lk} = \sum_i w_i (M_{Lk})_i \qquad \text{(D-8)}$$

where k is 1 or 2 and

$$w_i = \sigma_i^{-2} / \sum_j \sigma_j^{-2} \qquad \text{(D-9)}$$

The standard deviation of the resulting estimate was calculated from:

$$\sigma_{ML} = [\sum_j \sigma_j^{-2}]^{-1/2} \qquad \text{(D-10)}$$

This procedure follows that of EPRI (1986, p. 4-7) for the eastern U.S.

To avoid the bias introduced by uncertainty in M_L on the estimated rates and *b* values, "uniform" magnitude estimates were created. This followed the procedure of EPRI (1986, p. 4-7).

$$M_L^* = M_L + \beta \sigma_{ML}^2 / 2 \qquad \text{(D-11)}$$

where $\beta = b \ln 10$, with *b* the parameter of the exponential magnitude distribution. For typical *b* values of 0.75 to 0.9 this simplifies to the following, within reasonable approximation (for σ_{ML} = 0.6, the error is +0.05 magnitude units for $b = 0.75$, and -0.01 magnitude units for $b = 0.9$):

$$\left.\begin{aligned} M_{L1}^* &= M_{L1} + \sigma_{ML1}^2 \\ M_{L2}^* &= M_{L2} + \sigma_{ML2}^2 \end{aligned}\right\} \qquad \text{(D-12)}$$

Finally with respect to the catalog it was determined that, for subsequent analyses of detection probabilities, an average magnitude could be used (the average of the M_{L1} and M_{L2} analyses). Thus we defined

$$M_{L3} = (M_{L1} + M_{L2})/2 \qquad \text{(D-13)}$$

The reason this is an appropriate simplification is that the probabilities of detection depend, in the early years, on the earthquake being felt, and the corresponding size estimate is represented by I_o for the early earthquakes in the catalog. Thus in the early years the conversion of I_o to M_L is immaterial, the detection probabilities are governed by I_o. In the later years, and for smaller magnitudes, detection depends on instrumental coverage and magnitude level, and most of the recent earthquakes have instrumental magnitude assignments. These instrumental magnitudes do not change whether we are using the M_{L1} or M_{L2} magnitudes estimated from I_o, and the choice of

magnitude bins is arbitrary for these events. Thus in the later years the I_o to M_L conversion is not an issue; earthquakes are generally represented by an instrumental magnitude. Therefore, it is appropriate to base probabilities of detection on average magnitude values and to use these for both I_o to M_L conversions.

With magnitudes estimated for all events in the catalog, it was possible to identify swarms and sequences in Colorado that include obvious dependent events. These were initially identified visually, and were studied to see what had been published about each swarm or sequence. The following swarms and sequences were identified:

Rocky Mountain Arsenal, Colorado, 1961 to 1972: This series of earthquakes was caused by pumping liquid waste into a deep injection well. The series is well documented by Evans (1966), Healy et al. (1968), and Nicholson and Wesson (1990). It began with the initiation of pumping in November of 1961 (Evans, 1966), and continued until February of 1966 (Hsieh and Bredehoeft, 1981). The study by Hsieh and Bredehoeft (1981) on induced pressures concluded that changes in pore pressure were sufficiently high to induce earthquakes through 1972. Because the seismic hazard study is based on natural, tectonic earthquakes, these man-made events were deleted from the catalog (201 earthquakes between November 1961 and December 1972). All events in the catalog subsequent to 1972 in the Rocky Mountain Arsenal area were retained, with the exception of one M_L 2.8 event that was a foreshock of an M_L 3.8 earthquake that occurred in April of 1981 (Bollinger et al., 1983). Aftershocks of the 1981 shock were not listed in the USGS catalog and thus were not included in our Colorado catalog.

The treatment of current seismicity in the area of the Rocky Mountain Arsenal is important. There is general agreement that the earthquakes in the 1960s were caused by fluid injection (see, for example, Nicholson and Wesson, 1990, and Davis and Frohlich, 1993), but no definitive studies on the current, low level of seismicity in the region have been made. We know of no way to resolve definitively whether seismicity subsequent to 1972 in the area of the Rocky Mountain Arsenal is background seismicity due to normal tectonic loading or seismicity that could be induced by the fluid injection of the early- to mid-1960s after long delay. The following considerations, however, can be made. Aftershock studies of earthquakes document that aftershocks can continue for at least seven to nine years following a mainshock (see, for example, Gross and Kisslinger, 1994), although this usually happens only for large mainshocks (magnitudes of 6 or 7). Further, Dieterick (1994) presents a model and observations that indicate that the duration of aftershocks is related to the recurrence time of the mainshock; aftershock durations greater than a decade imply mainshock recurrence times greater than several hundred years. Attempts to fit the Rocky Mountain Arsenal sequence to aftershock models were unsuccessful; this included cases where the initiating event was assumed to be the start of deep well injection, the end of injection, and the largest induced earthquake. The sequence does not behave like an earthquake aftershock sequence in time, because the process of pore pressure build-up and diffusion does not change crustal stresses, either in space or time, the same way a mainshock does.

As noted above, the Rocky Mountain Arsenal seismicity was artificially induced. Studies of seismicity induced by reservoirs (Simpson et al., 1988) indicate two possible mechanisms: changes in elastic stresses caused by the weight of the reservoir on the earth's crust, and changes in pore water pressure caused by diffusion. It is likely that the latter mechanism is the cause of earthquakes where deep-well injection is associated with seismicity (see, for example, Nicholson and Wesson,

1990), and there can be some time delay between changes of pressure at the source (the reservoir or injection well) and the resulting seismicity. Eventually, changes in pressure stabilize, whether at new levels (as in the case of a reservoir) or at pre-existing levels (as in the case of an injection well where pumping has stopped). A model of pore-fluid diffusion and pressure changes induced by the Rocky Mountain Arsenal well (Hsieh and Bredehoeft, 1981) indicated that pressures were sufficient to induce earthquakes through 1972.

Of the 201 earthquakes removed from the catalog because of deep well injection, three occurred in 1970, five occurred in 1971, and two occurred in 1972. The occurrence of two events per year in 1972 cannot be definitively classified as induced rather than natural seismicity based on the rate of seismicity; it is the pore-fluid diffusion study of Hsieh and Bredehoeft (1981) that guides the designation of earthquakes through 1972 as being related to injection. We include the possibility that the 1972 events are natural earthquakes by allowing for variable *b*-values (and hence variable rates at magnitude 5), as discussed below.

As a result of these considerations, seismicity in the area of the Rocky Mountain Arsenal well was removed from the Colorado catalog from November 1961 through December 1972. While it is possible that subsequent seismicity might be related to injection, if this is the case the level of seismicity will decrease because of further pore-fluid diffusion, and the seismic hazard presented here will be slightly conservative.

Seismicity near the Rocky Mountain Arsenal is modeled in association with the RMA/Derby source, which is described in Appendix A on "Seismic Source Characterization." Seismicity parameters for the RMA/Derby source calculated from historical seismicity are described below, and an alternative derivation using slip rate is described in Appendix A.

Dulce, New Mexico, 1966: This was an aftershock sequence following the $M_L = 5.1$ earthquake on January 23, 1966 that lasted until January of 1967 (Herrmann et al., 1980; Kirkham and Rogers, 1985, p. 63). Ninety-four aftershocks were reported, and all were deleted from the catalog (the mainshock was retained).

Carbondale, Colorado, 1984: This was a swarm of 17 earthquakes that occurred in April and May of 1984 (Goter et al., 1988; Kirkham and Rogers, 1985, p. 85). Magnitudes ranged from 1.9 to 3.2. Sixteen of the events were deleted from the catalog and the largest ($M_L = 3.2$) was retained.

Crested Butte, Colorado, 1986: This was a swarm of 26 earthquakes of $M_L = 1.6$ to 3.5 that occurred between August and October of 1986 (Cranswick, 1988). Twenty-five events were deleted from the catalog and the largest ($M_L = 3.5$) was retained.

With the dependent foreshocks, aftershocks, and swarm events removed, it is possible to present some summary results for the Colorado catalog. Table D-1 shows a summary of earthquakes for magnitude M_{L1} by magnitude interval and time, and Table D-2 shows a similar summary for magnitude M_{L2}. Note that in Tables D-1 and D-2 the time steps are initially ten years, then five years, then one year. These data exhibit the usual characteristics of earthquake catalogs, that the small earthquakes are completely reported only recently, and earthquakes reported in the early years are relatively large. Table D-3 shows similar results for M_{L3}.

Figure D-6 shows "Stepp plots" of the data for magnitudes corresponding to I_o = III through VI. These follow the method of Stepp (1970) to identify periods of complete reporting. The method works backwards from the present, calculating the activity rate (number of observed events/time period), and the statistical standard deviation of the activity rate based on the number of observations. For the period when the observed rate is flat (within the statistical error) and the width of the one-sigma bounds is decreasing steadily, the observed activity rate is stationary for that magnitude level. Where the observed rate decreases, the cause is presumed to be incomplete reporting. From this analysis the following periods of stationarity are interpreted:

I_o	Magnitude M_{L1}	Magnitude M_{L2}	Period of Stationarity
III	3.0	2.3	7 years
IV	3.7	2.9	10 years
V	4.3	3.6	30 years (?)
VI	5.0	4.3	50 years

These interpretations are obviously uncertain. They are combined with other analyses of completeness in the next section to derive quantitative measures of completeness in the early years.

EARTHQUAKE CATALOG INCOMPLETENESS

All earthquake catalogs are incomplete because they do not contain every earthquake that has occurred in the study region over all of recorded time. For seismic hazard analysis the goal is to quantify this incompleteness so that rates of activity can be accurately estimated. In the early years of seismic hazard analysis only the most recent complete parts of the catalog were used; in more recent studies (e.g., EPRI, 1986, Section 4) the entire catalog is used, including times during which reporting has been only partially complete.

The primary method used to identify and evaluate historical earthquakes is through newspaper accounts (e.g., Dames & Moore, 1981; McGuire et al., 1982; Oaks and Kirkham, 1986). Newspapers have been better archived than personal accounts and are more readily available. In Colorado, substantial work has been done to locate earthquake reports in newspapers of the state.

In an attempt to use newspapers to quantify the completeness of the earthquake record, we developed a method to estimate P_d (M_L, t), the probability of detection of a randomly-located earthquake as a function of magnitude M_L and time, i.e., the probability that an earthquake occurring in Colorado of magnitude M_L at time t would be felt, reported, and included in today's catalog. Ultimately this analysis of newspaper data was discarded in favor of a purely empirical method of estimating P_d, but it is useful to describe the newspaper analysis as background for issues related to the correction of earthquake data for completeness.

To quantify P_d from newspapers, we obtained the location and history of currently-archived newspapers in Colorado from Library of Congress (1984), and performed a quantitative analysis to determine, for any M_L and time, whether that earthquake would have been sufficiently felt at

locations with newspapers to be reported and later included in a catalog of earthquakes. The criteria for being "sufficiently felt" were defined as follows:

1. One town with a currently-archived newspaper was within the first isoseismal of the earthquake (which is estimated to occur at a distance of 13 km), or

2. Three towns with currently-archived newspapers were within the felt area of the earthquake.

Figures D-7 through D-10 illustrate the locations of newspapers in Colorado in the years 1870, 1900, 1940, and 1960. For the calculations, the following equation was used to represent felt radius (in km) as a function of magnitude M_L:

$$r = 10^{0.03 + 0.41 M_L} \qquad \text{(D-14)}$$

which is derived from Kirkham and Rogers (1985, p. 92). Illustrations of this felt radius are shown in Figures D-7 through D-10 for magnitudes (M_{L3}) corresponding to I_o = II through VIII, for one hypothetical epicenter in western Colorado. In the analysis, hypothetical earthquakes were placed at grid points spaced 0.05 degrees apart (both for longitude and latitude) and probabilities were calculated for each year and magnitude level using the fraction of grid points that met the criteria defined above.

Results of the regional analysis are illustrated in Figure D-11, which shows P_d values as a function of I_o and time. For this calculation, M_{L3} values were used that corresponded to integer I_o values, using Equation (D-13). The correspondence is as follows:

I_o	M_{L3}
II	2.0
III	2.6
IV	3.3
V	4.0
VI	4.6
VII	5.3
VIII	6.0

If the P_d values shown in Figure D-11 are accurate, they should result in adjusted activity rates that are constant with time at each magnitude level. Figure D-12 shows the average seismicity rate of earthquakes calculated starting from different times in the past to the present, for I_o = III through VI. Smaller events (I_o = II) are not included because they are incomplete, even today. Larger events (I_o > VI) consist of only one earthquake, so a detailed analysis cannot be performed. Two curves are shown in each plot of Figure D-12: the "actual" curve shows rates calculated for each year as

$$\text{actual cumulative rate (year } i) = \{ \sum_{j=i}^{1992} (\text{no. earthquakes in year } j) \} / (1993 - i) \quad \text{(D-15)}$$

and the "adjusted" curve shows rates calculated for each year as

$$\text{adjusted cumulative rate (year } i) = \{ \sum_{j=i}^{1992} (\text{no. earthquakes in year } j) \} / \sum_{j=i}^{1992} P_d (M_L, j) \quad \text{(D-16)}$$

This corrects for the incompleteness in early years when the catalog is only partially complete. Note that Equation D-16 is <u>not</u> the same as adjusting the number of earthquakes in each year by (dividing by) P_d, summing those adjusted numbers, and dividing by the interval. Equation D-16 gives the maximum likelihood estimate for the rate, adjusted by P_d estimated for each magnitude and time interval. For the plots in Figure D-12, I_o = V and VI earthquakes were assumed to be complete since 1962, when the World-Wide Standardized Seismograph Network was installed, and I_o = IV earthquakes were assumed to be complete since 1974 when regional networks became common. While no regional network was established in Colorado in 1974, this date is consistent with the magnitude-completeness threshold indicated by Engdahl and Rinehart (1991, Figure 3). The decrease of the actual rates in Figure D-12 as the curves go to earlier times results from incomplete reporting of events (the numerator in Equation (D-16) is not as large as it should be).

Figure D-12 shows that the P_d values from Figure D-11 are not very accurate for the earlier times. If the catalog were complete throughout all time, or the P_d values were accurate to correct the catalog for incompleteness, we would expect to see a horizontal line for the adjusted average seismicity rate, equal to the rate observed in the recent past (excluding the most recent few years when the observation period is too small to establish any rate at all). For I_o = III and VI, the adjusted rates decrease at earlier times than the peak rate, and for I_o = IV and V the adjusted rates continue to increase at earlier times than the peak rate. This suggests that the newspaper analysis is over-correcting at some intensities and under-correcting at others.

As a result of the newspaper analysis, the P_d values in Figure D-11 were not used and a purely empirical approach was adopted to determine P_d (M_L, t) values that resulted in uniform adjusted rates of activity with time. A second requirement was that the estimates of rates for the lower magnitude values should be consistent with an exponential magnitude distribution. Accordingly, the historical record was divided into four periods and P_d values were calculated for each period by dividing the observed rate in that period by the highest rate observed in the most recent period. This ensured that adjusted activity rates in the prior years were consistent with recent history, when the catalog is believed to be most complete. In addition, we applied the logical constraint that the P_d for any time and I_o could not be lower than the P_d for that same time and a lower I_o. Table D-4 documents these P_d values, and Figure D-13 shows them graphically. The P_d value for I_o = III in the most recent period (P_d = 0.83) was calculated by determining that a rate of 4.5 events per year of I_o = III is consistent with rates observed for higher I_o and with an exponential magnitude distribution.

Figure D-14 shows the actual and adjusted average seismicity rates using the P_d values presented in Table D-4 and Figure D-13. The plots in this figure indicate that the adjusted rate is constant for the earlier times and approximately equal to the highest rate observed in recent times when the catalog is complete. This validates the time periods and P_d values in Table D-4.

The P_d values shown in Table D-4 and Figure D-13 are the values adopted to adjust earthquake rates in early years. These adjustments are used both in the historical seismic hazard analysis and in the calculation of activity rates and *b*-values for seismic sources (see the sections that follow). The advantage of using these P_d values is that, for small seismic sources, the entire time period of the catalog can be used for estimates of activity rate and *b*-value, not just the most recent complete time interval.

HISTORICAL EARTHQUAKE HAZARD

The historical seismic hazard is a useful way to give perspective on what the seismic hazard has been at the site and what might be reasonable levels of hazard from future earthquakes. The methodology follows that developed by Veneziano, Cornell, and O'Hara (1984). The method is summarized in Figure D-15 and a description of the steps involved follows.

Earthquakes in the vicinity of the site are assembled (Figure D-15a), and the distribution of possible ground motions at the site are estimated using a ground motion equation appropriate for the region (Figure D-15b). Any measure of ground motion can be used by the method; in this study we will use peak ground acceleration (PGA) and spectral velocity at 10 and 1 Hz, to cover the range of frequencies of engineering interest. In estimating ground motion amplitudes, randomness in the ground motion equation is taken into account, so that a range of possible amplitudes is produced by any one historical earthquake. (Each value in the range is weighted by its probability, as obtained from the ground motion equation. Thus, for example, if ten amplitudes are used to represent the range, each amplitude is assigned a value of 0.1) These estimated amplitudes from the historical earthquakes are ordered from highest to lowest, and a cumulative number of amplitudes is obtained by counting from the top down (Figure D-15c). In this way the randomness in the ground motion equation is incorporated. Finally, the cumulative number of observations is divided by the time period of the catalog to estimate annual frequencies with which amplitudes have occurred at the site (Figure D-15d).

The actual application is more complicated, because of several factors. First, realistic earthquake catalogs have different times of completeness for different magnitude levels, and these must be taken into account. This is done by accounting for the "equivalent period of completeness," as described below. Second, there is uncertainty in the ground motion estimation equation. This is handled by producing multiple historical hazard curves, one for each ground motion equation. Finally, any uncertainties in historical earthquake magnitudes and locations are incorporated into the analysis by weighting the available interpretations. This method is used so that we can evaluate the effect of uncertainties in the magnitude and location of the 1882 Colorado earthquake.

The results from this method are valid for annual probabilities that are no lower than the inverse of the number of years covered by the catalog, so we can only expect to accurately estimate annual probabilities down to about 0.01 per year with an earthquake history of 123 years. In fact the 30

years of complete data (see Table D-4) suggest that the accuracy for small earthquakes may be good for annual probabilities of about 0.03 or higher. The seismic hazard results from a range of earthquakes, both small and large, so the accuracy of the historical method is best stated as the range of probabilities of 0.01 to 0.03 and higher. Making certain that seismic hazard results are reasonable for these annual probabilities gives some constraint on the values that are reasonable at lower annual probabilities.

This method was applied to the Rocky Flats Plant using the following assumptions. First, all seven attenuation equations developed for this project (see Appendix E) for rock conditions were used to create historical seismic hazard curves. Second, separate analyses were run with the M_{L1} and M_{L2} magnitudes in the Colorado catalog. This created fourteen combinations of input parameters. Third, uncertainty in the location of the 1882 Colorado earthquake was accounted for by using multiple locations and weights on each. The uncertainty distribution was taken from Appendix C, as was the M_L estimate (mean magnitude of 6.3).

A fourth assumption is that the incompleteness in reporting of earthquakes (see the previous section) can be accounted for by correcting the *observed* number of historical earthquakes (of a given magnitude and at a given time) by $P_d(M_L,t)$ to obtain a best estimate of the *actual* number of earthquakes that occurred. To obtain an idea of the effect of $P_d(M_L,t)$, we calculate an equivalent period of completeness $T_{eq}(M_L)$ for each magnitude level. This is defined as

$$T_{eq}(M_L) = \int_{1870}^{1992} P_d(M_L, t)\, dt \qquad \text{(D-17)}$$

This definition is consistent with that of EPRI (1986, p. 4-20). The function previously defined for $P_d(M_L, t)$ is used in this assessment. This definition of $T_{eq}(M_L)$ means, for example, that if a 100-year catalog is 50 percent complete for magnitude M_L for the first 50 years, and is 100 percent complete for the second 50 years, T_{eq} = 75 years. Stated another way, the data available are equivalent to a complete catalog of 75 years duration. Calculated values of $T_{eq}(M_L)$ are as follows (see also Table D-4):

I_o	M_{L1}	M_{L2}	T_{eq}, years
III	3.0	2.3	14
IV	3.7	3.0	50
V	4.3	3.6	66
VI	5.0	4.3	86
VII	5.7	5.0	86
VIII	6.3	5.6	123

The number of observations is divided by T_{eq} to obtain an annual rate (see Figure D-15d), in a manner that is equivalent, for the historical analysis, to estimating maximum likelihood rates of seismicity (Equation D-16).

Figure D-16 shows the historical seismic hazard curves for PGA. The top plot indicates results for the M_{L1} magnitudes, the bottom plot for the M_{L2} magnitudes. The seven curves represent the range

of ground motion equations developed for this project. Figures D-17 and D-18 show similar results for 10 Hz and 1 Hz spectral velocity (5% damping). These figures show individual hazard results for each combination of inputs.

A more integrated summary of the historical seismic hazard is presented in Figures D-19, D-20, and D-21 for the three ground motion measures. These fractile seismic hazard curves were obtained by weighting the individual results using the following weights:

magnitudes M_{L1} =	0.5
magnitudes M_{L2} =	0.5
Total:	1.0
Campbell empirical attenuation:	0.167
Sadigh empirical attenuation:	0.167
Joyner-Boore empirical attenuation:	0.166
analytical attenuation no. 1:	0.023
analytical attenuation no. 2:	0.227
analytical attenuation no. 3:	0.227
analytical attenuation no. 4:	0.023
Total:	1.0

The above weights for attenuation equations were obtained by (a) giving equal weight to empirical vs. analytical attenuations, (b) weighting the three empirical equations equally, and (c) using weights on the analytical attenuation that capture the uncertainty in the median analytical attenuation function (see Appendix E). The fractiles represented in Figures D-19, D-20, and D-21 represent uncertainties caused by uncertainties in the magnitudes and attenuation equations. The reason that these fractile curves are more closely spaced than the individual curves (Figures D-16, D-17, and D-18) is that the extreme individual curves have low weight, in other words they are outside of the 10% and 90% fractiles. These fractiles are appropriate to compare to analytically-derived seismic hazard curves documented in the project.

ACTIVITY RATES AND *b*-VALUES

Rates of seismic activity and *b*-values are required for seismic sources in a seismic hazard analysis. The rate of seismic activity $\nu_{5.0}$ is the annual rate of earthquake occurrences with $M_L \geq 5.0$ in a source. The *b*-value is the slope of the exponential magnitude distribution:

$$\log N(M_L) = a - b\ M_L \qquad \text{(D-18)}$$

where $N(M_L)$ is the number of earthquakes over a defined time period with magnitude $\geq M_L$, and *a* is a constant (it is the antilog of the number of earthquakes at magnitude 0). If $N(M_L)$ is defined as the annual number of earthquakes in a seismic source, then $\nu_{5.0}$ is:

$$\nu_{5.0} = 10^{a - b \times 5.0} \qquad \text{(D-19)}$$

The rate $\nu_{5.0}$ and slope b are calculated using the maximum likelihood procedure, which in its simplest form has the following solution:

$$\nu_{5.0} = N(M_L \geq 5.0)/t \qquad \text{(D-20)}$$

$$b = \ln 10/(\overline{M_L} - m_o) \qquad \text{(D-21)}$$

where t is the period of the catalog and $\overline{M}_L$ is the average magnitude of earthquakes above m_o. In practical applications the magnitudes are grouped into bins because many of them have been converted from MM intensity, and the data set is not complete at all magnitude levels for the entire catalog. For these applications, Weichert (1980) provides a maximum likelihood solution requiring an iterative method. This method is implemented here, using for each magnitude level an equivalent period of completeness T_{eq} as defined previously (Equation D-17) and as used by EPRI (1986, p. 4-20).

The first analysis conducted here used the entire Colorado catalog, without seismic sources, and used magnitudes M^*_{L1} and M^*_{L2} as defined in Equation (D-12). The resulting b-value plots are shown in Figure D-22. The data are shown with one-standard-deviation error bars to indicate how disperse the observations are. The data point at the high magnitude end in each plot results from the 1882 earthquake. The fitted lines are the maximum likelihood solution (best estimate and $\pm$ 1.73 times one sigma) plotted through the mean magnitude of the data. The use of 1.73 times one sigma is discussed below.

The final step was to estimate rates and b-values for the individual seismic sources derived for this project. These sources are shown on Figure D-23. For Sources I, II, and III there is uncertainty on whether the 1882 earthquake occurred in that source. As a result, four basic estimates of $\nu_{5.0}$ and b were made for these three sources: for M^*_{L1} or M^*_{L2}, and with or without the 1882 earthquake. The resulting fits are shown in Figures D-24 through D-26 for Sources I, II, and III, respectively, and in Figures D-27 and D-28 for Sources IV and V. The results are presented in tabular form in Table D-5 for each source separately and for the Colorado catalog as a whole. In addition to $\nu_{5.0}$ and b, the standard deviations of the estimates are included. For Sources I and II, the coefficients of variation of $\nu_{5.0}$ and b are about 25%-30%; for Source III they are somewhat lower (more data are available for Source III). For Source V (Figure D-28), there were very few historical earthquakes. Hence we adopted a b-value of 0.75 for this source (a typical b-value for the entire catalog--see the bottom two rows of Table D-5). The low seismicity of Sources IV and V mean that they do not contribute significantly to the hazard at Rocky Flats, so the uncertainty in rate and b-value need not be extensively characterized for these sources.

A special study was made of seismicity in the vicinity of the Rocky Mountain Arsenal (RMA), because of the potential importance of this seismicity to seismic hazard at the RFP. This seismicity is shown on Figure D-29, and historical earthquakes are listed in Table D-7. For purposes of analyzing the historical seismicity, two areas were used to collect earthquakes for statistical analysis:

1. Region A: Events within 20 km of the linear representation of the RMA/Derby source (this includes all events listed in Table D-7 and shown in Figure D-29) and

2. Region B: Events within 5 km of the linear representation of the RMA/Derby source (this includes events within the elliptical region identified on Figure D-29 as "Geometry 1"). See Appendix A for a description of the RMA/Derby source location. An exception was that event 2, which occurred in 1916 and is located at 40°N, 105°W, was not considered in Region B because of low precision in the location estimate. With a large location uncertainty, it is more probable that event 2 occurred outside of Region B than inside. This event is considered within Region A.

These two hypotheses were investigated because it is not possible to determine precisely which events are associated with the RMA/Derby source and which are part of the off-fault background seismicity. The above assumptions are reasonable alternative interpretations given the uncertainties in epicentral locations (particularly for the pre-instrumental shocks) and the uncertainties in fault geometry at depth. Note that the difference in seismicity rates is generally less than a factor of two for the two regions.

Figures D-30 and D-31 show plots of the historical seismicity for Regions A and B, for M_{L1} and M_{L2}. For these applications there were insufficient earthquakes to establish a statistical *b*-value, so a value of 0.75 was chosen. This value is supported by the analysis of historical seismicity for the entire Colorado catalog, which indicates *b*-values of 0.72 and 0.81 depending on the MMI conversion used, and by the analysis of historical seismicity in Sources I to III, which indicate an average *b*-value of 0.74 (see Table D-5 for these specific values). Also, the uncertainties in the *b*-value were chosen to be consistent with $\sigma_b = 0.165$, which is the average σ_b for Sources I and II which have few data (see the results in Table D-5 for Sources I and II).

To calculate the rate of seismicity (number of events divided by T_{eq}) as shown in Figures D-30 and D-31, the period November 1961 through December 1972 was subtracted from T_{eq}. This is consistent with the removal of all events during this time period, and gives unbiased estimates of the observed rate of activity.

For purposes of seismic hazard calculations, two geometries for the RMA/Derby source were used, as follows:

1. RMA/Derby Source Geometry 1: This geometry uses the linear representation of the RMA/Derby source (see Appendix A) and assumes a 5 km region around that inferred location to delineate a source area (see Figure D-29). Because the style of faulting is unknown, as is the three-dimensional geometry, this area source is considered a reasonable representation of the fault geometry. (This geometry is identical to RMA/ Derby Region B described above and used to collect seismicity.)

2. RMA/Derby Source Geometry 2: This geometry recognizes that the inferred location of the RMA/Derby source may be incorrect, and uses an elliptical area around the Rocky Mountain Arsenal well to delineate the fault location (see the elliptical area extending northwest from the RMA well on Figure D-29). This area also represents uncertain fault location, strike, down-dip width, and style of faulting.

To calculate seismic hazards based on historical seismicity, the seismicity parameters from both Region A and Region B (described previously) were assigned to both RMA/Derby Source Geometry

1 and RMA/Derby Source Geometry 2. This was done because the inherent uncertainty in the location of the earthquake source, and the uncertainties in locations of historical earthquakes, are large enough that it was not felt appropriate to ascribe one region (for collecting earthquakes) to only one source geometry.

The RMA/Derby source is evaluated to have probability of activity of 0.5 (see Appendix A). For the case when the RMA/Derby source is considered active, the historical seismicity represented by it cannot also be assigned to the host source (which is Source I). Hence two additional analyses of historical seismicity were conducted for Source I, eliminating first the seismicity in Region A and then that in Region B. Both of these analyses resulted in rates of seismicity, *b*-values, and uncertainties such that the estimated rates of activity above $M_L = 5$ were similar to the rates estimated for Source I alone (without elimination of seismicity from Regions A and B). Because the RMA/Derby source produces seismic hazard that is higher than from Source I, it is an acceptable (and slightly conservative) approximation to use the Source I seismicity for all representations of Source I, even when the RMA/Derby source is active.

The final selection was to choose specific pairs of values of $\nu_{5.0}$ and *b* for each source to represent uncertainty in the entire estimation process. This uncertainty is contributed by three factors, which are weighted as follows:

I_o - M_L conversion (M^*_{L1} vs M^*_{L2}): weight 0.5 each

Uncertainty in rate and *b*-value (for Sources I, II and III, and Source I without the RMA/Derby source): use three values of *b* that represent the central value and alternative values of $\pm$ 1.73 σ, with weight of 0.666 on the central value and 0.167 on each alternative. These reflect the statistical uncertainty in *b*; the statistical uncertainty in the rate at the mean magnitude of the data is small (see Figures D-24 through D-26) and is ignored, and $\nu_{5.0}$ is calculated using alternative *b*-values plotted from the mean magnitude of the data.

Uncertainty in rate and *b*-value (for the RMA/Derby source): use three values of ν and *b* that represent the central value and alternative values of $\pm$ 1.73 σ, with weight of 0.666 on the central value and 0.167 on each alternative. Calculate the alternative values of ν at the magnitude used to estimate the rate; extrapolate using the central and alternative *b*-values to obtain nine values of $\nu_{5.0}$ and *b*. This procedure maintains the statistical correlation between ν and *b* so that the values of $\nu_{5.0}$ and *b* properly represent the joint uncertainty distribution.

Uncertainty in the location of the 1882 earthquake: assume in Source I with weight 0.18, in Source II with weight 0.35, and in Source III with weight 0.47 (these values are calculated from the results in Appendix C).

The I_o-M_L conversions have equal credibility, as discussed in previous sections. The uncertainty in *b* and, where applicable, in ν, is represented with a discrete distribution with three values, and the values selected above (number of standard deviations and weights) have the property that they reflect the second and fourth moments of a normal distribution accurately. (The first moment, the mean, is reflected accurately by choice of the central value, and the third moment, the skewness is zero by the choice of equal deviations from the mean. Thus all four moments of the distribution are

accurately represented.) This procedure is valid both for empirical distributions derived from many observations or for the selection of σ_b based on non-empirical considerations.
The explicit modeling of uncertainties in the *b*-values deserves further explanation. The modeled uncertainty coves a range of assumptions that might lead to higher or lower rates at **M** > 7.5, as follows:

- The completeness times selected by the empirical analysis described earlier may be too longs or short, meaning that the rate of activity should be higher or lower than estimated.

- The RMA/Derby source, and some other sources, may follow a characteristic distribution, so the rate for **M** > 5 should be higher than estimated by extrapolating seismicity at lower magnitudes using a standard *b*-value.

- Some distribution other than the exponential may govern seismicity over the short term. The exponential distribution has been found to work empirically for many regions, worldwide, but other distributions may be more appropriate for specific sources or times.

- For the RMA/Derby source, seismicity in 1972 (and, perhaps, earlier years) may have been natural, whereas that seismicity was treated as induced here.

All of these reasons emphasize that the extrapolation of small-earthquake seismicity rates to estimate rates for **M** > 5 is uncertain, and in many cases is difficult to quantify. The use of uncertain *b*-values and rates accounts for these uncertainties and allows a reasonable and justified hazard analysis to be conducted.

The uncertainty in the location of the 1882 earthquake was determined using the uncertainty analysis presented in Appendix C. This uncertainty analysis resulted in regions of Colorado where the 1882 earthquake might have occurred, and associated probabilities. Source I, II, and III were overlaid on these regions to determine the probability, based on the Appendix C analysis, that the 1882 earthquake occurred in each of those sources.

The final calculated values of $\nu_{5.0}$ and *b* are shown in Tables D-6 and D-8. Uncertainty in the rates $\nu_{5.0}$ and *b*-values were represented with multiple discrete values. The values and weights were chosen so that the original statistical uncertainty (from the maximum likelihood fits to the data) was replicated, i.e., the first four moments of the statistical distribution are duplicated by the discrete values and weights. Note that uncertainty in *b* translates to changes in $\nu_{5.0}$; in fact, this contributes to most of the σ_ν values shown in Table D-5. The additional uncertainty in $\nu_{5.0}$ caused by uncertainty in the rate at the average magnitude value is very small for Sources I through V (see the error bars in Figures D-24 through D-28 at the average magnitude level--where the curves cross). As a result the uncertainty in $\nu_{5.0}$ is calculated here from the uncertainty in *b*, for Sources I through V. For the RMA/Derby source the uncertainty in $\nu_{5.0}$ was large (because of the small number of events), so both σ_ν and σ_b were accounted for explicitly.

In Sources IV and V, very few earthquakes have occurred historically and the maximum likelihood estimates are not well-constrained. As an alternative, we use a *b*-value of 0.75 and calculate the rate at M_L = 5 using the rate observed for the lowest magnitude interval. This is a reasonable

approximation, and is justified because the distance of these sources from the Rocky Flats Plant, and their low rates of activity, mean that they will not contribute to the seismic hazard.

CONCLUSIONS

A uniform catalog of earthquakes for Colorado has been assembled from available sources (the U.S. Geological Survey, the Colorado Geological Survey, and published summaries of earthquakes). Estimates of local magnitude M_L from MM intensity I_o and body-wave magnitude m_b incorporate uncertainties explicitly.

An attempt to estimate the completeness of the earthquake catalog in early years using newspaper locations and dates of publication did not yield probabilities of detection that were consistent with the recent record. Therefore, a purely empirical analysis was used to calculate probabilities of detection for the early years. This allows all seismicity in small seismic sources to be used for the estimation of activity rate and *b*-value.

The historical seismic hazard method was applied, using the derived earthquake catalog and probabilities of detection. For the two magnitude conversions and seven attenuation equations this shows the historical hazard, and is accurate down to annual probabilities as low as 0.03 to 0.01.

The maximum likelihood method was used to calculate activity rates and *b*-values for the seismic sources specified for the hazard analysis. Alternative discrete sets of values are calculated for different I_o to M_L conversions, for different locations of the 1882 Colorado earthquake, and for different rates and *b*-values, representing statistical uncertainties in those parameters where appropriate. This gives a range of activity rates and *b*-values for the seismic hazard calculations.

REFERENCES

Bollinger, G.A. (1993). Reevaluation of the epicenter and magnitude for the 1882 Colorado earthquake, Appendix B to Task 7 Report on "Detailed Seismic Source Characterization," Rocky Flats Seismic Hazard Study.

Bollinger, G.A., M.J. Adams, R.F. Henrisey and C.J. Langer (1983). The Denver earthquake sequence of March-April 1981, *Earthquake Notes*, 54, 2, April-June, 3-12.

Chulick, J.A. and R.B. Herrmann (1986). The relation between m_{Lg} and M_L for California earthquakes: observations and modeling, *Earthquake Notes*, 57, 3, p. 95-102.

Cranswick, E. (1988). Microearthquakes recorded by a micro-array at a hard-rock site near Crested Butte, Colorado, *EOS* Abstracts, 69, 18, May 3.

Dames and Moore (1981). Geologic and seismologic investigations for Rocky Flats Plant, Rept to U.S. Dept. of Energy, July 9, Chapter 8, "1882 Earthquake Investigation."

Davis, S.D. and C. Frohlich (1993). Did (or will) fluid injection cause earthquakes? Criteria for a rational assessment, *Seism. Res. Letters*, 64, 3-4, 207-224, July-December.

Dieterich, J. (1994). A constitutive law for rate of earthquake production and its application to earthquake clustering, *Journ. Geophy. Res.*, 99, 2601-2618.

Engdahl, E.R. and W.A. Rinehart (1991). Seismicity Map of North America Project, *in* D.G. Slemmons, E.R. Engdahl, M.D. Zoback, and D.D. Blackwell, eds., Neotectonics of North America: Boulder, Colorado, Geological Society of America, Decade Map Volume 1.

EPRI (1986). Seismic hazard methodology for the central and eastern United States, Vol. 1: methodology, Elec. Power Res. Inst., Rept NP-4726, July, p. 4-7.

Evans, D. (1966). The Derby Earthquakes, *Mountain Geologist*, 3, 1, p. 23.

Goter, S.K., B.W. Presgrave, R.F. Henrisey and C.J. Langen (1988). The Carbondale, Colorado, earthquake swarm of April-May 1984, U.S. Geological Survey Open-File Rept. 88-417, 15 pp.

Gross, S.J. and C. Kisslinger (1994). Tests of models of aftershock rate decay, *Jour. Geophys. Res.*, in press.

Gutenberg, B. and C.F. Richter (1942). Earthquake magnitude, intensity, energy and acceleration, *Bull. Seis. Soc. Am.*, 32, p. 163-191.

Gutenberg, B. and C.F. Richter (1956). Earthquake magnitude, intensity, energy and acceleration (second paper), *Bull. Seis. Soc. Am.*, 46, 105-164.

Healy, J.H., W.W. Rubey, D.T. Griggs and C.B. Raleigh (1968). The Denver earthquakes, *Science*, 161, 3848, Sept. 27, p. 1301-1310.

Herrmann, R.B., J.W. Dewey, S.K. Park (1980). The Dulce, New Mexico earthquake of 23 January 1966, *Bull. Seis. Soc. Am.*, 70, 6, December, p. 2171-2183.

Herrmann, R.B. and O.W. Nuttli (1982). Magnitude: the relation of M_L to m_{bLg}, *Bull. Seis. Soc. Am.*, 72, 2, April, p. 389-398.

Hsieh, P.A. and J.D. Bredehoeft (1981). A reservoir analysis of the Denver earthquakes: a case of induced seismicity, *Jour. Geophys. Res.*, 86, B2, 903-920, February 10.

Kirkham, R.M. and W.P. Rogers (1985). Colorado earthquake data and interpretations--1867 to 1985, Colorado Geological Survey, Bull. 46.

Library of Congress (1984). Newspapers in microform, Library of Congress Catalogs, p. 119-139.

McGuire, R.K., A. Krusi and S.D. Oaks (1982). The Colorado earthquake of November 7, 1882: size, epicentral location, intensities, and possible causative fault, *Mountain Geologist*, 19, 1, January, p. 11-23.

Nicholson, C. and R.L. Wesson (1990). Earthquake hazard associated with deep well injection--a report to the U.S. Environmental Protection Agency, U.S. Geological Survey Bulletin 1951.

Oaks, S.D. and R.M. Kirkham (1986). Results of a search for felt reports for selected Colorado earthquakes, Colo. Geol. Survey, Info. Series 23.

Risk Engineering, Inc. (1989). Probabilistic seismic hazard evaluations at nuclear plant sites in the central and eastern United States: resolution of the Charleston earthquake issue, Elec. Power Res. Inst., Rept NP-6395-D, April.

Simpson, D.W., W.S. Leith and C.H. Scholz (1988). Two types of reservoir-induced seismicity, *Bull. Seis. Soc. Am.*, 78, 6, p. 2025-2040.

Stepp, J.C. (1970). Analysis of completeness of the earthquake sample in the Puget Sound area and its effect on statistical estimates of earthquake hazard, *Proc.*, First Intern. Microzonation Conf., Seattle, P. 897-909.

Stover, C.W., G. Reagor and S.T. Algermissen (1984). Seismicity Map of the State of Colorado, U.S. Geological Survey Map MF-1694.

Veneziano, D., C.A. Cornell and T.F. O'Hara (1984). Historical method of seismic hazard analysis, Elec. Power Res. Inst., Rept NP-3438, Palo Alto, May.

Weichert, D. (1980). Estimation of earthquake recurrence parameters for unequal observation periods for different magnitudes, *Bull. Seis. Soc. Am.*, 70, 4, p. 1337-1346.

TABLE D-1

EARTHQUAKE COUNTS BY MAGNITUDE INTERVAL AND TIME, USING M_{L1}

SOURCE FREQUENCY DISTRIBUTION PLOT OF EARTHQUAKES BY MAGNITUDE FOR COLORADO

BY DECADE BEFORE 1900, THEN BY FIVE YEARS TO 1970, THEN YEARLY

M>/=	2.00	2.67	3.33	4.00	4.67	5.33	6.00	6.67	7.33
but<	2.67	3.33	4.00	4.67	5.33	6.00	6.67	7.33	8.00
1870	.	.	1	.	2	.	.	.	.
1880	.	1	4	2	1	.	1	.	.
1890	.	.	2	3	1	.	.	.	.
1900	.	.	2	.	1	.	.	.	.
1905	.	1	.	1	.	.	.	.	.
1910	.	.	.	1	.	.	.	.	.
1915	.	1	1	.	.	.	.	.	.
1920	.	3	2	3	.	.	.	.	.
1925	.	.	1	2	.	.	.	.	.
1930	.	.	.	.	.	.	.	.	.
1935	.	.	.	.	.	.	.	.	.
1940	.	1	4	2	1	.	.	.	.
1945	.	1	4	.	.	.	.	.	.
1950	.	.	1	1	.	.	.	.	.
1955	.	2	3	.	2	.	.	.	.
1960	.	2	4	2	2	.	.	.	.
1965	2	12	7	3	.	.	.	.	.
1970	.	.	3	.	.	.	.	.	.
1971	.	.	1	2	.	.	.	.	.
1972	.	.	.	.	.	.	.	.	.
1973	.	5	1	.	1	.	.	.	.
1974	.	.	1	.	.	.	.	.	.
1975	.	.	1	.	.	.	.	.	.
1976	.	1	.	.	.	.	.	.	.
1977	1	1	.	.	.	.	.	.	.
1978	.	3	.	.	.	.	.	.	.
1979	1	3	.	1	.	.	.	.	.
1980	.	.	.	.	.	.	.	.	.
1981	1	1	1	.	.	.	.	.	.
1982	.	3	.	.	.	.	.	.	.
1983	.	.	2	1	.	.	.	.	.
1984	2	3	1	.	.	.	.	.	.
1985	.	2	.	.	.	.	.	.	.
1986	2	2	1	.	.	.	.	.	.
1987	2	2	.	.	.	.	.	.	.
1988	1	3	.	.	.	.	.	.	.
1989	4	3	.	.	.	.	.	.	.
1990	3	2	.	.	.	.	.	.	.
1991	7	.	1	.	.	.	.	.	.
1992	.	3	.	.	.	.	.	.	.
	26	61	49	24	11	0	1	0	0

TABLE D-2

EARTHQUAKE COUNTS BY MAGNITUDE INTERVAL AND TIME, USING M_{L2}

SOURCE FREQUENCY DISTRIBUTION PLOT OF EARTHQUAKES BY MAGNITUDE FOR COLORADO

BY DECADE BEFORE 1900, THEN BY FIVE YEARS TO 1970, THEN YEARLY

M>/=	1.26	1.93	2.59	3.26	3.93	4.59	5.26	5.93	6.59
but<	1.93	2.59	3.26	3.93	4.59	5.26	5.93	6.59	7.26
1870	.	.	1	.	2	.	.	.	.
1880	.	1	4	2	1	.	.	1	.
1890	.	.	2	3	1	.	.	.	.
1900	.	.	2	.	1	.	.	.	.
1905	.	1	.	1	.	.	.	.	.
1910	.	.	.	1	.	.	.	.	.
1915	.	1	1	.	.	.	.	.	.
1920	.	3	2	3	.	.	.	.	.
1925	.	.	1	2	.	.	.	.	.
1930	.	.	.	.	.	.	.	.	.
1935	.	.	.	.	.	.	.	.	.
1940	.	1	4	2	1	.	.	.	.
1945	.	1	4	.	.	.	.	.	.
1950	.	.	1	1	.	.	.	.	.
1955	.	2	3	.	2	.	.	.	.
1960	.	1	3	3	1	2	.	.	.
1965	.	3	6	12	2	1	.	.	.
1970	.	.	.	3	.	.	.	.	.
1971	.	.	.	2	1	.	.	.	.
1972	.	.	.	.	.	.	.	.	.
1973	.	4	2	.	1	.	.	.	.
1974	.	.	.	1	.	.	.	.	.
1975	.	.	.	1	.	.	.	.	.
1976	.	.	1	.	.	.	.	.	.
1977	.	1	1	.	.	.	.	.	.
1978	.	.	3	.	.	.	.	.	.
1979	.	.	3	1	1	.	.	.	.
1980	.	.	.	.	.	.	.	.	.
1981	.	1	1	1	.	.	.	.	.
1982	.	.	3	.	.	.	.	.	.
1983	.	.	.	2	1	.	.	.	.
1984	.	2	3	1	.	.	.	.	.
1985	.	.	2	.	.	.	.	.	.
1986	.	1	3	1	.	.	.	.	.
1987	.	2	2	.	.	.	.	.	.
1988	.	1	2	1	.	.	.	.	.
1989	.	3	4	.	.	.	.	.	.
1990	.	3	2	.	.	.	.	.	.
1991	.	6	1	1	.	.	.	.	.
1992	.	.	3	.	.	.	.	.	.
	0	38	70	45	15	3	0	1	0

TABLE D-3

EARTHQUAKE COUNTS BY MAGNITUDE INTERVAL AND TIME, USING M_{L3}

SOURCE FREQUENCY DISTRIBUTION PLOT OF EARTHQUAKES BY MAGNITUDE FOR COLORADO

BY DECADE BEFORE 1900, THEN BY FIVE YEARS TO 1970, THEN YEARLY

M>/=	1.63	2.30	2.96	3.63	4.30	4.96	5.63	6.30	6.96
but<	2.30	2.96	3.63	4.30	4.96	5.63	6.30	6.96	7.63
1870	.	.	1	.	2	.	.	.	.
1880	.	1	4	2	1	.	.	1	.
1890	.	.	2	3	1	.	.	.	.
1900	.	.	2	.	1	.	.	.	.
1905	.	1	.	1	.	.	.	.	.
1910	.	.	.	1	.	.	.	.	.
1915	.	1	1	.	.	.	.	.	.
1920	.	3	2	3	.	.	.	.	.
1925	.	.	1	2	.	.	.	.	.
1930	.	.	.	.	.	.	.	.	.
1935	.	.	.	.	.	.	.	.	.
1940	.	1	4	2	1	.	.	.	.
1945	.	1	4	.	.	.	.	.	.
1950	.	.	1	1	.	.	.	.	.
1955	.	2	3	.	2	.	.	.	.
1960	.	2	3	2	3	.	.	.	.
1965	2	2	12	6	2	.	.	.	.
1970	.	.	1	2	.	.	.	.	.
1971	.	.	.	3	.	.	.	.	.
1972	.	.	.	.	.	.	.	.	.
1973	.	4	2	.	1	.	.	.	.
1974	.	.	1	.	.	.	.	.	.
1975	.	.	.	1	.	.	.	.	.
1976	.	.	1	.	.	.	.	.	.
1977	1	.	1	.	.	.	.	.	.
1978	.	2	1	.	.	.	.	.	.
1979	.	2	2	1	.	.	.	.	.
1980	.	.	.	.	.	.	.	.	.
1981	1	1	.	1	.	.	.	.	.
1982	.	3	.	.	.	.	.	.	.
1983	.	.	2	1	.	.	.	.	.
1984	1	1	4	.	.	.	.	.	.
1985	.	1	1	.	.	.	.	.	.
1986	.	4	1	.	.	.	.	.	.
1987	.	4	.	.	.	.	.	.	.
1988	.	2	2	.	.	.	.	.	.
1989	2	4	1	.	.	.	.	.	.
1990	1	3	1	.	.	.	.	.	.
1991	2	5	1	.	.	.	.	.	.
1992	.	2	1	.	.	.	.	.	.
	10	52	63	32	14	0	0	1	0

TABLE D-4

EMPIRICAL P_d VALUES

		Period			
I_o	M_{L3}	1870-1939	1940-1961	1962-1985	1986-1992
III	2.6	0.02	0.05	0.24	0.83
IV	3.3	0.13	0.40	1.00	1.00
V	4.0	0.38	0.40	1.00	1.00
VI	4.6	0.47	1.00	1.00	1.00
VII	5.3	0.47	1.00	1.00	1.00
VIII	6.0	1.00	1.00	1.00	1.00

TABLE D-5

RATES, *b*-VALUES, AND UNCERTAINTIES

SOURCE	MAGNITUDE	1882 EQ	$\nu_{5.0}$	σ_ν	b	σ_b
I	M^*_{L1}	Y	.019	.0057	.6474	.1650
		N	.0082	.0026	.8533	.2099
	M^*_{L2}	Y	.0093	.0023	.6438	.1302
		N	.0039	.0010	.7967	.1587
II	M^*_{L1}	Y	.0199	.0058	.6584	.1595
		N	.0092	.0028	.8480	.1991
	M^*_{L2}	Y	.0081	.0020	.6707	.1341
		N	.0031	.0008	.8372	.1656
III	M^*_{L1}	Y	.1110	.0118	.7395	.0632
		N	.1004	.0107	.7643	.0650
	M^*_{L2}	Y	.0585	.0054	.6712	.0498
		N	.0527	.0049	.6898	.0511
IV	M^*_{L1}	N/A	.0250	.0072	.7500	.2000
	M^*_{L2}	N/A	.0007	.0002	1.1090	.2149
V	M^*_{L1}	N/A	.0024	--	.7500	.2000
	M^*_{L2}	N/A	.0013	--	.7500	.2000
COLORADO	M^*_{L1}	N/A	.1216	.0108	.8103	.0568
	M^*_{L2}	N/A	.0639	.0050	.7232	.0441

TABLE D-6

SOURCE PARAMETERS AND WEIGHTS

SOURCE	MAGNITUDE	1882 EQ	$v_{s,e}$	b	WEIGHT
I	$M^*_{1,1}$	Y	.0446	.3620	.01503
			.0190	.6474	.05994
			.0081	.9329	.01503
		N	.0278	.4902	.06847
			.0082	.8533	.27306
			.0024	1.2164	.06847
	$M^*_{1,2}$	Y	.0267	.4186	.01503
			.0093	.6438	.05994
			.0032	.8690	.01503
		N	.0153	.5221	.06847
			.0039	.7967	.27306
			.0010	1.0713	.06847
II	$M^*_{1,1}$	Y	.0458	.3825	.02923
			.0199	.6584	.11655
			.0087	.9343	.02923
		N	.0292	.5036	.05428
			.0092	.8480	.21645
			.0029	1.1924	.05428
	$M^*_{1,2}$	Y	.0244	.4387	.02923
			.0081	.6707	.11655
			.0027	.9027	.02923
		N	.0132	.5507	.05428
			.0031	.8372	.21645
			.0007	1.1237	.05428
III	$M^*_{1,1}$	Y	.1572	.6302	.03925
			.1110	.7395	.15651

TABLE D-6 (CONTINUED)

SOURCE	MAGNITUDE	1882 EQ	v_{50}	*b*	WEIGHT
			.0784	.8488	.03925
		N	.1443	.6519	.04426
			.1004	.7643	.17649
			.0698	.8768	.04426
	M_{12}^{*}	Y	.0881	.5850	.03925
			.0585	.6712	.15651
			.0389	.7574	.03925
		N	.0805	.6014	.04426
			.0527	.6898	.17649
			.0345	.7782	.04426
IV	M_{11}^{*}	N/A	.1200	.4040	.08350
			.0250	.7500	.33300
			.0052	1.0960	.08350
	M_{12}^{*}	N/A	.0051	.7372	.08350
			.0007	1.1090	.33300
			.0001	1.4808	.08350
V	M_{11}^{*}	N/A	.0114	.4040	.08350
			.0024	.7500	.33300
			.0005	1.0960	.08350
	M_{12}^{*}	N/A	.0115	.4040	.08350
			.0013	.7500	.33300
			.0002	1.0960	.08350

TABLE D-7

EARTHQUAKES NEAR ROCKY MOUNTAIN ARSENAL

EVENT NO.	DATE	LAT.	LON.	M_L	I_o	M_{L1}	M_{L2}
1	29-DEC-1902	39.70	105.00	--	4	3.67	2.93
2	12-OCT-1916	40.00	105.00	--	4	3.67	2.93
3	27-JAN-1923	39.70	105.00	--	F*	0	0
4	04-JAN-1924	39.70	105.00	--	F*	0	0
5	10-JUN-1978	39.79	104.87	2.9	4	2.90	2.90
6	02-APR-1981	39.91	104.95	3.8	6	3.80	3.80
7	16-SEP-1981	39.88	104.91	2.1	4	2.10	2.10
8	11-MAR-1982	39.86	104.85	2.8	3	2.80	2.80
9	18-SEP-1982	39.90	104.91	2.8	3	2.80	2.80
10	25-FEB-1984	39.92	105.02	2.5	3	2.50	2.50
11	08-NOV-1989	39.829	105.106	2.5	4	2.50	2.50

* Earthquakes listed as "Felt" in the catalog were not used in subsequent quantitative analyses.

TABLE D-8

RATES AND *b*-VALUES FOR RMA/DERBY SOURCE

Source	Seismicity	M_l	$\nu_{5.0}$	*b*-value	Weight*
RMA/Derby source	Region A	M^*_{L1}	.03307	.465	.0139
			.00906	.750	.0556
			.00248	1.036	.0139
			.02044	.465	.0556
			.00560	.750	.2222
			.00153	1.036	.0556
			.00781	.465	.0139
			.00214	.750	.0556
			.00059	1.036	.0139
RMA/Derby source	Region A	M^*_{L2}	.04094	.465	.0139
			.00690	.750	.0556
			.00116	1.036	.0139
			.02553	.465	.0556
			.00430	.750	.2222
			.00072	1.036	.0556
			.01012	.465	.0139
			.00171	.750	.0556
			.00029	1.036	.0139
RMA/Derby source	Region B	M^*_{L1}	.02633	.465	.0139
			.00721	.750	.0556
			.00198	1.036	.0139
			.01497	.465	.0556
			.00410	.750	.2222
			.00112	1.036	.0556
			.00360	.465	.0139
			.00099	.750	.0556
			.00027	1.036	.0139
RMA/Derby source	Region B	M^*_{L2}	.03057	.465	.0139
			.00515	.750	.0556
			.00087	1.036	.0139
			.01722	.465	.0556
			.00290	.750	.2222
			.00049	1.036	.0556
			.00387	.465	.0139
			.00065	.750	.0556
			.00011	1.036	.0139

* weights are rounded to nearest 0.0001

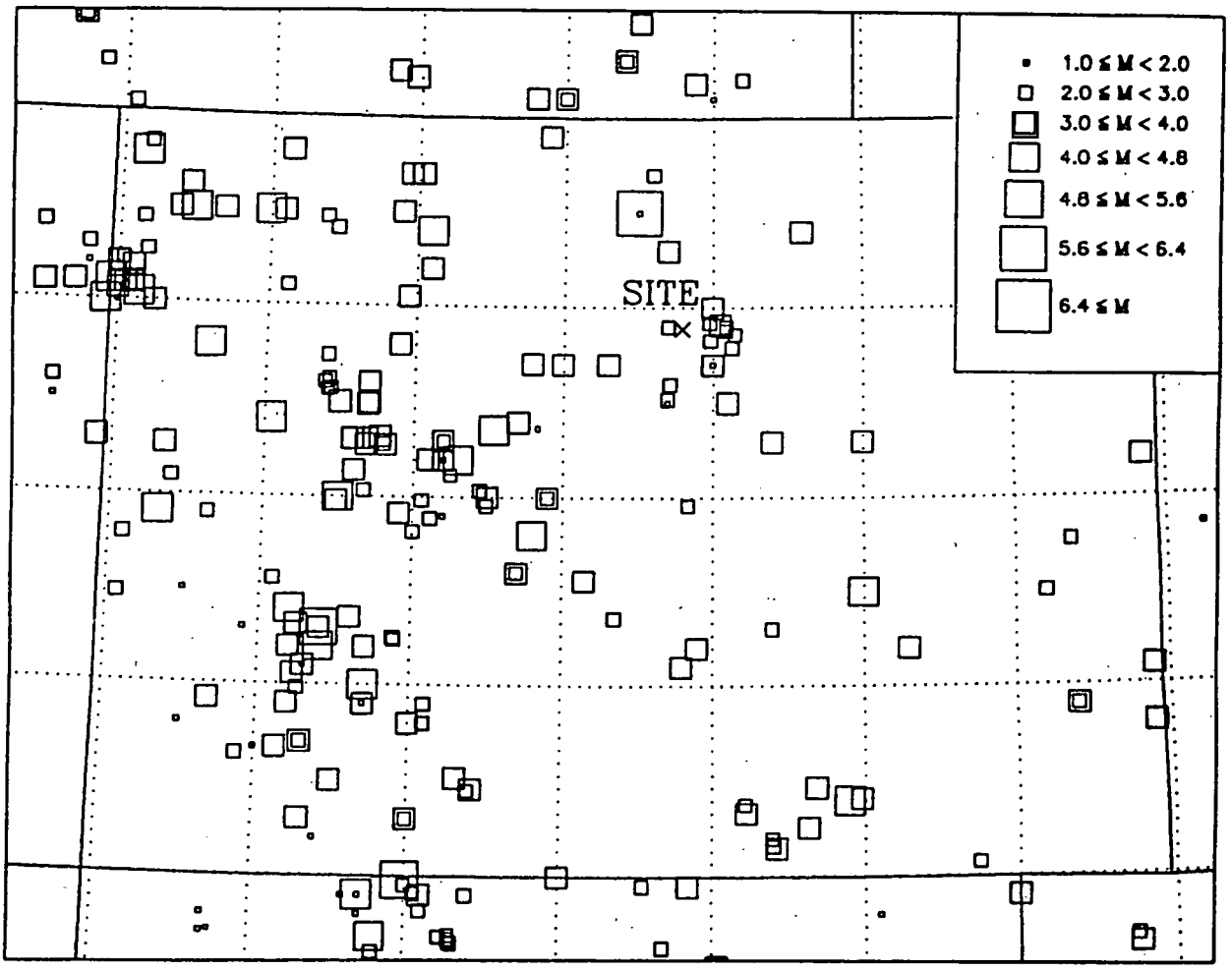

GREATER COLORADO SEISMICITY 1870 – MAY 1993

Figure D-1: Historical seismicity in Colorado.
Dotted lines indicate longitudes and latitudes.

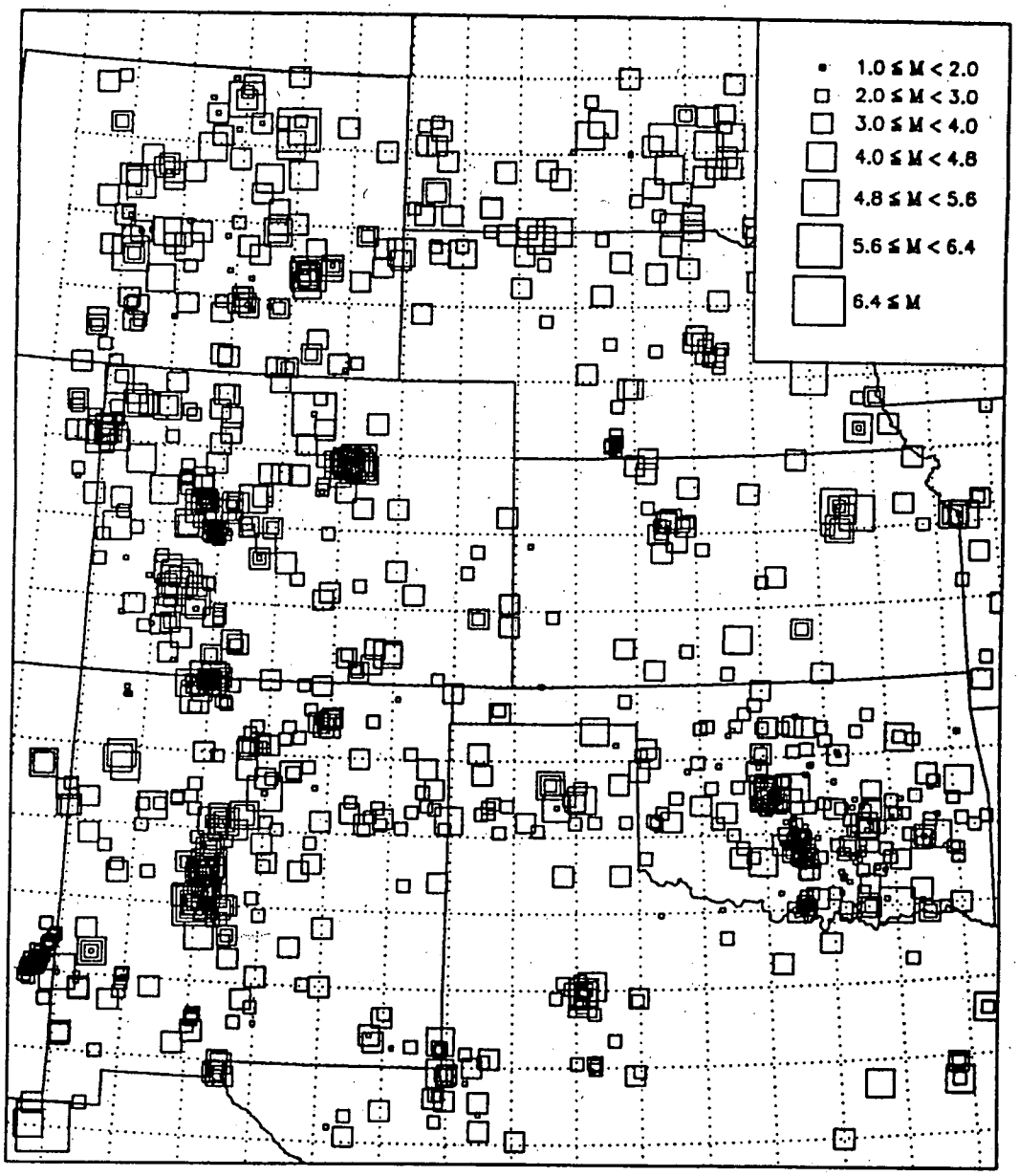

ROCKY MOUNTAIN – GREAT PLAINS 1830 – MAY 1993

Figure D-2: Rocky Mountain-Great Plains Catalog

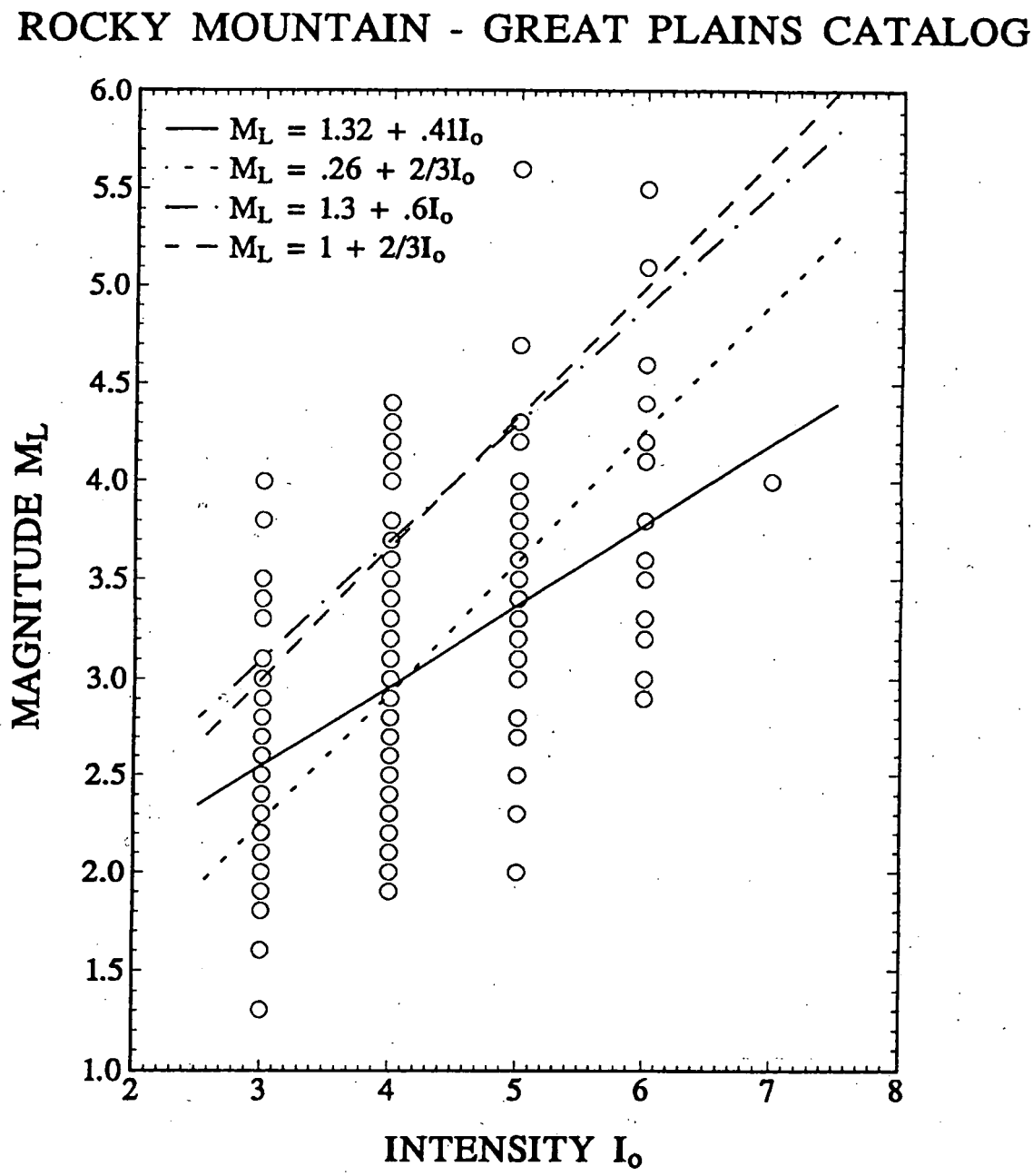

Figure D-3: M_L - I_o data and equations, this study.

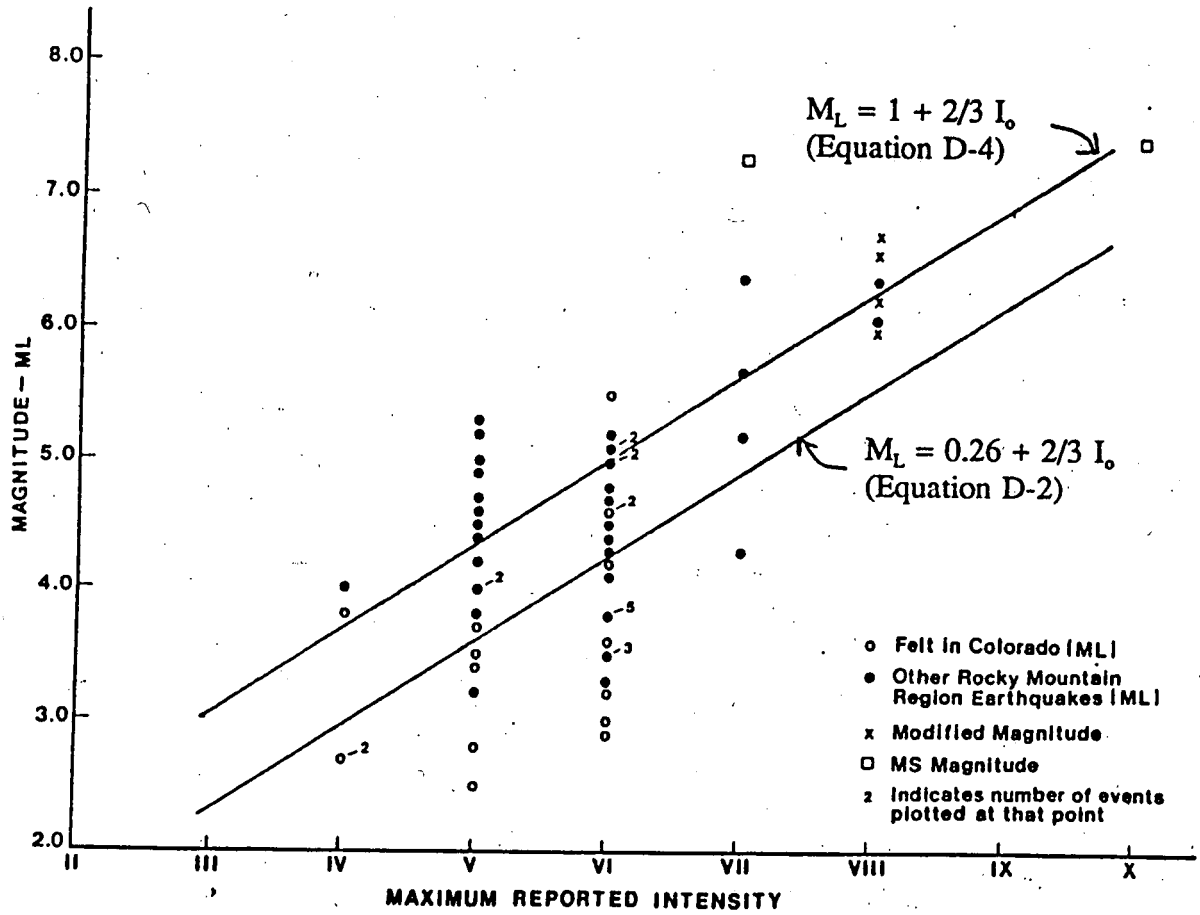

Figure D-4: M_L - I_o data (from Kirkham and Rogers, 1985, p. 98, with Equations (D-2) and (D-4) superimposed).

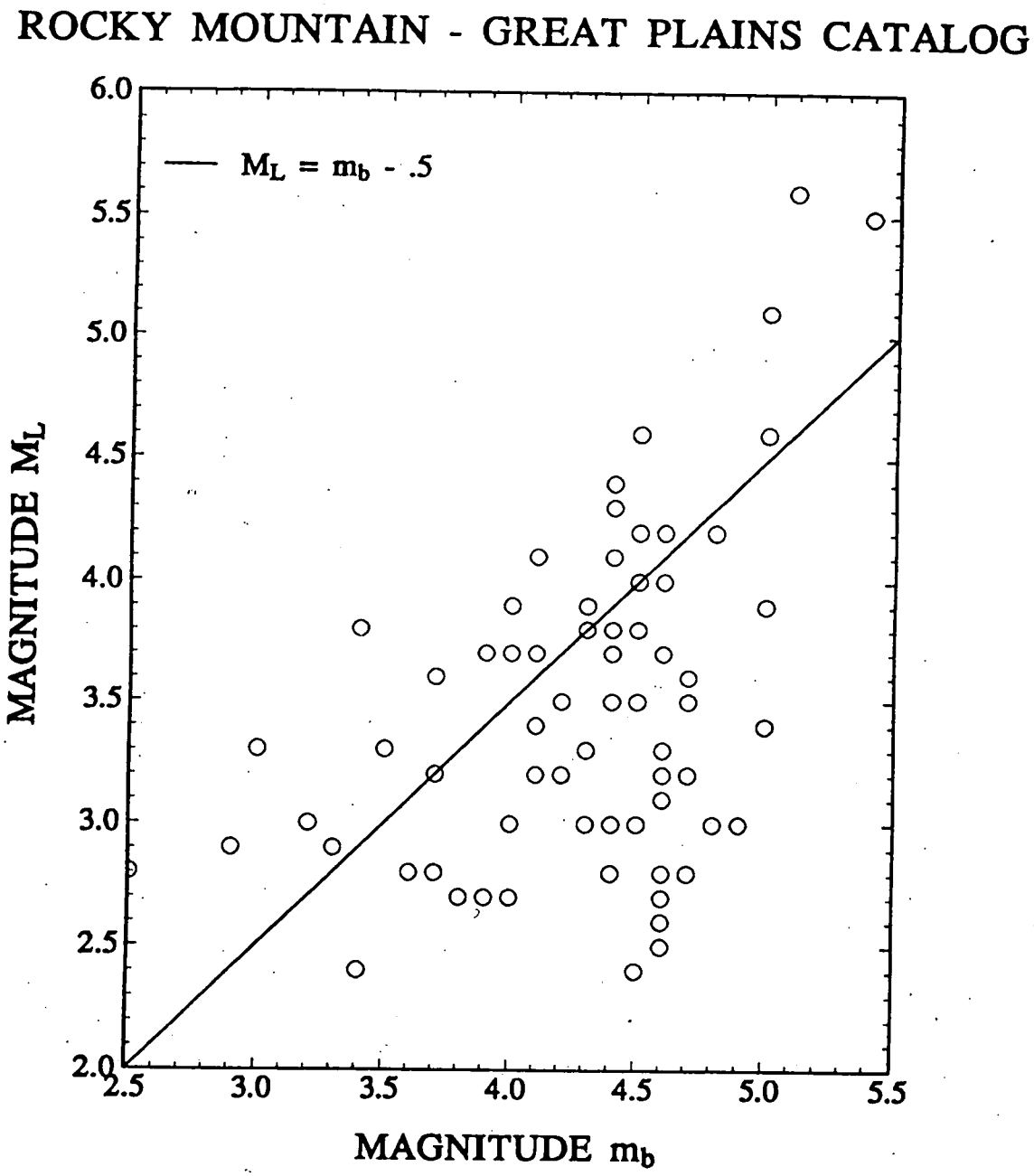

Figure D-5: M_L - m_b data and equations.

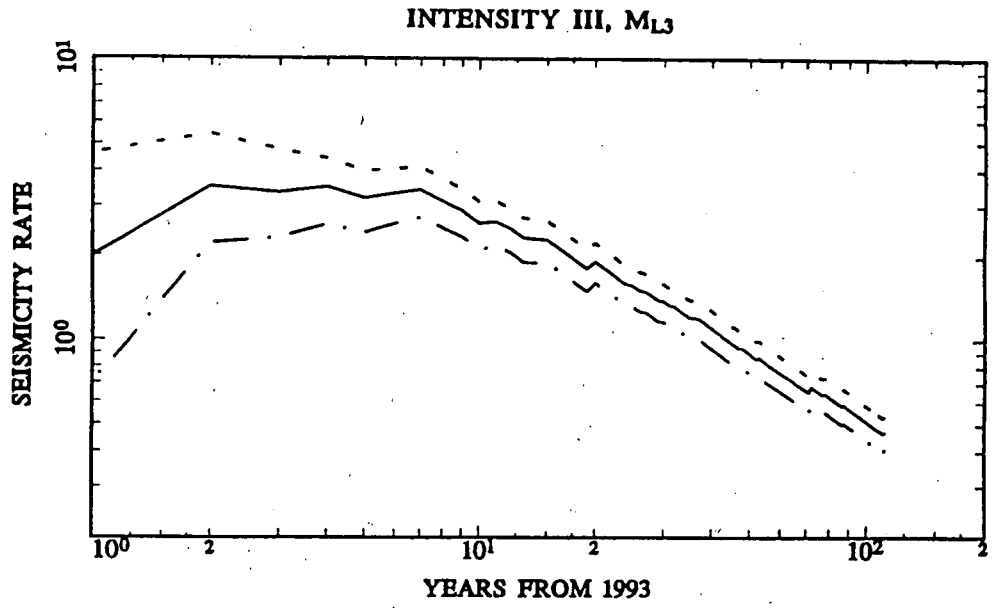

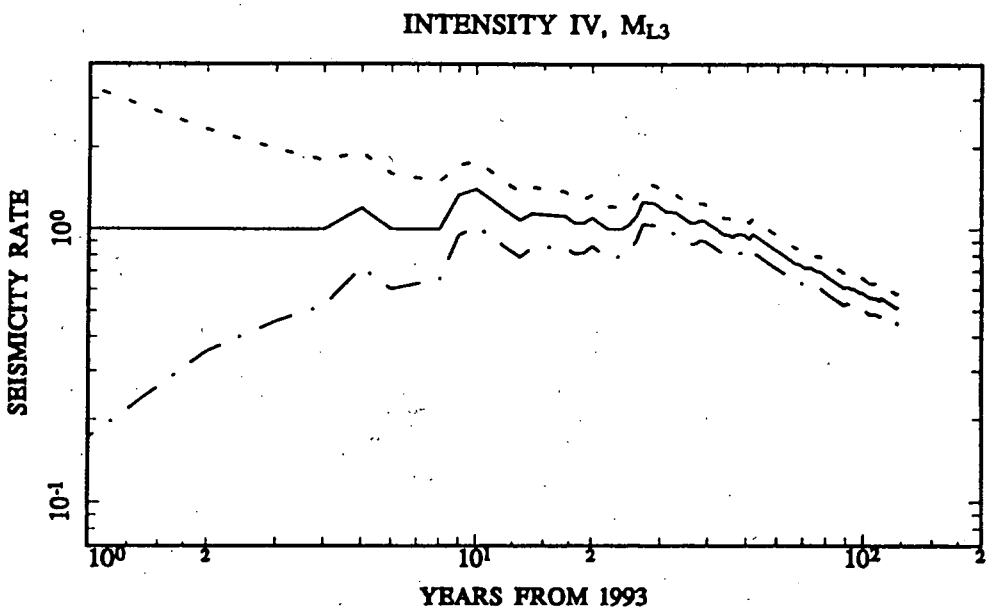

Figure D-6: (a): Stepp plot showing seismicity rate and uncertainty as a function of time interval for I_o = III.

(b): Stepp plot showing seismicity rate and uncertainty as a function of time interval for I_o = IV.

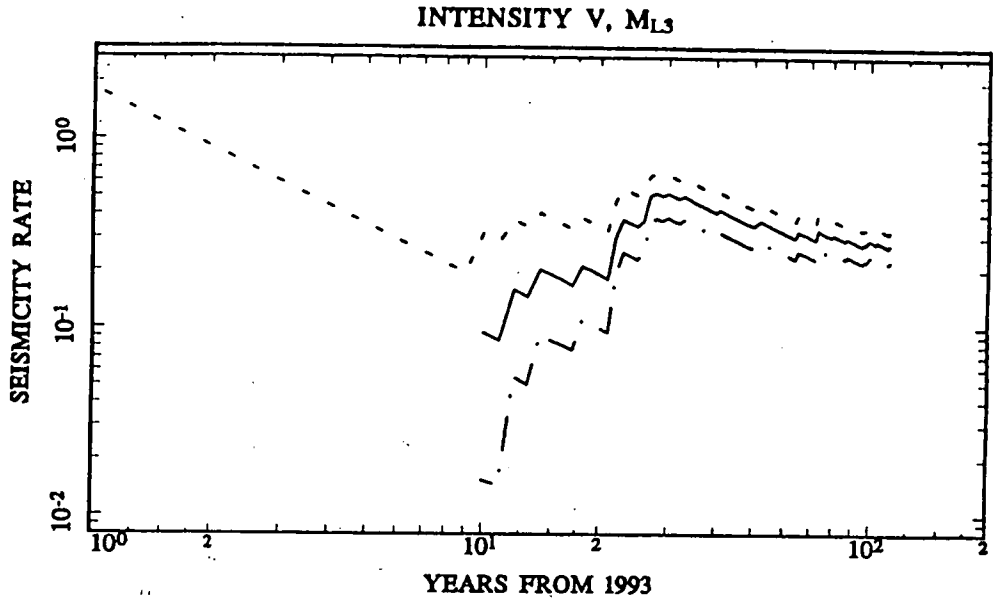

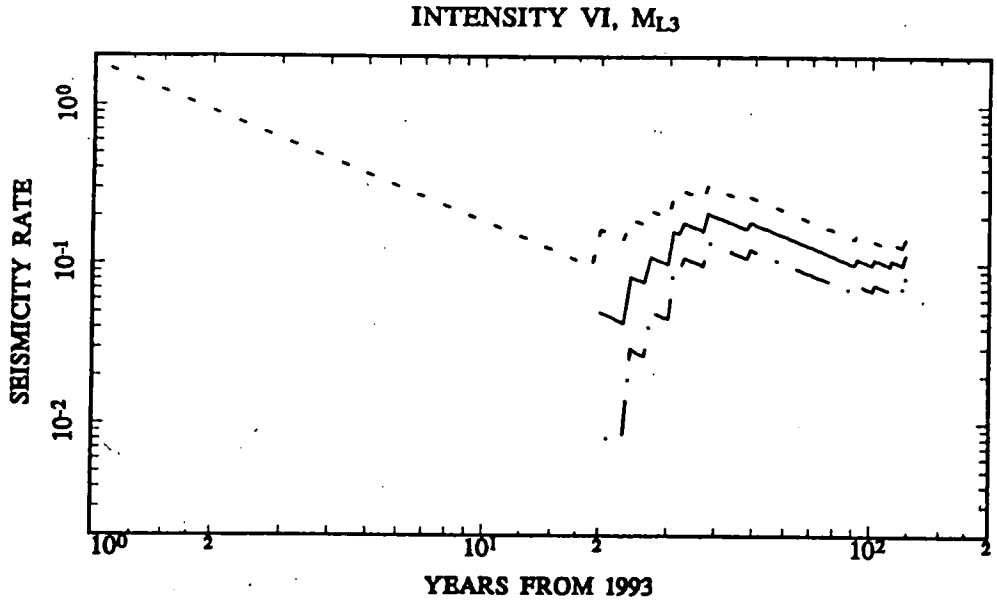

Figure D-6: (c): Stepp plot showing seismicity rate and uncertainty as a function of time interval for I_o = V.

(d): Stepp plot showing seismicity rate and uncertainty as a function of time interval for I_o = VI.

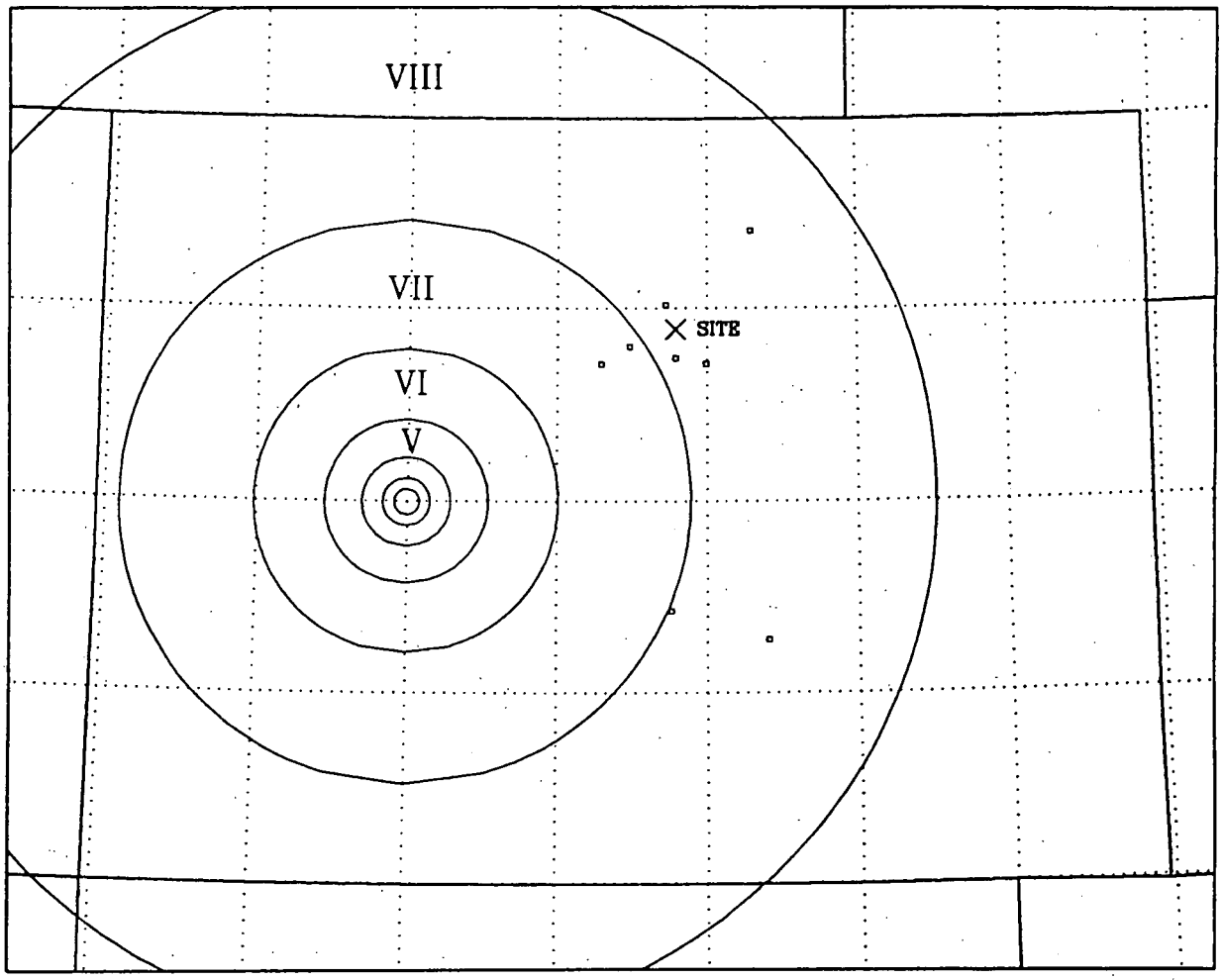

COLORADO NEWSPAPERS 1870

Figure D-7: Locations of Colorado newspapers in 1870 and felt areas for hypothetical earthquakes with I_o = II to VIII at the same location.

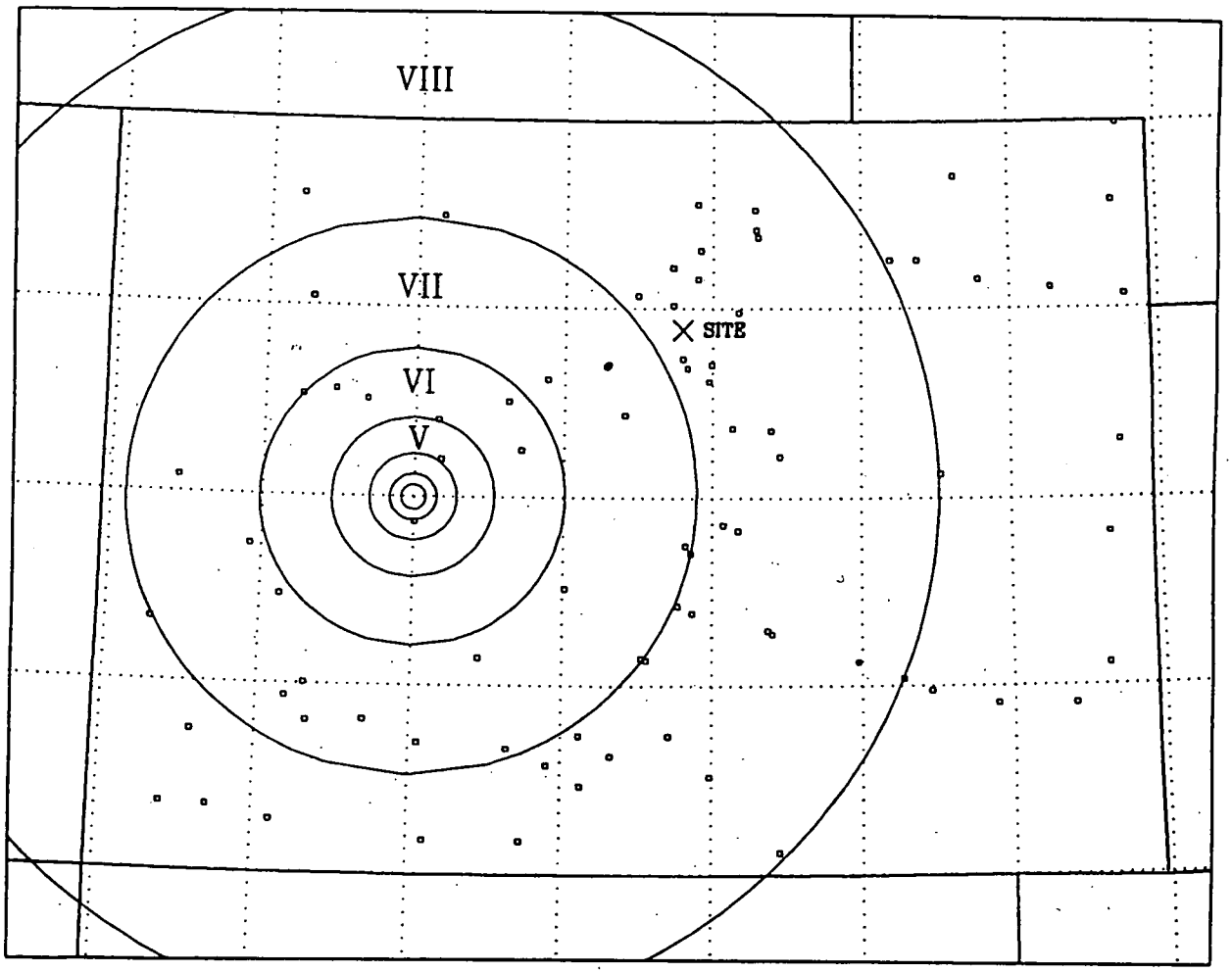

COLORADO NEWSPAPERS 1900

Figure D-8: Locations of Colorado newspapers in 1900 and felt areas for hypothetical earthquakes with I_o = II to VIII at the same location.

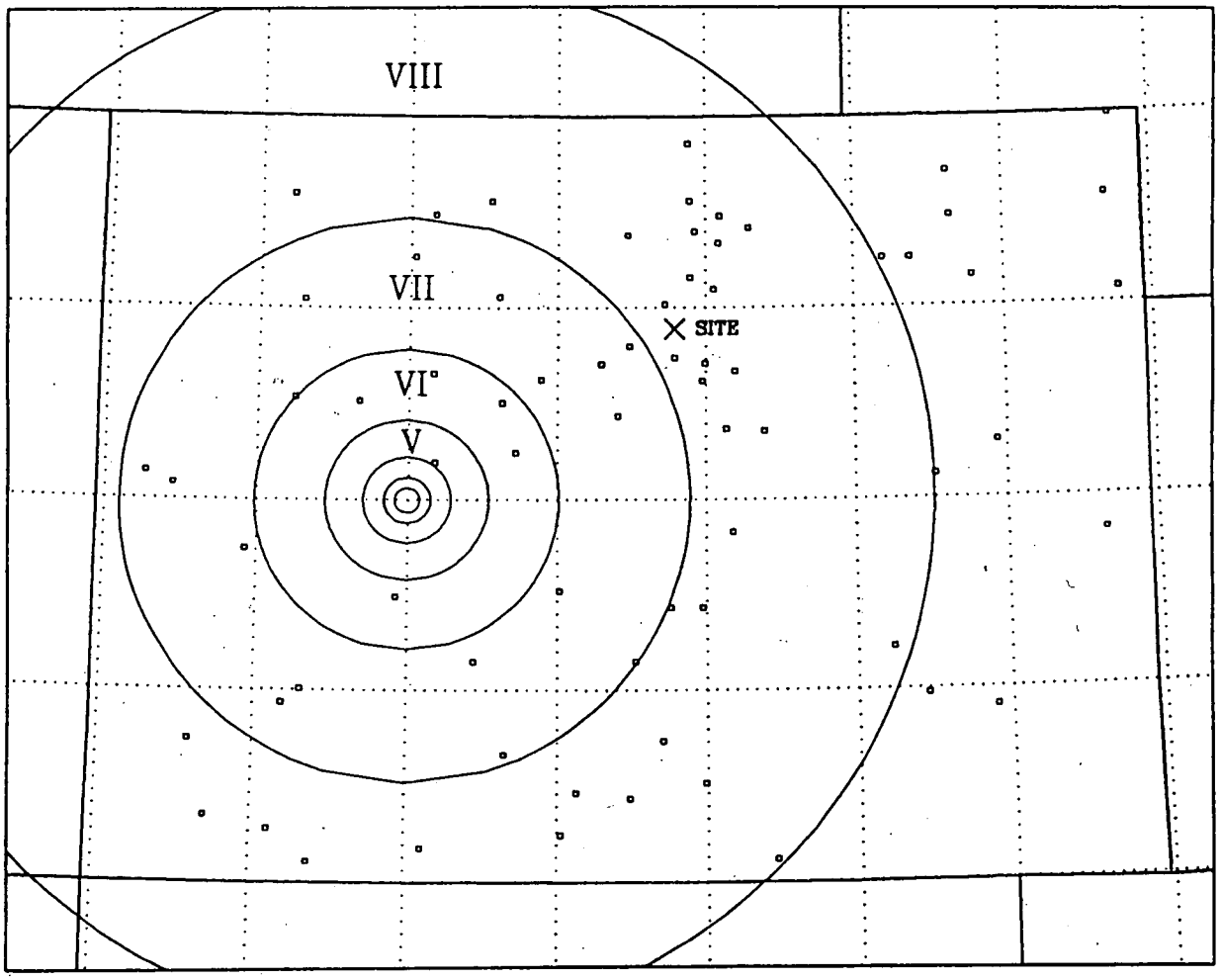

COLORADO NEWSPAPERS 1940

Figure D-9: Locations of Colorado newspapers in 1940 and felt areas for hypothetical earthquakes with I_o = II to VIII at the same location.

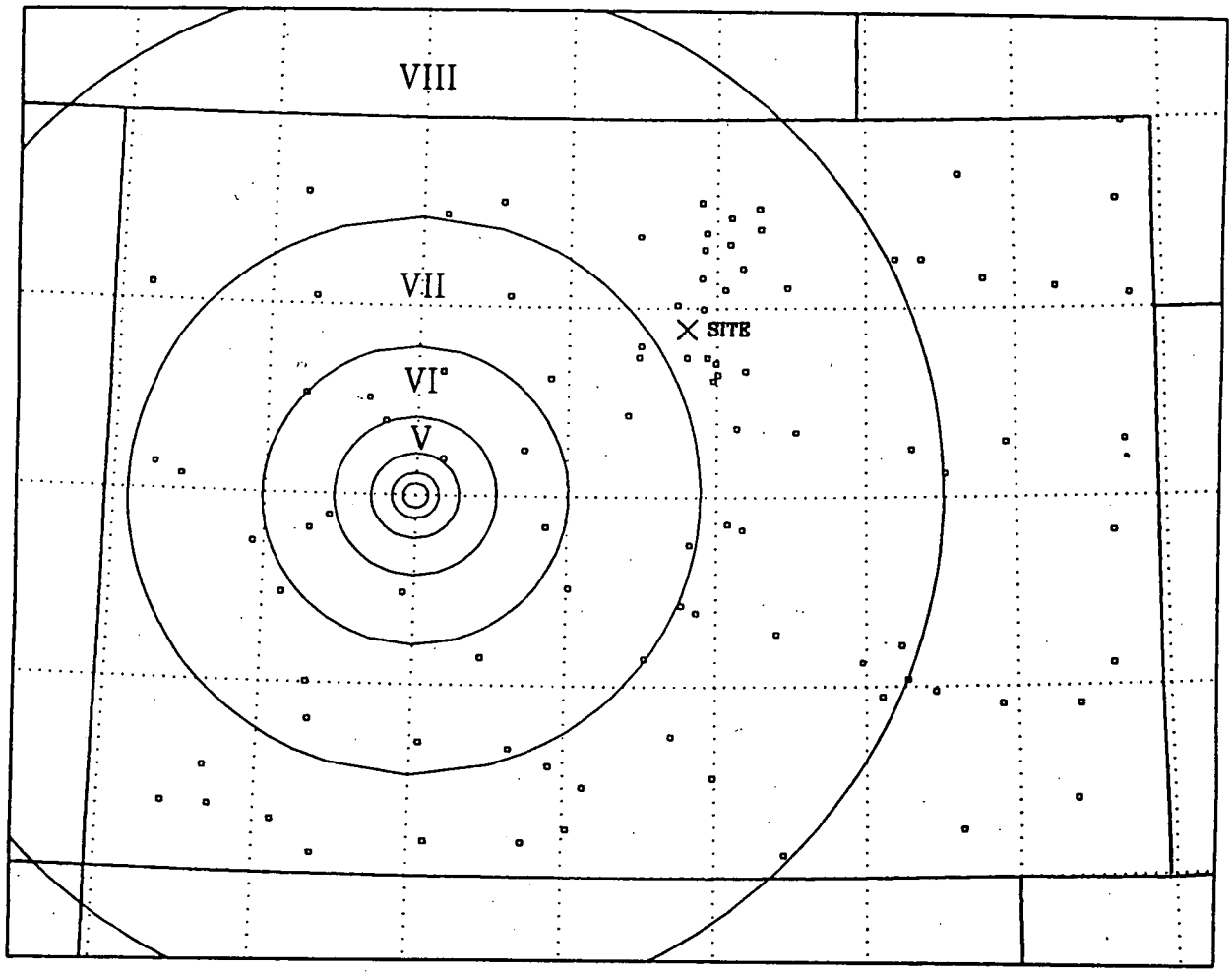

COLORADO NEWSPAPERS 1960

Figure D-10: Locations of Colorado newspapers in 1960 and felt areas for hypothetical earthquakes with I_o = II to VIII at the same location.

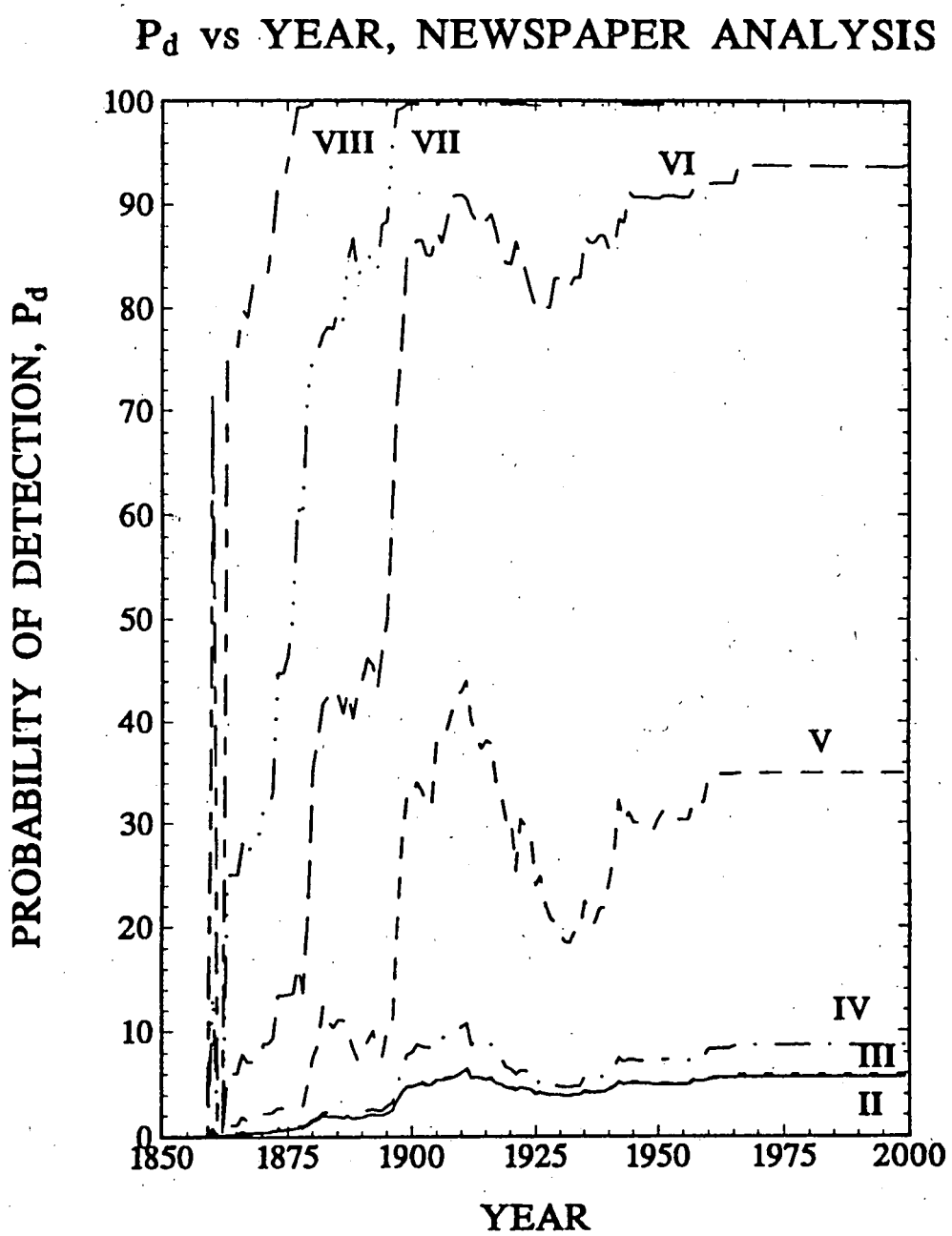

Figure D-11: P_d as a function of time, for the entire Colorado region, based on newspaper analysis.

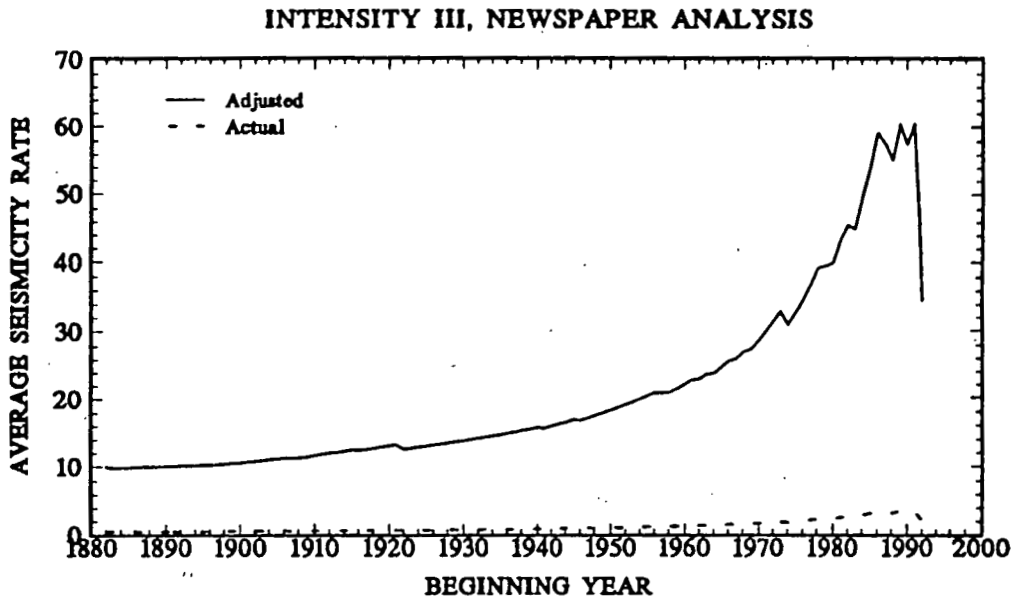

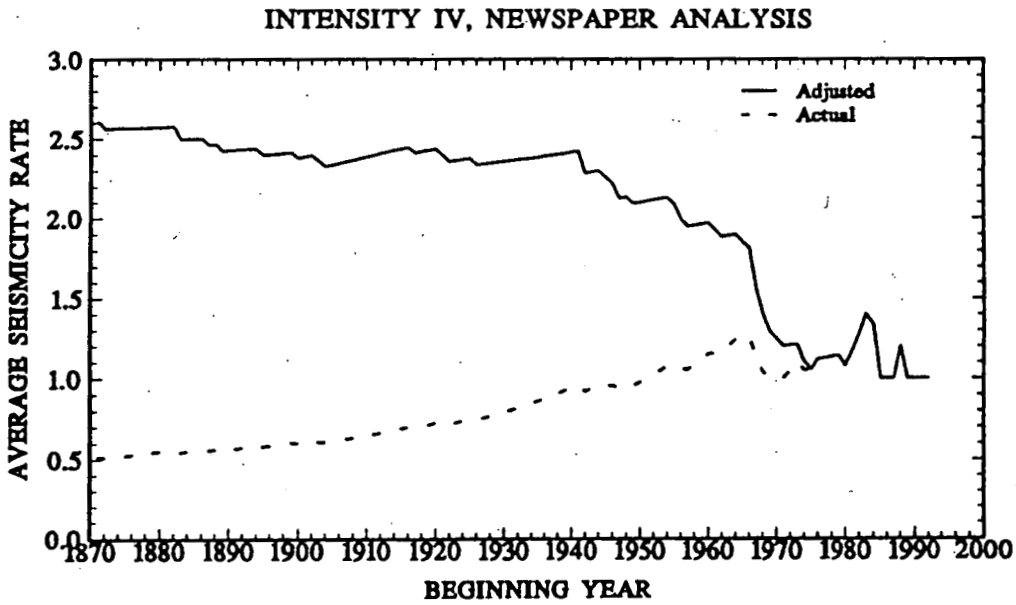

Figure D-12: (a): Actual and adjusted average seismicity rate from "Beginning Year" to 1993, I_o = III, newspaper analysis.

(b): Actual and adjusted average seismicity rate from "Beginning Year" to 1993, I_o = IV, newspaper analysis.

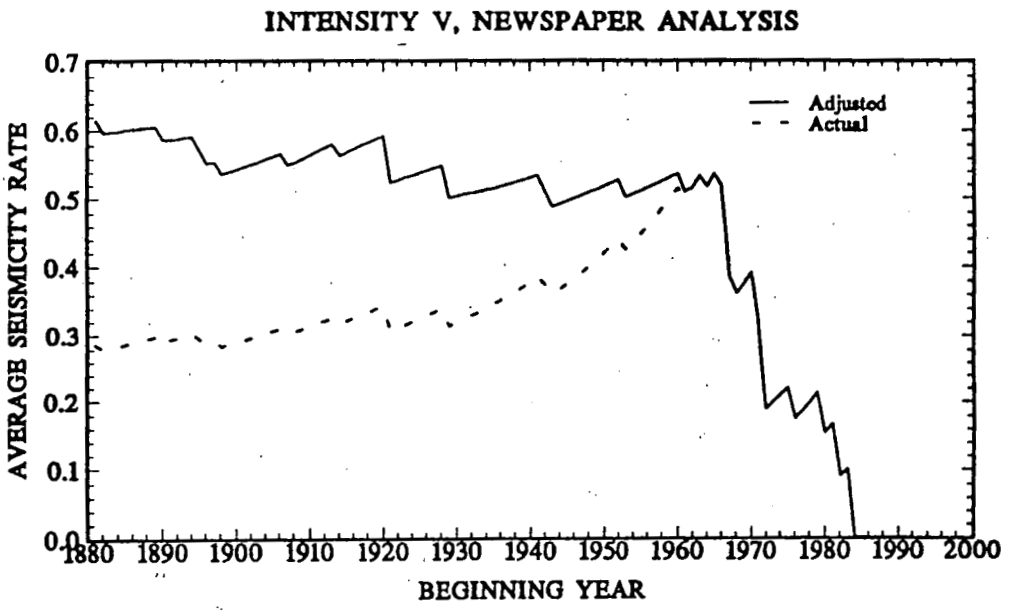

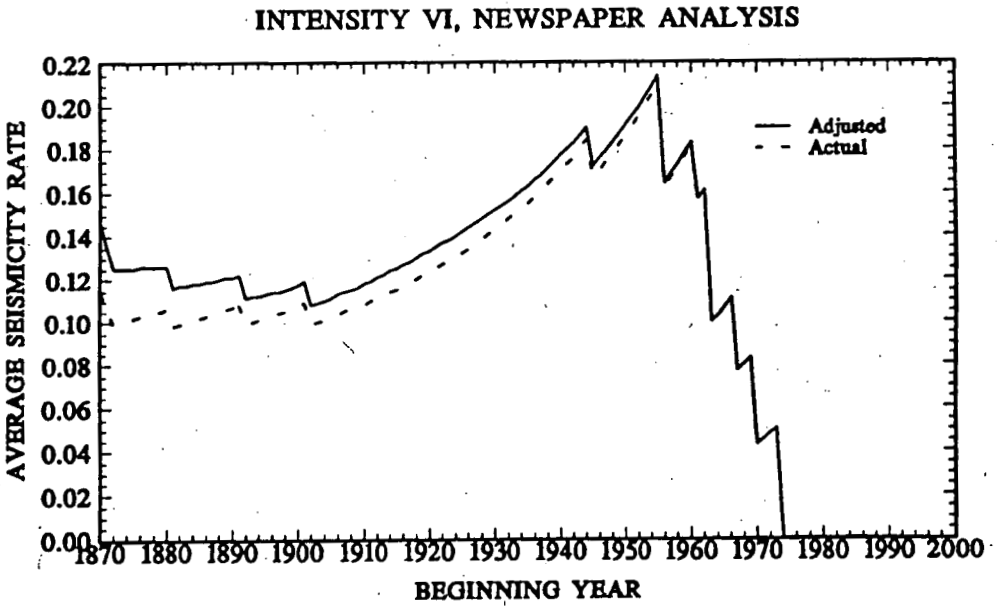

Figure D-12: (c): Actual and adjusted average seismicity rate from "Beginning Year" to 1993, I_o = V, newspaper analysis.

(d): Actual and adjusted average seismicity rate from "Beginning Year" to 1993, I_o = VI, newspaper analysis.

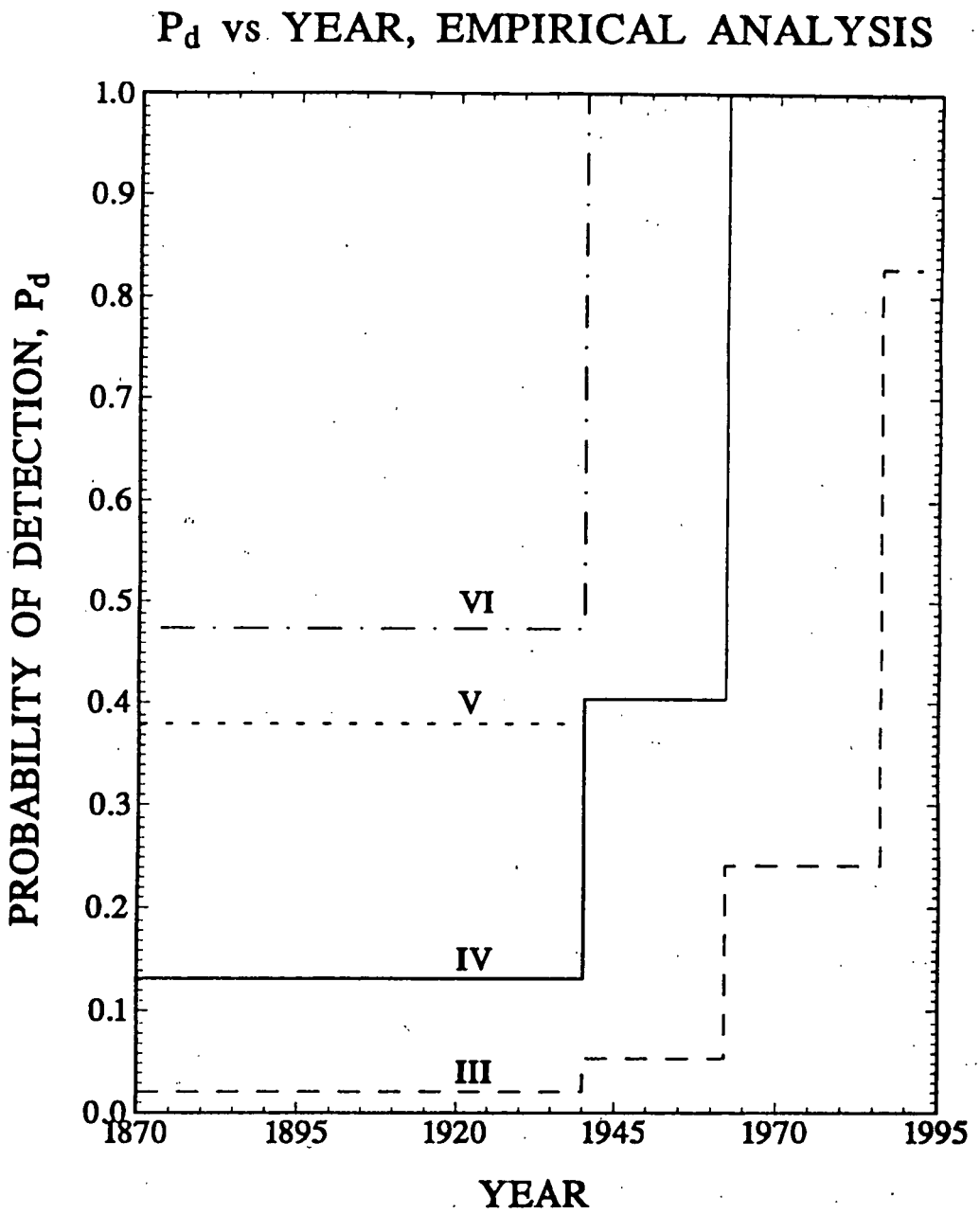

Figure D-13: P_d as a function of time, based on empirical analysis.

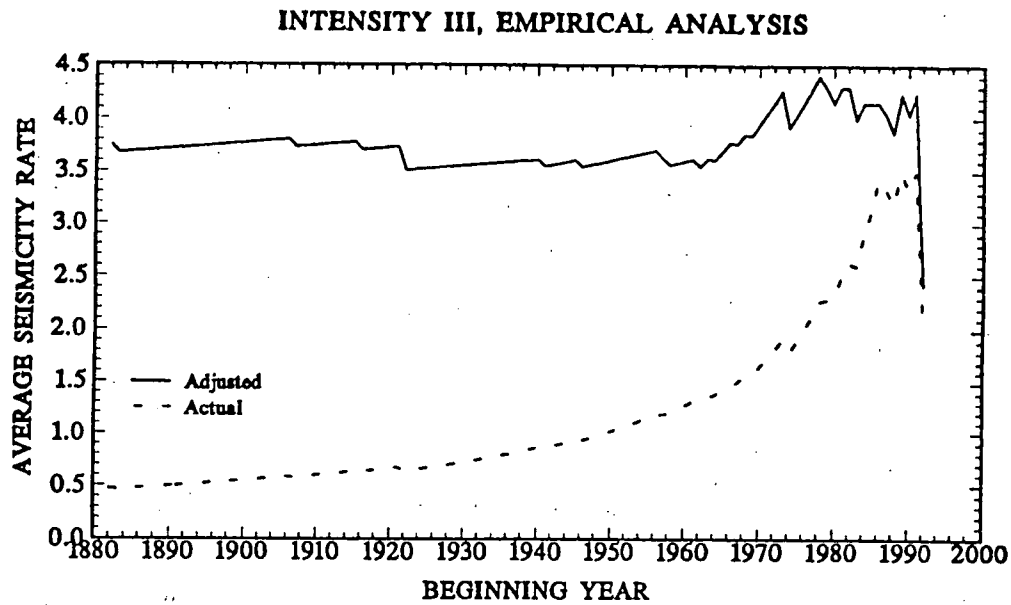

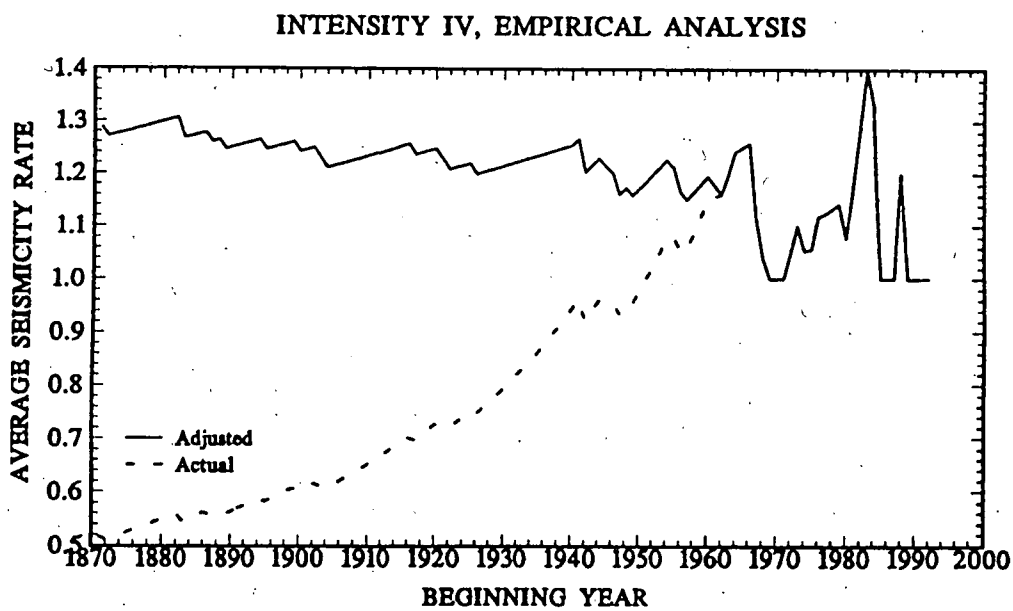

Figure D-14: (a): Actual and adjusted average seismicity rate from "Beginning Year" to 1993, I_o = III, empirical analysis.

(b): Actual and adjusted average seismicity rate from "Beginning Year" to 1993, I_o = IV, empirical analysis.

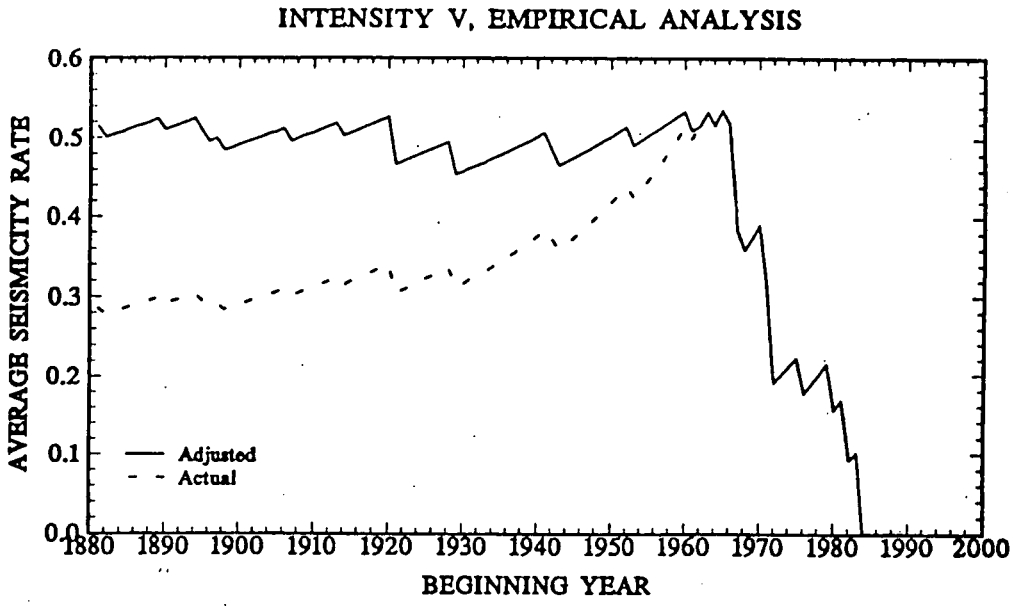

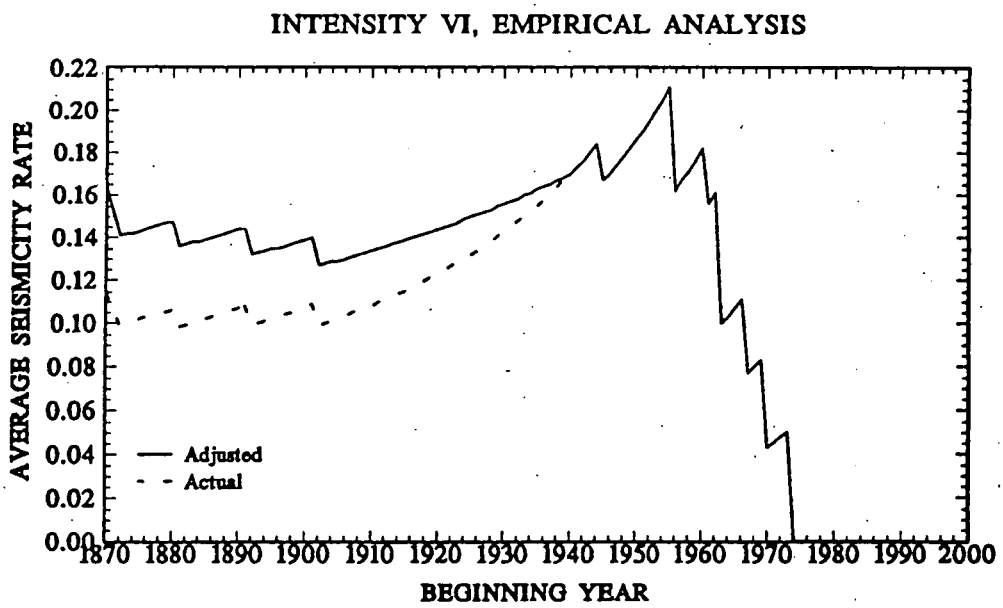

Figure D-14: (c): Actual and adjusted average seismicity rate from "Beginning Year" to 1993, I_o = V, empirical analysis.

(d): Actual and adjusted average seismicity rate from "Beginning Year" to 1993, I_o = VI, empirical analysis.

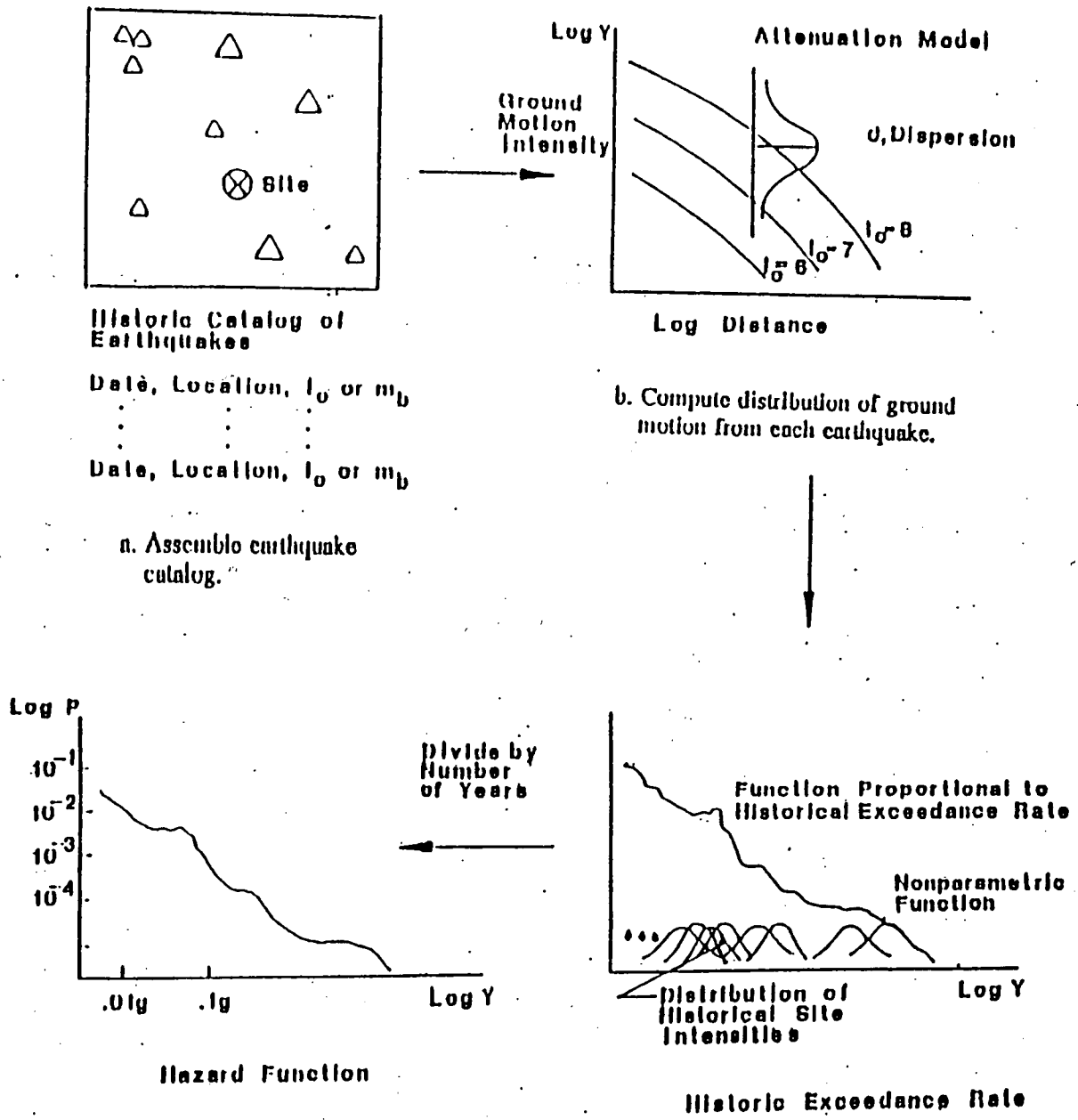

Figure D-15: Steps involved in historical seismic hazard method (from Veneziano et al., 1984).

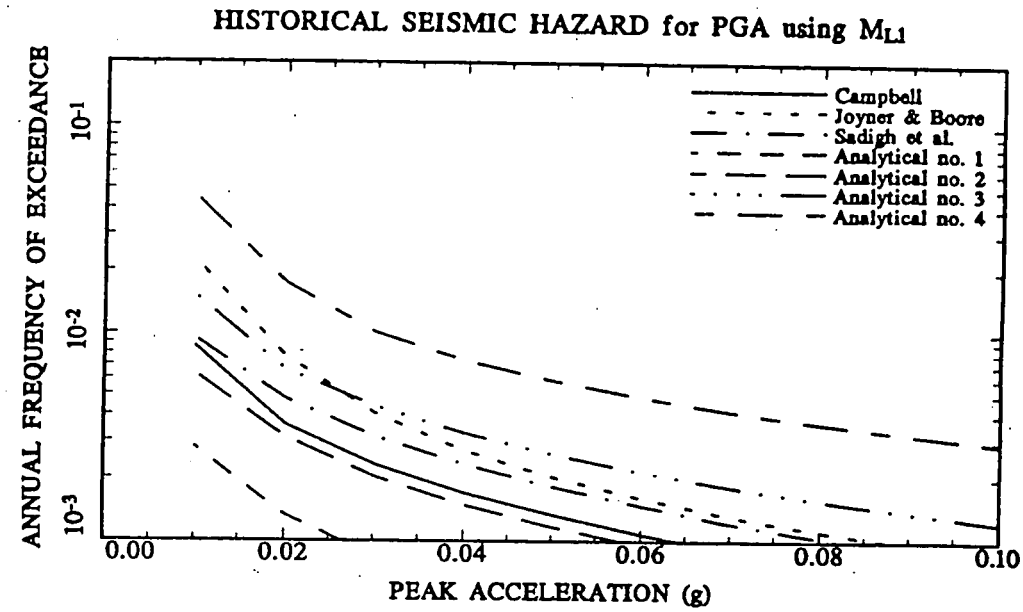

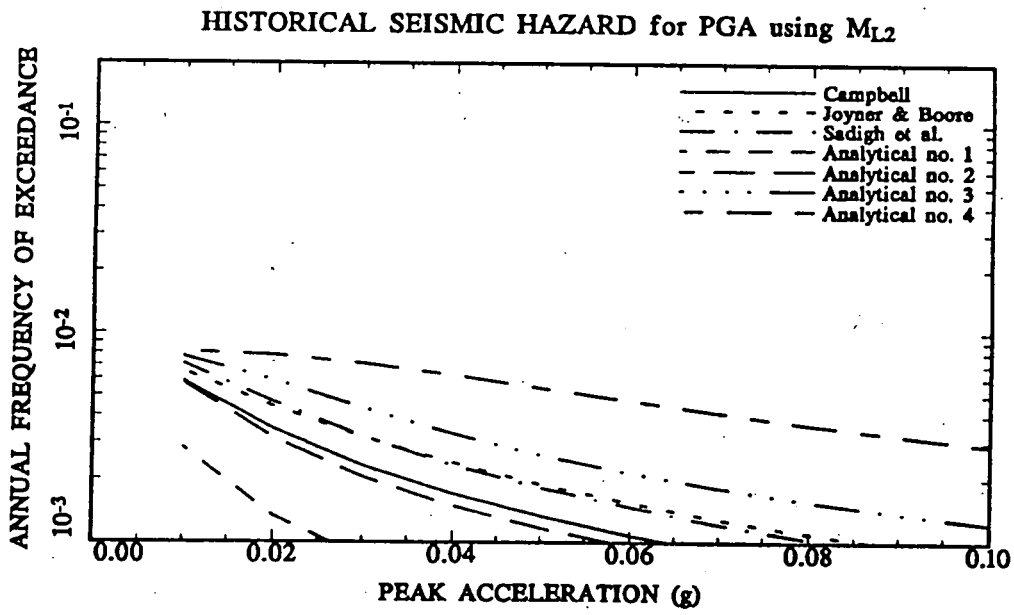

Figure D-16: (a): Historical seismic hazard, M_{L1}, for PGA.
(b): Historical seismic hazard, M_{L2}, for PGA.

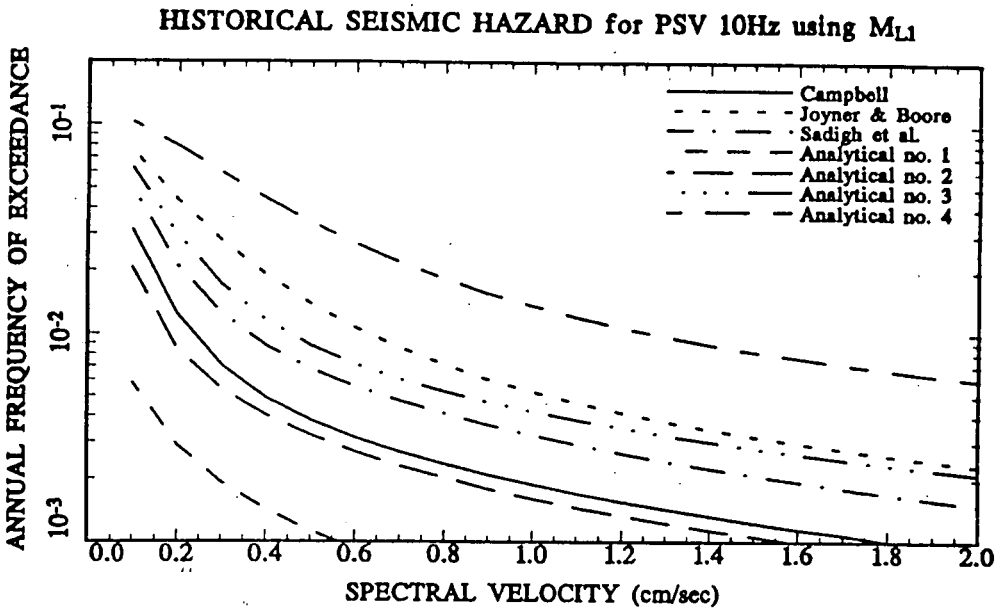

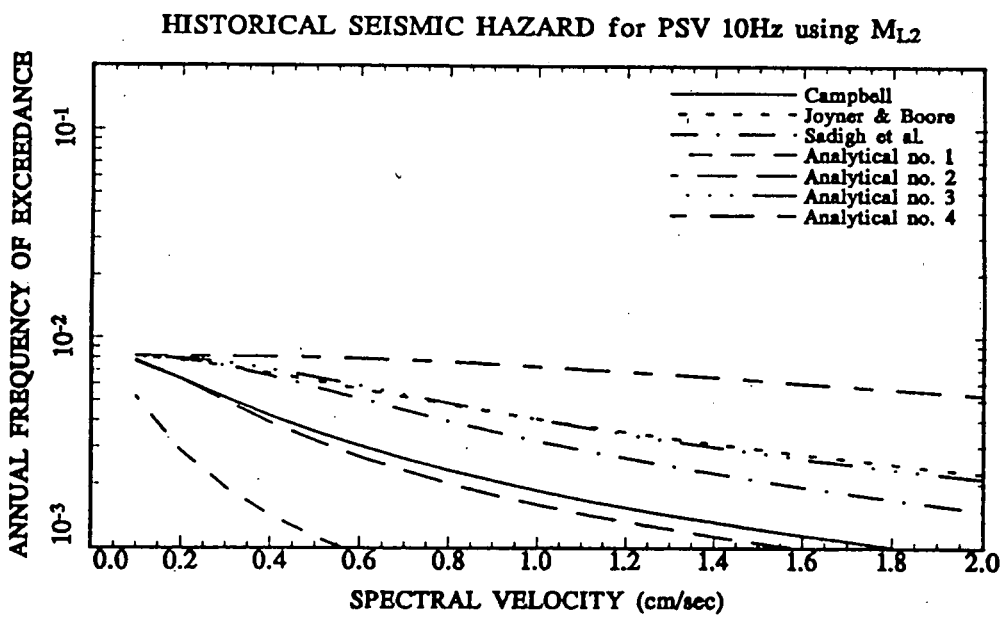

Figure D-17: (a): Historical seismic hazard, M_{L1}, for 10 Hz.
(b): Historical seismic hazard, M_{L2}, for 10 Hz.

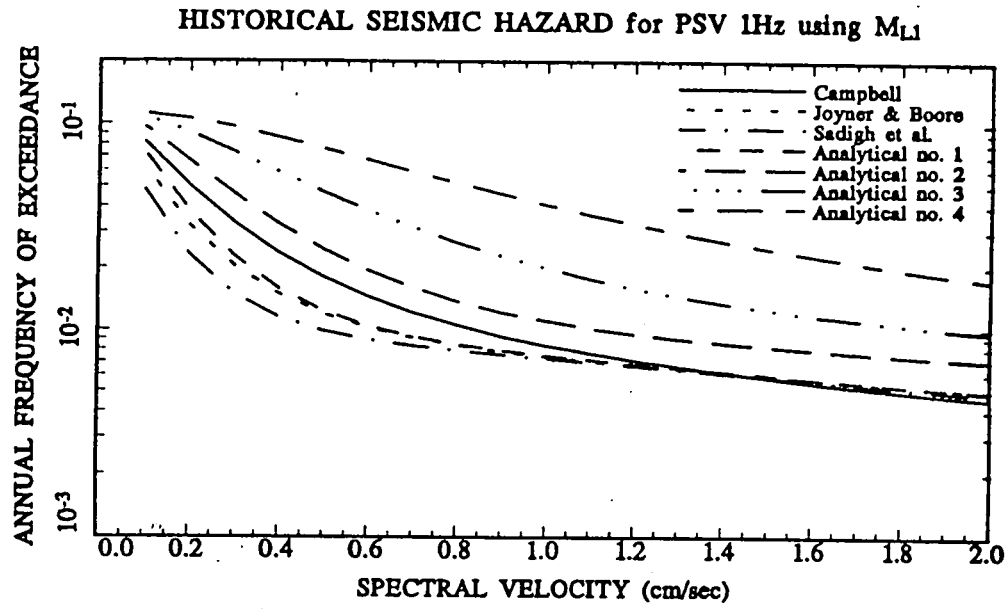

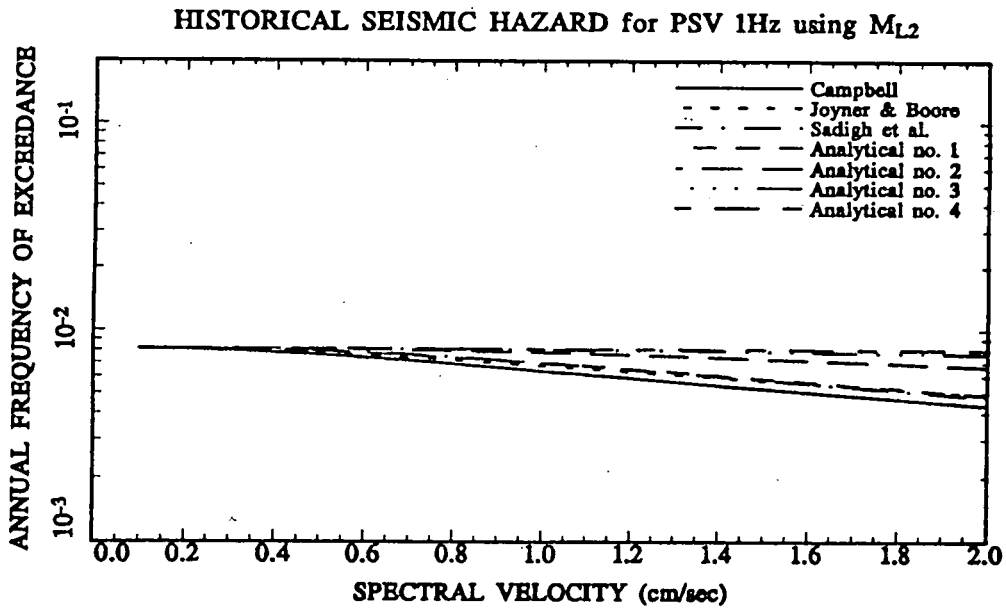

Figure D-18: (a): Historical seismic hazard, M_{L1}, for 1 Hz.
(b): Historical seismic hazard, M_{L2}, for 1 Hz.

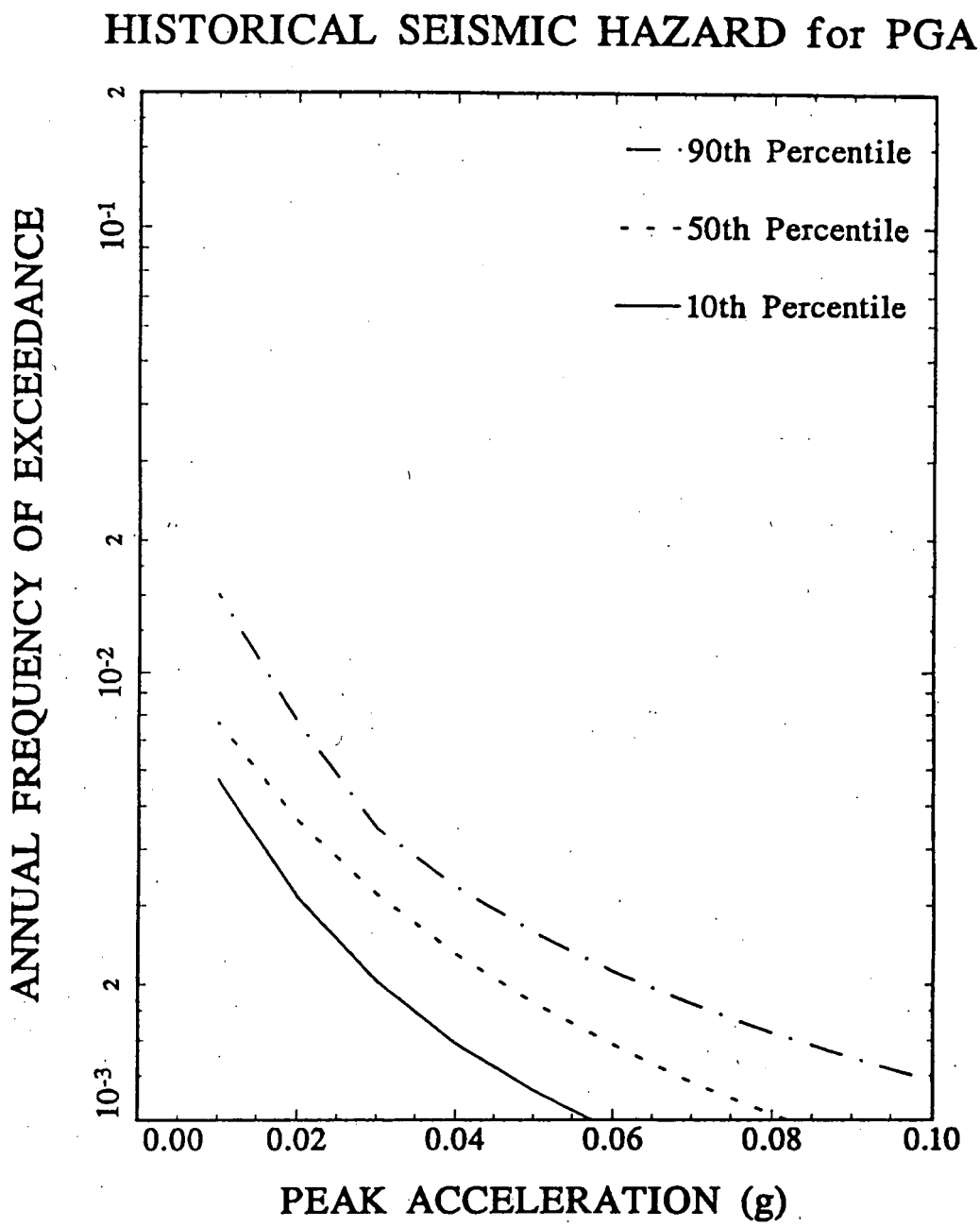

Figure D-19: Fractiles of historical seismic hazard for PGA.

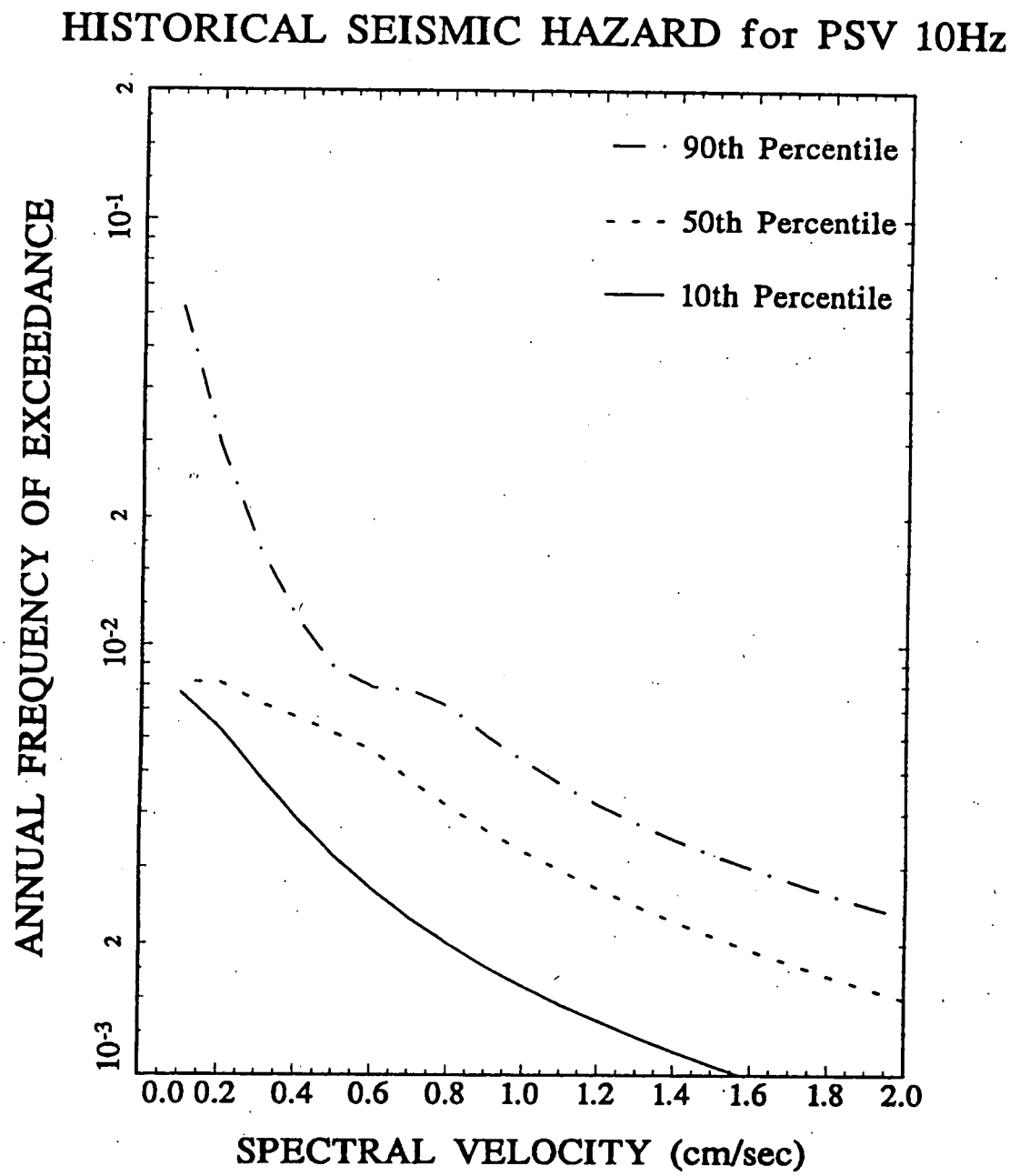

Figure D-20: Fractiles of historical seismic hazard for 10 Hz.

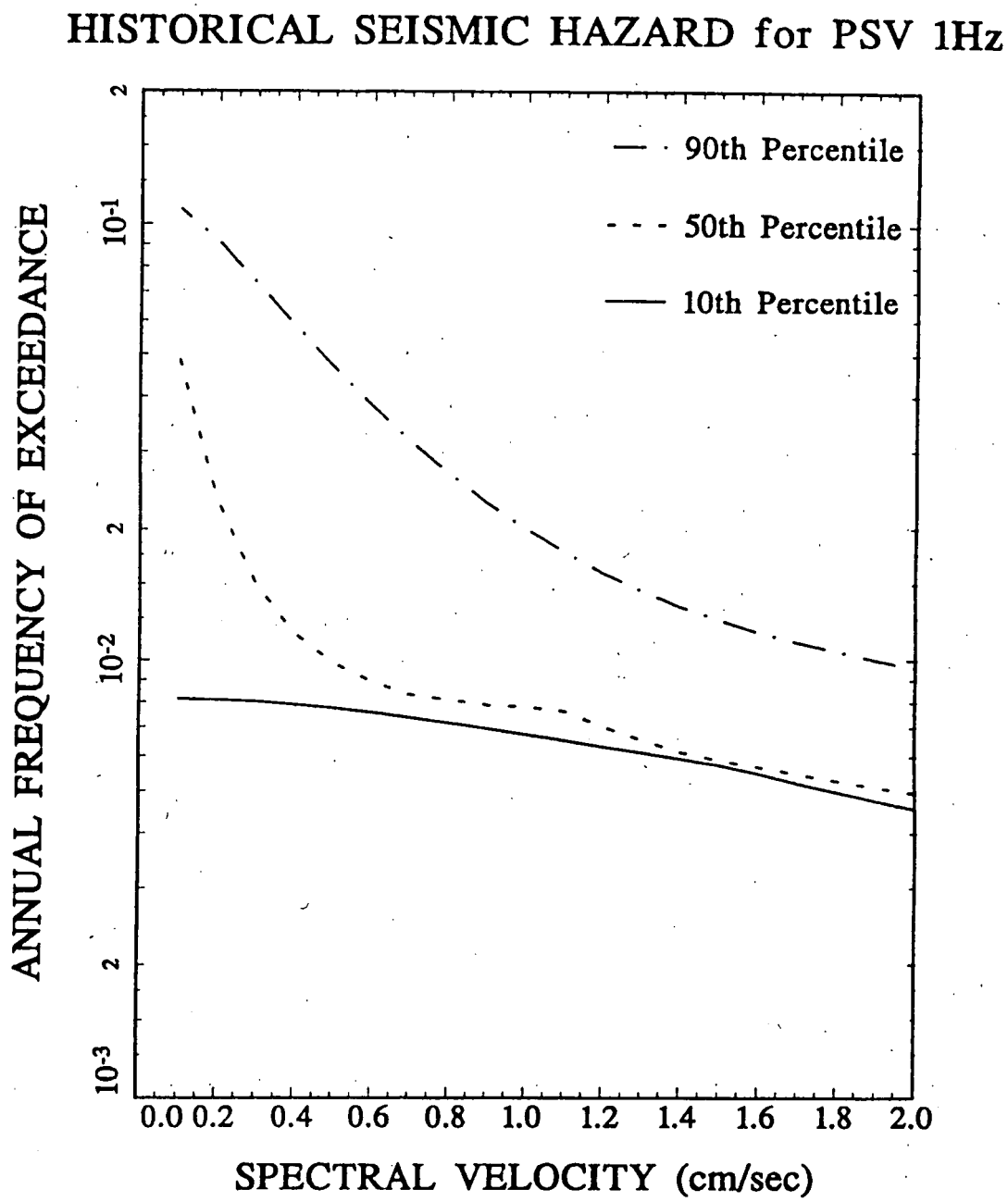

Figure D-21: Fractiles of historical seismic hazard for 1 Hz.

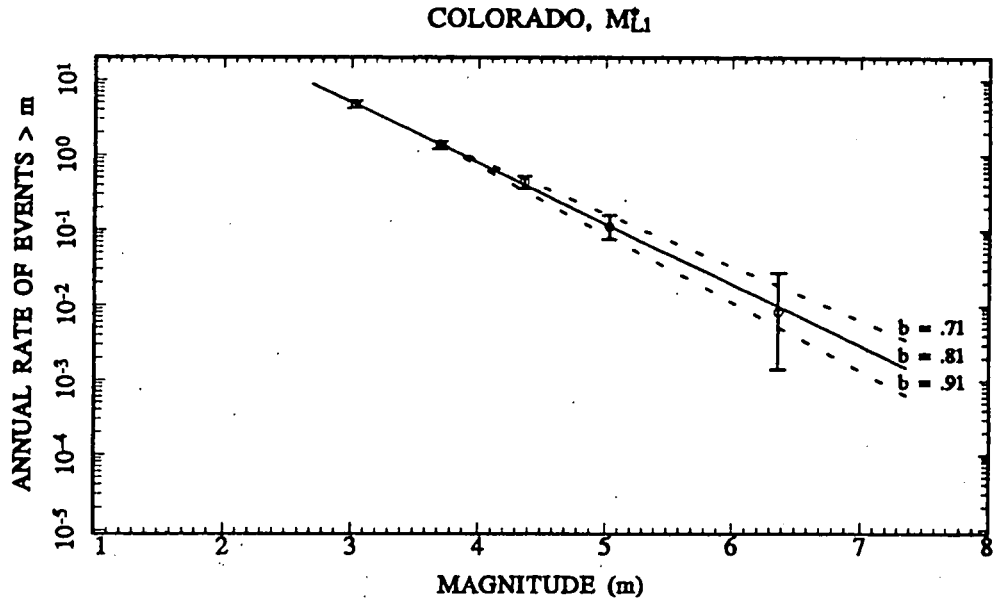

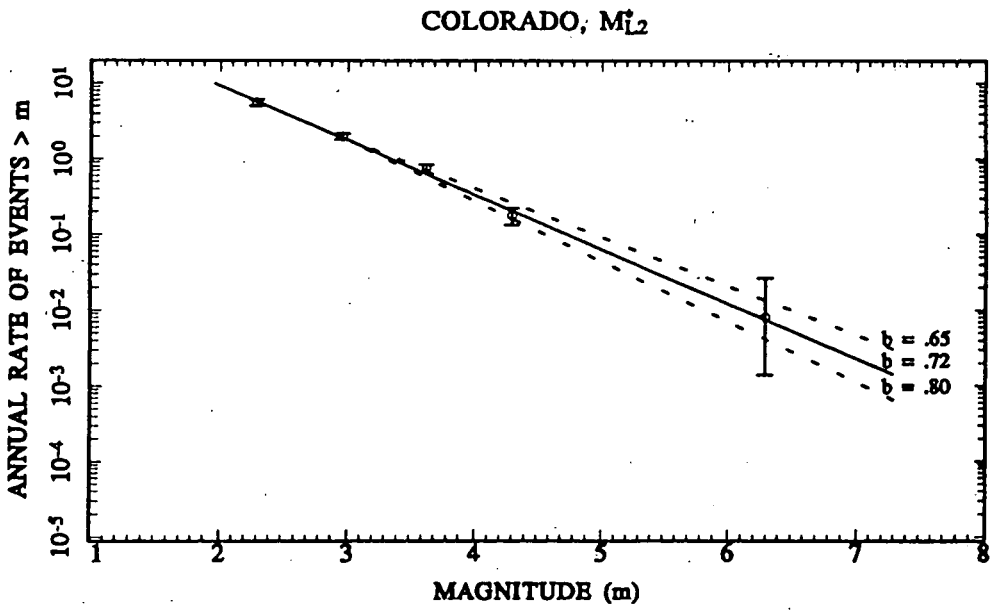

Figure D-22: (a): Historical seismicity for Colorado using M^*_{L1}.
(b): Historical seismicity for Colorado using M^*_{L2}.

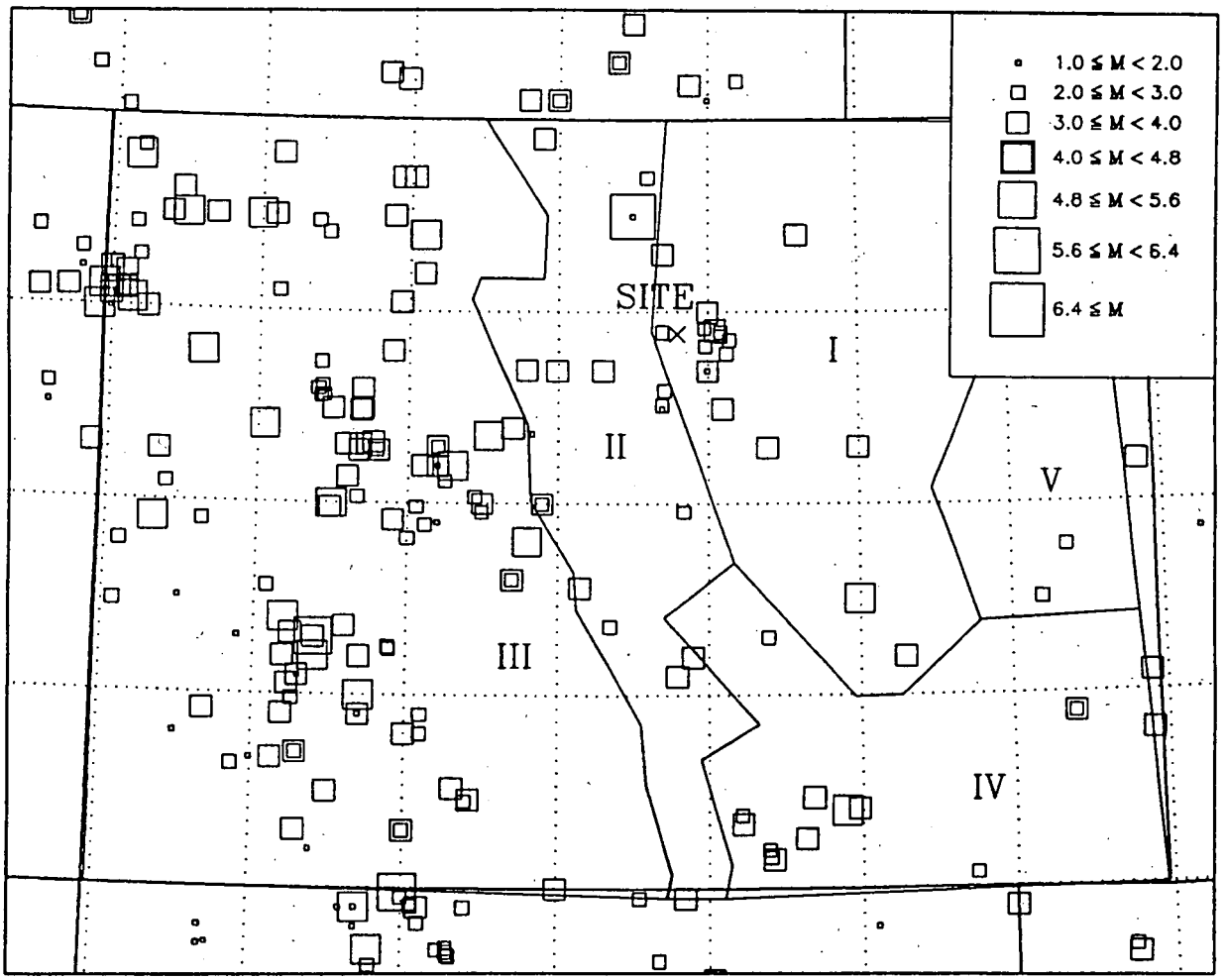

GREATER COLORADO SEISMICITY 1870 – MAY 1993

Figure D-23: Historical seismicity in Colorado and seismic sources.

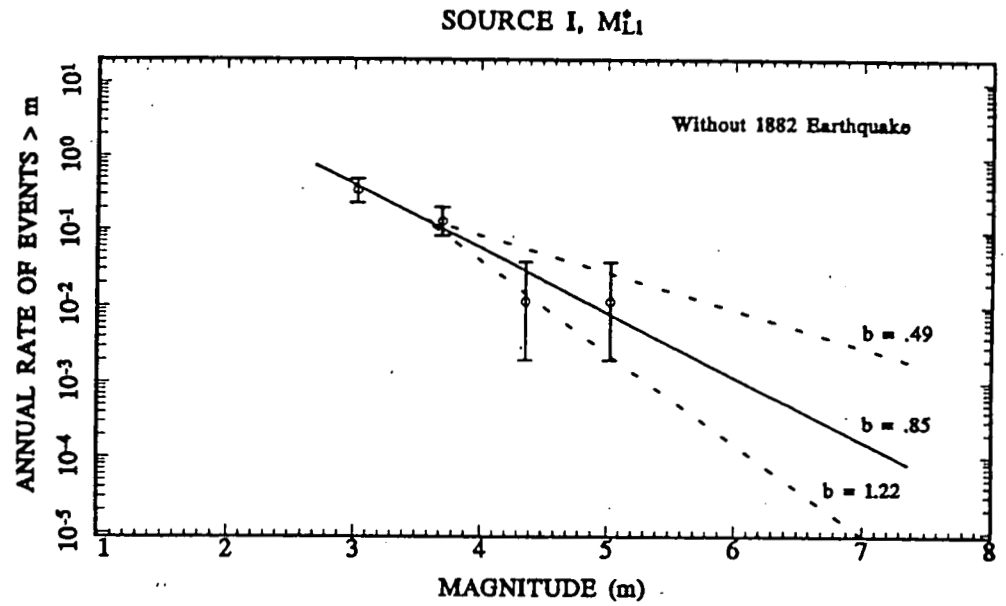

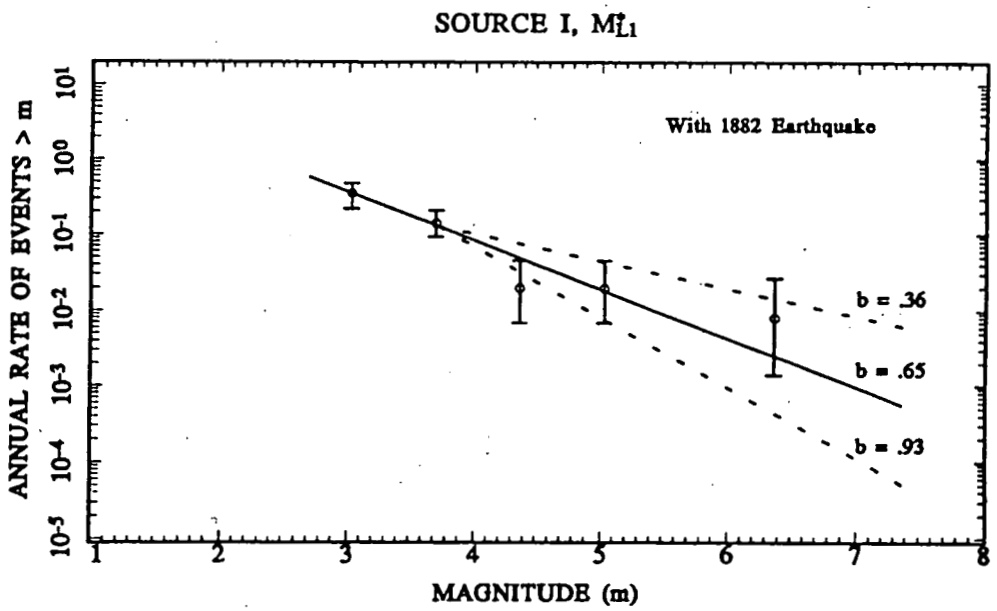

Figure D-24: (a) Historical seismicity for Source I using M^*_{L1}, without 1882 earthquake.
(b) Historical seismicity for Source I using M^*_{L1}, with 1882 earthquake.

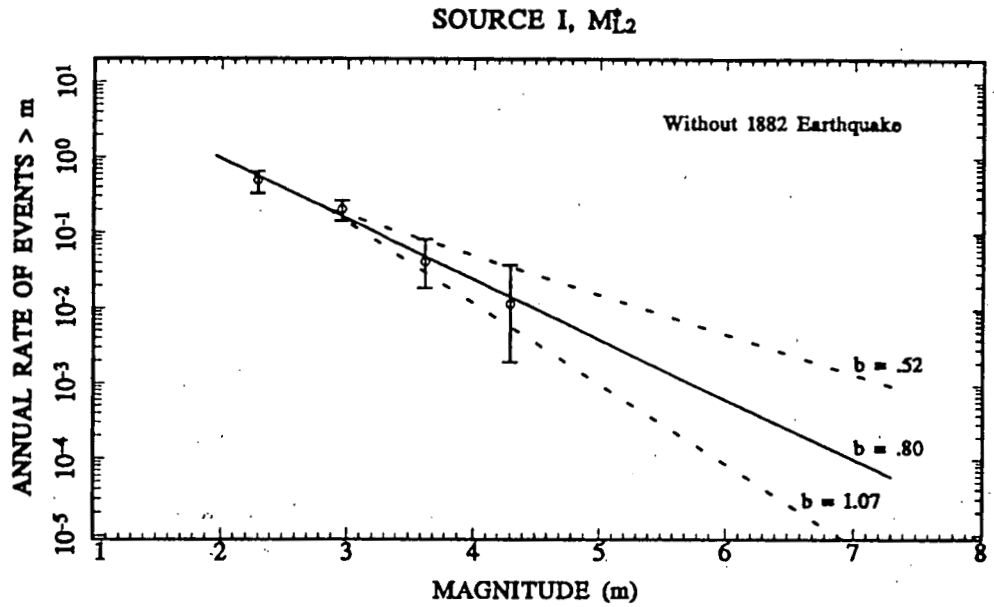

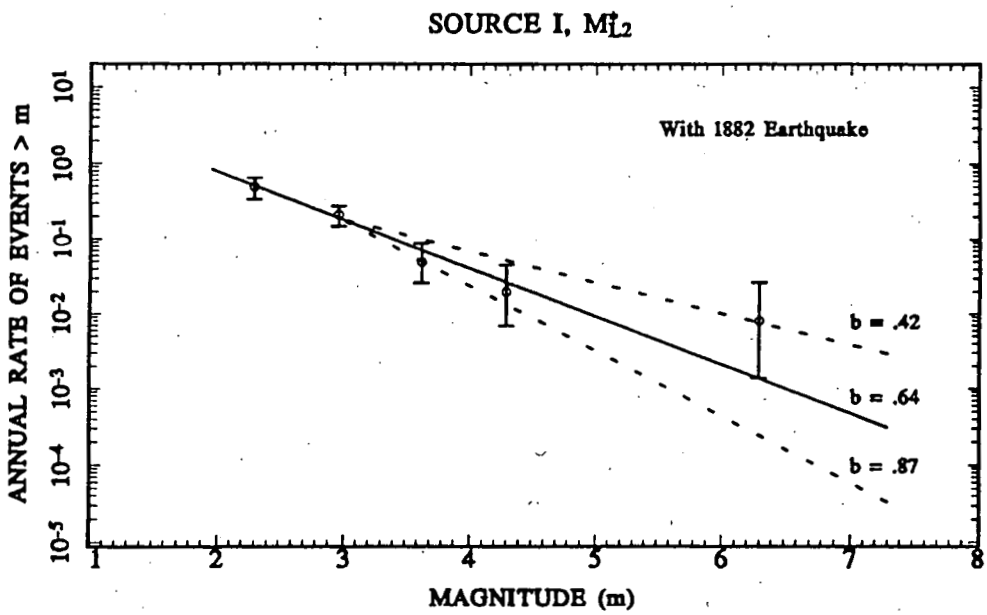

Figure D-24: (c) Historical seismicity for Source I using M^*_{L2}, without 1882 earthquake.
(d) Historical seismicity for Source I using M^*_{L2}, with 1882 earthquake.

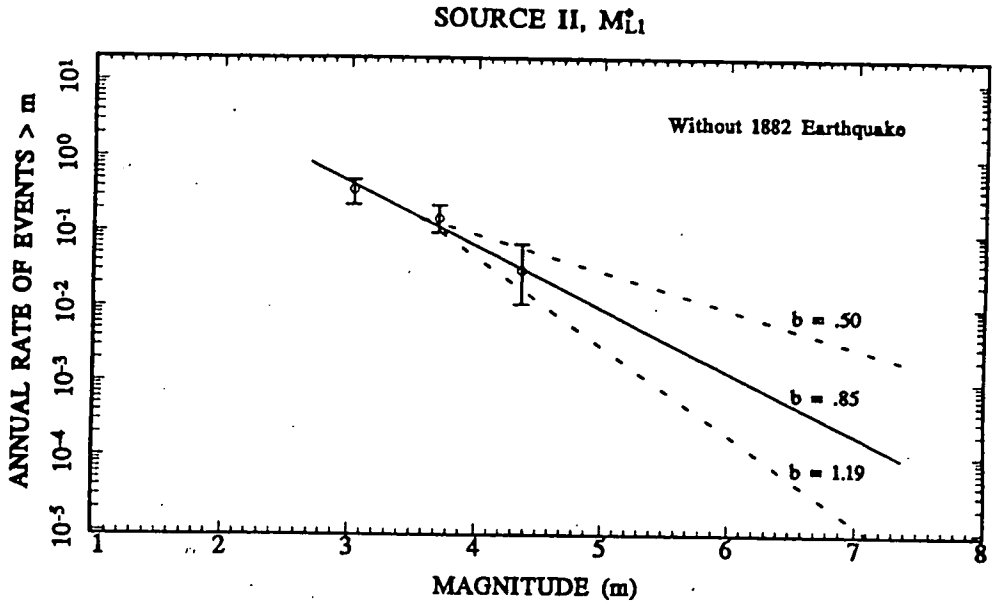

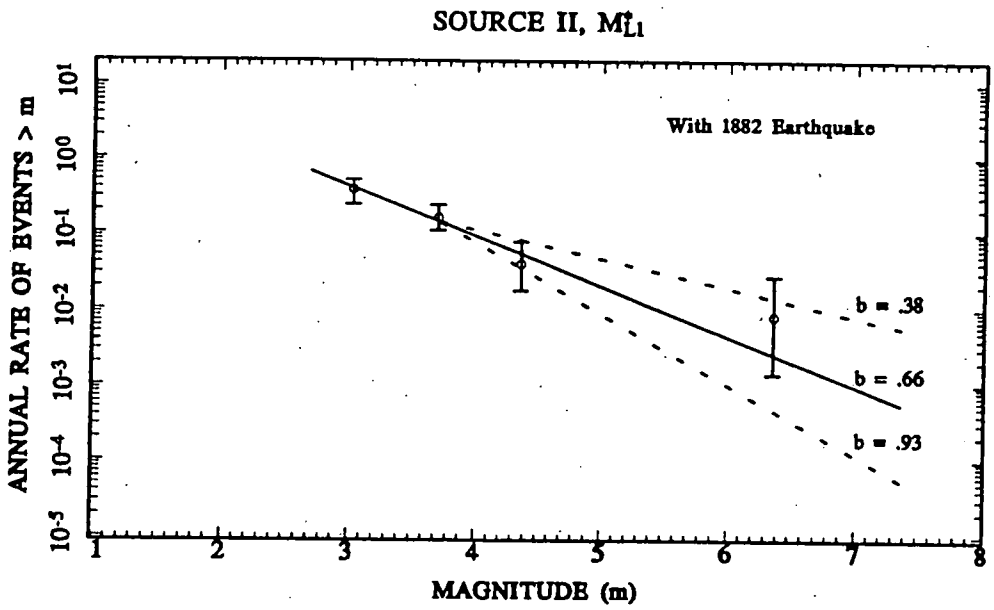

Figure D-25: (a) Historical seismicity for Source II using M^*_{L1}, without 1882 earthquake.
(b) Historical seismicity for Source II using M^*_{L1}, with 1882 earthquake.

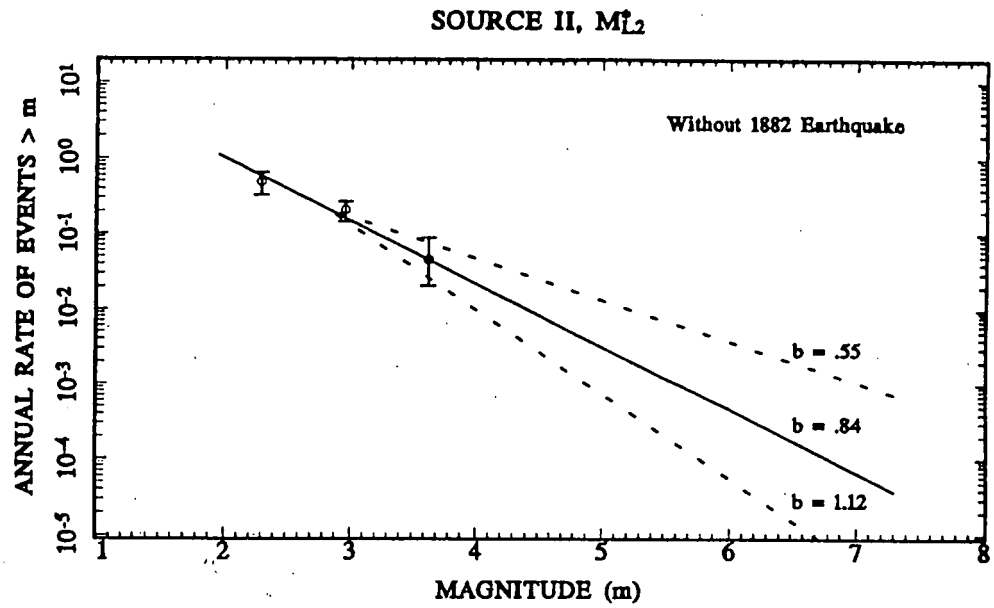

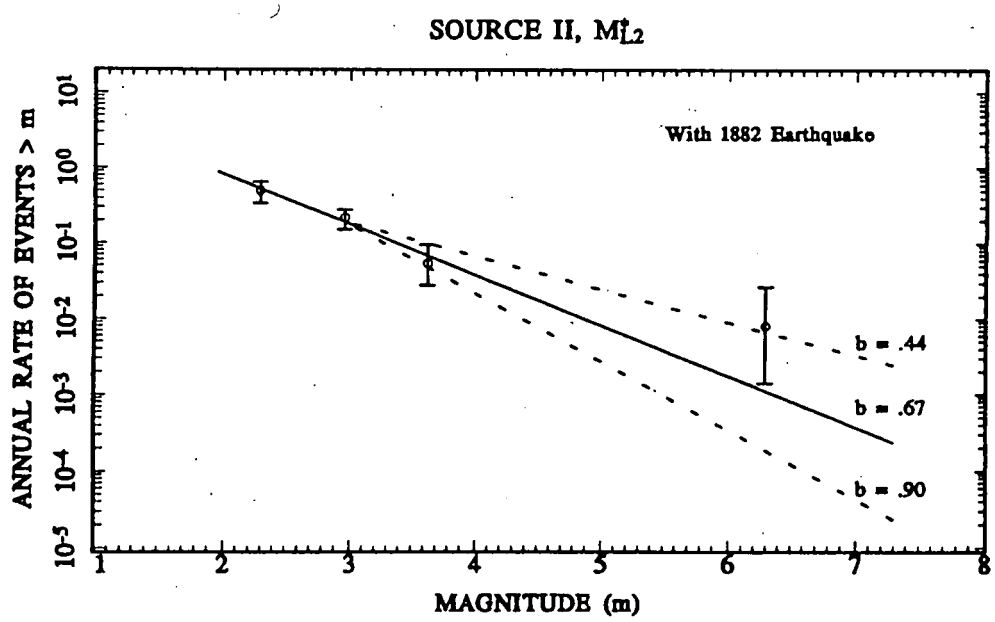

Figure D-25: (c) Historical seismicity for Source II using M^*_{L2}, without 1882 earthquake.
(d) Historical seismicity for Source II using M^*_{L2}, with 1882 earthquake.

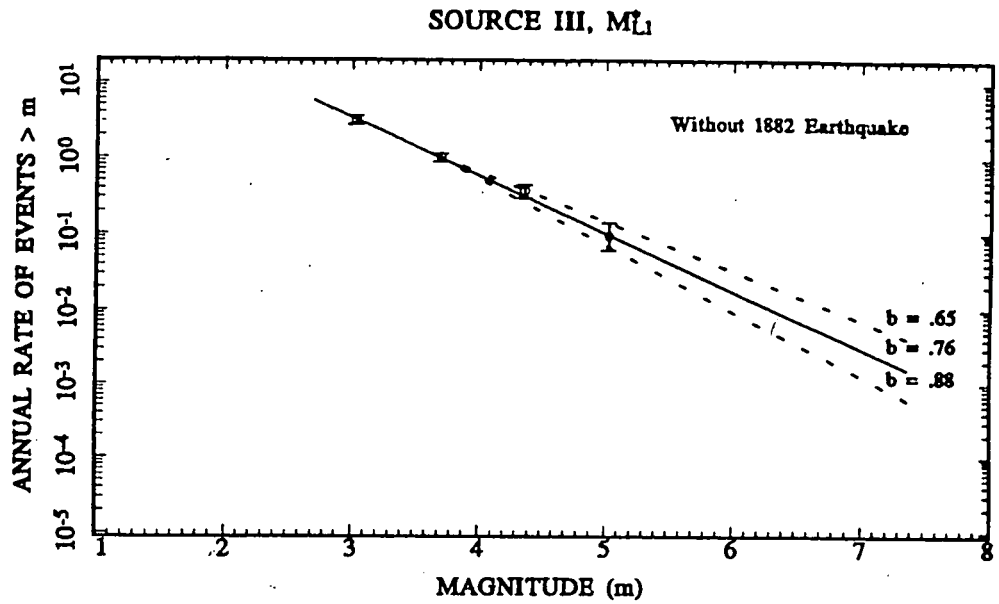

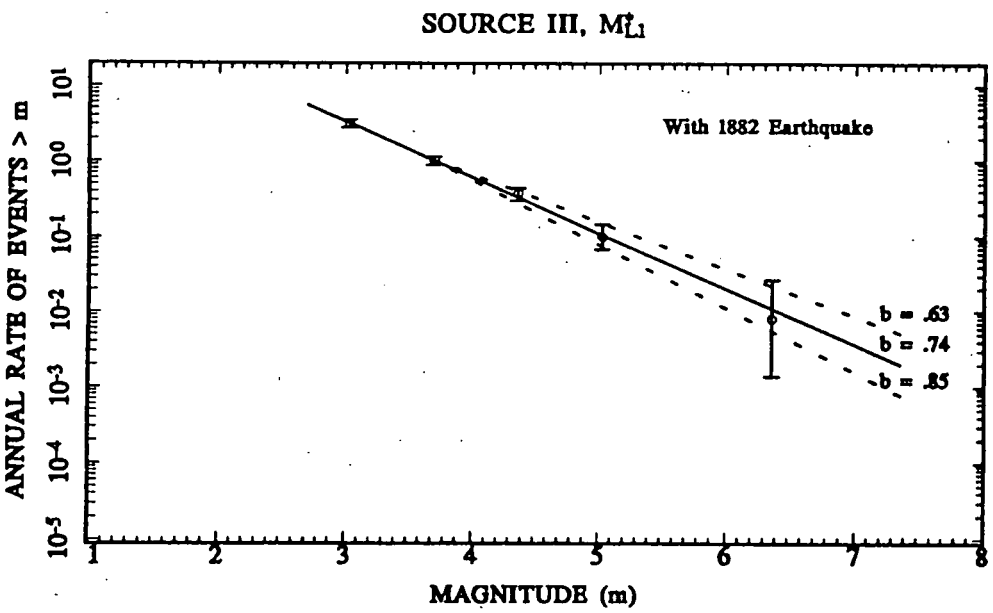

Figure D-26: (a) Historical seismicity for Source III using M^*_{L1}, without 1882 earthquake.
(b) Historical seismicity for Source III using M^*_{L1}, with 1882 earthquake.

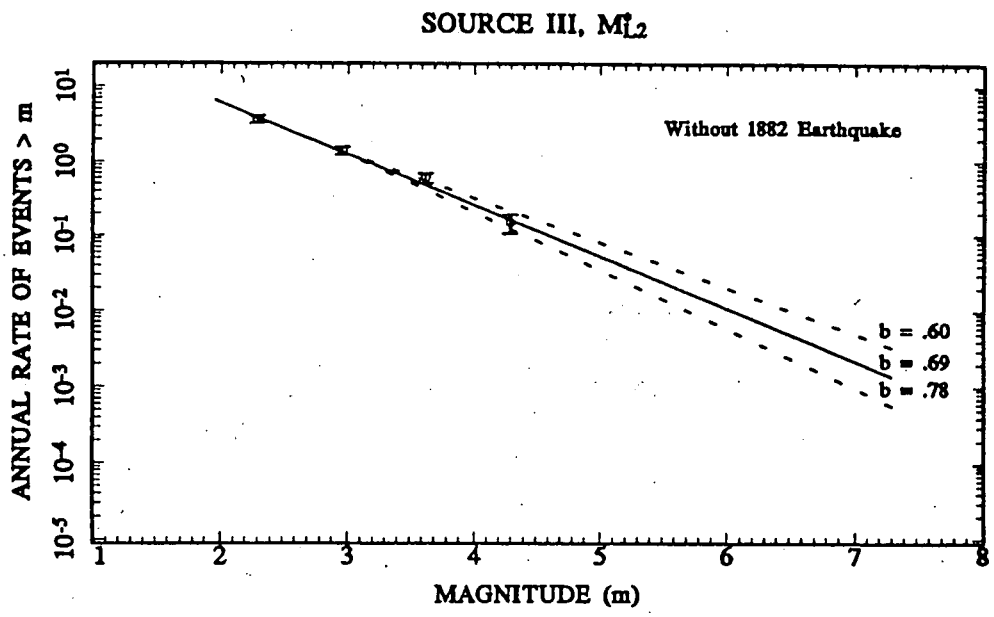

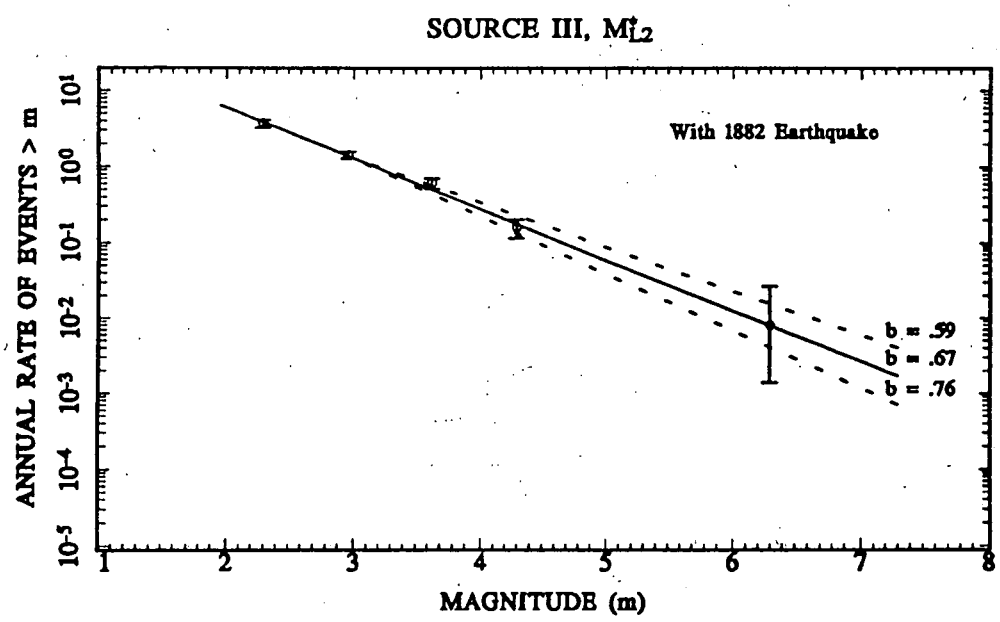

Figure D-26: (c) Historical seismicity for Source III using M^*_{L2}, without 1882 earthquake.
(d) Historical seismicity for Source III using M^*_{L2}, with 1882 earthquake.

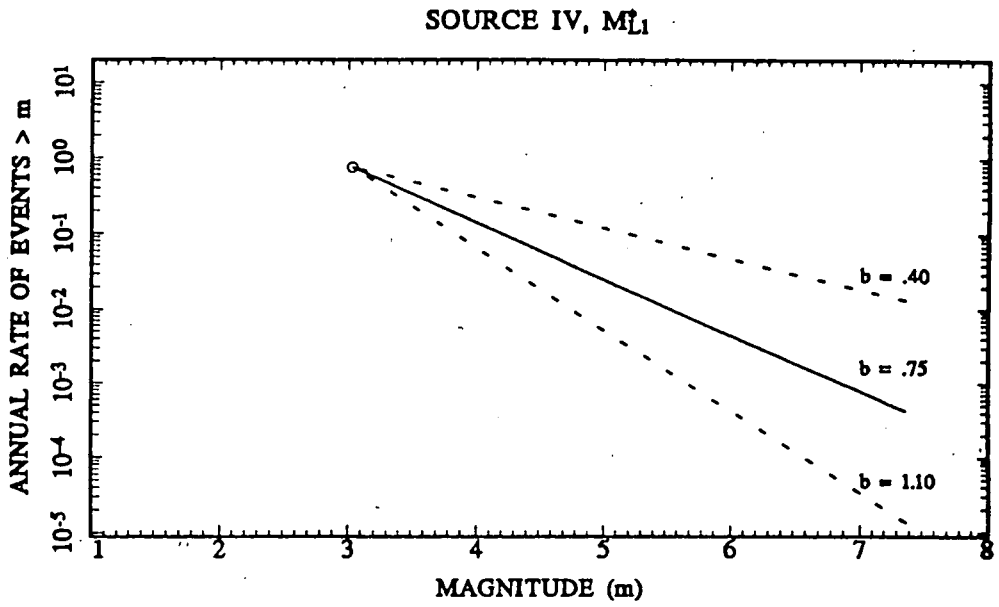

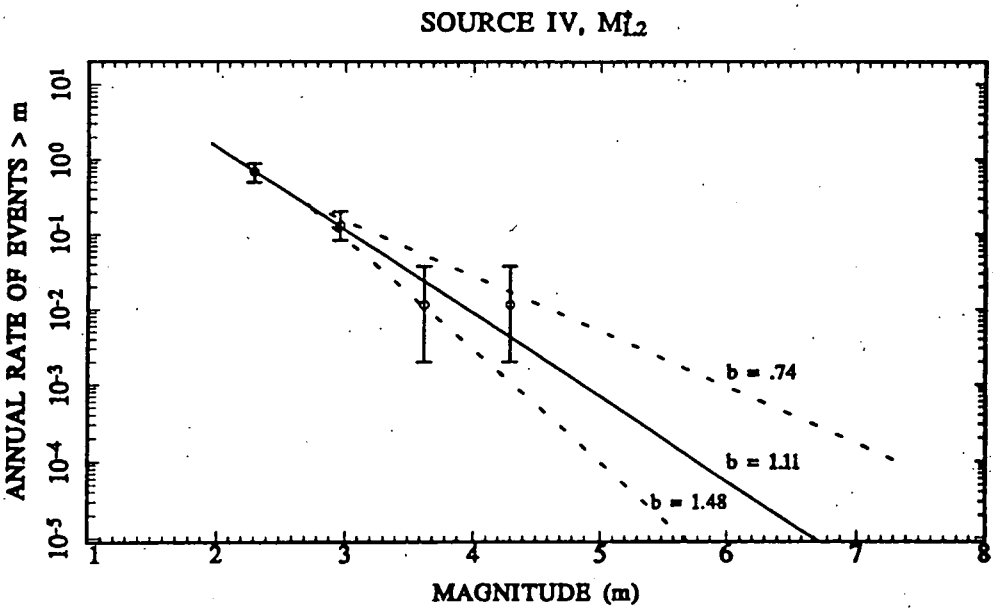

Figure D-27: (a): Historical seismicity for Source IV using M^*_{L1}.
(b): Historical seismicity for Source IV using M^*_{L2}.

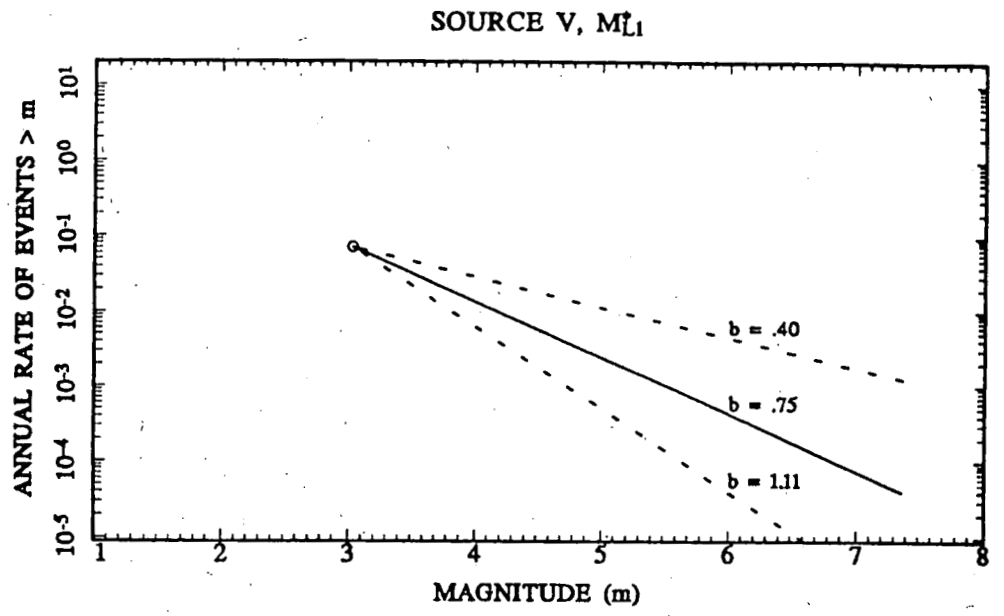

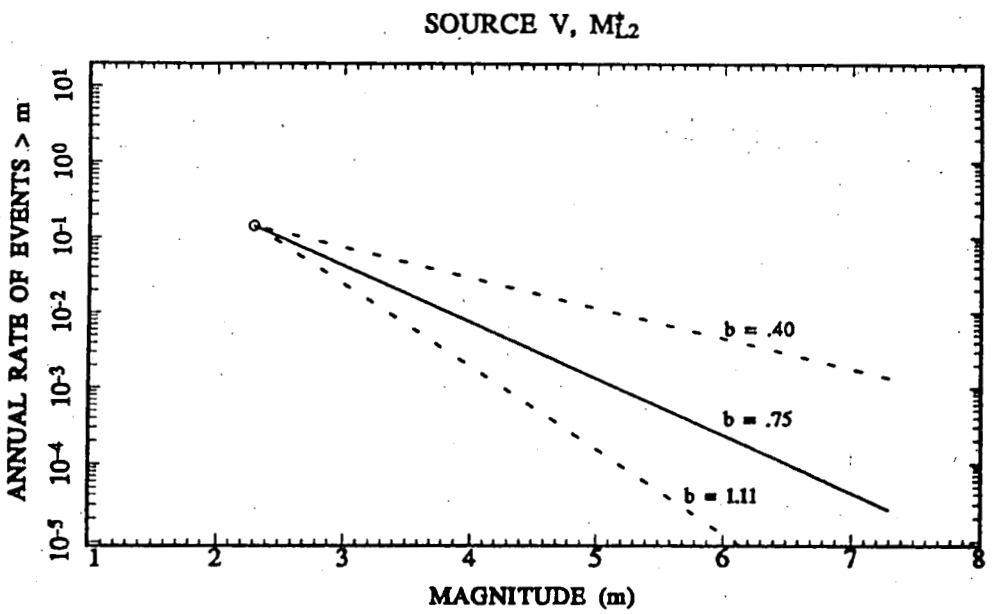

Figure D-28: (a): Historical seismicity for Source V using M^*_{L1}.
(b): Historical seismicity for Source V using M^*_{L2}.

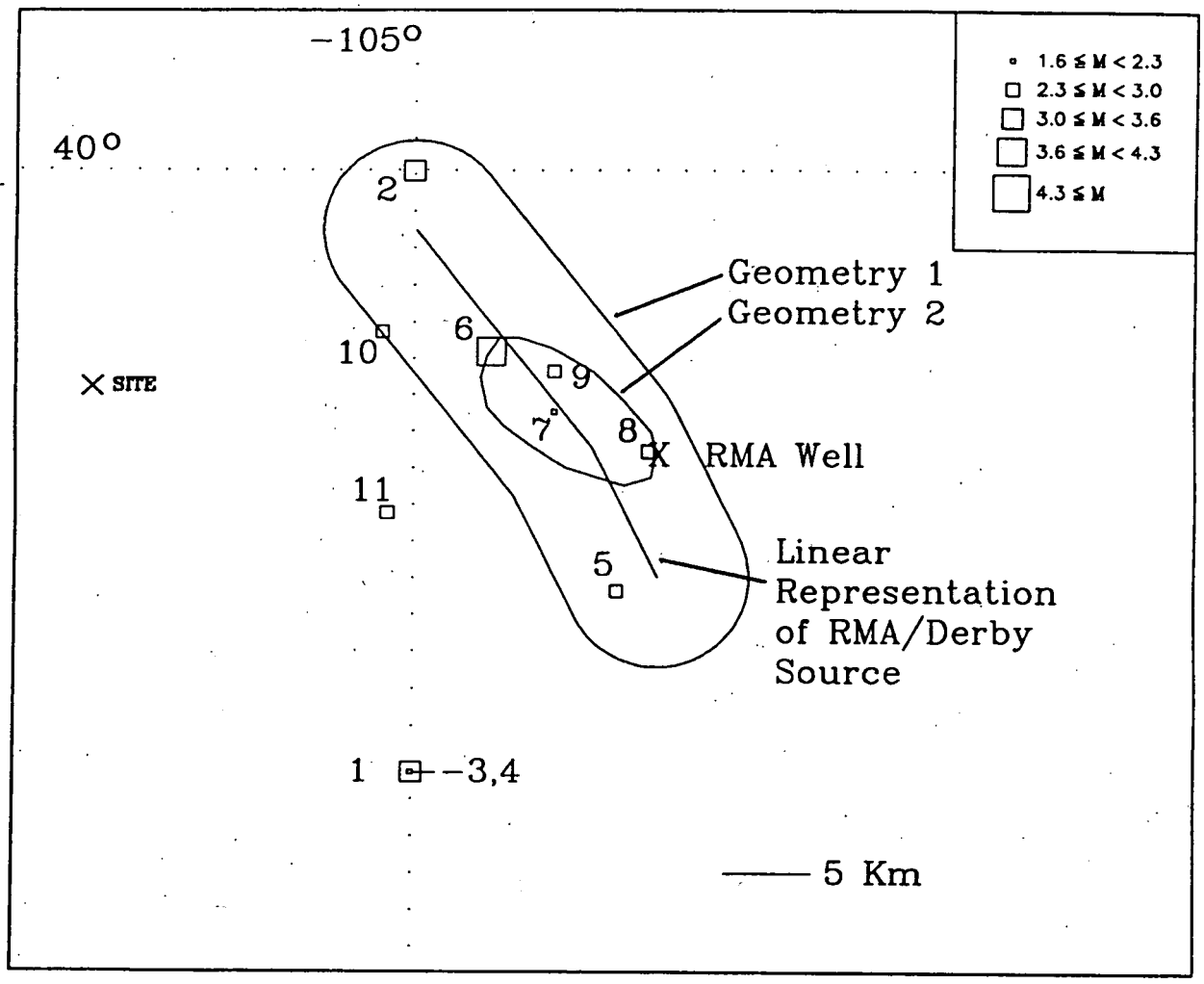

ROCKY MOUNTAIN ARSENAL/DERBY SEISMICITY

Figure D-29: Seismicity in vicinity of Rocky Mountain Arsenal.
Refer to Table D-7 for description of each event.

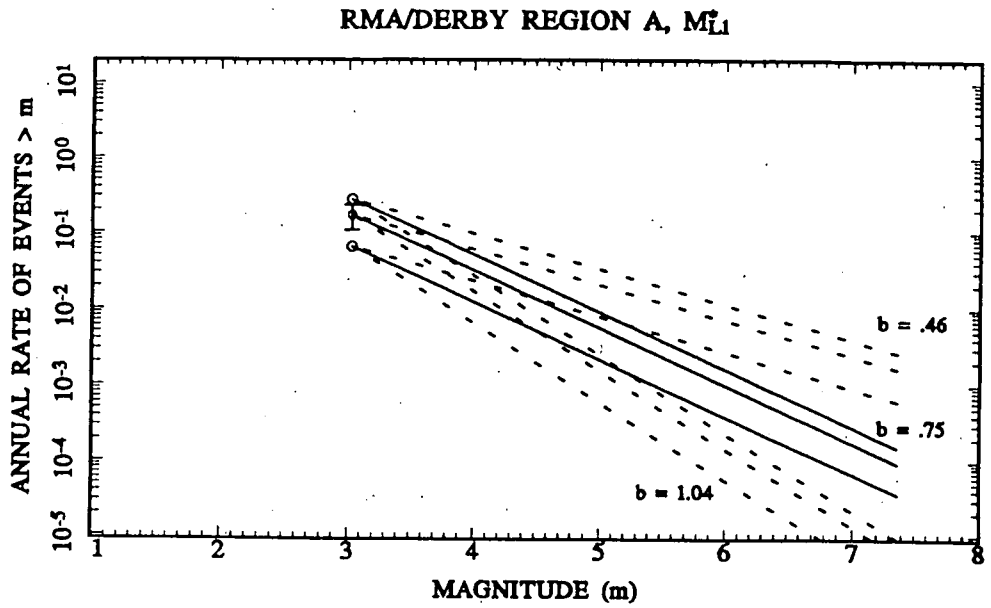

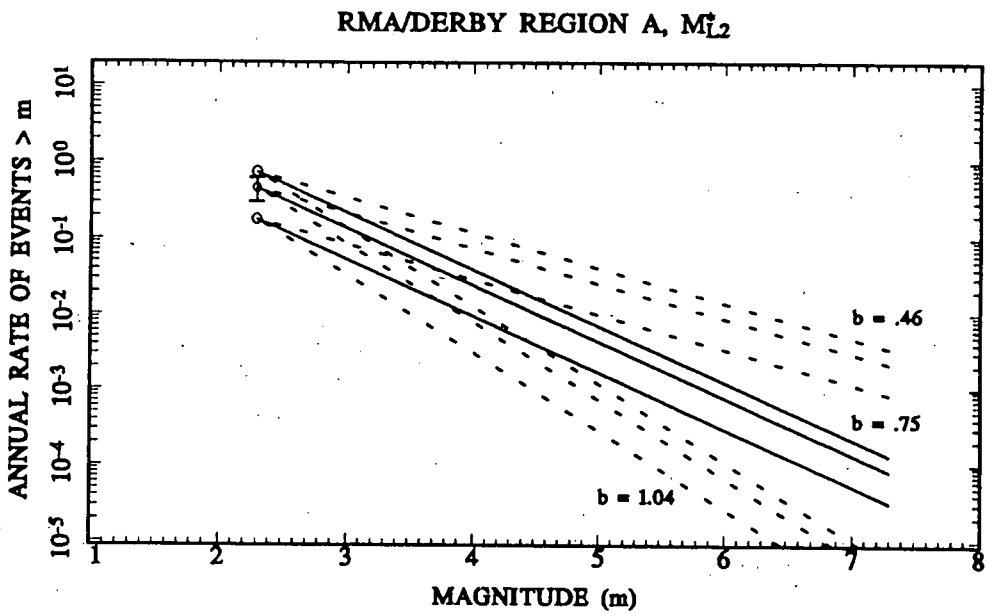

Figure D-30: *b*-value plot for RMA/Derby Region A
(a) Historical seismicity for Region A using M^*_{L1}.
(b) Historical seismicity for Region A using M^*_{L2}.

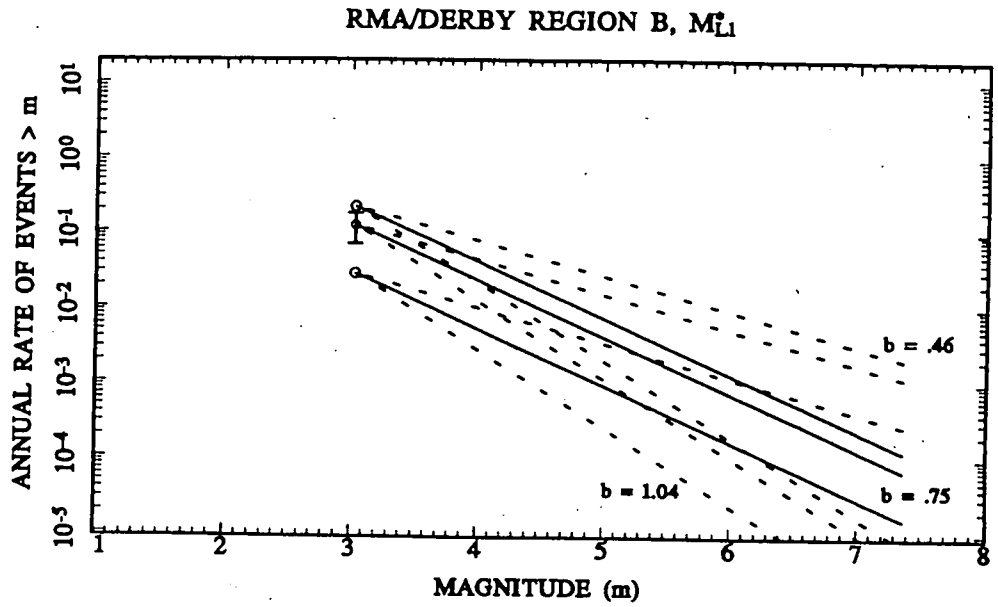

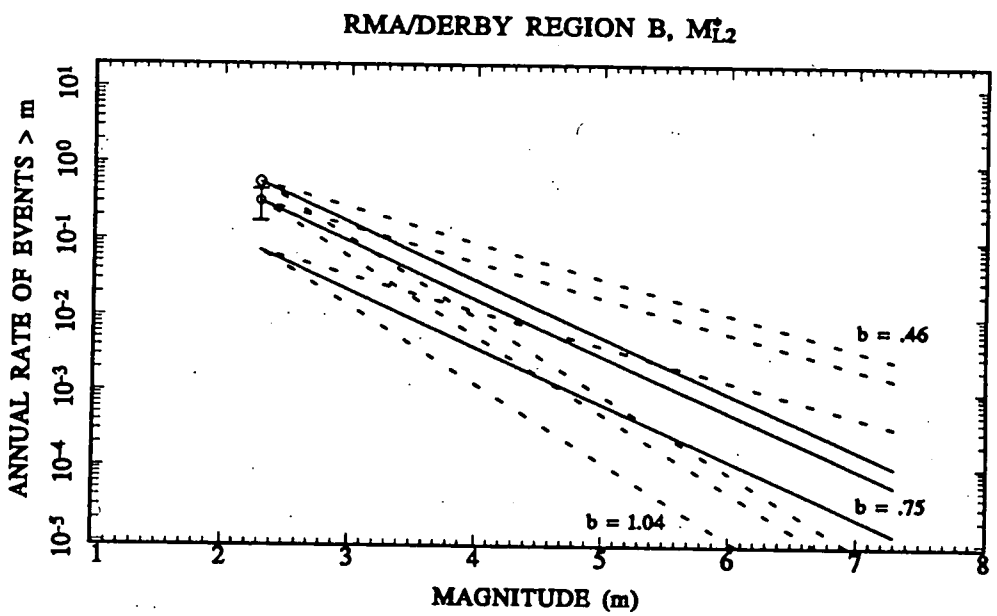

Figure D-31: *b*-value plot for RMA/Derby Region B
(a) Historical seismicity for Region B using M^*_{L1}.
(b) Historical seismicity for Region B using M^*_{L2}.

APPENDIX E

ATTENUATION RELATIONSHIPS

by

Risk Engineering, Inc.
Boulder, Colorado

EQE International, Inc.
Evergreen, Colorado

Pacific Engineering and Analysis Co.
El Cerrito, California

INTRODUCTION

The purpose of this Appendix is to derive methods of estimating seismic ground motions for rock conditions at Rocky Flats. For this purpose, estimates of crustal characteristics at deep depths (greater than several hundred feet) can be made on a regional basis using information such as sonic velocity logs from the Rocky Mountain Arsenal well. Site-specific information such as shear wave velocities measured at Rocky Flats in the top 100 feet of alluvium are not relevant to the estimation of rock ground motion; this information is used in Appendix F to estimate soil amplification factors for the shallow alluvium.

Because of the general lack of seismicity in Colorado, there are no strong motion records with which to make purely statistical estimates of ground shaking during future earthquakes. Therefore, equations must be adopted from other regions, modifying those equations to account for differences in the characteristics of the earth's crust that affect seismic waves, where these characteristics are known or can be estimated from seismological records, or from active testing (for example in wells). The purpose of this Appendix is to derive such equations for the estimation of ground motion at Rocky Flats. There are a range of possible methods of estimating strong ground motion at a site, from purely theoretical to purely empirical. These include the following:

(1) Purely deterministic methods start with a representation of fault rupture, propagate seismic waves through the earth's crust, and estimate theoretical time histories of motion at the site of interest.

(2) Analytical methods use a spectral representation of the seismic source and, through random vibration methods, estimate ground motion in the frequency domain, from which distributions of time-series maxima can be obtained. This method has proven to be accurate in California where abundant strong motion data are available for comparison.

(3) Modified-empirical methods start with empirical models obtained from strong motion data in other regions (e.g. California) and modify the attenuation equations based on estimated differences in regional attenuation.

(4) Purely empirical methods use data from the region of study to derive equations estimating ground motion as a function of magnitude and distance.

For this study option 1 is not appropriate because the sense of slip in source areas, and even on faults, in Colorado is ambiguous. Also, the regional crustal structure changes across the Colorado Front Range, and is not known well enough to justify deterministic ground motion estimates. Option 4 is not available because there are no strong motion records available from Colorado earthquakes. The only records that might have been useful were from the 1981 Derby earthquake aftershocks, but these records were inadequate to quantify ground motions to check attenuation equations.

Therefore for this study we concentrate on methods 2 and 3, which are the best available techniques. Using both methods and adopting the resulting ground motion equations in the seismic hazard estimates provides the most comprehensive and encompassing set of assumptions with which to calculate seismic hazard and assess its uncertainty.

The scope of this study is to quantify ground motion by horizontal peak ground acceleration (PGA) and by pseudo-relative velocity (PSV) for the frequency range 25 Hz to 1 Hz, for 5% of critical damping, for rock conditions. These are the standard parameters that are used for evaluation of seismic resistance of civil and mechanical structures and components. We also include methods to estimate vertical motions from horizontals, and methods to estimate response spectra for dampings other than 5%.

EMPIRICAL ESTIMATES OF GROUND MOTION

Since there were no empirical attenuation relationships available for the Rocky Flats region, the relationships of Sadigh et al. (1986), Joyner and Boore (1988), and Campbell (1993), which were developed for the western United States, were modified for use in this region. These relationships were selected from among those recently published in the literature by knowledgeable investigators and represent a diverse range of interpretations in data selection, parameter definitions, functional forms, and analysis techniques.

The ground-motion parameters of interest in this study were the horizontal components of peak ground acceleration (PGA) and 5% damped pseudorelative velocity (PSV) at frequencies of 1, 2.5, 5, 10, and 25 Hz (periods of 1, 0.4, 0.2, 0.1, and 0.04 sec). As applied to the Rocky Flats region, all of the selected attenuation relationships were considered to be appropriate for predicting ground motions on rock from earthquakes of magnitude 5 and greater located as far as several hundred kilometers from the site.

Two sets of empirical ground motion equations were developed. One set used fault distance to characterize source-to-site distance. A second set used epicentral distance as this measure of distance. The fault-distance models are appropriate for use with fault (extended) sources; the epicentral-distance models for use with areal (point) sources. Since none of the selected fault-distance relationships had associated epicentral-distance models, these latter relationships were developed by modifying the former to account for expected differences in scaling characteristics resulting from differences in the two distance measures.

In order to apply the selected attenuation relationships to the Rocky Flats region, modifications to account for potential regional differences in (1) anelastic attenuation, (2) stress drop, and (3) regional magnitude measures were considered. There is no difference in magnitude definition, i.e., the magnitude measure used in the empirical equations is consistent with the magnitudes used to quantify seismicity in the study region. An early study by Boore and Atkinson (1987) hypothesized that stress drops were higher in eastern North America than in western North America. However, later studies (Somerville et al., 1987; Boore et al., 1992; Silva, personal communication, 1993) used inversion methods to solve for stress drops from recorded motions, or determined the stress drop that is consistent with empirical attenuation equations, and found that stress drops in the two regions are essentially the same. The most recent major study that examined stress drops in the two regions (EPRI, 1993) found essentially the same stress drops. As a result, no modification for stress drop was applied to the relationships.

Anelastic Attenuation

Singh and Herrmann (1983) found significant regional differences in the anelastic attenuation of Lg coda waves throughout the United States. As a result, it was necessary to make modifications to the selected attenuation relationships to account for these differences. This was done by theoretically deriving anelastic attenuation terms for both California (the region representing the majority of strong-motion recordings used to develop each of the relationships) and the Rocky Flats region in a form consistent with that used to model anelastic attenuation in each of the relationships, then applying these terms to each relationship in a self-consistent manner.

The theoretically synthesized ground-motion data for each region were developed using the same stochastic simulation model used to develop the theoretical ground-motion models described later in this Appendix and the soil amplification factors described in Appendix F. Ground-motion data were synthesized for magnitudes ranging from 5 to 8 (in increments of 0.5) and distances ranging from 100 to 300 km (in increments of 50 km). Crustal attenuation in California was modeled by a frequency dependent quality factor (Q) of the form:

$$Q = 150\, f^{0.6} \qquad \text{(E-1)}$$

where f is the frequency of the wave in Hz and the constants represent a consensus based on the results of Singh and Herrmann (1983, Figures 13 and 14), Bakun and Joyner (1984, p. 1840), Nuttli (1986, Figure 5, p. 2144), and Hutton and Boore (1987, Table 2, n=1 based on the methodology used by Bakun and Joyner, 1984, p. 1840).

Singh and Herrmann (1983) found that crustal attenuation in the vicinity of the Front Range in Colorado was strongly dependent on azimuth, with travel paths from the west exhibiting higher attenuation than those from the east. Since only one set of attenuation relationships was to be used in the analyses, the lower attenuation associated with eastern Colorado was used to develop these relationships. Consistent with Singh and Herrmann (1983, Figures 13 and 14), this attenuation was modeled by a frequency dependent quality factor of the form:

$$Q = 800\, f^{0.3} \qquad \text{(E-2)}$$

Both of these relationships are considered appropriate for use with attenuation relationships that assume geometrical attenuation to be proportional to r^{-n}, where n is 1.

All three of the empirical attenuation relationships modified here were developed using a mix of data from soil and rock sites, which is standard practice. In order to replicate this mix of sites, the synthetic ground motion data were generated for both rock and soil sites, even though the ultimate use was to predict ground motions for rock conditions. This allows a comparison, Rocky Flats vs California, of ground motions under the same conditions for which the equations were derived. The resulting modification of the original equations is therefore consistent. For the synthetic soil ground motions, anelastic attenuation within alluvium was modeled using a kappa (κ) of 0.065 sec (Anderson and Hough, 1984, Table 1, p. 1984; Anderson, 1991, Table 2) for both Rocky Flats and California. A κ value of 0.04 sec (see the description of κ under "Analytical Estimates of Ground Motion" below) was used to represent anelastic attenuation in rock in both regions.

The assumption that kappa is about the same for alluvium or rock for both Rocky Flats and California is based on the similarity of the shear-wave velocity profiles in the two regions. The average shear-wave velocity in the upper 100 ft (30 m) of alluvium and weathered claystone at Rocky Flats, which is considered to be 'soil' for purposes of developing the soil amplification factors in Appendix F, is 1,065 ft/sec (325 m/sec), based on the median shear-wave velocity profile for the site (Figure F-4). This velocity falls in the range of shear-wave velocities defined by Boore et al. (1993) as Site Class C, which Boore et al. (1994) have shown is consistent with a generic soil site in California. The shear-wave velocity below 100 ft at Rocky Flats is found to be on the order of 2,000 ft/sec (610 m/sec). This velocity falls in the range of velocities defined by Boore et al. (1993) as Site Class B, which Boore et al. (1994) have shown is consistent with a generic rock site in California.

The synthetic ground motions indicated that anelastic attenuation was strongly magnitude dependent in both regions, especially for the high-frequency components of ground motion of interest in this study. This finding is consistent with previous results reported by Campbell (1991a,b). Neither Sadigh et al. (1986) nor Joyner and Boore (1988) considered this term to be magnitude dependent. Therefore, in order to be consistent with the way in which anelastic attenuation was modeled by each of the selected attenuation relationships, the following set of expressions was used to develop theoretical anelastic terms for both California and the Rocky Flats region:

$$\ln(y) = a + bM + cM^2 + f(r) \qquad \text{(E-3)}$$

$$f(r) \begin{cases} = -1.0 \ln(r) + \alpha' & \text{(Joyner and Boore)} \\ = -1.0 \ln(r) + (\alpha_1 + \alpha_2 M)r & \text{(Campbell)} \\ = d' \ln(r) & \text{(Sadigh et al.)} \end{cases}$$

where y is the ground-motion parameter of interest (PGA or PSV), M is moment magnitude, r is source-to-site distance (km), α' is the magnitude-independent coefficient of anelastic attenuation, $\alpha = \alpha_1 + \alpha_2 M$ is the magnitude-dependent coefficient of anelastic attenuation, and d' is the magnitude-independent coefficient of geometric attenuation, which in this case accounts for both anelastic and geometric attenuation. Each of the applications described below used this general form; details are given in the descriptions of Equations (E-4), (E-6), and (E-7). The quadratic

magnitude term in Equation (E-3) was necessary to remove the distance-independent magnitude scaling characteristics of the synthesized ground-motion data. The coefficients a, b, c, α', α_1, α_2 and d' were estimated by regression analysis using the method of least squares. The attenuation coefficients are summarized in Table E-1. An example of the difference in PGA that results from the difference in anelastic attenuation between California and eastern Colorado, using the attenuation relationship of Campbell (1993) for California and the modified version of this relationship for eastern Colorado (Equation E-7) is shown in Figure E-1. This figure indicates that the difference in the predicted value of PGA in the two regions becomes important only for distances beyond about 30 or 40 km.

Fault-Distance Models

The attenuation relationship developed by Sadigh et al. (1986, published in Joyner and Boore, 1988, Equation 9 and Table 5), as applied to the Rocky Flats region, is given by the expression,

$$\ln(y) = a + 1.1M + c_1(8.5-M)^{2.5} + d\ln(r) + 0.2F + g(r_o,r') + \epsilon \qquad \text{(E-4)}$$

where for rock sites:

$$r = r_o + 1.353\exp(0.406M) \qquad M < 6.5$$

$$r = r_o + 0.579\exp(0.537M) \qquad M \geq 6.5$$

$$g(r_o,r') = 0.00580r_o \qquad r_o < r'$$

$$g(r_o,r') = 0.00580r' + 0.349[\ln(r_o)-\ln(r')] \qquad r_o \geq r'$$

and for soil sites:

$$r = r_o + 0.8217\exp(0.4814M) \qquad M < 6.5$$

$$r = r_o + 0.3157\exp(0.6286M) \qquad M \geq 6.5$$

$$g(r_o,r') = 0.00560r_o \qquad r_o < r'$$

$$g(r_o,r') = 0.00560r' + 0.225[\ln(r_o)-\ln(r')]; \qquad r_o \geq r'$$

where y is the ground-motion parameter to be predicted (the average of the two horizontal components); M is moment magnitude; r_o is the shortest distance from the recording site to the fault rupture surface (km); r' is a reference distance (km); F is the style of faulting (F = 0 for strike-slip faults and F = 1 for reverse faults; for normal faults and faults whose style of faulting is unknown, F is assigned the value 0.5); ϵ is a random error term with a mean of zero and a standard deviation equal to $\sigma_{\ln y}$, the standard deviation of an individual prediction; $g(r_o,r')$ is a term used to correct for differences in regional attenuation; and a, c_1, d, $\sigma_{\ln y}$, and r' are given in Tables E-2 and E-3.

It is important to note that, while empirical soil attenuation equations are reported here, they are not used in calculating seismic hazard for the soil surface at Rocky Flats. Rather, a soil amplification

model is derived specific to the conditions at Rocky Flats (see Appendix F). The soil results reported here are used to estimate the uncertainties in soil amplification factors reported in Appendix F; that is the reason these soil results are included here.

Since there were no regression coefficients available for the 25 Hz component of PSV, this parameter was estimated by assuming that the 25 Hz value of PSA on soil, where PSA is pseudoabsolute acceleration ($2\pi f \cdot PSV/g$), is approximately 1% higher than the corresponding value of PGA on soil at $r_o = 0$ (Campbell, 1993), and that the 25 Hz value of PSA on rock is approximately 16% higher than the corresponding value of PGA on rock at $r_o = 0$, based on an extrapolation of the trend of Sadigh et al.'s results for the 3.3, 5 and 10 Hz components of PSV as suggested from the results of Campbell (1993, Equation 1, Table 1). The standard deviation of an individual prediction for the 25 Hz component of PSV was taken to be the average of those for the 10 Hz component of PSV and PGA, consistent with the results of Campbell (1993). Since there were no regression coefficients available for the 2.5 Hz component of PSV, values for these coefficients were estimated by averaging the coefficients from the 2 and 3.3 Hz components of PSV.

The geometric attenuation term given by the coefficient d in Equation (E-4) incorporates both geometric and anelastic attenuation. Its value was found to be strongly correlated with the near-source scaling characteristics of ln(y). Therefore, its value could not be modified to account for differences in anelastic attenuation without violating the near-source scaling characteristics of the model. In order to preserve these characteristics while at the same time maintain the original form of the relationship at large distances, regional differences in anelastic attenuation were taken into account by adding a distance-dependent attenuation correction term to the attenuation relationship [the function $g(r_o,r')$ in Equation (E-4)]. The value of this function at $r_o < r'$ represents the difference in the theoretically derived anelastic attenuation coefficients between California and the Rocky Flats region (α' in Table E-1), thereby preserving the near-source scaling characteristics of the model. It should be noted that only anelastic attenuation coefficients for PGA were used for this purpose to be consistent with the way in which the attenuation relationships were developed (K. Sadigh, personal communication, 1992).

The anelastic attenuation correction term for $r_o < r'$ could only be used to account for regional differences in anelastic attenuation at near-source distances; since at relatively large distances ($r_o \geq r'$) this term tended to "overcompensate" for regional differences in anelastic attenuation due to the use of a geometric attenuation term of the form d ln(r) to represent the far-field attenuation characteristics of the model. In order to avoid this overcompensation and at the same time assure that the attenuation relationship had the same functional form at large distances as intended by the original model, the attenuation characteristics of the model were modified to asymptotically approach the form d ln(r) beyond the reference distance r'. This reference distance was defined as the distance beyond which the rate of attenuation of ln(y) decreases, representing the distance at which the regional correction term begins to overcompensate for regional differences in anelastic attenuation.

Consistent with the intent of the attenuation correction term, the value of $g(r_o,r')$ at $r_o \geq r'$ represents the difference in the anelastic attenuation part of the theoretically derived PGA geometric attenuation coefficients for California and the Rocky Flats regions (d' in Table E-1). The coefficient of ln(r) in this function was estimated from the expression,

$$d_{rf} - d_{ca} = -[(1 + d'_{rf})/(1 + d'_{ca})](1 + d_{ca}) \qquad \text{(E-5)}$$

where d is the empirically derived geometric attenuation coefficient from Equation (E-4), d' is the theoretically derived geometric attenuation coefficient from Table E-1, and the subscripts 'rf' and 'ca' refer to Rocky Flats and California, respectively. The above expression assumes that the ratio of the anelastic attenuation part of the regional geometric attenuation terms is independent of the absolute value of the coefficients. The theoretical values themselves could not be used directly in Equation (E-4), since they were developed without consideration of near-source attenuation effects.

The attenuation relationship developed by Joyner and Boore (1988, Equation 5 and Table 2), as applied to the Rocky Flats region, is given by the expression,

$$\log(y) = a + b(M-6) + c(M-6)^2 - 1.0\log(r) + kr + s + \epsilon \qquad \text{(E-6)}$$
$$r = [r_o^2 + h^2]^{1/2}$$

where y is the ground-motion parameter to be predicted (the average of the two horizontal components, or what the authors refer to as the randomly oriented horizontal component); M is moment magnitude; r_o is the shortest distance from the recording site to the vertical projection of the earthquake fault rupture on the surface of the earth (km); k is the coefficient of anelastic attenuation (km^{-1}); s is the site correction for soil sites; ϵ is a random error term with a mean of zero and a standard deviation equal to $\sigma_{\log y}$, the standard deviation of an individual prediction; and a, b, c, k, s, h, and $\sigma_{\log y}$ are given in Table E-4.

Since there were no regression coefficients available for the 25 Hz component of PSV, this parameter was estimated by assuming that the 25 Hz value of PSA on soil is approximately 1% higher than the corresponding value of PGA on soil at $r_o = 0$ (Campbell, 1993, Equation 1, Table 1), and that the 25 Hz value of PSA on rock is approximately 8% higher than the corresponding value of PGA on rock at $r_o = 0$, based on an extrapolation of the trend of Joyner and Boore's results for the 5 and 10 Hz components of PSV as suggested from the results of Campbell (1993, Equation 1, Table 1). The standard deviation of an individual prediction for the 25 Hz component of PSV was taken as the average of those for the 10 Hz component of PSV and PGA, consistent with the results of Campbell (1993).

The anelastic attenuation coefficients (k) for California estimated by Joyner and Boore (1988) correspond to PSV attenuation rates that are substantially greater than those for PGA at all frequencies of interest. This results in unrealistic spectral shapes at large distances. Joyner (written communication, 1990) was consulted regarding this problem and recommended that these relationships only be used for predicting ground motions at sites located within 100 km of the fault.

Since we are interested in estimating ground motions from earthquakes located as far as several hundred kilometers from the Rocky Flats Plant, it is not appropriate to use Joyner and Boore's values for k as a reliable reference on which to base regional differences in anelastic attenuation. In comparing these values to the theoretically derived anelastic attenuation coefficients given in Table E-1, we found that Joyner and Boore's empirical estimates of PGA attenuate at a significantly lower rate and that their empirical estimates of PSV attenuate at a significantly higher rate than indicated by these theoretical estimates. Based on this comparison, we decided to use the magnitude-independent anelastic attenuation coefficients theoretically derived for the Rocky Flats region to define k. Since Joyner and Boore (1988) assumed that the rate of attenuation was

independent of site type, k was taken as the mean of the values of α' for soil and rock after converting them from natural to common logarithms (i.e., $k = \alpha'/\ln 10$).

The attenuation relationship developed by Campbell (1993, Equation 1 and Table 1), as applied in to the Rocky Flats region, is given by the expression,

$$\begin{aligned} \ln(y) = {} & \beta_o + 0.683M + \beta_1 \tanh[0.647(M - 4.7)] \\ & - 1.0 \ln(r) + \alpha r_o + [\beta_2 - 0.105 \ln(r_o)]S \\ & + 0.27F + \beta_3 \tanh[0.620D] + \epsilon \end{aligned} \qquad \text{(E-7)}$$

$$r = \{r_o^2 + [0.0586 \exp(0.683M)]^2\}^{1/2}$$

$$\alpha = \beta_4 + \beta_5 M$$

where y is the ground-motion parameter to be predicted (average of the two horizontal components); M is local Richter magnitude (M_L) for $M < 6.0$ and surface-wave magnitude (M_s) for $M \geq 6.0$, which is consistent with the definition of moment magnitude (M_w); r_o is the shortest distance from the recording site to the seismogenic rupture zone on the fault (km); S is site type (S = 0 for soil sites and S = 1 for rock sites); F is style of faulting (F = 0 for strike-slip faults and F = 1 for reverse, reverse-oblique, thrust, and thrust-oblique faults); α is the coefficient of anelastic attenuation (km^{-1}); D is the depth to basement rock beneath the site (km); ϵ is a random error term with a mean of zero and a standard deviation equal to $\sigma_{\ln y}$, the standard deviation of an individual estimate; tanh() is the hyperbolic tangent function; and β_o, β_1, ..., β_5 and $\sigma_{\ln y}$ are given in Table E-5.

As suggested by Campbell (1993, p. 3), if no other information was available, the average minimum depth to the top of the seismogenic rupture zone of a given earthquake was conservatively assumed to be dependent on magnitude based on the following relationship:

M	Depth (km)
5.0	7.3
5.5	5.8
6.0	3.5
6.5+	3.0

Bryant et al. (1981) estimated the depth to Precambrian basement beneath the Rocky Flats Plant to be approximately 13,000 ft. Thus, D was taken as 4 km. For normal faults and faults whose style of faulting was unknown, F was assigned the value 0.5.

The Campbell (1993) attenuation relationship was developed using anelastic attenuation coefficients derived for soil sites based on the same methods that were used in the present study. Therefore, the magnitude-dependent anelastic attenuation coefficients derived for soil for the Rocky Flats region (Table E-1) could be used without modification in the application of this relationship.

Epicentral-Distance Models

Since none of the selected attenuation relationships had corresponding epicentral-distance relationships, these latter relationships were developed from the selected fault-distance models based on the following assumptions: (1) the far-field magnitude and distance scaling characteristics of PGA and PSV are the same for both the fault-distance and epicentral-distance models, and (2) the attenuation of PGA and PSV is independent of magnitude (i.e., no near-source saturation effects), except where imposed by the coefficient of anelastic attenuation. The first assumption is justified on the basis that differences in distance measures, and thus differences in strong-motion scaling characteristics, become negligible at large distances. The second assumption is justified based on the form of attenuation relationships derived both theoretically (e.g., Boore and Atkinson, 1987, Equation 13a; Toro and McGuire, 1987, Equation 1 and Table 6; Boore and Joyner, 1991, Equation 10) and empirically (e.g., Atkinson, 1990, Equation 1; Dahle et al., 1990, Equation 4; see also Campbell, 1985).

The first assumption requires that the far-field amplitudes of PGA and PSV be the same as those given by the fault-distance models. However, the second assumption requires only that the far-field and near-source magnitude scaling characteristics of the two models be the same, and does not provide a basis for constraining the near-source amplitudes of PGA and PSV. In order to set the near-source level of the epicentral-distance models, we applied a near-field constraint based on the results of Campbell (1981, Equations 7 and 8), who developed both a fault-distance and an epicentral-distance attenuation relationship from the same set of strong-motion recordings. These relationships indicated that both models should give the same estimate of PGA at zero distance for a magnitude 6.8 earthquake.

Since Sadigh et al. (1986) used the same definition of fault distance as Campbell (1981), the above constraint could be applied directly to their fault-distance model. The other models, however, required some adjustment to account for the differences between their fault-distance measures and the distance measure used by Campbell (1981). Campbell (1993) used the shortest distance to the zone of seismogenic rupture as his definition of fault distance. He conservatively estimated this zone to be at least 3 km deep for a M6.8 earthquake. Based on this estimate, the Campbell (1993) epicentral-distance relationship was constrained to give the same estimate of PGA at an epicentral distance of 0 km as that predicted by the fault-distance relationship at a seismogenic distance of 3 km.

Joyner and Boore (1988) defined their fault-distance measure as the shortest distance to the surface projection of the earthquake fault rupture. That definition, together with the constraint that magnitude scaling be independent of distance, similar to that assumed for the epicentral-distance models, made it difficult to apply the same near-source constraint to their model as was applied to the other two relationships. Instead, we simply constrained the Joyner and Boore epicentral-distance model to give an estimate of PGA at M6.8 and zero distance that was halfway between those of the other two relationships.

Consistent with the above constraints, the following modifications were made to the selected fault-distance models to make them compatible with the use of epicentral distance: (1) Equation (E-4): $r = r_0 + 22.3$, $r' = 61.2$ km (soil), $r' = 66.5$ km (rock); (2) Equation (E-6): $h = 5.4$ (PGA), 3.2 (PSV, 1 Hz), 3.8 (PSV, 2.5 Hz), 6.4 (PSV, 5 Hz), 7.6 (PSV, 10 Hz), and 5.4 (PSV, 25 Hz); and (3)

Equation (E-7): $r = (r_o^2 + 6.8^2)^{1/2}$, $\ln(r_o) = \ln(r_o+1)$. In all of these relationships, r_o was redefined as epicentral distance (km).

Campbell (1981) found that the standard error of estimate of ln(y) was larger for point-source models than for fault-distance models. Using the same data base, he found that the variance associated with ln(y) increased by 0.13 when epicentral distance rather than fault distance was used as the measure of distance. Based on this result, the standard deviation of an individual prediction of ln(y) and log(y) was estimated from the expressions,

$$\sigma_{\ln y,e} = (\sigma_{\ln y,f}^2 + 0.13)^{1/2} \quad \text{(E-8)}$$

$$\sigma_{\log y,e} = (\sigma_{\log y,f}^2 + .025)^{1/2} \quad \text{(E-9)}$$

where the subscripts 'e' and 'f' refer to epicentral distance and fault distance, respectively.

The three attenuation equations are plotted in Figures E-2 through E-5 for comparison purposes. Figures E-2 and E-5 show predicted values of PGA vs. distance for m=5 and 6.5, respectively; Figures E-4 and E-5 show similar comparisons for 1 Hz PSV. The fault distance equations are shown in these plots; the epicentral distance equations are similar.

The attenuation relationships for rock site conditions were developed from recordings obtained on sites located on both soft rock (primarily sedimentary deposits) and hard rock (primarily crystalline rock). Therefore, they are considered appropriate for predicting ground motions on reasonably hard sedimentary rock. This would include the Upper Cretaceous deposits underlying the Rocky Flats site.

As indicated by the anelastic attenuation coefficients given in Tables E-4 and E-5, the high-frequency estimates of PSV attenuate more rapidly than PGA. As a result, it is possible for predicted values of PSV to be smaller than corresponding estimates of PGA at very large distances. Since by definition the high-frequency acceleration response of a single-degree-of- freedom oscillator cannot be less than PGA, estimates of PSA for frequencies of 5 Hz and higher were constrained to be greater than or equal to PGA in the application of Equations (E-6) through (E-7).

ANALYTICAL ESTIMATES OF GROUND MOTION

Introduction

The development of analytical estimates of ground motions for Rocky Flats using a stochastic model of ground motions is based in large part on the models, parameters, and insights obtained as part of an extensive study on earthquake ground-motion prediction for the central and eastern United States (EPRI, 1993). This study was sponsored by the United States Department of Energy and several electric utilities; we will refer to it as the EPRI-DOE study.

Modifications to the results from the EPRI-DOE study are required in order to incorporate site-specific information on crustal structure, anelastic attenuation, and near-site attenuation (κ).

Attenuation functions based on a stochastic model of ground motion are obtained in four steps, as follows:

1. Develop a characterization of the randomness and uncertainty in each of the main parameters of the stochastic model using both regional and site-specific information. For convenience, this characterization is in the form of a discrete distribution (i.e., multiple parameter values with associated weights). The combination of all possible values of the various model parameters is represented by a "logic tree."

2. Calculate the ground-motion amplitudes predicted by the stochastic model for each combination of model parameters.

3. Use least-squares regression to fit a simple functional form in terms of magnitude and distance to the log-ground-motion amplitudes obtained in Step 2 (considering their associated weights). This is done separately for each ground-motion measure (e.g., peak acceleration, 1-Hz spectral velocity, etc.).

4. Examine the regression residuals to determine the contribution of each parameter to the total variability. Use these results, together with the characterization of parameter randomness and uncertainty, to quantify the total randomness and uncertainty in ground motion amplitude and their possible dependence on magnitude and distance. Develop a functional form to represent the dependence of randomness on magnitude and distance. Construct a suite of alternative attenuation equations and associated weights in order to represent uncertainty.

Model Description

The stochastic model of earthquake ground motions uses Brune's (1970, 1971) representation of shear-wave energy generated at the seismic source, together with simple, yet physically sound, assumptions about geometric spreading and anelastic attenuation, to represent the Fourier amplitude of ground motion due to shear waves. This model is sometimes referred to as the Band-Limited White Noise (or BLWN) model or as the random-vibration (or RV) model. Using this spectrum and the associated duration, one calculates the root-mean-square (RMS) and peak amplitudes of ground response by assuming that the ground motion during the strong-shaking portion of an earthquake is a finite-duration segment of a gaussian random process. This model is attractive because it is based on seismological principles (yet it has few parameters, due to its highly simplified assumptions, because it follows a rigorous mathematical procedure to calculate time-domain amplitudes from Fourier amplitude and duration, and because it can predict virtually every measure of ground motion (e.g., acceleration, velocity, response spectra, seismograph response).

The stochastic model has been used extensively to predict ground motions in California (e.g., Hanks and McGuire, 1981; Boore, 1983; McGuire et al, 1984), in eastern North American (ENA; e.g., Boore and Atkinson, 1987; Toro and McGuire, 1987; McGuire et al., 1988; Boore and Joyner, 1991; EPRI, 1993), and in other regions (Wong et al., 1990; Bungum et al., 1992).

The stochastic model is particularly attractive for low-seismicity regions like the central and eastern United States, where there are few or no strong-motion recordings from magnitude and distances

of engineering interest. Because significant extrapolation of the data is required, one is more confident in performing this extrapolation using a model with a strong theoretical justification. In addition, seismological studies and analogies with other regions provide additional data that can be used in the development of parameters for the stochastic model.

The stochastic model represents the Fourier spectrum of ground acceleration, in an arbitrary horizontal direction, in the form:

$$a(f) = C \frac{f^2 M_0}{1 + (f/f_c)^2} G(R)\, A(f) \exp\left[-\frac{\pi f R}{\beta_0 Q(f)}\right] \exp[-\pi \kappa f] \qquad \text{(E-10)}$$

where

M_0 = seismic moment,
$G(R)$ = a function representing geometric-attenuation effects; the form of G(R) is discussed below,
β_0 = shear-wave velocity at the source,
$Q(f)$ = $Q_0 f^n$, frequency-dependent quality factor representing anelastic attenuation effects,
$A(f)$ = near-surface frequency-dependent amplification factor,
f_c = source corner frequency,
κ = parameter of the high-frequency truncation filter (Anderson and Hough, 1984; the κ term used here corresponds to Anderson and Hough's $\kappa(0)$), and
C = a constant that contains source-region density ρ_0 and shear-wave velocity terms and accounts for the free-surface effect (factor of 2), the source radiation pattern averaged over a sphere (0.55) (Boore, 1986), and the partition of energy into two horizontal components ($1/\sqrt{2}$).

Source scaling (i.e., the variation of spectral amplitude and shape with earthquake size) is controlled by the seismic moment M_0 and the corner frequency f_c. The seismic moment is a measure of earthquake size; it is related to moment magnitude **M** (the measure of earthquake size used in this study) by the relation (Hanks and Kanamori, 1979):

$$\log M_0 = 1.5M + 16.1 \qquad \text{(E-11)}$$

The corner frequency is related to the seismic moment by means of the stress drop $\Delta\sigma$ by the relationship (Brune, 1970, 1971):

$$f_c = \left(\frac{\Delta\sigma}{8.44 M_0}\right)^{1/3} \qquad \text{(E-12)}$$

Calculation of peak time-domain values requires the specification of the duration of strong ground motion, which is discussed below under "Geometric Attenuation, Duration and A(f)". These calculations are performed using random-vibration theory (see Boore, 1983; Boore and Joyner, 1984).

Geometric Attenuation, Duration, and A(f). Two models are available for the calculation of the geometric-attenuation term G(R). Based on modeling and observation, Herrmann (1985) proposed the form:

$$G(R)=\begin{cases} 1/R & R<100 \text{ km} \\ 0.01\dfrac{1}{\sqrt{R}} & R>100 \text{ km} \end{cases} \qquad \text{(E-13)}$$

and the associated duration $T=1/f_c+0.05R$. This form has been used by many investigators (e.g., Boore and Atkinson, 1987; Toro and McGuire, 1987; McGuire et al., 1988) and found to provide an adequate representation of observed ground motions.

More recently, Ou and Herrmann (1992; see EPRI, 1993, for revisions to this formulation) developed a procedure to calculate G(R) and T including the effect of a layered crustal structure. This formulation requires specification of the regional shear-wave velocity structure of the crust.

The amplification factor A(f) also depends on the crustal structure. In particular, A(f) depends on the shear-wave velocities and densities in the upper portion of the crust.

The selection of crustal velocity structure and geometric-attenuation formulation for this study is discussed in below under "Crustal Velocity Structure".

In summary, the key parameters for the stochastic model are magnitude and distance (independent variables), and stress-drop, crustal velocity structure, Q, κ and focal depth (parameters with variability. The variabilities of the latter parameters are described below.

Treatment of Physical Uncertainties

The variability of the model parameter values is separated into randomness and uncertainty. Randomness represents variability that is inherent to the parameter; uncertainty represents variability that is due to our lack of knowledge of the parameter. Therefore, randomness can be refined but not reduced, whereas uncertainty may be reduced in the future with additional information.

Stress-Drop. Following the EPRI-DOE study, the stress drop $\Delta\sigma$ is taken as lognormal with a median value of 120 bars and a total variability (randomness plus uncertainty) of 0.7 (natural-log units) The breakdown of this variability into randomness and uncertainty is magnitude-dependent, as follows:

$$\sigma_{r,\ln\Delta\sigma}(M) = \begin{cases} 0.684 & M<6 \\ \sqrt{(0.684)^2 - 0.436(M-6)} & 6<M<6.5 \\ 0.50 & M\geq 6.5 \end{cases} \qquad \text{(E-14)}$$

$$\sigma_{U,\ln\Delta\sigma}(M) = 0.15 \qquad M<6$$

$$= \sqrt{(0.15)^2 + 0.455\,(M-6)} \qquad 6<M<6.5 \qquad \text{(E-15)}$$

$$= 0.50 \qquad M \geq 6.5$$

This treatment is consistent with EPRI (1993). The total variability in $\ln(\Delta\sigma)$ is represented by five values with associated weights.

Crustal Velocity Structure. Because little information exists on direct measurements of shear-wave velocities for the regional crustal structure within 200 km of the Rocky Flats site, a derived model was developed based on measurements of compressional-wave velocities. For the crust beneath the sedimentary section, Precambrian basement, and below, the compressional-wave velocity and density models were based on deep refraction surveys described in Prodehl and Lipman (1989) and are appropriate for the central Plains. For the sedimentary section, the sonic velocity log for the Wildcat #1 borehole at the Rocky Mountain Arsenal was used. The sonic log was divided into three layers extending to a depth of about 4 km. The depth of the sedimentary column is based on reflection line RFD-1 of EBASCO (1991). Shear-wave velocities were then computed by assuming a Poisson solid. Table E-6 summarizes shear-wave velocities and densities as a function of depth. Based upon the compressional wave velocity data that are available in the region, as described above, and given that there are no site-specific shear- or compressional-wave measurements available, this is a reasonable and adequate interpretation of data to estimate shear wave velocities and densities.

Figure E-6 shows the variation of peak acceleration with distance for magnitude 6.5 and 10 km depth. These results were obtained using the revised Ou-Herrmann (1992) geometric-attenuation model and the crustal-structure model constructed above (labeled ROCK1; other models shown correspond to relevant regional models documented in Section 5 of EPRI, 1993). The changes in slope at 100 km for some of the models reflect crustal reflection phases that are stronger than direct arrivals for those crustal models. Figure E-7 shows results obtained using the Herrmann (1985; see Equation E-13) geometric-attenuation model compared to the ROCK1 results replotted from Figure E-5. The results obtained using the Herrmann (1985) formulation are higher than the results obtained from the ROCK1 crustal structure (except for distances less than 9 km, where the ROCK1 structure predicts slightly higher accelerations).

In view of these results, and because of the lack of direct shear-wave velocity measurements, the Herrmann (1985) formulation was selected because it leads to more robust ground-motion predictions. The lower predictions (relative to the ROCK1 curve) at distances less than 9 km are more than offset in the hazard calculations by higher predictions at distances greater than 9 km. This is evident because hazard calculations for sites within large areal sources indicate a mean distance of 20 to 30 km for earthquakes causing exceedences of ground motions with 100 to 10,000 year return periods. There are ten times as many earthquakes in the distance range 9-30 km, as in the range 0-9 km, for spatially-uniform seismicity, and higher estimates of ground motion for the

Herrmann model in the 9-30 km range, combined with the higher probability of occurrence, more than offset the slightly lower estimates of ground motion in the 0-9 km range.

The frequency-dependent amplification factor A(f) was computed from the crustal model derived above.

Parameter κ. κ represents attenuation in the shallow crust directly beneath the site. Values of κ in the 0.02-0.06 sec range are typical of sites in western North America (Boore, 1986; Silva and Darragh, 1993). The upper crust of the ROCK1 profile described above, consisting of sedimentary rocks to a depth of 13,000 feet, is similar to the upper crust in the crustal model used in the EPRI-DOE study (EPRI, 1993, Section 3.2.2.1) to model recordings from the 1989 Loma Prieta earthquake. Based on this similarity, a median κ value of 0.04 sec (in the center of the range for western North America) is adopted for Rocky Flats. The appropriateness of the kappa value of 0.04 sec is substantiated by the dependence of kappa on the average shear-wave velocity (over about 100 ft) shown in Figure E-8. The figure shows kappa values determined from strong motion data recorded at rock sites which have measured velocities to depths of about 100 ft. The average velocity over 100 ft of the Rocky Flats profile considered as firm rock (100-200) ft, Figure E-8) is about 2,300 ft/sec which corresponds to a kappa value of 0.035 sec. In view of the uncertainties involved, an average value of 0.04 sec is reasonable and consistent with the data in Figure E-8. Variability in κ is introduced by considering three equally weighted values of 0.02, 0.04, and 0.08 sec. This range of variability (in ln κ) is larger than the range considered in the EPRI-DOE study, because there is more uncertainty here (no direct observations of κ are available for Rocky Flats or the vicinity). To illustrate the effects of kappa on response spectra Figure E-9 shows 5% damped pseudo relative velocity computed using the point-source model with kappa values of 0.02, 0.04, and 0.08 sec. The effects of doubling kappa are large for frequencies exceeding about 2 Hz (Silva, 1993).

Because κ is primarily a site characteristic, 75% of its variability is considered uncertainty (which could in principle be resolved by site-specific measurements). The remaining 25% is considered randomness.

Q Models. The lower crust model described above is similar to that of the Midcontinent crust considered in the EPRI-DOE study. As a result, the three Q models used in the EPRI-DOE study (EPRI, 1993) for the Midcontinent (i.e., $Q(f)=400f^{0.4}$, $670f^{0.33}$, and $1000f^{0.3}$) are used for Rocky Flats. These Q models have the advantage of precedent, and there is no reason why they would not be applicable to the Rocky Flats region. Figure E-10 compares the three Q models with regional Q studies of Singh and Herrmann (1983) and Gupta et al. (1989), illustrating that the regional studies favor the second and third of the above models. Therefore, the three Q models given above are assigned weights of 0.2, 0.4, and 0.4, respectively.

The variability in Q represented by the above Q models and weights is considered to be equally divided between uncertainty and randomness.

Modeling. The modeling variability is determined from the misfit of modeled ground motion data with recorded data. The representation of modeling uncertainty and randomness obtained in Section 3 of the EPRI-DOE study (EPRI, 1993) is adopted for this study. They are of the form:

Modeling randomness:

$$\sigma_{r,modeling}(f) = 0.32 \qquad f \geq 9\text{Hz}$$
$$= 0.63 - 0.14 \ln(f) \qquad 1 \leq f < 9\text{Hz} \tag{E-16}$$

Modeling Uncertainty:

$$\sigma_{U,modeling} = 0.27 \tag{E-17}$$

where σ is in natural log units.

Thus, randomness in the predicted ground motions comes from parametric randomness in stress drop, kappa, and Q, and from modeling randomness. Uncertainty in the predicted ground motions comes from parametric uncertainty in stress drop, kappa, and Q, and from modeling uncertainty.

Functional Form of Predictive Equations. Practical considerations dictate that the ground-motion predictions for engineering applications must be in the form of relatively simple equations in terms of magnitude and distance. The functional form and number of terms in these equations must, however, be sufficient to match the main features of the ground motions predicted by the physical models described earlier, over the entire range of magnitudes, distances, and frequencies of engineering interest.

The functional form adopted here is the following:

$$\ln y = C_1 + C_2(M-6) + C_3(M-6)^2 - C_4 \ln R - (C_5 - C_4) \max\left[\ln\left(\frac{R}{100}\right), 0\right] - C_6 R + \epsilon_U + \epsilon_r \tag{E-18}$$

where y is pseudo spectral velocity (PSV; for 5% damping) or peak ground acceleration (in units of cm/sec or g, respectively), C_1 through C_6 are constants to be determined from the modeling results (see next section), M is moment magnitude, and R is hypocentral distance (km). This equation is slightly modified below so that it can use the closest distance to the fault rupture, for use with fault sources in the seismic-hazard calculations.

The quadratic magnitude term is needed in order to provide a better fit to the model predictions for low-frequency ground motions. The magnitude terms are of the form $(M-6)^n$ for the sake of numerical stability in the values of C_2 and C_3. The term in C_3 is not always present (it is not required for frequencies of 5 Hz or higher). The terms in C_4 and C_5 represent geometrical spreading with slopes C_4 (R < 100 km) and C_5 (R > 100 km). The model with two slopes provides a slightly better fit than a linear model to the crustal effects predicted by the ground-motion model in Equation E-13. Coefficient C_5 was fixed to its theoretical value of 0.83 (Nuttli, 1973).

Variability about these equations is represented by the quantities ϵ_r (randomness) and ϵ_U (uncertainty), which are assumed to follow normal distributions. The least-squares regression used

to fit the median model works with the total variability and does not distinguish between ϵ_r and ϵ_U. Randomness and uncertainty are determined after an analysis of the residuals.

Development of Median Attenuation Equations. The stochastic ground-motion model of Equation E-10 was used to calculate peak ground-motion amplitudes for all ground-motion measures considered in this study, for magnitudes and distances covering the range of engineering interest, and for all possible combinations of the model parameters described earlier. The weight assigned to each set of results is the product of the weights for the corresponding values of $\Delta\sigma$, κ, and Q. Values of coefficients C_1 through C_6 are obtained as a weighted least-squares fit to the calculated ground motions. This operation is performed separately for each ground-motion measure. The resulting coefficients are shown in Table E-7.

Treatment of Variability. Variability is separated into randomness and uncertainty. As described earlier, it is sometimes useful to separate it into parametric and modeling variabilities. The combined effect of all parametric variabilities is obtained by examining the residuals from the least-squares fit to model predictions. The modeling variability, which is obtained from comparisons of predictions to data, is added as a separate term.

To calculate the randomness and uncertainty in ground-motion amplitudes, the total parametric variability is decomposed into contributions from $\Delta\sigma$, κ, and Q. This is done by analyzing the regression residuals. These contributions are, in general, magnitude- and distance-dependent. Next, these contributions are divided into randomness and uncertainty by considering the partition of each parameter's variability between randomness and uncertainty. Finally, all contributions to randomness (including modeling randomness) are combined to obtain the total randomness. Similarly, all contributions to uncertainty are combined to obtain the total uncertainty.

Figures E-11 through E-22 illustrate the various contributions to randomness and uncertainty for the five spectral frequencies and for peak acceleration, for magnitude 6.5. There is only a moderate dependence on distance, except for 10 and 25 Hz where the contribution of κ decreases with increasing distance. Figures E-23 and E-24 illustrate the variation of the total randomness and total uncertainty with magnitude.

We develop a simplified characterization for the total randomness as follows. Distance dependence of the randomness is ignored and the values at 10 km are applied to all distances (this is slightly conservative). Magnitude dependence is characterized by using one value of σ_r for M<6, another value for M>6.5, and a linear transition between magnitudes 6 and 6.5. These values are shown in Table E-8.

The total uncertainty is characterized by one value of σ_U, which is calculated as the average of the values for magnitudes 6.0 and 6.5, for a distance of 10 km. These values are shown in Table E-9.

To characterize uncertainty in a manner that is compatible with most seismic-hazard analysis software (e.g., EPRI, 1986), the total uncertainty about the median attenuation function is represented by multiple attenuation functions (with associated weights). We construct these attenuation functions by characterizing the uncertainty as a discrete distribution, as described in Section 9.3.2.1 of the EPRI-DOE study (EPRI, 1993). Because we treat the total uncertainty as independent of magnitude and distance, this discrete distribution translates into multiple alternative

values of coefficient C_i in Equation E-18. These values are shown as $C_{1,1}$ through $C_{1,4}$ in Table E-7, with their associated weights.

The weights for each coefficient were calculated assuming that uncertainty is normally-distributed with respect to ln (ground motion), with a standard deviation as listed in Table E-9. This is a standard assumption for ground motion variability. The normal distribution was then represented with four discrete values and associated weights, the values and weights being chosen so that the first four moments of the normal distribution were maintained. These values, in terms of standard deviates of the normal distribution, are ± 0.74 and ± 2.33 with weights of 0.454 and 0.046, respectively. The corresponding coefficient values are shown in Table E-7.

Modification for Fault Rupture Distance. The results described up to this point assume that all seismic energy emanates from a point source. For magnitude 6, effects associated with the size of the fault rupture (as well as scaling effects of the type considered by Joyner, 1984), become moderately important. In these situations, distance is best characterized by the shortest distance to the fault rupture.

To obtain attenuation functions in terms of fault-rupture distance, we utilize a result obtained using an extended-rupture version of the stochastic model (Toro and McGuire, 1991). The effect of extended sources is introduced in point-source attenuation equations by replacing the terms in ln(R) in Equation E-18 with $\ln[R_f+0.006\exp(m_{Lg})]$, where m_{Lg} is the magnitude scale used in the central and eastern United States and R_f is distance to the fault rupture. Converting m_{Lg} in the above expression to moment magnitude in the range of moment magnitudes between 6 and 6.5 (applying Figure 4.1 of EPRI, 1993; EPRI version of report only), one obtains $\ln[R_f+0.089\exp(0.6M)]$.

Summary of Analytical Model

The analytically-derived attenuation equations for peak acceleration and spectral velocities at 1, 2.5, 5, 10, and 25 Hz, are in the form of Equation E-18, with coefficients given in Table E-7. Each value of coefficient C_i carries an associated weight, as shown also in Table E-7.

For use with faults, the two terms in ln(R) in Equation E-18 are replaced with the quantity

$$\ln\left[R_f + 0.089\ e^{0.6M}\right] \qquad \text{(E-19)}$$

where R_f is the shortest distance to the fault rupture.

Randomness is characterized as magnitude-dependent, as shown in Table E-8. There is one value for M<6, another value for M>6.5, and a linear transition between these values for magnitudes between 6 and 6.5.

Figures E-25 through E-28 show predictions of ground motion for the analytically-derived attenuation equations, for peak acceleration and 1 Hz spectral velocity, for magnitudes 5 and 6.5. The change in slope at 100 km is related to the C_4 and C_5 coefficients in Equation (E-18).

ESTIMATES OF SPECTRA

The seven ground motion attenuation equations described above were used to calculate spectra shapes for magnitude $\bar{M}$ and distance R that were found to be the average magnitude and distance of earthquakes causing ground motions with annual exceedence probabilities in the range 10^{-3} to 10^{-4}. From evaluations of seismic hazard conducted for Rocky Flats, this ground motion is on the order of 10-20 cm/sec for 10 Hz spectral velocity (5% damping), and the associated values are $\bar{M} \approx 5.9$ and $R \approx 27$ km, corresponding to an earthquake on the Derby Fault. Note that R included the depth of the event.

Figures E-29 through E-32 show the computed spectra for dampings of 2%, 5%, 7%, and 10%, corresponding to the seven equations described above for frequencies of 25 to 1 Hz. The spectra for 5% damping ($\xi = 0.05$) were computed from the equations directly; equations for other values of ξ were computed as follows.

For frequencies $1 \leq f < 5$ Hz, the procedure of Rosenblueth (1980) was followed. This scales the spectral velocity PSV at any frequency f and damping ξ by spectral velocity at $\xi = 0.05$ by:

$$PSV\ (f, \xi) = PSV\ (f, 0.05) \left[\frac{1 + 4.9\ \xi\ f\ T}{1 + 4.9 \times 0.05\ f\ T} \right]^{-0.41} \qquad \text{(E-20)}$$

where T is strong motion duration. For frequencies of 5 Hz and above, a procedure was developed using the concept of Vanmarcke (1976) that the response is controlled by a static portion (governed by PGA) and a dynamic portion (governed by equation E-20). This procedure provides a transition to the peak ground acceleration (PGA)-controlled portion of the spectrum in a realistic way as follows:

$$PSV\ (f, \xi) = \left\{ \left(\frac{PGA}{2\ \pi\ f} \right)^2 + \left[PSV\ (f, 0.05)^2 - \left(\frac{PGA}{2\ \pi\ f} \right)^2 \right] \left[\frac{1 + 4.9\ \xi\ f\ T}{1 + 4.9 \times 0.05\ f\ T} \right]^{-0.82} \right\}^{1/2}$$

(E-21)

where the second term on the right-hand-side (involving a subtraction) should not be less than 0.

These two equations allow estimation of dampings of 2%, 7%, and 10% from the predictive equations, which were developed for 5% damping. For the assumed magnitude of 5.9 and distance of 27 km, a strong motion duration of 4.5 sec was assumed based on experience and random vibration theory. This is 7% greater than the duration of 4.2 sec estimated from random vibration theory but is considered more realistic because it includes surface waves and refracted/reflected phases. The amplification factors are not highly sensitive to duration, as illustrated in Table E-10, which summarizes ratios of spectral velocities calculated using Equations E-20 and E-21 (assuming a dynamic amplification factor of 2 for illustration purposes for Equation E-21). This illustrates that the difference in absolute predicted amplitudes for dampings other than 0.05 is small, less than one percent, which is acceptable given the overall level of uncertainty in hazard.

VERTICAL GROUND MOTIONS

The estimation of vertical ground motions is made by factoring the horizontal motions. The procedure of using a fixed factor for all frequencies, magnitudes, and distances is modified here to account for the possibility that vertical motions may be comparable to, or higher than, horizontal motions for short source-to-site distances and large magnitude events (Abrahamson and Litehiser, 1989; EPRI, 1993).

We adopt here the recommendations of EPRI (1993) for vertical-to-horizontal (V/H) ratios. These were developed for eastern North America sites, but are appropriate for the RFP which is underlain by shallow alluvium over thick layers of sedimentary rocks. Specifically, for rock motions controlled by earthquakes on the Derby fault (which includes hazards of 2×10^{-4} per year or greater), vertical motions should be assumed to be 0.7 times the horizontal motions, for all frequencies. This follows EPRI (1993, Figure 6-56) for distances beyond 20 km, which is the case for mean distances for earthquakes on the Derby fault (see Table 3-5). For soil motions the same ratio of 0.7 may be used (see EPRI, 1993, Figure 6-58) except that the ratio increases from 0.7 at 20 Hz to 1.2 at 30 Hz and above.

For rock motions controlled by earthquakes on the Golden-Boulder fault, which are those with annual probability less than 2×10^{-4}, the associated magnitudes and distances are 6.1 to 6.6 and 7 to 15 km, respectively (see Table 3-5). For rock motions generated by these close events, the V/H ratio should be assumed to be 1.0 up to 20 Hz, increasing to 1.2 at 30 Hz and higher (see EPRI, 1993, Figure 6-56). For soil motion during these earthquakes, the V/H ratio should be 0.7 up to 10 Hz, increasing to 1.5 at 20 Hz and higher. This follows the EPRI (1993, Figure 6-58) recommendations for soil motions at high amplitudes (0.5g rock PGA and higher).

These recommendations are consistent with the empirical results of Abrahamson and Litehiser (1989), who found V/H ratios for PGA that increase for larger magnitudes and shorter distances. In particular the empirical results show V/H ratio that approach or exceed 1.0 for large magnitudes and short distances, and the above recommendations for vertical motions recognize this tendency for the ground motions expected at low probability levels for Rocky Flats.

CONCLUSIONS

This study derives seven equations for estimating ground shaking in the region of the Rocky Flats plant. Three of these are based on modifying empirical equations developed by other authors for California, using modifications that represent the attenuation inherent in the Rocky Mountain region. The other four are based on a theoretical model of ground shaking that has proven useful and accurate in California to estimate ground shaking, and that has been used in all parts of the U.S. to estimate ground shaking for critical facilities. This covers the range of methods by which ground motion might be estimated, and the range of applications by a variety of authors.

The empirically-based models are given by the following three equations (repeated from earlier in the text):

$$\ln(y) = a + 1.1M + c_1(8.5-M)^{2.5} + d\ln(r) + 0.2F + g(r_o,r') + \epsilon \qquad \text{(E-4)}$$

where r is the closest distance from the site to the fault rupture surface, and the other coefficients are defined following Equation (E-4) and in Tables E-2 and E-3 of the text.

$$\log(y) = a + b(M-6) + c(M-6)^2 - 1.0 \log(r) + kr + s + \epsilon \qquad \text{(E-6)}$$
$$r = [r_o^2 + h^2]^{1/2}$$

where r_o is the closest distance from the site to the vertical projection of the rupture on the earth's surface, and the other coefficients are defined following Equation (E-6) and in Table E-4 of the text.

$$\ln(y) = \beta_o + 0.683M + \beta_1 \tanh[0.647(M - 4.7)] \qquad \text{(E-7)}$$
$$- 1.0 \ln(r) + \alpha r_o + [\beta_2 - 0.105 \ln(r_o)]S$$
$$+ 0.27F + \beta_3 \tanh[0.620D] + \epsilon$$

where r_o is the closest distance from the site to the seismogenic rupture zone and the other coefficients are defined following Equation (E-7) and in Table E-5 of the text.

The analytical method for estimating ground motions is given by the following equation:

$$\ln y = C_1 + C_2(M-6) + C_3(M-6)^2$$
$$- C_4 \ln R - (C_5-C_4) \max[\ln(R/100), 0] - C_6R + \epsilon_U + \epsilon_r$$

where R is hypocentral distance and the coefficients are given in Table E-7. Four values of C_1 are shown in Table E-7, representing four equations (with weights) expressing uncertainty in ground motion estimates. When the earthquake is characterized by a fault rupture, the ln R term in Equation E-18 is replaced by $\ln[R_f + 0.089 \exp(0.6M)]$ where M is moment magnitude of the earthquake. It should be evident that uncertainty in the average depth of earthquake energy release will result in uncertainty in ground motion through the hypocentral distance R or through the depth term h.

As discussed in the Introduction, these two ground motion models represent a range of possible models that might be used. Arguments can be made for either model being more closely representative of ground motions. In fact the two methods yield very similar estimates of seismic hazard, so the combined seismic hazard estimate is not sensitive to the weights assigned to each set of equations. Indeed, the differences among the equations come from differences in preferred forms of equations and in the range of characteristics ($\Delta\sigma$, κ, and Q) that might be associated with future earthquakes and seismic wave transmission. None of this uncertainty can be resolved with currently available information, so the uncertainty is treated explicitly with multiple models. Because none of the models is preferred, we weight each method equally in the seismic hazard calculations, i.e., we apply a total weight of 1/2 to the empirically-based equations (1/3 each), and a total weight of 1/2 to the analytically-based equations (to accomplish this, the weights of Table E-7 are multiplied by 1/2).

REFERENCES

Abrahamson, N.A. and J.J. Litehiser (1989). Attenuation of Vertical Peak Acceleration, *Bull. Seism. Soc. Am.*, 79, 549-580.

Anderson, J.G. (1991). A preliminary descriptive model for the distance dependence of the spectral decay parameter in southern California, *Bull. Seism. Soc. Am.*, 81, 2186-2193.

Anderson, J.G. and S.E. Hough (1984). A Model for the Shape of the Fourier Amplitude Spectrum of Acceleration at High Frequencies, *Bull. Seism. Soc. Am.*, 74, 1969-1993.

Atkinson, G.M. (1990). A comparison of eastern North American ground motion observations with theoretical predictions, *Seismological Research Letters*, 61, 171-180.

Bakun, W.H. and W.B. Joyner (1984). The M_L scale in central California, *Bull. Seism. Soc. Am.*, 74, 1827-1843.

Boore, D.M. (1983). Stochastic simulation of high-frequency ground motions based on seismological models of the radiated spectra, *Bull. Seism. Soc. Am.*, 73, 1865-1894.

Boore, D.M. (1986). Short-period P- and S-wave radiation from large earthquakes: implications for spectral scaling relations, *Bull. Seism. Soc. Am.*, 76(1), 43-64.

Boore, D.M. and G.M. Atkinson (1987). Stochastic prediction of ground motion and spectral response parameters at hard-rock sites in eastern North America, *Bull. Seism. Soc. Am.*, 77, 440-467.

Boore, D.M. and W.B. Joyner (1984). A note on the use of random vibration theory to predict peak amplitudes of transient signals, *Bull. Seism. Soc. Am.*, 74, 2035-2039.

Boore, D.M. and W.B. Joyner (1991). Estimation of ground motion at deep soil sites in eastern North America, *Bull. Seism. Soc. Am.*, 81, 2167-2185.

Boore, D.M., W.B. Joyner and L. Wennerberg (1992). Fitting the Stochastic ω^{-2} source model to observed response spectra in western North America: trade-offs between $\Delta\sigma$ and κ" *Bull. Seism. Soc. Am.*, 82, 1956-1963.

Brune, J.N. (1970). Tectonic stress and the spectra of seismic shear waves from earthquakes, *J. Geophys. Res.*, 75, 4997-5009.

Brune, J.N. (1971). Correction, *J. Geophys. Res.*, 76, 5002.

Bryant, B., L.W. McGrew, and R. Wobus (1981). Geologic map of the Denver 1° x 2° quadrangle, north-central Colorado, U.S. Geological Survey, Miscellaneous Investigations Map M-1163, Scale 1:250,000.

Bungum, H., A. Dahle, G. Toro, R. McGuire and O.T. Gudmestad (1992). Ground motions from intraplate earthquakes, *Proc.*, Tenth World Conference on Earthquake Engineering, Balkema, Rotterdam, pp. 611-616.

Campbell, K.W. (1981). A ground motion model for the central United States based on near-source acceleration data, in *Proc., Conference on Earthquakes and Earthquake Engineering: The Eastern United States,* Ann Arbor Science Publishers, Ann Arbor, Michigan, 1, 213-232.

Campbell, K.W. (1985). Strong motion attenuation relations: a ten-year perspective, *Earthquake Spectra*, 1, 759-804.

Campbell, K.W. (1991a). Deterministic estimates of strong ground motion for the proposed low-level radioactive waste repository, Hudspeth County, Texas, Report Prepared for the Texas Low-Level Radioactive Waste Disposal Authority, Dames and Moore, Evergreen, Colorado.

Campbell, K.W. (1991b). The effect of anelastic attenuation on the attenuation of peak strong-motion parameters and response spectra (abstract), *Seismological Research Letters*, 62, 48.

Campbell, K.W. (1993). Empirical prediction of near-source ground motion from large earthquakes, in *Proc., International Workshop on Earthquake Hazard and Large Dams in the Himalaya*, the Indian National Trust for Art and Cultural Heritage (INTACH), January 15-16, 1993, New Delhi.

Dahle, A., H. Bungum and L.B. Kvamme (1990). Attenuation models inferred from intraplate earthquake recordings, *Earthquake Engineering and Structural Dynamics*, 19, 1125-1141.

Ebasco (1991). EG&G Rocky Flats line RFD-1, (unpublished seismic refection profile, processed by Vector Seismic Data Processing Inc.)

EPRI (1986). *Seismic Hazard Methodology for the Central and Eastern United States*. Technical Report NP-4726-A, Electric Power Research Institute, 1, Part 1: Methodology, 1, Part 2: Theory, 2: EQHAZARD Programmer's Manual, 3: EQHAZARD User's Manual, 4: Applications, 5 through 10: Tectonic Interpretations, 11: Nuclear Regulatory Commission Safety Review.

EPRI (1993). *Guidelines for Determining Design Basis Ground Motions*. Rept. TR-102293, Electric Power Research Inst., Palo Alto, California, Prepared for the Early Site Permit Demonstration Program (ESPDP), 5 volumes.

Gupta, I.N., K.L. McLaughlin, R.A. Wagner, R.S. Jih and T.W. McElfresh (1989). *Seismic wave attenuation in eastern North America*, Report NP-6304, Electric Power Research Inst., Palo Alto, California.

Hanks, T.C. and H. Kanamori (1979). A moment magnitude scale, *J. Geophys. Res.*, 84, 2348-2350.

Hanks, T.C. and R.K. McGuire (1981). Character of high-frequency ground motion, *Bull. Seism. Soc. Am.*, 71, 2071-2095.

Herrmann, R.B. (1985). An extension of the random vibration theory estimates of strong ground motion to large distances, *Bull. Seism. Soc. Am.*, 75, 1447-1453.

Hutton, L.K. and D.M. Boore (1987), The M_L scale in southern California, *Bull. Seism. Soc. Am.*, 77, 2074-2094.

Joyner, W.B. (1984). A scaling law for the spectra of large earthquakes, *Bull. Seism. Soc. Am.*, 74, 1167-1188.

Joyner, W.B. (1990). Memo from W.B. Joyner of the U.S. Geological Survey, Menlo Park, California, to E.V. Leyendecker of the U.S. Geological Survey, Golden, Colorado, dated April 11, 1990.

Joyner, W.B. and D.M. Boore (1988). Measurement, characterization, and prediction of strong ground motion, in *Proc., Conference on Earthquake Engineering and Soil Dynamics II - Recent Advances in Ground-Motion Evaluation*, Ed. by J.L. Von Thun, ASCE, New York, Geot. Special Pub. No. 20, 43-102.

McGuire, R.K., G.R. Toro and W.J. Silva (1988). *Engineering model of earthquake ground motion for eastern North America*, Rept. NP-6074, Electric Power Research Inst., Palo Alto, California.

Nuttli, O.W. (1973). Seismic wave attenuation and magnitude for eastern North America, *J. Geophys. Res.*, 78, 876-885.

Nuttli, O.W. (1986). Yield estimates of Nevada test site explosions obtained from seismic Lg waves, *J. Geophys. Res.*, 91, 2137-2151.

Ou, G.B. and R.B. Herrmann (1990). A statistical model for ground motion produced by earthquakes at local and regional distances, *Bull. Seism. Soc. Am.*, 80, 1397-1417.

Pakiser, L.C and W.D. Mooney (1989). Geophysical framework of the coterminous United States and adjacent Canada, *Geol. Soc. Am.*, Memoir 72, Boulder, Colorado.

Prodehl, C. and P.W. Lypman (1989). Crustal structure of the Rocky Mountain region, Chapter 14 of Geophysical Framework of the continental United States, L.C. Pakisir and W.D. Mooney, Editors, *Geol. Soc. Am.*, Memoir 172.

Rosenblueth, E. (1980). Characteristics of Earthquakes, In E. Rosenblueth, editor, *Design of Earthquake Resistant Structures*, chapter 1, Wiley.

Sadigh, K. (1992). Telephone conversation between K. Sadigh of Geomatrix Consultants and K.W. Campbell of EQE International, Inc., on September 16, 1992.

Sadigh, K., J. Egan and R. Youngs (1986). Specification of ground motion for seismic design of long period structures (abstract), *Earthquake Notes*, 57, 13 [attenuation relationships are documented in Joyner and Boore, 1988].

Silva, W.J. (1993). Factors controlling strong ground motions and their associated uncertainties," *ASCE Symposium on High Level Nuclear Waste Repositories*, 132-161.

Silva, W.J. (1993). Telephone conversation between W.J. Silva of Pacific Engineering, Inc. and K.W. Campbell of EQE International, Inc., on January 25, 1993.

Silva, W.J. and R.B. Darragh (1993). *Engineering characterization of earthquake strong ground motion recorded at rock sites*, Electric Power Research Inst., EPRI TR-102262, Palo Alto, California.

Singh, S. and R.B. Herrmann (1983). Regionalization of crustal Q in the continental United States, *J. Geophys. Res.*, 88, 527-538.

Somerville, P.G., J.P. McLaren, L.B. LeFevre, R.W. Burger and D.V. Helmburger (1987). Comparison of source scaling relations of eastern and western North American earthquakes, *Bull. Seism. Soc. Am.*, 77, 322-346.

Toro, G.R. and R.K. McGuire (1987). An investigation into earthquake ground motion characteristics in eastern North America, *Bull. Seism. Soc. Am.*, 77, 468-489.

Toro, G.R. and R.K. McGuire (1991). Evaluation of seismic hazard at the Paducah gaseous diffusion plant, *Proc., Third DOE Natural Phenomena Hazards Mitigation Conference*, St. Louis, Missouri, 157-165.

Vanmarcke, E.H. (1976). From Seismic Risk and Engineering Decision, Edited by C. Lomnitz and E. Rosenblueth, Elsevier Publishing Co., Amsterdam, London, New York.

Wong, I., W. Silva, R. Darragh, C. Stark, D. Wright, S. Jackson, G. Carpenter and R. Smith (1990). Site-specific ground motion predictions for a M 7 Basin and Range normal faulting earthquake in southeastern Idaho, *Proceedings, Fourth U.S. National Conference on Earthquake Engineering*, Memphis, Tennessee, 1, 617-626.

TABLE E-1

THEORETICALLY DERIVED ANELASTIC ATTENUATION COEFFICIENTS FOR CALIFORNIA AND EASTERN COLORADO

y	α_1	α_2	α'	d'
		California, Soil (Kappa=0.065)		
PGA	-0.01419	0.000950	-0.00801	-2.451
PSV(1 Hz)	-0.00642	0.0	-0.00642	-2.155
PSV(2.5 Hz)	-0.01043	0.000230	-0.00894	-2.611
PSV(5 Hz)	-0.01464	0.000650	-0.01042	-2.886
PSV(10 Hz)	-0.01658	0.001102	-0.00942	-2.713
PSV(25 Hz)	-0.01443	0.000971	-0.00812	-2.508
		California, Rock (Kappa=0.04)		
PGA	-0.01482	0.000941	-0.00870	-2.578
PSV(1 Hz)	-0.00644	0.0	-0.00644	-2.159
PSV(2.5 Hz)	-0.01023	0.000181	-0.00905	-2.630
PSV(5 Hz)	-0.01402	0.000465	-0.01100	-2.988
PSV(10 Hz)	-0.01753	0.001006	-0.01100	-3.047
PSV(25 Hz)	-0.01556	0.001001	-0.00906	-2.646
		Eastern Colorado, Soil (Kappa=0.065)		
PGA	-0.00398	0.000242	-0.00241	-1.436
PSV(1 Hz)	-0.00115	0.0	-0.00115	-1.208
PSV(2.5 Hz)	-0.00213	0.0	-0.00213	-1.383
PSV(5 Hz)	-0.00365	0.000068	-0.00321	-1.578
PSV(10 Hz)	-0.00532	0.000258	-0.00365	-1.661
PSV(25 Hz)	-0.00420	0.000257	-0.00253	-1.459
		Eastern Colorado, Rock (Kappa=0.04)		
PGA	-0.00445	0.000238	-0.00290	-1.525
PSV(1 Hz)	-0.00116	0.0	-0.00116	-1.209
PSV(2.5 Hz)	-0.00215	0.0	-0.00215	-1.387
PSV(5 Hz)	-0.00332	0.0	-0.00332	-1.598
PSV(10 Hz)	-0.00553	0.000161	-0.00449	-1.812
PSV(25 Hz)	-0.00525	0.000292	-0.00335	-1.609

TABLE E-2

COEFFICIENTS FOR THE FAULT-DISTANCE ATTENUATION RELATIONSHIP DERIVED FROM SADIGH ET AL. (1986)

y*	a	c_1	d	$\sigma_{\ln y}$ for M<6.5	$\sigma_{\ln y}$ for M≥6.5
			Soil Sites**		
PGA	-2.611	0.0	-1.75	1.26-0.14M	0.35
PSV(1 Hz)	3.075	-0.060	-1.75	1.62-0.18M	0.45
PSV(2.5 Hz)	2.486	-0.017	-1.75	1.535-0.170M	0.43
PSV(5 Hz)	1.745	0.0	-1.75	1.453-0.162M	0.40
PSV(10 Hz)	0.724	0.007	-1.75	1.332-0.148M	0.37
PSV(25 Hz)	-0.771	0.0	-1.75	1.296-0.144M	0.36
			Rock Sites		
PGA	-1.406	0.0	-2.05	1.26-0.14M	0.35
PSV(1 Hz)	3.674	-0.065	-2.05	1.62-0.18M	0.45
PSV(2.5 Hz)	3.466	-0.027	-2.05	1.535-0.170M	0.43
PSV(5 Hz)	2.962	-0.008	-2.05	1.453-0.162M	0.40
PSV(10 Hz)	2.060	0.007	-2.05	1.332-0.148M	0.37
PSV(25 Hz)	0.635	0.0	-2.05	1.296-0.144M	0.36

* PSV is in units of cm/sec; PGA is in units of g

** Soil coefficients are not used in hazard analysis, but are used to derive uncertainties in Appendix F.

TABLE E-3
VALUES OF THE REFERENCE DISTANCE r' FOR USE WITH THE FAULT-DISTANCE ATTENUATION RELATIONSHIP DERIVED FROM SADIGH ET AL. (1986)

M	r' (km)	M	r' (km)	M	r' (km)	M	r' (km)
	Soil Sites*				Rock Sites		
5.0	44.3	6.5	57.8	5.0	50.0	6.5	62.9
5.1	45.1	6.6	59.1	5.1	50.9	6.6	64.1
5.2	46.0	6.7	60.3	5.2	51.7	6.7	65.3
5.3	46.8	6.8	61.5	5.3	52.5	6.8	66.5
5.4	47.7	6.9	62.7	5.4	53.3	6.9	67.7
5.5	48.6	7.0	63.9	5.5	54.2	7.0	68.9
5.6	49.5	7.1	65.1	5.6	55.0	7.1	70.0
5.7	50.4	7.2	66.3	5.7	55.9	7.2	71.2
5.8	51.3	7.3	67.5	5.8	56.7	7.3	72.4
5.9	52.2	7.4	68.6	5.9	57.6	7.4	73.5
6.0	53.2	7.5	69.7	6.0	58.5	7.5	74.7
6.1	54.1	7.6	70.8	6.1	59.3	7.6	75.8
6.2	55.0	7.7	71.8	6.2	60.2	7.7	76.9
6.3	55.9	7.8	72.8	6.3	61.1	7.8	78.0
6.4	56.9	7.9	73.7	6.4	62.0	7.9	79.0
		8.0	74.5			8.0	80.1

* Soil coefficients are not used in hazard analysis, but are used to derive uncertainties in Appendix F.

TABLE E-4

COEFFICIENTS FOR THE FAULT-DISTANCE ATTENUATION RELATIONSHIP DERIVED FROM JOYNER AND BOORE (1988)

y*	a	b	c	k	s**	h	$\sigma_{\log y}$
PGA	0.43	0.23	0.0	-0.0012	0.0	8.0	0.28
PSV(1 Hz)	2.28	0.67	-0.17	-0.00050	0.27	4.7	0.33
PSV(2.5 Hz)	2.44	0.47	-0.13	-0.00093	0.10	5.7	0.31
PSV(5 Hz)	2.46	0.35	-0.09	-0.0014	-0.01	9.6	0.28
PSV(10 Hz)	2.16	0.25	-0.06	-0.0018	-0.02	11.3	0.28
PSV(25 Hz)	1.26	0.23	0.0	-0.0013	-0.03	8.0	0.28

* PSV is in units of cm/sec; PGA is in units of g
** s is set to zero for rock sites

TABLE E-5

COEFFICIENTS FOR THE FAULT-DISTANCE ATTENUATION RELATIONSHIP DERIVED FROM CAMPBELL (1993)

y*	β_o	β_1	β_2	β_3	β_4	β_5	$\sigma_{\ln y}$
PGA	-3.15	0.0	0.0	0.0	-0.00398	0.000242	0.50
PSV(1 Hz)	0.32	1.37	-0.41	0.57	-0.00115	0.0	0.72
PSV(2.5 Hz)	1.11	0.60	-0.46	0.12	-0.00213	0.0	0.65
PSV(5 Hz)	1.12	0.0	-0.21	0.0	-0.00365	0.000068	0.64
PSV(10 Hz)	0.14	0.0	0.08	0.0	-0.00532	0.000258	0.58
PSV(25 Hz)	-1.31	0.0	0.22	0.0	-0.00420	0.000257	0.53

* PSV is in units of cm/sec; PGA is in units of g

TABLE E-6

CRUSTAL VELOCITY MODEL

Depth Range (m)	Shear-Wave Velocity (m/sec)	Density (gm/cm^3)
0-305	1408	2.3
305-1829	1760	2.4
1829-3962	2600	2.45
3962-25,962	3580	2.73
25,962-40,962	3870	2.81
40,962-∞	4620	3.35

TABLE E-7

ATTENUATION COEFFICIENTS (SEE EQUATION E-18)

Ground Motion Measure	$C_{1,median}$	$C_{1,1}$ (0.046*)	$C_{1,2}$ (0.454)	$C_{1,3}$ (0.454)	$C_{1,4}$ (0.046)	C_2	C_3	C_4	C_5	C_6
1-Hz PSV	5.933	5.355	5.927	6.460	7.032	1.520	-0.289	1.047	0.830	8.28e-04
2.5-Hz PSV	5.822	5.193	5.845	6.452	7.104	1.136	-0.128	1.087	0.830	2.00e-03
5-Hz PSV	5.363	4.557	5.336	6.061	6.840	0.997	0.000	1.123	0.830	3.00e-03
10-Hz PSV	4.694	3.512	4.545	5.507	6.541	1.002	0.000	1.180	0.830	3.37e-03
25-Hz PSV	3.471	2.243	3.292	4.269	5.319	1.036	0.000	1.222	0.830	2.70e-03
Peak Accel.	1.249	.392	1.187	1.927	2.722	1.049	0.000	1.180	0.830	2.29e-03

* Quantities in parenthesis indicate weights for the alternative values of C_1.

TABLE E-8

CHARACTERIZATION OF RANDOMNESS
(standard deviation σ_r)

Ground-Motion Measure	$M \leq 6$	$M \geq 6.5$
1-Hz PSV	0.75	0.71
2.5-Hz PSV	0.70	0.63
5-Hz PSV	0.67	0.58
10-Hz PSV	0.68	0.58
25-Hz PSV	0.68	0.58
Peak Accel.	0.63	0.53

TABLE E-9

CHARACTERIZATION OF UNCERTAINTY
(standard deviation σ_u)

Ground-Motion Measure	σ_u
1-Hz PSV	0.36
2.5-Hz PSV	0.41
5-Hz PSV	0.49
10-Hz PSV	0.64
25-Hz PSV	0.66
Peak Accel.	0.50

Note: this uncertainty is captured by using multiple values of coefficient C_1.

TABLE E-10

RATIO OF PSV (f, ξ)/PSV (f, .05)

f	ξ	Ratio for 4.2 sec	Ratio for 4.5 sec	Percent Difference
1	0.02	1.1604	1.1675	-0.6%
1	0.07	0.9271	0.9249	0.2%
1	0.10	0.8452	0.8413	0.5%
5	0.02	1.2567	1.2615	-0.4%
5	0.07	0.9175	0.9168	0.1%
5	0.10	0.8399	0.8388	0.1%
10	0.02	1.2982	1.3015	-0.3%
10	0.07	0.9117	0.9113	0.0%
10	0.10	0.8312	0.8306	0.1%

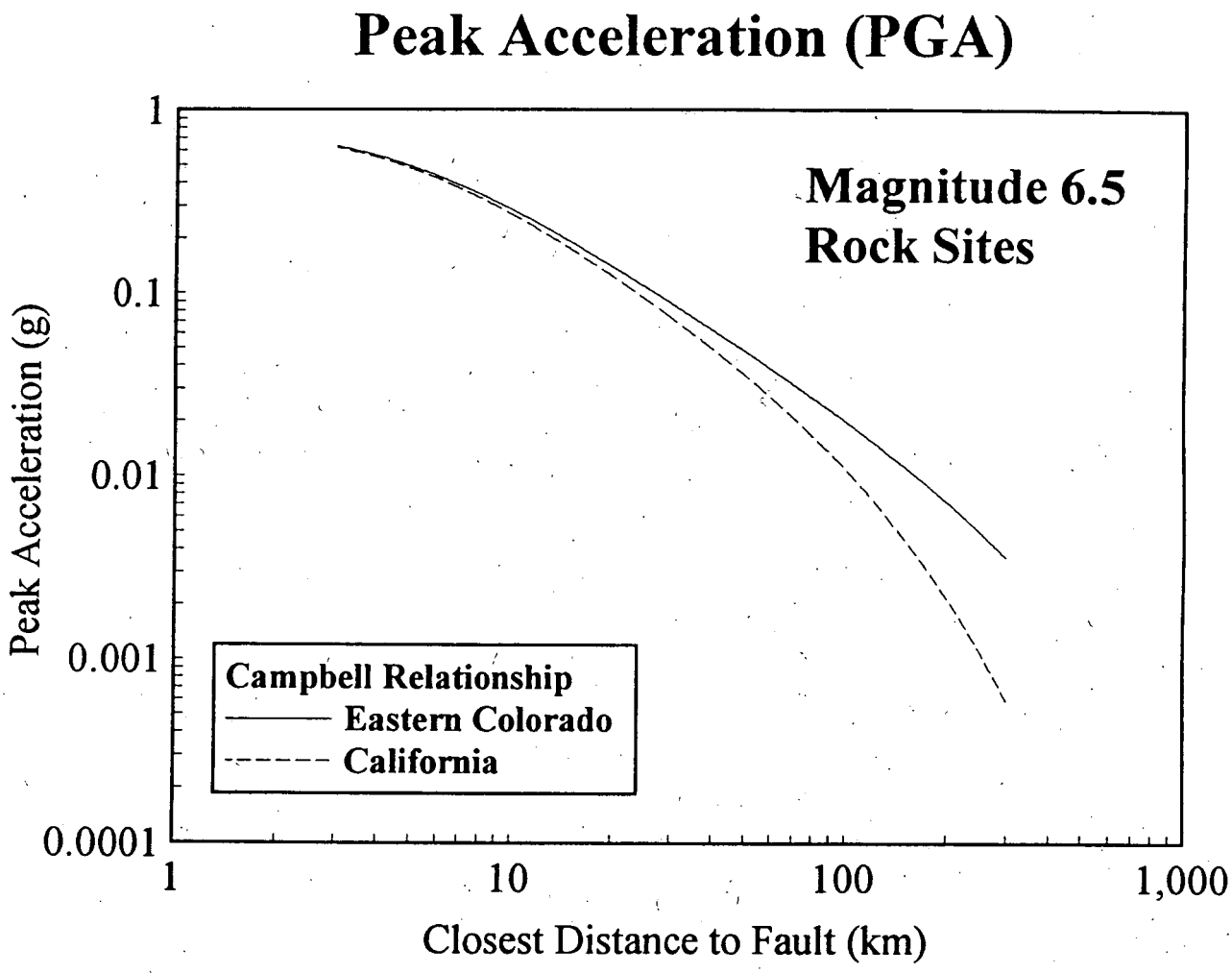

Figure E-1. Comparison of PGA attenuation for Colorado and California.

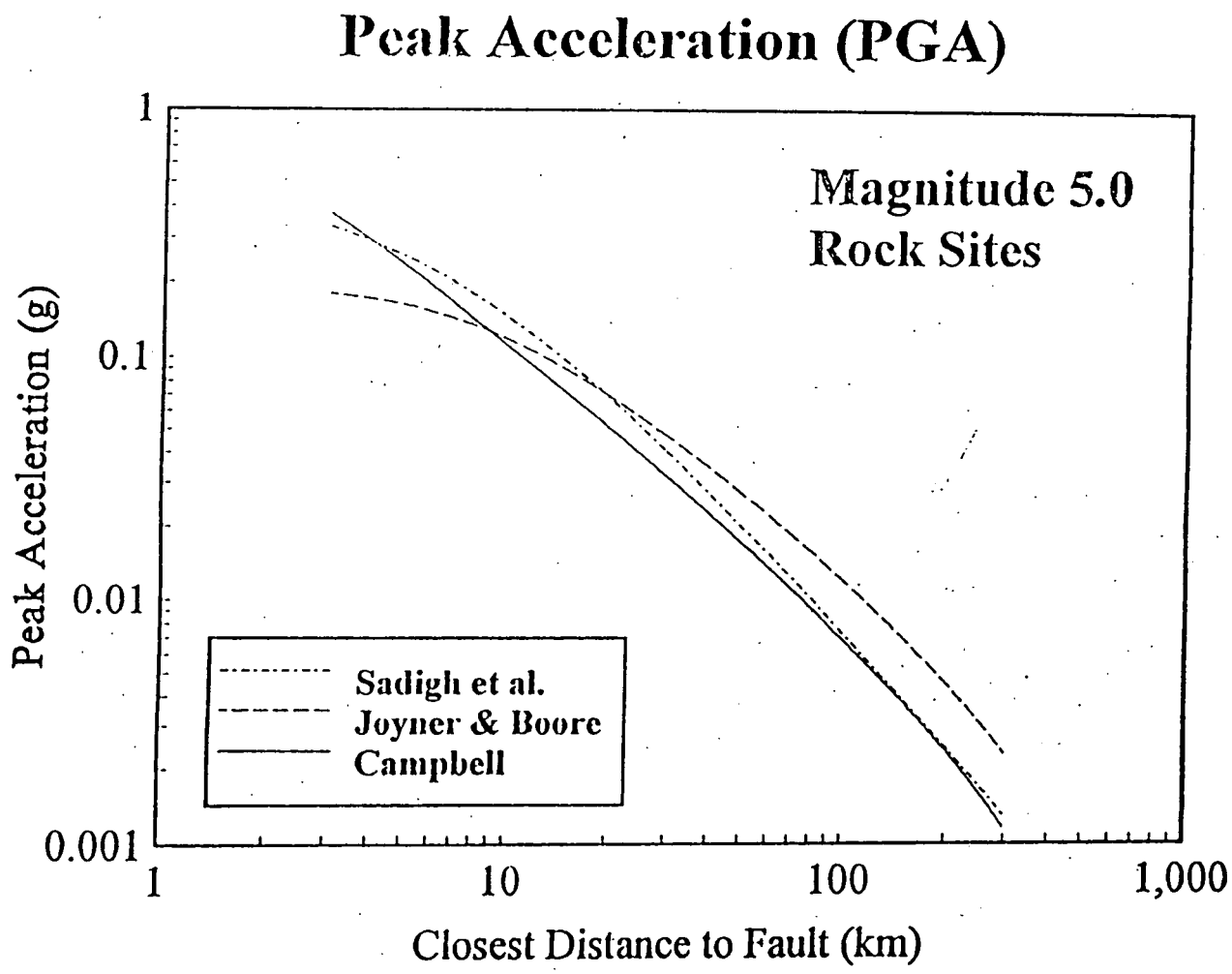

Figure E-2. Empirically based attenuation functions for rock; PGA predictions for magnitude 5.

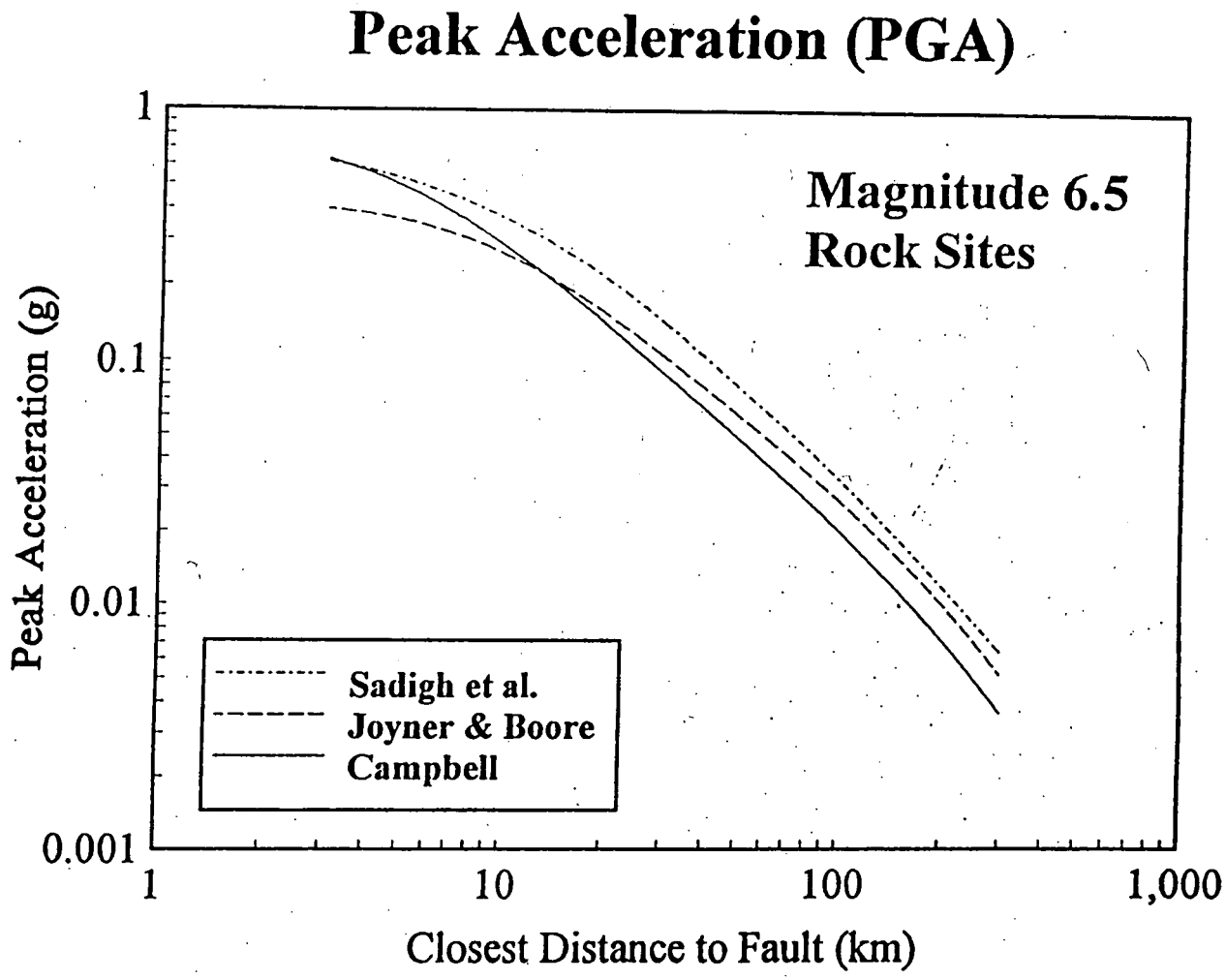

Figure E-3. Empirically based attenuation functions for rock; PGA predictions for magnitude 6.5.

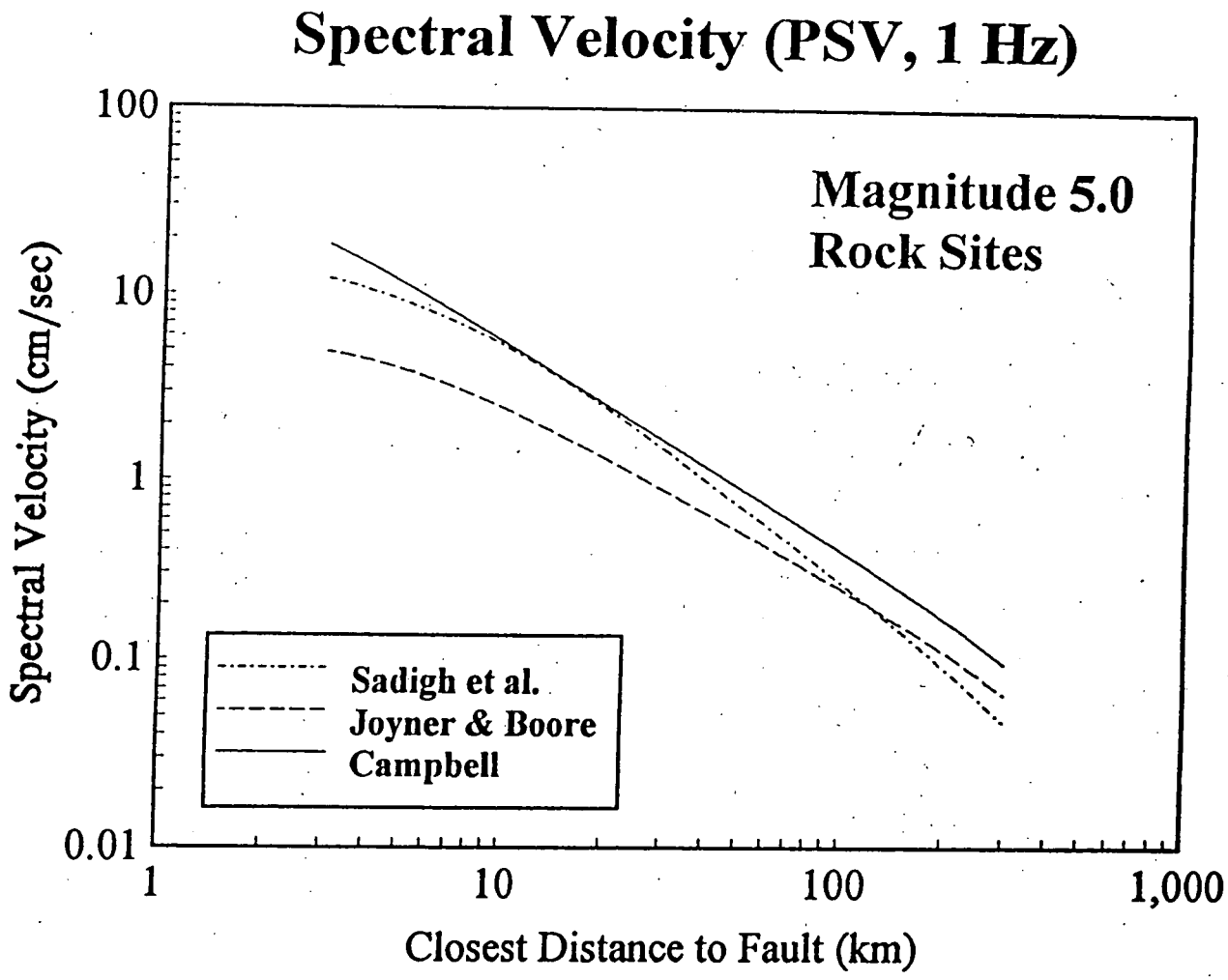

Figure E-4. Empirically based attenuation functions for rock; 1-Hz PSV predictions for magnitude 5.

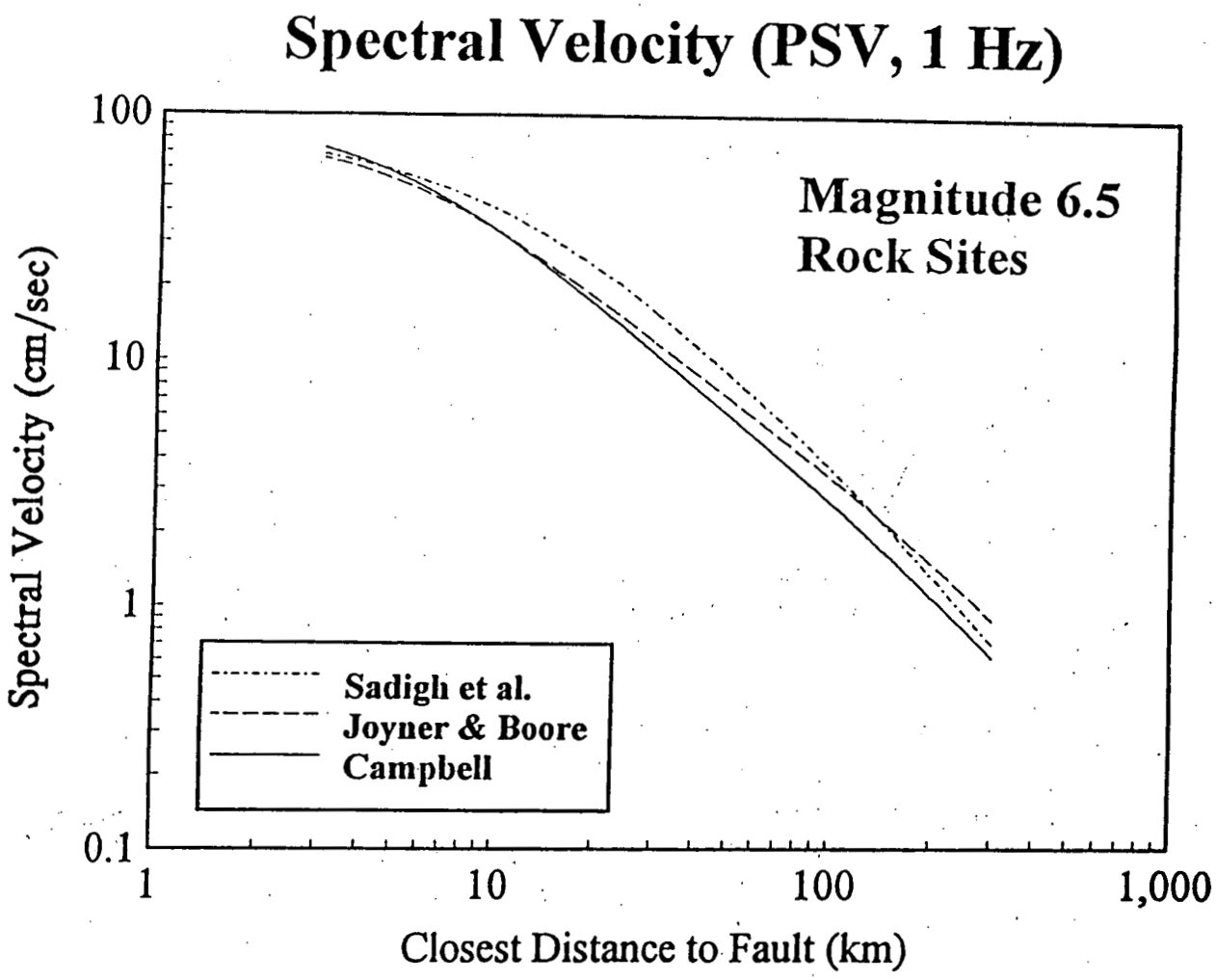

Figure E-5. Empirically based attenuation functions for rock; 1-Hz PSV predictions for magnitude 6.5.

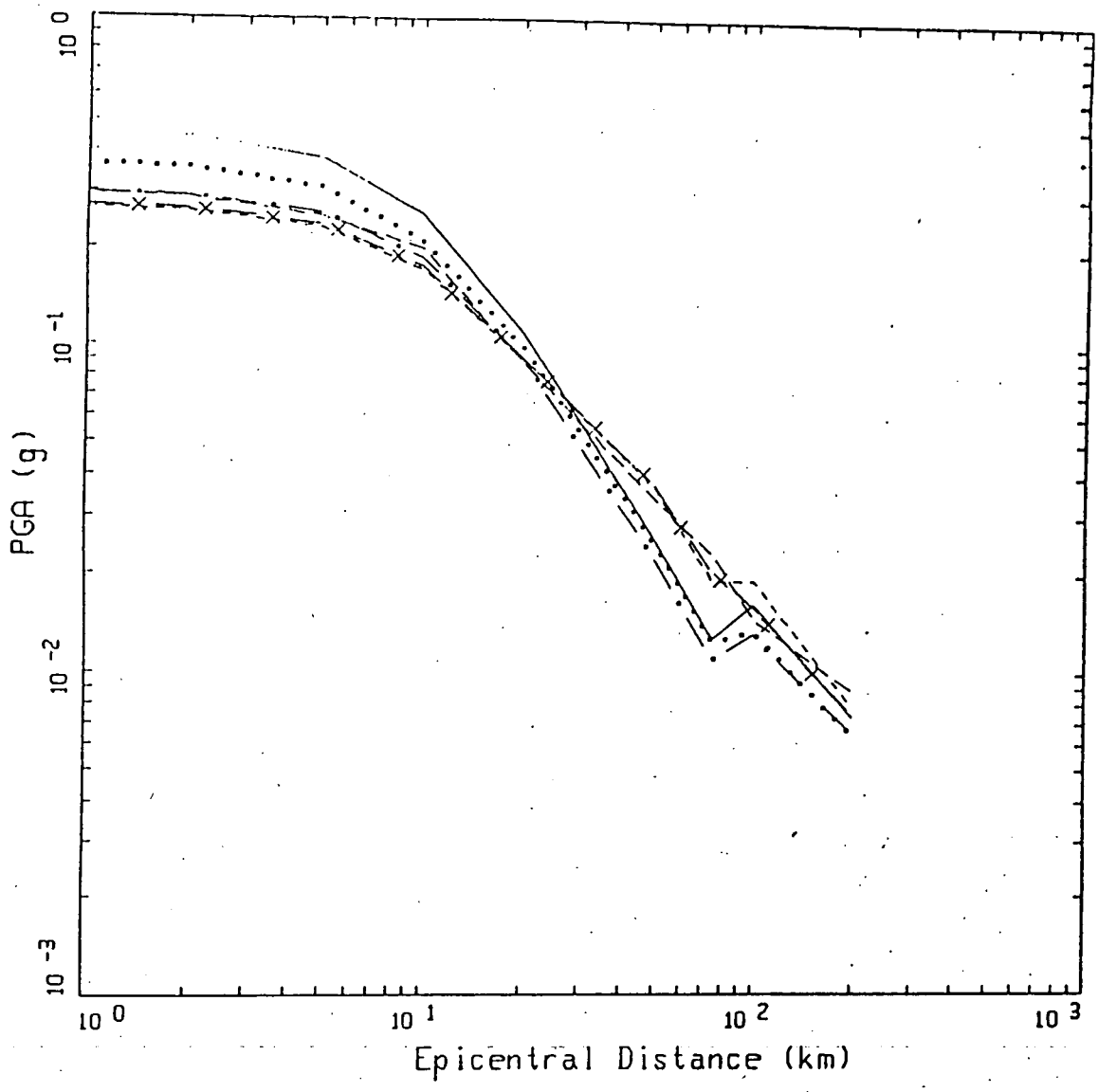

ROCKY FLATS ATTENUATION
OU & HERRMANN

LEGEND

———	M:6.5, Q:670, ETA:0.33, KAP:0.04 SEC, SD:120 BARS, H:10 KM, ROCK1 CRUST
• • • •	M:6.5, Q:670, ETA:0.33, KAP:0.04 SEC, SD:120 BARS, H:10 KM, ROCK2 CRUST
- - - - -	M:6.5, Q:670, ETA:0.33, KAP:0.04 SEC, SD:120 BARS, H:10 KM, MIDCONT CRUST
— — — -	M:6.5, Q:670, ETA:0.33, KAP:0.04 SEC, SD:120 BARS, H:9 KM, N. PLAINS CRUST
— • —	M:6.5, Q:670, ETA:0.33, KAP:0.04 SEC, SD:120 BARS, H:10 KM, C. PLAINS CRUST
— × —	M:6.5, Q:670, ETA:0.33, KAP:0.04 SEC, SD:120 BARS, H:10 KM, S. PLAINS CRUST

Figure E-6. Predicted peak accelerations using the Ou-Herrmann formulation. See text for description of crustal models.

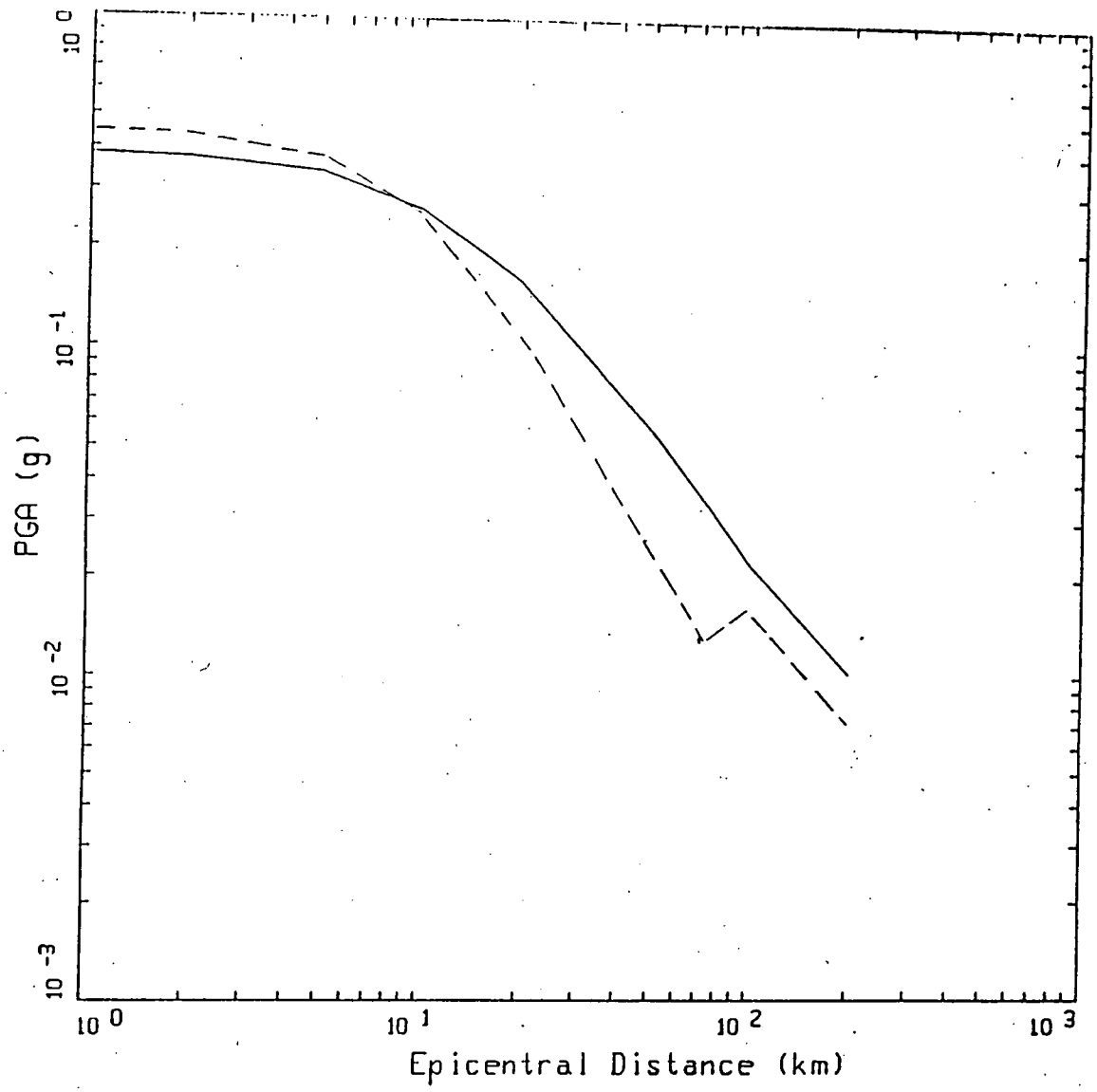

ROCKY FLATS ATTENUATION
1/R & 1/SQRT(R), 10 KM DEPTH

LEGEND

——— M=6.5, Q=670, ETA=0.33, KAP=0.04 SEC, SD=120 BARS, HERRMANN MODEL

- - - - M=6.5, Q=670, ETA=0.33, KAP=0.04 SEC, SD=120 BARS, ROCK 1 CRUST

Figure E-7. Predicted peak acceleration using the Herrmann (1985) formulation compared to predictions for the ROCK1 crust.

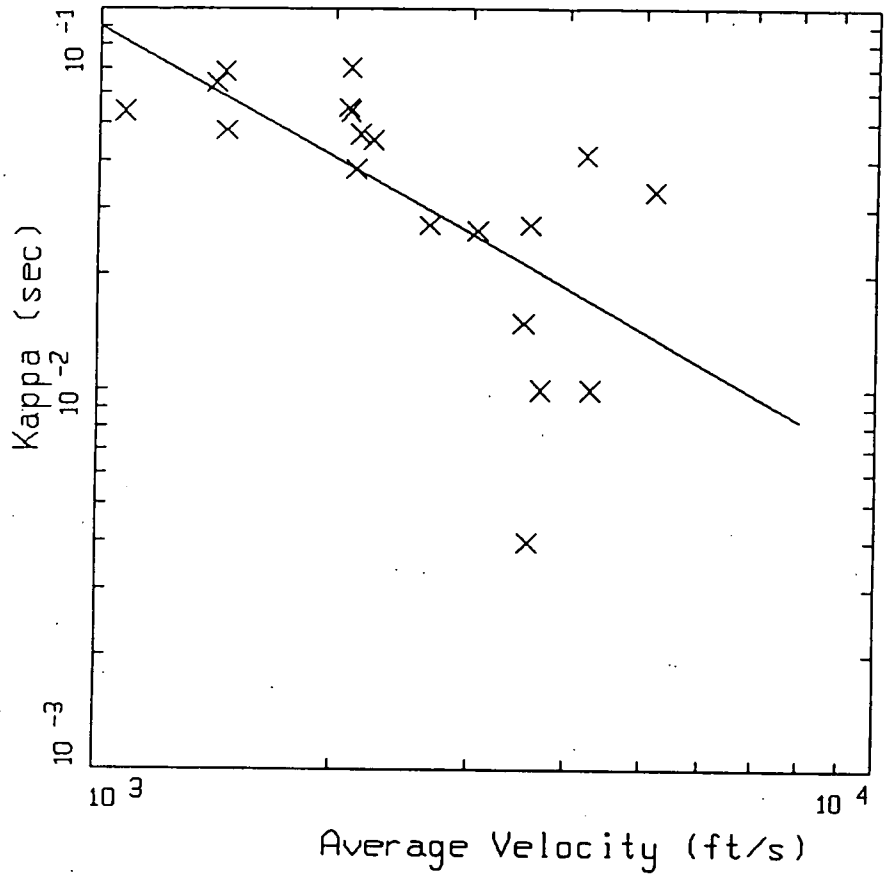

ROCK SITES (WNA)

KAPPA VS AVERAGE (OVER 100 FT) VELOCITY

LEGEND

× DATA

——— LOG(KAPPA) = 2.40939 - 1.15099 * LOG(VELOCITY IN FT/S)

Figure E-8. Kappa values plotted versus shear-wave velocities averaged over the top 100 ft for rock sites located in California.

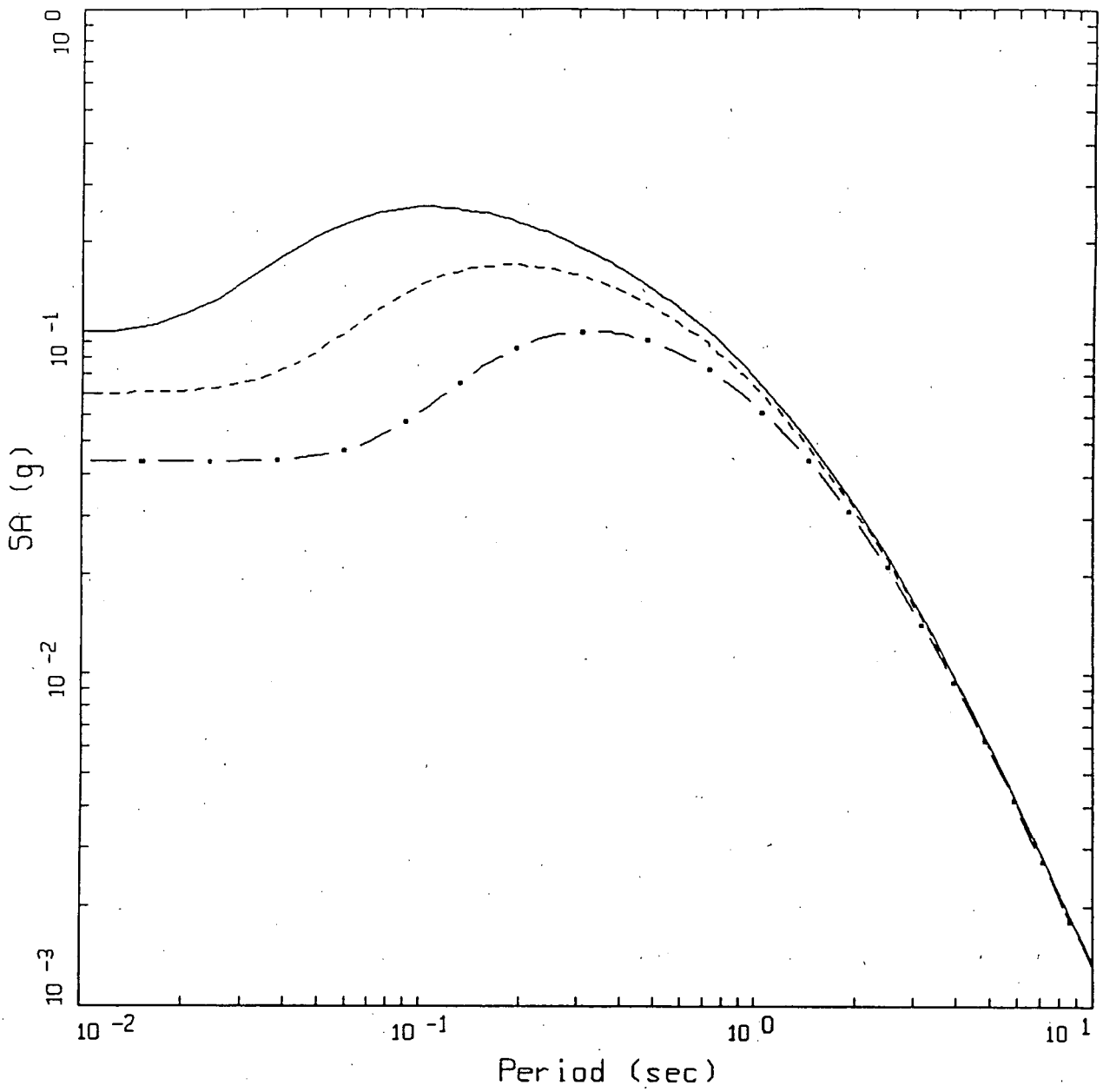

ROCKY FLATS: M=6.0, R=30 KM
SD=120 BARS, Q=670F^0.33

LEGEND

———	5 %, KAPPA=0.02 SEC
- - - - -	5 %, KAPPA=0.04 SEC
— • —	5 %, KAPPA=0.08 SEC

Figure E-9. Effects of kappa on 5% damped pseudo-relative response spectra computed using the point source stochastic model. A moment magnitude 6.0 earthquake is considered with a stress drop of 120 bars and a hypocentral distance of 30 km. The Q(f) model $670^{0.33}$.

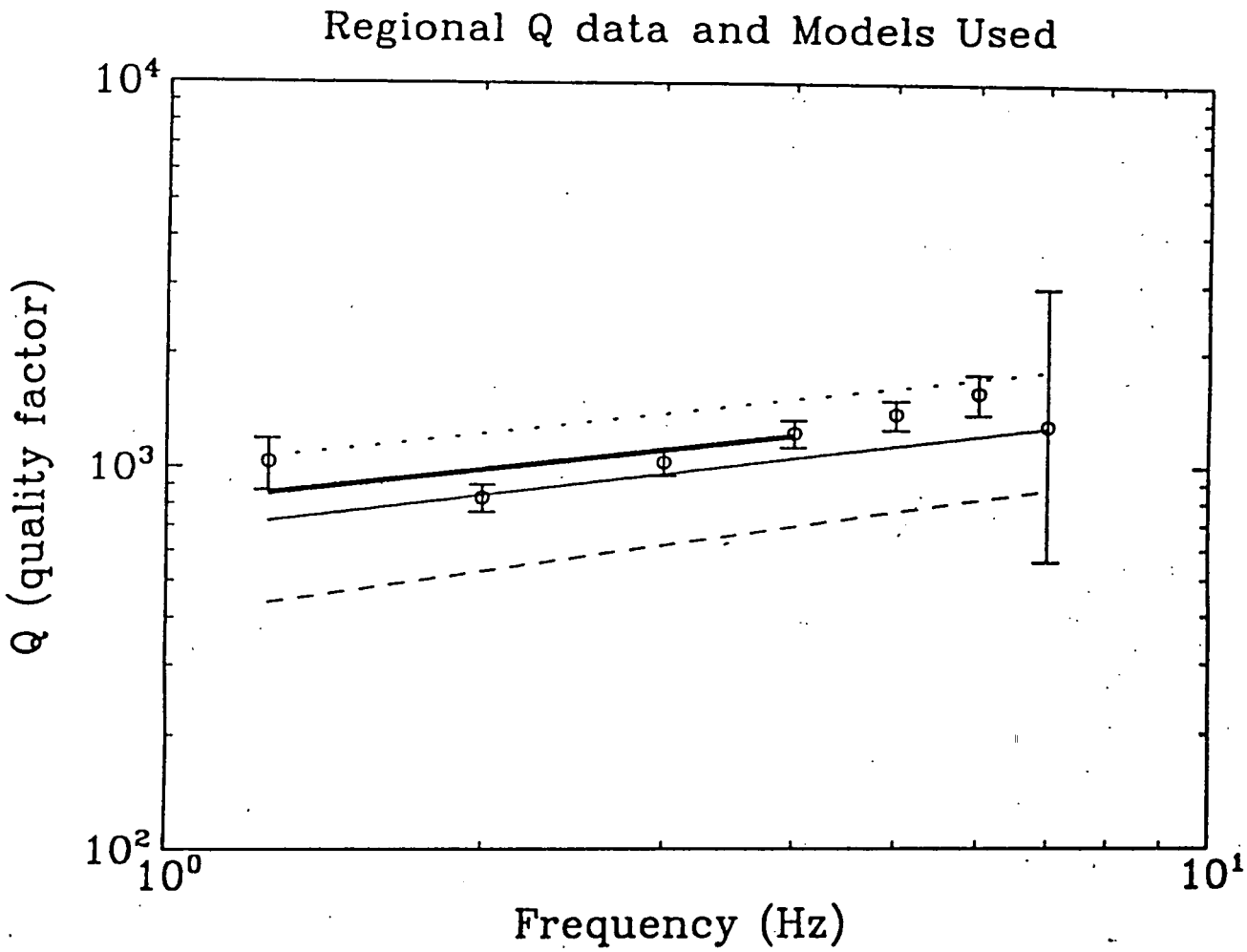

Figure E-10. Regional Q models and models used in this study. Thick line, Singh and Herrmann (1983); error bars, Gupta et al. (1989); thin lines, EPRI-DOE study and this study (used with weights of 0.2 (bottom), 0.4, and 0.4).

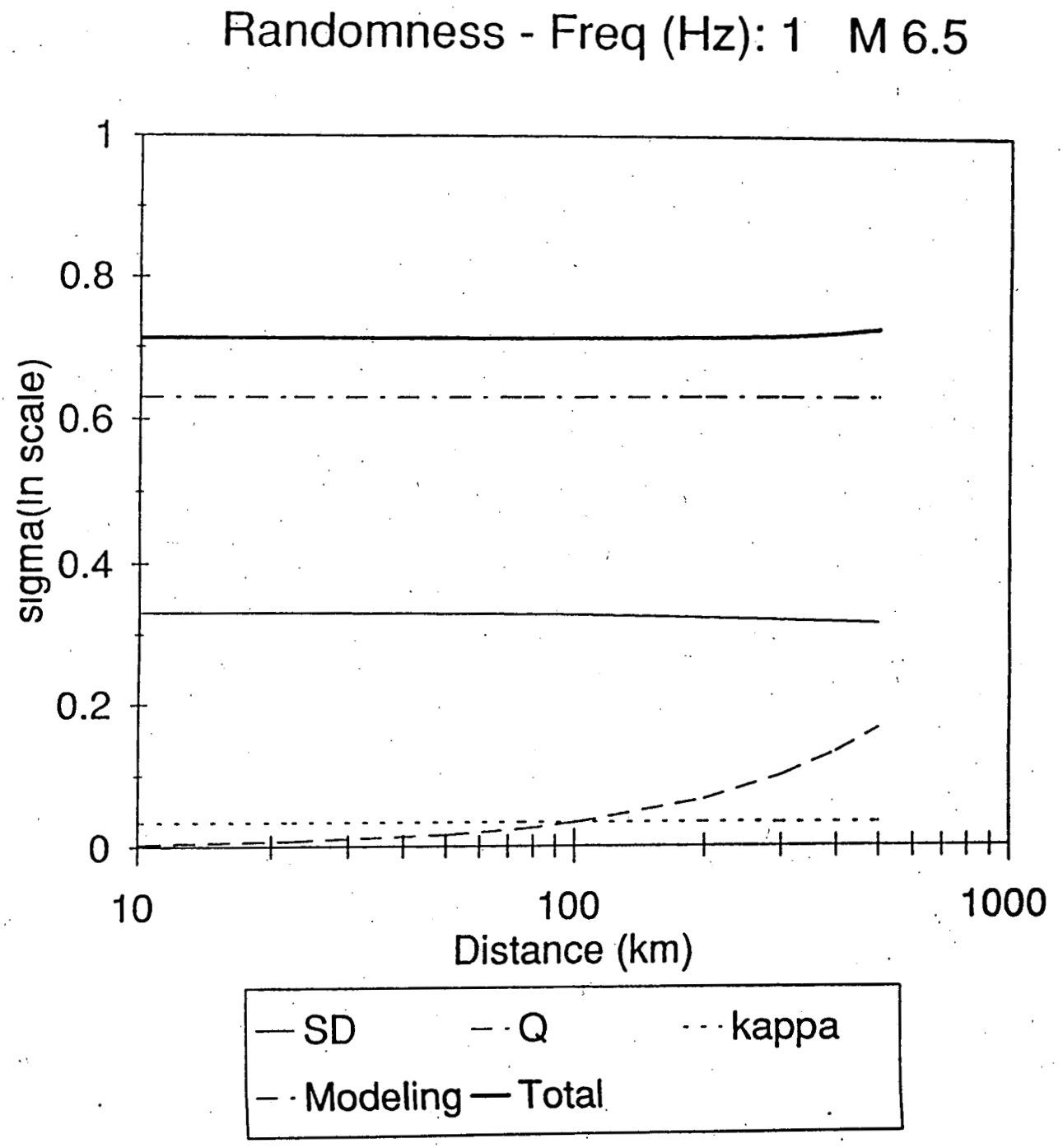

Figure E-11. Components of randomness plotted versus distance for 1-Hz PSV.

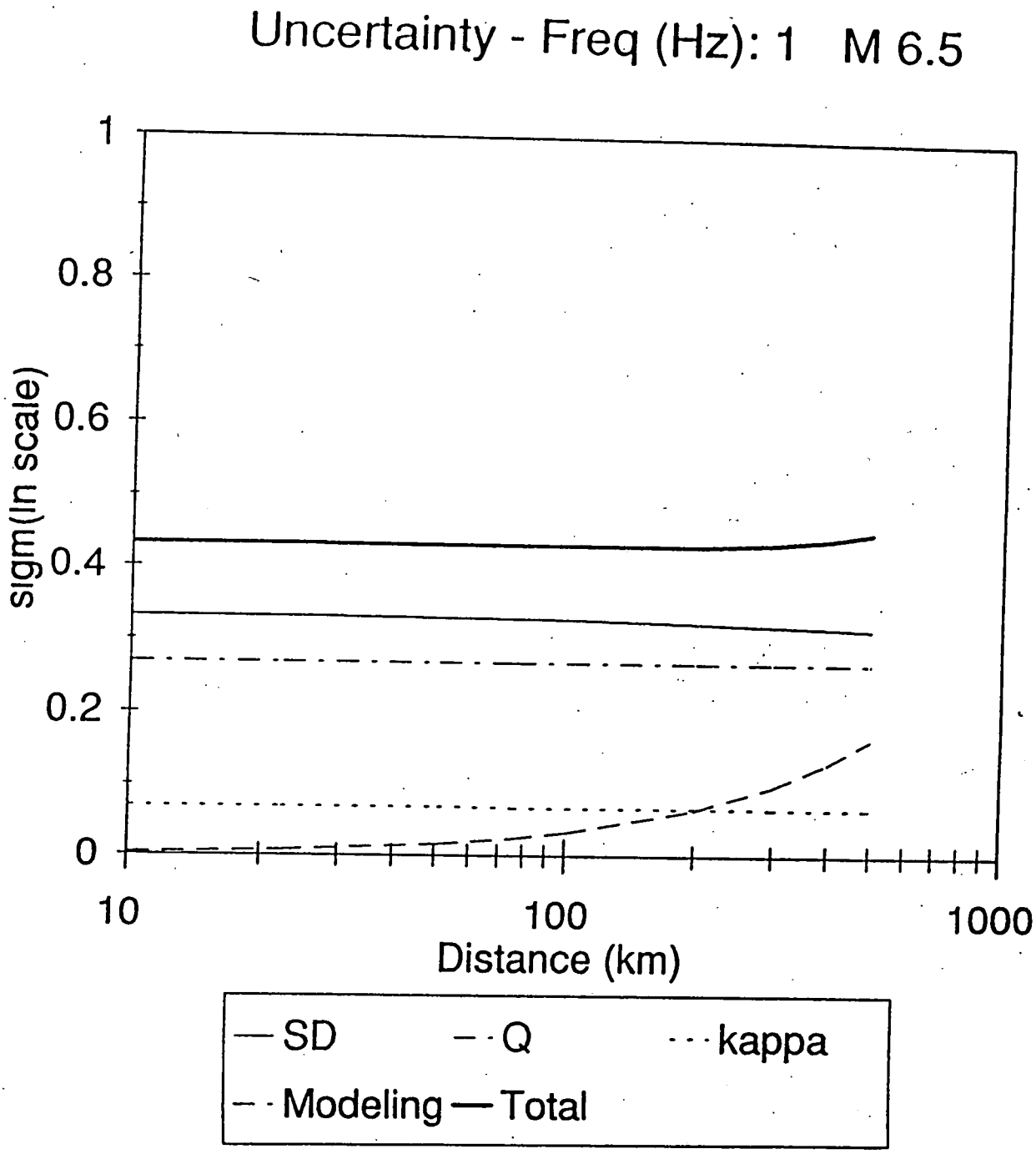

Figure E-12. Components of uncertainty plotted versus distance for 1-Hz PSV.

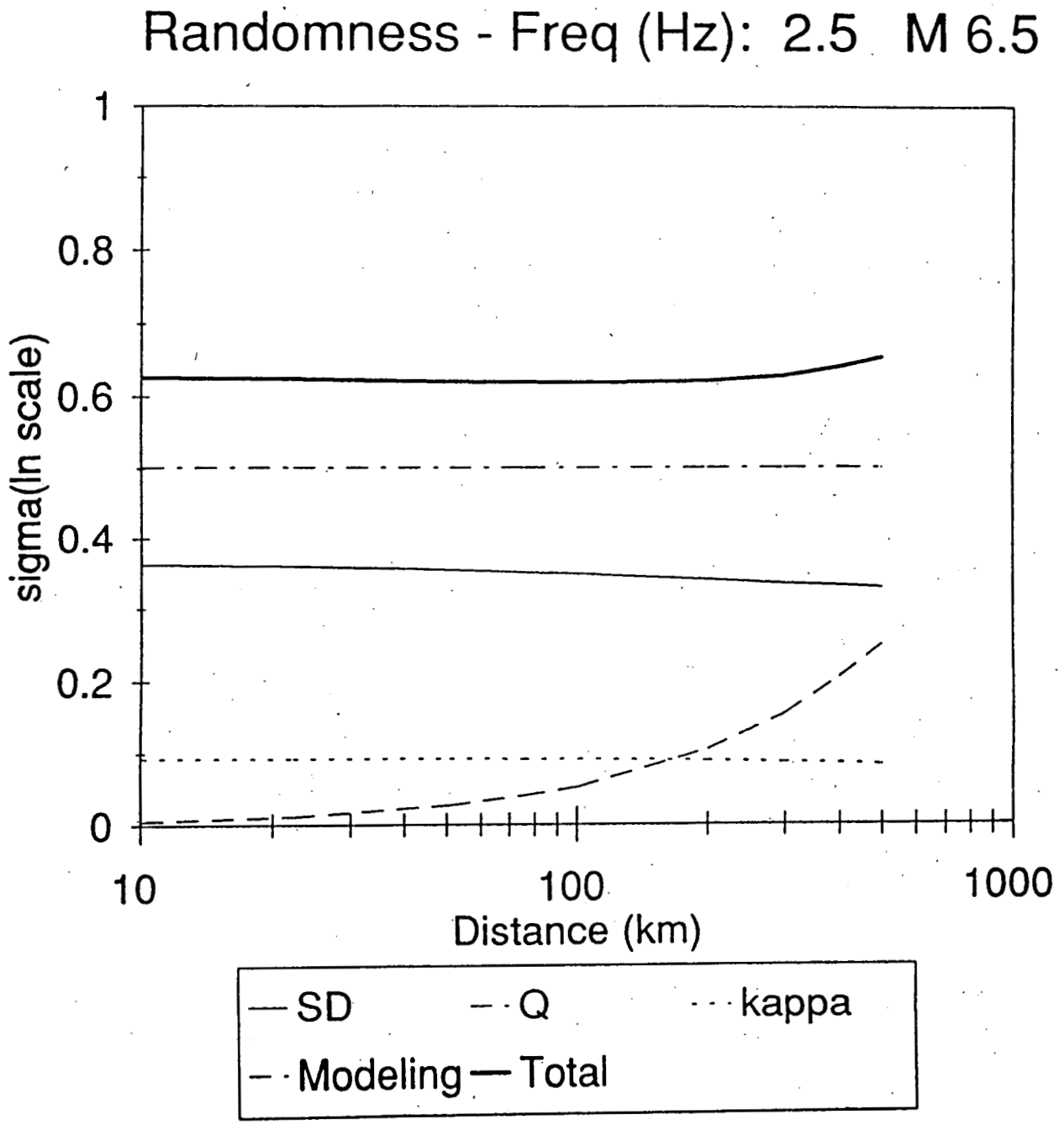

Figure E-13. Components of randomness plotted versus distance for 2.5 Hz PSV.

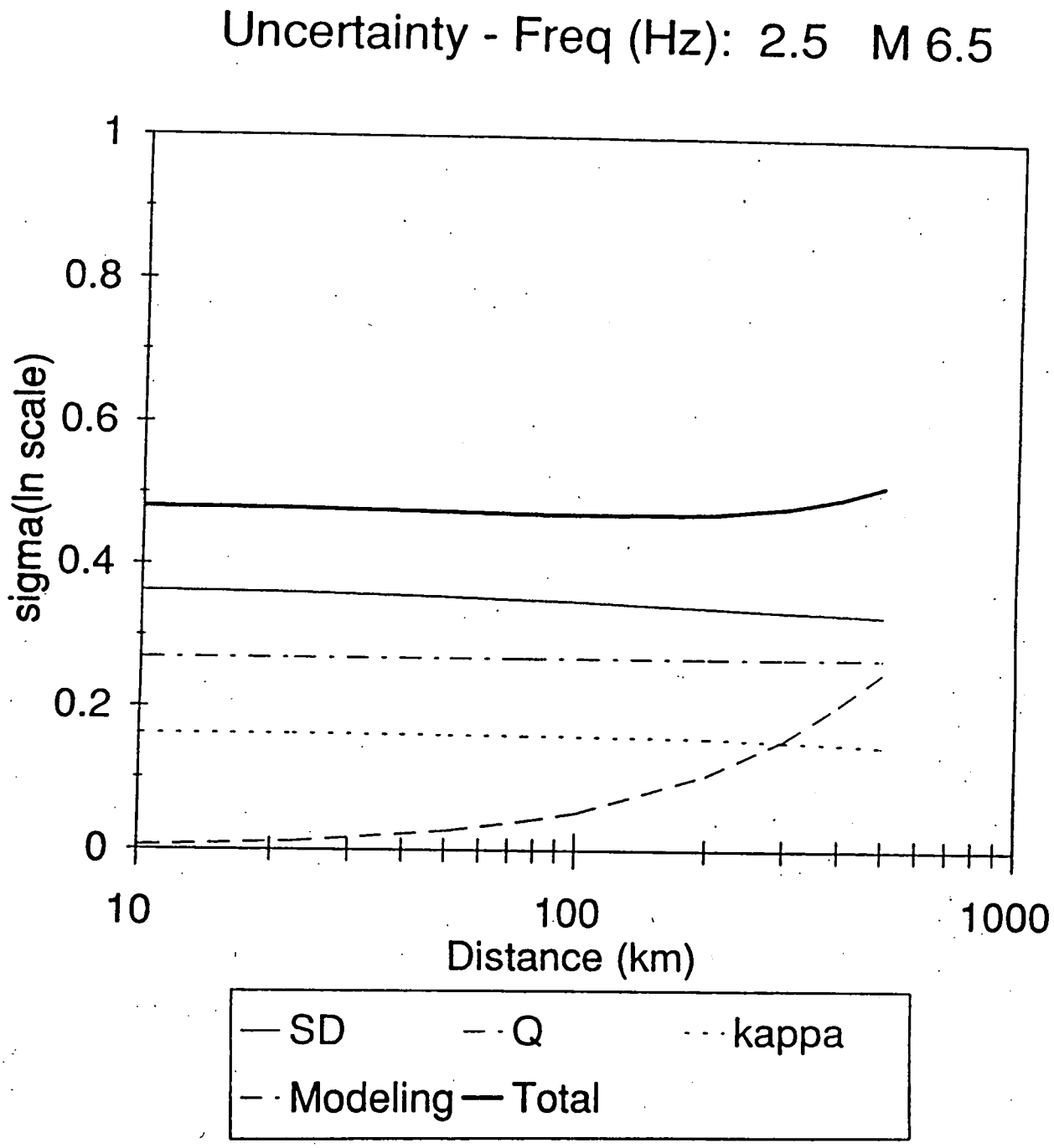

Figure E-14. Components of uncertainty plotted versus distance for 2.5 Hz PSV.

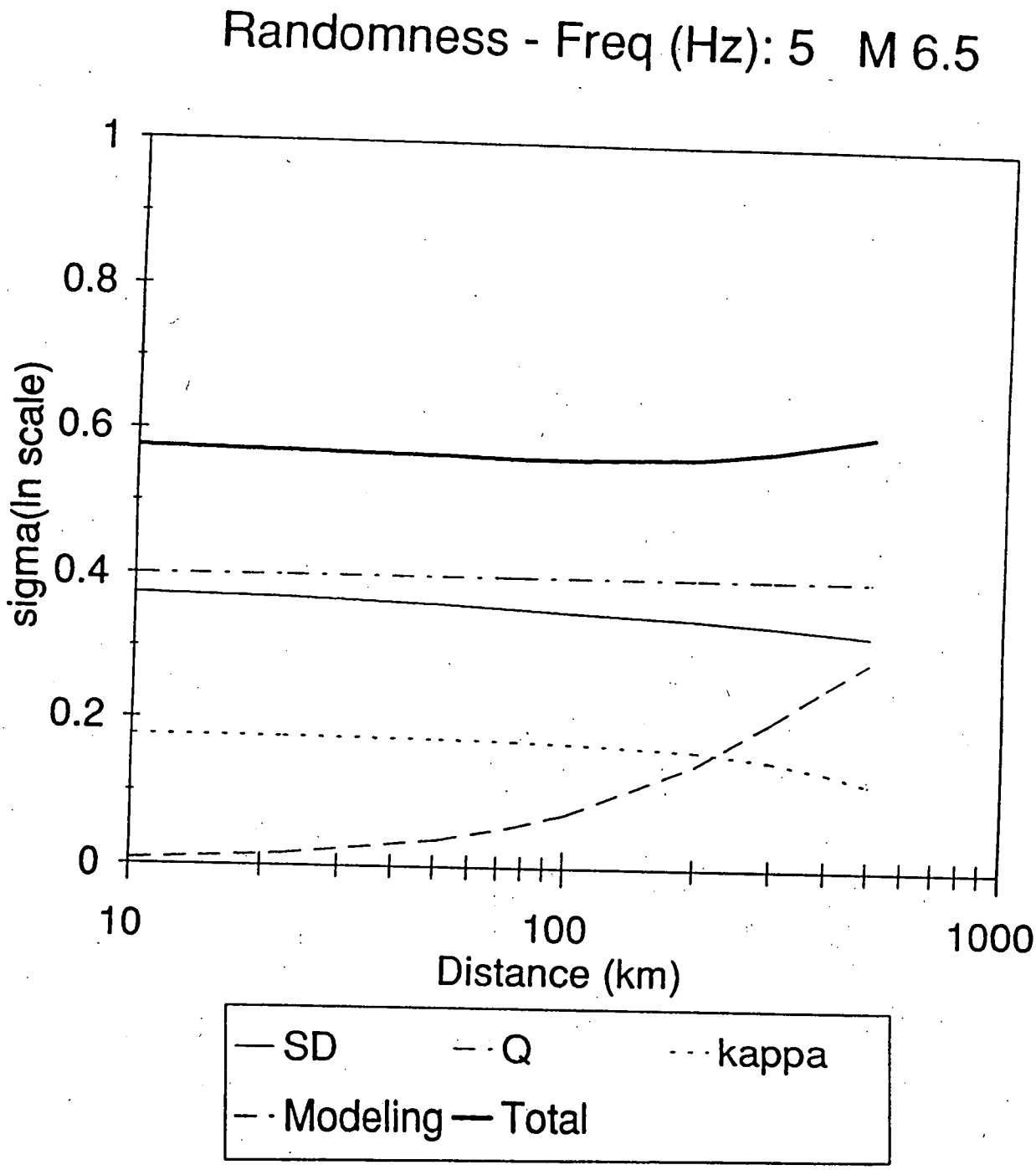

Figure E-15. Components of randomness plotted versus distance for 5 Hz PSV.

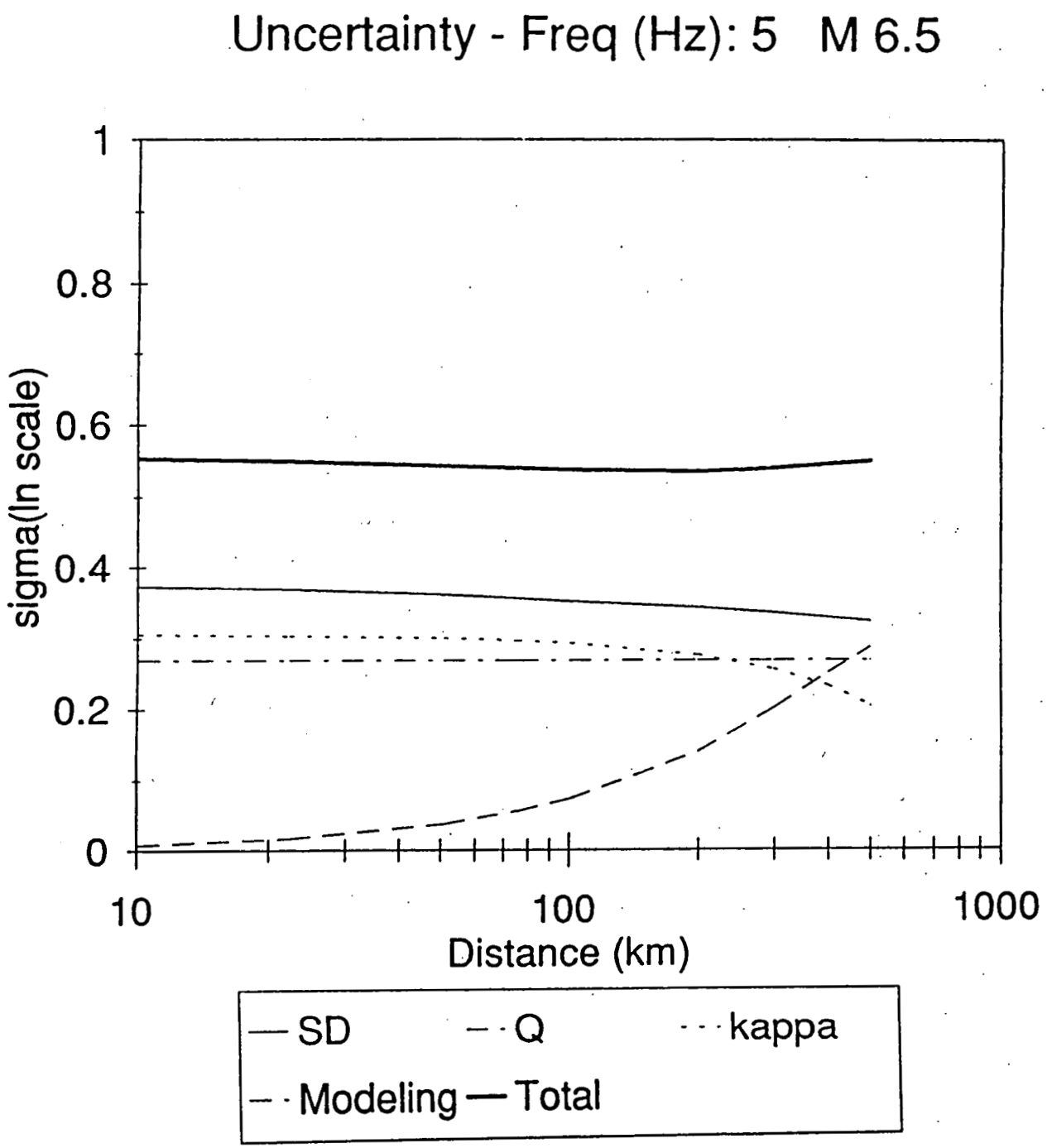

Figure E-16. Components of uncertainty plotted versus distance for 5 Hz PSV.

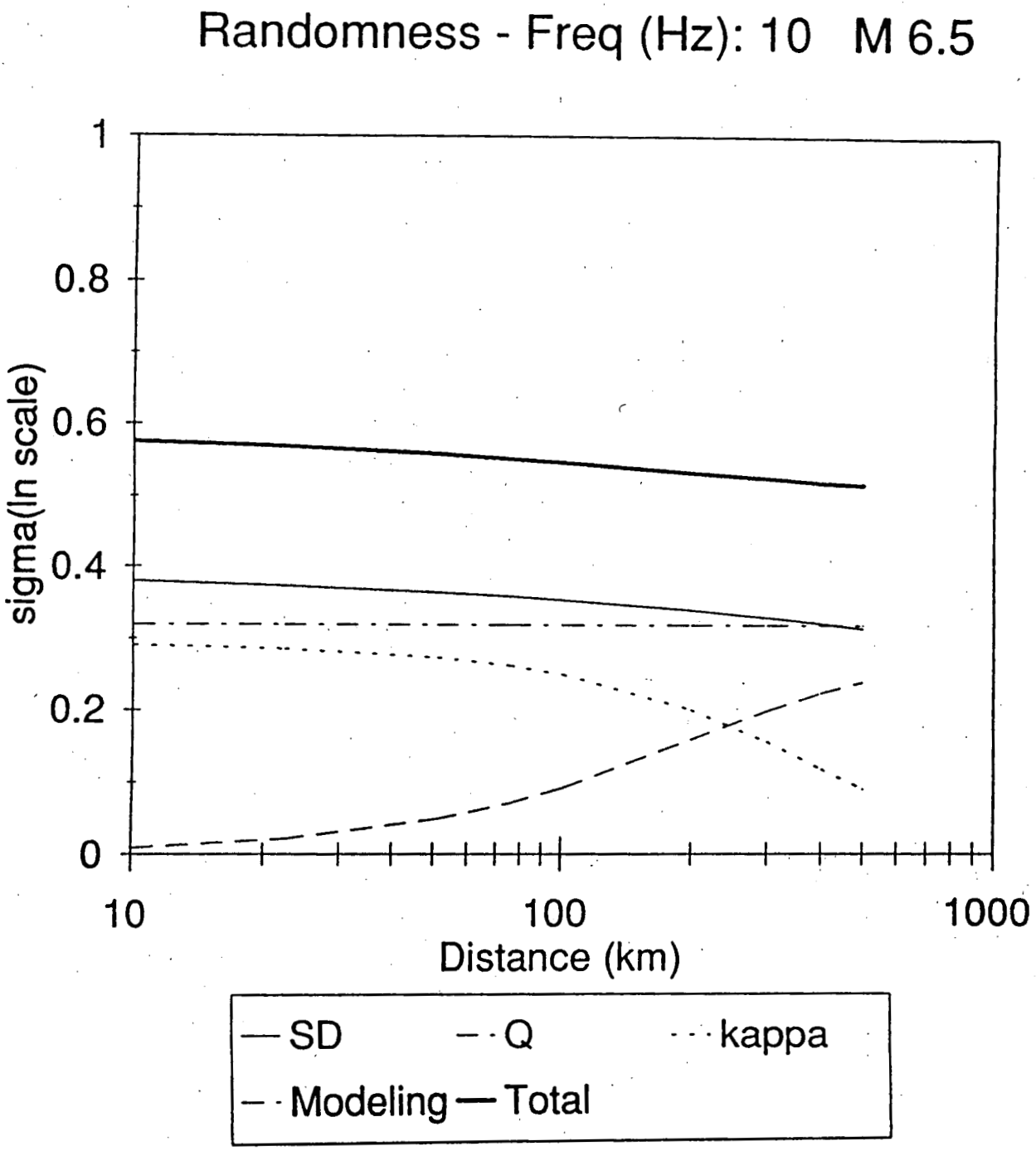

Figure E-17. Components of randomness plotted versus distance for 10 Hz PSV.

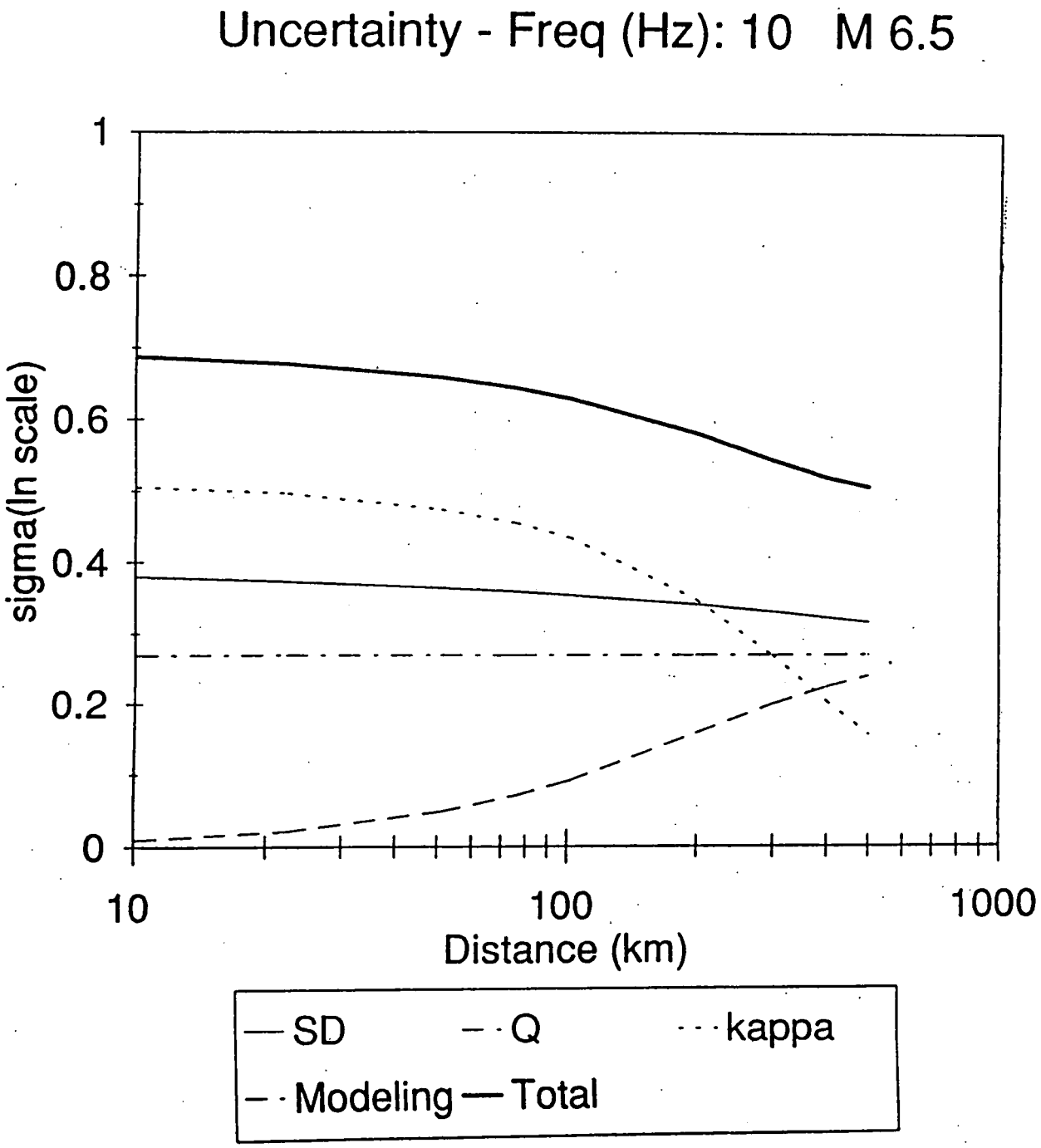

Figure E-18. Components of uncertainty plotted versus distance for 10 Hz PSV.

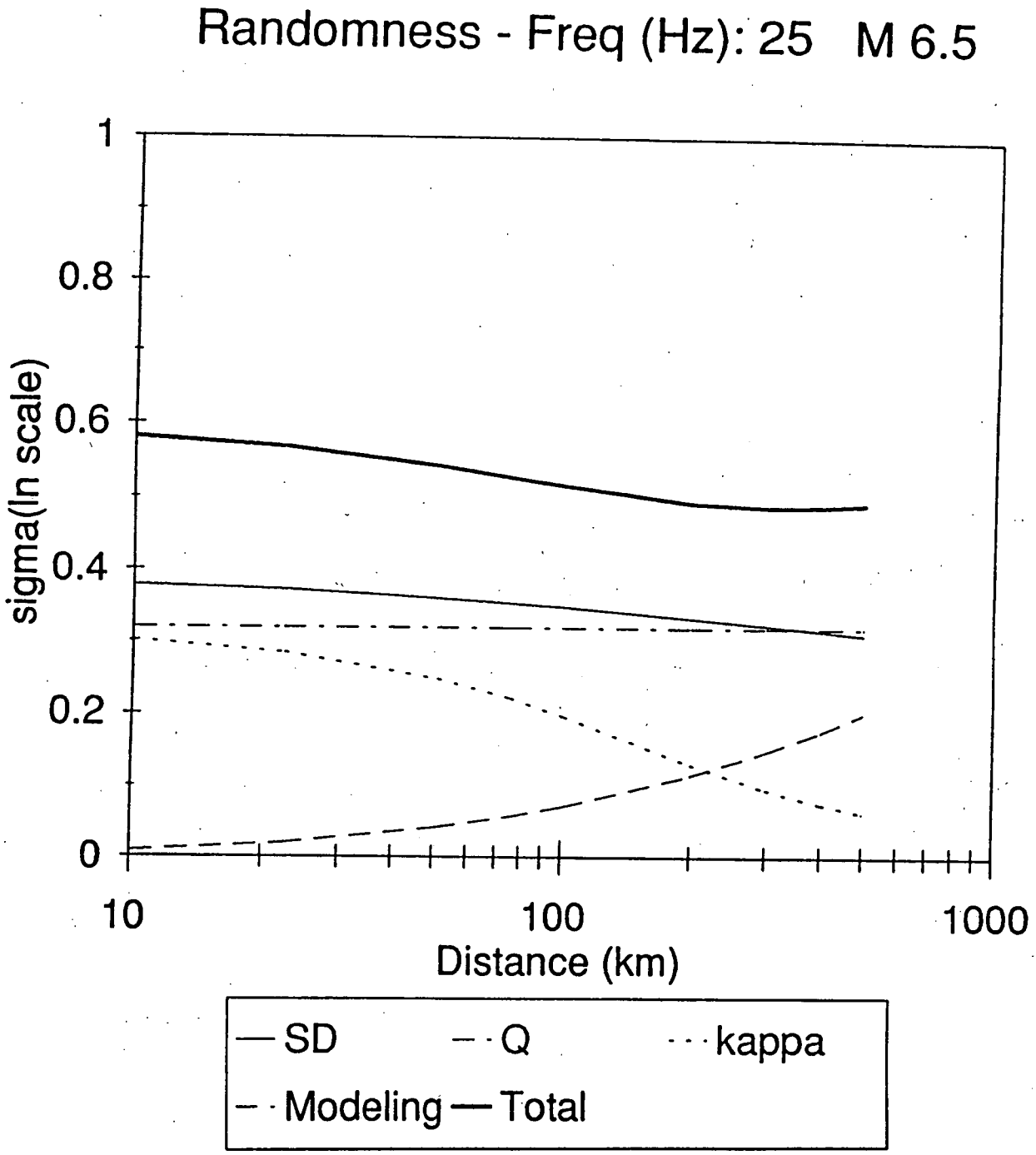

Figure E-19. Components of randomness plotted versus distance for 25 Hz PSV.

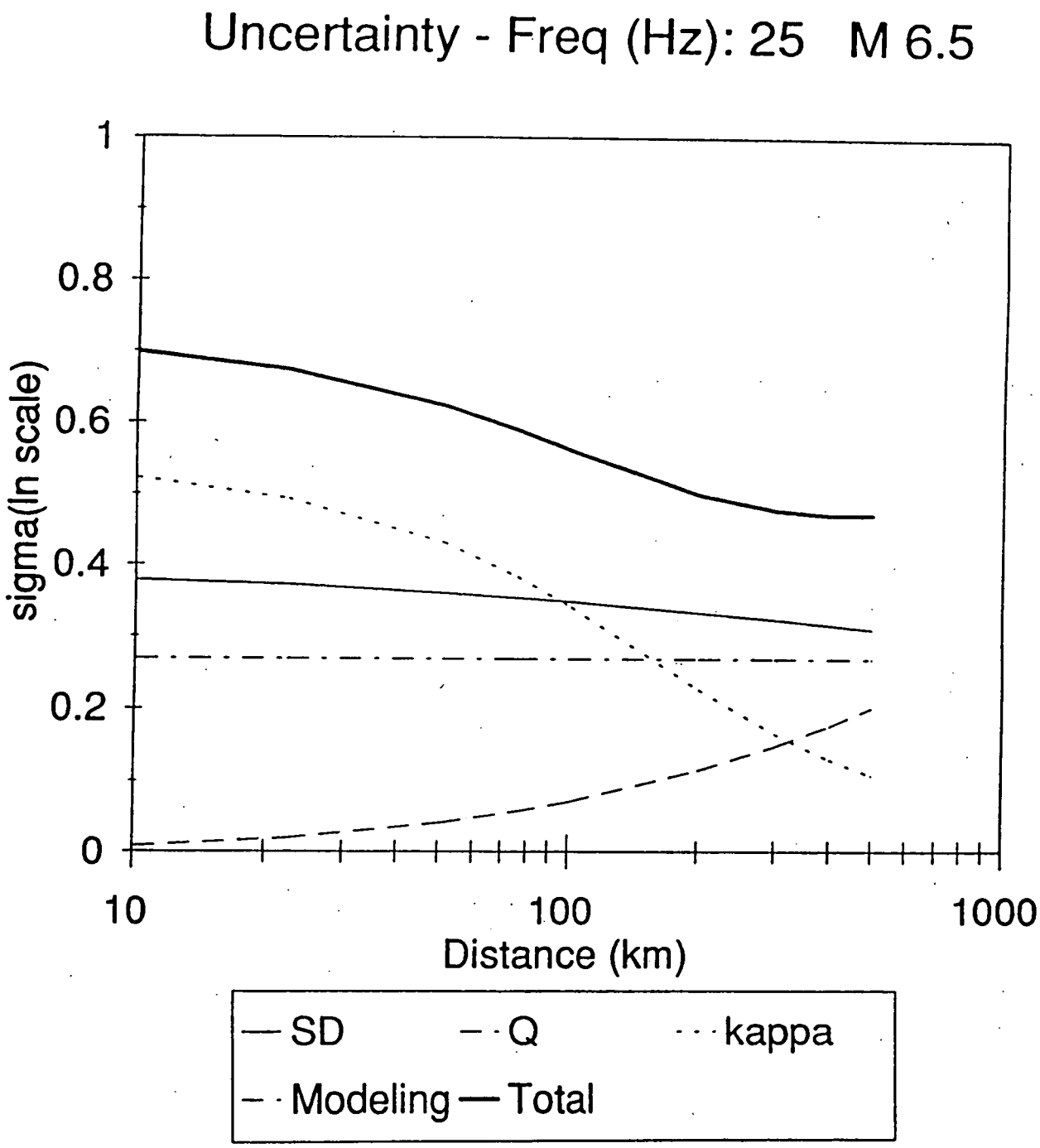

Figure E-20. Components of uncertainty plotted versus distance for 25 Hz PSV.

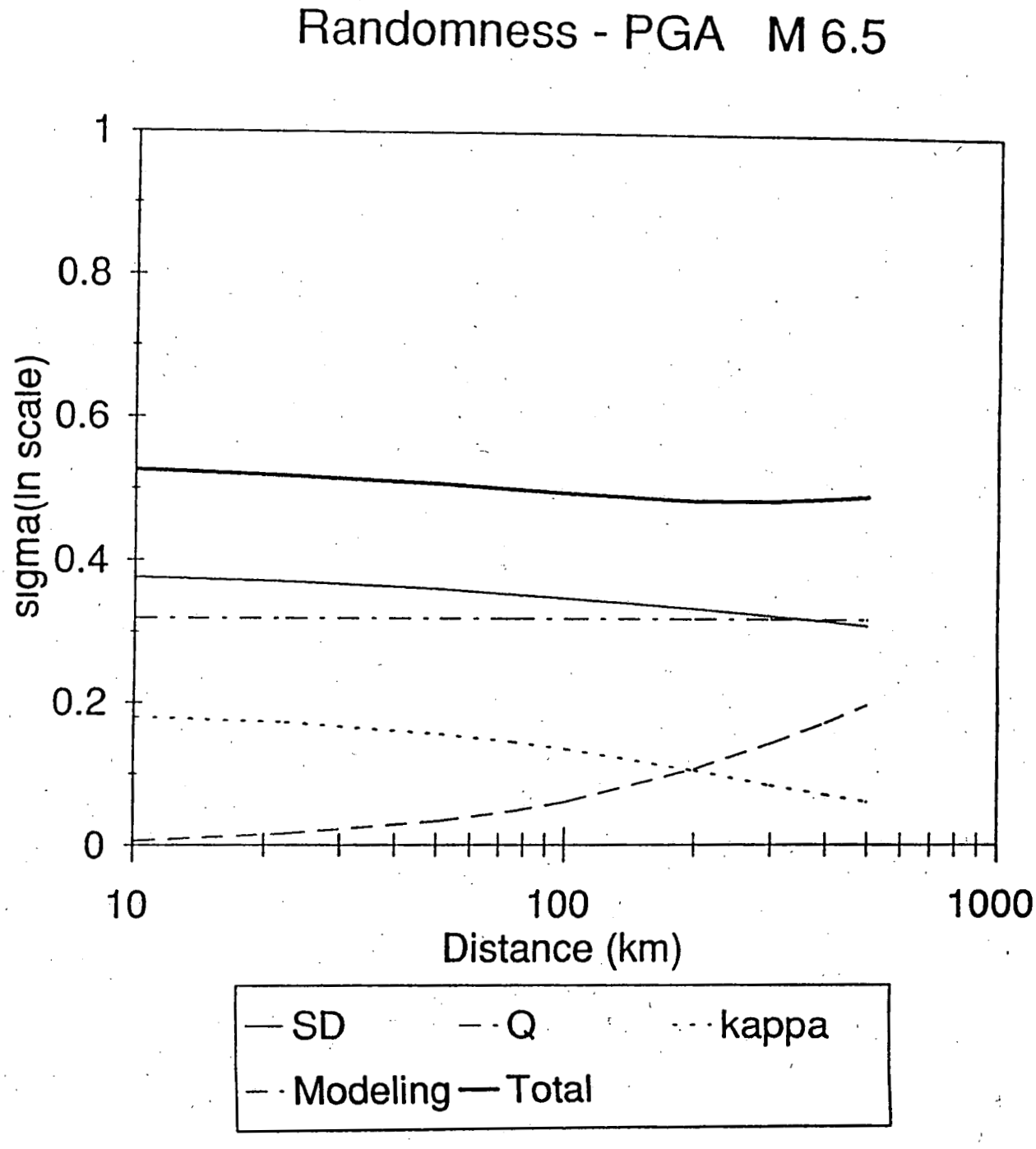

Figure E-21. Components of randomness plotted versus distance for PGA.

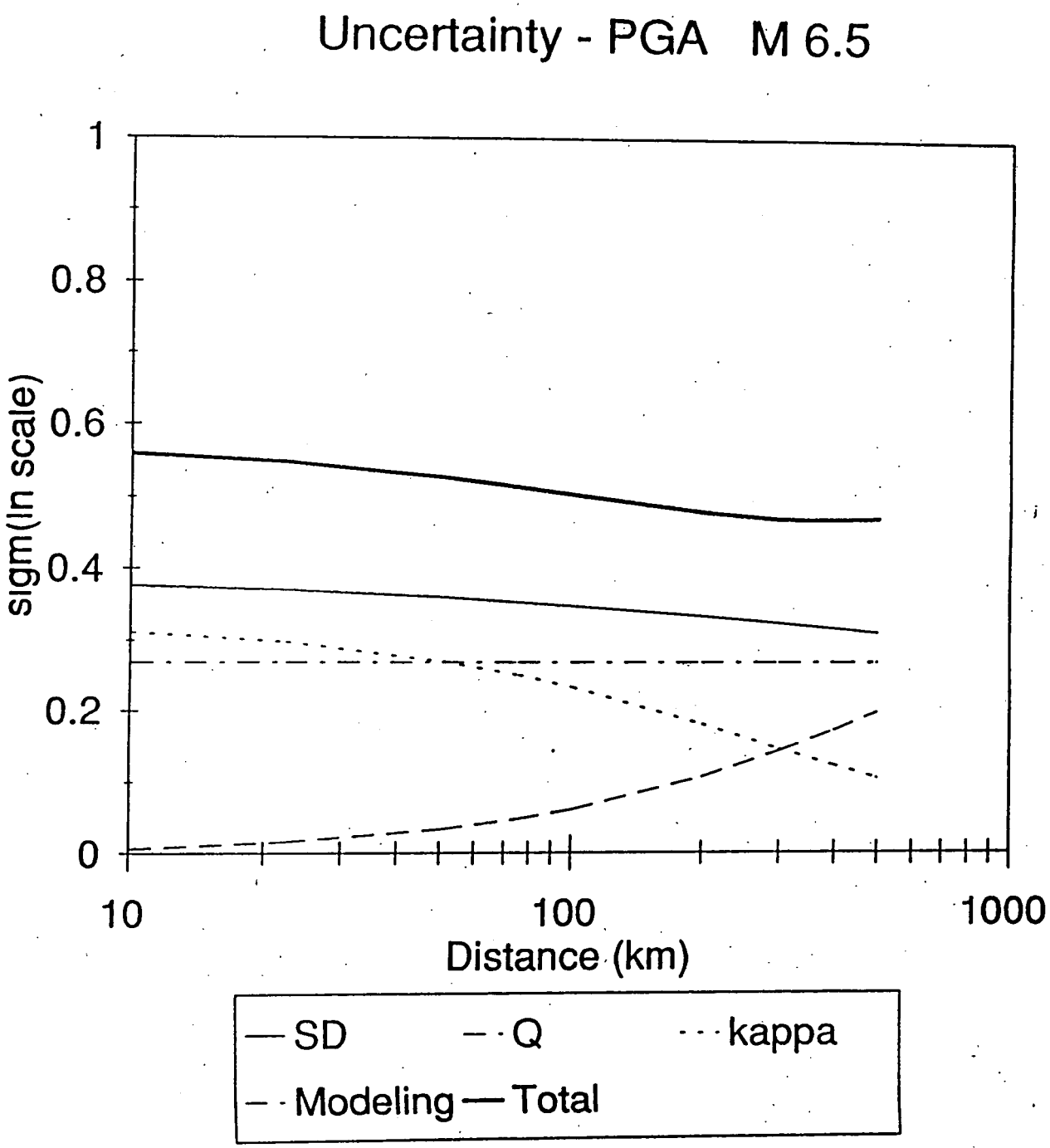

Figure E-22. 2% damped PSV spectra for M = 6.1, R = 20 km.

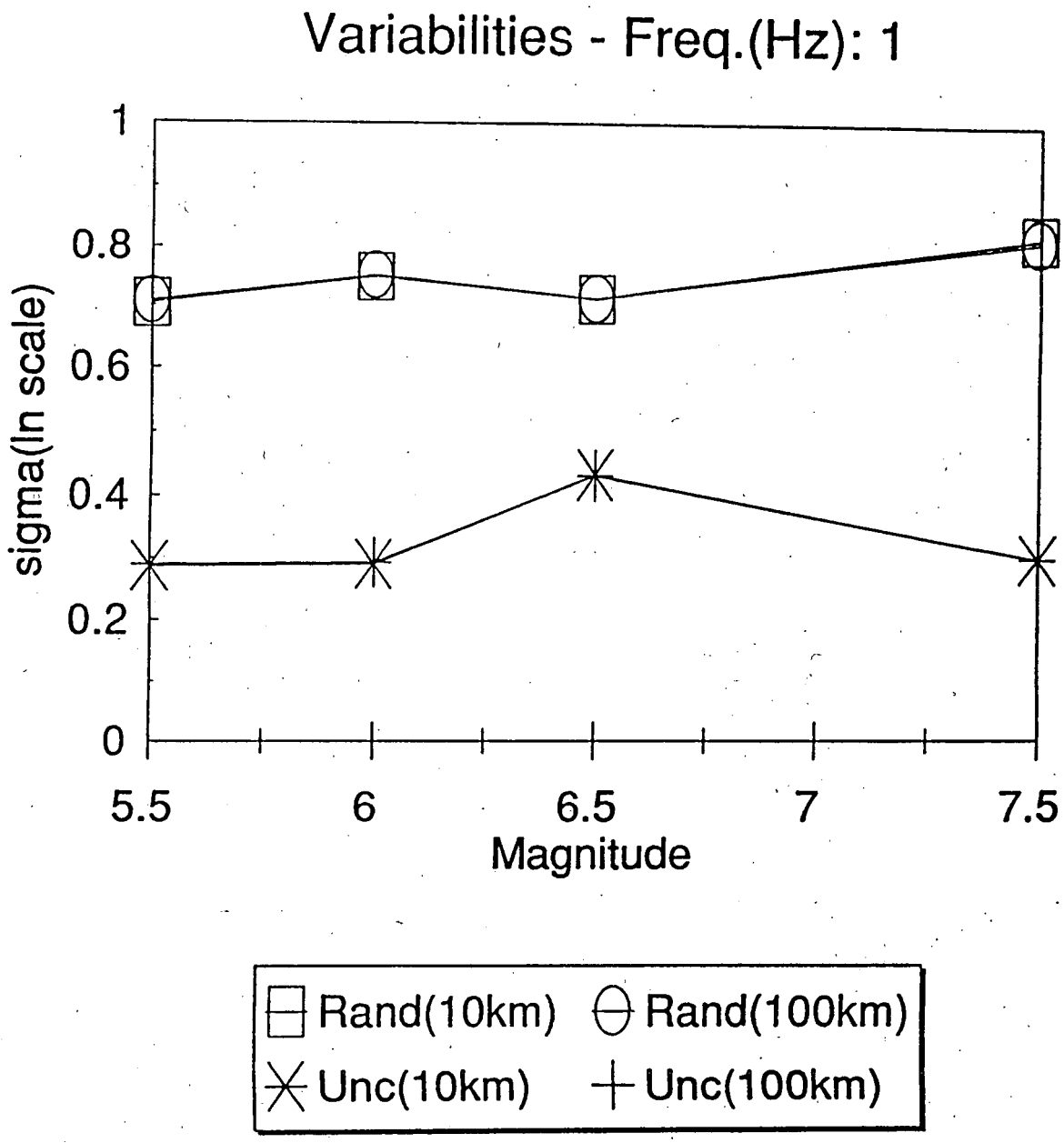

Figure E-23. Variation of randomness and uncertainty with magnitude for 1-Hz PSV.

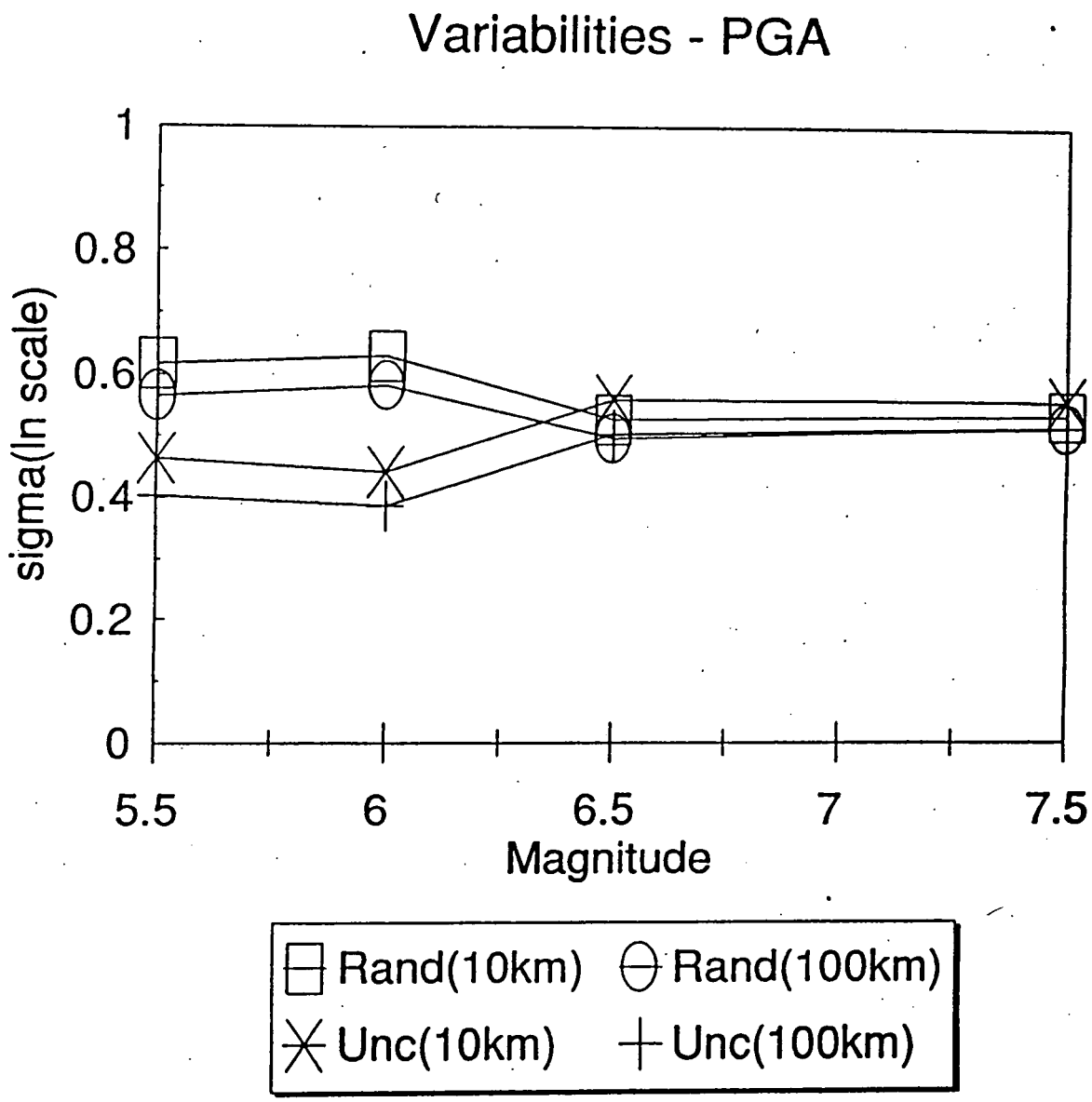

Figure E-24. Variation of randomness and uncertainty with magnitude for PGA.

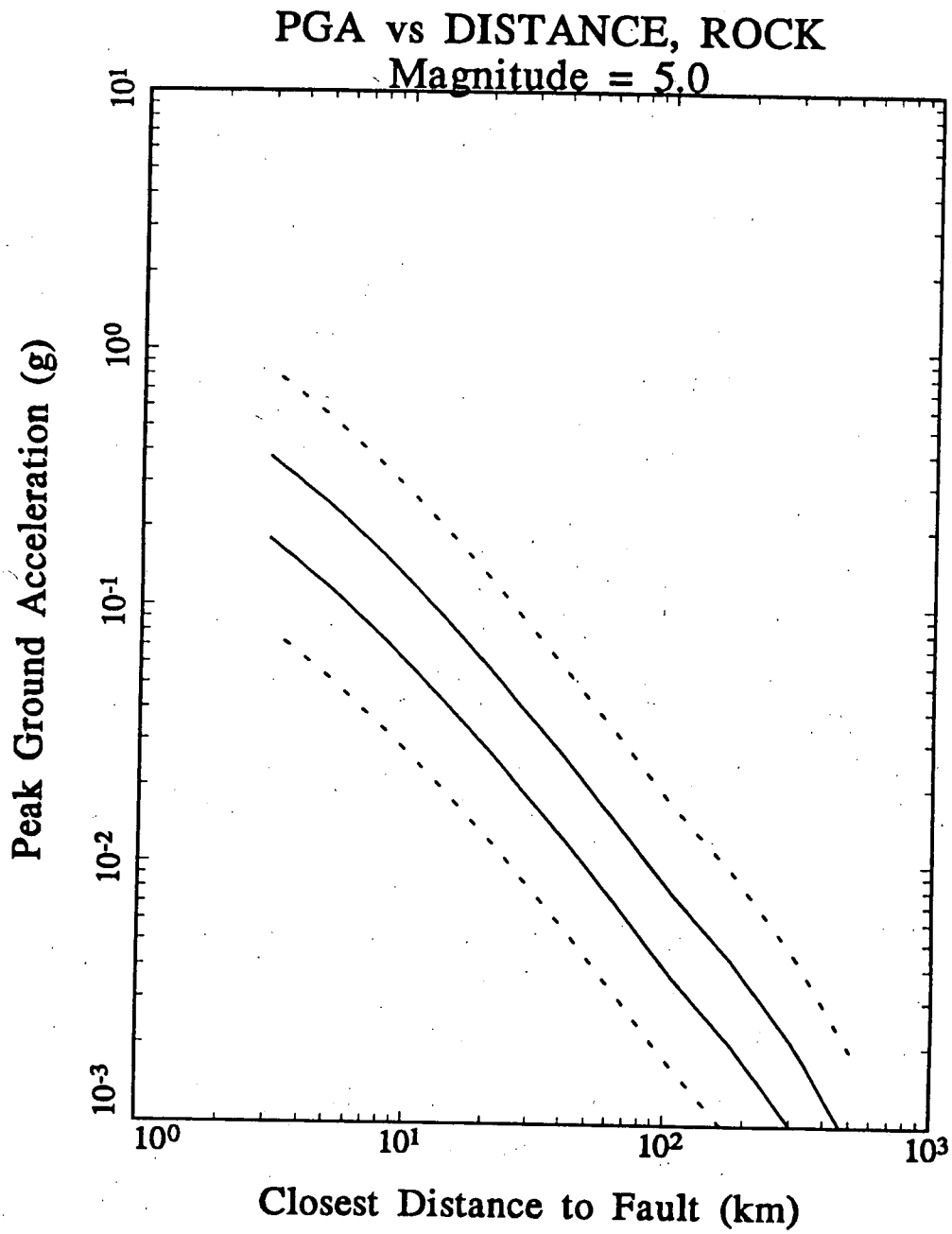

Figure E-25. Analytically based attenuation functions for rock; PGA predictions for magnitude 5. Weights: solid lines, 0.454; dashed lines, 0.046.

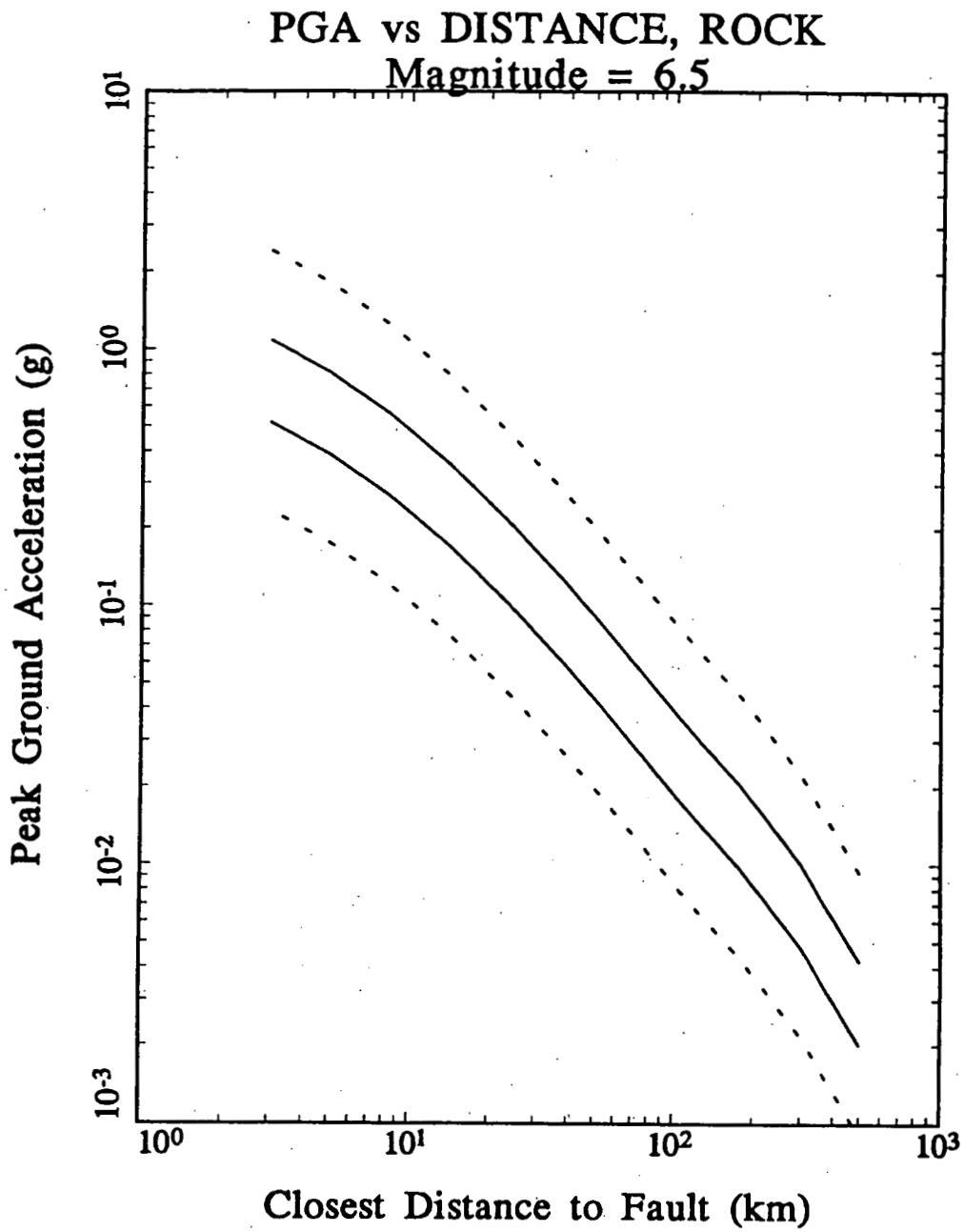

Figure E-26. Analytically based attenuation functions for rock;
PGA predictions for magnitude 6.5. Weights: solid lines, 0.454; dashed lines, 0.046.

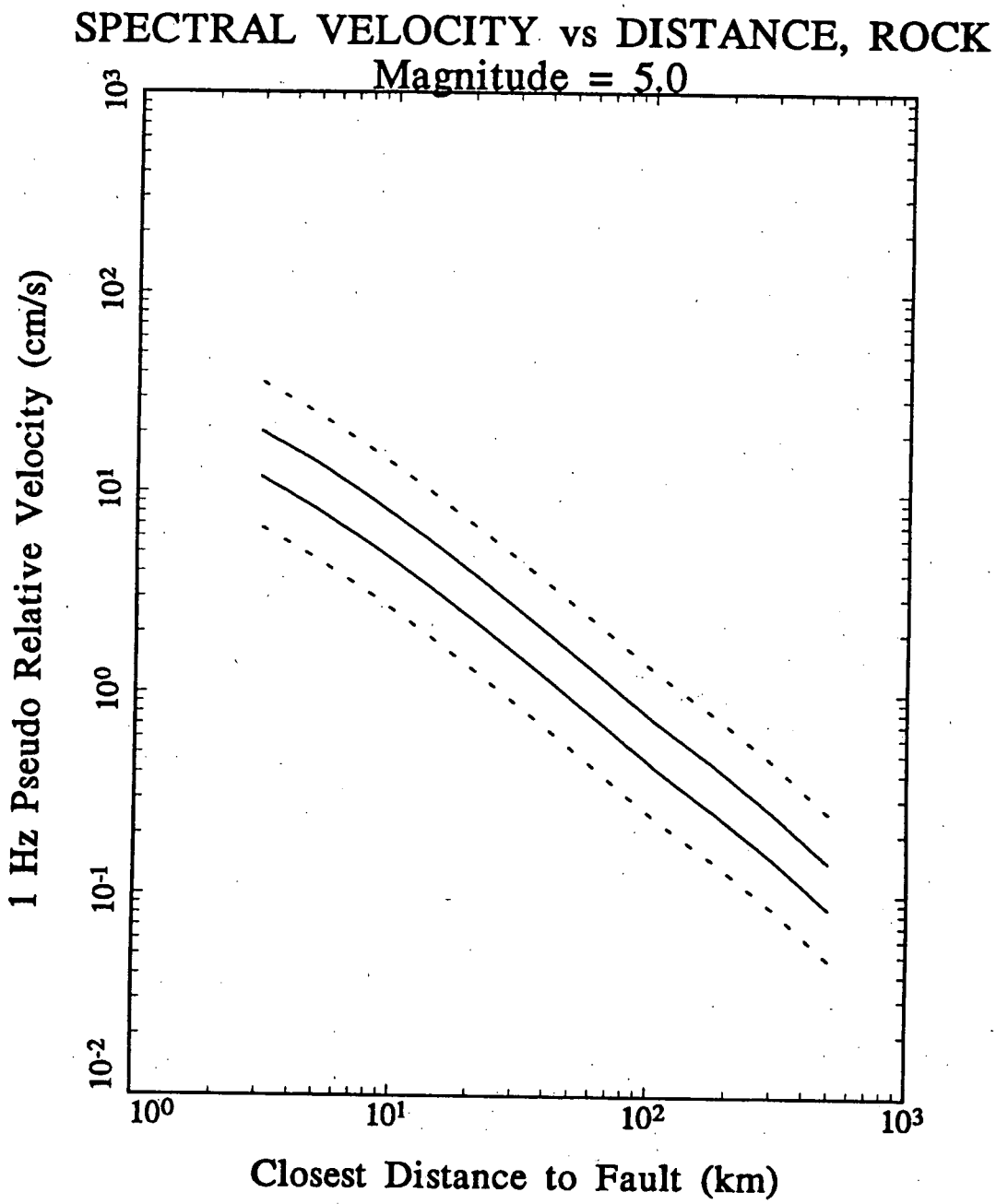

Figure E-27. Analytically based attenuation functions for rock; 1-Hz PSV prediction for magnitude 5. Weights: solid lines, 0.454; dashed lines, 0.046.

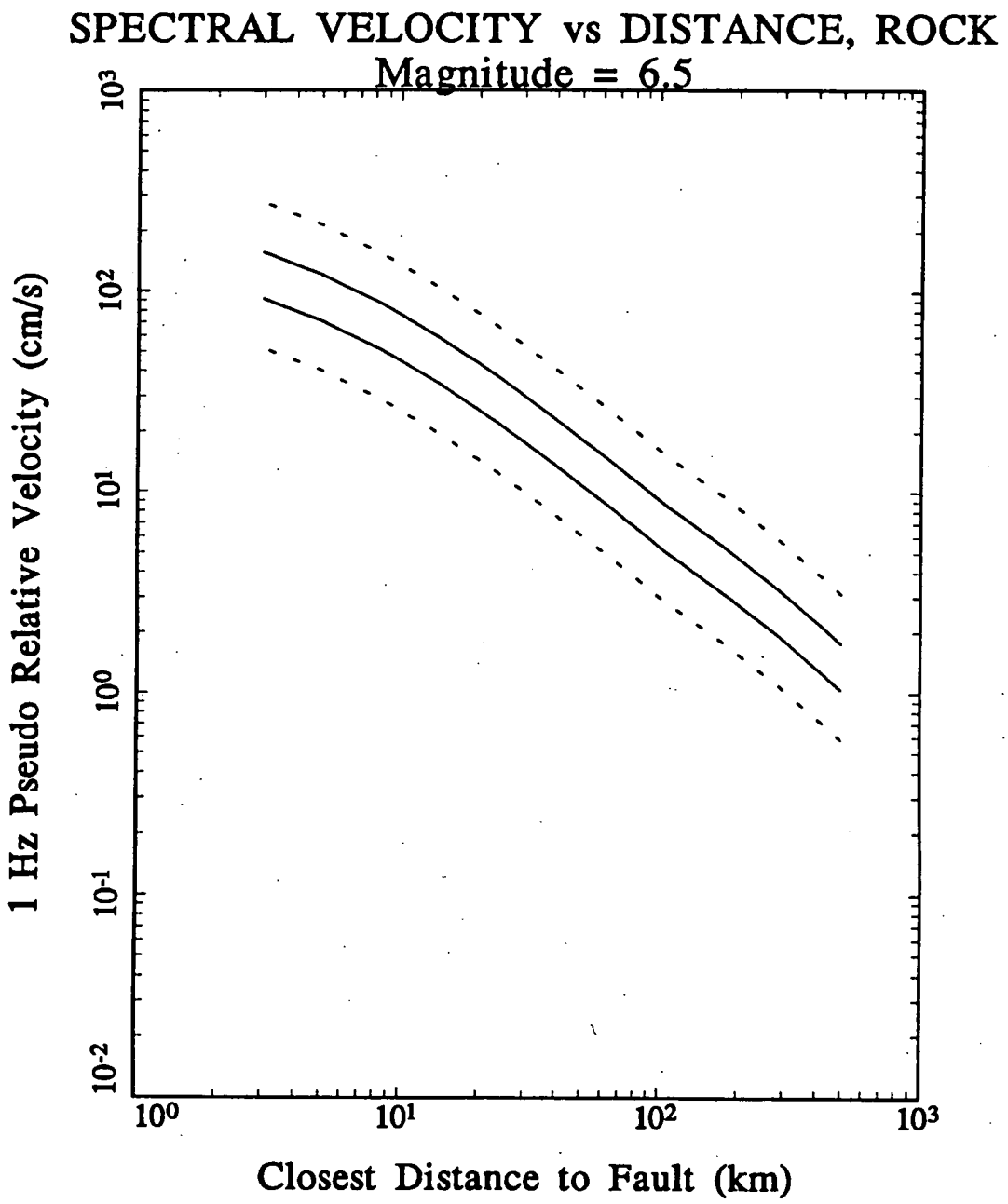

Figure E-28. Analytically based attenuation functions for rock;
1-Hz PSV prediction for magnitude 6.5. Weights: solid lines, 0.454; dashed lines, 0.046.

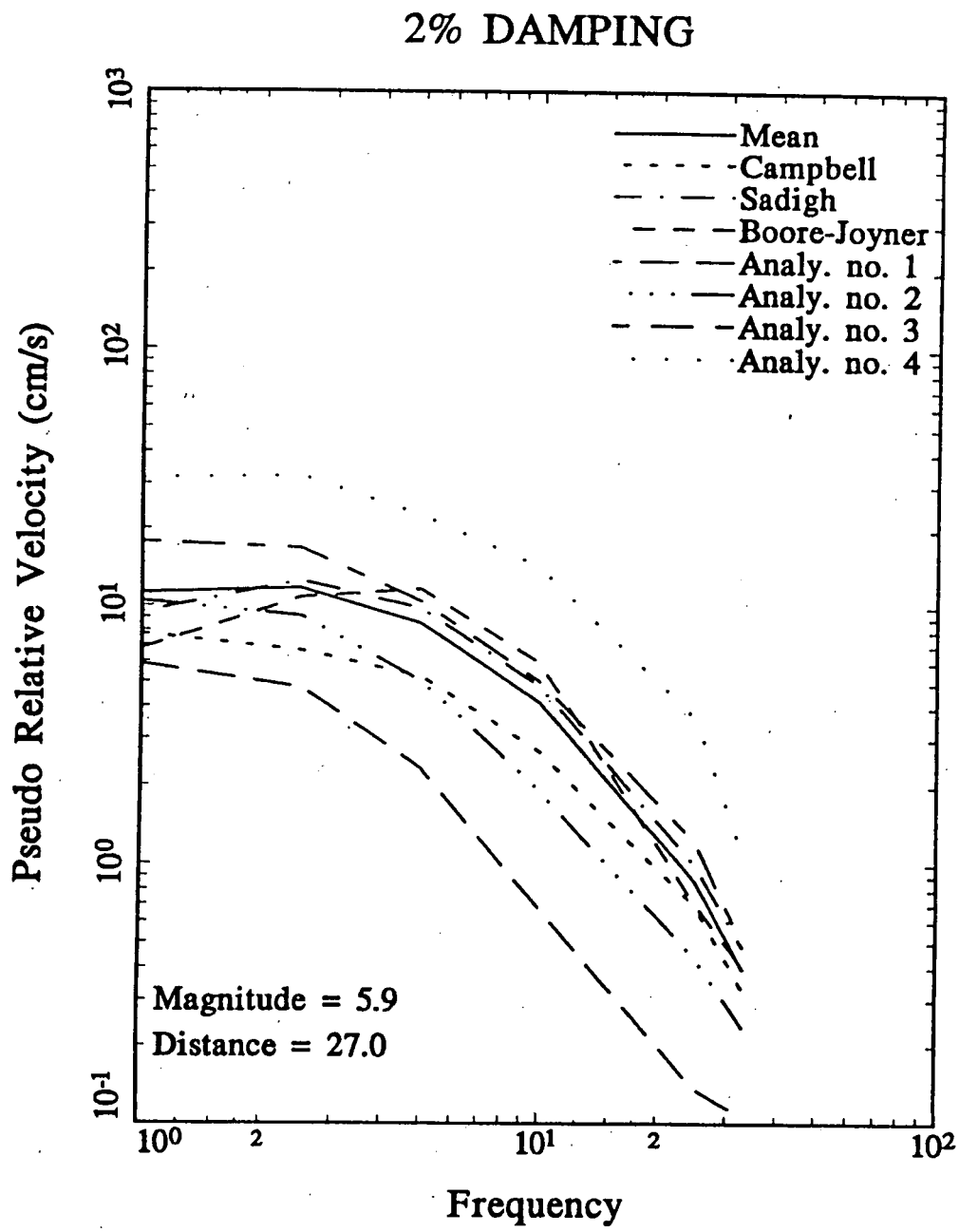

Figure E-29. 2% damped PSV spectra on rock for M = 5.9, R = 27 km.

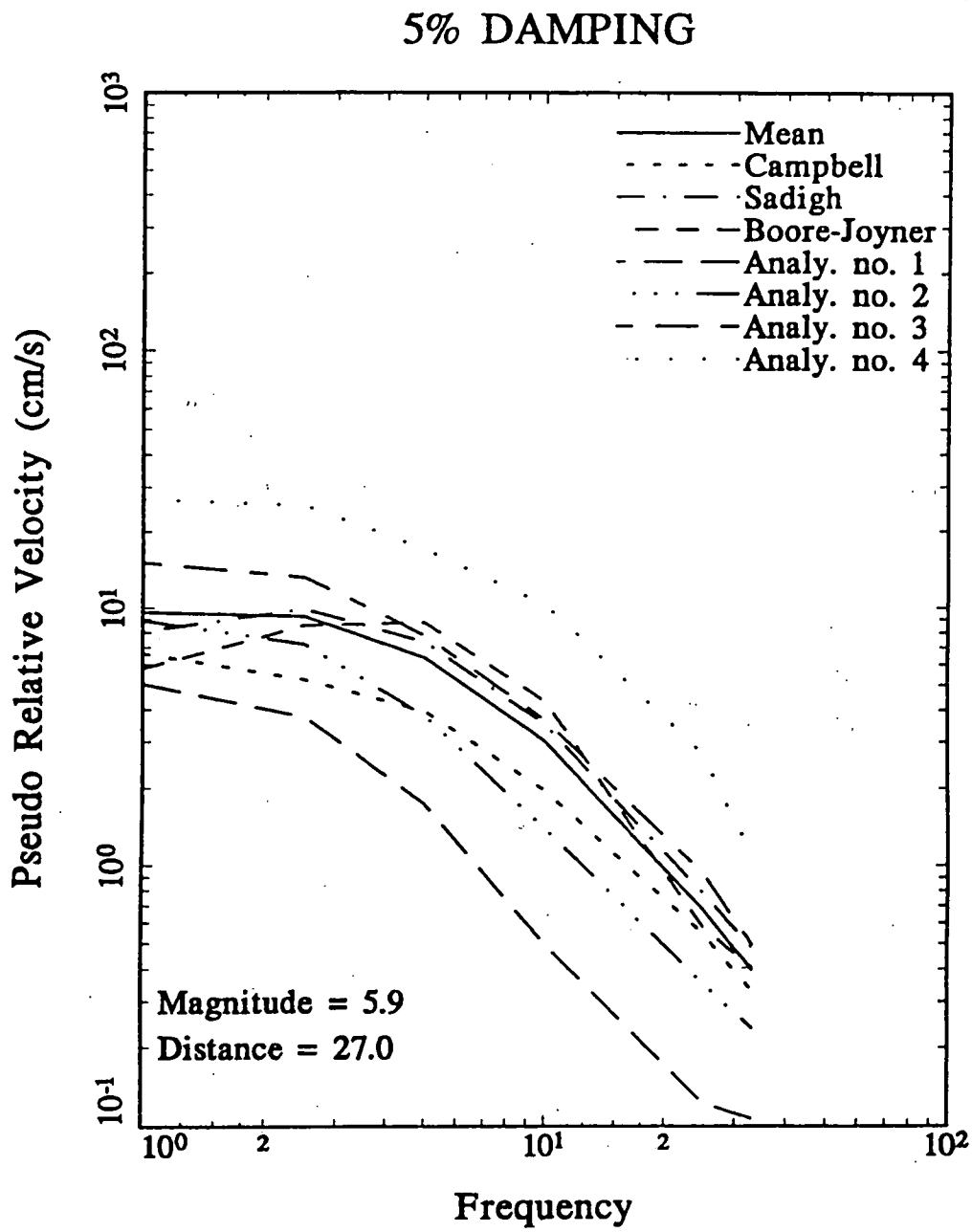

Figure E-30. 5% damped PSV spectra on rock for M = 5.9, R = 27 km.

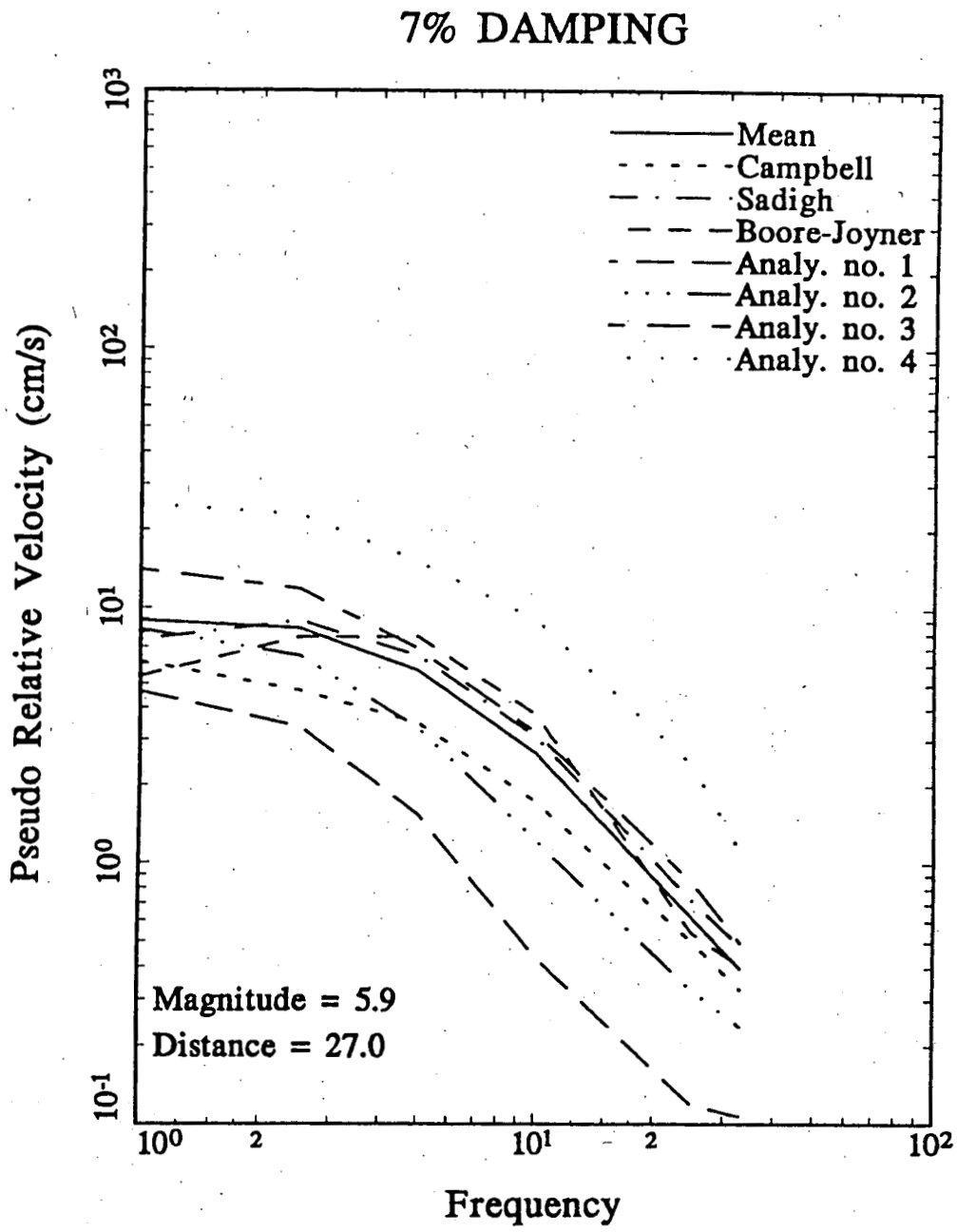

Figure E-31. 7% damped PSV spectra on rock for M = 5.9, R = 27 km.

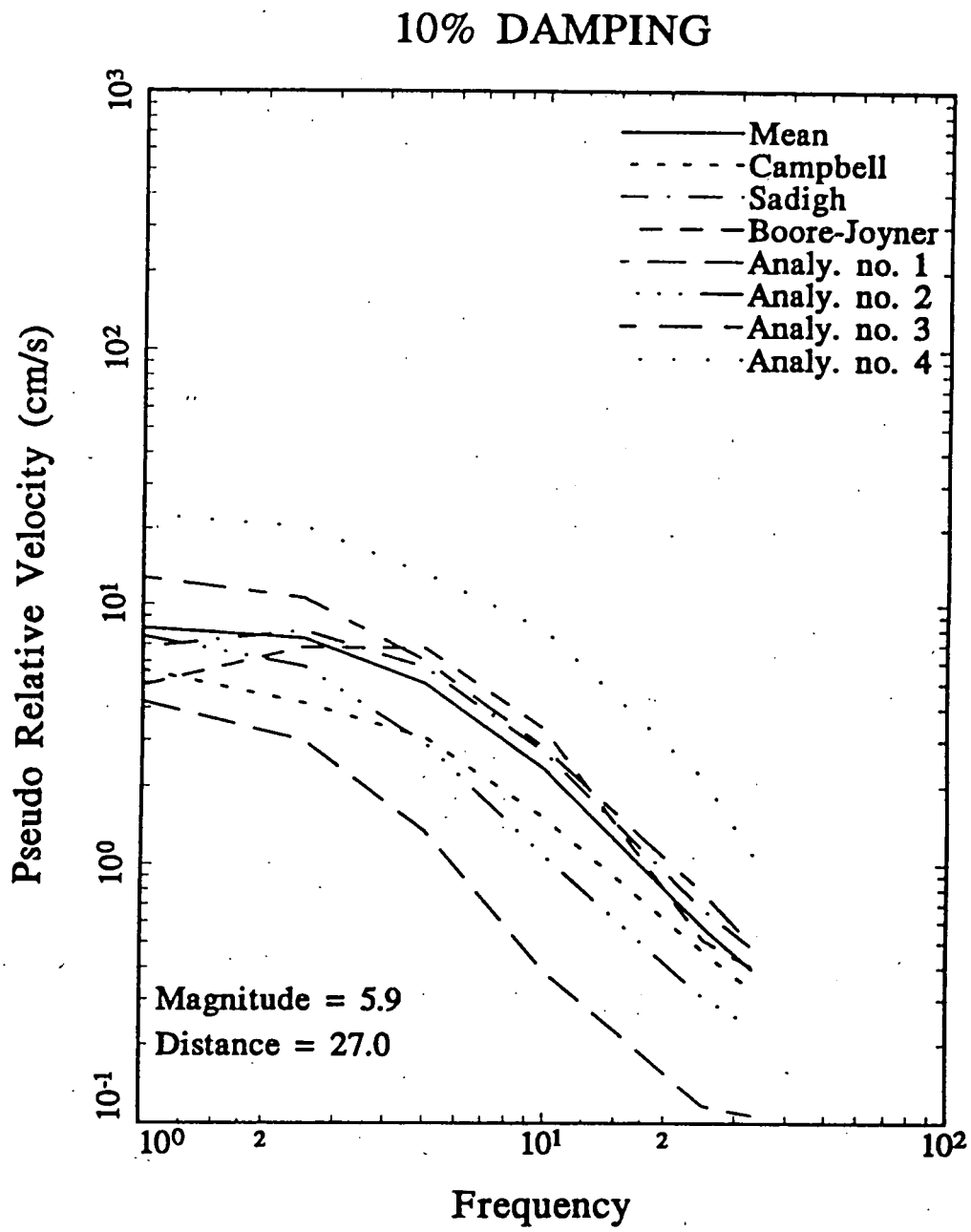

Figure E-32. 10% damped PSV spectra on rock for M = 5.9, R = 27 km.

APPENDIX F

SOIL AMPLIFICATION STUDIES

by

Risk Engineering, Inc.
Boulder, Colorado

EQE International, Inc.
Evergreen, Colorado

Pacific Engineering and Analysis Co.
El Cerrito, California

INTRODUCTION

For the purpose of site response analyses, the Rocky Flats site conditions consist generally of soil-like properties to a depth of about 100 feet. The shallow alluvium consists of sands, gravels, silts, and clays (EG&G Rocky Flats, Inc., 1993) with a thickness ranging from about 6 feet to over 20 feet (EG&G Rocky Flats, Inc., 1993). Below the alluvium, a weathered friable claystone bedrock is encountered. The weathered zone extends to depths of about 100 feet where the claystone reaches rock like properties. The claystone bedrock extends to depths exceeding 500 feet. The profile may be simply characterized as a three layer system consisting of alluvium, weathered bedrock, and bedrock. This profile has the capacity to amplify incoming seismic wave at certain frequencies, thereby modifying the characteristics of seismic rock motion that occurs at depth. This amplification must be considered in any analysis that represents the seismic hazard at the ground surface.

The purpose of this Appendix is to estimate quantitatively the effects that soils will have on incoming seismic motions. The most direct and non-controversial approach to account for the effects of surficial materials on strong ground motion is empirical. Ideally amplification factors could be developed based entirely upon observations of strong ground shaking at the site of interest. Past studies using data recorded on rock and on different classes of soil profiles, such as stiff soils and deep cohesionless soils, have demonstrated large differences in spectral amplification due to the presence of the soils (Seed et al., 1976; Mohraz, 1976; Joyner and Fumal, 1984; Schneider et al., 1993). These studies are extremely useful in showing general trends, but do not allow a direct application at any particular site because the general studies use a number of sites with a range of characteristics, not a set of identical sites.

There are no strong motion records available at the Rocky Flats Plant on which to base a purely empirical analysis. Therefore we estimate soil effects using an analytical model based on physical theory of dynamic soil behavior, and check these results for reasonableness and consistency using a model based on empirical trends. Both methods are described in this Appendix.

One of the most important parameters that influences soil amplification is the shear wave velocity of the in situ soil. Downhole shear wave velocity testing was performed at Rocky Flats in eight holes ranging in depth from about 20 ft to about 500 ft (Blackhawk, 1993, 1994). The hole locations are shown in Figure F-1 and surround the Protected Area of the Plant. No holes were drilled in the actual Protected Area due to access restrictions. As a result, no direct measurements of shear-wave velocities were available for the materials underlying the Protected Area. The available data should, however, be representative of the soil conditions in the general area. Profiles B, E, and J extended to about 145 ft while hole L had velocities logged to about 500 ft (Blackhawk, 1994, Figures 1 and 2). Profiles C, D, F, and G extend to depths of about 20 to 30 ft. The measured velocities for all holes are shown in Figure F-2 down to a depth of 200 ft. Hole L indicated uniform velocities below 160 ft down to the maximum hole depth of 500 ft. Profiles C and D have shear-wave velocities exceeding the compressional-wave velocities (Blackhawk, 1993), and are therefore considered unreliable; data from these holes are not used in developing a median profile, as discussed below.

EMPIRICAL ESTIMATES OF SOIL AMPLIFICATION

Methodology

There are no direct observations of soil amplification at Rocky Flats on which to base empirical estimates, so empirical estimates must be inferred and modeled from other observations, taking into account the available soil characteristics at Rocky Flats. The approach adopted for this study is consistent with that being recommended for an up-coming revision of the *NEHRP Recommended Provisions for the Development of Seismic Regulations for New Buildings*. Although not truly site-specific, the method uses the average shear-wave velocity in the upper 30 m (100 ft) of the site of interest to infer frequency dependent site amplification factors that are consistent with a generic site having the same average shear-wave velocity. Since the specific frequency response of the site is not accounted for in this methodology, it is recommended that the empirical results be used only as a check on the analytical procedure presented in the next section. The empirical method as applied in this study is based on an amplitude independent procedure that utilizes empirical regression models developed by Boore et al. (1993, 1994). Boore et al. (1993) developed attenuation relationships that included frequency dependent amplification factors for three site categories, referred to as Classes A, B and C. These site classes were defined in terms of the mean shear-wave velocity ($V_{s,30}$) in the upper 30 m (98.4 ft) of the soil deposit. Site classes were defined as having $V_{s,30}$ in the range >750 m/sec (2460 ft/sec) for Class A sites, 360 to 750 m/sec (1180 to 2460 ft/sec) for Class B sites, and 180 to 360 m/sec (590 to 1180 ft/sec) for Class C sites. The amplification factors were given by the expression,

$$A(f) = b_6(f)G_B + b_7(f)G_C \qquad \text{(F-1)}$$

where A(f) is a frequency dependent amplification factor, $G_B = 1$ for Class B sites, $G_C = 1$ for Class C sites, and $G_B = G_C = 0$ for Class A sites.

Boore et al. (1994) reanalyzed the data of Boore et al. (1993) and developed site amplification factors directly in terms of $V_{s,30}$. Since shear-wave velocities have been measured at Rocky Flats

(see Figure F-2), a modified version of this latter relationship was used to estimate empirical amplification factors at Rocky Flats. This relationship is given by the expression,

$$A(f) = b_v(f)[\log V_{s,30} - \log V_A(f)] \qquad \text{(F-2)}$$

where $V_A(f)$ is the average value of $V_{s,30}$ for Class A sites.

The amplification factors given by Equation (F-2) are calculated with respect to an average Class A site. In order to apply this relationship to the attenuation relationships for rock developed in Appendix E, it was necessary to adjust it to a reference site consistent with these relationships. Boore et al. (1993) compared predictions based on their new site classifications with those developed by Joyner and Boore (1988) for soil and rock. This latter relationship was one of those used to develop empirical attenuation relationships in Appendix E. They found that the rock predictions using the 1988 relationship were generally consistent with those for Class C sites for periods less than about 0.25 sec and generally consistent with those for Class B sites for periods greater than about 0.35 sec.

The agreement between the predictions for rock and those for Class C sites at the higher frequencies seems inconsistent, considering that predictions for Class C sites are in agreement with those for soil at all frequencies. The inconsistency arises from Joyner and Boore's (1988) results indicating that ground motions were similar on soil and rock at high frequencies. Although this similarity may be appropriate at high amplitudes for which nonlinear soil behavior becomes significant, it is not believed to be appropriate at smaller amplitudes. Since the procedure developed for estimating empirical soil amplification in the present study results in factors that are consistent with analytical results (also presented in this Appendix), it was assumed that rock as defined in the Joyner and Boore (1988) study corresponds to Class B sites of Boore et al. (1993, 1994) at all frequencies of interest.

A similar comparison could not be made for the other empirical rock attenuation relationships presented in Appendix E. However, since all of the relationships are based on the same general set of strong-motion recordings and all use about the same definition for rock, it is reasonable to assume that predictions from the rock relationships of Sadigh et al. (1986) and Campbell (1993) are also consistent with those for Class B sites.

To adjust Equation (F-2) to represent amplification with respect to rock, or equivalently Class B sites, we equated the right-hand side of Equation (F-2) to coefficient $b_6(f)$ and solved for $V_{s,30}$, thus obtaining an estimate for $V_B(f)$ to use in place of $V_A(f)$ in Equation (F-2). The resulting median estimate for A(f) is given by the expression,

$$A(f) = b_v(f)[\log V_{s,30} - \log V_B(f)] \qquad \text{(F-3)}$$

where the coefficients $b_v(f)$ and $V_B(f)$ are given in Table F-1.

An estimate of $V_{s,30}$ for the Rocky Flats Plant was developed from the median shear-wave velocity profile for the site using the same procedure that Boore et al. (1993, 1994) used to estimate $V_{s,30}$ for the recording sites used in their study. This procedure defines the mean shear-wave velocity as the depth (i.e., 30 m) divided by the mean travel time of vertically propagating shear waves over this

depth. Based on this procedure, the mean shear-wave velocity in the upper 30 m of the Rocky Flats site was found to be 1,065 ft/sec (324.8 m/sec).

The median soil amplification factors estimated using Equation (F-3) were found to have a dip in the amplification spectrum at 5 Hz. In order to produce a smooth spectrum, this value was replaced with the geometric average of the amplification factors at 2.5 and 10 Hz. The resulting median amplification factors are given in Table F-1.

Uncertainty

There are three sources of uncertainty in the median estimate of A(f). The first is the uncertainty in equating rock in the attenuation relationships of Sadigh et al. (1986), Joyner and Boore (1988), and Campbell (1993) to Class B sites of Boore et al. (1993, 1994). The second is the uncertainty in estimating A(f) from $V_{s,30}$ using Equation (F-3). The third is the uncertainty in the measured value of $V_{s,30}$ at the Rocky Flats Plant.

The first uncertainty associated with equating rock to Class B sites is known to be small for the Joyner and Boore (1988) attenuation relationship, since comparisons by Boore et al. (1993) demonstrated that the former resulted in predictions that are very nearly equivalent to or, in the case of the high frequencies, higher than those from the latter. Similar comparisons were not possible for the other two attenuation relationships, since their databases were not presented in such a form as to allow such a comparison to be made. However, since these relationships used similar databases and similar definitions of rock as the Joyner and Boore (1988) relationship, it is reasonable to assume that the errors in equating them to Class B sites should also be small.

The second source of uncertainty, the statistical error in estimating A(f) from Equation (F-3), was not addressed by Boore et al. (1994) and, therefore, could not be assessed directly. The third source of uncertainty, which includes both the error in the individual shear-wave velocity measurements at a given site at the Rocky Flats Plant as well as the site-to-site variability in the measured shear-wave velocity profiles at the various measurement sites within the Plant, was not formally estimated in the development of the median shear-wave velocity profile.

Since it was not possible to formally estimate the individual errors associated with the three sources of uncertainty, it was decided to use a statistical surrogate to estimate these uncertainties. A reasonable surrogate is the mean error in the soil amplification factors associated with predicting ground motions on soil from those on rock from the empirical attenuation relationships used to estimate ground motions for the Rocky Flats region in Appendix E. The average standard deviation of the natural logarithm of these amplification factors, averaged over magnitudes of 5 and 6.5 and distances of 5 and 50 km for all periods of interest, was estimated to be 0.22. The specific value assigned to this parameter is not critical, since the results are not very sensitive to its variation. For example, a $\pm$ 50% change in this parameter results in only about a $\pm$ 10% variation in the median plus and minus standard deviation amplification factors. Therefore, it is recommended that the standard deviation of ln A(f), $\sigma_{\ln A}$, be assigned the value 0.22 in all applications requiring an estimate of this uncertainty.

The median, median minus standard deviation, and median plus standard deviation estimates of the smoothed empirical soil amplification factors developed in this study are listed in Table F-1 and plotted in Figure F-3.

ANALYTICAL ESTIMATES OF SOIL AMPLIFICATION

Equivalent-Linear Computational Scheme

The computational scheme that has been most widely employed to evaluate one-dimensional site response assumes vertically-propagating plane shear waves. Departures of soil response from a linear constitutive relation are treated in an approximate manner through the use of the equivalent-linear approach.

The equivalent-linear approach, in its present form, was introduced by Seed and Idriss (1970). This scheme is a particular application of the general equivalent linear theory introduced by Iwan (1967). Basically, the approach is to approximate a second order nonlinear equation, over a limited range of its variables, by a linear equation. Formally this is done in such a way that an average of the difference between the two systems is minimized. For ground response modeling this is achieved by defining an effective strain which is assumed to exist for the duration of the excitation. This value is usually taken as 65% of the peak time-domain strain calculated at the midpoint of each layer, using a linear analysis. Modulus and damping curves are then used to define new parameters for each layer based on the effective strain computations. The linear response calculation is repeated, new effective strains evaluated, and iterations performed until the changes in parameters are below some tolerance level. Generally a few iterations are sufficient to achieve a strain-compatible linear solution.

This stepwise analysis procedure was formalized into a one-dimensional, vertically propagating shear-wave code called SHAKE (Schnabel et al., 1972). Subsequently, this code has become easily the most widely used analysis package for one-dimensional site response calculations.

The advantages of the equivalent-linear approach are that parameterization of complex nonlinear soil models is avoided and the mathematical simplicity of linear analysis is preserved. A truly nonlinear approach requires the specification of the shapes of hysteresis curves and their cyclic dependencies. In the equivalent-linear methodology the soil data are utilized directly and, because at each iteration the problem is linear and the material properties are frequency independent, the damping is rate independent and hysteresis loops close.

The most significant advantage of the equivalent-linear formulation is the preservation of the superposition principle. For linear systems, this principle permits spectral decomposition and frequency-domain solutions. One can then make use of the propagator matrix solution scheme (Haskell, 1960; Schnabel et al., 1972; Silva, 1976) for very efficient frequency domain solutions of the wave equation. The superposition principle then permits a spectral recomposition of the wavefields (sum over frequencies) through an inverse Fourier or Laplace transform. An important result is that the deconvolution process (i.e., propagating the control motion down rather than up) results in a unique solution. That is, for a given motion at the surface, within an equivalent-linear framework there is only one base motion (solution). In reality of course, if the soils are behaving

in a nonlinear fashion and have degraded, many different input motions at the base of the soil could result in a similar surface response.

While the assumptions of vertically propagating shear waves and equivalent-linear soil response certainly represent approximations to actual conditions, their combination has achieved demonstrated success in modeling observations of site effects (Schnabel et al., 1972; Schneider et al., 1993).

Stochastic Point-Source Computational Model

The computational scheme employed to compute the site response uses the stochastic point-source ground motion model (Boore, 1983; Silva and Green, 1989; Schneider et al., 1993) to generate the power spectral density and spectral acceleration of the rock or control motion. This motion or power spectrum is then propagated through the one-dimensional soil profile using the plane-wave propagators of Silva (1976). In this formulation only SH waves are considered. Arbitrary angles of incidence may be specified but normal incidence is used throughout the present analyses.

In order to treat possible material nonlinearities, the equivalent-linear formulation is employed. Random process theory is used to predict peak time domain values of shear strain based upon the shear strain power spectrum. In this sense the procedure is analogous to the program SHAKE except that peak shear strains in SHAKE are measured in the time domain. The purely frequency domain approach obviates a time domain control motion and, perhaps just as significant, eliminates the need for a suite of analyses based on input motions having the same response spectra but different time history characteristics. This arises because each time domain analysis may be viewed as one realization of a random process. In this case, several realizations of the random process must be sampled to have a statistically stable estimate of site response. The realizations are usually performed by employing different control motions with the same level of peak acceleration and spectral shape.

In the case of the frequency domain approach the estimates of peak shear strain as well as oscillator response are, as a result of the random process theory, fundamentally probabilistic in nature. Stable estimates of site response can then be computed by forming the ratio of spectral acceleration predicted at the surface of a soil profile to the spectral acceleration predicted for the control motion.

Soil Profile

The available shear wave profiles measured at Rocky Flats were described previously and are summarized in Figures F-1 and F-2. A median (logarithmic mean) profile was calculated based on the data from holes B, E, F, G, J, and L; this median is shown in Figure F-4 as a solid line.

To simplify the median profile for analyses, the thin low velocity layer near 25 ft was smoothed, as were the steps near 150 ft. For the site response analyses, bedrock is taken at a depth of 100 ft and with a velocity of 2000 ft/sec (610 m/sec). This is compatible with the analytically derived rock attenuation relation which represents a region specific crustal model with a shear wave velocity of 2000 ft/sec (610 m/sec). This base case profile is shown in Figure F-4 as a dashed line.

The base case profile is shown in Figure F-5 along with the measured profiles and is a good representation of an average profile for the purpose of site response analyses. To accommodate variations in velocity and layer thickness as well as profile depth which may be expected to occur over the site, response analyses are performed for a suite of 50 randomized profiles. The randomized profiles are produced by generating a velocity perturbation to the first layer assuming a lognormal distribution with a standard error (natural log) of 0.40. This perturbation velocity is then added to each layer resulting in a shift in the base case profile to higher or lower velocities. This process maintains the impedance contrasts between layers and results in a more conservative amplification than allowing the layers to vary individually. The bedrock velocity is independently varied assuming a smaller standard error (natural log) of 0.2 since the bedrock velocity is expected to vary less than the soil profile (EPRI, 1993).

The σ_{ln} of 0.40 (factor of 1.5) is chosen to be in general accord with the NRC guidelines which accommodate profile variation (velocity, layer thickness, and depth) in a deterministic manner by upper- and lower-bound analyses using a factor of 2 in shear modulus (1.4 in shear-wave velocity). The Monte Carlo approach permits true median and 1-sigma estimates of site amplification and, with a σ_{ln} of 0.4, results in variations similar to or larger than the NRC deterministic approach (Figure F-6). The uncertainty in soil amplification resulting from the randomized profiles as well as from randomized modulus reduction and damping curves (next section) are sufficient to accommodate variations in both layer thicknesses and material properties expected to occur over the site area. However, because velocity data were only available surrounding the site area (Figure F-1) and not at actual building locations, site (building) specific soil amplification factors should be computed if appropriate profiles are available. Recommendations for building-specific site response analyses are given in the conclusions of this Section.

Modulus Reduction and Damping Curves

The site is underlain by soils consisting of sands, gravels, silts, and clays over a soft friable claystone bedrock (EG&G Rocky Flats, Inc., 1993). Since laboratory dynamic testing was precluded due to environmental concerns, a set of generic modulus reduction and damping curves was adopted for the site response analyses. The curves selected were developed in a recent DOE/EPRI sponsored project (EPRI, 1993). As part of this project, laboratory testing was performed by Professor Ken Stokoe (EPRI, 1993) on soil samples taken from several sites which recorded significant levels of ground shaking. Modulus reduction and damping curves resulting from the laboratory resonant column and torsional shear tests were used to verify both equivalent-linear and nonlinear site response analyses (EPRI, 1993). Results from these analyses clearly demonstrated that both the equivalent-linear and nonlinear analyses provided equally good fits to the recorded motions and that the material nonlinearities, quantified through the laboratory testing program, accurately reflected in-situ high-strain dynamic soil properties. Based on this verification of the dynamic laboratory tests, a generic set of modulus reduction and damping curves were developed for application to soils comprised of sands, gravels, and low plasticity clays. The generic curves were based on the results of the laboratory testing program and were used to develop soil amplification factors for a suite a soils categories which include profiles comprised of materials like those which occur at Rocky Flats.

Figure F-7 shows the curves with the effects of confining pressure reflected in the depth ranges shown, with less damping and higher G/G_{max} for a given strain level as the depth increases.

In order to accommodate variability in the modulus reduction and damping curves for the site area, the curves were independently randomized about the base case values shown in Figure F-7. A lognormal distribution was assumed with a σ_{ln} of 0.35 at a cyclic shear strain of $3 \times 10^{-2}\%$ (EPRI, 1993). This distribution is based upon examining the variability in laboratory dynamic test results (EPRI, 1993) of materials sampled at the same site at close enough depths to ensure similar materials are sampled and that the effects of differences in confining pressures are not significant. Upper and lower bounds are placed on the randomized curves to preserve physically realizable variations. For a given depth range, the bounds are taken from the next shallower or deeper depth range depending on whether upper or lower modulus reduction or damping bounds are considered. For the shallowest and deepest ranges, the bounds are set to be symmetrical about the base case curves. The random curves are generated by sampling the transformed normal distribution with a σ_{ln} of 0.35, computing the change in normalized modulus reduction or percent damping at $3 \times 10^{-2}\%$ shear strain, and applying this factor at all strains. The random perturbation factor is reduced or tapered near the ends of the strain range to preserve the general shape of the median curves. Figures F-8, F-9, and F-10 show ten of the fifty realizations for each of the three sets of curves. As the figures show, the suites of curves are smooth and are constrained to preserve the general shape of the median curves.

Specification of Control Motion

Since the computational scheme used to compute the motions at the surface of the profiles does not require time histories for control motions, the point-source stochastic ground motion model may be used to define the outcrop power spectral density. In order that the outcrop motions used to excite the soil profile are in general accord with the analytical attenuation model for rock motions, the base case source and propagation path parameters listed in Table F-2 were used. These are the same values used in developing the motions for the analytical attenuation relation.

Development of Site Amplification Factors

Site amplification factors are computed as the ratio of the 5% damped spectral pseudo acceleration (PSA) at the surface of each site for each randomized profile to the 5% damped PSA for the bedrock (outcrop) motion. In addition, both peak acceleration and peak velocity were computed for the site and outcrop as well. Levels of input motion (rock outcrop) of 0.01, 0.05, 0.1, 0.2, 0.3, 0.4, 0.5, 0.75, and 1.0g were used to accommodate effects of material nonlinearity upon site response. The varying levels of control or rock outcrop motion are intended to reflect the effects of magnitude or distance on the soil profile. Table F-2 shows the magnitudes (M), distances (R), peak accelerations, and peak particle velocities of the outcrop motions. Also shown are the predominant frequencies, estimated from the random process theory, associated with the peak accelerations and peak particle velocities. The outcrop ratios of peak velocity to peak acceleration (V/A) display expected magnitude dependency and weak dependence upon distance.

Amplification Factors

The amplification factors, 5% damped PSA(soil)/PSA(rock), were computed at 89 frequencies from approximately 0.25 Hz to 100 Hz. The frequency range of interest is from 0.5 Hz to 25 Hz and more specifically at discrete frequencies of 0.5, 1.0, 2.5, 5, 10, and 25 Hz. Figures F-11 through F-19 show the median and $\pm$ 1 sigma amplification factors for each control motion level and Table

F-3 summarizes the values at the suite of discrete frequencies along with factors for peak ground acceleration and peak particle velocity.

The largest amplification, about 1.75, occurs near 4 Hz (Figure F-11) at the median profile fundamental resonance for the lowest control motion (0.01g). At higher levels of motion, the fundamental resonance shifts to lower frequency and is smaller in amplitude. Accompanying the shift in the resonance to lower frequencies as the profiles soften with increased input motions is a reduction in amplification at higher frequencies. This results from the increased damping in the profiles at the higher strain levels. The increase in the amplification factors with increasing frequency beyond about 10 Hz is due to the soil response spectral acceleration beginning to saturate to peak acceleration (i.e. response accelerations are driven by, and are close to, peak ground acceleration) at lower frequencies than for the control motion response spectra. The increased damping at the higher input levels is causing the spectra computed at the soil surface to attenuate at frequencies above about 10 Hz. This effect is illustrated in Figure F-20 which shows a comparison of the soil and rock (control motion) 5% damped spectral accelerations. The median soil spectrum exceeds the rock spectrum at low frequency with a broad maximum near 3 Hz. Beyond that the soil spectrum decreases with increasing frequency falling to the level of the rock spectrum near 10 Hz. At higher frequencies, the soil spectrum rapidly saturates to peak acceleration while the rock spectrum continues to decrease, saturating near 30 Hz.

The largest uncertainty (σ_{ln}) is about 0.40 and occurs near the fundamental resonance of the median profile where the soil column is, on average, having its greatest amplification effect. The amplification factors for peak acceleration (Table F-3) range from 1.55 for the lowest input motion to 0.98 for a 1g control motion. The average value is about 1.3. Peak velocity amplification averages somewhat less, about 1.2. The predominant effects of the soil column are at the higher frequencies (> 2 Hz) associated with peak acceleration.

EFFECTS OF FRONT RANGE BEDROCK GEOLOGY

Effects of Non-Horizontal Interfaces

There is some concern that the geometry of the Colorado Front Range bedrock structures may lead to amplified ground motions at sites close to where sedimentary units have been juxtaposed against older igneous and metamorphic units. Consideration of ground motions for these bedrock geometries is fundamentally an assessment of departure in response from the classical vertically propagating plane shear-wave one-dimensional model (Seed and Idriss, 1970; Schnabel et al., 1972). The main effect of the curvature of the sediment-basement interface is the generation of surface waves and trapped body waves that propagate in sedimentary rocks and superpose with the vertically-propagating shear waves. This may result in an amplification of motion as well as increased duration over one-dimensional site response effects alone.

Observations suggest that the simple one-dimensional model works well in predicting local site effects at locations away from dipping interfaces (King and Tucker, 1984). This observation is also predicted in modeling (Bard and Gariel, 1986). Edge effects, associated with rapid changes in the depth to basement may give rise to the local generation of surface waves which, because of material damping, do not significantly alter the spectral content of motions some distance from the edges

(Tucker and King, 1984). Additionally, long period body waves incident at shallow angles to a basin structure may become trapped and propagate across the basin as surface waves until reaching the thinning margin when they escape as body waves (Vidale and Helmburger, 1988). In the basin, these locally generated surface waves can give rise to amplifications and increased durations not predicted by vertically propagating shear waves.

An important aspect of these basin effects is that both modeling and observations indicate they are present and show similar characteristics for incident SH as well as incident SV wavefields (Tucker and King, 1984; Kawase and Aki, 1989; Vidale and Helmberger, 1988; Silva, 1991). Incident SH-waves give rise to Love type surface waves and trapped SH body waves while incident SV-waves generate Rayleigh type surface waves, trapped SV body waves, and scattered or converted P-waves. Incident P-waves, as well as scattered P-waves, are of little concern since their amplitudes are much smaller than S-waves, particularly in the frequency range which excites surface waves (Kawase and Aki, 1989). The similarity of basin response due to incident SH or SV waves indicates that the use of more straightforward analyses involving incident SH waves will reveal expected amplitudes and characteristic frequencies of structure generated surface waves and trapped body waves. As a result, an SH analysis for a given structure and suite of incidence angles can characterize stable features of basin response indicating whether enhanced motions over direct S-waves and one-dimensional effects may be of concern for design ground motions. Naturally if an SH wave analyses indicates stable features of basin induced motions in the frequency range of interest to structures, systems, or components a more complete analysis is warranted. Because the current analysis is simply one of determining whether or not basin response may be an issue of concern at the Rocky Flats Plant for frequencies of 1 Hz and greater, only an SH wave analysis will be performed.

Since little information exists on direct measurements of shear-wave velocities for the regional crustal structure (deeper than 500 ft) within about 200 km of the Denver area, the 1-dimensional model was developed based upon measured compressional-wave velocities. For the crust beneath the sedimentary section, Precambrian basement and below, the compressional-wave velocity and density models were based on deep refraction surveys described in Prodehl and Lypman (1989) and are appropriate to the Central Plains. For the sedimentary section, the sonic velocity log for the Wildcat #1 borehole at the Rocky Mountain Arsenal was used. The sonic log was divided into three layers extending to a depth of about 4 km. The depth of the sedimentary column at Rocky Flats is based on reflection line RFD-1 of Ebasco (1991). Shear-wave velocities were then computed by assuming a Poisson solid for the entire crust. The entire crustal profile is shown in Figure F-21.

The 2-dimensional crustal model is based on the reflection line RFD-1 of Ebasco (1992) which shows the eastward dipping interface between the sedimentary and crystalline rock units along the Front Range. Since the analysis procedure to assess the effects of the dipping interface will consist of ratios of motions (Fourier amplitude spectra) computed using 2-dimensional and 1-dimensional structures, details in the velocity gradient for the sedimentary rock column (top 4 km shown in Figure F-21) need not be considered. The use of ratios also cancels out the effect of source mechanism making the results independent of fault type. Simplified crustal model consists of a sedimentary block with an average shear-wave velocity of 2.05 km/sec (6724 ft/sec) in contact with crystalline rock with a shear-wave velocity of 3.58 km/sec (11,740 ft/sec) (layer 4 of the crustal model in Figure F-21). The crustal model is shown in Figure F-22 along with the inferred trace of the Front Range Fault (see Appendix A). It should be pointed out that a 2-D model of a complicated geological problem such as this may not bring out all the ground motion amplification that might

occur. Therefore these results should be viewed as an approximate evaluation consistent with the scope of the project that is not definitive.

Analytical Model

The computational algorithm used to model the effects of the 2-dimensional structure is an elastic explicit time-domain-finite-difference formulation (Vidale and Helmberger, 1988). The algorithm was developed by Dr. John Vidale who is currently at USGS (Menlo Park). The computer code, AMOD is fourth order in accuracy of spatial derivatives resulting in minimal grid dispersion. Absorbing boundary conditions are imposed on the sides and bottom of the finite difference grid. In the SH mode implemented here the top of the grid has free surface boundary conditions (reflection coefficient is equal to 1). In the analyses, the source is input as plane SH waves incident at specified angles from either the left (western) or right (eastern) side of the grid.

Code Validation

To validate the 2-dimensional code AMOD, identical runs using the structure shown in Figure F-22 were made with AMOD and an independently developed code which solves the same equations of motion but using different computational algorithms. This code was developed by Professor Jerry Schuster at the University of Utah. Professor Schuster's code has been extensively tested against analytical results and has been published in reviewed papers (Schuster et al., 1990). A comparison of Professor Schuster's code to several other 2 dimensional modeling methods using the same basin structure (Salt Lake Basin) as well as to recorded ground motion data has been recently performed (Schuster et al., 1990). The results showed good agreement between the different methods and to the recorded motions.

The comparison between the AMOD results and those of Professor Schuster's code are shown in Figure F-23 for each of the 7 site locations. The incidence angle is 32 degrees for a plane wave source located to the west of the Front Range. In the figure, the AMOD results are plotted as a solid line with Professor Schuster's results overplotted with a dashed line. The two results are nearly identical and illustrate very close agreement for two independently formulated finite difference solutions to the wave equations.

Results of Analytical Analyses

The 2-dimensional finite element grid used in assessing the effects of the dipping contact between the sedimentary and crystalline basement rock units is shown in Figure F-22. Because there is some uncertainty as to the actual location of the contact relative to the Rocky Flats Plant Site (Site 4, Figure F-22), computations are also made for three sites on either side of the plant location. The sites are spaced at 1 km intervals and the motions are averaged over the seven sites.

To assess the effects of the dipping interface, Fourier amplitude spectra are computed at each site using both the 2-dimensional crustal structure and a 1-dimensional structure for the same angle of incidence. The 1-dimensional structure consists of simply the sedimentary rock layer over the granitic basement. Taking the ratios of the 2-dimension simulations to the 1-dimension simulations isolates the effects of the dipping structure.

For completeness, a source west of the plant site, representative of the Front Range Fault, and a source to the east, representative of the Derby Fault, are considered. In the analyses, incident inclined plane SH waves are considered. For the Front Range Fault (Figure F-22), angles of incidence are computed based upon assumed source depths of 5, 10, and 15 km and fault dips of 30°, 45°, and 60° (Table F-4). These values of dip span the range of expected angles (see Appendix A). The Derby Fault is considered a vertical fault with a source depth of 10 km. Angles of incidence are computed for epicentral distances of 15, 20, and 30 km (Table F-4). This range covers the distance of the mapped surface trace of the fault from the plant site (see Appendix A). The fault lies off the eastern side of Figure F-22.

Results of the analyses for the Front Range Fault are shown in Figure F-24. The Fourier amplitude spectra computed for each angle of incidence (Table F-4) are averaged over the sites. The ratios of 2-dimensional to 1-dimensional analyses are then averaged over incidence angles assuming a lognormal distribution. The resulting median ratio and sigma values are smoothed over 7 points (0.5 Hz). The sigma values should be viewed as approximate since they are based on a limited number of analyses (Table F-4). Figure F-24 shows a small peak in the median amplification of about 30% at low frequencies (around 0.6 Hz). This effect is likely due to the generation of surface waves along the dipping interface. Since this is an elastic calculation, the effects of damping would tend to reduce the amplification slightly. The small peak near 10 Hz is not considered significant and would likely be completely eliminated if the effects of damping, particularly at high levels of strain, were considered. Figure F-25 shows the results of analyses for the Derby Fault (eastern sources). Interestingly, the most significant feature is a deamplification for frequencies near about 2 Hz. In addition, the uncertainty appears to be greater. The trough may be due to a cancellation effect of scattered surface waves propagating from west-to-east after being generated along the dipping interface by the westward propagating primary wavefield. The greater uncertainty may simply be due to fewer analyses (3 compared to 9, Table F-4). In order to assess the effects of uncertainties in the crustal velocities, sedimentary rock and crystalline basement, the suites of analyses were repeated for upper- and lower-bounds on shear-wave velocities (Table F-5). These bounds in velocities were based on Prodehl and Lypman (1989) and represent the variability in crustal velocities based on compressional-wave refraction surveys in the Central Plains. A constant Poissons' ratio of 0.25 was used in deriving the range in shear-wave velocities based upon the range in compressional-wave velocities.

Figure F-26 shows the resulting Fourier amplitude spectral ratio computed for the Front Range Fault (averaged over site and incidence angle) which includes the seven velocity cases shown in Table F-5. As expected, the peak near 0.6 hz is broadened and slightly reduced and the total uncertainty has increased. The analogous results for the Derby Fault are shown in Figure F-27. In this case, the trough has broadened and become less deep. Finally, Figure F-28 shows an average over both eastern sources (Derby Fault) and western sources (Front Range Fault). Here the slight amplification at low frequencies due to western source and the slight deamplification near 2 Hz for eastern source is still apparent.

OBSERVATIONS OF EARTHQUAKE INTENSITY

A source of data that has been used to infer trends in ground motion attenuation is observed Modified Mercalli Intensity (MMI) data. Kirkham and Rogers (1985; p. 92-96) use MMI

observations to conclude that focusing and wave guide effects are a possible explanation for elongated trends of MMI parallel to the Front Range. These focusing and wave guide effects may be caused by Front Range faulting, shearing, mineralized zones, and igneous dikes, they conclude.

Also, Kirkham and Rogers (1986, p. 134) state that the 1882 Colorado earthquake may have characteristics similar to the October 18, 1984 Laramie Mountains earthquake in Wyoming. They cite Oaks et al. (1985), who state that the MMI patterns for the two events are similar. Kirkham and Rogers (1986, p. 134) also cite damage in Golden during the 1984 shock, and mention wave path and focusing effects that might cause higher-than-expected ground motions in the Front Range area.

To quantify the possible effect of focusing and wave guide effects along the Front Range, we have examined the MMI data from the Laramie Mountains earthquake (see Figure F-29). These data were digitized, the distance to the epicenter was computed, and least-squares regression analysis was used to examine the attenuation of MMI data. The following form of attenuation equation was used:

$$I_s = C_1 + C_2 \ln \Delta + C_3 \Delta \qquad \text{(F-4)}$$

where I_s is MMI at each site, Δ is epicentral distance, and the constants are obtained from the regression analysis. Three sets of MMI data were used: (a) all data with MMI ≥ 2; (b) data with MMI ≥ 2 in the "Front Range," defined as latitudes from 38.7° to 42.4°N and longitudes from 104° to 105.5°W; (c) all data with MMI ≥ 2 except "Front Range" data as just defined. Regression analysis was performed on each set of data, resulting in the following equations:

All data:

$$I_s = 9.904 - 1.044 \ln \Delta - 0.00263 \Delta \qquad \text{(F-6)}$$

Front Range data:

$$I_s = 10.542 - 1.243 \ln \Delta - 0.00068 \Delta \qquad \text{(F-7)}$$

All data except Front Range:

$$I_s = 9.354 - 0.889 \ln \Delta - 0.00387 \Delta \qquad \text{(F-8)}$$

The data and equations are plotted on Figure F-30. The Front Range data indicates faster attenuation, if anything, than the entire data set (the C_2 coefficient is more negative for the Front Range data). Examination of the standard errors in the coefficients indicates that there is not a statistically-significant difference, implying that attenuation along the Front Range is not different from other directions, at least for this earthquake.

CONCLUSIONS

For the purpose of site response analyses, the Rocky Flats site conditions consist generally of soil-like properties to a depth of about 100 feet. The shallow alluvium consists of sands, gravels, silts,

and clays (EG&G Rocky Flats, Inc., 1993) with a thickness ranging from about 6 feet to over 20 feet (EG&G Rocky Flats, Inc., 1993). Below the alluvium, a weathered friable claystone bedrock is encountered. The weathered zone extends to depths of about 100 feet where the claystone reaches rock like properties. The claystone bedrock extends to depths exceeding 500 feet. The profile may be simply characterized as a three layer system consisting of alluvium, weathered bedrock, and bedrock. This profile has the ability to amplify incoming seismic wave energy, from that recorded on a solid rock outcrop. There are no strong motion records at Rocky Flats, so estimates of the amount of amplification must be based on inference and modeling from other empirical studies and from analytical models.

The empirical model used here extends empirical observations of soil response in California, and accounts for the average shear wave velocity observed in the top 30 m of material at Rocky Flats. The resulting empirical soil amplification factors are amplitude-independent, and indicate a maximum amplification for frequencies between 1 and 2.5 Hz (a factor of 1.34 to 1.38). The specific amplification factors and uncertainties are presented in Table F-1.

The analytical technique used here employs a stochastic point-source computational model that uses the equivalent-linear formulation to treat the non-linear response of horizontally layered soils to vertically propagating shear waves. The analysis is done in the frequency domain, using a power spectrum representation of the input motion, which can be scaled to represent different amplitudes of input. The resulting analytical soil amplification factors are amplitude-dependent, and are shown in Table F-3 along with uncertainty factors. The largest amplification occurs at about 4 Hz for very low levels of input motion (1%g), and shifts to lower frequencies at higher amplitudes of motion. At 0.3g input motion, for example, the peak amplification (a factor of 1.68) occurs at about 2.5 Hz.

These soil amplification factors allow rock seismic hazard curves to be translated into hazard curves on the soil surface. The two methods indicate consistent results in terms of the frequencies at which amplification will occur and the general level of amplification that will occur. Because the analytical site-specific soil amplification factors accommodate nonlinear soil response, they are used to modify the bedrock seismic hazard results for the effects of the local soils. The empirical results are used to check the analytical results for consistency and reasonableness. Table F-6 summarizes both the empirical and analytical amplification factors for all frequencies and input motion levels. The factors are most consistent at amplitudes of 0.1g to 0.5g, which are the amplitudes generally of interest for structural evaluations of seismic safety. At higher amplitudes the analytical procedure accounts for soil non-linearity at the higher frequencies, and indicates, in some cases, amplification factors less than unity. Figure F-31 compares the empirical, analytical, and average results graphically, for 0.1g and 0.5g input motions.

For building design or site specific analyses that employ soil structure interaction (SSI) investigations or detailed building-specific soil columns, it is recommended that the rock outcrop motions be used as control motions. The control point should be taken at a depth of about 100 feet with a bedrock velocity of 2000 ft/sec (610 m/sec) and the base case profile used (Figure F-4). If a local building specific profile is used, it should extend to a depth where the material has a velocity of about 2000 ft/sec (610 m/sec). For profiles which do not extend to a sufficient depth, they may be merged to the base case profile. The rock motions (both horizontal and vertical) should be propagated to the surface using an appropriate computational scheme that can accommodate both

horizontal and vertical motions. This approach reflects state-of-practice site specific analyses and is the only approach available.

For a generic analysis of structures at the soil surface, the soil motions (both horizontal and vertical) presented in this report may be used. These represent the effects of soil for the base case profile (Figure F-4) and represent an average conversion of horizontal to vertical motions. Therefore, these motions are appropriate for a generic analysis.

Two techniques were used to examine possible amplification along the Front Range caused by geometry of the bedrock geology, wave guide, and/or focusing effects. Analytically, a two-dimensional model of the bedrock geometry was developed and used to calculate spectra of rock surface motions and to compare these to one-dimensional analysis results. These calculations were repeated for faults both west and east of the Rocky Flats Plant, and for a range of incidence angles. The overall results, averaged over source geometry, source depth, and incidence angle indicate no amplification at frequencies above 1 Hz. Empirically, the MMI pattern from the 1984 Laramie Mountains earthquake was examined; a least-squares regression analysis indicated that MMI values in the Front Range do not attenuate more slowly than all data taken as a whole. Thus we conclude both from analysis and empirical data studies that general amplification of ground motion in the Front Range due to geometrical wave propagation effects is not a significant factor in seismic hazard at Rocky Flats. To the extent that amplification or de-amplification occur because of bedrock geometry, they are in a general sense included in, and accounted for, by randomness and uncertainty already modeled in the attenuation equations.

REFERENCES

Bard, P.Y. and J. Gariel (1986). "The seismic response of two-dimensional sedimentary deposits with large vertical velocity gradients," *Bull. Seism. Soc. Am.*, 76, 343-366.

Blackhawk (1993). "Shear wave velocity investigation Rocky Flats Plant, Golden, Colorado," Coleman Energy and Environmental Systems--Blackhawk Geosciences Division Report to EG&G Rocky Flats, Inc., Golden, Colorado, Subcontract No. ASC-340290ST4.

Blackhawk (1994). "Shear wave velocity investigation Rocky Flats Plant, Golden, Colorado," Coleman Energy and Environmental Systems--Blackhawk Geosciences Division Report to EG&G Rocky Flats, Inc., Golden, Colorado, Subcontract No. ASC-340290ST4.

Boore, D.M. (1983). "Stochastic simulation of high-frequency ground motions based on seismological models of the radiated spectra," *Bull. Seism. Soc. Am.*, 73(6), 1865-1894.

Boore, D.M., W.B. Joyner and T.E. Fumal (1993). "Estimation of Response Spectra and Peak Accelerations From Western North American Earthquakes: An Interim Report," US Geological Survey Open-File Report 93-509.

Boore, D.M., W.B. Joyner and T.E. Fumal (1994). "Estimation of Response Spectra and Peak Accelerations From Western North American Earthquakes: An Interim Report, Part 2," US Geological Survey Open-File Report 94-127.

Campbell, K.W. (1993). "Empirical Prediction of Near-Source Ground Motion From Large Earthquakes, in *Proceedings,* International Workshop on Earthquake Hazard and Large Dams in the Himalayas, The Indian National Trust for Art and Cultural Heritage (INTACH), New Delhi (in press).

Ebasco (1991). "Task 3, Shallow, High-Resolution Seismic Reflection Profiling in Operable Unit 2 (903 Pad, East Trenches, and Mound) at the Rocky Flats Plant, Final Report," report prepared for EG&G Rocky Flats and U.S. DOE.

EG&G Rocky Flats, Inc. (1993). "Well abandonment and replacement program," EG&G Rocky Flats, Inc. Golden, Colorado, Final Report

Electric Power Research Institute (1993). "Guidelines for determining design basis ground motions," Palo Alto, California, Electric Power Research Institute, vol. 1, EPRI TR-102293.

Haskell, N.A. (1960). "Crustal reflection of plane SH waves," *J. Geophys. Res.*, 65:4147-4150.

Iwan, W.D. (1967). "On a class of models for the yielding behavior of continuous and composite systems," *J. Appl. Mech.*, 34:612-617.

Joyner, W.B. and T.E. Fumal (1984). "Use of measured shear-wave velocity for predicting geologic site effects on strong ground motion," *Proceedings,* Eighth World Conf. on Earthquake Engin., San Francisco, 2:777-783.

Joyner, W.B. and D.M. Boore (1988). "Measurement, Characterization, and Prediction of Strong Ground Motion," in *Proceedings,* Conference on Earthquake Engineering and Soil Dynamics II--Recent Advances in Ground-Motion Evaluation, J.L. Von Thun, ed., American Society of Civil Engineers, Park City, Utah, Geotechnical Special Publication No. 20, p. 43-102.

Kawase, H. and K. Aki (1989). "A study on the response of a soft basin for incident *S, P,* and Rayleigh waves with special reference to the long duration observed in Mexico City," *Bull. Seism. Soc. Am.*, 79(5), 1361-1382.

King, J.L. and B.E. Tucker (1984). "Observed variations of earthquake motion across a sediment-filled valley," *Bull. Seism. Soc. Am.*, 74, 137-151.

Kirkham, R.M. and W.P. Rogers (1985). *Colorado Earthquake Data and Interpretations: 1867 to 1985*, Colorado Geological Survey, Bulletin 46.

Kirkham, R.M. and W.P. Rogers (1986). "An Interpretation of the November 7, 1882 Colorado Earthquake," *Contributions to Colorado Seismicity and Tectonics--A 1986 Update*, Colorado Geological Survey, Special Publication 28, p. 125-134.

Mohraz, B. (1976). "A study of earthquake response spectra for different geological conditions," *Bull. Seism. Soc. Am.*, 66(3):915-935.

Oaks, S.D., M.G. Hopper, L.M. Barnhard and S.T. Algermissen (1985). "November 7, 1882, Colorado Earthquake Reinterpreted in Light of the October 18, 1984, Wyoming Earthquake," *Earthquake Notes*, Vol. 55, p. 24.

Prodehl, C. and P.W. Lypman (1989). Chapter 14, Crustal Structure of the Rocky Mountain Region, in Geophysical Framework of the Continental United States, L.C. Paskisir and W.D. Mooney, Editors, Geol. Soc. Am. Memoir 172.

Sadigh, K., J. Egan and R. Youngs (1986). "Specification of Ground Motion for Seismic Design of Long Period Structures," *Earthquake Notes,* Vol. 57, p. 13 (as published in Joyner and Boore, 1988).

Schnabel, P.B., J. Lysmer and H.B. Seed (1972). "SHAKE: A computer program for earthquake response analysis of horizontally layered sites," Earthquake Engin. Res. Center, Univ. of Calif. at Berkeley, UBC/EERC 72-12.

Schneider, J.F., W.J. Silva, and C.L. Stark (1993). "Ground motion model for the 1989 M 6.9 Loma Prieta earthquake including effects of source, path and site," *Earthquake Spectra,* 9(2), 251-287.

Schuster, G., H. Benz, M. Murphy, J. Hill, C. Sikorski and C.-W. Tsay (1990). "Prediction of seismic ground amplification by forward modeling techniques," *Geotech. Environmental Geophysics,* Stanley H. Ward, ed., 3:1-21.

Seed, H.B. and I.M. Idriss (1970). "Soil moduli and damping factors for dynamic response analyses," Earthquake Engin. Res. Center, Univ. of Calif. at Berkeley, UBC/EERC 70-10.

Seed, H.B., C. Ugas and J. Lysmer (1976). "Site-dependent spectra for earthquake-resistant design," *Bull. Seism. Soc. Am.*, 66:221-243.

Silva, W.J. (1976). "Body waves in a layered anelastic solid," *Bull. Seis. Soc. Am.*, 66(5):1539-1554.

Silva, W.J. (1991). "Global characteristics and site geometry," *Proceedings: NSF/EPRI Workshop on Dynamic Soil Properties and Site Characterization,* Electric Power Res. Inst., EPRI NP-7337.

Silva, W.J. and R.K. Green (1989). "Magnitude and distance scaling of response spectral shapes for rock sites with applications to North American tectonic environment," *Earthquake Spectra,* 5(3), 591-624.

Tucker, B.E. and J.L. King (1984). "Dependence of sediment-filled valley response on the input amplitude and the valley properties," *Bull. Seism. Soc. Am.*, 74, 153-165.

Vidale, J.E. and D.V. Helmberger (1988). "Elastic finite-difference modeling of the 1971 San Fernando, California earthquake," *Bull. Seism. Soc. Am.*, 78(1), 122-141.

TABLE F-1

EMPIRICAL AMPLIFICATION FACTORS

Frequency (Hz)	$b_v(f)$	$V_B(f)$ (m/sec)	$V_B(f)$ (ft/sec)	Amplification Factors Median	Median-σ_{lnA}	Median+σ_{lnA}
0.5	-0.655	469.0	1539	1.27	1.02	1.59
1	-0.698	515.5	1691	1.38	1.11	1.72
2.5	-0.487	592.4	1944	1.34	1.08	1.67
5	-0.292	492.9	1617	1.26	1.01	1.57
10	-0.212	726.7	2348	1.19	0.95	1.48
25	-0.371	512.2	1680	1.18	0.95	1.48
PGA	-0.371	512.2	1680	1.18	0.95	1.48

TABLE F-2

MAGNITUDES (M) AND DISTANCES USED IN OUTCROP MOTIONS

A(g)	f_p*(Hz)	V**(cm/sec)	f_p*(Hz)	V/A(cm/sec/g)	M	R(km)
0.01	4.31	1.02	1.35	102.00	6.0	155.75
0.05	5.47	4.10	1.58	82.00	6.0	58.19
0.10	5.87	7.81	1.66	78.10	6.0	31.81
0.20	6.13	15.18	1.70	75.90	6.0	16.77
0.30	6.22	22.53	1.72	75.10	6.0	11.40
0.40	6.00	37.84	1.36	94.60	6.5	12.52
0.50	5.87	57.67	1.11	115.34	7.0	14.31
0.75	5.95	85.64	1.13	114.19	7.0	9.69
1.00	5.89	132.10	0.98	132.10	7.5	10.27

- Predominant frequencies associated with peak acceleration and peak particle velocity estimated by random process theory.

V** Peak Velocity

Outcrop motions are computed using a source region shear-wave velocity and density of 3.87 km/sec and 2.81 cgs, a stress drop of 120 bars, a kappa value of 0.04 sec, and a $Q(f) = 670\ f^{0.33}$.

TABLE F-3

MEDIAN AMPLIFICATION FACTORS AND STANDARD DEVIATIONS COMPUTED FOR 5% DAMPED RESPONSE SPECTRA, PEAK ACCELERATION, AND PEAK VELOCITY

Frequencies (Hz)	Amplification Factors		(Rock Outcrop)[1] (g)
	Median	Sigma[2]	
0.5	1.03	0.04	0.01
	1.04	0.04	0.05
	1.05	0.06	0.10
	1.07	0.09	0.20
	1.09	0.13	0.30
	1.12	0.17	0.40
	1.12	0.15	0.50
	1.17	0.17	0.75
	1.18	0.13	1.00
1.0	1.10	0.10	0.01
	1.13	0.14	0.05
	1.16	0.19	0.10
	1.22	0.22	0.20
	1.26	0.21	0.30
	1.29	0.23	0.40
	1.33	0.23	0.50
	1.49	0.30	0.75
	1.54	0.28	1.00
2.5	1.61	0.35	0.01
	1.66	0.35	0.05
	1.70	0.35	0.10
	1.73	0.33	0.20
	1.68	0.31	0.30
	1.58	0.32	0.40
	1.51	0.33	0.50
	1.17	0.31	0.75
	1.05	0.31	1.00

TABLE F-3 (CONT.)

MEDIAN AMPLIFICATION FACTORS AND STANDARD DEVIATIONS COMPUTED FOR 5% DAMPED RESPONSE SPECTRA, PEAK ACCELERATION, AND PEAK VELOCITY

Frequencies (Hz)	Amplification Factors		(Rock Outcrop)[1] (g)
	Median	Sigma[2]	
5.0	1.71	0.20	0.01
	1.66	0.19	0.05
	1.59	0.17	0.10
	1.45	0.20	0.20
	1.30	0.27	0.30
	1.14	0.36	0.40
	1.07	0.37	0.50
	0.82	0.41	0.75
	0.74	0.40	1.00
10.0	1.52	0.20	0.01
	1.42	0.16	0.05
	1.33	0.15	0.10
	1.16	0.21	0.20
	1.01	0.29	0.30
	0.90	0.34	0.40
	0.84	0.33	0.50
	0.65	0.38	0.75
	0.59	0.38	1.00
25.0	1.54	0.23	0.01
	1.47	0.19	0.05
	1.40	0.17	0.10
	1.26	0.16	0.20
	1.15	0.19	0.30
	1.08	0.21	0.40
	1.04	0.20	0.50
	0.88	0.21	0.75
	0.83	0.20	1.00

TABLE F-3 (CONT.)

MEDIAN AMPLIFICATION FACTORS AND STANDARD DEVIATIONS COMPUTED FOR 5% DAMPED RESPONSE SPECTRA, PEAK ACCELERATION, AND PEAK VELOCITY

	Amplification Factors		(Rock Outcrop)[1] (g)
	Median	Sigma[2]	
PGA	1.55	0.24	0.01
	1.54	0.21	0.05
	1.50	0.19	0.10
	1.42	0.17	0.20
	1.33	0.19	0.30
	1.24	0.20	0.40
	1.20	0.19	0.50
	1.03	0.19	0.75
	0.98	0.18	1.00
PGV	1.21	0.15	0.01
	1.28	0.17	0.05
	1.30	0.17	0.10
	1.32	0.17	0.20
	1.33	0.16	0.30
	1.25	0.12	0.40
	1.20	0.10	0.50
	1.19	0.10	0.75
	1.15	0.07	1.00

[1]For levels of control motion between those shown, linear interpolation may be used to determine the appropriate amplification factors.
[2]Sigma (ln)

TABLE F-4

SUMMARY OF INCIDENCE ANGLES

Fault	Dip (deg.)	Source Depth (km)	Incidence Angle (deg.)
Front Range	30	5	73
	30	10	69
	30	15	66
	45	5	69
	45	10	61
	45	15	57
	60	5	54
	60	10	66
	60	15	48
Derby	90	10 (15)*	56
	90	10 (20)*	63
	90	10 (30)*	72

*Source depth fixed, epicentral distance varied

TABLE F-5

SUMMARY OF VELOCITIES

Case	Sedimentary Rock km/sec (ft/sec)	Crystalline Basement km/sec (ft/sec)
1	2.05 (6720)	3.58 (11,700)
2	1.64 (5380)	3.58 (11,700)
3	2.46 (5860)	3.58 (11,700)
4	2.05 (6720)	2.86 (9,380)
5	2.05 (6720)	4.30 (14,100)
6	1.64 (5380)	4.30 (14,100)
7	2.46 (5860)	2.86 (9,380)
median	2.05 (6720)	3.50 (11,500)
upper range	2.46 (5860)	4.30 (14,100)
lower range	1.64 (5380)	2.86 (9,380)

TABLE F-6

SUMMARY OF EMPIRICAL AND ANALYTICAL AMPLIFICATION FACTORS

		AMPLIFICATION FACTOR	
FREQUENCY (Hz)	ROCK OUTCROP (g)	EMPIRICAL	ANALYTICAL
0.5	0.01	1.27	1.03
	0.05	1.27	1.04
	0.10	1.27	1.05
	0.20	1.27	1.07
	0.30	1.27	1.09
	0.40	1.27	1.12
	0.50	1.27	1.12
	0.75	1.27	1.17
	1.00	1.27	1.18
1.0	0.01	1.38	1.10
	0.05	1.38	1.13
	0.10	1.38	1.16
	0.20	1.38	1.22
	0.30	1.38	1.26
	0.40	1.38	1.29
	0.50	1.38	1.33
	0.75	1.38	1.49
	1.00	1.38	1.54
2.5	0.01	1.34	1.61
	0.05	1.34	1.66
	0.10	1.34	1.70
	0.20	1.34	1.73
	0.30	1.34	1.68
	0.40	1.34	1.58
	0.50	1.34	1.51
	0.75	1.34	1.17
	1.00	1.34	1.05

		AMPLIFICATION FACTOR	
FREQUENCY (Hz)	ROCK OUTCROP (g)	EMPIRICAL	ANALYTICAL
5.0	0.01	1.26	1.71
	0.05	1.26	1.66
	0.10	1.26	1.59
	0.20	1.26	1.45
	0.30	1.26	1.30
	0.40	1.26	1.14
	0.50	1.26	1.07
	0.75	1.26	0.82
	1.00	1.26	0.74
10.0	0.01	1.19	1.52
	0.05	1.19	1.42
	0.10	1.19	1.33
	0.20	1.19	1.16
	0.30	1.19	1.01
	0.40	1.19	0.90
	0.50	1.19	0.84
	0.75	1.19	0.65
	1.00	1.19	0.59
25	0.01	1.18	1.54
	0.05	1.18	1.47
	0.10	1.18	1.40
	0.20	1.18	1.26
	0.30	1.18	1.15
	0.40	1.18	1.08
	0.50	1.18	1.04
	0.75	1.18	0.88
	1.00	1.18	0.83
PGA	0.01	1.18	1.55
	0.05	1.18	1.54
	0.10	1.18	1.50
	0.20	1.18	1.42
	0.30	1.18	1.33
	0.40	1.18	1.24
	0.50	1.18	1.20
	0.75	1.18	1.03
	1.00	1.18	0.98

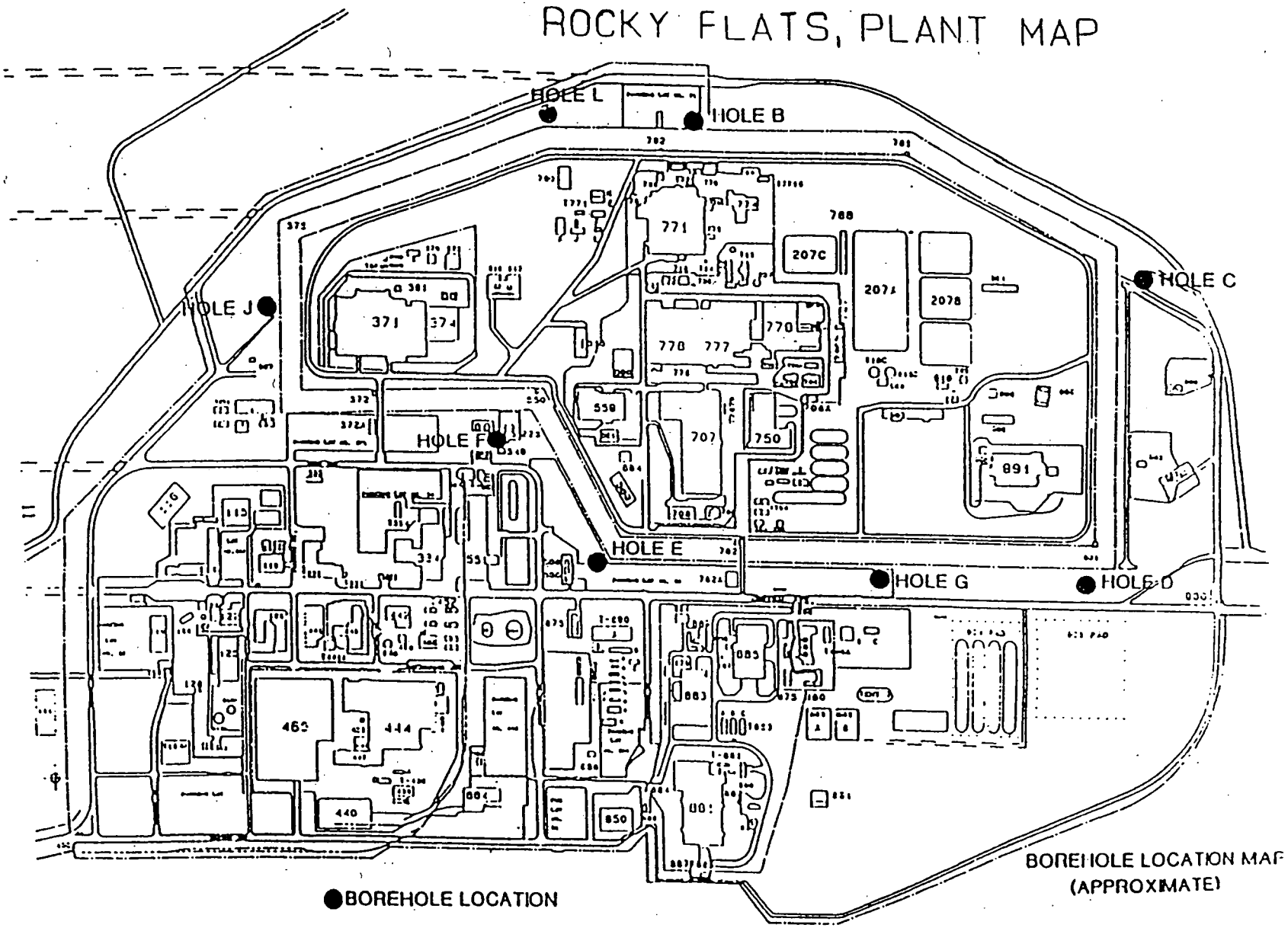

Figure F-1. Plan view of Rocky Flats Plant showing borehole locations where downhole velocities were obtained (Blackhawk, 1994).

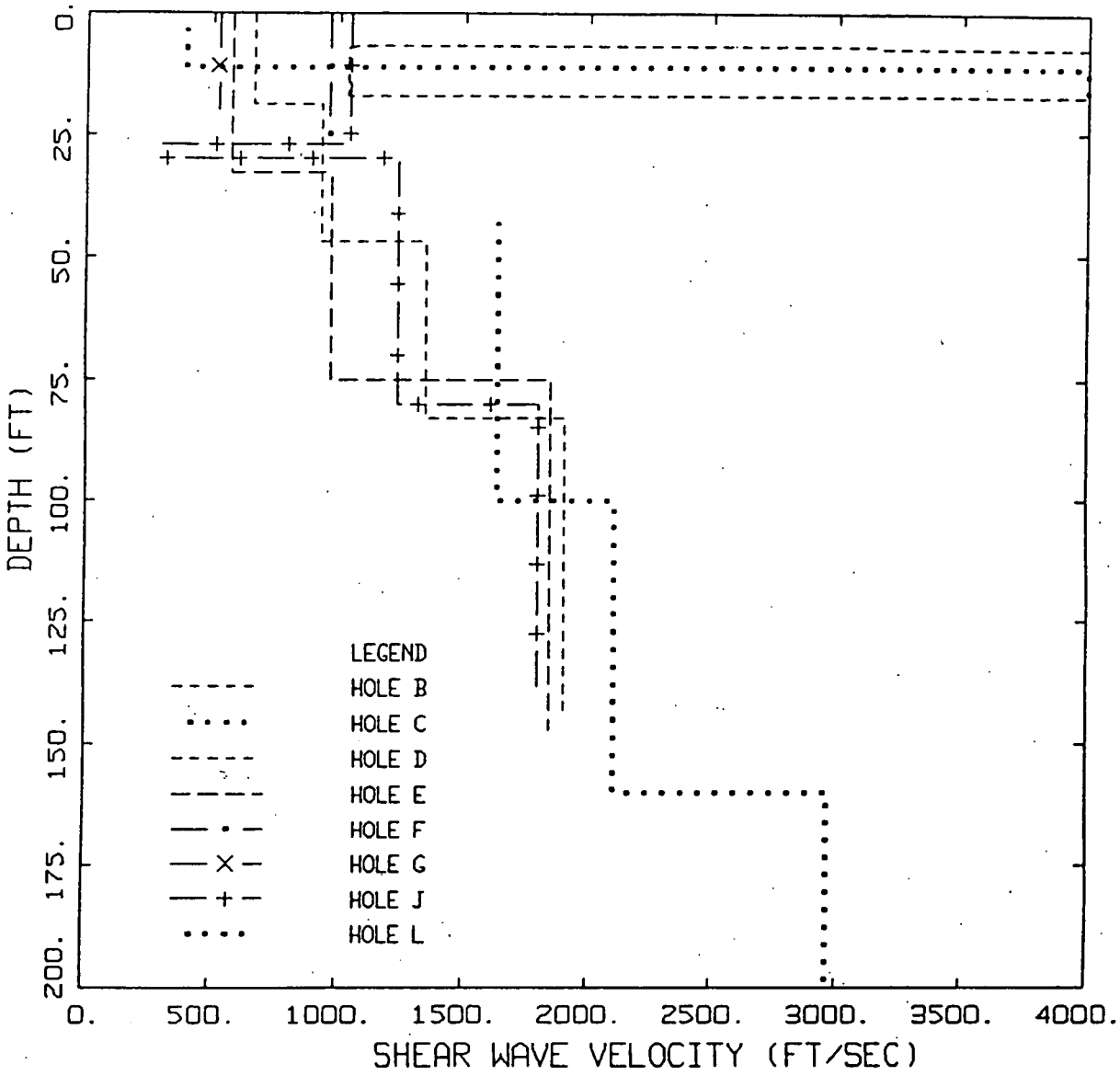

ROCKY FLATS VELOCITY PROFILES

Figure F-2. Downhole shear wave velocity profiles corresponding to Figure 1 boreholes. Profiles C and D have shear-wave velocities of 6,452 ft/sec and 11,111 ft/sec respectively and are truncated for plotting.

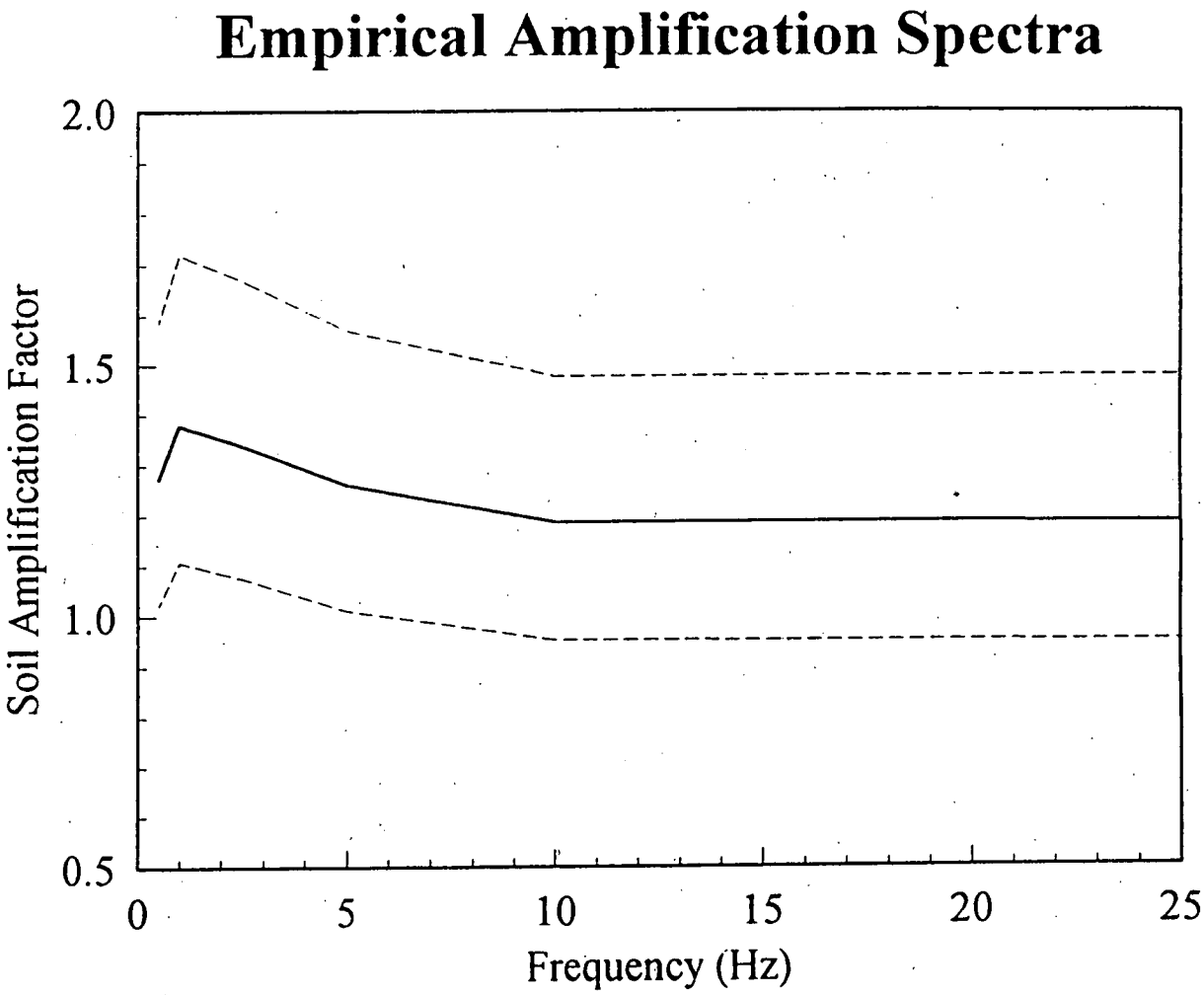

Figure F-3. Smoothed empirical soil amplification factors for Rocky Flats: the solid line is the median amplification spectrum; the dashed lines are the median plus and minus standard deviation amplification spectra.

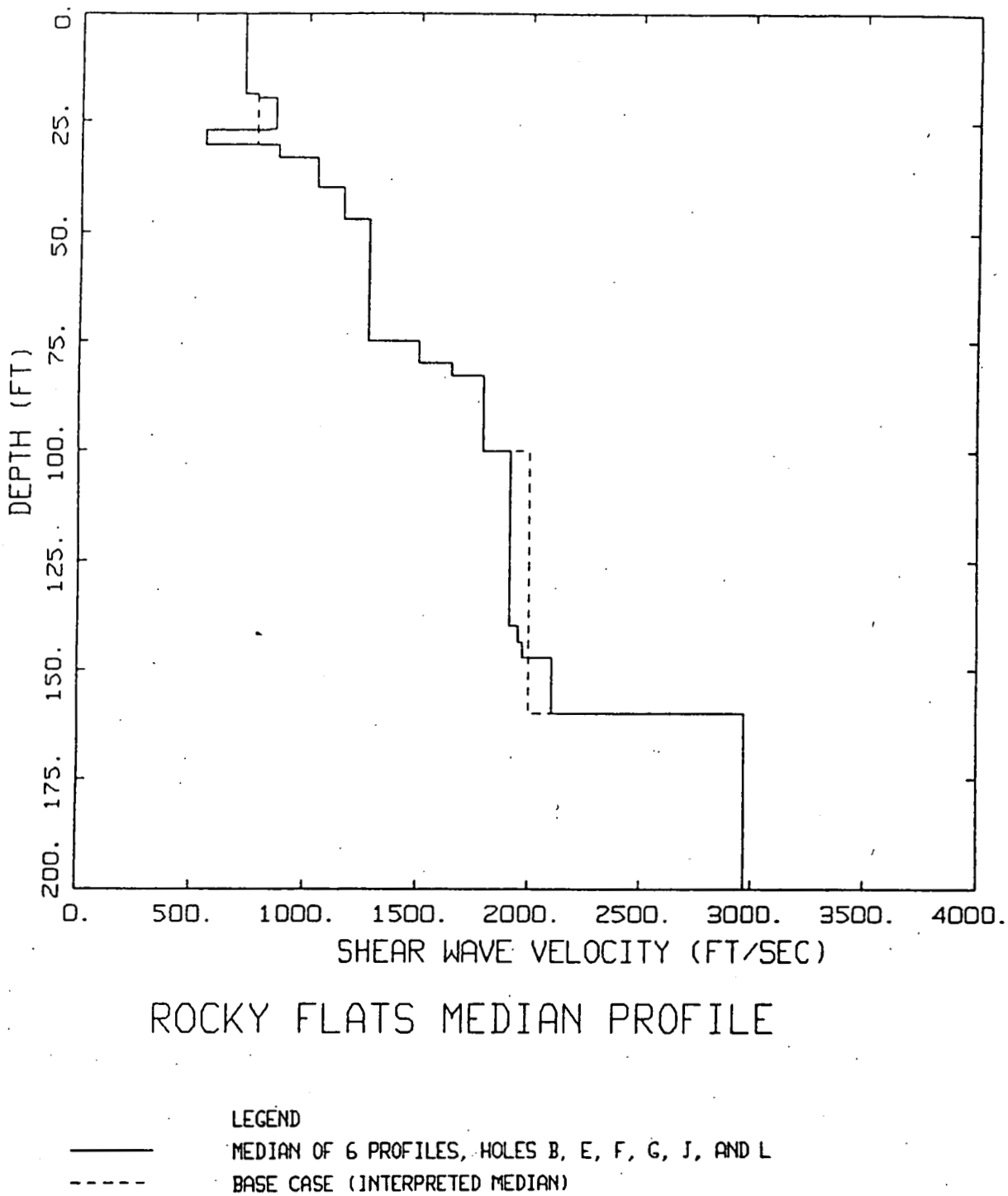

Figure F-4. Median shear-wave velocity profile based on data from holes B, E, F, G, J, and L (solid line). Profiles C and D are considered unreliable and were not used in computing the median profile. The base case profile used for analyses is shown as the dashed line.

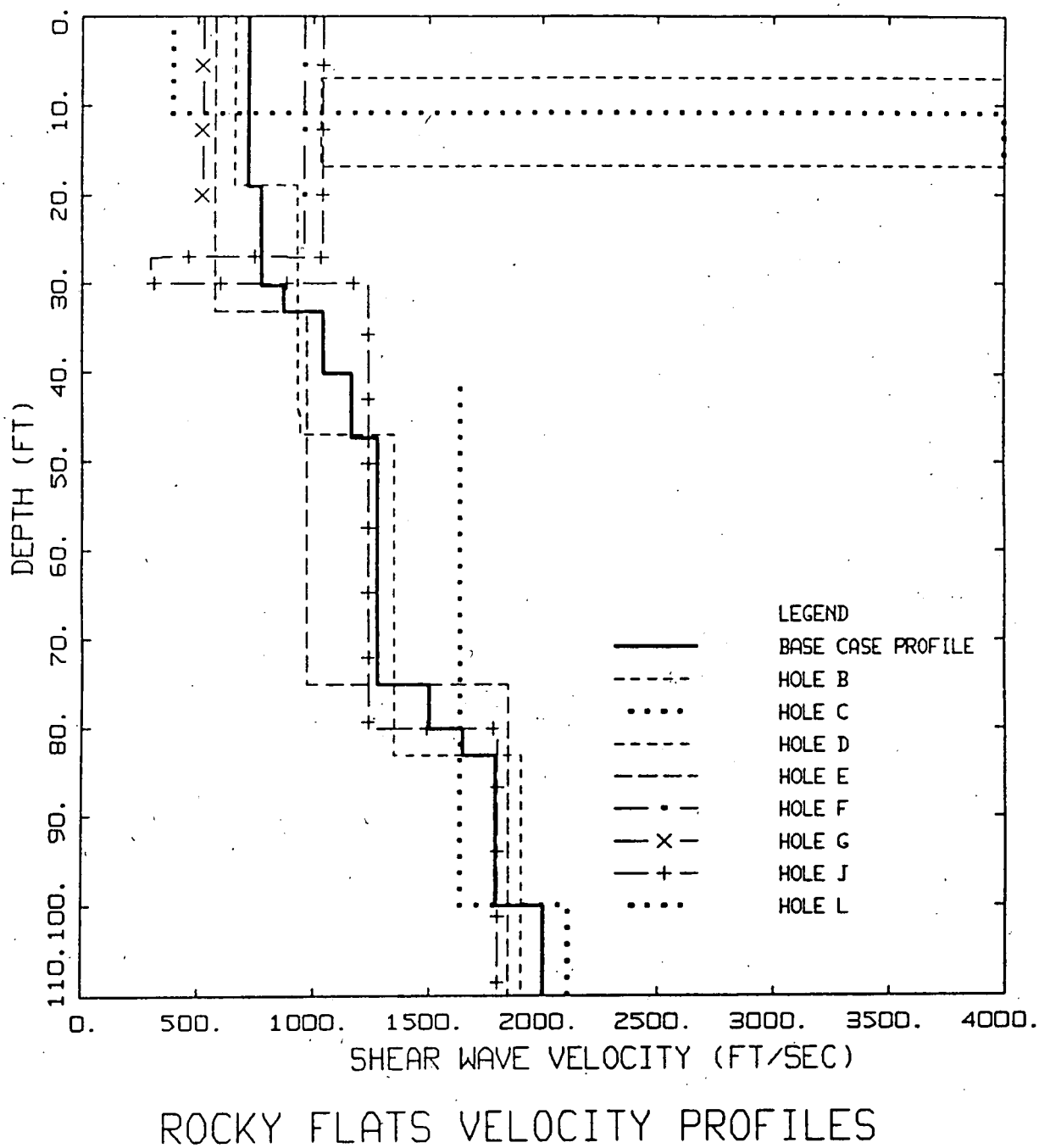

Figure F-5. Base case profile (heavy line) along with the measured profiles.

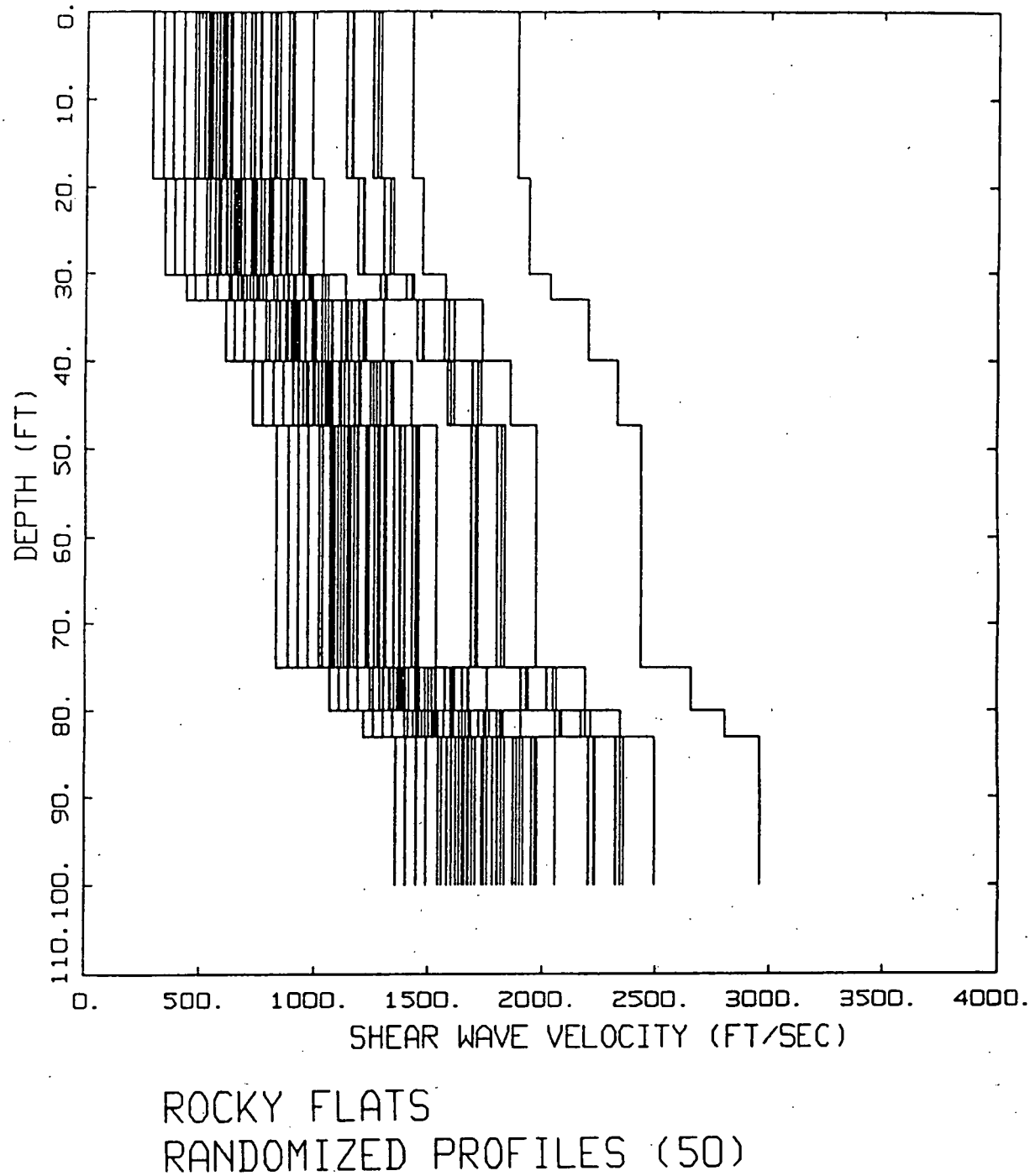

Figure F-6. Suite of 50 randomized profiles generated from the base case profile (Figure F-4).

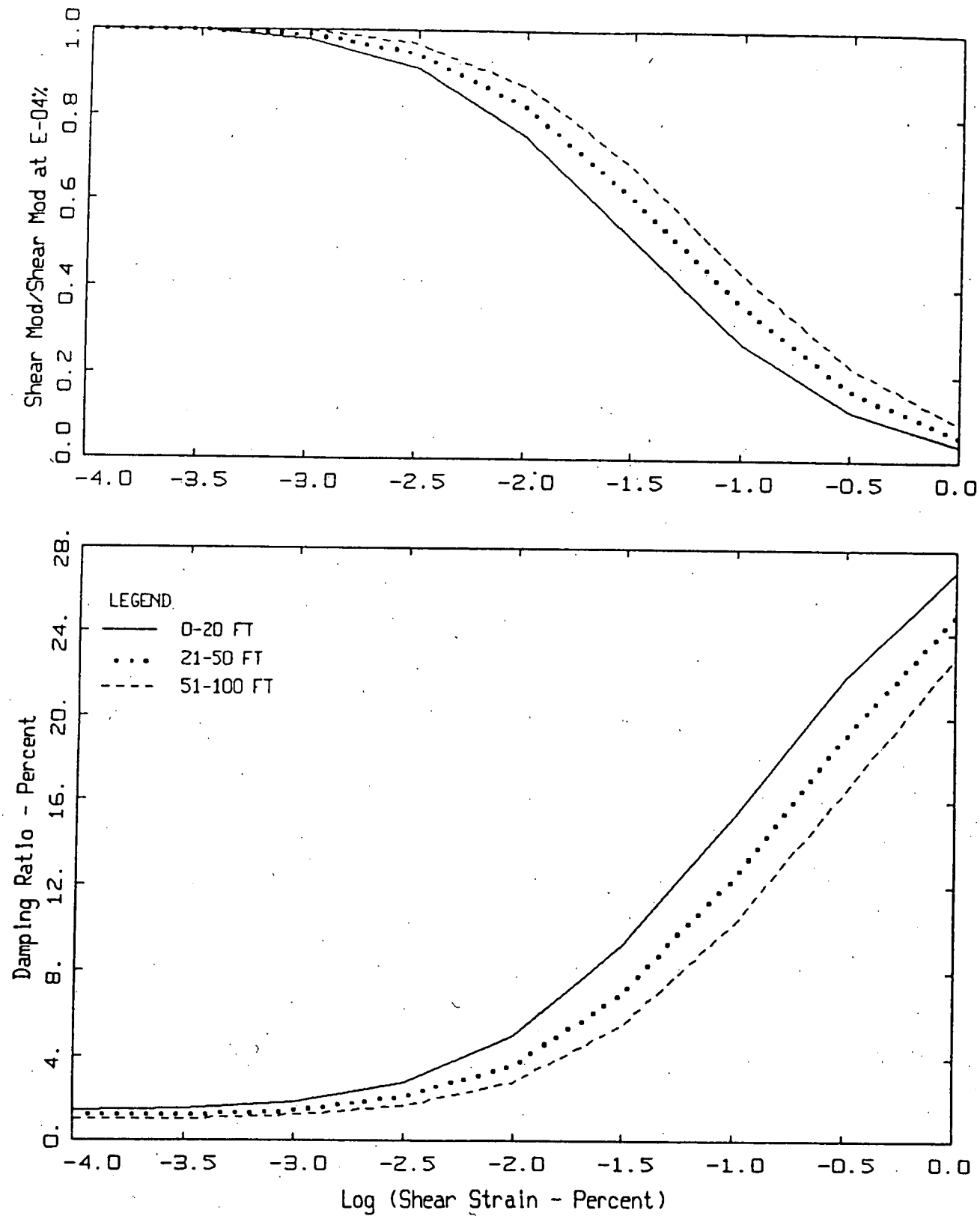

Figure F-7. Depth dependent modulus reduction and damping curves appropriate for soils comprised of sands, gravels, and low plasticity clays (EPRI, 1993).

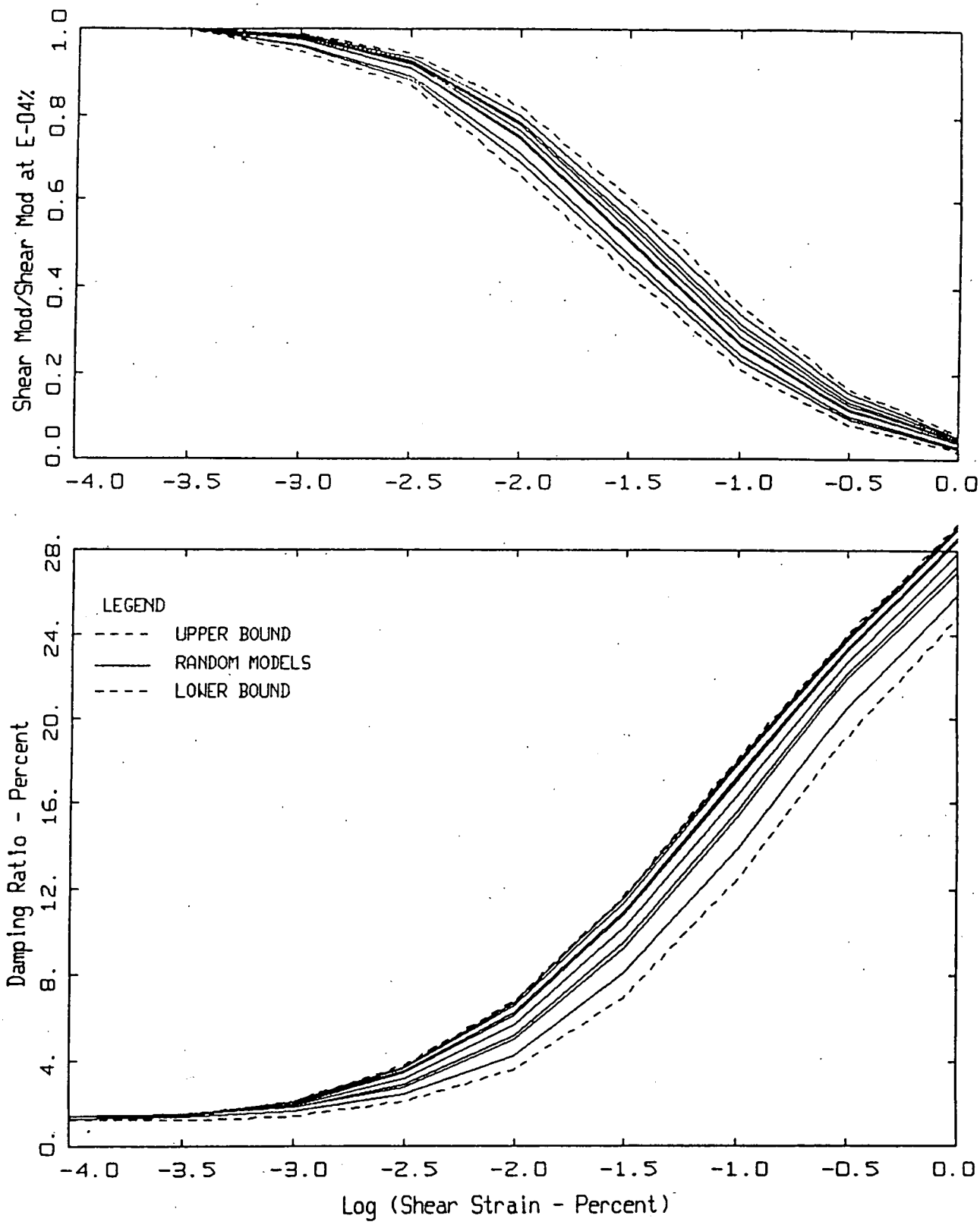

Figure F-8. Example of randomized modulus reduction and damping curves (10) taken from the suite of 50 used in the analyses. Dashed lines are upper- and lower-bounds. Depth range is 0-20 ft.

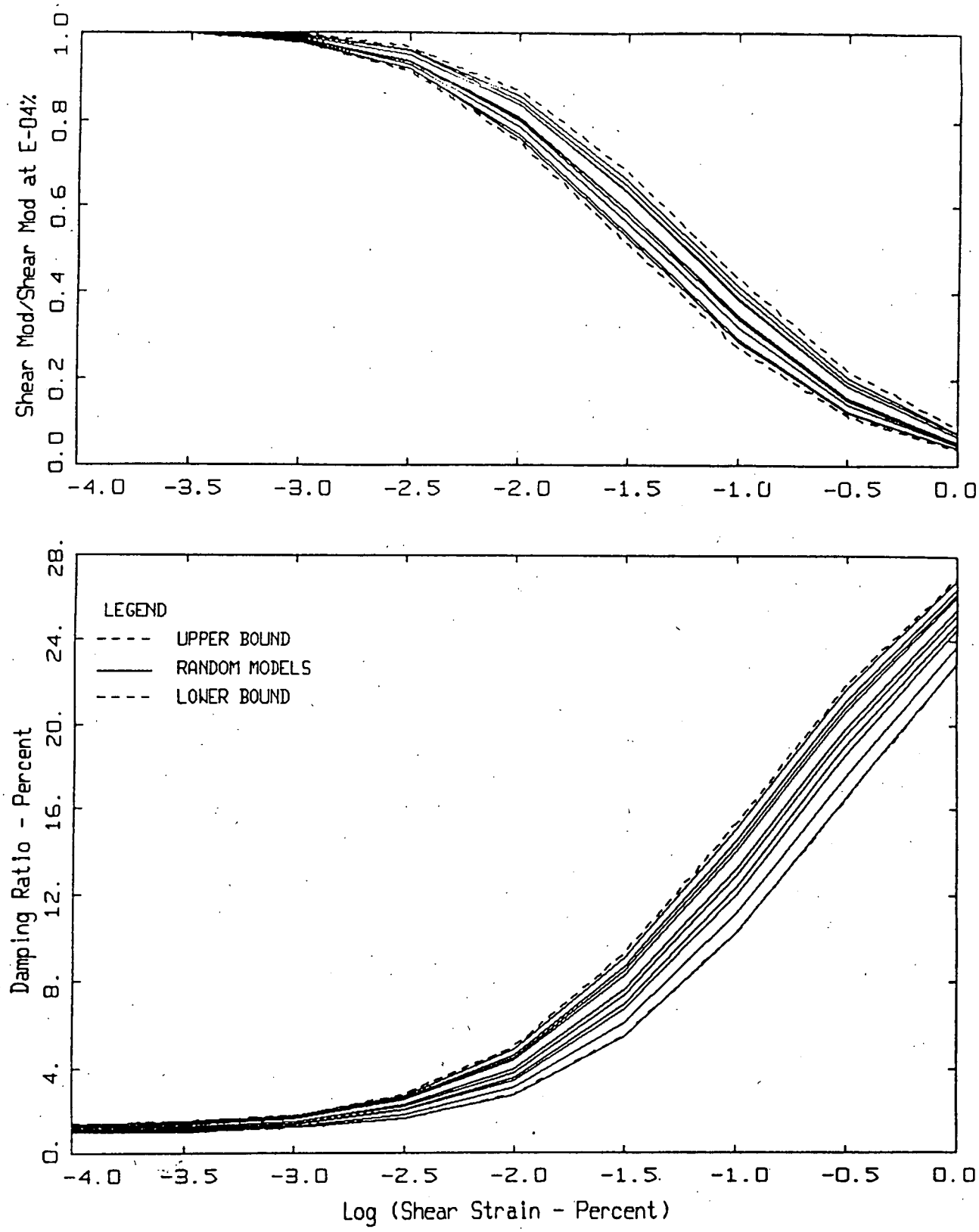

Figure F-9. Example of randomized modulus reduction and damping curves (10) taken from the suite of 50 used in the analyses. Dashed lines are upper- and lower-bounds. Depth range is 21-50 ft.

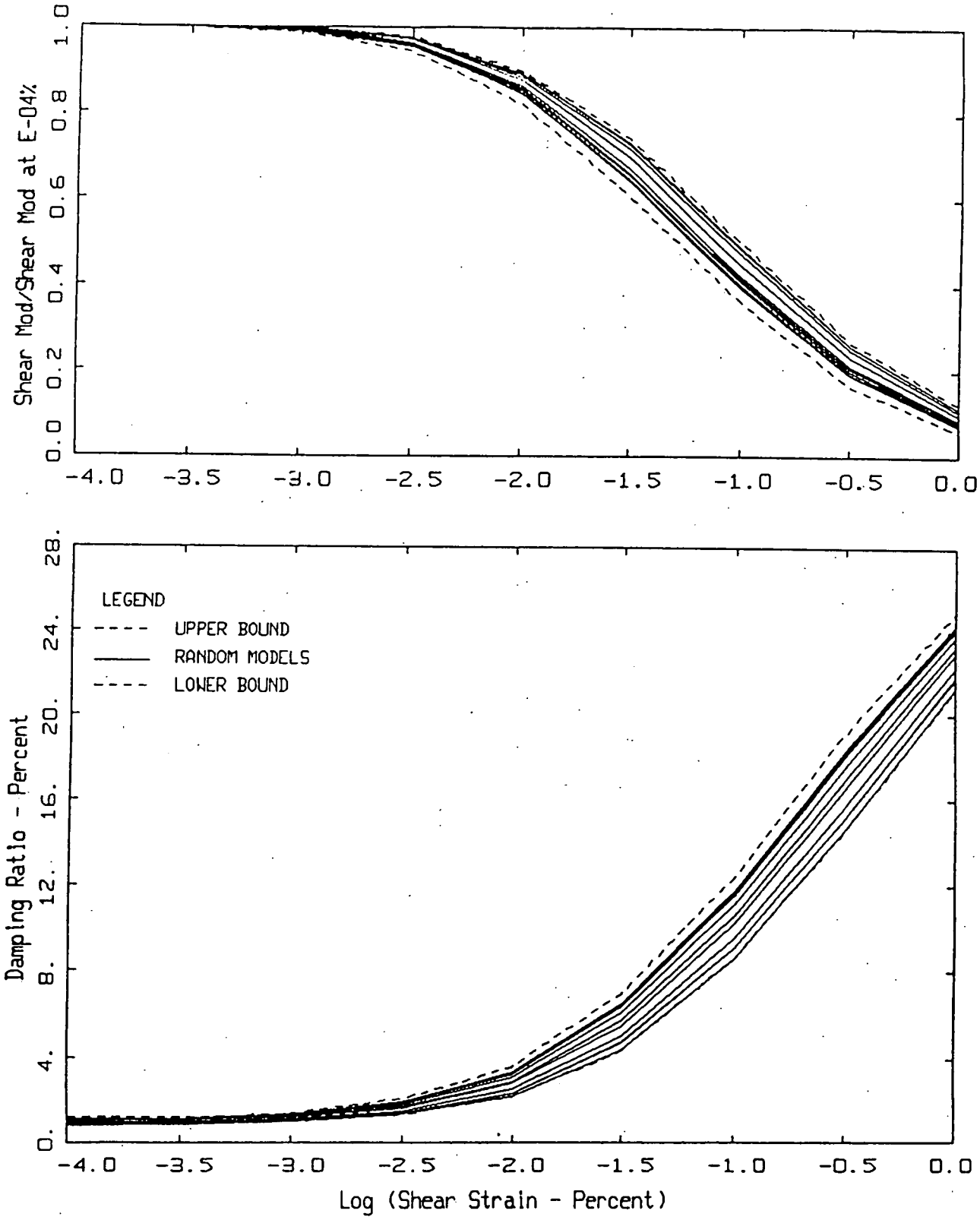

Figure F-10. Example of randomized modulus reduction and damping curves (10) taken from the suite of 50 used in the analyses. Dashed lines are upper- and lower-bounds. Depth range is 51-100 ft.

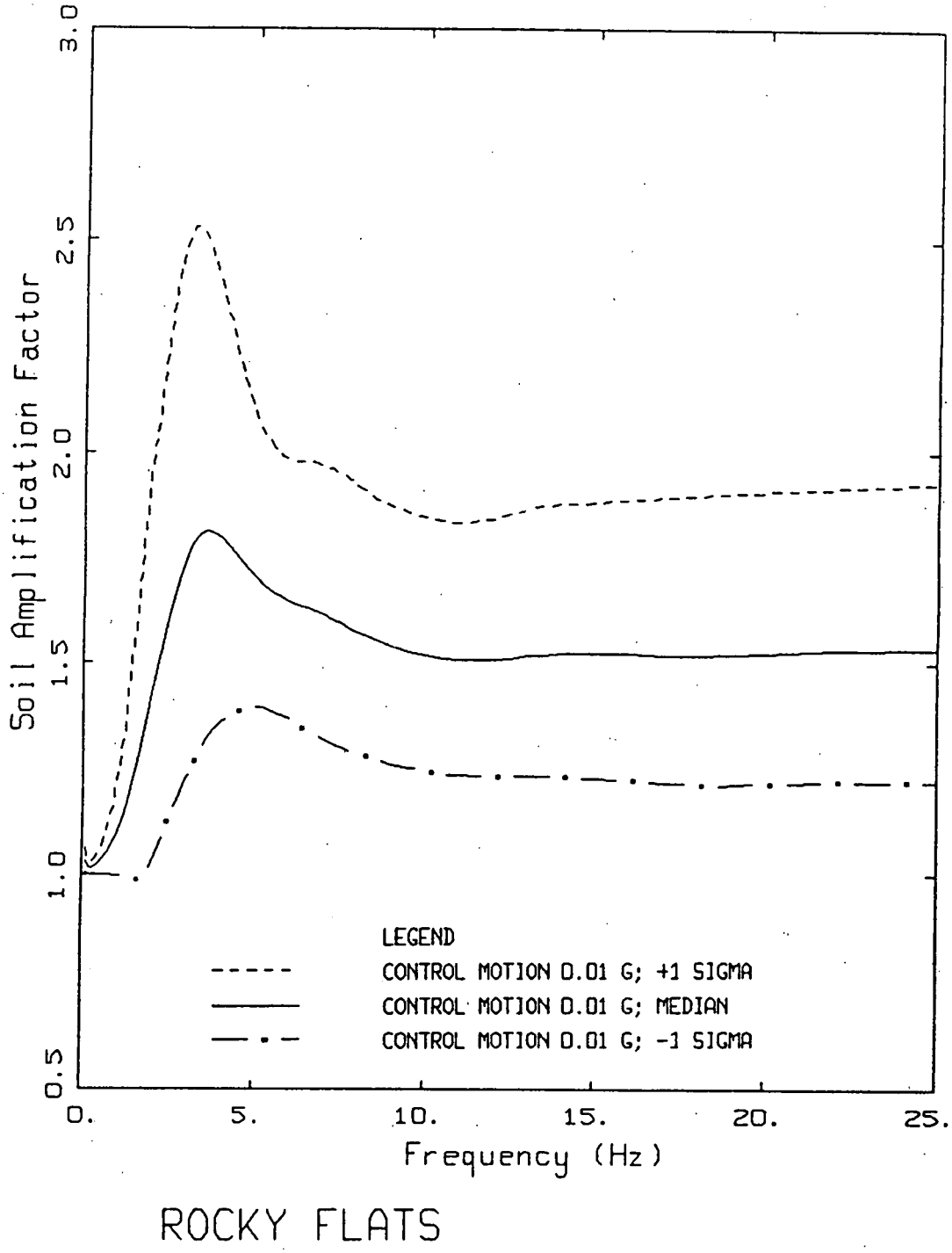

Figure F-11. Median and 1 sigma amplification factors for 5% damped response spectra. Control motion is 0.01g.

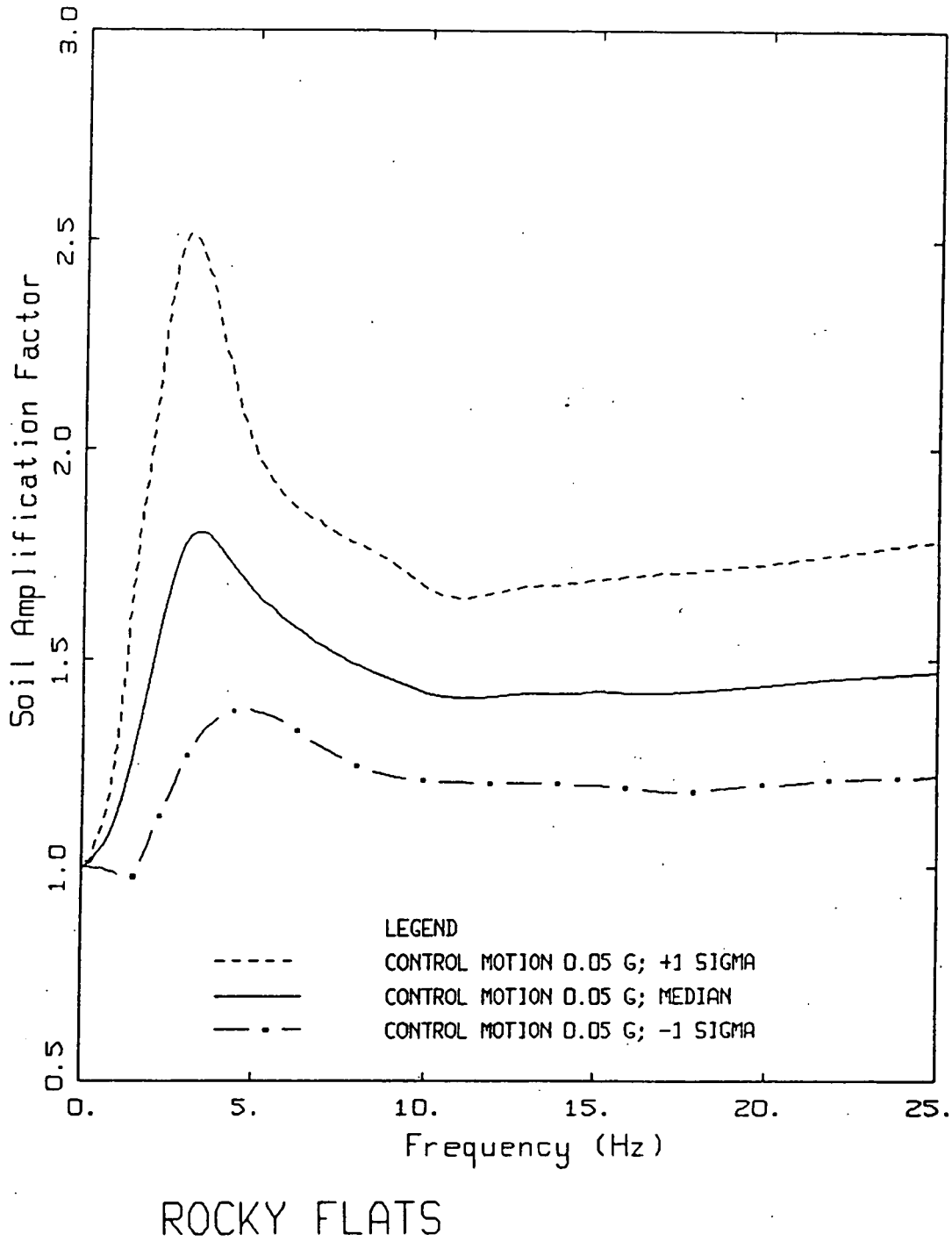

Figure F-12. Median and 1 sigma amplification factors for 5% damped response spectra. Control motion is 0.05g.

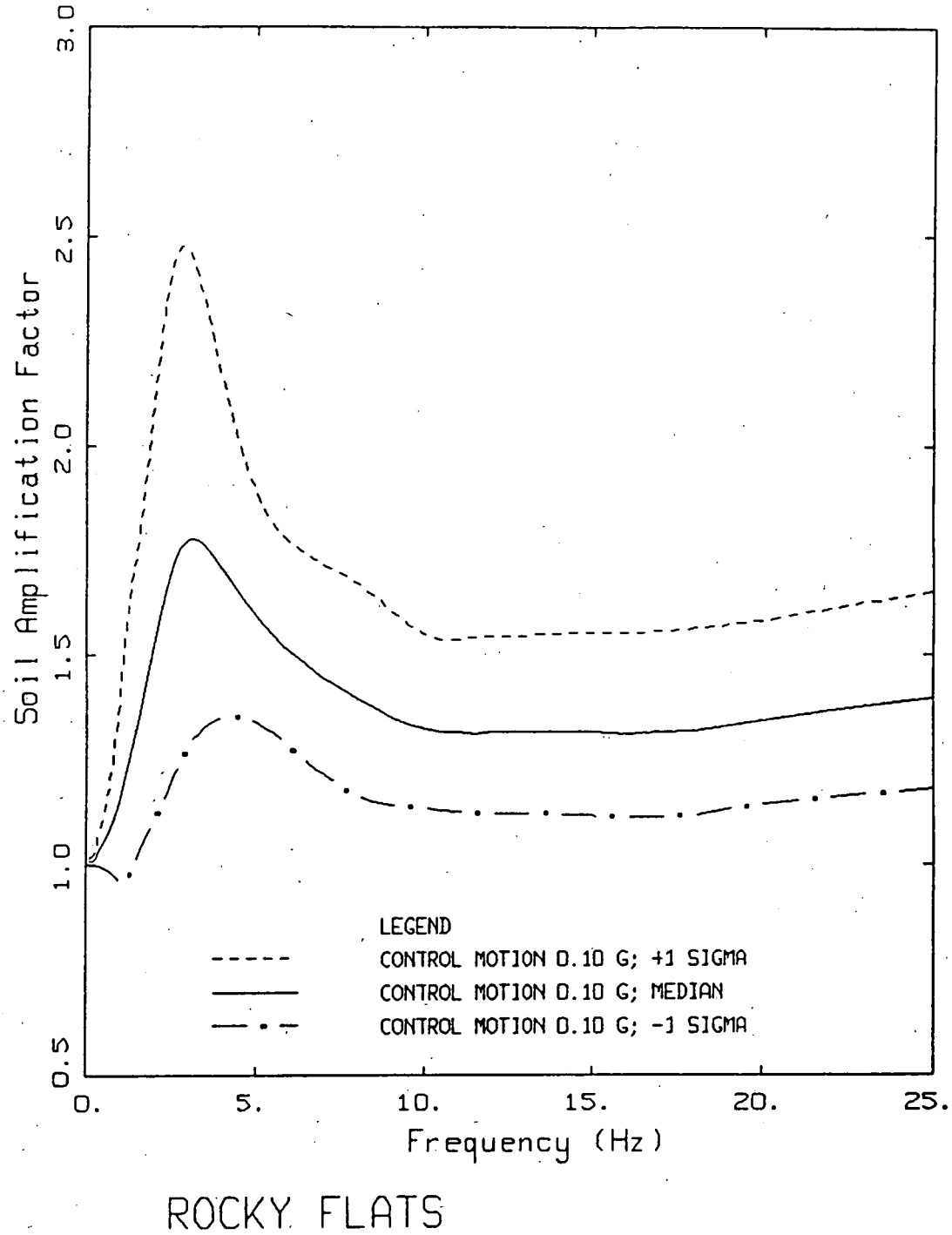

Figure F-13. Median and 1 sigma amplification factors for 5% damped response spectra. Control motion is 0.10g.

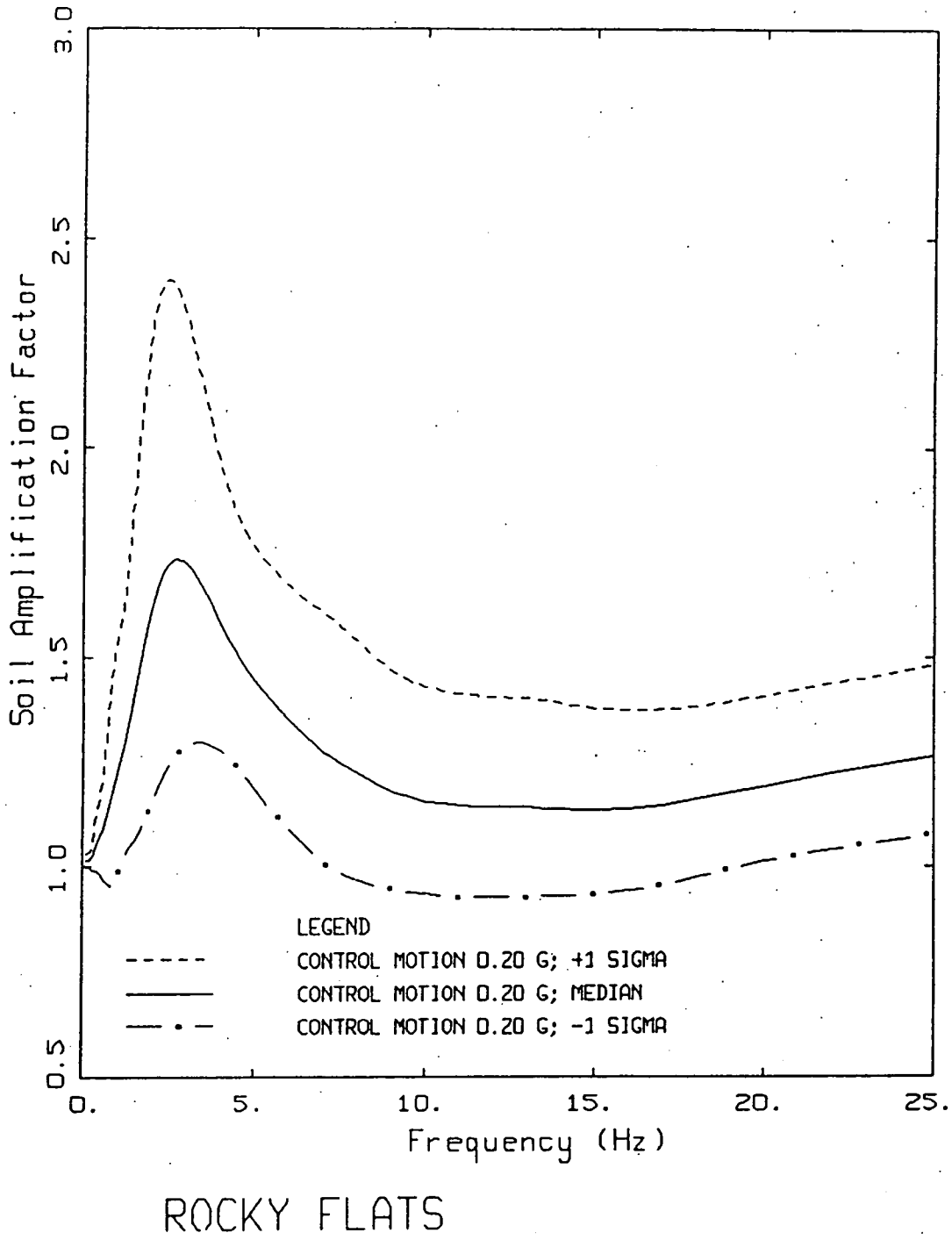

Figure F-14. Median and 1 sigma amplification factors for 5% damped response spectra. Control motion is 0.20g.

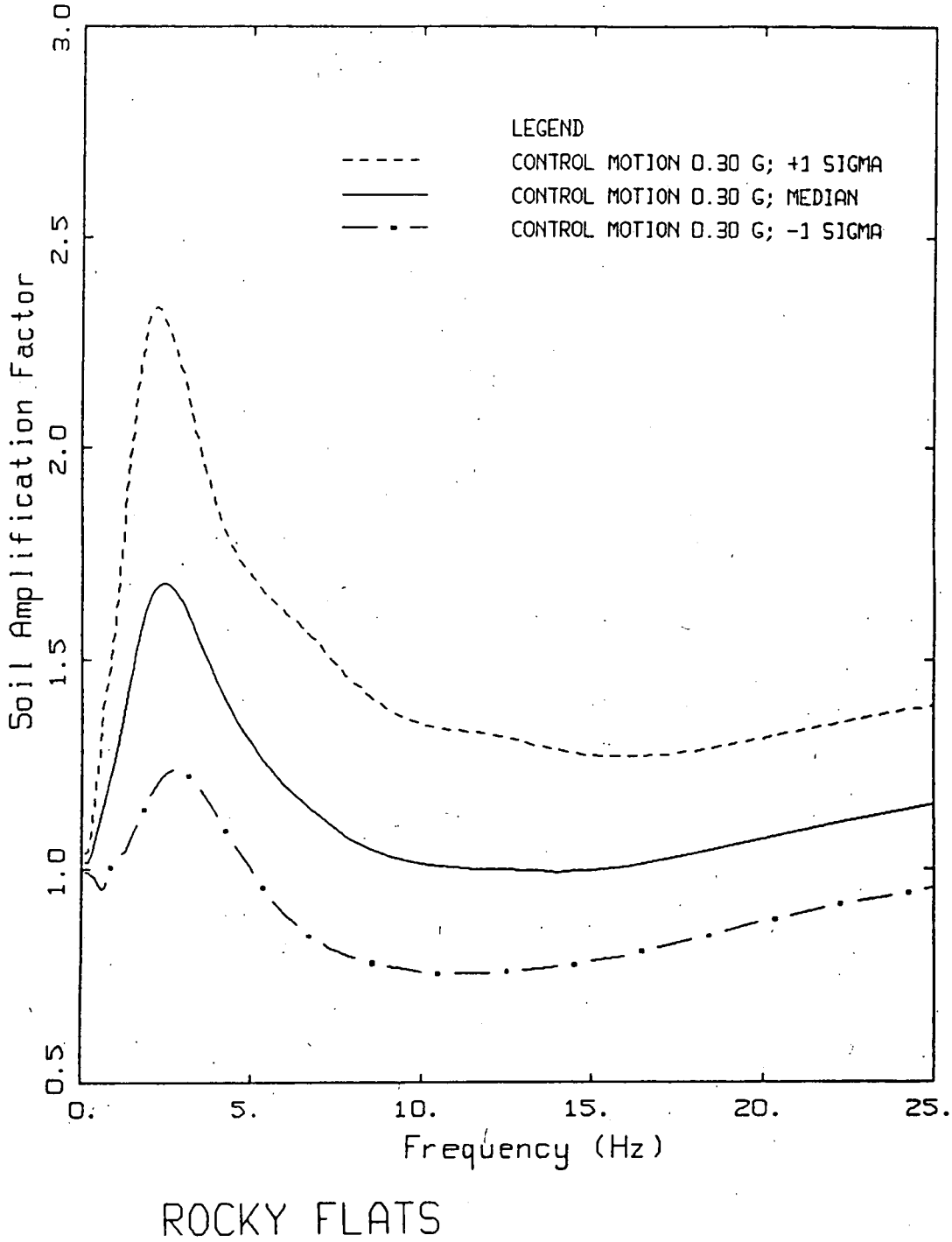

Figure F-15. Median and 1 sigma amplification factors for 5% damped response spectra. Control motion is 0.30g.

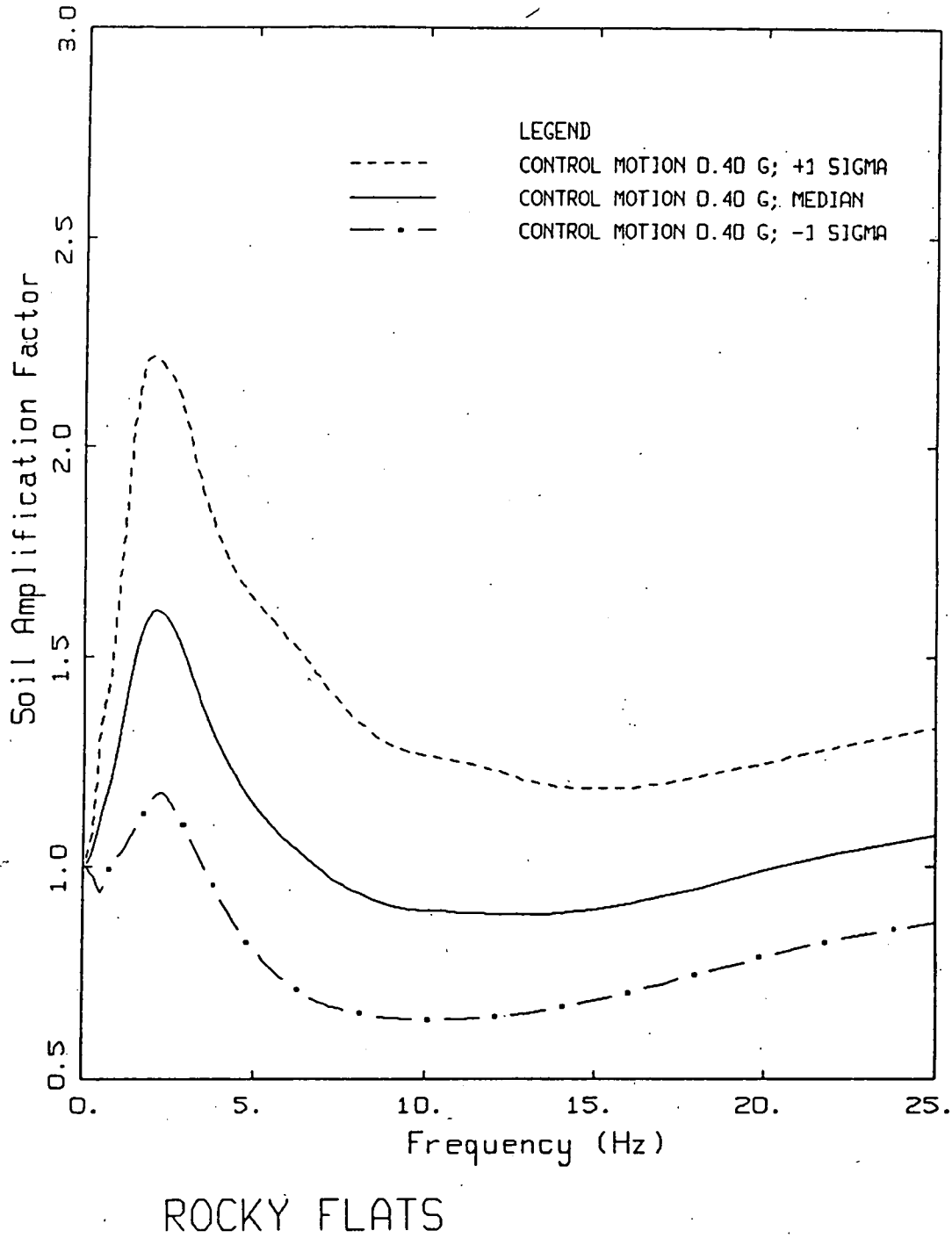

Figure F-16. Median and 1 sigma amplification factors for 5% damped response spectra. Control motion is 0.40g.

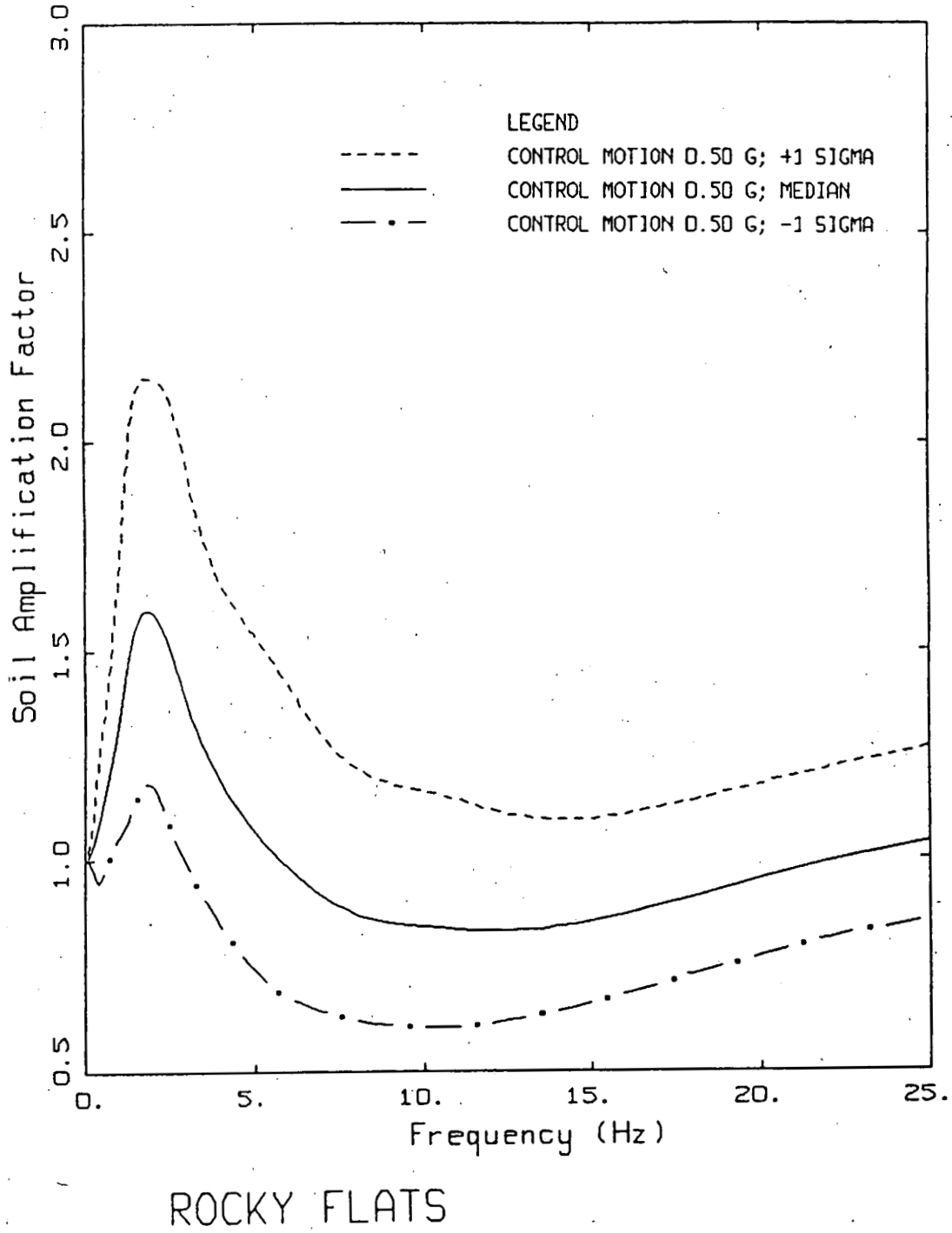

Figure F-17. Median and 1 sigma amplification factors for 5% damped response spectra. Control motion is 0.50g.

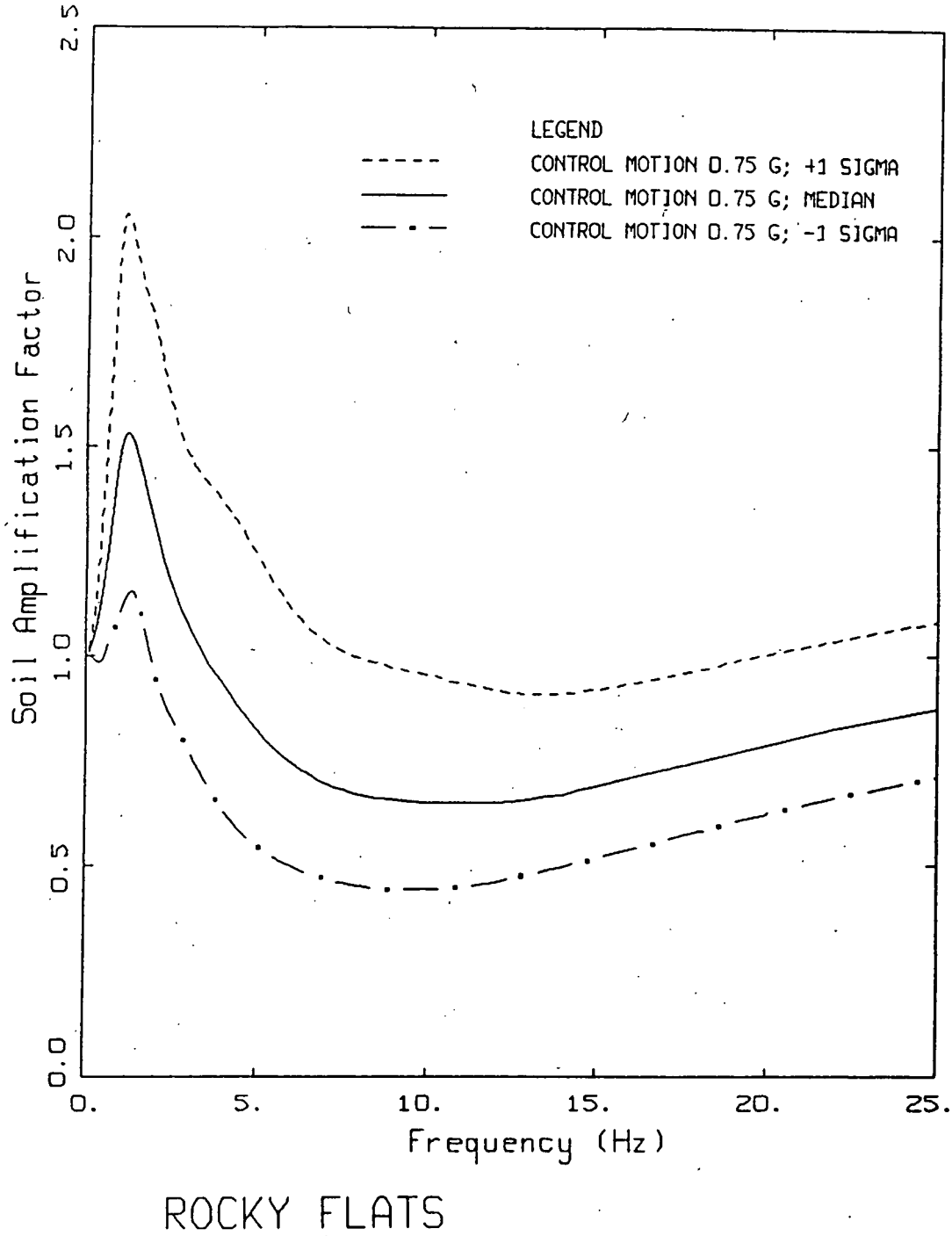

Figure F-18. Median and 1 sigma amplification factors for 5% damped response spectra. Control motion is 0.75g.

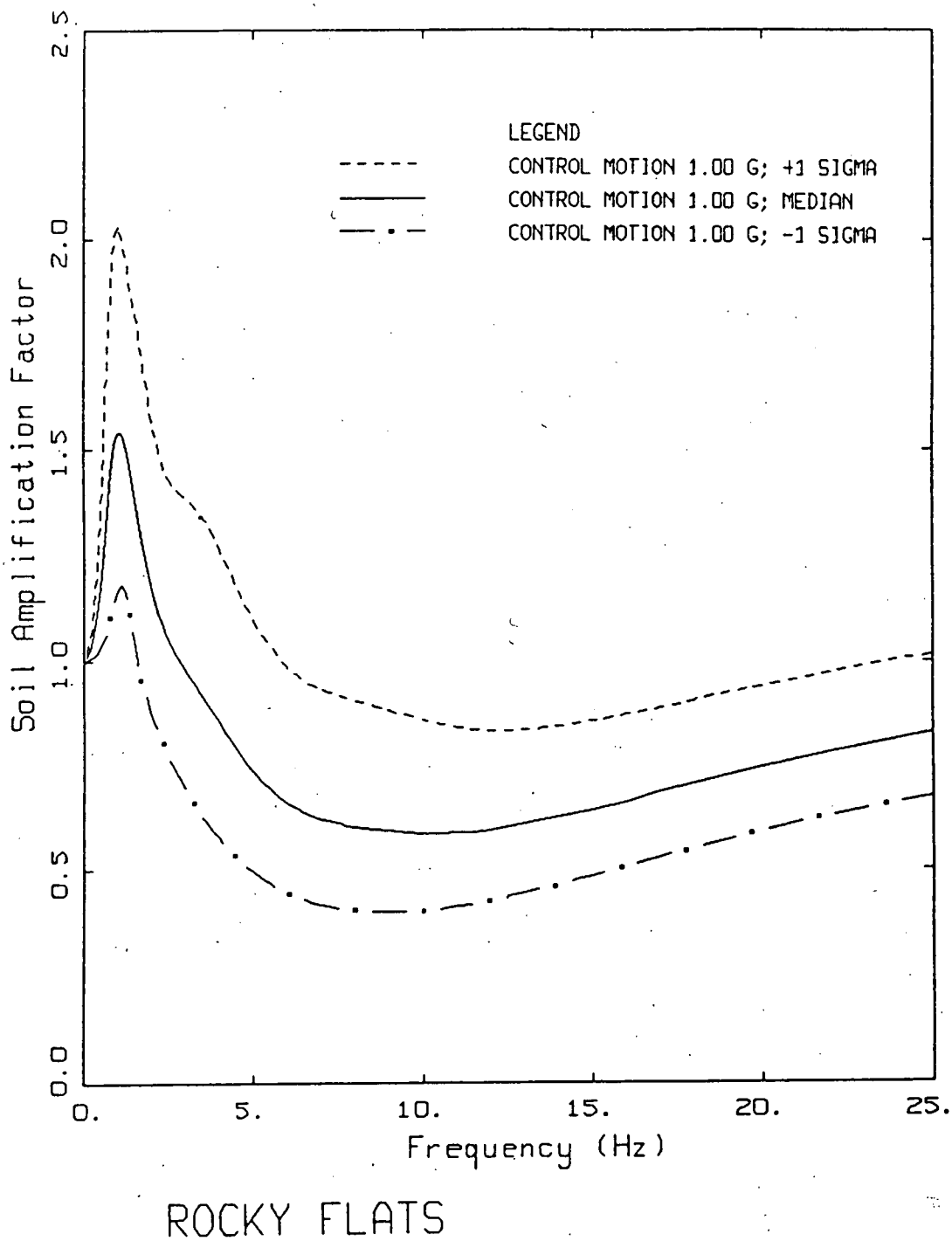

Figure F-19. Median and 1 sigma amplification factors for 5% damped response spectra. Control motion is 1.00g.

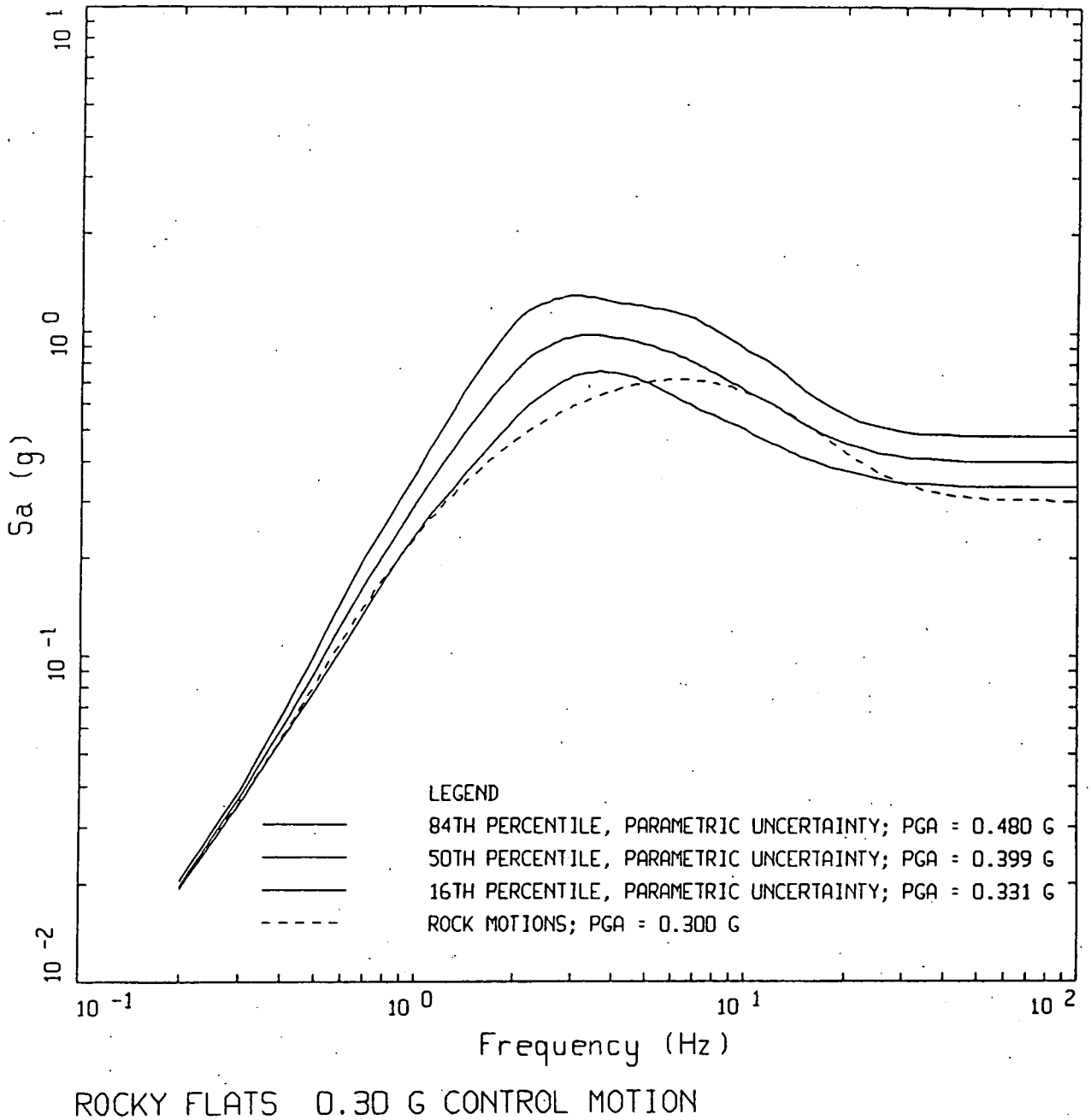

Figure F-20. Plot of median and ± 1 sigma soil motions for an input control motion (rock) of 0.3g (dashed line).

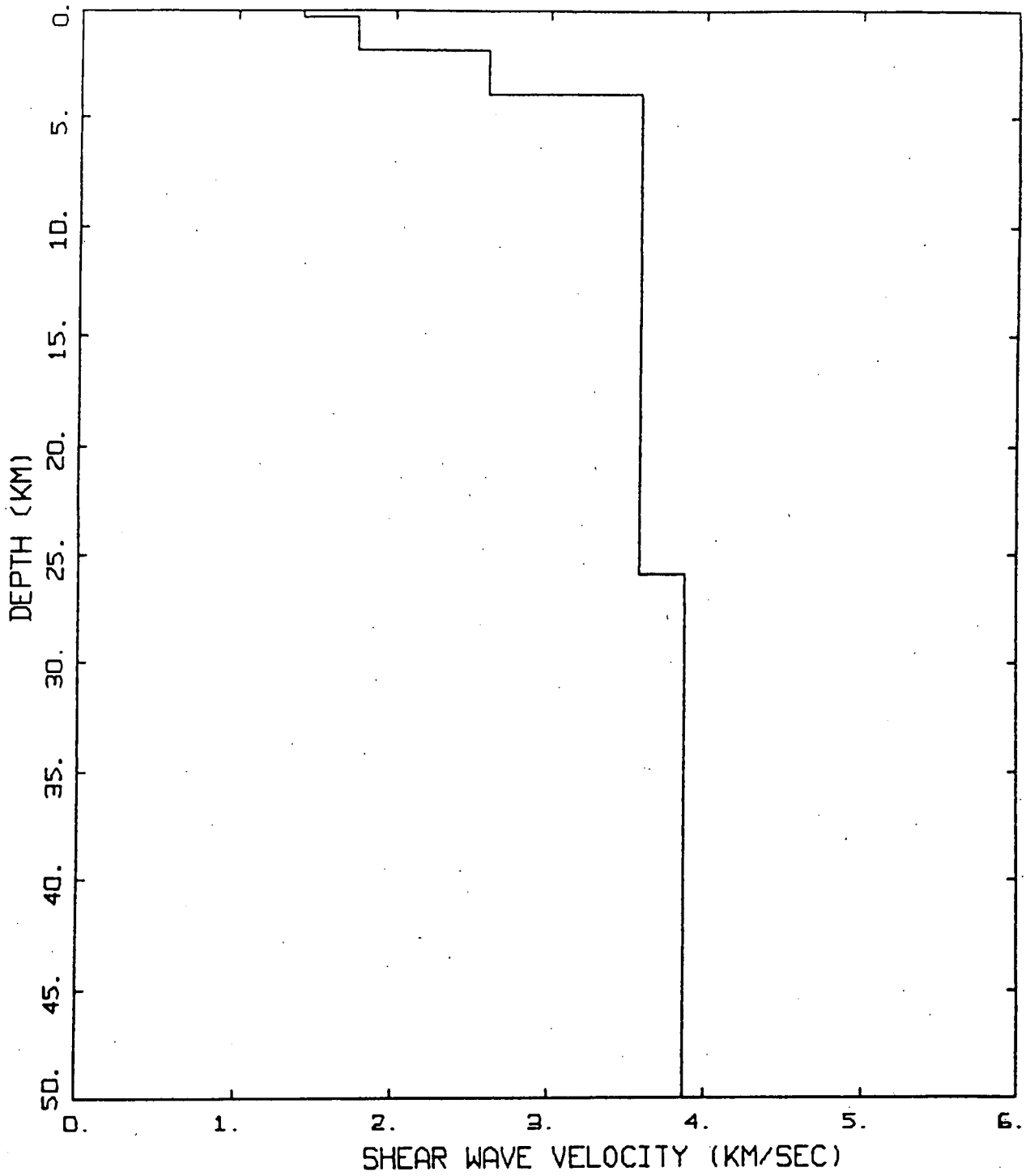

S-WAVE CRUSTAL PROFILE
ROCKY FLATS

Figure F-21. One-dimensional shear-wave velocity profile for the Rocky Flats crust.

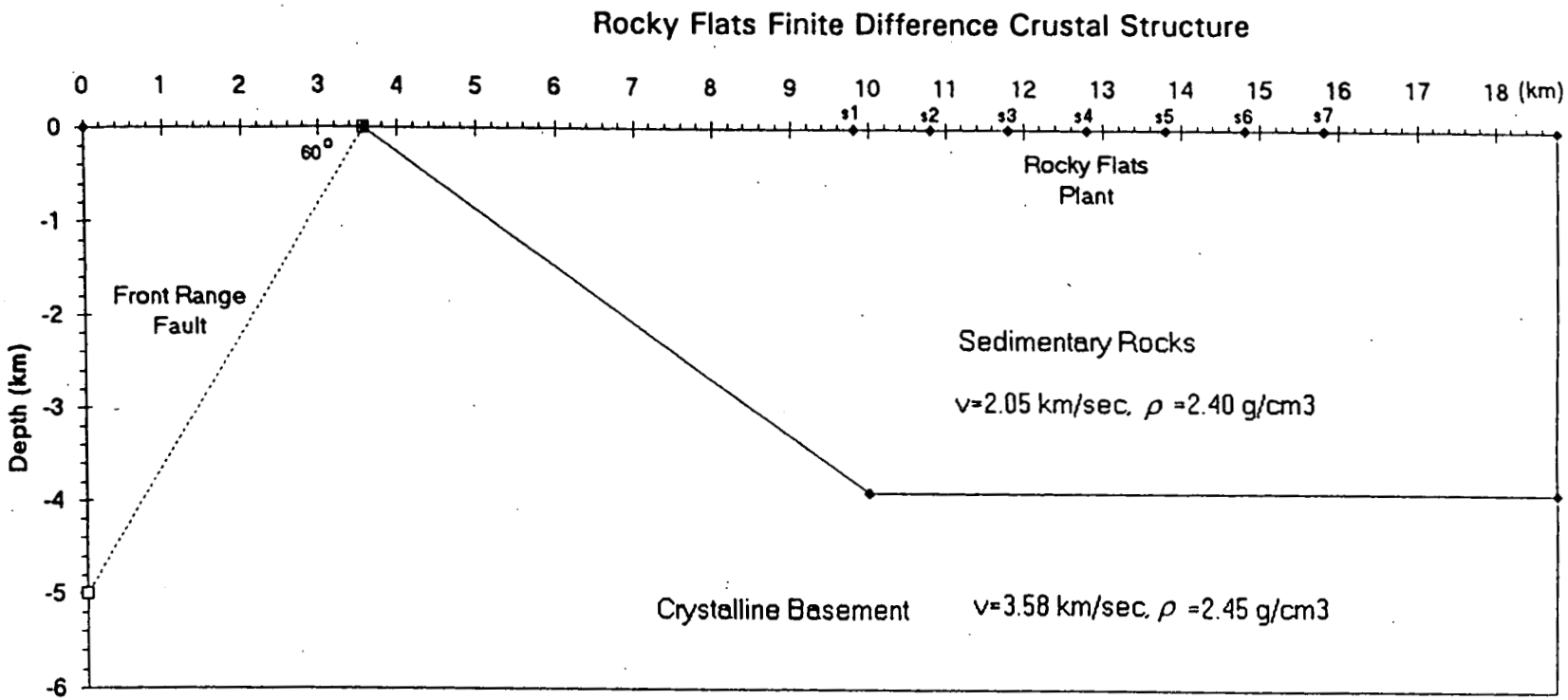

Figure F-22. Two-dimensional crustal structure used in the elastice finite difference computations.

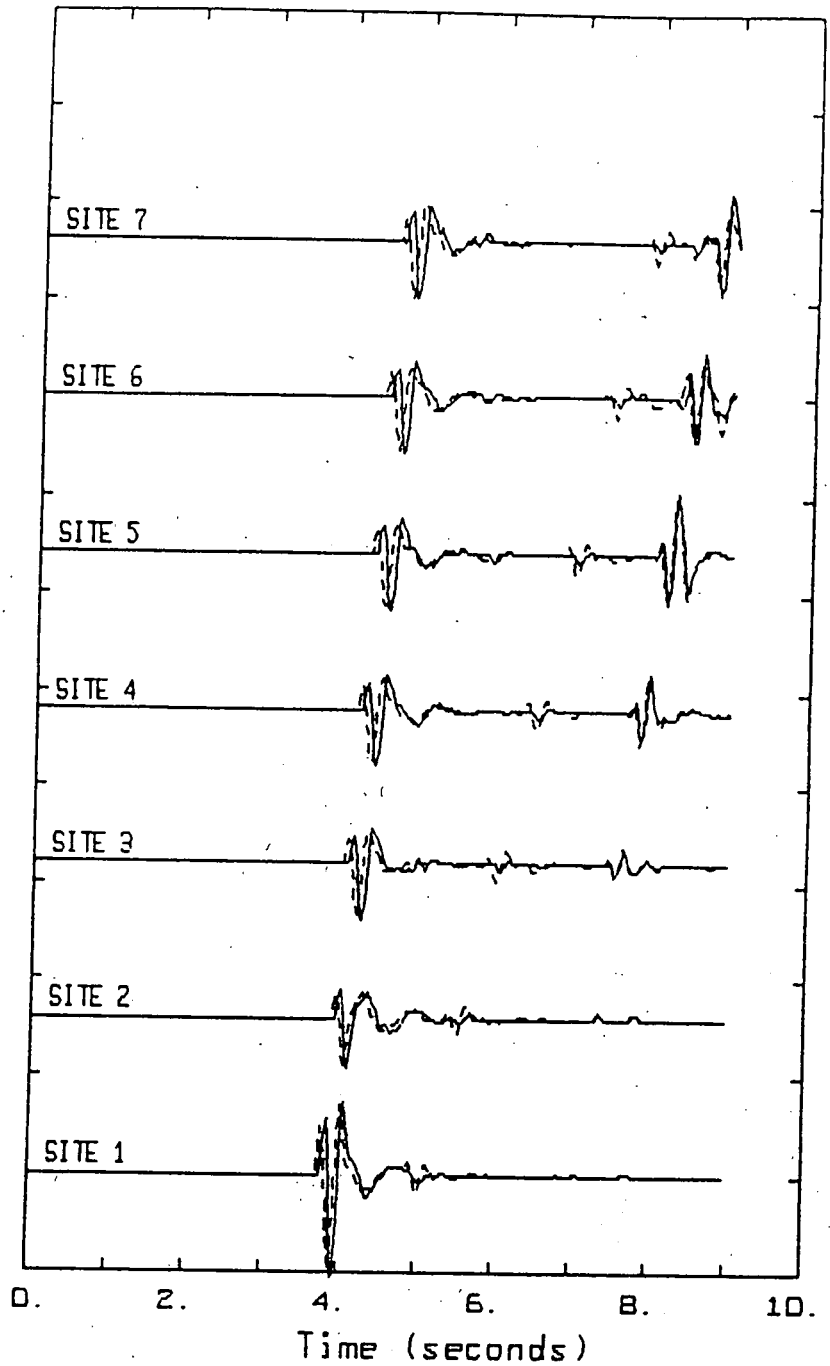

AMOD VERIFICATION 2D MODEL

INCIDENCE ANGLE = 32.0 DEG DT=.03 SEC

Figure F-23. Validation of computer code AMOD. Solid lines are motions computed at the seven site locations (Figure F-22) for a plane wave source incident from the west at 32°. The dashed lines are results from the finite difference code developed by Professor Jerry Schuster at University of Utah for the same model and input source function.

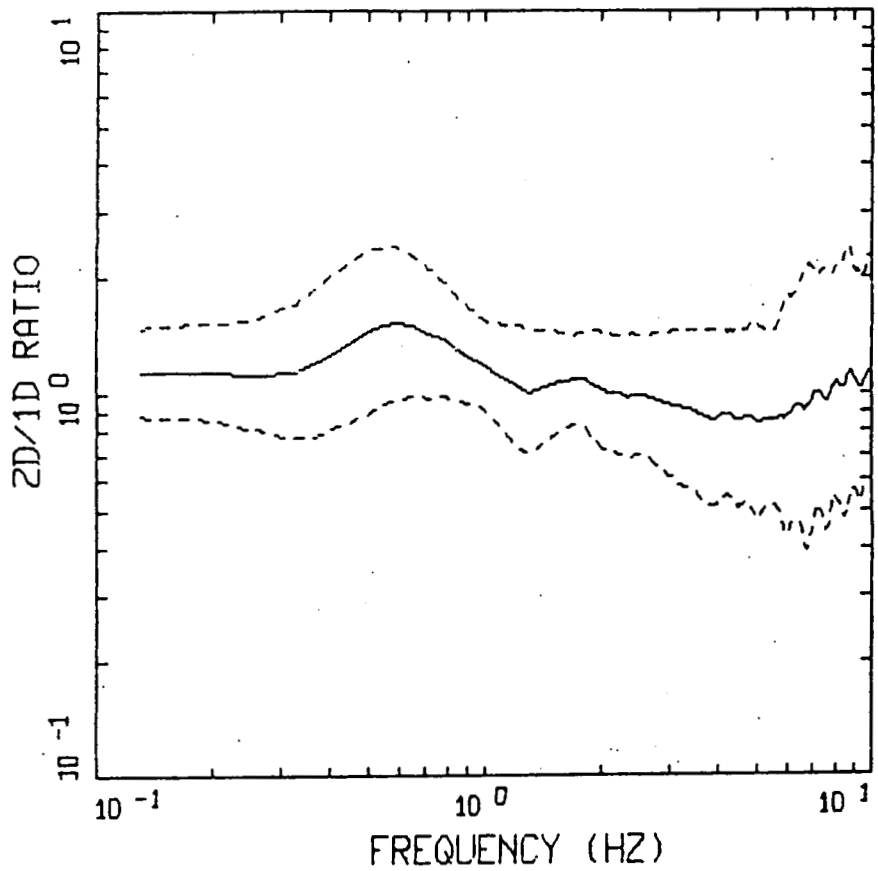

ROCKY FLATS: RATIO 2D/1D ALL SITES
FRONT RANGE FAULT

LEGEND

- - - - - 84TH PERCENTILE (7 points smoothing)
——— 50TH PERCENTILE (7 points smoothing)
- - - - - 16TH PERCENTILE (7 points smoothing)

Figure F-24. Fourier amplitude spectral ratio for western sources (Front Range Fault) averaged over the seven sites (Figure F-22) and nine incidence angles (Table F-4). The ratio has been smoothed with a 0.5 Hz triangular window.

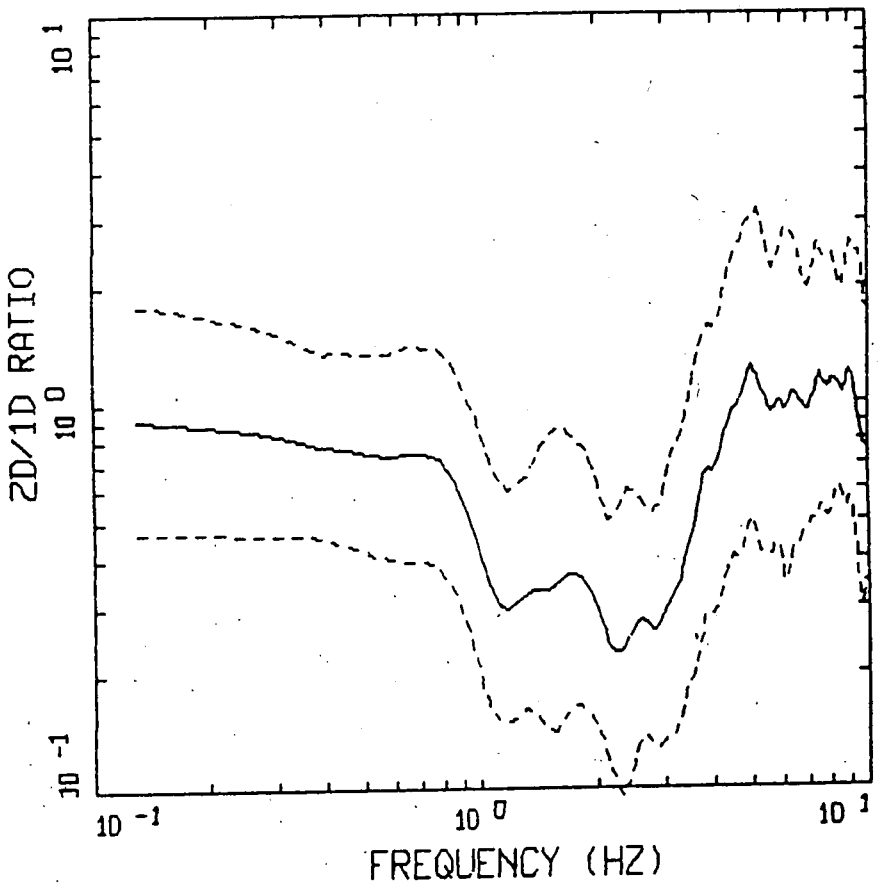

ROCKY FLATS: RATIO 2D/1D ALL SITES
ROCKY MOUNTAIN ARSENAL FAULT

LEGEND

- - - - -	84TH PERCENTILE (7 points smoothing)
———	50TH PERCENTILE (7 points smoothing)
- - - - -	16TH PERCENTILE (7 points smoothing)

Figure F-25. Fourier amplitude spectral ratio for eastern sources (Derby Fault) averaged over the seven sites (Figure F-22) and three incidence angles (Table F-4). The ratio has been smoothed with a 0.5 Hz triangular window.

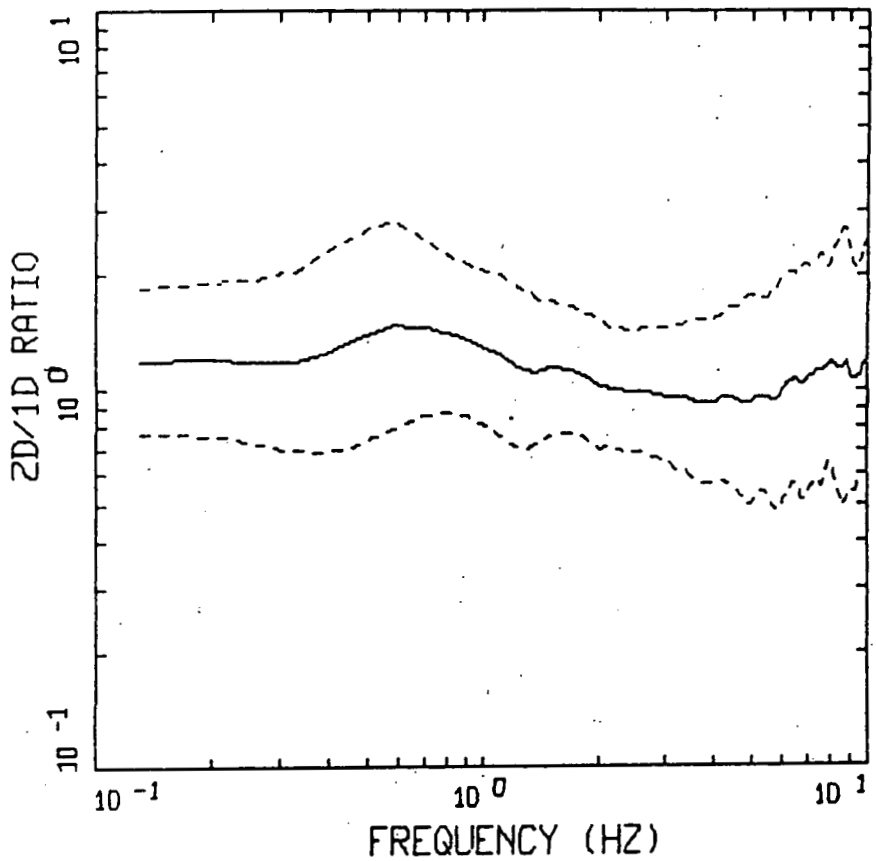

ROCKY FLATS: RATIO 2D/1D ALL SITES
FRONT RANGE FAULT, VARIABLE VELOCITIES

LEGEND

-----	84TH PERCENTILE (7 points smoothing)
———	50TH PERCENTILE (7 points smoothing)
-----	16TH PERCENTILE (7 points smoothing)

Figure F-26. Fourier amplitude spectral ratio for western sources (Front Range Fault) averaged over the seven sites (Figure F-22), nine incidence angles (Table F-4), and seven crustal velocity cases (Table F-5). The ratio has been smoothed with a 0.5 Hz triangular window.

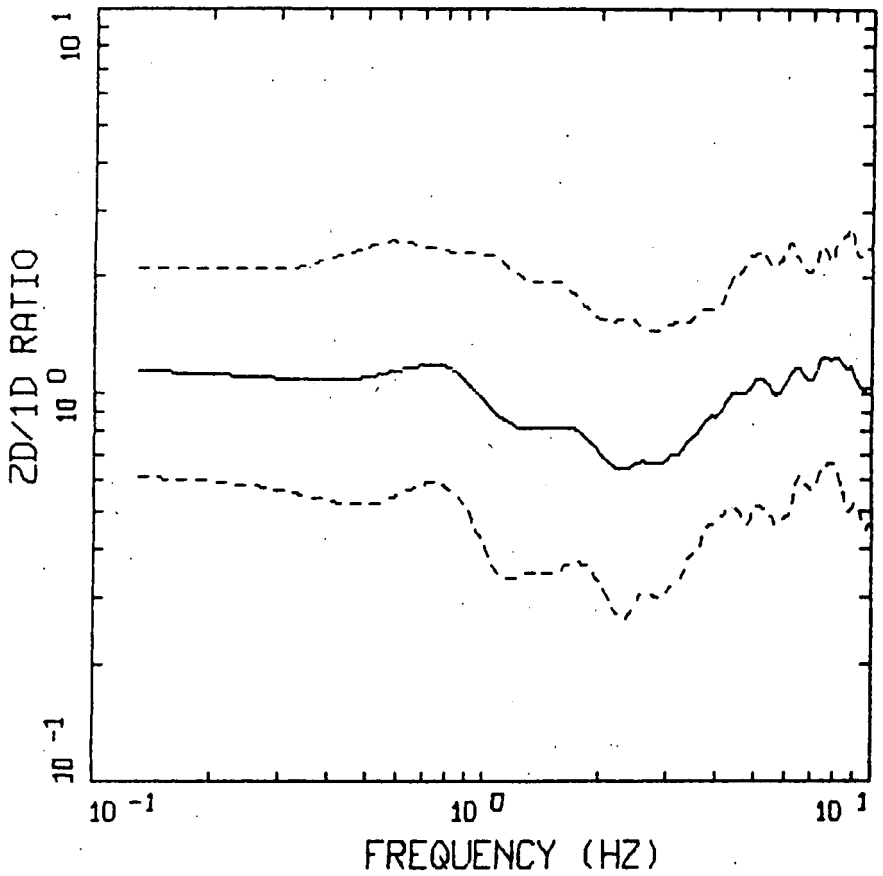

ROCKY FLATS: RATIO 2D/1D ALL SITES
ROCKY MOUNTAIN ARSENAL FAULT, VARIABLE VELOCITIES

LEGEND

- - - - - 84TH PERCENTILE (7 points smoothing)
——— 50TH PERCENTILE (7 points smoothing)
- - - - - 16TH PERCENTILE (7 points smoothing)

Figure F-27. Fourier amplitude spectral ratio for eastern sources (Derby Fault) averaged over the seven sites (Figure F-22), three nine incidence angles (Table F-4), and seven crustal velocity cases (Table F-5). The ratio has been smoothed with a 0.5 Hz triangular window.

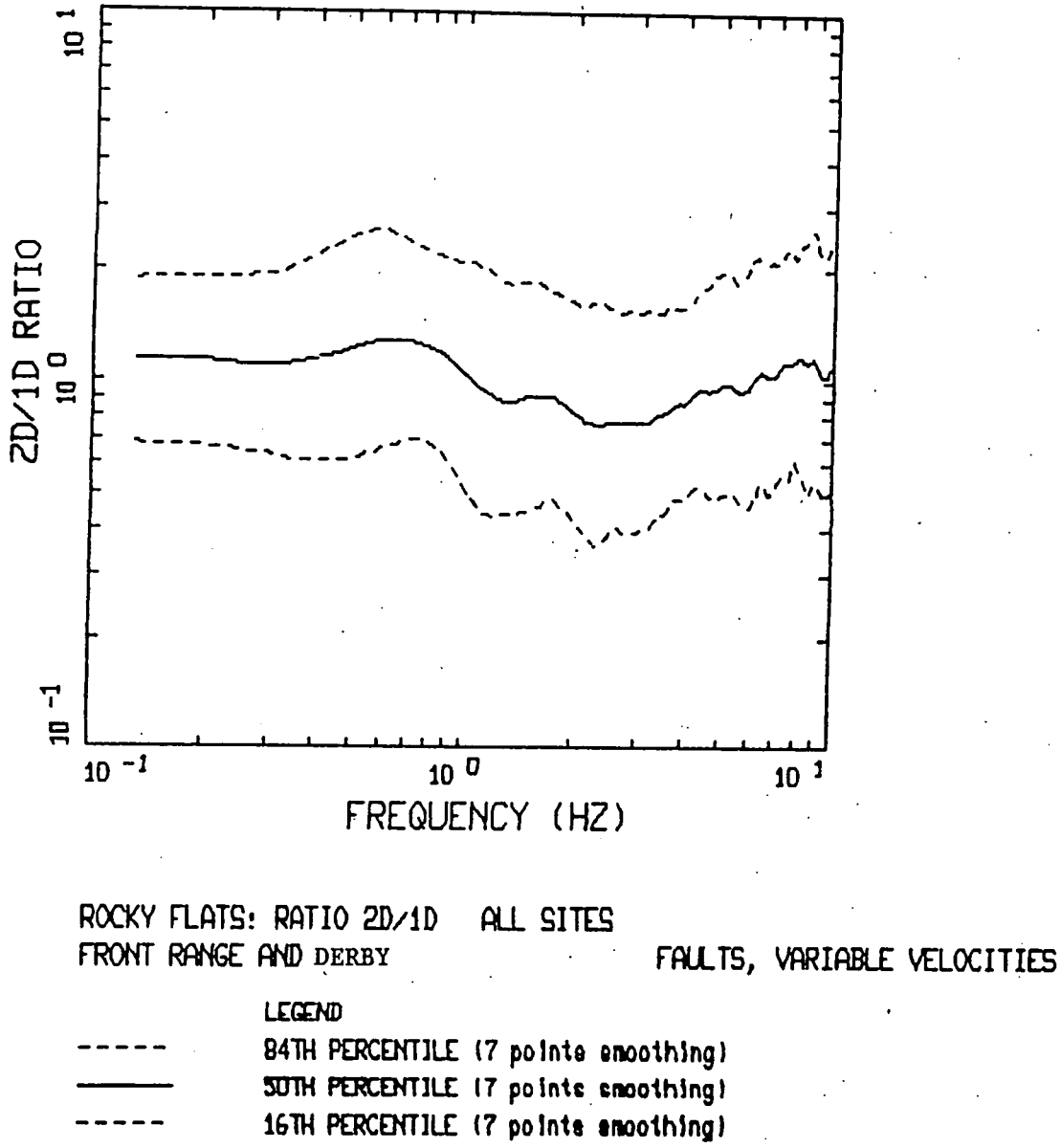

Figure F-28. Fourier amplitude spectral ratio for western and eastern sources (Front Range and Derby Faults) averaged over the seven sites (Figure F-22), incidence angles (Table F-4), and seven crustal velocity cases. The ratio has been smoothed with a 0.5 Hz triangular window.

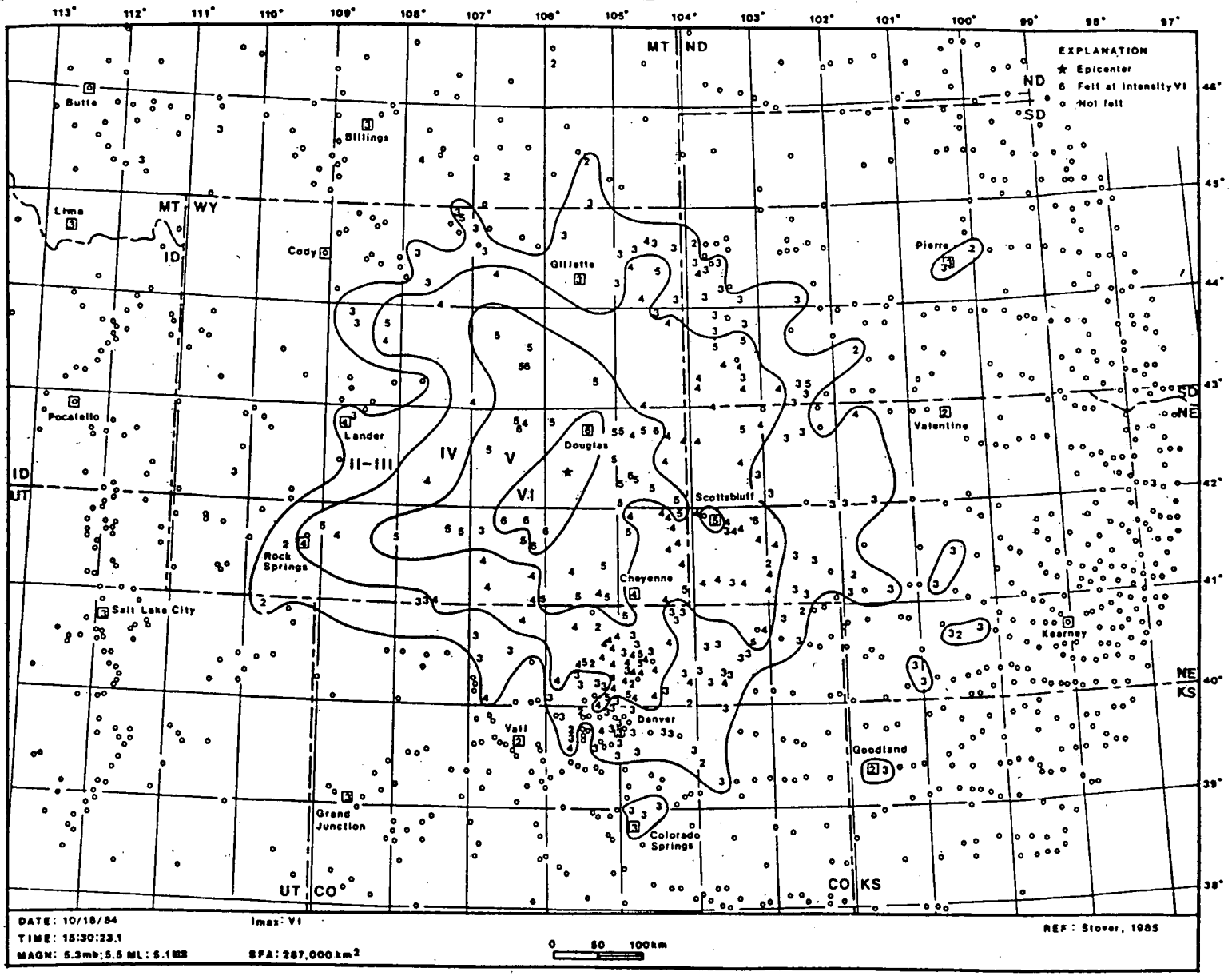

Figure F-29. Isoseismal map for the 1984 Laramie Mountains, Wyoming earthquake (from Kirkham and Rogers, 1986).

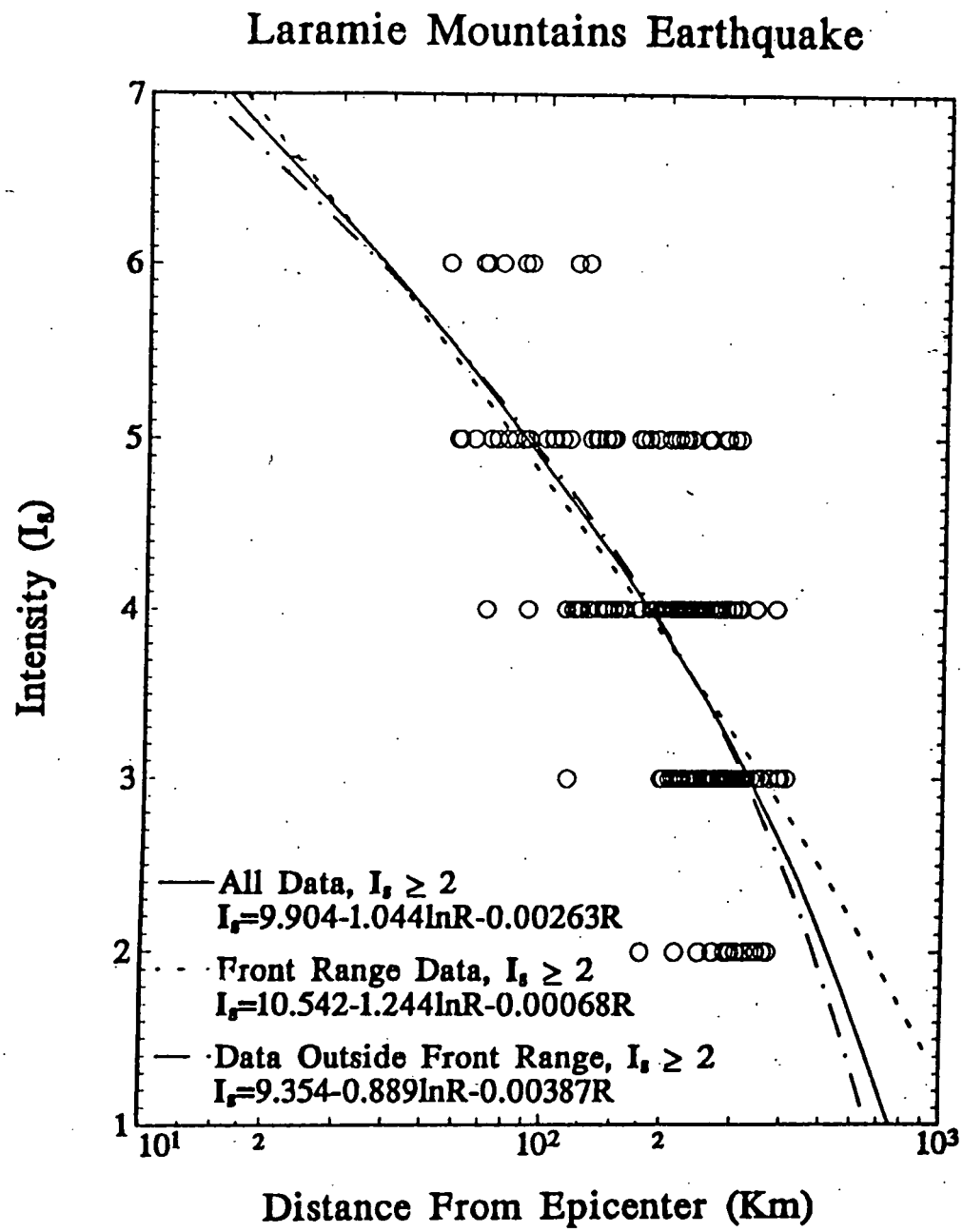

Figure F-30. MMI data from Laramie Mountains earthquake, and equations fit to sets of data.

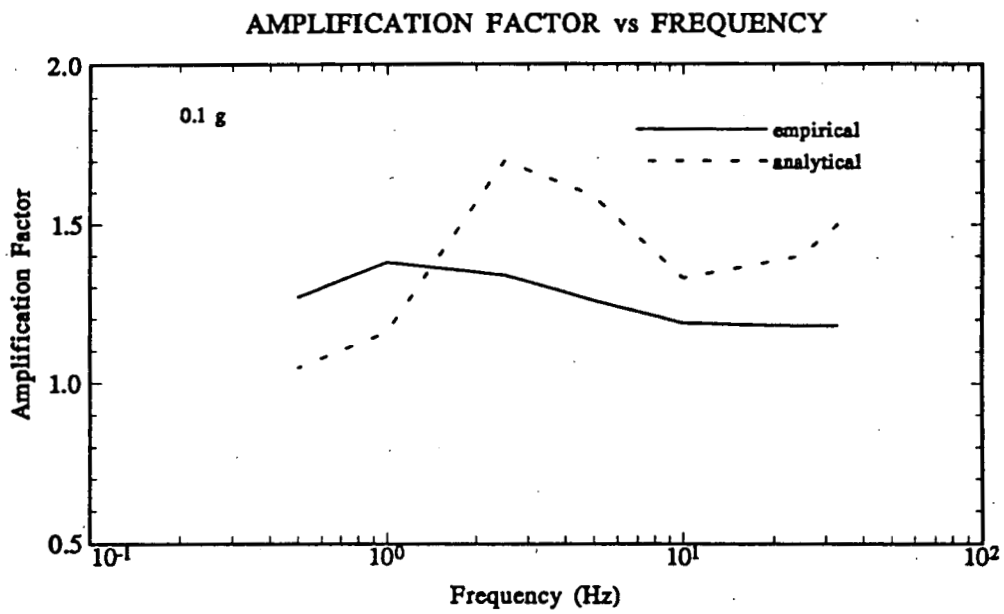

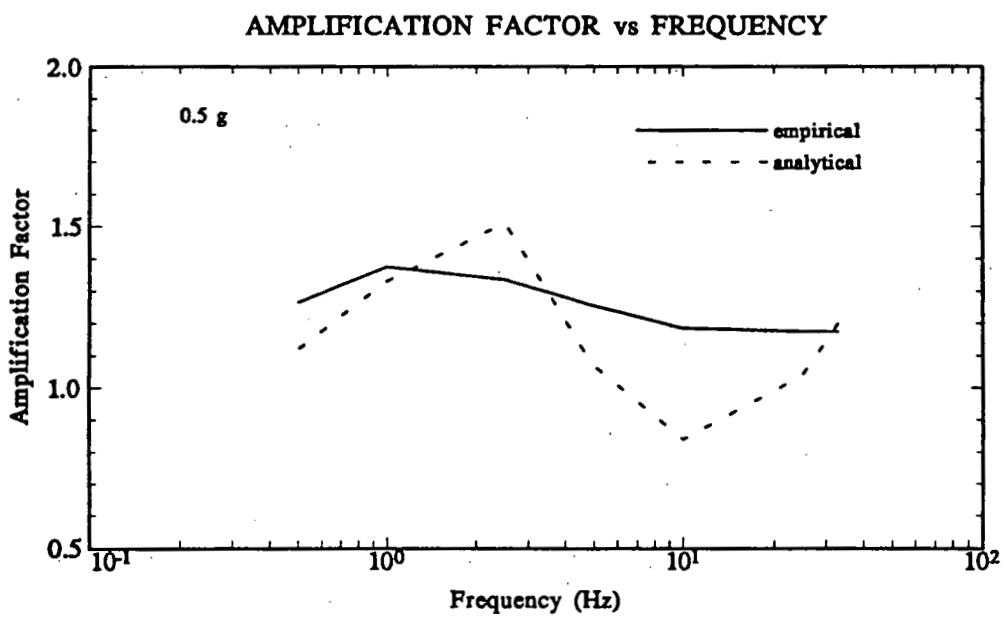

Figure F-31. Empirical and analytical soil amplification factors for 0.1g and 0.5g input motions.

APPENDIX G

SOIL LIQUEFACTION POTENTIAL

by

Geomatrix Consultants, Inc.
San Francisco, California

INTRODUCTION

This Appendix describes work undertaken to investigate the possibility of earthquake-induced soil liquefaction within the maximum security area at the Rocky Flats Plant (RFP). This work was conducted and reported by Geomatrix Consultants, Inc.

A prior study (Blume, 1974) at Rocky Flats Plant site area concluded that "For this site, liquefaction is not a problem because of the absence of loose sands of any kind beneath this Plutonium Facility." Other studies performed at Rocky Flats Plant have come to similar conclusions (TERA, 1976; Wassenaar, 1987). The purpose of this study is to review available subsurface and site geologic information, including previous reports containing foundation, geologic, seismic, geotechnical, or other subsurface information at the Rocky Flats Plant site area in order to fully disclose the potential for liquefaction, if any, and the likely extent of any area involved.

SUMMARY OF SITE GEOLOGY

The Rocky Flats Plant site is located on the western edge of the Colorado Piedmont section of the Great Plains Physiographic Province (Hunt, 1974). The Colorado Piedmont lies adjacent to the southern Rocky Mountains and is drained by the South Platte and Arkansas rivers. Tertiary bedrock has been stripped from much of this region and the section is eroded below the High Plains by as much as 450 meters (Osterkamp and others, 1987). The plant site sits on a geomorphic surface comprised of a gravel-capped pediment surface (Rocky Flats alluvial surface) that is adjacent to the base of the Colorado Front Range. Erosional remnants of the Rocky Flats surface slope gently east towards the central Denver Basin. It is dissected along its eastern edge by the heads of several small intermittent (seasonal) streams.

The gravel that caps the pediment surface was deposited in the very early Pleistocene (1 to 2.5 million years ago) and is identified as the Rocky Flats Alluvium (Blume, 1974; Ebasco, 1992). It consists predominantly of bouldery and cobbly, silty, clayey, and sandy gravel. The gravel is predominantly quartzite, containing sizeable percentages of schist, gneiss, and granite. The Rocky Flats Alluvium ranges in thickness from less than 1 foot to over 100 feet to the west of the site, averaging about 10 feet, across the width of the Rocky Flats Plant. The bedrock surface has a relief of about 50 feet. Details of the material characteristics of Rocky Flats Alluvium are provided (see page G-3, Subsurface Site Conditions).

The underlying bedrock consists of Cretaceous-age (65 to 135 million years ago) sedimentary strata, including, in descending order, the Arapahoe Formation, the Laramie Formation, the Fox Hill Sandstone, and the Pierre Shale. These sedimentary formations dip to the east at angles ranging from about 76 degrees west of the Rocky Flats alluvial surface to less than 5 degrees east of the surface. In the plant site area, bedrock dips about 1 to 5 degrees to the east, on average. Locally, dips may be steeper (e.g., 10 to 20 degrees).

The Arapahoe Formation, which immediately underlies the Rocky Flats Alluvium at the Rocky Flats Plant, is approximately 0 to 120 feet thick and consists of claystone with interbedded sandstone and siltstone. Underlying the Arapahoe Formation is the Laramie Formation, which is approximately 600 to 800 feet thick. The upper several hundred feet of the Laramie is composed chiefly of clay shale, sandy shale, and claystone containing some lenticular beds of sandstone, while the lower couple of hundred feet is sandstone separated by thin beds of shale, clay, and coal. Underlying the Laramie is the Fox Hills Sandstone, which is estimated to be about 100 feet thick under the Rocky Flats Plant. Underlying the Fox Hills Sandstone is the Pierre Shale, which is about 8000 feet thick. A more detailed discussion of site geology may be found in Ebasco (1992).

METHODOLOGY AND SCOPE OF GEOTECHNICAL DATA REVIEW

To evaluate the liquefaction potential of the alluvial deposits within the maximum security area at the Rocky Flats Plant site area, a review was performed of geotechnical information for sites within the north plant site area and in the near vicinity. Since 1951 and the inception of the Rocky Flats Plant, there have been numerous investigations and test holes to aid in the design and construction of site facilities. Although not every geotechnical report at the plant site was reviewed, a review of reports relevant to the assessed plant area provided adequate data on which to base our analyses and conclusions. Geotechnical reports for sites within and surrounding the maximum security area were examined and reports with boring information which were believed to have material property data representative of subsurface conditions were selected for incorporation into our evaluations.

Our review included 22 soil investigation reports for individual buildings, utilities, roads, parking lots, holding ponds, storage tanks, or other conventional surface facility structures; six geophysical data/seismic line reports; four seismic risk/hazard, seismic design criteria, and geologic investigation reports; and one ground water monitoring report. Various maps and aerial photographs were also reviewed. The documents reviewed are listed in the references. Individual soil investigation reports contained logs of borings and test pits for as few as one or two subsurface locations to more than 60 locations. It should be noted that because the plant site area is relatively flat and located in competent material for relatively shallow lightly-loaded foundations, exploration generally was done using hollow-stem augers (continuous flight augers). Sampling generally was performed by the standard split-spoon or thin brass liner method. Penetration resistance measured when a 140-pound hammer is dropped a distance of 30 inches on a 2-inch diameter sampler is designated as a Standard Penetration Test (SPT). Undisturbed sampling was difficult to perform in the gravelly materials, where standard penetration tests generally indicated competent dense or hard materials. Consequently, testing of samples usually consisted of index property tests, such as gradation tests on the granular materials, and unit weight, plasticity tests (Atterberg limits), and occasional unconfined tests on more cohesive samples. A tabulation of data collected listing the boring number, reference, blow count elevation or depth, depth to ground water, the soil type according to the Unified Soil Classification System, fines content, and blow count is provided at the end of

this document (Table G-1). The locations of 150 borings used in this study are shown in Plate G-1. The borings are randomly located throughout the study area and should be representative of subsurface materials.

SUBSURFACE SITE CONDITIONS

Based on our review of previous investigations for the plant, the logs of borings and laboratory tests revealed the following about the general subsurface conditions at the Rocky Flats Plant site area.

- Three units/formations were encountered in the shallow borings drilled at the site: (1) compacted and uncompacted fill consisting of random fill derived from bedrock and alluvial materials; (2) alluvial materials consisting primarily of clayey sands and gravels, and gravelly sandy clays; (3) bedrock of the Arapahoe formation consisting primarily of claystone with interbeds of siltstone and sandstone.

- The alluvial (Rocky Flats Alluvium) soils, which are of primary concern for the liquefaction assessment, consist of interbedded and lenticular layers of silty, sandy, and gravelly clay; clayey, silty, and gravelly sand; and clayey, silty, and sandy gravel. However, sandy and gravelly clay and well-graded bouldery and cobbly, silty, clayey, and sandy gravel predominate these deposits. Typically, the sandy gravels and gravelly sands with clays are well-graded and consist of 25 to 40% gravels, 40 to 50% sand, and 20 to 30% clays (ATEC, 1987; Chen, 1972). (It should be noted that size of the soil sampler limits the maximum particle size of the sample obtained. Samples are typically finer grained materials.) The Rocky Flats Alluvium is generally medium dense to very dense. The thickness of the alluvium in the plant site area ranges from 0 to 30 feet, averaging about 10 feet.

In particular, methodical review of the blowcount data (penetration resistance) and laboratory test data revealed the following.

- Of the 22 soils investigation reports reviewed, 18 had boring log data with information on the penetration resistance of the overlying Rocky Flats Alluvium. Each report reviewed had one boring to tens of borings within or surrounding the Rocky Flats Plant site. Nine of the 18 reports were for facilities within the area of interest; the other half of the reports were for facilities relevant to the site but outside or surrounding the area of interest.

- A total of 150 boring logs (Plate G-1) had penetration values in the alluvial deposits; 91 of the borings were within the area of interest and 59 were in the surrounding area. The boring logs contained penetration values (blows/foot) for 189 sampling locations within the area of interest and 138 locations in the surrounding area, or a total of 327 penetration values within the alluvial deposits (refer to Table G-1). All of the borings were generally shallow (less than 15 feet) and were performed using a hollow stem auger or continuous flight auger. Penetration sampling was generally performed using a 140-pound weight falling a distance of 30 inches. Standard split-spoon and brass liner samplers were generally used, although the sampling method was not always specifically indicated in the boring logs. Blowcount data (blows/foot) were reported for the last 12 inches of penetration, but often the number of blows were reported for lesser amounts of penetration when experiencing refusal during drilling (for example, per 3, 6, or 9 inches of penetration for up to 50 blows).

- Of the 150 borings reviewed for penetration test measurements, 75 borings reported water in the holes. Water levels were generally taken during drilling and occasionally measurements were taken several days to a week after drilling. Although the borings were drilled at various times of the year, the depths to observed ground water (in general) ranged between 3 and 25 feet. Average levels are between 5 and 10 feet deep. WCC (1986) in their investigation of Buildings 707, 779, 776, and 777, note: "Free water was found in 5 of the 10 holes at depths of between 7 and 15 feet [for drilling performed between November 10 to 14, 1986]. We have no data on ground water level fluctuations at the site, but our experience in the Rocky Flats area indicates that in wetter seasons and wetter years, a ground water level rise to just below the existing ground surface can occur."

- Of the 327 penetration resistance measurements taken, approximately 105 samples were in generally clayey materials (Unified Soil Classification System = CL), 91 samples were in generally sandy materials (SC/SM); 91 samples were in generally gravelly materials (GC/GM), 34 samples were from fill constructed from bedrock or gravelly clay materials, and 5 samples were not clearly classified. The majority of the sandy materials that were sampled and tested were found to be well-graded and clayey and gravelly in nature (e.g., clayey sand with gravel). Likewise the majority of clayey materials tend to be stiff to very stiff and gravelly in nature (e.g., sandy clay with gravel). The gravels tend to be well-graded and clayey as well (e.g., clayey gravel with sand).

- Blowcounts within the clayey materials ranged from 4 to more than 50 blows/foot, averaging 28 ± 14 blows/foot. This average blow count and the standard deviation are conservative and were calculated assuming a value of 50 (refusal was noted when the actual blows/foot was equal to or exceeded 50). In clayey materials, refusal is often defined as penetration values greater than 30. In the clayey material, 39 of 105 blowcounts measured were greater than 30, and 21 of 105 blowcounts were greater than 50.

- Blowcounts within the sandy materials ranged from 4 to more than 50, averaging 38 ± 14 blows/foot. As in the case of the clayey materials, this average and standard deviation are conservative and were calculated assuming a value of 50 when the actual blows/foot exceeded 50. Of the 91 blowcounts in sandy material, 42 (or 46%) had blowcounts that are interpreted as meeting refusal (i.e., $N > 50$ blows/foot).

- Blowcounts within the gravelly material ranged from 3 to more than 50 blows/foot and averaging 41 ± 13 blows/foot. These average and standard deviations are conservative and were calculated assuming a value of 50 when the actual blows/foot usually exceeded 50. In these materials, 55 of 91 blowcounts were greater than 50.

- Blowcounts within the cohesive fill ranged from 3 to more than 50, averaging 14 ± 11. Only 2 of the 34 blowcounts in fill met refusal.

A summary of the penetration results on samples from the alluvium and fill materials is presented in Table G-2.

Based on the measured penetration test values summarized above and relationships by Terzaghi and Peck (1967) for soil consistency versus blowcount, it can be concluded that the clayey materials are generally very stiff; the sandy materials are generally medium dense to very dense; the gravelly

materials are generally medium dense to very dense; and the fill (usually cohesive), range from soft to hard, but on the average is stiff. There are very few isolated pockets of loose sand and gravel as shown on Plate G-1. These pockets occur at random locations and depths and do not appear to represent an identifiable deposit or layer.

The discussion on ground water above is based on investigations that were performed prior to construction of additional buildings, storm drains, and regrading work, as well as an ongoing extensive ground water monitoring and treatment program in the RFP Site area. Based on a review of the Ground Water Protection and Monitoring Program Plan report (EG&G, 1991), ground water in the alluvium is variable, although it generally becomes shallower from west to east as the alluvial material thins. Seeps are common at the base of the Rocky Flats Alluvium at the contact with claystones, in stream drainages. The report indicates that much of the ground water within the alluvial unit becomes surface water or evaporates where it discharges from seeps along slopes and in drainage valleys. Based on the above discussion, ground water in the Rocky Flats Plant site area is generally found at depths of 5 to 10 feet and is perched within the varied and individual layers of more pervious sands or gravels above clay layers or the claystone bedrock. A map showing the ground water elevation contours within the Rocky Flats Plant site is shown in Figure G-1. The ground water contours shown in Figure G-1 were used as a basis for selecting a conservative ground water depth of 5 feet for the liquefaction analyses.

ASSESSMENT OF POTENTIAL FOR LIQUEFACTION

During an earthquake event, ground shaking can generate pore water pressures in a saturated soil deposit, thus reducing its intergranular stress. In saturated sands, this reduction in intergranular stress may result in significant loss of shear strength. If the intergranular stress and strength of the soil are significantly reduced compared to pre-earthquake static conditions, then soil becomes liquefied. The degree of pore water pressure buildup and subsequent loss of strength in the material depends on both the density of the soil and the level and duration of shaking at the site. Liquefaction is defined as the temporary loss of strength in saturated cohesionless soils due to repeated or cyclic loading. The assessment of the potential for liquefaction commonly utilizes three techniques: (1) mapping/identifying liquefaction susceptibility based on geologic criteria; (2) estimating liquefaction susceptibility based on simple geotechnical criteria; and (3) determining liquefaction susceptibility based on empirical correlations using in-situ evaluations of penetration resistance.

Each of these techniques was used to evaluate the liquefaction potential of the alluvial deposits at the Rocky Flats Plant site. Each method is described briefly in the following sections. Conclusions regarding the liquefaction potential of the site soils also are presented.

Evaluation Based on Geologic Criteria

Mapping liquefaction susceptibility based on geologic criteria basically involves superposition of three steps: (1) mapping surface geologic deposits based on age and their susceptibility to liquefaction; (2) mapping the depth to ground water; and (3) mapping results of ground motion hazards studies. From these maps the susceptibility of liquefaction can be classified as very low, low, moderate, or high, based on criteria determined from observed performances during previous earthquakes (National Research Council, 1985). Liquefaction susceptibility maps are not a

substitute for site specific evaluations of liquefaction hazards, but they do indicate areas where site-specific evaluations may be desirable.

The National Research Council (1985), after the study by Youd and Perkins (1978) on liquefaction susceptibility in the San Fernando Valley, California, indicated: "Deposits older than late Pleistocene [10,000 to 130,000 years ago] are assumed to be not susceptible to liquefaction on the basis of experience during actual earthquakes." Youd and Perkins (1978) concluded that late Pleistocene deposits with depth to ground water from 0 to 10 feet have a "low" susceptibility to liquefaction, and that late Pleistocene deposits with depth to ground water from 10 to 30 feet have a "nil" susceptibility to liquefaction. Therefore, based on the age of the Rocky Flats Alluvium (1 to 2.5 million years old), the 0 to 10 feet depth of ground water at the site, and the conclusions of the National Research Council (1985), the liquefaction susceptibility of the site soils is negligible based on simple geologic criteria only.

Based on Simple Geotechnical Criteria

A simple geotechnical method to estimate liquefaction susceptibility at a site is based on the gradation (or grain size characteristics) of the soils. In general, only cohesionless soils are susceptible to liquefaction; while clays and gravels are not. Example gradation curves of soils which have liquefied in past earthquakes are shown in Figure G-2. Clean sands are the most susceptible to liquefaction. The presence of fines, particularly plastic fines, makes it more difficult for sand particles to come free of each other and seek denser arrangements during earthquake shaking (NRC, 1985). However, nonplastic fines may not have as much of this restraining effect, so silts and silty sands are more susceptible to liquefaction than soils having plastic fines. Seed and Idriss (1982) reported that the great majority of clayey soils will not liquefy during earthquakes. They also noted that certain types of clayey materials (with percent finer than 0.005 mm <15%; Liquid Limit <35; and water content >90% of Liquid Limit) may be vulnerable to strength loss during earthquakes. None of the stiff to very stiff clays encountered at the site, however, have characteristics similar to those described above.

In addition to the presence of fines, the rate at which excess pore pressures can be dissipated during and after strong earthquake shaking is important. Seed et al. (1976) showed that soils with D_{20} > 0.7 mm are not subject to liquefaction provided there are no strata of low-permeability material present to inhibit drainage. For gravelly soils, it is important to consider the relative density of the soils. In recent years, a number of cases in which earthquake-induced liquefaction of gravelly deposits has been described in the literature (Andrus and Youd, 1989, 1987; Harder, 1988; Hynes-Griffin, 1988; Youd et al., 1978). However, Valera and Kaneshiro (1991), after a review of all the suspected cases involving liquefaction of gravelly soils, found that one or more of the following conditions were observed.

> *All gravel deposits were loose to very loose. In the best-documented case where SPT or equivalent SPT were measured in the gravelly deposits which liquefied, values ranged from 1 to 15 blows per foot.*
>
> *In the clean gravel deposits, the quantity of sand filling the voids was insufficient to fill the voids between contacting gravel particles, allowing the larger particles to contact each other in a "clast-supported structure."*

In the silty/sandy gravel deposits the larger gravel particles were simply floating without direct contact with each other in a silty sand matrix. Thus, liquefaction behavior was controlled by the fine matrix and not by the gravel particles.

Based on review of the borings, laboratory tests, and soil descriptions from the borings drilled into the alluvium in the plant site area, about one-third of the materials are sandy, while the remaining materials are predominantly stiff clays and dense gravels not subject to liquefaction. Of the sandy materials, there appears to be few deposits of clean sands; the sands that are present are often clayey or gravelly and are dense. Based on gradation characteristics alone and a simple overview of the geotechnical data, one would conclude that the susceptibility to liquefaction is negligible.

Evaluations Based on Correlations to Standard Penetration Resistance

The potential for liquefaction of saturated cohesionless soil strata may be examined using simplified procedures currently in practice. The use of SPT data to assess liquefaction potential due to an earthquake is considered a reasonable and acceptable engineering procedure (Seed et al., 1985; National Research Council, 1985). This is because many of the factors affecting the SPT results similarly affect the liquefaction resistance of sandy soils. Furthermore, the evaluation procedure is based on the actual performance of soil deposits during worldwide historical earthquakes.

The potential for liquefaction at a particular site is evaluated by comparing the earthquake-induced shear stresses with those required to cause liquefaction. These latter stresses are determined by correlation with soils at other sites that have similar penetration resistance values and whose behavior has been observed during earthquakes.

The earthquake-induced shear stresses can be calculated from site response computations employing wave propagation techniques, or from the simplified procedures developed on the basis of response computations performed for a large number of soil deposits.

The simplified method requires knowing the peak earthquake-induced ground surface acceleration, the total and effective stress conditions at various depths within the soil profile, and the standard penetration resistance, $(N_1)_{60}$. The cyclic stress ratio (τ_h/σ_o') induced by an earthquake in the field, can be calculated using the following equation (Seed et al., 1985):

$$\frac{\tau_h}{\sigma_o'} = 0.65 \frac{a_{max}}{g} \cdot \frac{\sigma_o}{\sigma_o'} \cdot r_d \qquad \text{(G-1)}$$

where a_{max} = the maximum acceleration at the ground surface
σ_o = the total overburden pressure on the layer under consideration
σ_o' = the initial effective overburden pressure on the layer under consideration
τ_h = the horizontal shear stress
r_d = a stress reduction factor that ranges from a value of 1 at the ground surface to about 0.9 at a depth of 35 feet.

The potential for liquefaction at a soil site is evaluated based on empirical correlations between the cyclic stress ratio and $(N_1)_{60}$ values indicating the observed occurrence, or non-occurrence, of

liquefaction in sand deposits during historical earthquakes. The correlation for magnitude 7.5 earthquakes for materials having various fines contents is shown on Figure G-3.

The curves shown on Figure G-3, which were presented by Seed and Idriss (1982) and Seed et al. (1985), relate the cyclic stress ratio required to cause initial liquefaction, to the standard penetration resistance value, $(N_1)_{60}$. The value of $(N_1)_{60}$, which is the penetration resistance corrected to an effective overburden pressure of 1 ton per square foot, can be obtained from the results of the Standard Penetration Test (SPT), N, using the relationship:

$$N_1 = C_N \cdot N \qquad \text{(G-2)}$$

where C_N is a function of the effective overburden pressure at the depth where N is measured, and the approximate relative density of the sand. Relationship of C_N values versus effective overburden pressure were developed from the results of studies conducted at the U.S. Army Corps of Engineers Waterways Experiment Station (Marcuson and Bieganouski, 1977) and later used by Seed and Idriss (1982). These relationships are presented on Figure G-4.

SPT measurements for liquefaction assessments are normally obtained with rotary wash drilling methods, in which water or drilling fluid fills the hole, keeping the test material of interest confined. When ground water is present, the water or drilling fluid prevents blow outs of saturated sand deposits and prevents the loosening of the soil by the upward flow of water. All borings reviewed for the Rocky Flats Plant Site were drilled using a hollow-stem or flight auger. The N values recorded in saturated deposits using auger drilling techniques may not be equivalent to the N-value recorded in the same sand using rotary wash techniques (i.e., the N value using auger drilling techniques may be lower). Consequently, all interpretations of the available data likely will be conservative.

In addition to overburden effects, the N_1 value is corrected to obtain the $(N_1)_{60}$ value corresponding to a 60% hammer efficiency. The correction factor that is used depends on the hammer energy ratio, or the hammer drop and hammer type. Other effects such as the effect of fines content, rod stiffness, and sampler diameter also are considered to obtain the $(N_1)_{60}$ values.
For a given value of peak ground surface acceleration and the total and effective static stresses at the depth of interest, a value of the induced cyclic stress ratio can be computed. Using this value of cyclic stress ratio and a plot such as Figure G-3 for the appropriate magnitude earthquake, a critical value of the $(N_1)_{60}$ blowcount can be determined, such that those materials having a value greater than the critical $(N_1)_{60}$ likely would not liquefy, and those having a value less than the critical $(N_1)_{60}$ likely would liquefy. By comparing the critical blowcount $(N_1)_{60}$ with the measured $(N_1)_{60}$ of the material, it is possible to assess whether liquefaction would be expected.

For the purposes of this study, penetration measurements were only corrected for overburden effects. The "corrected" N_1 values for the sandy materials having SPT blowcounts less than or equal 50 (Figure G-5) were plotted at the corresponding test depth. The N_1 blowcounts were then compared to the critical value of $(N_1)_{60}$ computed for three levels of ground shaking: a 0.2g, 0.4g, and 0.6g peak ground acceleration from a Magnitude 6.5 earthquake. The critical blowcount induced by these three levels of ground shaking are plotted in Figure G-5, along with the N_1 blowcounts from the SPT measurements for comparison. The critical blowcounts were computed assuming a water table depth of 5 feet.

Based on a comparison of the N_1 blowcounts with the critical blowcounts shown on Figure G-5, the susceptibility to liquefaction at the site is judged to be low, especially when one considers that these sandy materials constitute less than 15% of the alluvial deposits at the site. If one further considers that the site material are predominantly clayey in nature, the blowcounts adjusted for fines content would be much higher than those shown on Figure G-5. For the Magnitude 6.5 earthquake with a peak ground acceleration of 0.6g, less than 3% of all the penetration resistance test samples would be subject to liquefaction. The locations of samples shown on Figure G-5 to have a potential for liquefaction are presented on Plate G-1 for the three assumed levels of peak ground acceleration.

As can be seen on Plate G-1, the locations of these potentially liquefiable samples cannot be correlated with one another. The locations are at various depths and scattered randomly throughout the site. Where blowcounts may be particularly low at one borehole location, they are absent in an adjacent borehole. In addition, four of the low blowcount locations are at a shallow depth (less than 5 feet). The blowcounts also have not been corrected for fines content. Consequently, it can be concluded that the looser sands are confined to small lenses or isolated pockets within the Rocky Flats Alluvium. This is consistent with the character and description of alluvial deposits at Rocky Flats.

SUMMARY AND CONCLUSIONS

Based on the measured penetration resistance values and material consistency relationships, the clayey materials at the site are generally very stiff; the sandy materials are generally medium dense to very dense, the gravelly materials are generally medium dense to very dense; and the fill is usually cohesive, ranging from soft to hard, but on the average stiff. There are very few isolated pockets of soft clay or loose sand and gravel. The blowcount values in the sandy soils that did not meet refusal represent less than 15% of all data reviewed, and on average represent medium-dense materials. Based on the age of the Rocky Flat Alluvium and the conclusions of the National Research Council (1985), the susceptibility to liquefaction of the site is judged to be negligible. About one-third of the materials at the plant site area are sandy and the rest are predominantly clay and dense gravels that are not subject to liquefaction. Of the sandy materials, there appear to be few deposits of clean sand and the sands that are present are often clayey or gravelly and dense. Based on gradation alone and a simple overview of the geotechnical data, one would conclude that the susceptibility to liquefaction is negligible.

The comparison of $(N_1)_{60}$ blowcounts with the critical blowcounts where liquefaction would be triggered, shows the susceptibility to liquefaction at the site is low, especially when one considers that these sandy materials constitute less than 15% of the terrace deposits at the site. For a Magnitude 6.5 earthquake having a peak ground acceleration of 0.6g, only about 3% of all the samples reviewed would be subject to liquefaction. This is a very conservative estimate because our analyses do not take into account the correction factors that would increase the blowcount value for fine contents nor the perched nature of the ground water. Assuming saturated steady state shallow conditions for a perched groundwater table is very conservative. In addition, the loose sand deposits, which represent less than 3% of all penetration tests, are confined to lenses scattered throughout the site. They do not appear to represent a unique/identifiable deposit or layer within the Rocky Flats Alluvium.

Since there is no or negligible chance of liquefaction at the Rocky Flats Plant Site, there will be no liquefaction induced ground settlement. It should be noted that poorly consolidated soils and poorly compacted fills may be subject to earthquake-related ground failures such as lurching, heave, cracking and settlement. In our review of the boring logs, we noted some claystone fills with low blowcount measurements (on the order of 3) indicating that these materials may be soft. Consequently, some earthquake-induced settlement may occur in these areas.

REFERENCES

Air Products and Chemicals, Inc. (1989). Specifications for civil and underground construction of 184M standard nitrogen plant at Rocky Flats (00-9-6732).

Andrus, R.D. and T.L. Youd (1987). Subsurface investigation of a liquefaction-induced lateral spread, Thousand Springs Valley, Idaho, U.S. Army Corps of Engineers, Geotechnical Laboratory Miscellaneous Paper GL-87-8, 131 p.

Andrus, R.D. and T.L. Youd (1989). Penetration tests in liquefiable gravels, Twelfth International Conference on Soil Mechanics and Foundation Engineering, Rio de Janeiro, August.

Aguirre Engineers, Inc. (1988). Subsurface investigation and engineering analysis report, Electrical system upgrade, Phase 1 and Phase 2, Rocky Flats Plant, Jefferson County, Colorado, prepared for Black and Veatch Engineers-Architects.

ATEC Associates (1987). Geotechnical engineering investigation, Rocky Flats - Building no. 772, Appendix 5.7, Soil investigation report, p. 5-6, Drawing 1, boring logs B-1 through B-4.

ATEC Associates (1988). Geotechnical report for Building 116, Appendix 4.8.

ATEC Associates (1989). Geotechnical engineering investigation, nitrogen production facility, Rocky Flats Plant, Jefferson County, Colorado, drawing 1, boring logs B-1 through B-3.

ATEC Associates (1992). Geotechnical engineering investigation, Rocky Flats Building 374 addition, Jefferson County, Colorado, boring logs B-1 through B-3.

Blume, [URS/John A. Blume & Assoc.] (1972). Supplement no. 1 to Seismic and geological investigations and design criteria for Rocky Flats plutonium recovery and waste treatment facility.

Blume, [URS/John A. Blume & Assoc.] (1974). Seismic and geologic investigations and design criteria for Rocky Flats plutonium recovery and waste treatment facility, report prepared for CF Braun & Company.

Chen & Associates (1986). Soil and foundation investigation and pavement design, proposed buildings 569 and 570, Rocky Flats Plant, Golden, Colorado, report prepared for Rockwell International, figs. 1-3.

Chen & Associates (1972). Soils and foundation investigation for Building 123, the proposed low radiation surveillance laboratory, Rocky Flat Plant, Golden, Colorado, May 23.

CTL/Thompson Inc. (1980). Soils investigation, proposed perimeter security zone (PSZ) stations 82+86.3 to 107+94.42 & 0+00 to 3+83.62, borrow area and parking lot no. 71, a portion of safeguards and site security upgrading, report prepared for Richard Weingardt Consultants.

Dames & Moore (1981). Final Report, Geological and seismologic investigations for Rocky Flats Plant for U.S. Dept. of Energy, v. 1, p. 3.0-6 - 3.0-10, fig. 3-2.

Ebasco (1990). Geologic characterization report, Appendix E, Seismic data reprocessing, prepared for US DOE-Rocky Flats Plant.

Ebasco (1990). Draft Report, Task 2, Addendum, Vertical Seismic Profile of Well 56-89BR at the Rocky Flats Plant, June.

Ebasco (1991). Task 3, Shallow, high-resolution seismic reflection profiling in operable unit 2 (903 pad, east trenches, and mound) at the Rocky Flats Plant, final report, prepared for EG&G Rocky Flats and U.S. DOE.

Ebasco (1992). Phase II geologic characterization data acquisition; surface geologic mapping of the Rocky Flats Plant and vicinity, Jefferson and Boulder counties, Colorado, March.

Engineering-Science, Inc. (1990). Specifications and drawings, Remedial action, 881 Hillside, 881 effluent storage tanks, plates 1 through 4, 8 & 9.

EG&G Rocky Flats, Inc. (1991). Final ground water protection and monitoring program plan, prepared for U.S. Department of Energy, Rocky Flats, Golden, CO, Nov. 27.

Ground Water Protection and Monitoring Program Plan, Third Quarter; Well and Piezometer Locations, Individual Hazardous Substance Sites (map) (2 copies).

Harder, L.F., Jr. (1988). Use of penetration tests to determine the liquefaction potential of soils during earthquake shaking: Ph.D. Dissertation, University of California, Berkeley.

Hunt, C.B. (1974). *Natural regions of the United States and Canada,* San Francisco, W.H. Freeman and Company, 725 p.

Hynes-Griffin, M.E. (1988). Pore pressure generation characteristics of gravel under un-drained cyclic loading: Ph.D. Dissertation, University of California, Berkeley.

Marcuson, W.F., III. and W.A. Beiganousky (1977). SPT and relative density in course sands, *Journal of the Geotechnical Engineering Division*, ASCE 103 (GT11), p. 1295-1309.

Merrick & Co. (1989). Title II Submittal - Phase I, Foundation and site work, Replace tanks T66, T67, and T68, figs. 1 - 4.

National Research Council (1985). *Liquefaction of soils during earthquakes,* National Academy Press, Washington, D.C.

Osterkamp, W.R., M.M. Fenton, T.C. Gustavson, R.F. Hadley, V.T. Holliday, R.B. Morrison and T.J. Toy (1987). Great Plains, *in* W.L. Graf, ed., Geomorphic Systems of North America, Boulder, Colorado, Geological Society of America, Centennial Special Volume 2, p. 163-210.

Rocky Flats Plant Area Plot Plan.

R.V. Lord & Associates (1972). Subsurface soil investigation for the proposed Fuel Oil Storage Tank in the vicinity of Central Avenue and 7th Street, June 14.

R.V. Lord & Associates (1976). Subsurface soil and groundwater investigation for existing Building 928, December 1.

Seed, H.B., K. Tokimatsu, L.F. Harder and R.M. Chung (1985). Influence of SPT procedures in soil liquefaction resistance evaluations, *Journal of the Geotechnical Engineering Division,* ASCE, v. 111, no. 12, p. 1425-1445, December.

Seed, H.B., P.P. Martin and J. Lysmer (1976). Pore pressure changes during soil liquefaction, *Journal of the Geotechnical Engineering Division*, ASCE 102 (GTM), p. 246-270.

Seed, H.B. and I.M. Idriss (1982). Ground Motions and Soil Liquefaction during Earthquakes, monograph series, Earthquake Engineering Research Institute, Berkeley, California.

Tera Advanced Services Corp. (1982). Seismic hazard analysis for the Bendix, Los Alamos, Mound, Pantex, Rocky Flats, Sandia-Albuquerque, Sandia-Livermore, and Pinella's sites, final report.

TERA (1976). Seismic Hazard Study, pages III-38, III-41, III-42, III-60 through III-66.

TERA Corporation (1978). Seismic risk analysis for Rocky Flats, Colorado, report prepared for Lawrence Livermore Laboratory.

Terzaghi, K. and R.B. Peck (1967). *Soil mechanics in engineering practice,* John Wiley & Sons, New York, 729 p.

Valera, J.E. and J.Y. Kaneshiro (1991). Liquefaction Analysis for Rubber Dam and Review of Case Histories of Liquefaction of Gravels, Proceedings: 2nd International Conference on Recent Advances in Geotechnical Earthquake Engineering and Soil Dynamics, March 11-15, St. Louis Missouri, Paper No. 3.7, p. 347-356.

Wassenaar (1987). Soil and foundation study for proposed protection clothing and decontamination center, Rocky Flats Facility, Jefferson County, Colorado, pp. 4-6, figs. 1 - 3, 5, and 6.

Woodward-Clyde Consultants, Inc. (1986). Geotechnical services for seismic retrofit on Buildings 707, 779, and 776/777 at Rocky Flats Plant, Jefferson County, Colorado, pp. 2, 4, 5, figs. 1 & 2.

Youd, T.L., J.C. Tinsley, D.M. Perkins, E.J. King and R.F. Preston (1978). Liquefaction Potential Map of San Fernando Valley, California, pp. 268-278 in *Proceedings of the Second*

International Conference on Microzonation for Safety Construction--Research and Applications, Volume 1, National Science Foundation, Washington, D.C.

TABLE G-1
TABULATION OF BORINGS REVIEWED TO ADDRESS SOIL LIQUEFACTION CONCERNS ROCKY FLATS PLANT SITE AREA

Blow Count Elevation (ft)	Blow Count Depth (ft)	Depth or GWL Elevation (ft)	Unified Soil Classification System	Fines Content ≤ #200 Sieve	N Blows/foot or (Blows/Inches)	Boring No.*	Reference
6004	10	6004	GC		26/6	TH-1 (1-1)	TERA (1976)
6000	14	6004	SC, Cobbly/Gravelly		70/6	TH-1 (1-1)	TERA (1976)
5986	28	6004	SC, Cobbly/Gravelly		66/12	TH-1 (1-1)	TERA (1976)
5995	3	5976	GC		30/12	TH-2 (1-2)	TERA (1976)
5985	13	5976	SC, Cobbly/Gravelly		30/9	TH-2 (1-2)	TERA (1976)
6010	10	6015	GC		5/11	TH-3 (1-3)	TERA (1976)
6004	15	6015	SC, Cobbly/Gravelly		15/12	TH-3 (1-3)	TERA (1976)
6000	19	6015	SC, Cobbly/Gravelly		17/12	TH-3 (1-3)	TERA (1976)
5996	23	6015	SC, Cobbly/Gravelly		21/12	TH-3 (1-3)	TERA (1976)
6015	9	6018	SC, Cobbly/Gravelly		38/9	TH-4 (1-4)	TERA (1976)
6006	20	6018	GC		50/6	TH-4 (1-4)	TERA (1976)
5996	30	6018	GC		43/6	TH-4 (1-4)	TERA (1976)
5988	38	6018	GC		60/5	TH-4 (1-4)	TERA (1976)
5987	4	5983	CL, Stiff Clay		12/12	TH-5 (1-5)	TERA (1976)
5983	8	5983	CL, Stiff Clay		6/12	TH-5 (1-5)	TERA (1976)
5975	16	5983	CL, Stiff Clay		25/12	TH-5 (1-5)	TERA (1976)
5590	4	5577	GM		25/9	TB-1 (2-1)	Wassenaar (1987)
5585	9	5577	CL/SM/GM Clay, Stiff to very stiff		11/12	TB-1 (2-1)	Wassenaar (1987)
5580	14	5577	CL/SM/GM Clay, Stiff to very stiff		14/12	TB-1 (2-1)	Wassenaar (1987)

* Number in parenthesis indicates Boring Location on Plate 1.

TABLE G-1 (continued)
TABULATION OF BORINGS REVIEWED TO ADDRESS SOIL LIQUEFACTION CONCERNS ROCKY FLATS PLANT SITE AREA

Blow Count Elevation (ft)	Blow Count Depth (ft)	Depth or GWL Elevation (ft)	Unified Soil Classification System	Fines Content ≤ #200 Sieve	N Blows/foot or (Blows/inches)	Boring No.*	Reference
5575	19	5577	SM/GM med. dense		20/9	TB-1 (2-1)	Wassenaar (1987)
5592	1	5582	GC		18/12	TB-2 (2-2)	Wassenaar (1987)
5589	4	5582	GC		26/9	TB-2 (2-2)	Wassenaar (1987)
5584	9	5582	CL/SM/GM Stiff to very stiff		22/12	TB-2 (2-2)	Wassenaar (1987)
5579	14	5582	CL/SM/GM Stiff to very stiff		22/12	TB-2 (2-2)	Wassenaar (1987)
5595	1	5578	GC		21/12	TB-3 (2-3)	Wassenaar (1987)
5592	4	5578	GC		50/4	TB-3 (2-3)	Wassenaar (1987)
5587	9	5578	GC		22/6	TB-3 (2-3)	Wassenaar (1987)
5582	14	5578	CL/SM/GM Stiff to very stiff		22/9	TB-3 (2-3)	Wassenaar (1987)
5577	19	5578	CL/SM/GM Stiff to very stiff		14/12	TB-3 (2-3)	Wassenaar (1987)
5591	4	5578	GC		20/9	TB-4 (2-4)	Wassenaar (1987)
5586	9	5578	CL/SM/GM Stiff to very stiff		19/12	TB-4 (2-4)	Wassenaar (1987)
5581	14	5578	CL/SM/GM Stiff to very stiff		18/12	TB-4 (2-4)	Wassenaar (1987)
6029	5	6005	SC, Gravelly Sand w/Clay		50/11	B-1 (3-1)	ATEC (1988)
6024	10	6005	SC, Gravelly Sand w/Clay		50/12	B-1 (3-1)	ATEC (1988)
6019	15	6005	SC, Gravelly Sand w/Clay		50/8	B-1 (3-1)	ATEC (1988)
6014	20	6005	SC, Gravelly Sand w/Clay		50/6	B-1 (3-1)	ATEC (1988)
6009	25	6005	SC, Gravelly Sand w/Clay		50/15	B-1 (3-1)	ATEC (1988)
6004	30	6005	SC, Gravelly Sand w/Clay		50/4	B-1 (3-1)	ATEC (1988)
6026	5	---	Not Noted		50/7	B-3 (3-2)	ATEC (1988)

* Number in parenthesis indicates Boring Location on Plate 1.

TABLE G-1 (continued)
TABULATION OF BORINGS REVIEWED TO ADDRESS SOIL LIQUEFACTION CONCERNS ROCKY FLATS PLANT SITE AREA

Blow Count Elevation (ft)	Blow Count Depth (ft)	Depth or GWL Elevation (ft)	Unified Soil Classification System	Fines Content ≤ #200 Sieve	N Blows/foot or (Blows/Inches)	Boring No.*	Reference
6021	10	---	Not Noted		50/12	B-3 (3-2)	ATEC (1988)
6016	15	---	Not Noted		50/9	B-3 (3-2)	ATEC (1988)
6021	5	---	SC, Gravelly Sand w/Clay		50/15	B-5 (3-3)	ATEC (1988)
6016	10	---	SC, Gravelly Sand w/Clay		50/9	B-5 (3-3)	ATEC (1988)
6011	15	---	SC, Gravelly Sand w/Clay		50/9	B-5 (3-3)	ATEC (1988)
---	5	---	SC, Sand w/Gravel & Clay	25	50/12	B-1 (4-1)	Air Products (1989)
---	5	---	SC Cobbles		50/9	B-2 (4-2)	Air Products (1989)
---	10	---	SC Cobbles	14	50/5	B-2 (4-2)	Air Products (1989)
---	5	---	GC	18	50/10	B-3 (4-3)	Air Products (1989)
---	5	10' deep	GC		50	B-1A (4-4)	Air Products (1989)
---	10	10' deep	GC		50/6	B-1A (4-4)	Air Products (1989)
---	15	10' deep	GC	21	38	B-1A (4-4)	Air Products (1989)
---	20	10' deep	GC		43	B-1A (4-4)	Air Products (1989)
---	5	---	SC, Gravelly Sand w/Clay		38	B-2A (4-5)	Air Products (1989)
---	10	---	SC, Gravelly Sand w/Clay	17	50/8	B-2A (4-5)	Air Products (1989)
---	15	---	SC, Gravelly Sand w/Clay		48	B-2A (4-5)	Air Products (1989)
---	5	10' deep	SC, Gravelly Sand w/Clay	29	28	B-3A (4-6)	Air Products (1989)
---	10	10' deep	SC, Gravelly Sand w/Clay		50/7	B-3A (4-6)	Air Products (1989)
---	15	10' deep	SC, Gravelly Sand w/Clay		40	B-3A (4-6)	Air Products (1989)
5980	4	---	Fill		26/12	TH-1 (G-1)	Woodward-Clyde (1986)

* Number in parenthesis indicates Boring Location on Plate 1.

TABLE G-1 (continued)
TABULATION OF BORINGS REVIEWED
TO ADDRESS SOIL LIQUEFACTION CONCERNS
ROCKY FLATS PLANT SITE AREA

Blow Count Elevation (ft)	Blow Count Depth (ft)	Depth or GWL Elevation (ft)	Unified Soil Classification System	Fines Content ≤ #200 Sieve	N Blows/foot or (Blows/inches)	Boring No.*	Reference
5975	9	---	CL, Stiff to very stiff		16/12	TH-1 (G-1)	Woodward-Clyde (1986)
5983	4	---	Fill		12/3	TH-2 (5-2)	Woodward-Clyde (1986)
5979	4	---	Fill		3/12	TH-3 (5-3)	Woodward-Clyde (1986)
5978	4	5966	Fill		20/12	TH-3A (5-4)	Woodward-Clyde (1986)
5973	9	5966	SC,GC,SM		45/12	TH-3A (5-4)	Woodward-Clyde (1986)
5975	4	5970	SC,GC,SM		36/12	TH-4 (5-5)	Woodward-Clyde (1986)
5970	9	5970	SC,GC,SM		13/12	TH-4 (5-5)	Woodward-Clyde (1986)
5974	4	---	SC,GC,SM		24/9	TH-5 (5-6)	Woodward-Clyde (1986)
5969	9	---	CL		20/12	TH-5 (5-6)	Woodward-Clyde (1986)
5975	4	5970	Fill		8/12	TH-6 (5-7)	Woodward-Clyde (1986)
5970	9	5970	CL/SC,GC,SM		36/12	TH-6 (5-7)	Woodward-Clyde (1986)
5984	4	5973	Fill		18/12	TH-7 (5-8)	Woodward-Clyde (1986)
5977	11	5973	SC,GC,SM		51/12	TH-7 (5-8)	Woodward-Clyde (1986)
5973	15	5973	CL		20/12	TH-7 (5-8)	Woodward-Clyde (1986)
5985	4	---	Fill		13/12	TH-8 (5-9)	Woodward-Clyde (1986)
5980	9	---	SC,GC,SM		13/12	TH-8 (5-9)	Woodward-Clyde (1986)
5984	4	---	SC,GC,SM		36/12	TH-9 (G-10)	Woodward-Clyde (1986)
5983	4	---	CL		14/12	TH-10 (G-11)	Woodward-Clyde (1986)
5978	9	---	CL		23/12	TH-10 (G-11)	Woodward-Clyde (1986)
5985	4	---	Fill		12/12	TH-11 (G-12)	Woodward-Clyde (1986)

* Number in parenthesis indicates Boring Location on Plate 1.

TABLE G-1 (continued)
TABULATION OF BORINGS REVIEWED
TO ADDRESS SOIL LIQUEFACTION CONCERNS
ROCKY FLATS PLANT SITE AREA

Blow Count Elevation (ft)	Blow Count Depth (ft)	Depth or GWL Elevation (ft)	Unified Soil Classification System	Fines Content ≤ #200 Sieve	N Blows/foot or (Blows/Inches)	Boring No.*	Reference
5985	4	5982	SC,GC,GM		12/12	TH-12 (G-13)	Woodward-Clyde (1986)
5980	9	5982	SC,GC,GM		16/12	TH-12 (G-13)	Woodward-Clyde (1986)
5975	14	5982	CL		18/12	TH-12 (G-13)	Woodward-Clyde (1986)
5984	4	---	SC,GC,SM		9/12	TH-13 (G-14)	Woodward-Clyde (1986)
5984	4	---	SC,GC,SM		36/12	TH-14 (G-15)	Woodward-Clyde (1986)
95	5	90-92	GC	20	47/12	Hole 1 (6-1)	Chen (1986)
90	10	90-92	GC		66/12	Hole 1 (6-1)	Chen (1986)
96	5	91	CL	39	21/12	Hole 2 (6-2)	Chen (1986)
91	10	91	GC		40/12	Hole 2 (6-2)	Chen (1986)
95	5	96	GC	26	30/12	Hole 3 (6-3)	Chen (1986)
90	10	96	GC		45/12	Hole 3 (6-3)	Chen (1986)
97	2	---	GC	40	50/15	Hole 4 (6-4)	Chen (1986)
95	5	---	GC		50/11	Hole 4 (6-4)	Chen (1986)
65.4	1	42-51	Fill	24	8/12	Hole 2 (7-1)	Merrick (1989)
61	5	42-51	SC		14/12	Hole 2 (7-1)	Merrick (1989)
56	10	42-51	SC	37	17/12	Hole 2 (7-1)	Merrick (1989)
---	4	---	Clayey Gravel Fill		6	B-1 (8-1)	ATEC (1987)
---	7	---	Claystone Fill	70	6	B-1 (8-1)	ATEC (1987)
---	11	---	Claystone Fill		6	B-1 (8-1)	ATEC (1987)
---	15	---	Claystone Fill		9	B-1 (8-1)	ATEC (1987)

* Number in parenthesis indicates Boring Location on Plate 1.

TABLE G-1 (continued)
TABULATION OF BORINGS REVIEWED TO ADDRESS SOIL LIQUEFACTION CONCERNS ROCKY FLATS PLANT SITE AREA

Blow Count Elevation (ft)	Blow Count Depth (ft)	Depth or GWL Elevation (ft)	Unified Soil Classification System	Fines Content ≤ #200 Sieve	N Blows/foot or (Blows/inches)	Boring No.*	Reference
---	20	---	Claystone Fill		23	B-1 (8-1)	ATEC (1987)
---	25	---	Claystone Fill	54	13	B-1 (8-1)	ATEC (1987)
---	30	---	Claystone Fill		13	B-1 (8-1)	ATEC (1987)
---	4	25' deep	Sandy Gravel Fill w/Clay	21	9	B-2 (8-2)	ATEC (1987)
---	7	25' deep	Sandy Gravel Fill w/Clay		8	B-2 (8-2)	ATEC (1987)
---	11	25' deep	Claystone Fill		10	B-2 (8-2)	ATEC (1987)
---	20	25' deep	Claystone Fill		5	B-2 (8-2)	ATEC (1987)
---	26	25' deep	Claystone Fill		50/0	B-2 (8-2)	ATECE (1987)
---	4	23' deep	Claystone Fill		4	B-3 (8-3)	ATEC (1987)
---	10	23' deep	Claystone Fill		5	B-3 (8-3)	ATEC (1987)
---	20	23' deep	Claystone Fill		3	B-3 (8-3)	ATEC (1987)
---	3	---	Fill, Clay		14	B-1 (9-1)	ATEC (1992)
---	5	---	Fill, Clay		24	B-1 (9-1)	ATEC (1992)
---	10	---	SW/SC, Fill w/Gravel		98/10	B-1 (9-1)	ATEC (1992)
---	15	---	CL, Clay		40	B-1 (9-1)	ATEC (1992)
---	20	---	CL, Clay		35	B-1 (9-1)	ATEC (1992)
---	3	24' deep	Fill, Clay w/Gravel		10	B-2 (9-2)	ATEC (1992)
---	5	24' deep	Clay, CL		13	B-2 (9-2)	ATEC (1992)
---	10	24' deep	Clay, CL		19	B-2 (9-2)	ATEC (1992)
---	15	24' deep	Clay, CL		22	B-2 (9-2)	ATEC (1992)

* Number in parenthesis indicates Boring Location on Plate 1.

TABLE G-1 (continued)
TABULATION OF BORINGS REVIEWED TO ADDRESS SOIL LIQUEFACTION CONCERNS ROCKY FLATS PLANT SITE AREA

Blow Count Elevation (ft)	Blow Count Depth (ft)	Depth or GWL Elevation (ft)	Unified Soil Classification System	Fines Content ≤ #200 Sieve	N Blows/foot or (Blows/Inches)	Boring No.*	Reference
---	20	24' deep	Clay, CL		32	B-2 (9-2)	ATEC (1992)
---	25	24' deep	Sand & Gravel		14	B-2 (9-2)	ATEC (1992)
---	3	25' deep	Fill, Clay		10	B-3 (9-3)	ATEC (1992)
---	5	25' deep	Fill, Clay		16	B-3 (9-3)	ATEC (1992)
---	10	25' deep	Fill, Sand & Gravel		21	B-3 (9-3)	ATEC (1992)
---	15	25' deep	Clay, CL		16	B-3 (9-3)	ATEC (1992)
---	20	25' deep	Sand & Gravel w/Clay		34	B-3 (9-3)	ATEC (1992)
---	25	25' deep	Sand & Gravel w/Clay		48	B-3 (9-3)	ATEC (1992)
---	5	22-23' deep	GC, Sandy Gravel w/Clay	25	50/8	B-1 (10-1)	ATEC (1989)
---	10	22-23' deep	GC, Sandy Gravel w/Clay		50/11	B-1 (10-1)	ATEC (1989)
---	15	22-23' deep	CH, v. stiff clay		32	B-1 (10-1)	ATEC (1989)
---	20	22-23' deep	GC, Sandy Gravel w/Clay		50	B-1 (10-1)	ATEC (1989)
---	25	22-23' deep	GC, Sandy Gravel w/Clay		44	B-1 (10-1)	ATEC (1989)
---	5	---	CL, Sandy Clay	55	21	B-2 (10-2)	ATEC (1989)
---	10	---	CL, Sandy Clay		22	B-2 (10-2)	ATEC (1989)
---	15	---	CL, Sandy Clay		29	B-2 (10-2)	ATEC (1989)
---	3	---	SC, loose sand w/Gravel & Clay	14	10	B-3 (10-3)	ATEC (1989)
---	6	---	GC, Dense to v. Dense Sandy Gravel w/Clay	26	18	B-3 (10-3)	ATEC (1989)

* Number in parenthesis indicates Boring Location on Plate 1.

TABLE G-1 (continued)
TABULATION OF BORINGS REVIEWED TO ADDRESS SOIL LIQUEFACTION CONCERNS ROCKY FLATS PLANT SITE AREA

Blow Count Elevation (ft)	Blow Count Depth (ft)	Depth or GWL Elevation (ft)	Unified Soil Classification System	Fines Content ≤ #200 Sieve	N Blows/foot or (Blows/inches)	Boring No.*	Reference
---	11	---	GC, Dense to v. Dense Sandy Gravel w/Clay		50/8	B-3 (10-3)	ATEC (1989)
---	16	---	GC, Dense to v. Dense Sandy Gravel w/Clay		20	B-3 (10-3)	ATEC (1989)
5989	3	---	SC-GC, Sand & Gravel		29	1 (11-1)	ESI (1990)
5988	4	---	SC-GC, Sand & Gravel		50/10	1 (11-1)	ESI (1990)
5989	4	---	SC-GC, Sand & Gravel		52	2 (11-2)	ESI (1990)
5980	9	---	SC-GC, Sand & Gravel		50/10	2 (11-2)	ESI (1990)
5989	4	---	SC-GC, Sand & Gravel	50	38	3 (11-3)	ESI (1990)
5980	9	---	SC-GC, Sand & Gravel		50/8	3 (11-3)	ESI (1990)
5989	4	---	SC-GC, Sand & Gravel	40	36	4 (11-4)	ESI (1990)
5989	4	---	SC-GC, Sand & Gravel		33	5 (11-5)	ESI (1990)
5988	4	---	SC-GC, Sand & Gravel		50/11	6 (11-6)	ESI (1990)
5983	9	---	SC-GC, Sand & Gravel		24	6 (11-6)	ESI (1990)
---	5	---	CL		30/12	TH-201 (12-1)	CTL/Thompson (1980)
---	5	---	CL-GC-SC		21/12	TH-202 (12-2)	CTL/Thompson (1980)
---	5	---	CL-GC-SC		19/12	TH-203 (12-3)	CTL/Thompson (1980)
---	5	---	CL-GC-SC	34	21/12	TH-204 (12-4)	CTL/Thompson (1980)
---	10	---	CL-GC-SC		41/6	TH-204 (12-4)	CTL/Thompson (1980)
---	5	---	CL	28	6/12	TH-206 (12-5)	CTL/Thompson (1980)
---	10	---	CL		11/12	TH-206 (12-5)	CTL/Thompson (1980)

* Number in parenthesis indicates Boring Location on Plate 1.

TABLE G-1 (continued)
TABULATION OF BORINGS REVIEWED TO ADDRESS SOIL LIQUEFACTION CONCERNS ROCKY FLATS PLANT SITE AREA

Blow Count Elevation (ft)	Blow Count Depth (ft)	Depth or GWL Elevation (ft)	Unified Soil Classification System	Fines Content ≤ #200 Sieve	N Blows/foot or (Blows/Inches)	Boring No.*	Reference
---	5	---	CL	79	20/12	TH-207 (12-6)	CTL/Thompson (1980)
---	10	---	CL-GC-SC	17	50/11	TH-207 (12-6)	CTL/Thompson (1980)
---	4	---	GC-SC	19	43/9	TH-208A (12-7)	CTL/Thompson (1980)
---	9	---	GC-SC		48/9	TH-208A (12-7)	CTL/Thompson (1980)
---	14	---	GC-SC	21	44/9	TH-208A (12-7)	CTL/Thompson (1980)
---	19	---	GC-SC		41/9	TH-208A (12-7)	CTL/Thompson (1980)
---	4	---	GC-SC		26/12	TH-209 (12-8)	CTL/Thompson (1980)
---	9	---	GC-SC		42/9	TH-209 (12-8)	CTL/Thompson (1980)
---	14	---	GC-SC	20	40/9	TH-209 (12-8)	CTL/Thompson (1980)
---	19	---	GC-SC		50/6	TH-209 (12-8)	CTL/Thompson (1980)
---	24	---	GC-SC		50/9	TH-209 (12-8)	CTL/Thompson (1980)
---	5	---	Fill		9/12	TH-210 (12-9)	CTL/Thompson (1980)
---	10	---	Fill	46	23/12	TH-210 (12-9)	CTL/Thompson (1980)
---	15	---	Fill		14/12	TH-210 (12-9)	CTL/Thompson (1980)
---	20	---	Clay		27/9	TH-210 (12-9)	CTL/Thompson (1980)
---	25	---	Clay		14/12	TH-210 (12-9)	CTL/Thompson (1980)
---	5	---	SC, Gravelly Sand w/Clay		50/10	B-1 (13-1)	ATEC (1989)
---	10	---	SC, Gravelly Sand w/Clay		50/7	B-1 (13-1)	ATEC (1989)
---	15	---	SC, Gravelly Sand w/Clay	30	50/6	B-1 (13-1)	ATEC (1989)
---	20	---	SC, Clayey Sand		8/12	B-1 (13-1)	ATEC (1989)

* Number in parenthesis indicates Boring Location on Plate 1.

TABLE G-1 (continued)
TABULATION OF BORINGS REVIEWED TO ADDRESS SOIL LIQUEFACTION CONCERNS ROCKY FLATS PLANT SITE AREA

Blow Count Elevation (ft)	Blow Count Depth (ft)	Depth or GWL Elevation (ft)	Unified Soil Classification System	Fines Content ≤ #200 Sieve	N Blows/foot or (Blows/Inches)	Boring No.*	Reference
---	25	---	CL, w/Gravel		50/7	B-1 (13-1)	ATEC (1989)
---	30	---	CL, w/Gravel		49	B-1 (13-1)	ATEC (1989)
---	5	---	GC	24	63	B-2 (13-2)	ATEC (1989)
---	10	---	SC	30	50/5	B-2 (13-2)	ATEC (1989)
6005	3	5994	GM		37	TH-1 (14-1)	RV LORD (1972)
6003	5	5994	CL		43	TH-1 (14-1)	RV LORD (1972)
5997	11	5994	GM		32	TH-1 (14-1)	RV LORD (1972)
5993	15	5994	GM		50/9	TH-1 (14-1)	RV LORD (1972)
6004	5	5997	CL w/Gravel		50/7	TH-2 (14-2)	RV LORD (1972)
5999	10	5997	CL w/Gravel		39/12	TH-2 (14-2)	RV LORD (1972)
5994	15	5997	CL		26/12	TH-2 (14-2)	RV LORD (1972)
6002	5	5993	CL		52	TH-3 (14-3)	RV LORD (1972)
5997	10	5993	CL		34	TH-3 (14-3)	RV LORD (1972)
5992	15	5993	SM		35	TH-3 (14-3)	RV LORD (1972)
---	9	---	SC-GC	14	25/9	1 (1G-1)	Chen & Assoc. (1972)
---	14	---	SC-GC	13	30/6	1 (1G-1)	Chen & Assoc. (1972)
---	4	---	SC-GC	24	25/10	2 (15-2)	Chen & Assoc. (1972)
---	14	---	SC-GC		23/6	2 (15-2)	Chen & Assoc. (1972)
5970	4	5967-5971	GC		50/6	TH-1 (16-1)	RV LORD (1976)
5969	4	5971	GC		50/11	TH-2 (16-2)	RV LORD (1976)

* Number in parenthesis indicates Boring Location on Plate 1.

TABLE G-1 (continued)
TABULATION OF BORINGS REVIEWED TO ADDRESS SOIL LIQUEFACTION CONCERNS ROCKY FLATS PLANT SITE AREA

Blow Count Elevation (ft)	Blow Count Depth (ft)	Depth or GWL Elevation (ft)	Unified Soil Classification System	Fines Content ≤ #200 Sieve	N Blows/foot or (Blows/Inches)	Boring No.*	Reference
5971	5	5971	GC		30/12	TH-3 (16-3)	RV LORD (1976)
5972	5	---	GC		31/12	TH-4 (16-4)	RV LORD (1976)
5968	5	5966	GC		32/12	TH-5 (16-5)	RV LORD (1976)
---	4	---	CL-SC	67	12	1 (17-1)	Aguirre (1988)/Phase II
---	4	5'-7' deep	CL-SC		15	2 (17-2)	Aguirre (1988)/Phase II
---	9	5'-7' deep	CL		22	2 (17-2)	Aguirre (1988)/Phase II
---	4	5'-7' deep	CL	88.7	19	3 (17-3)	Aguirre (1988)/Phase II
---	9	5'-7' deep	CL		32	3 (17-3)	Aguirre (1988)/Phase II
---	4	5'-7' deep	SC/SM	20.4	39	4 (17-4)	Aguirre (1988)/Phase II
---	4	7'-8' deep	CL	98	34	6 (17-5)	Aguirre (1988)/Phase II
---	9	7'-8' deep	GC	35	50/0	6 (17-5)	Aguirre (1988)/Phase II
---	4	7' deep	CL		34	7 (17-6)	Aguirre (1988)/Phase II
---	9	7' deep	CL	66.4	32	7 (17-6)	Aguirre (1988)/Phase II
---	4	---	CL		32	8 (17-7)	Aguirre (1988)/Phase II
---	4	7'-9' deep	GC		50/0	9 (17-8)	Aguirre (1988)/Phase II
----	9	7'-9' deep	GC	16.7	23	9 (17-8)	Aguirre (1988)/Phase II
---	4	---	GC		50/8	10 (17-9)	Aguirre (1988)/Phase II
---	9	---	GC		50/10	10 (17-9)	Aguirre (1988)/Phase II
---	4	6'-8' deep	CL		50	11 (17-10)	Aguirre (1988)/Phase II
---	9	6'-8' deep	CL	31.5	50	11 (17-10)	Aguirre (1988)/Phase II

* Number in parenthesis indicates Boring Location on Plate 1.

TABLE G-1 (continued)
TABULATION OF BORINGS REVIEWED TO ADDRESS SOIL LIQUEFACTION CONCERNS ROCKY FLATS PLANT SITE AREA

Blow Count Elevation (ft)	Blow Count Depth (ft)	Depth or GWL Elevation (ft)	Unified Soil Classification System	Fines Content ≤ #200 Sieve	N Blows/foot or (Blows/Inches)	Boring No.*	Reference
---	4	8' deep	CL/SC		50	13 (17-11)	Aguirre (1988)/Phase II
---	4	10' 2-days 3'-14 days 7'-36 days	GC		50/0	18 (17-12)	Aguirre (1988)/Phase II
---	4	5' deep	GC		5	19 (17-13)	Aguirre (1988)/Phase II
---	9	5' deep	GC		11	19 (17-13)	Aguirre (1988)/Phase II
---	4	7'-9' deep	GC	0.5	18	20 (17-14)	Aguirre (1988)/Phase II
---	4	3'-'6 deep	GC		14	21 (17-15)	Aguirre (1988)/Phase II
---	4	3'-5' deep	CL		6	22 (17-16)	Aguirre (1988)/Phase II
---	9	---	CL		50/11	25 (17-17)	Aguirre (1988)/Phase II
---	4	4'-8' deep	SP/SM		50/9	26 (17-18)	Aguirre (1988)/Phase II
---	9	4'-8' deep	SM/CL	8.8	50/10	26 (17-18)	Aguirre (1988)/Phase II
---	4	---	CL		16	27 (17-19)	Aguirre (1988)/Phase II
---	9	---	GC	7.0	50/0	27 (17-19)	Aguirre (1988)/Phase II
---	4	---	CL		50	28 (17-20)	Aguirre (1988)/Phase II
---	4	10' deep	CL/SC	48.1	50/8	29 (17-21)	Aguirre (1988)/Phase II
---	9	10' deep	?		50/11	29 (17-21)	Aguirre (1988)/Phase II
---	4	9' deep	CL	19.6	15	30 (17-22)	Aguirre (1988)/Phase II
---	9	9' deep	CL	27.9	26	30 (17-22)	Aguirre (1988)/Phase II
---	4	8' deep	GC	23.5	50/8	31 (17-23)	Aguirre (1988)/Phase II
---	9	8' deep	CL/GC		46	31 (17-23)	Aguirre (1988)/Phase II

* Number in parenthesis indicates Boring Location on Plate 1.

TABLE G-1 (continued)
TABULATION OF BORINGS REVIEWED TO ADDRESS SOIL LIQUEFACTION CONCERNS ROCKY FLATS PLANT SITE AREA

Blow Count Elevation (ft)	Blow Count Depth (ft)	Depth or GWL Elevation (ft)	Unified Soil Classification System	Fines Content ≤ #200 Sieve	N Blows/foot or (Blows/Inches)	Boring No.*	Reference
---	4	---	CL		26	32 (17-24)	Aguirre (1988)/Phase II
---	9	---	CL		23	32 (17-24)	Aguirre (1988)/Phase II
---	4	---	CL		19	33 (17-25)	Aguirre (1988)/Phase II
---	9	---	CL		17	33 (17-25)	Aguirre (1988)/Phase II
---	4	5'-8' deep	CL	99.1	13	34 (17-26)	Aguirre (1988)/Phase II
---	9	5'-8' deep	CL		17	34 (17-26)	Aguirre (1988)/Phase II
---	4	---	CL-SC		16	37 (17-27)	Aguirre (1988)/Phase II
---	9	---	CL-SC		10	37 (17-27)	Aguirre (1988)/Phase II
---	4	8' deep	CL		45	38 (17-28)	Aguirre (1988)/Phase II
---	9	8' deep	CL		30	38 (17-28)	Aguirre (1988)/Phase II
---	4	10' deep	CL	80.5	18	39 (17-29)	Aguirre (1988)/Phase II
---	9	10' deep	CL		12	39 (17-29)	Aguirre (1988)/Phase II
---	4	7' deep	CL		29	40 (17-30)	Aguirre (1988)/Phase II
---	9	7' deep	CL		26	40 (17-30)	Aguirre (1988)/Phase II
---	4	---	CL		18	41 (17-31)	Aguirre (1988)/Phase II
---	4	7' deep	CL		40	42 (17-32)	Aguirre (1988)/Phase II
---	9	7' deep	GC		50/8	42 (17-32)	Aguirre (1988)/Phase II
---	4	6' deep	CL		50/9	43 (17-33)	Aguirre (1988)/Phase II
---	9	6' deep	SC	56.2	43	43 (17-33)	Aguirre (1988)/Phase II
---	4	---	SP/SM		37	45 (17-34)	Aguirre (1988)/Phase II

* Number in parenthesis indicates Boring Location on Plate 1.

TABLE G-1 (continued)
TABULATION OF BORINGS REVIEWED
TO ADDRESS SOIL LIQUEFACTION CONCERNS
ROCKY FLATS PLANT SITE AREA

Blow Count Elevation (ft)	Blow Count Depth (ft)	Depth or GWL Elevation (ft)	Unified Soil Classification System	Fines Content ≤ #200 Sieve	N Blows/foot or (Blows/Inches)	Boring No.*	Reference
---	9	---	SP/SM		39	45 (17-34)	Aguirre (1988)/Phase II
---	4	8' deep	GC		50/6	46 (17-35)	Aguirre (1988)/Phase II
---	4	8' deep	SM	45.0	30	48 (17-36)	Aguirre (1988)/Phase II
---	4	8' deep	CL		50/7	50 (17-37)	Aguirre (1988)/Phase II
---	4	6' deep	CL/SP/SM		6	53 (17-38)	Aguirre (1988)/Phase II
---	4	9' deep	GC	31.6	50/7	54 (17-39)	Aguirre (1988)/Phase II
---	9	9' deep	GC		50/1	54 (17-39)	Aguirre (1988)/Phase II
---	4	4' deep	CL		37	55 (17-40)	Aguirre (1988)/Phase II
---	9	4' deep	GC		50/6	55 (17-40)	Aguirre (1988)/Phase II
---	4	---	GC/CL	62.8	50/8	56 (17-41)	Aguirre (1988)/Phase II
---	9	---	GC		50/8	56 (17-41)	Aguirre (1988)/Phase II
---	4	---	GC		50/8	57 (17-42)	Aguirre (1988)/Phase II
---	9	---	GC		35	57 (17-42)	Aguirre (1988)/Phase II
---	4	9' deep	GC	22.9	17	59 (17-43)	Aguirre (1988)/Phase II
---	9	9' deep	GC		50/8	59 (17-43)	Aguirre (1988)/Phase II
---	4	7' deep	GC		50/10	61 (17-44)	Aguirre (1988)/Phase II
---	4	8' deep	CL		17	62 (17-45)	Aguirre (1988)/Phase II
---	4	4' deep	GC		50/7	64 (17-46)	Aguirre (1988)/Phase II
---	4	7' deep	CL		17	66 (17-47)	Aguirre (1988)/Phase II
---	9	7' deep	CL		20	66 (17-47)	Aguirre (1988)/Phase II

* Number in parenthesis indicates Boring Location on Plate 1.

TABLE G-1 (continued)
TABULATION OF BORINGS REVIEWED TO ADDRESS SOIL LIQUEFACTION CONCERNS ROCKY FLATS PLANT SITE AREA

Blow Count Elevation (ft)	Blow Count Depth (ft)	Depth or GWL Elevation (ft)	Unified Soil Classification System	Fines Content ≤ #200 Sieve	N Blows/foot or (Blows/inches)	Boring No.*	Reference
---	4	---	Sand		33	1 (18-1)	Aguirre (1988)/Phase I
---	9	---	GC	22	60/6	1 (18-1)	Aguirre (1988)/Phase I
---	4	4' deep	GC	22	3	2 (18-2)	Aguirre (1988)/Phase I
---	9	4' deep	GC		12	2 (18-2)	Aguirre (1988)/Phase I
---	4	---	GC		50/7	3 (18-3)	Aguirre (1988)/Phase I
---	9	---	GC		50/9	3 (18-3)	Aguirre (1988)/Phase I
---	4	---	SM	35	50/6	4 (18-4)	Aguirre (1988)/Phase I
---	9	---	SM	18	50/11	4 (18-4)	Aguirre (1988)/Phase I
---	4	4' deep	GC		34	5 (18-5)	Aguirre (1988)/Phase I
---	9	4' deep	GC	11	50/7	5 (18-5)	Aguirre (1988)/Phase I
---	4	---	SM	28	50/5	6 (18-6)	Aguirre (1988)/Phase I
---	9	---	SM		50/7	6 (18-6)	Aguirre (1988)/Phase I
---	4	---	GC		38/9	7 (18-7)	Aguirre (1988)/Phase I
---	9	---	SM	30	50/5	7 (18-7)	Aguirre (1988)/Phase I
---	4	---	GC		50/6	8 (18-8)	Aguirre (1988)/Phase I
---	9	---	SM		40/8	8 (18-8)	Aguirre (1988)/Phase I
---	4	4' deep	GC		39/7	9 (18-9)	Aguirre (1988)/Phase I
---	9	4' deep	SM		24	9 (18-9)	Aguirre (1988)/Phase I
---	4	8' deep	GC		40	10 (18-10)	Aguirre (1988)/Phase I
---	9	8' deep	SM	32	39	10 (18-10)	Aguirre (1988)/Phase I

* Number in parenthesis indicates Boring Location on Plate 1.

TABLE G-1 (continued)
TABULATION OF BORINGS REVIEWED TO ADDRESS SOIL LIQUEFACTION CONCERNS ROCKY FLATS PLANT SITE AREA

Blow Count Elevation (ft)	Blow Count Depth (ft)	Depth or GWL Elevation (ft)	Unified Soil Classification System	Fines Content ≤ #200 Sieve	N Blows/foot or (Blows/inches)	Boring No.*	Reference
---	4	---	SM		50/7	11 (18-11)	Aguirre (1988)/Phase I
---	9	---	SM	37	50/7	11 (18-11)	Aguirre (1988)/Phase I
---	4	---	CL		50/13	12 (18-12)	Aguirre (1988)/Phase I
---	9	---	CL		50/8	12 (18-12)	Aguirre (1988)/Phase I
---	4	4' deep	GC		50	13 (18-13)	Aguirre (1988)/Phase I
---	9	4' deep	CL/SP/SM		50/8	13 (18-13)	Aguirre (1988)/Phase I
---	4	---	SM	16	50/7	14 (18-14)	Aguirre (1988)/Phase I
---	4	4' deep	SM		4	15 (18-15)	Aguirre (1988)/Phase I
---	9	4' deep	GC		34/11	15 (18-15)	Aguirre (1988)/Phase I
---	4	---	SM		50/6	16 (18-16)	Aguirre (1988)/Phase I
---	4	---	CL		4	17 (18-17)	Aguirre (1988)/Phase I
---	9	---	CL		12	17 (18-17)	Aguirre (1988)/Phase I
---	4	---	CL/SC		12	18 (18-18)	Aguirre (1988)/Phase I
---	4	9' deep	SP		20	19 (18-19)	Aguirre (1988)/Phase I
---	9	9' deep	CL		23	19 (18-19)	Aguirre (1988)/Phase I
---	4	9' deep	GC	19	50	20 (18-20)	Aguirre (1988)/Phase I
---	4	6' deep	CL		34/7	21 (18-21)	Aguirre (1988)/Phase I
---	4	---	GC/SC		50/9	22 (18-22)	Aguirre (1988)/Phase I
---	9	---	SM		16	22 (18-22)	Aguirre (1988)/Phase I
---	4	9' deep	CL/SC	28	14	23 (18-23)	Aguirre (1988)/Phase I

* Number in parenthesis indicates Boring Location on Plate 1.

TABLE G-1 (continued)
TABULATION OF BORINGS REVIEWED
TO ADDRESS SOIL LIQUEFACTION CONCERNS
ROCKY FLATS PLANT SITE AREA

Blow Count Elevation (ft)	Blow Count Depth (ft)	Depth or GWL Elevation (ft)	Unified Soil Classification System	Fines Content ≤ #200 Sieve	N Blows/foot or (Blows/Inches)	Boring No.*	Reference
---	4	---	SP/SM		50/7	24 (18-24)	Aguirre (1988)/Phase I
---	9	---	SP/SM		50/5	24 (18-24)	Aguirre (1988)/Phase I
---	4	---	SP/SM/GC		50/9	25 (18-25)	Aguirre (1988)/Phase I
---	9	---	GC		50/5	25 (18-25)	Aguirre (1988)/Phase I
---	4	7' deep	SM		38	26 (18-26)	Aguirre (1988)/Phase I
---	9	7' deep	SM		50/9	26 (18-26)	Aguirre (1988)/Phase I
---	4	---	CL/GC		50/9	27 (18-27)	Aguirre (1988)/Phase I
---	9	---	CL/SP/SM		50/11	27 (18-27)	Aguirre (1988)/Phase I
---	4	---	GC		50/9	28 (18-28)	Aguirre (1988)/Phase I
---	9	---	CL/SP/SM	32	50/9	28 (18-28)	Aguirre (1988)/Phase I
---	4	---	SP/SM		21	29 (18-29)	Aguirre (1988)/Phase I

* Number in parenthesis indicates Boring Location on Plate 1.

TABLE G-2

SUMMARY OF STANDARD PENETRATION TEST RESULTS
IN ALLUVIUM AND FILL MATERIALS

	No. of Samples	Range of Measured SPT Values (Blows/ft)	Average SPT Value (Blows/ft)	Standard Deviation (Blows/ft)
ALLUVIUM				
a) Clayey portion	105	4 to > 50	28	14
b) Sandy portion	91	4 to > 50	38	14
c) Gravelly portion	91	3 to > 50	41	13
FILL	34	3 to > 50	14	11

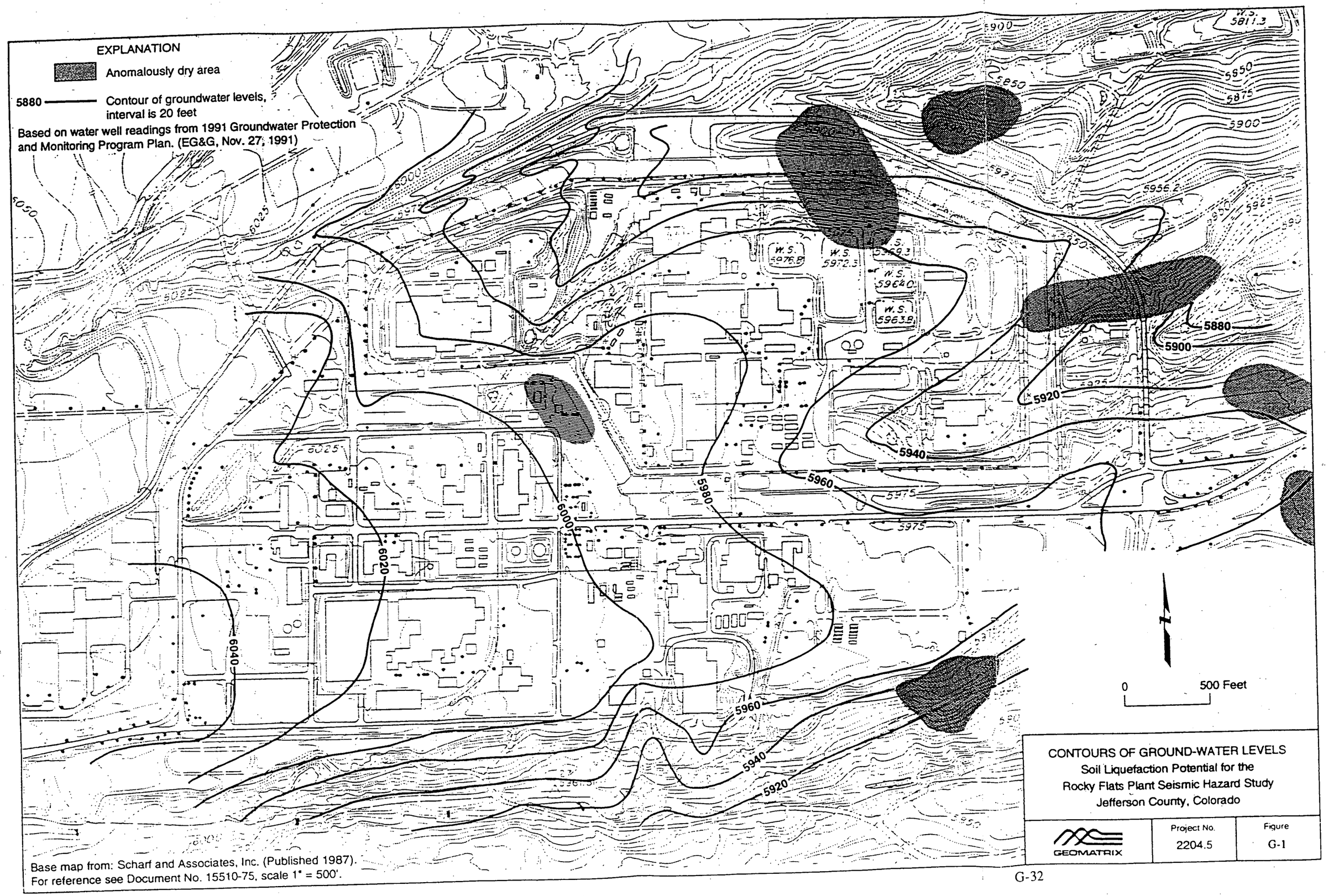
EXPLANATION
Anomalously dry area
5880 Contour of groundwater levels, interval is 20 feet
Based on water well readings from 1991 Groundwater Protection and Monitoring Program Plan. (EG&G, Nov. 27, 1991)
5880
5900
5920
5940
5960
5980
6000
6020
6040
0
500 Feet
CONTOURS OF GROUND-WATER LEVELS
Soil Liquefaction Potential for the
Rocky Flats Plant Seismic Hazard Study
Jefferson County, Colorado
GEOMATRIX
Project No.
2204.5
Figure
G-1
Base map from: Scharf and Associates, Inc. (Published 1987).
For reference see Document No. 15510-75, scale 1" = 500'.

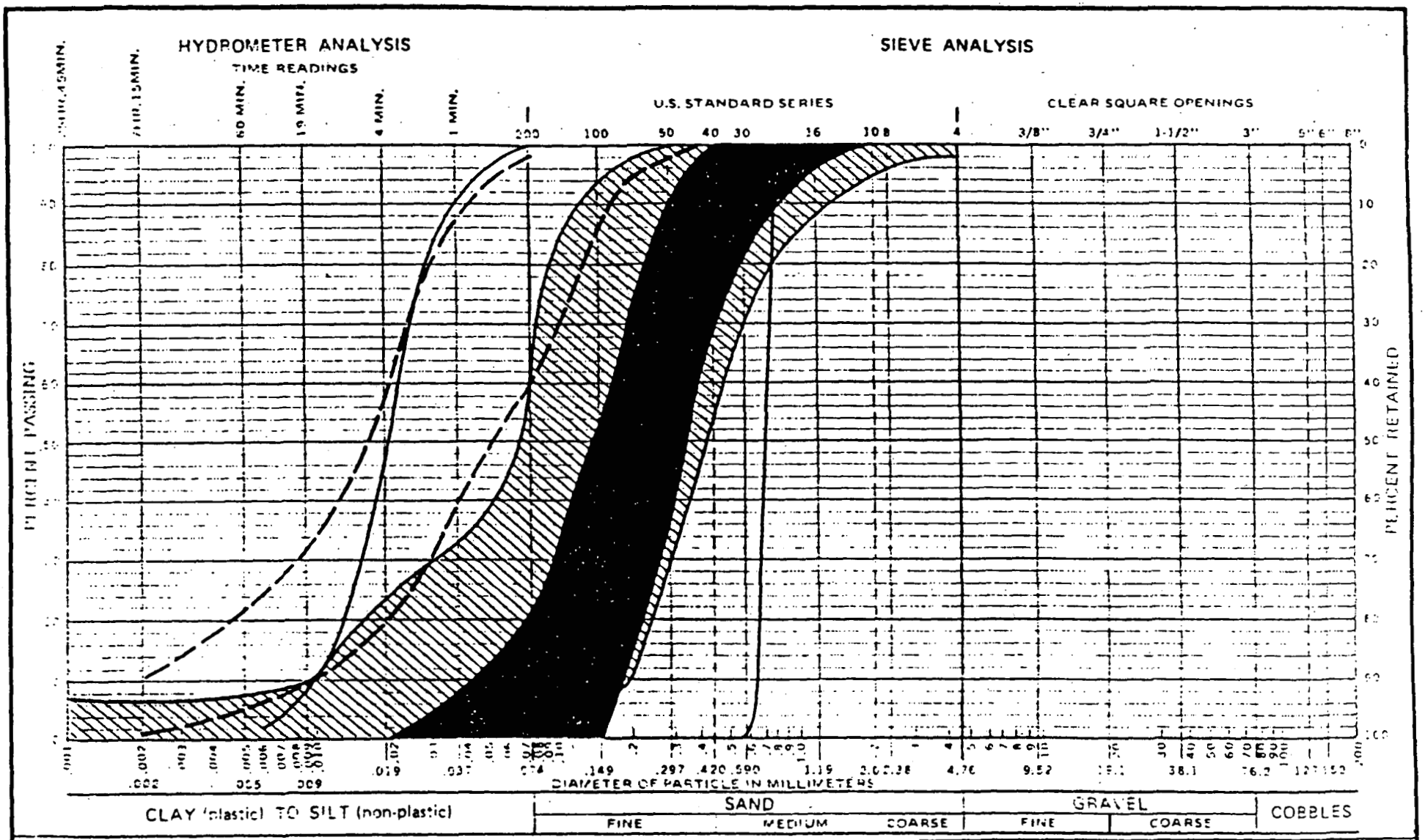

KEY

- Most liquefiable soils based on laboratory tests. Lee and Fitton (1968)
- Sands at Niigata in 15 to 30 feet depth range. Seed and Idriss (1967)
- Envelope of 19 curves of sands that liquefied during earthquakes in Japan. Kishida (1969)
- Envelope of 7 curves of silts that liquefied during Western Argentina earthquake of 1977. Youd (1982)

GRADATION OF LIQUEFIABLE SANDY AND SILTY SOILS

Soil Liquefaction Potential for the
Rocky Flats Plant Seismic Hazard Study
Jefferson County, Colorado

GEOMATRIX	Project No.	Figure
	2204.5	G-2

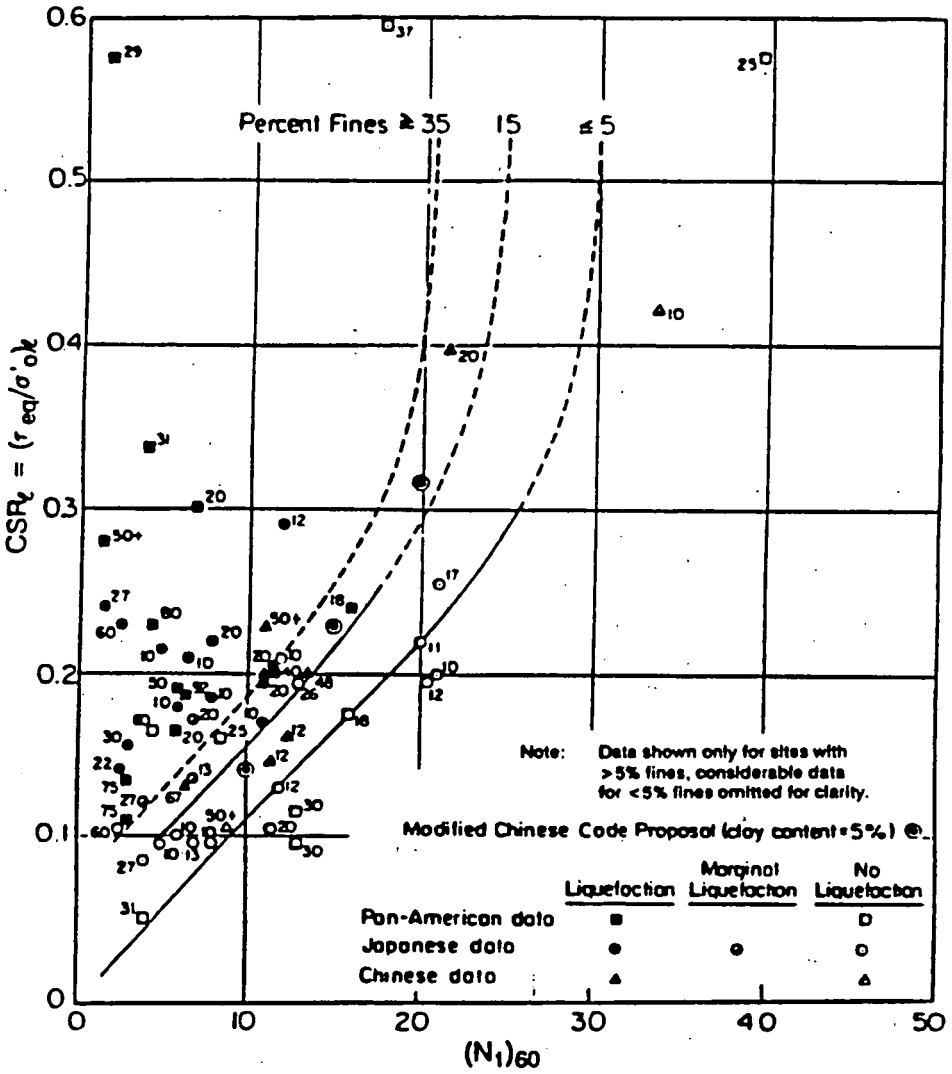

Figure G-3. Relationship between Cyclic Stress Ratio Causing Liquefaction and $(N_1)_{60}$. Values for M = 7 1/2 Earthquakes (After Seed et al., 1985).

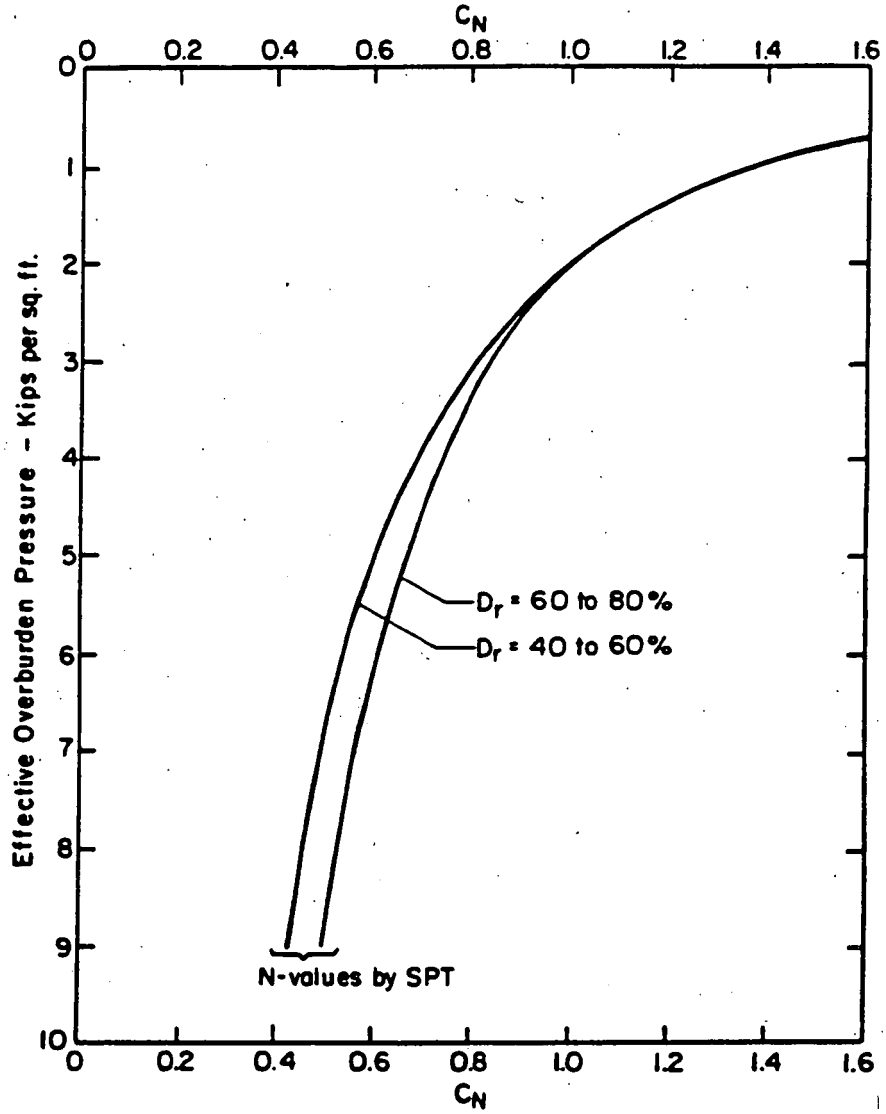

Figure G-4. Chart for values of overburden correction factor C_N. Source: Seed et al. (1985) based on data and analyses from Marcuson and Mieganousky (1977).

Rocky Flats Plant Site Area
Liquefaction Assessment

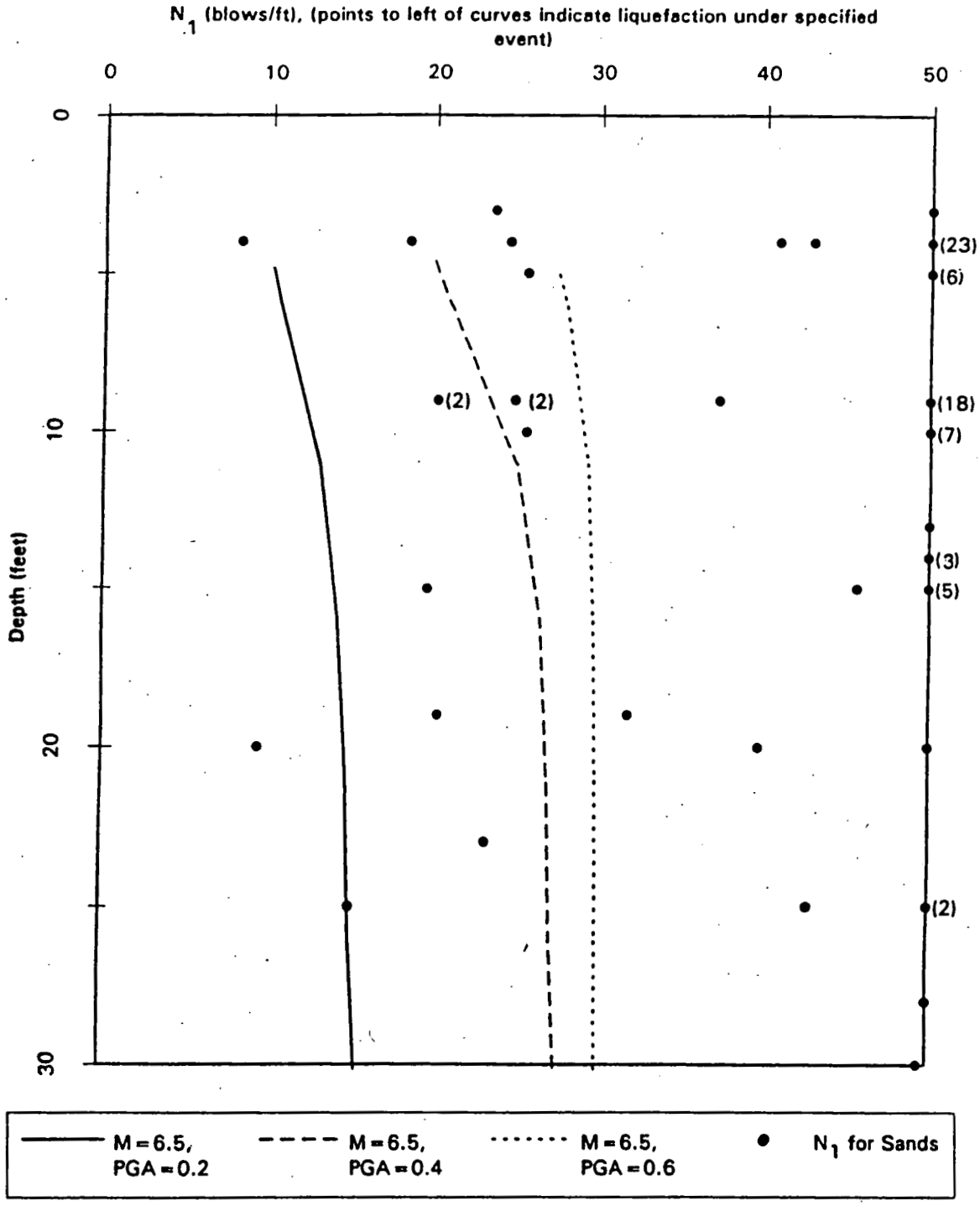

Figure G-5. Blowcounts, N_1 (blows/foot) versus Depth, with N_1 critical for Three Selected Earthquakes. Number in ( ) indicates number of points with same blowcount or greater.

APPENDIX H

STABILITY OF GEOTECHNICAL STRUCTURES

by

Geomatrix Consultants, Inc.
San Francisco, California

INTRODUCTION

This Appendix covers the evaluation of man-made and natural slopes at the Rocky Flats plant for possible damage (settlement, sliding, lurching, etc.) during earthquakes. This work was conducted and reported by Geomatrix Consultants, Inc., San Francisco.

The topography at the Rocky Flats Plant site is relatively flat. However, the Rocky Flats Alluvium and the underlying bedrock formations have been dissected by several streams and drainage channels, a process that has created natural slopes and topographic relief as much as 50 feet high. Grading, excavation, and filling related to construction of plant buildings also has created man-made slopes and embankments that are as much as 30 feet in height.

Based on an examination of topographic maps of the plant site, we identified locations that exhibit the highest topographic relief and steepest slopes in the vicinity of the plant structures. We developed profiles typical of these slopes, having various subsurface conditions, to evaluate the seismic stability of the slopes under several postulated levels of earthquake ground shaking.

We performed a site reconnaissance and reviewed previous geotechnical and geologic investigations of the plant site to assess subsurface and ground water conditions for use in the seismic stability evaluations of the slopes.

The following pages present a summary of general geologic conditions at the plant site, an assessment of typical subsurface soil and ground water conditions that may underlie those slopes, estimates of shear strength parameters for the various materials comprising those slopes, and assessment of the seismic stability under various levels of earthquake ground shaking. We assess slope stability in terms of the potential for permanent downslope displacements given a specified level of ground shaking.

SUMMARY OF SITE GEOLOGY

The Rock Flats Plant site is located on the western edge of the Colorado Piedmont section of the Great Plains Physiographic Province (Hunt, 1974). The Colorado Piedmont lies adjacent to the southern Rocky Mountains and is drained by the South Platte and Arkansas rivers. Tertiary bedrock has been stripped from much of this region and the section is eroded below the High Plains by as much as 450 meters (Osterkamp and others, 1987). The plant site sits on a geomorphic surface comprised of a gravel-capped pediment surface (Rocky Flats alluvial surface)

that is adjacent to the base of the Colorado Front Range. Erosional remnants of the Rocky Flats surface slope gently east towards the central Denver Basin. It is dissected along its eastern edge by the heads of several small intermittent (seasonal) streams.

The gravel that caps the pediment surface was deposited in the very early Pleistocene (1 to 2.5 million years ago) and is identified as the Rocky Flats Alluvium (Blume, 1974; Ebasco, 1992). It consists predominantly of bouldery and cobbly, silty, clayey, and sandy gravel. The gravel is predominantly quartzite, containing sizeable percentages of schist, gneiss, and granite. The surface deposits range in thickness from less than 1 foot to over 100 feet to the west of the site, averaging about 10 feet, across the width of the Rocky Flats Plant. The bedrock surface has a relief of about 50 feet. Details of the material characteristics of Rocky Flats Alluvium are provided in the soil liquefaction assessment (Appendix G) report.

The underlying bedrock consists of Cretaceous-age sedimentary strata, including, in descending order, the Arapahoe Formation, the Laramie Formation, the Fox Hill Sandstone, and the Pierre Shale. These sedimentary formations dip to the east at angles ranging from about 76 degrees west of the Rocky Flats alluvial surface to less than 5 degrees east of the surface. In the plant site area, bedrock dips about 1 to 5 degrees to the east, on average. Locally, dips may be steeper (e.g., 10 to 20 degrees).

The Arapahoe Formation, which immediately underlies the Rocky Flats Alluvium at the Rocky Flats Plant, is approximately 0 to 120 feet thick and consists of claystone with interbedded sandstone and siltstone. Underlying the Arapahoe Formation is the Laramie Formation, which is approximately 600 to 800 feet thick. The upper several hundred feet of the Laramie is composed chiefly of clay shale, sandy shale, and claystone containing some lenticular beds of sandstone, while the lower couple of hundred feet is sandstone separated by thin beds of shale, clay, and coal. Underlying the Laramie is the Fox Hills Sandstone, which is estimated to be about 100 feet thick under the Rocky Flats Plant. Underlying the Fox Hills Sandstone is the Pierre Shale, which is about 8000 feet thick. A more detailed discussion of site geology may be found in Ebasco (1992).

The following general observations about the topography, drainage, and slope stability of the plant site are based on field observations made adjacent to the plant site by URS/J. Blume (1974). Because of its inherent strength, the Rocky Flats Alluvium forms a scarp that has a distinct break in slope at the contact where it overlies bedrock. Springs and seeps are common along the contact between the permeable sands and gravels of the Rocky Flats Alluvium and the underlying impermeable shales, especially where the alluvium projects like fingers over the bedrock. A predominant growth of brush and grass is found at this spring line. A number of recent landslides and many areas suggestive of old landslides are associated with the spring line. Most of the slides developed exclusively in the shales, but some included blocks of the overlying alluvium. The north slopes of the stream valleys seem to be more affected by sliding and are also steeper than the south slopes (URS/J. Blume, 1974). These landslides, primarily slumps, probably occurred in response to oversteepening of the slopes by the eroding streams. The slides are reported to include the residual and slopewash soils and portions of bedrock. Thin, poorly stratified alluvial soils, primarily silty, clayey, and gravelly sands, blanket the floor of the stream valleys (Wassenaar, 1987).

Few of these features were observed during our present study, mainly in the steep walls of a stream outside the plant's north perimeter road. However, because of extensive grading and filling related

to construction activities within the plant area and the installation of culverts, drainage channels, and storm drains, the recent incidence of these shallow landslides in natural slopes within the plant area has been negligible.

METHODOLOGY AND SCOPE OF GEOTECHNICAL DATA REVIEW

To evaluate the seismic stability of geotechnical structures at the Rocky Flats Plant site area, a review was performed of geotechnical information for sites within the plant area and in the near vicinity. Since 1951 and the inception of the Rocky Flats Plant, there have been numerous investigations and test holes to aid in the design and construction of site facilities. Although not every geotechnical report at the plant site was reviewed, a review of reports relevant to the assessed plant area provided adequate data on which to base our analyses and conclusions. Geotechnical reports for sites within and surrounding the maximum security area were examined and reports with boring information which were believed to have material property data representative of subsurface conditions were selected for incorporation into our evaluations.

Our review included 22 soil investigation reports for individual buildings, utilities, roads, parking lots, holding ponds, storage tanks, or other conventional surface facility structures; six geophysical data/seismic line reports; four seismic risk/hazard, seismic design criteria, and geologic investigation reports; and one ground water monitoring report. Various maps and aerial photographs were also reviewed. The documents reviewed are listed in the references. The soil investigation reports, themselves, contained logs of borings and test pits for as few as one or two subsurface locations to more than 60 locations. It should be noted that because the plant site area is relatively flat and located in competent material for relatively shallow lightly-loaded foundations, exploration generally was done using hollow-stem augers (continuous flight augers). Sampling generally was performed by the standard split-spoon or thin brass liner method. Penetration resistance measured when a 140-pound hammer is dropped a distance of 30 inches on a 2-inch diameter sampler is designated as a Standard Penetration Test (SPT). Undisturbed sampling was difficult to perform in the gravelly materials, where standard penetration tests generally indicated competent dense or hard materials. Consequently, testing of samples usually consisted of index property tests, such as gradation tests on the granular materials, and unit weight, plasticity tests (Atterberg limits), and occasional unconfined tests on more cohesive samples. A tabulation of data collected listing the boring number, reference, blow count elevation or depth, depth to ground water, the soil type according to the Unified Soil Classification System, fines content, and blow count was presented in the soil liquefaction assessment (Appendix G) report.

SUBSURFACE SITE CONDITIONS

A description of our review of the subsurface conditions at the Rocky Flats Plant area was presented in the soil liquefaction assessment (Appendix G).

Three units/formations were encountered in the borings drilled at the site: (1) compacted and random fill derived from bedrock and alluvial materials; (2) alluvium consisting primarily of clayey sands and gravels, and gravelly sandy clays; (3) bedrock of the Arapahoe formation consisting primarily of claystone with interbeds of siltstone and sandstone.

A description of the ground water conditions at the plant site was presented in the soil liquefaction assessment (Appendix G) report. Based on a review of the Ground Water Protection and Monitoring Program Plan (EG&G, 1991), the water table depth in the alluvium is variable, although it generally becomes shallower from west to east as the alluvial material thins. Seeps are common at the base of the Rocky Flats alluvium at the contact with claystones, in stream drainages. The report indicates that much of the ground water within the alluvium unit becomes surface water or evaporates where it discharges from seeps along slopes and in drainage valleys. A map showing the ground water table elevation contours within the Rocky Flats Plant site is shown on Figure H-1. This figure was used in assessing the ground water conditions at selected profiles used in the seismic stability evaluations.

SHEAR STRENGTH PROPERTIES

A number of profiles were identified at several locations throughout the plant site that represent the steepest slopes and largest topographic relief in the vicinity of the plant structures. These slopes are listed in Table H-1; their locations are presented on Figure H-2. Cross-sections through each of the profiles listed in Table H-1 are presented in Addendum H-1 to this report. No borings were available at the immediate locations of these slopes, however the general subsurface conditions underlying these sites were inferred on the basis of an assessment of geotechnical data available in their general vicinity and a review of aerial photographs of the plant site at various stages of construction.

Table H-1 shows that the subsurface soils underlying these slopes can be classified as (a) alluvium, (b) compacted fill or random fill, and (c) claystone of the Arapahoe Formation. For the purpose of the stability evaluations, the shear strength parameters for these materials were estimated based on our review of available geotechnical data.

The properties of the alluvium and the fill materials were based on evaluations of the Standard Penetration Tests (SPTs) performed during previous investigations. The properties of the claystone were estimated using unconfined compression test results reported by URS/J. Blume (1974), and Woodward-Clyde Consultants (1986), as well as review of published data on similar materials.

The alluvium was assumed to consist predominantly of clayey sands and gravels. Average SPT blowcounts estimated from our review of previous investigations were on the order of about 40 blows/ft. Using the correlation charts of Schmertman (1975), a friction angle, ϕ, for the sandy and gravelly alluvium was estimated at 45 degrees. Because one-third of the SPT samples recovered from the alluvial materials were representative of clayey (cohesive) soil, alternative strength parameters also were assumed for performing parametric analyses. The strength parameters for the clayey alluvium are: a cohesion, c, of 200 psf and a friction angle, ϕ, of 38 degrees.

Compacted and random fills at the site consist of stiff sandy/gravelly clays derived from the underlying claystone bedrock. An average blowcount estimated for the fill material is 14 blows/ft. Using correlations of Terzaghi and Peck (1967) a cohesion value, c, for the stiff cohesive fill is conservatively estimated at 1000 psf. The relatively low value of c selected for the fill material is intended to account for the possible existence of uncompacted random fill at certain locations.

The shear strength properties for the claystone bedrock were conservatively obtained using the results of unconfined compressive tests on samples that failed along an "old fracture surface." Values of unconfined compressive strength from tests performed by URS/J. Blume (1974) ranged from 2300 to 12,300 psf. Values reported by Woodward-Clyde (1986) on samples of the weathered claystone ranged from 4800 to 10,600 psf. Based on these test results, a value of cohesion, c, of 1000 psf and friction angle of 20 degrees were selected for use in the stability analyses.

The shear strength parameters for the various material types comprising the slopes, that were selected for use in the stability analyses, are summarized below:

Material Type	Unit Weight (pcf)	Cohesion - C (psf)	Friction Angle ϕ
Alluvium (sandy gravels)	120	0	45
Alluvium (gravelly, sandy clays)	120	200	38
Fill Material	120	1000	0
Claystone	130	1000	20

EVALUATION OF SEISMIC STABILITY

The seismic stability of the slopes was assessed for their potential to undergo permanent deformations due to earthquake shaking. The permanent deformations (i.e., cumulative downslope displacements) were estimated using the concept of yield seismic coefficient. This concept and the nature of these deformations are further explained below.

A simple procedure was developed by Newmark (1965) to estimate the amount of deformation that a slope might undergo as a result of strong earthquake ground shaking. The method has been modified and improved by various investigators (Ambraseys, 1973; Sarma, 1975; Franklin and Chang, 1977; Makdisi and Seed, 1978). The approach adopted here is that of Makdisi and Seed (1978). The method provides an estimate of permanent deformations in soils that neither liquefy nor undergo a significant loss of strength under cyclic loading (Seed, 1979).

The Makdisi and Seed method analyzes potential sliding masses as acted on by three forces: driving force from the weight of the soil, driving force from earthquake inertia, and resisting force from soil shear strength. For a given potential sliding mass, shear strength characteristics, and earthquake shaking conditions, these forces and the corresponding yield seismic coefficient can be calculated using slope stability analyses. The yield seismic coefficient is the acceleration that produces a large enough driving force from inertia to make the factor of safety of the slope equal to one.

When using this method, it is important to note that when the total driving force becomes equal to or greater than the total resisting force, this does not, by itself, necessarily imply slope "failure." Rather, because of the transient nature of the driving force from earthquake inertia, the likely consequence is a permanent displacement of the soil mass, with the magnitude of the displacement depending on the intensity and duration of earthquake shaking.

Three primary parameters affect the seismically induced displacement of a given sliding mass (Makdisi and Seed, 1978): (1) the yield seismic coefficient for the sliding mass; (2) the maximum acceleration induced by the earthquake; and (3) the duration of ground shaking, as reflected by the magnitude of the earthquake. If values of the above parameters are known for a given potential sliding mass, it is possible to estimate a range for the seismically induced displacement for that mass.

As mentioned previously, the yield seismic coefficient, k_y, is defined as the horizontal acceleration, applied to a potential sliding mass, that results in a factor of safety of 1.0. The yield seismic coefficient is estimated using slope stability analyses that employ limit equilibrium techniques.

The slopes, listed in Table H-1 and presented in Addendum H-1, range in height from 14 to 30 feet; most are between 20 and 30 feet. All of the slopes, with the exception of two, have inclinations of about 2.0H to 1.0V or flatter. The slope at location 4 had an inclination of 1.5H to 1.0V; however, a retaining crib wall supports half the height of the slope. At location 6; the lower two-thirds of the slope has an inclination of 1.6H to 1.0V; the upper third portion has an inclination of 3.5H to 1.0V.

For purposes of the stability analyses, two slope heights were considered: 20 and 30 feet. A uniform slope inclination of 2.0H to 1.0V was assumed. Soil profiles were chosen to represent the following subsurface conditions:

1. slopes located in cohesionless alluvial materials
2. slopes located in cohesive alluvial materials
3. slopes located in fill
4. slopes located in claystone formations.

Ground water conditions within these slopes were estimated from the contour elevations presented on Figure H-1 and are shown in the profile cross-sections in Addendum H-1. As can be seen from these figures, the ground water table in all cases is at or below the level of the toe of the slope. However, to account for possible fluctuations in ground water levels and for purposes of the seismic slope stability evaluations, two conditions of the ground water table were conservatively assumed within the slope: a water level at a depth of 10 feet below the crest of the slope, and another at 20 feet.

In all, stability analyses were performed on 16 different profiles.

Stability analyses were performed using the computer program PCSTABL 5M developed at Purdue University (Achilleos, 1988). The program uses two-dimensional limit equilibrium techniques and the method of slices. These methods include the simplified Bishop method, simplified Janbu method, and Spencer's method. Options are available for circular and non-circular slip surfaces. Factors of safety were computed using Bishop's simplified method for

circular slip surfaces. The program searches for the slip surface with the minimum factor of safety. Three hundred trial surfaces were generated for each slope profile that was analyzed. A horizontal seismic coefficient was applied in the analysis and the value that results in a factor of safety of one corresponds to the yield seismic coefficient.

The shear strength parameters used in the stability evaluations were presented on page H-3 (Subsurface Site Conditions). The results of the stability analyses for the sixteen different profiles evaluated, are presented in Table H-2 in terms of the yield horizontal seismic coefficient. The results are presented for four soil profiles, two slope heights, and two assumed depths of the ground water table. Computer printouts of the results of the stability computations are presented in Addendum H-2 to this report.

The values of yield seismic coefficient presented in Table H-2 were used in the procedure presented by Makdisi and Seed (1978) to estimate earthquake-induced permanent displacement. Charts used in this procedure are shown on Figure H-3 (presented in Seed, 1979). For a given potential sliding surface, the ratio of yield seismic coefficient to the maximum induced acceleration, k_y/k_m, is used in the chart to estimate permanent displacement.

For the purposes of this evaluation, three levels of peak ground acceleration: 0.2g, 0.4g, and 0.6g, were assumed to occur at the plant site due to a Magnitude 6.5 earthquake occurring on a nearby seismic source. The estimated permanent displacements for each slope profile for the postulated earthquake ground motions are summarized in Table H-3. The estimates were made using the mean curve of Makdisi and Seed (1978) shown on Figure H-3(b).

The results presented in Table H-3 show that permanent displacements for a 30-foot-high slope consisting of sandy and gravelly alluvium, where the water table is conservatively assumed to be 10 feet below the crest of the slope, range between 2 cm (for a peak ground acceleration of 0.2 g) and about 28 cm (for a peak acceleration level of 0.6 g). The corresponding displacements for a 20-foot-high slope range from 0 to 3 cm. Alternatively when using shear strength properties representative of the sandy/gravelly clay alluvium, estimated displacement for the 30-foot-high slope (with a water table at 10 feet depth) range between 0 and 10 cm. Relations showing permanent displacements as a function of peak ground acceleration are shown on Figures H-4 and H-5. When the water table is assumed at a depth of 20 feet below the crest of the slope, the estimated displacements are negligible

For 30-foot-high slopes comprised of fill, the estimated displacements range from 0 to 16 cm, the corresponding displacements for 20-foot-high slopes are 0 to 8 cm (Figure H-6).

Estimated displacements for slope profiles in the claystone formation were negligible. It should be noted that although estimated displacements for cut slopes made in the Arapahoe claystone were negligible, there may be cases where the slope stability in these formations may be dependent on the geometry and orientation of weak bedding planes. However, strength parameters used in the stability analyses were based on a conservative estimate of the shear strength of claystone measured on "old fracture surfaces."

SUMMARY AND CONCLUSIONS

An assessment was made of the seismic stability of natural and man-made slopes at the Rocky Flats Plant site. The assessment involved a review of previous geotechnical studies performed for plant facilities. A number of profiles located in areas that exhibit the largest topographic relief and steepest slopes were selected for this study. Based on a review of subsurface data, representative slope profiles were selected and evaluated for seismic stability.

Because shear strength properties for the subsurface materials were unknown, shear strength parameters used in the stability evaluations were conservatively estimated using published correlations with standard penetration test data. For slope profiles located within the claystone formations, shear strength parameters were conservatively estimated using results of laboratory unconfined compressive strength tests on samples containing "old failure planes." The shear strength of the fill material was conservatively selected to reflect the possible existence of random uncompacted fill at certain locations.

The seismic stability of the representative slope profiles was assessed based on their potential to undergo permanent displacements under several levels of ground shaking. Peak ground acceleration levels of 0.2g, 0.4g, and 0.6g were assumed to occur at the plant site during a magnitude M 6.5 earthquake originating on a nearby seismic source.

Estimated permanent displacements were strongly affected by the assumed depth of the water table. When assuming a ground water table at a depth of 20 feet below the crest of the slope, estimated displacements were generally negligible, except for the fill slopes where maximum displacement ranged between 8 and 16 cm (at a peak acceleration level of 0.6 g).

When the ground water table is assumed at a depth of 10 feet below the crest of the slope, estimated maximum displacements (at a peak acceleration of 0.6 g) for a 30-foot-high slope in alluvium material ranged between 10 and 28 cm. The displacements would be manifested in surface slumping and sloughing.

It should be noted that because detailed shear strength properties of the subsurface materials are lacking, we selected conservative estimates of shear strength parameters for use in the stability analyses.

REFERENCES

Achilleos, B. (1988). Users Guide for PCSTABL 5M, Purdue University, West Lafayette, Indiana, December.

Ambraseys, N.N. (1973). Dynamics and response of foundation materials in epicentral regions of strong earthquakes, *Proceedings of the 5th World Conference on Earthquake Engineering*, Rome.

Air Products and Chemicals, Inc. (1989). Specifications for civil and underground construction of 184M standard nitrogen plant at Rocky Flats (00-9-6732).

Aguirre Engineers, Inc. (1988). Subsurface investigation and engineering analysis report, Electrical system upgrade, Phases I and II, Rocky Flats Plant, Jefferson County, Colorado, prepared for Black and Veatch Engineers-Architects.

ATEC Associates (1987). Geotechnical engineering investigation, Rocky Flats - Building no. 772, Appendix 5.7, Soil investigation report, p. 5-6, Drawing 1, boring logs B-1 thru B-4.

ATEC Associates (1988). Geotechnical report for Building 116, Appendix 4.8.

ATEC Associates (1989). Geotechnical engineering investigation, nitrogen production facility, Rocky Flats Plant, Jefferson County, Colorado, drawing 1, boring logs B-1 thru B-3.

ATEC Associates (1992). Geotechnical engineering investigation, Rocky Flats Building 374 addition, Jefferson County, Colorado, boring logs B-1 thru B-3.

Blume, [URS/John A. Blume & Assoc.] (1972). Supplement no. 1 to Seismic and geological investigations and design criteria for Rocky Flats plutonium recovery and waste treatment facility.

Blume, [URS/John A. Blume & Assoc.] (1974). Seismic and geologic investigations and design criteria for Rocky Flats plutonium recovery and waste treatment facility, report prepared for CF Braun & Company.

Chen & Associates (1972). Soils and foundation investigation for Building 123, the proposed low radiation surveillance laboratory Rocky Flat Plant, Golden, Colorado, May 23.

Chen & Associates (1986). Soil and foundation investigation and pavement design, proposed buildings 569 and 570, Rocky Flats Plant, Golden, Colorado, report prepared for Rockwell International, figs. 1-3.

CTL/Thompson Inc. (1980). Soils investigation, proposed perimeter security zone (PSZ) stations 82+86.3 to 107+94.42 & 0+00 to 3+83.62, borrow area and parking lot no. 71, a portion of safeguards and site security upgrading, report prepared for Richard Weingardt Consultants.

Dames & Moore (1981). Final Report, Geological and seismologic investigations for Rocky Flats Plant for U.S. Dept. of Energy, v. 1, p. 3.0-6 - 3.0-10, fig. 3-2.

Ebasco (1990). Geologic characterization report, Appendix E, Seismic data reprocessing, prepared for US DOE-Rocky Flats Plant.

Ebasco (1990). Draft Report, Task 2, Addendum, Vertical Seismic Profile of Well 56-89BR at the Rocky Flats Plant, June.

Ebasco (1991). Task 3, Shallow, high-resolution seismic reflection profiling in operable unit 2 (903 pad, east trenches, and mound) at the Rocky Flats Plant, final report, prepared for EG&G Rocky Flats and U.S. DOE.

Ebasco (1992). Phase II geologic characterization data acquisition; surface geologic mapping of the Rocky Flats Plant and vicinity, Jefferson and Boulder counties, Colorado, March.

EG&G Rocky Flats, Inc. (1990). Draft Report, Task 2, Addendum, Vertical Seismic Profile of Well 56-89BR at the Rocky Flats Plant, June.

EG&G Rocky Flats, Inc. (1991). Final ground water protection and monitoring program plan, prepared for U.S. Department of Energy, Rocky Flats, Golden, CO, Nov. 27.

EMC Engineers (1987). Soil and foundation study for proposed protection clothing and decontamination center, Rocky Flats Facility, Jefferson County, Colorado, pp. 4-6, figs. 1 - 3, 5, and 6.

Engineering-Science, Inc. (1990). Specifications and drawings, Remedial action, 881 Hillside, 881 effluent storage tanks, plates 1 thru 4, 8 & 9.

Franklin, A.G. and F.K. Chang (1977). Earthquake resistance of earth and rockfill dams; permanent displacement of earth embankments by Newmark sliding block analysis: Miscellaneous Paper S-71-17, Report 5, U.S. Army Engineer Waterways Experiment Station, CE, Vickburg.

Ground water Protection and Monitoring Program Plan, Third Quarter; Well and Piezometer Locations, Individual Hazardous Substance Sites (map) (2 copies).

Hunt, C.B. (1974). *Natural regions of the United States and Canada*, San Francisco, W.H. Freeman and Company, 725 p.

Makdisi, F.I. and H.B. Seed (1978). Simplified procedure for estimating dam and embankment earthquake-induced deformations, *Journal of Geotechnical Engineering*, v. 104, no. GT7, Proceedings Paper 13,898, p. 849-867.

Merrick & Co. (1989). Title II Submittal - Phase I, Foundation and site work, Replace tanks T66, T67, and T68, figs. 1 - 4

Newmark, N.M. (1965). Effects of earthquakes on dams and embankments, *Geotechnique*, 15, n. 2, p. 139-160.

Osterkamp, W.R., M.M. Fenton, T.C. Gustavson, R.F. Hadley, V.T. Holliday, R.G. Morrison and T.J. Toy (1987). Great Plains, *in* W.L. Graf, ed., Geomorphic Systems of North America: Boulder, Colorado, Geological Society of America, Centennial Special Volume 2, p. 163-210.

Rocky Flats Plant Area Plot Plan.

R.V. Lord & Associates (1972). Subsurface soil investigation for the proposed Fuel Oil Storage Tank in the vicinity of Central Avenue and 7th Street, June 14.

R.V. Lord & Associates (1976). Subsurface soil and groundwater investigation for existing Building 928, December 1.

Sarma, S.K. (1975). Seismic stability of earth dams and embankments, *Geotechnique*, 25, n. 4, p. 743-761.

Schmertmann, J.H. (1975). The measurement of in situ shear strength, ASCE Geotechnical Engineering Division Specialty Conference on In Situ Measurement of Soil Properties, North Carolina State University, Raleigh.

Seed, H.B. (1979). Considerations in the earthquake-resistant design of earth and rockfill dams: 19th Rankine Lecture of the British Geotechnical Society, *Geotechnique*, v. xxix, n. 3, September.

TERA Advanced Services Corp. (1982). Seismic hazard analysis for the Bendix, Los Alamos, Mound, Pantex, Rocky Flats, Sandia-Albuquerque, Sandia-Livermore, and Pinella's sites, final report.

TERA (1976). Seismic Hazard Study, pages III-38, III-41, III-42, III-60 thru III-66.

TERA Corporation (1978). Seismic risk analysis for Rocky Flats, Colorado, report prepared for Lawrence Livermore Laboratory.

Terzaghi, K. and R.B. Peck (1967). *Soil mechanics in engineering practice*, John Wiley & Sons, New York, 729 p.

Wassenaar (1987). Soil and foundation study for proposed protection clothing and decontamination center, Rocky Flats Facility, Jefferson County, Colorado, pp. 4-6, figs. 1 - 3, 5, and 6.

Woodward-Clyde Consultants, Inc. (1986). Geotechnical services for seismic retrofit on Buildings 707, 779, and 776/777 at Rocky Flats Plant, Jefferson County, Colorado, pp. 2, 4, 5, figs. 1 & 2.

TABLE H-1

CHARACTERISTICS OF SLOPES INVESTIGATED
AT ROCKY FLATS PLANT SITE

Location	Height (feet)	Slope	Description of Subsurface Materials
1.* East of Building 374	30	2.0H:1.0V	Compacted fill
2. North of Buildings 517/518	30	2.0H:1.0V with berm at 1/3 height	Compacted fill
3. West of Building 790	24	1.9H:1.0V	Cut slope in claystone of Arapahoe Formation
4. Adjacent to west wall of Building 771	20	1.5H:1.0V with 10-ft crib retaining wall	Compacted/random fill
4a. West of Building 771	20	2.3H:1.0V	Natural slope or cut in alluvial deposits
5. East of Building 575	17	2.0H:1.0V	Compacted/random fill
6. North embankment of Sage Avenue south of Building 991	30	1.6H:1.0V (lower 2/3) 3.5H:1.0V (upper 1/3)	Compacted fill
7. North of Building 991	14	4.H:1.0V and 2.0H:1.0V	Compacted fill and alluvium
8. South of Building 881	30	2.7H:1.0V	Alluvium or claystone of Arapahoe Formation
9. Northwest of Building 995	14	2.5H:1.0V	Claystone of Arapahoe Formation
10. Road embankments southeast of Building 995	20 30	2.0H:1.0V (west) 3.0H:1.0V (east)	Compacted fill

* Number indicates location of slope on Figure H-2.

TABLE H-2

ESTIMATED YIELD SEISMIC COEFFICIENTS FOR SEVERAL SLOPE PROFILES

Profile	Height (feet)	Yield Seismic Coefficient, k_y (g)	
		Water Level at 20 Feet Below Ground Surface	Water Level at 10 Feet Below Ground Surface
Alluvium (c=0, ϕ=45°)	30	0.42	0.12
Alluvium (c=0, ϕ=45°)	20	0.49	0.33
Alluvium (c=200 psf, ϕ=38°)	30	0.47	0.23
Alluvium (c=200 psf, ϕ=38°)	20	0.52	0.40
Fill	30	0.17	0.17
Fill	20	0.24	0.24
Claystone	30	0.51	0.43
Claystone	20	0.55	0.51

Note: Slope inclination: 2.0H:1.0V

255

TABLE H-3

ESTIMATED EARTHQUAKE-INDUCED PERMANENT DISPLACEMENTS AT SEVERAL SLOPE PROFILES

Profile	Height (feet)	Permanent Displacements (cm)	
		Water Level at 20 Feet Below Ground Surface	Water Level at 10 Feet Below Ground Surface
Alluvium (c=0, ϕ=45°)	30	Negligible	2-28 cm (see Fig. 6-4)
Alluvium (c=0, ϕ=45°)	20	Negligible	0-3 cm (see Fig. 6-4)
Alluvium (c=200 psf, ϕ=38°)	30	Negligible	0-10 cm (see Fig. 6-5)
Alluvium (c=200 psf, ϕ=38°)	20	Negligible	0-2 cm (see Fig. 6-5)
Fill	30	0-16 cm (see Fig. 6-6)	0-16 cm (see Fig. 6-6)
Fill	20	0-6 cm (see Fig. 6-6)	0-8 cm (see Fig. 6-6)
Claystone	30	Negligible	Negligible
Claystone	20	Negligible	Negligible

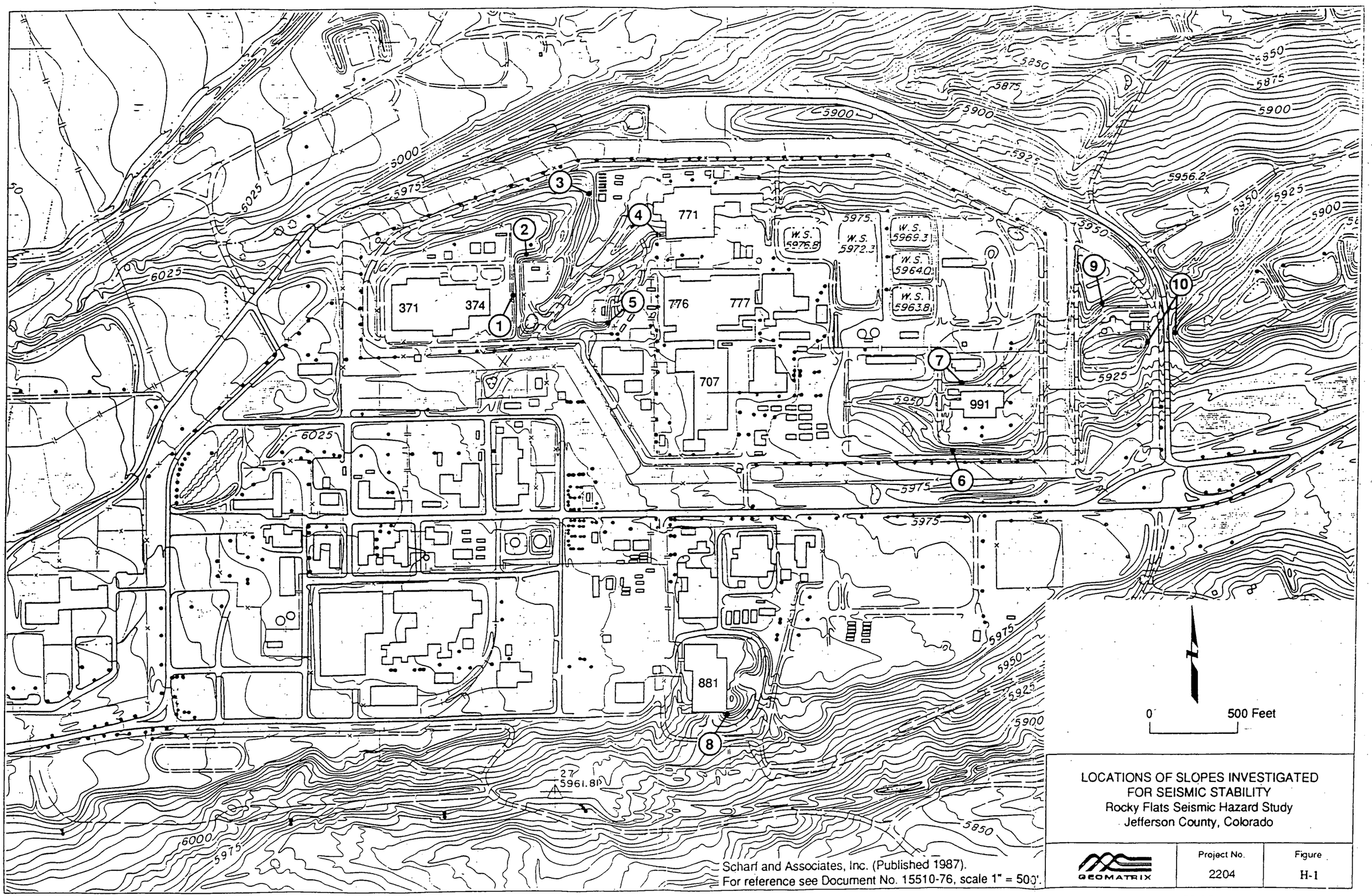

LOCATIONS OF SLOPES INVESTIGATED
FOR SEISMIC STABILITY
Rocky Flats Seismic Hazard Study
Jefferson County, Colorado

Scharf and Associates, Inc. (Published 1987).
For reference see Document No. 15510-76, scale 1" = 500'.

GEOMATRIX	Project No.	Figure
	2204	H-1

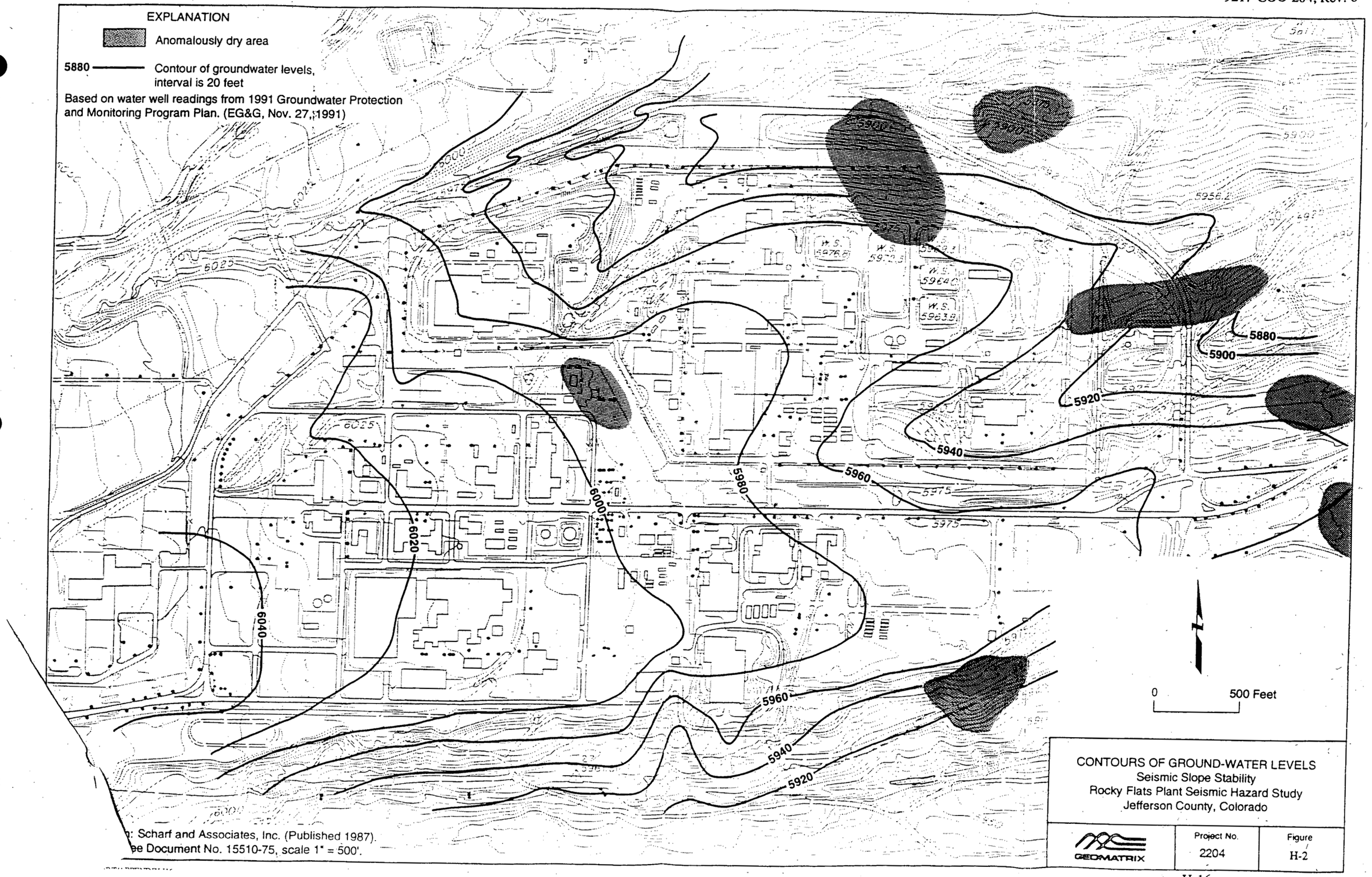
EXPLANATION
Anomalously dry area
5880 Contour of groundwater levels, interval is 20 feet
Based on water well readings from 1991 Groundwater Protection and Monitoring Program Plan. (EG&G, Nov. 27, 1991)
5880
5900
5920
5940
5960
5980
6000
6020
6040
5960
5940
5920
0
500 Feet
n: Scharf and Associates, Inc. (Published 1987).
ee Document No. 15510-75, scale 1" = 500'.
CONTOURS OF GROUND-WATER LEVELS
Seismic Slope Stability
Rocky Flats Plant Seismic Hazard Study
Jefferson County, Colorado
GEOMATRIX
Project No.
2204
Figure
H-2

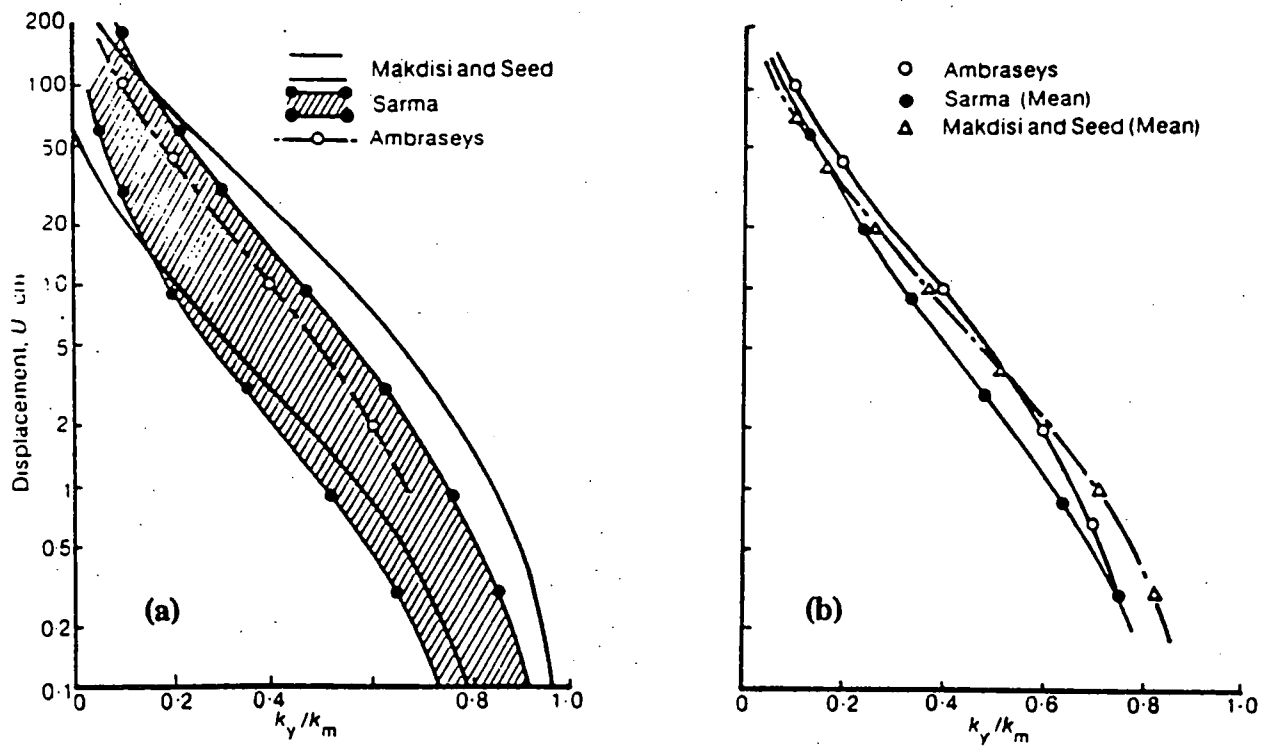

Figure H-3. Computed displacements of embankment dams subjected to magnitude 6 1/2 earthquakes for soils having little or no strength loss due to earthquake-induced shaking (from Seed, 1979).

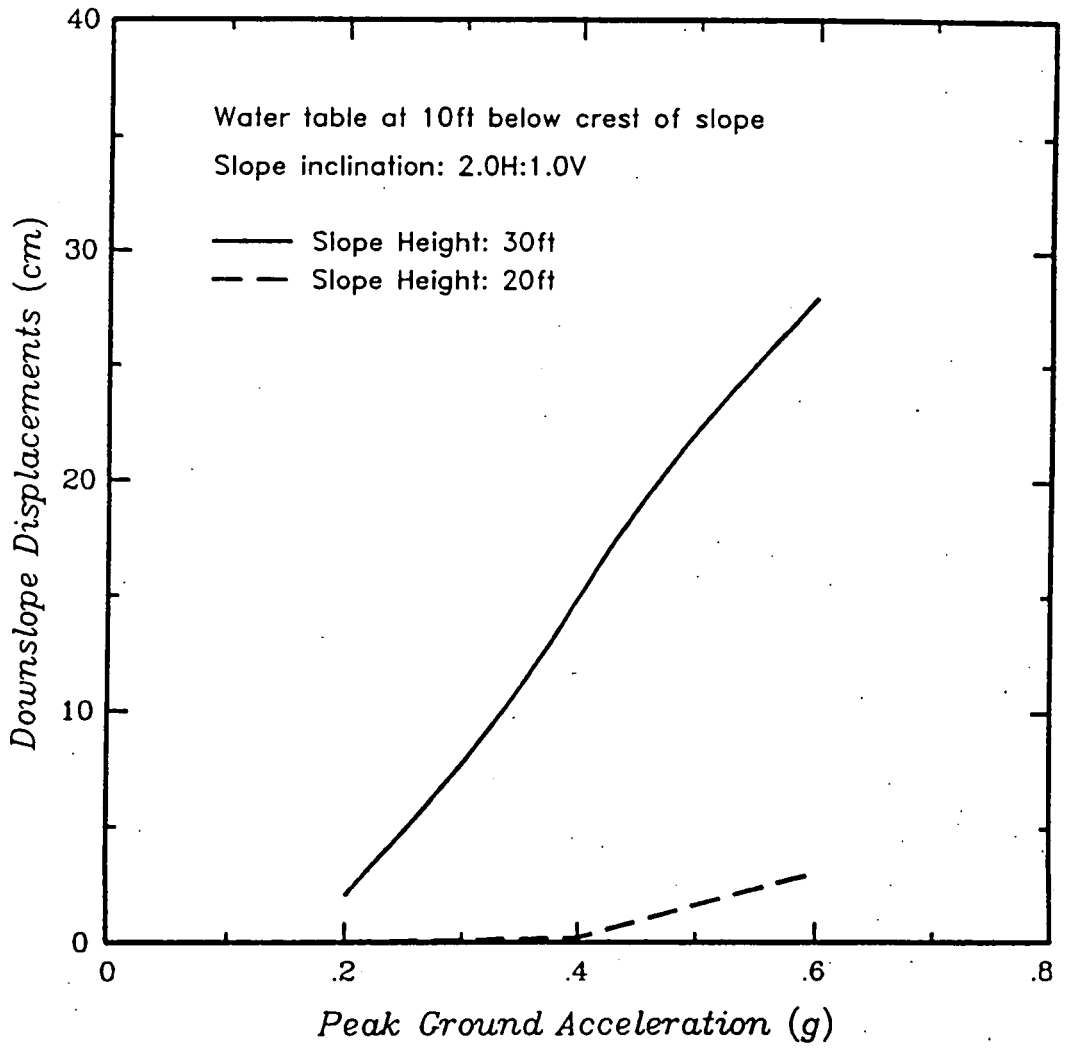

Figure H-4. Downslope displacements for slopes in cohesionless alluvium during magnitude 6 1/2 earthquake.

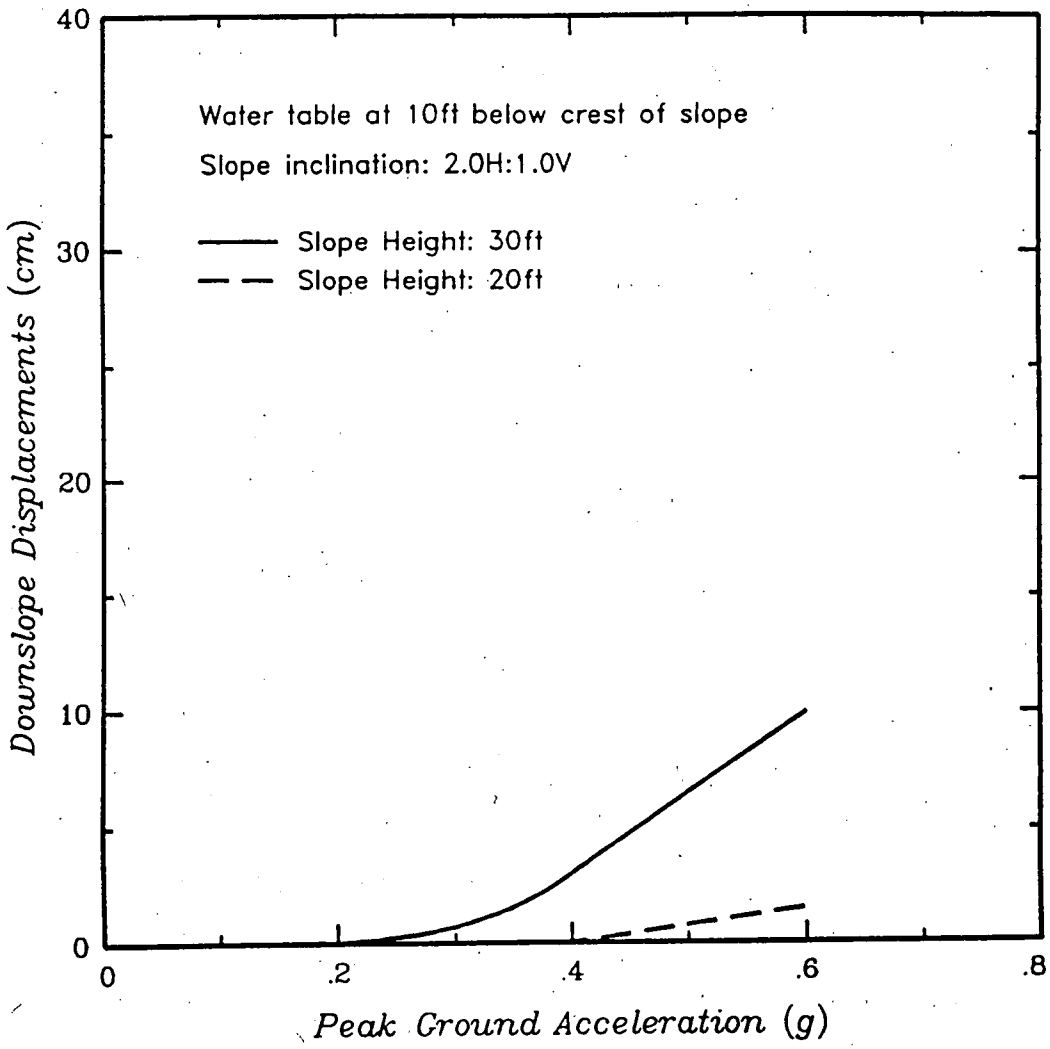

Figure H-5. Downslope displacements for slopes in cohesive alluvium during magnitude 6 1/2 earthquake.

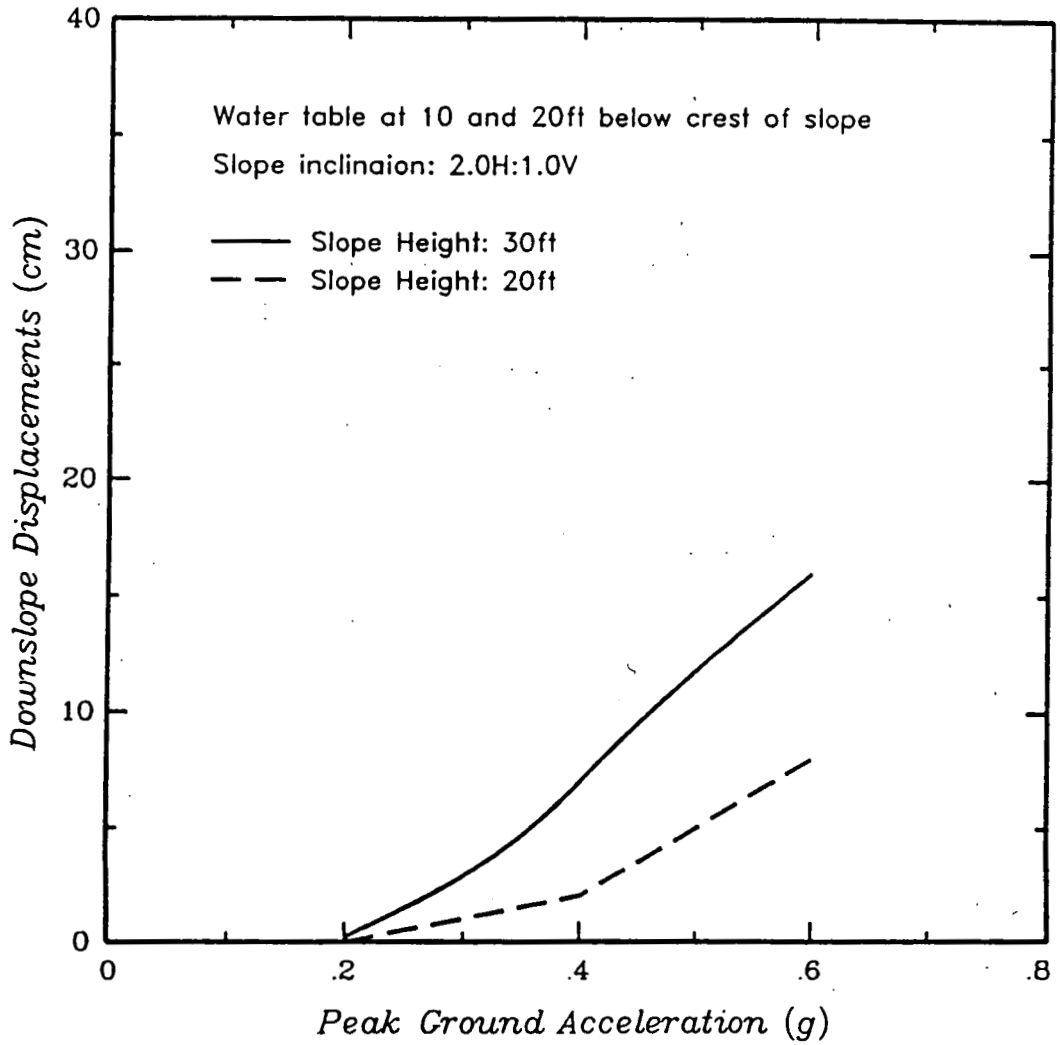

Figure H-6. Downslope displacements for slopes in fill during magnitude 6 1/2 earthquake.

ADDENDUM H-1

SOIL PROFILES SELECTED FOR EVALUATION OF SEISMIC STABILITY

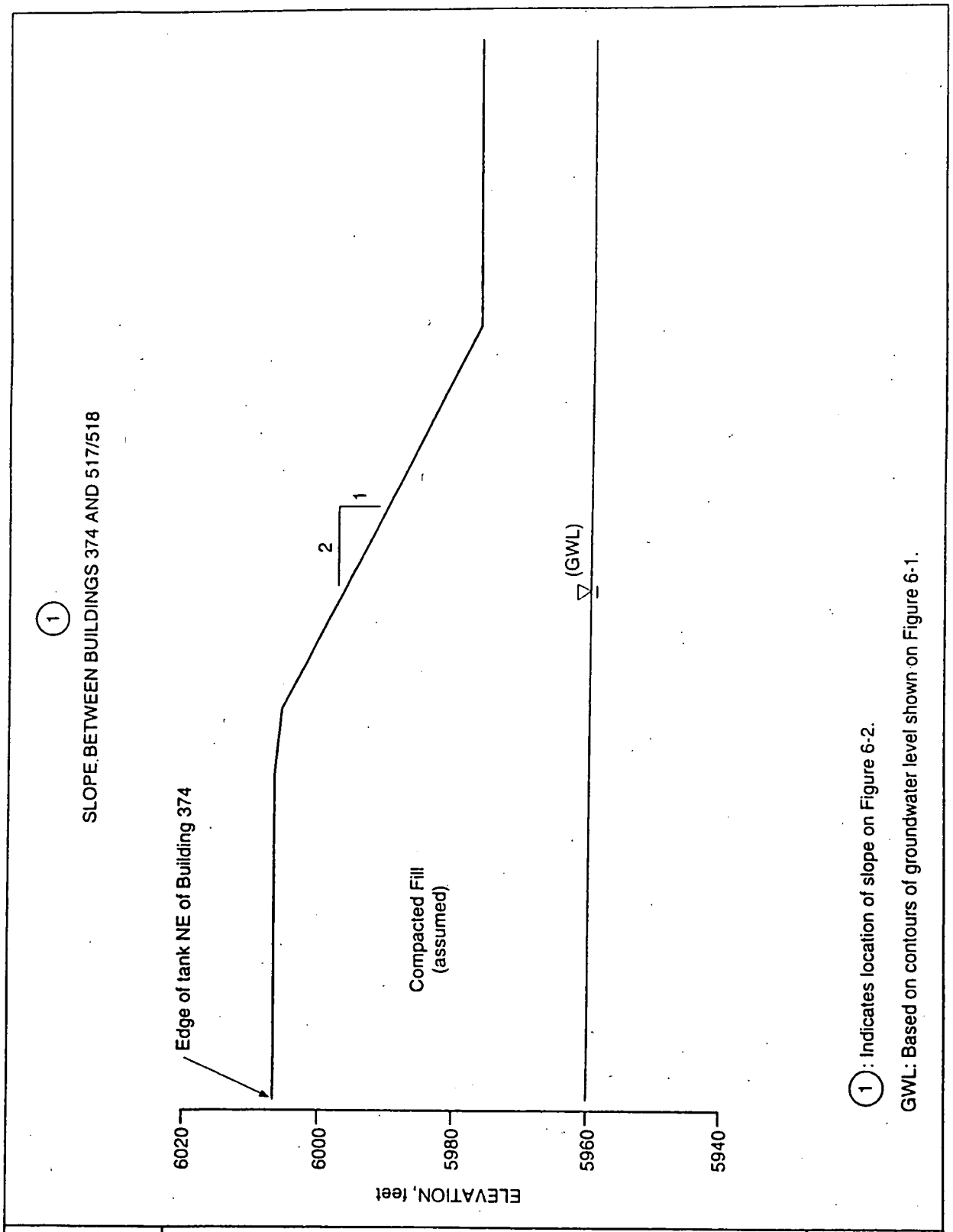

GEOMATRIX

CROSS-SECTION OF SLOPE AT LOCATION 1
Rocky Flats Seismic Hazard Study
Jefferson County, Colorado

Figure 6A-1

Project No. 2204

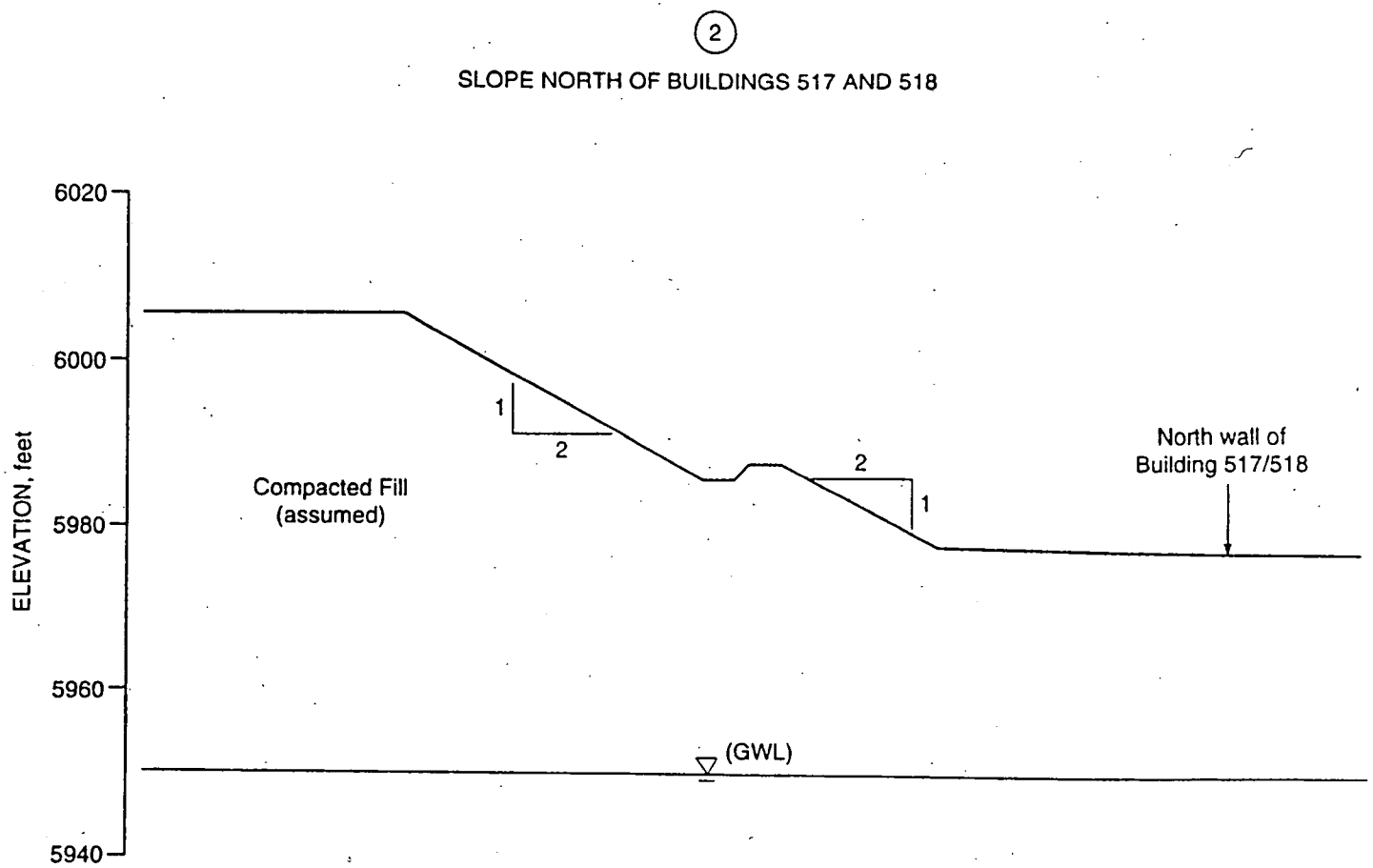

2 : Indicates location of slope on Figure 6-2.

GWL: Based on contours of groundwater level shown on Figure 6-1.

GEOMATRIX

CROSS-SECTION OF SLOPE AT LOCATION 2
Rocky Flats Seismic Hazard Study
Jefferson County, Colorado

Figure 6A-2

Project No. 2204

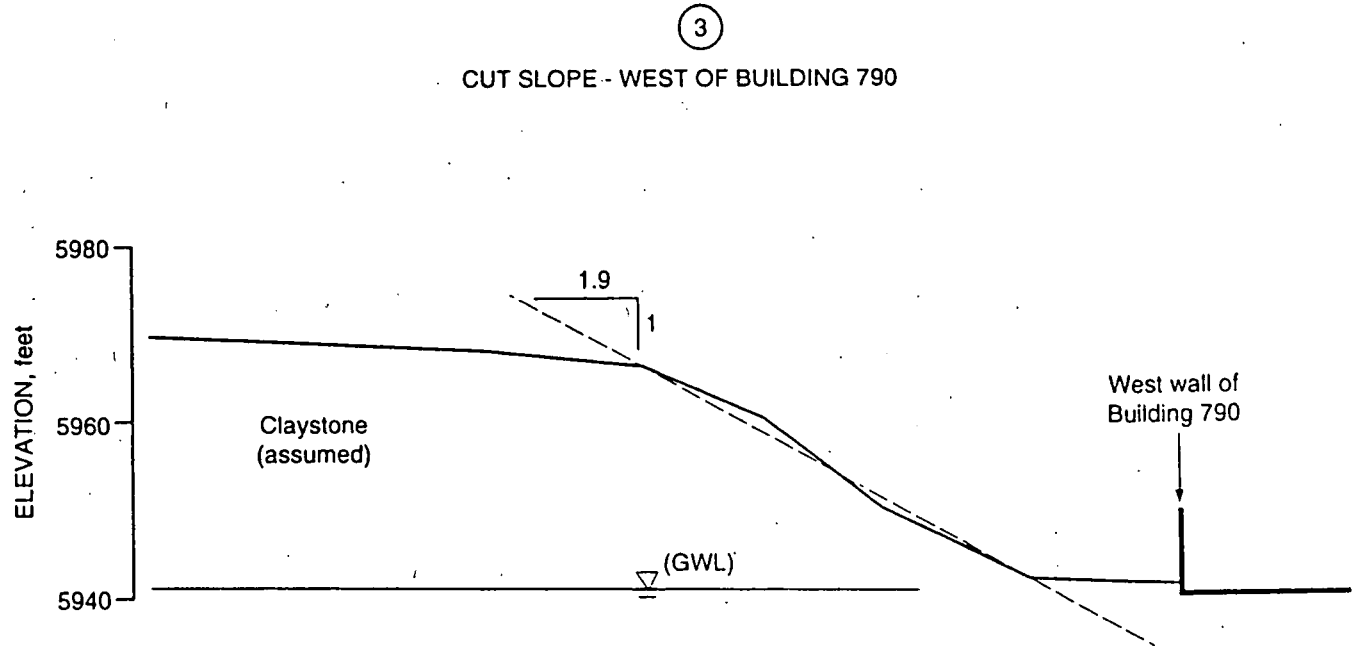

3 : Indicates location of slope on Figure 6-2.

GWL: Based on contours of groundwater level shown on Figure 6-1.

GEOMATRIX

CROSS-SECTION OF SLOPE AT LOCATION 3
Rocky Flats Seismic Hazard Study
Jefferson County, Colorado

Figure 6A-3

Project No. 2204

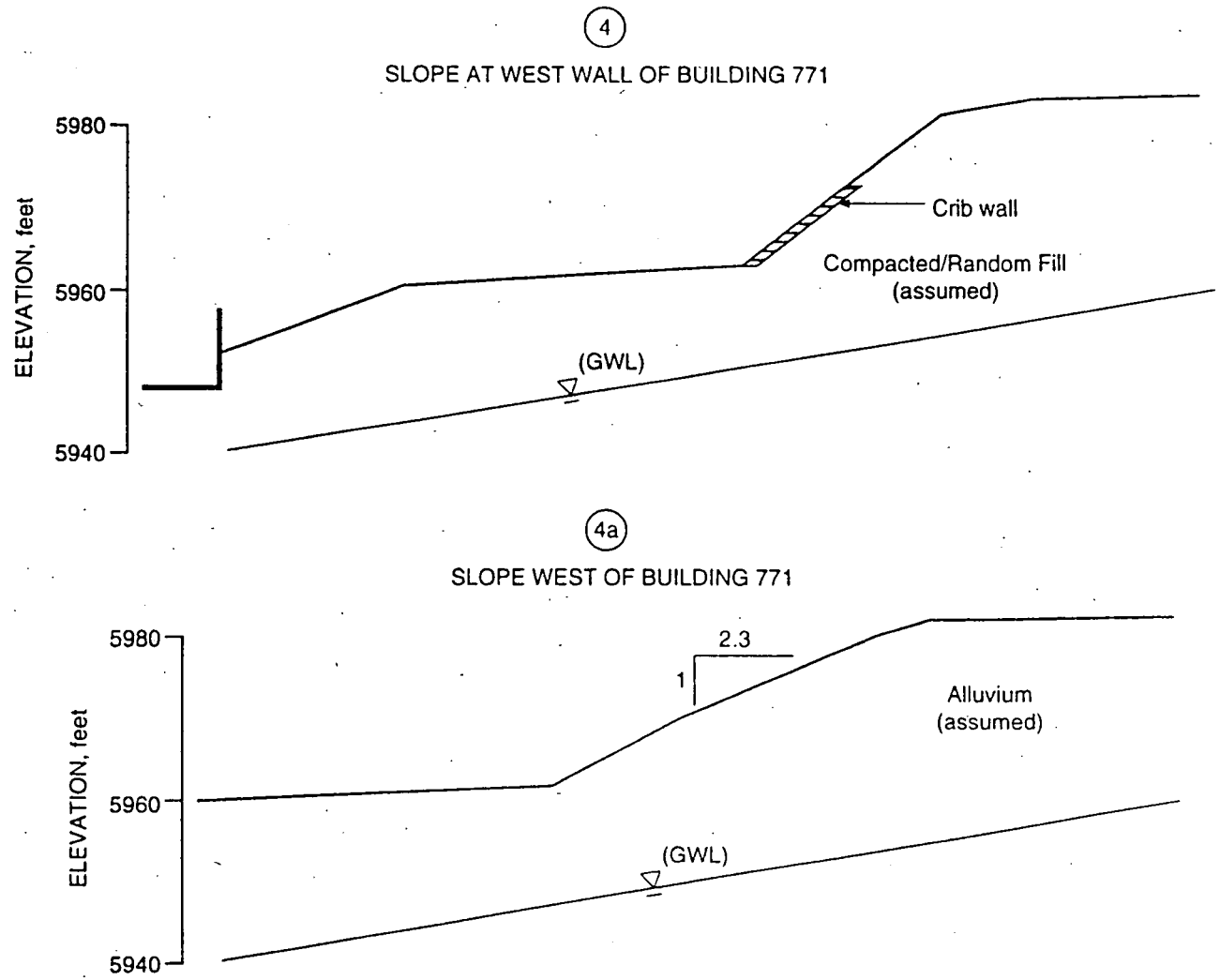

4 : Indicates location of slope on Figure 6-2.

GWL: Based on contours of groundwater level shown on Figure 6-1.

GEOMATRIX

CROSS-SECTION OF SLOPES AT LOCATION 4
Rocky Flats Seismic Hazard Study
Jefferson County, Colorado

Figure 6A-4

Project No. 2204

(5)

SLOPE EAST OF BUILDING 575

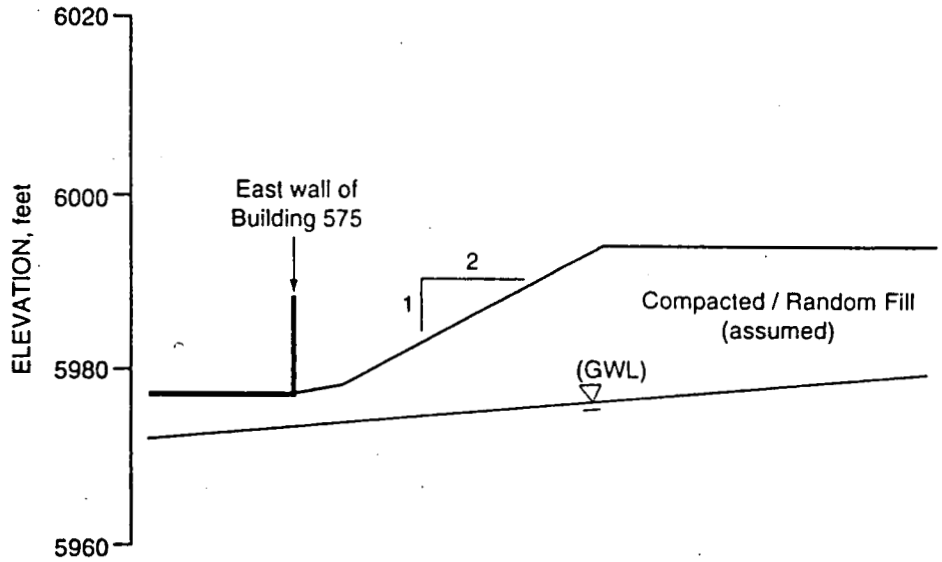

(5): Indicates location of slope on Figure 6-2.

GWL: Based on contours of groundwater level shown on Figure 6-1.

GEOMATRIX

CROSS-SECTION OF SLOPE AT LOCATION 5
Rocky Flats Seismic Hazard Study
Jefferson County, Colorado

Figure 6A-5

Project No. 2204

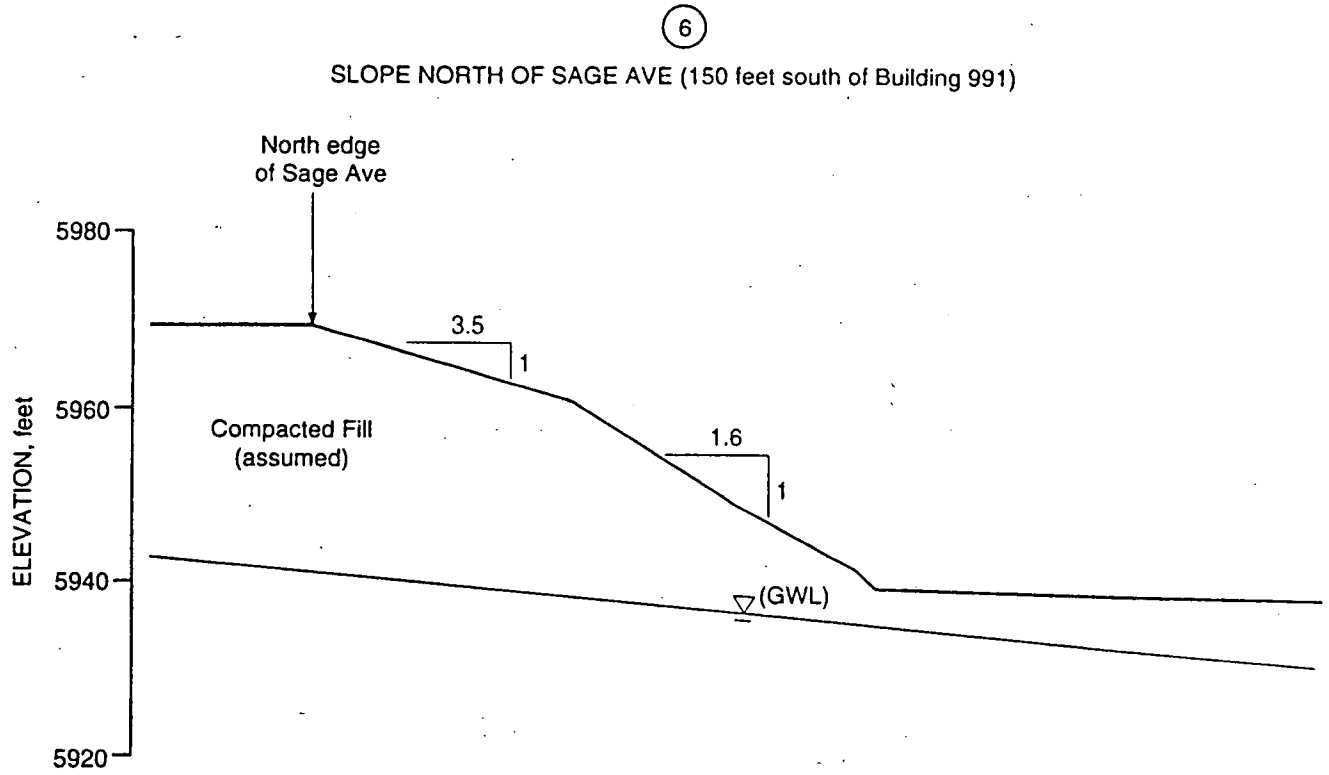

6 : Indicates location of slope on Figure 6-2.

GWL: Based on contours of groundwater level shown on Figure 6-1.

GEOMATRIX

CROSS-SECTION OF SLOPE AT LOCATION 6
Rocky Flats Seismic Hazard Study
Jefferson County, Colorado

Figure 6A-6

Project No. 2204

7

SLOPE NORTH OF BUILDING 991 (south of Building 980)

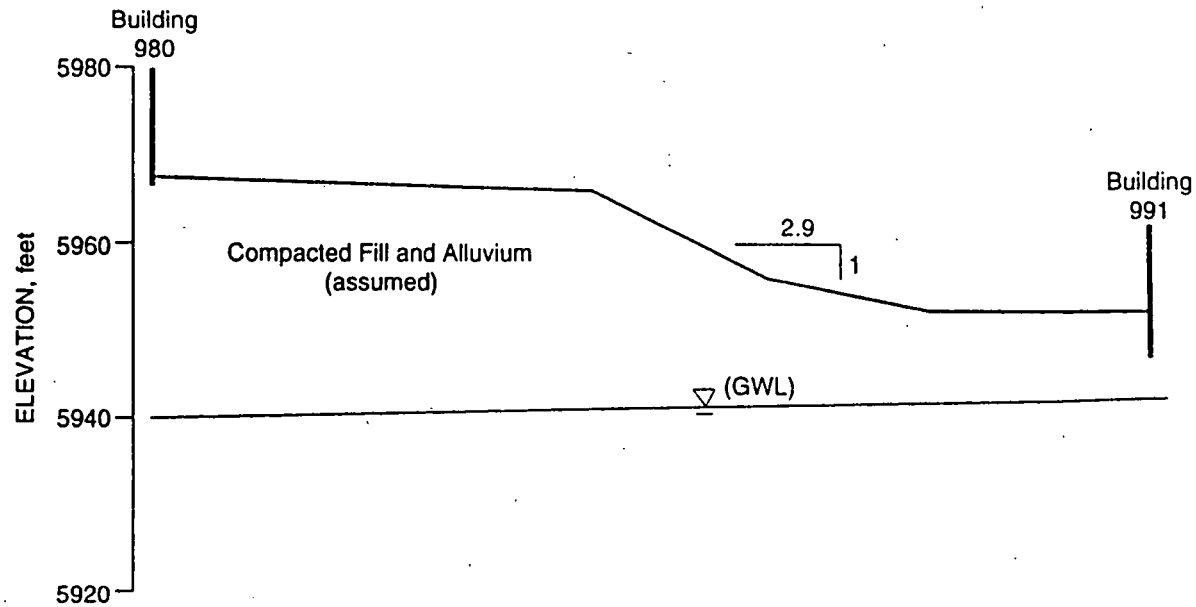

7: Indicates location of slope on Figure 6-2.

GWL: Based on contours of groundwater level shown on Figure 6-1.

GEOMATRIX

CROSS-SECTION OF SLOPE AT LOCATION 7
Rocky Flats Seismic Hazard Study
Jefferson County, Colorado

Figure 6A-7

Project No. 2204

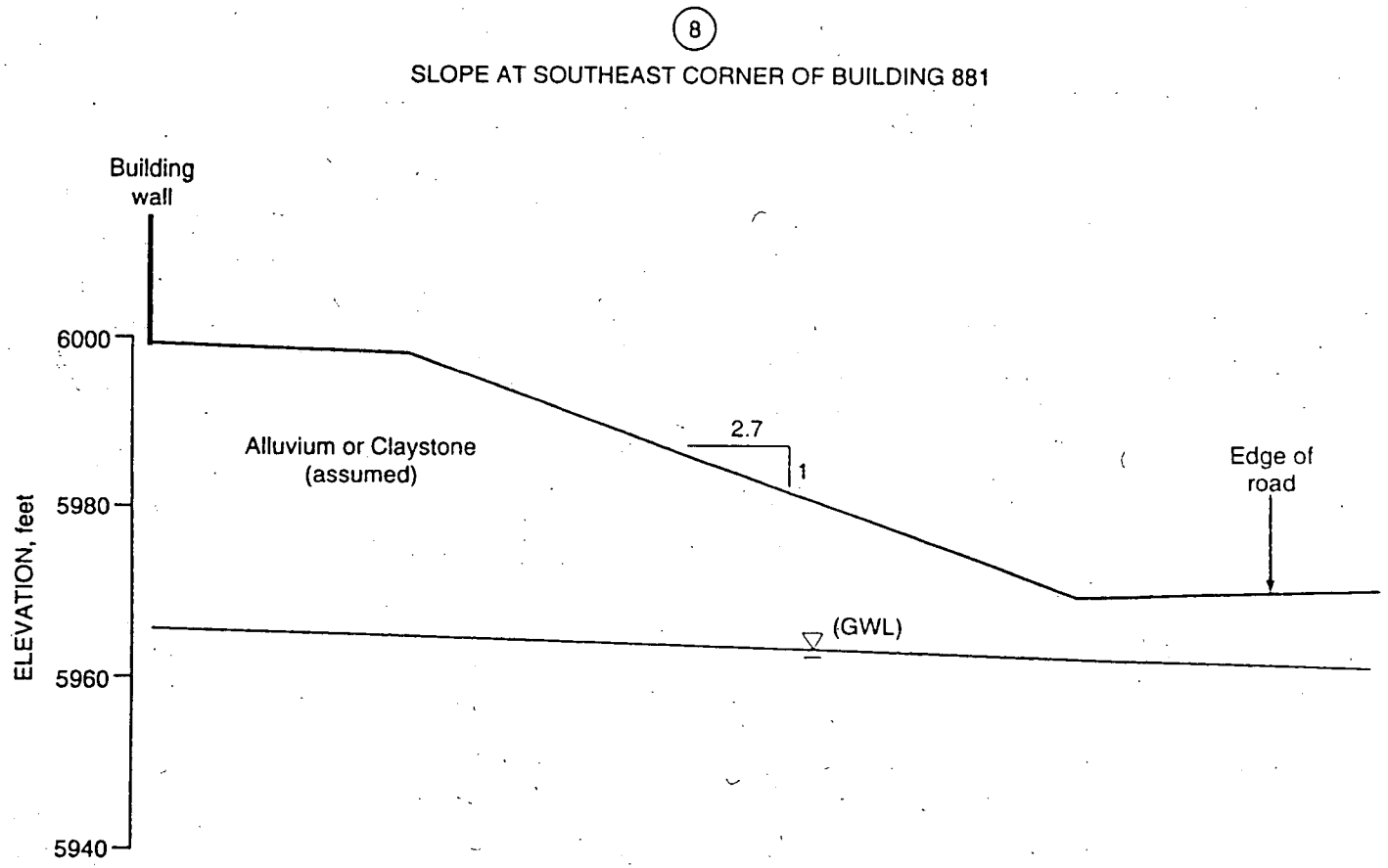

8: Indicates location of slope on Figure 6-2.

GWL: Based on contours of groundwater level shown on Figure 6-1.

GEOMATRIX

CROSS-SECTION OF SLOPE AT LOCATION 8
Rocky Flats Seismic Hazard Study
Jefferson County, Colorado

Figure 6A-8

Project No. 2204

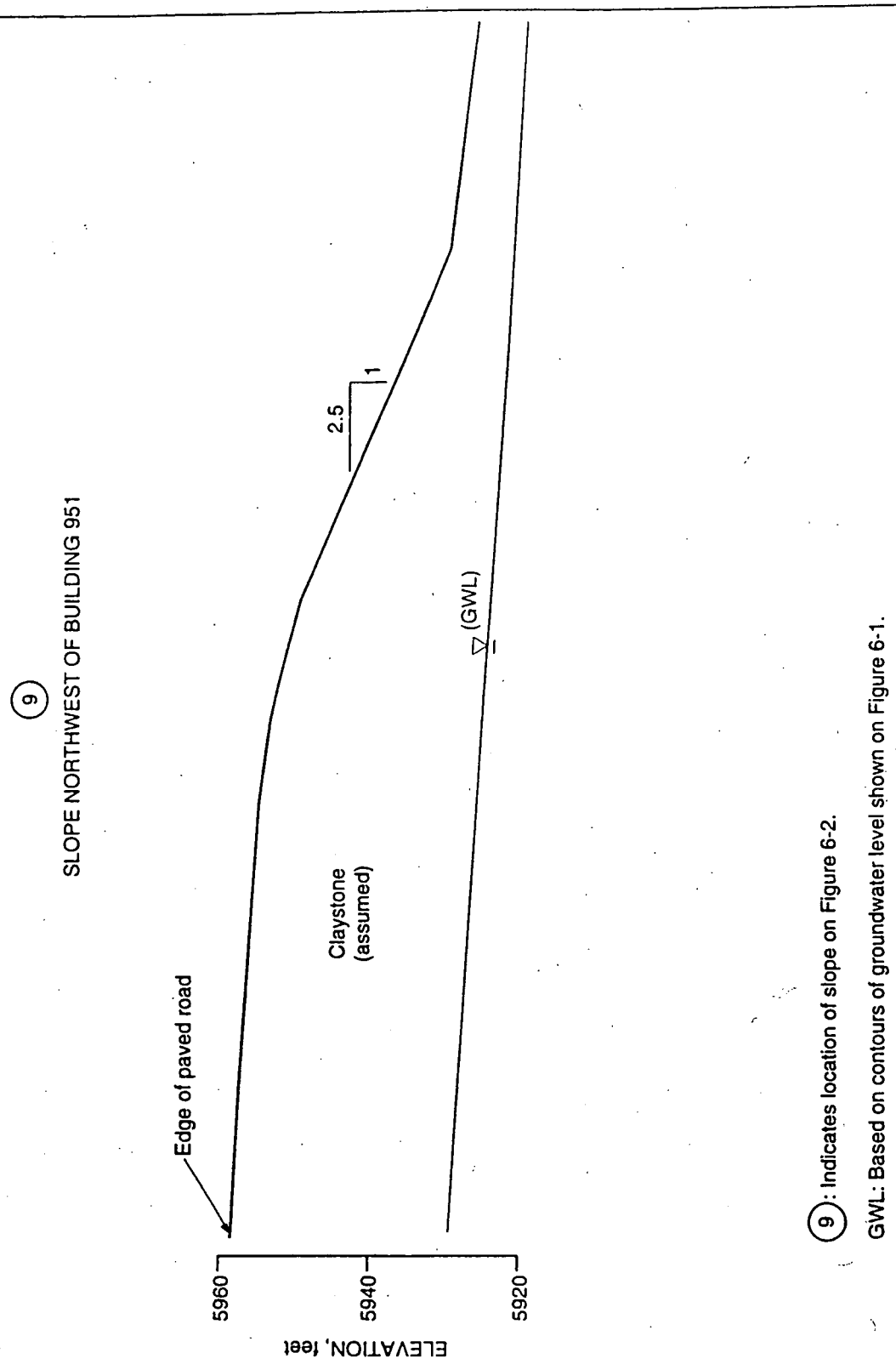

9 : Indicates location of slope on Figure 6-2.

GWL: Based on contours of groundwater level shown on Figure 6-1.

GEOMATRIX

CROSS-SECTION OF SLOPE AT LOCATION 9
Rocky Flats Seismic Hazard Study
Jefferson County, Colorado

Figure 6A-9

Project No. 2204

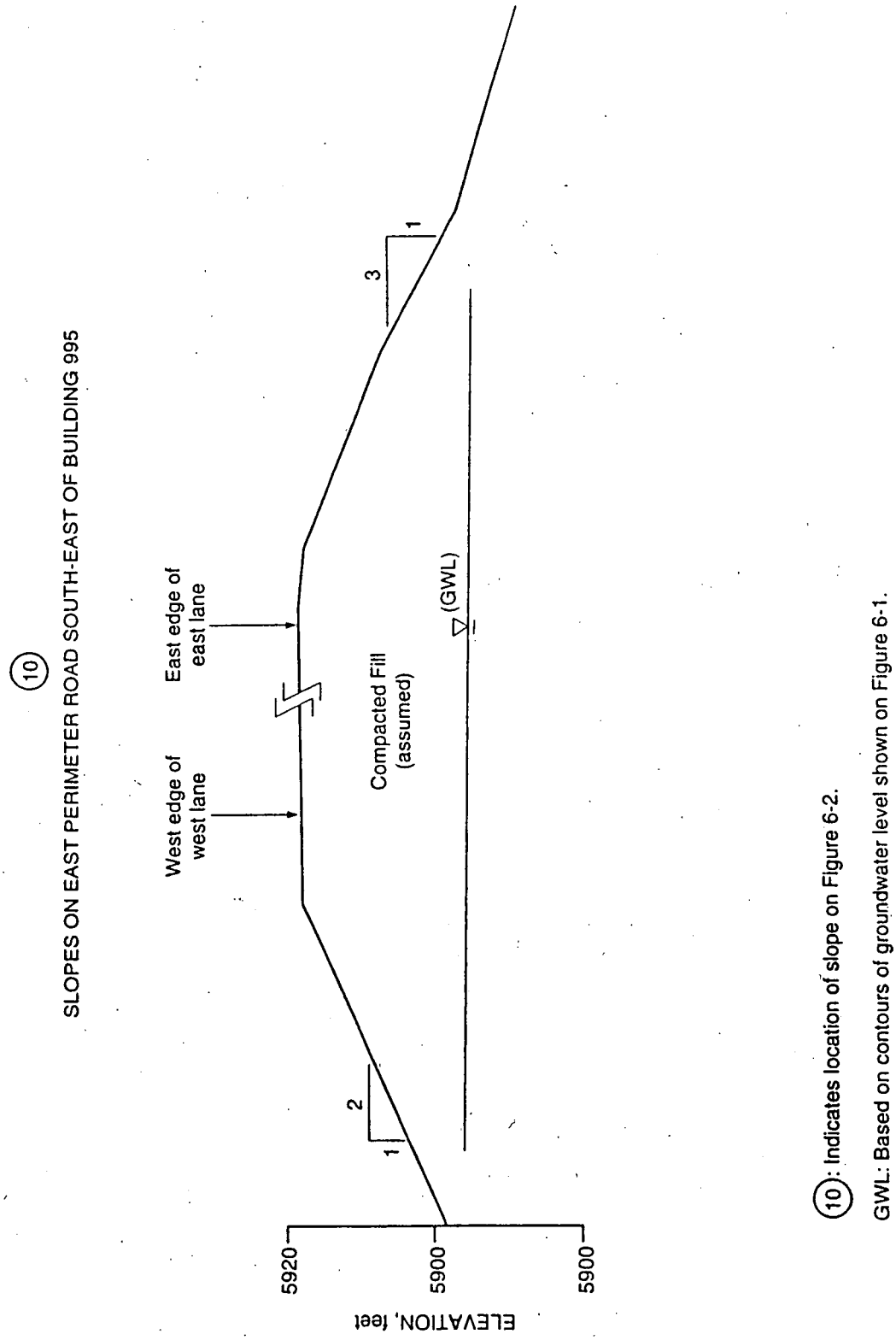

10: Indicates location of slope on Figure 6-2.

GWL: Based on contours of groundwater level shown on Figure 6-1.

GEOMATRIX

CROSS-SECTION OF SLOPE AT LOCATION 10
Rocky Flats Seismic Hazard Study
Jefferson County, Colorado

Figure 6A-10

Project No. 2204

ADDENDUM H-2

COMPUTER PRINTOUTS OF SLOPE STABILITY ANALYSES

** PCSTABL5M **

by
Purdue University

--Slope Stability Analysis--
Simplified Janbu, Simplified Bishop
or Spencer's Method of Slices

Run Date: 10/06/93
Time of Run: 4:40
Run By: ZLW
Input Data Filename: 1230alh.in1
Output Filename: 1230alh.out

PROBLEM DESCRIPTION PCSTABL5M : 30 ft, 1:2 slope, Aluvium 1, H. WT

BOUNDARY COORDINATES

3 Top Boundaries
3 Total Boundaries

Boundary No.	X-Left (ft)	Y-Left (ft)	X-Right (ft)	Y-Right (ft)	Soil Type Below Bnd
1	.00	100.00	60.00	100.00	1
2	60.00	100.00	120.00	130.00	1
3	120.00	130.00	180.00	130.00	1

ISOTROPIC SOIL PARAMETERS

1 Type(s) of Soil

Soil Type No.	Total Unit Wt. (pcf)	Saturated Unit Wt. (pcf)	Cohesion Intercept (psf)	Friction Angle (deg)	Pore Pressure Param.	Pressure Constant (psf)	Piez. Surface No.
1	120.0	120.0	.0	45.0	.00	.0	1

1 PIEZOMETRIC SURFACE(S) HAVE BEEN SPECIFIED

Unit Weight of Water = 62.40

Piezometric Surface No. 1 Specified by 4 Coordinate Points

Point No.	X-Water (ft)	Y-Water (ft)
1	.00	100.00
2	60.00	100.00
3	100.00	120.00
4	180.00	120.00

A Horizontal Earthquake Loading Coefficient
Of .115 Has Been Assigned

A Vertical Earthquake Loading Coefficient
Of .000 Has Been Assigned

Cavitation Pressure = .0 psf

A Critical Failure Surface Searching Method, Using A Random Technique For Generating Circular Surfaces, Has Been Specified.

300 Trial Surfaces Have Been Generated.

30 Surfaces Initiate From Each Of 10 Points Equally Spaced
Along The Ground Surface Between X = .00 ft.
and X = 59.00 ft.

Each Surface Terminates Between X = 121.00 ft.
and X = 180.00 ft.

Unless Further Limitations Were Imposed, The Minimum Elevation
At Which A Surface Extends Is Y = .00 ft.

10.00 ft. Line Segments Define Each Trial Failure Surface.

Following Are Displayed The Ten Most Critical Of The Trial Failure Surfaces Examined. They Are Ordered - Most Critical First.

** Safety Factors Are Calculated By The Modified Bishop Method **

Failure Surface Specified By 11 Coordinate Points

Point No.	X-Surf (ft)	Y-Surf (ft)
1	45.89	100.00
2	52.66	99.87
3	62.69	97.32
4	72.63	94.02
5	82.41	100.17
6	94.80	103.61
7	103.62	108.32
8	111.71	114.20
9	118.90	121.15
10	122.09	129.02
11	125.63	130.00

Circle Center At X = 65.4 ; Y = 169.4 and Radius, 72.1

*** 1.002 ***

Individual data on the 14 slices

Width Ft(m)	Weight Lbs(kg)	Water Force Top Lbs(kg)	Water Force Bot Lbs(kg)	Tie Force Norm Lbs(kg)	Tie Force Tan Lbs(kg)	Earthquake Force Hor Lbs(kg)	Earthquake Force Ver Lbs(kg)	Surcharge Load Lbs(kg)
9.8	1190.8	.0	632.2	.0	.0	136.9	.0	.0
2.3	1123.0	.0	585.2	.0	.0	129.1	.0	.0
5.7	2652.8	.0	1245.1	.0	.0	305.3	.0	.0
10.0	9135.3	.0	4287.0	.0	.0	1050.6	.0	.0
9.8	13076.6	.0	6260.7	.0	.0	1503.8	.0	.0
9.4	12831.3	.0	7392.7	.0	.0	1705.6	.0	.0
5.2	8554.1	.0	4537.7	.0	.0	983.7	.0	.0
3.6	5887.9	.0	3238.7	.0	.0	677.1	.0	.0
8.1	12186.2	.0	5552.5	.0	.0	1402.9	.0	.0
6.0	7389.8	.0	1510.6	.0	.0	849.8	.0	.0
1.2	1223.0	.0	.0	.0	.0	140.6	.0	.0
1.1	1038.9	.0	.0	.0	.0	119.6	.0	.0
5.1	2558.6	.0	.0	.0	.0	294.3	.0	.0
.6	33.2	.0	.0	.0	.0	3.8	.0	.0

Failure Surface Specified By 11 Coordinate Points

Point No.	X-Surf (ft)	Y-Surf (ft)
1	45.89	100.00
2	52.42	99.32
3	62.44	97.05
4	72.71	94.81
5	85.19	100.20
6	94.03	104.20
7	103.88	108.66
8	112.20	114.20
9	119.77	120.74
10	124.46	128.17
11	127.73	130.00

Circle Center At X = 63.9 ; Y = 177.7 and Radius, 79.8

*** 1.007 ***

Failure Surface Specified By 11 Coordinate Points

Point No.	X-Surf (ft)	Y-Surf (ft)
1	45.89	100.00
2	55.71	98.14
3	65.70	97.57
4	75.67	98.31
5	85.26	100.33
6	87.99	101.23
7	103.85	108.10
8	116.13	113.70
9	119.61	120.34
10	124.17	127.89
11	127.57	130.00

Circle Center At X = 65.1 ; Y = 174.3 and Radius, 76.8

*** 1.017 ***

Failure Surface Specified By 12 Coordinate Points

Point No.	X-Surf (ft)	Y-Surf (ft)
1	39.33	100.00
2	49.11	99.89
3	59.05	99.84
4	69.05	99.87
5	78.99	99.98
6	88.75	100.19
7	98.53	103.38
8	107.89	107.60
9	115.82	112.78
10	123.79	118.85
11	131.03	125.74
12	134.84	130.00

Circle Center At X = 63.8 ; Y = 188.8 and Radius, 92.1

*** 1.127 ***

Failure Surface Specified By 12 Coordinate Points

Point No.	X-Surf (ft)	Y-Surf (ft)
1	32.78	100.00
2	45.17	98.57
3	55.05	97.50
4	61.63	96.81
5	71.60	95.57
6	81.68	94.54
7	81.68	96.69
8	81.68	100.13
9	99.85	104.88
10	107.80	110.82
11	115.03	117.84
12	121.10	125.78
	123.47	130.00

Circle Center At X = 61.7 ; Y = 164.5 and Radius, 70.7

*** 1.128 ***

Failure Surface Specified By 13 Coordinate Points

Point No.	X-Surf (ft)	Y-Surf (ft)
1	19.67	100.00
2	29.48	98.10
3	39.43	97.01
4	46.42	96.76
5	56.41	97.32
6	66.31	98.74
7	79.06	100.96
8	88.58	103.99
9	97.84	107.79
10	106.74	112.35
11	115.23	117.63
12	123.55	123.60
13	130.51	130.00

Circle Center At X = 47.5 ; Y = 217.1 and Radius, 120.4

*** 1.140 ***

Failure Surface Specified By 13 Coordinate Points

Point No.	X-Surf (ft)	Y-Surf (ft)
1	26.22	100.00
2	36.13	98.65
3	46.11	98.07
4	56.11	98.23
5	66.07	99.16
6	75.93	100.87
7	85.63	103.27
8	95.12	106.42
9	104.37	110.38
10	113.25	114.83
11	121.78	120.07
12	129.89	125.89
13	134.77	130.00

Circle Center At X = 48.9 ; Y = 229.8 and Radius, 131.7

*** 1.143 ***

Failure Surface Specified By 12 Coordinate Points

Point No.	X-Surf (ft)	Y-Surf (ft)
1	45.89	100.00
2	55.57	97.48
3	65.26	96.24
4	75.26	96.28
5	85.40	97.61
6	95.08	100.21
7	104.30	104.03
8	113.87	109.01
9	120.65	115.06
10	128.07	122.10
11	132.93	129.98
12	134.20	130.00

Circle Center At X = 70.2 ; Y = 173.5 and Radius, 77.4

*** 1.145 ***

Failure Surface Specified By 11 Coordinate Points

Point No.	X-Surf (ft)	Y-Surf (ft)
1	45.89	100.00
2	55.22	99.40
3	65.01	97.37
4	75.00	93.86
5	82.83	89.19
6	87.55	84.03
7	103.55	102.38
8	111.68	108.15
9	118.80	115.18
10	124.68	123.27
11	128.05	130.00

Circle Center At X = 72.5 ; Y = 155.0 and Radius, 61.1

*** 1.170 ***

Failure Surface Specified By 13 Coordinate Points

Point No.	X-Surf (ft)	Y-Surf (ft)
1	32.78	100.00
2	42.33	99.03
3	52.15	97.18
4	62.13	94.46
5	72.46	90.90
6	81.66	86.58
7	91.82	80.60
8	100.87	102.88
9	109.62	107.83
10	117.76	113.67
11	125.18	120.32
12	131.78	127.88
13	133.26	130.00

Circle Center At X = 63.3 ; Y = 181.3 and Radius, 86.9

*** 1.171 ***

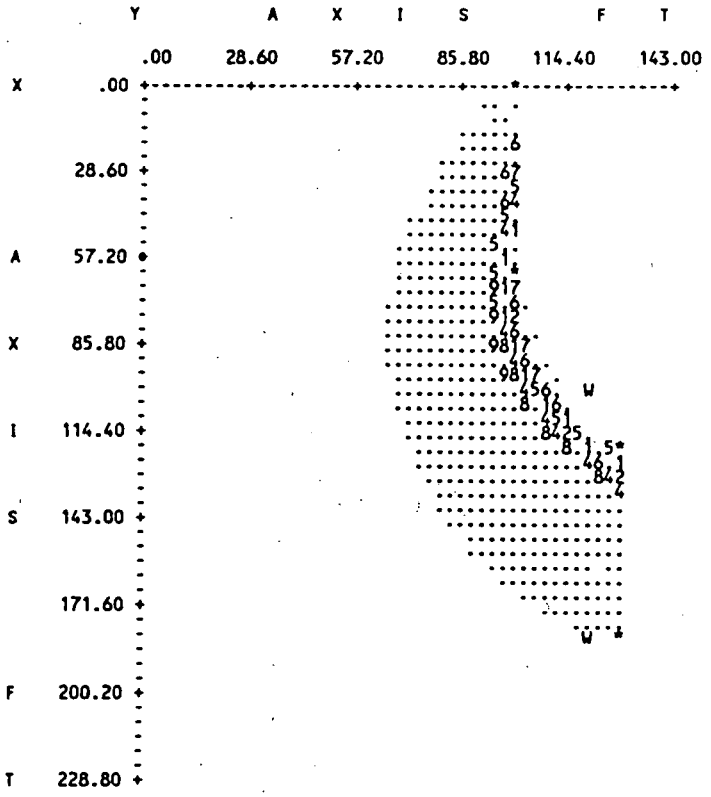

** PCSTABL5M **
by
Purdue University

--Slope Stability Analysis--
Simplified Janbu, Simplified Bishop
or Spencer's Method of Slices

Run Date: 10/06/93
Time of Run: 4:40
Run By: ZLW
Input Data Filename: 1230a2h.in1
Output Filename: 1230a2h.out

PROBLEM DESCRIPTION PCSTABL5M : 30 ft, 1:2 slope, Aluvium 2, H.WT

BOUNDARY COORDINATES

3 Top Boundaries
3 Total Boundaries

Boundary No.	X-Left (ft)	Y-Left (ft)	X-Right (ft)	Y-Right (ft)	Soil Type Below Bnd
1	.00	100.00	60.00	100.00	1
2	60.00	100.00	120.00	130.00	1
3	120.00	130.00	180.00	130.00	1

ISOTROPIC SOIL PARAMETERS

1 Type(s) of Soil

Soil Type No.	Total Unit Wt. (pcf)	Saturated Unit Wt. (pcf)	Cohesion Intercept (psf)	Friction Angle (deg)	Pore Pressure Param.	Pressure Constant (psf)	Piez. Surface No.
1	120.0	120.0	200.0	38.0	.00	.0	1

1 PIEZOMETRIC SURFACE(S) HAVE BEEN SPECIFIED

Unit Weight of Water = 62.40

Piezometric Surface No. 1 Specified by 4 Coordinate Points

Point No.	X-Water (ft)	Y-Water (ft)
1	.00	100.00
2	60.00	100.00
3	100.00	120.00
4	180.00	120.00

A Horizontal Earthquake Loading Coefficient
Of .230 Has Been Assigned

A Vertical Earthquake Loading Coefficient
Of .000 Has Been Assigned

Cavitation Pressure = .0 psf

A Critical Failure Surface Searching Method, Using A Random
Technique for Generating Circular Surfaces, Has Been Specified.

300 Trial Surfaces Have Been Generated.

30 Surfaces Initiate From Each Of 10 Points Equally Spaced
Along The Ground Surface Between X = .00 ft.
and X = 59.00 ft.

Each Surface Terminates Between X = 121.00 ft.
and X = 180.00 ft.

Unless Further Limitations Were Imposed, The Minimum Elevation
At Which A Surface Extends Is Y = .00 ft.

10.00 ft. Line Segments Define Each Trial Failure Surface.

Following Are Displayed The Ten Most Critical Of The Trial
Failure Surfaces Examined. They Are Ordered - Most Critical
First.

* * Safety Factors Are Calculated By The Modified Bishop Method * *

Failure Surface Specified By 11 Coordinate Points

Point No.	X-Surf (ft)	Y-Surf (ft)
1	45.89	100.00
2	52.68	97.37
3	62.66	97.32
4	72.23	98.06
5	85.41	100.17
6	94.80	103.61
7	103.62	108.32
8	111.71	114.20
9	118.60	121.15
10	125.06	129.02
11	125.63	130.00

Circle Center At X = 65.4 ; Y = 169.4 and Radius, 72.1

*** 1.021 ***

Individual data on the 14 slices

Width Ft(m)	Weight Lbs(kg)	Water Force Top Lbs(kg)	Water Force Bot Lbs(kg)	Tie Force Norm Lbs(kg)	Tie Force Tan Lbs(kg)	Earthquake Force Hor Lbs(kg)	Earthquake Force Ver Lbs(kg)	Surcharge Load Lbs(kg)
9.8	1190.6	.0	632.2	.0	.0	573.8	.0	.0
7.8	1124.0	.0	585.2	.0	.0	558.3	.0	.0
5.3	2057.8	.0	1275.1	.0	.0	610.6	.0	.0
5.7	6335.3	.0	4287.0	.0	.0	2101.1	.0	.0
10.0	9133.3	.0	7220.7	.0	.0	3007.9	.0	.0
9.8	13076.6	.0	9280.7	.0	.0	3711.2	.0	.0
6.6	14831.3	.0	7585.7	.0	.0	3417.7	.0	.0
2.3	8557.1	.0	2535.7	.0	.0	1067.4	.0	.0
3.2	6883.9	.0	4338.7	.0	.0	1354.3	.0	.0
3.6	5086.2	.0	5750.5	.0	.0	1304.2	.0	.0
8.1	12166.2	.0	5750.5	.0	.0	2805.8	.0	.0
6.0	7369.8	.0	1510.6	.0	.0	1665.7	.0	.0
1.2	1243.0	.0	.0	.0	.0	281.3	.0	.0
1.1	1039.9	.0	.0	.0	.0	250.3	.0	.0
5.1	2556.9	.0	.0	.0	.0	586.5	.0	.0
.6	33.2	.0	.0	.0	.0	7.6	.0	.0

Failure Surface Specified By 11 Coordinate Points

Point No.	X-Surf (ft)	Y-Surf (ft)
1	45.89	100.00
2	52.71	98.14
3	62.70	97.57
4	72.67	98.31
5	85.46	100.33
6	94.91	103.62
7	103.85	108.10
8	112.13	113.70
9	118.61	120.34
10	126.17	127.88
11	127.57	130.00

Circle Center At X = 65.1 ; Y = 174.3 and Radius, 76.8

*** 1.022 ***

Failure Surface Specified By 12 Coordinate Points

Point No.	X-Surf (ft)	Y-Surf (ft)
1	45.89	100.00
2	52.77	97.48
3	62.76	96.94
4	72.79	96.28
5	85.40	97.61
6	95.06	100.21
7	103.30	104.03
8	113.87	109.01
9	120.93	115.06
10	128.04	122.10
11	132.16	126.08
12	134.20	130.00

Circle Center At X = 70.2 ; Y = 173.5 and Radius, 77.4

*** 1.025 ***

Failure Surface Specified By 11 Coordinate Points

Point No.	X-Surf (ft)	Y-Surf (ft)
1	45.89	100.00
2	52.75	98.32
3	62.74	97.95
4	72.71	98.81
5	85.49	100.90
6	94.93	104.20
7	103.88	108.66
8	112.20	114.20
9	118.77	120.74
10	126.46	128.17
11	127.73	130.00

Circle Center At X = 63.9 ; Y = 177.7 and Radius, 79.8

*** 1.030 ***

Failure Surface Specified By 11 Coordinate Points

Point No.	X-Surf (ft)	Y-Surf (ft)
1	45.89	100.00
2	55.92	96.40
3	65.01	92.37
4	75.00	93.96
5	82.83	95.18
6	84.55	98.03
7	87.55	98.03
8	103.55	102.38
9	111.68	108.15
10	118.80	115.18
11	122.88	123.27
	128.05	130.00

Circle Center At X = 72.5 ; Y = 155.0 and Radius, 61.1

*** 1.038 ***

Failure Surface Specified By 11 Coordinate Points

Point No.	X-Surf (ft)	Y-Surf (ft)
1	59.00	100.00
2	68.82	98.09
3	78.80	97.53
4	88.77	98.33
5	98.34	100.48
6	107.92	103.93
7	116.75	108.63
8	124.86	114.48
9	132.10	121.37
10	138.34	129.19
11	138.82	130.00

Circle Center At X = 77.9 ; Y = 171.0 and Radius, 73.5

*** 1.038 ***

Failure Surface Specified By 12 Coordinate Points

Point No.	X-Surf (ft)	Y-Surf (ft)
1	45.89	100.00
2	52.66	97.48
3	62.63	96.98
4	72.63	97.09
5	82.39	98.27
6	85.31	100.50
7	104.76	103.77
8	113.81	108.04
9	122.34	113.25
10	130.27	119.35
11	137.49	126.26
12	140.64	130.00

Circle Center At X = 69.7 ; Y = 189.5 and Radius, 92.6

*** 1.053 ***

Failure Surface Specified By 13 Coordinate Points

Point No.	X-Surf (ft)	Y-Surf (ft)
1	39.33	100.00
2	48.71	96.33
3	58.49	94.31
4	68.42	93.39
5	78.41	93.77
6	88.37	95.43
7	97.83	98.39
8	106.92	102.56
9	115.39	107.88
10	123.09	114.26
11	129.89	121.58
12	135.69	129.74
13	135.83	130.00

Circle Center At X = 70.5 ; Y = 169.9 and Radius, 76.6

*** 1.055 ***

Failure Surface Specified By 12 Coordinate Points

JAN 1995
RECEIVED
Environmental
Library

Point No.	X-Surf (ft)	Y-Surf (ft)
1	39.33	100.00
2	46.11	97.88
3	52.05	94.87
4	59.03	92.87
5	66.02	90.87
6	78.22	97.18
7	88.73	100.16
8	98.23	103.38
9	107.28	107.60
10	115.84	112.78
11	123.79	118.85
12	131.03	125.74
	134.64	130.00

Circle Center At X = 63.8 ; Y = 188.8 and Radius, 92.1

*** 1.056 ***

Failure Surface Specified By 12 Coordinate Points

Point No.	X-Surf (ft)	Y-Surf (ft)
1	52.44	100.00
2	61.08	96.89
3	71.85	95.35
4	81.84	95.11
5	91.77	95.27
6	101.44	98.82
7	110.69	103.70
8	119.22	107.84
9	127.01	114.13
10	133.82	121.45
11	138.52	129.22
12	139.71	130.00

Circle Center At X = 78.5 ; Y = 166.0 and Radius, 71.0

*** 1.059 ***

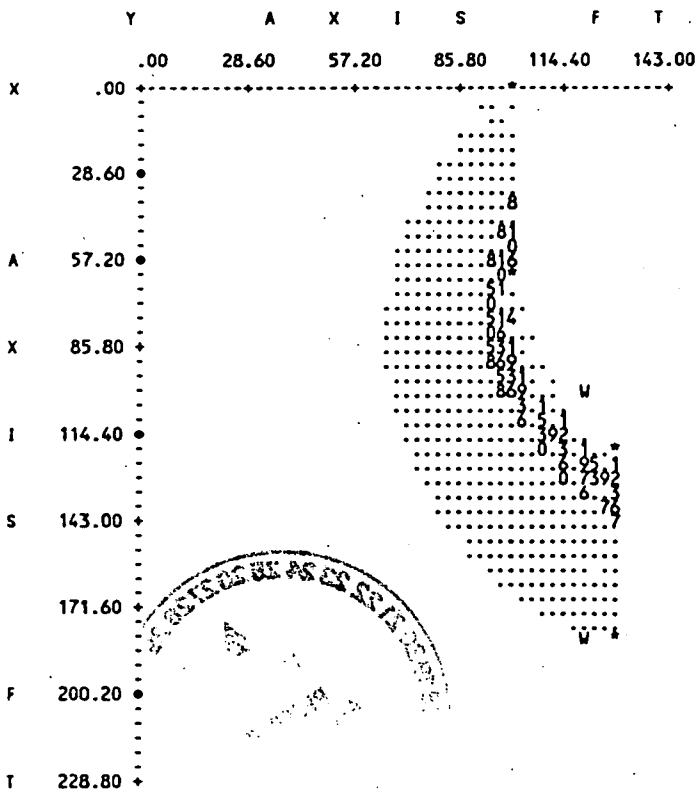

** PCSTABL5M **

by
Purdue University

--Slope Stability Analysis--
Simplified Janbu, Simplified Bishop
or Spencer's Method of Slices

Run Date: 10/06/93
Time of Run: 4:40
Run By: ZLW
Input Data Filename: 1230flh.inl
Output Filename: 1230flh.oul

PROBLEM DESCRIPTION PCSTABL5M : 30 ft, 1:2 slope, FILL, H. W

BOUNDARY COORDINATES

3 Top Boundaries
3 Total Boundaries

Boundary No.	X-Left (ft)	Y-Left (ft)	X-Right (ft)	Y-Right (ft)	Soil Type Below Bnd
1	.00	100.00	60.00	100.00	1
2	60.00	100.00	120.00	130.00	1
3	120.00	130.00	180.00	130.00	1

ISOTROPIC SOIL PARAMETERS

1 Type(s) of Soil

Soil Type No.	Total Unit Wt. (pcf)	Saturated Unit Wt. (pcf)	Cohesion Intercept (psf)	Friction Angle (deg)	Pore Pressure Param.	Pressure Constant (psf)	Piez. Surface No.
1	120.0	120.0	1000.0	.0	.00	.0	1

1 PIEZOMETRIC SURFACE(S) HAVE BEEN SPECIFIED

Unit Weight of Water = 62.40

Piezometric Surface No. 1 Specified by 4 Coordinate Points

Point No.	X-Water (ft)	Y-Water (ft)
1	.00	100.00
2	60.00	100.00
3	100.00	120.00
4	180.00	120.00

A Horizontal Earthquake Loading Coefficient
Of .165 Has Been Assigned

A Vertical Earthquake Loading Coefficient
Of .000 Has Been Assigned

Cavitation Pressure = .0 psf

A Critical Failure Surface Searching Method, Using A Random
Technique For Generating Circular Surfaces, Has Been Specified.

300 Trial Surfaces Have Been Generated.

30 Surfaces Initiate From Each Of 10 Points Equally Spaced
Along The Ground Surface Between X = .00 ft.
and X = 59.00 ft.

Each Surface Terminates Between X = 121.00 ft.
and X = 180.00 ft.

Unless Further Limitations Were Imposed, The Minimum Elevation
At Which A Surface Extends Is Y = .00 ft.

10.00 ft. Line Segments Define Each Trial Failure Surface.

Following Are Displayed The Ten Most Critical Of The Trial
Failure Surfaces Examined. They Are Ordered - Most Critical
First.

** Safety Factors Are Calculated By The Modified Bishop Method **

Failure Surface Specified By 22 Coordinate Points

Point No.	X-Surf (ft)	Y-Surf (ft)
1	6.56	100.00
2	13.69	92.99
3	21.46	86.70
4	29.80	81.18
5	38.63	76.49
6	47.87	72.66
7	57.44	69.72
8	67.24	67.75
9	77.18	66.71
10	87.18	66.63
11	97.14	67.51
12	106.97	69.33
13	116.56	72.10
14	125.89	75.77
15	137.76	80.51
16	143.22	85.69
17	151.10	91.85
18	158.35	98.74
19	164.90	106.30
20	170.70	114.44
21	175.69	123.11
22	178.83	130.00

Circle Center At X = 83.0 ; Y = 170.6 and Radius, 104.1

*** .994 ***

Individual data on the 25 slices

Width Ft(m)	Weight Lbs(kg)	Water Force Top Lbs(kg)	Water Force Bot Lbs(kg)	Tie Force Norm Lbs(kg)	Tie Force Tan Lbs(kg)	Earthquake Force Hor Lbs(kg)	Earthquake Force Ver Lbs(kg)	Surcharge Load Lbs(kg)
7.1	5860.3	.0	2186.6	.0	.0	493.2	.0	.0
7.8	9470.8	.0	6336.3	.0	.0	1562.7	.0	.0
8.3	16071.2	.0	10021.0	.0	.0	2651.9	.0	.0
8.8	22427.3	.0	13206.8	.0	.0	3700.5	.0	.0
9.2	28188.5	.0	15863.9	.0	.0	4651.1	.0	.0
9.6	33047.8	.0	17968.3	.0	.0	5426.9	.0	.0
9.9	36386.0	.0	19681.9	.0	.0	5949.2	.0	.0
7.2	28632.6	.0	13816.8	.0	.0	4773.9	.0	.0
6.6	46301.3	.0	21829.6	.0	.0	7654.6	.0	.0
10.0	53301.2	.0	24945.8	.0	.0	8792.7	.0	.0
10.0	58588.6	.0	27535.5	.0	.0	9667.2	.0	.0
2.9	17661.6	.0	8207.2	.0	.0	2914.5	.0	.0
7.0	44205.5	.0	22214.6	.0	.0	7328.6	.0	.0
6.6	63634.5	.0	30753.8	.0	.0	10269.7	.0	.0
3.2	23100.1	.0	10818.5	.0	.0	3811.5	.0	.0
5.8	38135.2	.0	17928.3	.0	.0	6257.3	.0	.0
6.6	55537.6	.0	26183.2	.0	.0	9163.7	.0	.0
8.7	77573.8	.0	23086.7	.0	.0	7844.7	.0	.0
8.3	77273.6	.0	19285.8	.0	.0	6728.8	.0	.0
7.6	38622.2	.0	15213.6	.0	.0	2980.2	.0	.0
7.2	30183.1	.0	12526.6	.0	.0	3566.3	.0	.0
6.6	21613.8	.0	10907.8	.0	.0	2554.2	.0	.0
5.8	13663.0	.0	6009.8	.0	.0	810.2	.0	.0
3.5	7810.3	.0	1112.3	.0	.0	209.2	.0	.0
1.8	1812.3	.0	.0	.0	.0	213.8	.0	.0
3.1	1295.9	.0	.0	.0	.0		.0	.0

Failure Surface Specified By 23 Coordinate Points

Point No.	X-Surf (ft)	Y-Surf (ft)
1	.00	100.00
2	7.55	93.55
3	15.21	87.11
4	23.16	81.75
5	32.32	77.16
6	41.85	73.36
7	51.41	70.44
8	61.19	68.38
9	71.15	67.19
10	81.12	66.90
11	91.10	67.51
12	100.99	69.00
13	110.70	71.37
14	120.17	74.61
15	129.30	78.67
16	138.04	83.54
17	146.30	89.17
18	152.03	95.52
19	161.16	102.53
20	167.63	110.15
21	173.20	118.32
22	178.21	126.97
23	179.82	130.00

Circle Center At X = 79.4 ; Y = 178.6 and Radius, 111.7

*** .995 ***

Failure Surface Specified By 23 Coordinate Points

Point No.	X-Surf (ft)	Y-Surf (ft)
1	.00	100.00
2	7.22	93.10
3	15.08	86.89
4	23.26	81.43
5	32.30	76.76
6	41.53	72.92

7	51.08	69.94
8	60.86	67.85
9	70.79	66.00
10	80.78	65.48
11	90.76	67.03
12	100.64	68.58
13	110.33	71.95
14	118.72	74.58
15	127.67	78.59
16	136.04	79.59
17	137.31	83.39
18	145.67	88.33
19	153.28	92.83
20	160.26	98.86
21	166.55	105.77
22	172.10	110.78
23	176.87	119.09
	177.78	127.87
		130.00

Circle Center At X = 78.8 ; Y = 175.4 and Radius, 109.0

*** .997 ***

Failure Surface Specified By 22 Coordinate Points

Point No.	X-Surf (ft)	Y-Surf (ft)
1	6.56	100.00
2	13.79	93.09
3	21.65	86.91
4	30.06	81.50
5	38.95	76.92
6	48.23	73.20
7	57.82	70.38
8	67.67	68.49
9	77.60	67.54
10	87.60	67.55
11	97.55	68.50
12	107.37	70.40
13	116.86	73.23
14	126.29	77.95
15	135.53	79.55
16	143.13	81.55
17	147.53	84.93
18	151.38	89.16
19	158.61	93.15
20	165.15	100.07
21	170.93	107.63
22	175.95	115.79
	178.44	124.28
		130.00

Circle Center At X = 82.5 ; Y = 172.2 and Radius, 104.8

*** .999 ***

Failure Surface Specified By 22 Coordinate Points

Point No.	X-Surf (ft)	Y-Surf (ft)
1	6.56	100.00
2	13.93	93.03
3	21.76	86.59
4	29.98	81.07
5	38.50	76.34
6	47.25	72.52
7	57.32	69.37
8	67.14	67.64
9	77.09	67.21
10	87.09	66.75
11	97.07	69.78
12	106.84	71.80
13	116.40	75.29
14	125.62	77.73
15	135.51	79.60
16	142.70	81.35
17	150.39	86.95
18	157.42	93.37
19	163.45	100.45
20	169.22	108.22
21	173.87	116.58
22	175.72	125.23
		130.00

Circle Center At X = 81.7 ; Y = 168.0 and Radius, 101.4

*** 1.003 ***

Failure Surface Specified By 22 Coordinate Points

Point No.	X-Surf (ft)	Y-Surf (ft)
1	.00	100.00
2	7.39	93.23
3	15.32	87.17
4	23.80	81.87
5	32.72	77.37
6	42.03	73.71
7	51.63	70.92
8	61.45	69.05
9	71.40	68.04
10	81.40	67.97
11	91.37	68.83
12	101.21	70.60
13	110.85	73.26

14	120.20	76.80
15	129.19	81.18
16	137.73	86.38
17	145.76	92.32
18	153.21	99.01
19	160.02	106.34
20	166.12	114.26
21	171.47	122.71
22	175.19	130.00

Circle Center At X = 77.1 ; Y = 176.4 and Radius, 108.5

*** 1.015 ***

Failure Surface Specified By 20 Coordinate Points

Point No.	X-Surf (ft)	Y-Surf (ft)
1	26.22	100.00
2	33.34	89.89
3	37.17	82.32
4	40.17	86.26
5	43.64	81.44
6	46.67	77.08
7	48.08	73.72
8	49.29	71.41
9	51.21	70.18
10	53.71	70.03
11	107.67	70.98
12	111.26	73.00
13	116.37	76.09
14	136.09	80.16
15	142.71	83.26
16	153.72	91.24
17	160.07	98.06
18	166.36	105.62
19	172.22	113.88
20	176.65	122.70
	179.89	130.00

Circle Center At X = 94.0 ; Y = 161.4 and Radius, 91.5

*** 1.018 ***

Failure Surface Specified By 20 Coordinate Points

Point No.	X-Surf (ft)	Y-Surf (ft)
1	26.22	100.00
2	33.58	89.53
3	37.22	87.58
4	40.25	82.23
5	43.37	78.12
6	46.87	74.05
7	48.65	72.83
8	49.60	71.60
9	50.60	71.07
10	108.54	72.04
11	113.31	75.20
12	117.79	78.38
13	136.87	82.56
14	143.46	87.68
15	153.76	93.68
16	160.77	100.51
17	167.31	108.07
18	173.01	116.29
19	177.80	125.06
20	179.84	130.00

Circle Center At X = 93.2 ; Y = 165.4 and Radius, 93.6

*** 1.025 ***

Failure Surface Specified By 20 Coordinate Points

Point No.	X-Surf (ft)	Y-Surf (ft)
1	19.67	100.00
2	27.08	89.28
3	35.16	83.57
4	43.48	82.33
5	53.68	78.20
6	65.37	73.04
7	75.14	72.88
8	83.07	71.74
9	85.07	71.63
10	102.03	72.36
11	111.82	74.51
12	121.30	77.47
13	130.58	81.40
14	139.32	86.26
15	147.51	92.00
16	155.06	98.55
17	161.90	105.85
18	167.94	113.82
19	173.13	122.37
20	176.73	130.00

Circle Center At X = 88.1 ; Y = 168.0 and Radius, 96.5

*** 1.027 ***

Failure Surface Specified By 21 Coordinate Points

Point No.	X-Surf (ft)	Y-Surf (ft)
1	13.11	100.00
2	20.21	92.96
3	28.02	86.71
4	36.46	81.35
5	45.42	76.92
6	54.81	73.47
7	64.52	71.06
8	74.45	69.70
9	84.45	69.41
10	94.36	70.20
11	104.22	72.05
12	113.76	74.97
13	122.99	78.85
14	131.73	83.72
15	139.88	89.50
16	147.38	96.13
17	154.12	103.52
18	160.02	111.56
19	165.03	120.24
20	169.07	129.39
21	169.27	130.00

Circle Center At X = 82.1 ; Y = 162.4 and Radius, 93.0

*** 1.037 ***

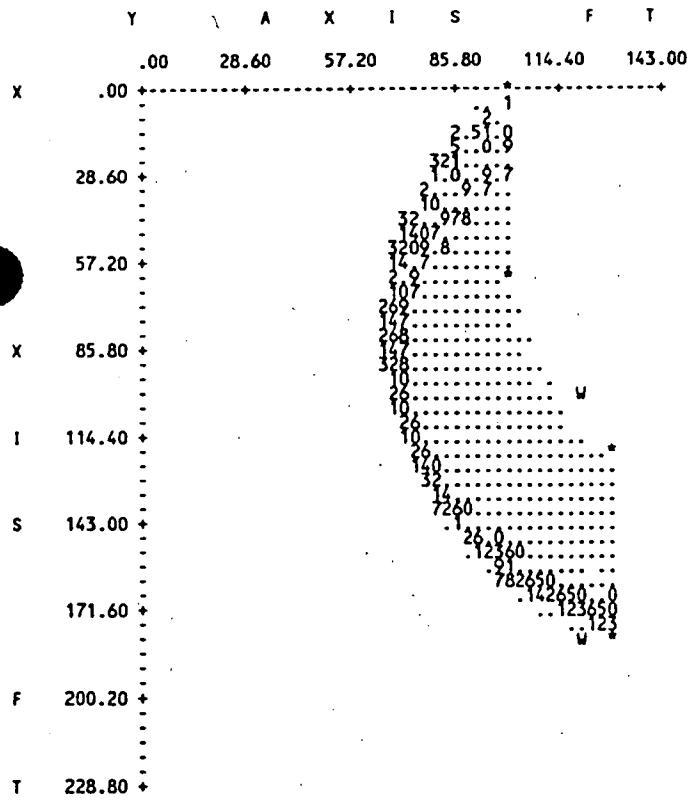

** PCSTABL5M **
by
Purdue University

--Slope Stability Analysis--
Simplified Janbu, Simplified Bishop
or Spencer's Method of Slices

Run Date: 10/06/93
Time of Run: 4:40
Run By: ZLW
Input Data filename: 1230csh.in1
Output Filename: 1230csh.out

PROBLEM DESCRIPTION PCSTABL5M : 30 ft, 1:2 slope, CLAYSTONE, H. WT

BOUNDARY COORDINATES

3 Top Boundaries
3 Total Boundaries

Boundary No.	X-Left (ft)	Y-Left (ft)	X-Right (ft)	Y-Right (ft)	Soil Type Below Bnd
1	.00	100.00	60.00	100.00	1
2	60.00	100.00	120.00	130.00	1
3	120.00	130.00	180.00	130.00	1

ISOTROPIC SOIL PARAMETERS

1 Type(s) of Soil

Soil Type No.	Total Unit Wt. (pcf)	Saturated Unit Wt. (pcf)	Cohesion Intercept (psf)	Friction Angle (deg)	Pore Pressure Param.	Pressure Constant (psf)	Piez. Surface No.
1	130.0	130.0	1000.0	20.0	.00	.0	1

1 PIEZOMETRIC SURFACE(S) HAVE BEEN SPECIFIED

Unit Weight of Water = 62.40

Piezometric Surface No. 1 Specified by 4 Coordinate Points

Point No.	X-Water (ft)	Y-Water (ft)
1	.00	100.00
2	60.00	100.00
3	100.00	120.00
4	180.00	120.00

A Horizontal Earthquake Loading Coefficient
Of .425 Has Been Assigned

A Vertical Earthquake Loading Coefficient
Of .000 Has Been Assigned

Cavitation Pressure = .0 psf

A Critical Failure Surface Searching Method, Using A Random
Technique For Generating Circular Surfaces, Has Been Specified.

300 Trial Surfaces Have Been Generated.

30 Surfaces Initiate From Each Of 10 Points Equally Spaced
Along The Ground Surface Between X = .00 ft.
and X = 59.00 ft.

Each Surface Terminates Between X = 121.00 ft.
and X = 180.00 ft.

Unless Further Limitations Were Imposed, The Minimum Elevation
At Which A Surface Extends Is Y = .00 ft.

10.00 ft. Line Segments Define Each Trial Failure Surface.

Following Are Displayed The Ten Most Critical Of The Trial
Failure Surfaces Examined. They Are Ordered - Most Critical
First.

** Safety Factors Are Calculated By The Modified Bishop Method **

Failure Surface Specified By 21 Coordinate Points

Point No.	X-Surf (ft)	Y-Surf (ft)
1	13.11	100.00
2	21.11	94.00
3	29.62	88.75
4	36.57	84.28
5	39.88	80.23
6	47.48	77.83
7	57.38	77.81
8	67.57	77.87
9	77.57	77.94
10	87.57	77.94
11	97.57	77.50
12	107.07	77.15
13	116.74	77.16
14	126.15	79.69
15	135.21	83.08
16	143.81	87.31
17	153.89	87.33
18	156.02	88.11
19	159.63	101.60
20	163.83	111.74
21	169.85	119.49
22	172.25	122.37
23	178.58	127.77
24	179.79	130.00

Circle Center At X = 83.7 ; Y = 185.9 and Radius, 111.2

*** 1.005 ***

Individual data on the 24 slices

Width Ft(m)	Weight Lbs(kg)	Water Force Top Lbs(kg)	Water Force Bot Lbs(kg)	Tie Force Norm Lbs(kg)	Tie Force Tan Lbs(kg)	Earthquake Force Hor Lbs(kg)	Earthquake Force Ver Lbs(kg)	Surcharge Load Lbs(kg)
8.0	3119.7	.0	1871.8	.0	.0	1325.6	.0	.0
8.5	8540.7	.0	5382.6	.0	.0	4052.8	.0	.0
8.6	15686.5	.0	8417.3	.0	.0	6669.8	.0	.0
8.3	23970.5	.0	10950.2	.0	.0	9027.2	.0	.0
9.7	25637.3	.0	12071.2	.0	.0	11018.0	.0	.0
2.6	22253.9	.0	3580.2	.0	.0	3124.7	.0	.0
6.3	17352.1	.0	10517.2	.0	.0	10150.6	.0	.0
7.3	23884.3	.0	14217.4	.0	.0	16893.8	.0	.0
9.0	30750.1	.0	17563.9	.0	.0	20061.2	.0	.0
10.0	37200.7	.0	20383.5	.0	.0	22582.7	.0	.0
10.0	43135.0	.0	23021.7	.0	.0	2723.6	.0	.0
2.8	15820.2	.0	8755.2	.0	.0	17605.2	.0	.0
7.1	41577.6	.0	17520.3	.0	.0	25403.1	.0	.0
9.2	39775.1	.0	23247.6	.0	.0	8803.0	.0	.0
3.3	20712.8	.0	8284.3	.0	.0	16315.9	.0	.0
8.1	38390.3	.0	15510.8	.0	.0	15737.0	.0	.0
9.1	47722.9	.0	21718.3	.0	.0	23707.5	.0	.0
8.6	45171.3	.0	18833.2	.0	.0	12183.9	.0	.0
8.2	36902.5	.0	12263.3	.0	.0	15062.6	.0	.0
7.6	28338.8	.0	11636.3	.0	.0	12033.9	.0	.0
7.0	19853.8	.0	7382.5	.0	.0	8437.7	.0	.0
6.3	11826.2	.0	2738.5	.0	.0	5027.7	.0	.0
.3	262.6	.0	9.6	.0	.0	196.6	.0	.0
5.3	4170.3	.0	.0	.0	.0	1776.2	.0	.0
1.2	178.7	.0	.0	.0	.0	76.0	.0	.0

Failure Surface Specified By 23 Coordinate Points

Point No.	X-Surf (ft)	Y-Surf (ft)
1	.00	100.00
2	7.35	93.22
3	15.27	87.11
4	23.71	81.75
5	33.59	77.16
6	41.85	73.38
7	51.41	70.44
8	61.19	68.38
9	71.15	67.19
10	81.12	66.90
11	91.10	67.53
12	100.99	69.00
13	110.70	71.37
14	120.17	74.67
15	129.30	78.87
16	138.04	83.94
17	146.30	89.17
18	154.03	95.52
19	161.16	102.53
20	167.63	110.15
21	173.20	118.32
22	178.21	126.67
23	179.82	130.00

Circle Center At X = 79.4 ; Y = 178.6 and Radius, 111.7

*** 1.005 ***

Failure Surface Specified By 22 Coordinate Points

Point No.	X-Surf (ft)	Y-Surf (ft)
1	.00	100.00
2	7.77	93.70
3	16.06	88.11
4	24.81	83.28
5	33.96	79.24
6	43.43	76.03
7	53.15	73.68
8	63.04	72.17

9	73.02	71.56
10	83.01	71.84
11	82.95	73.00
12	102.74	75.03
13	112.31	77.82
14	121.59	81.35
15	130.50	86.19
16	138.88	91.69
17	146.85	97.33
18	154.36	103.35
19	161.34	111.60
20	167.63	119.62
21	172.84	132.85
22	173.69	130.00

Circle Center At X = 74.9 ; Y = 184.3 and Radius, 112.7

*** 1.010 ***

Failure Surface Specified By 21 Coordinate Points

Point No.	X-Surf (ft)	Y-Surf (ft)
1	6.56	100.00
2	13.08	94.77
3	23.99	90.23
4	33.23	86.40
5	42.97	83.31
6	52.72	80.97
7	62.34	79.40
8	72.31	78.61
9	82.31	78.61
10	92.28	79.39
11	102.15	80.94
12	111.88	83.27
13	121.39	86.36
14	130.63	90.18
15	139.55	94.71
16	148.08	99.92
17	156.17	105.79
18	163.78	112.28
19	170.86	119.35
20	177.37	126.97
21	179.59	130.00

Circle Center At X = 77.4 ; Y = 206.0 and Radius, 127.4

*** 1.011 ***

Failure Surface Specified By 23 Coordinate Points

Point No.	X-Surf (ft)	Y-Surf (ft)
1	.00	100.00
2	7.64	93.10
3	15.08	86.89
4	23.46	81.43
5	32.30	76.76
6	41.53	72.92
7	51.08	69.94
8	60.86	67.85
9	70.79	66.68
10	80.78	66.38
11	90.76	67.03
12	100.64	68.59
13	110.33	71.05
14	119.76	74.38
15	128.84	78.59
16	137.51	83.59
17	145.67	89.33
18	153.28	95.82
19	160.59	102.86
20	166.55	110.79
21	172.10	119.08
22	176.87	127.87
23	177.78	130.00

Circle Center At X = 78.8 ; Y = 175.4 and Radius, 109.0

*** 1.012 ***

Failure Surface Specified By 22 Coordinate Points

Point No.	X-Surf (ft)	Y-Surf (ft)
1	.00	100.00
2	7.38	93.23
3	15.32	87.17
4	23.80	81.87
5	32.72	77.37
6	42.03	73.71
7	51.63	70.92
8	61.45	68.05
9	71.20	68.04
10	81.20	69.07
11	91.37	68.83
12	101.31	70.99
13	110.85	74.68
14	120.20	79.80
15	129.18	81.19
16	137.73	86.38

17	145.76	92.34
18	153.51	86.07
19	160.02	99.97
20	166.15	106.32
21	171.47	113.29
22	175.19	122.71
		130.00

Circle Center At X = 77.1 ; Y = 176.4 and Radius, 108.5

*** 1.014 ***

Failure Surface Specified By 21 Coordinate Points

Point No.	X-Surf (ft)	Y-Surf (ft)
1	6.56	100.00
2	14.57	93.63
3	22.54	88.01
4	31.30	83.18
5	40.77	79.20
6	48.97	76.08
7	56.72	73.87
8	64.67	72.58
9	69.63	72.22
10	77.03	72.79
11	80.91	72.29
12	85.50	74.70
13	109.30	78.02
14	118.64	80.16
15	127.73	83.20
16	136.38	87.69
17	144.53	91.52
18	153.11	101.52
19	156.04	108.73
20	162.27	116.55
21	169.51	122.83
	173.42	130.00

Circle Center At X = 78.5 ; Y = 179.3 and Radius, 107.0

*** 1.016 ***

Failure Surface Specified By 21 Coordinate Points

Point No.	X-Surf (ft)	Y-Surf (ft)
1	.00	100.00
2	8.28	94.36
3	16.89	89.48
4	26.08	85.30
5	35.47	81.88
6	45.12	79.27
7	54.95	77.41
8	64.90	76.38
9	72.89	76.18
10	84.87	76.79
11	87.77	78.23
12	102.52	80.23
13	112.05	83.50
14	123.30	83.30
15	132.50	84.85
16	140.70	87.11
17	148.72	103.06
18	156.27	108.64
19	163.23	116.85
20	169.58	122.34
21	173.36	130.00

Circle Center At X = 72.4 ; Y = 197.9 and Radius, 121.8

*** 1.016 ***

Failure Surface Specified By 19 Coordinate Points

Point No.	X-Surf (ft)	Y-Surf (ft)
1	19.67	100.00
2	27.88	92.58
3	37.58	88.58
4	45.72	83.38
5	53.16	83.30
6	57.03	86.10
7	67.02	79.80
8	77.83	78.42
9	87.82	77.97
10	97.81	78.47
11	104.70	79.89
12	114.42	82.24
13	123.88	85.26
14	132.99	89.61
15	142.77	87.57
16	149.89	100.31
17	157.47	106.80
18	164.24	113.98
19	170.70	121.77
	176.13	130.00

Circle Center At X = 84.6 ; Y = 184.6 and Radius, 106.6

*** 1.018 ***

Failure Surface Specified By 20 Coordinate Points

Point No.	X-Surf (ft)	Y-Surf (ft)
1	19.67	100.00
2	27.81	92.20
3	36.57	89.19
4	46.56	85.03
5	55.01	81.25
6	64.16	79.38
7	74.66	77.82
8	84.61	77.44
9	94.60	77.20
10	104.50	77.29
11	114.25	77.62
12	123.88	81.82
13	132.80	84.88
14	141.77	88.88
15	150.27	93.95
16	158.93	98.72
17	167.43	103.75
18	174.17	109.23
19	170.39	113.34
20	176.02	121.27
	175.82	126.85
	176.02	130.00

Circle Center At X = 84.8 ; Y = 182.8 and Radius, 105.4

*** 1.018 ***

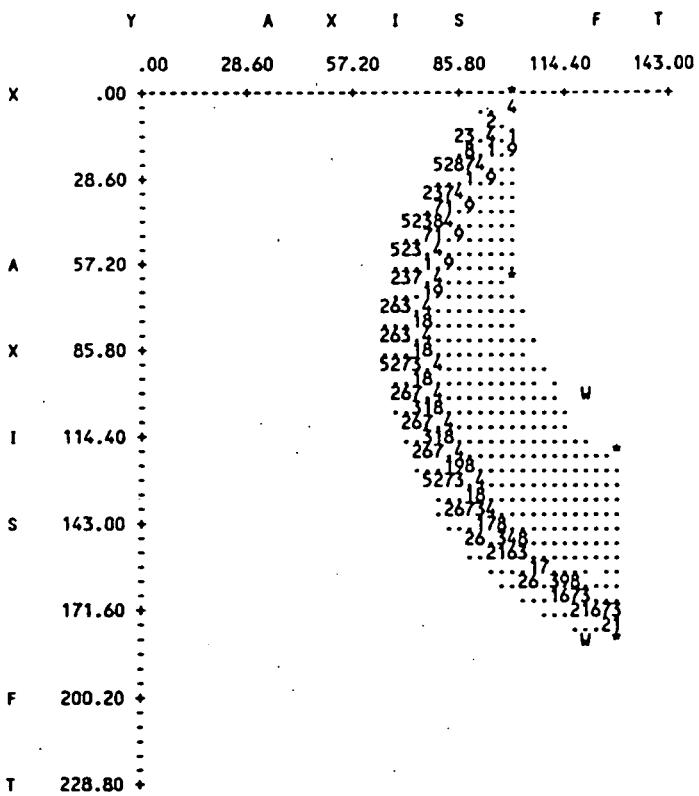

** PCSTABL5M **

by
Purdue University

--Slope Stability Analysis--
Simplified Janbu, Simplified Bishop
or Spencer's Method of Slices

Run Date: 10/06/93
Time of Run: 4:40
Run By: ZLW
Input Data Filename: 1230all.in
Output Filename: 1230all.out

PROBLEM DESCRIPTION PCSTABL5M : 30 ft, 1:2 slope, Aluvium 1, L. WT

BOUNDARY COORDINATES

3 Top Boundaries
3 Total Boundaries

Boundary No.	X-Left (ft)	Y-Left (ft)	X-Right (ft)	Y-Right (ft)	Soil Type Below Bnd
1	.00	100.00	60.00	100.00	1
2	60.00	100.00	120.00	130.00	1
3	120.00	130.00	180.00	130.00	1

ISOTROPIC SOIL PARAMETERS

1 Type(s) of Soil

Soil Type No.	Total Unit Wt. (pcf)	Saturated Unit Wt. (pcf)	Cohesion Intercept (psf)	Friction Angle (deg)	Pore Pressure Param.	Pressure Constant (psf)	Piez. Surface No.
1	120.0	120.0	.0	45.0	.00	.0	1

1 PIEZOMETRIC SURFACE(S) HAVE BEEN SPECIFIED

Unit Weight of Water = 62.40

Piezometric Surface No. 1 Specified by 2 Coordinate Points

Point No.	X-Water (ft)	Y-Water (ft)
1	.00	100.00
2	180.00	100.00

A Horizontal Earthquake Loading Coefficient
Of .420 Has Been Assigned

A Vertical Earthquake Loading Coefficient
Of .000 Has Been Assigned

Cavitation Pressure = .0 psf

A Critical Failure Surface Searching Method, Using A Random Technique For Generating Circular Surfaces, Has Been Specified.

300 Trial Surfaces Have Been Generated.

30 Surfaces Initiate From Each Of 10 Points Equally Spaced
Along The Ground Surface Between X = .00 ft.
and X = 59.00 ft.

Each Surface Terminates Between X = 121.00 ft.
and X = 180.00 ft.

Unless Further Limitations Were Imposed, The Minimum Elevation
At Which A Surface Extends Is Y = .00 ft.

10.00 ft. Line Segments Define Each Trial Failure Surface.

Following Are Displayed The Ten Most Critical Of The Trial Failure Surfaces Examined. They Are Ordered - Most Critical First.

* * Safety Factors Are Calculated By The Modified Bishop Method * *

Failure Surface Specified By 14 Coordinate Points

Point No.	X-Surf (ft)	Y-Surf (ft)
1	13.11	100.00
2	22.87	97.81
3	32.77	96.72
4	42.76	96.85
5	52.75	97.10
6	62.70	97.17
7	72.52	99.04
8	82.15	101.72
9	91.52	105.17
10	100.31	109.38
11	108.30	114.32
12	117.39	119.82
13	125.32	122.26
14	129.27	130.00

Circle Center At X = 44.7 ; Y = 217.5 and Radius, 121.7

*** 1.004 ***

Individual data on the 16 slices

Width Ft(m)	Weight Lbs(kg)	Water Force Top Lbs(kg)	Water Force Bot Lbs(kg)	Tie Force Norm Lbs(kg)	Tie Force Tan Lbs(kg)	Earthquake Force Hor Lbs(kg)	Earthquake Force Ver Lbs(kg)	Surcharge Load Lbs(kg)
6.8	1283.2	.0	684.0	.0	.0	539.0	.0	.0
6.8	3426.1	.0	1800.5	.0	.0	1440.2	.0	.0
10.0	7626.2	.0	2511.1	.0	.0	1944.3	.0	.0
10.0	7828.6	.0	2511.7	.0	.0	2028.0	.0	.0
4.2	3054.7	.0	1597.6	.0	.0	1283.0	.0	.0
2.7	1181.6	.0	504.0	.0	.0	496.3	.0	.0
6.8	6718.2	.0	1183.4	.0	.0	2821.7	.0	.0
3.5	3149.1	.0	107.1	.0	.0	1322.6	.0	.0
6.2	6435.2	.0	.0	.0	.0	2702.8	.0	.0
6.4	11238.3	.0	.0	.0	.0	4720.1	.0	.0
6.1	11712.0	.0	.0	.0	.0	4919.0	.0	.0
8.7	11087.8	.0	.0	.0	.0	4656.9	.0	.0
8.3	9496.0	.0	.0	.0	.0	3888.3	.0	.0
2.4	2469.6	.0	.0	.0	.0	1037.2	.0	.0
5.3	3786.5	.0	.0	.0	.0	1590.3	.0	.0
3.9	884.4	.0	.0	.0	.0	371.5	.0	.0

Failure Surface Specified By 14 Coordinate Points

Point No.	X-Surf (ft)	Y-Surf (ft)
1	13.11	100.00
2	22.91	98.01
3	32.87	96.60
4	42.83	96.37
5	52.83	96.72
6	62.82	97.72
7	72.76	97.69
8	82.57	99.77
9	91.61	102.53
10	100.70	105.87
11	109.12	110.02
12	117.45	114.87
13	125.67	120.39
14	129.44	122.57
		126.54
		130.00

Circle Center At X = 43.3 ; Y = 223.4 and Radius, 127.1

*** 1.004 ***

Failure Surface Specified By 15 Coordinate Points

Point No.	X-Surf (ft)	Y-Surf (ft)
1	.00	100.00
2	9.81	98.02
3	19.73	96.78
4	29.71	96.18
5	39.71	96.37
6	49.68	97.00
7	59.58	98.53
8	69.39	100.52
9	78.97	103.26
10	88.38	106.65
11	97.54	110.67
12	106.40	115.30
13	114.93	120.52
14	123.09	126.30
15	127.63	130.00

Circle Center At X = 33.6 ; Y = 243.9 and Radius, 147.8

*** 1.004 ***

Failure Surface Specified By 13 Coordinate Points

Point No.	X-Surf (ft)	Y-Surf (ft)
1	19.67	100.00
2	29.76	98.10
3	39.73	97.01
4	49.42	96.76

5	58.41	97.34
6	66.31	98.74
7	75.06	100.98
8	86.58	103.88
9	87.84	107.29
10	106.74	112.35
11	113.23	115.63
12	123.25	125.60
13	130.51	130.00

Circle Center At X = 47.5 ; Y = 217.1 and Radius, 120.4

*** 1.010 ***

Failure Surface Specified By 14 Coordinate Points

Point No.	X-Surf (ft)	Y-Surf (ft)
1	13.11	100.00
2	22.60	96.85
3	32.36	94.62
4	42.28	93.40
5	52.28	93.14
6	62.25	93.86
7	72.11	95.55
8	81.75	98.19
9	91.02	101.77
10	100.03	106.25
11	108.28	111.58
12	116.39	117.71
13	123.25	124.58
14	128.36	130.00

Circle Center At X = 49.9 ; Y = 194.9 and Radius, 101.8

*** 1.010 ***

Failure Surface Specified By 14 Coordinate Points

Point No.	X-Surf (ft)	Y-Surf (ft)
1	19.67	100.00
2	29.07	96.60
3	38.80	94.28
4	48.73	93.07
5	58.72	92.97
6	68.67	93.99
7	78.44	96.12
8	87.91	99.33
9	96.97	103.58
10	105.48	108.82
11	113.36	114.98
12	120.50	121.98
13	126.81	129.72
14	128.98	130.00

Circle Center At X = 54.6 ; Y = 182.0 and Radius, 89.1

*** 1.014 ***

Failure Surface Specified By 14 Coordinate Points

Point No.	X-Surf (ft)	Y-Surf (ft)
1	19.67	100.00
2	29.36	97.67
3	39.27	96.16
4	49.26	95.55
5	59.25	95.83
6	69.18	97.00
7	78.97	99.03
8	88.55	101.93
9	97.82	105.66
10	106.74	110.20
11	115.21	115.51
12	123.18	121.54
13	130.58	128.32
14	132.19	130.00

Circle Center At X = 51.1 ; Y = 208.2 and Radius, 112.6

*** 1.021 ***

Failure Surface Specified By 12 Coordinate Points

Point No.	X-Surf (ft)	Y-Surf (ft)
1	32.78	100.00
2	42.17	96.57
3	51.95	94.50
4	61.63	93.81
5	71.90	94.54
6	81.68	96.69
7	91.06	100.13

8	99.85	104.88
9	107.90	110.82
10	115.03	117.84
11	121.10	125.78
12	123.47	130.00

Circle Center At X = 61.7 ; Y = 164.5 and Radius, 70.7

*** 1.028 ***

Failure Surface Specified By 14 Coordinate Points

Point No.	X-Surf (ft)	Y-Surf (ft)
1	13.11	100.00
2	23.04	98.82
3	33.03	98.59
4	43.03	98.37
5	53.01	98.00
6	63.93	100.27
7	75.75	102.13
8	85.45	104.58
9	91.97	107.23
10	101.30	111.97
11	110.38	115.41
12	118.21	120.12
13	127.72	125.36
14	134.33	130.00

Circle Center At X = 37.2 ; Y = 262.7 and Radius, 164.5

*** 1.029 ***

Failure Surface Specified By 14 Coordinate Points

Point No.	X-Surf (ft)	Y-Surf (ft)
1	19.67	100.00
2	28.86	96.07
3	38.46	93.26
4	48.32	91.60
5	58.31	91.12
6	68.29	91.85
7	78.11	93.66
8	87.62	96.71
9	96.75	100.84
10	105.31	106.01
11	113.20	112.19
12	120.30	118.19
13	126.53	127.02
14	128.37	130.00

Circle Center At X = 57.4 ; Y = 175.4 and Radius, 84.3

*** 1.037 ***

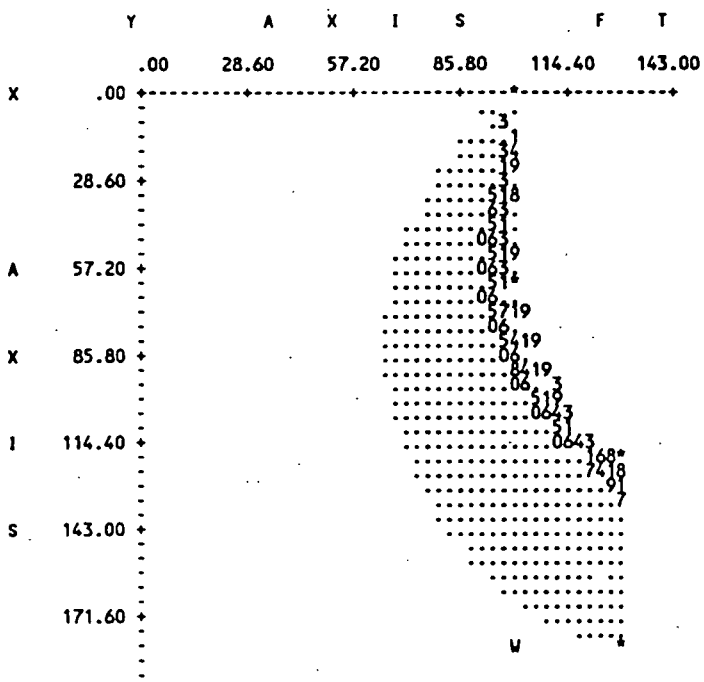

F 200.20 +

T 228.80 +

** PCSTABL5M **

by
Purdue University

--Slope Stability Analysis--
Simplified Janbu, Simplified Bishop
or Spencer's Method of Slices

Run Date: 10/06/93
Time of Run: 4:40
Run By: JLW
Input Data Filename: 1230a2l.inl
Output Filename: 1230a2l.oul

PROBLEM DESCRIPTION PCSTABL5M : 30 ft, 1:2 slope, Aluvium 2, Low.WT

BOUNDARY COORDINATES

3 Top Boundaries
3 Total Boundaries

Boundary No.	X-Left (ft)	Y-Left (ft)	X-Right (ft)	Y-Right (ft)	Soil Type Below Bnd
1	.00	100.00	60.00	100.00	1
2	60.00	100.00	120.00	130.00	1
3	120.00	130.00	180.00	130.00	1

ISOTROPIC SOIL PARAMETERS

1 Type(s) of Soil

Soil Type No.	Total Unit Wt. (pcf)	Saturated Unit Wt. (pcf)	Cohesion Intercept (psf)	Friction Angle (deg)	Pore Pressure Param.	Pressure Constant (psf)	Piez. Surface No.
1	120.0	120.0	200.0	38.0	.00	.0	1

1 PIEZOMETRIC SURFACE(S) HAVE BEEN SPECIFIED

Unit Weight of Water = 62.40

Piezometric Surface No. 1 Specified by 2 Coordinate Points

Point No.	X-Water (ft)	Y-Water (ft)
1	.00	100.00
2	180.00	100.00

A Horizontal Earthquake Loading Coefficient
Of .470 Has Been Assigned

A Vertical Earthquake Loading Coefficient
Of .000 Has Been Assigned

Cavitation Pressure = .0 psf

A Critical Failure Surface Searching Method, Using A Random
Technique For Generating Circular Surfaces, Has Been Specified.

300 Trial Surfaces Have Been Generated.

30 Surfaces Initiate From Each Of 10 Points Equally Spaced
Along The Ground Surface Between X = .00 ft.
and X = 59.00 ft.

Each Surface Terminates Between X = 121.00 ft.
and X = 180.00 ft.

Unless Further Limitations Were Imposed, The Minimum Elevation
At Which A Surface Extends Is Y = .00 ft.

10.00 ft. Line Segments Define Each Trial Failure Surface.

Following Are Displayed The Ten Most Critical Of The Trial
Failure Surfaces Examined. They Are Ordered - Most Critical
First.

* * Safety Factors Are Calculated By The Modified Bishop Method * *

Failure Surface Specified By 17 Coordinate Points

Point No.	X-Surf (ft)	Y-Surf (ft)
1	6.56	100.00
2	15.40	85.32
3	27.29	81.57
4	27.69	81.25
5	34.23	88.65
6	37.03	82.06
7	37.34	87.60
8	54.31	86.88
9	54.88	85.98
10	63.08	85.92
11	63.22	85.95
12	63.27	86.35
13	83.47	88.35
14	83.37	87.15
15	83.37	87.87
16	102.67	87.24
17	111.57	89.40
18	119.69	104.80
19	127.84	110.87
20	135.10	117.87
21	141.84	125.43
22	144.89	130.00

Circle Center At X = 56.9 ; Y = 189.7 and Radius, 102.8

*** 1.001 ***

Individual data on the 19 slices

Slice No.	Width Ft(m)	Weight Lbs(kg)	Water Force Top Lbs(kg)	Water Force Bot Lbs(kg)	Tie Force Norm Lbs(kg)	Tie Force Tan Lbs(kg)	Earthquake Force Hor Lbs(kg)	Earthquake Force Ver Lbs(kg)	Surcharge Load Lbs(kg)
1	8.3	2388.3	.0	1384.0	.0	.0	1127.2	.0	.0
2	8.3	5010.3	.0	3802.2	.0	.0	3265.2	.0	.0
3	6.7	10843.8	.0	5848.5	.0	.0	5096.6	.0	.0
4	6.8	13958.2	.0	7208.7	.0	.0	6219.9	.0	.0
5	7.7	15087.3	.0	7609.3	.0	.0	6785.0	.0	.0
6	10.0	15867.6	.0	7771.5	.0	.0	7108.4	.0	.0
7	7.7	8922.7	.0	4249.5	.0	.0	3408.9	.0	.0
8	7.3	7325.6	.0	3783.0	.0	.0	3287.9	.0	.0
9	6.9	20180.8	.0	7895.4	.0	.0	11116.4	.0	.0
10	6.8	23631.1	.0	6832.7	.0	.0	11998.3	.0	.0
11	6.3	25358.1	.0	3721.7	.0	.0	12339.2	.0	.0
12	6.2	25867.2	.0	2774.2	.0	.0	12437.8	.0	.0
13	7.7	12201.6	.0	381.5	.0	.0	5928.9	.0	.0
14	4.7	12327.7	.0	.0	.0	.0	5720.4	.0	.0
15	4.3	12274.3	.0	.0	.0	.0	10406.8	.0	.0
16	8.2	22142.2	.0	.0	.0	.0	475.2	.0	.0
17	.2	1011.8	.0	.0	.0	.0	7327.2	.0	.0
18	7.2	16016.0	.0	.0	.0	.0	4967.3	.0	.0
19	7.0	9845.8	.0	.0	.0	.0	1506.3	.0	.0
20	6.2	3205.0	.0	.0	.0	.0	2.6	.0	.0
21	.2	5.5	.0	.0	.0	.0			

Failure Surface Specified By 17 Coordinate Points

Point No.	X-Surf (ft)	Y-Surf (ft)
1	6.56	100.00
2	15.40	85.32
3	27.29	81.57
4	27.69	81.25
5	34.23	88.65
6	37.03	82.06
7	53.88	85.98
8	53.88	85.98
9	63.08	85.92
10	63.22	85.95
11	63.27	86.35
12	83.47	88.35
13	83.37	87.15
14	83.37	87.87
15	102.67	87.24
16	111.57	89.40
17	119.69	104.80
18	127.84	110.87
19	135.10	117.87
20	141.84	125.43
21	144.89	130.00

Circle Center At X = 59.6 ; Y = 189.9 and Radius, 104.3

*** 1.002 ***

Failure Surface Specified By 18 Coordinate Points

Point No.	X-Surf (ft)	Y-Surf (ft)
1	.00	100.00
2	8.63	85.15
3	17.89	81.10
4	27.38	87.88
5	37.08	85.32
6	46.89	87.02
7	56.87	83.44
8	66.93	83.73
9	76.87	87.81
10	86.69	86.87
11	96.23	89.90
12	105.48	93.69
13	114.38	98.62
14	122.82	103.59
15	130.76	109.67
16	138.13	116.44
17	144.89	123.83
18	149.54	130.00

Circle Center At X = 58.6 ; Y = 195.4 and Radius, 112.0

*** 1.003 ***

Failure Surface Specified By 17 Coordinate Points

Point No.	X-Surf (ft)	Y-Surf (ft)
1	.00	100.00
2	8.82	95.29
3	18.05	91.75
4	29.61	88.35
5	37.31	85.55
6	47.39	85.76
7	57.40	85.71
8	67.35	85.31
9	77.15	88.16
10	86.75	88.95
11	95.07	91.35
12	104.93	93.97
13	113.33	97.52
14	121.77	101.82
15	129.17	107.80
16	132.87	112.40
17	138.10	130.00

Circle Center At X = 53.1 ; Y = 188.8 and Radius, 103.4

*** 1.003 ***

Failure Surface Specified By 15 Coordinate Points

Point No.	X-Surf (ft)	Y-Surf (ft)
1	13.11	100.00
2	22.16	95.74
3	31.60	92.45
4	41.34	90.18
5	51.26	88.95
6	61.28	88.77
7	71.22	89.65
8	81.04	91.57
9	90.56	94.52
10	99.78	98.47
11	108.51	103.36
12	116.66	109.14
13	124.17	115.75
14	130.93	123.12
15	136.02	130.00

Circle Center At X = 57.9 ; Y = 183.4 and Radius, 94.6

*** 1.005 ***

Failure Surface Specified By 17 Coordinate Points

Point No.	X-Surf (ft)	Y-Surf (ft)
1	.00	100.00
2	8.83	95.31
3	18.09	91.52
4	27.67	88.65
5	37.48	86.74
6	47.44	85.80
7	57.44	85.84
8	67.38	86.82
9	77.18	88.86
10	86.74	91.81
11	95.96	95.68
12	104.75	100.44
13	113.04	106.05
14	120.73	112.43
15	127.76	119.55
16	131.05	127.32
17	135.82	130.00

Circle Center At X = 52.0 ; Y = 187.4 and Radius, 101.7

*** 1.006 ***

Failure Surface Specified By 16 Coordinate Points

Point No.	X-Surf (ft)	Y-Surf (ft)
1	13.11	100.00
2	21.96	95.32
3	31.26	91.22
4	40.80	88.00
5	50.77	87.70
6	60.76	86.87
7	70.72	87.42
8	80.61	89.04
9	90.34	91.73
10	99.53	95.42
11	108.37	100.06
12	116.68	105.70
13	124.38	112.29
14	131.18	119.41
15	137.22	127.35
16	138.85	130.00

Circle Center At X = 60.6 ; Y = 179.3 and Radius, 92.5

*** 1.006 ***

Failure Surface Specified By 15 Coordinate Points

Point No.	X-Surf (ft)	Y-Surf (ft)
1	19.67	100.00
2	28.73	95.26
3	38.19	92.54
4	47.95	90.37
5	57.86	89.27
6	67.86	89.26
7	77.83	90.34
8	87.60	92.50
9	97.07	95.71
10	106.14	99.63
11	114.69	105.11
12	123.62	111.19
13	132.85	118.10
14	142.28	125.76
15	139.11	130.00

Circle Center At X = 63.0 ; Y = 180.8 and Radius, 91.7

*** 1.008 ***

Failure Surface Specified By 19 Coordinate Points

Point No.	X-Surf (ft)	Y-Surf (ft)
1	.00	100.00
2	8.65	94.98
3	17.70	90.73
4	27.10	87.30
5	36.75	84.66
6	46.60	82.99
7	56.57	82.17
8	66.57	82.16
9	76.53	83.07
10	86.37	84.85
11	96.01	87.50
12	105.39	90.98
13	114.22	95.29
14	123.03	100.35
15	131.17	106.19
16	138.77	112.67
17	145.76	119.82
18	152.09	127.55
19	153.76	130.00

Circle Center At X = 61.2 ; Y = 195.4 and Radius, 113.4

*** 1.010 ***

Failure Surface Specified By 18 Coordinate Points

Point No.	X-Surf (ft)	Y-Surf (ft)
1	6.56	100.00
2	15.82	95.53
3	25.33	91.57
4	34.93	88.14
5	44.57	85.89
6	54.27	84.52
7	63.99	84.06
8	73.65	84.47
9	83.57	85.76
10	93.32	88.00
11	102.87	91.07
12	112.07	94.99
13	120.83	99.72
14	129.20	105.22
15	137.02	111.45
16	144.25	118.36
17	150.83	125.88
18	153.82	130.00

Circle Center At X = 63.9 ; Y = 195.0 and Radius, 110.9

*** 1.011 ***

```
        Y            A     X     I     S            F     T

          .00     28.60     57.20     85.80    114.40    143.00
X     .00 +----------+---------+---------+----*----+----------+
          -                                   1
          -                                 3
          -                                 5
          -                                 8
          -                                 5
    28.60 +                                 3.8
```

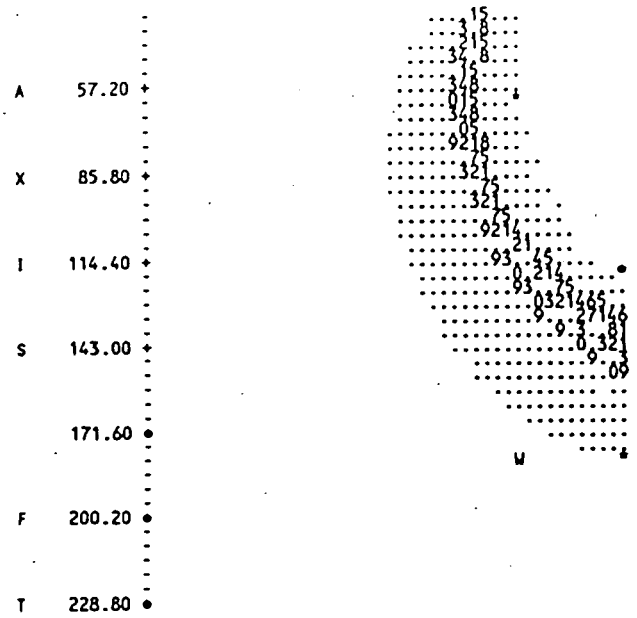
A 57.20
X 85.80
I 114.40
S 143.00
171.60
F 200.20
T 228.80
W

** PCSTABL5M **

by
Purdue University

--Slope Stability Analysis--
Simplified Janbu, Simplified Bishop
or Spencer's Method of Slices

Run Date: 10/06/93
Time of Run: 4:40
Run By: ZLW
Input Data Filename: 1230fll.inl
Output Filename: 1230afl.oul

PROBLEM DESCRIPTION PCSTABL5M : 30 ft, 1:2 slope, FILL, Low. WT

BOUNDARY COORDINATES

3 Top Boundaries
3 Total Boundaries

Boundary No.	X-Left (ft)	Y-Left (ft)	X-Right (ft)	Y-Right (ft)	Soil Type Below Bnd
1	.00	100.00	60.00	100.00	1
2	60.00	100.00	120.00	130.00	1
3	120.00	130.00	180.00	130.00	1

ISOTROPIC SOIL PARAMETERS

1 Type(s) of Soil

Soil Type No.	Total Unit Wt. (pcf)	Saturated Unit Wt. (pcf)	Cohesion Intercept (psf)	Friction Angle (deg)	Pore Pressure Param.	Pressure Constant (psf)	Piez. Surface No.
1	120.0	120.0	1000.0	.0	.00	.0	1

1 PIEZOMETRIC SURFACE(S) HAVE BEEN SPECIFIED

Unit Weight of Water = 62.40

Piezometric Surface No. 1 Specified by 2 Coordinate Points

Point No.	X-Water (ft)	Y-Water (ft)
1	.00	100.00
2	180.00	100.00

A Horizontal Earthquake Loading Coefficient
Of .165 Has Been Assigned

A Vertical Earthquake Loading Coefficient
Of .000 Has Been Assigned

Cavitation Pressure = .0 psf

A Critical Failure Surface Searching Method, Using A Random
Technique For Generating Circular Surfaces, Has Been Specified.

300 Trial Surfaces Have Been Generated.

30 Surfaces Initiate From Each Of 10 Points Equally Spaced
Along The Ground Surface Between X = .00 ft.
and X = 59.00 ft.

Each Surface Terminates Between X = 121.00 ft.
and X = 180.00 ft.

Unless Further Limitations Were Imposed, The Minimum Elevation
At Which A Surface Extends Is Y = .00 ft.

10.00 ft. Line Segments Define Each Trial Failure Surface.

Following Are Displayed The Ten Most Critical Of The Trial
Failure Surfaces Examined. They Are Ordered - Most Critical
First.

** Safety Factors Are Calculated By The Modified Bishop Method **

Failure Surface Specified By 22 Coordinate Points

Point No.	X-Surf (ft)	Y-Surf (ft)
1	6.56	100.00
2	13.68	93.88
3	21.46	87.70
4	29.80	81.18
5	37.63	76.18
6	38.63	76.21
7	47.87	72.66
8	57.37	69.74
9	67.24	67.75
10	77.18	66.71
11	87.18	66.63
12	97.17	67.51
13	106.97	69.33
14	116.59	72.10
15	125.89	75.77
16	134.79	80.31
17	143.22	85.69
18	151.10	91.85
19	158.35	98.74
20	164.90	106.30
21	170.70	114.44
22	175.69	123.11
23	178.83	130.00

Circle Center At X = 83.0 ; Y = 170.6 and Radius, 104.1

*** .994 ***

Individual data on the 24 slices

Width Ft(m)	Weight Lbs(kg)	Water Force Top Lbs(kg)	Water Force Bot Lbs(kg)	Tie Force Norm Lbs(kg)	Tie Force Tan Lbs(kg)	Earthquake Force Hor Lbs(kg)	Earthquake Force Ver Lbs(kg)	Surcharge Load Lbs(kg)
7.1	2886.5	.0	2186.8	.0	.0	494.9	.0	.0
7.8	6470.8	.0	6339.3	.0	.0	1562.7	.0	.0
8.3	16071.9	.0	10021.0	.0	.0	2651.9	.0	.0
8.8	22727.3	.0	13206.6	.0	.0	3900.5	.0	.0
8.2	28188.5	.0	15863.8	.0	.0	4651.1	.0	.0
9.2	33047.8	.0	17828.3	.0	.0	5521.0	.0	.0
2.9	9389.0	.0	4981.9	.0	.0	1376.2	.0	.0
7.0	28932.7	.0	12718.9	.0	.0	4773.6	.0	.0
6.6	26361.6	.0	10446.3	.0	.0	5624.6	.0	.0
7.7	53301.3	.0	20707.0	.0	.0	8797.7	.0	.0
10.0	58588.6	.0	20549.4	.0	.0	8667.2	.0	.0
9.8	62067.4	.0	18705.7	.0	.0	10241.1	.0	.0
9.6	63634.5	.0	18673.8	.0	.0	10499.7	.0	.0
3.4	23100.1	.0	6837.5	.0	.0	3811.5	.0	.0
5.9	39133.9	.0	10029.3	.0	.0	6757.3	.0	.0
8.7	52232.2	.0	13703.2	.0	.0	8165.7	.0	.0
8.4	47623.8	.0	10606.7	.0	.0	7873.7	.0	.0
7.3	38692.2	.0	7003.8	.0	.0	6228.8	.0	.0
7.2	30183.1	.0	2933.6	.0	.0	4980.2	.0	.0
1.1	4008.3	.0	65.2	.0	.0	661.4	.0	.0
5.5	17603.3	.0	.0	.0	.0	2904.9	.0	.0
5.8	13663.0	.0	.0	.0	.0	2254.2	.0	.0
5.0	6722.8	.0	.0	.0	.0	1109.6	.0	.0
3.1	1295.9	.0	.0	.0	.0	213.8	.0	.0

Failure Surface Specified By 23 Coordinate Points

Point No.	X-Surf (ft)	Y-Surf (ft)
1	.00	100.00
2	7.35	93.22
3	15.27	87.11
4	23.71	81.75
5	32.59	77.18
6	41.85	73.38
7	51.41	70.42
8	61.19	68.38
9	71.12	67.18
10	81.15	66.90
11	91.10	67.51
12	100.99	69.00
13	110.70	71.37
14	120.17	74.67
15	128.30	78.67
16	136.04	83.34
17	142.30	88.17
18	147.03	93.22
19	151.16	102.53
20	157.93	110.15
21	173.40	118.32
22	178.41	126.07
23	179.82	130.00

Circle Center At X = 79.4 ; Y = 178.6 and Radius, 111.7

*** .995 ***

Failure Surface Specified By 23 Coordinate Points

Point No.	X-Surf (ft)	Y-Surf (ft)
1	.00	100.00
2	7.64	93.10
3	15.08	86.89
4	23.58	81.43
5	32.30	76.76
6	41.53	72.92
7	51.08	69.92
8	60.86	67.85
9	70.79	66.66

10	80.78	66.39
11	90.76	67.03
12	100.64	69.52
13	110.33	71.03
14	118.76	74.38
15	126.84	78.52
16	137.31	83.39
17	143.67	86.33
18	153.28	95.85
19	160.26	102.29
20	166.55	110.76
21	172.10	119.08
22	176.87	127.87
23	177.78	130.00

Circle Center At X = 78.8 ; Y = 175.4 and Radius, 109.0

*** .997 ***

Failure Surface Specified By 22 Coordinate Points

Point No.	X-Surf (ft)	Y-Surf (ft)
1	6.56	100.00
2	13.78	93.09
3	21.15	87.91
4	30.03	85.50
5	38.89	84.92
6	48.23	84.20
7	59.23	83.38
8	67.87	80.78
9	77.64	80.57
10	87.60	81.55
11	97.90	80.50
12	107.37	80.40
13	116.26	77.33
14	124.24	76.62
15	133.13	81.55
16	143.53	89.96
17	151.38	93.15
18	158.61	100.07
19	165.15	107.63
20	170.93	115.76
21	175.92	124.17
22	178.44	130.00

Circle Center At X = 82.5 ; Y = 172.2 and Radius, 104.8

*** .999 ***

Failure Surface Specified By 22 Coordinate Points

Point No.	X-Surf (ft)	Y-Surf (ft)
1	6.56	100.00
2	13.63	93.03
3	21.38	86.57
4	29.68	81.07
5	38.30	76.35
6	47.75	72.52
7	57.43	69.32
8	67.14	69.64
9	77.09	67.71
10	87.09	66.75
11	97.04	67.80
12	106.84	69.78
13	116.40	69.79
14	125.62	72.73
15	137.51	76.60
16	143.70	81.35
17	150.39	86.85
18	157.42	83.34
19	163.75	100.75
20	168.25	108.32
21	173.87	116.58
22	175.72	125.79
		130.00

Circle Center At X = 81.7 ; Y = 168.0 and Radius, 101.4

*** 1.003 ***

Failure Surface Specified By 22 Coordinate Points

Point No.	X-Surf (ft)	Y-Surf (ft)
1	.00	100.00
2	7.38	93.23
3	15.32	87.17
4	23.80	81.87
5	32.72	77.37
6	42.03	73.71
7	51.63	70.92
8	61.45	69.05
9	71.40	68.02
10	81.40	67.87
11	91.37	68.83
12	101.31	70.60
13	110.85	73.86
14	120.50	76.80
15	129.18	81.19
16	137.73	86.38

17	145.76	92.34
18	153.21	99.01
19	160.05	106.34
20	166.15	113.29
21	171.47	122.03
22	175.19	130.00

Circle Center At X = 77.1 ; Y = 176.4 and Radius, 108.5

*** 1.015 ***

Failure Surface Specified By 20 Coordinate Points

Point No.	X-Surf (ft)	Y-Surf (ft)
1	26.22	100.00
2	33.47	92.97
3	41.13	85.76
4	46.47	81.44
5	53.27	77.08
6	58.03	73.72
7	68.08	71.41
8	77.78	71.41
9	87.71	70.18
10	87.71	70.03
11	107.67	70.98
12	117.66	73.00
13	126.87	76.09
14	136.09	80.19
15	144.71	85.26
16	153.72	91.52
17	162.06	98.42
18	160.04	98.06
19	172.57	105.64
20	179.89	113.88
	176.65	122.70
	179.89	130.00

Circle Center At X = 94.0 ; Y = 161.4 and Radius, 91.5

*** 1.018 ***

Failure Surface Specified By 20 Coordinate Points

Point No.	X-Surf (ft)	Y-Surf (ft)
1	26.22	100.00
2	33.58	93.53
3	41.82	87.59
4	50.25	82.23
5	59.37	78.12
6	68.87	75.01
7	78.65	72.93
8	88.60	71.90
9	98.60	71.94
10	108.54	73.04
11	118.31	75.20
12	127.79	78.38
13	136.87	82.56
14	145.46	87.68
15	153.49	93.68
16	160.77	100.51
17	167.31	108.07
18	173.01	116.29
19	177.80	125.06
20	179.84	130.00

Circle Center At X = 93.2 ; Y = 165.4 and Radius, 93.6

*** 1.024 ***

Failure Surface Specified By 20 Coordinate Points

Point No.	X-Surf (ft)	Y-Surf (ft)
1	19.67	100.00
2	27.08	93.29
3	35.12	87.37
4	43.78	82.33
5	52.89	78.20
6	62.37	75.04
7	72.17	72.88
8	82.13	71.74
9	92.07	71.63
10	102.03	72.59
11	111.82	74.51
12	121.39	77.77
13	130.58	81.40
14	139.32	86.32
15	147.51	89.60
16	155.01	92.00
17	161.86	95.55
18	167.80	105.85
19	172.73	113.83
20	176.73	122.96
		130.00

Circle Center At X = 88.1 ; Y = 168.0 and Radius, 96.5

*** 1.027 ***

Failure Surface Specified By 21 Coordinate Points

Point No.	X-Surf (ft)	Y-Surf (ft)
1	13.11	100.00
2	20.21	92.86
3	28.02	86.71
4	36.46	81.65
5	45.41	77.77
6	54.81	75.07
7	64.55	73.66
8	74.45	73.70
9	84.36	75.21
10	94.39	78.20
11	104.26	82.05
12	113.79	87.62
13	122.99	94.85
14	131.73	103.65
15	139.89	113.50
16	147.38	124.13
17	154.12	135.45
18	160.02	147.39
19	165.03	159.84
20	169.07	172.39
21	169.27	185.00

Circle Center At X = 82.1 ; Y = 162.4 and Radius, 93.0

*** 1.037 ***

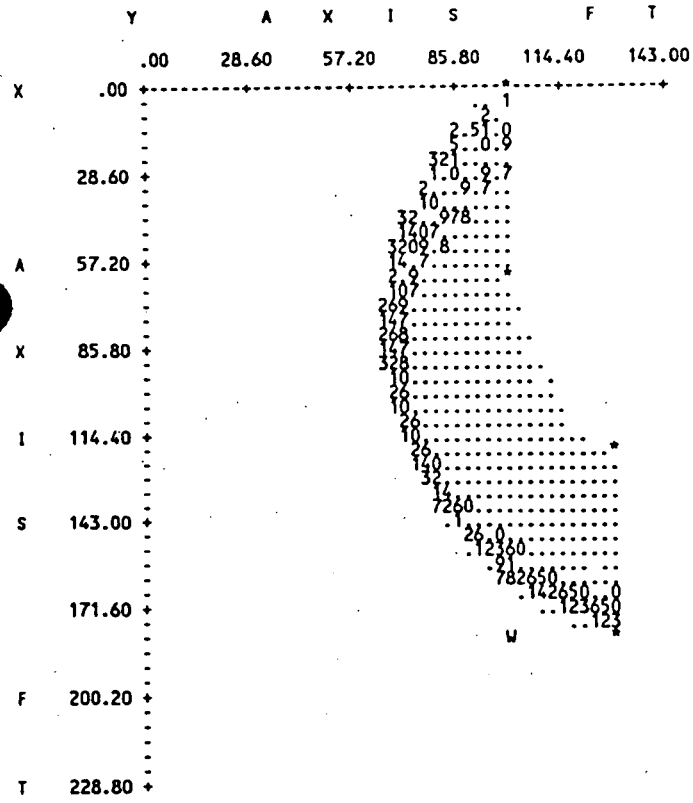

** PCSTABL5M **

by
Purdue University

--Slope Stability Analysis--
Simplified Janbu, Simplified Bishop
or Spencer's Method of Slices

Run Date: 10/06/93
Time of Run: 4:40
Run By: ZLW
Input Data Filename: 1230csl.in1
Output Filename: 1230csl.out

PROBLEM DESCRIPTION PCSTABL5M : 30 ft, 1:2 slope, CLAYSTONE, L. WT

BOUNDARY COORDINATES

3 Top Boundaries
3 Total Boundaries

Boundary No.	X-Left (ft)	Y-Left (ft)	X-Right (ft)	Y-Right (ft)	Soil Type Below Bnd
1	.00	100.00	60.00	100.00	1
2	60.00	100.00	120.00	130.00	1
3	120.00	130.00	180.00	130.00	1

ISOTROPIC SOIL PARAMETERS

1 Type(s) of Soil

Soil Type No.	Total Unit Wt. (pcf)	Saturated Unit Wt. (pcf)	Cohesion Intercept (psf)	Friction Angle (deg)	Pore Pressure Param.	Pressure Constant (psf)	Piez. Surface No.
1	120.0	120.0	1000.0	20.0	.00	.0	1

1 PIEZOMETRIC SURFACE(S) HAVE BEEN SPECIFIED

Unit Weight of Water = 62.40

Piezometric Surface No. 1 Specified by 2 Coordinate Points

Point No.	X-Water (ft)	Y-Water (ft)
1	.00	100.00
2	180.00	100.00

A Horizontal Earthquake Loading Coefficient
Of .505 Has Been Assigned

A Vertical Earthquake Loading Coefficient
Of .000 Has Been Assigned

Cavitation Pressure = .0 psf

A Critical Failure Surface Searching Method, Using A Random
Technique For Generating Circular Surfaces, Has Been Specified.

300 Trial Surfaces Have Been Generated.

30 Surfaces Initiate From Each Of 10 Points Equally Spaced
Along The Ground Surface Between X = .00 ft.
and X = 59.00 ft.

Each Surface Terminates Between X = 121.00 ft.
and X = 180.00 ft.

Unless Further Limitations Were Imposed, The Minimum Elevation
At Which A Surface Extends Is Y = .00 ft.

10.00 ft. Line Segments Define Each Trial Failure Surface.

Following Are Displayed The Ten Most Critical Of The Trial
Failure Surfaces Examined. They Are Ordered - Most Critical
First.

** Safety Factors Are Calculated By The Modified Bishop Method **

Failure Surface Specified By 23 Coordinate Points

Point No.	X-Surf (ft)	Y-Surf (ft)
1	.00	100.00
2	7.35	93.22
3	15.27	87.11
4	23.71	81.72
5	32.59	77.10
6	41.85	73.38
7	51.41	70.74
8	61.19	69.38
9	71.15	69.40
10	81.12	70.80
11	91.10	73.51
12	100.99	77.00
13	110.70	81.37
14	120.17	86.61
15	129.30	92.67
16	138.04	99.51
17	146.30	107.17
18	154.03	115.52
19	161.16	124.53
20	167.63	134.15
21	173.40	144.32
22	178.41	154.97
23	179.82	156.00

Circle Center At X = 79.4 ; Y = 178.6 and Radius, 111.7

*** 1.003 ***

Individual data on the 25 slices

ice o.	Width Ft(m)	Weight Lbs(kg)	Water Force Top Lbs(kg)	Water Force Bot Lbs(kg)	Tie Force Norm Lbs(kg)	Tie Force Tan Lbs(kg)	Earthquake Force Hor Lbs(kg)	Earthquake Force Ver Lbs(kg)	Surcharge Load Lbs(kg)
1	7.3	2800.5	.0	2119.1	.0	.0	1510.5	.0	.0
2	7.8	6351.2	.0	6137.1	.0	.0	4726.5	.0	.0
3	7.7	12321.9	.0	9131.1	.0	.0	7926.2	.0	.0
4	8.4	15763.7	.0	9615.0	.0	.0	9760.7	.0	.0
5	8.9	21905.6	.0	12822.0	.0	.0	11062.3	.0	.0
6	9.3	27479.3	.0	15433.9	.0	.0	13877.2	.0	.0
7	9.6	32522.3	.0	17527.2	.0	.0	16272.3	.0	.0
8	8.6	31399.7	.0	16888.4	.0	.0	15856.8	.0	.0
9	1.2	4557.3	.0	2309.4	.0	.0	2301.5	.0	.0
0	9.9	42055.8	.0	20102.2	.0	.0	21236.2	.0	.0
1	10.0	49195.3	.0	20552.3	.0	.0	24843.8	.0	.0
2	10.0	54920.7	.0	20464.2	.0	.0	27734.9	.0	.0
3	9.9	59051.3	.0	19809.5	.0	.0	29820.9	.0	.0
4	9.7	61473.8	.0	18902.6	.0	.0	31044.3	.0	.0
5	9.3	61036.9	.0	16572.4	.0	.0	30823.6	.0	.0
6	.2	1107.0	.0	279.0	.0	.0	559.0	.0	.0
7	9.1	58497.5	.0	14576.0	.0	.0	29541.2	.0	.0
8	8.7	51251.2	.0	11788.6	.0	.0	25881.8	.0	.0
9	8.3	43285.8	.0	8513.6	.0	.0	21859.3	.0	.0
0	7.7	34921.8	.0	4777.3	.0	.0	17635.5	.0	.0
1	4.6	17634.9	.0	894.1	.0	.0	8905.5	.0	.0
2	2.6	8827.7	.0	.0	.0	.0	4778.2	.0	.0
3	6.5	18380.2	.0	.0	.0	.0	9282.0	.0	.0
4	5.8	10907.4	.0	.0	.0	.0	5508.2	.0	.0
5	5.0	4421.9	.0	.0	.0	.0	2233.0	.0	.0
6	1.4	255.5	.0	.0	.0	.0	129.0	.0	.0

Failure Surface Specified By 23 Coordinate Points

Point No.	X-Surf (ft)	Y-Surf (ft)
1	.00	100.00
2	7.94	93.10
3	15.08	86.89
4	23.36	81.33
5	32.30	76.76
6	41.53	73.02
7	51.08	69.97
8	60.88	67.85
9	70.79	66.66
10	80.78	66.39
11	90.76	67.03
12	100.64	68.56
13	110.33	71.05
14	119.76	74.38
15	128.84	78.56
16	137.51	83.58
17	145.67	89.33
18	153.28	95.82
19	160.28	102.99
20	166.55	110.76
21	172.10	119.08
22	176.87	127.89
23	177.78	130.00

Circle Center At X = 78.8 ; Y = 175.4 and Radius, 109.0

*** 1.009 ***

Failure Surface Specified By 22 Coordinate Points

Point No.	X-Surf (ft)	Y-Surf (ft)
1	.00	100.00
2	7.39	93.23
3	15.35	87.17
4	23.80	81.87
5	32.72	77.37
6	42.03	73.71
7	51.63	70.92

8	61.45	69.02
9	71.70	68.04
10	81.70	67.07
11	91.37	66.83
12	101.21	70.60
13	110.85	73.26
14	120.20	76.80
15	128.19	81.19
16	135.73	86.38
17	143.70	89.37
18	153.21	96.01
19	160.02	102.34
20	169.16	113.26
21	171.17	127.71
22	175.19	130.00

Circle Center At X = 77.1 ; Y = 176.4 and Radius, 108.5

*** 1.013 ***

Failure Surface Specified By 22 Coordinate Points

Point No.	X-Surf (ft)	Y-Surf (ft)
1	.00	100.00
2	7.77	93.70
3	16.06	88.11
4	24.81	83.28
5	33.99	79.27
6	43.43	76.03
7	53.15	73.69
8	63.04	72.17
9	73.02	71.56
10	83.01	71.87
11	92.95	73.00
12	102.74	75.03
13	112.31	77.92
14	121.50	81.65
15	130.50	86.19
16	138.98	91.29
17	146.95	97.53
18	152.32	104.25
19	157.36	111.60
20	161.14	119.52
21	167.23	127.95
22	173.69	130.00

Circle Center At X = 74.9 ; Y = 184.3 and Radius, 112.7

*** 1.014 ***

Failure Surface Specified By 22 Coordinate Points

Point No.	X-Surf (ft)	Y-Surf (ft)
1	6.56	100.00
2	13.78	93.09
3	21.65	86.91
4	30.06	81.50
5	38.95	76.92
6	48.23	73.20
7	57.82	70.38
8	67.64	68.49
9	77.60	67.57
10	87.60	67.55
11	97.55	68.50
12	107.37	70.40
13	116.96	73.23
14	126.27	76.95
15	135.13	81.55
16	143.53	86.96
17	151.38	93.15
18	158.61	100.07
19	165.15	107.63
20	170.93	115.79
21	175.92	124.46
22	178.44	130.00

Circle Center At X = 82.5 ; Y = 172.2 and Radius, 104.8

*** 1.021 ***

Failure Surface Specified By 22 Coordinate Points

Point No.	X-Surf (ft)	Y-Surf (ft)
1	6.56	100.00
2	13.78	93.09
3	21.66	86.70
4	30.80	81.78
5	40.63	79.29
6	50.87	79.69
7	61.34	82.44
8	71.74	87.73
9	82.18	96.71
10	92.18	99.83
11	102.14	97.51
12	111.97	92.33
13	121.56	84.10
14	130.82	73.77
15	134.79	80.31

16	143.22	85.69
17	151.10	91.85
18	158.35	98.72
19	164.90	106.30
20	170.70	114.44
21	175.69	123.11
22	178.83	130.00

Circle Center At X = 83.0 ; Y = 170.6 and Radius, 104.1

*** 1.023 ***

Failure Surface Specified By 21 Coordinate Points

Point No.	X-Surf (ft)	Y-Surf (ft)
1	13.11	100.00
2	20.12	92.00
3	26.64	88.75
4	38.37	82.26
5	47.88	80.63
6	57.48	77.83
7	67.38	75.67
8	77.57	74.87
9	87.54	74.74
10	97.21	75.50
11	107.07	77.15
12	116.14	79.60
13	126.15	83.08
14	135.21	87.31
15	143.86	92.33
16	152.02	98.11
17	159.63	104.69
18	168.83	111.74
19	172.05	119.49
20	178.56	127.77
21	179.79	130.00

Circle Center At X = 83.7 ; Y = 185.9 and Radius, 111.2

*** 1.024 ***

Failure Surface Specified By 21 Coordinate Points

Point No.	X-Surf (ft)	Y-Surf (ft)
1	6.56	100.00
2	13.67	93.63
3	22.34	88.01
4	31.30	83.18
5	40.47	79.20
6	49.97	76.08
7	59.72	73.87
8	69.64	72.58
9	79.63	72.22
10	89.61	72.78
11	99.50	74.29
12	109.20	76.70
13	118.64	80.02
14	127.73	84.16
15	136.38	89.20
16	144.53	95.09
17	152.11	101.52
18	159.04	108.73
19	165.27	116.55
20	170.74	124.92
21	173.42	130.00

Circle Center At X = 78.5 ; Y = 179.3 and Radius, 107.0

*** 1.026 ***

Failure Surface Specified By 22 Coordinate Points

Point No.	X-Surf (ft)	Y-Surf (ft)
1	.00	100.00
2	7.28	93.15
3	15.20	87.03
4	23.69	81.71
5	32.60	77.22
6	41.83	73.62
7	51.56	70.93
8	61.71	69.18
9	71.37	68.40
10	81.37	68.58
11	91.31	69.72
12	101.09	71.81
13	110.62	74.83
14	118.81	78.76
15	126.59	83.56
16	136.86	89.18
17	144.23	95.57
18	151.50	102.68
19	157.91	110.43
20	163.45	118.75
21	168.17	127.57
22	169.18	130.00

Circle Center At X = 74.5 ; Y = 171.9 and Radius, 103.5

*** 1.029 ***

Failure Surface Specified By 21 Coordinate Points

Point No.	X-Surf (ft)	Y-Surf (ft)
1	.00	100.00
2	8.28	97.39
3	16.68	89.78
4	25.08	85.30
5	33.49	81.88
6	41.92	79.57
7	50.35	77.41
8	58.80	76.38
9	67.26	76.18
10	75.72	76.78
11	84.17	78.23
12	92.62	80.56
13	101.05	83.50
14	109.47	87.30
15	117.88	91.85
16	126.28	97.11
17	134.67	103.06
18	143.04	109.64
19	151.39	116.82
20	159.72	124.54
21	173.36	130.00

Circle Center At X = 72.4 ; Y = 197.9 and Radius, 121.8

*** 1.029 ***

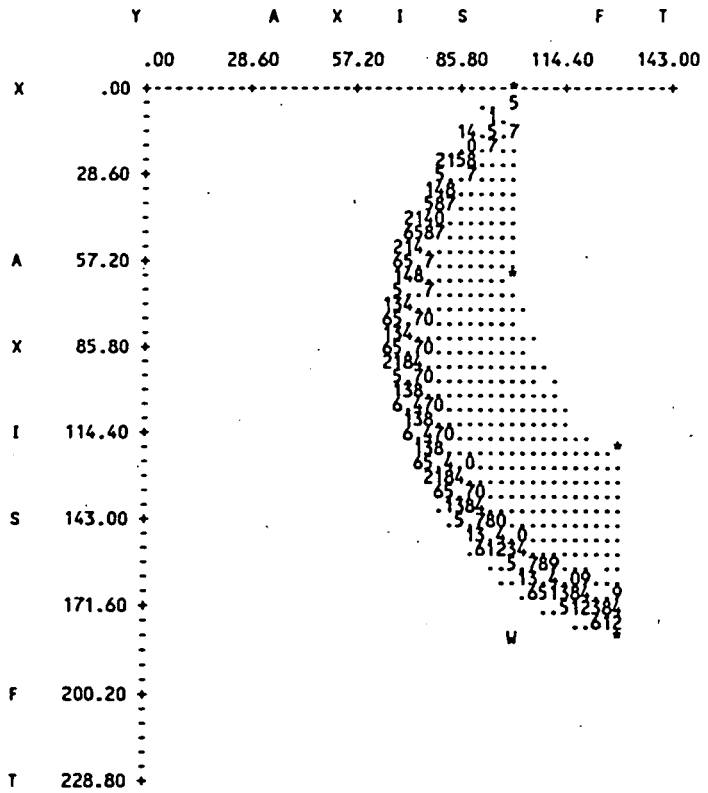

** PCSTABL5M **

by
Purdue University

--Slope Stability Analysis--
Simplified Janbu, Simplified Bishop
or Spencer's Method of Slices

Run Date: 10/06/93
Time of Run: 4:40
Run By: ZLW
Input Data Filename: 1220alh.in1
Output Filename: 1220alh.out

PROBLEM DESCRIPTION PCSTABL5M : 20 ft, 1:2 slope, ALLUVIUM 1
, H. WT

BOUNDARY COORDINATES

3 Top Boundaries
3 Total Boundaries

Boundary No.	X-Left (ft)	Y-Left (ft)	X-Right (ft)	Y-Right (ft)	Soil Type Below Bnd
1	.00	100.00	60.00	100.00	1
2	60.00	100.00	100.00	120.00	1
3	100.00	120.00	180.00	120.00	1

ISOTROPIC SOIL PARAMETERS

1 Type(s) of Soil

Soil Type No.	Total Unit Wt. (pcf)	Saturated Unit Wt. (pcf)	Cohesion Intercept (psf)	Friction Angle (deg)	Pore Pressure Param.	Pressure Constant (psf)	Piez. Surface No.
1	120.0	120.0	.0	45.0	.00	.0	1

1 PIEZOMETRIC SURFACE(S) HAVE BEEN SPECIFIED

Unit Weight of Water = 62.40

Piezometric Surface No. 1 Specified by 4 Coordinate Points

Point No.	X-Water (ft)	Y-Water (ft)
1	.00	100.00
2	60.00	100.00
3	80.00	110.00
4	180.00	110.00

A Horizontal Earthquake Loading Coefficient
Of .330 Has Been Assigned

A Vertical Earthquake Loading Coefficient
Of .000 Has Been Assigned

Cavitation Pressure = .0 psf

A Critical Failure Surface Searching Method, Using A Random
Technique For Generating Circular Surfaces, Has Been Specified.

300 Trial Surfaces Have Been Generated.

30 Surfaces Initiate From Each Of 10 Points Equally Spaced
Along The Ground Surface Between X = .00 ft.
and X = 59.00 ft.

Each Surface Terminates Between X = 121.00 ft.
and X = 180.00 ft.

Unless Further Limitations Were Imposed, The Minimum Elevation
At Which A Surface Extends Is Y = .00 ft.

10.00 ft. Line Segments Define Each Trial Failure Surface.

Following Are Displayed The Ten Most Critical Of The Trial
Failure Surfaces Examined. They Are Ordered - Most Critical
First.

* * Safety Factors Are Calculated By The Modified Bishop Method * *

Failure Surface Specified By 12 Coordinate Points

Point No.	X-Surf (ft)	Y-Surf (ft)
1	26.22	100.00
2	26.05	99.15
3	26.00	97.65
4	26.00	96.15
5	62.27	97.65
6	62.86	99.15
7	82.58	101.47
8	92.07	104.63
9	104.26	108.38
10	113.08	113.28
11	121.47	118.72
12	123.12	120.00

Circle Center At X = 53.1 ; Y = 214.7 and Radius, 117.8

*** .990 ***

Individual data on the 15 slices

Slice No.	Width Ft(m)	Weight Lbs(kg)	Water Force Top Lbs(kg)	Water Force Bot Lbs(kg)	Tie Force Norm Lbs(kg)	Tie Force Tan Lbs(kg)	Earthquake Force Hor Lbs(kg)	Earthquake Force Ver Lbs(kg)	Surcharge Load Lbs(kg)
1	6.8	1085.8	.0	759.1	.0	.0	361.3	.0	.0
2	6.8	2825.8	.0	1777.1	.0	.0	892.5	.0	.0
3	10.0	5552.9	.0	3450.1	.0	.0	1773.9	.0	.0
4	2.0	3702.2	.0	2330.8	.0	.0	1162.7	.0	.0
5	2.0	3396.6	.0	1730.1	.0	.0	865.6	.0	.0
6	8.8	8769.0	.0	3870.9	.0	.0	2263.7	.0	.0
7	7.1	8402.3	.0	3377.8	.0	.0	2177.5	.0	.0
8	5.1	7040.3	.0	2633.6	.0	.0	1531.7	.0	.0
9	3.6	7093.7	.0	2332.7	.0	.0	1340.7	.0	.0
10	9.5	13700.8	.0	4336.4	.0	.0	2550.7	.0	.0
11	4.2	7740.3	.0	1432.3	.0	.0	522.0	.0	.0
12	3.3	6302.4	.0	676.1	.0	.0	5023.3	.0	.0
13	2.7	3430.3	.0	134.4	.0	.0	2912.8	.0	.0
14	6.2	6171.0	.0	.0	.0	.0	1132.0	.0	.0
15	8.4	4023.8	.0	.0	.0	.0	2036.4	.0	.0
	1.6	126.1	.0	.0	.0	.0	1327.9	.0	.0

Failure Surface Specified By 9 Coordinate Points

Point No.	X-Surf (ft)	Y-Surf (ft)
1	52.44	100.00
2	62.31	97.85
3	72.19	97.19
4	82.15	98.02
5	91.88	100.33
6	101.19	104.08
7	109.77	109.19
8	117.52	115.47
9	121.64	120.00

Circle Center At X = 71.6 ; Y = 163.9 and Radius, 66.8

*** .999 ***

1

Failure Surface Specified By 11 Coordinate Points

Point No.	X-Surf (ft)	Y-Surf (ft)
1	32.78	100.00
2	42.17	96.57
3	51.92	94.36
4	61.88	93.40
5	71.87	93.70
6	81.75	95.27
7	91.35	98.07
8	100.52	102.06
9	109.11	107.18
10	117.08	113.35
11	123.55	120.00

Circle Center At X = 64.5 ; Y = 172.3 and Radius, 78.9

*** 1.003 ***

Failure Surface Specified By 13 Coordinate Points

Point No.	X-Surf (ft)	Y-Surf (ft)
1	19.67	100.00
2	29.53	97.07
3	39.02	95.04
4	48.86	93.93
5	58.86	93.75
6	68.83	94.50
7	78.72	96.17
8	88.43	98.75
9	97.83	102.27
10	106.85	106.54
11	115.42	111.68
12	123.49	117.58
13	126.20	120.00

Circle Center At X = 55.9 ; Y = 201.2 and Radius, 107.5

*** 1.022 ***

Failure Surface Specified By 13 Coordinate Points

Point No.	X-Surf (ft)	Y-Surf (ft)
1	19.67	100.00
2	26.00	99.40
3	38.66	63.84
4	48.55	62.37
5	58.57	61.02
6	68.53	62.56
7	78.36	64.33
8	87.69	67.14
9	97.20	100.97
10	105.97	105.78
11	113.16	111.52
12	121.68	118.10
13	123.42	120.00

Circle Center At X = 57.4 ; Y = 183.9 and Radius, 92.0

*** 1.024 ***

Failure Surface Specified By 10 Coordinate Points

Point No.	X-Surf (ft)	Y-Surf (ft)
1	45.89	100.00
2	52.85	98.82
3	65.86	68.64
4	75.79	69.40
5	85.64	101.12
6	95.28	103.77
7	104.62	107.34
8	113.58	111.79
9	122.07	117.08
10	125.87	120.00

Circle Center At X = 62.9 ; Y = 201.8 and Radius, 103.2

*** 1.028 ***

Failure Surface Specified By 10 Coordinate Points

Point No.	X-Surf (ft)	Y-Surf (ft)
1	45.89	100.00
2	52.91	98.92
3	65.71	68.34
4	75.69	67.38
5	85.96	67.12
6	95.52	69.18
7	104.59	101.69
8	113.47	105.27
9	121.79	109.86
10	127.27	115.41
		120.00

Circle Center At X = 67.6 ; Y = 187.3 and Radius, 89.9

*** 1.033 ***

Failure Surface Specified By 10 Coordinate Points

Point No.	X-Surf (ft)	Y-Surf (ft)
1	45.89	100.00
2	52.92	98.95
3	65.73	67.75
4	75.75	68.50
5	85.64	68.70
6	95.29	102.23
7	104.64	105.76
8	113.58	110.25
9	121.99	115.88
10	127.40	120.00

Circle Center At X = 66.5 ; Y = 192.3 and Radius, 94.6

*** 1.036 ***

Failure Surface Specified By 9 Coordinate Points

Point No.	X-Surf (ft)	Y-Surf (ft)

1	52.44	100.00
2	62.24	97.97
3	72.21	97.30
4	82.19	97.88
5	91.98	100.03
6	101.41	103.35
7	110.29	107.67
8	118.47	113.69
9	125.25	120.00

Circle Center At X = 72.2 ; Y = 170.8 and Radius, 73.5

*** 1.037 ***

Failure Surface Specified By 14 Coordinate Points

Point No.	X-Surf (ft)	Y-Surf (ft)
1	13.11	100.00
2	22.00	98.85
3	35.33	97.54
4	45.33	97.09
5	55.51	97.50
6	65.50	97.79
7	75.14	97.97
8	84.93	97.99
9	94.51	98.83
10	100.81	102.52
11	109.72	107.00
12	118.28	107.95
13	128.28	118.53
14	128.28	120.00

Circle Center At X = 53.9 ; Y = 206.8 and Radius, 114.3

*** 1.050 ***

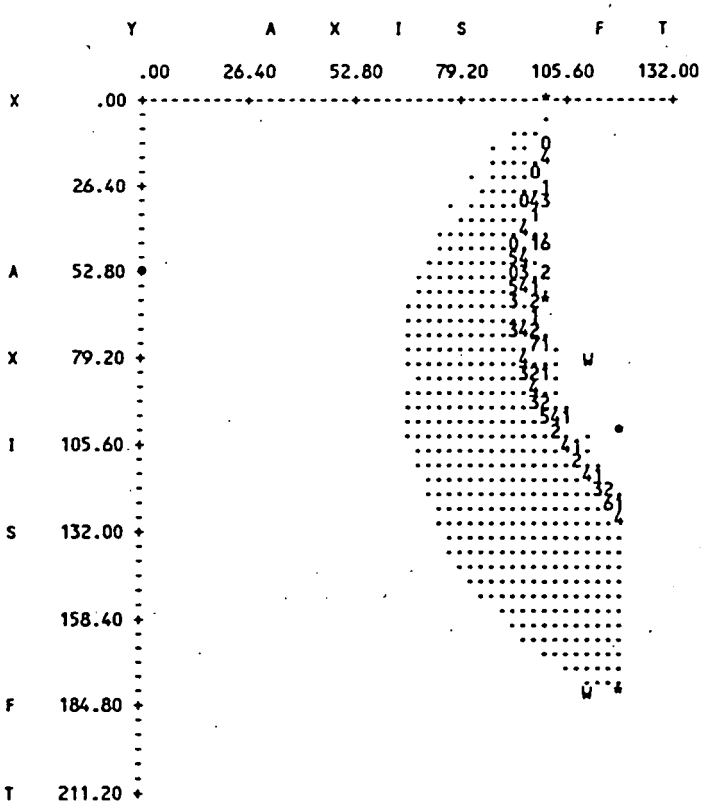

** PCSTABL5H **

by
Purdue University

--Slope Stability Analysis--
Simplified Janbu, Simplified Bishop
or Spencer's Method of Slices

Run Date: 10/06/93
Time of Run: 4:40
Run By: ZLW
Input Data Filename: 1220a2h.inl
Output Filename: 1220a2h.oul

PROBLEM DESCRIPTION PCSTABL5H : 20 ft, 1:2 slope, ALLU. 2, H
. WT

BOUNDARY COORDINATES

3 Top Boundaries
3 Total Boundaries

Boundary No.	X-Left (ft)	Y-Left (ft)	X-Right (ft)	Y-Right (ft)	Soil Type Below Bnd
1	.00	100.00	60.00	100.00	1
2	60.00	100.00	100.00	120.00	1
3	100.00	120.00	180.00	120.00	1

ISOTROPIC SOIL PARAMETERS

1 Type(s) of Soil

Soil Type No.	Total Unit Wt. (pcf)	Saturated Unit Wt. (pcf)	Cohesion Intercept (psf)	Friction Angle (deg)	Pore Pressure Param.	Pressure Constant (psf)	Piez. Surface No.
1	120.0	120.0	200.0	38.0	.00	.0	1

1 PIEZOMETRIC SURFACE(S) HAVE BEEN SPECIFIED

Unit Weight of Water = 62.40

Piezometric Surface No. 1 Specified by 4 Coordinate Points

Point No.	X-Water (ft)	Y-Water (ft)
1	.00	100.00
2	60.00	100.00
3	80.00	110.00
4	180.00	110.00

A Horizontal Earthquake Loading Coefficient
Of .400 Has Been Assigned

A Vertical Earthquake Loading Coefficient
Of .000 Has Been Assigned

Cavitation Pressure = .0 psf

A Critical Failure Surface Searching Method, Using A Random
Technique For Generating Circular Surfaces, Has Been Specified.

300 Trial Surfaces Have Been Generated.

30 Surfaces Initiate From Each Of 10 Points Equally Spaced
Along The Ground Surface Between X = .00 ft.
and X = 59.00 ft.

Each Surface Terminates Between X = 121.00 ft.
and X = 180.00 ft.

Unless Further Limitations Were Imposed, The Minimum Elevation
At Which A Surface Extends Is Y = .00 ft.

10.00 ft. Line Segments Define Each Trial Failure Surface.

Following Are Displayed The Ten Most Critical Of The Trial
Failure Surfaces Examined. They Are Ordered - Most Critical
First.

* * Safety Factors Are Calculated By The Modified Bishop Method * *

Failure Surface Specified By 9 Coordinate Points

Point No.	X-Surf (ft)	Y-Surf (ft)
1	52.44	100.00
2	65.21	97.85
3	72.19	97.19
4	82.15	98.02
5	91.88	100.33
6	101.16	104.08
7	109.77	109.19
8	117.52	115.47
9	121.64	120.00

Circle Center At X = 71.6 ; Y = 163.9 and Radius, 66.8

*** 1.008 ***

Individual data on the 12 slices

ice o.	Width Ft(m)	Weight Lbs(kg)	Water Force Top Lbs(kg)	Water Force Bot Lbs(kg)	Tie Force Norm Lbs(kg)	Tie Force Tan Lbs(kg)	Earthquake Force Hor Lbs(kg)	Earthquake Force Ver Lbs(kg)	Surcharge Load Lbs(kg)
1	7.9	753.0	.0	399.5	.0	.0	301.2	.0	.0
2	6.2	626.1	.0	312.7	.0	.0	250.5	.0	.0
3	10.0	7278.7	.0	3212.4	.0	.0	2911.5	.0	.0
4	7.8	7677.2	.0	2242.4	.0	.0	3071.0	.0	.0
5	7.8	7864.5	.0	4638.0	.0	.0	3146.8	.0	.0
6	6.5	3231.8	.0	1968.3	.0	.0	1303.7	.0	.0
7	6.7	10731.0	.0	6782.9	.0	.0	4292.4	.0	.0
8	6.1	15562.8	.0	4383.3	.0	.0	6233.1	.0	.0
9	1.2	3229.9	.0	478.6	.0	.0	808.0	.0	.0
10	6.6	13863.4	.0	2110.6	.0	.0	5231.8	.0	.0
11	1.0	1562.0	.0	35.0	.0	.0	576.8	.0	.0
12	6.7	5659.5	.0	.0	.0	.0	2343.8	.0	.0
12	4.1	1117.9	.0	.0	.0	.0	447.1	.0	.0

Failure Surface Specified By 11 Coordinate Points

Point No.	X-Surf (ft)	Y-Surf (ft)
1	32.78	100.00
2	45.17	96.57
3	51.62	94.36
4	61.88	93.40
5	71.88	93.70
6	81.75	95.27
7	91.35	98.07
8	100.52	102.06
9	109.11	107.18
10	116.98	113.35
11	123.55	120.00

Circle Center At X = 64.5 ; Y = 172.3 and Radius, 78.9

*** 1.011 ***

Failure Surface Specified By 9 Coordinate Points

Point No.	X-Surf (ft)	Y-Surf (ft)
1	52.44	100.00
2	65.57	97.87
3	75.21	97.30
4	85.19	97.98
5	91.98	100.01
6	101.41	103.35
7	110.29	107.67
8	118.47	113.69
9	125.25	120.00

Circle Center At X = 72.2 ; Y = 170.8 and Radius, 73.5

*** 1.026 ***

Failure Surface Specified By 11 Coordinate Points

Point No.	X-Surf (ft)	Y-Surf (ft)
1	45.89	100.00
2	57.62	96.40
3	67.68	94.67
4	77.66	93.57
5	87.92	93.34
6	97.86	94.61
7	103.82	100.31
8	112.59	105.36
9	120.37	111.63
10	127.14	119.00
11	127.81	120.00

Circle Center At X = 74.6 ; Y = 160.5 and Radius, 66.9

*** 1.026 ***

Failure Surface Specified By 13 Coordinate Points

Point No.	X-Surf (ft)	Y-Surf (ft)
1	19.67	100.00
2	28.20	99.17
3	38.50	97.35
4	48.37	93.58
5	58.33	90.88
6	68.31	87.65
7	78.21	86.70
8	87.89	83.19
9	97.25	80.71
10	106.18	103.22
11	114.57	108.69
12	122.33	114.98
13	127.32	120.00

Circle Center At X = 59.9 ; Y = 183.9 and Radius, 93.0

*** 1.027 ***

Failure Surface Specified By 13 Coordinate Points

Point No.	X-Surf (ft)	Y-Surf (ft)
1	19.67	100.00
2	29.00	99.40
3	38.66	98.84
4	48.55	95.37
5	58.57	91.83
6	68.54	91.56
7	78.52	92.56
8	88.36	87.33
9	97.98	87.14
10	107.20	100.97
11	115.97	105.78
12	124.16	111.33
13	125.42	120.00

Circle Center At X = 57.4 ; Y = 183.9 and Radius, 92.0

*** 1.033 ***

Failure Surface Specified By 14 Coordinate Points

Point No.	X-Surf (ft)	Y-Surf (ft)
1	19.67	100.00
2	28.85	99.04
3	38.38	93.01
4	48.16	90.94
5	58.10	89.85
6	68.10	89.79
7	78.06	90.99
8	87.88	85.34
9	97.47	85.39
10	106.73	99.17
11	115.58	103.86
12	123.89	109.20
13	131.62	115.34
14	135.88	120.00

Circle Center At X = 64.0 ; Y = 190.0 and Radius, 100.3

*** 1.033 ***

Failure Surface Specified By 14 Coordinate Points

Point No.	X-Surf (ft)	Y-Surf (ft)
1	19.67	100.00
2	29.01	99.23
3	38.65	93.78
4	48.51	93.10
5	58.48	91.37
6	68.48	91.32
7	78.40	92.82
8	88.16	85.02
9	97.67	85.14
10	106.82	102.17
11	115.53	107.07
12	123.73	112.79
13	131.37	118.29
14	132.02	120.00

Circle Center At X = 60.9 ; Y = 193.9 and Radius, 102.5

*** 1.034 ***

Failure Surface Specified By 14 Coordinate Points

Point No.	X-Surf (ft)	Y-Surf (ft)
1	13.11	100.00
2	22.25	93.85
3	31.75	92.81
4	41.63	90.63
5	51.73	89.41
6	61.43	89.18
7	71.40	89.93
8	81.25	91.65
9	90.86	94.34
10	100.21	97.66
11	109.33	102.28
12	117.56	107.85
13	125.73	114.02
14	131.67	120.00

Circle Center At X = 58.8 ; Y = 190.6 and Radius, 101.5

*** 1.034 ***

Failure Surface Specified By 15 Coordinate Points

Point No.	X-Surf (ft)	Y-Surf (ft)
1	13.11	100.00
2	22.19	94.74
3	31.59	93.37
4	41.37	90.87
5	51.56	88.72
6	61.19	88.49
7	71.15	89.95
8	81.07	88.41
9	90.95	89.84
10	100.75	92.53
11	100.18	96.55
12	109.65	99.77
13	117.86	104.85
14	125.87	110.72
15	133.40	117.39
15	135.81	120.00

Circle Center At X = 61.4 ; Y = 190.7 and Radius, 102.8

*** 1.037 ***

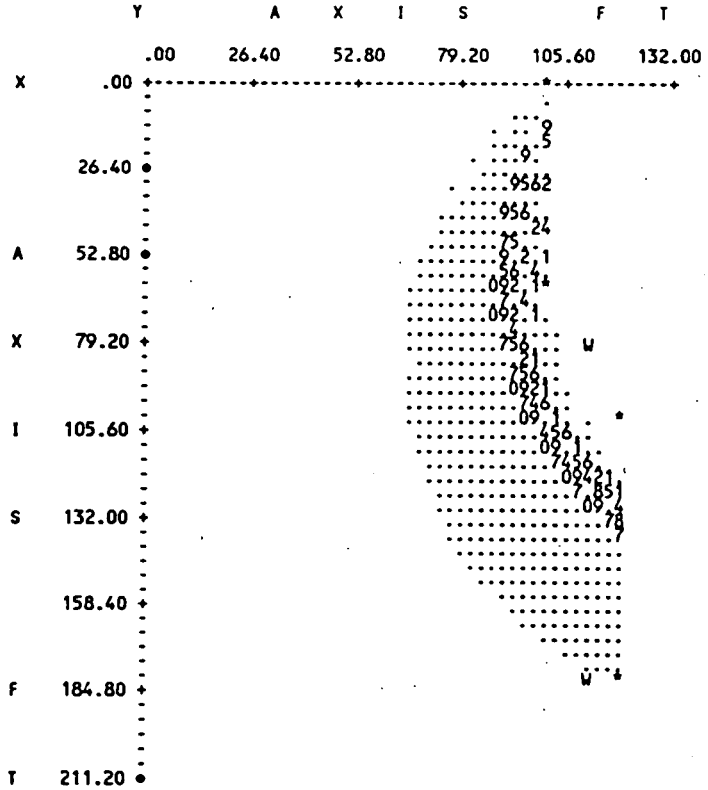

** PCSTABL5M **

by
Purdue University

--Slope Stability Analysis--
Simplified Janbu, Simplified Bishop
or Spencer's Method of Slices

Run Date: 10/06/93
Time of Run: 4:40
Run By: ZLW
Input Data Filename: 1220flh.in1
Output Filename: 1220flh.out

PROBLEM DESCRIPTION PCSTABL5M : 20 ft, 1:2 slope, FILL, H. W T

BOUNDARY COORDINATES

3 Top Boundaries
3 Total Boundaries

Boundary No.	X-Left (ft)	Y-Left (ft)	X-Right (ft)	Y-Right (ft)	Soil Type Below Bnd
1	.00	100.00	60.00	100.00	1
2	60.00	100.00	100.00	120.00	1
3	100.00	120.00	180.00	120.00	

ISOTROPIC SOIL PARAMETERS

1 Type(s) of Soil

Soil Type No.	Total Unit Wt. (pcf)	Saturated Unit Wt. (pcf)	Cohesion Intercept (psf)	Friction Angle (deg)	Pore Pressure Param.	Pressure Constant (psf)	Piez. Surface No.
1	120.0	120.0	1000.0	.0	.00	.0	1

1 PIEZOMETRIC SURFACE(S) HAVE BEEN SPECIFIED

Unit Weight of Water = 62.40

Piezometric Surface No. 1 Specified by 4 Coordinate Points

Point No.	X-Water (ft)	Y-Water (ft)
1	.00	100.00
2	60.00	100.00
3	80.00	110.00
4	180.00	110.00

A Horizontal Earthquake Loading Coefficient
Of .240 Has Been Assigned

A Vertical Earthquake Loading Coefficient
Of .000 Has Been Assigned

Cavitation Pressure = .0 psf

A Critical Failure Surface Searching Method, Using A Random
Technique for Generating Circular Surfaces, Has Been Specified.

300 Trial Surfaces Have Been Generated.

30 Surfaces Initiate From Each Of 10 Points Equally Spaced
Along The Ground Surface Between X = .00 ft.
and X = 59.00 ft.

Each Surface Terminates Between X = 121.00 ft.
and X = 180.00 ft.

Unless Further Limitations Were Imposed, The Minimum Elevation
At Which A Surface Extends Is Y = .00 ft.

10.00 ft. Line Segments Define Each Trial Failure Surface.

Following Are Displayed The Ten Most Critical Of The Trial
Failure Surfaces Examined. They Are Ordered - Most Critical
First.

* * Safety Factors Are Calculated By The Modified Bishop Method * *

Failure Surface Specified By 22 Coordinate Points

Point No.	X-Surf (ft)	Y-Surf (ft)
1	.00	100.00
2	7.35	93.69
3	15.67	87.66
4	23.88	81.67
5	32.30	77.00
6	41.11	73.11
7	51.62	70.03
8	60.47	67.49
9	70.87	66.39
10	80.86	65.86
11	90.85	66.19
12	100.78	67.38
13	110.57	69.43
14	120.14	72.32
15	129.43	76.05
16	138.37	80.51
17	146.88	85.69
18	154.91	91.45
19	162.39	98.38
20	169.27	105.62
21	175.49	113.44
22	179.84	120.00

Circle Center At X = 82.0 ; Y = 181.3 and Radius, 115.5

*** .998 ***

Individual data on the 25 slices

ice	Width Ft(m)	Weight Lbs(kg)	Water Force Top Lbs(kg)	Water Force Bot Lbs(kg)	Tie Force Norm Lbs(kg)	Tie Force Tan Lbs(kg)	Earthquake Force Hor Lbs(kg)	Earthquake Force Ver Lbs(kg)	Surcharge Load Lbs(kg)
).	7.4	2000.5	.0	2716.9	.0	.0	2157.7	.0	.0
)	7.5	6371.3	.0	6147.6	.0	.0	2241.6	.0	.0
)	8.4	15752.6	.0	8742.0	.0	.0	3780.9	.0	.0
)	8.8	21627.9	.0	12897.0	.0	.0	5251.8	.0	.0
)	8.5	27575.6	.0	15563.2	.0	.0	6218.1	.0	.0
)	9.5	32755.0	.0	17236.5	.0	.0	6789.7	.0	.0
)	9.5	34431.7	.0	17407.7	.0	.0	7852.1	.0	.0
)	8.8	35231.1	.0	17807.5	.0	.0	8013.2	.0	.0
)	9.0	3762.5	.0	20175.3	.0	.0	10225.6	.0	.0
)	9.1	42653.8	.0	21370.2	.0	.0	10628.1	.0	.0
)	9.1	4253.0	.0	2320.6	.0	.0	1005.1	.0	.0
)	9.0	4263.0	.0	2720.6	.0	.0	1005.1	.0	.0
)	10.0	59257.1	.0	27470.6	.0	.0	13500.6	.0	.0
)	9.5	55652.1	.0	24871.4	.0	.0	13798.8	.0	.0
)	9.8	4033.2	.0	2861.1	.0	.0	1187.0	.0	.0
)	9.8	7597.0	.0	5923.8	.0	.0	1523.1	.0	.0
)	9.8	60726.0	.0	27775.9	.0	.0	13273.5	.0	.0
)	9.9	59382.2	.0	27313.3	.0	.0	13275.7	.0	.0
)	9.0	51082.6	.0	22327.5	.0	.0	12260.4	.0	.0
)	8.0	37740.7	.0	19800.5	.0	.0	10737.8	.0	.0
)	8.5	37654.2	.0	16761.6	.0	.0	2032.0	.0	.0
)	9.0	30107.3	.0	13263.7	.0	.0	7225.8	.0	.0
)	7.5	22402.7	.0	9338.9	.0	.0	5377.5	.0	.0
)	6.9	14869.6	.0	4998.5	.0	.0	3568.7	.0	.0
)	3.5	5101.6	.0	765.6	.0	.0	1224.5	.0	.0
)	2.7	2721.8	.0	.0	.0	.0	653.2	.0	.0
)	4.3	1711.2	.0	.0	.0	.0	410.7	.0	.0

Failure Surface Specified By 22 Coordinate Points

Point No.	X-Surf (ft)	Y-Surf (ft)
1	.00	100.00
2	7.22	93.10
3	15.06	86.87
4	23.21	81.36
5	32.21	76.61
6	41.39	72.66
7	50.89	69.54
8	60.63	67.27
9	70.53	65.88
10	80.52	65.39
11	90.51	65.77
12	100.43	67.01
13	110.20	69.11
14	119.75	72.04
15	129.08	75.78
16	137.85	80.60
17	146.29	86.00
18	154.17	92.12
19	161.50	98.95
20	168.20	106.35
21	174.21	114.34
22	177.74	120.00

Circle Center At X = 81.2 ; Y = 177.9 and Radius, 112.6

*** .999 ***

Failure Surface Specified By 22 Coordinate Points

Point No.	X-Surf (ft)	Y-Surf (ft)
1	6.56	100.00
2	13.78	93.88
3	21.67	87.66
4	30.35	81.11
5	39.75	75.34
6	49.73	70.40
7	57.25	69.34

8	67.01	67.17
9	76.03	65.62
10	82.03	65.26
11	82.61	69.20
12	106.79	67.13
13	116.69	70.17
14	125.02	73.31
15	135.00	77.70
16	143.64	82.72
17	151.70	88.65
18	150.17	85.05
19	152.38	102.93
20	165.59	110.08
21	172.53	116.09
22	178.01	118.44
	178.83	120.00

Circle Center At X = 85.4 ; Y = 173.0 and Radius, 107.5

*** 1.005 ***

Failure Surface Specified By 22 Coordinate Points

Point No.	X-Surf (ft)	Y-Surf (ft)
1	6.56	100.00
2	13.76	93.09
3	21.63	86.89
4	30.00	81.42
5	38.85	76.78
6	48.09	73.02
7	57.94	69.66
8	67.22	67.88
9	77.35	66.72
10	87.35	66.48
11	87.35	67.15
12	107.20	68.75
13	116.88	71.24
14	126.29	74.62
15	135.55	78.85
16	143.88	83.80
17	153.12	89.71
18	156.68	86.25
19	172.68	99.47
20	169.81	101.36
21	172.81	111.28
22	178.33	116.69
	178.52	120.00

Circle Center At X = 85.0 ; Y = 174.9 and Radius, 108.5

*** 1.011 ***

Failure Surface Specified By 21 Coordinate Points

Point No.	X-Surf (ft)	Y-Surf (ft)
1	6.56	100.00
2	13.63	92.93
3	21.34	86.57
4	29.63	80.97
5	38.41	76.18
6	47.61	72.29
7	57.14	69.33
8	66.91	67.13
9	76.85	65.92
10	86.87	65.78
11	86.83	66.50
12	106.97	68.19
13	116.32	70.82
14	125.67	74.37
15	134.93	78.76
16	143.16	84.01
17	151.14	90.04
18	158.50	96.81
19	165.18	104.23
20	171.12	112.20
21	175.75	120.00

Circle Center At X = 84.0 ; Y = 170.4 and Radius, 104.7

*** 1.013 ***

Failure Surface Specified By 22 Coordinate Points

Point No.	X-Surf (ft)	Y-Surf (ft)
1	.00	100.00
2	7.38	93.23
3	15.30	87.13
4	23.74	81.79
5	32.63	77.23
6	41.86	73.43
7	51.42	70.49
8	61.23	68.31
9	71.16	67.21
10	81.15	66.89
11	91.13	67.46
12	101.03	68.92
13	110.75	71.25
14	120.23	74.44
15	129.39	78.46
16	138.15	83.27

17	146.46	88.84
18	154.23	95.13
19	161.42	102.09
20	167.96	109.65
21	173.80	117.77
22	175.12	120.00

Circle Center At X = 79.7 ; Y = 179.2 and Radius, 112.3

*** 1.017 ***

Failure Surface Specified By 21 Coordinate Points

Point No.	X-Surf (ft)	Y-Surf (ft)
1	13.11	100.00
2	20.36	93.01
3	28.24	86.25
4	36.68	81.69
5	45.80	77.07
6	55.62	73.42
7	65.95	70.74
8	76.39	68.98
9	86.96	68.18
10	97.38	68.39
11	107.89	69.31
12	117.07	71.61
13	123.59	74.99
14	132.78	78.67
15	141.53	83.44
16	149.78	89.10
17	157.77	95.33
18	165.43	102.68
19	170.70	110.47
20	176.19	118.83
21	178.80	120.00

Circle Center At X = 87.5 ; Y = 171.0 and Radius, 102.9

*** 1.035 ***

Failure Surface Specified By 21 Coordinate Points

Point No.	X-Surf (ft)	Y-Surf (ft)
1	.00	100.00
2	7.98	93.15
3	15.18	87.01
4	23.01	81.33
5	32.30	77.36
6	41.78	73.34
7	51.37	70.50
8	61.18	68.27
9	71.13	67.78
10	81.13	67.48
11	91.00	68.33
12	100.24	70.11
13	110.21	72.80
14	119.81	76.38
15	128.67	80.81
16	137.38	86.05
17	145.37	92.07
18	152.78	98.81
19	159.69	106.21
20	165.30	114.20
21	169.07	120.00

Circle Center At X = 77.0 ; Y = 174.5 and Radius, 107.1

*** 1.036 ***

Failure Surface Specified By 21 Coordinate Points

Point No.	X-Surf (ft)	Y-Surf (ft)
1	.00	100.00
2	7.12	93.01
3	15.95	86.75
4	23.31	81.28
5	32.16	76.60
6	41.41	72.82
7	50.99	69.92
8	60.80	68.00
9	70.72	67.01
10	80.75	66.98
11	90.71	67.92
12	100.53	69.80
13	110.12	72.63
14	119.40	76.38
15	128.27	80.97
16	136.66	86.41
17	144.48	92.64
18	151.68	99.58
19	158.17	107.18
20	163.90	115.39
21	166.50	120.00

Circle Center At X = 76.0 ; Y = 170.7 and Radius, 103.8

*** 1.040 ***

Failure Surface Specified By 21 Coordinate Points

Point No.	X-Surf (ft)	Y-Surf (ft)
1	.00	100.00
2	7.33	83.19
3	15.26	87.10
4	23.73	81.79
5	32.68	77.28
6	41.97	73.62
7	51.58	70.88
8	61.41	69.07
9	71.37	68.12
10	81.37	68.14
11	91.32	69.10
12	101.14	70.99
13	110.74	73.79
14	120.04	77.47
15	128.95	82.02
16	137.39	87.37
17	145.30	93.50
18	152.58	100.34
19	159.22	107.83
20	165.11	115.91
21	167.54	120.00

Circle Center At X = 76.1 ; Y = 174.6 and Radius, 106.6

*** 1.046 ***

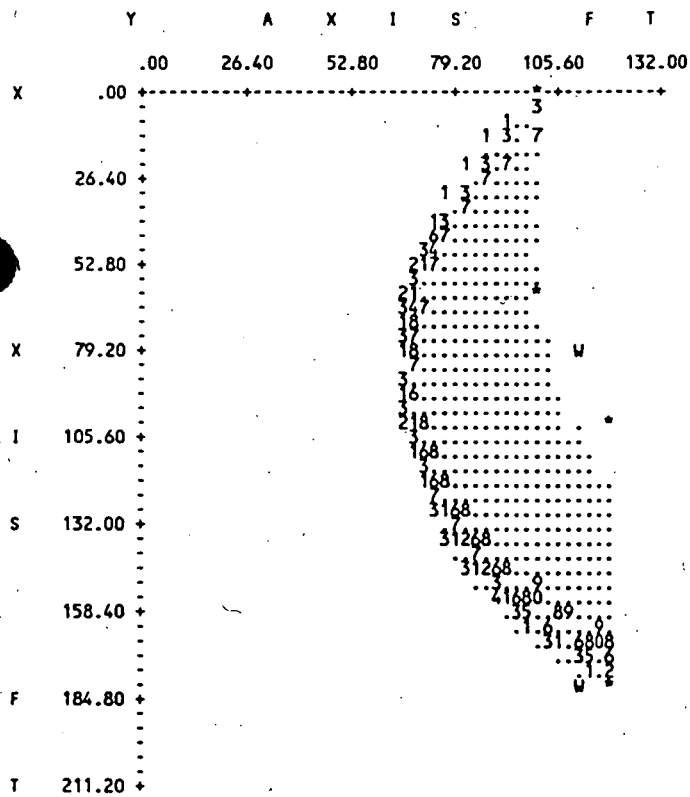

** PCSTABL5M **

by
Purdue University

--Slope Stability Analysis--
Simplified Janbu, Simplified Bishop
or Spencer's Method of Slices

Run Date: 10/06/93
Time of Run: 4:40
Run By: ZLW
Input Data Filename: 1220csh.in1
Output Filename: 1220csh.out

PROBLEM DESCRIPTION PCSTABL5M : 20 ft, 1:2 slope, CLAYSTONE, H. WT

BOUNDARY COORDINATES

3 Top Boundaries
3 Total Boundaries

Boundary No.	X-Left (ft)	Y-Left (ft)	X-Right (ft)	Y-Right (ft)	Soil Type Below Bnd
1	.00	100.00	60.00	100.00	1
2	60.00	100.00	100.00	120.00	1
3	100.00	120.00	180.00	120.00	1

ISOTROPIC SOIL PARAMETERS

1 Type(s) of Soil

Soil Type No.	Total Unit Wt. (pcf)	Saturated Unit Wt. (pcf)	Cohesion Intercept (psf)	Friction Angle (deg)	Pore Pressure Param.	Pressure Constant (psf)	Piez. Surface No.
1	130.0	130.0	1000.0	20.0	.00	.0	1

1 PIEZOMETRIC SURFACE(S) HAVE BEEN SPECIFIED

Unit Weight of Water = 62.40

Piezometric Surface No. 1 Specified by 4 Coordinate Points

Point No.	X-Water (ft)	Y-Water (ft)
1	.00	100.00
2	60.00	100.00
3	80.00	110.00
4	180.00	110.00

A Horizontal Earthquake Loading Coefficient
Of .510 Has Been Assigned

A Vertical Earthquake Loading Coefficient
Of .000 Has Been Assigned

Cavitation Pressure = .0 psf

A Critical Failure Surface Searching Method, Using A Random
Technique For Generating Circular Surfaces, Has Been Specified.

300 Trial Surfaces Have Been Generated.

30 Surfaces Initiate From Each Of 10 Points Equally Spaced
Along The Ground Surface Between X = .00 ft.
and X = 59.00 ft.

Each Surface Terminates Between X = 121.00 ft.
and X = 180.00 ft.

Unless Further Limitations Were Imposed, The Minimum Elevation
At Which A Surface Extends Is Y = .00 ft.

10.00 ft. Line Segments Define Each Trial Failure Surface.

Following Are Displayed The Ten Most Critical Of The Trial
Failure Surfaces Examined. They Are Ordered - Most Critical
First.

* * Safety Factors Are Calculated By The Modified Bishop Method * *

Failure Surface Specified By 22 Coordinate Points

Point No.	X-Surf (ft)	Y-Surf (ft)
1	.00	100.00
2	7.35	93.22
3	15.25	87.09
4	23.72	81.67
5	32.50	77.00
6	41.21	73.11
7	51.22	70.03
8	60.67	67.79
9	70.87	66.39
10	80.86	65.86
11	90.85	66.18
12	100.78	67.38
13	110.57	69.43
14	120.14	72.32
15	129.43	76.02
16	138.37	80.51
17	146.88	85.79
18	154.91	91.73
19	162.39	98.39
20	169.32	105.62
21	175.69	113.44
22	179.84	120.00

Circle Center At X = 82.0 ; Y = 181.3 and Radius, 115.5

*** .995 ***

Individual data on the 25 slices

ice o.	Width Ft(m)	Weight Lbs(kg)	Water Force Top Lbs(kg)	Water Force Bot Lbs(kg)	Tie Force Norm Lbs(kg)	Tie Force Tan Lbs(kg)	Earthquake Force Hor Lbs(kg)	Earthquake Force Ver Lbs(kg)	Surcharge Load Lbs(kg)
1	7.3	3239.8	.0	2116.9	.0	.0	1652.3	.0	.0
2	7.9	10119.5	.0	6144.6	.0	.0	5160.9	.0	.0
3	8.2	17082.3	.0	8746.0	.0	.0	8703.3	.0	.0
4	8.4	23751.1	.0	12892.0	.0	.0	12113.1	.0	.0
5	8.5	30873.6	.0	15562.2	.0	.0	15235.5	.0	.0
6	8.5	37673.9	.0	17236.5	.0	.0	17832.5	.0	.0
7	8.8	35330.5	.0	17407.7	.0	.0	18023.2	.0	.0
8	9.0	4077.1	.0	1807.5	.0	.0	2078.3	.0	.0
9	9.0	44176.9	.0	20145.1	.0	.0	23550.1	.0	.0
10	9.1	48328.4	.0	21370.2	.0	.0	25157.5	.0	.0
11	9.0	4878.3	.0	2320.6	.0	.0	2521.0	.0	.0
12	10.0	60970.1	.0	27240.9	.0	.0	31079.5	.0	.0
13	9.9	60616.9	.0	27871.4	.0	.0	30914.6	.0	.0
14	9.8	5347.3	.0	2861.1	.0	.0	2725.6	.0	.0
15	9.8	65679.8	.0	25023.8	.0	.0	33479.9	.0	.0
16	9.6	61173.0	.0	27715.9	.0	.0	31182.9	.0	.0
17	9.3	55313.3	.0	25313.7	.0	.0	28232.7	.0	.0
18	9.3	55276.3	.0	26357.5	.0	.0	28213.9	.0	.0
19	8.9	48469.1	.0	19800.5	.0	.0	24703.6	.0	.0
20	8.5	40792.0	.0	16761.6	.0	.0	20803.3	.0	.0
21	8.0	32616.3	.0	13263.7	.0	.0	16633.3	.0	.0
22	7.3	24276.9	.0	9338.9	.0	.0	12379.2	.0	.0
23	6.0	16108.7	.0	4998.5	.0	.0	8215.4	.0	.0
24	3.5	5529.7	.0	765.6	.0	.0	2818.6	.0	.0
25	2.7	2948.7	.0	.0	.0	.0	1503.8	.0	.0
26	4.3	1853.8	.0	.0	.0	.0	945.5	.0	.0

Failure Surface Specified By 22 Coordinate Points

Point No.	X-Surf (ft)	Y-Surf (ft)
1	.00	100.00
2	7.22	93.10
3	15.06	86.87
4	23.21	81.36
5	32.21	76.61
6	41.39	72.66
7	51.89	69.54
8	60.23	67.27
9	70.63	65.88
10	80.63	65.39
11	90.55	65.99
12	100.33	67.37
13	110.20	69.61
14	119.73	72.71
15	128.98	76.67
16	137.85	80.60
17	146.26	85.00
18	154.17	89.75
19	161.50	98.96
20	168.20	106.35
21	174.21	114.34
22	177.74	120.00

Circle Center At X = 81.2 ; Y = 177.9 and Radius, 112.6

*** 1.001 ***

Failure Surface Specified By 22 Coordinate Points

Point No.	X-Surf (ft)	Y-Surf (ft)
1	.00	100.00
2	7.38	93.23
3	15.30	87.13
4	23.74	81.76
5	32.63	77.21
6	41.89	73.43
7	51.45	70.49

8	61.23	68.41
9	71.16	67.31
10	81.15	66.89
11	91.13	67.76
12	101.03	68.92
13	110.75	71.25
14	120.23	74.77
15	129.30	78.44
16	138.15	83.37
17	146.39	88.87
18	154.39	95.93
19	161.23	103.08
20	167.86	106.95
21	173.80	117.07
22	175.12	120.00

Circle Center At X = 79.7 ; Y = 179.2 and Radius, 112.3

*** 1.004 ***

Failure Surface Specified By 21 Coordinate Points

Point No.	X-Surf (ft)	Y-Surf (ft)
1	.00	100.00
2	7.77	93.70
3	16.04	88.08
4	24.76	83.19
5	33.88	79.05
6	43.39	75.70
7	53.61	73.17
8	65.81	71.47
9	76.78	70.61
10	86.78	70.60
11	95.74	71.43
12	103.60	73.12
13	112.28	75.64
14	121.71	78.87
15	130.82	83.09
16	139.55	87.87
17	147.83	93.57
18	155.61	99.86
19	162.82	106.79
20	169.42	114.30
21	173.63	120.00

Circle Center At X = 77.9 ; Y = 188.0 and Radius, 117.5

*** 1.004 ***

Failure Surface Specified By 22 Coordinate Points

Point No.	X-Surf (ft)	Y-Surf (ft)
1	6.56	100.00
2	13.79	93.09
3	21.63	86.82
4	30.00	81.22
5	38.85	76.26
6	48.09	72.02
7	57.64	68.56
8	67.42	65.88
9	77.32	64.16
10	87.35	63.48
11	97.36	63.15
12	107.20	63.75
13	116.88	65.27
14	126.29	67.63
15	135.35	70.85
16	143.99	74.86
17	152.12	79.71
18	159.68	85.25
19	166.61	91.27
20	172.84	97.38
21	178.33	103.64
22	178.52	120.00

Circle Center At X = 85.0 ; Y = 174.9 and Radius, 108.5

*** 1.013 ***

Failure Surface Specified By 22 Coordinate Points

Point No.	X-Surf (ft)	Y-Surf (ft)
1	6.56	100.00
2	13.69	92.99
3	21.44	86.68
4	29.75	81.11
5	38.54	76.34
6	47.73	72.40
7	57.25	69.34
8	67.01	67.17
9	76.93	65.92
10	86.93	65.56
11	96.91	66.20
12	106.79	67.73
13	116.46	70.14
14	125.82	73.31
15	135.00	77.70
16	143.64	82.72

17	151.79	88.52
18	159.36	95.05
19	166.30	102.28
20	172.53	110.08
21	178.01	118.42
22	178.83	120.00

Circle Center At X = 85.4 ; Y = 173.0 and Radius, 107.5

*** 1.015 ***

Failure Surface Specified By 21 Coordinate Points

Point No.	X-Surf (ft)	Y-Surf (ft)
1	6.56	100.00
2	14.67	89.23
3	23.32	87.88
4	31.57	85.08
5	40.36	82.00
6	48.82	79.45
7	56.94	75.17
8	65.73	73.39
9	74.40	71.83
10	82.70	71.53
11	88.39	71.50
12	96.35	72.67
13	109.11	74.72
14	118.87	77.63
15	127.23	81.41
16	136.82	84.01
17	142.28	85.37
18	153.18	87.37
19	160.53	104.26
20	167.24	111.67
21	173.23	119.88
	173.47	120.00

Circle Center At X = 81.3 ; Y = 182.7 and Radius, 111.4

*** 1.016 ***

Failure Surface Specified By 21 Coordinate Points

Point No.	X-Surf (ft)	Y-Surf (ft)
1	.00	100.00
2	8.28	92.38
3	16.67	89.75
4	25.02	85.76
5	33.38	81.66
6	41.98	78.89
7	50.79	76.83
8	59.77	76.93
9	67.69	75.59
10	75.67	75.07
11	82.67	75.36
12	92.61	76.32
13	104.14	78.65
14	114.10	80.86
15	123.52	82.31
16	132.66	83.58
17	141.45	83.05
18	149.84	88.49
19	157.78	104.57
20	165.22	111.25
21	172.12	118.29
	173.35	120.00

Circle Center At X = 76.0 ; Y = 203.2 and Radius, 128.2

*** 1.016 ***

Failure Surface Specified By 21 Coordinate Points

Point No.	X-Surf (ft)	Y-Surf (ft)
1	.00	100.00
2	7.28	93.37
3	15.54	87.46
4	24.13	85.31
5	33.13	77.87
6	42.50	74.46
7	52.15	71.83
8	62.00	70.09
9	71.86	69.26
10	81.66	69.35
11	91.21	70.34
12	101.73	72.25
13	111.33	75.67
14	120.64	78.70
15	128.57	83.20
16	136.05	88.29
17	142.02	92.54
18	149.36	101.39
19	157.12	104.68
20	165.15	112.67
21	168.22	120.00

Circle Center At X = 76.0 ; Y = 178.4 and Radius, 109.2

*** 1.018 ***

Failure Surface Specified By 21 Coordinate Points

Point No.	X-Surf (ft)	Y-Surf (ft)
1	.00	100.00
2	8.11	84.15
3	16.67	88.98
4	25.63	87.27
5	37.82	80.84
6	47.76	77.83
7	57.31	75.82
8	57.66	75.81
9	67.18	77.51
10	74.17	77.03
11	82.16	77.37
12	84.08	75.51
13	103.89	77.53
14	113.50	80.30
15	122.84	83.80
16	131.66	88.18
17	140.50	93.33
18	148.28	98.67
19	156.94	98.37
20	156.37	105.36
21	163.50	112.39
	170.04	116.84
	170.08	120.00

Circle Center At X = 75.0 ; Y = 195.3 and Radius, 121.3

*** 1.019 ***

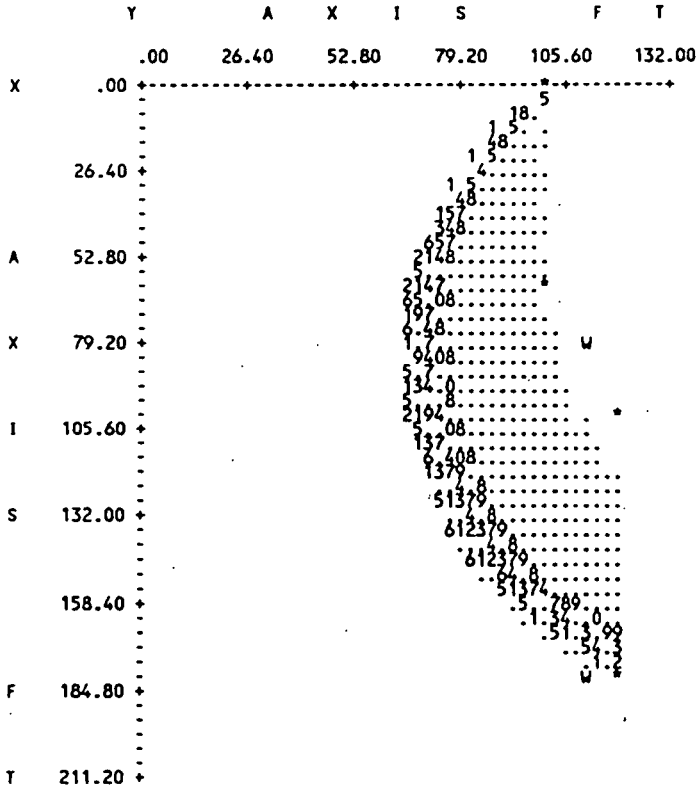

** PCSTABL5M **
by
Purdue University

--Slope Stability Analysis--
Simplified Janbu, Simplified Bishop
or Spencer's Method of Slices

Run Date: 10/06/93
Time of Run: 4:40
Run By: ZLW
Input Data Filename: 1220all.inl
Output Filename: 1220all.oul

PROBLEM DESCRIPTION PCSTABL5M : 20 ft, 1:2 slope, ALLUVIUM 1
, L. WT

BOUNDARY COORDINATES

3 Top Boundaries
3 Total Boundaries

Boundary No.	X-Left (ft)	Y-Left (ft)	X-Right (ft)	Y-Right (ft)	Soil Type Below Bnd
1	.00	100.00	60.00	100.00	1
2	60.00	100.00	100.00	120.00	1
3	100.00	120.00	180.00	120.00	1

ISOTROPIC SOIL PARAMETERS

1 Type(s) of Soil

Soil Type No.	Total Unit Wt. (pcf)	Saturated Unit Wt. (pcf)	Cohesion Intercept (psf)	Friction Angle (deg)	Pore Pressure Param.	Pressure Constant (psf)	Piez. Surface No.
1	120.0	120.0	.0	45.0	.00	.0	1

1 PIEZOMETRIC SURFACE(S) HAVE BEEN SPECIFIED

Unit Weight of Water = 62.40

Piezometric Surface No. 1 Specified by 2 Coordinate Points

Point No.	X-Water (ft)	Y-Water (ft)
1	.00	100.00
2	180.00	100.00

A Horizontal Earthquake Loading Coefficient
Of .485 Has Been Assigned

A Vertical Earthquake Loading Coefficient
Of .000 Has Been Assigned

Cavitation Pressure = .0 psf

A Critical Failure Surface Searching Method, Using A Random
Technique For Generating Circular Surfaces, Has Been Specified.

300 Trial Surfaces Have Been Generated.

30 Surfaces Initiate From Each Of 10 Points Equally Spaced
Along The Ground Surface Between X = .00 ft.
and X = 59.00 ft.

Each Surface Terminates Between X = 121.00 ft.
and X = 180.00 ft.

Unless Further Limitations Were Imposed, The Minimum Elevation
At Which A Surface Extends Is Y = .00 ft.

10.00 ft. Line Segments Define Each Trial Failure Surface.

Following Are Displayed The Ten Most Critical Of The Trial
Failure Surfaces Examined. They Are Ordered - Most Critical
First.

* * Safety Factors Are Calculated By The Modified Bishop Method * *

Failure Surface Specified By 13 Coordinate Points

Point No.	X-Surf (ft)	Y-Surf (ft)
1	19.67	100.00
2	20.00	99.20
3	28.09	93.84
4	28.53	93.34
5	28.27	91.83
6	28.23	92.26
7	68.32	92.33
8	78.36	92.32
9	87.38	97.17
10	97.60	100.97
11	105.97	105.78
12	114.16	111.56
13	121.68	118.10
	123.42	120.00

Circle Center At X = 57.4 ; Y = 183.9 and Radius, 92.0

*** 1.007 ***

Individual data on the 15 slices

ice No.	Width Ft(m)	Weight Lbs(kg)	Water Force Top Lbs(kg)	Water Force Bot Lbs(kg)	Tie Force Norm Lbs(kg)	Tie Force Tan Lbs(kg)	Earthquake Force Hor Lbs(kg)	Earthquake Force Ver Lbs(kg)	Surcharge Load Lbs(kg)
1	0.3	2014.4	.0	1122.7	.0	.0	977.0	.0	.0
2	0.7	5661.0	.0	3075.6	.0	.0	2745.6	.0	.0
3	0.6	8201.9	.0	2313.8	.0	.0	3977.9	.0	.0
4	10.0	8738.8	.0	2612.5	.0	.0	4237.8	.0	.0
5	1.5	1206.5	.0	733.0	.0	.0	682.5	.0	.0
6	8.5	10046.8	.0	4101.5	.0	.0	4872.7	.0	.0
7	8.8	15667.8	.0	2080.8	.0	.0	7598.9	.0	.0
8	6.6	18250.4	.0	2660.2	.0	.0	8851.4	.0	.0
9	6.9	17182.3	.0	666.3	.0	.0	8878.2	.0	.0
10	5.3	7022.7	.0	.0	.0	.0	2387.5	.0	.0
11	2.8	5900.3	.0	.0	.0	.0	2861.6	.0	.0
12	2.0	11353.3	.0	.0	.0	.0	5506.4	.0	.0
13	8.2	11160.7	.0	.0	.0	.0	5412.8	.0	.0
14	4.5	4685.0	.0	.0	.0	.0	2272.2	.0	.0
15	1.7	197.9	.0	.0	.0	.0	96.0	.0	.0

Failure Surface Specified By 14 Coordinate Points

Point No.	X-Surf (ft)	Y-Surf (ft)
1	13.11	100.00
2	22.60	96.85
3	32.33	92.75
4	32.53	93.09
5	32.50	92.30
6	62.20	92.72
7	72.14	93.65
8	81.93	95.96
9	91.51	98.83
10	100.81	102.52
11	109.74	107.00
12	118.26	112.25
13	126.28	118.22
14	128.28	120.00

Circle Center At X = 53.9 ; Y = 206.8 and Radius, 114.3

*** 1.022 ***

Failure Surface Specified By 13 Coordinate Points

Point No.	X-Surf (ft)	Y-Surf (ft)
1	19.67	100.00
2	20.63	97.07
3	32.02	95.04
4	28.96	93.53
5	58.02	93.73
6	68.93	94.50
7	78.79	96.12
8	88.45	98.75
9	97.83	102.21
10	106.85	106.54
11	115.32	111.68
12	123.26	117.59
13	126.20	120.00

Circle Center At X = 55.9 ; Y = 201.2 and Radius, 107.5

*** 1.023 ***

Failure Surface Specified By 14 Coordinate Points

Point No.	X-Surf (ft)	Y-Surf (ft)
1	13.11	100.00
2	22.40	96.30
3	32.00	93.29
4	31.82	91.61
5	31.78	90.66
6	61.78	90.66
7	71.73	91.60
8	81.55	93.48

9	91.15	86.29
10	100.47	89.88
11	109.34	104.25
12	117.77	109.82
13	125.65	116.08
14	129.80	120.00

Circle Center At X = 56.7 ; Y = 195.8 and Radius, 105.3

*** 1.030 ***

Failure Surface Specified By 13 Coordinate Points

Point No.	X-Surf (ft)	Y-Surf (ft)
1	19.67	100.00
2	28.80	96.17
3	38.50	93.35
4	48.34	91.58
5	58.33	90.88
6	68.31	91.25
7	78.21	92.70
8	87.89	95.18
9	97.25	98.71
10	106.18	103.22
11	114.57	108.66
12	123.33	114.99
13	127.32	120.00

Circle Center At X = 59.9 ; Y = 183.9 and Radius, 93.0

*** 1.032 ***

Failure Surface Specified By 12 Coordinate Points

Point No.	X-Surf (ft)	Y-Surf (ft)
1	26.22	100.00
2	36.05	98.14
3	46.00	97.12
4	56.00	96.95
5	65.97	97.62
6	75.86	99.13
7	85.58	101.47
8	95.07	104.63
9	104.26	108.58
10	113.08	113.28
11	121.47	118.72
12	123.12	120.00

Circle Center At X = 53.1 ; Y = 214.7 and Radius, 117.8

*** 1.037 ***

Failure Surface Specified By 11 Coordinate Points

Point No.	X-Surf (ft)	Y-Surf (ft)
1	32.78	100.00
2	42.17	96.57
3	51.92	94.36
4	61.88	93.40
5	71.87	93.70
6	81.75	95.27
7	91.35	98.07
8	100.52	102.06
9	109.11	107.18
10	116.98	113.35
11	123.55	120.00

Circle Center At X = 64.5 ; Y = 172.3 and Radius, 78.9

*** 1.041 ***

Failure Surface Specified By 14 Coordinate Points

Point No.	X-Surf (ft)	Y-Surf (ft)
1	13.11	100.00
2	22.22	95.95
3	31.75	92.81
4	41.51	90.63
5	51.43	89.41
6	61.43	89.18
7	71.40	89.93
8	81.25	91.65
9	90.86	94.32
10	100.21	97.92
11	109.13	102.48
12	117.52	107.85
13	125.43	114.02
14	131.67	120.00

Circle Center At X = 58.8 ; Y = 190.6 and Radius, 101.5

*** 1.044 ***

Failure Surface Specified By 15 Coordinate Points

Point No.	X-Surf (ft)	Y-Surf (ft)
1	.00	100.00
2	9.81	98.06
3	19.71	96.68
4	29.68	95.87
5	39.68	95.63
6	49.67	95.97
7	59.63	96.88
8	69.52	98.36
9	79.31	100.40
10	88.97	103.00
11	98.46	106.15
12	107.73	109.84
13	116.82	114.05
14	125.63	118.78
15	127.62	120.00

Circle Center At X = 38.8 ; Y = 270.1 and Radius, 174.4

*** 1.046 ***

Failure Surface Specified By 13 Coordinate Points

Point No.	X-Surf (ft)	Y-Surf (ft)
1	13.11	100.00
2	23.04	98.82
3	33.03	98.97
4	43.03	98.22
5	53.01	98.89
6	63.01	98.84
7	72.94	100.00
8	82.79	101.73
9	92.52	104.03
10	102.11	106.89
11	111.51	110.30
12	120.70	114.25
13	129.62	118.72
	121.86	120.00

Circle Center At X = 38.0 ; Y = 270.6 and Radius, 172.4

*** 1.046 ***

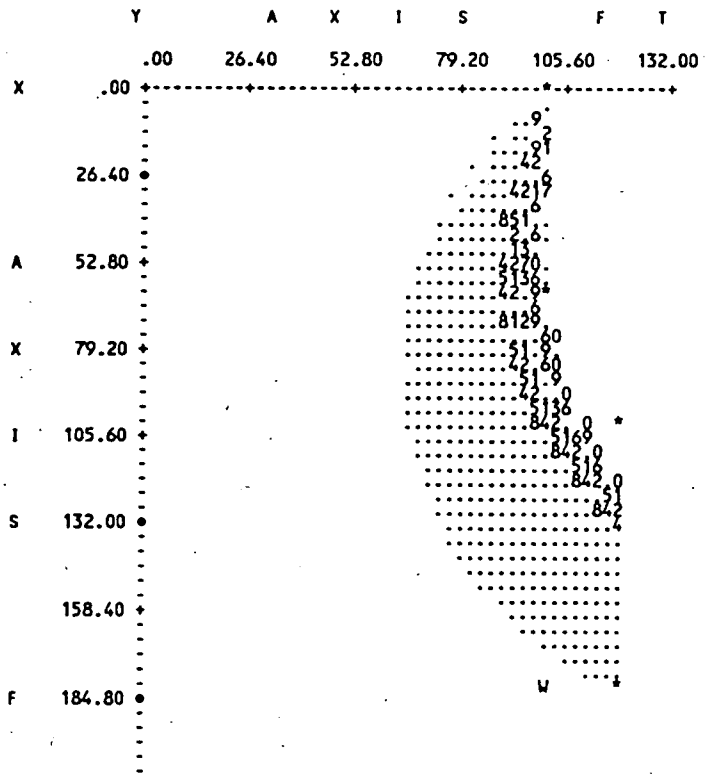

T 211.20 +

** PCSTABL5M **

by
Purdue University

--Slope Stability Analysis--
Simplified Janbu, Simplified Bishop
or Spencer's Method of Slices

Run Date: 10/06/93
Time of Run: 4:40
Run By: ZLW
Input Data Filename: 1220a2l.inl
Output Filename: 1220a2l.oul

PROBLEM DESCRIPTION PCSTABL5M : 20 ft, 1:2 slope, ALLU. 2, L
. WT

BOUNDARY COORDINATES

3 Top Boundaries
3 Total Boundaries

Boundary No.	X-Left (ft)	Y-Left (ft)	X-Right (ft)	Y-Right (ft)	Soil Type Below Bnd
1	.00	100.00	60.00	100.00	1
2	60.00	100.00	100.00	120.00	1
3	100.00	120.00	180.00	120.00	1

ISOTROPIC SOIL PARAMETERS

1 Type(s) of Soil

Soil Type No.	Total Unit Wt. (pcf)	Saturated Unit Wt. (pcf)	Cohesion Intercept (psf)	Friction Angle (deg)	Pore Pressure Param.	Pressure Constant (psf)	Piez. Surface No.
1	120.0	120.0	200.0	38.0	.00	.0	1

1 PIEZOMETRIC SURFACE(S) HAVE BEEN SPECIFIED

Unit Weight of Water = 62.40

Piezometric Surface No. 1 Specified by 2 Coordinate Points

Point No.	X-Water (ft)	Y-Water (ft)
1	.00	100.00
2	180.00	100.00

A Horizontal Earthquake Loading Coefficient
Of .520 Has Been Assigned

A Vertical Earthquake Loading Coefficient
Of .000 Has Been Assigned

Cavitation Pressure = .0 psf

A Critical Failure Surface Searching Method, Using A Random
Technique For Generating Circular Surfaces, Has Been Specified.

300 Trial Surfaces Have Been Generated.

30 Surfaces Initiate From Each Of 10 Points Equally Spaced
Along The Ground Surface Between X = .00 ft.
and X = 59.00 ft.

Each Surface Terminates Between X = 121.00 ft.
and X = 180.00 ft.

Unless Further Limitations Were Imposed, The Minimum Elevation
At Which A Surface Extends Is Y = .00 ft.

10.00 ft. Line Segments Define Each Trial Failure Surface.

Following Are Displayed The Ten Most Critical Of The Trial
Failure Surfaces Examined. They Are Ordered - Most Critical
First.

* * Safety Factors Are Calculated By The Modified Bishop Method * *

Failure Surface Specified By 16 Coordinate Points

Point No.	X-Surf (ft)	Y-Surf (ft)
1	.00	100.00
2	8.83	95.31
3	18.06	91.74
4	27.60	88.46
5	37.37	86.34
6	47.30	85.13
7	57.30	85.03
8	67.28	85.52
9	77.16	86.97
10	86.86	89.40
11	96.30	92.70
12	105.40	96.85
13	114.08	101.81
14	122.27	107.55
15	129.90	114.01
16	135.79	120.00

Circle Center At X = 55.5 ; Y = 193.9 and Radius, 109.1

*** .996 ***

Individual data on the 18 slices

ice No.	Width Ft(m)	Weight Lbs(kg)	Water Force Top Lbs(kg)	Water Force Bot Lbs(kg)	Tie Force Norm Lbs(kg)	Tie Force Tan Lbs(kg)	Earthquake Force Hor Lbs(kg)	Earthquake Force Ver Lbs(kg)	Surcharge Load Lbs(kg)
1	8.8	2783.8	.0	1762.0	.0	.0	1201.6	.0	.0
2	8.5	4323.5	.0	4127.9	.0	.0	3808.5	.0	.0
3	9.5	11767.6	.0	6267.7	.0	.0	5978.6	.0	.0
4	9.8	14778.7	.0	7862.9	.0	.0	7682.9	.0	.0
5	9.8	16686.7	.0	8900.5	.0	.0	8832.7	.0	.0
6	10.0	18014.0	.0	9371.5	.0	.0	9367.3	.0	.0
7	2.7	2804.9	.0	2550.2	.0	.0	2575.3	.0	.0
8	7.3	17791.5	.0	6722.3	.0	.0	7535.6	.0	.0
9	9.9	23597.3	.0	8604.0	.0	.0	12270.6	.0	.0
10	9.7	22564.3	.0	8371.9	.0	.0	15817.5	.0	.0
11	9.7	20699.0	.0	7585.8	.0	.0	17577.0	.0	.0
12	3.4	11933.0	.0	3738.9	.0	.0	5863.1	.0	.0
13	5.1	15788.0	.0	1939.1	.0	.0	8215.5	.0	.0
14	2.4	17776.2	.0	1057.1	.0	.0	9210.0	.0	.0
15	3.3	3665.4	.0	624.3	.0	.0	2362.0	.0	.0
16	3.3	1726.3	.0	.0	.0	.0	3778.7	.0	.0
17	8.5	13056.5	.0	.0	.0	.0	7867.7	.0	.0
18	7.8	8772.1	.0	.0	.0	.0	4390.7	.0	.0
19	5.9	2114.3	.0	.0	.0	.0	1099.4	.0	.0

Failure Surface Specified By 17 Coordinate Points

Point No.	X-Surf (ft)	Y-Surf (ft)
1	.00	100.00
2	8.82	95.29
3	18.03	91.39
4	27.55	88.33
5	37.31	86.14
6	47.22	84.84
7	57.21	84.44
8	67.20	84.93
9	77.10	86.32
10	86.84	88.60
11	96.33	91.72
12	105.51	95.73
13	114.28	100.53
14	122.59	106.09
15	130.36	112.38
16	137.54	118.34
17	138.11	120.00

Circle Center At X = 56.7 ; Y = 195.5 and Radius, 111.1

*** .996 ***

Failure Surface Specified By 18 Coordinate Points

Point No.	X-Surf (ft)	Y-Surf (ft)
1	.00	100.00
2	8.75	95.15
3	17.87	91.05
4	27.30	87.72
5	36.87	85.16
6	46.62	83.48
7	56.48	82.68
8	66.38	82.77
9	76.25	83.73
10	86.02	85.57
11	95.65	88.25
12	105.09	91.78
13	114.32	96.14
14	123.25	101.31
15	131.82	107.27
16	139.97	113.98
17	147.65	121.39
18	149.42	120.00

Circle Center At X = 62.4 ; Y = 202.1 and Radius, 119.7

*** 1.003 ***

Failure Surface Specified By 16 Coordinate Points

Point No.	X-Surf (ft)	Y-Surf (ft)
1	6.56	100.00
2	15.50	95.53
3	24.81	91.86
4	34.42	89.10
5	44.23	87.18
6	54.18	86.15
7	64.18	86.03
8	74.15	86.80
9	84.01	88.47
10	93.68	91.02
11	103.08	94.43
12	112.14	98.67
13	120.77	103.71
14	128.92	109.50
15	136.52	116.01
16	140.41	120.00

Circle Center At X = 60.5 ; Y = 196.7 and Radius, 110.8

*** 1.005 ***

Failure Surface Specified By 17 Coordinate Points

Point No.	X-Surf (ft)	Y-Surf (ft)
1	6.56	100.00
2	15.40	95.34
3	24.73	91.78
4	34.19	89.39
5	43.63	88.31
6	53.85	88.03
7	63.84	88.95
8	73.83	89.15
9	83.73	88.54
10	93.47	88.81
11	103.07	91.24
12	112.15	94.90
13	120.94	100.66
14	129.27	106.19
15	137.08	112.27
16	142.30	116.32
17	144.86	120.00

Circle Center At X = 63.2 ; Y = 196.7 and Radius, 112.1

*** 1.008 ***

Failure Surface Specified By 18 Coordinate Points

Point No.	X-Surf (ft)	Y-Surf (ft)
1	.00	100.00
2	8.65	94.08
3	17.68	90.68
4	27.04	87.15
5	36.65	84.71
6	46.46	83.47
7	56.40	83.35
8	66.38	84.07
9	76.38	84.58
10	86.38	84.85
11	96.05	86.13
12	105.90	88.10
13	114.87	91.65
14	123.77	96.38
15	132.31	101.59
16	140.38	107.51
17	147.93	114.07
18	153.69	120.00

Circle Center At X = 64.9 ; Y = 201.7 and Radius, 120.6

*** 1.009 ***

Failure Surface Specified By 15 Coordinate Points

Point No.	X-Surf (ft)	Y-Surf (ft)
1	13.11	100.00
2	22.19	93.24
3	31.37	86.87
4	41.47	82.02
5	51.16	88.36
6	61.17	87.97
7	71.17	88.41
8	81.04	89.84
9	90.75	92.23
10	100.18	95.55
11	109.23	99.77
12	117.86	104.85
13	126.04	110.74
14	133.40	117.39
15	135.81	120.00

Circle Center At X = 61.4 ; Y = 190.7 and Radius, 102.8

*** 1.012 ***

Failure Surface Specified By 14 Coordinate Points

Point No.	X-Surf (ft)	Y-Surf (ft)
1	13.11	100.00
2	25.25	95.05
3	31.75	92.81
4	41.51	90.63
5	51.43	89.41
6	61.43	89.18
7	71.40	89.03
8	81.25	91.65
9	90.86	94.37
10	100.21	97.56
11	109.13	102.28
12	117.56	107.85
13	125.43	114.02
14	131.67	120.00

Circle Center At X = 58.8 ; Y = 190.6 and Radius, 101.5

*** 1.013 ***

Failure Surface Specified By 19 Coordinate Points

Point No.	X-Surf (ft)	Y-Surf (ft)
1	.00	100.00
2	8.62	94.93
3	17.82	90.56
4	26.94	87.02
5	36.53	84.08
6	46.30	82.00
7	56.22	80.72
8	66.21	80.25
9	76.20	80.58
10	86.14	81.71
11	95.95	83.65
12	105.57	86.39
13	114.94	89.85
14	124.01	94.08
15	132.70	99.03
16	140.96	104.69
17	148.74	110.92
18	155.99	117.83
19	157.94	120.00

Circle Center At X = 67.1 ; Y = 204.1 and Radius, 123.9

*** 1.014 ***

Failure Surface Specified By 18 Coordinate Points

Point No.	X-Surf (ft)	Y-Surf (ft)
1	6.56	100.00
2	15.37	95.53
3	24.30	91.31
4	33.96	87.08
5	43.67	84.28
6	53.54	83.55
7	63.51	83.07
8	73.51	83.17
9	83.51	83.27
10	93.36	84.45
11	103.31	85.89
12	112.98	88.75
13	122.40	91.82
14	131.50	95.86
15	139.92	100.85
16	147.65	106.92
17	154.38	109.56
18	159.68	116.73
19	153.30	117.02
20	153.81	120.00

Circle Center At X = 67.7 ; Y = 202.1 and Radius, 119.0

*** 1.017 ***

```
          Y           A     X     I     S           F     T.

          .00      26.40     52.80     79.20     105.60     132.00
X       .00 +---------+---------+---------+--------*-+---------+
            -                                       4
            -                                     .1.
            -                                    :0 7
            -                                   :31 ..
            -                                   7
      26.40 +                                  .21 ...
            -                                  7
            -                                 .:314...
```

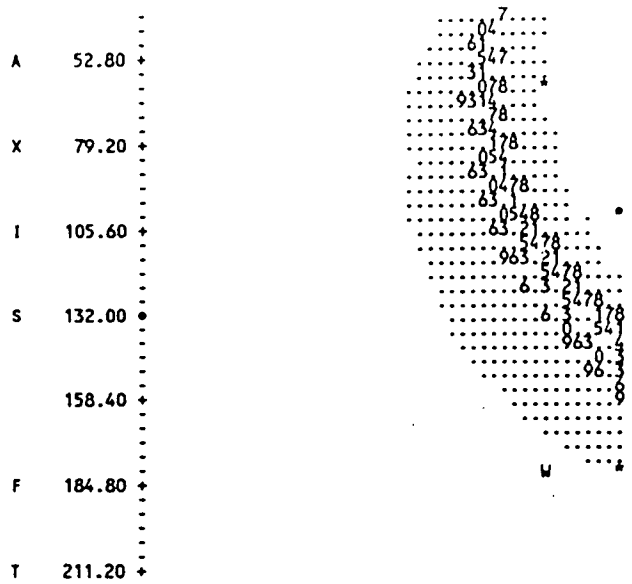
A 52.80
X 79.20
I 105.60
S 132.00
158.40
F 184.80
T 211.20

** PCSTABL5M **

by
Purdue University

--Slope Stability Analysis--
Simplified Janbu, Simplified Bishop
or Spencer's Method of Slices

Run Date: 10/06/93
Time of Run: 2:40
Run By: ZLW
Input Data Filename: 1220fil.in
Output Filename: 1220fil.out

PROBLEM DESCRIPTION PCSTABL5M : 20 ft, 1:2 slope, FILL, L. W T

BOUNDARY COORDINATES

3 Top Boundaries
3 Total Boundaries

Boundary No.	X-Left (ft)	Y-Left (ft)	X-Right (ft)	Y-Right (ft)	Soil Type Below Bnd
1	.00	100.00	60.00	100.00	1
2	60.00	100.00	100.00	120.00	1
3	100.00	120.00	180.00	120.00	1

ISOTROPIC SOIL PARAMETERS

1 Type(s) of Soil

Soil Type No.	Total Unit Wt. (pcf)	Saturated Unit Wt. (pcf)	Cohesion Intercept (psf)	Friction Angle (deg)	Pore Pressure Param.	Pressure Constant (psf)	Piez. Surface No.
1	120.0	120.0	1000.0	.0	.00	.0	1

1 PIEZOMETRIC SURFACE(S) HAVE BEEN SPECIFIED

Unit Weight of Water = 62.40

Piezometric Surface No. 1 Specified by 2 Coordinate Points

Point No.	X-Water (ft)	Y-Water (ft)
1	.00	100.00
2	180.00	100.00

A Horizontal Earthquake Loading Coefficient
Of .240 Has Been Assigned

A Vertical Earthquake Loading Coefficient
Of .000 Has Been Assigned

Cavitation Pressure = .0 psf

A Critical Failure Surface Searching Method, Using A Random
Technique For Generating Circular Surfaces, Has Been Specified.

300 Trial Surfaces Have Been Generated.

30 Surfaces Initiate From Each Of 10 Points Equally Spaced
Along The Ground Surface Between X = .00 ft.
and X = 59.00 ft.

Each Surface Terminates Between X = 121.00 ft.
and X = 180.00 ft.

Unless Further Limitations Were Imposed, The Minimum Elevation
At Which A Surface Extends Is Y = .00 ft.

10.00 ft. Line Segments Define Each Trial Failure Surface.

Following Are Displayed The Ten Most Critical Of The Trial
Failure Surfaces Examined. They Are Ordered - Most Critical
First.

** Safety Factors Are Calculated By The Modified Bishop Method **

Failure Surface Specified By 22 Coordinate Points

Point No.	X-Surf (ft)	Y-Surf (ft)
1	.00	100.00
2	7.35	93.22
3	15.25	87.06
4	23.66	81.67
5	32.50	77.00
6	41.71	73.11
7	51.22	70.03
8	60.97	67.79
9	70.87	66.39
10	80.86	65.86
11	90.85	66.19
12	100.78	67.38
13	110.57	69.43
14	120.17	72.32
15	128.73	76.05
16	136.37	80.51
17	142.88	85.70
18	149.81	91.73
19	153.39	98.36
20	156.27	105.62
21	162.46	113.44
22	179.84	120.00

Circle Center At X = 82.0 ; Y = 181.3 and Radius, 115.5

*** .998 ***

Individual data on the 24 slices

ce	Width Ft(m)	Weight Lbs(kg)	Water Force Top Lbs(kg)	Water Force Bot Lbs(kg)	Tie Force Norm Lbs(kg)	Tie Force Tan Lbs(kg)	Earthquake Force Hor Lbs(kg)	Earthquake Force Ver Lbs(kg)	Surcharge Load Lbs(kg)
	7.3	2990.5	.0	2116.9	.0	.0	717.7	.0	.0
	7.9	6321.1	.0	6147.6	.0	.0	2241.9	.0	.0
	8.4	15752.6	.0	9746.0	.0	.0	3780.6	.0	.0
	8.8	21925.1	.0	12892.0	.0	.0	5261.8	.0	.0
	9.2	27575.6	.0	15565.2	.0	.0	6618.1	.0	.0
	9.5	32457.0	.0	17736.5	.0	.0	7789.7	.0	.0
	8.8	32621.1	.0	17407.4	.0	.0	7829.1	.0	.0
	1.0	3763.5	.0	1993.2	.0	.0	903.2	.0	.0
	9.9	42627.6	.0	20536.2	.0	.0	10229.5	.0	.0
	10.0	50096.9	.0	21137.7	.0	.0	12023.3	.0	.0
	10.0	52252.7	.0	21200.6	.0	.0	13500.6	.0	.0
	9.1	55667.1	.0	19122.0	.0	.0	13429.0	.0	.0
	.8	7633.2	.0	1602.5	.0	.0	1184.0	.0	.0
	9.8	60587.0	.0	19712.8	.0	.0	14573.3	.0	.0
	8.6	56739.7	.0	18173.3	.0	.0	13575.5	.0	.0
	9.3	51085.2	.0	16117.2	.0	.0	12260.2	.0	.0
	8.6	47720.7	.0	13560.5	.0	.0	10737.8	.0	.0
	8.5	37652.2	.0	10521.6	.0	.0	9037.0	.0	.0
	8.0	30107.5	.0	7023.7	.0	.0	7225.8	.0	.0
	9.5	22405.7	.0	3092.9	.0	.0	5377.2	.0	.0
	1.2	5881.6	.0	115.5	.0	.0	931.7	.0	.0
	5.3	10987.7	.0	.0	.0	.0	2637.0	.0	.0
	2.3	7823.7	.0	.0	.0	.0	1877.6	.0	.0
	2.5	1961.2	.0	.0	.0	.0	470.7	.0	.0
	4.3	1711.2	.0	.0	.0	.0	410.7	.0	.0

Failure Surface Specified By 22 Coordinate Points

Point No.	X-Surf (ft)	Y-Surf (ft)
1	.00	100.00
2	7.24	93.10
3	15.06	86.87
4	23.31	81.36
5	32.21	76.61
6	41.39	72.69
7	50.89	69.54
8	60.63	67.27
9	70.53	65.88
10	80.52	65.38
11	90.51	65.74
12	100.43	67.01
13	110.20	69.14
14	119.75	72.14
15	128.68	75.98
16	137.85	80.60
17	146.26	86.00
18	157.17	92.12
19	157.50	98.92
20	168.20	106.35
21	172.51	114.34
22	177.74	120.00

Circle Center At X = 81.2 ; Y = 177.9 and Radius, 112.6

*** .999 ***

Failure Surface Specified By 22 Coordinate Points

Point No.	X-Surf (ft)	Y-Surf (ft)
1	6.56	100.00
2	13.09	93.89
3	21.44	88.68
4	30.75	84.11
5	38.57	78.34
6	47.24	73.20
7	57.25	69.34
8	67.01	67.37
9	76.93	65.92
10	86.93	65.59

11	96.91	64.20
12	106.79	67.73
13	116.49	70.17
14	125.92	73.51
15	135.00	77.70
16	143.94	82.72
17	151.79	88.52
18	159.36	95.05
19	166.30	102.28
20	172.53	110.08
21	178.01	118.44
22	178.83	120.00

Circle Center At X = 85.4 ; Y = 173.0 and Radius, 107.5

*** 1.005 ***

Failure Surface Specified By 22 Coordinate Points

Point No.	X-Surf (ft)	Y-Surf (ft)
1	6.56	100.00
2	13.78	93.09
3	21.63	86.89
4	30.00	81.42
5	38.85	76.76
6	48.09	72.92
7	57.64	69.28
8	67.42	67.88
9	77.35	66.75
10	87.35	66.18
11	97.32	67.15
12	107.20	69.75
13	116.88	71.24
14	126.29	74.62
15	135.35	78.85
16	143.96	83.86
17	152.12	89.71
18	159.68	96.25
19	166.61	103.47
20	172.84	111.28
21	178.33	119.64
22	178.52	120.00

Circle Center At X = 85.0 ; Y = 174.9 and Radius, 108.5

*** 1.011 ***

Failure Surface Specified By 21 Coordinate Points

Point No.	X-Surf (ft)	Y-Surf (ft)
1	6.56	100.00
2	13.63	92.23
3	21.37	84.27
4	29.73	86.37
5	38.63	80.07
6	38.71	76.18
7	47.61	72.24
8	57.14	69.23
9	66.91	67.13
10	76.85	65.26
11	86.84	65.75
12	96.82	66.50
13	106.67	68.19
14	116.32	70.82
15	125.67	74.35
16	134.65	78.76
17	143.16	84.01
18	151.14	90.04
19	158.50	96.81
20	165.18	103.25
21	171.12	110.28
	175.75	120.00

Circle Center At X = 84.0 ; Y = 170.4 and Radius, 104.7

*** 1.013 ***

Failure Surface Specified By 22 Coordinate Points

Point No.	X-Surf (ft)	Y-Surf (ft)
1	.00	100.00
2	7.38	93.23
3	15.30	87.15
4	23.74	81.79
5	32.63	77.21
6	41.89	73.43
7	51.45	70.78
8	61.33	68.71
9	71.17	67.31
10	81.16	67.89
11	91.13	69.67
12	101.03	69.49
13	110.73	69.39
14	120.23	71.27
15	129.39	74.77
16	137.95	79.39
17	146.15	83.37
18	154.27	88.84
19	161.42	93.13
		102.09

300

20	167.96	109.65
21	173.80	117.77
22	175.12	120.00

Circle Center At X = 79.7 ; Y = 179.2 and Radius, 112.3

*** 1.017 ***

Failure Surface Specified By 21 Coordinate Points

Point No.	X-Surf (ft)	Y-Surf (ft)
1	13.11	100.00
2	20.36	93.11
3	28.24	86.95
4	36.68	81.56
5	39.60	77.07
6	45.82	73.44
7	54.55	70.74
8	62.39	68.98
9	67.36	68.18
10	84.36	68.36
11	87.38	68.51
12	104.38	69.51
13	117.07	71.61
14	133.56	74.66
15	143.78	78.67
16	151.59	84.67
17	171.58	88.10
18	172.19	92.54
19	172.73	95.53
20	174.43	103.68
21	174.90	110.47
22	175.18	118.83
23	176.80	120.00

Circle Center At X = 87.5 ; Y = 171.0 and Radius, 102.9

*** 1.035 ***

Failure Surface Specified By 21 Coordinate Points

Point No.	X-Surf (ft)	Y-Surf (ft)
1	.00	100.00
2	7.26	93.15
3	15.18	87.01
4	23.61	81.63
5	32.50	77.06
6	41.78	73.34
7	51.37	70.50
8	61.18	68.57
9	71.13	67.56
10	81.13	67.48
11	81.10	68.33
12	100.94	70.11
13	110.57	72.80
14	118.61	76.38
15	128.87	80.81
16	139.38	86.05
17	142.39	89.07
18	153.76	98.81
19	156.18	102.21
20	165.50	112.50
21	169.07	120.00

Circle Center At X = 77.0 ; Y = 174.5 and Radius, 107.1

*** 1.036 ***

Failure Surface Specified By 21 Coordinate Points

Point No.	X-Surf (ft)	Y-Surf (ft)
1	.00	100.00
2	7.15	93.01
3	14.95	86.75
4	23.31	81.26
5	32.16	76.60
6	41.41	72.82
7	50.99	69.94
8	60.80	68.00
9	70.75	67.01
10	80.75	66.98
11	80.71	67.83
12	100.53	69.60
13	110.16	72.93
14	118.39	76.39
15	128.27	80.97
16	136.66	86.41
17	137.79	89.24
18	151.68	99.64
19	154.17	99.58
20	163.90	107.19
21	166.50	115.39
22		120.00

Circle Center At X = 76.0 ; Y = 170.7 and Radius, 103.8

*** 1.040 ***

Failure Surface Specified By 21 Coordinate Points

Point No.	X-Surf (ft)	Y-Surf (ft)
1	.00	100.00
2	7.33	83.18
3	15.26	81.10
4	23.73	81.79
5	32.69	77.28
6	41.97	73.67
7	51.58	70.88
8	61.41	69.04
9	71.37	68.13
10	81.37	68.14
11	91.32	69.10
12	101.14	70.99
13	110.74	73.79
14	120.04	77.47
15	128.95	82.02
16	137.36	87.37
17	145.30	93.50
18	152.59	100.34
19	159.22	107.83
20	165.11	115.81
21	167.54	120.00

Circle Center At X = 76.1 ; Y = 174.6 and Radius, 106.6

*** 1.046 ***

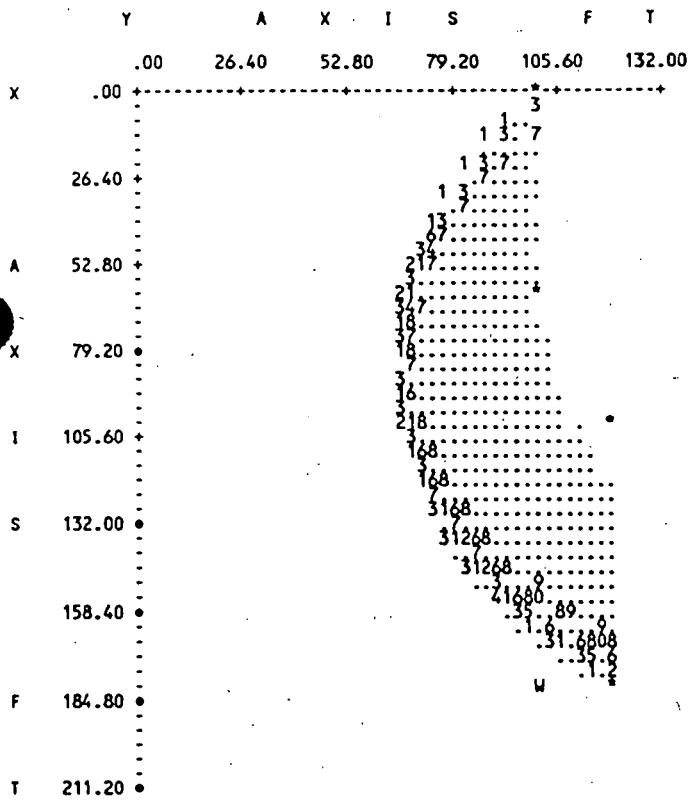

** PCSTABL5M **

by
Purdue University

--Slope Stability Analysis--
Simplified Janbu, Simplified Bishop
or Spencer's Method of Slices

Run Date: 10/06/93
Time of Run: 4:40
Run By: JLW
Input Data Filename: 1220csl.in1
Output Filename: 1220csl.ou1

PROBLEM DESCRIPTION PCSTABL5M : 20 ft, 1:2 slope, CLAYSTONE, L. WT

BOUNDARY COORDINATES

3 Top Boundaries
3 Total Boundaries

Boundary No.	X-Left (ft)	Y-Left (ft)	X-Right (ft)	Y-Right (ft)	Soil Type Below Bnd
1	.00	100.00	60.00	100.00	1
2	60.00	100.00	100.00	120.00	1
3	100.00	120.00	180.00	120.00	1

ISOTROPIC SOIL PARAMETERS

1 Type(s) of Soil

Soil Type No.	Total Unit Wt. (pcf)	Saturated Unit Wt. (pcf)	Cohesion Intercept (psf)	Friction Angle (deg)	Pore Pressure Param.	Pressure Constant (psf)	Piez. Surface No.
1	130.0	130.0	1000.0	20.0	.00	.0	1

1 PIEZOMETRIC SURFACE(S) HAVE BEEN SPECIFIED

Unit Weight of Water = 62.40

Piezometric Surface No. 1 Specified by 2 Coordinate Points

Point No.	X-Water (ft)	Y-Water (ft)
1	.00	100.00
2	180.00	100.00

A Horizontal Earthquake Loading Coefficient
Of .545 Has Been Assigned

A Vertical Earthquake Loading Coefficient
Of .000 Has Been Assigned

Cavitation Pressure = .0 psf

A Critical Failure Surface Searching Method, Using A Random
Technique For Generating Circular Surfaces, Has Been Specified.

300 Trial Surfaces Have Been Generated.

30 Surfaces Initiate From Each Of 10 Points Equally Spaced
Along The Ground Surface Between X = .00 ft.
and X = 59.00 ft.

Each Surface Terminates Between X = 121.00 ft.
and X = 180.00 ft.

Unless Further Limitations Were Imposed, The Minimum Elevation
At Which A Surface Extends Is Y = .00 ft.

10.00 ft. Line Segments Define Each Trial Failure Surface.

Following Are Displayed The Ten Most Critical Of The Trial
Failure Surfaces Examined. They Are Ordered - Most Critical
First.

* * Safety Factors Are Calculated By The Modified Bishop Method * *

Failure Surface Specified By 22 Coordinate Points

Point No.	X-Surf (ft)	Y-Surf (ft)
1	.00	100.00
2	7.35	93.66
3	15.23	87.09
4	23.66	81.67
5	32.50	77.00
6	41.71	73.11
7	51.22	70.03
8	60.67	67.79
9	70.87	66.39
10	80.86	65.86
11	90.85	66.19
12	100.78	67.38
13	110.57	69.43
14	120.14	72.32
15	129.43	76.02
16	138.37	80.51
17	146.88	85.76
18	154.91	91.73
19	162.39	98.38
20	169.27	105.62
21	175.46	113.44
22	179.84	120.00

Circle Center At X = 82.0 ; Y = 181.3 and Radius, 115.5

*** .996 ***

Individual data on the 24 slices

ce	Width Ft(m)	Weight Lbs(kg)	Water Force Top Lbs(kg)	Water Force Bot Lbs(kg)	Tie Force Norm Lbs(kg)	Tie Force Tan Lbs(kg)	Earthquake Force Hor Lbs(kg)	Earthquake Force Ver Lbs(kg)	Surcharge Load Lbs(kg)
	7.3	3330.8	.0	2116.9	.0	.0	1762.7	.0	.0
	7.9	10119.5	.0	8122.6	.0	.0	6515.1	.0	.0
	8.4	17065.3	.0	9726.0	.0	.0	9300.6	.0	.0
	8.8	23731.1	.0	12892.0	.0	.0	12944.4	.0	.0
	9.2	29873.6	.0	15563.2	.0	.0	16281.1	.0	.0
	9.5	35161.7	.0	17739.5	.0	.0	18163.2	.0	.0
	9.8	35339.5	.0	17407.4	.0	.0	19260.0	.0	.0
	1.0	4077.1	.0	1993.2	.0	.0	2222.0	.0	.0
	9.9	46176.6	.0	20538.2	.0	.0	25166.3	.0	.0
	10.0	54271.6	.0	21137.7	.0	.0	29578.0	.0	.0
	10.0	60940.1	.0	21200.6	.0	.0	33212.4	.0	.0
	9.1	60616.9	.0	19122.0	.0	.0	33036.2	.0	.0
	.8	5344.3	.0	1602.5	.0	.0	2912.6	.0	.0
	9.8	65646.8	.0	19712.8	.0	.0	35777.5	.0	.0
	9.6	61143.0	.0	18173.3	.0	.0	33322.6	.0	.0
	9.3	55342.3	.0	16117.4	.0	.0	30161.6	.0	.0
	8.9	48465.1	.0	13560.5	.0	.0	26415.6	.0	.0
	8.5	40792.0	.0	10521.6	.0	.0	22231.7	.0	.0
	8.0	32616.3	.0	7023.7	.0	.0	17775.6	.0	.0
	7.5	23272.8	.0	3092.6	.0	.0	13228.7	.0	.0
	6.6	7506.7	.0	115.5	.0	.0	2291.6	.0	.0
	5.3	11903.3	.0	.0	.0	.0	6487.3	.0	.0
	3.2	8475.4	.0	.0	.0	.0	4619.1	.0	.0
	2.3	1853.8	.0	.0	.0	.0	1010.3	.0	.0

Failure Surface Specified By 22 Coordinate Points

Point No.	X-Surf (ft)	Y-Surf (ft)
1	.00	100.00
2	7.67	93.10
3	15.06	86.87
4	23.21	81.36
5	32.21	76.61
6	41.39	72.66
7	50.89	69.34
8	60.63	67.27
9	70.53	65.88
10	80.52	65.37
11	90.51	65.74
12	100.43	67.01
13	110.20	69.14
14	119.75	72.14
15	128.98	75.98
16	137.85	80.60
17	146.28	86.00
18	154.17	92.13
19	161.50	98.92
20	168.20	106.35
21	174.51	114.34
22	177.74	120.00

Circle Center At X = 81.2 ; Y = 177.9 and Radius, 112.6

*** 1.002 ***

Failure Surface Specified By 22 Coordinate Points

Point No.	X-Surf (ft)	Y-Surf (ft)
1	.00	100.00
2	7.36	93.23
3	15.30	87.15
4	23.77	81.79
5	33.63	77.21
6	41.80	73.43
7	51.45	70.28
8	61.33	68.21
9	71.17	67.31
10	81.15	66.89

11	91.13	67.46
12	101.03	68.92
13	110.75	71.25
14	120.23	74.44
15	129.39	78.49
16	138.15	83.37
17	146.49	88.84
18	154.23	95.13
19	161.42	102.09
20	167.96	109.65
21	173.80	117.77
22	175.12	120.00

Circle Center At X = 79.7 ; Y = 179.2 and Radius, 112.3

*** 1.005 ***

Failure Surface Specified By 21 Coordinate Points

Point No.	X-Surf (ft)	Y-Surf (ft)
1	.00	100.00
2	7.77	93.70
3	16.02	88.08
4	24.76	83.19
5	33.88	79.05
6	43.38	75.70
7	53.62	73.17
8	64.81	71.47
9	76.78	70.61
10	88.78	70.60
11	99.72	71.42
12	109.60	73.13
13	118.28	75.84
14	125.71	78.97
15	130.82	83.09
16	139.55	87.97
17	147.83	93.57
18	155.61	99.86
19	162.82	106.79
20	169.42	114.30
21	173.63	120.00

Circle Center At X = 77.9 ; Y = 188.0 and Radius, 117.5

*** 1.007 ***

Failure Surface Specified By 22 Coordinate Points

Point No.	X-Surf (ft)	Y-Surf (ft)
1	6.56	100.00
2	13.79	93.09
3	21.63	86.89
4	30.00	81.52
5	38.85	76.76
6	48.06	72.92
7	57.62	69.96
8	67.22	67.88
9	77.32	66.72
10	87.35	66.48
11	97.32	67.12
12	107.20	68.75
13	116.88	71.24
14	126.29	74.62
15	135.35	78.85
16	143.99	83.86
17	152.12	89.61
18	159.68	96.21
19	166.61	103.57
20	172.84	111.28
21	178.33	119.27
22	178.52	120.00

Circle Center At X = 85.0 ; Y = 174.9 and Radius, 108.5

*** 1.016 ***

Failure Surface Specified By 22 Coordinate Points

Point No.	X-Surf (ft)	Y-Surf (ft)
1	6.56	100.00
2	13.69	92.99
3	21.47	86.68
4	29.75	81.11
5	38.54	76.34
6	47.73	72.40
7	57.25	69.34
8	67.03	67.14
9	76.93	65.92
10	86.93	65.56
11	96.93	66.20
12	106.79	67.73
13	116.49	70.17
14	125.92	73.51
15	135.00	77.70
16	143.64	82.72
17	151.79	88.55
18	159.38	95.16
19	166.30	102.26

20	172.53	110.08
21	178.01	118.22
22	178.83	120.00

Circle Center At X = 85.4 ; Y = 173.0 and Radius, 107.5

*** 1.018 ***

Failure Surface Specified By 21 Coordinate Points

Point No.	X-Surf (ft)	Y-Surf (ft)
1	.00	100.00
2	7.49	93.37
3	15.56	87.46
4	24.13	82.31
5	33.13	77.97
6	42.50	74.46
7	52.15	71.83
8	62.00	70.09
9	71.96	69.26
10	81.96	69.35
11	91.91	70.34
12	101.73	72.25
13	111.33	75.04
14	120.64	78.70
15	129.57	83.20
16	138.05	88.29
17	146.02	92.54
18	153.39	101.29
19	160.12	108.68
20	166.15	116.67
21	168.22	120.00

Circle Center At X = 76.0 ; Y = 178.4 and Radius, 109.2

*** 1.019 ***

Failure Surface Specified By 21 Coordinate Points

Point No.	X-Surf (ft)	Y-Surf (ft)
1	.00	100.00
2	7.29	93.15
3	15.18	87.01
4	23.61	81.63
5	32.50	77.06
6	41.78	73.34
7	51.37	70.50
8	61.18	68.57
9	71.13	67.56
10	81.13	67.48
11	91.10	68.33
12	100.94	70.11
13	110.57	72.80
14	119.91	76.38
15	128.87	80.81
16	137.38	86.05
17	145.37	92.07
18	152.76	98.81
19	159.48	106.21
20	165.50	114.20
21	169.07	120.00

Circle Center At X = 77.0 ; Y = 174.5 and Radius, 107.1

*** 1.019 ***

Failure Surface Specified By 21 Coordinate Points

Point No.	X-Surf (ft)	Y-Surf (ft)
1	6.56	100.00
2	14.27	93.63
3	22.52	87.88
4	31.22	83.09
5	40.34	79.00
6	49.82	75.75
7	59.53	73.36
8	69.41	71.87
9	79.40	71.33
10	89.38	71.60
11	99.33	72.74
12	109.11	74.67
13	118.67	77.63
14	127.93	81.56
15	136.82	86.01
16	145.66	91.37
17	153.18	97.37
18	160.33	104.26
19	167.22	111.67
20	173.23	119.66
21	173.47	120.00

Circle Center At X = 81.3 ; Y = 182.7 and Radius, 111.4

*** 1.022 ***

Failure Surface Specified By 21 Coordinate Points

Point No.	X-Surf (ft)	Y-Surf (ft)
1	.00	100.00
2	7.33	99.19
3	13.26	97.10
4	23.73	91.79
5	33.69	87.28
6	41.87	83.64
7	51.58	78.88
8	61.21	74.04
9	71.37	69.12
10	81.37	69.16
11	91.32	70.10
12	101.17	74.99
13	110.74	79.72
14	120.04	84.47
15	129.85	89.02
16	139.38	93.37
17	143.30	95.50
18	156.59	100.34
19	162.22	107.83
20	165.11	115.91
21	167.54	120.00

Circle Center At X = 76.1 ; Y = 174.6 and Radius, 106.6

*** 1.022 ***

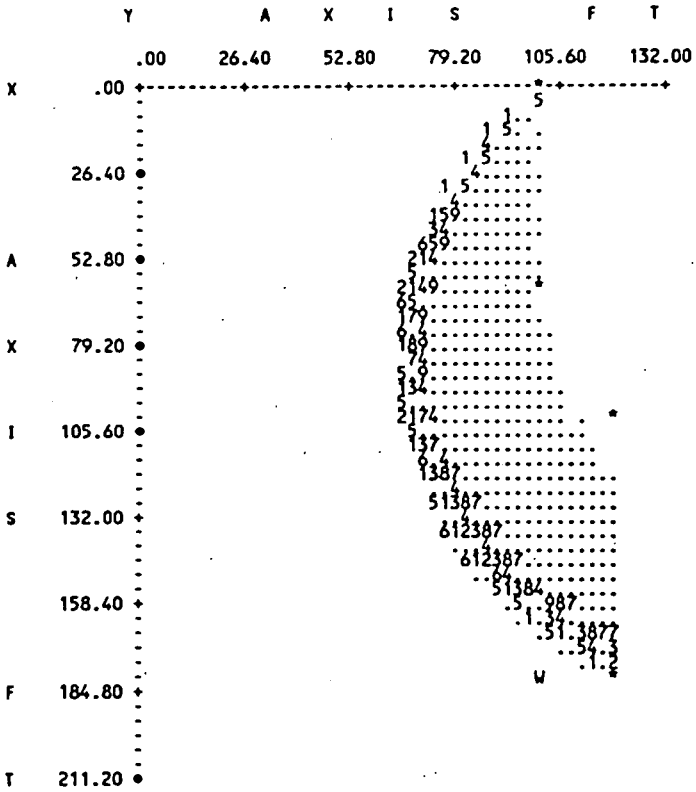

APPENDIX I

DEVELOPMENT OF ARTIFICIAL EARTHQUAKE GROUND MOTIONS

by

Risk Engineering, Inc.
Boulder, Colorado

INTRODUCTION

This Appendix documents the development of artificial time histories compatible with the mean uniform-hazard spectra, for rock-outcrop site conditions and for multiple return periods (i.e., 500, 1000, 2500, 5000, and 10,000 years).

The artificial time histories are generated by adjusting the frequency content of the real ground-motion time history in order to match the target response spectrum, while meeting the requirements in Section 3.7.1 of the NRC Standard Review Plan. These adjustments are made in a manner that preserves the time-domain "character" of the real ground motions.

GROUND MOTION CHARACTERISTICS

The target response spectra for horizontal motions and 5 percent damping are the mean uniform hazard spectra listed in Table 3-2. The spectral velocity at 33 Hz is taken as PGA/(2πx33 Hz), which is consistent with Appendix E.

Target spectra for vertical motions are calculated from the corresponding horizontal spectra by using factors in the EPRI (1993) recommendations, which are described in Appendix E. For ground motions, representing all return periods (corresponding to an earthquake in the RMA/Derby source), the V/H ratio is taken as 0.7 for all frequencies and for PGA.

Target spectra for damping ratios of 2, 7, 10, 12, and 15 percent are obtained using Equations E-20 and E-21 in Appendix E. Following Appendix E, a strong-motion duration of 4.5 sec is assumed in applying these equations.

The target power spectral density function (psdf; also required by the criteria in the NRC Standard Review Plan, NRC, 1989) is calculated from the target response spectrum for 5% damping using the procedure in Section A-2 of Sewell et al. (1991). This procedure recognizes that the mean-square oscillator response at frequency f may be approximated as the sum of two terms, as follows: (1) a dynamic term, which is proportional to the psdf at frequency f, and (2) a static term, which is proportional to the integral of the psdf over frequencies lower than f. Replacing the integral with a summation, one can solve sequentially for the target psdf associated with a given response spectrum, by advancing from the lowest to the highest frequencies of interest. In these calculations,

we use Boore and Joyner's (1984) expression for non-stationary oscillator response, rather than Equations A-3 through A-6 of Sewell et al. (1991).

According to the seismic-hazard results in Section 3 of this report, ground motions for all return periods are dominated by events in the RMA/Derby source (M ~ 5.9, R ~ 27 km). The strong-motion durations associated with this magnitude-distance combination is 4.2 sec (obtained using the equation $T = 1/f_o + 0.05\ R$ by Herrmann, 1985, where f_o is the corner frequency, assuming a stress drop of 120 bars).

METHODOLOGY

1. Select several strong-motion records with magnitudes and distances consistent with those that dominate seismic hazard at the site, for the return periods of interest.

2. Perform iterative adjustments to the frequency content of these ground motions to obtain a close match to the target spectra and PGA, while meeting the enveloping requirements (NRC, 1989) with respect to both response spectrum at multiple damping ratios and power spectrum. These adjustments are performed using multiple causal filters, thus preserving the general time-domain "character" of the original ground motions.

3. Select the artificial time histories with the closest match to the target spectra. High-pass filtering of the filtered record may be required in order to remove spurious low frequencies (< 0.5 Hz) introduced during the filtering.

4. Verify that the selected artificial motions meet the NRC requirements with respect to response spectra and power spectra. In addition, the artificial ground motions were checked for compliance with the requirements in Section 2.3 of ASCE 4-86 (ASCE, 1986), including the requirement of independence between the time histories for different components.

SELECTION OF REAL RECORDS

Table I-1 lists the records used as starting points in the development of the selected artificial ground motions. Records from the 1984 Morgan Hill earthquake were selected for both horizontal and vertical components at all return periods, in order to obtain strong-motion durations longer than 4 seconds (using Kennedy et al., 1984, definition of duration). The strong motions listed in Table I-1 are shorter than the minimum 6 seconds required by the NRC (1989; see below), but these shorter durations are justified on the basis of the magnitudes that dominate seismic hazard at the Rocky Flats Plant (as compared to California sites).

NRC REQUIREMENTS

The most important requirements in Section 3.7.1 of the NRC Standard Review Plan (NRC, 1989) for artificial ground motions are summarized below:

1. Consistency between the artificial and target spectra must be checked at frequencies specified in Table 3.7.1-1 of NRC (1989) or at frequencies with a spacing of 10% or less. We consider frequencies between 0.5 and 33 Hz, with a 10% spacing. The spectrum of the artificial ground motion may be lower than the target spectrum at no more than five points and cannot be lower than the target by more than 10%.

2. The power spectral density function of the artificial ground motion must exceed 80% of the theoretical spectral density function derived from the target spectrum. We calculate the power spectra of the artificial ground motions using the procedure in Appendix A of Philippacopolous (1989), as suggested in NRC (1989).

3. The strong-motion duration (or stationary-phase duration) should be between 6 and 15 seconds. Different durations may be used if justified by site-specific information.

RESULTS

The figures that follow show the generated time histories (Figures I-1--I-15), response spectra (Figures I-16--I-30), and power spectra (Figures I-31--I-45) for two horizontal components and one vertical component, and for five return periods. In Figures I-16 through I-45, the dashed lines indicate the smooth target spectra; the solid lines indicate the spectra calculated from the records. The numbers in each panel in Figures I-16 through I-30 denote damping ratios.

The artificial time histories of acceleration and velocity retain the time-domain character of the original ground motions. The response spectra of the artificial motions provide a reasonable match to the target response spectra, especially for damping ratios of 5% or higher. It is difficult to obtain a closer match because of the requirement on the power spectrum.

REFERENCES

American Society of Civil Engineers (1986). *ASCE Standard: Seismic Analysis of Safety-Related Nuclear Structures and Commentary on Standard for Seismic Analysis of Safety Related Structures*, ASCE 4-86.

Boore, D.M. and W.B. Joyner (1984). A Note on the Use of Random Vibration Theory to Predict Peak Amplitudes of Transient Signals, *Bull. Seism. Soc. Am.*, Vol. 74, No. 5, October, pp. 2035-2039.

EPRI (1993). *Guidelines for Determining Design Basis Ground Motions, Volume 1: Method and Guidelines for Estimating Earthquake Ground Motion in Eastern North America*, Electric Power Research Institute, TR-102293, Project 3302, November.

Herrmann, R.B. (1985). An extension of random vibration theory estimates of strong ground motion to large distances, *Bull. Seism. Soc. Am.*, 75, 1447-1453.

Kennedy, R.P., S.A. Short, K.L. Merz, F.J. Tokarz, I.M. Idriss, M.S. Power and K. Sadigh (1984). *Engineering Characterization of Ground Motion, Task I: Effects of Characteristics of Free Field Motions on Structural Response*, Technical Report NUREG/CR-3805, U.S. Nuclear Regulatory Commission.

Nuclear Regulatory Commission (1989). *Standard Review Plan, Part 3.7.1 Seismic Design Parameters, Revision 2*, NUREG-0800, Office of Nuclear Reactor Regulation, August.

Philippacopolous, A.J. (1989). *Recommendations for Resolution of Public Comments on USI A-40, Seismic Design Criteria*, Technical Report NUREG/CR-5374, U.S. Nuclear Regulatory Commission, June.

Sewell, R.T., G.R. Toro and R.K. McGuire (1991). *Impact of Ground Motion Characteristics on Conservatism and Variability in Seismic Risk Estimates*, Final Report to the U.S. Nuclear Regulatory Commission, Contract NRC-04-89-098, Risk Engineering, Inc., May.

Vanmarcke, E.H. and S.P. Lai (1980). Strong-motion duration and rms amplitude of earthquake records, *Bull. Seism. Soc. Am.*, 70, 1293-1307.

TABLE I-1

REAL RECORDS USED IN THE DEVELOPMENT OF ARTIFICIAL GROUND MOTIONS

EVENT	M	RECORD	RUPTURE DISTANCE	COMP	DURATION*	USED FOR
1984 Morgan Hill	6.1	Gavilan College	16.2	N67	5.1/3.0	First Horizontal Component, all return periods
		Gilroy Array No. 2	15.1	N0	6.8/3.2	Second Horizontal Component, all return periods
		Gilroy Array No. 1	16.2	UP	4.5/2.6	Vertical Component, all return periods

* The first duration measure is calculated following Kennedy et al., 1984. The second duration measure is calculated following Vanmarcke and Lai (1980).

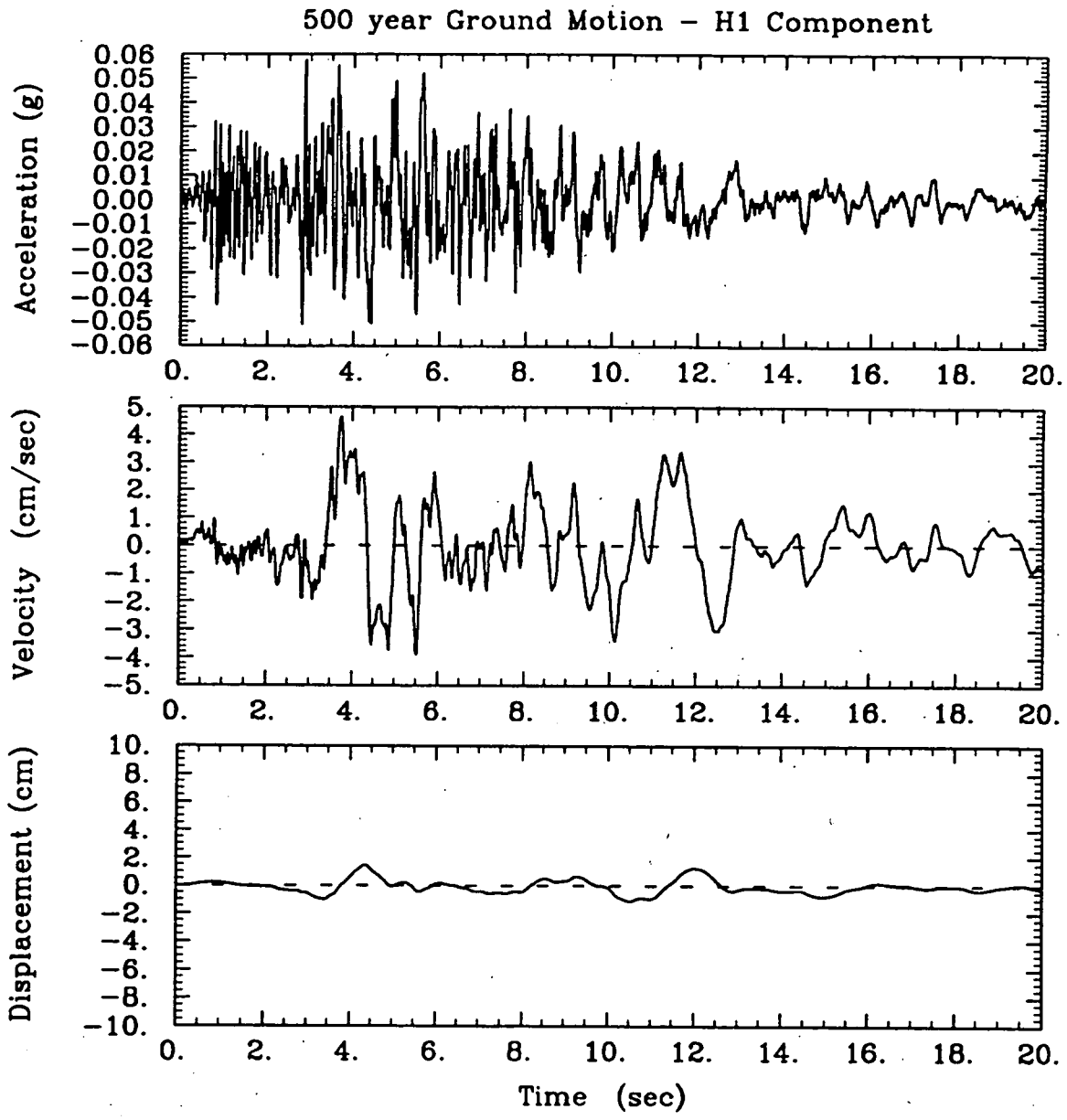

Figure I-1. Time histories of artificial acceleration, velocity, and displacement. Return period: 500 years; component: first horizontal.

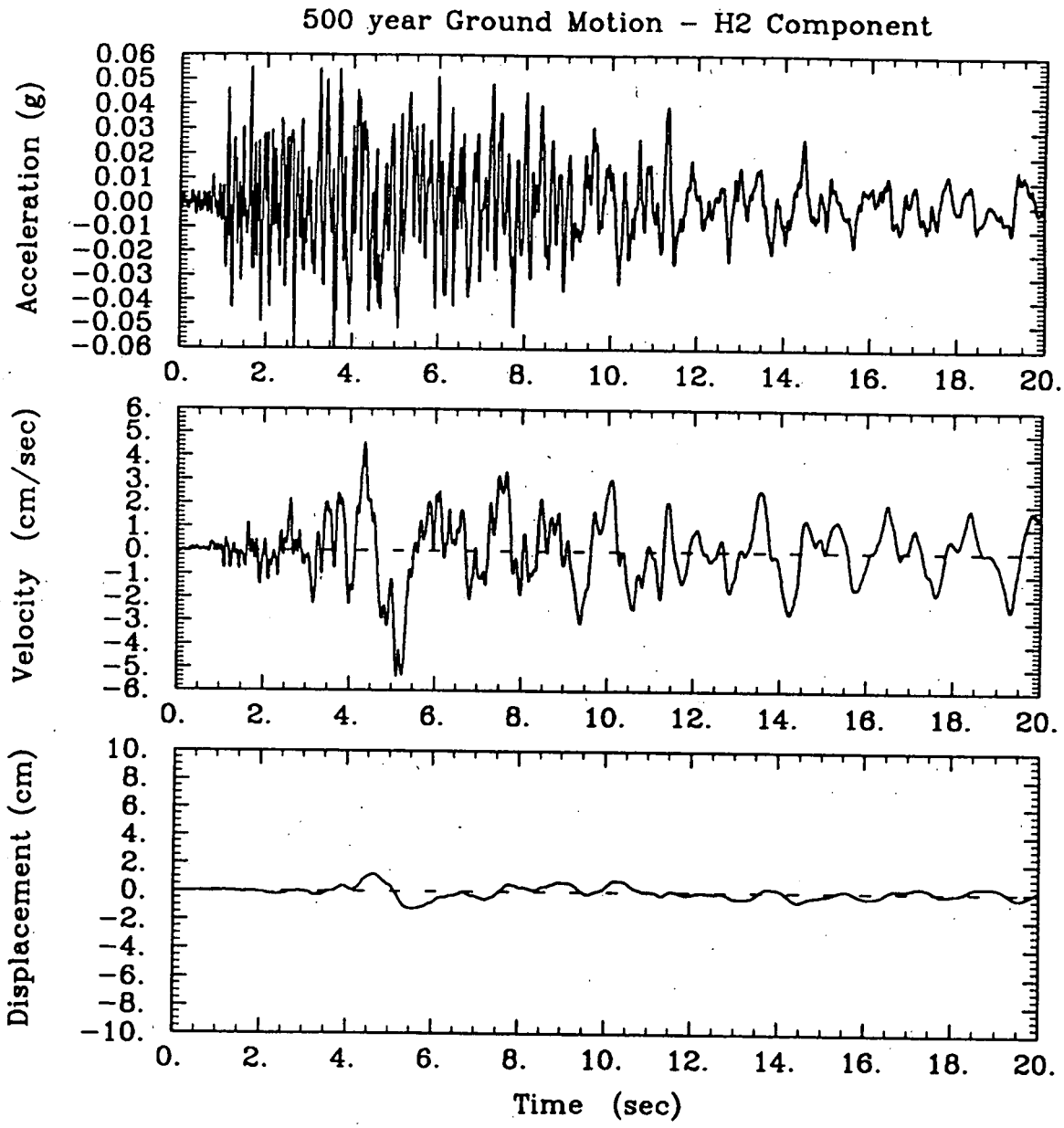

Figure I-2. Time histories of artificial acceleration, velocity, and displacement. Return period: 500 years; component: second horizontal.

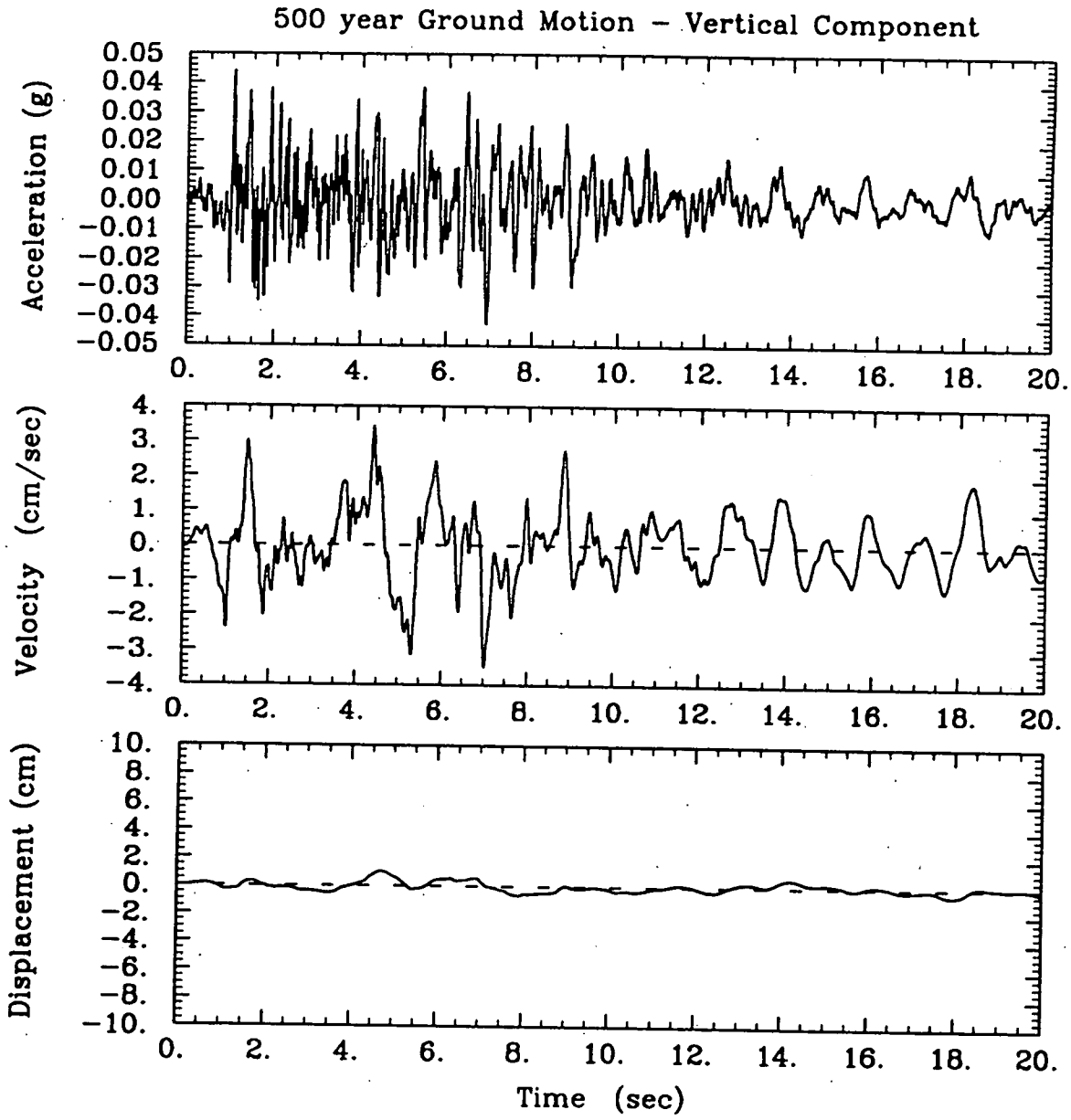

Figure I-3. Time histories of artificial acceleration, velocity, and displacement. Return period: 500 years; component: vertical.

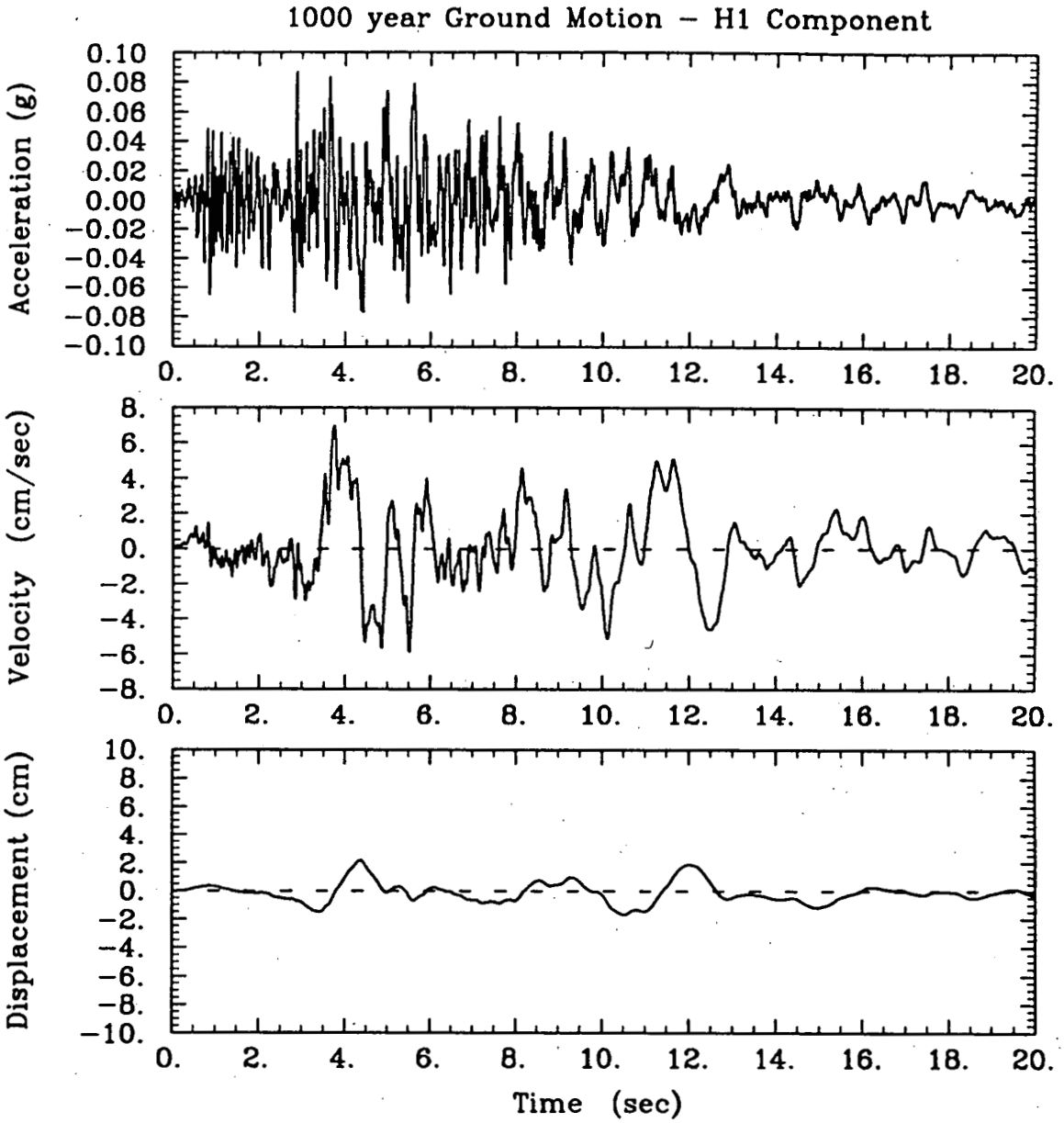

Figure I-4. Time histories of artificial acceleration, velocity, and displacement. Return period: 1000 years; component: first horizontal.

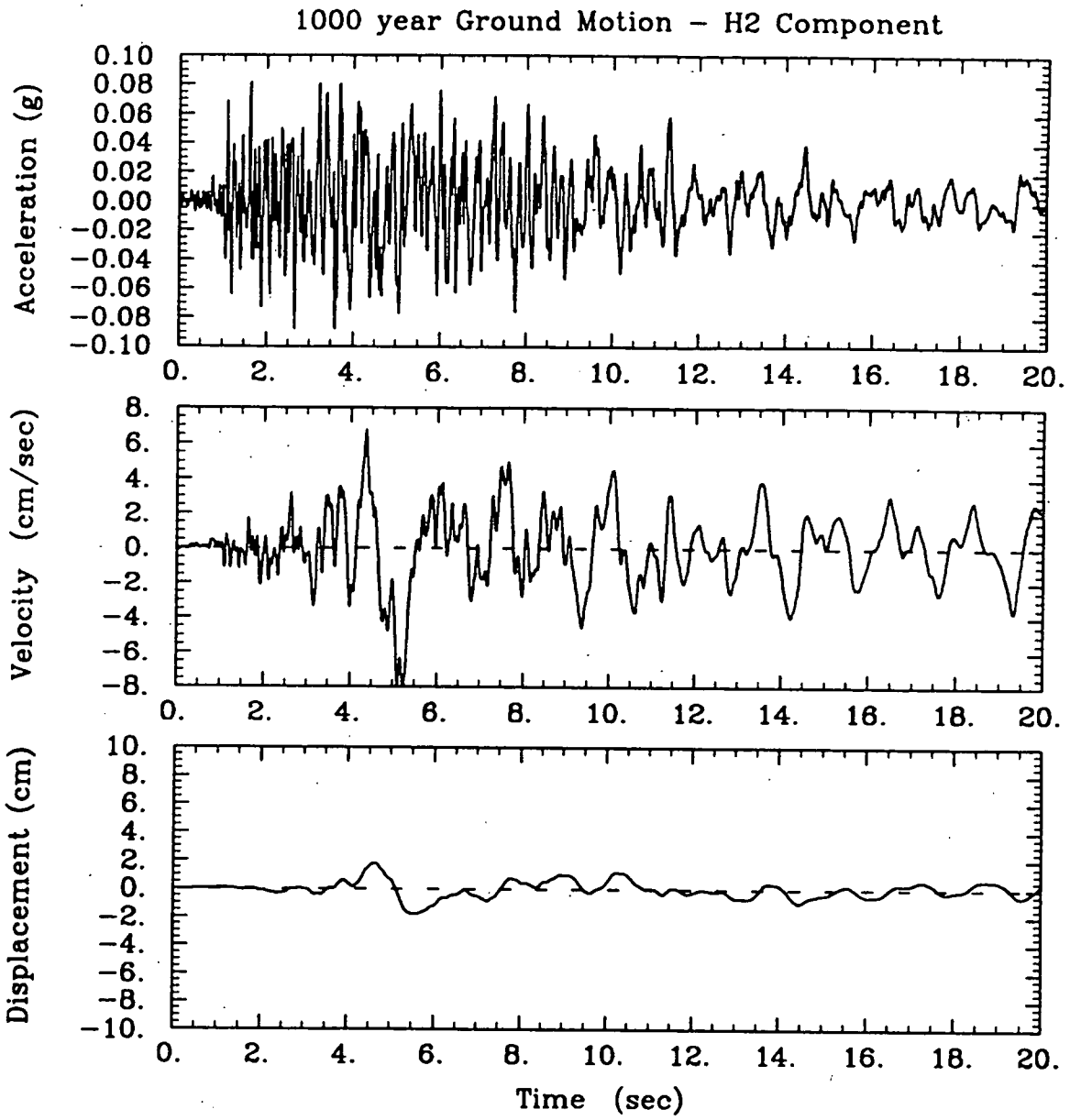

Figure I-5. Time histories of artificial acceleration, velocity, and displacement. Return period: 1000 years; component: second horizontal.

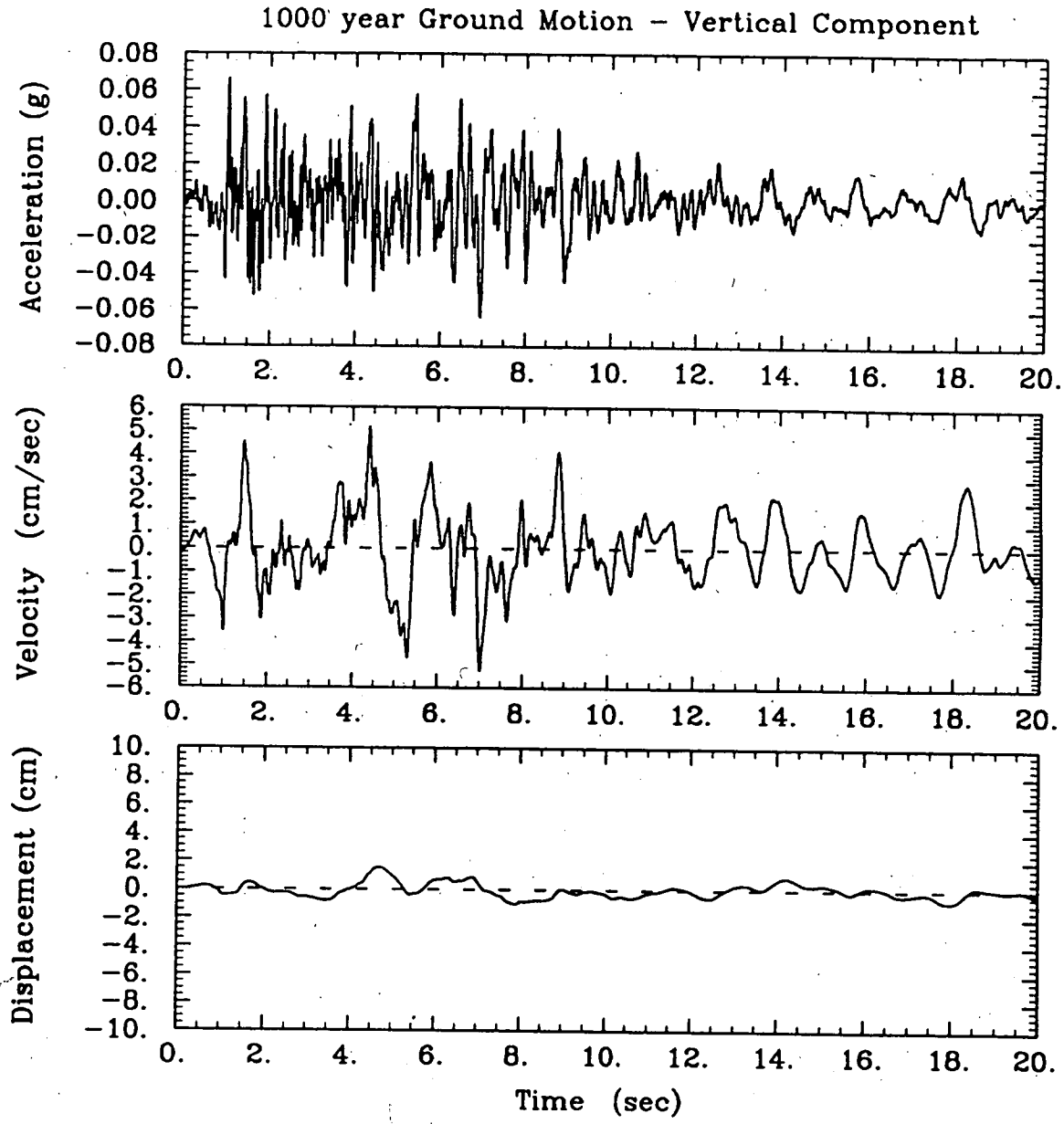

Figure I-6. Time histories of artificial acceleration, velocity, and displacement. Return period: 1000 years; component: vertical.

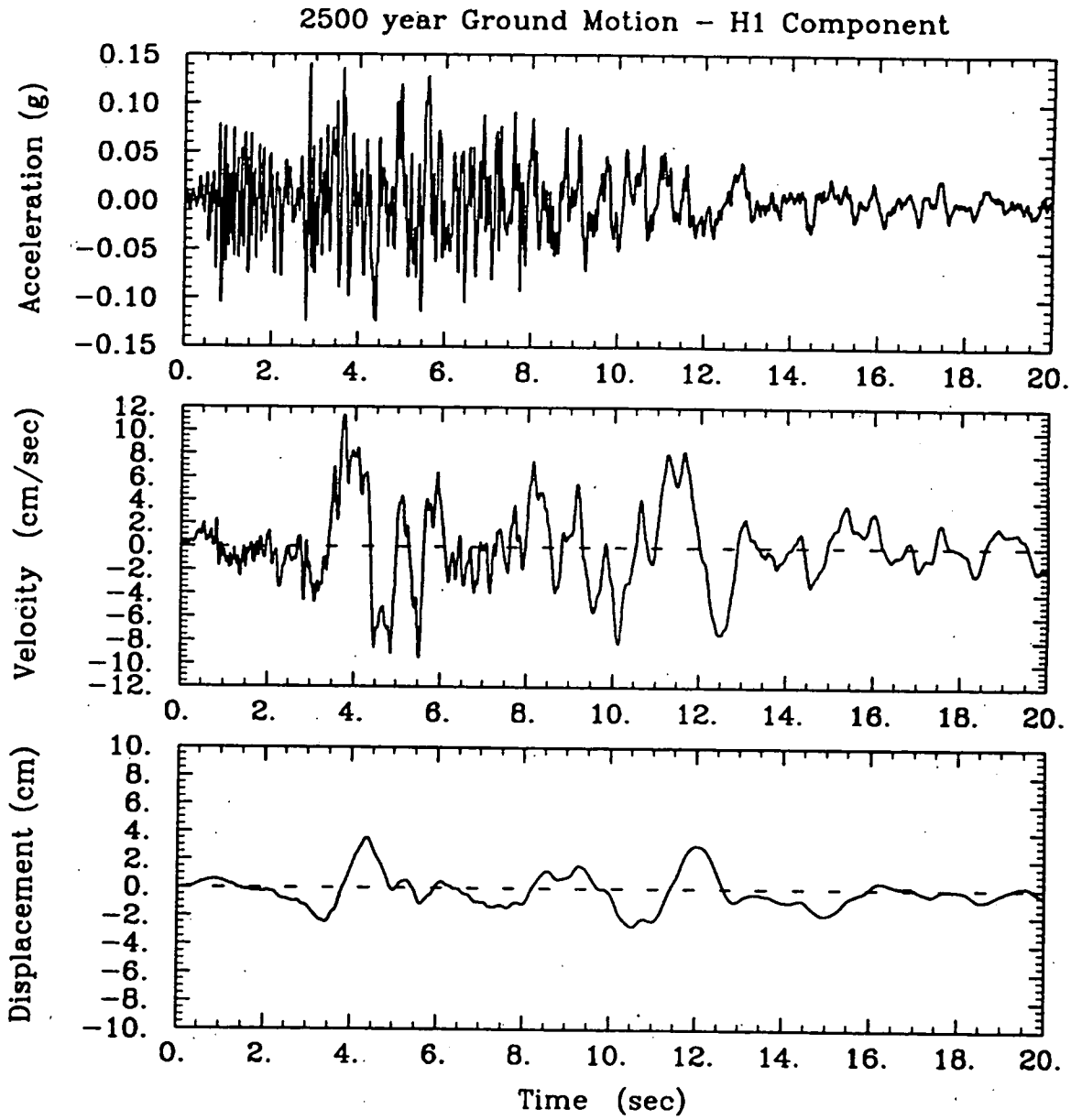

Figure I-7. Time histories of artificial acceleration, velocity, and displacement. Return period: 2500 years; component: first horizontal.

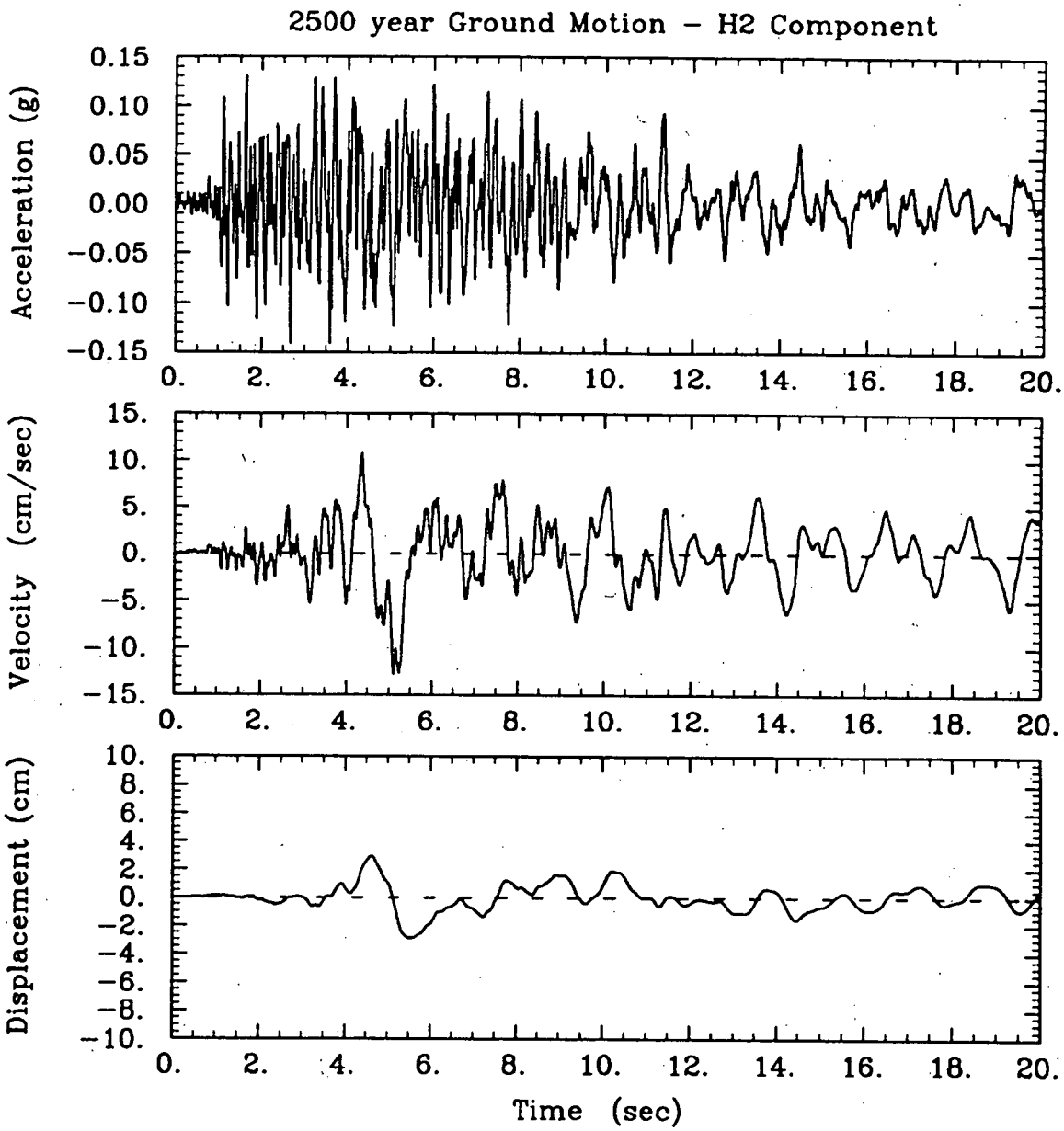

Figure I-8. Time histories of artificial acceleration, velocity, and displacement. Return period: 2500 years; component: second horizontal.

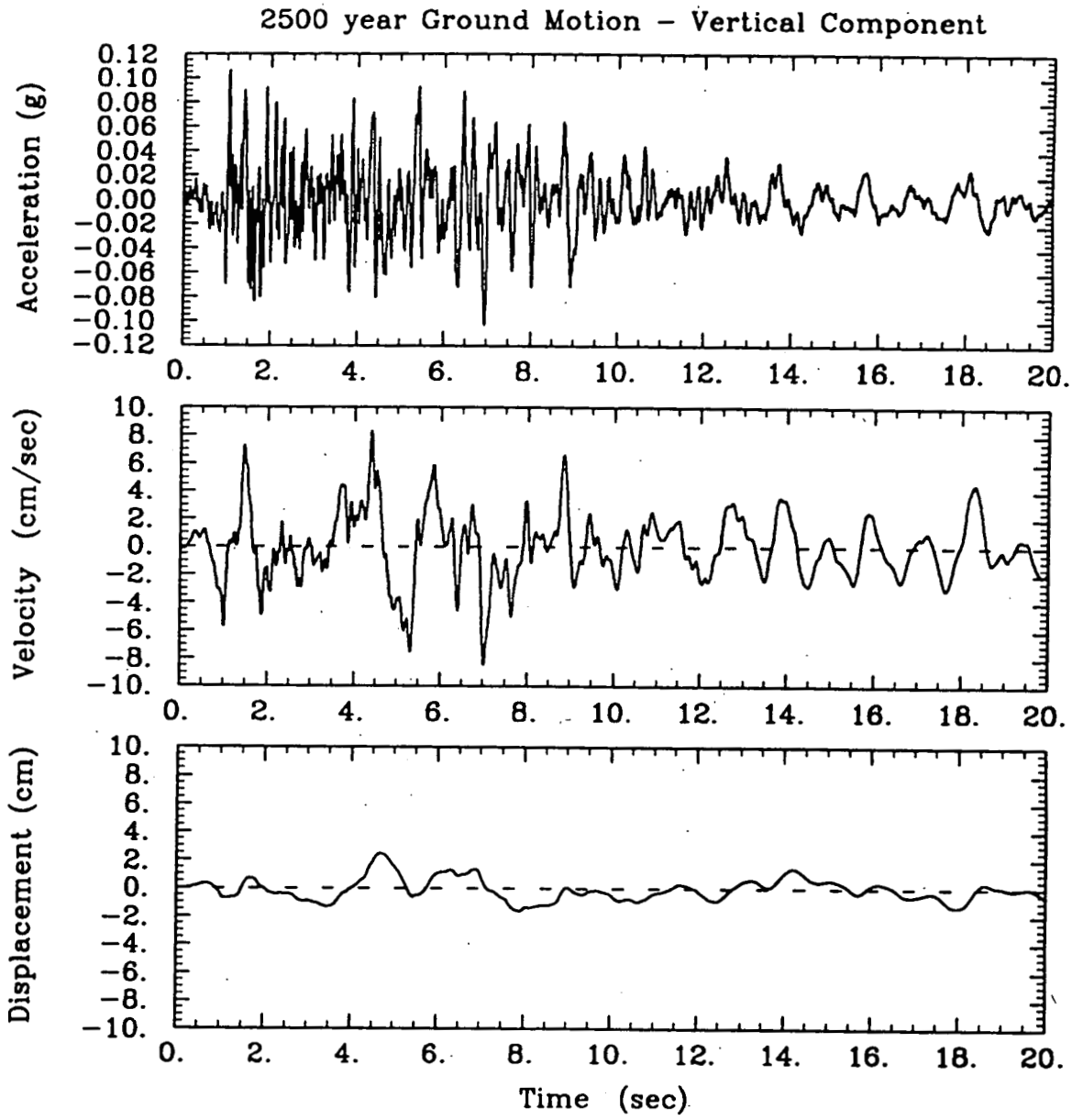

Figure I-9. Time histories of artificial acceleration, velocity, and displacement. Return period: 2500 years; component: vertical.

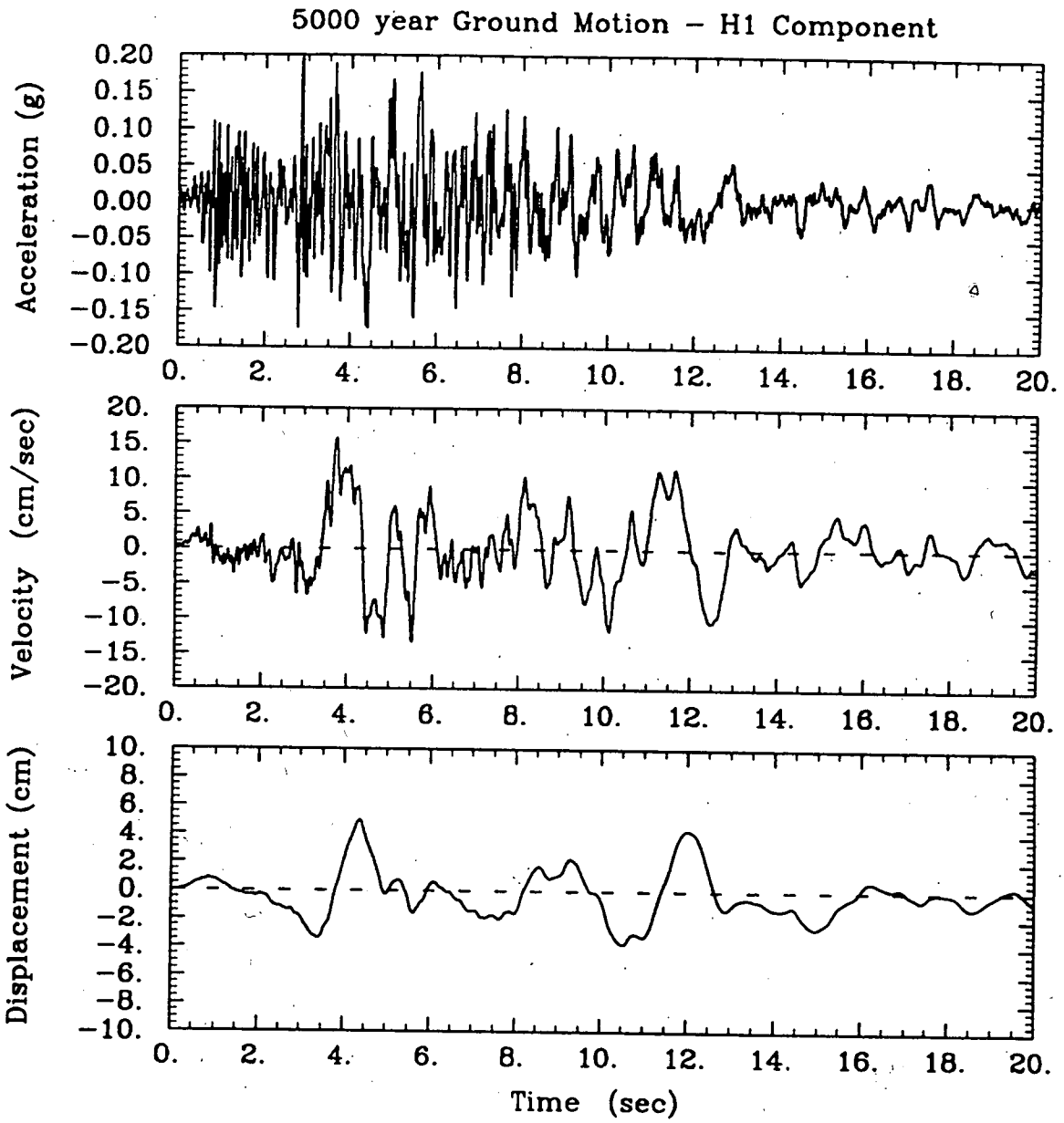

Figure I-10. Time histories of artificial acceleration, velocity, and displacement. Return period: 5000 years; component: first horizontal.

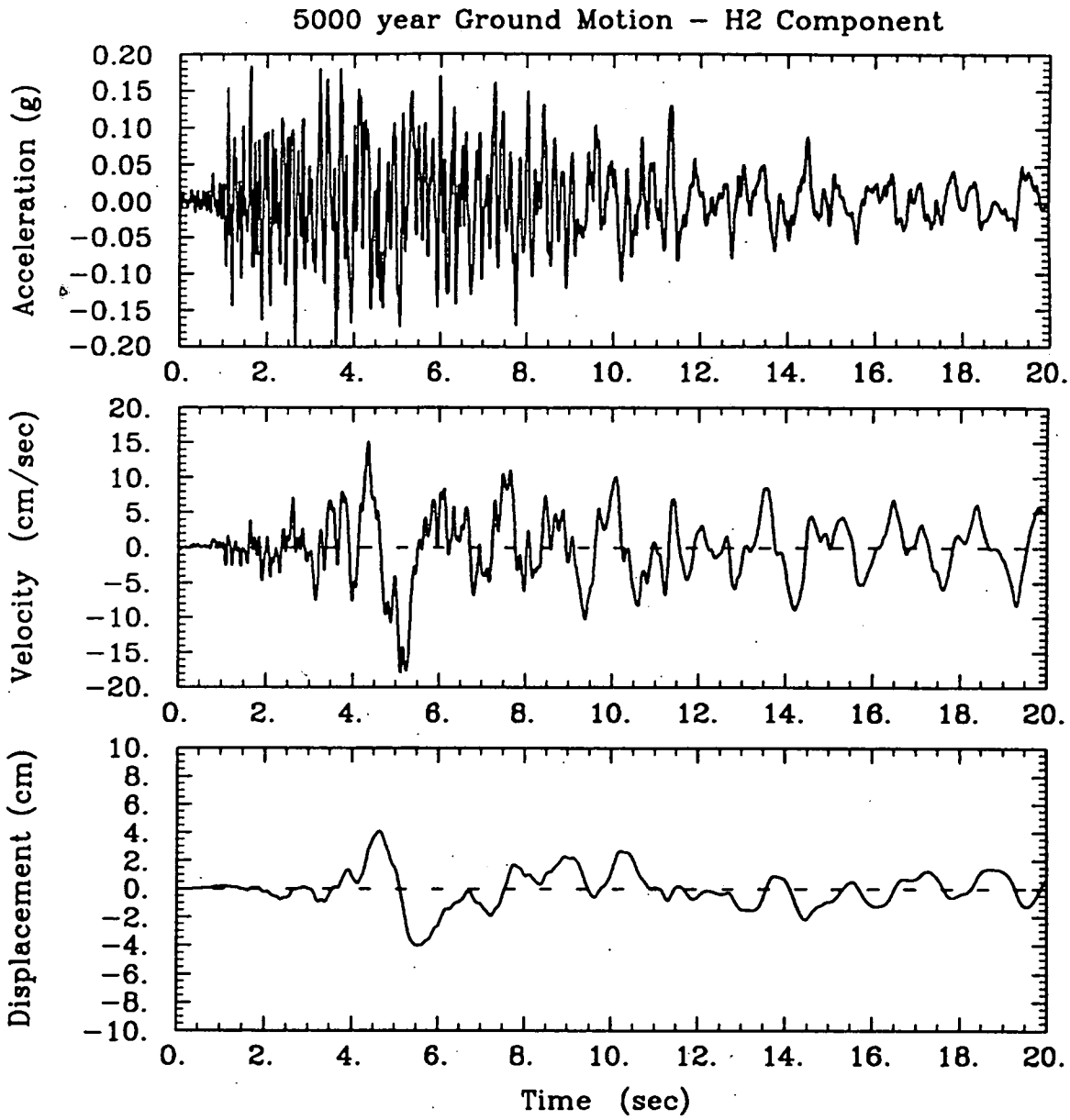

Figure I-11. Time histories of artificial acceleration, velocity, and displacement. Return period: 5000 years; component: second horizontal.

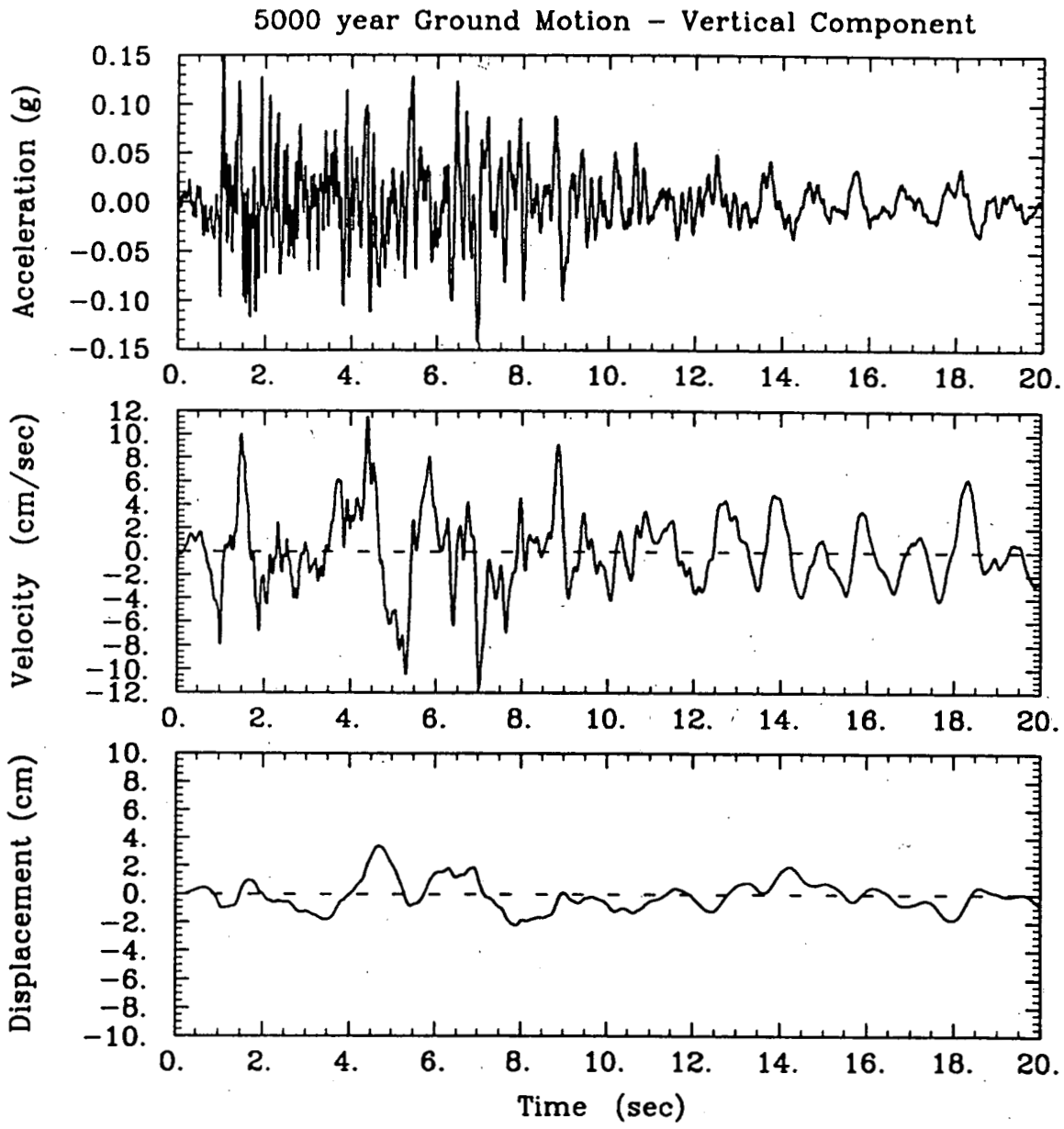

Figure I-12. Time histories of artificial acceleration, velocity, and displacement. Return period: 5000 years; component: vertical.

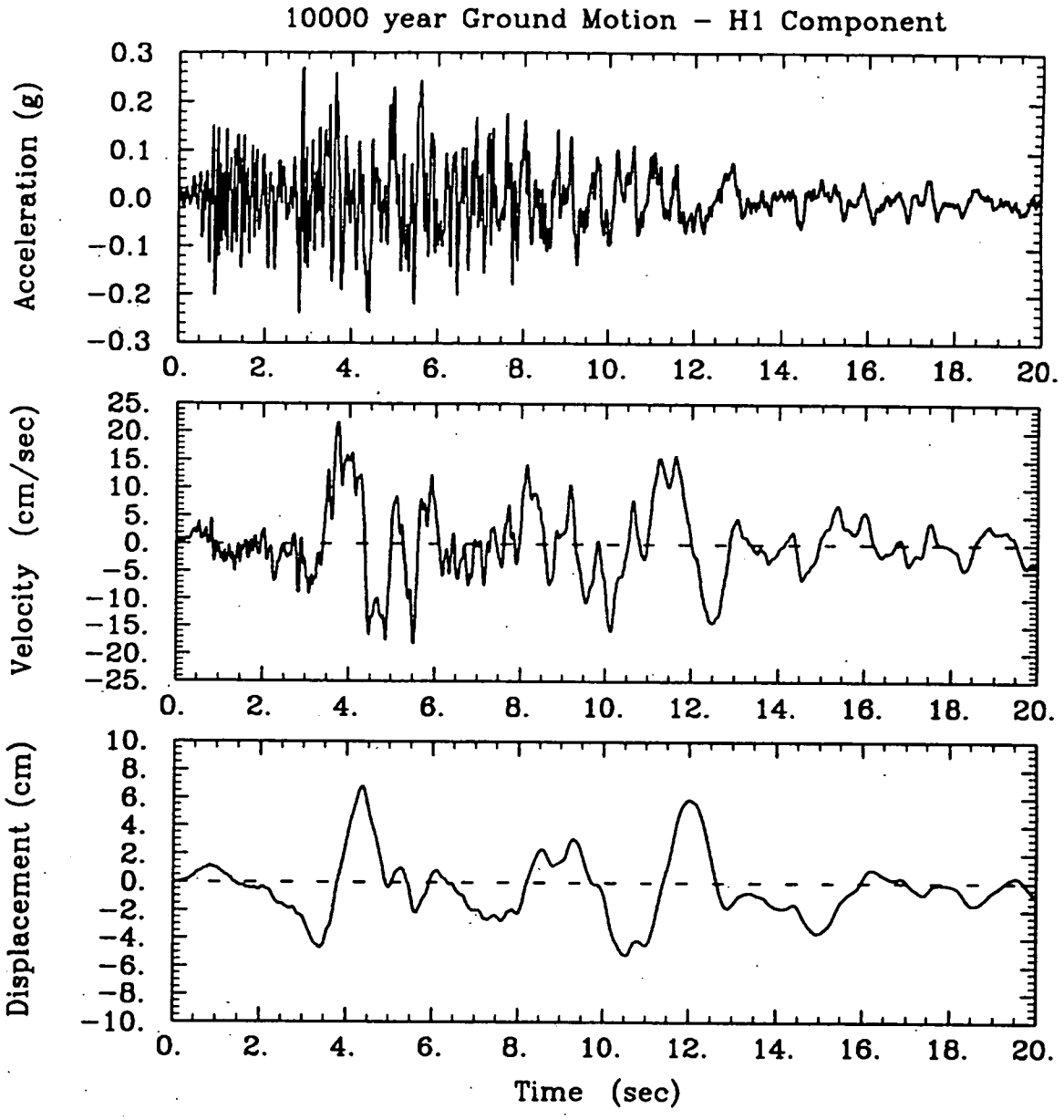

Figure I-13. Time histories of artificial acceleration, velocity, and displacement. Return period: 10,000 years; component: first horizontal.

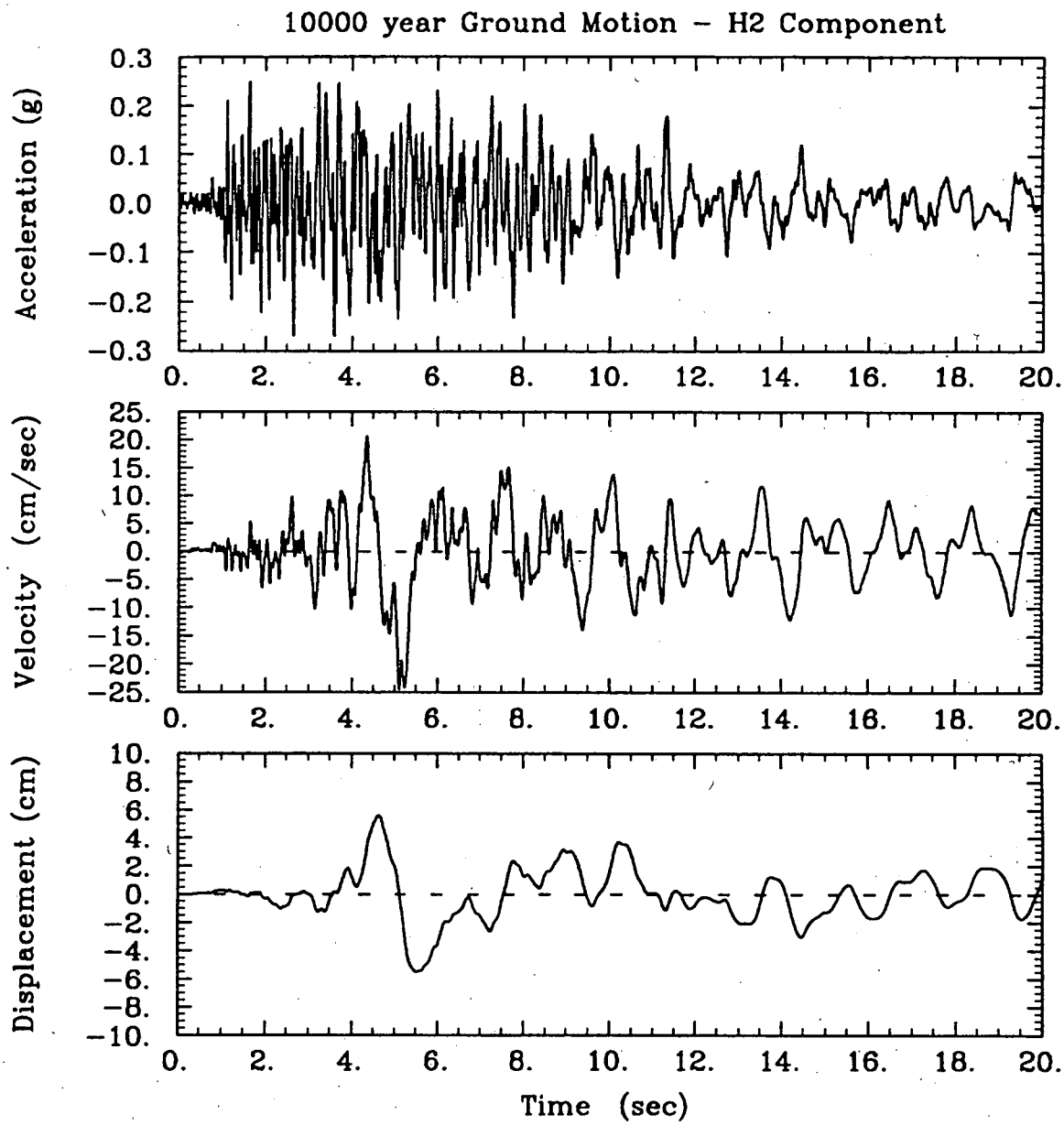

Figure I-14. Time histories of artificial acceleration, velocity, and displacement. Return period: 10,000 years; component: second horizontal.

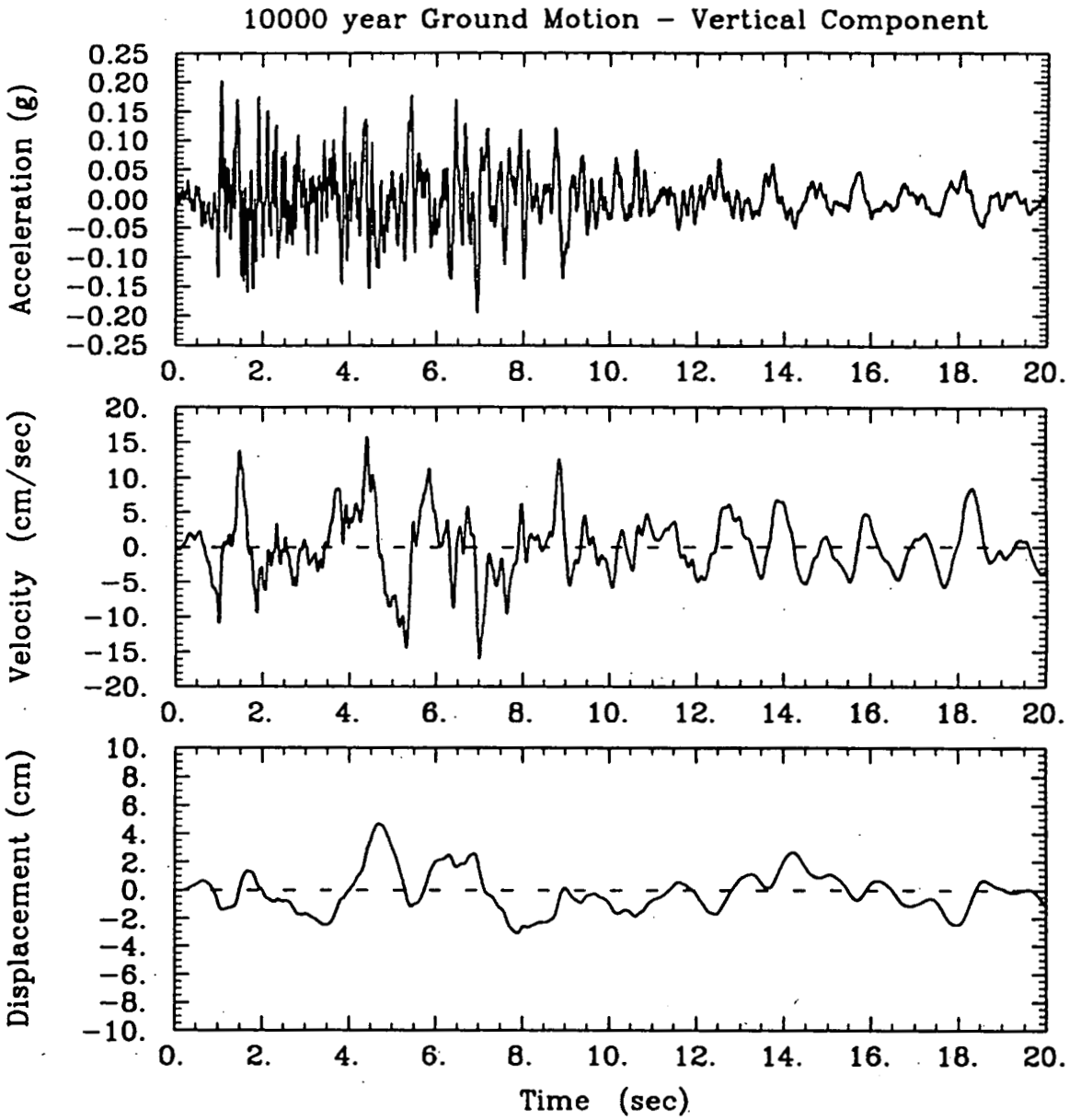

Figure I-15. Time histories of artificial acceleration, velocity, and displacement. Return period: 10,000 years; component: vertical.

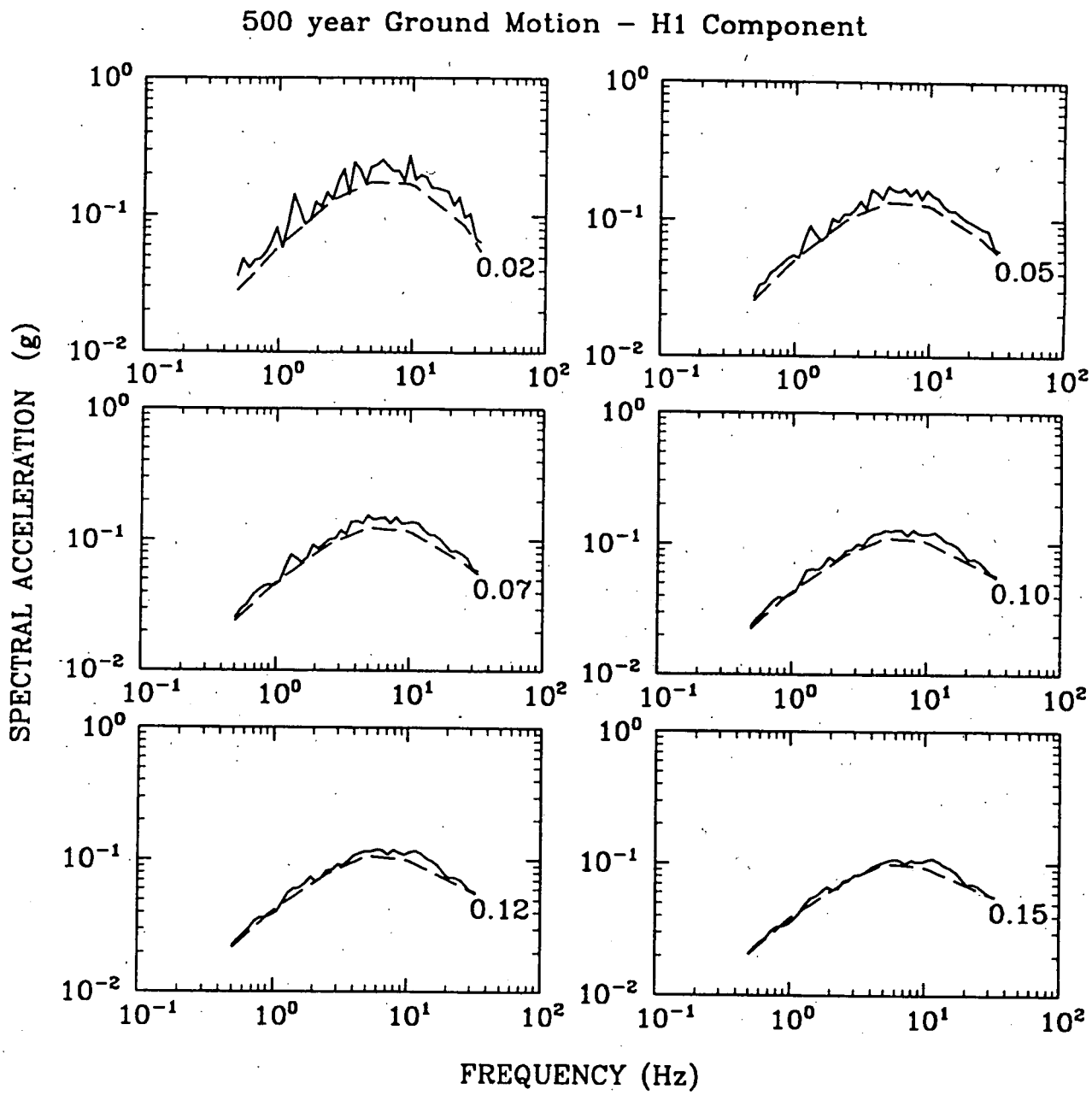

Figure I-16. Response spectra of artificial ground motions are compared to the target spectra. Return period: 500 years; component: first horizontal. Damping values are indicated on each panel.

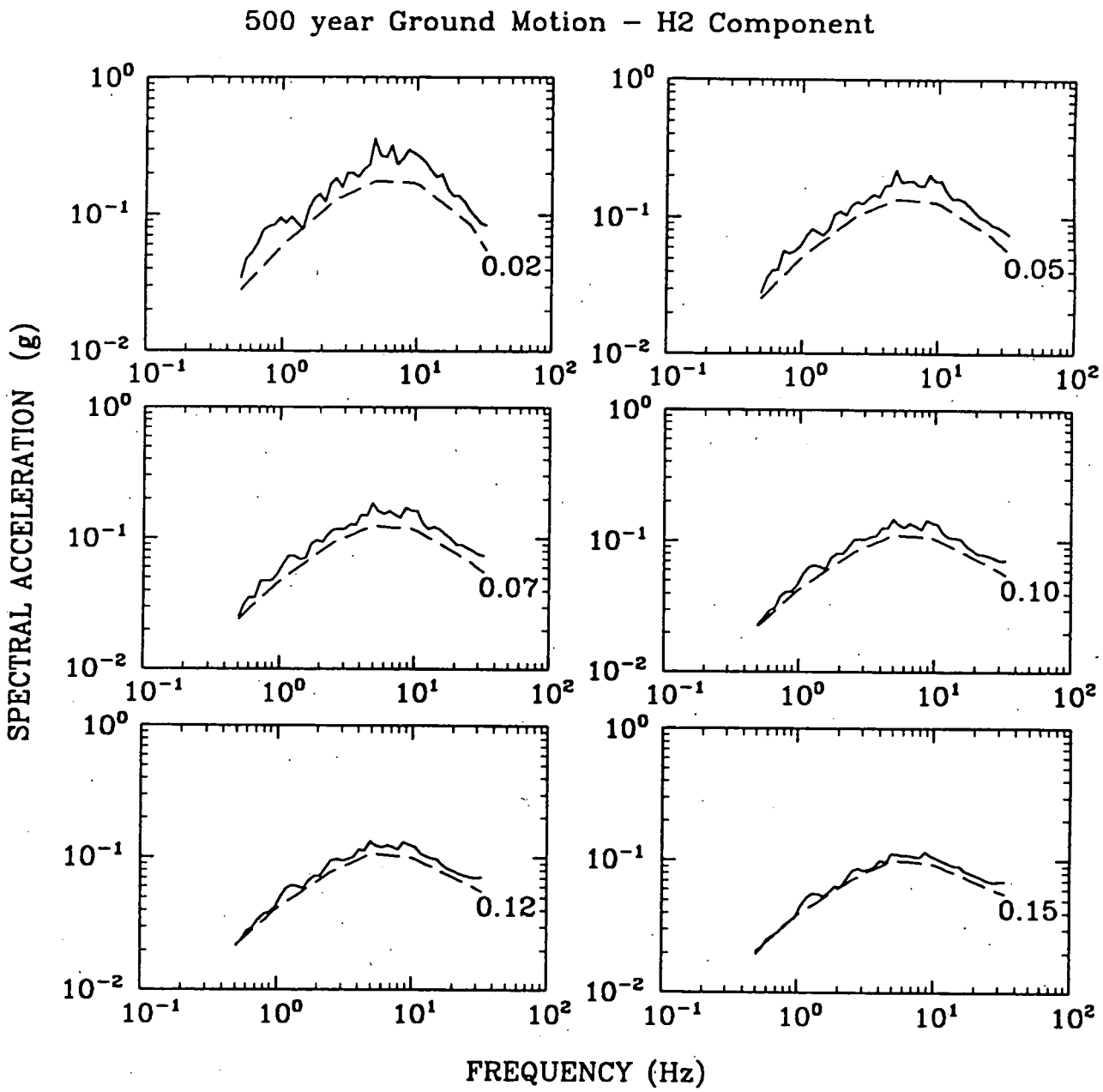

Figure I-17. Response spectra of artificial ground motions are compared to the target spectra. Return period: 500 years; component: second horizontal. Damping values are indicated on each panel.

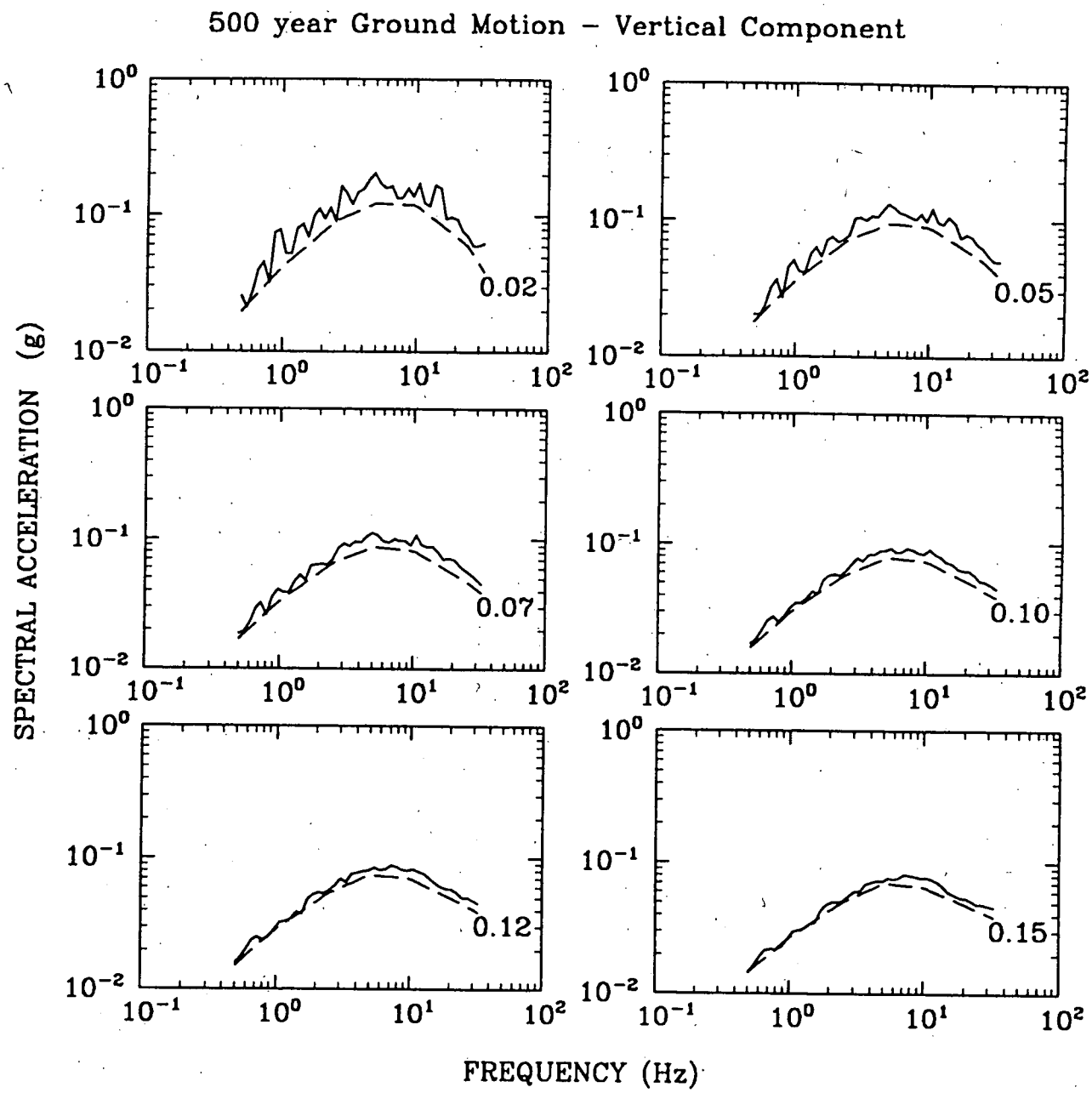

Figure I-18. Response spectra of artificial ground motions are compared to the target spectra. Return period: 500 years; component: vertical. Damping values are indicated on each panel.

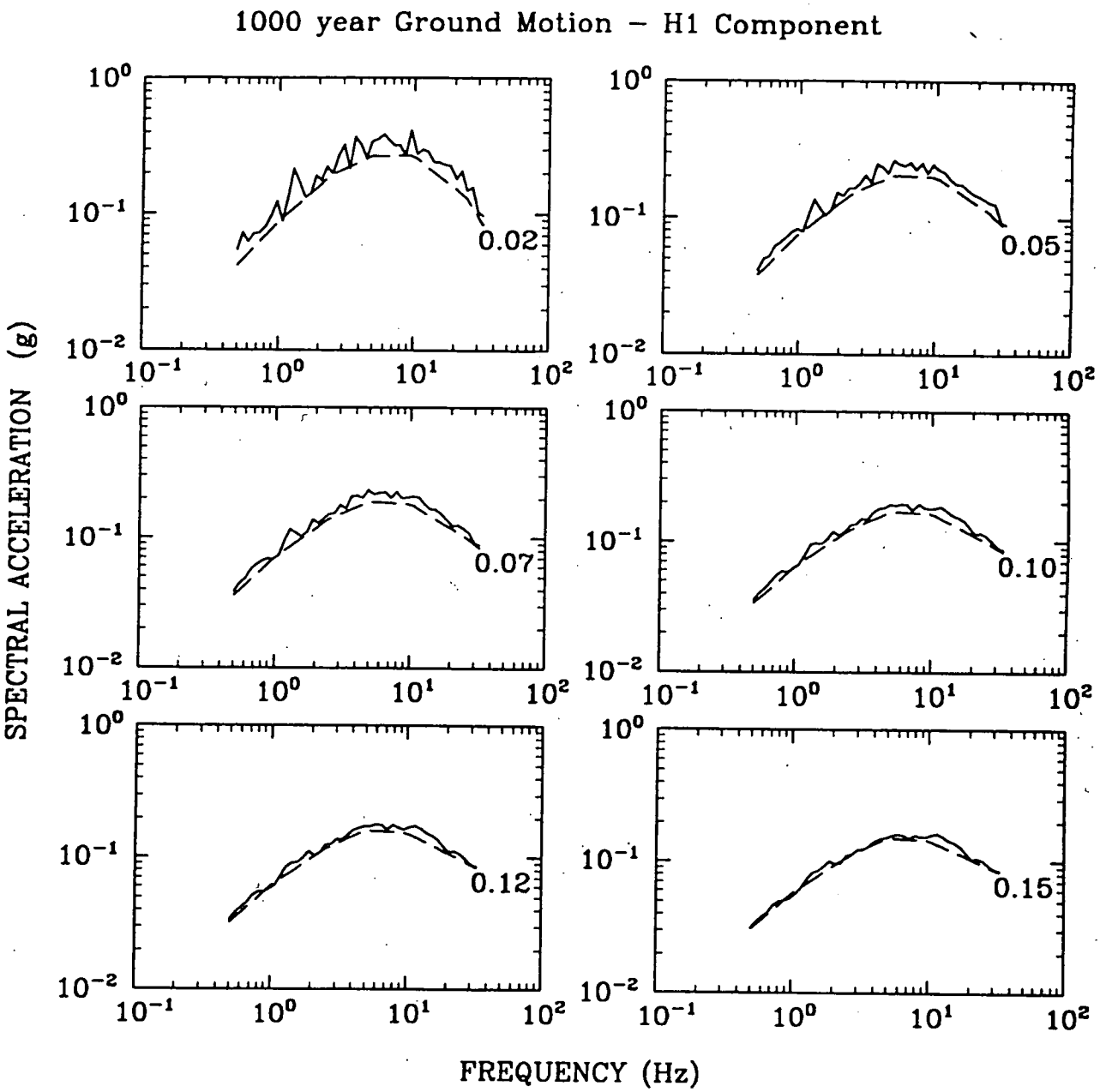

Figure I-19. Response spectra of artificial ground motions are compared to the target spectra. Return period: 1000 years; component: first horizontal. Damping values are indicated on each panel.

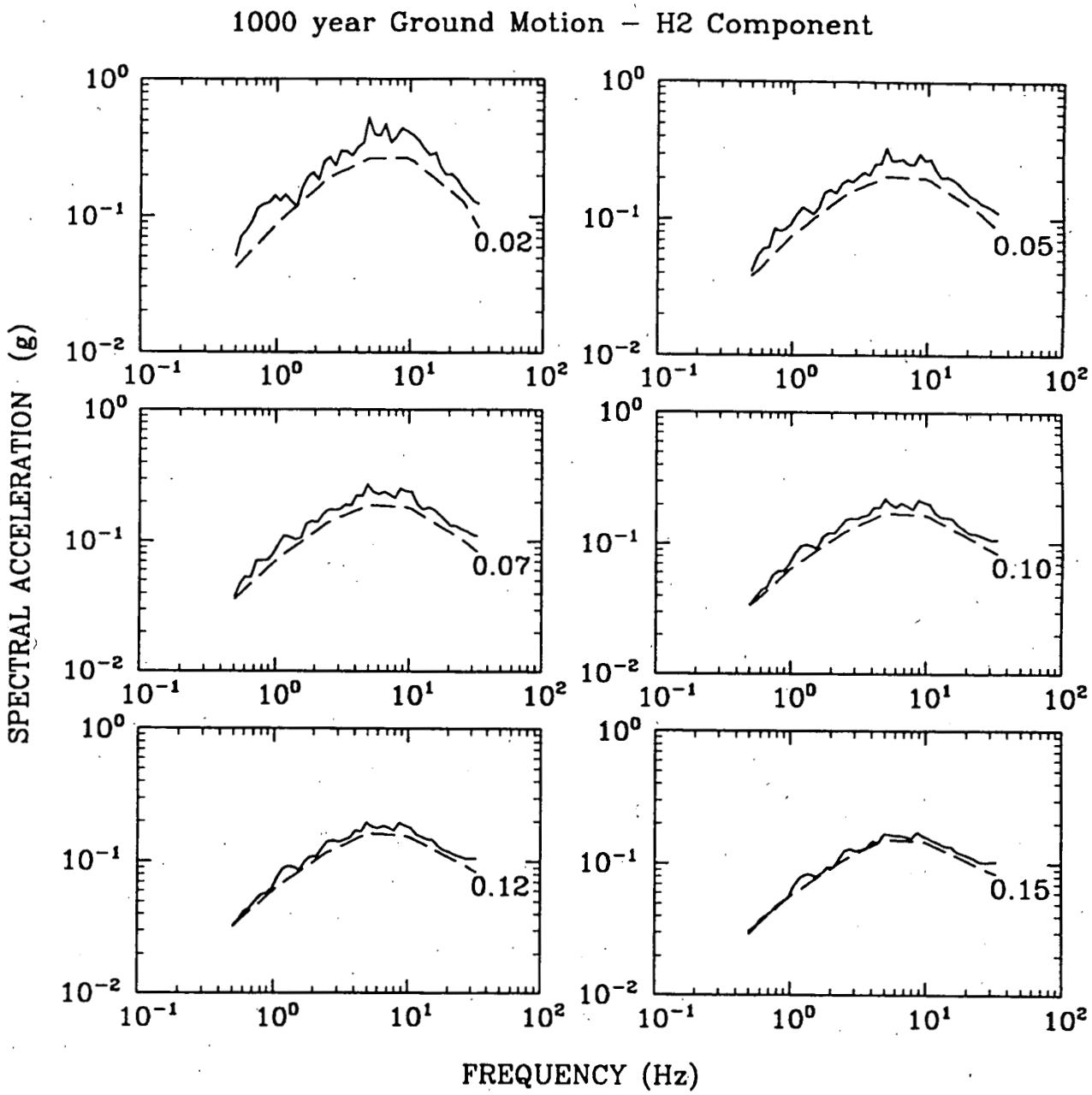

Figure I-20. Response spectra of artificial ground motions are compared to the target spectra. Return period: 1000 years; component: second horizontal. Damping values are indicated on each panel.

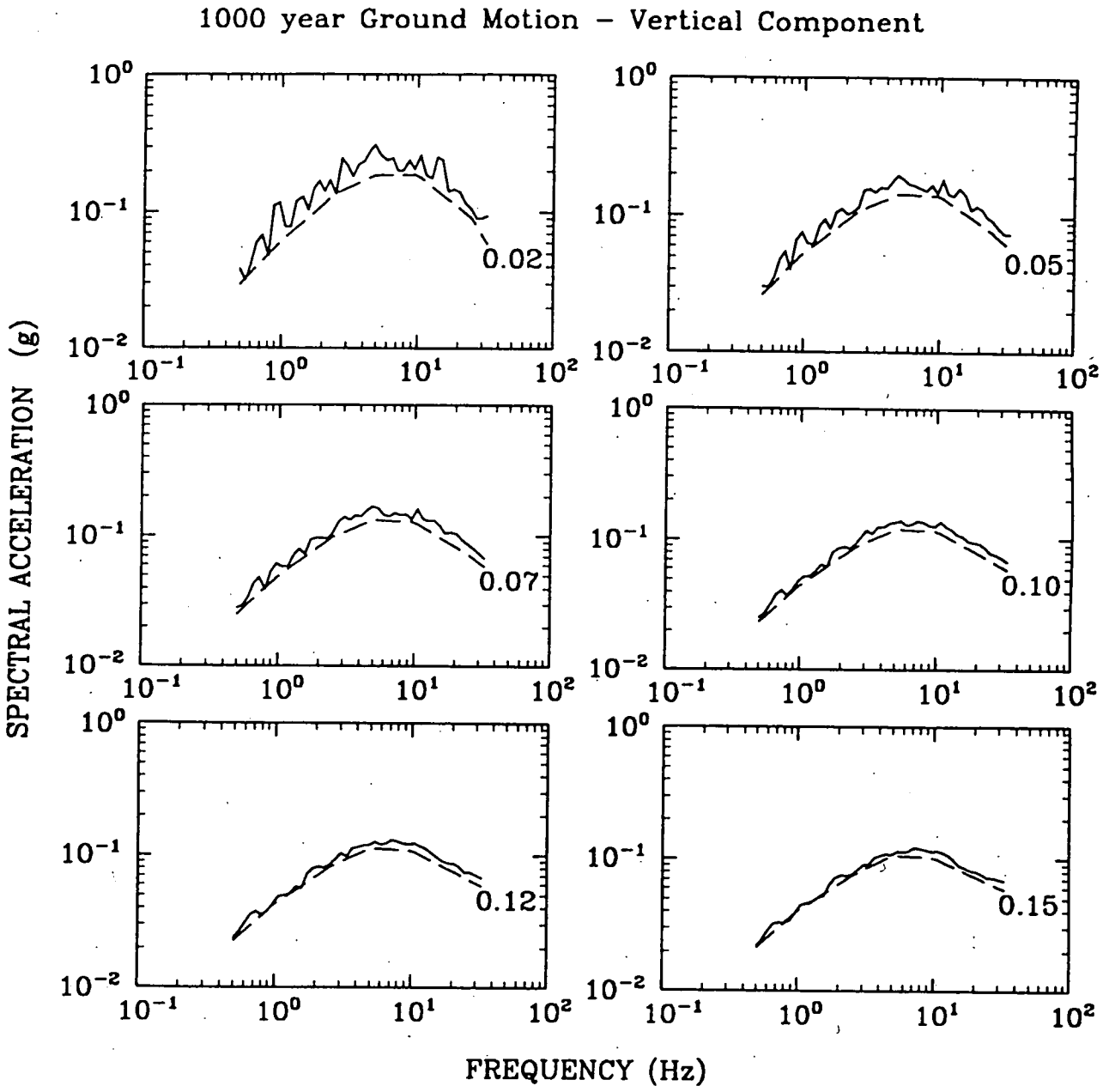

Figure I-21. Response spectra of artificial ground motions are compared to the target spectra. Return period: 1000 years; component: vertical. Damping values are indicated on each panel.

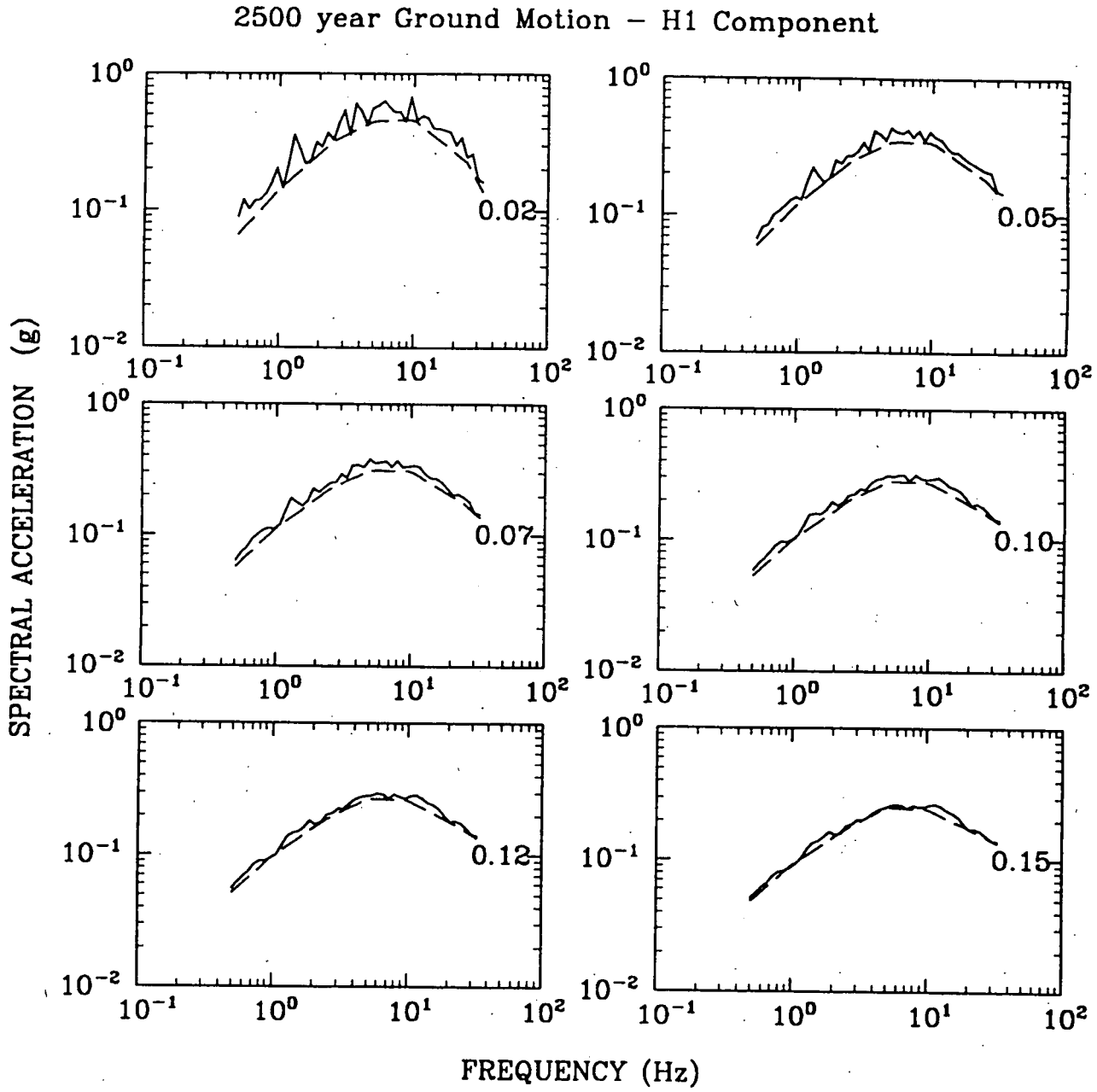

Figure I-22. Response spectra of artificial ground motions are compared to the target spectra. Return period: 2500 years; component: first horizontal. Damping values are indicated on each panel.

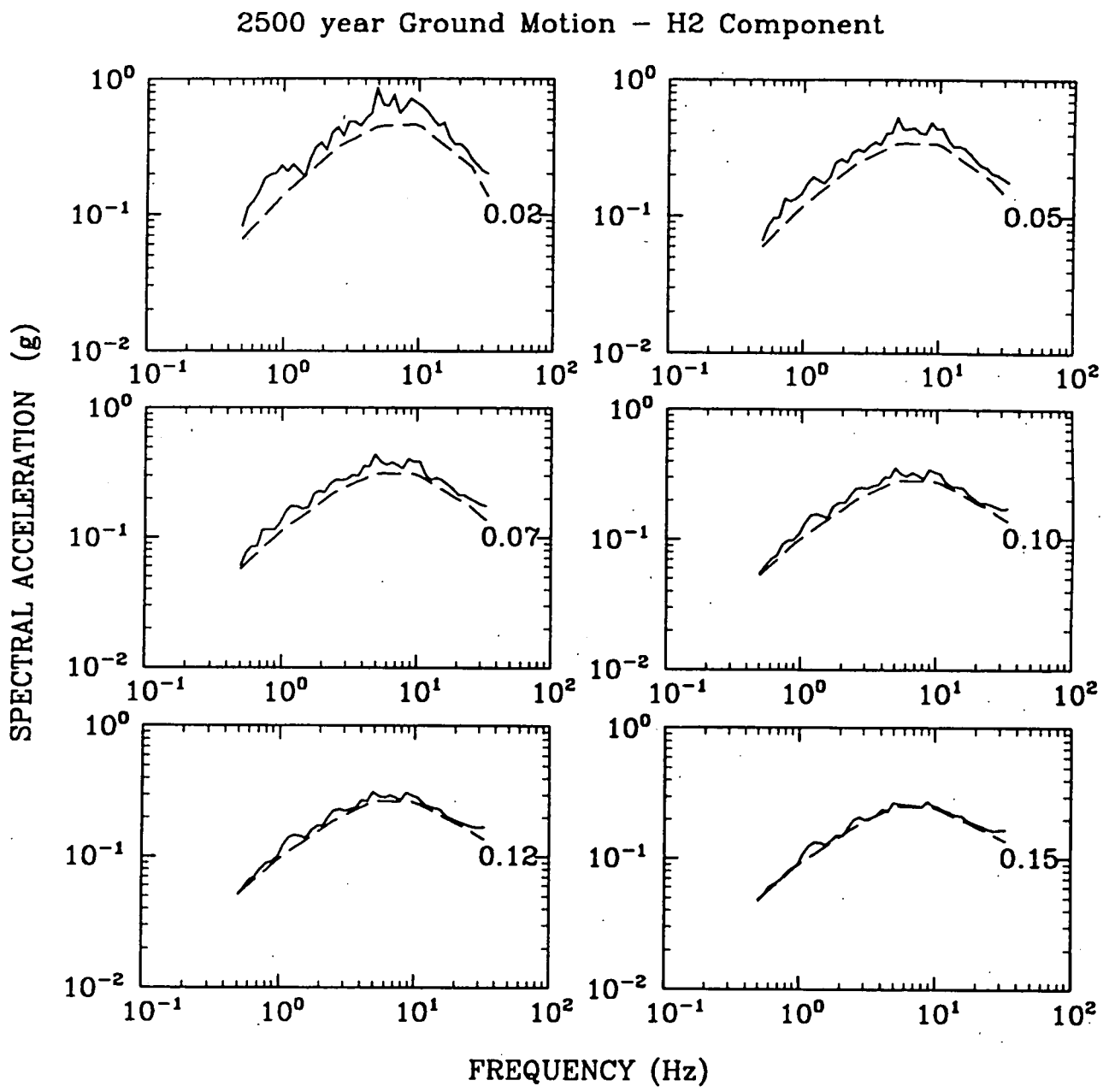

Figure I-23. Response spectra of artificial ground motions are compared to the target spectra. Return period: 2500 years; component: second horizontal. Damping values are indicated on each panel.

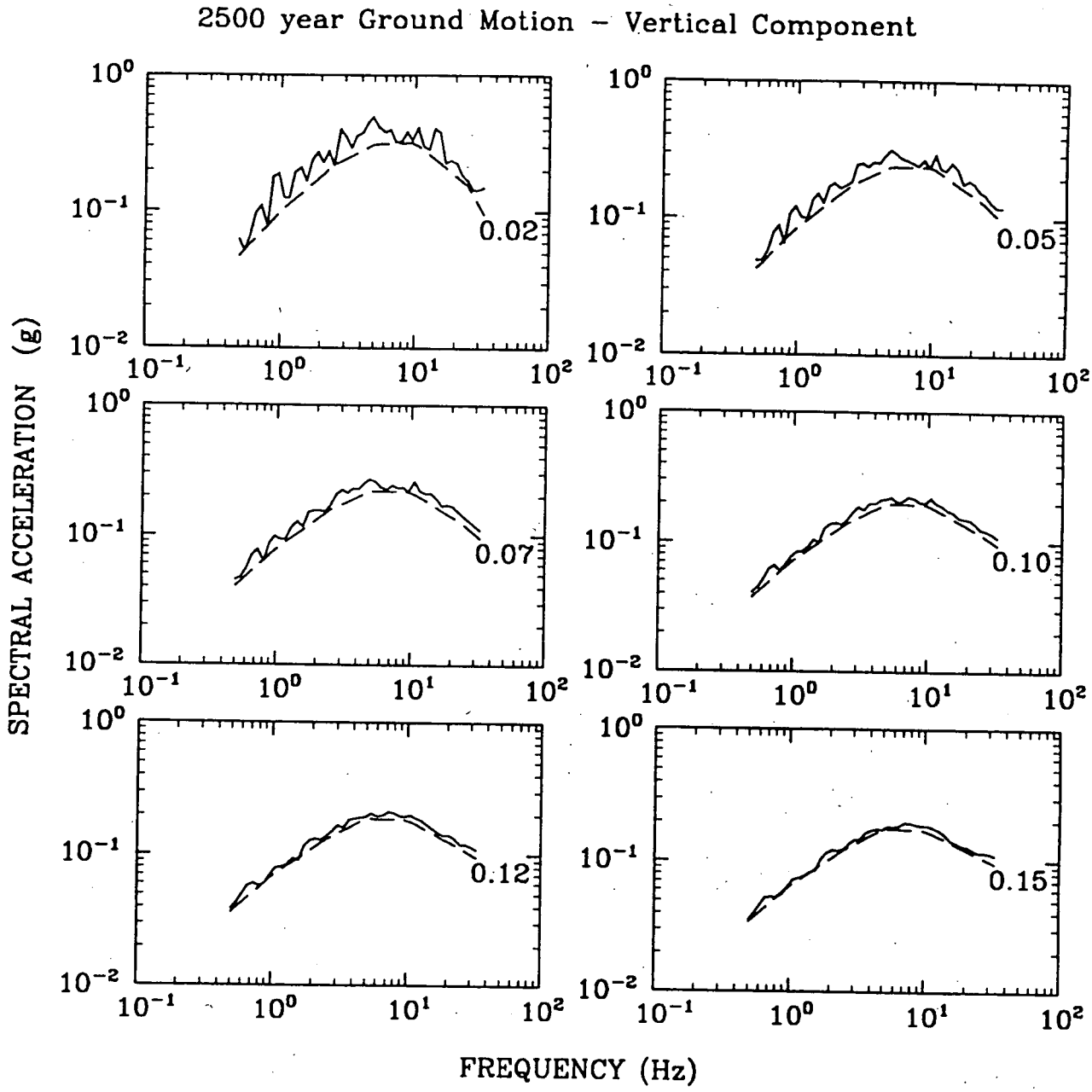

Figure I-24. Response spectra of artificial ground motions are compared to the target spectra. Return period: 2500 years; component: vertical. Damping values are indicated on each panel.

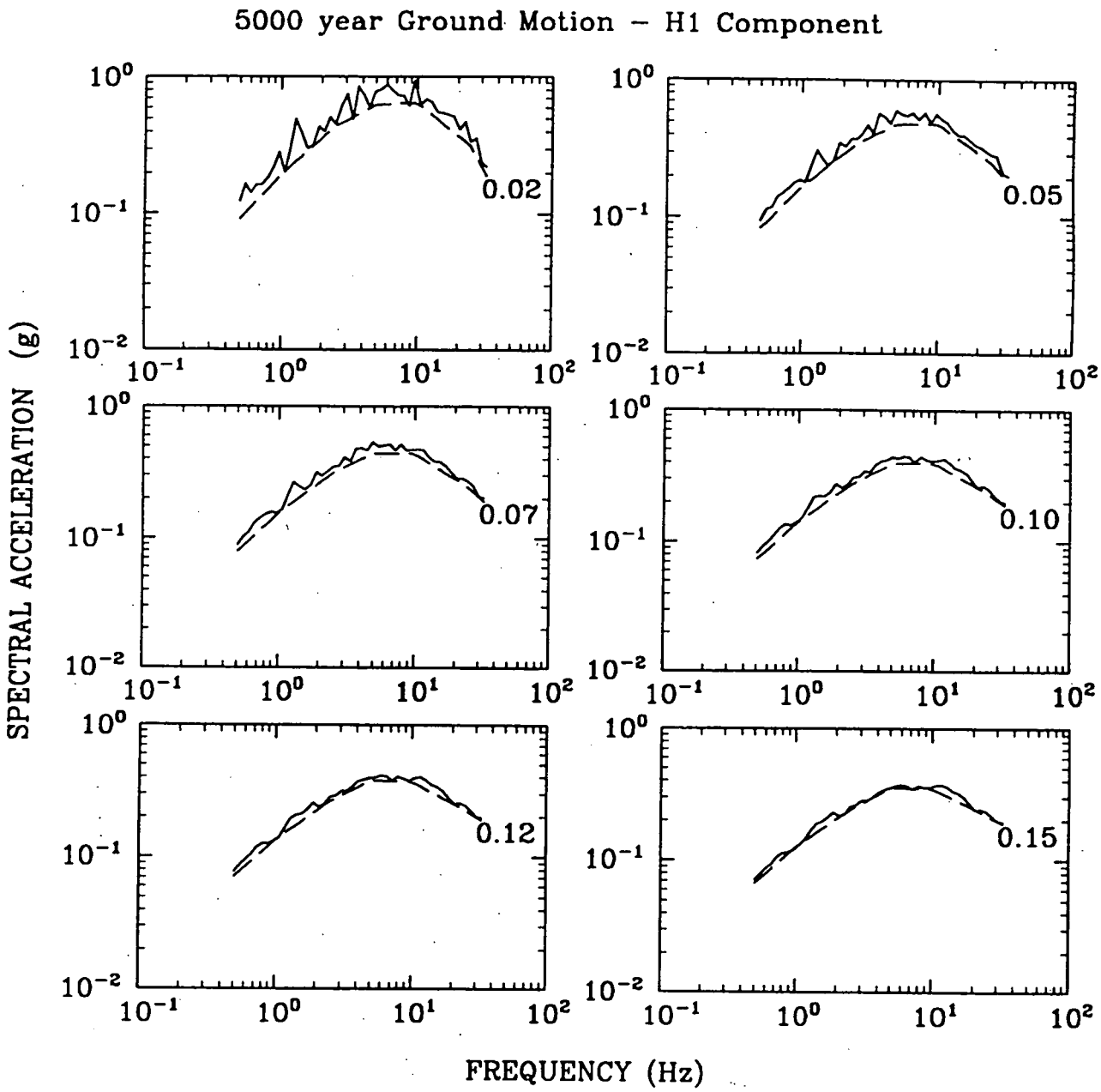

Figure I-25. Response spectra of artificial ground motions are compared to the target spectra. Return period: 5000 years; component: first horizontal. Damping values are indicated on each panel.

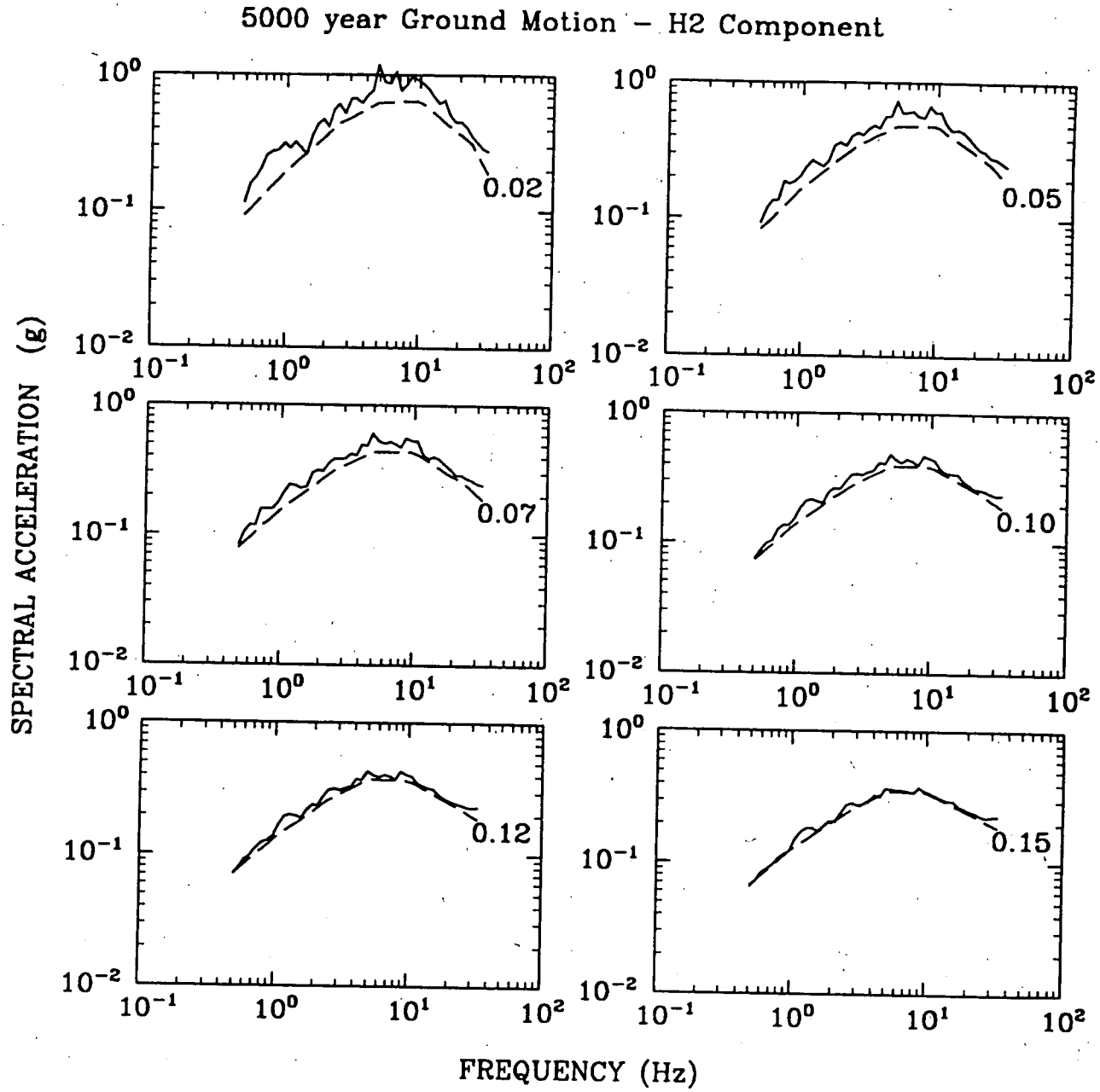

Figure I-26. Response spectra of artificial ground motions are compared to the target spectra. Return period: 5000 years; component: second horizontal. Damping values are indicated on each panel.

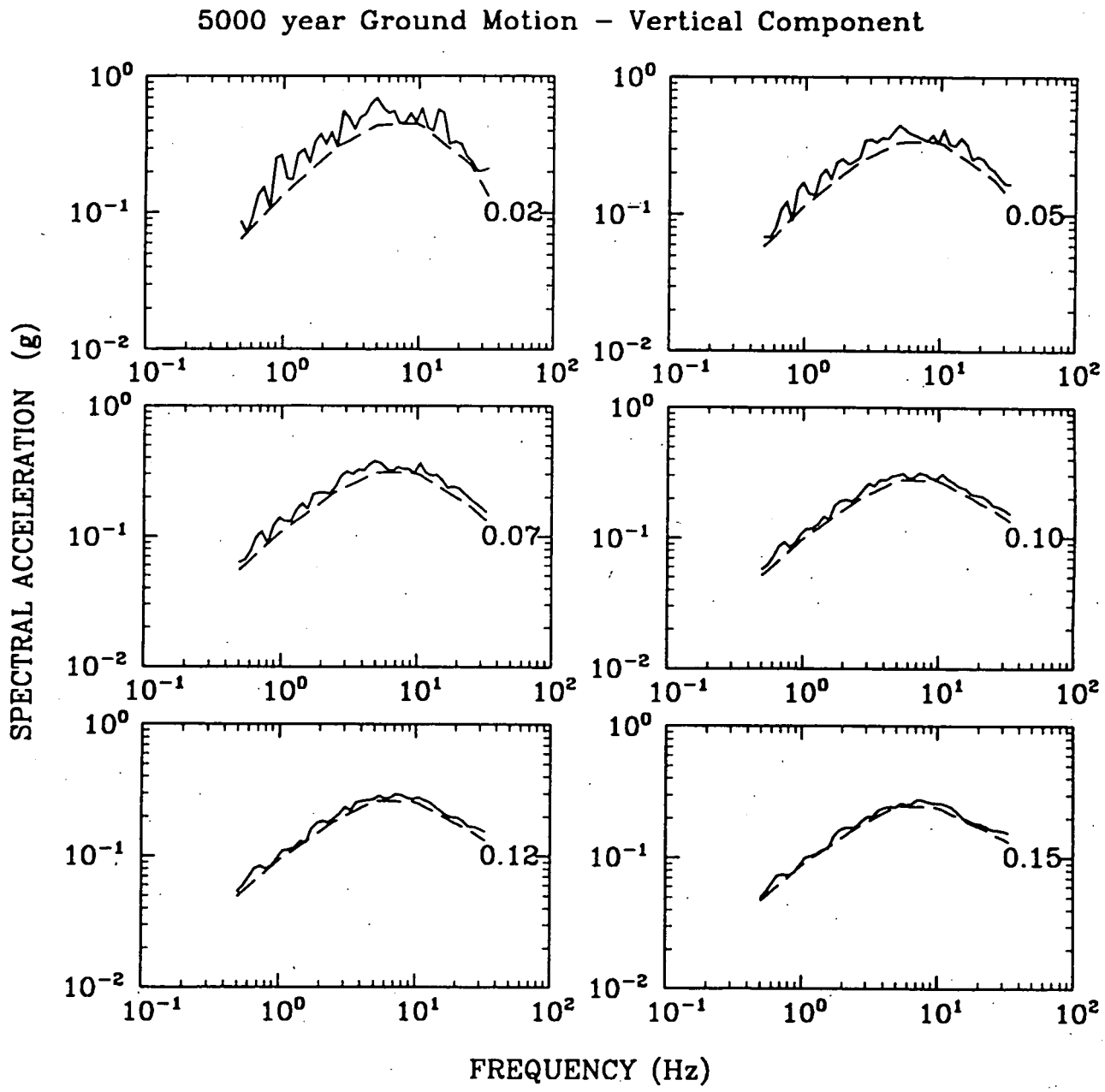

Figure I-27. Response spectra of artificial ground motions are compared to the target spectra. Return period: 5000 years; component: vertical. Damping values are indicated on each panel.

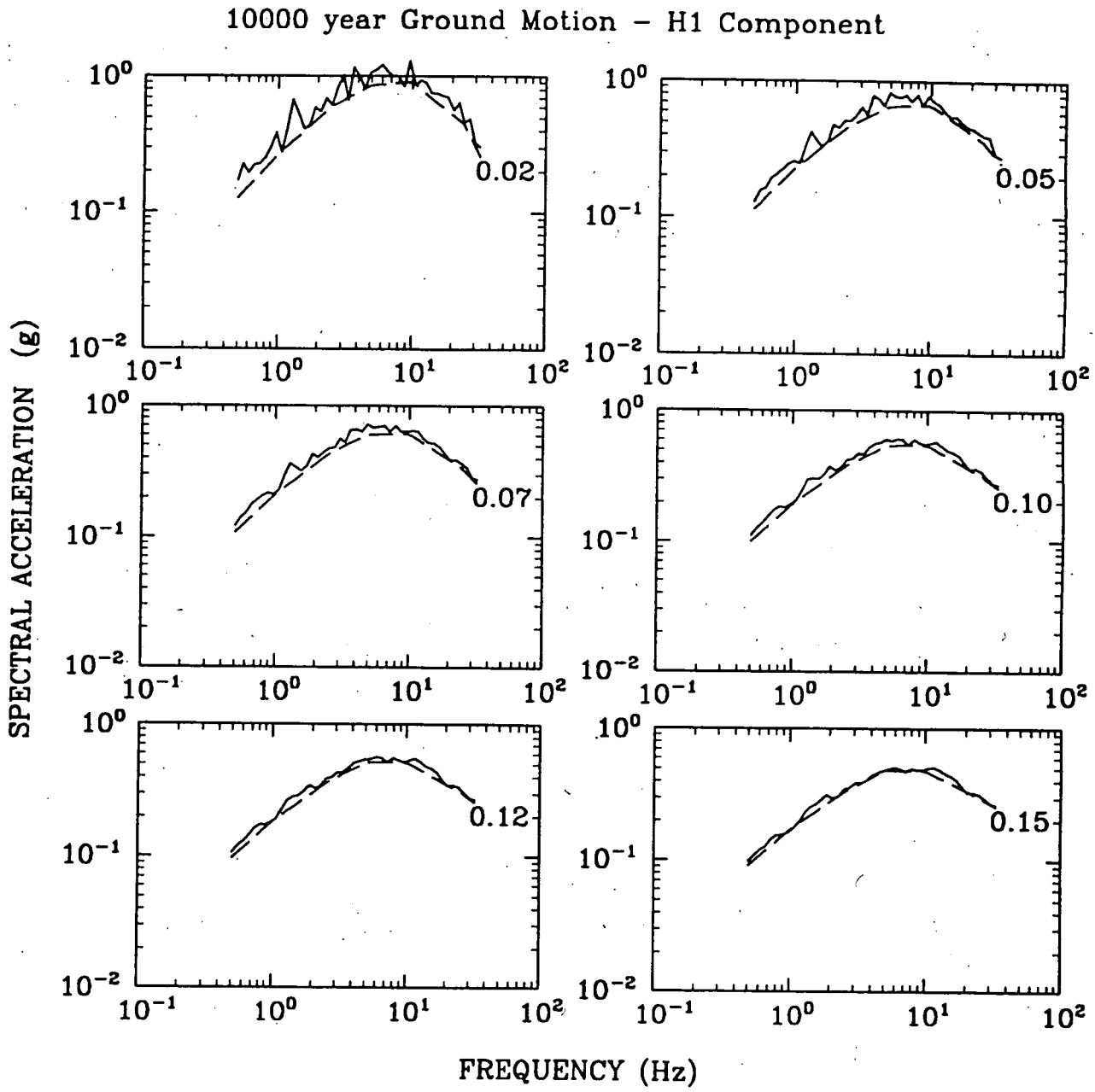

Figure I-28. Response spectra of artificial ground motions are compared to the target spectra. Return period: 10,000 years; component: first horizontal. Damping values are indicated on each panel.

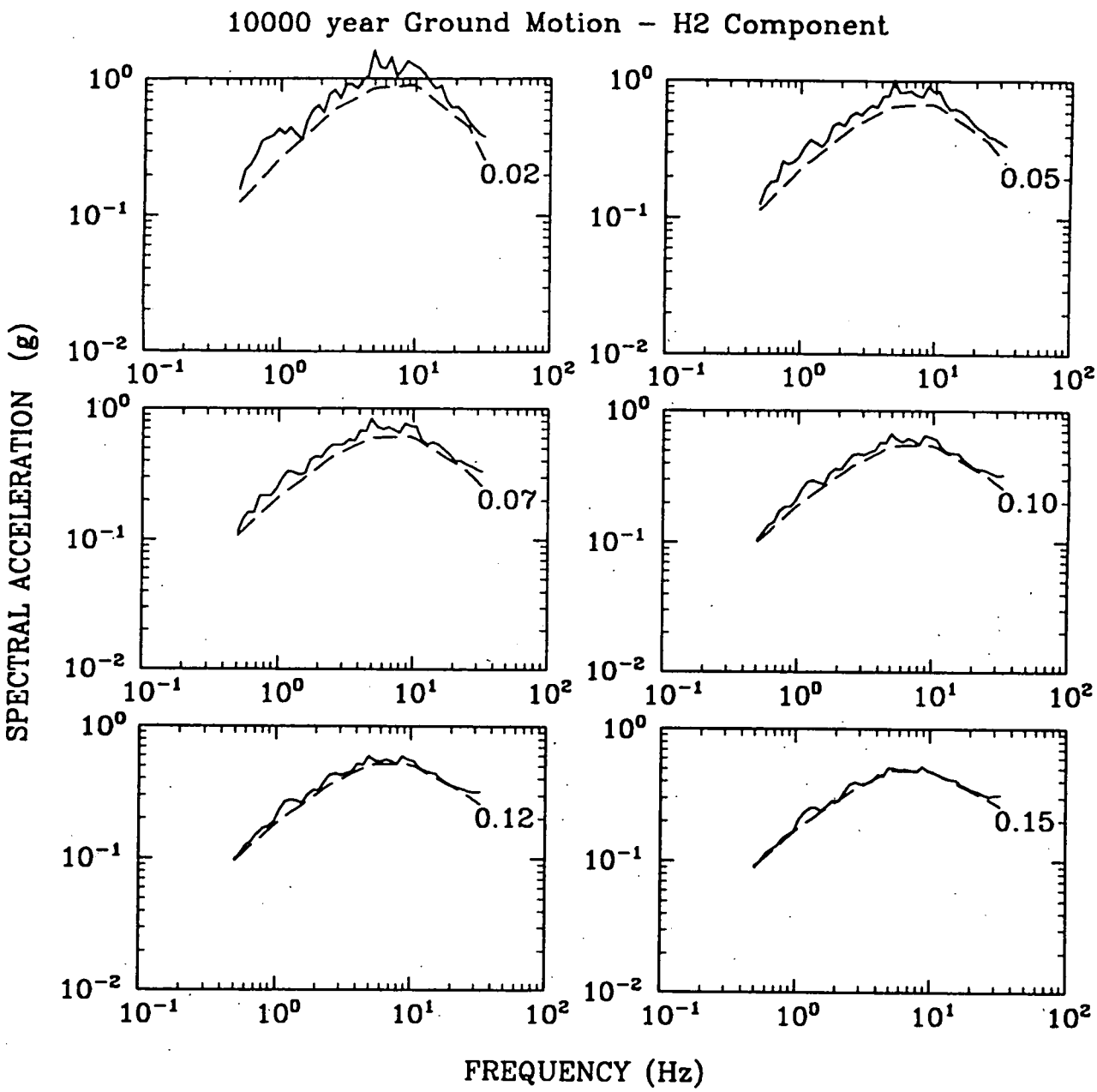

Figure I-29. Response spectra of artificial ground motions are compared to the target spectra. Return period: 10,000 years; component: second horizontal. Damping values are indicated on each panel.

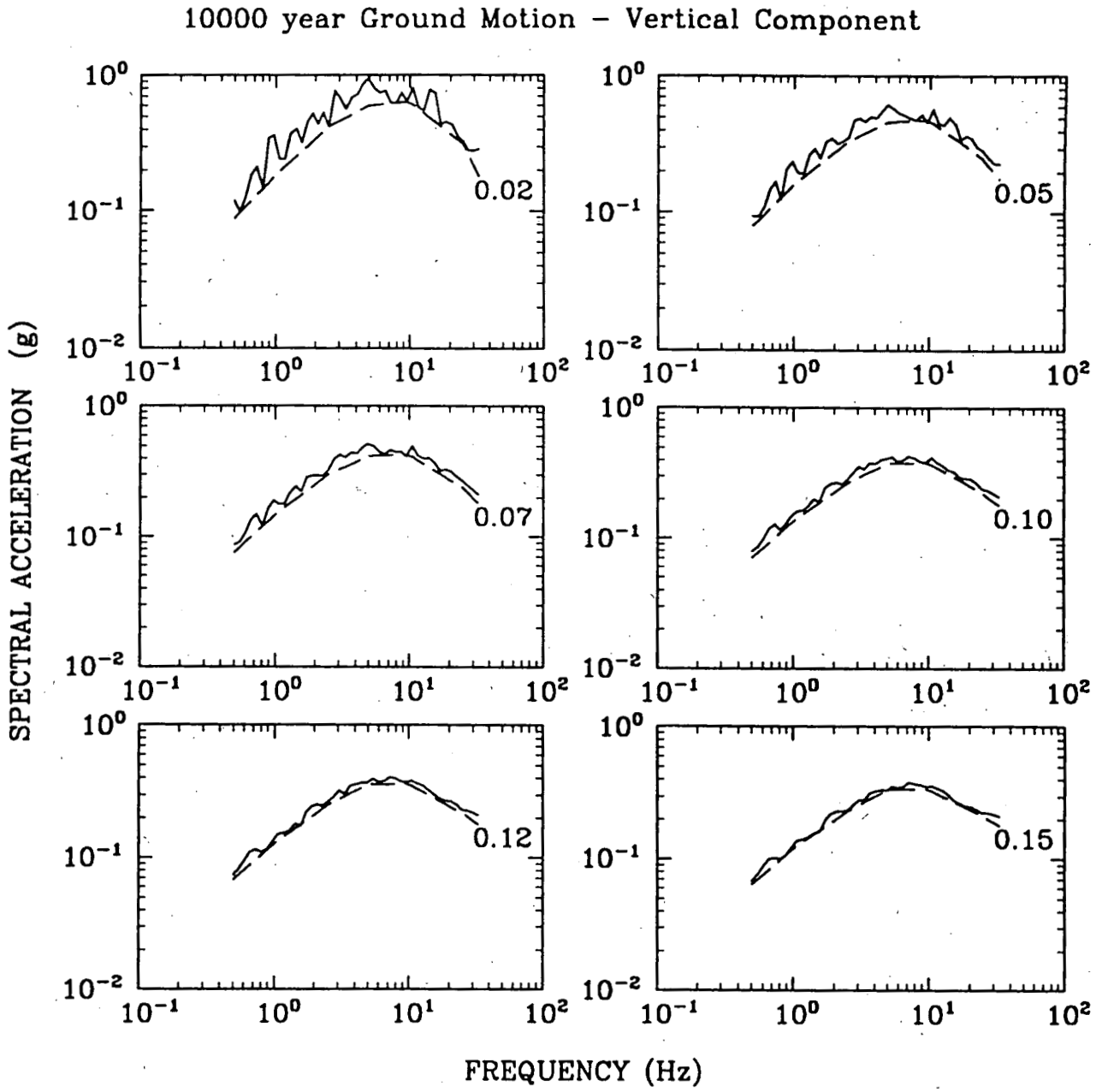

Figure I-30. Response spectra of artificial ground motions are compared to the target spectra. Return period: 10,000 years; component: vertical. Damping values are indicated on each panel.

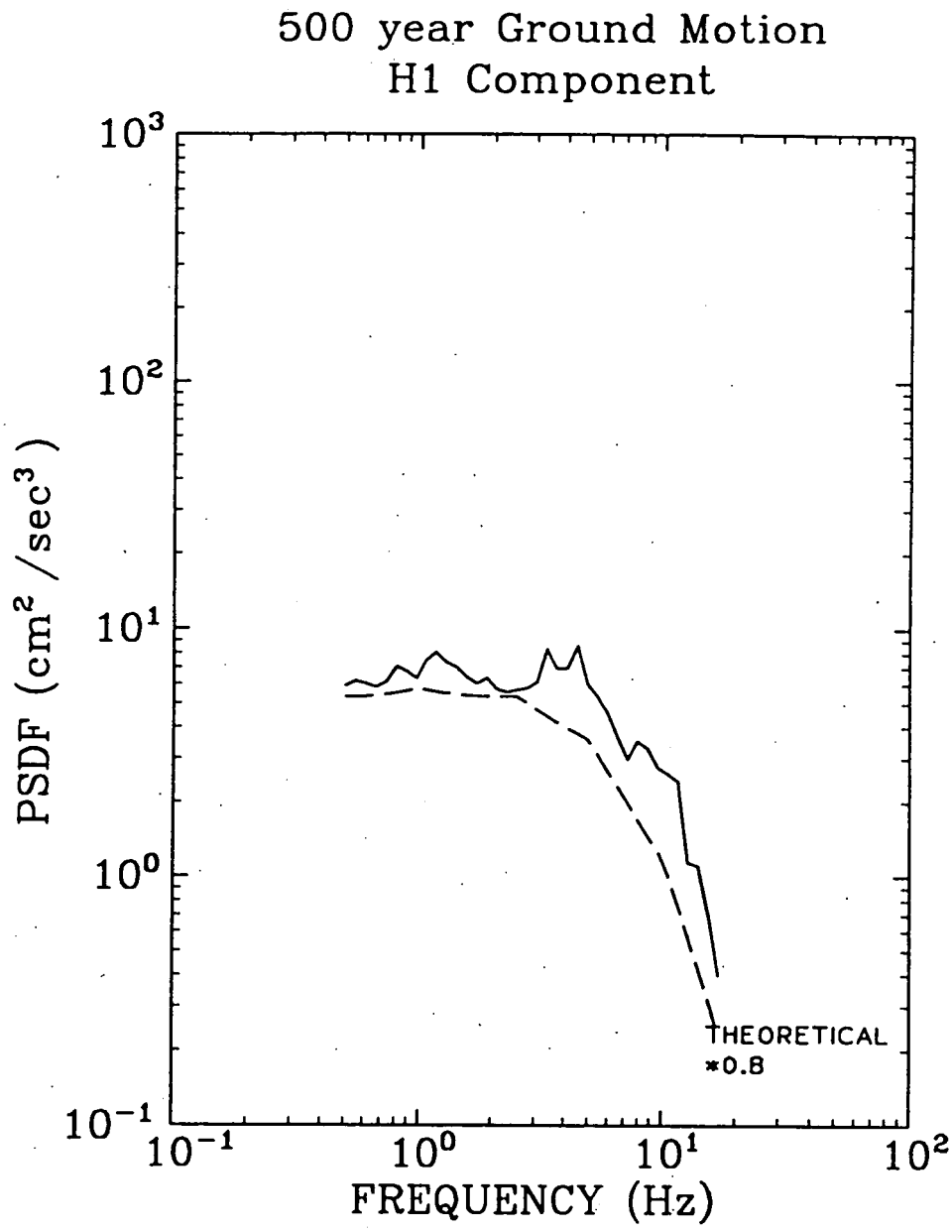

Figure I-31. Spectral density function of artificial ground motion is compared to the target spectral density function. Return period: 500 years; component: first horizontal.

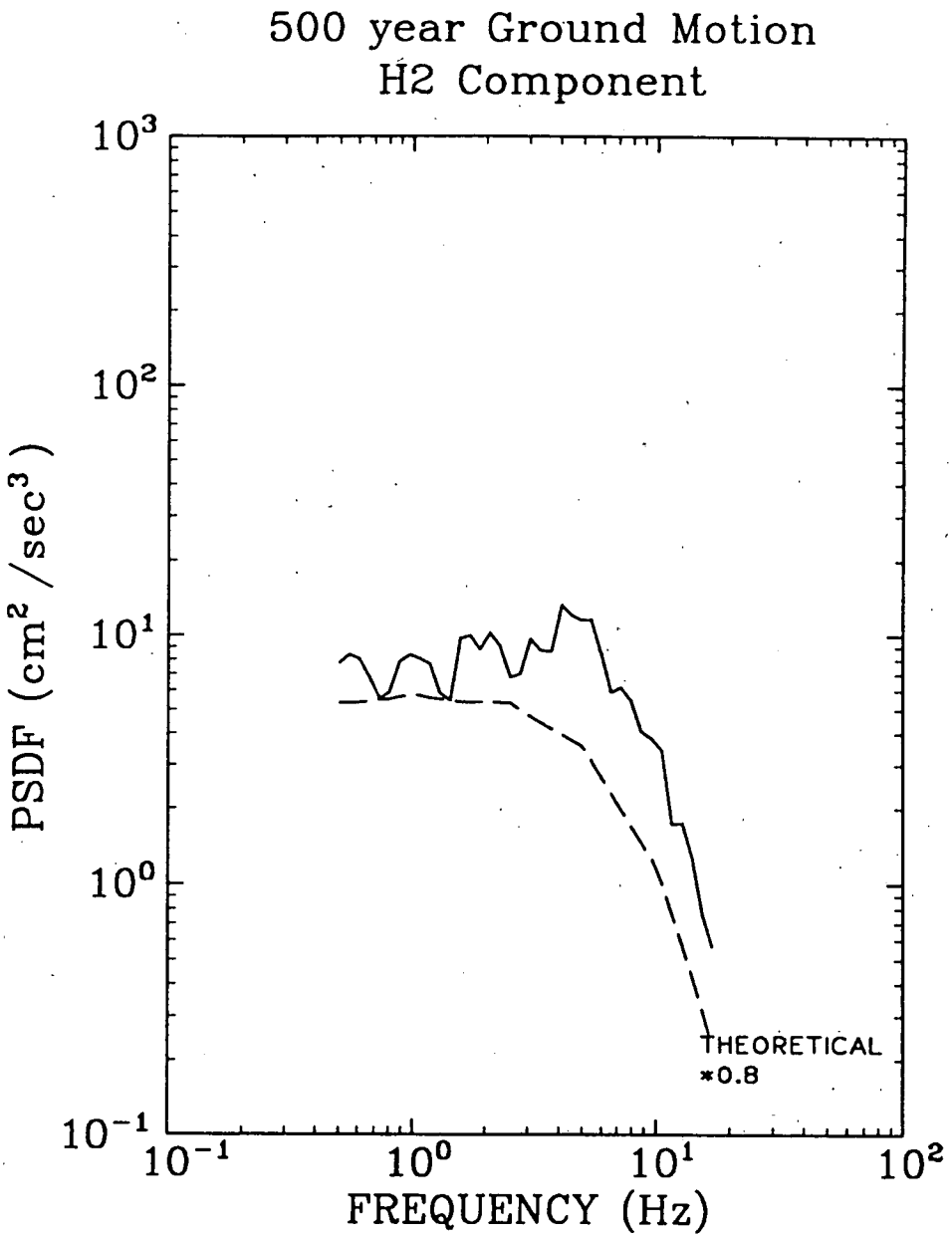

Figure I-32. Spectral density function of artificial ground motion is compared to the target spectral density function. Return period: 500 years; component: second horizontal.

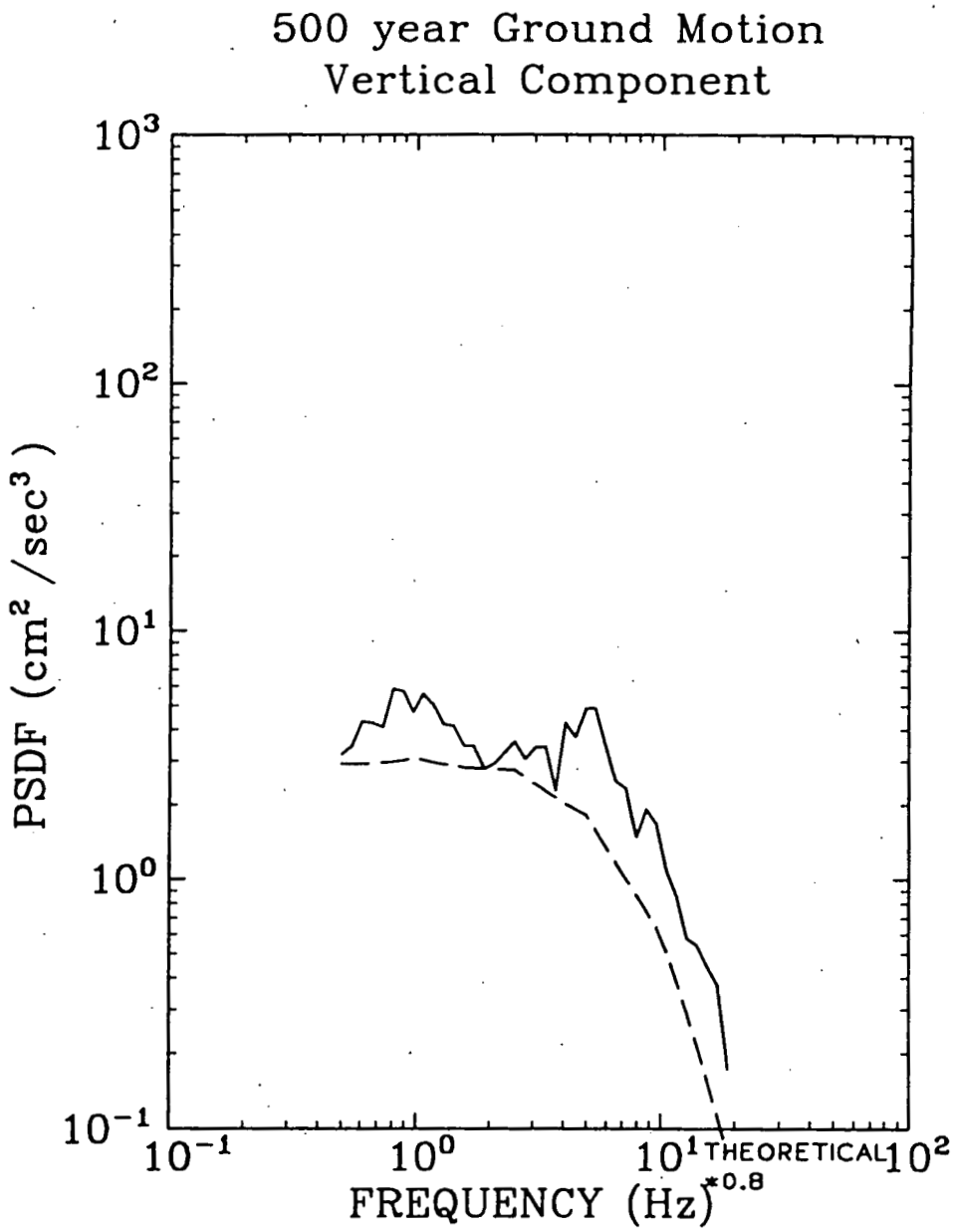

Figure I-33. Spectral density function of artificial ground motion is compared to the target spectral density function. Return period: 500 years; component: vertical.

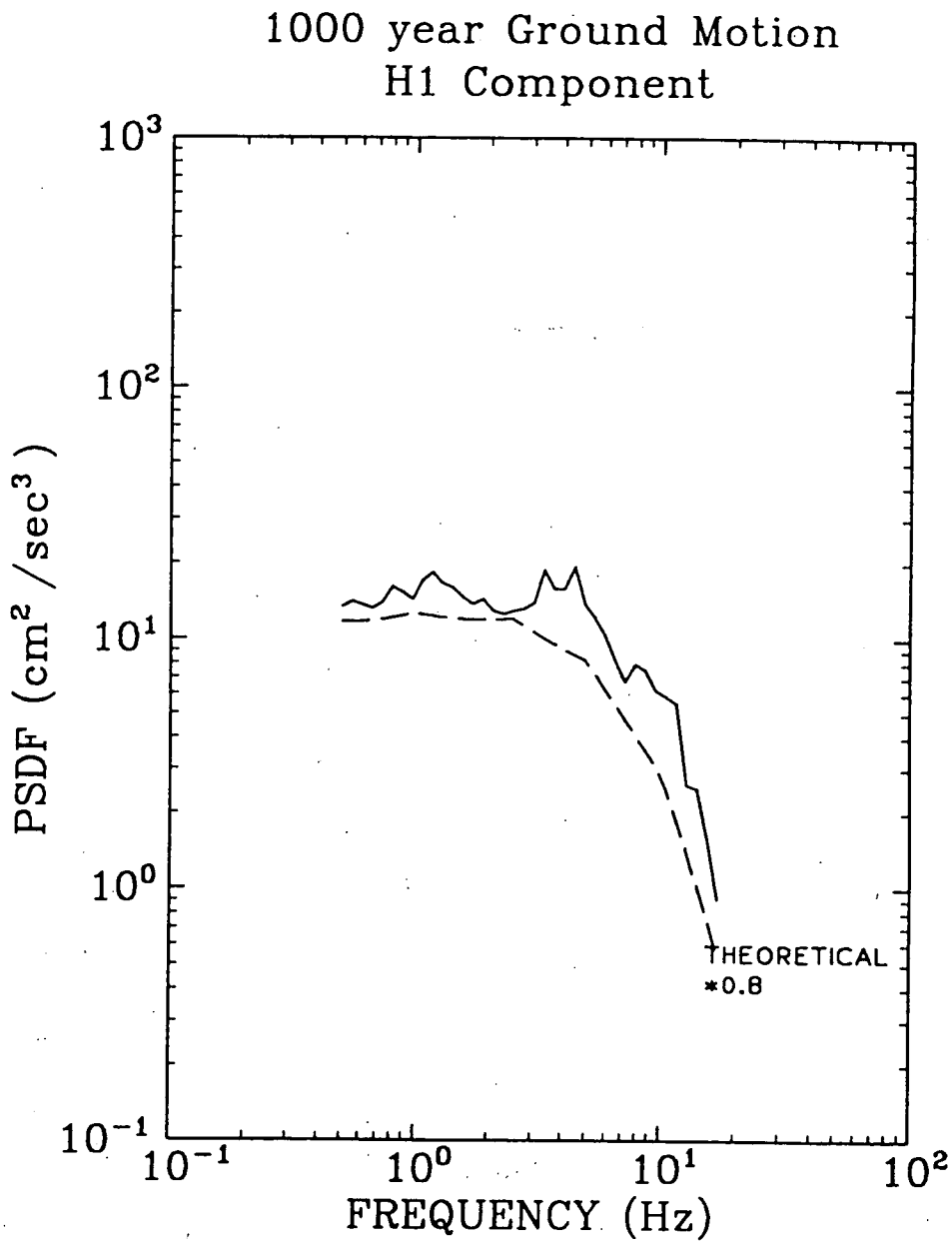

Figure I-34. Spectral density function of artificial ground motion is compared to the target spectral density function. Return period: 1000 years; component: first horizontal.

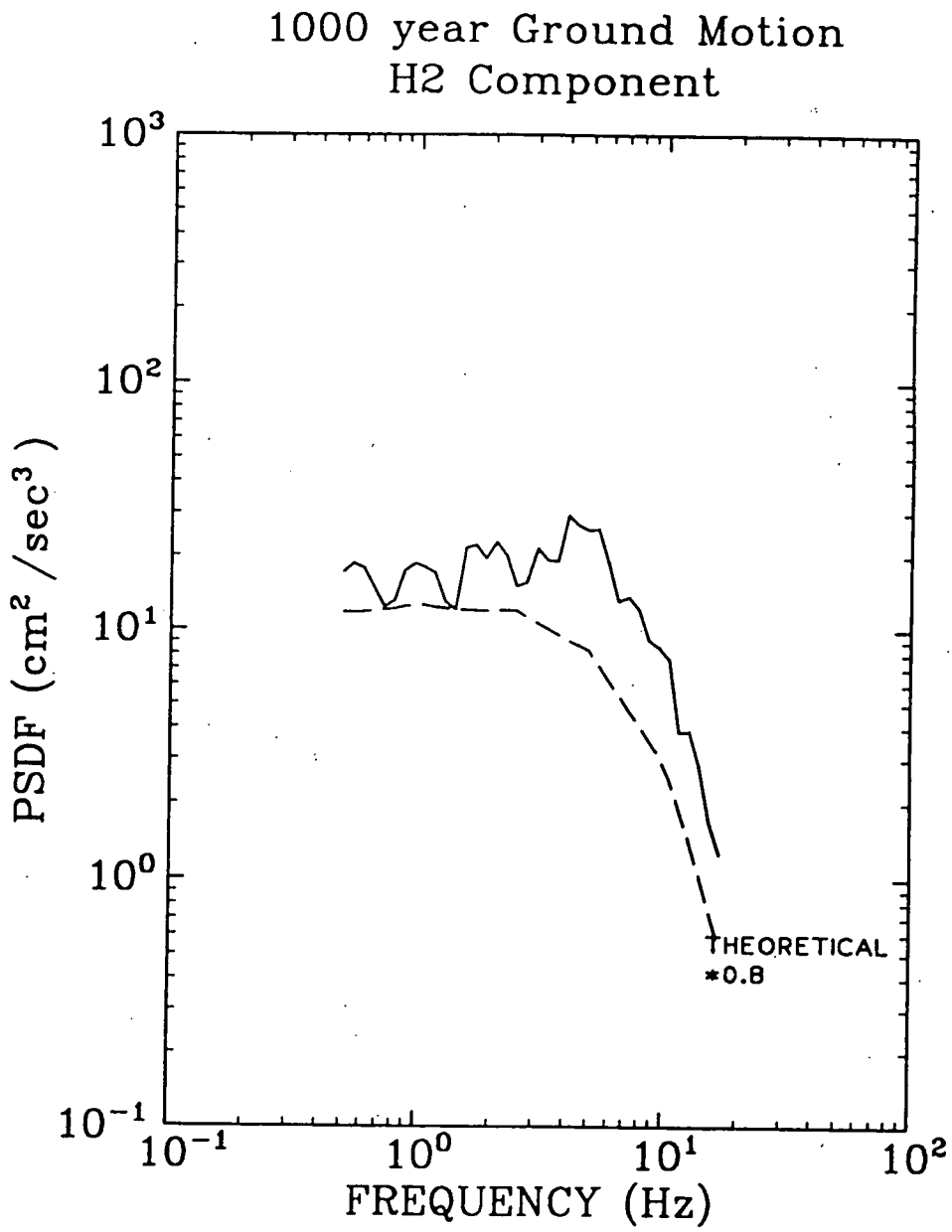

Figure I-35. Spectral density function of artificial ground motion is compared to the target spectral density function. Return period: 1000 years; component: second horizontal.

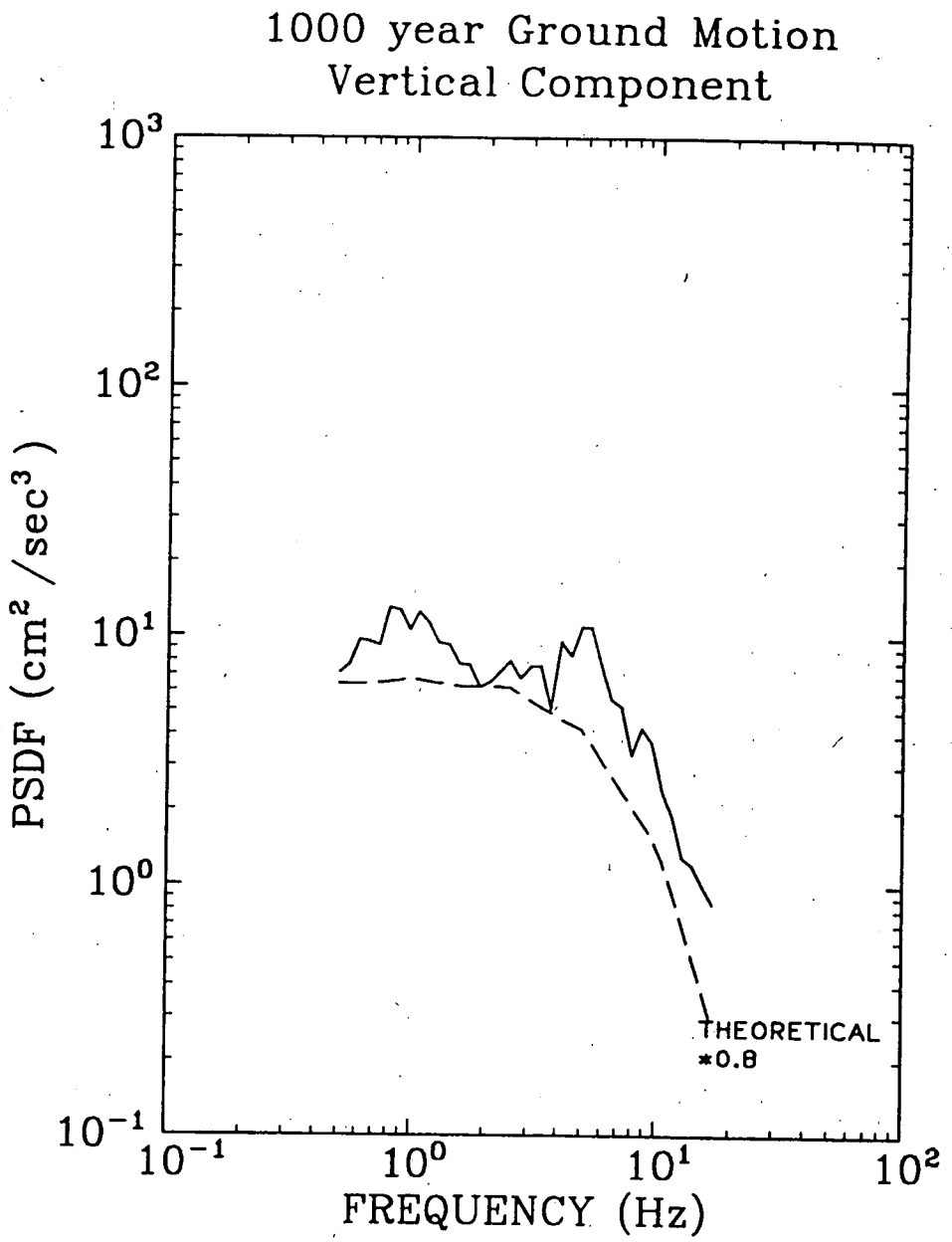

Figure I-36. Spectral density function of artificial ground motion is compared to the target spectral density function. Return period: 1000 years; component: vertical.

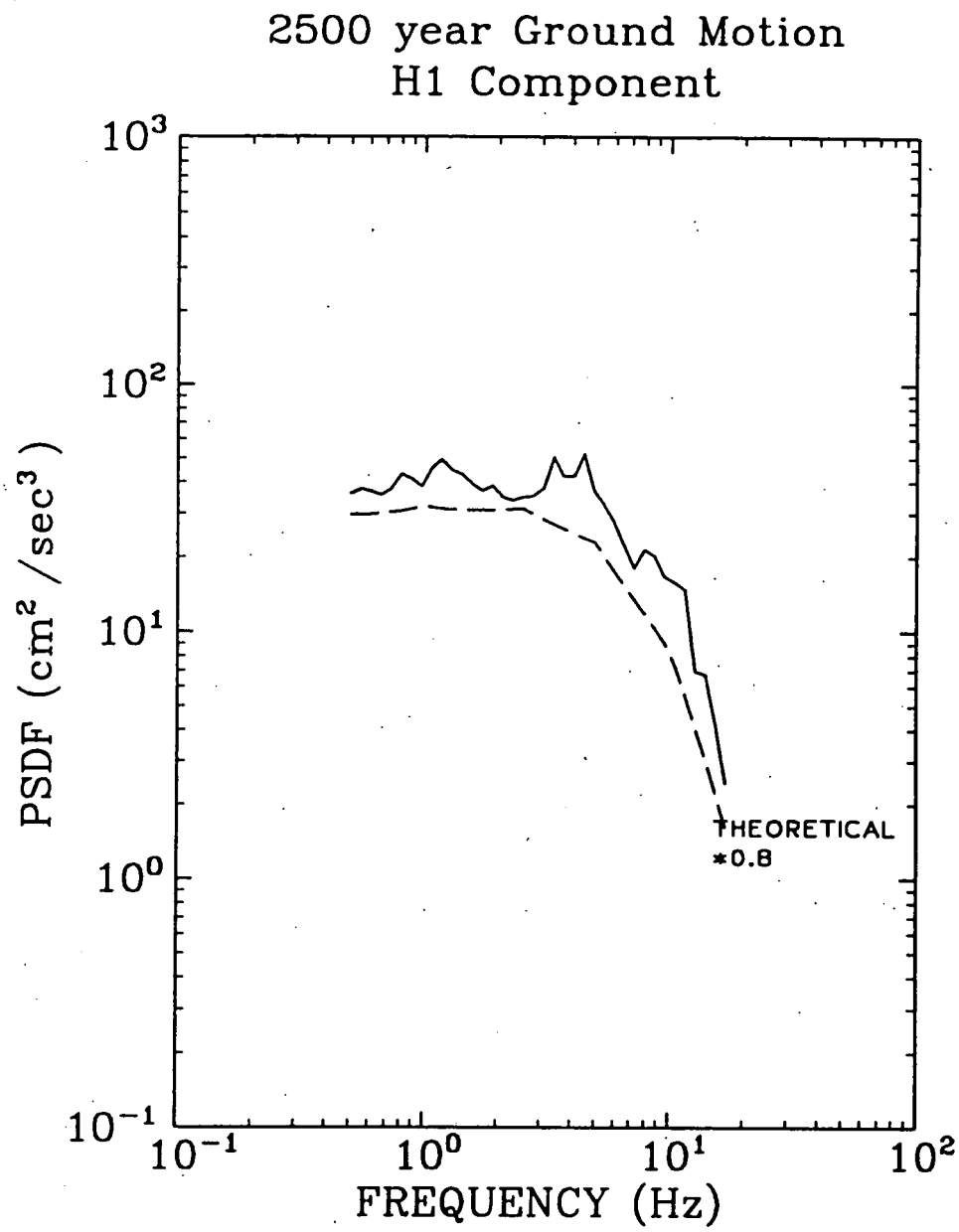

Figure I-37. Spectral density function of artificial ground motion is compared to the target spectral density function. Return period: 2500 years; component: first horizontal.

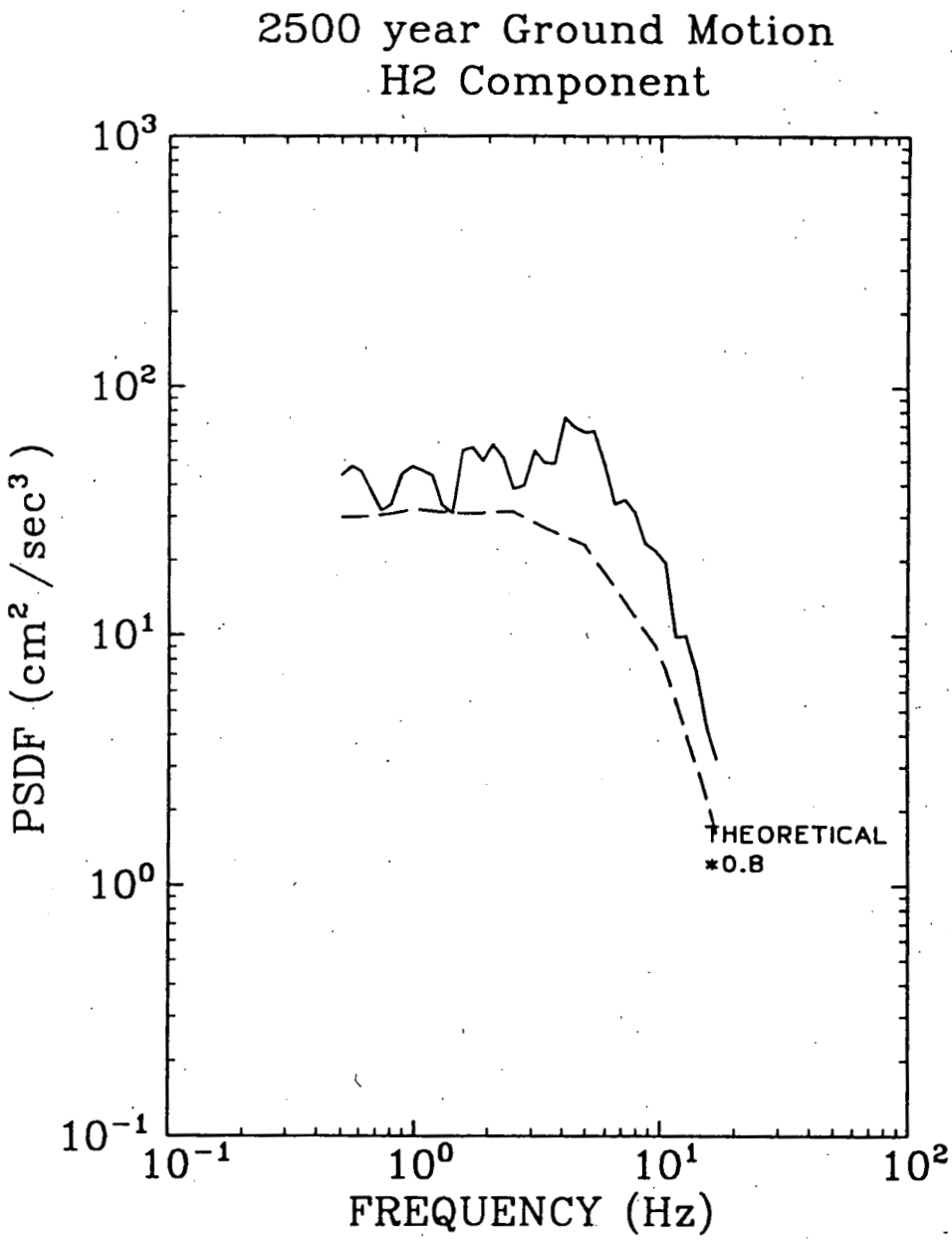

Figure I-38. Spectral density function of artificial ground motion is compared to the target spectral density function. Return period: 2500 years; component: second horizontal.

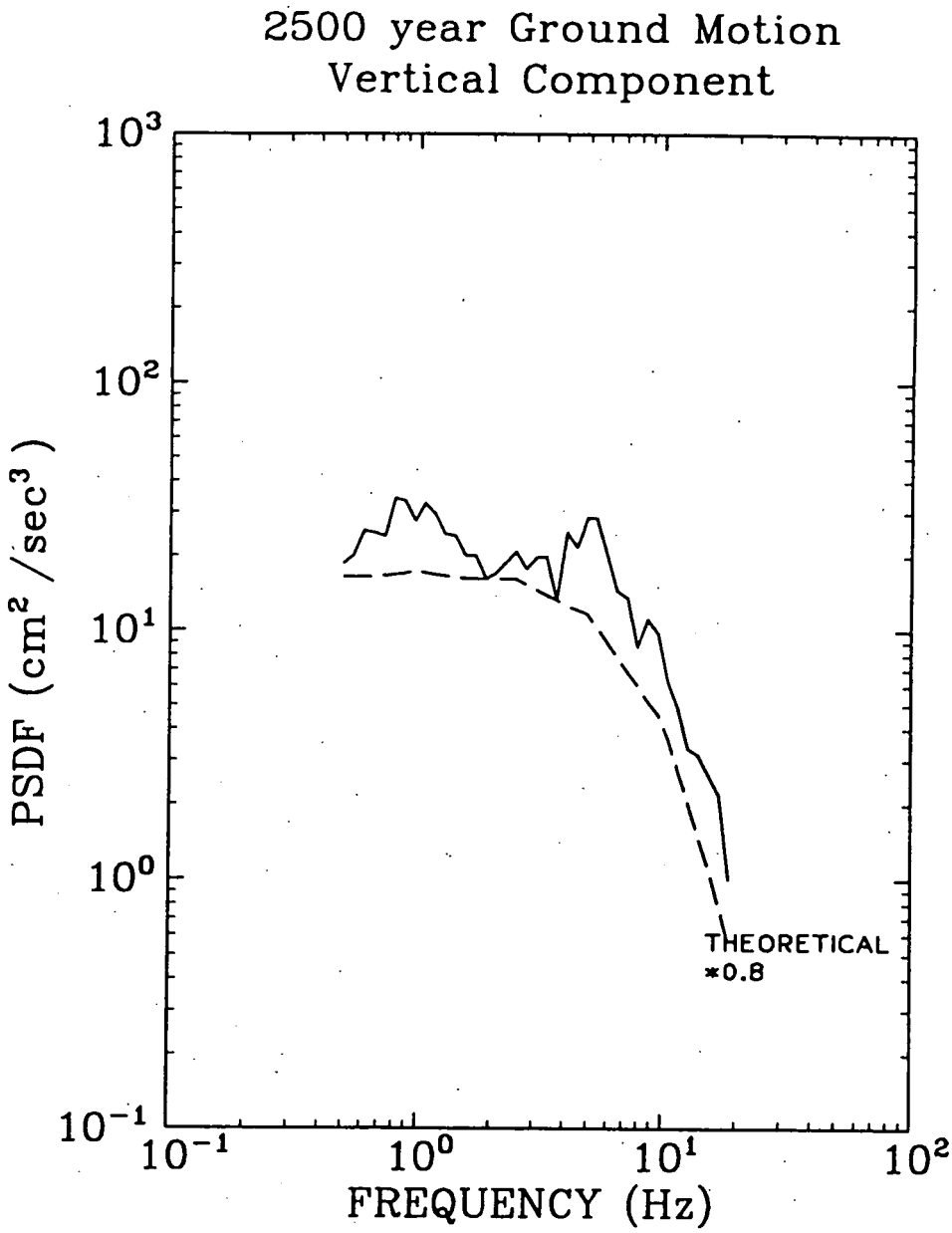

Figure I-39. Spectral density function of artificial ground motion is compared to the target spectral density function. Return period: 2500 years; component: vertical.

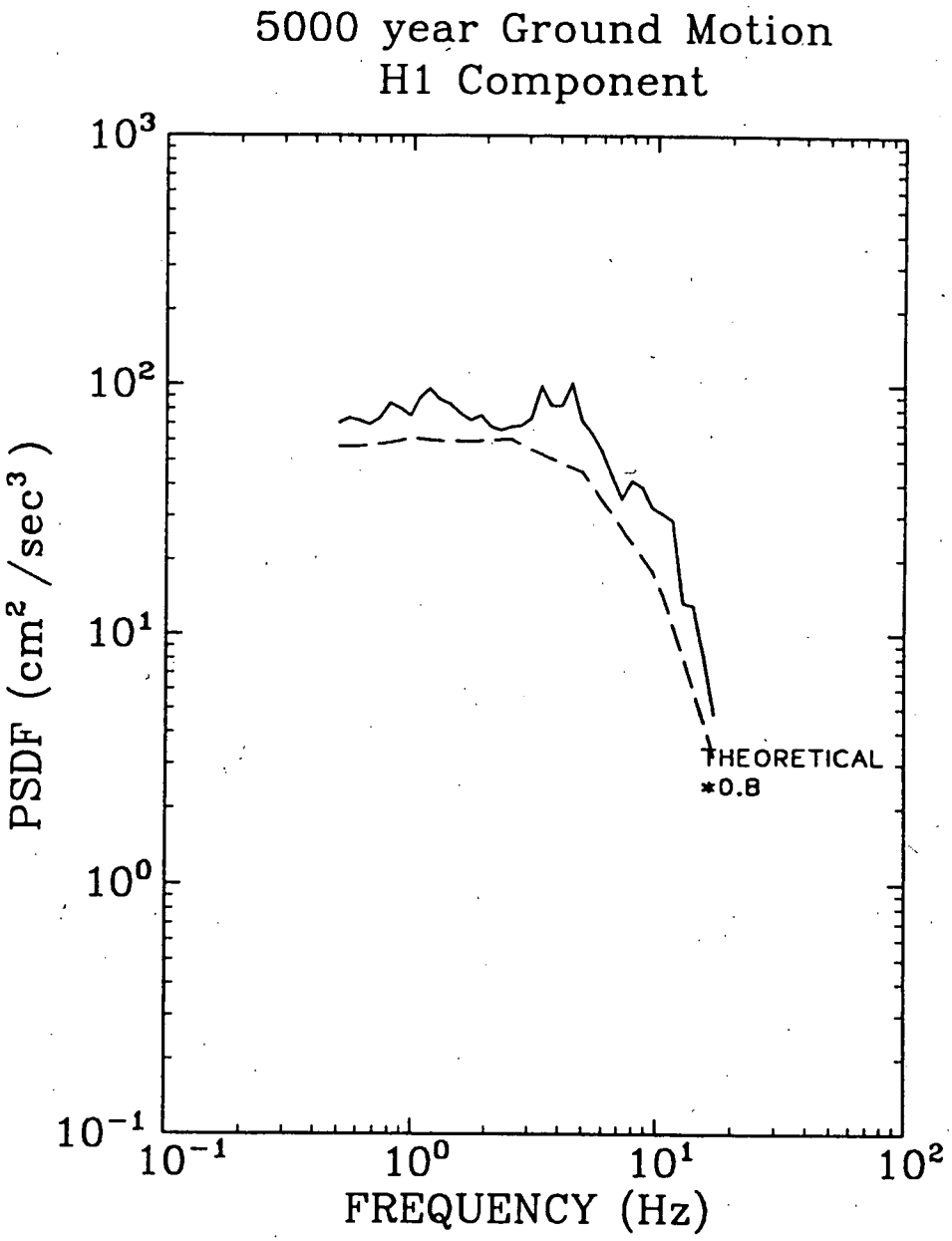

Figure I-40. Spectral density function of artificial ground motion is compared to the target spectral density function. Return period: 5000 years; component: first horizontal.

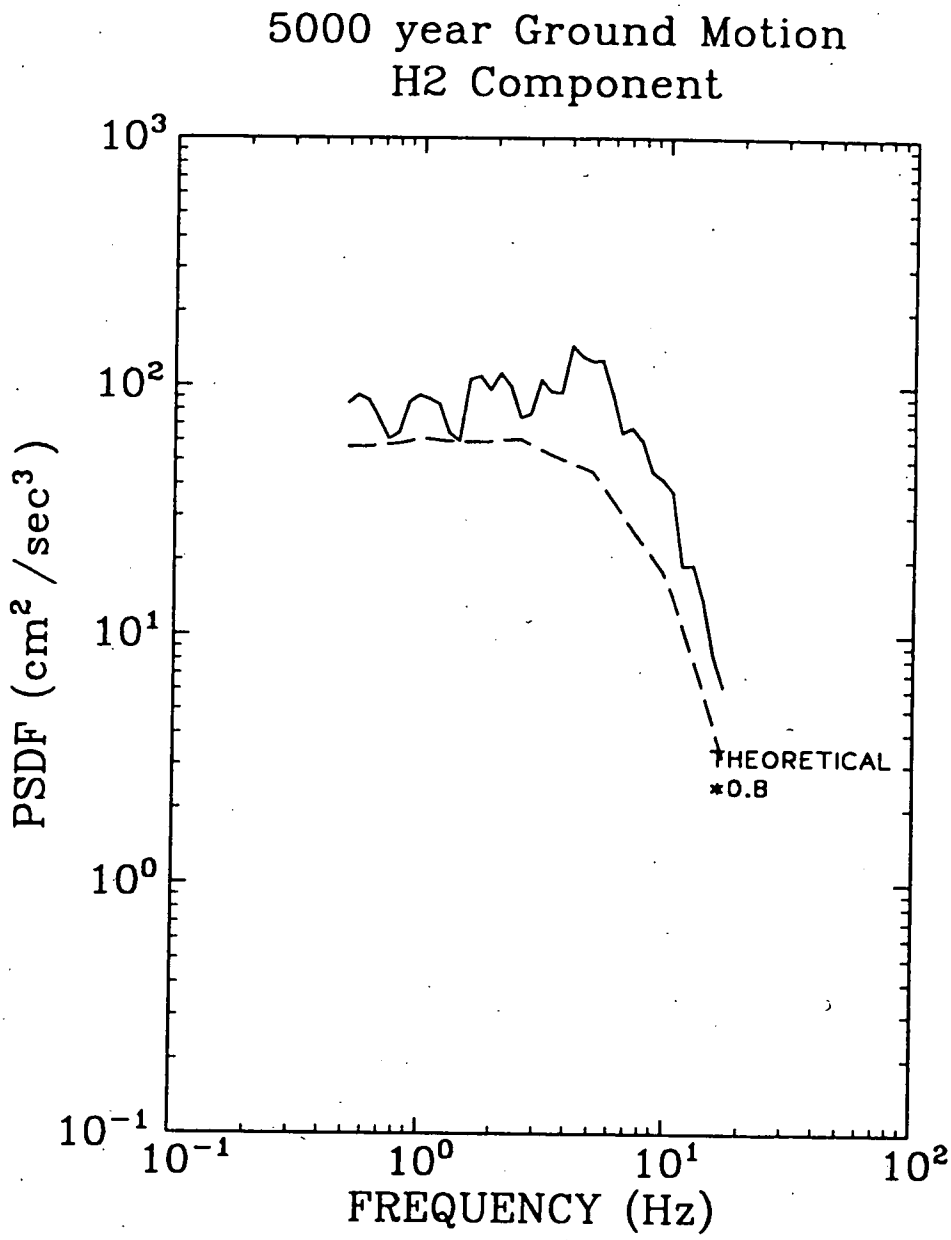

Figure I-41. Spectral density function of artificial ground motion is compared to the target spectral density function. Return period: 5000 years; component: second horizontal.

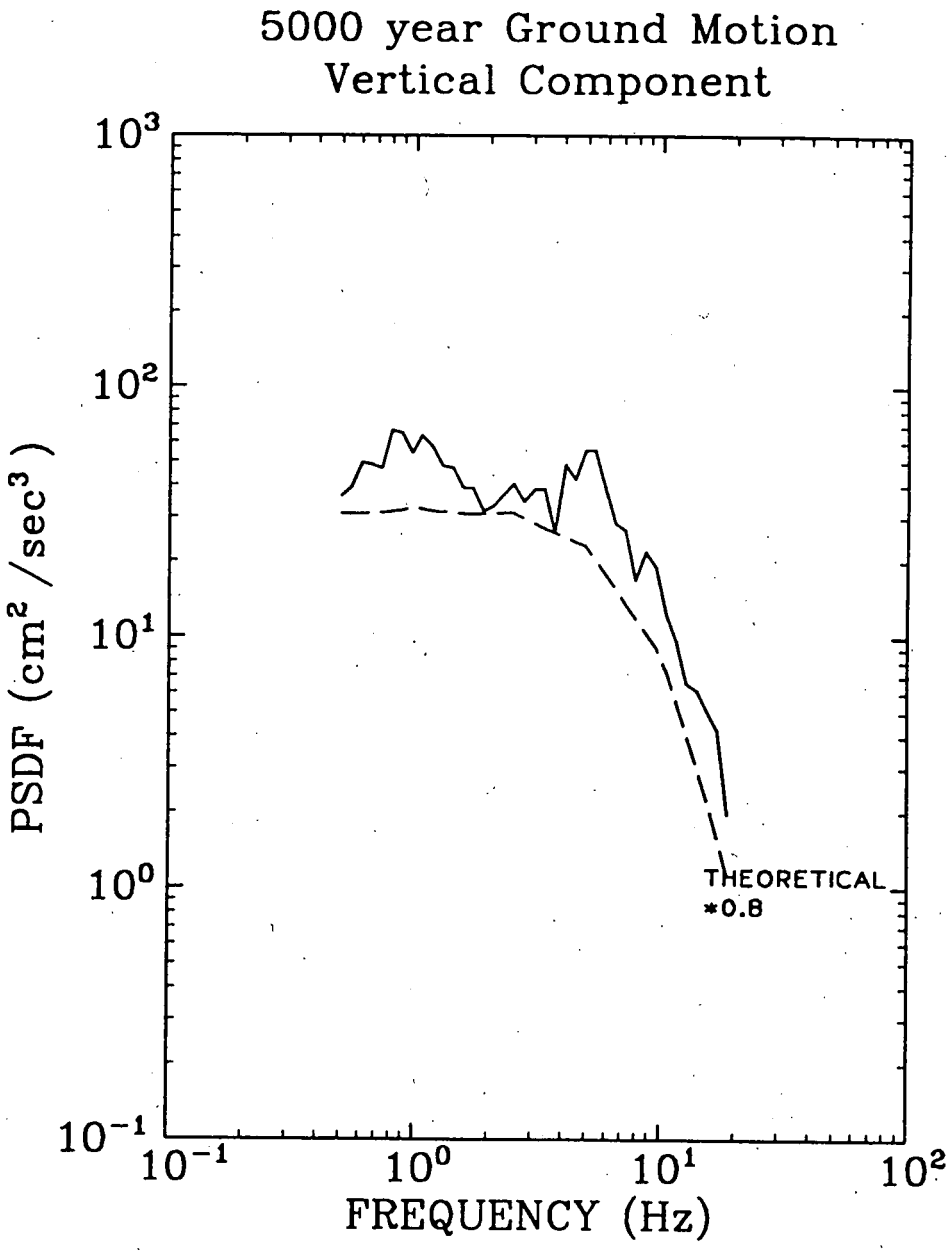

Figure I-42. Spectral density function of artificial ground motion is compared to the target spectral density function. Return period: 5000 years; component: vertical.

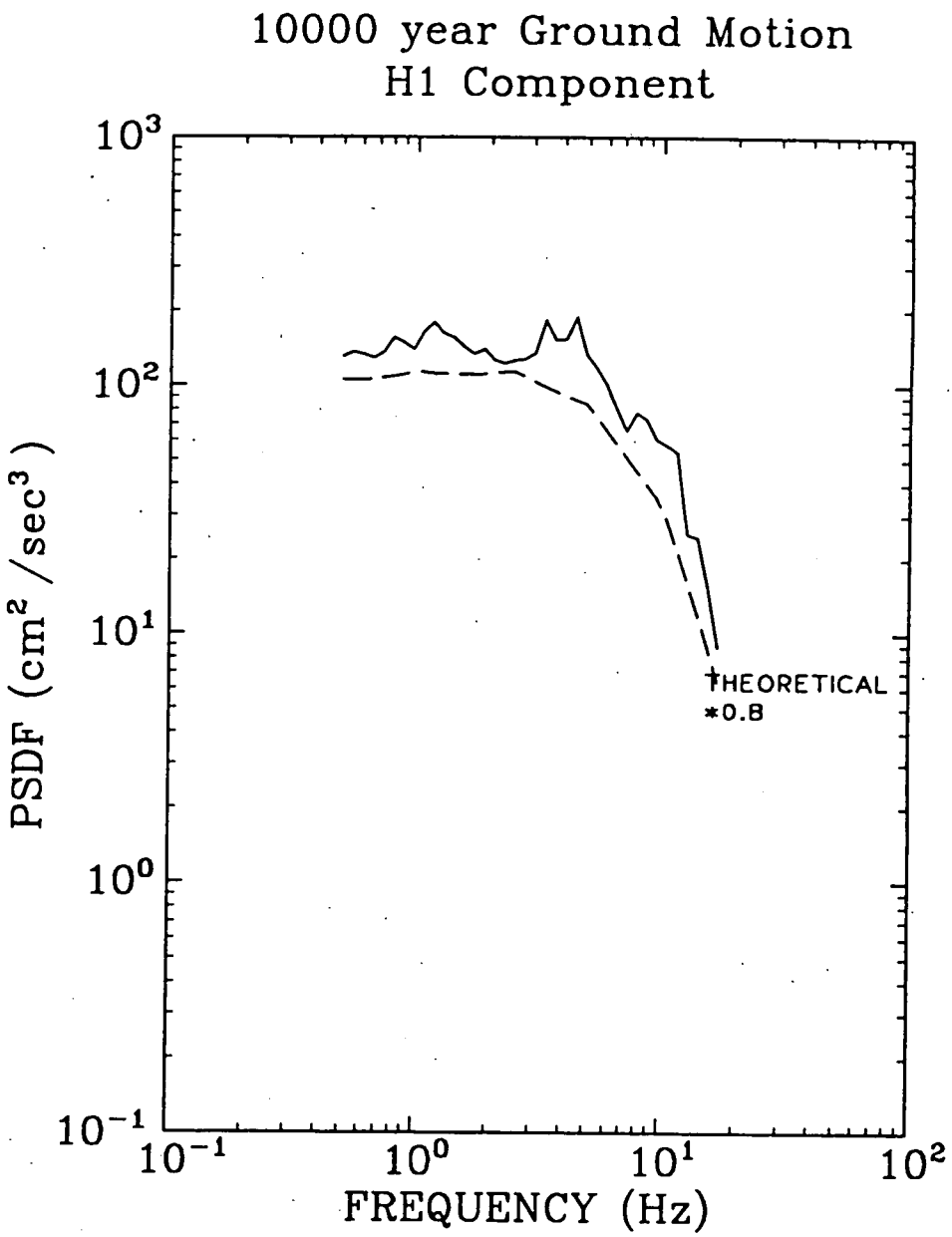

Figure I-43. Spectral density function of artificial ground motion is compared to the target spectral density function. Return period: 10,000 years; component: first horizontal.

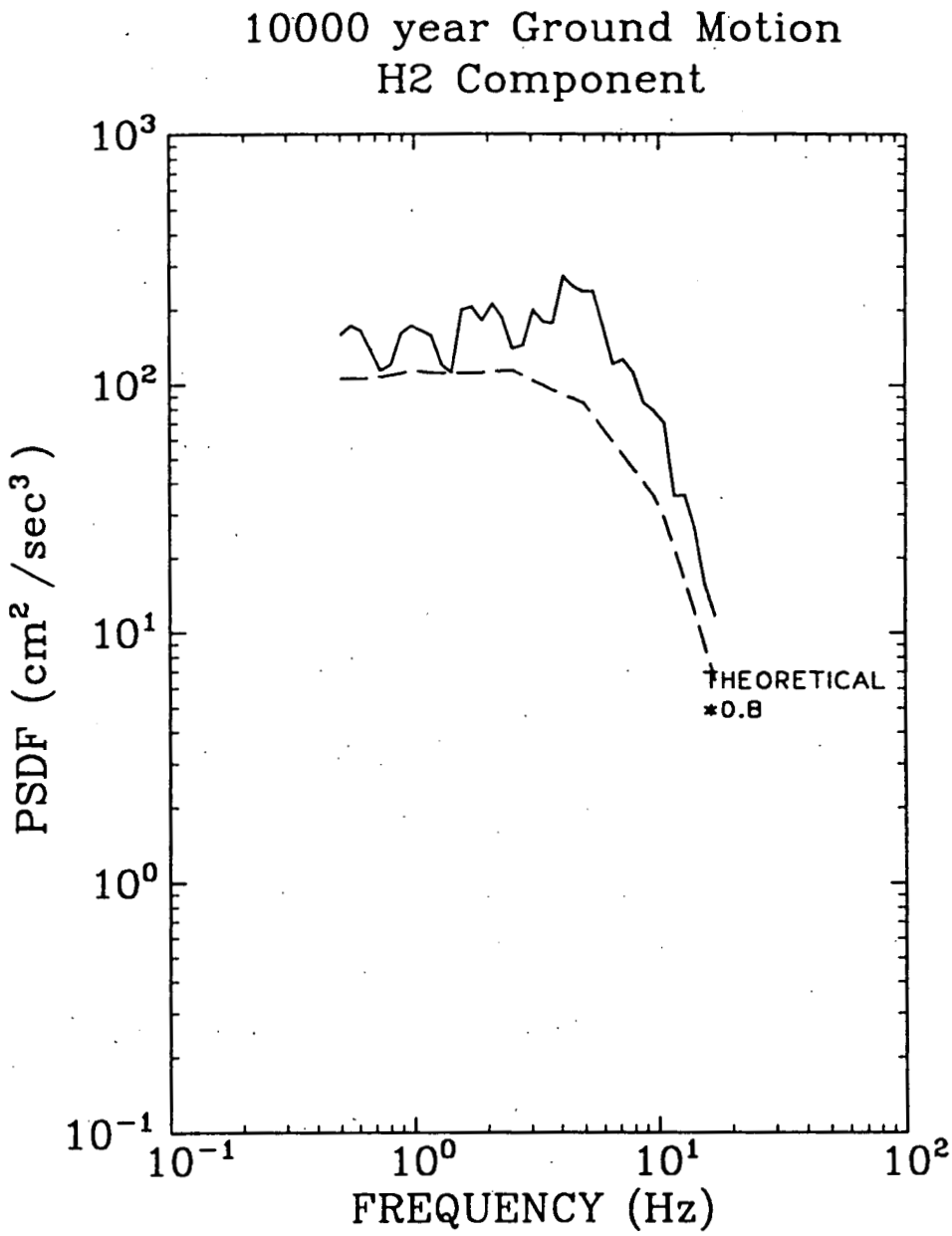

Figure I-44. Spectral density function of artificial ground motion is compared to the target spectral density function. Return period: 10,000 years; component: second horizontal.

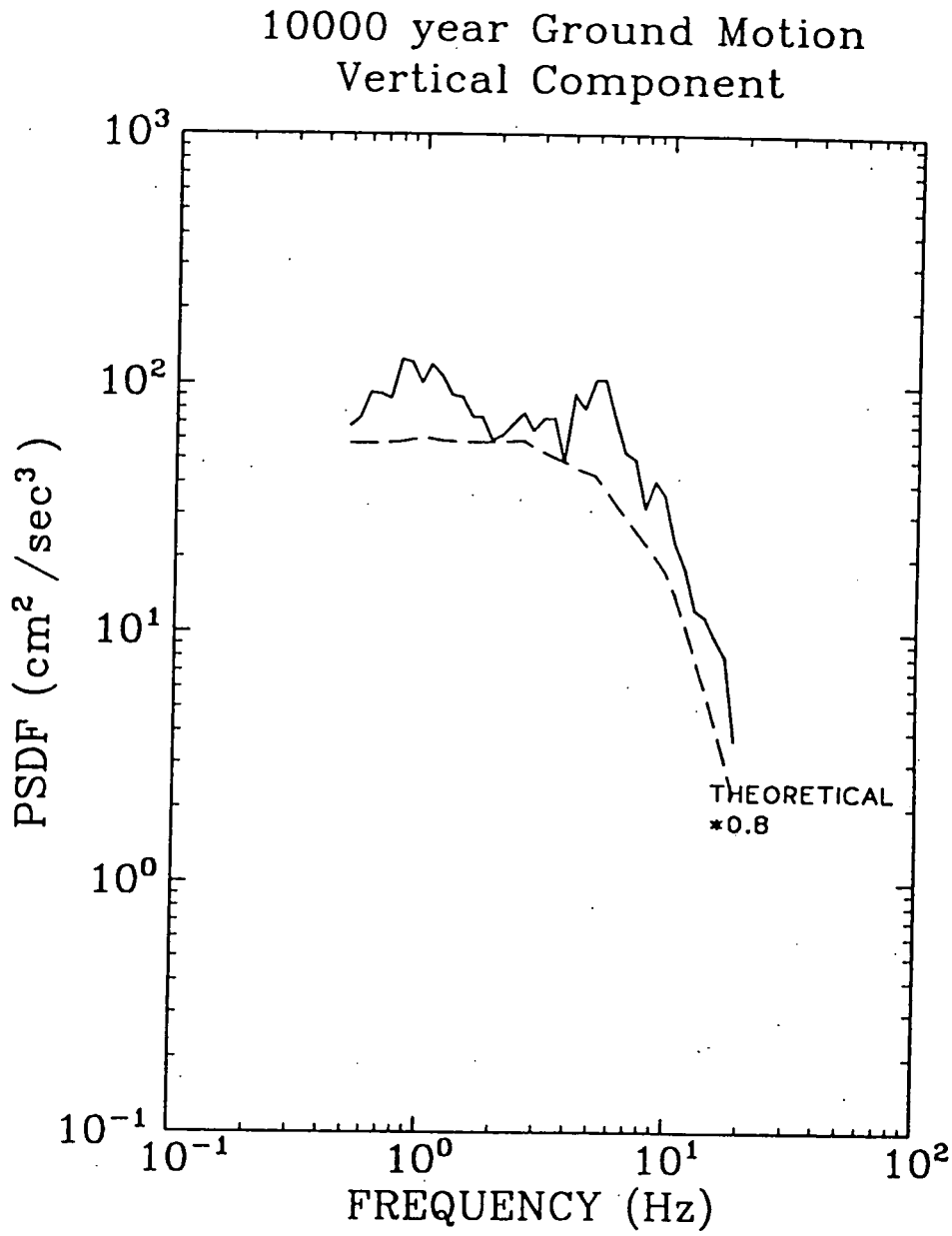

Figure I-45. Spectral density function of artificial ground motion is compared to the target spectral density function. Return period: 10,000 years; component: vertical.

APPENDIX J

DETERMINISTIC GROUND MOTION

by

Risk Engineering, Inc.
Boulder, Colorado

INTRODUCTION

A probabilistic seismic hazard analysis (PSHA) integrates over all earthquake magnitudes and locations to calculate a combined frequency of exceeding various ground motions levels. In this integration process the concept of a single design event used to generate a deterministic ground motion is lost, because the probabilistic result represents a combination of possible occurrences.

Two methods are available to derive deterministic spectra from PSHA applications. First, the hazard results can be "deaggregated" to determine a dominant earthquake magnitude and distance; this event can then be used to generate deterministic ground motions or spectral shapes. Second, the PSHA hazard results can be ignored and the faults and area sources identified as capable can be used to specify a maximum magnitude and closest distance for deterministic ground motion calculation. Both methods are pursued in this Appendix; final deterministic ground motions are recommended using the deaggregation process (the first of the two procedures described above).

As background for deaggregation of hazard results, the Aki committee (NRC, 1988) recommended that a "recursive" PSHA be performed using the dominant earthquake at any particular hazard level. The dominant earthquake was recommended to be the mean magnitude $\overline{M}$ and distance $\overline{R}$ of the seismic event that caused a ground motion exceedence at the chosen return period. The concept of $\overline{M}$ and $\overline{R}$ was introduced by McGuire and Shedlock (1981) in the context of evaluating uncertainties in hazard. These values of $\overline{M}$ and $\overline{R}$ can be used to generate deterministic ground motions for design or analysis.

Independently, Kameda and his co-workers in Japan have examined the concept of $\overline{M}$ and $\overline{R}$ for single-hypothesis PSHA, i.e., without uncertainties in inputs (Ishikawa and Kameda, 1988, 1991, 1993). They have recommended that $\overline{M}$ and $\overline{R}$ be determined for each seismic zone that contributes to hazard and be used with attenuation equations to calculate ground motions. These motions must be scaled to give the same amplitudes as the seismic hazard results, which can then be used as design ground motions with an associated $\overline{M}$ and $\overline{R}$.

There are distinct advantages of developing one or a few "design events" based on hazard results that can be used for detailed analysis and decision-making. One obtains an intuitive feel for the earthquake that is dominating the hazard at the chosen probability level. This event can be associated with a known earthquake fault or area source and can be ascribed familiar characteristics such as a magnitude, distance, azimuth, depth and stress drop. Also, more detailed analyses can be

performed for the design event, for example by generating durations and time histories of motion for non-linear structural analysis.

DEAGGREGATION OF PSHA RESULTS

Methodology

The deaggregation procedure shows the contribution to seismic hazard by magnitude and distance values. This deaggregation process allows us to see the contributions of each fault and area source, both separately and together, and allows the choice of one or a few deterministic earthquakes (M and R values) for which ground motions can be calculated. The mean magnitude $\overline{M}$ and distance $\overline{R}$ are obtained as one simple summary result of this deaggregation process, as are other measures such as the modal (most likely) values of $\hat{M}$ and $\hat{R}$ where the maximum contribution to hazard is made. The chosen deterministic ground motions are the ones recommended for evaluation of plant structures and equipment.

The methodology for determining the M and R contributions is to compile the contribution to hazard in discrete magnitude and distance bins, and to plot these contributions both marginally (vs. M and R separately) and jointly (vs. M and R together). Mathematically, the integrand in the seismic hazard equation (Equation 2-1 of the main report) is maintained separately for discrete M and R bins; the hazard value in each M-R bin is renormalized by the total hazard, which creates a bi-variate discrete probability distribution. For plotting marginal distributions (vs. M and R), the discrete values are divided by the M or R bin size, as appropriate, to obtain probability density; for plotting joint distribution the renormalized hazard values are plotted as percent contributions to the total hazard. A simple summary of these distributions is $\overline{M}$ and $\overline{R}$, which are the means of the marginal distributions with respect to M and R, respectively, but these single values do not reflect the range of magnitudes and distances that contribute to the hazard. It is important to note that the contribution by M and R will change as the ground motion measure changes (high vibrational frequencies are affected differently than low vibrational frequencies) and as the hazard level changes. In general low hazard levels (high ground motions) are dominated by larger magnitudes and closer distances, than are high hazard levels (low ground motions).

Application

Results of the deaggregation process for the RFP are presented first by separate source for the PGA level corresponding to 10^{-4} annual probability, and then are presented for all sources combined for that same ground motion. Combined results are then presented for all sources for the PGA level corresponding to 10^{-3} annual probabilities, and for PSV(1 Hz) at 10^{-4} and 10^{-3} annual probability.

Table J-1 summarizes the contributions by source to the hazard for 0.25g PGA, which corresponds approximately to the 10^{-4} annual probability level. The individual values of $\overline{M}$ and $\overline{R}$ are shown for each source, as well as the overall $\overline{M}$ and $\overline{R}$ value. As noted in the main report, the RMA/Derby source dominates the hazard for this level of ground motion.

The contributions to 0.25g PGA hazard by magnitude and distance for Source I are illustrated in Figures J-1a and J-1b. The primary contribution comes from the small magnitudes, with lesser contributions from magnitudes as high as 7.0. Recall from the description of Source I (see Appendix A) that the upper-bound magnitude of Source I is represented with a discrete distribution using values of M_{max} = 5.5, 6.0, 6.5 and 7.0. These values correspond to the levels at which the distribution in Figure J-1a decreases. Figure J-1b shows that the primary contribution comes from distances in the range 10 to 25 km, and this is a common result for a host source. Note that the distance plotted is hypocentral distance, and two depths (10 and 15 km) are used to represent earthquake occurrences for area sources, so no contribution is obtained for distances less than 10 km.

Figures J-2 an J-3 illustrate the distributions for Sources II and III, respectively. In Figure J-3b the large distance of Source III is evident, and events must have large magnitudes (Figure J-3a) to contribute to the hazard.

Figure J-4 shows the contribution by **M** and R for the RMA/Derby source. Magnitudes of 5.5 to 6.0 dominate (Figure J-4a), and the changes in the distribution correspond to discrete values of M_{max}. The distance contribution comes from 20 to 35 km, which is the distance of this source.

Figures J-5 and J-6 show the contributions by **M** and R for the Rock Creek and Golden-Boulder faults, respectively. These faults are close to the RFP, so the distance distributions are peaked at short distances. The Golden-Boulder fault has a dominant contributions from magnitudes in the range 6.2 to 7.2, which reflect both the M_{max} values and the use of the characteristic magnitude distribution for faults.

The combined distributions by **M** and R are shown in Figure J-7a and J-7b, respectively. These distributions weight all sources by their contributions to hazard, so the RMA/Derby source dominates these total distributions (see the contributions listed on Table J-1). In particular the peak in the distance distribution (Figure J-8b) at 25 km comes from the RMA/Derby source.

Additional perspective is gained by plotting the two-dimensional distribution, percent contribution to hazard vs **M** and R, as shown in Figure J-8. Again the dominance of the RMA/Derby source is evident at 25 km. Note that the contribution to total hazard in Figure J-8 is proportional to the <u>volume</u> under each peak, just as it is proportional to the <u>area</u> under the curves of Figure J-7b. Stated another way, the hazard contribution <u>by source</u> is not proportional to the height of the highest peak in Figure J-8 at 25 km vs. the height of the highest peak at some other distance (although the contribution of each discrete **M**-R bin is certainly proportional to the value plotted for that bin).

Results are presented in Figure J-9 for PGA at 0.08g, which corresponds to approximately 10^{-3} annual probability. The contribution by fault is shown in Table J-1, and the RMA/Derby source dominates the hazard. Only the total distribution for all sources is presented, for the sake of brevity, but the domination of the RMA/Derby source is clear from Figure J-9 and also from Figure J-10, which shows the distribution by **M** and R.

For PSV(1 Hz), contributions to hazard for 35 cm/s and 12 cm/s by source are shown in Table J-2. These levels correspond approximately to 10^{-4} and 10^{-3} annual probability, respectively. The total distributions by **M** and R are illustrated in Figures J-11 through J-14, which are similar to the plots

shown for PGA. Note in comparing the magnitude distributions (e.g., Figure J-11a vs. Figure J-7a, or Figure J-13a vs. J-9a) that the distribution is shifted to somewhat higher magnitudes, as is expected for PSV(1 Hz) vs. PGA. The distance distributions are similar.

The contribution plotted at 100 km on Figure J-13b and J-14 comes from Source III, and this is actually the contribution for distances of 100 km and greater. The actual distance distribution for Source III is distributed over a wide range of distances, as the value of R=197.9 in Table J-2 indicates, so the contribution from any one distance bin is small. This source contributes 38% of the hazard for the 10^{-3} annual probability level, as shown in Table J-2.

Over all natural frequencies and annual probabilities, the RMA/Derby source generally dominates the hazard for the ground motion measures and amplitudes examined here. From these results we derive deterministic ground motions using the following steps for 10^{-3} annual probability:

1. For both PGA and PSV(1 Hz), select the most likely magnitude $\hat{\mathbf{M}}$ and distance $\hat{\mathbf{R}}$ corresponding to an earthquake on the RMA/Derby source. The $\hat{\mathbf{M}}$ and $\hat{\mathbf{R}}$ values are read from Figures J-10 and J-14. For both PGA and PSV(1 Hz), $\hat{\mathbf{M}} = 5.9$ and $\hat{\mathbf{R}} = 27$ km are obtained.

2. Compute an average spectrum over all ground motion attenuation equations for these values of $\hat{\mathbf{M}}$ and $\hat{\mathbf{R}}$.

3. Rescale this average deterministic spectrum so it corresponds to the 10^{-3} ground motion calculated from the PSHA for PGA and PSA(1 Hz), respectively. (In this case the calculated PGA exactly equaled the 10^{-3} PGA from the hazard analysis, so no scaling by PGA was necessary).

4. The spectrum scaled to PSA(1 Hz) results in slightly higher ground motions, so use it (as the envelope of the two) for the 10^{-3} spectrum.

The average, scaled and envelope spectrum values are shown in Table J-3, and are plotted in Figures J-15 and J-16.

This deterministic spectral shape can be used for all probability levels down to 10^{-4}, because the RMA/Derby source still dominates the hazard down to that level. Values for the 10^{-4} spectrum are listed in Table J-4, and the spectra are plotted in Figures J-17 and J-18.

For deterministic spectra we recommend that the shapes and amplitudes shown in Tables J-3 and J-4 and Figures J-15 through J-18 be used. These correspond to a recognizable seismic source that generally dominates earthquake hazard at the RFP, they represent realistic ground motions, and they correspond to identified annual probability values. As such, they are also useful for deriving other representations of ground shaking such as duration and artificial motions.

USE OF CAPABLE FAULTS AND AREA SOURCES

Background

To place the PSHA results in perspective we derive spectra corresponding to earthquakes on identified faults that are assessed to be capable using deterministic criteria. The regulations of the Nuclear Regulatory Commission have been widely applied in past studies in this context.

Through the multiple applications of Appendix A to 10 CFR Part 100 and application of Standard Review Plan 2.5.2 by the Nuclear Regulatory Commission staff (NRC, 1990), a variety of approaches have developed to conduct deterministic analyses. For example, a method to develop deterministic site-specific ground motions for a site lying within a regional seismic source zone (host zone) was developed (Kimball, 1983) and has been applied at several plant sites (e.g., Power et al., 1981). Although the NRC allows for a deterministic evaluation of ground motions to evaluate seismic margins as part of the IPEEE (Individual Plant Examination for External Events) program (NRC, 1991), 10 CFR 100 Appendix A has not been used for a license application since the early 1980's.

Beginning in the early 1980's and continuing to the present (e.g., probabilistic seismic risk analysis in IPEEE; NRC, 1991), the NRC has encouraged the application of probabilistic methodologies in characterizing ground motions for design evaluations. Further, Appendix B to 10 CFR 100 was developed to replace Appendix A and includes the requirement for both a probabilistic hazard analysis as well as a `deterministic check' to be conducted by the staff. Draft Regulatory Guide 1015 provides detailed information on how the probabilistic seismic hazard analysis should be conducted and includes disaggregation of the seismic hazard curves to assess the dominant contributors to the hazard and to, in turn, use these contributors in a deterministic sense to develop design ground motions.

DOE Standard 1020 is now being developed to specify the procedures for conducting ground motion analyses for evaluation of seismic design values at DOE sites. Although these standards are only in draft form, they include the requirement to conduct probabilistic seismic hazard analyses (Draft Standard 1023) and will likely include a requirement to conduct a `deterministic check' as well (Kimball, pers. comm.). In anticipation of the requirements that will ultimately come out of the finalization of the standards, we provide in this section an `Appendix A' deterministic evaluation that follows the procedures developed and applied in the past by licensing precedent for commercial nuclear power plants.

The basic Appendix A procedure consists of the following steps: 1) identify capable faults and other capable seismic sources, 2) define the closest distance of the capable seismic sources to the site, 3) define the maximum magnitudes associated with each seismic source, 4) calculate ground motions for each capable source and determine the source-ground motion combination that leads to the largest ground motions at the site. These steps are discussed below.

Capable Faults and Capable Sources

The criteria for evaluating fault capability in 10 CFR 100 Appendix A include assessments of the recency of displacement, association with macro- and microseismicity, and structural association

with another capable fault. Draft Appendix B includes these same criteria but revises slightly the ages for assessing recency. These criteria are those that have been evaluated explicitly in assessing the `activity' of faults in the probabilistic analysis (see Appendix A). Further, these are the criteria that have been given the highest weight in assessing activity; two other criteria are added that might give an indication of possible activity, but these are given relatively lesser weight.

Each of the capability criteria have been evaluated for each seismic source and the degree to which each potential source satisfies the criteria has been documented in Appendix A to this report. For the probabilistic analysis, the uncertainty in assessing activity has been quantified and is included explicitly into the analysis. That is, the relative weight of the various activity criteria has been quantified and the probability that each criterion applies to a particular fault is given and the technical basis for the assessment is documented. For the deterministic evaluation of capability, there is no opportunity to provide a probability of capability; each fault/source must be characterized as either capable or not capable. In making this assessment the uncertainties in evaluating the capability of any given fault or potential source are not incorporated explicitly into the analysis.

Consistent with the application of 10 CFR 100 Appendix A, the capability of each fault and potential source is evaluated using the criteria given in Appendix A to this report and documented for each fault/source. The probability of activity of each fault and potential source is discussed in the main report and is summarized in Table 2-1. The assessment of greater than 0.5 means that it is more likely that the fault/source is active (capable in this case) than that it is not. Accordingly, any fault/source that has a probability of activity of 0.5 or greater is assessed to be capable. Likewise, a fault/source with a probability of activity of less than 0.5 means that the fault/source is judged for the deterministic analysis to not be capable. These definitions are consistent with the applications of the `active/not active' probabilities used in the probabilistic analysis, and are consistent with similar analyses conducted for nuclear power plants (Pacific Gas and Electric, 1988).

Following the procedure given above, the only fault assessed to be capable is the RMA/Derby source. As discussed in detail in Appendix A, this source is, in fact, not a known or mapped fault but is a zone of concentrated seismicity. In spite of the fact that the geologic evidence of faulting is lacking, the occurrence of seismicity (non-injection related) is judged to provide overriding evidence for the presence of a capable source in the vicinity of the Rocky Mountain Arsenal.

The other faults considered in the probabilistic analysis are judged to not be capable. That is, the activity criteria considered for each fault result in the assessment of probability of activity that is less than 0.5. Likewise, the local source zone, which accounts for a family of northeast-trending faults in the site vicinity, is judged to not be capable.

All of the regional seismic source zones, including the Denver Basin source zone (Source Zone I) are judged to be capable, because of the occurrence of low levels of microseismicity and possible macroseismicity (e.g. the 1882 Colorado earthquake).

The closest distance of the RMA/Derby source and other capable seismic sources to the site is given in Table J-5. The distance of the host zone (Source I) to the site is assessed to be 15 km based on the application of Standard Review Plan 2.5.2 and described in Kimball (1983). Note that this distance is consistent with the range of distances contributing to hazard from Source I (see Figure J-1a).

Maximum Magnitudes

Maximum earthquake magnitudes are assessed for each capable source. The evaluation of maximum magnitudes for the probabilistic analysis is described in detail in Appendix A to the report and, because the analysis is probabilistic, results in a probabilistic distribution of maximum magnitudes that includes the uncertainties in the assessment. For the deterministic analysis a single value of maximum magnitude must be selected for each capable source. Because the probabilistic analysis is aimed at arriving at a best estimate of maximum magnitude and the associated uncertainties, the average or mean estimate of the maximum magnitude distribution is the most appropriate estimate of the maximum magnitude for the deterministic analysis. The upper bound to the probabilistic distribution on maximum magnitude is a low likelihood assessment and is not an appropriate estimate for the deterministic analysis. Regulatory precedent for the use of a selected deterministic maximum magnitude that is a central value in the maximum magnitude distribution is given in the Diablo Canyon Long Term Seismic Program (Pacific Gas and Electric, 1988).

Ground Motion Assessment

Deterministic spectra for 5% damping calculated for the RMA/Derby source and for Sources I through V are illustrated in Figures J-19 through J-24. These have been calculated using the magnitudes and distances listed in Table J-5. Both median (50%) and 84% spectra are shown, as there is precedent for using both in deterministic evaluations. These spectra represent the weighted average of the seven attenuation equations developed in this study to estimate ground motion on rock.

SUMMARY

Deterministic ground motions have been derived for the RFP using two methods. The first is to deaggregate the hazard results to determine the critical magnitudes and distances that contribute to hazard. For the RFP the relevant source is the RMA/Derby source. This source generally dominates hazards at annual probability levels of down to 10^{-4}, and indicates a modal magnitude and distance of $\hat{\mathbf{M}} = 5.9$ and $\hat{\mathbf{R}} = 27$ km. (Source III also contributes, and dominates the hazard for natural frequencies around 1 Hz and annual probabilities around 10^{-3}.) The second method follows deterministic procedures used by the U.S. Nuclear Regulatory Commission and derives estimates of the largest magnitudes that could occur at the closest distance for all capable faults and area sources.

Comparisons of rock spectra are shown in Figures J-25 and J-26 for 10^{-3} and 10^{-4} annual probabilities, respectively. The spectra shown are the deterministic spectra derived in this Appendix (and documented in Tables J-3 and J-4), the uniform hazard spectra documented in the main report, and the median deterministic spectra calculated for the RMA/Derby source and for Sources I, II, and III. It is clear that the deterministic spectra derived here closely match the uniform hazard spectrum. The individual deterministic spectra for the RMA/Derby source and Sources I and II exceed the 10^{-3} deterministic spectrum but are bounded by the 10^{-4} deterministic spectrum. This reflects the low recurrence rate on the RMA/Derby source and the fact that a maximum magnitude earthquake on that structure would be a very low probability event.

To derive deterministic ground motions the recommended procedure is to use the deaggregated hazard results to develop a spectral shape, anchor this to the PGA and PSV(1 Hz) amplitudes corresponding to the desired annual probability, and choose a spectrum that anchors the hazard values for the chosen annual probability. This is a reasonable procedure because the spectrum representing the deterministic event comes from the seismic source that generally dominates hazard over most frequencies and annual probabilities of interest. Thus this spectrum, when scaled by PGA, gives reasonable estimates of the low frequency portion of the spectrum (and similarly for high frequencies when scaled by PSV(1 Hz)). Anchoring the spectrum to selected annual probability values means that amplitudes consistent with those values will be obtained over all frequencies.

Alternatives, such as using unscaled amplitudes or using deterministic, worst case earthquakes, do not take into account the seismic activity of each fault or area source. Thus a fault that has very low activity but has the potential to generate large magnitudes could dominate a deterministic calculation of ground motion, when the real shaking, should it occur, likely will come from a different fault with a higher rate of activity. The methodology recommended here incorporates both the rates of seismic activity and probability of activity and leads to the most realistic deterministic ground motions consistent with the seismic hazard.

REFERENCES

Ishikawa, Y. and H. Kameda (1988). Hazard-consistent magnitude and distance for extended seismic risk analysis, *Proc.*, 9th World Conf. on Earth. Eng., II:89-94.

Ishikawa, Y. and H. Kameda (1991). Probability-based determination of specific scenario earthquakes, *Proc.*, 4th Intern. Conf. on Seismic Zonation, II:3-10.

Ishikawa, Y. and H. Kameda (1993). Scenario earthquakes vs. probabilistic seismic hazard, *Proc.*, ICOSSAR '93 Conf., Innsbruck.

Kimball, J.K. (1983). The use of site dependent spectra, Proceedings of the U.S. Geological Survey Workshop on Site Specific Effects of Soil and Rock on Ground Motions and the Implications for Earthquake-Resistant Design, U.S. Geological Survey Open-File Report 83-845, p. 401-422.

McGuire, R.K. and K.M. Shedlock (1981). Statistical Uncertainties in Seismic Hazard Evaluations in the United States, *Bull. Seism. Soc. Am.*, Vol. 71, No. 4, pp. 1287-1308, August.

National Research Council (1988). Probabilistic seismic hazard analysis, Rept. of the Panel on Seismic Hazard Analysis, National Academy Press, Wash., DC, 97.

Pacific Gas and Electric Company (1988). Final Report of the Diablo Canyon Long Term Seismic Program, U.S. Nuclear Commission Docket Nos. 50-275 and 50-323, Section 3, July 1988.

Power, M.S., K.J. Coppersmith, R.R. Youngs, D.P. Schwartz and F.H. Swan (1981). Seismic Exposure Analysis for the WNP-2 and WNP-3/4 Sites, Appendix 2.5K to Amendment No. 18 Final Safety Analysis Report WNP-2, for Washington Public Power Supply System, Richland, Washington, September.

United States Nuclear Regulatory Commission (NRC) (1990). Standard Review Plan, Office of Nuclear Reactor Regulation, NUREG-0800, Rev. 2, 2.5.2 Vibratory Ground Motion, 15p.

United States Nuclear Regulatory Commission (NRC) (1991). Procedural and Submittal Guidance for the Individual Plant Examination of External Events (IPEEE) for Severe Accident Vulnerabilities, NUREG-1407, 27p.

TABLE J-1

$\bar{M}$ AND $\bar{R}$ SOURCE FOR PGA

Freq.	Ground Motion	Source	Prob.	Cont. to Hazard*	$\bar{M}$	$\bar{R}$
PGA	.25g	Source I	3.14×10^{-5}	30%	5.57	21.8
		Source II	1.66×10^{-5}	16%	5.86	35.5
		Source III	8.61×10^{-7}	1%	6.82	134.6
		RMA/Derby	4.15×10^{-5}	39%	5.68	26.5
		Rock Creek	6.68×10^{-6}	6%	5.74	2.1
		Golden-Boulder	8.75×10^{-6}	8%	6.52	8.4
		All	1.06×10^{-4}	100%	5.76	24.4
	.08g	Source I	2.71×10^{-4}	25%	5.50	35.8
		Source II	2.74×10^{-4}	25%	5.72	49.3
		Source III	7.03×10^{-5}	6%	6.49	153.1
		RMA/Derby	4.54×10^{-4}	41%	5.53	27.3
		Rock Creek	8.74×10^{-6}	1%	5.68	2.5
		Golden-Boulder	1.80×10^{-5}	2%	6.14	13.9
		All	1.10×10^{-3}	100%	5.64	42.5

* Individual contributions do not sum to exactly 100% because of rounding.

TABLE J-2

$\bar{M}$ AND $\bar{R}$ BY SOURCE FOR PSV(1 Hz)

Freq.	Ground Motion	Source	Prob.	Cont. to Hazard*	$\bar{M}$	$\bar{R}$
1 Hz	35 cm/s	Source I	1.91×10^{-5}	19%	5.93	33.0
		Source II	2.27×10^{-5}	22%	6.15	49.9
		Source III	1.88×10^{-5}	18%	6.77	174.5
		RMA/Derby	2.93×10^{-5}	29%	5.91	26.7
		Rock Creek	4.80×10^{-6}	5%	5.85	1.8
		Golden-Boulder	7.79×10^{-6}	8%	6.68	9.4
		All	1.02×10^{-4}	100%	6.18	57.6
	12cm/s	Source I	1.56×10^{-4}	16%	5.77	50.4
		Source II	2.20×10^{-4}	23%	5.98	64.2
		Source III	3.67×10^{-4}	38%	6.56	197.9
		RMA/Derby	2.11×10^{-4}	22%	5.71	27.2
		Rock Creek	7.60×10^{-6}	1%	5.73	2.3
		Golden-Boulder	1.39×10^{-5}	1%	6.39	14.1
		All	9.75×10^{-4}	100%	6.11	103.1

* Individual contributions do not sum to exactly 100% because of rounding.

TABLE J-3

DETERMINISTIC ROCK SPECTRA** FOR 10^{-3} ANNUAL PROBABILITY

$\hat{M}$	$\hat{R}$	Spectrum	PGA	PSA (25 Hz)	PSA (10 Hz)	PSA (5 Hz)	PSA (2.5 Hz)	PSA (1 Hz)
5.9	27 km	average	.083	.109	.193	.205	.150	.063
		scaled to PGA = .083*	.083	.109	.193	.205	.150	.063
		scaled to PSA(1 Hz) = .075*	.099	.131	.231	.246	.180	.075
10^{-3} envelope			.099	.131	.231	.246	.180	.075

* These are the ground motion values corresponding to 10^{-3} annual probability.

** PGA and PSA are listed in units of g.

TABLE J-4

DETERMINISTIC ROCK SPECTRA** FOR 10^{-4} ANNUAL PROBABILITY

$\hat{M}$	$\hat{R}$	Spectrum	PGA	PSA(25 Hz)	PSA(10 Hz)	PSA(5 Hz)	PSA(2.5 Hz)	PSA(1 Hz)
5.9	27 km	average	.083	.109	.193	.205	.150	.063
		scaled to PGA = .256*	.256	.336	.594	.631	.462	.194
		scaled to PSA(1 Hz) = .226*	.298	.391	.693	.736	.539	.226
10^{-4} envelope			.298	.391	.693	.736	.539	.226

* These are the ground motion values corresponding to 10^{-4} annual probability.

** PGA and PSA are listed in units of g.

TABLE J-5

CAPABLE SOURCES FOR 10 CFR 100 APPENDIX A ASSESSMENT

CAPABLE SOURCE	MEAN MAXIMUM MAGNITUDE	CLOSEST DISTANCE (km)
RMA/Derby	6.2	13
Source Zone I	5.8	15
Source Zone II	6.2	16
Source Zone III	7.0	85
Source Zone IV	5.8	142
Source Zone V	5.8	170

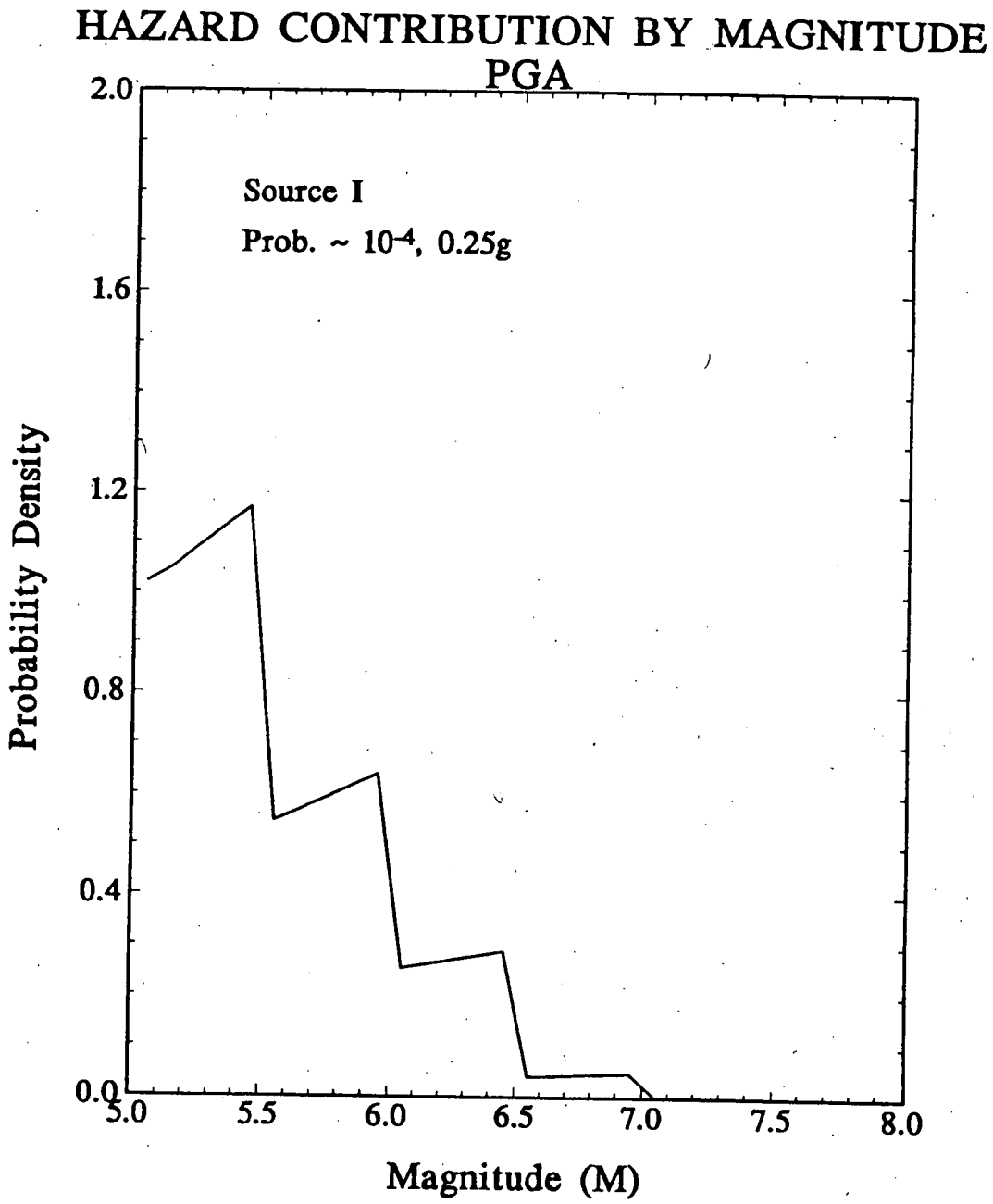

Figure J-1a. Contribution to hazard by magnitude for PGA = 0.25g, Source I.

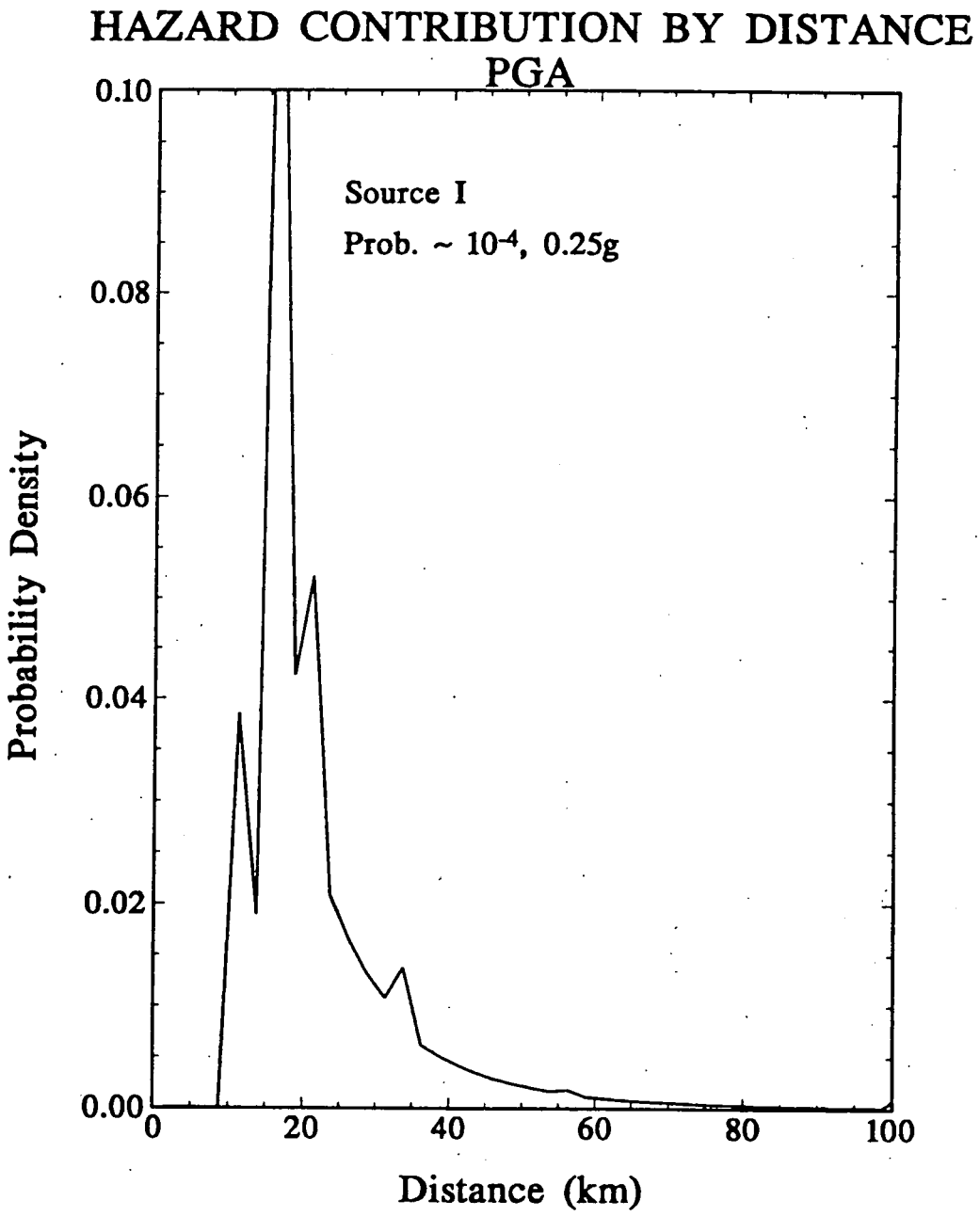

Figure J-1b. Contribution to hazard by distance for PGA = 0.25g, Source I.

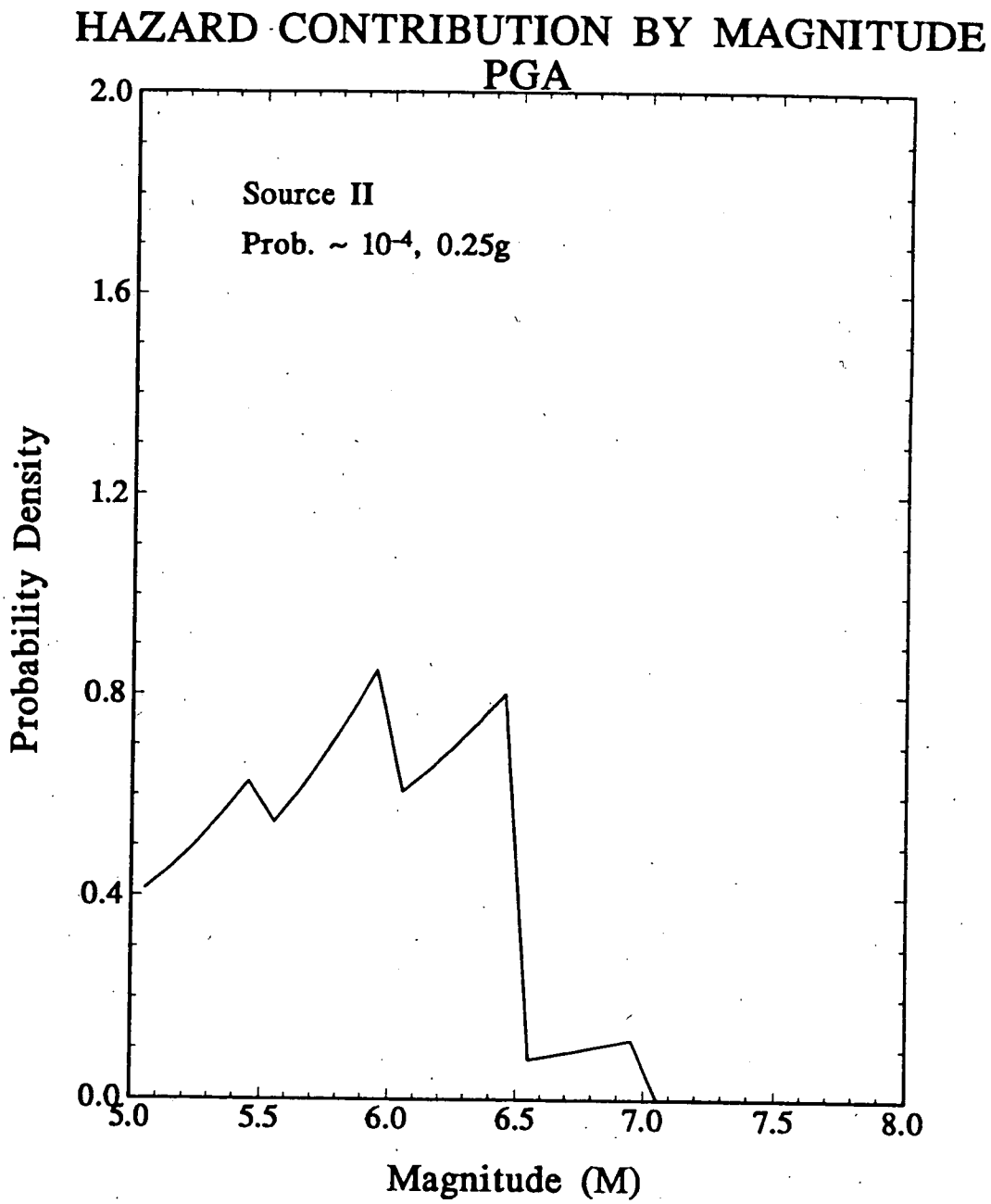

Figure J-2a. Contribution to hazard by magnitude for PGA = 0.25g, Source II.

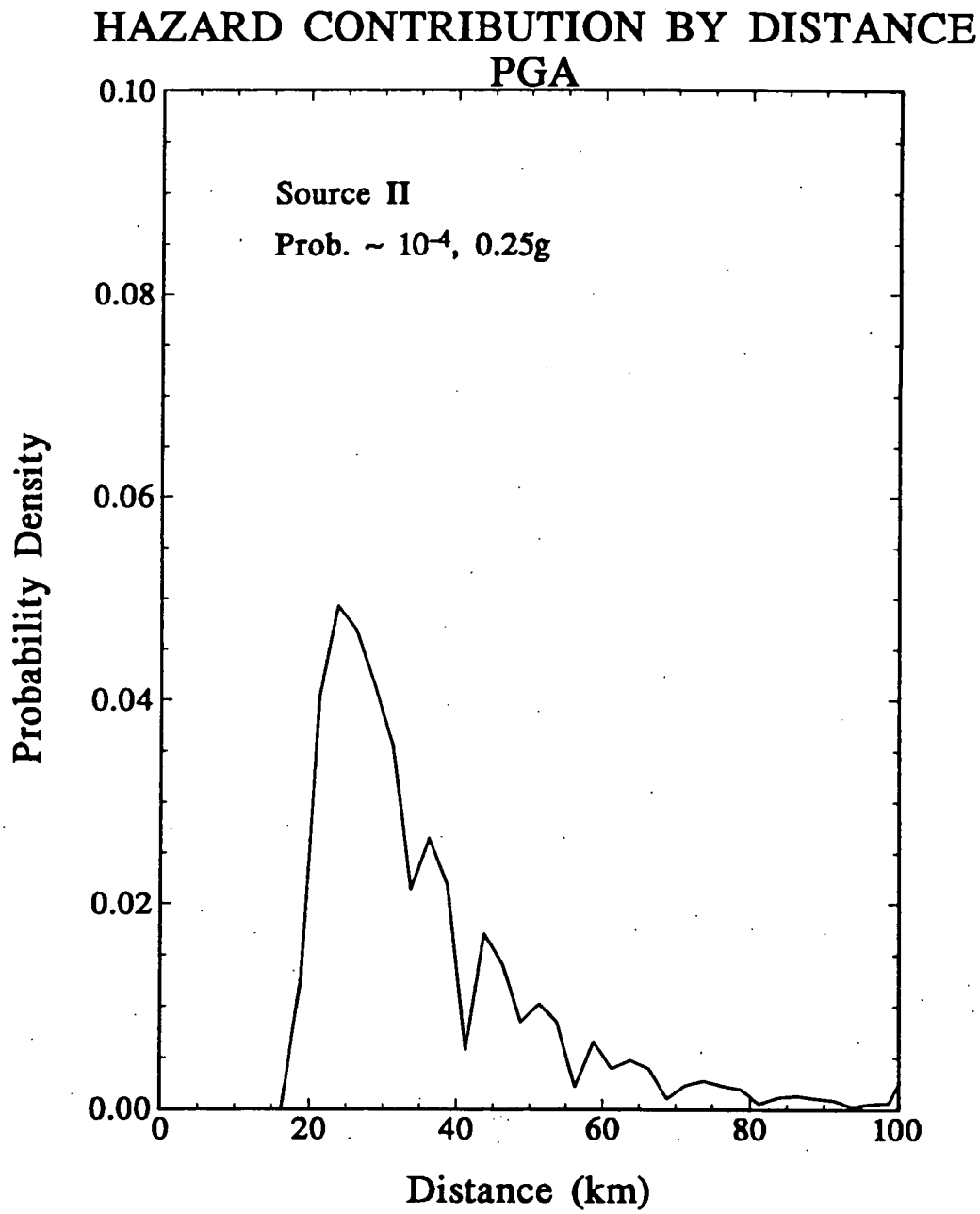

Figure J-2b. Contribution to hazard by distance for PGA = 0.25g, Source II.

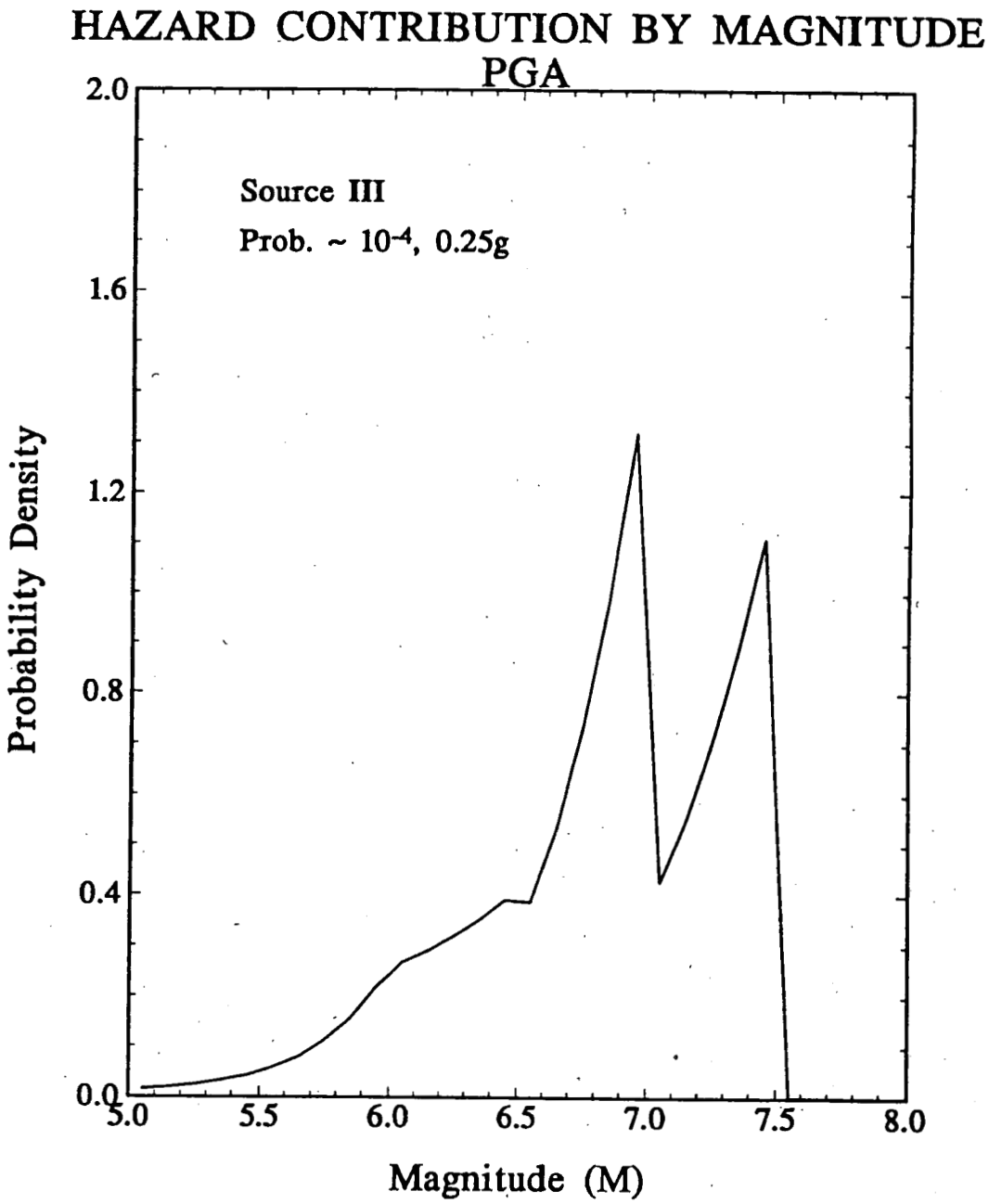

Figure J-3a. Contribution to hazard by magnitude for PGA = 0.25g, Source III.

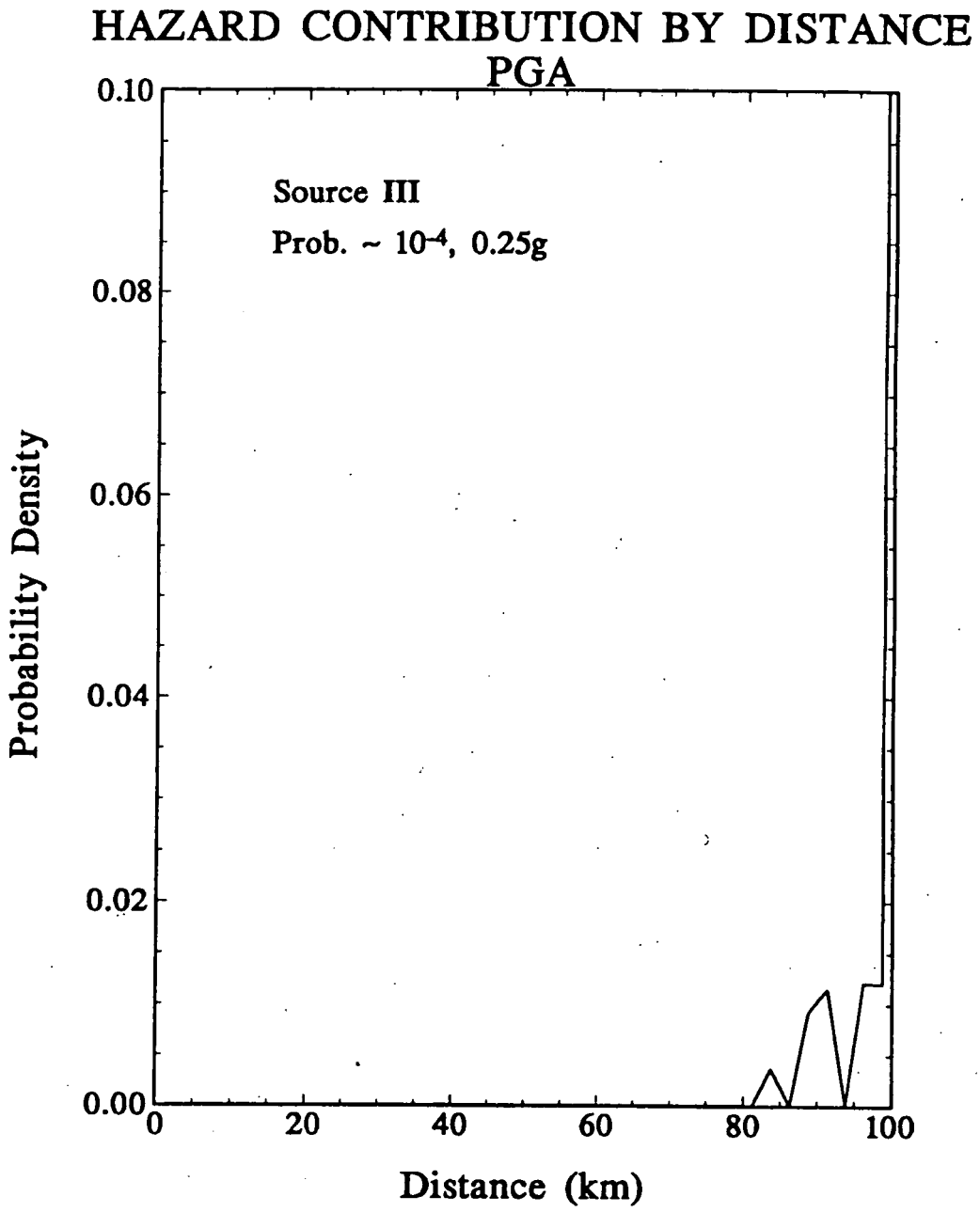

Figure J-3b. Contribution to hazard by distance for PGA = 0.25g, Source III.

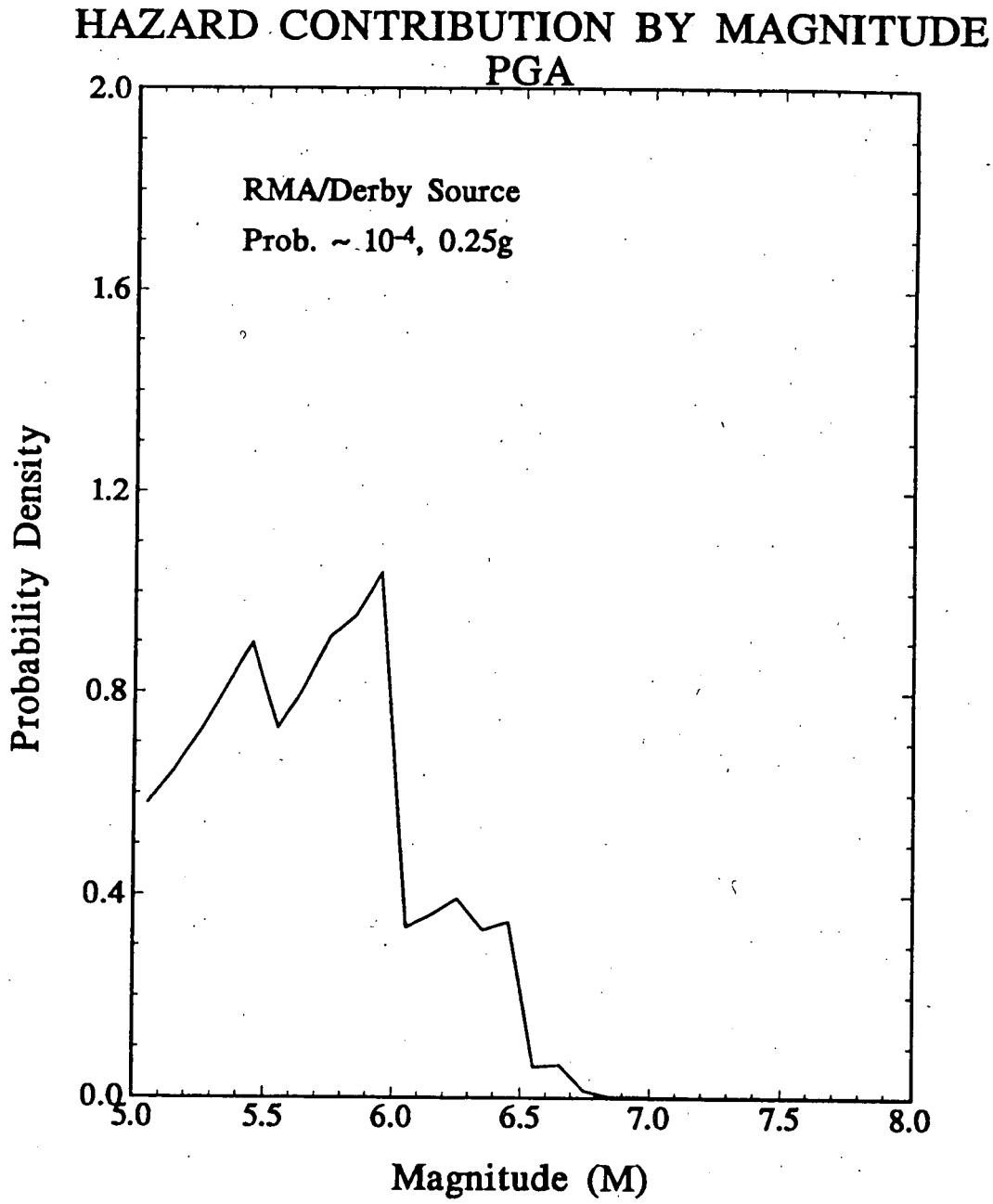

Figure J-4a. Contribution to hazard by magnitude for PGA = 0.25g, RMA/Derby source.

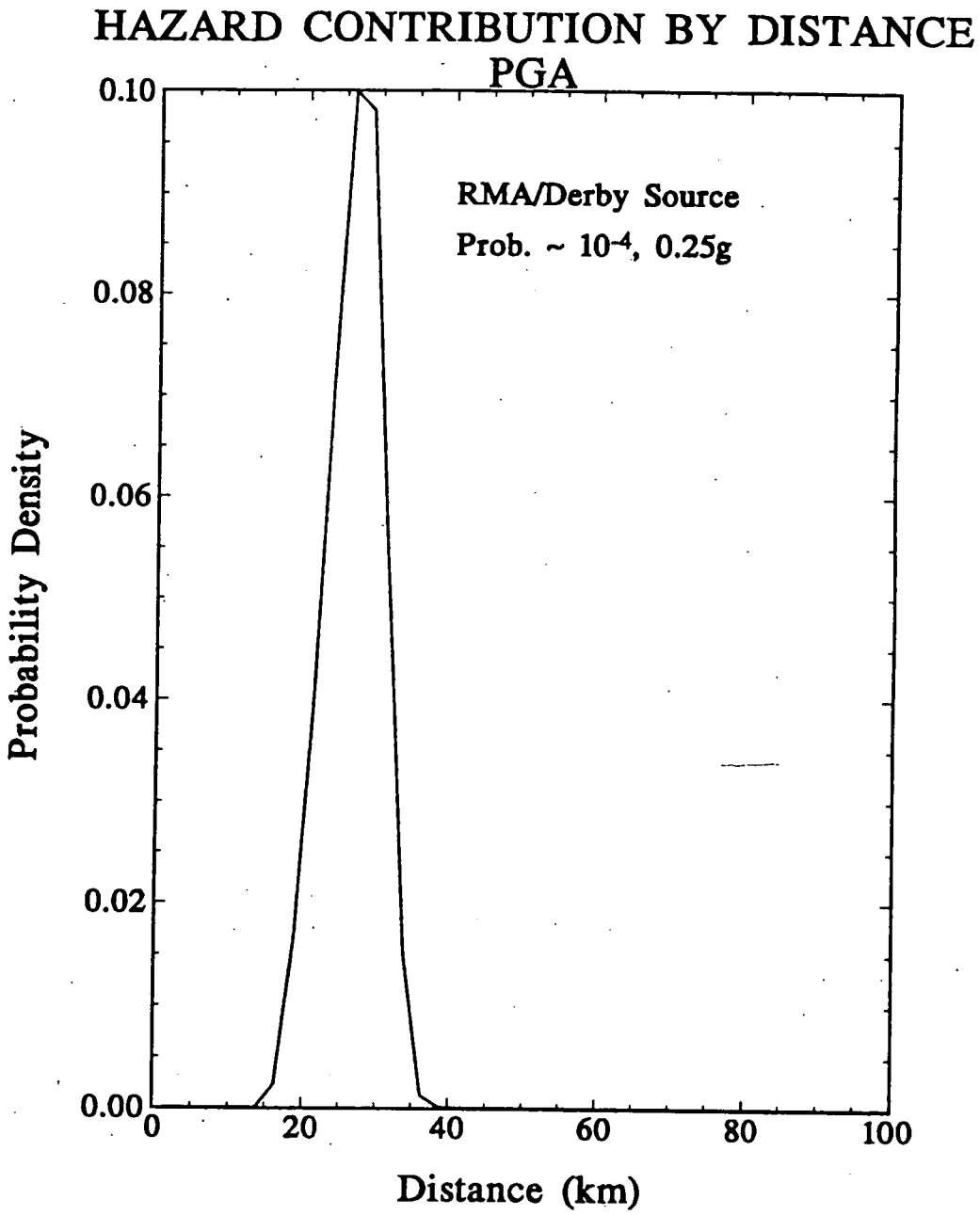

Figure J-4b. Contribution to hazard by distance for PGA = 0.25g, RMA/Derby source.

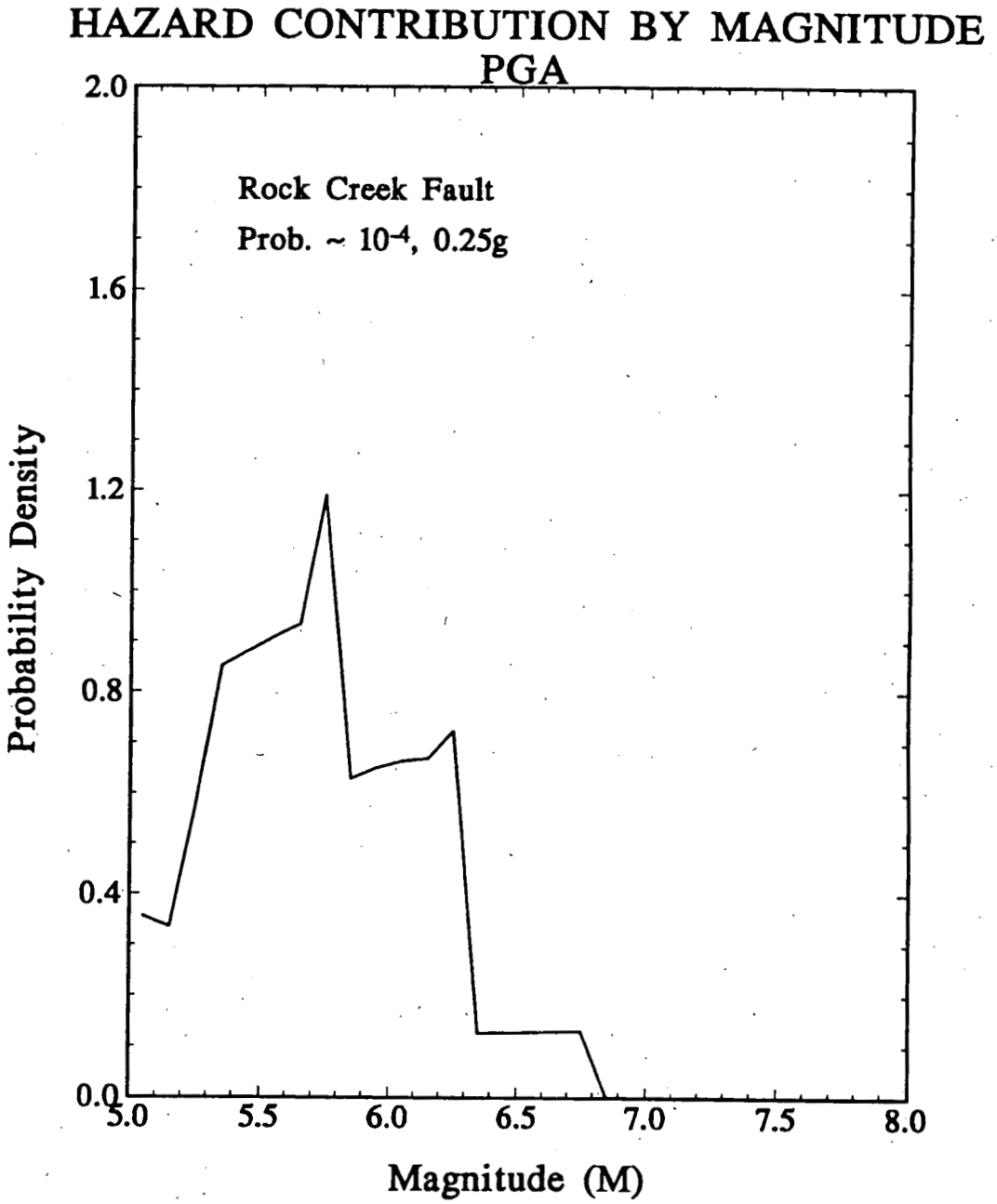

Figure J-5a. Contribution to hazard by magnitude for PGA = 0.25g, Rock Creek fault.

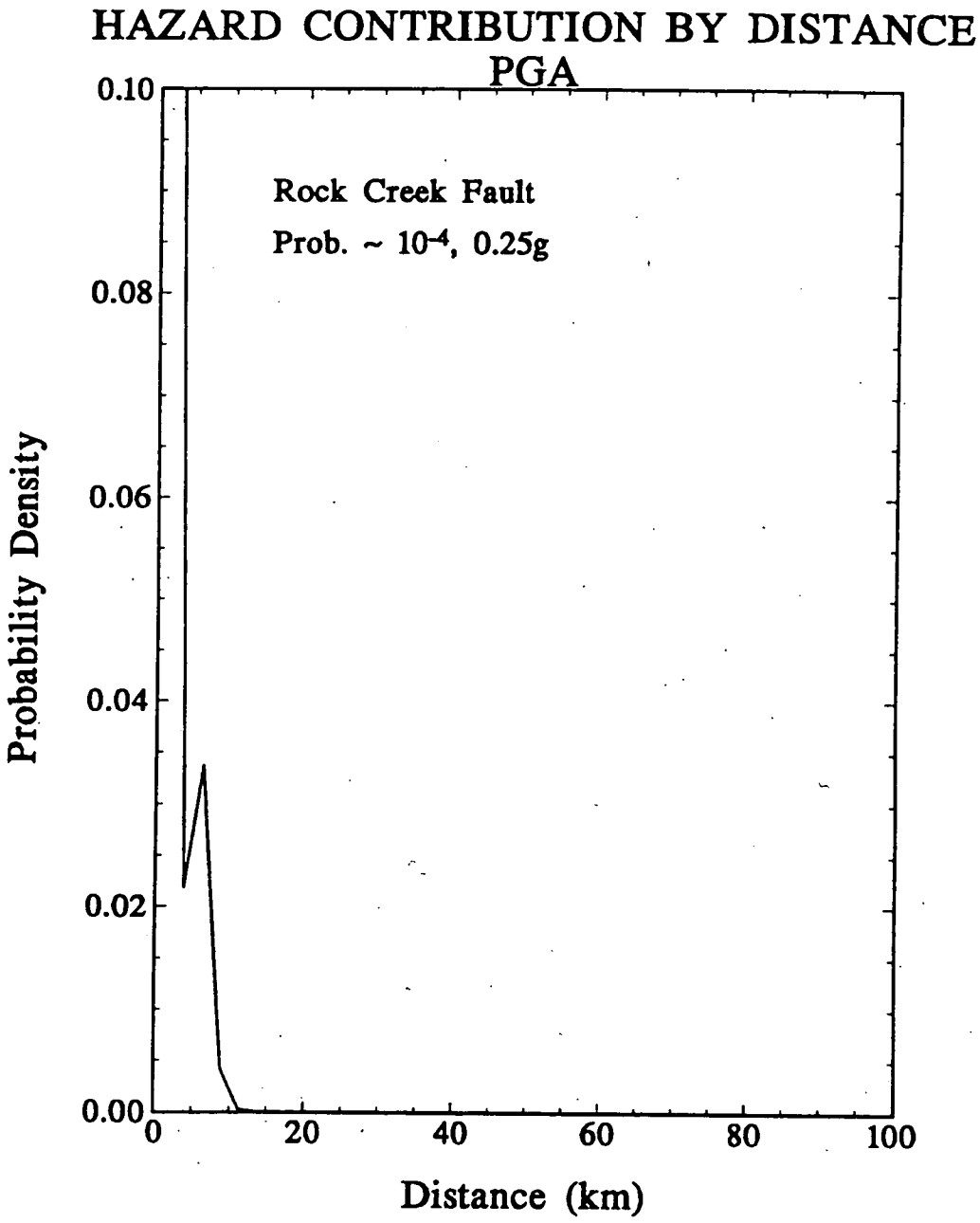

Figure J-5b Contribution to hazard by distance for PGA = 0.25g, Rock Creek fault.

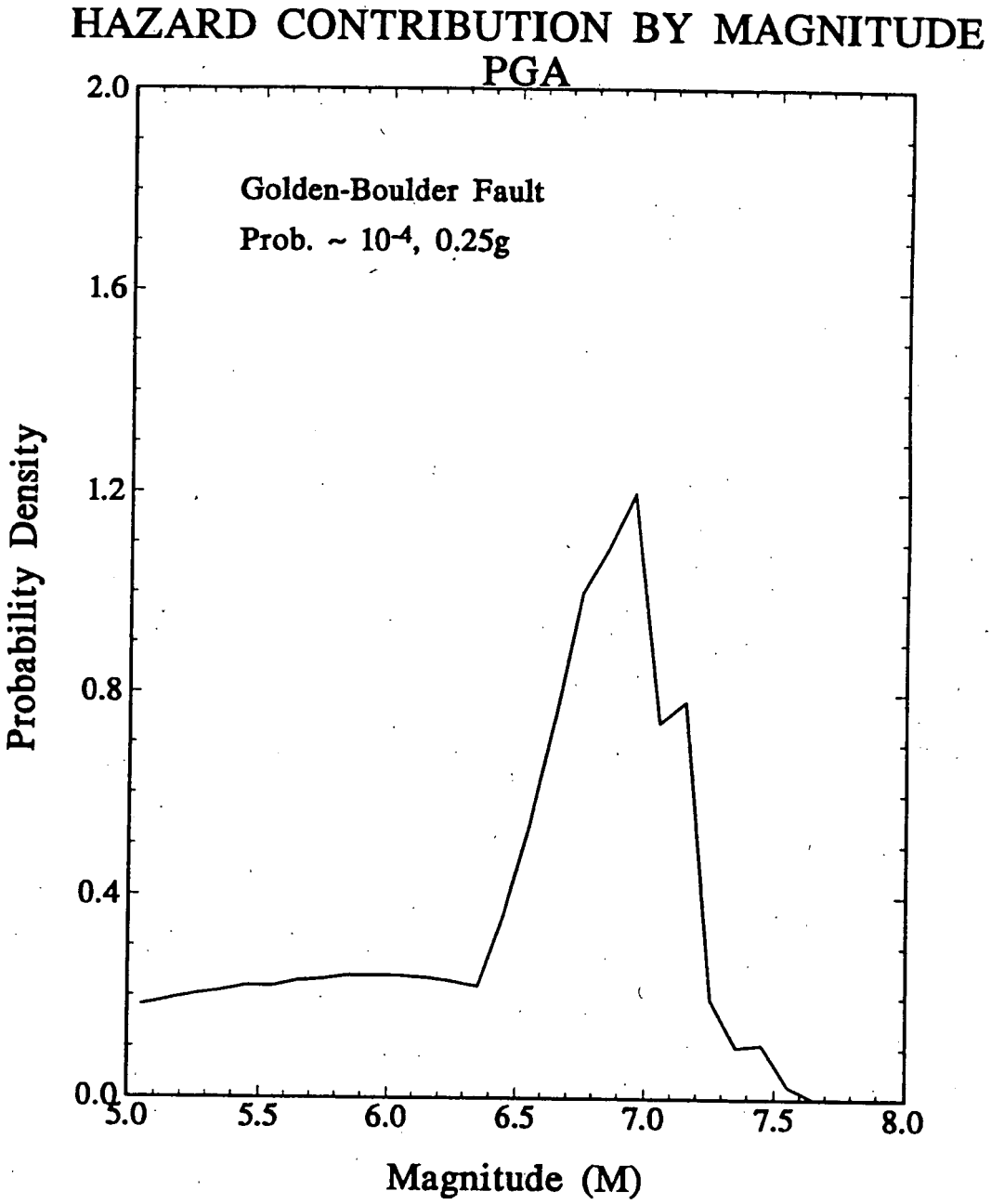

Figure J-6a. Contribution to hazard by magnitude for PGA = 0.25g, Golden-Boulder fault.

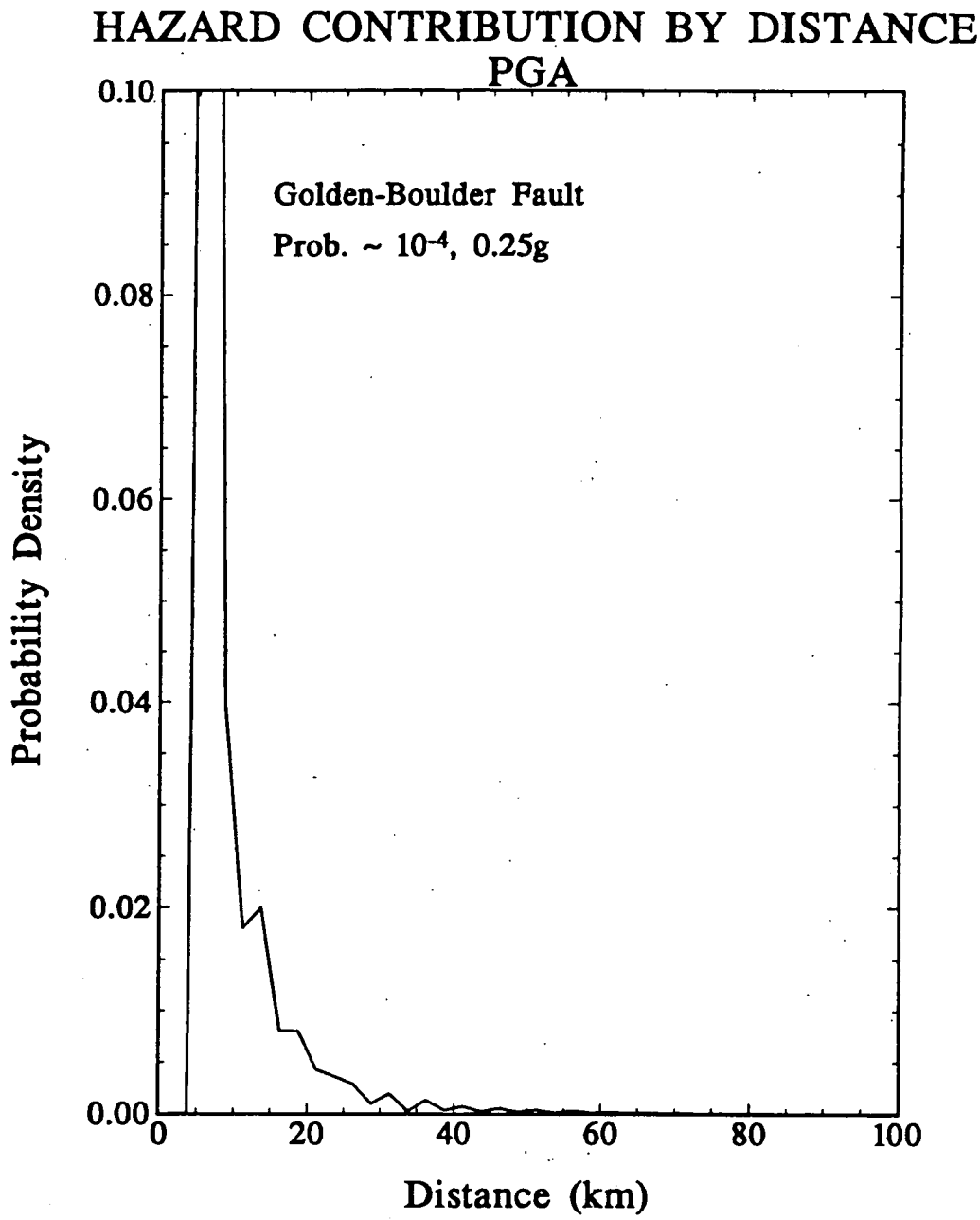

Figure J-6b. Contribution to hazard by distance for PGA = 0.25g, Golden-Boulder fault.

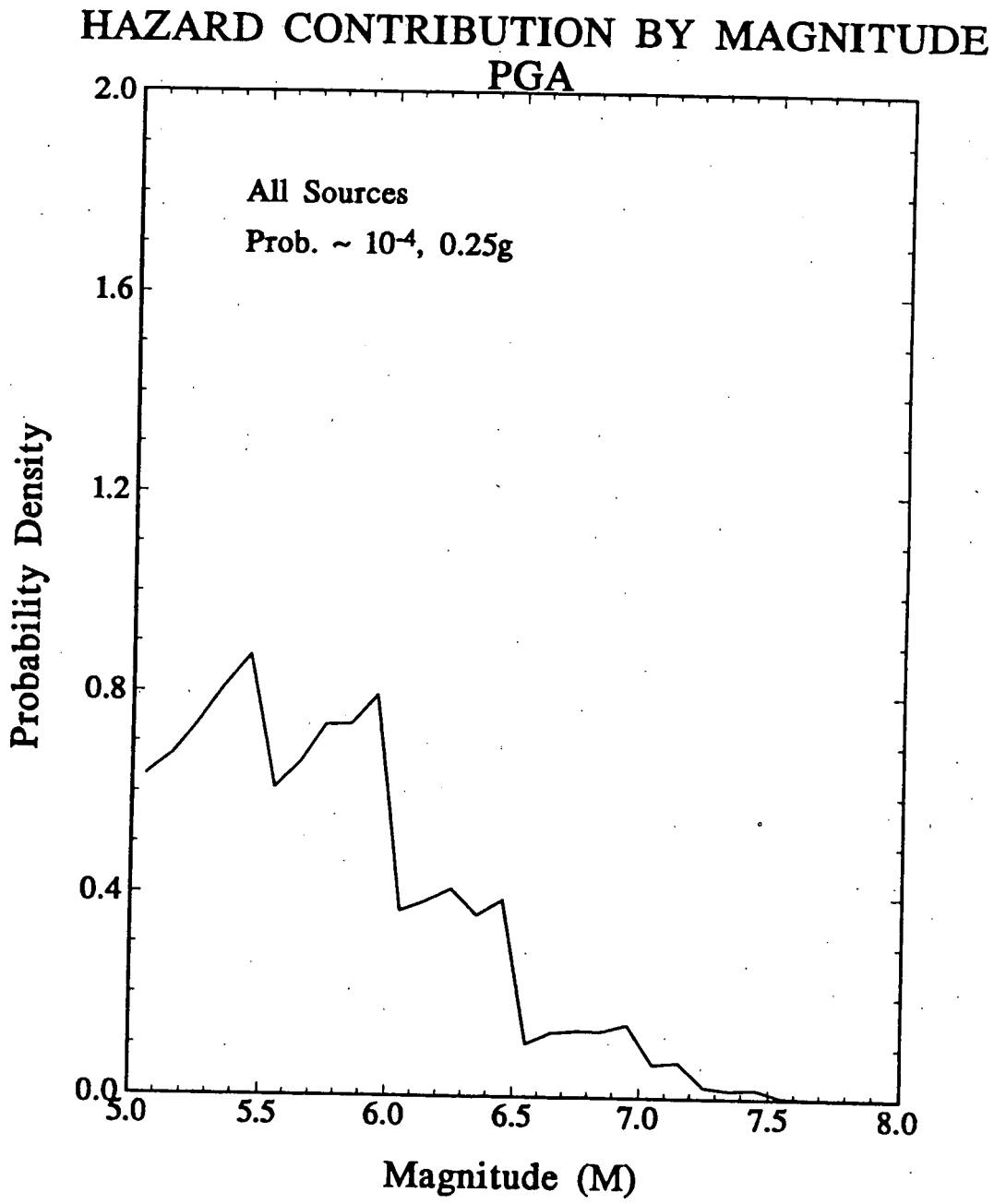

Figure J-7a. Contribution to hazard by magnitude for PGA = 0.25g, all sources.

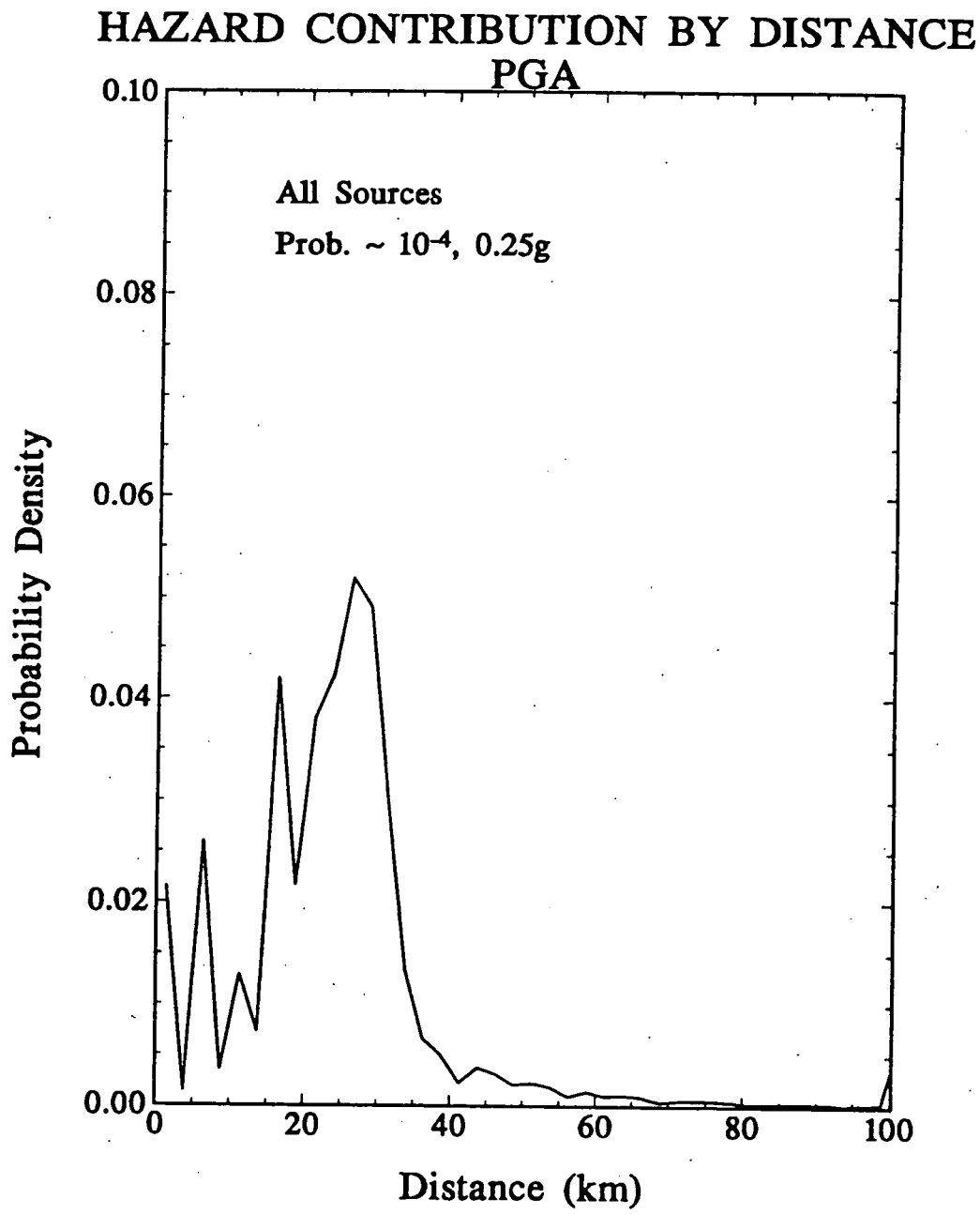

Figure J-7b. Contribution to hazard by distance for PGA = 0.25g, all sources.

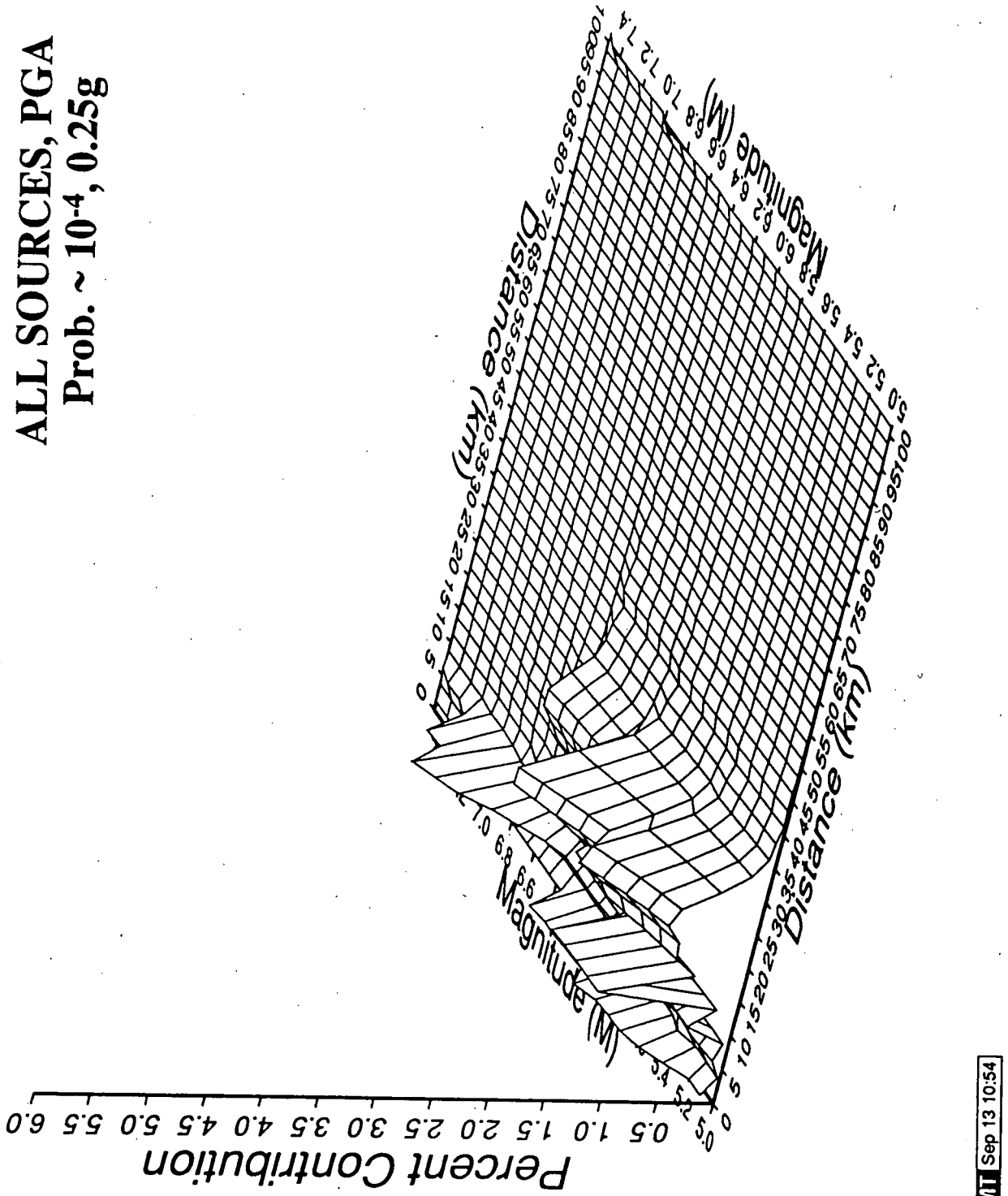

GMT Sep 13 10:54

Figure J-8. Contribution to hazard by magnitude and distance for PGA = 0.25g, all sources.

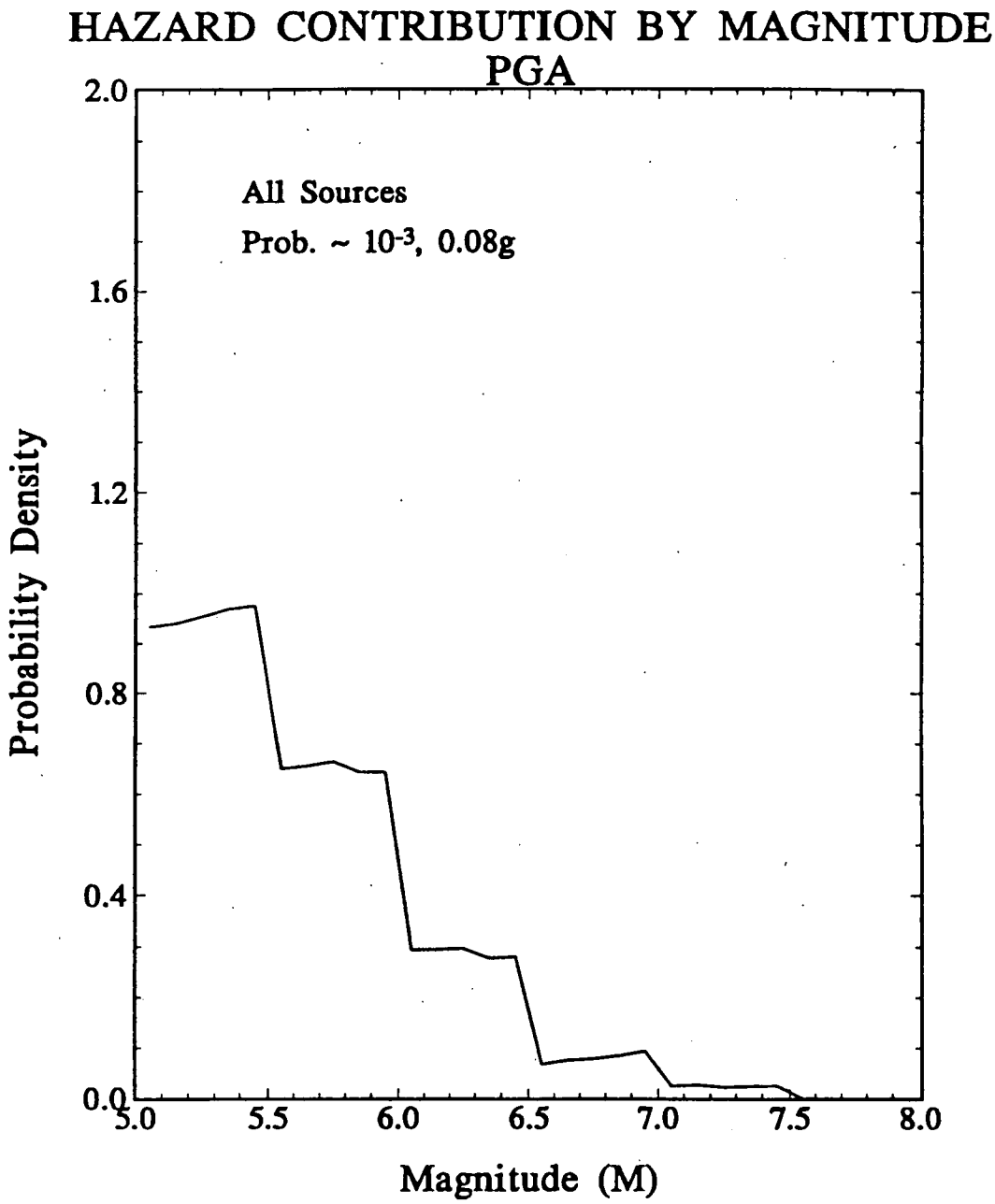

Figure J-9a. Contribution to hazard by magnitude for PGA = 0.08g, all sources.

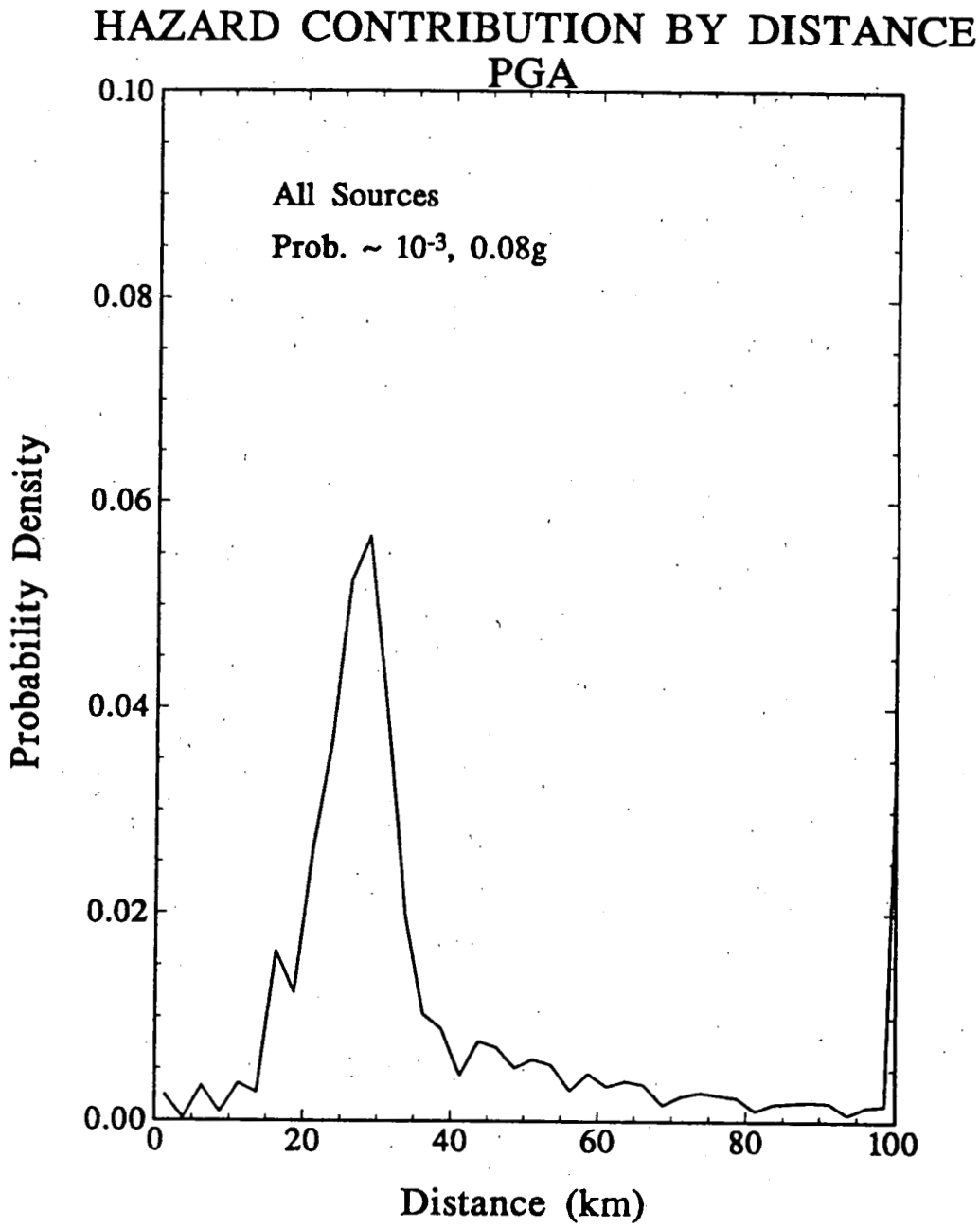

Figure J-9b. Contribution to hazard by distance for PGA = 0.08g all sources.

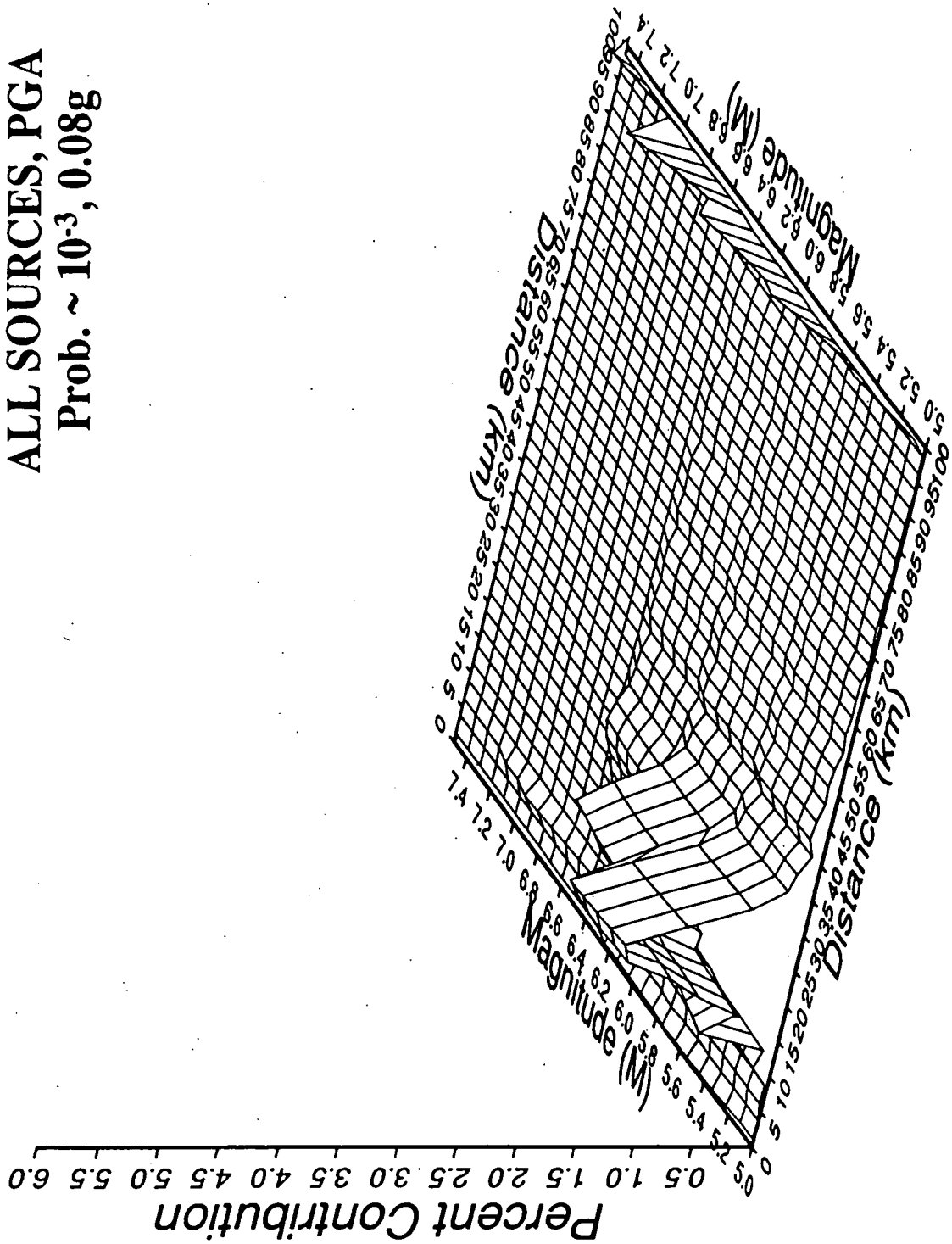

GMT Sep 13 10:54

Figure J-10. Contribution to hazard by magnitude and distance for PGA = 0.08g, all sources.

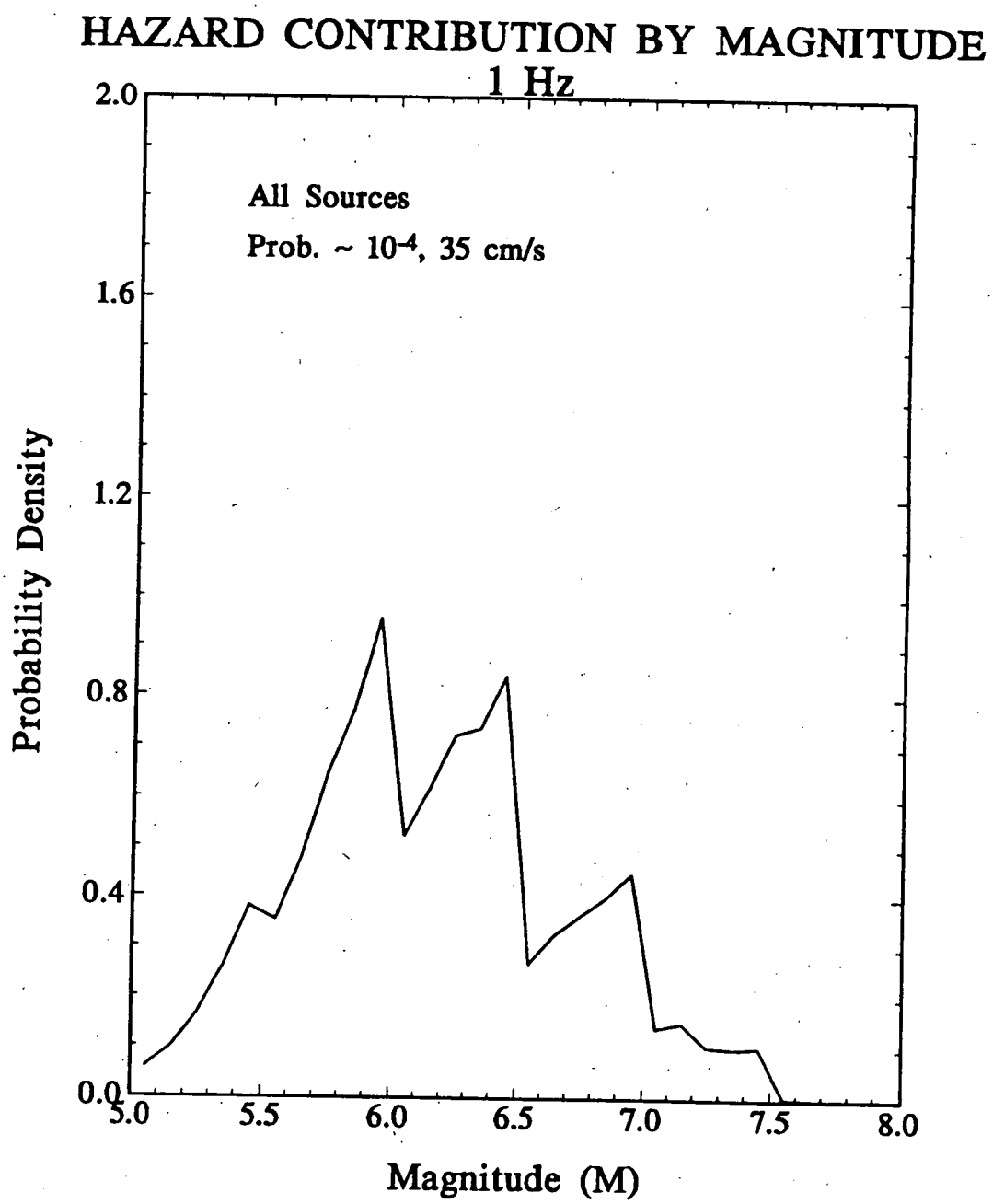

Figure J-11a. Contribution to hazard by magnitude for PSV(1 Hz) = 35 cm/s, all sources.

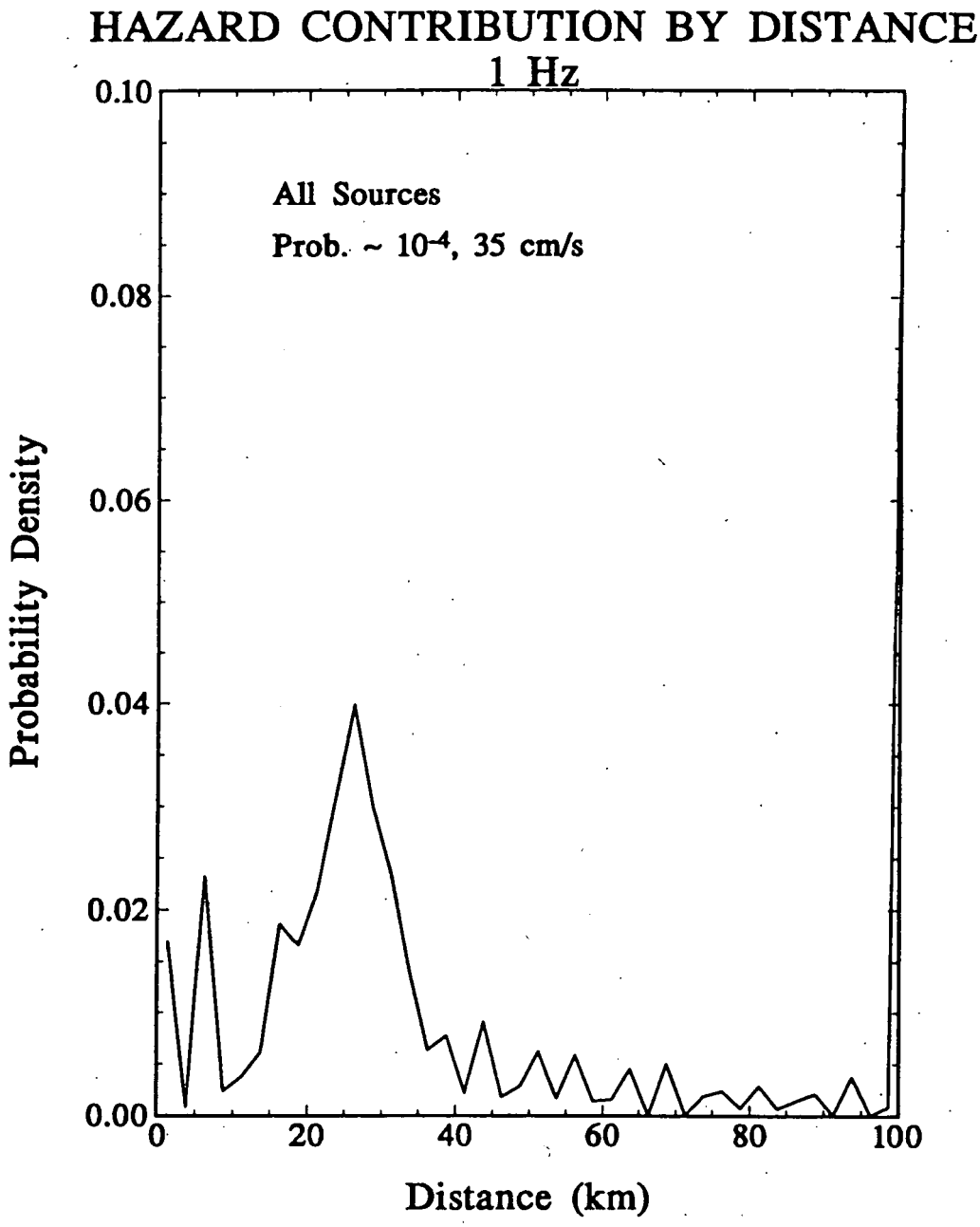

Figure J-11b. Contribution to hazard by distance for PSV(1 Hz) = 35 cm/s, all sources.

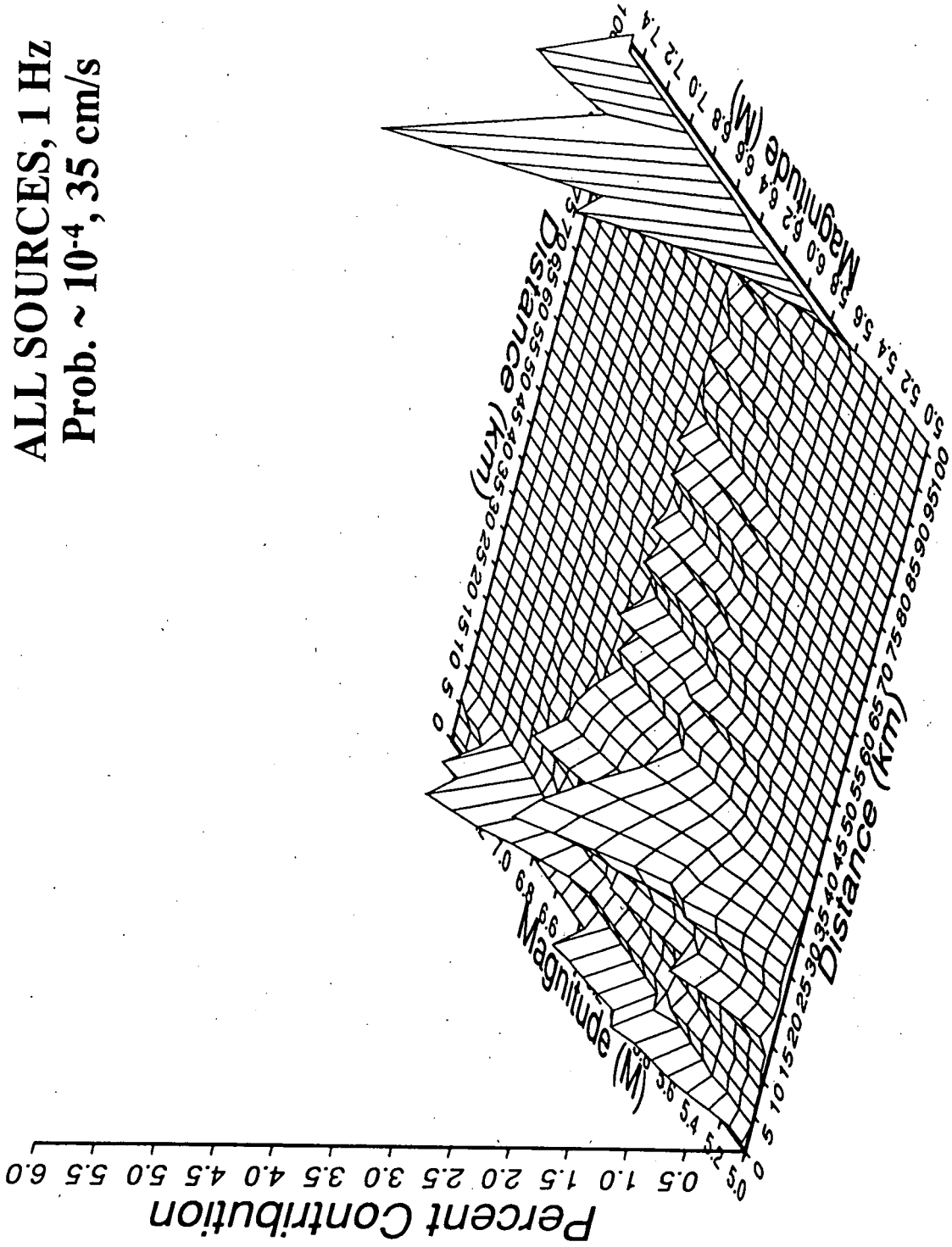

Figure J-12. Contribution to hazard by magnitude and distance for PSV(1 Hz) = 35 cm/s, all sources.

GMT Sep 13 10:55

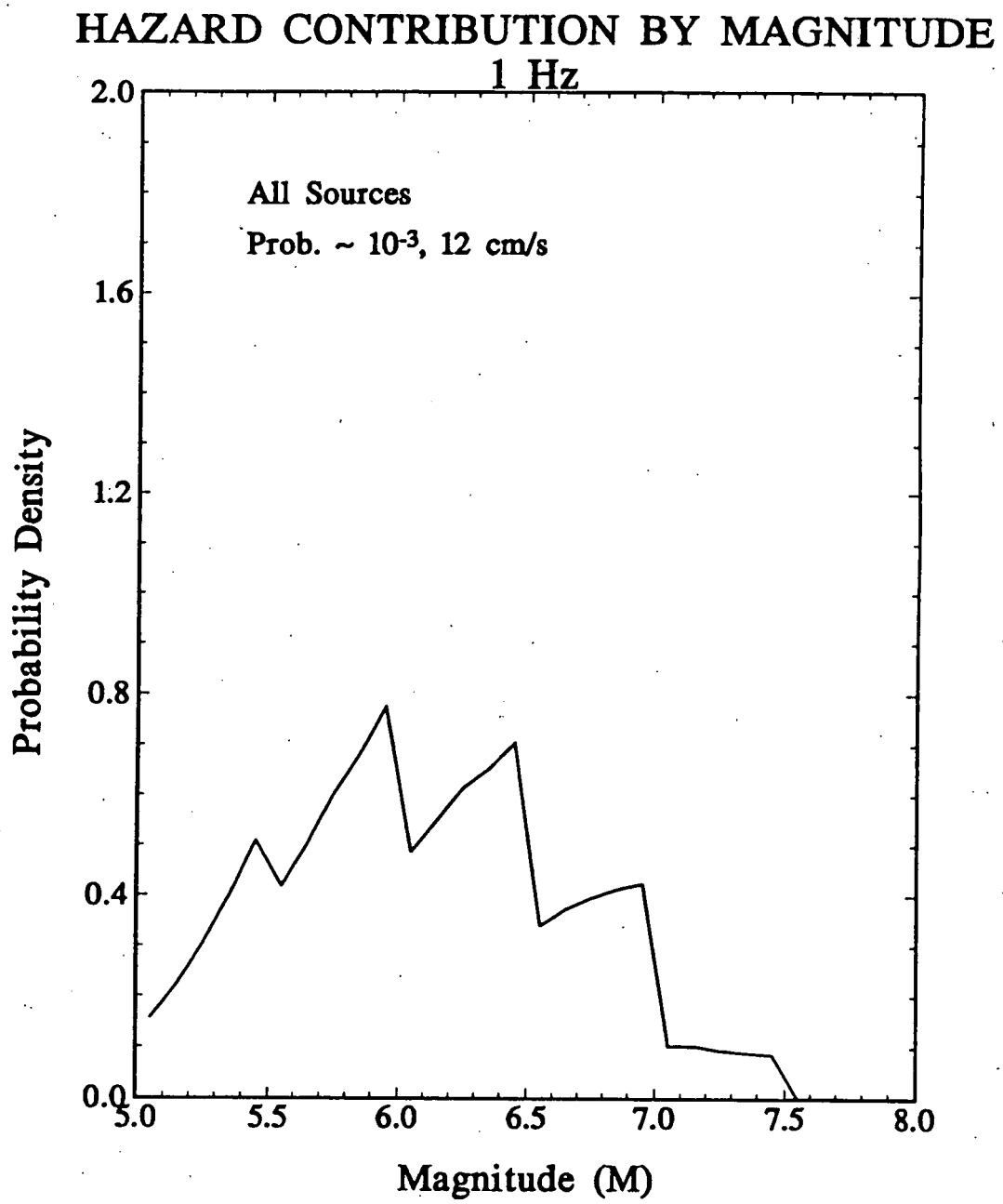

Figure J-13a. Contribution to hazard by magnitude for PSV(1 Hz) = 12 cm/s, all sources.

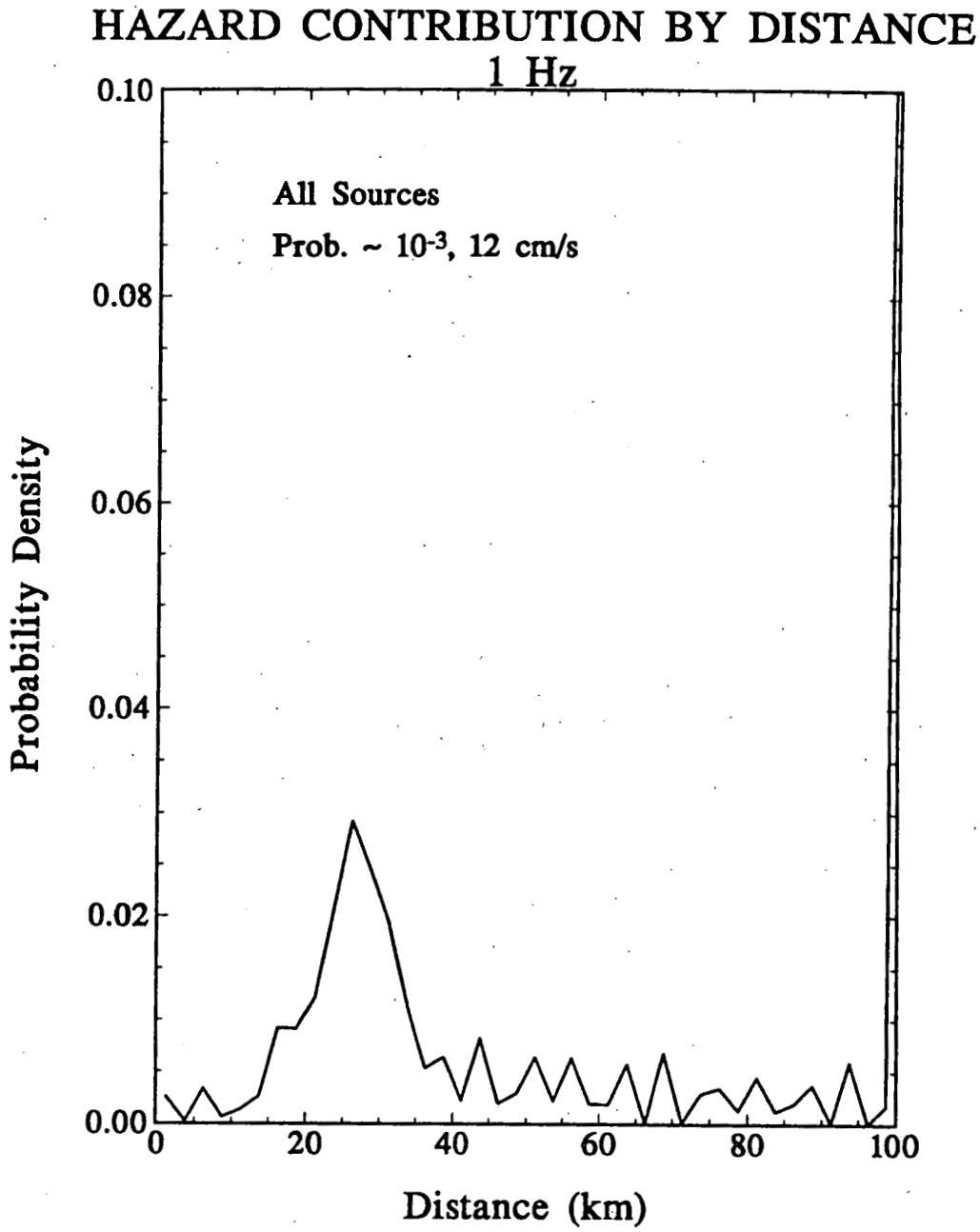

Figure J-13b. Contribution to hazard by distance for PSV(1 Hz) = 12 cm/s, all sources.

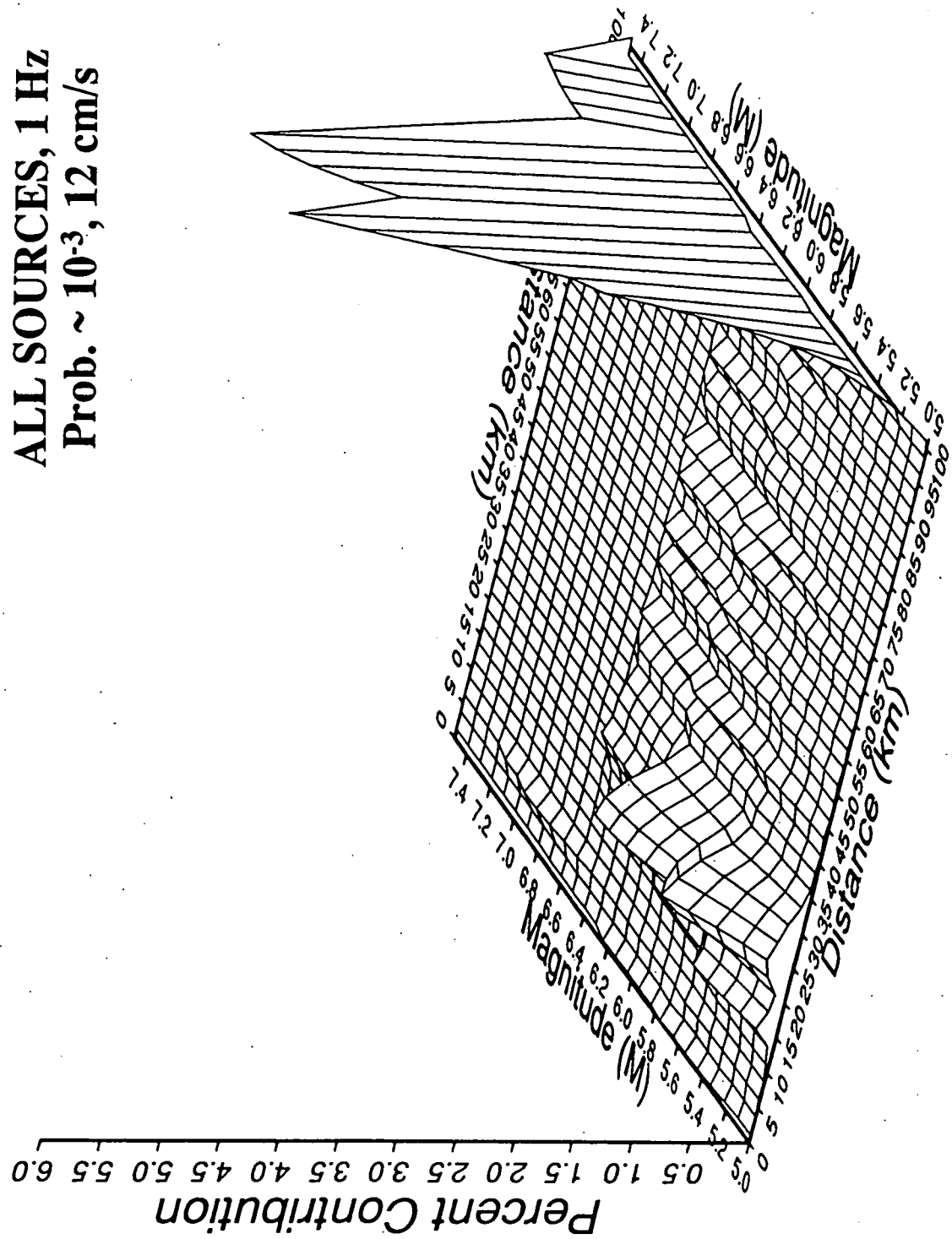

Figure J-14. Contribution to hazard by magnitude and distance for PSV(1 Hz) = 12 cm/s, all sources.

GMT Sep 13 10:55

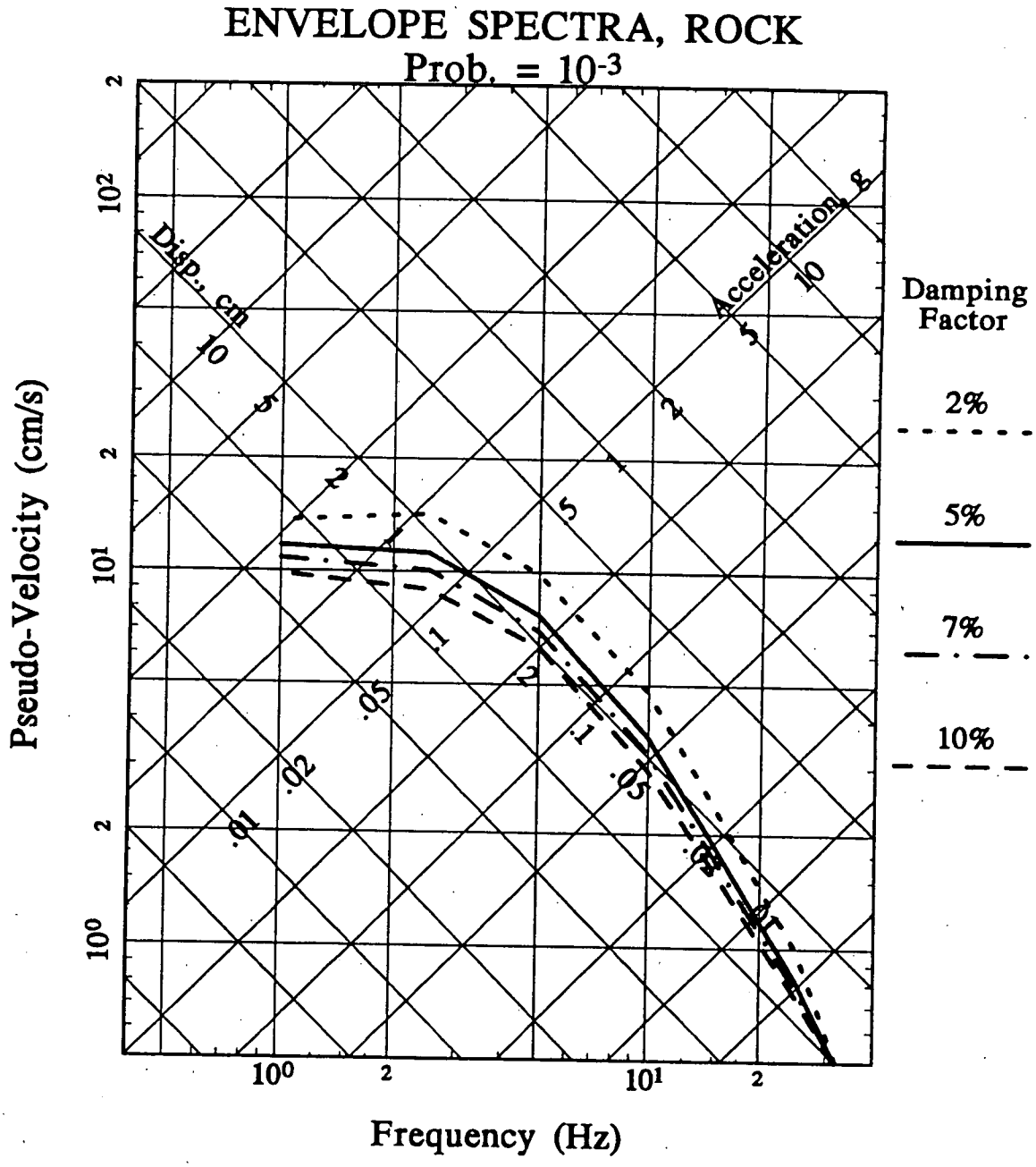

Figure J-15. Recommended deterministic tripartite spectra for 10^{-3} annual probability.

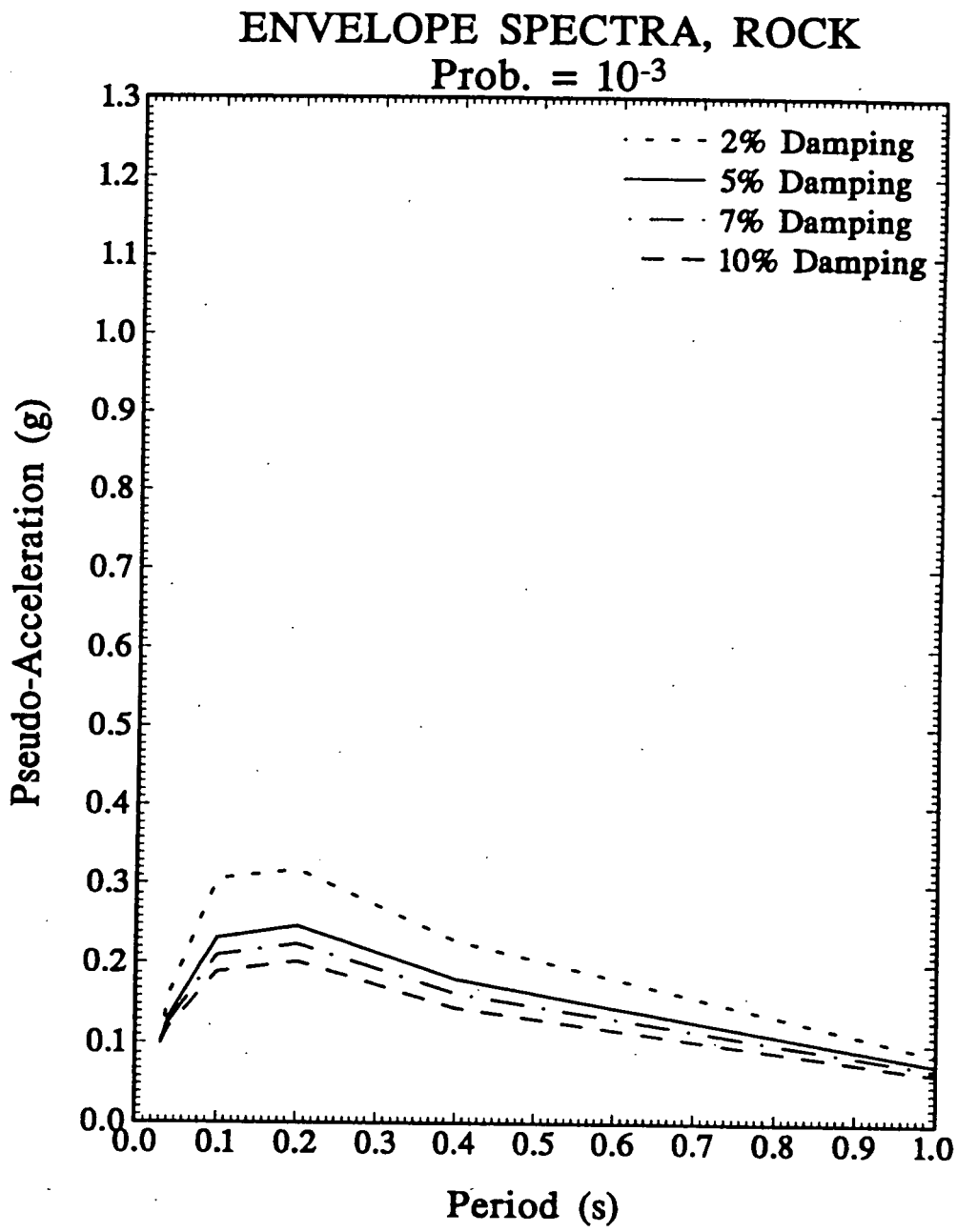

Figure J-16. Recommended deterministic pseudo-acceleration spectra for 10^{-3} annual probability.

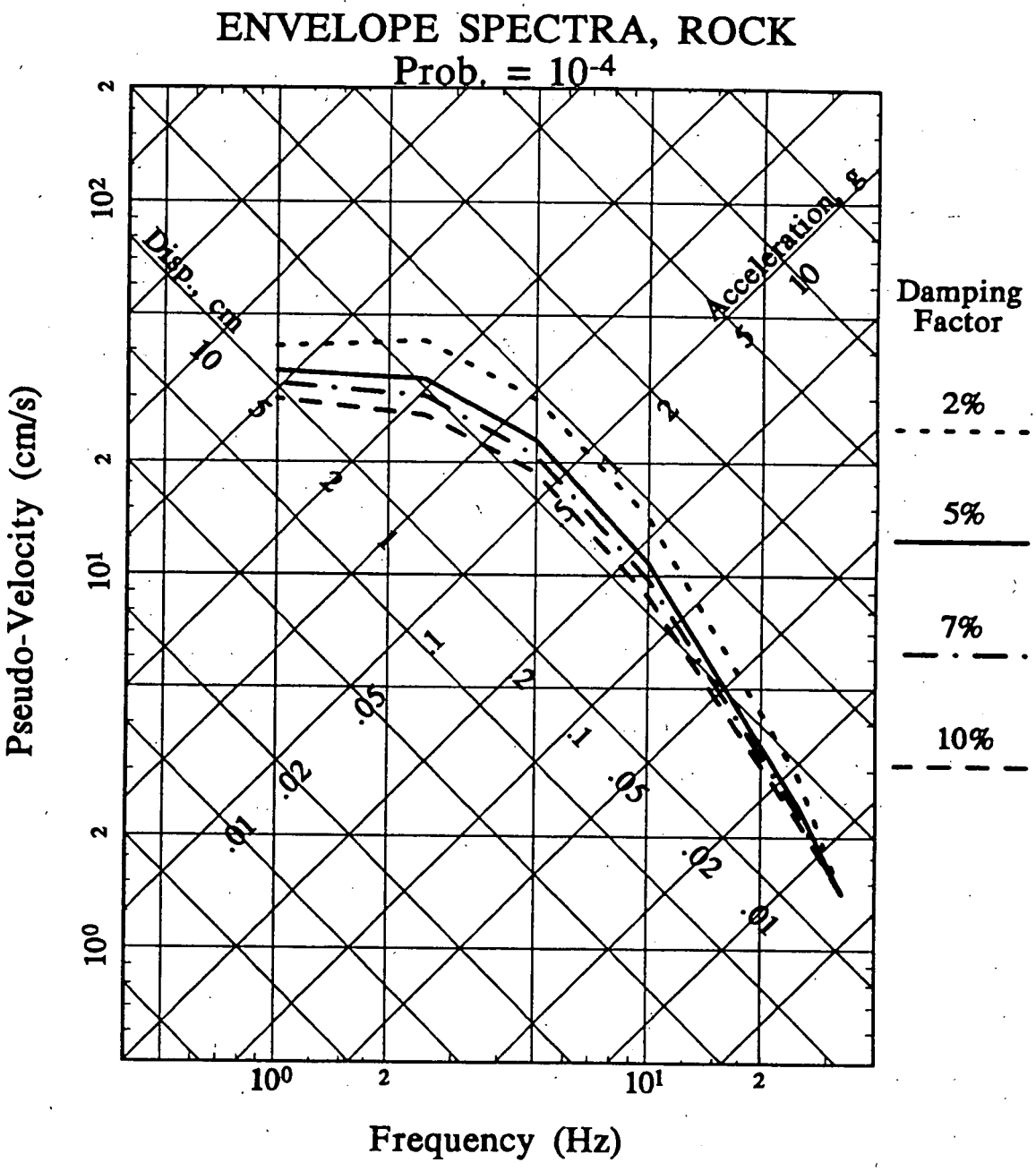

Figure J-17. Recommended deterministic tripartite spectra for 10^{-4} annual probability.

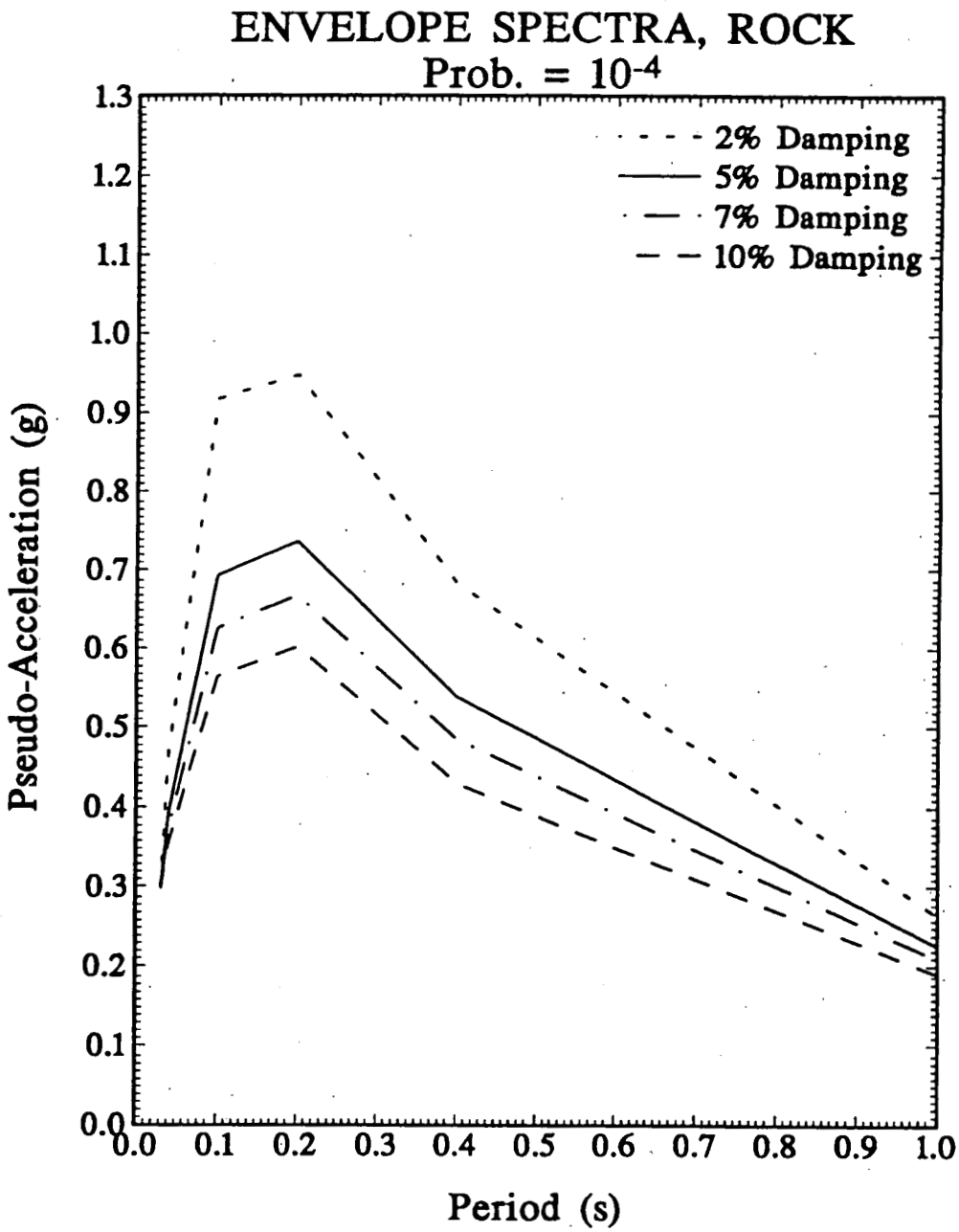

Figure J-18. Recommended deterministic pseudo-acceleration spectra for 10^{-4} annual probability.

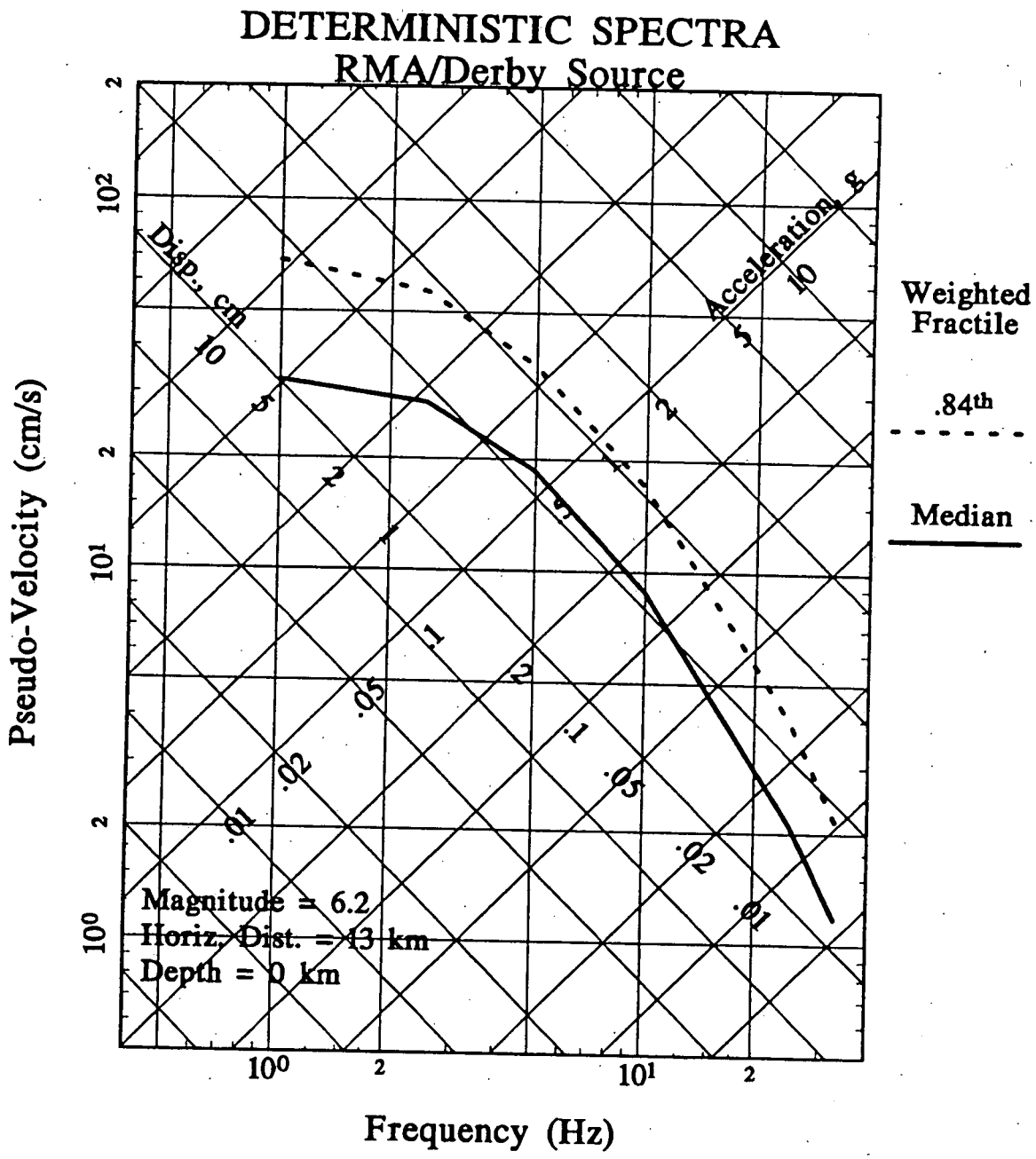

Figure J-19. Predicted 50% and 84% spectrum (5% damping) for RMA/Derby source.

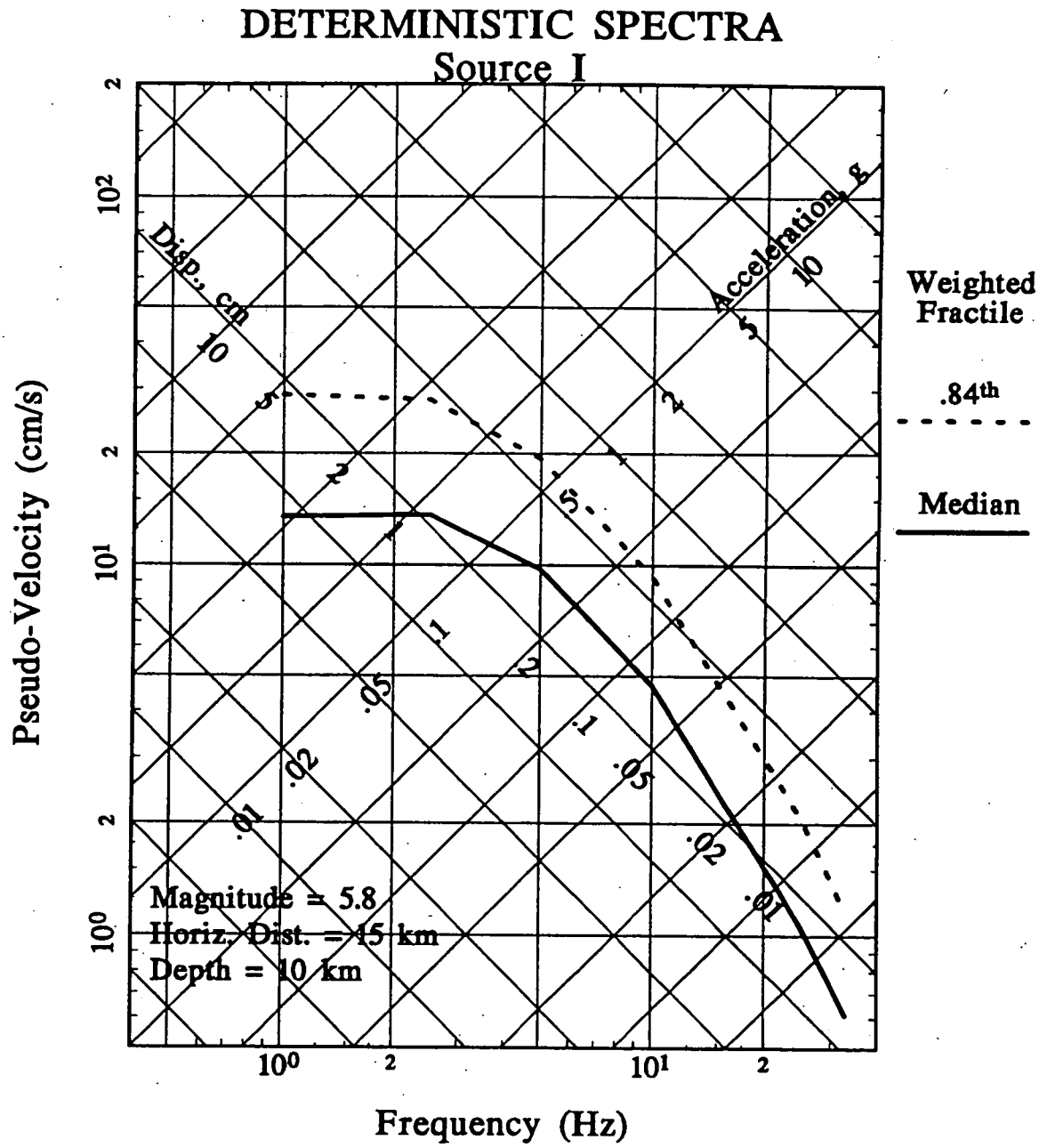

Figure J-20. Predicted 50% and 84% spectrum (5% damping) for Source I.

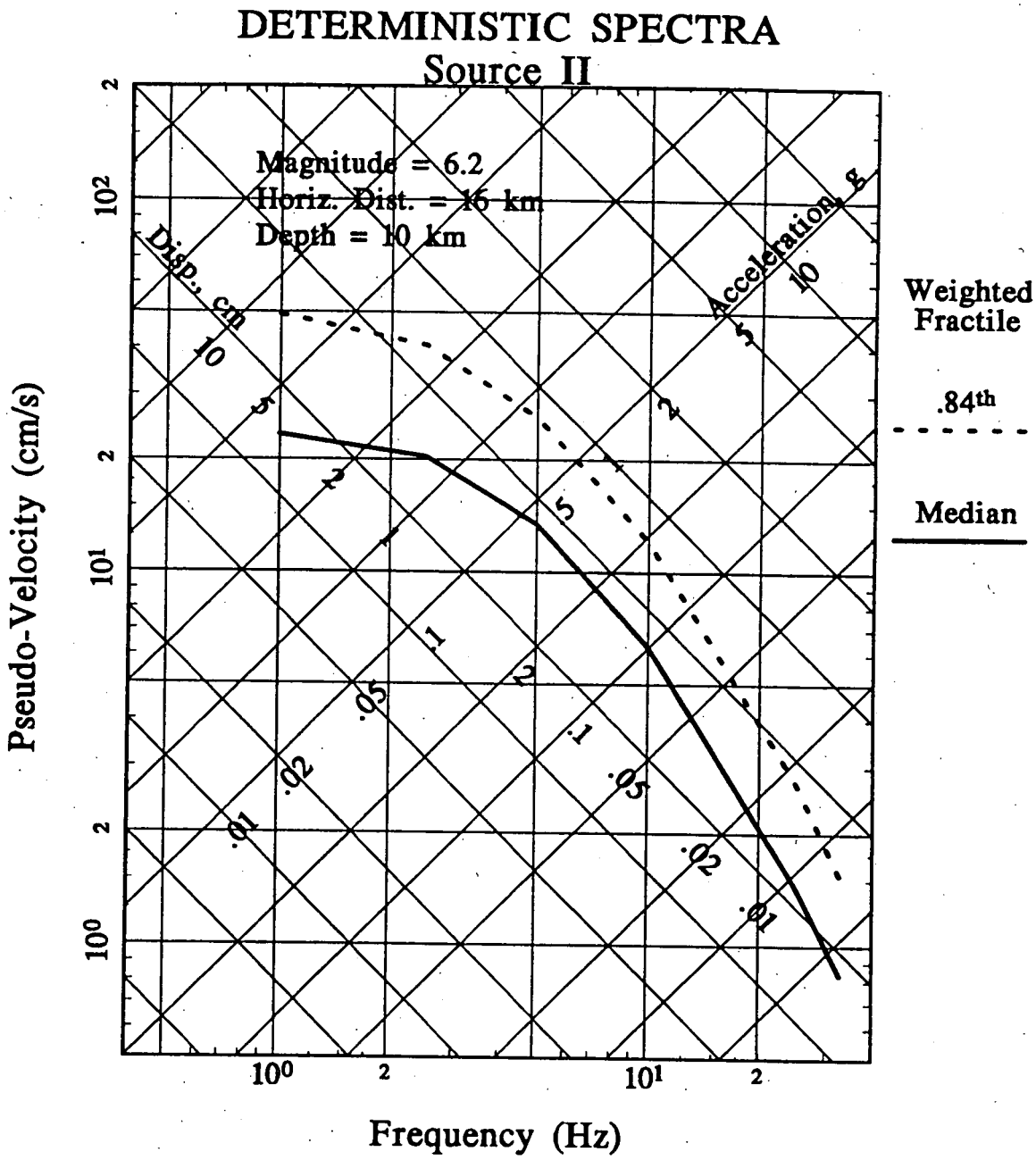

Figure J-21. Predicted 50% and 84% spectrum (5% damping) for Source II.

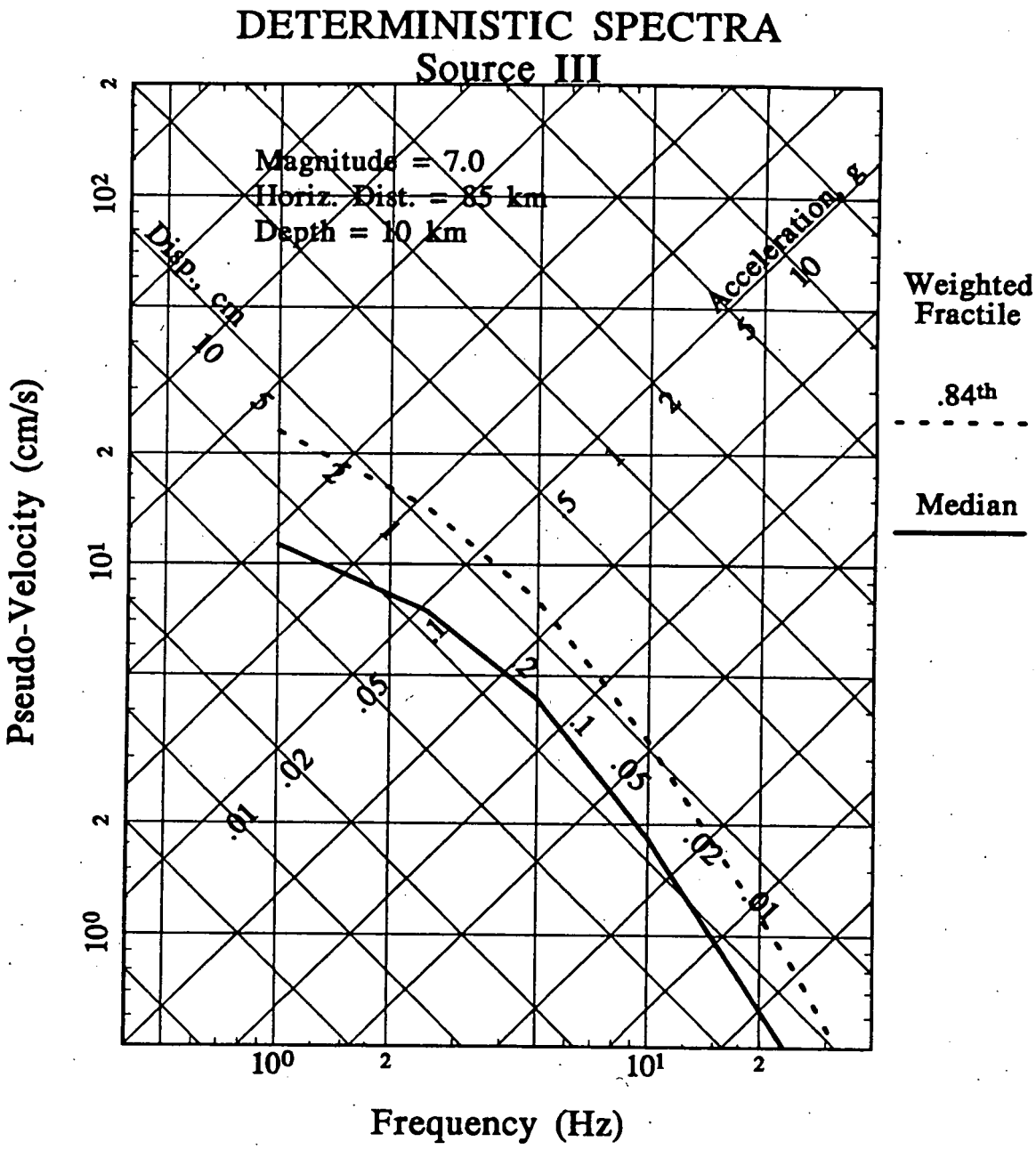

Figure J-22. Predicted 50% and 84% spectrum (5% damping) for Source III.

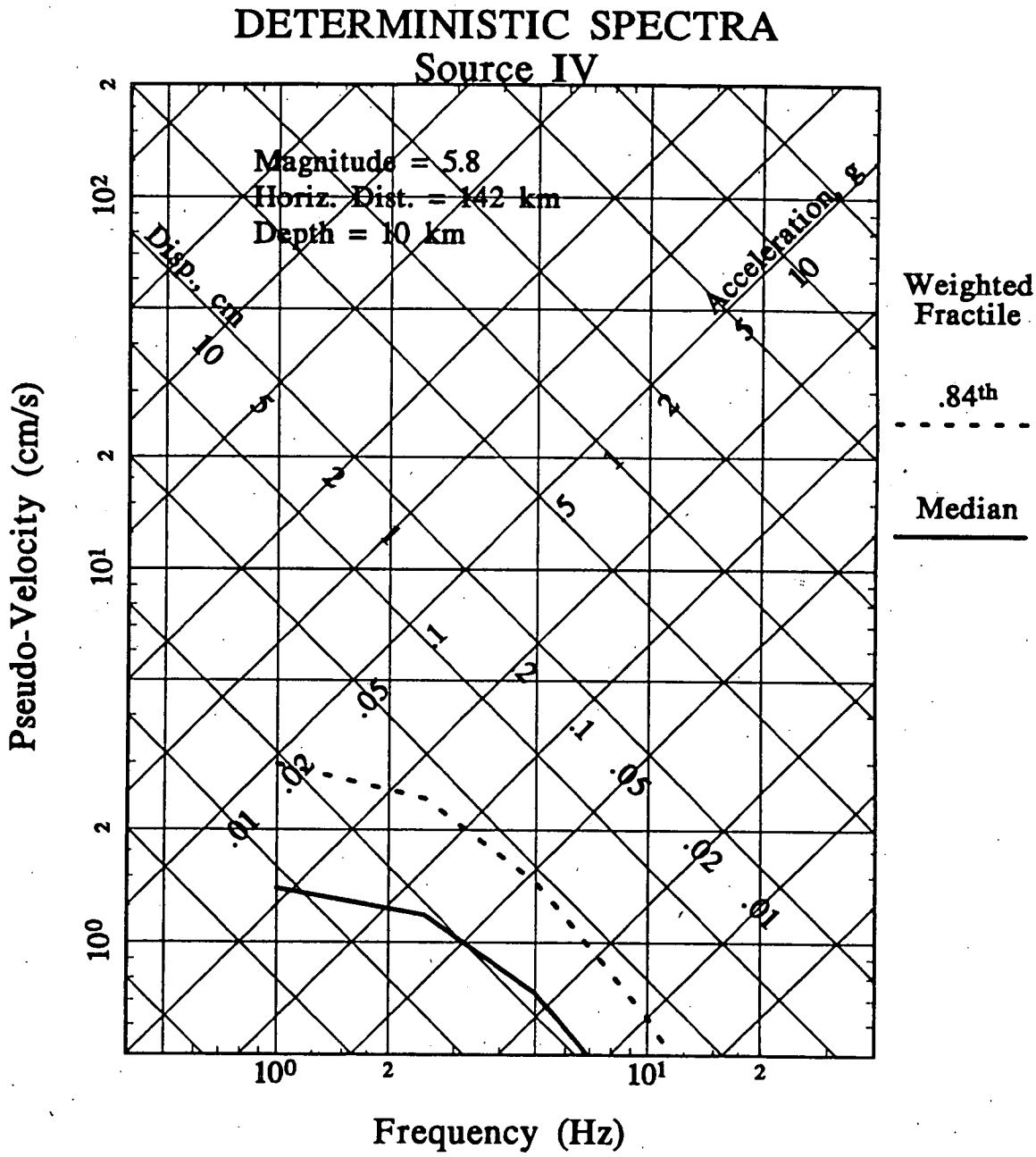

Figure J-23. Predicted 50% and 84% spectrum (5% damping) for Source IV.

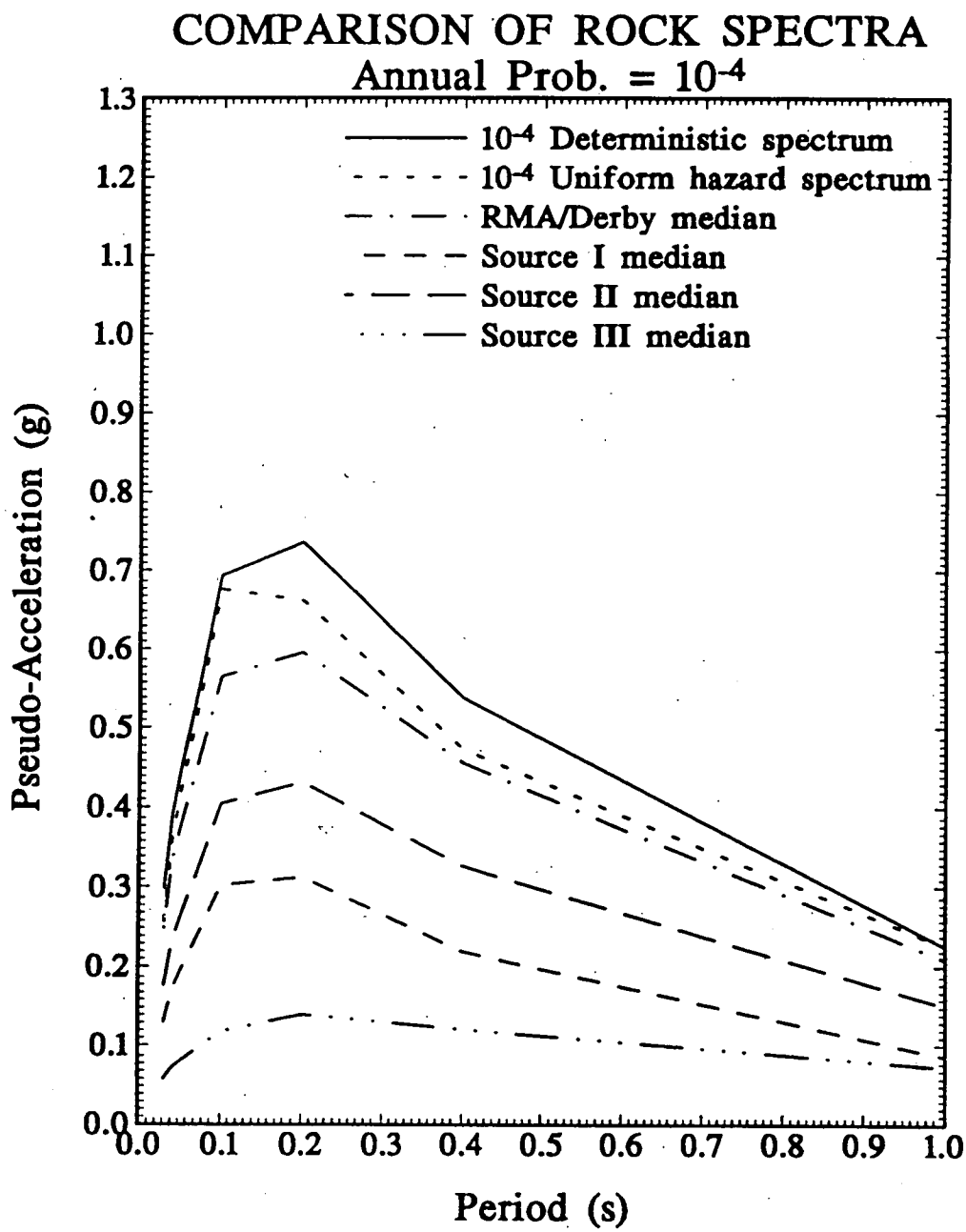

Figure J-26. Comparison of 10^{-4} rock spectra.